FAA CENTER OF EXCELLENCE FOR ALTERNATIVE JET FUELS & ENVIRONMENT

Annual Technical Report

2017

For the period

October 1, 2016 – September 30, 2017

Boston University
Georgia Institute of Technology
Massachusetts Institute of Technology
Missouri University of Science and Technology
Oregon State University
Pennsylvania State University
Purdue University
Stanford University
University of Dayton
University of Hawaii
University of Illinois
University of North Carolina
University of Pennsylvania
University of Tennessee
University of Washington
Washington State University

This work was funded by the US Federal Aviation Administration (FAA) Office of Environment and Energy as a part of ASCENT Project AJFE under FAA Award Number 13-C. Any opinions, findings, and conclusions or recommendations expressed in this material are those of the authors and do not necessarily reflect the views of the FAA or other ASCENT Sponsors.

Table of Contents

Overview

This report covers the period October 1, 2016 through September 30, 2017. The Center was established by the authority of FAA solicitation 13-C-AJFE-Solicitation. During that time the ASCENT team launched a new website, which can be viewed at ascent.aero. The next meeting will be hosted by the Massachusetts Institute of Technology, April 3-4, 2018 in Boston.

Over the last year, the ASCENT team has made great strides in research, outreach, and education. The team's success includes the following:

- **43 research projects.**

The projects can be divided into five categories: tools, operations, noise, emissions, and alternative fuels. See the project category descriptions for more detail on each category and a summary of the projects. Funding for these projects comes from the FAA in partnership with Transport Canada.

- **110 publications, reports, and presentations by the ASCENT team.**

Each project report includes a list of publications, reports, and presentations published between June 2015 and December 2017. A comprehensive list of the publications, reports, and presentations is available in the publications index on page 726.

- **105 students participated in aviation research with the ASCENT team.**

Each project report includes the names and roles of the graduate and undergraduate students in the investigator's research. Students are selected by the investigators to participate in this research.

- **72 industry partners involved in ASCENT.**

ASCENT's industry partners play an important role in the Center. The 72 members of the ASCENT Advisory Board provide insight into the view of stakeholders, provide advice on the activities and priorities of the Center's co-directors, and ensure research will have practical application. The committee does not influence FAA policy. Industry partners also play a direct role in some of the research projects, providing resources and expertise to the project investigators.

Leadership

Dr. Michael Wolcott
Center Director and Technical Lead for Alternative Jet Fuels Research
Washington State University
(509) 335-6392
wolcott@wsu.edu

Dr. R. John Hansman
Center Co-Director and Technical Lead for Environmental Research
Massachusetts Institute of Technology
(617) 253-2271
rjhans@mit.edu

Dr. John Holladay
Federal Research Laboratories and Agency Liaison
john.holladay@pnnl.gov

Dr. James Hileman
Chief Scientific and Technical Advisor for Environment and Energy
Office of Environment and Energy
Federal Aviation Administration
james.hileman@faa.gov

Research Topics

Research projects within ASCENT are divided into five categories: tools, operations, noise, emissions, and alternative fuels.

Tools

Research within the tools category involves researching current systems to understand the short- and long-term effects of new technologies. The ASCENT ream is working to develop tools to model and assess new and existing aircraft technology.

Projects include:

- 010 - Aircraft Technology Modeling and Assessment
- 011 - Rapid Fleet-wide Environmental Assessment Capability
- 035 – Airline Flight Data Examination to Improve Flight Performance Modeling
- 036 – Parametric Uncertainty Assessment for AEDT 2b
- 037 – CLEEN II Technology Modeling and Assessment
- 045 – Takeoff/Climb Analysis to Support AEDT APM Development
- 046 – Surface Analysis to Support AEDT APM Development

Operations

Research within the operations category involves improving aviation operations to reduce negative impacts on local communities, the environment, and the economy. The ASCENT team is working to develop efficient gate-to-gate aircraft operations, develop evaluation tools for aircraft performance, and explore new operations procedures.

Projects include:

- 015 - Cruise Altitude and Speed Optimization
- 016 - Airport Surface Movement Optimization
- 023 - Analytical Approach for Quantifying Noise from Advanced Operational Procedures

Noise

Research within the noise category involves researching noise pollution caused by the aviation industry. The ASCENT team is working to understand the impact of noise pollution on health, create tools for analyzing aircraft noise, understand how specific variables impact noise, and conduct outreach and education about aircraft noise reduction.

Projects include:

- 003 - Cardiovascular Disease and Aircraft Noise Exposure
- 004 - Estimate of Noise Level Reduction
- 005 - Noise Emission and Propagation Modeling
- 006 - Rotorcraft Noise Abatement Operating Conditions Modeling
- 007- Civil, Supersonic Over Flight, Sonic Boom (Noise) Standards Development
- 008 - Noise Outreach
- 017 - Pilot Study on Aircraft Noise and Sleep Disturbance
- 023 - Analytical Approach for Quantifying Noise from Advanced Operational Procedures
- 038 – Rotorcraft Noise Abatement Procedures Development
- 040 – Quantifying Uncertainties in Predicting Aircraft Noise in Real-world Situations
- 041 – Identification of Noise Acceptance Onset for Noise Certification Standards of Supersonic Airplane
- 042 – Acoustical Mode of Mach Cut-off
- 043 – Noise Power Distance Re-Evaluation

Emissions

Research within the emissions category focuses on reducing emissions from the aviation industry. The ASCENT team is working to analyze data and improve models to better understand the effect of airplane emissions, create and refine analysis techniques, and understand how policy changes could affect emissions.

Projects include:

- 002 - Ambient Conditions Corrections for Non-Volatile PM Emissions Measurements
- 013 - Micro-Physical Modeling & Analysis of ACCESS 2 Aviation Exhaust Observations
- 014 - Analysis to Support the Development of an Aircraft CO2 Standard
- 018 - Health Impacts Quantification for Aviation Air Quality Tools
- 019 - Development of Aviation Air Quality Tools for Airport-Specific Impact Assessment: Air Quality Modeling
- 020 - Development of NAS wide and Global Rapid Aviation Air Quality
- 021 - Improving Climate Policy Analysis Tools
- 022 - Evaluation of FAA Climate Tools
- 024 - Emissions Data Analysis for CLEEN, ACCESS, and Other Recent Tests
- 039 – Naphthalene Removal Assessment
- 048 – Analysis to Support Development of an Engine nvPM Emissions Standards

Alternative Fuels

Research within the alternative fuels category addresses the challenges associated with the creation and accessibility of alternative fuels. The ASCENT team is working to improve the feasibility of renewable fuels, understand how alternative fuels will affect emissions, air quality, and performance, and create standards for alternative fuel certification.

Projects include:

- 001 - Alternative Jet Fuel Supply Chain Analysis
- 021 - Improving Climate Policy Analysis Tools
- 024 - Emissions Data Analysis for CLEEN, ACCESS, and Other Recent Tests
- 025 - National Jet Fuels Combustion Program – Area #1: Chemical Kinetics Combustion Experiments
- 026 - National Jet Fuels Combustion Program – Area #2: Chemical Kinetics Model Development and Evaluation
- 027 - National Jet Fuels Combustion Program – Area #3: Advanced Combustion Tests
- 028 - National Jet Fuels Combustion Program – Area #4: Combustion Model Development and Evaluation
- 029 - National Jet Fuels Combustion Program – Area #5: Atomization Tests and Models
- 030 - National Jet Fuels Combustion Program – Area #6: Referee Swirl-Stabilized Combustor Evaluation/Support
- 031 - Alternative Jet Fuels Test and Evaluation
- 032 - Worldwide LCA of GHG Emissions from Petroleum Jet Fuel
- 033 - Alternative Fuels Test Database Library
- 034 - National Jet Fuels Combustion Program – Area #7: Overall Program Integration and Analysis

Project 001(A) Alternative Jet Fuel Supply Chain Analysis

Washington State University

Project Lead Investigator

Michael P. Wolcott
Regents Professor
Department of Civil & Environmental Engineering
Washington State University
PO Box 642910
Pullman, WA 99164-2910
509-335-6392
wolcott@wsu.edu

University Participants

Washington State University

- P.I.(s): Michael P. Wolcott, Regents Professor; Christina Sanders, Acting Director, DGSS; Manuel Garcia-Perez, Associate Professor; and Xiao Zhang, Associate Professor
- FAA Award Number: 13-C-AJFE-WaSU-013
- Period of Performance August 1st, 2017 to July 31st, 2018
- Task(s):
    - WSU 1. Design cases– Garcia-Perez, Zhang
    - WSU 2. Evaluation of the most promising biorefinery concepts for AJF production. Garcia-Perez, Zhang
    - WSU 3. Supplement and maintain the current inventory of biorefinery infrastructure identified in the conversion design cases that are useful for production of AJF. Wolcott
    - WSU 4. Community Social Asset Assessment Gaffney
    - WSU.5 Refine and deploy the facility siting tools for determining regional demand and potential conversion sites to be used in regional analyses. Wolcott
    - WSU.6 Refinery to Wing Stakeholder Assessment. Gaffney
    - WSU.7 Supply Chain analysis. Wolcott-Garcia-Perez
    - WSU. 8 Analytical support for regional CAAFI and USDA jet fuel project. Wolcott

Project Funding Level

$396,037 FAA funding and $396,037 matching funds. State committed graduate school contributions for four PhD students. Faculty time, Michael Wolcott, Manuel Garcia-Perez and Xiao Zhang are contributing to cost shared.

Investigation Team

- Michael Wolcott, Project Director/Principal Investigator
- Christina Sanders, Co-Project Director(s) /Co-Principal Investigator (Co-PI)
- Season Hoard, Co-Project Director(s)/Co-Principal Investigator (Co-PI)
- Manuel Garcia-Perez, Co-project Director(s)/Co-Principal Investigator
- Xiao Zhang, Co-project Director(s)/Co-principal Investigator
- Paul Smith, Faculty
- Michael Gaffney, faculty
- Kristin Brandt, Staff Engineer
- Natalie Martinkus, Staff Engineer
- Sarah Dossey, Staff Engineer
- Scott Geleynse, post-doctoral (100 %)
- Dane Camenzind, Graduate Student
- Lina Pilar Martinez Valencia, Graduate Student
- Tanzil Abid Hossain, Graduate Student

- Anamaria Paiva, Graduate Student
- Daniel Mueller, Graduate Student
- Kelly Nguyen, Graduate Student

Collaborating Researchers

- Burton English, University of Tennessee
- Kristin C. Lewis, Volpe

Project Overview

As part of an effort to realize an "aviation system in which air traffic will move safely, swiftly efficiently, and seamlessly around the globe", the Federal Aviation Administration (FAA) has set a series of goals and supporting outcomes, strategies, and performance metrics (Hileman et al 2013). The goal entitled, "Sustaining our Future" outlines a number of strategies that are collectively aimed at reducing the environmental and energy impacts of the aviation system. To achieve this goal, the FAA set an aspirational goal of aviation utilizing 1 billion gallons of AJF by the year 2018. This goal was created from an economic, emissions, and overall feasibility perspective (Richard 2010, Staples et al. 2014).

Current approaches to supply chain analysis for AJF optimizes transportation logistics of feedstocks to refinery and refinery to wing (Bond et al 2014). One of the largest barriers to large scale production of all bio-fuels is the high capital cost of greenfield facilities translating to risk in the investment community (Huber et al 2007). The capital cost of cellulosic ethanol plants range from $ 10-13/gal capacity (Hileman and Stratton, 2014). The additional process steps required to convert the intermediate to a drop in AJF could increase this cost to over $ 25/gal capacity (Hileman 2014).

The realities of these initial commercialization efforts into second-generation biofuel have led to studies that envision alternate conversion scenarios including transitioning existing facilities (Brown 2013). Gevo is employing retrofit strategies of corn ethanol plants for producing isobuthanol, a potential intermediate for the alcohol-to-jet process of producing iso-paraffinic kerosene (Pearlson 2011, Pearlson et al 2013). Research to envision scenarios to achieve the FAA aspirational goal of AJF consumption relied upon "switching" scenarios where existing and planned capacity would be used for producing the drop-in fuel (Malina et al 2012). All of these approaches require identifying existing industrial assets to target for future AJF production. Siting becomes, not just an exercise of optimizing feedstock transportation, but aligning this critical factor with a host of existing infrastructure, markets within regions with the proper social capital for developing this new industry (Seber et al 2014, Henrich et al 2007).

Up to now all the AJF supply chain analyses published have been limited to standalone jet fuel production technologies that do not generate bio-products. The potential techno-economic and environmental benefits of using existing industrial infrastructure and the production of coproducts on the development of jet fuel production scenarios has to be considered in future studies.

The design cases of the standalone AJF production facilities will be used in supply chain evaluations. Community Social Asset Modeling (CAAM): Social Asset modeling is not well-developed, and efforts are likely hampered by the difficulty in quantifying social assets when compared to improved environmental performance or a reduction in biofuel costs that may be observed by optimizing economic and environmental constraints. However, considering the community characteristics of a potential site is important when determining preferred locations for a new biorefinery. Community resistance or enthusiasm for the biofuels industry can play a large role in the success or failure of a facility (Martinkus et al 2014). CAAM efforts conducted within this project will inform disciplinary applications and advances. It is clear that social factors can have a significant effect – positive or negative – on project adoption and implementation, especially high technology or energy-related projects (Lewis et al 2012, Martinkus et al 2012). Accounting for social factors to inform selection of sites and implementation decisions to maximize positive social support and minimize opposition and social negatives can significantly enhance project success. The CAAM model originally piloted in the NARA project is designed to provide a quantitative rating of select social factors at the county level (Martinkus et al 2014).

This research is targeted at identifying the key barriers in regional supply chains that must be overcome to produce 1-billion gallons of alternative jet fuel. This overall goal is addressed by developing tools to support the AJF supply chain assessment by the Volpe Center. Our effort will provide facility siting analyses that assess (a) conversion design cases combined with (b) regional supply chain assets and (c) social capacity assessments for communities to act collectively for development goals.

Finally, a refinery-to-wing stakeholder assessment will support modeling and accounting of AJF distribution for downstream fuel logistics.

Task #1: Design Cases

Washington State University

Objective(s)

Continuation from previous years

Our team will complete the reviews and final report of the design cases for six standalone AJF technologies and four important industries (sugarcane, pulp and paper, corn ethanol and petroleum refineries) developed in previous years and will start developing the design cases for targeted co-products that could improve the economic viability of AJFs.

New Tasks

(1) New case design report "Alternative Jet Fuel Supply Chain Analysis: hydrothermal liquefaction processing of tall oil for jet fuel production". This work involved collecting primary data, establishing process flow diagram and conducting a detailed TEA. This task will be carried out in collaboration with PNNL HTL group. **(2)** Conduct detailed TEA analyses of integrating lignin co-products technologies in Alcohol-to-Jet pathway to determine the potential to lower fuel cost to $2.00/gge.**(3)** New design case reports on technology review and process evaluation of lipid conversion processes (HEFA, CH, SBI, Forge, Tyton, decarboxylation) and new technologies for the production of alternative lipids (HTL and sugars to lipid). **(4)** Conduct detailed TEA analysis integrating lignin co-products technologies in biorefinery cases integrated with the corn ethanol, and the sugarcane industry

Research Approach

Background

The design cases developed for AJFs and for existing industrial infrastructure, are being used in the development of supply chains and on the identification of synergisms that could eventually lead to the construction of integrated systems of AJF production that take advantage of the infrastructure in a given region. Analysis of the location of existing infrastructure showed that the United States can be divided in regions dominant biomass of the region. So, we believe that a viable approach to evaluate the synergism between the AJF pathways, the existing infrastructure and the co-products is to generate advanced biorefinery concepts around the Petroleum Refineries, Pulp and Paper Mills, Sugar Cane Mills, and Corn Ethanol Mills. Then we will compare the biorefinery concepts developed for each of these technologies to decide the most promising ones. The most promising biorefinery concepts for the synergistic production of AJFs and co-products with these industries will then be used in the supply chain analyses.

Standalone design case reports are generated by conducting reviews of research related to each in academic literature and public information available from commercial interests developing the technology. The reports are meant to detail the processes involved in each conversion pathway and outline the technology readiness and particular barriers to implementation. Publically available information on the commercial processes and research literature will provide the foundation of information later used in modeling efforts. Where detailed process engineering information is lacking, new models will be built to estimate the parameters needed to complete assessments such as techno-economic modeling, lifecycle analysis, and supply chain modeling. Aspen Plus is primarily used to generate process models and details including mass balances, energy balances, energy requirements, and equipment size and cost. These results will also aim to provide the basis for comparative analysis between design cases, identifying key advantages and markets for each technology.

Each design case has the following components: (1) Feedstock requirement (Availability and feedstock composition) (2) Flow diagram of technology (3) Companies commercializing the technology (level of maturity) (4) Current location of units in the United States (In case of an existing technology it will be the inventory of units that could be retrofitted) (5) Literature review on papers reporting data relevant to the operation of the technology (operating conditions, type of reactor used, catalysts, yield of products) (6) Properties of jet fuel produced (7) Identification of potential intermediates (bio-oil, sugars, densified feedstock); current and potential uses of wastes and effluents; and co-products (biochemicals, carbon, etc.) that can be obtained from the technology.

Last year we continued refining the design cases developed for four standalone AJF technologies: Alcohol to Jet (ATJ), Hydrotreated Depolymerized Cellulosic Jet (HDCJ), Direct Sugars to Hydrocarbons (DSHC), Synthetic kerosene and Synthetic Aromatic Kerosene (SK&SAK), as well as for four important industries; sugarcane, pulp and paper, corn ethanol and petroleum refineries. We have addressed all the comments received from our internal reviewers, and from our industrial reviewers. In the last six months we have been standardizing the design cases so that they can be used by our partners. The design case for the Hydrotreated depolymerized cellulosic jet consisting in a literature review, the mass and energy balances and the economic analysis was submitted in October. The design case for the Virent technology and the Alcohol to Jet technology are under review and will be submitted before the end of the year. The design cases for three of the industrial infrastructure (corn ethanol, and sugarcane mill) are completed and will be soon submitted for review and standardization. We are currently working to submit for revisions and standardization the petroleum refinery design case by March 2018. We are drafting a manuscript of integration of ATJ technologies in chemical pulp mill infrastructure. At the request of FAA, this year we started developing design cases for HEFA and FT. The first draft of these design cases will be available by the end of the year. We are also working in a literature review of other technologies for lipid conversion (CH, SBI, Forge, Tyton, decarboxylation) and new technologies for the production of alternative lipids (HTL and sugars to lipid). This literature review will be completed by the summer 2018.

We are working on completing a design case report of "lignin co-products opportunities from advanced fermentations based AJF processes".

We are working with PNNL to complete a case design report on HTL for AJF conversion. This work involved collecting primary data, establishing process flow diagrams for several feedstocks including, municipal waste (primary and secondary), Algae and tall oil, and conducting a detailed TEA. We have discussed the draft report with PNNL. We will also work with PNNL to help identify ways to improve HTL conversion efficiency.

Responsible: Manuel Garcia-Perez, Xiao Zhang and Michael Wolcott

Milestone(s)

Literature search complete for all pathways and design cases. Draft design cases complete for all pathways and design cases. Internal review by team members and external reviews completed. We are currently standardizing all the design cases and one design case for alternative jet fuel production was released for use by team members early in October. Three more will be released by the end of the year. The design cases for the corn ethanol and the sugarcane industry are under review by the standardization team. The design case for the petroleum refinery will be available by the summer 2018. The design cases for HEFA and micro-reactors FT are under construction and should be completed by the end of the year. We will complete the design cases report for Lignin co-products, pulp and paper mills by the end of this year. A detailed HTL designed cased report will be completed by March 31st 2018.

Major Accomplishments

Models were developed for the main AJF production technologies and for relevant technologies that can be used as baseline for the synthesis of biorefinery concepts. The methodology for these models is providing data to form a baseline for comparative analysis with other design cases. Key process variations have been identified in several design cases and have been modeled to determine their effects on process economics and viability, as well as to identify the key barrier toward commercialization in complete biorefinery concepts.

Data generated from the design cases were also supplied to A01 partners to assist with supply chain, techno-economic models by improving the conversion and cost figures database values. Evaluations of the effects of process variations on the chemical properties of products generated are being used to provide insight into the challenges that will be faced when blending the AJFs into commercial jet fuel.

Most of the design cases have undergone external review and are currently under review by the standardization team for public release.

Publications

Scott Geleynse, Kristin Brandt, Manuel Garcia-Perez, Michael Wolcott, Xiao Zhang, The Alcohol to Jet Conversion Strategy for Drop in Biofuels. Evaluation of Technical Aspects and Economics (manuscript reviewed by Gevo and John Holladay at

PNNL, currently under review by FAA, a copy of draft manuscript was also sent to LanzaTech). To be submitted for Journal publication by the end of Nov. 2017.

Outreach Efforts
None – Task in Progress

Awards
None – Task in Progress

Student Involvement
Several graduate (Scott Geleynse, Mond Guo, Carlos Alvarez Vasco, Ruoshui Ma, Kelly Nguyen, Tanzil Hossain, Anamaria Paiva, Lina Martines) and undergraduate students participated in the creation, editing and updating of the design cases for standalone AJF technologies, for relevant existing infrastructure and for co-products from lignin.

Plans for Next Period
Complete the design cases for HEFA and FT-micro-reactors. Literature review on other technologies for alternative jet fuel production from lipids. Release of all design cases for standalone AJF production technologies, for relevant infrastructure and for co-products from lignin.

Task #2: Evaluation of the Most Promising Biorefinery Concepts for AJF Production
Washington State University

Objective(s)

Continuation from previous years
This year we will complete the evaluation of biorefinery scenarios for AJF production in corn ethanol, sugarcane and pulp and paper mills and petroleum refineries. Last year we advanced the analysis for corn ethanol and pulp and paper mills. This year we should complete the analysis for sugarcane and petroleum refineries.

New Tasks
Conduct detailed TEA analyses of integrating lignin co-products technologies Direct Sugars to Hydrocarbons (DSHC) pathway to determine the potential to lower fuel cost to $2.00/gge.

Research Approach

Background
In this task we are using the design cases of existing infrastructure, AJF production technology and co-products identified to generate new biorefinery concepts for Petroleum Refineries, Pulp and Paper Mills, Sugarcane Mills and dry corn mills. The results from this effort will allow us to identify and select the most commercially feasible biorefinery concepts. Major technical gaps/barriers toward commercialization of each of the biorefinery concepts will also be revealed from the results of this study.

Integration of process technologies through a similar approach to the standalone design cases is assessed. Further evaluation of integration concepts will be developed by pairing standalone cases with these opportunities to evaluate the economic and environmental advantage of the integration approaches. During this period we conducted detailed analyses of alcohol to jet conversion (ATJ) and integration with pulp mill operations. We have also investigated the potential of lignin co-products contribution to the overall process economy.

A dry grind corn ethanol mill (DGCEM) with a capacity of 80 million gallons of ethanol per year (MGY) was studied in order to evaluate potential bio-refinery scenarios for AJF production. Five alternative jet fuel (AJF) technologies were studied: Virent's BioForming, "Gevo" alcohol to jet (ATJ), direct sugar to hydrocarbon (DSHC), fast pyrolysis (FP) and Fischer-Tropsch (FT). A standardized methodology was adopted to evaluate twelve integration scenarios between DGCEM and AJF

technologies in terms of minimum fuel selling price (MFSP) and greenhouse gas (GHG) emission. The total alternative jet fuel production capacity ranged from 25 MGY to 50 MGY. Eight scenarios resulted in cost reduction opportunities in capital expenditure (CAPEX) and operational expenditure (OPEX) leading to reduced MFSPs in the range of 6% to 29%. Four scenarios resulted in negative GHG emission. A performance evaluation revealed that integration scenario of fast pyrolysis provided the better results in cost and GHG emission reduction. We are currently conducting similar analyses for a corn ethanol plant and petroleum refineries. The comparison of sugarcane bio-refinery concepts for aviation fuel production has progressing well. In January 2018 we plan to start will the analysis of petroleum refineries biorefinery concepts.

We will complete a draft paper of integration of ATJ technologies in pulp mill infrastructure this year. We will then apply this methodology for analyzing other advanced fermentation technology (direct sugar to hydrocarbon by Amyris) in pulp mill next year. We will also expand the lignin co-product analysis to all other AJF pathways.

Major Accomplishments

Economic models and Life Cycle Assessments were used to support the selection of the most promising bio-refinery concepts for the corn ethanol plant. A manuscript on corn ethanol bio-refineries will be submitted shortly.

Publications

We plan to complete the manuscript preparations of “integration of ATJ to pulp mill infrastructure” and “Lignin co-products opportunities to improve AJF production in advanced fermentation conversion pathways” by June 30th 2018.

- Tanzil, AH, Zhang X, Wolcott M, Garcia-Perez: Evaluation of Biorefinery Alternatives for the Production of Jet Fuels in a Dry Corn Ethanol Plant. Paper to be submitted to Biofuels, Bioproducts and Biorefinery, 2018
- Martinkus, N., Rijkoff, S.A.M., Hoard, S.A., Shi, W., Smith, P., Gaffney, M. & Wolcott, M. (2017). Biorefinery site selection using a stepwise biogeophysical and social analysis approach. Biomass and Bioenergy, 97, 139-148. doi:10.1016/j.biombioe.2016.12.022
- Rijkhoff, S.A.M., Hoard, S., Gaffney, M.J. & Smith, P.M. (2017). Communities ready for takeoff: Integrating social assets for biofuel site-selection modeling. Politics and the Life Sciences, 36(1):14-26. doi:10.1017/pls.2017.6

Outreach Efforts

Tanzil, AH, Geleynse S, Garcia-Perez M, Zhang X, Wolcott M: Alternative Jet Fuel Production in Integrated Biorefuneries Using Existing Dry Corn Mill: Cost Reduction Opportunities. ASCENT Meeting, September 27-28, 2016

Awards

None

Student Involvement

Graduate students Scott Geleynse, Senthil Subramaniam, Kelly Nguyen, Abid Tanzil Houssain, Lina Martinez Valencia, Anamaria Paiva, and Ruoshui Ma have received trained working in this project. An undergraduate student, Kitana Kaiphanliam, funded under an NSF REU grant assisted with building techno-economic models for co-products production scenarios.

Plans for Next Period

Next period Dr. Garcia-Perez’s team will focus on the potential cost reductions if alternative jet fuels are integrated with a petroleum refinery. Dr. Zhang’s team will complete the HTL case design report and lignin analysis report.

Task #3: Supplement and Maintain the Current Inventory of Bio-Refinery Infrastructure Identified In the Conversion Design Cases That Are Useful For Production of AJF

Washington State University

Objective(s)

Continuation from previous years
This task requires annual evaluation of the database to add or eliminate new and closed facilities in each category so that the geospatially specific assets are current with reality.

Research Approach

Background
Utilizing existing infrastructure assets is key to retrofit approaches to developing the industry. In order to differentiate between the relative value of different options, the specific assets must be valued with respect to their potential use within a conversion pathway. Regional databases of industrial assets that might be utilized by a developing AJF industry, have been assessed on a national level. These baseline databases are compiled from a variety of sources that include industry associations, universities, and news outlets. These databases will be expanded, refined, and validated as the conversion design cases articulate additional needs for the regional analyses.

Milestone(s)
National databases are compiled, geolocated, validated and shared for biodiesel, corn ethanol, energy pellet, pulp & paper, and sugar mill production. We are evaluating the database to add or eliminate new and closed facilities in each category so that the geospatially specific assets are current with reality.

A regional supply chain analysis was completed for eastern Washington and western Montana using forest harvest residuals as the feedstock. This analysis included market fuel demand, potential siting assets and feedstock availability. A siting tool was developed to help determine if the most economical site was a greenfield, co-location or conversion of an existing facility. This tool includes the impact of operating costs including electricity rate, natural gas rate and delivered feedstock cost. Capital costs are included by applying a factored approach to estimating capital costs and accounts for infrastructure that would be included at an existing facility such as service facilities, equipment costs, buildings and yard improvements. The siting tool combines the operating and capital cost components in a cost-weighted equation. The results of the equation allow for quantitative comparison of multiple locations based on both operating and capital costs.

Major Accomplishments
The national databases have been compiled, validated, and shared with the A01 teams. All of the metadata is complete for use in the regional analyses.

Publications
None – these are shared assets for later analyses

Outreach Efforts
Nothing to report

Awards
None – these are shared assets for later analyses

Student Involvement
Dane Camenzind, Master's student in Civil Engineering, validated the operating status of previously identified production facilities, compiled and geolocated MSW incinerators and landfill gas to energy facilities and worked to assemble and update all county level feedstock information.

Natalie Martinkus, Ph.D. candidate in Civil Engineering (degree completed), developed the siting decision matrix as a portion of her dissertation.

Plans for Next Period

Additional refinements will be completed for the siting tool. GIS analysis will be completed after tool is finalized. We plan to continue the annual evaluation of the database to add or eliminate new and close facilities in each category so that the geospatially specific assets are current with reality.

Task #4: Continue Work On Social Asset Decision Tools Developed In Phase 1 For Plant Siting (Community Asset & Attribute Model—CAAM); Including Additional Validation And Incorporation Of Multi-Decision Making Tools. Extend Application To Another US Region In Coordination With Other Team Members (Inland Northwest, Appalachian Region). Prepare For Extension Nationally & Replication in Select Countries

Washington State University

Objective(s)

Continue to build on social asset decision tools for plant siting (Community Asset & Attribute Model—CAAM) through addition of political capital. Prepare for extension nationally & replication for Canada, and select EU countries.

Research Approach

Based on key measures of social, cultural, human, and political capitals, WSU has developed and refined a Community Asset and Attribute Model (CAAM). The first tool was initially applied to the NARA region, and the refined tool that added more complete measures of social, cultural, and human capital was deployed in two sub-regions of NARA in the Pacific Northwest. The initial measure of political capital has now been added to the CAAM, and the tool can be used across the continental United States. The refined CAAM (excluding the political capital) has been used to assess social capacity for biorefinery siting in two separate studies, including retrofitting paper mill facilities in the Pacific Northwest. Ground-truthing analysis was used to assess the role of social, cultural and human capitals in the success or failure of biofuel related projects in both the NARA and BANR regions. This ground-truthing analysis supported the role of CAAM measures in project success, and suggested opportunities to further improve the CAAM which we are currently working to incorporate. The CAAM has undergone another refinement and now includes measurements for political capital. The ways in which each capital is measured have also been altered for each capital. This overhaul necessitates another effort to validate the model, which is currently underway. Work is also underway to develop approaches to apply the CAAM strategically providing guidance to stakeholders on methods of approaching communities and stakeholders to aid successful development and implementation.

Milestone(s)

The validated CAAM model based on county-level comparative rankings on Social, Human Cultural, and Political Capitals is tested and available for use.

Major Accomplishments

A paper on the refined CAAM will be published by Politics and the Life Sciences in 2017, the manuscript details the model's measurements of cultural, human, and social capital and presents validation of the model based on case studies from the Pacific Northwest. A step-wise analysis that combines biogeophysical and social assets to examine retrofitting pulp mills in the Pacific Northwest has been published in Biomass and Bioenergy. The updated CAAM with the addition of political capital was also presented at the WSU Sustainability Fair.

Publications

Peer-reviewed journal publications:

Martinkus, N. Rijkhoff, S.A.M., Hoard, S.A., Shi, W., Smith, P., Gaffney, M., & Wolcott, M. (submitted, R&R). Biorefinery Site Selection Using a Stepwise Biogeophysical and Social Analysis Approach. *Biomass and Bioenergy.*

Rijkhoff, S.A.M., Hoard, S., Gaffney, M., Smith, P. (submitted). Communities Ready for Takeoff: Integrating Social Assets for Biofuel Site-selection Modeling. *Politics and Life Sciences.*

Outreach Efforts

Mueller, D., Hoard, S., Sanders, C., & Gaffney, M. *The Community Assets and Attributes Model: Refining and Updating Measurements for Social Assets*. Fall 2017 ASCENT Advisory Committee Meeting. Alexandria, VA.

Mueller, D., Hoard, S., Sanders, C., Gaffney, M., & Smith, P. *Strategic Applications of the Community Assets and Attribute Model*. Washington State University Sustainability Fair. Pullman, WA.

Awards

None

Student Involvement

Daniel Mueller, Ph.D. candidate in political science at WSU and research assistant on this project, will continue validation efforts for the CAAM and has developed measurements for political capital. He will also continue work on developing strategic applications of the CAAM.

Kelli Roemer, Master's student of natural resources at the University of Idaho, has completed validation work of the CAAM as part of her thesis work. She has completed her thesis, receiving her M.S.

Plans for Next Period

Subsequent development of the CAAM will include further validation efforts of the overhauled version of the model that now includes political capital and new measurements for the other social assets. Strategic application of the CAAM will also be examined, which includes developing strategies to go beyond the model's ability to quantitatively identify ideal communities and include considerations for political support of biofuels and the potential for sustainable outcomes. This year the CAAM model will be further developed by incorporating multi-method decision-making tools, including semi-quantitative weighting approaches, for better inclusion in current biogeophysical, economic, and systems analysis.

Task #5: Refine and Deploy the Facility Siting Tools for Determining Regional Demand and Potential Conversion Sites to Be Used in Regional Analyses

Washington State University

Objective(s)

Continuation from last year

Develop readiness level tools for regional projects.

Research Approach

The CAAM model developed under the NARA project, and refined for ASCENT applications, provides county-level data collected from national datasets (to conduct a preliminary assessment of community characteristics for now four (Cultural, Social, Human, Political) of the seven "Community Capitals" framework (Emery and Flora. 2006)."

To help improve facility siting tools, prior CAAM models (focusing on 3 assets: social, cultural, and human capital) have been added to biogeophysical assets to assess suitability of communities in the Pacific Northwest for bio-refineries. Expanding on these analysis, our CAAM measures have been added to a decisional support tool to assess re-purposing pulp mills in the Pacific Northwest for a biorefinery. These approaches have been utilized for cellulosic Alcohol to Jet supply chains in the Pacific Northwest, and we will work to demonstrate the tool for supply chain and siting analysis for the alternative jet fuel production using FOGs converted from HEFA in the Inland Northwest.

Milestone(s)
CAAM has been updated with four capitals, and readiness level tools for regional projects are being developed.

Major Accomplishments
During this reporting period, ground truthing of CAAM has been completed, and a Master's thesis based on this analysis was completed this summer. Further validation and refinement has led to the incorporation in an updated Decision Support Tool for the Pacific Northwest and the addition of political capital. National datasets on voting trends in local and national elections are currently being assessed for incorporation in strategic intervention modeling.

Publications
None

Outreach Efforts
None

Awards
None

Student Involvement
Daniel Mueller, Ph.D. candidate in Political Science, now holds a funded Research Assistant appointment working on this project, and has been primarily responsible for acquisition of new primary data, further validation of the model, and the (continuing) development of the fourth iteration of the CAAM.

Kelli Roemer, Master's student of natural resources at the University of Idaho, is continuing validation work of the CAAM as part of her thesis work.

Plans for Next Period
In the next year, the new iteration of the CAAM that includes updated data and the addition of political capital will be validated and applied in the NARA and BANR regions, with expansion to at least one additional U.S. region (Inland Northwest and potentially Central Appalachian Region in cooperation with Team members). This model is based upon the addition of measurements for political capital, development of more refined measurement of capital comparative ranking beyond dichotomous outperform/under-perform ratings using standard deviations to examine distance from regional average and impact on successful development and implementation, alternative measurements for cultural capital and slight changes in measurements for human and social capitals, and final validation, after statistical confirmation, using selected case studies to confirm the efficacy of the model.

The updated CAAM is available for use nationally, allowing comparison of counties against defined regional norms on cultural, social, human, and political capital scales that have been statistically tested and validated through triangulated testing with external data. The new version of the CAAM allows for further enhancing predictive capacity through the development of strategic applications of the model, including, for example, the level of political support for biofuels in any given community.

Task #6: Refinery to Wing Stakeholder
Washington State University
This is a shared task lead by Penn State University. The reporting is provided in Award No. 13-C-AJFE-PSU-002.

Objective(s)

Continuation from last year
Extend Stakeholder assessment to a limited sample of informed stakeholders in the remaining sections of the country to provide insight into market & industry dynamics which will help optimize successful outcomes.

Research Approach
The team will collect primary data via interviews and surveys to better understand the awareness, opinions, and perspectives of key aviation fuel supply chain stakeholders regarding to the potential impacts and key success factors for an economically viable biojet fuel production industry in the United States, and specifically the Pacific Northwest and US Midwest region. These aviation fuel supply chain stakeholders include airport management, FBOs, other aviation fuel handlers, relevant airlines, and CAAFI personnel. Data collection to assess aviation fuel supply chain stakeholder opinions, awareness, and perceptions regarding factors impacting the adoption and diffusion of AJF in the Pacific Northwest region has been completed, and Midwest region analysis is continuing. A national survey of aviation management is being developed and will be fielded in early 2018 after consultation with CAAFI and FAA. A survey to replace interviews in the Midwest Region is currently being developed, and will be deployed in other regions when complete.

Milestone(s)
Assessment in the Pacific Northwest region of stakeholder perceptions using interviews and a survey of airport management have been completed, resulting in one published paper and a manuscript currently submitted. Interview requests for stakeholders in the Midwest have been sent out, and there has been a limited response. One interview has already been conducted.

Major Accomplishments
The team has completed stakeholder assessment interviews and surveys in the Pacific Northwest, publishing a paper on interview results from this region. A second manuscript is currently submitted for publication detailing the survey results from stakeholders in the same region. Interview contacts in the Midwest have been established and a third round of interview requests has been sent. We have received potential contacts from an interview participant, and are working to include these contacts to get corporate participation from key fuel distributors in the region.

Publications
Smith, P.M., Gaffney, M.J., Shi, W., Hoard, S., Ibarrola Armendariz, I., Mueller, D.W., 2017. Drivers and barriers to the adoption and diffusion of sustainable jet fuel (SJF) in the U.S. Pacific Northwest. *Journal of Air Transport Management, 58*, 113-124.

Outreach Efforts
None

Awards
None

Student Involvement
Daniel Mueller, Ph.D. candidate in political science at WSU and research assistant on this project, has aided in writing and publishing NARA interview results and is currently involved in the interview process for the Midwest, gathering contact information, aiding in question development, and contacting potential interviewees.

Plans for Next Period
The next year will see the completion of the stakeholder assessment in the Midwest, with the team continuing to gather contact information of stakeholders in the region. A national survey has also been developed, and will be sent out to aviation management stakeholders throughout the country. Plans are currently underway to replicate the research in Canada.

Task #7: Supply Chain Analysis
Washington State University-Volpe

Objective(s)

Continuation from previous years
Use the design cases developed in previous years for standalone alternative jet fuel production technologies to estimate production volumes and breakeven price for all the facilities identified by the Volpe Center. This effort will continue toward the continual refinement of the FAA aspirational jet fuel production goal.

Research Approach
We use the conversion design cases for standalone alternative jet fuel production technologies to estimate production volumes and breakeven price for all the facilities identified by the Volpe Center in their AFTOT analysis. Geospatially specific layers are produced for waste feedstock and incorporated into the AFTOT analysis.

Milestone(s)
Our team provided Volpe data developed in previous years for standalone alternative jet fuel production technologies to estimate production volumes and breakeven price. A nation-wide analysis to estimate the ability to produce 1-billion gals of AJF in the US.

Major Accomplishments
WSU and the Volpe AFTOT analysis team has teamed with the NREL BSM team for a joint analysis of the ability to reach 1-billion gallon of AJF production in the US.

Publications
A publication has been prepared and is in review.

Outreach Efforts
None

Awards
None

Student Involvement
A graduate student (Lina Martinez) is receiving training (taking courses) to contribute in this task.

Plans for Next Period
Participate in the development of supply chain analysis tasks.

Task #8: Analytical Support for Regional CAAFI and USDA Jet Fuel Project
Washington State University

Objective(s)

Continuation from previous years
Develop a readiness level tool to assess the status of regional alternatives jet production projects. In addition, use the supply chain and standalone design cases to support the USDA BANR project in TEA and supply chain analysis. This regional CAP project focuses on the use of softwood forest salvage feedstock for fuels via a catalyzed pyrolysis conversion pathway.

Research Approach
We will develop readiness level tools for regional projects to assess their status of developing fuel project and assist in understanding critical missing components. This tool will take similar form and approaches to the CAAFI Feedstock and Fuel Readiness Levels and will be used to assist CAAFI in understanding the stage of development for projects of interest and assess critical gaps. In addition, we will assist the regional USDA BANR team in deploying TEA and Supply Chain analysis to

their project. This effort is structured around using softwood forest salvage feedstock with a thermochemical conversion process to produce fuels and coproducts.

Milestone(s)

We are progressing on the use of the supply chain and standalone design cases to support the USDA BANR project in TEA and supply chain analysis. We have supported the BANR team in creating TEAs for the technologies under consideration.

Major Accomplishments

In collaboration with the USDA BANR project and attending their annual meeting to coordinate analysis. We currently await their completion of beetle-killed softwood estimates to complete the supply chain analysis.

Publications

None

Outreach Efforts

None

Awards

None

Student Involvement

None

Plans for Next Period

To complete a supply chain analysis that assesses the role of depots. Draft paper to be complete by end of next quarter.

References

Bond JQ, Upadhye AA, Olcay H, Tompsett GA, Jae J, Xing R, Alonso DM, Wang D, Zhang T, Kumar R, Foster A, Sen SM, Maravalias CT, 13 R, Barret SR, Lobo R, Wayman CE, Dumesic JA, Huber GW. (2014). Production of renewable jet fuel range alkanes and commodity chemicals from integrated catalytic processing of biomass. Energy Environ. Sci, 7:1500.

Brown, N. (2013). FAA Alternative Jet Fuel Activities. Overview. Presented to: CLEEN Consortium, November 20, 2013.

Henrich E. (2007). The status of FZK concept of biomass gasification. 2nd European Summer School on Renewable Motor Fuels. Warsaw, Poland 29-31, August 2007.

Hileman JI, De la Rosa-Blanco E, Bonnefoy PA, Carter NA: The carbón dioxide challenge facing aviation. (2013). Progress in Aerospace Sciences. 63:84-95.

Hileman, J. I., and R. W. Stratton. (2014). "Alternative jet fuel feasibility." Transport Policy, 34:52-62.

Hileman J. (2013). Overview of FAA Alternative Jet Fuel Activities. Presentation to the Biomass R&D Technical Advisory Committee, Washington DC, August 14, 2013.

Huber GW, Corma A. (2007). Synergies between Bio- and Oil Refineries for the Production of Fuels from Biomass. Angewandte Chemie. 46(38):7184-7201.

Lewis, K; S Mitra, S Xu, L Tripp, M Lau, A Epstein, G Fleming, C Roof. (2012) Alternative jet fuel scenario analysis report. No. DOT/FAA/AEE/2011-05.(http://ntl.bts.gov/lib/46000/46500/46597/DOT-VNTSC-FAA-12-01.pdf) (Retrieved on 2014-07)

Malina R. (2012). HEFA and F-T jet fuel cost analyses. Laboratory for Aviation and the Environment. MIT, Nov 27, 2012.

Martinkus, N., Kulkarni, A., Lovrich, N., Smith, P., Shi, W., Pierce, J., & Brown, S. An Innovative Approach to Identify Regional Bioenergy Infrastructure Sites. Proceedings of the 55th International Convention of Society of Wood Science and Technology, August 27-31, 2012 - Beijing, CHINA.

Martinkus, N., Shi, W., Lovrich, N., Pierce, J., Smith, P., and Wolcott, M. (2014). Integrating biogeophysical and social assets into biomass-to-biofuel supply chain siting decisions. Biomass and Bioenergy, 66:410-418.

Pearlson MN. (2011). A Techno-economic and Environmental Assessment of Hydroprocessed Renewable Distillate Fuels. MSc Thesis in Technology and Policy, MIT.

Pearlson M, Wollersheim C, Hileman J. (2013). A techno-economic review of hydroprocessed renewable esters and fatty acids for het fuel production. Biofuels, Bioproducts and Biorefining, 7(1):89-96.

Richard TL: Challenges in Scaling Up Biofuels Infrastructure. (2010). Science, 329:793.

Seber G, Malina R, Pearlson MN, Olcay H, Hileman JI, Barret SRH. (2014). Environmental and Economic Assessment of Producing hydroprocessed jet and diesel fuel from waste oil and tallow. Biomass and Bioenergy 67:108-118.

Spath P, Aden A, Eggeman M, Ringer B, Wallace B, Jechura J. (2005). Biomass to Hydrogen Production detailed Design and Economic Utilizing the Battelle Columbus Laboratory Indirectly Heated Gasifier. Technical Report NREL/TP-510-37408.

Staples MD, Malina R, Olcay H, Pearlson MN, Hileman JI, Boies A, Barrett SRH. (2014). Lifecycle greenhouse gas footprint and minium selling price of renewable diesel and jet fuel from fermentation and advanced fermentation technologies. Energy & Environmental Science, 7:1545.

Project 001(B) Alternative Jet Fuel Supply Chain Analysis

University of Hawaii

Project Lead Investigator

University of Hawaii Lead:
Scott Q. Turn
Researcher
Hawaii Natural Energy Institute
University of Hawaii
1680 East-West Rd., POST 109; Honolulu, HI 96822
(808) 956-2346
sturn@hawaii.edu

University Participants

University of Hawaii

- P.I.(s): Scott Q. Turn, Researcher
- FAA Award Number: 13-C-AJFE-UH, Amendment 005
- Period of Performance: 10/1/15 to 9/30/18
- Task(s):
    1. Informing Regional Supply Chains
    2. Identification of Supply Chain Barriers in the Hawaiian Islands

University of Hawaii

- P.I.(s): Scott Q. Turn, Researcher
- FAA Award Number: 13-C-AJFE-UH, Amendment 007
- Period of Performance: 10/1/16 to 9/30/18
- Task(s):
    1. Informing Regional Supply Chains
    2. Support of Indonesian Alternative Jet Fuel Supply Initiatives

University of Hawaii

- P.I.(s): Scott Q. Turn, Researcher
- FAA Award Number: 13-C-AJFE-UH, Amendment 008
- Period of Performance: 8/1/17 to 9/30/18
- Task(s):
    1. National lipid supply availability analysis
    2. Hawaii regional project

Project Funding Level

Under **FAA Award Number 13-C-AJFE-UH, Amendment 005**, the Alternative Jet Fuel Supply Chain Analysis-Tropical Region Analysis project received $75,000 in funding from the FAA and cost share funding of $75,000 from the State of Hawaii.

Under **FAA Award Number 13-C-AJFE-UH, Amendment 007**, the Alternative Jet Fuel Supply Chain Analysis-Tropical Region Analysis project received $100,000 in funding from the FAA and cost share funding of $75,000 from the State of Hawaii and $25,000 of in-kind cost match in the form of salary support for Scott Turn from the University of Hawaii.

Under **FAA Award Number 13-C-AJFE-UH, Amendment 008**, the Alternative Jet Fuel Supply Chain Analysis-Tropical Region Analysis project received $125,000 in funding from the FAA and cost share funding of $125,000 from the State of Hawaii.

Investigation Team

Lead
Scott Turn – University of Hawaii

Other Lead Personnel
Tim Rials and Burt English (UT Co-PIs)
Manuel Garcia-Perez (WSU Co-PI)
Kristin Lewis (Volpe PI)
Michael Wolcott (WSU PI)

UH Investigation Team
Under **FAA Award Number 13-C-AJFE-UH, Amendment 005**, Task 1 and Task 2 includes
Dr. Scott Turn, Researcher, Hawaii Natural Energy Institute, UH
Dr. Trevor Morgan, Assistant Researcher, Hawaii Natural Energy Institute, UH
Dr. Richard Ogoshi, Assistant Researcher, Department of Tropical Plant and Soil Sciences, UH
Dr. Adel H. Youkhana, Junior Researcher, Department of Tropical Plant and Soil Sciences, UH

Under **FAA Award Number 13-C-AJFE-UH, Amendment 007**, Task 1 and Task 2 includes
Dr. Scott Turn, Researcher, Hawaii Natural Energy Institute, UH
Dr. Trevor Morgan, Assistant Researcher, Hawaii Natural Energy Institute, UH
Dr. Richard Ogoshi, Assistant Researcher, Department of Tropical Plant and Soil Sciences, UH
Dr. Adel H. Youkhana, Junior Researcher, Department of Tropical Plant and Soil Sciences, UH
Ms. Sharon Chan, Junior Researcher, Hawaii Natural Energy Institute, UH

Under **FAA Award Number 13-C-AJFE-UH, Amendment 008**, Task 1 and Task 2 includes
Dr. Scott Turn, Researcher, Hawaii Natural Energy Institute, UH
Dr. Trevor Morgan, Assistant Researcher, Hawaii Natural Energy Institute, UH

Project Overview

Under **FAA Award Number 13-C-AJFE-UH, Amendment 005**, the research effort has two objectives. The first objective is to develop information on regional supply chains for use in creating scenarios of future alternative jet fuel production in tropical regions. Outputs from this project may be used as inputs to regional supply chain analyses being developed by the FAA and Volpe Center. The second objective is to identify the key barriers in regional supply chains that must be overcome to produce significant quantities of alternative jet fuel in the Hawaiian Islands and similar tropical regions.

The **FAA Award Number 13-C-AJFE-UH, Amendment 005** project goals are to:

- Review and summarize:
  - the available literature on biomass feedstocks for the tropics,
  - the available literature on pretreatment and conversion technologies for tropical biomass feedstocks,
  - the available literature on geographic information systems data sets available for assessment of alternative jet fuel production systems in the tropics.
- Identify alternative jet fuel supply chain barriers in the Hawaiian islands

Under **FAA Award Number 13-C-AJFE-UH, Amendment 007**, the research effort has two objectives. The first objective is to develop information on regional supply chains for use in creating scenarios of future alternative jet fuel production in tropical regions. Outputs from this project may be used as inputs to regional supply chain analyses being developed by the FAA and Volpe Center. Included in this objective is the development of fundamental property data for tropical biomass resources to support supply chain analysis. The second objective is to support the Memorandum of Understanding between the Federal Aviation Administration (FAA) and Indonesian Directorate General of Civil Aviation (DGCA) to promote developing and using sustainable, alternative aviation fuels.

The **FAA Award Number 13-C-AJFE-UH, Amendment 007** project goals are to:

- Support the Volpe Center and Commercial Aviation Alternative Fuels Initiative (CAAFI) Farm to Fly 2.0 supply chain analysis.
- Use GIS-based estimates of fiber crop production potential to develop preliminary technical production estimates of jet fuel in Hawaii.
- Develop fundamental property data for tropical biomass resources.
- Transmit data and analysis results to other ASCENT Project 1 researchers to support improvement of existing tools and best practices.
- Support Indonesian alternative jet fuel supply initiatives

Under **FAA Award Number 13-C-AJFE-UH, Amendment 008**, the research effort has two objectives. The first objective is to support a national lipid supply availability analysis that will inform industry development and guide policy. The second objective is to conduct a targeted supply chain analysis for alternative jet fuel production facility based on a Hawaii regional project

The **FAA Award Number 13-C-AJFE-UH, Amendment 008** project goals are to:

- Support ASCENT partners conducting the national lipid supply availability analysis by contributing information on tropical oilseed availability.
- Evaluate supply chains for targeted waste streams and purpose grown crops in Hawaii to a location in the principal industrial park on the island of Oahu.

Task #0.1: Informing Regional Supply Chains

University of Hawaii

Objective(s)

This task included two activities, (1) a review of the archival literature on existing tropical crops and potential new crops that could provide feedstocks for AJF production and (2) a review of relevant pretreatment and conversion technology options and experience with feedstocks identified in (1).

Research Approach

Activity 1. The archival literature will be reviewed to construct an updated database of relevant citations for the tropical crops identified in section 8; new potential energy crops will be identified and added to the database. Available information on agronomic practices, crop rotations, and harvest techniques will be included. The database will be shared with and serve as a resource for the Project 1 team and Volpe Center analyses of regional supply chains.

Activity 2. A database of relevant pretreatment and conversion technology options and experience with potential tropical feedstock materials will be assembled from the archival literature and from existing Project 1 team shared resources. Of particular interest are inventories of material and energy flows associated with the pretreatment and conversion unit operations, fundamental to the design of sustainable systems and the underlying analysis. Pairings of pretreatment and conversion technology options provide the starting point for evaluation of tropical biorefineries that can be integrated into ASCENT Project 1 team and Volpe Center activities.

Milestone(s)

Task 1, Activity 1: Identify target list of databases to search for relevant literature.
Task 1, Activity 1: Interim report summarizing progress on literature search.
Task 1, Activity 2: Identify target list of databases to search for relevant literature.
Task 1, Activity 2: Interim report summarizing progress on literature search.
Task 1, Activity 3: Identify target list of databases to search for relevant literature.
Task 1, Activity 3: Interim report summarizing progress on literature search.

Major Accomplishments

This work is largely completed. A report was produced for each of the two activities. The two reports were combined to form a manuscript that is currently under review by co-author Prof. Manuel Garcia-Perez (WSU). The manuscript will be submitted to the *Journal of Renewable and Sustainable Energy Reviews* when review by FAA program managers is completed.

Publications
None

Outreach Efforts
None

Awards
None

Student Involvement
None

Plans for Next Period
During the next period, the manuscript will be submitted to the *Journal of Renewable and Sustainable Energy Reviews* when review by FAA program managers is completed.

Task #0.2: Identification of Supply Chain Barriers in the Hawaiian Islands
University of Hawaii

Objective(s)
Identify the key barriers in regional supply chains that must be overcome to produce significant quantities of alternative jet fuel in the Hawaiian Islands and similar tropical regions.

Research Approach
UH developed the Hawaii Bioenergy Master Plan for the State of Hawaii [1]. Completed in 2009, UH was tasked with determining whether Hawaii had the capability to produce 20% of land transportation fuels and 20% of electricity from biobased resources. Toward this end, the plan included assessments of (1) land and water resources that could support biomass feedstock production, (2) potential biomass resources and their availabilities, (3) technology requirements, (4) infrastructure requirements to support logistics, (5) economic impacts, (6) environmental impacts, (7) availability of human capital, (8) permitting requirements, and (9) limitations to developing complete value chains for biomass based energy systems. In keeping with the stakeholder driven development of the Hawaii Bioenergy Master Plan, barriers to development of regional supply chains for ASCENT will be identified by interacting with key stakeholder groups. Green Initiative for Fuels Transition Pacific (GIFTPAC) meetings are held quarterly and are attended by biofuel development interests in Hawaii including representatives of large landowners, producers of first generation biofuels, petroleum refiners, electric utilities, the State Energy Office, U.S. Pacific Command, biofuel entrepreneurs, county government officials, and the University of Hawaii. Additional stakeholders are invited as necessary to fill information and value chain gaps. These meetings are excellent opportunities to receive stakeholder input, identify barriers to supply chain development, and organize data collection efforts that span supply chain participants.

Milestone(s)
Include a description of any and all milestones reached in this research according to previously indicated timelines.

Task 2: Introduce activities at next regularly scheduled GIFTPAC meeting after contract executed.
Task 2: Interim report outlining two tropical supply chain scenarios developed in consultation with Project 1 team, and with input from GIFTPAC participants.

Major Accomplishments
This task is largely completed. A stakeholder meeting was held and documented in a report. The stakeholders identified barriers to alternative jet fuel production in Hawaii and ranked the barriers in order of importance as indicated below:

Economic constraints [e.g., high costs of entry for production factors such as land] throughout the whole production chain

- Issues associated with access to capital including high initial risks and uncertain return on investment

- Insufficient government support in the form of incentives and favorable policies to encourage long-term private investment
- Cost, availability and competition for water
- Alternative jet fuel production technologies are emerging but have not yet demonstrated full commercial viability
- Insufficient or inadequate infrastructure [harbors, roads, fuel distribution infrastructure, irrigation systems] to support the whole production chain

Several of the barriers are held in common with other locations in the continental U.S. but those related to water and infrastructure bear unique characteristics of an island state.

Publications
None

Outreach Efforts
This activity engaged stakeholders to identify barriers to alternative jet fuel production in Hawaii. Preparation included reviewing stakeholder lists from previous activities. Facilitators appropriate to the stakeholder group were retained. The stakeholder meeting included a presentation about the larger ASCENT program's scope and goals and the other aspects of the UH ASCENT project.

Awards
None

Student Involvement
None

Plans for Next Period
This task is complete but stakeholder outreach activities will continue under other tasks outlined below.

Task #0.3: Informing Regional Supply Chains
University of Hawaii

Objective(s)
Building on FY16 activities, additional supporting analysis will be conducted for proposed supply chains in Hawaii, including:

- 0.3.1 Support Volpe Center and Commercial Aviation Alternative Fuels Initiative (CAAFI) Farm to Fly 2.0 supply chain analysis.
- 0.3.2 Use GIS-based estimates of fiber crop production potential to develop preliminary technical production estimates of jet fuel in Hawaii.
- 0.3.3 Develop fundamental property data for tropical biomass resources.
- 0.3.4 Transmit data and analysis results to support improvement of existing tools (e.g. POLYSIS).

Research Approach
Activity 0.3.2 has been conducted using geographic information system (GIS) data to identify areas suitable for purpose grown crop production of feedstocks for AJF production in Hawaii. The approach has been to use GIS layers for land capability class (LCC), slope, and zoning as preliminary screens for suitability. Lands are classified by NRCS with ratings from 1 to 6. LCC's from 1 to 3 are generally suitable for agricultural production and LCC of 4 can be productive with proper management. The slopes of terrains impact aspects of production including mechanization and erodibility. An elevation GIS layer was used to derive a slope layer. Zoning layers were acquired from State and County GIS offices. Only agricultural zoning was deemed suitable for this analysis. The EcoCrop model was used to develop yield models for the crops selected in Task 0.1 based on the annual rainfall and mean minimum monthly temperature data. EcoCrop includes

model parameters on sugarcane, banagrass, five species of eucalyptus, leucaena, pongamia, jatropha, and sorghum. The parameters for sugarcane will be used to provide a base case assessment for comparison with historical sugar cane acreage and yield. Using sensitivity analysis, the model can be tuned to account for the differences between parameters developed from global sugar production and a century of production experience in Hawaii that was refined through plant breeding to adapt sugarcane varieties to a wide variety of agro-ecosystems. Model results across all of the potential feedstocks will be used to identify land use patterns that would match plants with environmental conditions toward maximizing productivity in support of AJF production.

Pongamia will be the initial focus of Activity 0.3.3. Pongamia is an oil seed bearing, leguminous tree that has production potential in Hawaii and Florida. The tree produces pods containing oil bearing seeds. Pods, oil seed cake, and oil will be evaluated from a number of trees growing on the island of Oahu. Fundamental measurements of chemical composition will be conducted and reported. Development of coproducts from the pods and oil seed cake will be explored.

Milestone(s)

Identify target opportunities to augment POLYSYS, AFTOT, and conversion modules
Review previously developed GIS information layers for tropical fiber crops and identify updating requirements
Preliminary estimates of AJF technical potential in Hawaii based on previously developed GIS information layers

Major Accomplishments

The GIS based analysis of AJF production potential is ongoing. The assessment of potential lands meeting requirements for land capability class, slope, and land use zoning was completed. The EcoCrop model is being implemented to predict yield as a function of the minimum average monthly temperature and the annual rainfall. This will allow prescription of potential AJF feedstock crops on land areas capable of supporting their production under both rain-fed and irrigated conditions. This analysis will provide information necessary in determining cropping patterns and assessing transport costs to processing facility locations. The EcoCrop model's prediction of sugarcane potential was determined and the results were compared with historic sugarcane acreage, both rainfed and irrigated. EcoCrop upper and lower values for temperature and rainfall that support optimal sugarcane production were varied to calibrate the prediction against historic acreage. The difference between the EcoCrop values and those representative of Hawaii conditions can be attributed to improvements due to plant breeding and unique combinations of environmental conditions. An example of the latter is the relatively young volcanic soils present in high rainfall areas on the island of Hawaii that allow for high drainage rates and accommodate sugar production. Similar analysis has begun with for *Eucalyptus grandis* and *Eucalyptus saligna*, the former suited for planting at lower, warmer, wetter locations and the latter better suited for cooler, drying sites.

Additional seeds and pods were collected from the pongamia tree on the University of Hawaii campus and the Ke`ehi Lagoon Beach Park. Two oil seed presses were acquired and safety documents were developed. Soxhlet extraction methods were reviewed and apparatus assembled.

Publications

None

Outreach Efforts

Outreach in this task has focused on interactions with Terviva, a startup company that has identified pongamia germplasm production and marketing as the central focus of their business plan.

Awards

None

Student Involvement

None

Plans for Next Period

The GIS analysis of AJF production will continue to include the remaining AJF crops and provide State-wide working maps for each of the species.

The pongamia oil seeds and husks will be analyzed to determine oil content and potential for coproduct development. Differences between pongamia tree germplasms located on the island of Oahu will be determined to compare oil component profiles and coproduct potential.

Task #0.4: Support of Indonesian alternative jet fuel supply initiatives

University of Hawaii

Objective(s)

This task supports the Memorandum of Understanding between the Federal Aviation Administration (FAA) and Indonesian Directorate General of Civil Aviation (DGCA) to promote development and use of sustainable, alternative aviation fuels. Under the coordination of the FAA, efforts to establish points of contact and coordinate with Indonesian counterparts are ongoing.

Research Approach

This task will support the Memorandum of Understanding between the Federal Aviation Administration (FAA) and Indonesian Directorate General of Civil Aviation (DGCA) to promote development and use of sustainable, alternative aviation fuels. This will begin with working with the FAA to establish points of contact to coordinate efforts with Indonesian counterparts. The Indonesian Aviation Biofuels and Renewable Energy Task Force (ABRETF) membership includes Universitas Indonesia, Institut Teknologi Bandung, and Universitas Padjadjaran. A prioritized list of tasks will be developed in consultation with Indonesian counterparts and data required to inform sustainability and supply analyses and potential sources of information will be identified. This could include data collection on Indonesian jet fuel use and resources for alternative jet fuel production, airport locations and annual and monthly jet fuel consumption patterns. Characterization of sustainable biomass resources with potential for use in producing alternative jet fuel supplies could include developing preliminary GIS mapping information of their locations and distributions and preliminary estimates of their technical potentials.

Milestone(s)

Identify points of contact at Indonesian universities participating in ABRETF; identify research needs and develop project plan. Develop data on potential project.

Major Accomplishments

The PI travelled to Jakarta in the first week of August, 2017, and met with Cesar Velarde Catolfi-Salvoni (ICAO), Wendy Aritenang (ICAO), Dr. Ridwan Rachmat (Head of Research Collaboration, Indonesian Agency for Agricultural Research and Development), Sylvia Ayu Bethari (Head of Aviation Fuel Physical & Chemical Laboratory, Research and Development Centre for Oil and Gas Technology), Dr. Ina Winarni (Forest Product Research and Development Center, Ministry of Environment and Forestry), and Dr. SD Sumbogo Murti (Center of Technology Energy Resources and Chemical Industry, Agency for the Assessment and Application of Technology). The activities of the tropical supply chain analysis effort were presented to the group followed by a general discussion. The conclusion from this introductory meeting was that the Indonesian counterparts would seek agreement on how to move forward with future cooperation.

Publications

None

Outreach Efforts

The PI travelled to Jakarta in the first week of August, 2017, and met with Cesar Velarde Catolfi-Salvoni (ICAO), Wendy Aritenang (ICAO), Dr. Ridwan Rachmat (Head of Research Collaboration, Indonesian Agency for Agricultural Research and Development), Sylvia Ayu Bethari (Head of Aviation Fuel Physical & Chemical Laboratory, Research and Development Centre for Oil and Gas Technology), Dr. Ina Winarni (Forest Product Research and Development Center, Ministry of Environment and Forestry), and Dr. SD Sumbogo Murti (Center of Technology Energy Resources and Chemical Industry, Agency for the Assessment and Application of Technology). The activities of the tropical supply chain analysis effort were presented to the group followed by a general discussion. The conclusion from this introductory meeting was that the Indonesian counterparts would seek agreement on how to move forward with future cooperation.

Awards
None

Student Involvement
None

Plans for Next Period
The PI will continue to develop the cooperative research agenda between UH and Indonesian universities through continued dialog with FAA, ICAO, and the Indonesian Directorate General of Civil Aviation.

Task #2.2: National lipid supply availability analysis
University of Hawaii

Objective(s)
Activities under this task will support ASCENT partners working on a national lipid supply availability analysis by sharing data on tropical oilseed availability developed under previous year's activities.

Research Approach
Activities under this task will support ASCENT partners working on a national lipid supply availability analysis by sharing data on tropical oilseed availability developed under previous year's activities. This support will include estimates of pongamia production capability in the State in addition to assessments of waste cooking oil and tallow.

Milestone(s)
Milestones will coincide with lead institution, WSU, schedule for the national lipid supply analysis.

Major Accomplishments
None – Task in progress

Publications
None

Outreach Efforts
None

Awards
None

Student Involvement
None

Plans for Next Period
Efforts in the next period will include conducting production estimates of oil seed crops in Hawaii and assessing waste oil supplies. Information will be provided to the lead institution, WSU.

Task #3.2: Hawaii Regional Project

University of Hawaii

Objective(s)

A supply chain based on fiber feedstocks transported to a conversion facility located at Campbell Industrial Park (CIP) on Oahu will be evaluated (Figure 1). CIP is the current site of two oil refineries. Construction and demolition (C&D) wood waste from PVT Landfill could be primary source of feedstock. Other sources will be evaluated from elsewhere on Oahu and from outer islands, including MSW stream from outer islands and mining of current stocks of waste in place. Waste streams and purpose grown crops form the basis for a hub and spoke supply system with the hub located on Oahu. Pipelines for jet fuel transport are in place from CIP to Daniel K. Inouye International Airport and adjacent Joint Base Pearl Harbor/Hickam. Other coproduct off-takers for alternative diesel fuel (ADF) include Hawaiian Electric Co. and several military bases (Schofield Barracks (~50 MW alternative fuel-capable power plant under development), Kaneohe Marine Corp Base, etc.). Hawaii Gas (local gas utility) is also seeking alternative sources of methane if methane or feedstock suitable for methane production is available as a coproduct. Hawaii Gas currently off takes feedstock (naphtha) from refinery.

Figure 1. Possible locations of value chain participants for fiber based AJF production facility located at Campbell Industrial Park, Oahu.

Research Approach

Task 3.2.G1. Analysis of feedstock-conversion pathway efficiency, product slate (including co-products), maturation
Building on activities from previous years, additional supporting analysis will be conducted for proposed supply chains in Hawaii, including:

- 3.2.G1.1 Assess feedstock suitability for conversion processes (characterization, conversion efficiencies, contaminants, etc.) [UH and WSU (Manuel Garcia-Perez)]
- 3.2.G1.2 Acquire data re. feedstock size reduction, particle size of materials, bulk densities [UH, WSU (Manuel Garcia-Perez)]
- 3.2.G1.3 Evaluate coproducts at every step of the supply chain. [A01 team]

Task 3.2.G2. Scoping of techno-economic analysis (TEA) issues
This task will determine the current TEA status of targeted AJF production technologies that use fiber feedstocks as production inputs. [UH, WSU (Manuel Garcia-Perez), Purdue (Wally Tyner)]

Task 3.2.G3. Screening level greenhouse gas (GHG) life cycle assessment (LCA)
This task will conduct screening level GHG LCA on the proposed target supply chains and AJF conversion technologies.

Sub-tasks:

- 3.2.G3.1 Assess MIT waste based GHG LCA tools in context of Hawaii application. [MIT (Mark Staples)]
- 3.2.G3.2 Assess requirements to link previously completed eucalyptus energy and GHG analysis to the edge of the plantation with available GHG LCA info for conversion technology options. [MIT (Mark Staples), UH]
- 3.2.G3.3 Identify and fill information/data gaps

Task 3.2.G4. Identification of supply chain participants/partners

Sub-tasks:

- 3.2.G4.1 Define C&D landfill case
- 3.2.G4.2 Identify eucalyptus in existing plantations – landowners, leaseholder/feedstock producer, harvesting contractor, trucking, etc. [UH]
- 3.2.G4.3 Define other feedstock systems as identified. [A01 Team]

Task 3.2.G5. Develop appropriate stakeholder engagement plan

Sub-tasks:

- 3.2.G5.1 Review stakeholder engagement methods and plans from past work to establish baseline methods [UH, WSU (Season Hoard)].
- 3.2.G5.2 Identify and update engagement strategies based on updated CAAM/Outreach support tool [UH, WSU (Season Hoard)]

Task 3.2.G6. Identify and engage stakeholders

Sub-tasks:

- 3.2.G6.1 Identify stakeholders along the value chain and create database based on value chain location. [UH]
- 3.2.G6.2 Conduct stakeholder meeting using instruments developed in Task 3.2G5. [UH, WSU (Season Hoard)]
- 3.2.G6.3 Analyze stakeholder response and feedback to process. [UH, WSU (Season Hoard)]

Task 3.2.G7. Acquire transportation network and other regional data needed for FTOT and other modeling efforts

Sub-tasks:

- 3.2.G7.1 Acquire necessary data to evaluate harbor capacities and current usage. [UH, Volpe (Kristin Lewis), WSU (Mike Wolcott)]
- 3.2.G7.2 Acquire data on interisland transport practices. [UH, Volpe (Kristin Lewis), WSU (Mike Wolcott)]

Task 3.2.G8. Evaluate infrastructure availability

Sub-tasks:

- 3.2.G8.1 Evaluate interisland shipping options and applicable regulation. [UH, Volpe (Kristin Lewis), WSU (Mike Wolcott)]
- 3.2.G8.2 Evaluate transport or conveyance options from conversion location to end user and applicable regulation. [UH, Volpe (Kristin Lewis), WSU (Mike Wolcott)]

Task 3.2.G9. Evaluate feedstock availability

Sub-tasks:

- 3.2.G9.1 Refine/groundtruth prior evaluations of options for purpose grown feedstock supply [UH]
- 3.2.G9.2 Conduct projections of C&D waste supply moving forward and mining of waste in place on Oahu, MSW and mining of waste in place on other islands [UH]

Task 3.2.G10. Develop regional proposal
This task will use the information collected in Tasks 3.2.G1 through 3.2.G9 to develop a regional project proposal.

Milestone(s)

One milestones is associated with each of the subtask activities identified in the research approach section above.

Major Accomplishments

None, project is being initiated.

Publications

None

Outreach Efforts

None

Awards

None

Student Involvement

None

Plans for Next Period

During the next period, activities will begin toward completing subtasks identified in the research approach section above.

Project 001(C) Alternative Jet Fuel Supply Chain Analysis

Purdue University

Project Lead Investigator

Wallace E. Tyner
James and Lois Ackerman Professor
Department of Agricultural Economics
Purdue University
403 West State Street
West Lafayette, IN 47907-2056
765-494-0199
wtyner@purdue.edu

University Participants

Purdue University

- Wallace E. Tyner, James and Lois Ackerman Professor
- FAA Award Number: 13-C-AJFE-PU
- Period of Performance: July 14, 2014 – August 31, 2018
- Task(s):

1. **Lead: Tyner; supported by graduate students)** – Develop stochastic techno-economic models for relevant pathways and identify key stochastic variables to be modeled for assessing risk in conversion pathways. This work will lead to our capability to compare pathways, their expected economic cost plus the inherent uncertainty in each pathway.
2. **Lead: Tyner; supported by Taheripour, Zhao, and Malina (Hasselt University)** – life cycle and production potential analysis of alternative aviation biofuel pathways in coordination with ICAO-AFTF. Work with the CAEP/AFTF life cycle assessment committee (WP3) on issues such as system boundaries, induced land use change, LCA methodology, and pathway GHG emissions assessment.
3. **Lead**: **Tyner; supported by Zhao, Taheripour, and post doc** – Develop estimates of land use change associated emissions for aviation biofuels for the ICAO Alternative Fuels Task Force.
4. **Lead: Tyner** - provide support for the other ASCENT universities on aviation biofuels policy analysis.
5. **Lead: Tyner** – provide support for the Farm to Fly initiative as needed.

Project Funding Level

Amendment 3 - $250,000, Amendment 6 - $110,000, Amendment 10 - $230,000, Amendment 15 - $373,750, Amendment 19 - $400,000.
Current cost sharing is from Oliver Wyman

Investigation Team

Wallace E. Tyner – PI – James and Lois Ackerman Professor
Farzad Taheripour – Research Associate Professor – involved in several aspects of the project, but especially life cycle analysis and land use change
David Cui – post doc, GTAP-BIO model modifications and simulations
Xin Zhao – PhD student Purdue University – stochastic techno-economic analysis and GTAP ILUC analysis
Elspeth McGarvey – MS student, Purdue University - stochastic techno-economic analysis
Jeremiah Stevens – MS student, Purdue University – stochastic techno-economic analysis

Project Overview

This project has five main components. First is advancement of stochastic techno-economic analysis for aviation biofuel pathways. Second is life cycle and production potential analysis of alternative aviation biofuel pathways in coordination

with ICAO-AFTF. The third component also involves working with ICAO-AFTF but specifically on estimation of land use change associated emissions for aviation biofuels. The fourth and fifth components are smaller. The fourth is to provide support for the policy sub-group in AFTF. The fifth will be providing support for "Farm to Fly 2.0" (F2F2). F2F2 is a collaboration of government and industry to enable commercially viable, sustainable bio-jet fuel supply chains in the U.S. at the state and regional level that are able to support the goal of one billion gallons of bio-jet fuel production capacity and use by 2018.To support this effort, Purdue would provide necessary analytical support to this process.

Task #1: Develop Stochastic Techno-Economic Models for Relevant Pathways and Identify Key Stochastic Variables to Be Modeled For Assessing Risk in Conversion Pathways

Purdue University

Objective(s)

Develop stochastic techno-economic models for relevant pathways and identify key stochastic variables to be modeled for assessing risk in conversion pathways. This work will lead to our capability to compare pathways, their expected economic cost, plus the inherent uncertainty in each pathway.

Research Approach

For each pathway being evaluated, we develop a stochastic model that covers the entire pathway so that it can be used for both techno-economic and life cycle analysis. Over this period, we have evaluated alcohol to jet and the Catalytic Hydrothermolosis (CH) processes. We have also developed some new approaches to stochastic TEA.

Milestone(s)

We continue to get refereed journal papers published in the area of stochastic techno-economic analysis. See the publications in the publications section below.
Two other papers on quantifying stochastic TEA were published. See publications below.

Major Accomplishments

See the publications section below.

Publications

Zhao, Xin, Guolin Yao, and Wallace E. Tyner. "Quantifying breakeven price distributions in stochastic techno-economic analysis." *Applied Energy* 183 (2016) 318-326.

Bann, Seamus J., Robert Malina, Pooja Suresh, Matthew Pearlson, Wallace E. Tyner, James I. Hileman, and Steven Barrett. "The costs of production of alternative jet fuel: A harmonized stochastic assessment." *Bioresource Technology* 227 (2017), 179-187.

Yao, Guolin, Mark D. Staples, Robert Malina, and Wallace E. Tyner. "Stochastic techno-economic analysis of alcohol-to-jet fuel production." *Biotechnology for Biofuels* 10:18 (2017), 13 pages.

Outreach Efforts

Tyner made a presentation on stochastic TEA for aviation biofuels at the DOE workshop on aviation biofuels in Macon, GA

Awards

Tyner was named a fellow of the American Association for the Advancement of Science (AAAS) awarded in February 2017 at the AAAS meetings in Boston.
Tyner was named one of the top 100 people in the Advanced Bioeconomy by *Biofuels Digest*.

Student Involvement

Xin Zhao – PhD student, Purdue University

Elspeth McGarvey – MS student, Purdue University
Jeremiah Stevens – MS student, Purdue University
The students have worked on the stochastic techno-economic analysis and induced land use change.

Plans for Next Period
We will continue stochastic TEA, with the next pathway to be completed being pennycress to jet fuel. We also anticipate an analysis of the quantitative potential for camelina based jet fuel.

Task #2: Life Cycle and Production Potential Analysis of Alternative Aviation Biofuel Pathways in Coordination with ICAO-AFTF
Purdue University

Objective(s)
Work with the CAEP/AFTF life cycle assessment committee (WP3) on issues such as system boundaries, induced land use change, LCA methodology, and pathway GHG emissions assessment.

Research Approach
There are many varied assignments and pieces under this task. For life cycle analysis, working with other team members, we use standard approaches for consequential LCA. For system boundaries, we have investigated the consequences of different approaches to defining system boundaries. For estimating induced land use change, we use the GTAP model and have modified it to improve land allocation at the extensive and intensive margins (see task 4).

Milestone(s)
Tyner participated in the AFTF meetings in Montreal in October 2016 and February 2016. He has been involved in many of the tasks and document preparation for the meetings. In Montreal, Tyner and Zhao gave presentations on the improvements in induced land use change modeling and the work plan for the ILUC sub-group.

Major Accomplishments
AFTF is making progress on core LCA, induced land use change, and sustainability.

Publications
There have been numerous working papers and information papers produced for the AFTF work.

Outreach Efforts
None

Awards
See awards under Task 1

Student Involvement
Xin Zhao has been involved in the AFTF ILUC work

Plans for Next Period
In the next period, we will be doing further model improvements and additional test simulations for multiple aviation biofuel pathways and regions. We have also been working with the International Institute for Applied Systems Analysis on comparing model results from their GLOBIOM model with GTAP-BIO. That work will continue in 2017-2018.

Task #3: Develop Estimates of Land Use Change Associated Emissions for Aviation Biofuels for the ICAO Alternative Fuels Task Force

Purdue University

Objective(s)

Develop estimates of land use change associated emissions for aviation biofuels for the ICAO Alternative Fuels Task Force

Research Approach

We use the updated and modified GTAP-BIO model to produce preliminary estimates of induced land use change for AFTF. We are also working with IIASA and Hugo Valin to evaluate differences between results obtained with GTAP-BIO and GLOBIOM.

Milestone(s)

None

Major Accomplishments

Most of the accomplishments under this task are in the form of work progress of ICAO/CAEP/AFTF. Some of the working papers and information papers we have produced in 2016/17 are listed in this section and in the overall publication list at the end of this report.

Publications

CAEP/11 ILUC Task Group. Development of Test Model Simulations to Be Used in Studying Induced Land Use Change from Aviation Biofuels Production. *CAEP/11-AFTF/2-WP/3.* Oct 2016.

CAEP/11 ILUC Task Group. Preliminary Simulation Test Results for Estimation of Land Use Change Emission Values for Aviation Biofuels Production. *CAEP/11-AFTF/3-WP/4.* Jan 2017.

CAEP/11 ILUC Task Group. Preliminary GTAP-BIO Simulation Results for Estimation of Land Use Change Emission Values for Aviation Biofuels Production. *CAEP/11-AFTF/4-WP/06.* May 2017.

CAEP/11 ILUC Task Group. Summary Comparison of GTAP-BIO and GLOBIOM Models and Results. *CAEP/11-AFTF/4-IP/07.* May 2017.

Taheripour, F., Cui, H., & Tyner, W. E. (2017). An Exploration of Agricultural Land use Change at the Intensive and Extensive Margins: Implications for Biofuels Induced Land Use Change. In Z. Qin, U. Mishra, & A. Hastings (Eds.), *Bioenergy and Land Use Change*: American Geophysical Union (Wiley).

Taheripour, F., Zhao, X., & Tyner, W. E. (2017). The impact of considering land intensification and updated data on biofuels land use change and emissions estimates. *Biotechnology for Biofuels*, *10*(1), 191.

Outreach Efforts

Xin Zhao made a poster presentation of the aviation biofuels induced land use change work at the April 2017 ASCENT meeting.

Xin Zhao presented our induced land use change work at the September 2017 ASCENT meeting.

Awards

See task 1.

Student Involvement

Xin Zhao – PhD student, Purdue University

Plans for Next Period
We will be producing induced land use change emission estimates for the AFTF April 2018 meeting.

Task #4: Provide Support for the Other ASCENT Universities on Aviation Biofuels Policy Analysis
Purdue University

Objective(s)
To provide support for the other ASCENT universities on aviation biofuels policy analysis.

Research Approach
We develop spreadsheet models of various pathways incorporating risk analysis. The output of the risk analysis is the distribution of net present value (NPV), internal rate of return (IRR), and the probability the investment will lose money. Being able to provide a distribution of financial outputs is immensely valuable to private sector investors and other players. The analysis outputs can also be used to help target future research to areas where the research outcome could be expected to have a high payoff. We have been working with WSU on stochastic TEA and expect in the next year to work with WSU, PSU, Hawaii, and Tennessee on stochastic TEA and risk analysis.

In addition, we now can develop distributions of breakeven prices that reflect the uncertainty in the input distributions. A distribution of breakeven prices is a very effective way to communicate the relative level of pathway cost as well as its uncertainty.

Any of the stochastic techno-economic analyses can be used with policy overlays to conduct evaluations of alternative policy options. The stochastic models can also be used to examine the impacts of alternative feedstock contracting mechanisms for feedstocks without effective hedging alternatives available, such as the cellulosic feedstocks or new lipids such as pennycress. If desired, we can work with the ICAO/AFTF policy sub-group to develop such policy case studies.

Milestone(s)
We have published papers on stochastic TEA (see the publications in task 1) and are now assisting researchers at other universities in doing this type of analysis using the approaches we have developed.

Major Accomplishments
We have provided guidance to ASCENT partners and have helped them to build stochastic TEA models for their pathways under investigation.

Publications
None

Outreach Efforts
None

Awards
See task 1.

Student Involvement
Elspeth McGarvey – MS student, Purdue University
Jeremiah Stevens – MS student, Purdue University

Plans for Next Period
We will be working with researchers at other universities to do stochastic TEA and to develop policy overlays for the models.

Task #5: Provide Support for the Farm to Fly Initiative As Needed

Purdue University

Objective(s)

To provide support for the Farm to Fly initiative as needed.

Research Approach

This activity is a general support for other initiatives. Our main role is to consult with other projects and activities and provide assistance as needed.

Milestone(s)

There has been little activity under this task in this reporting period.

Major Accomplishments

None

Publications

Perkis, David F., and Wallace E. Tyner. "Developing a Cellulosic Aviation Biofuel Industry in Indiana: A Market and Logistics Analysis." *Energy*, forthcoming 2017.

Zhao, Xin, Guolin Yao, and Wallace E. Tyner. "Quantifying breakeven price distributions in stochastic techno-economic analysis." *Applied Energy* 183 (2016) 318-326.

Bann, Seamus J., Robert Malina, Pooja Suresh, Matthew Pearlson, Wallace E. Tyner, James I. Hileman, and Steven Barrett. "The costs of production of alternative jet fuel: A harmonized stochastic assessment." *Bioresource Technology* 227 (2017), 179-187.

Taheripour, F., Cui, H., & Tyner, W. E. (2017). An Exploration of Agricultural Land use Change at the Intensive and Extensive Margins: Implications for Biofuels Induced Land Use Change. In Z. Qin, U. Mishra, & A. Hastings (Eds.), *Bioenergy and Land Use Change*: American Geophysical Union (Wiley).

Yao, Guolin, Mark D. Staples, Robert Malina, and Wallace E. Tyner. "Stochastic techno-economic analysis of alcohol-to-jet fuel production." *Biotechnology for Biofuels* 10:18 (2017), 13 pages.

Taheripour, F., Zhao, X., & Tyner, W. E. (2017). The impact of considering land intensification and updated data on biofuels land use change and emissions estimates. *Biotechnology for Biofuels*, *10*(1), 191.

Perkis, David F., and Wallace E. Tyner. "Developing a Cellulosic Aviation Biofuel Industry in Indiana: A Market and Logistics Analysis." *Energy*, forthcoming 2017.

CAEP/11 ILUC Task Group. Development of Test Model Simulations to Be Used in Studying Induced Land Use Change from Aviation Biofuels Production. *CAEP/11-AFTF/2-WP/3.* Oct 2016.

CAEP/11 ILUC Task Group. Preliminary Simulation Test Results for Estimation of Land Use Change Emission Values for Aviation Biofuels Production. *CAEP/11-AFTF/3-WP/4.* Jan 2017.

CAEP/11 ILUC Task Group. Preliminary GTAP-BIO Simulation Results for Estimation of Land Use Change Emission Values for Aviation Biofuels Production. *CAEP/11-AFTF/4-WP/06.* May 2017.

CAEP/11 ILUC Task Group. Summary Comparison of GTAP-BIO and GLOBIOM Models and Results. *CAEP/11-AFTF/4-IP/07.* May 2017.

Outreach Efforts
None

Awards
See task 1.

Student Involvement
None

Plans for Next Period
We will continue to be available to other projects and universities as needed in the regional and national analysis related to "Farm to Fly."

Project 001(D) Alternative Jet Fuel Supply Chain Analysis

Pennsylvania State University

Project Lead Investigator

Investigating Team:

- Leads: Katherine Y. Zipp – PSU

Other Lead Personnel:

- Tom Richard – PSU, Caroline E. Clifford – PSU, Lara Fowler – PSU, Michael P. Wolcott – WSU, Manuel Garcia-Perez – WSU, Tim Rials – UT, Burt English – UT, Kristin Lewis – Volpe

Penn State Lead:

Katherine Y. Zipp
Assistant Professor of Environmental and Resource Economics
Department of Agricultural Economics, Sociology, and Education
The Pennsylvania State University
112-F Armsby
University Park, PA 16802
814.863.8247
kyz1@psu.edu

University Participants

Penn State University

- Project Co-Director: Katherine Y. Zipp, PSU
- Other researchers: Tom Richard – PSU, Caroline E. Clifford – PSU, Lara Fowler – PSU
- FAA Award Number: FAA Cooperative Agreement No. 13-C-AJFE-PSU, Amendment 028
- Period of Performance: August 1, 2016 – July 31, 2017

Project Funding Level

FAA Funding: $200,000.
Matching: Penn State - $200,000
Total Funding: $400,000

Investigation Team

1.5.1 (Lead: Richard; supported by Zipp, Rials, and English) – Delineate the sustainability impacts associated with various feedstock choices (switchgrass, oilseeds and winter grasses) including land-use effects for the mid-Atlantic region, including the Chesapeake Bay watershed.

1.5.2 (Lead: Zipp, supported by Richard and Lewis) - Evaluate the supply chains associated with switchgrass, oilseeds and winter grasses for the mid-Atlantic region.

3.3.1 (Lead: Clifford; supported by Garcia-Perez) - Report on preprocessing requirements and refinery insertion points for various bio-oil and biomass feeds.

3.3.3 (Lead: Garcia-Perez, supported by Clifford) – Simulate satellite biomass-to-liquid processing (e.g. gasification/F-T catalysis, pyrolysis, hydrothermal liquefaction or vegetable oil processing)

7.1.4 (Lead: Richard, supported by Wolcott) - Updated Data Management Plan and Status Report

8.1.0 (Lead: Zipp, supported by Fowler, and Richard) - Analysis of ecosystem service valuation, law and policy drivers, and potential policy design of water quality improvements associated with perennial grasses and cover crops.

Project Overview

1.5.1 Delineate sustainability impacts associated with various feedstocks, including land use effects for mid-Atlantic region/Chesapeake Bay watershed. Includes subtasks addressing erosion and sediment delivery and water quality.

1.5.2 Evaluate the supply chains associated with switchgrass, oilseeds and winter grasses for the mid-Atlantic region.

3.3.1 Report on preprocessing requirements and refinery insertion points for various bio-oil and biomass feeds.

3.3.3 Simulate satellite biomass-to-liquid processing (e.g. gasification/F-T catalysis, pyrolysis, hydrothermal liquefaction or vegetable oil processing)

7.1.4 Updated Data Management Plan and Status Report

8.1.0 Analysis of ecosystem service valuation, law and policy drivers, and potential policy design of water quality improvements associated with perennial grasses and cover crops. Includes subtasks 8.1.1, a literature review, and 8.1.2, a report analyzing Chesapeake Bay opportunities as a co-product market opportunity.

Task #1.5:

- **1.5.1 Delineate Sustainability Impacts Associated with Various Feedstocks, Including Land Use Effects for Mid-Atlantic Region/Chesapeake Bay Watershed**
- **1.5.2 Evaluate the Supply Chains Associated with Switchgrass, Oilseeds and Winter Grasses for the Mid-Atlantic Region**

Penn State

Objective(s)

Evaluate the supply chains associated with switchgrass, oilseeds and winter grasses for the mid-Atlantic region.

Research Approach

Using the model developed in Task 8.1, we determined the price-supply curves to determine crop acreages at different price points. See Task 8.1 for a description of the returns to biomass needed to induce conversion.

Milestone(s)

Determined the returns needed to induce farmers to convert to switchgrass. This is the first step to estimate the price-supply curves.

Major Accomplishments

Economic model to motivate land use conversion has been developed and demonstrated at ASCENT and CAAFI meetings

Publications

N/A

Outreach Efforts

Economic model to motivate land use conversion has been demonstrated at CAAFI meetings.

Awards

N/A

Student Involvement
One graduate student is a major contributor to this project, drafting both the literature review, and the coding to estimate our model.

Plans for Next Period
Future work will couple these results on farmer adoption of switchgrass with a more accurate model of water quality benefits and use the value of these water quality benefits to offer optimal payments to farmers for these services.

References
See Task 8.1

Task #3.3:

- **3.3.1 Report On Preprocessing Requirements and Refinery Insertion Points for Various Bio-Oil and Biomass Feeds**
- **3.3.3 Simulate Satellite Biomass-to-Liquid Processing (e.g. Gasification/F-T Catalysis, Pyrolysis, Hydrothermal Liquefaction or Vegetable Oil Processing)**

Penn State and Washington State

Objective(s)
Evaluate commercial options for biofuel intermediates insertion into petroleum refineries for conversion to AJF.

Research Approach
Using an extensive literature review, PSU identified and evaluated commercial biomass feedstocks and bio-based intermediates that could be inserted in a refinery or be converted to alternative jet fuel with minimal processing. The evaluation considered bio-based liquids at three insertion points: 1) “bio-crude” introduced at the front of the refinery for crude processing with petroleum, 2) refinery-ready liquids inserted after crude processing and utilizing conversion and/or finishing unit operations to upgrade the bio-based liquids into fuels, and 3) blend-ready fuels that are inserted during blending to upgrade low-value refinery streams, improve specifications, and take advantage of blending, storage and distribution capacity. Unit operations and process opportunities and constraints were assessed for a range of bio-based liquids relevant to alternative jet fuels.

Milestone(s)
Currently we are working on report focused on oxygen removal of bio-based fuels and intermediates.

Major Accomplishments
The accomplishments of this task (Task 3.3) will provide the project and stakeholders with a clearer understanding of the options, pros and cons of integrating bio-based feedstocks in a conventional petroleum refinery. Oxygen in biomass intermediates may discourage petroleum-refining facilities from pursuing the use of intermediates, so how to remove the oxygen is critical. We are working on a literature review of how to remove oxygen using conventional processes and catalysts as well as suggesting alternative catalysts.

Publications
A Technical Report was developed for discussion with Delta Airlines. We have written a publication on this material that will be submitted in the next couple of months.

Outreach Efforts
We are currently working on a publication to submit in late 2017 to the journal *Energy and Fuels*.

Awards
N/A

Student Involvement
N/A

Plans for Next Period
The literature review of how to remove oxygen using conventional processes and catalysts as well as alternative catalysts will be completed and submitted for publication.

References
See technical report.

Task #7.1.4: Updated Data Management Plan and Status Report
Penn State and Washington State and ORNL

Objective(s)
Update Data Management Plan and provide status report.

Research Approach
The primary goal of this task is to develop a common framework that facilitates transparent and open data access for supply chain model intercomparison and improvement, specifically targeting the needs and opportunities of the AJF sector. This effort requires coordination of all team members, many of whom have independent models and datasets, some of which are proprietary. The team developed a consensus approach to data use and model access and then established appropriate agreements and documentation.

Milestone(s)
This year we transitioned the data management plan to be administered by staff at Washington State University. The ASCENT01 data management system is being evaluated as a model for other ASCENT projects.

Major Accomplishments
PIs and students working on the project have reviewed signed the Data Use Agreement document and the Data Use Acknowledgement document, file naming conventions and meta data documentation have been developed, and over 2200 files have been uploaded into the system. Most of these files are journal articles, but 70 of the files are datasets that have been classified and logged in our Common Data needs document for internal data sharing and eventual public release.

Publications
None

Outreach Efforts
N/A

Awards
N/A

Student Involvement
N/A

Plans for Next Period
Continue to encourage participation, now under the auspices of Washington State University.

Task #8.1: Analysis of Ecosystem Service Valuation, Law and Policy Drivers, and Potential Policy Design of Water Quality Improvements Associated With Perennial Grasses and Cover Crops
Penn State

Objective(s)
Analysis of Ecosystem service valuation and policy design of water quality improvements associated with perennial grasses and cover crops. Includes subtasks 8.1.1 (Literature review) and 8.1.2 (Report analyzing Chesapeake Bay opportunities as a co-product market opportunity.

Research Approach
Drawing on scholarly literature, government reports, legislation and policy documents, we have investigated the legal and policy incentives for ecosystem services for the Chesapeake Bay region. To operationalize those policies in an economic farmer decision framework, we developed a land use conversion contract model following the general land conversion model by (Song, Zhao, & Swinton, 2011), while also incorporating subsidies in the form of payments for ecosystem services and incentive compatibility constraints. Specifically, we expanded the model by considering that the potential payoff for farmers who choose to initiate land use conversion and adopt biofuel crops consists of not only the monetary values of crop outputs, but also a one-time lump-sum payment and subsidies that are depended on the consequential environmental benefits. We also extended the model to offer targeted payments to farmers based on the predicted effectiveness of improving water quality benefits based on the farmer's location. Figure 1 provides an example of delivery factors that represent the proportion of nitrogen pollution in each area reaching the Chesapeake Bay (Environmental Protection Agency, 2010). We use this information to target payments for environmental services based on the benefits provided by planting switchgrass. For example, to reduce nitrogen concentrations in the Chesapeake Bay it will be more effective to reduce nitrogen in the red counties compared to the blue counties.

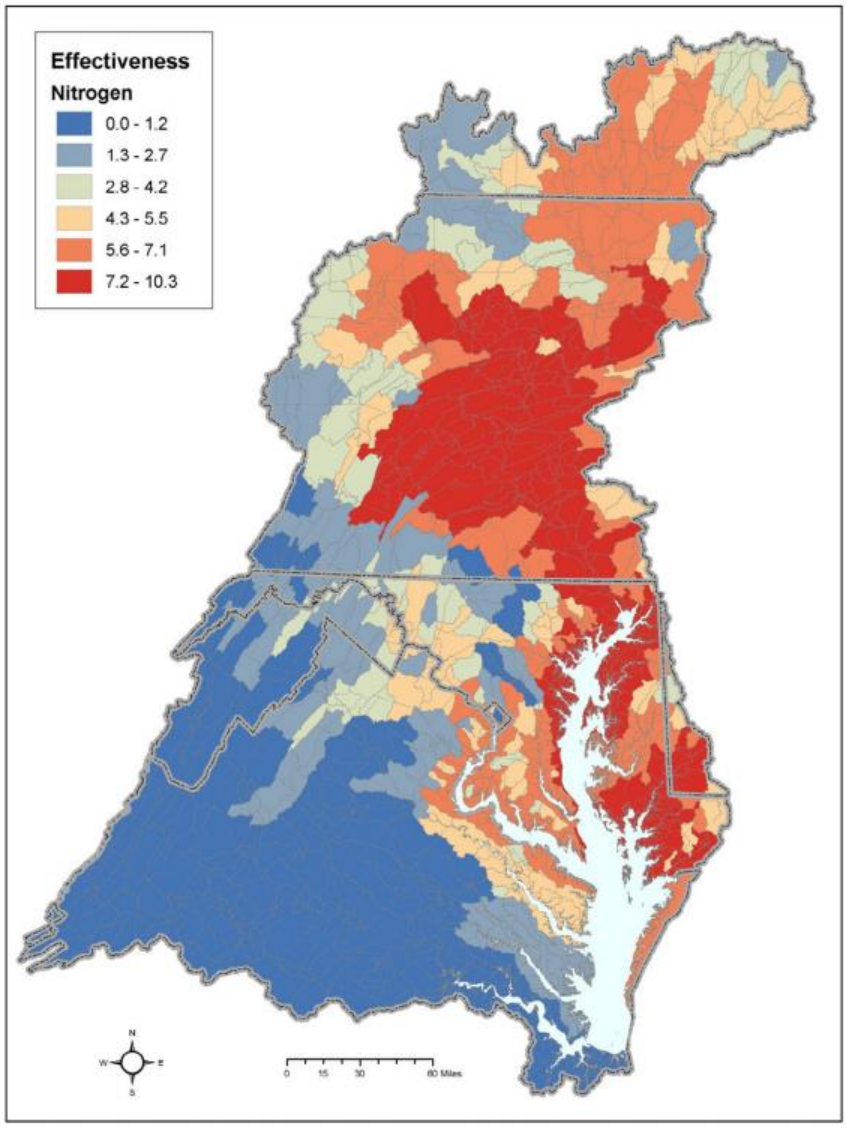

Figure 6-5. Relative effectiveness illustrated geographically by subbasins across the Chesapeake Bay watershed for nitrogen.

(Environmental Protection Agency, 2010)

The one-time lump-sum welfare transfer (denoted as T_{cs}) includes monetary compensation as well as technological assistance from government agencies to offset any fixed costs that farmers might incur if they convert their cropland from a corn-soybean rotation (denoted as *c*) to biofuel crops such as switchgrass (denoted as *s*). For simplicity, consider that $\{c, s\}$ is the only set of crop choices for a risk-neutral farmer with a unit of cropland, and any one-time land use conversion from *i* to *j* would incur a lump-sum cost $C_{ij}, i, j \in \{c, s\}$. Hence, it is necessary that $T_{cs} \geq C_{cs}$ holds for any conversion from *c* to *s* in order for farmers to participate. We compare a uniform payment to all farmers versus a targeted payment for the environmental services provided to the Chesapeake Bay (see Figure 1).

The farmer's payoff is consisted of two components. First, the monetary values of crop *i* outputs in period *t* is denoted by $\pi_i(t)$ which follows a stochastic process with evolution of a general form (Song et al., 2011), as follows:

(1) $$d\pi_i(t) = \theta_i(\pi_i, t)dt + \sigma_i(\pi_i, t)d\varepsilon_i,\ i \in \{c, s\}$$

where the drift term $\theta_i(\pi_i, t)$and variance $\sigma_i(\pi_i, t)$ are observable nonrandom functions, and $d\varepsilon_i$ is the increment of a Wiener process[1] which assumes that farmers would be able to learn about and predict future returns in each new period based on information updated in previous period. The correlation coefficient between *c* and *s* is denoted as ρ, such that $\mathrm{E}[d\varepsilon_c d\varepsilon_s] = \rho dt$. Farmers' expected present value payoff from crop returns on land use *i* at period *t* is denoted $V^i(\pi_c(t), \pi_s(t))$, which depends on the distribution of future returns of both land uses and farmers make decisions between keeping land use *i* or convert it into alternative *j* (Song et al., 2011), as:

(2) $$V^i(\pi_c(t), \pi_s(t)) = max\begin{Bmatrix} \pi_i(t)dt + e^{-rdt}EV^i[\pi_c(t+dt) \times \pi_s(t+dt)], \\ V^j(\pi_c(t), \pi_s(t)) - C_{ij} \end{Bmatrix}$$

Second, farmers who agree to convert land use from corn-soybean to switchgrass (thus a $c \to s$ process) can receive, by the end of each period *t* of this particular conversion process, a subsidy from government agencies based on the generated environmental values. Switchgrass and many other biofuels have the potential to provide a variety of environmental benefits such as soil nitrogen sequestration, water nutrient reduction, and biodiversity conservation. These benefits, although often not traded with market values, can be utilized by government agencies and regulators as a part of the efforts on environmental protection and ecosystem restoration. For simplicity, we denote the environmental performance level of land use alternative *i* as a stochastically continuous and twice differentiable function $\phi_i(e_t), i \in \{c, s\}$, such that:

$$\frac{d\phi_s(e_t)}{dt} > 0, \quad \frac{d^2\phi_s(e_t)}{dt^2} \leq 0$$
$$\frac{d\phi_c(e_t)}{dt} \leq 0, \quad \frac{d^2\phi_c(e_t)}{dt^2} \leq 0$$

This restriction allows us to differentiate the environmental performance of the two land uses so that switchgrass would generate increasing environmental benefits, while corn would generate limited (but not necessarily negative) environmental benefits.

Suppose that $\phi_i(e_t)$ is observable to government agencies at the end of period *t*, and a subsidy is paid to farmers based on the perceived environmental performance level. Without loss of generality, we define a subsidy rate, m, as a per unit compensation rate paid to farmers according to the perceived environmental performance level at the end of period *t*. Hence, the total subsidies paid to farmers in each possible land use scenario in period *t* are as follows:

(3-1) grow corn in period $t-1$, and convert land use to switchgrass in period t:

$$-C_{cs} + T_{cs} + m\phi_s(e_t) = m\phi_s(e_t), \text{ since } T_{cs} = C_{cs}$$

(3-2) grow switchgrass in period $t-1$ and period t:

$$m\phi_s(e_t)$$

(3-3) grow corn in period $t-1$ and period t:

$$m\phi_c(e_t)$$

[1] The Wiener pdf is $f_{W_t}(x) = \frac{1}{\sqrt{2\pi t}}\exp(-\frac{x^2}{2t})$, following normal distribution with zero mean and variance *t* at any fixed period *t*. The covariance between any *s* and *t* is $cov(W_s, W_t) = \min(s, t)$, and $corr(W_s, W_t) = \sqrt{\frac{\min(s,t)}{\max(s,t)}}$.

(3-4) grow switchgrass in period $t-1$, and convert land use to corn in period t:

$$-C_{sc} + m\phi_c(e_t)$$

Since we assume that $\phi_s(e_t)$ is increasing over time, it is necessary that the total subsidy paid to farmers of land use type s by government at the end of each period t is strictly higher than farmers of land use type c.

Hence, the optimal land use decision problem in Equation (2), for value functions V^i and $V^j, i,j \in \{c,s\}$, must satisfy the following conditions along with the IC and IR constraints:

(4-1) $$LV^i\big(\pi_c(t),\pi_s(t)\big) \geq 0, i,j \in \{c,s\}$$

where $LV^i\big(\pi_c(t),\pi_s(t)\big)$ is the second order Taylor expansion of $V^i\big(\pi_c(t),\pi_s(t)\big)$ by applying Ito's lemma, as:

$$LV^i\big(\pi_c(t),\pi_s(t)\big) = rV^i(\pi_c,\pi_s) - \pi_i(t) - \sum_{p=c,s}\alpha_p(\pi_p,t)\frac{\partial V^i}{\partial \pi_p} - \sum_{p=c,s}\frac{\sigma_p^2(\pi_p,t)}{2}\frac{\partial^2 V^i}{\partial \pi_p \partial \pi_p}$$

$$-\rho\sigma_c(\pi_c,t)\sigma_s(\pi_s,t)\frac{\partial^2 V^i}{\partial \pi_c \partial \pi_s}$$

(4-2) $$V^i(\pi_c,\pi_s) \geq V^j(\pi_c,\pi_s) - C_{ij}, i,j \in \{c,s\}\ and\ i \neq j$$

(4-3) Either (4-1) or (4-2) holds with strict equality.

Data

We collected the following data to estimate the supply of switchgrass by water quality benefits provided to the Chesapeake Bay. Through personal communication with Jeff Sweeney at the Chesapeake Bay Program Office of the Environmental Protection Agency, we obtained data on the effectiveness of reducing nitrogen in each county to Chesapeake Bay water quality goals (Figure 1). For this first step, we focused on nitrogen reduction but other water quality goals could be considered. For each of the effectiveness categories, we also needed data on corn yields, prices, and profits and potential switchgrass yields, prices, and profits. We also need the variance of these estimates. We obtained these data from personal communication with Laurence Eaton at the Oak Ridge National Lab (Daly, Halbleib, Hannaway, & Eaton, n.d.).

Parameter Calibration and Estimation

The model can be parameterized and solved by collocation using OSSOLVER (Fackler, 2008) and estimated with CompEcon package in Matlab (Miranda & Fackler, 2002). Value functions can be approximated using a linearized combination of a sequence of known basis functions, such as:

(5) $$\widehat{V^i}(\pi_c,\pi_s) = \sum_{j_c=1}^{n_c}\sum_{j_s=1}^{n_s} c_{j_c j_s}\psi_{j_c j_s}(\pi_c,\pi_s)$$

where $c_{j_c j_s}$ is obtained when the decision optimality conditions are satisfied. The optimal decision rule is determined by solving and evaluating the approximated value functions at $\{c,s\}$ as well as the return minus the conversion costs, and based on the results the best payoffs from converting are then compared with the best payoffs from not converting (Fackler, 2008).

The empirical method involves solving the parameters in the return equation and calibrating parameters in the value functions. Return from land use is assumed to follow stochastic processes, with unknown parameters including the drift term θ_i, variance σ_i and correlation between the two alternatives ρ, which can be re-parameterized by linearization approximation. Two stochastic processes are often used. If return follows geometric Brownian motion (GBM), the analytical representation is as follows:

(6) $$d\pi_i = \theta_i\pi_i dt + \sigma_i\pi_i d\varepsilon_i,\ i \in \{c,s\}$$

Discrete approximation of the inter-temporal return difference gives:

(7) $$\ln \pi_{i,t} - \ln \pi_{i,t-1} = \left(\theta_i - \frac{\sigma_i^2}{2}\right) + \sigma_i \varepsilon_i,\ i \in \{c, s\}$$

Denote $\alpha_i = \theta_i - \frac{\sigma_i^2}{2}$, then α_i, σ_i and ρ can be estimated by maximum likelihood estimates.

If the returns follow mean reversion (MR), the analytical representation is as follows:

(8) $$d\pi_i = \theta_i(\tilde{\pi_i} - \pi_i)dt + \sigma_i \pi_i d\varepsilon_i,\ i \in \{c, s\}$$

where $\tilde{\pi_i}$ is the historically observed average return of land use *i*, and θ_i here measures speed of reversion. Discrete approximation of the inter-temporal return difference gives:

(9) $$\frac{\pi_{i,t} - \pi_{i,t-1}}{\pi_{i,t-1}} = \theta_i\left(\tilde{\pi_i} - \pi_{i,t-1}\right) + \sigma_i \varepsilon_i$$
$$= \theta_i \tilde{\pi_i} - \theta_i \pi_{i,t-1} + \sigma_i \varepsilon_i, \qquad i \in \{c, s\}$$

Denote $\beta_{1i} = \theta_i \tilde{\pi_i}$, $\beta_{2i} = -\theta_i$, , then β_{1i}, β_{2i}, σ_i and ρ can be estimated.

Parameters

Table 1: Parameter estimates

Parameter	Seg0-1	Seg1-2	Seg2-3	Seg3-4	Seg4-5	Seg>5
alpha_c	0.086	0.080	0.081	0.079	0.079	0.068
sigma_c	0.181	0.160	0.176	0.193	0.159	0.147
alpha_s	-0.006	-0.005	-0.006	-0.008	0.000	-0.009
sigma_s	0.086	0.078	0.086	0.101	0.063	0.060
rho_t	0.671	0.655	0.646	0.722	0.609	0.451

Table 2: The net present value (NPV) of corn and switchgrass returns by nitrogen reduction bins.

Weighted Base Year NPV(2012 in $2016)	Seg(0-1)	Seg(1-2)	Seg(2-3)	Seg(3-4)	Seg(4-5)	Seg(>5)
Corn	$ 368.54	$ 572.46	$ 306.01	$ 508.77	$ 523.18	$ 284.32
Switchgrass	$ 113.22	$ 183.69	$ 136.62	$ 156.42	$ 171.10	$ 84.55

Preliminary Results

The preliminary results[2] are presented as conversion boundaries. If a farmer is growing corn-soybeans they will convert to growing switchgrass when annual returns to switchgrass are above the line b^{CS}. If a farmer is growing switchgrass they will convert to growing corn-soybeans when annual returns to corn-soybeans are greater than the line b^{SC}. Because of uncertainty, risk, and the option value (the value of continuing the current use and having the option of converting crops in the future when it is more profitable to do so) the annual returns to switchgrass have to be higher than the net present value (b^{CS}_{NPV}) of the annual returns to switchgrass to induce conversion.

[2] These results are preliminary so please do not cite.

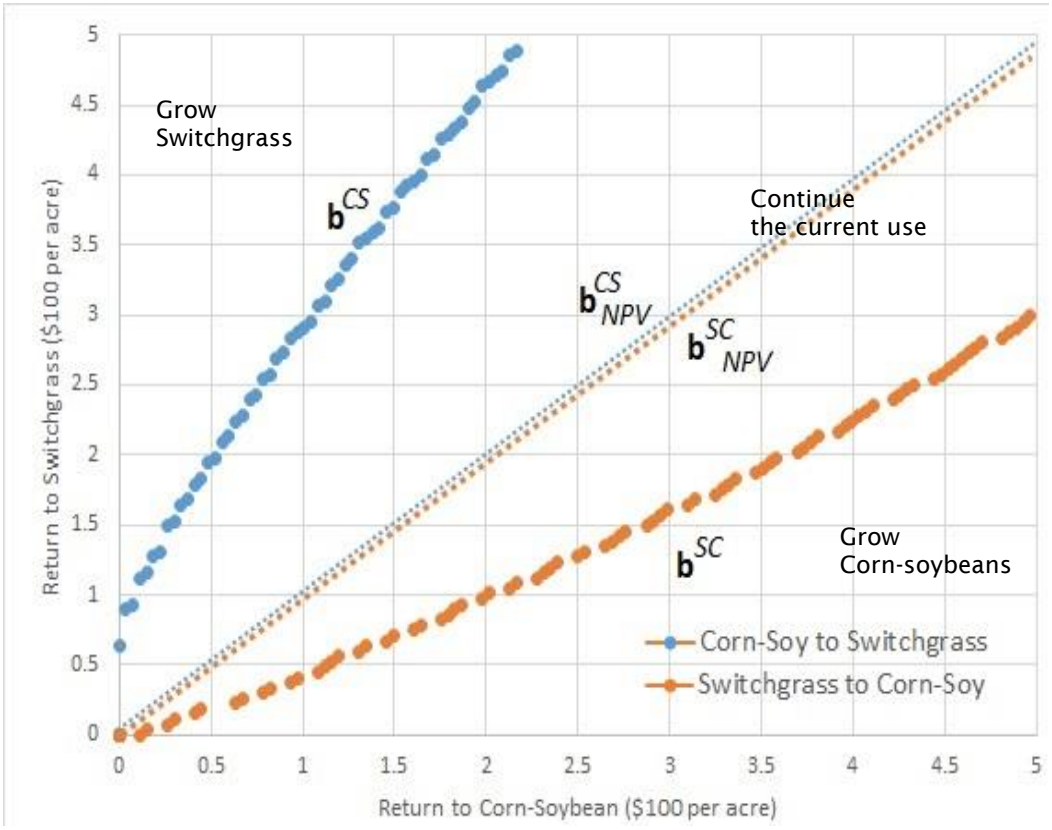

Figure 1: Replicate of the baseline model in (Song et al., 2011)

First, we replicated the baseline model in (Song et al., 2011). The optimality condition for conversion decisions are solved using Compecon toolbox (Miranda & Fackler, 2002) in MATLAB. The nodal points for the state variables (returns to corn-soybean and switchgrass, respectively) are evenly scattered over a revenue interval [0, 5] in hundred dollars ($100) in $1982. The output diagram shows the two boundaries in solid lines for conversions from corn-soybean to switchgrass (b^{cs}) and from switchgrass to corn-soybean (b^{sc}).

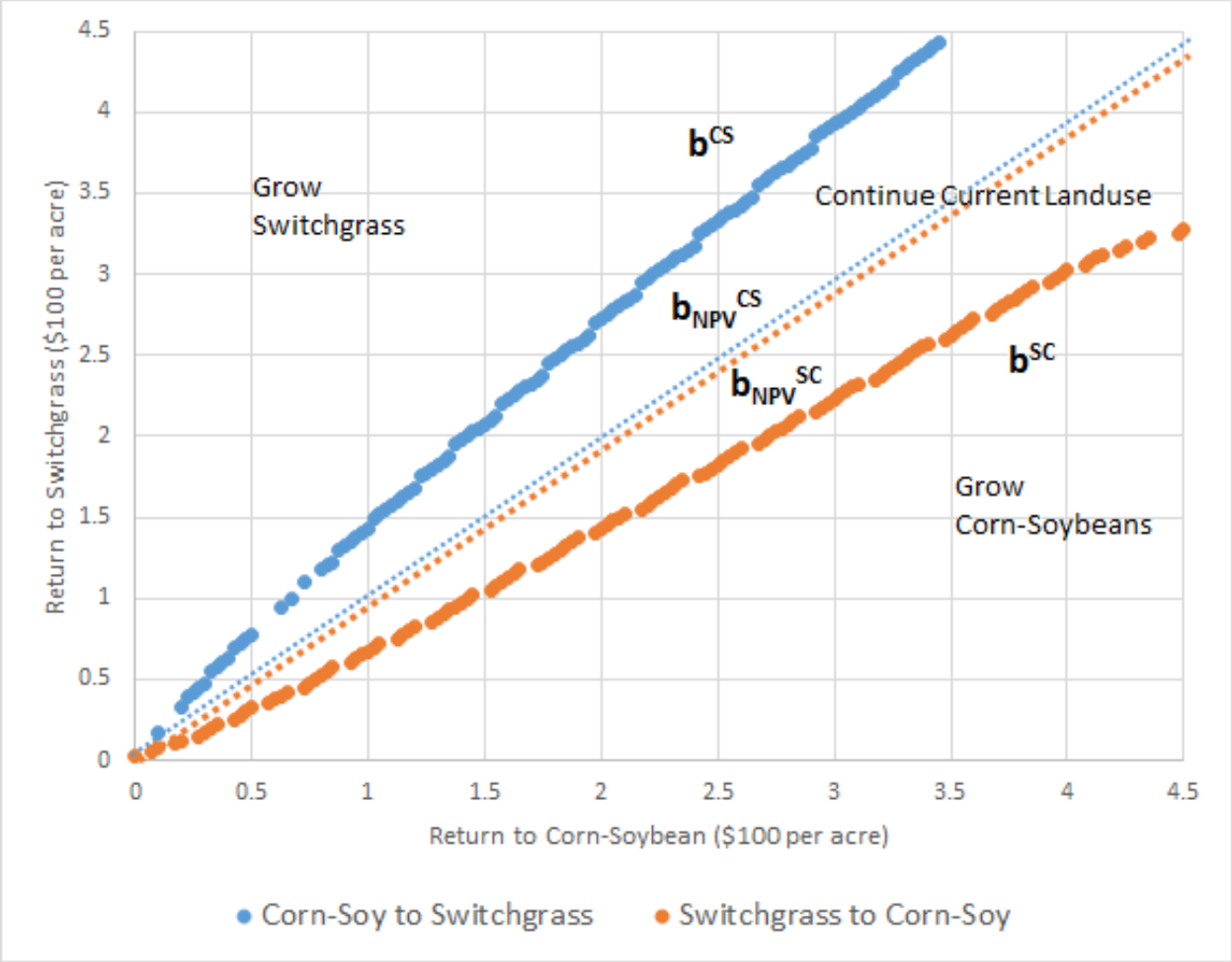

Figure 2: Subsidy to Switchgrass: $100 per acre from (Woodbury et al., n.d.)

In this modification, we applied a subsidy of $100 per acre to farmers if the crops are converted from corn-soybean to switchgrass.

Converting all units to 2016$, without a government subsidy if farmers can earn $230/acre per year with a corn-soybean rotation and $337/acre per year with switchgrass, then they will not convert to switchgrass unless they can earn more than $512/acre per year. Uncertainty, risk, and the option value to convert in the future increase the minimum return from switchgrass needed to induce farmers to convert to switchgrass. With a $100/acre per year payment for ecosystem services (PES) subsidy, farmers would only need $399/acre per year returns to convert their land to switchgrass. Therefore, farmers do need more than the real annual returns to incentivize them to grow switchgrass but a $100/acre subsidy for ecosystem services reduces the uncertainty and risk and therefore reduces the returns need to convert by more than $100/acre.

Table 3: Estimated total switchgrass acreage, nitrogen (N) reduction, and the percent of the Pennsylvania (PA) nitrogen (N) reduction goals

Time period	Outcome	No PES	Uniform Payment	Targeted Payment Aggregated
10 Years	Switchgrass (acre)	3877.41	7575.53	18911.00
	N Reduction (tons)*	69.79	136.36	340.40
	% PA N Goal**	0.49%	0.96%	2.39%
20 Years	Switchgrass (acre)	4502.17	6547.34	20178.00
	N Reduction (tons)*	81.04	117.85	363.2
	Pct. of PA N Goal**	0.57%	0.83%	2.55%
30 Years	Switchgrass (acre)	3751.34	5956.20	16753.00
	N Reduction (tons)*	67.52	107.21	301.55
	% PA N Goal**	0.47%	0.75%	2.12%

*Woodbury et al (2017) suggests that switchgrass can generate nitrogen reduction of 18kg/acre per year on fertilized agricultural land.
**According to the PA government, its goal is to reduce nitrogen by 31.4 million pounds (14242.8 tons) by 2025. (Hunter-Davenport, Brady, & Shader, 2016)

Milestone(s)
A draft of a review of the ecosystem benefits of perennial grasses and winter cover crops (water quality improvements, soil improvements, and biodiversity improvements) has been started. A manuscript to estimate the effects of payments for ecosystem services (PES) subsidies on the willingness to convert to biomass is under preparation. A white paper summarizing the legal and policy incentives for ecosystem services for the Chesapeake Bay Region has been finalized.

Major Accomplishments
N/A

Publications
A formal publication on the legal and policy incentives for the Chesapeake Bay Region is underway.

Outreach Efforts
N/A

Awards
N/A

Student Involvement
One graduate student is a major contributor to this project, drafting both the literature review, and the coding to estimate our model.

Plans for Next Period
Continue to work on a publication on the relationship between payments for ecosystem services (PES) and willingness to convert to biomass. Work to complete a national survey of current and proposed state and federal programs, and other legal and policy incentives, which monetize ecosystem services,

References
Daly, C., Halbleib, M., Hannaway, D., & Eaton, L. (n.d.). Environmental Limitation Mapping of Potential Biomass Resources across the Conterminous United States. *Global Climate Change Biology-Bioenergy*.

Environmental Protection Agency. (2010). *Chesapeake Bay TMDL Document*.

Fackler, P. L. (2008). Solving Optimal Switching Models. *Working Paper. North Carolina State University*. Retrieved from http://www4.ncsu.edu/unity/users/p/pfackler/www/ECG766/switch.pdf

Hunter-Davenport, B., Brady, T., & Shader, N. (2016). Pennsylvania Unveils Comprehensive Strategy to Improve Water Quality in state and Chesapeake Bay Watershed. Retrieved November 3, 2017, from http://www.media.pa.gov/pages/Agriculture_details.aspx?newsid=385

Miranda, M. J., & Fackler, P. L. (2002). *Applied Computational Economics and Finance*. Cambridge: MIT Press.

Song, F., Zhao, J., & Swinton, S. M. (2011). Switching to Perennial Energy Crops Under Uncertainty and Costly Reversibility. *American Journal of Agricultural Economics*, *93*(3), 768–783. https://doi.org/10.1093/ajae/aar018

Project 001(E) Alternative Jet Fuel Supply Chain Analysis

University of Tennessee

Project Lead Investigator

Timothy Rials
Professor and Director
Center for Renewable Carbon
University of Tennessee
2506 Jacob Dr. Knoxville, TN 37996
865-946-1130
trials@utk.edu

University Participants

University of Tennessee

- P.I.(s): Burton English, Professor
- FAA Award Number: 11712069
- Period of Performance: [August 1, 2016 to September, 30, 2017]
- Task(s):
    1. Task 1.1: Assess and inventory regional forest and agricultural biomass feedstock options.
    2. Task 1.2: Delineate the sustainability impacts associated with various feedstock choices including land use effects.
    3. Task 4: Biorefinery Infrastructure and Siting (Supporting Role)

Project Funding Level

Total Estimated Project Funding: $100,000
Total Federal and Non-Federal Funds: $200,000
Faculty salary was provided by The University of Tennessee, Institute of Agriculture in support of the project.

Investigation Team

- Tim Rials – Project Director(s)/Principal Investigator (PD/PI)
- Burton English – Co-Principal Investigator (Co PD/PI)
- Chris Clark – Faculty
- Lixia He – Other Professional
- Kim Jensen – Faculty
- Dayton Lambert – Faculty
- Jim Larson – Faculty
- Ed Yu – Faculty
- Evan Markel – Graduate Student
- Katryn Pasaribu – Graduate Student
- Umama Rahman – Graduate Student
- Bijay Sharma – Graduate Student

Project Overview

The University of Tennessee will lead the Feedstock Production (Task 1) component of the project. This component targets the need to assess and inventory regional forest and agricultural biomass feedstock options (1.1); and, the goal to delineate the sustainability impacts associated with various feedstock choices, including land use effects. Additionally, The University of Tennessee will support activities in Task 4 (Biorefinery Infrastructure and Siting) with information and insights on regional demand centers for aviation fuels and current supply chain infrastructure, as required.

Task #1.1: Assess and Inventory Regional Forest and Agricultural Biomass Feedstock Options

University of Tennessee

Objective(s)

As the markets for lignocellulosic biomass (LCB) feedstock, i.e. grasses, short-rotation woody crops, and agricultural residues, are currently not well established, it is important to evaluate the feasibility of supplying those LCB feedstocks. The opportunity cost of converting the current agricultural lands to LCB feedstocks production will be estimated. In addition, the production, harvest, storage and transportation cost of the feedstocks are included in the assessment. A variety of potential crop and biomass sources will be considered in the feedstock path including:

Oilseed crops: Potentials include: Mustard/Crambe (*Sinapsis alba/Crambe abyssinicia*); Pennycress (*Thlaspi arvense*) (Rapeseed/Canola (*Brassica napus/B. campestris*); Safflower (*Carthamus tinctorius*); Sunflower (*Helianthus spp.*); Soybean (*Glycine max*); Camelina (*Camelina sativa*)

Perennial grasses: Switchgrass (*Panicum virgatum*); Miscanthus (*Miscanthus sinensis*); Energy Cane (*Saccharum complex*)

Short-rotation woody crops: Poplar (*Populus species*); Willow (*Salix species*); Loblolly pine (*Pinus taeda*); Sweetgum (*Liquidambar styraciflua*); Sycamore (*Plantanus occidentalis*)

Agricultural residue: Wheat straw; Corn stover

Forest residue: Logging and Processing Residue

POLYSYS will be used to estimate and assess the supply and availability of these feedstock options at regional and national levels. This U.S. agricultural sector model forecasts changes in commodity prices and net farm income over time.

County level estimates of all-live total woody biomass, as well as average annual growth, removals, and mortality will be obtained from the Forest Inventory and Analysis Database (FIADB). Mill residue data will be obtained from the USFS FIA Timber Product Output (TPO) data. The ForSEAM model will be used to estimate and predict logging residues. ForSEAM uses U.S. Forest Service FIA data to project timber supply based on USGPM demand projections. Specific tasks related to this objective are outlined below. These supply curves will be placed in POLYSYS and estimates into the future will be made.

Research Approach

1. Using an existing model, POLYSYS, the price for a commodity or annual demands for feedstock are exogenously determined and placed into the model. For this year, analysis was conducted for a model cover crop – pennycress, an oil feedstock. A solution was generated that estimated the supply curve that pennycress might take ranging from $0.00 to $0.50 per pound. The feedstock streams were placed in ASCENT 1's Database. It was presented twice before the ASCENT 1 research team.
2. Completed the development of pennycress budgets and the fact sheet.
3. Added cover crops Camelina, winter rye, and triticale to the potential feedstock candidates list and developed fact sheets for these crops. We are investigating yields
4. Address comments from 1 and develop new target pathway
5. Used the approach shown in Figure 1 and Figure 2.

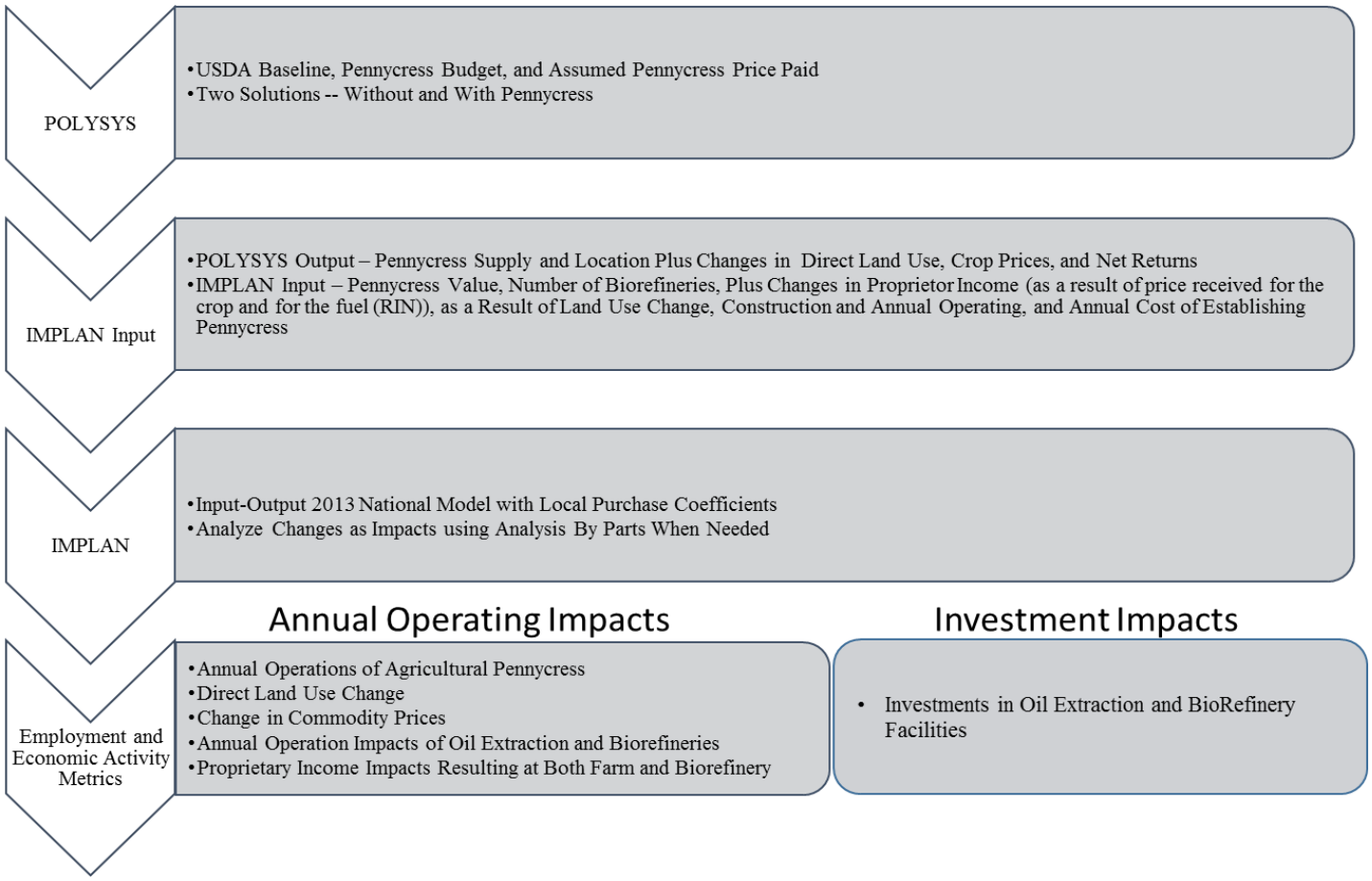

Figure 1. Approach to estimate economic impacts of using pennycress as a biofuels feedstock.

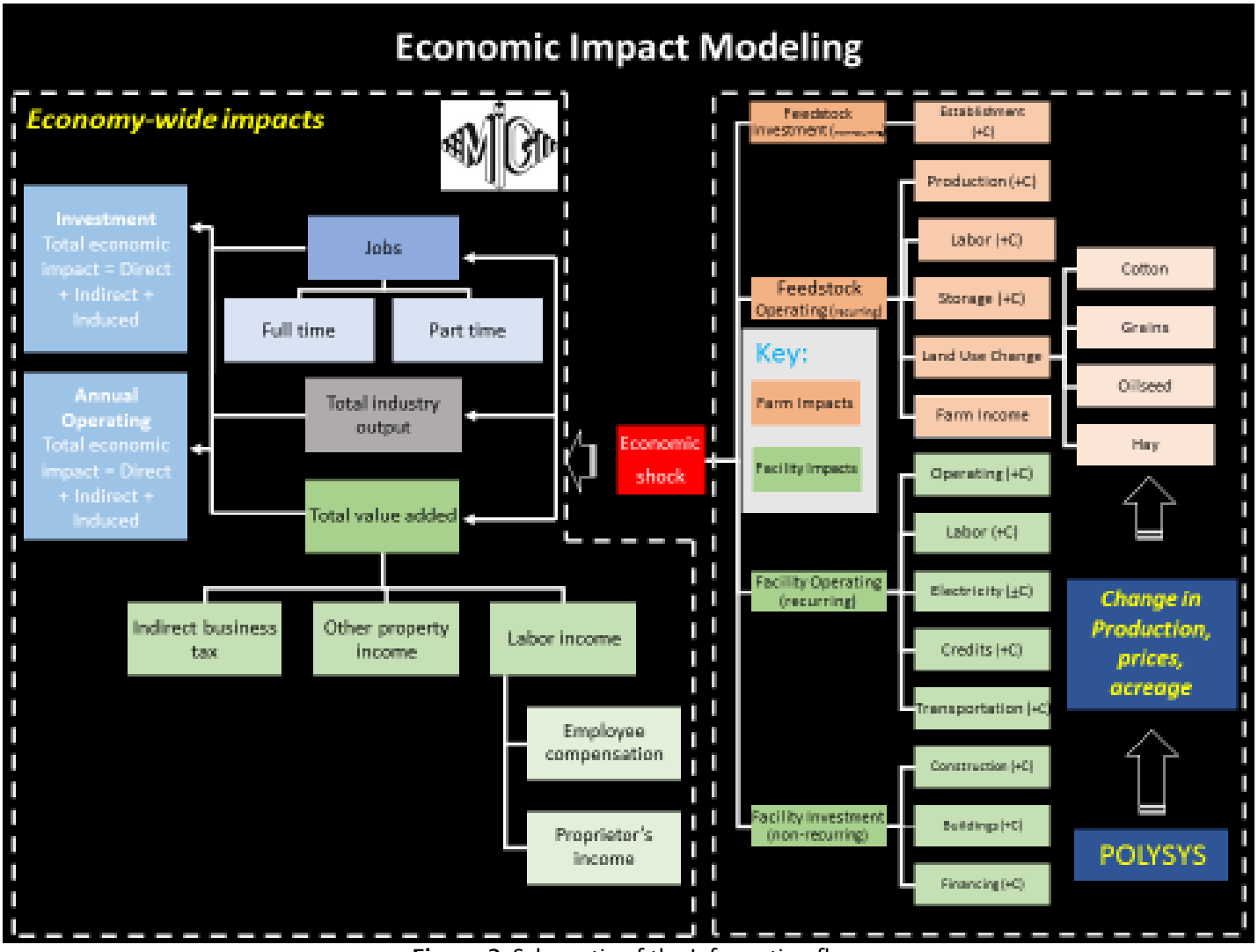

Figure 2. Schematic of the Information flow

Findings (1)

- Pennycress has the potential to supply both oil and biomass to the biofuels market.
- Pennycress is a winter crop that is typically planted in September and harvested the following May.
- It can be seeded in a corn stand via air and harvested before soybeans are planted.
- Following harvest, seed crushing and pre-processing, pennycress offers a suitable oil to allow conversion to a Hydro-processed Ester and Fatty Acid (HEFA) fuel.
- HEFA fuels are a second-generation alternative fuel that can be blended at 50/50 ratio with conventional jet fuels.
- Pennycress budget see Table 1. Other cover crops cost under review.

Table 1. Pennycress budget

	Units	$/Unit	$/Acre	
Pennycress [1]	lbs	1193	$0.20	$238.60
				$225.00
Seed [2]	lbs	5	$2.50	$12.50
Fertilizer & Lime	Acre	1	$28.50	$28.50
Chemical [3]	Acre	1	$0.00	$0.00
Repair & Maintenance [4]	Acre	1	$10.46	$10.46
Fuel, Oil & Filter [4, 9]	Acre	1	$5.90	$5.90
Operator Labor [4, 9]	Acre	1	$5.33	$5.33
Machinery Rental [5]	Acre	1	$10.00	$10.00
Crop Insurance [6]	Acre	1	$0.00	$0.00
Operating Interest [7, 9]	percent	$72.69	6.00%	$2.18
Other Variable Costs	Acre	1	$0.00	$0.00
				$74.87
				$163.73
Machinery [4, 9]				
Capital Recovery	Acre	1	$23.25	$23.25
Other Fixed Machinery Costs	Acre	1	$0.00	$0.00
Property Taxes	Acre	1	$0.00	$0.00
Insurance (Non-Machinery)	Acre	1	$0.00	$0.00
Other Fixed Costs [8]	Acre	1	$0.00	$0.00
				$23.25
				$140.49

- The breakeven price for various yields are displayed in Table 2.

Table 2. Breakeven Price For Selected Yield

Yield (lbs)	Variable Cost	Total Specified Cost
	($/lbs)	($/lbs)
800	$0.09	$0.12
900	$0.08	$0.11
1,000	$0.07	$0.10
1,100	$0.07	$0.09
1,200	$0.06	$0.08
1,300	$0.06	$0.08
1,400	$0.05	$0.07
1,500	$0.05	$0.07
1,600	$0.05	$0.06

Hydroprocessing Scenario

1. Conversion process was assumed to be a Hydro Processed Renewable Distillate Facility
2. Conversion rate 7.22 gallons jet fuel /100 pounds of oil plus other energy fuels
3. Requiring 58.8 million gallons per year of oil.
4. Need 1.84 crush facilities to meet the demand of the biorefinery.
5. Production at $0.20/pound of pennycress seed is estimated to require 22.1 million acres which will yield an average of 1300 pounds/acre.
6. 22 conversion facilities and 41 oil extraction facilities will be required.
7. Estimated the economic impact of the hydro-processing and crush facilities.
8. Partial equilibrium simulation results from POLYSYS suggest that pennycress has the potential to supply approximately 800 million gallons nationally to an alternative aviation fuel industry. The economic impact of this industry has the potential to increase national economic activity by almost $19 billion and add 66,000 jobs. Many of these jobs will occur in rural areas; therefore adding value to pennycress seed by converting the oil into biofuel could enhance rural American economies.

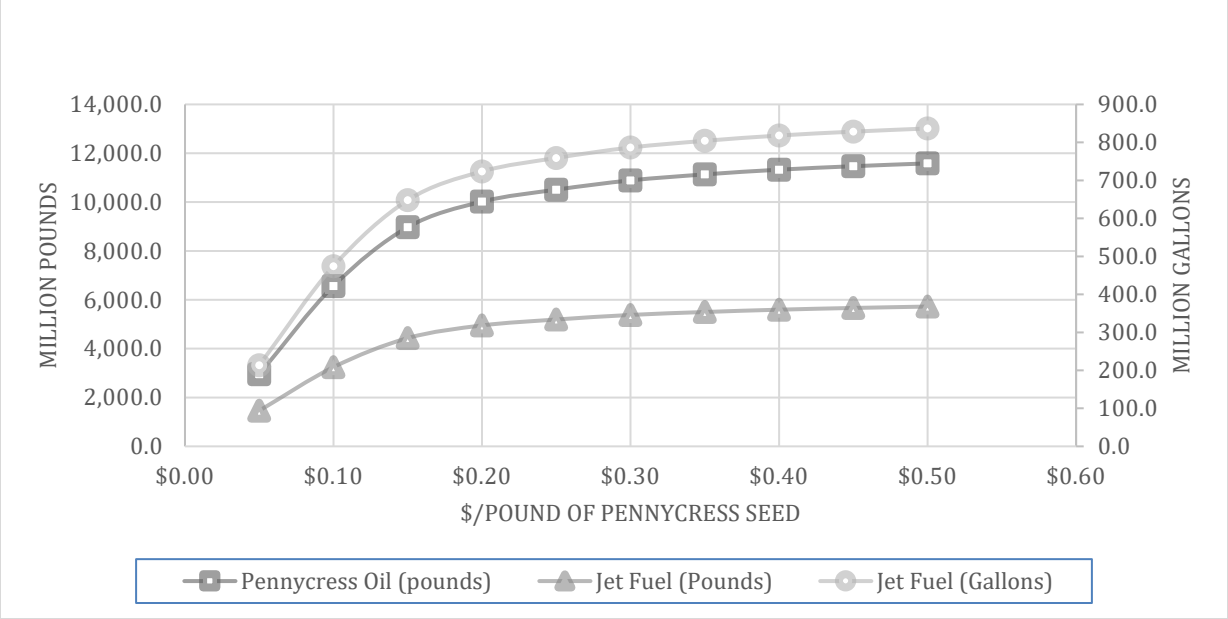

Figure 3. Pennycress and jet fuel production at different feedstock prices

Milestone(s)

Generated data passed on to ASCENT 1 database for pennycress feedstock.
Pennycress pathway developed
Other cover crops costs have been derived

Major Accomplishments

1. Completed Journal Article for submittal.
2. Developed 2 posters examining impacts of feedstock risk.
3. Evaluated the impact of BCAP on cellulosic feedstock risk
4. Developed economic multipliers for

- FT-SPK; Feedstock - Conversion temp. - 1200~1600 deg. C; Product - jet and naphtha; I have an excel model of economic analysis; and
- ATJ-SPK; Feedstock - yeast biocatalyst converts purified sugar to **ethanol**, followed by oligomerization and hydrogenation; Product - jet fuel;

Publications

None

Outreach Efforts

None

Awards

None

Student Involvement

We have had a PhD student, Evan Markel, working on this project. He is gathering information on Pennycress and developing an analysis looking at pennycress as a feedstock. Another Ph.D. student, Katryn Pasaribu, along with a Masters student, Umama Rahman, worked on the cover crop spreadsheets, and Bijay Sharma worked on risk analysis.

Plans for Next Period

Complete cover crop analysis for feedstock costs and yields. Develop POLYSYS analysis for both camellia and winter rye. Upload information gained into Box. Present material on Webina in March or April.

Task #1.2: Delineate the Sustainability Impacts Associated with Various Feedstock Choices Including Land Use Effects

University of Tennessee

Objective(s)

Environmental Sustainability – Regarding environmental sustainability, the impacts associated with LCB feedstock production, such as greenhouse gas (GHG) flux and soil erosion are estimated based on local geographic characteristics. The GHG flux related to land use change and LCB feedstock production is analyzed using the POLYSYS model. Different agricultural land use systems have varied effects on soil erosion or soil loss. The impact on soil erosion from different LCB feedstock productions is simulated with the Universal Soil Loss Equation and the 1997 NRI data base.

The SPARROW module generates ex ante forecasts of the impacts land use changes have on water quality and is fine tuned for the Southeast. While the geographic resolution is flexible and can be expanded to model all 48 contiguous states, this has not been attempted. Input from the deterministic models (POLYSYS) provides data for the SPARROW analysis. The approach we use is entirely general. The SPARROW model has been calibrated to analyze changes in water quality as determined by land use driven by demand for cellulosic bioenergy in the Southeast.

Economic/Social Sustainability – The IO analysis provides estimates of output, employment and income multipliers, which measure the response of the economy to a change in demand or production[9, 22]. The economic multipliers measure the indirect and induced effects of a change in final demand (direct effects) for a particular industry (for example, the introduction of biorefineries and preprocessing facilities in a region). The indirect effects are the secondary effects or production changes when input demands change due to the impact of the directly-affected industry (for example, construction sector, agriculture producers, and transportation sectors). The induced effects represent the response by all local industries caused by changes in expenditures by households and inter-institutional transfers generated from the direct and indirect effects of the change in final demand. Projections of changes in jobs (job creation), economic activity, The FT-SPK and ATJ-SPK multipliers have been estimated for the entire 48 contiguous states and maps developed that will allow estimation of the economic impacts of the direct investment and operating transactions to be reflected in the economic impacts of a given area within the country. The model regions are the 187 Bureau of Economic Analysis (BEA) regions in the country. This was completed and information available for Total Industry Output, Value Added, and Employment.

Research Approach

Develop impact analysis for economic and environmental parameters.

IO Analysis

For the ASCENT TEA's developed by WSU, estimate the impacts for Total Industry Output, Value Added, and Employment. Using the Bureau of Economic Analysis (BEA) regions, develop a spatial surface of the multipliers for three indicator for both investment (one time) impacts and annual operating impacts. These impacts will be developed for the conversion facility, feedstocks, land use change, proprietor income and transportation,

Environmental Parameters

Access database is developed with soil characteristics and climate characteristics defined (RKLS factors in the Universal Soil Loss Equation). Soils were identified for crop land, CRP land, and pasture land for each agricultural Statistical District in the U. S using the 1997 NRI. A C factor by crop was estimated from the same dataset for conventional, reduced, and no Tillage practices. The P factor was assumed to equal 1. For any new crop, a C factor will need to be defined. Based on

information from the IBSS project, a C factor of 0.04 is used for switchgrass. Note: Schwartz found a much smaller C factor in his research.

C factors for cover crops are not readily available so some assumptions will be required. A C factor for a corn Soybean rotation ranges from 0.1 to 0.45 depending on tillage and cover. With winter cover this range should be lower than 0.1.

Work with SPARROW has not been undertaken at this point in time. It is ready for use for the Southeast region, but to this point we have been conducting national studies.

Carbon emissions information is needed from MIT. This will be pursued this year. However, we have carbon emissions coefficients in POLYSYS and those are available to indicate percent changes as a result of changes in land use as well as input application.

Milestone(s)

1. Completed conversion facility economic impact analysis for FT and ATJ – SPK technologies. See Figure 4.
2. Developed ACCESS data base for Soil Erosion Estimation.

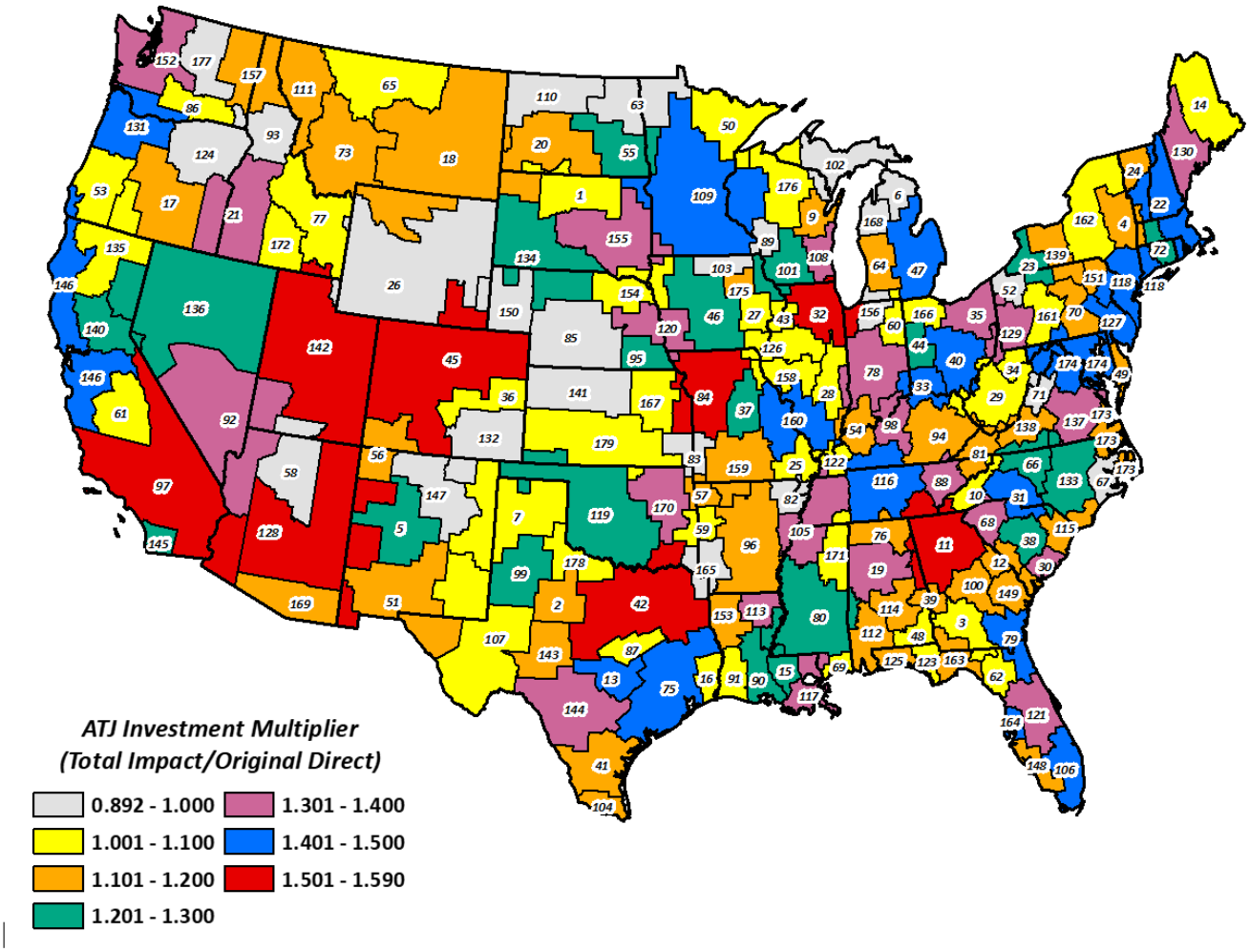

Figure 4. Projected ATJ Investment Total Industry Output Multiplier

Major Accomplishments
Plant run

Publications
None

Outreach Efforts
None

Awards
None

Student Involvement
None

Plans for Next Period
Develop impact analysis for economic and environmental parameters.

Task #4: Biorefinery Infrastructure and Siting (Supporting Role)
Washington State University

Objective(s)
The University of Tennessee team will play a supporting role in this task. Several models are available to contribute to the effort, including: 1) BioSAT (currently available for the 33 Eastern states), 2) BioFLAME (we hope to expand its geographic scope from its current southeast U.S. regional focus to the contiguous 48 states).

Research Approach
Provide feedstock information (location, price, quantity) to ASCENT Database
Contact WSU for ASCENT conversion technologies
Pennycress feedstock information provided to VOLPE and the BOX

Milestone(s)
WSU provided ATJ and FT – SPK TEAs for economic indicator development
Economic indicators are developed for those two technologies.

Major Accomplishments
None

Publications
None

Outreach Efforts
None

Awards
None

Student Involvement
None

Plans for Next Period
None

Project 001(F) Alternative Jet Fuel Supply Chain Analysis

Massachusetts Institute of Technology

Project Lead Investigator

PI: Prof. Steven Barrett
Raymond L. Bisplinghoff Professor of Aeronautics and Astronautics
Director, Laboratory for Aviation and the Environment
Massachusetts Institute of Technology
77 Massachusetts Ave, Building 33-322, Cambridge, MA 02139
+1 (617) 452-2550
sbarrett@mit.edu

Co-PI: Dr. Raymond L. Speth
Research Scientist
Associate Director, Laboratory for Aviation and the Environment
Massachusetts Institute of Technology
77 Massachusetts Ave, Building 33-322, Cambridge, MA 02139
+1 (617) 253-1516
speth@mit.edu

University Participants

Massachusetts Institute of Technology

- P.I.(s): Steven R.H. Barrett, Professor
- FAA Award Number: 13-C-AJFE-MIT, Amendment Nos. 003, 012, 016, 028, and 033
- Period of Performance: [August 1, 2014 to August 31, 2018]
- Tasks (note that the tasks listed here are relevant only to the reporting period, 10/01/2016 – 09/31/2017):
    1. LCA methodology development and default core LCA emissions value calculation for use under CORSIA
    2. Regionalized assessment of AJF from MSW production technologies
    3. Assessment of long term potential for AJF production in the US
    4. Time- and path-dependence of AJF technologies, including the effects of learning-by-doing on production costs and environmental performance
    5. Assessment of the impact of policies on the economic viability of AJF in the context of AFTF
    6. Additional support of FAA in the context of AFTF
    7. Collaborate with ASCENT 21 to capture non-CO_2 lifecycle emissions in APMT-IC
    8. Collaborate with WSU to facilitate development of Aspen HEFA model

Hasselt University (sub-award from MIT)

- P.I.(s): Steven R.H. Barrett, Professor
- Period of Performance: [August 1, 2014 to August 31, 2018]
- Tasks (note that the tasks listed here are relevant only to the reporting period, 10/01/2016 – 09/31/2017):
    1. LCA methodology development and default core LCA emissions value calculation for use under CORSIA
    2. Regionalized assessment of AJF from MSW production technologies
    3. Assessment of the impact of policies on the economic viability of AJF in the context of AFTF
    4. Additional support of FAA in the context of AFTF

Project Funding Level

$1,660,000 FAA funding and $1,660,000 matching funds. Sources of match are approximately $296,000 from MIT, plus 3rd party in-kind contributions of $326,000 from Byogy Renewables, Inc. and $1,038,000 from Oliver Wyman Group.

Investigation Team

Principal Investigator: Prof. Steven Barrett (MIT)
Co-Principal Investigator: Dr. Raymond Speth (MIT)
Co-Investigators: Dr. Mark Staples, Dr. Florian Allroggen (MIT)
Graduate Research Assistants: Timothy Galligan, Cassandra Rosen, Paula do Vale Pereira, Juju Wang (MIT)

The research will partly be conducted through a sub-award with Hasselt University (Belgium), led by Prof. Robert Malina, and Hasselt University post-doctoral researchers Marieke Franck and Hakan Olcay.

Project Overview

The overall objectives of ASCENT Project 1 for the reporting period October 1, 2016 to September 30, 2017 are to derive information on regional supply chains to create scenarios for future alternative jet fuel (AJF) production, to identify the key supply chain-related obstacles that must be overcome for commercial scale production of AJF in the near term, and to achieve large-scale replacement of conventional jet fuel with AJF in the longer term.

Following these overall objectives, MIT's work under ASCENT Project 1 during AY 2016/2017 (from 09/01/2016 to 08/31/2017), as defined in the Grant Proposal Narrative for that period, was focused on: 1) supporting US participation in the International Civil Aviation Organization Committee for Aviation Environmental Protection Alternative Fuels Task Force (ICAO CAEP AFTF) to develop a methodology for appropriate accounting of AJF life cycle greenhouse gas (GHG) emissions under the Carbon Offsetting and Reduction Scheme for International Aviation (CORSIA); 2) to support FAA assessment of policy options for AJF in the context of AFTF; 3) build upon and extend previous work to estimate the economic production costs and life cycle GHG benefits of AJF production from MSW; 4) assess the long term potential for AJF production in the US; 5) and explore the time- and path-dependent characteristics of AJF technologies, including the effects of learning-by-doing on production costs and environmental performance.

MIT's work under ASCENT 1 during AY 2017/2018 (from 09/01/2017 to 08/31/2018), as defined in the Grant Proposal Narrative for that period, is focused on: 1) supporting US participation in ICAO CAEP AFTF by applying the developed LCA methodology to calculate default core LCA GHG emissions values for use under CORSIA; 2) support FAA work to calculate induced land use change (ILUC) emissions of AJF and assess sustainability certification schemes for potential inclusion under CORSIA; 3) quantify and assess the impact of various policy options on the financial viability of AJF to provide guidance to States that are party to CORSIA; 4) collaborate with ASCENT Project 21 to capture the climate impacts of non-CO_2 lifecycle emission from petroleum jet fuels and AJF in the Aviation environmental Portfolio Management Tool - Impacts Climate (APMT-IC); 5) collaborate with Washington State University (WSU) to facilitate development of an Aspen model of the hydroprocessed esters and fatty acids (HEFA) fuel production process; 6) and to provide additional (including in-person) support to FAA for decision-making in the context of AFTF.

In order to capture work that occurred during the reporting period (from 10/01/2016 to 09/30/2017) and overlaps with both funding periods, MIT's work under ASCENT Project 1 is described here under the following eight task categories:

1. AY 2016/2017 Task 1 & AY 2017/2018 Task 1 – LCA methodology development and default core LCA emissions value calculation for use under CORSIA
2. AY 2016/2017 Task 3 – Regionalized assessment of AJF from MSW production technologies
3. AY 2016/2017 Task 4 – Assessment of long term potential for AJF production in the US
4. AY 2016/2017 Task 5 – Time- and path-dependence of AJF technologies, including the effects of learning-by-doing on production costs and environmental performance
5. AY 2016/2017 Task 2 & AY 2017/2018 Task 3 – Assessment of the impact of policies on the economic viability of AJF in the context of AFTF
6. AY 2017/2018 Tasks 2 & 6 – Additional support of FAA in the context of AFTF
7. AY 2017/2018 Task 4 – Collaborate with ASCENT 21 to capture non-CO_2 lifecycle emissions in APMT-IC

8. AY 2017/2018 Task 5 - Collaborate with WSU to facilitate development of Aspen HEFA model

Because 11 of the 12 months of the reporting period correspond to AY 2016/2017, the bulk of this annual report focuses on work accomplished during that period of time. The plan to accomplish the remaining tasks under ASCENT 1 for AY 2017/2018 is also summarized.

Task #1: LCA Methodology Development and Default Core LCA Emissions Value Calculation for Use under CORSIA

Massachusetts Institute of Technology

Objective(s)

The overall objective of this task is to provide support to the FAA for its engagement with ICAO CAEP AFTF, specifically on the development of a methodology for appropriate accounting of AJF lifecycle GHG emissions under CORSIA, and applying the method to calculate AJF default core LCA emissions values for use under CORSIA.

Research Approach

During this reporting period, significant progress has been made on the work of the core LCA Task Group of AFTF. The MIT ASCENT Project 1 team has been key to this progress in terms of development of the methodology to calculated LCA values, and the application of the method been instrumental in that work. These two task items are described below.

Core LCA Methodology Development

Guidance document

In preparation for the AFTF/2 meeting in October 2016, the MIT ASCENT Project 1 team prepared a guidance document. The purpose of this document was to summarize the agreed-upon core LCA methodology of CORSIA for those wishing to participate in the calculation and submission of default values to AFTF. Although the LCA methodology had already been documented in a number of information papers (IPs), these documents could not be distributed beyond technical experts nominated to AFTF. In addition, the guidance document defines the relevance, adequacy, quality, transparency and accessibility requirements of LCA data submitted to AFTF, in order for it to be considered in the calculation of core LCA values.

At the AFTF/2 meeting, feedback on this document was elicited from AFTF, and the feedback was incorporated to generate a final draft of the guidance document following the meeting. Coming to agreement on the guidance document was a key step towards calculating default core LCA values for use in CORSIA, as it defined the rules by which the analysis would be carried out.

Geographical aggregation study

During AY 2016/2017, the MIT ASCENT Project 1 team carried out an analysis to quantify the sensitivity of core LCA results to regional specificity, in order to inform the level of geographical aggregation to which default LCA values should be calculated.

The sensitivity analysis of LCA results to geographic variation was carried out by altering regionally specific parameters. The starting point for calculations were USA default values in GREET. This USA-specific data was then replaced with parameters relevant for different geographic regions, to generate LCA results for the same pathway in different world regions, and compared to each other. Data for different regions were collected from publically available and region-specific models, government documents, and peer-reviewed literature.

The parameters modified within each pathway varied based on the feedstock and conversion technology of interest. However, generally speaking, the primary drivers of emissions were identified to be agricultural productivity, process efficiencies, and the emission factors associated with utility inputs, as documented in CAEP/11-AFTF/01-IP/7. The parameters affecting the agricultural productivity include crop yield, nutrient application rates, and farming energy demand. Process efficiency includes both pre-processing of feedstock and fuel production process. Emissions factors were relevant for inputs such as electricity, hydrogen, and natural gas.

Several conclusions were drawn from the regional sensitivity analyses. First, regional variation was shown to have a relatively minor impact on LCA emissions within each specific pathway. For waste HEFA pathways, where no emissions are associated with feedstock production, the regional differences resulted in a total range of variability in LCA emissions of less than 1.2 gCO_2e/MJ. For oil crop HEFA pathways, LCA emissions varied less than 4.7 gCO_2e/MJ due to regional-specificity. The geographic variation in the LCA results for oil crop HEFA pathways showed up primarily in the feedstock production step however, because emissions from feedstock-to-fuel conversion dominate overall emissions and are relatively constant between pathways, little geographic variation was observed in the overall LCA emissions. For the FT pathways, where electricity and heat demand is met within the process through co-generation, regional-specificity resulted in variability of LCA emission of less than 3.6 gCO_2e/MJ. Compared to the 89 gCO_2e/MJ baseline for petroleum jet fuel, the sensitivity to regional variation observed for the HEFA and FT pathways was relatively small. These results are shown in Figure 1.

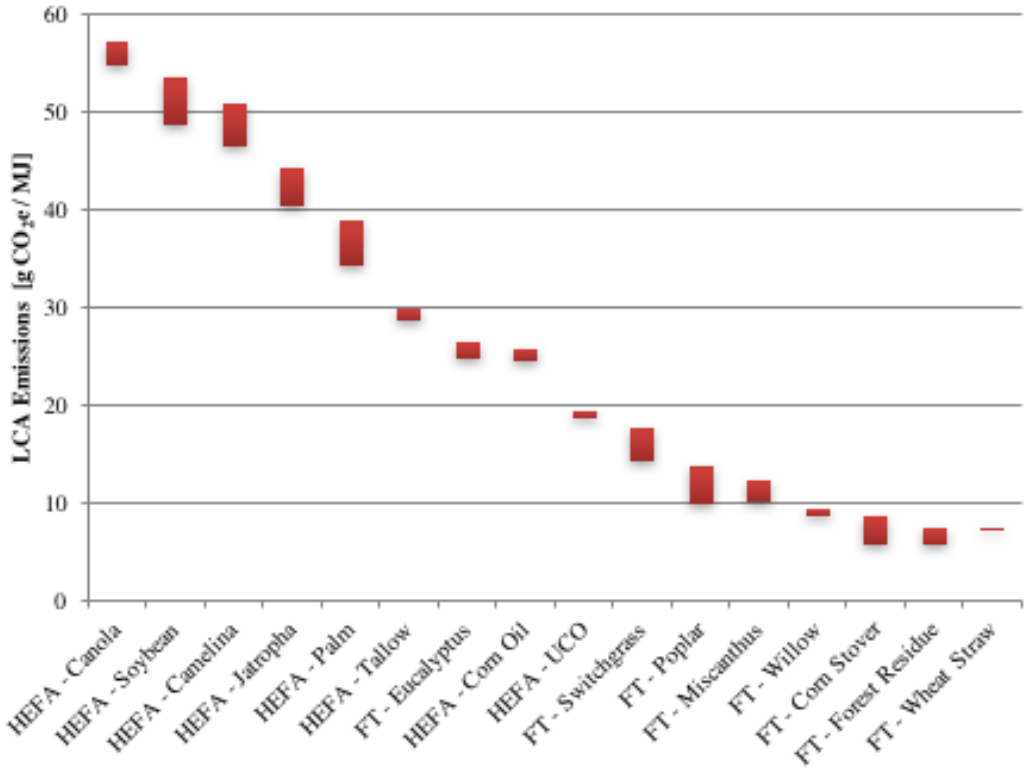

Figure 1: LCA emissions of HEFA and FT pathways. The whiskers indicate variability due to regional specificity for each feedstock-to-fuel pathway.

One the basis of this analysis, it was determined by AFTF that a single global value would be calculated for the default core LCA value of different feedstock-to-fuel pathways.

Calculation of Default Core LCA Emissions Values

Based on the agreed core LCA methodology, and the use of a single global value for default core LCA emissions of different feedstock-to-fuel pathways, significant progress was made during AY 2016/2017 on the calculation of default LCA values for different AJF pathways under CORSIA.

In advance of the AFTF/4 meeting in June 2017, the Core LCA Task Group carried out analysis according to the following agreed upon principles:

- Core default LCA values are calculated at a global level of resolution
- A pathway is defined as a feedstock and conversion technology pairing for which emissions vary by <10% of the conventional jet fuel baseline (8.9 gCO_2e/MJ)

- Default values are calculated as the mid-point of the range of results for a given pathway

Under the leadership of the MIT ASCENT Project 1 team, a number of institutions contributed to the work on the Task Group on this analysis, including the European Union Joint Research Centre, Argonne National Laboratory, and the University of Toronto. Analysis efforts focused first on waste and residue pathways, because these do not require ILUC values to be completed and included in the Standards and Recommended Practices (SARP) document. Institutions volunteered to act as lead and verifying analysts on the identified waste and residue pathways, as indicated in Table 1.

Table 1: List of first priority feedstock-to-fuel pathways for development of core LCA default values and responsible AFTF member organizations

Technology	Feedstock	Lead	Verifier
FT	Herbaceous energy crops	MIT/JRC	ANL
	Short rotation wood crops		
	Agricultural residues		
	Forest residues		
	MSW	MIT	
HEFA	Tallow	MIT/JRC	ANL
	UCO		
	PFAD	ANL	U Toronto
	Corn oil		
	Tall oil	JRC	ANL
ATJ	Agricultural residues	MIT	JRC
	Forest residues		

Two models were used for LCA calculations. The GREET® (the Greenhouse gasses, Regulated Emissions, and Energy use in Transportation) (Argonne National Laboratory, 2015) model has been used for the analyses by ANL, MIT and University of Toronto. GREET is a peer-reviewed, publicly available, and editable software. JRC used the E3 Database model for their calculations (Ludwig-Bolkow Systemtechnik GMBH, 2006). Over the course of the analysis performed for AFTF, the original database was reviewed and updated to respond to AFTF-specific requirements. Lifecycle inventory datasets for the various AJF pathways were inputs for these LCA models, and were put together collaboratively based on information from the different experts within the Modelling Subgroup. This data is documented in detail in CAEP/11-AFTF/4-IP/4. The functional unit was defined as one mega joule (MJ) of delivered jet fuel energy (lower heating value), and the LCA results are presented in terms of the amount of GHG emissions for each functional unit (gCO_2e/MJ).

The process of calculating the default core LCA values proceeded as follows. Immediately following the AFTF/3 meeting in February 2017, the lead institutions started their calculations. In March 2017, the verifying institutions reviewed the calculations of the lead organizations. In April 2017, discrepancies between lead and verifying calculations were discussed and reconciled by the Core LCA Modelling Subgroup. The results of the analysis are summarized in Table 2, which are the default core LCA values agreed to by AFTF and submitted to Steering Group for approval in September 2017.

Table 2: Default core LCA values for selected AJF pathways [gCO2e/MJ]

Technology	Feedstock	Sub-feedstock type		Data source	Model	Data points	Mid-point value
FT	Herbaceous energy crops	Switchgrass		MIT	GREET	12.7	**10.4**
				JRC	GREET	12.7	
				JRC	E3	11.3	
		Miscanthus		MIT	GREET	10.7	
				JRC	GREET	8.0	
	Short rotation woody crops	Poplar		MIT	GREET	9.9	**12.2**
				JRC	GREET	13.0	
				JRC	E3	16.5	
		Willow		MIT	GREET	7.8	
				JRC	GREET	9.7	
		Eucalyptus		MIT/ANL	GREET	9.1	
				JRC	E3	16.6	
	Agricultural residues	Corn stover (without nutrient replacement)		MIT	GREET	6.5	**7.7**
				JRC	GREET	5.4	
				JRC	E3	9.7	
		Wheat straw (without nutrient replacement)		MIT	GREET	6.6	
				JRC	GREET	10.0	
				JRC	E3	5.5	
	Forest residues			MIT	GREET	6.1	**8.3**
				JRC	GREET	7.1	
				JRC	E3	10.5	
	MSW	Non-biogenic C content	NBC = 0%	MIT	GREET data implemented in Suresh (2016) model	5.2	**5.2**
			NBC > 0%			NBC*170.5+5.2	**NBC*170.5+5.2**
HEFA	Tallow	Boundary starts at tallow rendering		MIT	GREET	25.3	**22.5**
				JRC	E3	19.8	
	UCO			MIT	GREET	14.8	**13.9**
				JRC	E3	13.0	
	PFAD	Boundary starts at PFAD production		ANL	GREET	24.3	**20.7**
				JRC	GREET	21.8	
				JRC/ANL	E3/GREET	17.0	
	Corn oil	Boundary starts at corn oil production		ANL	GREET	17.5	**17.2**
				JRC	GREET	16.8	
ATJ	Agricultural residues	Corn stover (without nutrient replacement)		MIT	GREET	31.9	**29.3**
				JRC	E3	25.9	
				JRC	GREET	30.0	
	Forest Residues			MIT	GREET	24.7	**23.8**
				JRC	E3	22.8	

Milestone(s)

The work described above on this task represents the achievement of MS 1, 2 and 3 as defined in the AY 2016/2017 Grant Proposal. The revised guidance document on calculation of core LCA values for AJF under CORSIA was submitted to AFTF, and the status and progress on core LCA default value calculations was presented to AFTF at meetings in October 2016, February 2017, and June 2017.

Major Accomplishments

The major accomplishments during this period of performance was the submission of a finalized guidance document to AFTF, outlining the methodology for the calculation of core LCA values under CORSIA. In addition, as of June 2017, the MIT-led core LCA Task Group had agreed upon core LCA values for 11 feedstock-to-fuel AJF production pathways. This progress will enable the inclusion and use of these fuels as soon as CORSIA goes into effect.

Publications

Peer reviewed publications

Staples, M.D., R. Malina, P. Suresh, J.I. Hileman, S.R.H. Barrett (*in revision*) "Aviation CO_2 emission reductions from the use of alternative jet fuels." *Energy Policy*.

Written reports

CAEP/11-AFTF/4-IP/04, Calculation of core default LCA values for selected pathways under CORSIA, presented at AFTF/4, June 2017, Montreal, Canada

CAEP/11-AFTF/4-WP/02, Progress update on core LCA task, presented at AFTF/4, June 2017 Montreal, Canada.

CAEP/11-AFTF/3-IP/02, Core LCA Task Group – study of pathway aggregation, February 2017, Montreal, Canada.

CAEP/11-AFTF/3-WP/02, Progress update on core LCA task group, February 2017, Montreal, Canada.

CAEP/11-AFTF/2-IP/04, Core LCA Task Group – study of pathway aggregation, October 2016 Montreal, Canada.

CAEP/11-AFTF/2-WP/02, Report on Core LCA Task, October 2016, Montreal, Canada.

CAEP/11-AFTF/2-IP/03, Guidance Document for Calculation and Submission of Alternative Jet Fuel Lifecycle Analysis Data for Default Values under the Global Market-based Measure, October, 2016, Montreal, Canada.

Outreach Efforts

Progress on these tasks were communicated during weekly briefing calls with the FAA and other US delegation members to AFTF, numerous AFTF teleconferences between in-person meetings, as well as at in-person meetings of AFTF in October 2016, February 2017, and June 2017. In addition, MIT presented this work to ASCENT in a poster at the April 2017 biannual meeting, and in a presentation at the September 2017 biannual meeting. MIT also briefed the entire A001 team on these topics on the January 9 and 23, 2017 ASCENT Project 1 teleconferences.

Awards

None.

Student Involvement

During the reporting period of AY 2016/2017, the majority of the analysis work was carried out by Cassandra Rosen, who finished her Masters at MIT in June 2017. Going forward, the MIT graduate students involved in this task will be Paula do Vale Pereira and Juju Wang, both funded under ASCENT Project 1.

Plans for Next Period

In the coming year, the MIT ASCENT Project 1 team will continue its work in AFTF. Default core LCA values will be calculated and proposed for additional pathways, and the results will be presented at AFTF/5 and AFTF/6 in October 2017 and April 2018, respectively. In addition, Prof. Robert Malina from Hasselt University will continue to lead the core LCA Task Group, and Dr. Mark Staples will lead a small group responsible for defining a methodology for assigning landfilling and recycling emissions credits to fuels derived from MSW feedstocks. The work of the core LCA Task Group will be summarized in a draft technical report delivered to the Steering Group 3 meeting in June 2018, and MIT will take the lead in writing this report.

References

Argonne National Laboratory. (2015) Greenhouse gases, Regulated Emissions, and Energy use in Transportation (GREET) Model. [Online]. http://greet.es.anl.gov/

Ludwig-Bolkow Systemtechnik GMBH. (2006) E3 Database. [Online]. http://www.e3database.com/

Task #3: Regionalized Assessment of AJF from MSW Production Technologies

Massachusetts Institute of Technology

Objective(s)

The objective of this task is to build upon previous work, in order to quantify the performance of AJF derived from MSW as a function of geographical location.

Research Approach

Introduction

Over the previous two years of ASCENT Project 1, a model was developed that quantifies the US-average costs of production and lifecycle GHG emissions of several pathways for MSW conversion into liquid transportation fuels, accounting for parameter uncertainty with a Monte Carlo framework (Suresh 2016). This previous analysis focused on three thermochemical conversion pathways: conventional gasification and Fischer-Tropsch (FT MD), plasma gasification and Fischer-Tropsch (Plasma FT MD) and conventional gasification, catalytic alcohol synthesis and alcohol- to-jet-upgrading (ATJ MD). These conversion pathways were chosen as they are well-suited to deal with the heterogeneous composition of MSW feedstock.

All three technology pathways demonstrate significant environmental potential, even when accounting for the foregone landfill gas recovery when discarded MSW is used as a feedstock: all of the conversion pathways considered are expected to have lower lifecycle GHG emissions compared to conventional middle distillate (MD) fuels.

The estimated probability of a positive NPV ranges from 0.1 to 14% in the Suresh (2016) analysis. Sensitivity analysis revealed that the results are sensitive to changes in the MSW composition, the waste management strategy that is displaced, plant scale and fuel yield, co-product allocation method, and transportation distance. It should be noted that these conversion pathways are not yet commercialized, which means that the calculated probability of a positive NPV may represent an underestimation of the commercialized version of the technology. Moreover, the possibility of a positive NPV when taking a societal perspective (societal opportunity cost of capital, social cost of GHG emissions) ranges between 67 to 93%. As mentioned before, this model was US-average specific and the estimated probabilities are sensitive to changes in the parameters. It is therefore highly relevant to allow for spatial variation within the US. The next section describes how the original modeling tool was adapted to reflect geographical variation within the US.

Methods

A state specific model was developed, based on the US average model, in order to estimate the GHG emissions (gCO_2eq/MJ) resulting from the production of ATJ MD from MSW as a function of lovation. Spatial variation between the US states was introduced in the following parameters: pre-processed and dried MSW characteristics (carbon content, non-biogenic portion carbon content) and GHG emissions factors (replaced waste management strategy credit, recycling credit, average grid electricity). During the analysis, it became apparent that not all states could be assessed due to lack of data. Therefore, for the states/regions/counties that do report on their MSW data, one specific state/region/county was carefully selected per NERC region.

The most recent published report on MSW from EPA dates from 2014, therefore 2014 has been chosen to serve as the base year for the analysis. When further breakdown of the data is unavailable, 2014 national averages for MSW generation[1] have been used to estimate the landfilled values (e.g. to calculate the share of PET in landfilled plastic bottles or films). When selecting a specific state/region/county to represent a certain NERC region, the following items were taken into account:

- Data from 2014 has been chosen to minimize efforts to estimate the composition for that year
- When data is unavailable for the year 2014, the most recent data to that year was selected and adjusted (this process is described below)
- Statewide data has been favored over data from any other region
- When data appeared to be unreliable or of poor quality, the state/region was not considered

As can be seen in Table 3[2], this selection method resulted in 8 states/regions/counties that were included in the analysis out of a pool of 27. The following states have been selected: Texas, Florida, Minnesota, Vermont, Michigan, Missouri, Kansas and California (indicated in bold in Table 3). As mentioned before, each of them represent a different NERC region.

Table 3. The US regions for which the MSW data has been collected. Bold rows indicate those used for this analysis.

No.	NERC Region	State	Data Year
1	**ERCOT**	**Texas**[1]	**2014**
2	**FRCC**	**Florida**	**2014**
3	MRO	Iowa	2011
4	**MRO**	**Minnesota**	**2012**
5	MRO	Nebraska[1]	2014
6	MRO	Wisconsin	2009
7	NPCC	Connecticut	2009
8	NPCC	Maine	2011
9	NPCC	Massachusetts	2013
10	NPCC	New York[1]	2013
11	**NPCC**	**Vermont**	**2012**
12	RFC	D.C.	2007
13	RFC	Delaware	2016
14	RFC	Indiana	2009
15	RFC	Maryland[1]	2012
16	**RFC**	**Michigan**	**2014**
17	SERC	Arkansas	2010
18	SERC	Georgia	2004
19	SERC	Illinois[1]	2014
20	**SERC**	**Missouri**	**2008**
21	SERC	North Carolina[1]	2010
22	SERC	Tennessee	2005
23	**SPP**	**Kansas**	**2012**
24	**WECC**	**California**	**2014**
25	WECC	Colorado[1]	2016
26	WECC	Oregon	2010
27	WECC	Washington	2016

[1]Data available for a county, region or city.

Next, the following approach was applied to adjust MSW quantities from a different year into 2014 data, when data specific to 2014 was unavailable. The equations make use of real GDP per capita data (rGDP/c) and MSW quantities for both the state/region/county and the US.

[1] Generation data was used as it offered a more complete data breakdown than reported national landfilled values. Note that the previous MSW analysis by MIT was based on the national averages reported for the year 2013.

[2] Table 3 is based on the survey conducted in 2011 by the Earth Engineering Center (Shin, 2014) as this survey resulted in a collection of MSW characterization information from 27 U.S. regions, most of which represent states.

		Year	
		20xx	2014
Region	rGDP/c	G_{R1}	G_{R2}
	MSW Quantity	Q_{R1}	Q_{R2}
US average	rGDP/c	G_{U1}	G_{U2}
	MSW Quantity	Q_{U1}	Q_{U2}

$$\frac{R_2}{R_1} = \frac{U_2}{U_1}$$

where,

$$R_1 = \frac{Q_{R1}}{G_{R1}} \; R_2 = \frac{Q_{R2}}{G_{R2}}$$

$$U_1 = \frac{Q_{U1}}{G_{U1}} \; U_2 = \frac{Q_{U2}}{G_{U2}}$$

When data from a state is to be used to represent a NERC region (e.g, in the case of Texas), the compositions are assumed for the region that the state belongs to, and the quantities have been estimated for the state based on the relative total landfilled MSW amounts. This, however, does not affect the calculated GHG emissions results.

These categories, which represent one of the ways the EPA breaks down the MSW, are defined as follows:

- Paper and paperboard
- Glass
- Metals
- Plastics
- Rubber and leather
- Textiles
- Wood
- Other materials
- Food wastes
- Yard trimmings
- Miscellaneous inorganic wastes

These categories are further broken down as shown in Table 4. MSW characterization has been reported by the authorities in many different categories that do not necessarily line up with the ones shown in this table. Hence, a careful consideration has been taken to re-group all the data into these categories.

The reported data typically includes information about the MSW quantity generated, composted, recycled, combusted and landfilled. The reported combusted data indicates the amount of MSW that is utilized in waste-to-energy facilities. There is also a part of MSW which is used as process fuel in the recycling plants, which is included in the recycled and/or combusted MSW datasets. Therefore, these two sources of potential feedstocks could be considered unavailable for fuel production. However, to be consistent with the previous analysis by MIT on MSW, the combusted MSW data has been taken into account in this analysis as a potentially available feedstock, along with the landfilled quantities, for conversion into MD fuels. This assumption plays an important role in the calculation of the avoided landfill credits. On the other hand, any other MSW combustion process is not accounted for explicitly in the official reports, and they are assumed to have been reported as part of the landfilled data.

When composition of combusted and landfilled MSW is not provided separately (which has been the case for all the 8 states chosen here), aggregate composition has been assumed to be the same. Typically, composition data is available for the

disposed/discarded MSW, which includes the combusted (if any[3]) and landfilled quantities, along with an overall ratio defining how much is combusted and how much is landfilled. (Note that, however, even though the compositions are kept the same, as mentioned above, whether the feedstock scope is expanded to include the combusted MSW or not will still affect the GHG results through combustion and recycling credits.) When this ratio is not explicit, total combusted MSW quantities estimated for the year 2011 by Shin (2014) have been considered, which are then extrapolated to 2014 using the relations described above.

Note also that the MSW reported under construction and demolition (C&D) has been excluded from the data used for this analysis, as this was the case in the EPA reports.

[3] Some states don't have any waste-to-energy facilities, e.g. Kansas, Missouri, Texas and Vermont. Their reported disposal data then represents the landfilled quantities.

Table 4: Categories utilized to re-group reported MSW data for consistency.

Material	Breakdown level I	Breakdown level II
Paper and paperboard	Newsprint Paper Containers & Packaging	
Glass		
Metals	Ferrous (iron and steel)	Steel cans and packaging Steel ingot
	Aluminum	Aluminum cans and packaging Aluminum ingot (durable goods) Aluminum (nondurable)
	Other nonferrous	Lead Other nonferrous metals
Plastics	PET HDPE PVC LDPE/LLDPE PLA PP PS Other resins	
Rubber and leather	Rubber Leather	*Partial breakdown below**
Textiles Wood Other materials Food wastes Yard trimmings Miscellaneous inorganic wastes Mixed MSW		
*Carpet and rugs *Rubber in tires	*As a whole included in Rubber and leather* *Only rubber content is included in Rubber and leather*	

As mentioned above, the carbon footprint of electricity has also been varied throughout the NERC regions in the calculations. For this, NERC region-specific data have been extracted out of the ECOINVENT database. Avoided landfill credits and recycling credits have been calculated using EPA's WARM model for the year 2014 (v14). For comparison purposes among the NERC regions and with the US average, the calculations have been calculated for a single feedstock-to-jet fuel pathway, instead of all three: conventional gasification, catalytic alcohol synthesis and alcohol-to-jet upgrading (ATJ MD).

Results

Table 5 represents the assumed MSW composition for the 8 states/NERC regions that were selected for this report.

Table 5: Landfilled MSW characterization (tons) and combusted-to-landfilled ratio for the states/NERC regions in consideration.

	California WECC	Florida FRCC	Kansas SPP	Michigan RFC	Minnesota MRO	Missouri SERC	Texas ERCOT	Vermont NPCC
Paper and paperboard	5170	3570	1580	1620	400	850	4660	100
Glass	740	440	180	160	40	180	800	10
Metals	920	1230	220	280	80	240	880	10
Plastics	3100	1260	900	1050	300	660	2630	50
Rubber and leather	1210	120	90	680	80	20	300	10
Textiles	1190	590	190	270	70	210	590	30
Wood	510	0	40	390	90	40	310	0
Other materials	1080	120	280	300	150	220	2280	70
Food wastes	5380	1530	830	1010	300	670	5290	60
Yard trimmings	2060	1150	310	550	40	100	1350	20
Miscellaneous inorganic wastes	2460	1800	190	1160	10	190	960	10
Total	23800	11800	4800	7500	1600	3400	20100	400
Combusted-to-Landfilled	4%	30%	0%	19%	82%	0%	0%	0%

Table 6 presents the preliminary results for each NERC region compared to the US average. The calculations include a Monte Carlo analysis, therefore the results are displayed by a mean value accompanied by a percent standard deviation. Moreover, these preliminary results are displayed for two different allocation methods. Energy allocation refers to the calculations where emissions of producing all the co-products are allocated based on the relative energy content of each product. Displacement, on the other hand, refers to the system expansion technique applied for the electricity and higher alcohol co-products, where excess generated electricity is assumed to displace US average grid electricity, and higher alcohols are assumed to displace virgin higher alcohol production from fossil energy.

The results range from 12.1 to 54.6 gCO_2e/MJ for when an energy allocation is applied for all the co-products. The values that involve system expansion, on the other hand, do not differ much from these results. The fact that all the values for the NERC regions except for SERC (Missouri) have come below the US average indicates that some, if not all, of the 8 states chosen are not representative of the respective NERC region average.

Table 6. Preliminary lifecycle GHG emissions (gCO_2eq/MJ) for producing ATJ MD fuels from disposed MSW in the NERC regions. Results are provided using two different allocation methods. See text for details.

	Energy allocation		Displacement	
	Mean	**%Std. Dev.**	**Mean**	**%Std. Dev.**
California-WECC	35.2	15.3	34.4	15.3
Florida-FRCC	12.1	12.1	11.5	12.2
Kansas-SPP	42.8	10.7	41.8	10.5
Michigan-RFC	45.3	19.9	44.4	19.8
Minnesota-MRO	49.7	13.3	48.6	13.1
Missouri-SERC	54.6	11.6	53.9	11.3
Texas-ERCOT	31.9	11.5	31.1	11.5
Vermont-NPCC	23.5	10.6	22.5	10.6
US	52.8	13.3	52.0	13.1

Milestone(s)
This analysis, and it's documentation in this report, represents completion of MS 6 from the AY 2016/2017 Grant Proposal Narrative.

Major Accomplishments
This work has quantified the regionalized lifecycle GHG emissions for MSW-derived drop-in MD fuels, in 8 NERC regions around the US. The variation between the analyzed regions (e.g. Florida-FRCC at 12.1 gCO_2e/MJ vs. Missouri-SERC at 54.6 gCO_2e/MJ) demonstrates the importance of region specificity in assessing the emissions from this pathway.

Publications
None.

Outreach Efforts
None.

Awards
None.

Student Involvement
This work was carried out by Marieke Franck and Hakan Olcay, both post-doctoral researchers at Hasselt University, and was supervisor by Prof. Robert Malina of Hasselt University.

Plans for Next Period
The analysis described here represents completion of the work on this task for ASCENT Project 1.

References
Shin, D. (2014). Generation and Disposition of Municipal Solid Waste (MSW) in the United States–A National Survey. Master of Science thesis submitted to the Department of Earth and Environmental Engineering Fu Foundation School of Engineering and Applied Science, Columbia University.

Suresh, P. Environmental and economic assessment of alternative jet fuel derived from municipal solid waste. Master's Thesis submitted to the Massachusetts Institute of Technology (2016).

Task #4: Assessment of Long Term Potential for AJF Production in the US
Massachusetts Institute of Technology

Objective(s)
For AY 2016/2017 Task 4, the objective of the funded work is to assess the long-term production potential of AJF in the US. The analysis leverages the modeling framework developed for the Fuel Production Assessment carried out by MIT in the context of AFTF during CAEP/10. Estimates of GHG emissions reductions associated with different scenarios of AJF deployment are provided, with the tradeoffs between increased AJF production and increased fuel emissions quantified.

Research Approach

Introduction
Air travel accounts for approximately 3% of total GHG emissions within the United States (US), and the Federal Aviation Administration (FAA) expects continued growth at a 2.6% annual rate over the next 20 years (Federal Aviation Administration, 2015; OAR,OTAQ US EPA, n.d.). Emissions from petroleum jet fuel into the atmosphere contribute to global warming, and therefore replacement of petroleum jet fuel with AJF has been identified by the EPA as a primary area of focus for abatement of aviation GHG emissions (OA US EPA, n.d.).

This analysis aims to determine the future availability of AJF that can be produced in the United States, limited by land use constraints and the availability of wastes and residues for conversion to AJF. The inclusion of land use change (LUC) emissions into the calculation allows for accurate determination of AJF emissions. Previous work to assess the availability of AJF in the United States has focused on economic feasibility, and climate assessments have only considered the life cycle emissions of AJF, without any consideration for the emissions associated with converting land for feedstock cultivation. This analysis assesses the maximum AJF production limit not constrained by economic limitations, and quantifies the maximum climate benefits that could be achieved by total replacement of petroleum derived jet fuel with AJF.

Methods

The analysis considers a number of feedstock resource pools for conversion to AJF. AJF production levels, using three fuel conversion pathways, are quantified for three scenarios defined in the below, and the climate impacts of each scenario are assessed.

The largest potential source of AJF is the cultivation of energy crops. The FORE-SCE model results from the US Geological Survey describe land use patterns in 2050 across the US (Sohl et al., 2014). Land uses unavailable or unsuitable for energy crop cultivation, such as cropland, developed areas, and protected areas, are not considered for energy crop production. Crop specific suitability, determined by soil and climate characteristics, is available from the Global Agro-Ecological Zone (GAEZ) model from the United Nations' Food and Agriculture Organization (FAO). A lower threshold on suitability for agriculture is applied on a crop by crop basis to eliminate areas of low productivity. Crop specific yield data from the US Department of Agriculture (USDA) is extrapolated temporally to 2050, and capped by the agro-climatically attainable rain-fed yield available from the GAEZ model (USDA, n.d.). Lignocellulosic energy crop yields from literature are used, due to an absence of historical yield data (Baskaran, Jager, Schweizer, & Srinivasan, 2010; Lewandowski, Scurlock, Lindvall, & Christou, 2003). The highest producing crop is chosen at each location, with both maximum AJF and maximum transportation fuel (AJF, diesel, and naphtha) cases considered. The combination of optimal crop choices and available land quantifies potential feedstock production levels for conversion to AJF.

Agricultural residues from different crop types, as a function of yield, are also quantified as a potential feedstock for AJF production. The energy crop production levels from the previous step are used in combination with future USDA crop estimates (USDA, 2017). From the literature, a residue yield per unit of agricultural yield is found for each crop (Lal, 2005). Sustainable residue removal rates from the literature are used to determine the portion of generated residue that can be extracted for generation of AJF (Muth, Bryden, & Nelson, 2013).

Additionally, forestry and wood processing residues are a potential source of bioenergy feedstocks for AJF production. Residue fractions for harvested wood, which includes treetops and branches left behind, and processed wood products, such as the chips and dust generated in sawmills and the production of plywood, are available from the literature (Searle & Malins, 2013; Smeets & Faaij, 2007). This literature also contains the portion of residue that is recoverable from each source. Historical production data from the US Forest Service is used to estimate lumber and engineered products production (Howard, 2016). Finally, estimates of the residues diverted for char and pellets from the literature are not considered available for AJF production (McKeever, 2004).

Waste fats, oils, and greases (FOGs) include tallow from slaughtered livestock and waste grease from food production. USDA data from 2016 is used to estimate per capita livestock production in 2050 (USDA-NASS, 2017). Waste grease availability is available from the National Renewable Energy Lab (NREL), also on a per capita basis (Wiltsee, 1998). For each analysis scenario, literature estimates of annual population growth are applied to current US population to estimate the population in 2050 (Gaffin, Rosenzweig, Xing, & Yetman, 2004). From the calculated quantity of waste FOG generation, it is assumed that 100% of tallow is collected, and that 85% of waste grease is collected, based on data from the US Department of Energy (Moore & Myers, 2010). An ECOFYS consultancy fact sheet estimates the portion of collected waste FOGs in the EU diverted for feed and oleochemical products, and it is assumed that the remainder is available for conversion to AJF (Peters, Koop, & Warmerdam, 2011).

Per capita Municipal Solid Waste (MSW) estimates from the International Energy Agency (IEA) are combined with 2050 population estimates to estimate total quantity of MSW produced (IEA, 2016). Based on EPA data, the composition of MSW and landfill rate by component are determined (USEPA, 2016). The availability of MSW for conversion to AJF is quantified using component energy content from the US Energy Information Administration (EIA) (U.S. Department of Energy, 2007).

The calculated feedstock quantities are fed into either advanced fermentation (AF), Fischer-Tropsch (FT), or hydro-processed esters and fatty acids (HEFA), fuel conversion pathways. The conversion efficiencies and product slates of these conversion technologies are well characterized in the literature (Pearlson, Wollersheim, & Hileman, 2012; Staples et al., 2014; Stratton, Wong, Hileman, & Stratton, 2011; Suresh et al., 2016). Additionally, each feedstock-fuel pathway has lifecycle emissions quantified in scientific literature; for energy crop cultivation requiring a land use change (LUC), emissions factors from the Global Trade Analysis Project (GTAP) emissions factor model are used.

Results

The potential quantity of AJF production is dependent on a number of assumptions. Three scenarios are defined in Table 7, outlining the assumptions of interest, in order to capture the range of.

Table 7: Scenarios investigated for AJF production potential in the US

Scenario	Description	Technological/ economic development	Land use decision criteria	Hay/pasture land availability	Ag. residue removal rate	Agro-climatic suitability threshold
A	Highest AJF potential	SRES B1	Max. AJF	20%	50%	Moderate
B	Baseline	SRES A2	Max. Transportation Fuel	10%	30%	Moderate
C	Lowest AJF potential	SRES A1B	Max. Transportation Fuel	0%	10%	Good

For each scenario, the total AJF production potential is shown in Figure 2, broken out by fuel pathway.

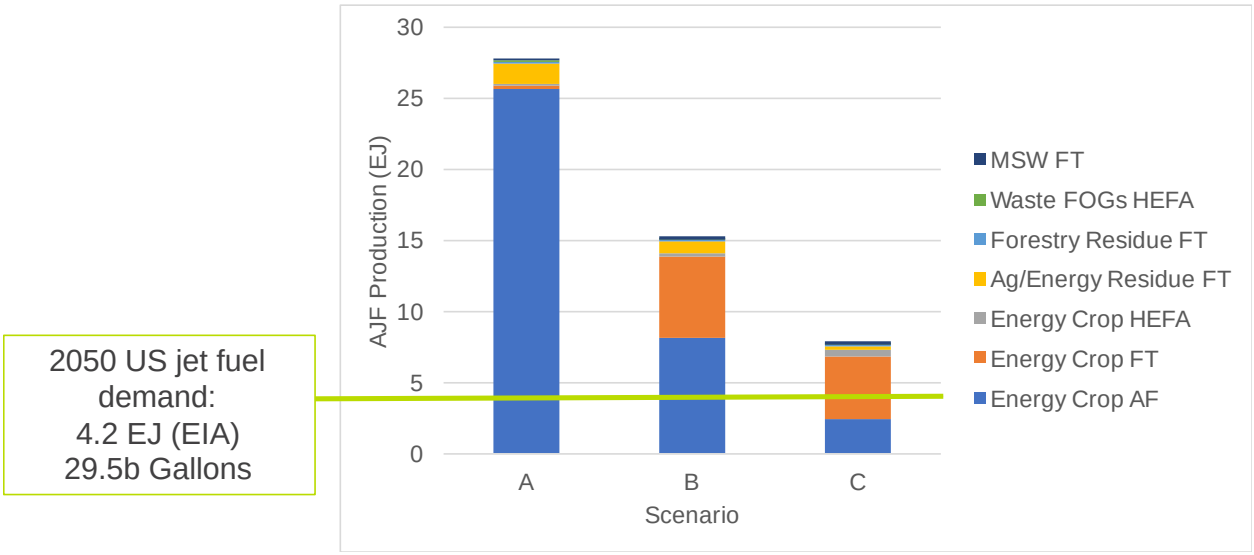

Figure 2: AJF production potential by fuel pathway for each analysis scenario

Table shows the areas required for energy crop cultivation to attain the energy crop AJF levels of Figure 1. Expected area of food crops in 2050 are provided in Table as a reference.

Table 8: Land area used for energy crop cultivation

Scenario	Energy Crop Area (10^6 ha)	Food Crop Area (10^6 ha)
A	217	130
B	188	145
C	120	150

The climate impacts of each feedstock-fuel pathway depend on lifecycle emissions and land use change emissions, for energy crops. Figure 3 presents AJF emissions on a per unit basis plotted against cumulative AJF production. These results from the baseline scenario are ordered from lowest to highest emissions; also shown are jet fuel demand and petroleum jet fuel emissions.

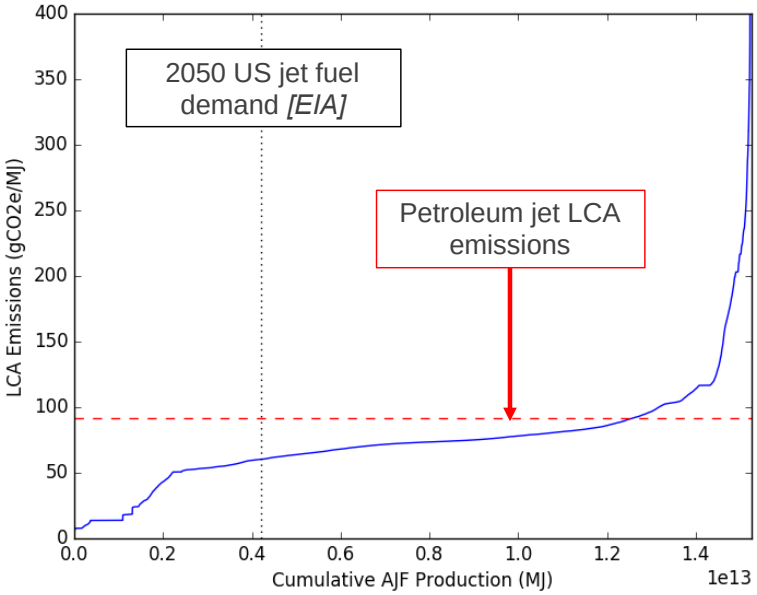

Figure 3: Fuel lifecycle emissions (including LUC emissions)

For the baseline scenario, a mixed use of all AJF feedstock-fuel pathways results in an emissions savings of 42% compared to petroleum jet fuel. Offsetting demand using the lowest emitting pathway results in the largest possible reduction of GHG emissions from jet fuel. Table presents the US aviation sector emissions savings for three levels of fuel demand replacement using the lowest emitting pathways.

Table 9: Potential aviation sector emissions savings with partial offset of petroleum fuel

2050 Jet Fuel Demand Satisfied	Potential Emissions Savings
25%	22%
50%	39%
100%	59%

AJF from wastes and residues have emissions lower than most feedstocks cultivated on converted land, due to the absence of LUC emissions. They also only require collection of existing material, rather than expanding crop area. The potential AJF production levels from wastes and residues are presented in Figure 3, broken out by feedstock.

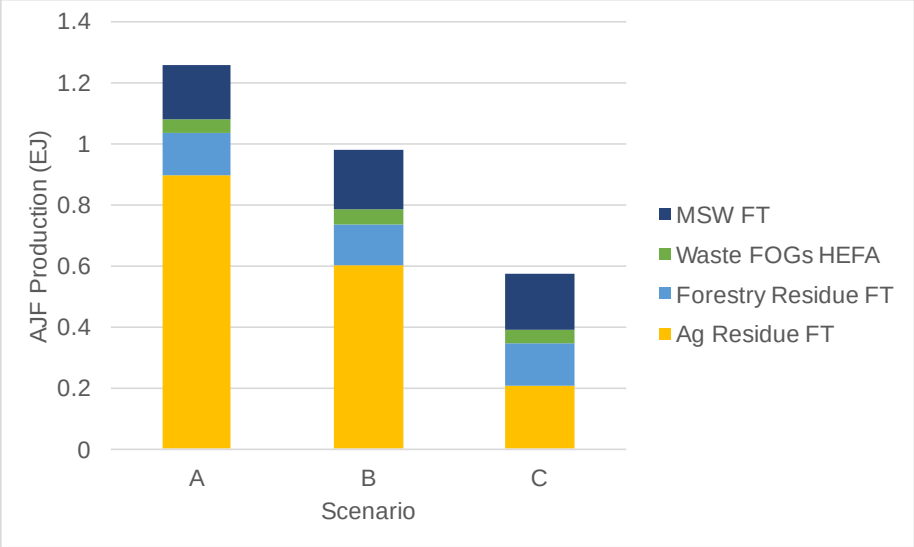

Figure 4: AJF availability from waste and residue sources for each analysis scenario

Table presents the US aviation sector emissions savings associated with complete realization of waste and residue derived AJF.

Table 10: US aviation sector emissions savings from waste and residue derived AJF

Scenario	Percent of Demand Satisfied	Sector Emissions Saved
A	30%	23%
B	23%	17%
C	14%	9%

Milestone(s)

This analysis was completed and presented to the FAA in September of 2016, and will be documented in an MIT Master's thesis to be submitted in January 2018. This represents completion of MS 4 in the AY 2016/2017 Grant Proposal Narrative.

Major Accomplishments

During this period, the production potential of AJF in 2050 in the United States has been quantified across scenarios assuming different economic, climate, and land use assumptions. The potential of AJF to reduce GHG emissions from the US aviation sector is quantified.

Publications

Peer reviewed journal publications

T. Galligan, M. Staples, R. Speth, S. Barrett. "The potential of bio- and waste- derived jet fuel to reduce US aviation sector emissions in 2050" (*in preparation*)

Written reports

T. Galligan, "The potential of bio- and waste- derived jet fuel to reduce aviation sector emissions in 2050," Master of Science thesis, Department of Aeronautics and Astronautics, Massachusetts Institute of Technology, 2017. (*in preparation*)

Outreach Efforts

Long-Term Alternative Jet Fuel Production in the United States. Presented by Mark Staples at ASCENT biannual meeting in September 2017, Alexandria, VA.

Long-Term Alternative Jet Fuel Production in the United States. Presented by Timothy Galligan on teleconference with Jim Hileman, Fabio Grandi, Dan Williams of the FAA, September 19, 2017.

Long-Term Alternative Jet Fuel Production in the United States. Presentation given on weekly ASCENT-1 teleconference, May 1, 2017.

National assessment of alternative jet fuel production potential. Poster presented at ASCENT biannual meeting in April 2017, Alexandria, VA.

Awards

None.

Student Involvement

Tim Galligan, Masters student at MIT's Department of Aeronautics and Astronautics carried out the majority of the analysis, constituting his master's thesis. He is expected to graduate in January of 2018.

Plans for Next Period

The work is being prepared for submission to a peer reviewed journal and as Tim Galligan's master's thesis. The complete work will be available on the website of the Lab for Aviation and the Environment at MIT.

References

Baskaran, L., Jager, H., Schweizer, P., & Srinivasan, R. (2010). Progress toward Evaluating the Sustainability of Switchgrass as a Bioenergy Crop using the SWAT Model. Transactions Of The ASABE, 53(5), 1547–1556. https://doi.org/10.13031/2013.34905

Federal Aviation Administration. (2015). FAA Aerospace Forecast: 2016-2036. FAA Aerospace Forecast, 3–94. https://doi.org/10.1017/CBO9781107415324.004

Gaffin, S. R., Rosenzweig, C., Xing, X., & Yetman, G. (2004). Downscaling and geo-spatial gridding of socio-economic projections from the IPCC Special Report on Emissions Scenarios (SRES). Global Environmental Change, 14(2), 105–123. https://doi.org/10.1016/j.gloenvcha.2004.02.004

Howard, J. L. (2016). U . S . Timber Production , Trade , Consumption , and Price Statistics , 1965 – 2013, (February), 1965–2013.

IEA. (2016). Annex I : Municipal solid waste potential in cities, 1–9.

Lal, R. (2005). World crop residues production and implications of its use as a biofuel. Environment International, 31(4), 575–584. https://doi.org/10.1016/j.envint.2004.09.005

Lewandowski, I., Scurlock, J. M. O., Lindvall, E., & Christou, M. (2003). The development and current status of perennial rhizomatous grasses as energy crops in the US and Europe. Biomass and Bioenergy, 25(4), 335–361. https://doi.org/10.1016/S0961-9534(03)00030-8

McKeever, D. B. (2004). Inventories of Woody Residues and Solid Wood Waste in the United States, 2002. The Ninth International Conference on Inorganic-Bonded Composite Materials Conference, 1–12. Retrieved from http://www.fpl.fs.fed.us/documnts/pdf2004/fpl_2004_mckeever002.pdf

Moore, T., & Myers, E. H. (2010). An Assessment of the Restaurant Grease Collection and Rendering Industry in South Carolina.

Muth, D. J., Bryden, K. M., & Nelson, R. G. (2013). Sustainable agricultural residue removal for bioenergy: A spatially comprehensive US national assessment. Applied Energy, 102, 403–417. https://doi.org/10.1016/j.apenergy.2012.07.028

Pearlson, M., Wollersheim, C., & Hileman, J. (2012). A techno-economic review of hydroprocessed renewable esters and fatty acids for jet fuel production. Biofuels, Bioproducts and Biorefining, 6(3), 89–96. https://doi.org/10.1002/bbb.1378

Peters, D., Koop, K., & Warmerdam, J. (2011). Info sheet 10 : Animal fats. Retrieved from http://www.dekra-certification.com/en/c/document_library/get_file?uuid=1d9c4007-1551-4329-a288-98601ac43e32&groupId=3762595

Searle, S., & Malins, C. (2013). Availability of cellulosic residues and wastes in the EU. International Council on Clean Transportation, Washington, USA, (October), 1–7. Retrieved from http://biorefiningalliance.com/wp-content/uploads/2014/02/ICCT_EUcellulosic-waste-residues_20131022.pdf

Smeets, E. M. W., & Faaij, A. P. C. (2007). Bioenergy potentials from forestry in 2050: An assessment of the drivers that determine the potentials. Climatic Change, 81(3–4), 353–390. https://doi.org/10.1007/s10584-006-9163-x

Sohl, T. L. T. T. L., Sayler, K. L. K. K. L., Bouchard, M. A. M., Reker, R. R., Friesz, A. M., Bennett, S. L., … Van Hofwegen, T. (2014). Spatially explicit modeling of 1992-2100 land cover and forest stand age for the conterminous United States. Ecological Applications, 24(5), 1015–1036. https://doi.org/10.1890/13-1245.1

Staples, M. D., Malina, R., Olcay, H., Pearlson, M. N., Hileman, J. I., Boies, A., & Barrett, S. R. H. (2014). Lifecycle greenhouse gas footprint and minimum selling price of renewable diesel and jet fuel from fermentation and advanced fermentation production technologies. Energy Environ. Sci., 7(5), 1545–1554. https://doi.org/10.1039/C3EE43655A

Stratton, R. W., Wong, H. M., Hileman, J. I., & Stratton, R. W. (2011). Quantifying Variability in Life Cycle Greenhouse Gas Inventories of Alternative Middle Distillate Transportation Fuels Citation " Quantifying Variability in Life Cycle Greenhouse Gas Inventories of Alternative Middle Distillate Transportation Fuels ." Acc. Environmental Science & Technology, 45(10), 4637–4644. Retrieved from http://search.ebscohost.com/login.aspx?direct=true&db=bth&AN=61438139&site=ehost-live

Suresh, P., Staples, M. D., Blazy, D., Pearlson, M. N., Barrett, S. R. H., & Malina, R. (2016). Environmental and economic assessment of jet fuel from municipal solid waste. Massachusetts Institute of Technology.

U.S. Department of Energy. (2007). Methodology for Allocating Municipal Solid Waste to Biogenic and Non-Biogenic Energy. Energy Information Administration: Office of Coal, Nuclear, Electric and Alternate Fuels, (May), 1–18. Retrieved from https://www.eia.gov/totalenergy/data/monthly/pdf/historical/msw.pdf

US EPA, O. (n.d.). Regulations for Greenhouse Gas Emissions from Aircraft. Retrieved from https://www.epa.gov/regulations-emissions-vehicles-and-engines/regulations-greenhouse-gas-emissions-aircraft

US EPA, O. (n.d.). Sources of Greenhouse Gas Emissions. Retrieved from https://www.epa.gov/ghgemissions/sources-greenhouse-gas-emissions

USDA. (n.d.). USDA/NASS QuickStats. Retrieved October 31, 2017, from https://quickstats.nass.usda.gov/

USDA. (2017). USDA Agricultural Projections to 2026. United States Department of Agriculture (USDA).

USDA-NASS. (2017). Livestock Slaughter. https://doi.org/0499-0544

USEPA. (2016). Advancing sustainable materials management: 2014 fact sheet. United States Environmental Protection Agency, Office of Land and Emergency Management, Washington, DC 20460, (November), 22. Retrieved from https://www.epa.gov/sites/production/files/2016-11/documents/2014_smmfactsheet_508.pdf

Wiltsee, G. (1998). Urban Waste Grease Resource Assessment. City, (November). https://doi.org/10.2172/9782

Task #5: Time- and Path-Dependent Characteristics of AJF Technologies, Including the Effects of Learning-By-Doing on Production Costs and Environmental Performance

Massachusetts Institute of Technology

Objective(s)

The purpose of this task is to carry out an assessment of AJF technologies that accounts for the time- and path-dependence of technology maturation.

Research Approach

Introduction

Anticipated growth in crude oil and conventional jet fuel prices could decrease the relative cost premium of AJF [US EIA 2015], and the societal benefits of GHG emissions mitigation are expected to grow in future years as physical and economic systems become more stressed by climate change [US IAWG 2015]. In addition, learning-by-doing, also referred to as learning curve effects, could contribute to a reduction in the production costs of AJF as experience with the technologies accumulates, as has been empirically observed in the analogous corn ethanol [Chen & Khanna 2012, Hettinga et al. 2009], sugarcane ethanol [van de Wall Bake et al 2009, Goldemberg et al. 2004] and vegetable oil biodiesel industries [Berghout 2008, Nogueira et al. 2016]. Insofar as learning-by-doing contributes to improvements in efficiency and a reduction in process input requirements, the lifecycle environmental impact of AJF fuel production may also improve over time. All of these time-dependent factors indicate that the climate damages mitigated by replacing conventional jet with AJF may exceed the additional cost premium of producing AJF at some point in the future, even if that is not the case today.

Therefore, the aim of this analysis is to test the hypothesis that the societal benefits of a policy of large-scale AJF adoption outweigh the societal costs, in terms of the climate damages and fuel production costs attributable to aviation, when changes over time are taken into account. A system dynamics approach is used to capture the time- and path-dependence of the societal climate and fuel production costs of AJF and conventional jet outlined above, as well as potential non-linearities and feedbacks associated with large-scale adoption of AJF fuels. These include the impacts of AJF feedstock demand on agricultural commodity prices and ultimately AJF production costs, the potential for CO_2 emissions from land use change (LUC), and the impact of fuel price on commercial aviation demand. The results of this cost-benefit assessment (CBA) identify the AJF production pathway characteristics that drive the balance of costs and benefits to society, in terms of climate damages and fuel production costs, attributable to aviation.

Methods

This analysis builds off of existing studies to quantify the lifecycle GHG emissions and production costs of various feedstock-to-fuel AJF technologies, both in terms of n^{th} plant performance and the potential for improvement as limited by thermodynamic and stoichiometric characteristics. The data sources for the pathways considered are summarized in Table 61. Further detail on the lifecycle emissions and production costs of these feedstock to fuel pathways assumed for n^{th} and optimal plant performance are detailed in Staples (2017).

Table 61: Feedstock-to-fuel pathway scope, data sources, and simplifying assumptions

Fuel production technology	Feedstock	TEA data source	LCA data source
HEFA	Soybean oil	Bann et al. (2017)	Stratton et al. (2011) GREET1 2015
	Rapeseed oil	Assumed equivalent to soybean oil HEFA pathway from Bann et al. (2017)*	
	Palm oil		
	Jatropha oil		
	Tallow	Bann et al. (2017)	Seber et al. (2014)
	Yellow grease		
AF	Sugarcane	Bann et al. (2017)	Staples et al. (2014) Trivedi et al. (2015)
	Corn grain		
	Herbaceous lignocellulosic crop		
	Agricultural residue	Assumed equivalent to herbaceous lignocellulosic crop AF pathway from Bann et al. (2017)*	
FT	Herbaceous lignocellulosic crop	Assumed equivalent to MSW FT pathway, plus additional feedstock cost and minus revenue from scrap, from Bann et al. (2017)*	Stratton et al. (2011) GREET1 2015
	Agricultural residue		
	Woody lignocellulosic crop		
	Forestry residue		
	MSW	Bann et al. (2017)	Suresh (2016)
FP	Agricultural residue	Bann et al. (2017)	Assumed equivalent to renewable diesel pyrolysis pathway in GREET1 2015†
	Forestry residue	Assumed equivalent to agricultural residue FP pathway from Bann et al. (2017)*	
APP	Woody lignocellulosic crop	Bann et al. (2017)	Olcay et al. (2013)
	Forestry residue		
HTL	Woody lignocellulosic crop	Bann et al. (2017)	Assumed equivalent to analogous FT pathways in GREET1 2015†
	Forestry residue		
*Denotes simplfying assumption for TEA data coverage			
†Denotes simplifying assumption for LCA data coverage			

As noted above, there may be time- and path-dependence associated with the environmental and economic performance of AJF. Therefore, this analysis uses a stochastic system dynamics model the non-linearities and feedbacks of large-scale AJF adoption, and the resulting impacts on the societal climate change and fuel production costs of commercial aviation. For example, the effect of learning-by-doing on the performance characteristics of advanced biofuel production is captured by the formulation given below, based on Vimmerstedt et al (2015) and Newes et al. (2011):

$$M = \begin{cases} 1 - (1 - M_0)\left(\frac{L^*}{E}\right)^{\left(\frac{1-PR}{ln2}\right)} & \text{for } E \geq L^* \\ M_0 & \text{otherwise} \end{cases}$$

$$L^* = \max\{L, E_0\}$$

$$m = m_{\text{early}} \cdot (1 - M) + m_{\text{minimum}} \cdot M$$

where

M	= degree of maturity, ϵ (0,1)
M_0	= initial maturity, ϵ (0,1)
L	= min. experience required for learning, units of cumulative production
L^*	= effective min. experience required for learning, units of cumulative production
E	= cumulative experience, units of cumulative production
E_O	= initial cumulative experience, units of production
PR	= progress ratio, percentage of maturity gap, (1-M), remaining after each doubling of cumulative production
m_{early}	= MSP or LCA characteristic of interest, nth plant
m_{minimum}	= MSP or LCA characteristic of interest, minimum
m	= MSP or LCA characteristic of interest

This formulation is more meaningful than the single factor learning curve, traditionally used to model learning-by-doing of energy technologies, because a single factor learning curve implicitly has an asymptote of zero. By using the above formulation, however, the parameter *m* asymptotically approaches the minimum case value, which is defined by physical or practical limits on the degree to which that characteristic may improve over time.

The degree of maturity of feedstock requirements *(f)*, non-feedstock operating costs (OpEx), non-MD fuel revenue *(R)*, and lifecycle GHG emissions, are modeled as a function of cumulative production of MD fuels. In contrast, the maturity of the capital cost is modeled as a function of the cumulative number of facilities constructed, meaning that there are two parallel learning processes modeled. The nth plant value of each MSP or LCA characteristic is assumed to correspond to initial maturity, M_0, of 50%, which is then used to calculate m_{early}. Initial cumulative experience, E_0, is assumed to be zero. A progress ratio *(PR)* of 90% is assumed based on a review of empirical studies of learning-by-doing for biofuel production, meaning that 90% of the gap between *m* and m_{minimum} remains after each doubling of cumulative production.

The minimum cumulative volume of MD fuel production required for learning-by-doing to take place is assumed to be 6.4 million metric tonnes of MD, equivalent to the annual production of approximately 30 medium-sized (5000 bpd) bio-refineries. Similarly, the minimum cumulative number of MD fuel production facilities required for learning-by-doing to begin taking place for CapEx is assumed to be 30. These values of *L* were selected for the two learning processes to reflect an established commercial drop-in MD fuel production industry, where the next unit of production (in terms of fuel volume or production facility) could be considered *"nth"*.

In addition to learning curve effects, using a system dynamics approach enabled the inclusion of non-linear and feedback mechanisms, including: the demand elasticity of the price of agricultural commodities; the impact of incremental feedstock demand on LUC emissions; and the price elasticity of demand for aviation services. These are further documented in Staples (2017).

A simplified representation of the system dynamics model, in the form of a causal loop diagram, is given in Figure 5. This figure shows two re-enforcing loops, and two balancing loops.

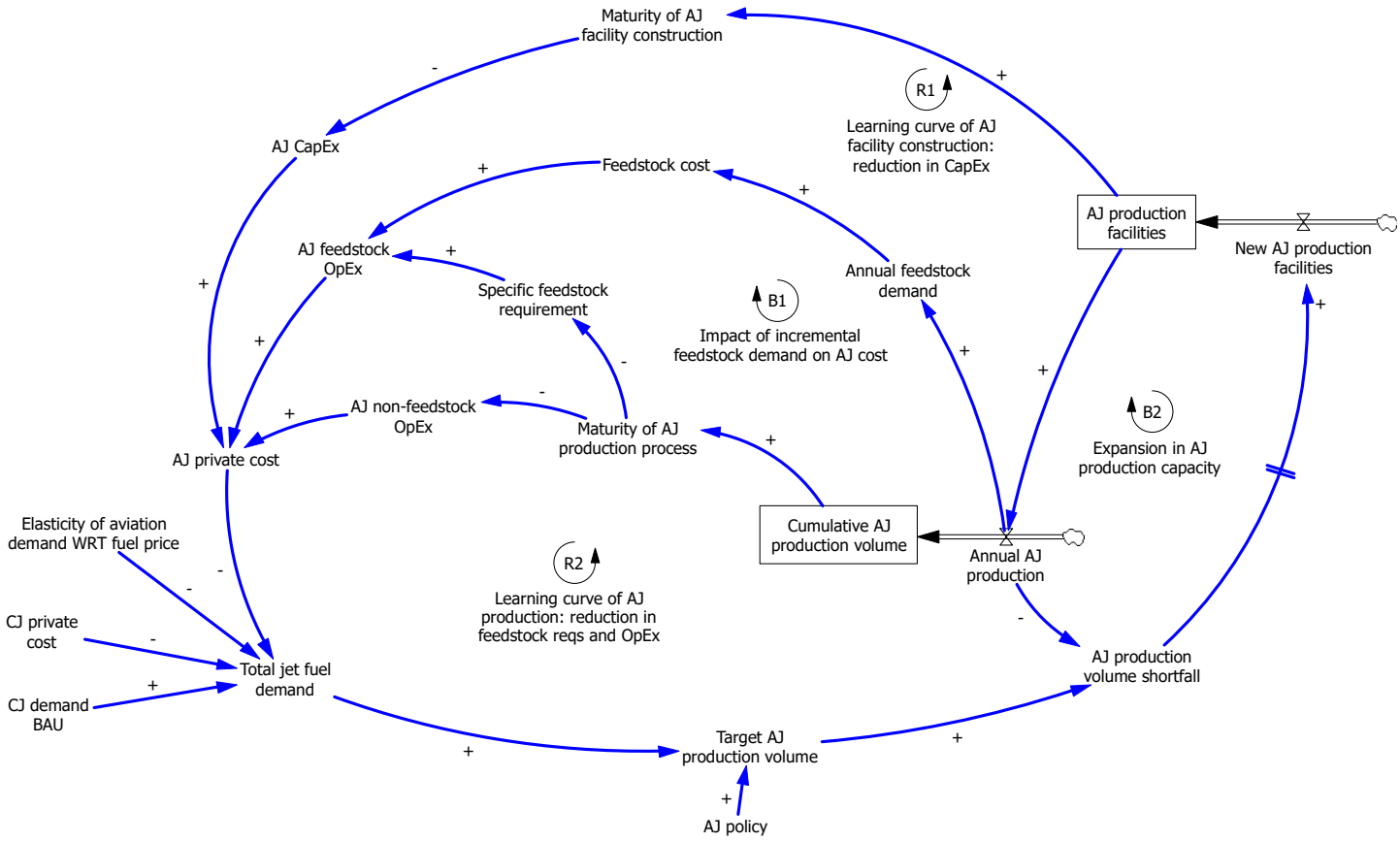

Figure 5: Simplified causal loop diagram of the system dynamics model

The resulting climate impacts of emissions from the business-as-usual and policy cases are monetized using version 23 of APMT-IC. Commodity prices and conventional jet fuel demand are modeled as Geometric Brownian Motion processes, in order to capture stochasticity in the analysis. The methods and selected analysis runs are described in greater detail in Staples (2017).

Results

The results of this analysis are given in terms of the NPV of costs to society. These results are shown for three AJF pathways of interest, and are broken out in a stepwise manner to illustrate the contribution of different impacts on the change in NPV of societal climate damages and fuel production costs of aviation, over the modeled assessment period of 2015-2050. These results are shown in Figure 6.

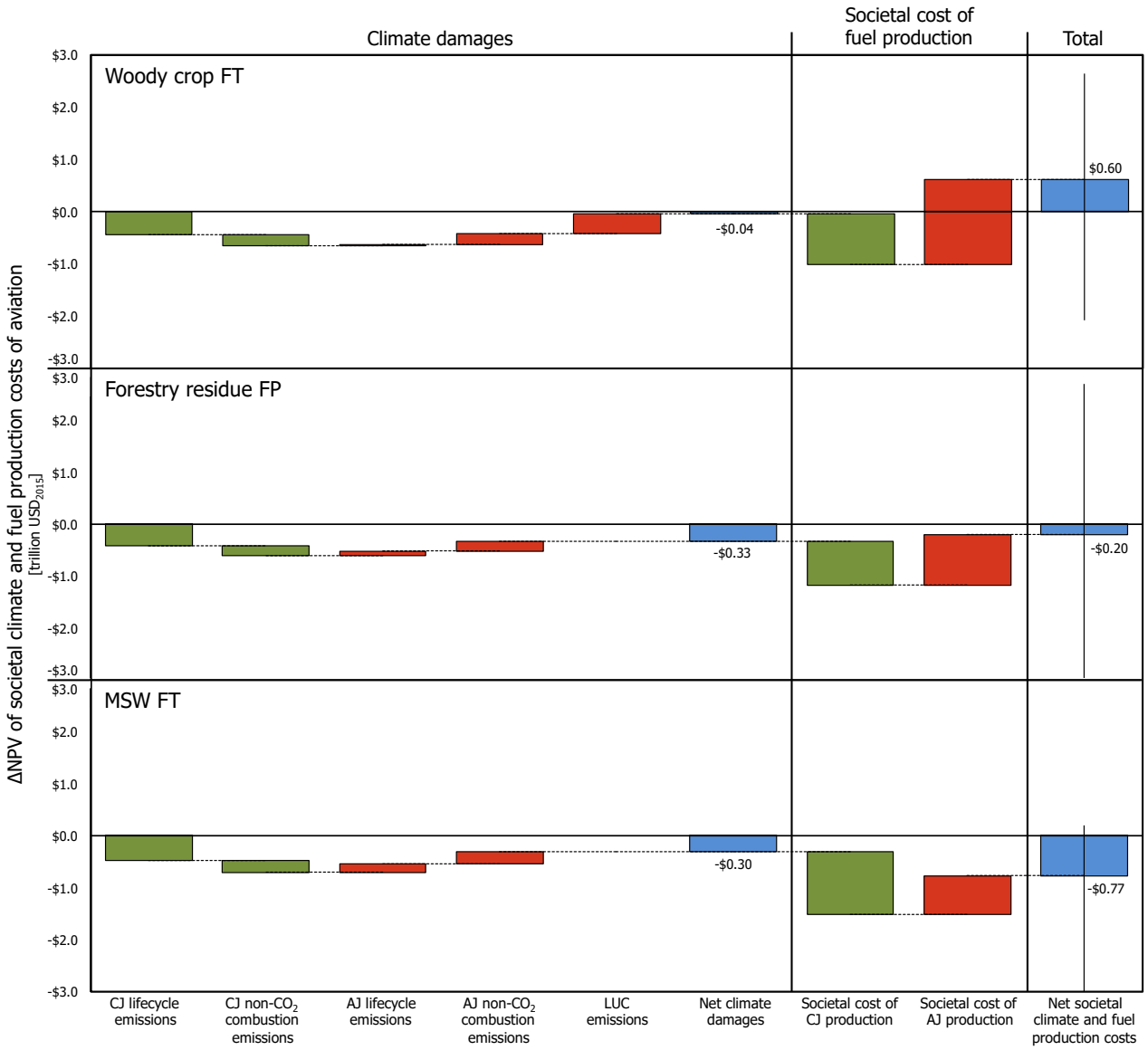

Figure 6: Change in NPV of societal climate and fuel production costs of aviation, 2015-2050. The 95% confidence interval is shown only for net results. Forestry residue FP and MSW FT 2.5th percentiles are at -3.2 and -5.6 trillion USD_{2015}, respectively, but are not shown for practical representation of the results.

Additional results are given in Staples (2017). Sensitivity analysis indicates the importance of the selected societal discount rate, the LUC emissions associated with incremental feedstock demand, and the initial feedstock price, in driving the results shown here. Therefore, a trade-space analysis of these parameters was carried out for the three pathways of interest. These results are now shown here, but are documented in Staples (2017), along with a discussion of the results.

Milestone(s)

The milestone on this task is the completion of the analysis, as described above. This work was presented in a thesis defense in December 2016, and is fully documented in an MIT PhD dissertation, available publically via MIT DSpace. Documentation of this work in the MIT dissertation constitutes completion of MS 4 from the AY 2016/2017 Grant Proposal Narrative.

Major Accomplishments

The major accomplishment on this task is completion of the analysis, and it's documentation in an accepted MIT PhD dissertation.

Publications

This work is documented in the following MIT PhD dissertation: Staples, M. Bioenergy and its use to mitigate the climate impact of aviation. PhD Dissertation submitted to the Massachusetts Institute of Technology (2017). The write-up for the dissertation is currently under revision and preparation for submission to a peer-reviewed journal.

Outreach Efforts

This work was presented at the PhD dissertation defense of Mark Staples, on December 15, 2016 at MIT. Dr. James Hileman was in attendance, as he served as a PhD committee member.

Awards

None.

Student Involvement

This work was carried out by Mark Staples, who was an MIT PhD student until January 15, 2017. As of January 16, 2017, he became research staff at MIT and continues to work on ASCENT Project 1.

Plans for Next Period

Completion of this analysis constitutes the conclusion of this task under ASCENT Project 1. The researchers who carried out this work will be moving forwards with this work to aim for peer-revied publication of the analysis.

References

Bann, S; Malina, R; Staples, M; Suresh, P; Pearlson, M; Tyner, W; Hileman, J; Barrett, S, The costs of production of alternative jet fuel: A harmonized stochastic assessment. Bioresource Technology, 227: 1790187 (2017).

Berghout, N.A. (2008). Technological learning in the German biodiesel industry. (Masters thesis submitted to Utrecht University, Netherlands) Retrieved from https://www.researchgate.net/publication/235704228_Technological_learning_in_the_German_biodiesel_industry_An_experience_curve_approach_to_quantify_reductions_in_production_costs_energy_use_and_greenhouse_gas_emissions.

Chen, X. & Khanna, M. (2012). Explaining the reductions in US corn ethanol processing costs: testing competing hypotheses. Energy Policy, 44, 153-159. DOI: 10.1016/j.enpol.2012.01.032

Goldemberg, J., Teixeira Coelho, S., Nastari, P.M. & Lucon, O. (2004). Ethanol learning curve – the Brazilian experience. Biomass and Bioenergy, 26, 301-304. DOI: 10.1016/S0961-9534(03)00125-9

Hettinga, W.G., Junginger, H.M., Dekker, S.C., Hoogwijk, M., McAloon, A.J., & Hicks, K.B. (2009). Understanding the reductions in US corn ethanol production costs: an experience curve approach. Energy Policy, 37, 190-203. DOI: 10.1016/j.enpol.2008.08.002

Newes, E., Inman, D. & Bush, B. (2011). Understanding the developing cellulosic biofuels industry through dynamic modeling, in: *Economic effects of biofuel production.* Dos Santos Bernardes, M.A. (ed.), InTech. DOI: 10.5772/17090.

Nogueira, L.A.H., Capaz, R.S., Souza, S.P. & Seabra, J.E.A. (2016). Biodiesel program in Brazil: learning curve over ten years (2005-2015). Biofuels, Bioproducts and Biorefining, 10(6), 728-737. DOI: 10.1002/bbb.1718

Olcay, H; Seber, G; Malina, R. Life Cycle Analysis for Fully-Synthetic Jet Fuel Production, MIT Support for Honeywell Continuous Lower Energy, Emissions and Noise (CLEEN) Technologies Development, Report to the FAA (2013).

Seber, G; Malina, R; Pearlson, M; Olcay, H; Hileman, J; Barrett, S. Environmental and economic assessment of producing hydroprocessed jet and diesel fuel from waste oils and tallow, Biomass and Bioenergy Vol. 67 (2014).

Staples, M. Bioenergy and its use to mitigate the climate impact of aviation. PhD Dissertation submitted to the Massachusetts Institute of Technology (2017).

Stratton, R; Wong, H; Hileman, J. Quantifying Variability in Life Cycle Greenhouse Gas Inventories of Alternative Middle Distillate Transportation Fuels, in: Environmental Science & Technology, Vol. 45 (2011).

Suresh, P. Environmental and economic assessment of alternative jet fuel derived from municipal solid waste. Masters Thesis submitted to the Massachusetts Institute of Technology (2016).

Trivedi, P; Malina, R; Barrett, S. Environmental and economic tradeoffs of using corn stover for liquid fuels and power production, in: Energy and Environmental Science, Vol. 8, pp. 1428-1437 (2015).

United States Energy Information Agency (US EIA) (2015). Annual energy outlook 2015 with projections to 2040. Retrieved from: https://www.eia.gov/forecasts/archive/aeo15/pdf/0383(2015).pdf

United States Government Interagency Working Group on Social Cost of Carbon (2015). Technical update of the social cost of carbon for regulatory impact analysis – under Executive Order 12866. Retrieved from: https://www.whitehouse.gov/sites/default/files/omb/inforeg/scc-tsd-final-july-2015.pdf

van den Wall Bake, J.D., Junginger, M., Faaij, A., Poot, T. & Walter, A. (2009). Explaining the experience curve: cost reductions of Brazilian ethanol from sugarcane. Biomass and Bioenergy, 33, 644-658. DOI: 10.1016/j.biombioe.2008.10.006

Vimmerstedt, L.J., Bush, B. & Peterson, S.O. (2015). Dynamic modeling of learning in emerging energy industries: the example of advanced biofuels in the United States. Paper presented at the *33rd International Conference of the System Dynamics Society*, Cambridge, MA, July 19-23, 2015.

Task #2 & Task #3: Assessment of the Impact of Policies on the Economic Viability of AJF in the Context of AFTF

Massachusetts Institute of Technology

Objective(s)

The purpose of this task is to evaluate policies being considered to support development of AJF production by States that are party to CORSIA, in terms of the impact of the policies of interest on the economic viability of different AJF technologies.

Research Approach

Introduction

AFTF was tasked with providing guidance to CAEP on potential policies and approaches to deploy sustainable AJF. In order to fulfill this mandate, the Policy Task Group of AFTF compiled a summary of past and existing biofuels policies. This process was intended to identify policies which have been effective in developing nascent biofuels industries in the past, and to inform the design of appropriate policy measures specific to aviation in the future. In order to take the findings of this work a step further, during AY 2017/2018 the MIT ASCENT Project 1 team will carry out stochastic techno-economic analysis (TEA) on a number of specific case studies, to provide quantitative guidance to FAA and CAEP on the impact of policies to encourage AJF production.

Background

In the past, the FAA has funded TEAs for a wide set of feedstock-to-fuel pathways to convert biomass or industrial and household wastes into AJF. The resulting literature (eg. Bann et al., 2017, Yao et al., 2017; Suresh, 2016; Pearlson et al., 2013, Seber et al., 2014; Bond et al. 2014; Staples et al. 2014) shows that AJF will remain costlier to produce than conventional jet fuel in the short- to medium term. However, a number of policy measures exist that could potentially improve the economic viability of these technologies. Such measures include, for example, loan guarantees, public offtake agreements, alternative fuel production or use mandates, production or consumption subsidies, tax breaks, carbon taxation or carbon offsetting mandates. In the US, for example, support is provided to AJF production, inter alia, through the Farm to Fly Program and its associated loan guarantees and support for alternative aviation fuel R&D and pilot plant development, the Renewable Fuels Standard, and by offtake agreements of the US military. In the EU, AJF use reduces the amount of

emission certificates an airline needs to surrender under the EU Emission Trading Scheme. For international aviation, the upcoming CORSIA regulation will provide an incentive for the use of AJF by reducing the CO_2 offsetting requirements of airlines.

To date, the monetary impact of only some of these options have been studied for a limited set of feedstock-to-fuel production pathways (Bann et al. 2017, Bittner et al. 2015). However, the available evidence points to heterogeneity in the cost-effectiveness of these policy measures. Therefore, during AY 2017/2018 the MIT ASCENT Project 1 team (in collaboration with Purdue University and Hasselt University) plans to conduct a comprehensive analysis of a wide set of policy options and feedstock-to-fuel pathways using a consistent set of assumptions. This will be done using the harmonized stochastic TEA model developed at MIT (Bann et al. 2017). The model will be augmented to account for the policy measures identified by the Policy Task Group of AFTF, and will quantify the changes in net present value (i.e. financial performance of an AJF production facility) and AJF minimum selling prices resulting from these policies. We will also assess combinations of policy measures, for example, loan guarantees coupled with offtake agreements and a carbon offsetting system. The results of this task will provide insight into the absolute and relative effectiveness of different policy measures for enhancing the economic viability of alternative aviation fuels, both in isolation and in the form of bundles of different policy options. The results of these analysis will be used to inform the work of the Policy Task Group of AFTF. AFTF will use this work to provide guidance to ICAO CAEP on policies to encourage the use of AJF in international aviation.

Milestone(s)

The MIT ASCENT Project 1 team contributed to the identification of past and existing biofuels policies by the Policy Task Group of AFTF, and has volunteered to contribute to the quantitative stochastic TEA analysis of the group. The bulk of this work will be carried out in AY 2017/2018.

Major Accomplishments

This task falls under the work plan for AY 2017/2018. Therefore, the major accomplishments for this work will occur in the next period.

Publications

None.

Outreach Efforts

This work plan was discussed with the other technical experts of AFTF during the AFTF/4 meeting in June 2017, in Montreal.

Awards

None.

Student Involvement

The MIT graduate students involved in this task will be Paula do Vale Pereira and Juju Wang, both funded under ASCENT Project 1.

Plans for Next Period

This work will be discussed during the AFTF/5 meeting in October 2017 in Brasilia. Following AFTF/5, a list of case studies of particular interest to the Policy Task Group will be proposed by MIT and discussed with the Policy Task Group. The MIT team will then use the stochastic TEA model to quantify the impacts of the relevant policies on NPV and MSP of the selected AJF technologies.

This work will be summarized in an Information Paper and a Working Paper presented to AFTF/6 in April, 2018.

References

Bann, S; Malina, R; Staples, M; Suresh, P; Pearlson, M; Tyner, W; Hileman, J; Barrett, S, The costs of production of alternative jet fuel: A harmonized stochastic assessment. Bioresource Technology, 227: 1790187 (2017).

Bittner, A, Tyner, WE., Zhao, X, Field to flight: A techno-economic analysis of the corn stover to aviation biofuels supply chain. Biofuels, Bioprod. Bioref., 9: 201–210 (2015).

Bond, J; Upadhye, A; Olcay, H; Tompsett, G; Jae, J; Xing, R; Alonso, D; Wang, D; Zhang, T; Kumar, R; Foster, A; Sen, S; Maravelias, C; Malina, R; Barrett, S; Lobo, R; Wyman, C; Dumesic, J; Huber, G. Production of renewable jet fuel range alkanes and commodity chemicals from integrated catalytic processing of biomass, In: Energy and Environmental Science, Vol. 7 (2014).

Pearlson, M; Wollersheim, C; Hileman, J. A Techno-economic Review of Hydroprocessed Renewable Esters and Fatty Acids for Jet Fuel Production, Biofuels Bioprod. Biorefining 7, 89 (2013).

Seber, G; Malina, R; Pearlson, M; Olcay, H; Hileman, J; Barrett, S. Environmental and economic assessment of producing hydroprocessed jet and diesel fuel from waste oils and tallow, Biomass and Bioenergy Vol. 67 (2014).

Staples, M; Malina, R; Olcay, H; Pearlson, M; Hileman, J; Boies, A; Barrett, S. Lifecycle Greenhouse Gas Footprint and Minimum Selling Price of Renewable Diesel and Jet Fuel from Fermentation and Advanced Fermentation Production Technologies, Energy and Environmental Science, 7, 1545 (2014).

Suresh, P. Environmental and economic assessment of alternative jet fuel derived from municipal solid waste. Master's Thesis submitted to the Massachusetts Institute of Technology (2016).

Yao, G; Staples, M. / Malina, R; Tyner, WE: Stochastic Techno-Economic Analysis of Alcohol- to-Jet Fuel Production, in: Biotechnology for Biofuels, Vol. 10, 18 (2017).

Task #2 & Task #6: Additional Support of FAA in the Context of AFTF

Massachusetts Institute of Technology

Objective(s)

The objective of this task is to provide support to the FAA in the context of AFTF beyond the major LCA and policy analysis tasks outlined above. Specifically, this task will support the work of the induced land use change (ILUC) and sustainability task groups, and provide in-person support for FAA decision-making at meetings of AFTF and CAEP.

Research Approach

ILUC Task Group

The ILUC Task Group is responsible for the calculation of ILUC emissions factors, which are added to the core LCA values. Purdue University and the University of Toronto currently lead this task within AFTF. The MIT ASCENT Project 1 team will support the work of the ILUC Task Group by: providing relevant pathway and technology-specific data (e.g. expected fuel yields, fuel product slates) and scenario assumptions (e.g. anticipated global fuel production volumes) for ILUC analysis such that the work is consistent with the work of the LCA Task Group; identifying additional pathways for which ILUC values may be required (e.g. fuels derived from valuable by-product feedstocks, such as palm fatty-acid distillates or corn oil); and contributing to discussion on comparison of ILUC results from the GTAP and GLOBIOM models.

Sustainability Task Group

In order to qualify under CORSIA, AJFs have to satisfy sustainability criteria beyond the CO_2 reductions that are captured in the LCA and ILUC emissions analyses. These criteria encompass environmental, social and economic aspects. Over the previous year, the Sustainability Task Group of AFTF developed these criteria, which were finalized and presented to ICAO steering group in September 2017 in the SARPs appendix. However, no decision has been made yet on how fuel producers and airlines can prove that their AJF adheres to these criteria. In AY 2017/18, the MIT ASCENT Project 1 team will work with the Sustainability Task Group to contribute to proposing and evaluating different options for the recognition of existing sustainability certification schemes under CORSIA, as a means to meet the sustainability criteria defined by AFTF.

In-person Support
The MIT ASCENT Project 1 team will provide in-person support for FAA decision-making for purposes of the AFTF. The principal investigator from Hasselt University will continue serve as the co-lead of the task group on core LCA emission values, and a team member from the MIT ASCENT Project 1 team will lead the modeling work of the AFTF Task Group for Core LCA. Team members will lead and take part in ICAO CAEP AFTF in-person meetings in fall 2017 and spring and summer 2018, and will participate in other in-person meetings of AFTF or the U.S. delegation, such as the ICAO Alternative Fuels Conference in Mexico in fall 2017, as requested by FAA. Furthermore, team members will participate in teleconferences, virtual meetings, and the preparation of information and working papers.

Milestone(s)
This task falls under the work plan for AY 2017/2018. Therefore, the major milestones for this work will occur in the next period.

Major Accomplishments
This task falls under the work plan for AY 2017/2018. Therefore, the major accomplishments for this work will occur in the next period.

Publications
None.

Outreach Efforts
None.

Awards
None.

Student Involvement
The MIT graduate students involved in this task will be Paula do Vale Pereira and Juju Wang, both funded under ASCENT Project 1.

Plans for Next Period
Please see the task description above under “Research Approach”.

Task #4: Collaborate With ASCENT 21 to Capture Non-CO_2 Lifecycle Emissions in APMT-IC
Massachusetts Institute of Technology

Objective(s)
The objective of this task is to collaborate with Project A021 to incorporate non-CO_2 lifecycle GHG emissions into APMT-IC, and to evaluate the impact that the choice of climate metric has on results and conclusions from APMT-IC.

Research Approach
The MIT ASCENT Project 1 team will collaborate with the Project A021 team to properly represent AJF in the APMT-IC module. AMPT-IC was developed by MIT under the Partnership for AiR Transportation Noise and Emissions Reduction (PARTNER) to quantify the environmental impacts of policies influencing aircraft operations and the resulting changes in health and welfare outcomes for climate, air quality and noise. Currently, APMT-IC represents the differences between petroleum-derived jet fuels and AJF in terms of lifecycle CO_2-equivalent emissions, where the CO_2e value of CH_4 and N_2O emissions are calculated on the basis of 100-year global warming potential (GWP) equivalents. While this approach is useful as a first-order approximation to quantify the lifecycle climate impacts of different jet fuels, the use of 100-year GWP to capture non-CO_2 emissions misrepresents the climate impacts. For instance, the atmospheric background concentrations, radiative forcing, and atmospheric lifetime of CH_4 and N_2O are fundamentally different than those of CO_2. Using an equivalency metric that

depends on an arbitrarily defined time horizon, such as the GWP-100, masks these physical differences, and that could distort the results at each step of the analysis. In order to better reflect non-CO_2 lifecycle emissions in APMT-IC, it is proposed under ASCENT Project 21 to model lifecycle CH_4 and N_2O emissions to quantify their impacts on radiative forcing.

The MIT A001 team will contribute to this task by providing lifecycle emissions inventories for petroleum and AJF, disaggregated by emissions species, to the Project A021 team. This data will be used to verify and validate the modifications made to APMT-IC. The results will be used to evaluate the impact that the choice of climate metric has on results and conclusions from APMT-IC, and to enhance the ability to assess policies influencing the use of AJF.

Milestone(s)
This task falls under the work plan for AY 2017/2018. Therefore, the major milestones for this work will occur in the next period.

Major Accomplishments
This task falls under the work plan for AY 2017/2018. Therefore, the major accomplishments for this work will occur in the next period.

Publications
None.

Outreach Efforts
None.

Awards
None.

Student Involvement
This modifications to APMT-IC will be carried out by Carla Grobler, a graduate student at MIT, who is primarily funded by Project A021. Lifecycle emissions inventories for petroleum-derived jet fuel and AJF will be provided by Paula do Vale Pereira and Juju Wang, the MIT graduate students funded under ASCENT Project 1.

Plans for Next Period
Please see the task description above under “Research Approach”.

Task #5: Collaborate With WSU to Facilitate Development of Aspen HEFA Model
Massachusetts Institute of Technology

Objective(s)
The objective of this task is to collaborate with Washington State University (WSU) ASCENT Project 1 team to facilitate development of an Aspen model of the HEFA fuel production process.

Research Approach
Under this task, the MIT ASCENT Project 1 team will facilitate development of an Aspen model of the HEFA fuel production process by the ASCENT Project 1 research team at WSU. The HEFA model developed by WSU will leverage the model described in Pearlson et al. (2013), and will contain greater fidelity on the hydro-deoxygenation, isomerization and catalytic cracking unit processes than the original analysis. The purpose of this task is to build up a modeling tool suited for use in WSU’s lipid-focused advanced supply chain deployment support project, which is Task 3.1 of the ASCENT Project 1 Regional Project Planning numbering system.

Milestone(s)
This task falls under the work plan for AY 2017/2018. Therefore, the major milestones for this work will occur in the next period.

Major Accomplishments
This task falls under the work plan for AY 2017/2018. Therefore, the major accomplishments for this work will occur in the next period.

Publications
None.

Outreach Efforts
None.

Awards
None.

Student Involvement
None.

Plans for Next Period
Please see the task description above under “Research Approach”.

Project 002 Ambient Conditions Corrections for Non-volatile PM Emissions Measurements.

Missouri University of Science and Technology, Aerodyne Research Inc., NASA, General Electric, and Honeywell.

Project Lead Investigator

Philip D. Whitefield
Professor of Chemistry and Dir. Center for Research in Energy and Environment (CREE)
Chemistry
Missouri University of Science and Technology
400 W 11th Street, Rolla, MO 65409
573-341-4420
pwhite@mst.edu

University Participants

Missouri University of Science and Technology

- Philip D. Whitefield, Professor of Chemistry and Dir. Center for Research in Energy and Environment (CREE)
- FAA Award Number: 13-C-AJFE-MST amendments: 002,003,005,008 and 010
- Period of Performance: 9/18/2014 – 12/31/2019
- Tasks:
  1. Ambient conditions corrections measurements using the NASA LDI combustor rig
  2. Ambient conditions corrections measurements using the GEAE combustor rig
  3. Engine to engine variability at Honeywell
  4. Ground-based nvPM emissions from an IAE V2527-A5 engine burning four different fuel types.

Project Funding Level

PROJECT	FUNDING	MATCHING	SOURCE
13-C-AJFE-MST-002	1,573,000.00	1,288,836.34	EMPA LETTER
		300,000.00	TRANSPORT CANADA
13-C-AJFE-MST-003	500,000.00	500,000.00	EMPA LETTER
13-C-AJFE-MST-005	500,000.00	500,000.00	EMPA LETTER
13-C-AJFE-MST-008	579,234.00	579,234.00	EMPA LETTER
13-C-AJFE-MST-010	725,500.00	725,500.00	EMPA LETTER

Investigation Team

Professor Philip Whitefield (all tasks), Dr. Prem Lobo, Research Scientist (tasks 1,2), Dr. Wenyan Liu, Research Chemist (task 4), Steven Achterberg, Research Technician (tasks 1,2,4), Max Trueblood, Research Technician (tasks 1,2,4), Dr. Richard Miake-Lye and Dr. Zenhong Yu, sub-contractors (tasks 1,2,3,4) and (tasks (1,2,4) respectively.

Project Overview

The International Civil Aviation Organization (ICAO) has approved publication of the revised ICAO Annex 16 Vol. II specifying a standardized sampling system for the measurement of non-volatile particulate matter (nvPM) from aircraft engines for use in certification. The Missouri University of Science and Technology (Missouri S&T) owns and operates the

ICAO Annex 16 Vol. II compliant, North American mobile reference system (NARS) to measure nvPM emissions from the exhaust of aircraft engines. The work under this project exploits the use of the NARS to address issues associated with ambient conditions corrections, engine to engine variability and fuel formulation sensitivity.

Task1 and Task 2
Ambient Conditions Corrections measurements. A key consideration for the development of the nvPM emissions standard is the impact of ambient condition variability on the nvPM emissions. Combustor rigs at: (1) the NASA Glenn Research Center, Cleveland, OH and (2) GEAE Cincinnati, OH, have been identified as a suitable test vehicle for these types of measurements. Since we had an imminent opportunity at NASA in the late summer of 2016 and at GEAE in March/April 2017, funds were redirected from the original Engine to Engine Variability Study to support these tests. The redirection of funds allowed us to complete both tests and provide valuable information to the ICAO/CAEP process as they develop the nvPM emissions standard.

Task 3
Additional testing has taken place at Honeywell as part of a series of measurements to acquire certification-like data on a set of engines identified by ICAO Committee on Aviation Environmental Protection Working Group 3 (Emissions Technical) Particulate Matter Task Group (CAEP/WG3/PMTG to be representative of the commercial fleet, for entry into the nvPM values database. The engine-to-engine variability of nvPM emissions data from a sample of a large number of engines is required in order to assess the characteristic variability of these engines, which is critical in establishing a regulatory limit for nvPM number- and mass-based emissions. The measurement activity in this task will be undertaken by Honeywell personnel under sub-contract to MS&T. Technical oversight will be provided by the MS&T team.

Task 4
The North American Reference System (NARS) and its ancillary equipment will be used to characterize the ground-based nvPM emissions from an IAE V2527-A5 engine burning four different fuel types. This work will be conducted as part of the NASA/DLR ND MAX campaign.

Task #1: Ambient Conditions Corrections for nvPM – NASA LDI Combustor Rig

Missouri University of Science and Technology

Objective(s)

As part of the standard setting process, corrections for measured nvPM emissions at various ambient conditions, similar to those employed for gaseous species, will need to be developed. Missouri S&T is currently working with NASA to conduct an nvPM emissions measurement campaign in NASA's LDI (Lean Direct Injection) combustor rig to acquire data that will be used to develop first order ambient conditions corrections of nvPM number- and mass-based emissions. These first order corrections will need to be validated in subsequent tests to evaluate their applicability to a range of turbofan engines. Missouri S&T will review data from this and other engines tests conducted over a wide range of ambient conditions to validate the methodology and the model developed in previous campaign with GE Aviation.

Research Approach

The system is designed to operate in parallel with existing International Civil Aviation Organization (ICAO) Annex 16 compliant combustion gas sampling systems used for emissions certification from aircraft engines captured by conventional (Annex 16) gas sampling rakes (ICAO, 2008). The certification measurements of nvPM emissions will be performed using the SAE defined nvPM sampling system.

The Missouri University of Science and Technology (Missouri S&T) owns and operates an Annex 16 compliant, North American mobile reference system to measure nvPM emissions from the exhaust of aircraft engines. The nvPM system consists of three sections – collection, transfer, and measurement – connected in series (Figure 1). A description of each section is provided below.

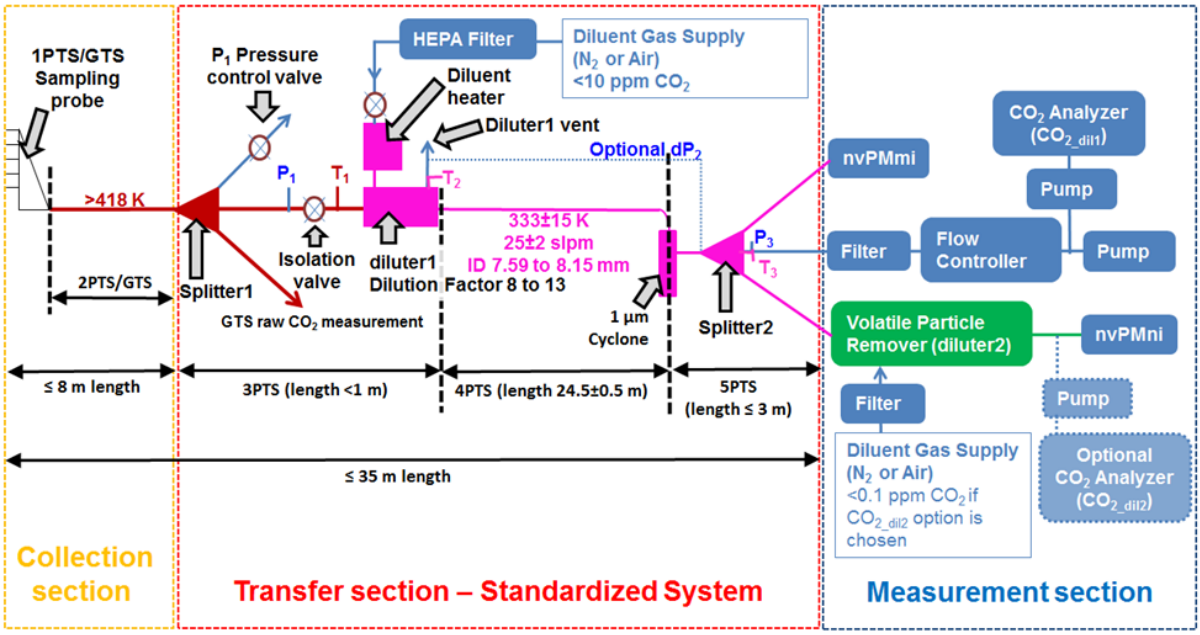

Figure 1: Components of an ICAO Annex 16 Vol.II Appendix 7 Compliant nvPM system

Collection section
The collection section consists of the probe rake system and up to 8m of stainless sample line heated to 160˚C.

Transfer section
The transfer section consists of a three way sample splitter, a PM sample eductor/dilutor, flow controllers, and sample line heater controllers The first sub-component of the transfer section is a three way sample splitter which divides the total exhaust gas sample from the rake into three flow streams. The first is the required flow of exhaust for the Annex 16 combustion gas sample. The second is the PM sample and the third is an excess flow dump line controlled with a pressure relief valve. The PM sample is diluted by a factor 8-13 with dry nitrogen (heated to 60˚C) by means of an eductor/dilutor. The diluted PM sample with a flow rate 25 ± 2 SLPM is transferred by an electrically heated, temperature controlled conductive, grounded, carbon loaded PTFE PM sample transfer line 25m in length, maintained at 60˚C to a 1µm cyclone and then a second three way splitter to direct the sample to the number and mass measurement devices in the measurement system.

Measurement section
The measurement section consists of a volatile particle remover and a particle number measurement device, a mass measurement device and a mass flow controller, pump and CO_2 detector as specified by Annex 16

As part of evaluating the methodology and the robustness of the system described in Annex 16, the North American nvPM reference system has been deployed at several OEM facilities in North America as well as the SR Technics maintenance facility in Zurich, Switzerland. These demonstration/inter-comparison studies served to provide information regarding the variability of the individual sampling and measurement systems. Additional testing at OEM facilities has also be conducted to acquire QL2 data on a set of engines identified to be representative of the commercial fleet for entry into the nvPM values database. Datasets from these initial measurement activities are being used by the ICAO Committee on Aviation Environmental Protection (CAEP) and their PM Task Group (PMTG) as they consider future aviation PM regulations. The data will be used by PMTG to develop a metric on which the regulation for nvPM emissions will be based.
In this task Missouri S&T and its sub-contractor Aerodyne Research Inc. will use the North American Reference System as described above to develop a dataset for the development of an ambient conditions corrections methodology validation. Representative data and a summary of conclusions from the study can be found in reference 1.

Ref 1 – Presentation on Project 2 at the ASCENT Advisory board Meeting in Washington DC, April 2017.

Milestone(s)

Measurement campaign completed (October 2016)
Data delivered to NASA (October 2016)
NASA/MS&T team presented results to CAEP (spring 2017)
NASA final report in preparation.

Major Accomplishments

Critical data on nvPM ambient conditions corrections was acquired using the NASA LDI combustor. These data were used to inform CAEP WG3 as it strives to establish regulatory standards for nvPM emissions from commercial transport aircraft.

Publications

None

Outreach Efforts

A summary of the findings from this task was presented at:

(1) The SAE E31 Meeting in Madrid, Spain, January 2017
(2) ASCENT Advisory Board Meeting in April 2017

Awards

None

Student Involvement

No graduate students were employed in this task however four undergraduate research assistants were employed in pre- and post-test activities including individual component testing and calibration and data reduction and interpretation.

Plans for Next Period

Additional ambient condition correction testing is anticipated during the next year. Potential test vehicles are being pursued at Pratt and Whitney, Rolls Royce and Honeywell.

Task #2: Ambient Conditions Corrections for nvPM – GE Combustor Rig

Missouri University of Science and Technology

Objective(s)

As part of the standard setting process, corrections for measured nvPM emissions at various ambient conditions, similar to those employed for gaseous species, will need to be developed. Missouri S&T is currently working with GE Aviation to conduct an nvPM emissions measurement campaign in GEAE combustor rig to acquire data that will be used to develop first order ambient conditions corrections of nvPM number- and mass-based emissions. These first order corrections will need to be validated in subsequent test to evaluate its applicability to a range of turbofan engines. Missouri S&T will review data from other engines tests conducted over a wide range of ambient conditions to validate the methodology and the model developed in previous campaign with GE Aviation.

Research Approach

ICAO has published Annex 16 Vol II Appendix 7 detailing the sampling system for the measurement of non-volatile particulate matter (nvPM) from aircraft engines. The system is designed to operate in parallel with existing International Civil Aviation Organization (ICAO) Annex 16 compliant combustion gas sampling systems used for emissions certification from aircraft engines captured by conventional (Annex 16) gas sampling rakes (ICAO, 2008). The certification measurements of nvPM emissions will be performed using the SAE defined nvPM sampling system.

The Missouri University of Science and Technology (Missouri S&T) owns and operates the Annex 16 compliant, North American mobile reference system to measure nvPM emissions from the exhaust of aircraft engines. The nvPM system

consists of three sections – collection, transfer, and measurement – connected in series (Figure 1). A description of each section is provided below.

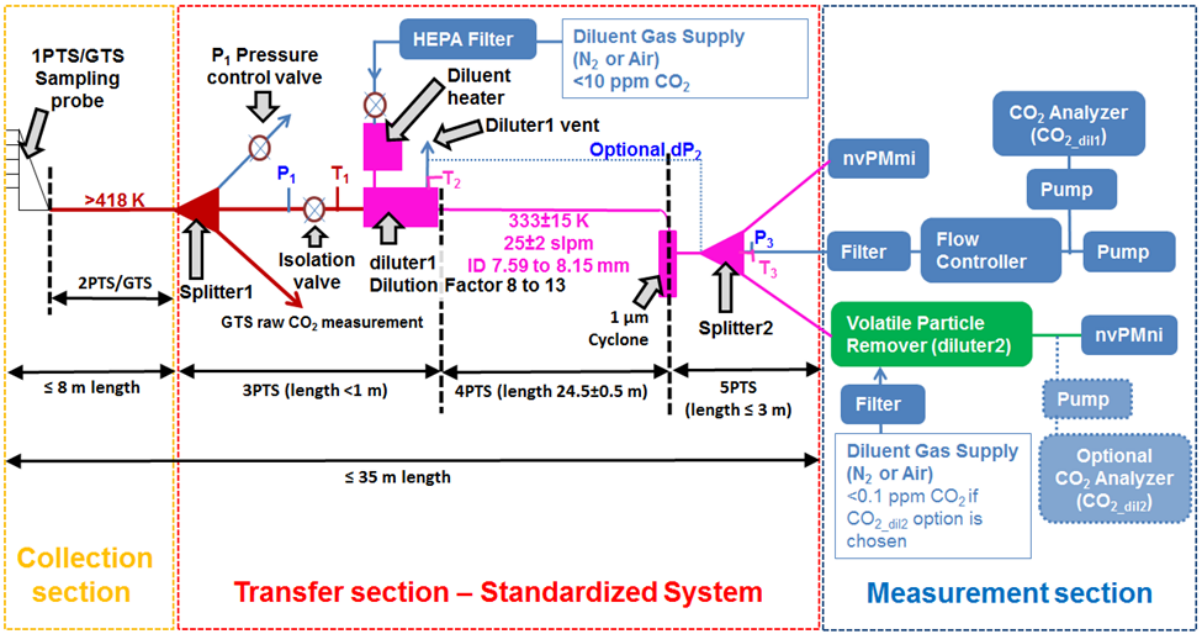

Figure 2: Components of an ICAO Annex 16 Vol.II Appendix 7 Compliant nvPM system

Collection section
The collection section consists of the probe rake system and up to 8m of stainless sample line heated to 160˚C.

Transfer section
The transfer section consists of a three way sample splitter, a PM sample eductor/dilutor, flow controllers, and sample line heater controllers The first sub-component of the transfer section is a three way sample splitter which divides the total exhaust gas sample from the rake into three flow streams. The first is the required flow of exhaust for the Annex 16 combustion gas sample. The second is the PM sample and the third is an excess flow dump line controlled with a pressure relief valve. The PM sample is diluted by a factor 8-13 with dry nitrogen (heated to 60˚C) by means of an eductor/dilutor. The diluted PM sample with a flow rate 25 ± 2 SLPM is transferred by an electrically heated, temperature controlled conductive, grounded, carbon loaded PTFE PM sample transfer line 25m in length, maintained at 60˚C to a 1µm cyclone and then a second three way splitter to direct the sample to the number and mass measurement devices in the measurement system.

Measurement section
The measurement section consists of a volatile particle remover and a particle number measurement device, a mass measurement device and a mass flow controller, pump and CO_2 detector as specified by AIR6241.

As part of evaluating the methodology and the robustness of the system described in AIR6241, the North American nvPM reference system has been deployed at several OEM facilities in North America as well as the SR Technics maintenance facility in Zurich, Switzerland. These demonstration/inter-comparison studies served to provide information regarding the variability of the individual sampling and measurement systems. Additional testing at OEM facilities has also be conducted to acquire QL2 data on a set of engines identified to be representative of the commercial fleet for entry into the nvPM values database. Datasets from these initial measurement activities are being used by the ICAO Committee on Aviation Environmental Protection (CAEP) and their PM Task Group (PMTG) as they consider future aviation PM regulations. The data will be used by PMTG to develop a metric on which the regulation for nvPM emissions will be based.

In this task Missouri S&T and its sub-contractor Aerodyne Research Inc. with use the North American Reference System as described above to develop a dataset for the development of an ambient conditions corrections methodology. Reference 1.

Milestone(s)
Measurement campaign completed (April 2017)
NARS Data delivered to GE (April 2017)
Ancillary size distribution data to GE (October 2017)

Major Accomplishments
Critical data on nvPM ambient conditions corrections was acquired using the GE combustor. These data were used to inform CAEP WG3 as it strives to establish regulatory standards for nvPM emissions from commercial transport aircraft.

Publications
None

Outreach Efforts
This work was reported at the ASCENT advisory board meetings held in Washington DC in April and September 2017

Awards
None

Student Involvement
No graduate students were employed in this task however four undergraduate research assistants were employed in pre- and post-test activities including individual component testing and calibration and data reduction and interpretation.

Plans for Next Period
Additional ambient condition correction testing is anticipated during the next year. Potential test vehicles are being pursued at Pratt and Whitney, Rolls Royce and Honeywell.

Ref 1 – Presentation on Project 2 at the ASCENT Advisory board Meeting in Washington DC, April 2017.

Task #3: Engine to Engine Variability at Honeywell
Missouri University of Science and Technology

Objective(s)
The objective of this effort is to gather emissions data from at least 20 Honeywell commercial propulsion engines of the same type to assess engine-to-engine variability and to derive characteristic nvPM emissions.

Research Approach
Experience has shown that manual calibration of the currently accepted standard systems for measuring nvPM from aero-engines is problematic. The current accepted method for assuring that nvPM measurements are valid is to perform a back-to-back measurement with a known good measurement system or “gold standard system.” The North American reference system for nvPM, operated by MS&T has been compared with a similar European system and now serves as the reference “gold” system in the United States and Canada. In July and August, 2014, Honeywell performed a correlation test with the North American reference system at the Honeywell facility in Phoenix, Arizona. This test was performed on a development HTF7500 engine using the Honeywell Mobile Emissions Facility 2, (MES2). MES2 is equipped to measure nvPM, gaseous emissions and smoke. The North American reference system was plumbed in parallel to MES2 and nvPM results were measured sequentially from the Honeywell system and the MS&T system. Data was sampled at the four International Civil Aviation Organization (ICAO) landing and take-off (LTO) conditions. Emissions samples were drawn from the Honeywell emissions sampling system (a cruciform mixed exhaust rake with 16 sampling ports on four arms at four radii) and two core engine sampling rakes with six radial ports per rake. Test results were analyzed and reported to the FAA.

In support of the anticipated 2019 ICAO/FAA Part 34 certification standard, Honeywell received a request for proposal from the FAA in January 2016 to measure engine-to- engine variability of non-volatile particulate matter emissions data from a sample of 20 Honeywell engines in order to assess the characteristic variability of these engines. The FAA proposed work included the following items.

(a) Obtain nvPM mass and number emissions from 20 turbofan engines, which contain the same model and type with the standardized draft ICAO Annex 16 Appendix 7 compliant nvPM measurement system, along with ICAO Annex 16 compliant gaseous emissions (possibly obtained during green runs).

(b) Use a single-point probe positioned at a spot in the exhaust stream that is representative of the average emissions in the exit plane. A certification-type probe is preferable, if the added cost is not prohibitive.

(c) Vary the rated thrust from idle to 100 percent at 10 percent increments. After the engine stabilizes at each thrust point, hold the throttle at that thrust point for approximately 3 minutes so that nvPM and gaseous emissions can be acquired.

(d) Use limited release Non-Disclosure Agreement (NDA) as needed. Ensure that the nvPM and gaseous emissions data are available from the 20 engines for analysis to derive characteristic nvPM mass and number emissions indices (EIs) or any other emissions metric as needed.

In response to this request, Honeywell proposed conducting nvPM emissions sampling during break-in (green run) testing of new AS907-2-1A type production engines. This required the redesign of the HTF7500 sampling rake in order for it to be compatible with the AS907-2-1A engine short mixer design. During testing, two of the existing fixed AS907-2-1A Station 6 (core exit) thermocouple (TC) probes were replaced with these new core exhaust emissions sampling rakes.

Honeywell used their existing mobile emissions facility, MES2, certified for ICAO emissions testing. Under this program, Honeywell also procured one standardized draft Annex 16 Appendix 7 compliant nvPM mass measurement system and installed it in MES2 system to support this testing. Reference 2.

Task 3.1 – Procurement of nvPM Emissions Test Equipment

Honeywell shall design and fabricate nvPM emissions rakes required to gather data from new Honeywell AS907-2-1A engines. These are Station 6 (core exit) emissions sampling rakes compatible with the AS907-2-1A engine short mixer configuration. Two rakes will be installed for testing, with each rake configured with six dial sampling ports. An exhaust sample from both rakes is averaged and analyzed through the compliant Honeywell emissions measurement system MES2. Honeywell will complete design drawings for the engine Station 6 exhaust emissions rakes and fabricate four, which consists of two for testing with two spares. One standardized draft Annex 16 Appendix 7 compliant nvPM mass measurement system shall be purchased and installed in Honeywell's existing mobile emissions facility, MES2.

Task 3.2 – Engine nvPM Emissions Testing

Honeywell shall obtain nvPM and gaseous emissions from a minimum of 20 AS907-2-1A type turbofan engines during production break-in testing, using MES2. This facility is fully compliant with the draft ICAO Annex 16 Appendix 7 nvPM measurement system and is also ICAO Annex 16 compliant for the gaseous emissions system. In addition, with nvPM and gaseous emissions, Honeywell will also report derived smoke number (SN) from the optical smoke meter (OSM). Honeywell will not perform or report filter smoke measurements to minimize the analysis time per engine condition.

To minimize impact on the critical HTF7000 production engine break-in test schedule, the nvPM emissions test plan will align with the existing break-in run test schedule which includes a 3-minute hold at the end of each power point tested. This program will obtain nvPM mass and gaseous emissions samples at the end of these 3-minute periods. The proposed 11-point nvPM and gaseous emissions sampling test matrix is shown in Table 1. Prior to each green run test, technicians will replace two of the fixed AS907-2-1A Station 6 (core exit) TC probes with the exhaust emissions sampling rakes.

Table 1. nvPM Mass and Emissions Sampling Test Matrix.

Test Condition/	Approximate Maximum Thrust, Percent	Stabilizing Time Prior to nvPM Sampling, minutes
Ground idle (GI)	4	3
17,600	8	3
20,600	16	3
22,600	29	3
23,600	38	3
24,600	52	3
25,600	72	3
26,300	90	3
26,900	97	3
Maximum takeoff (MTO)	100	3
1,100 lb/hr	33	3
GI	4	3

Since agreement with production is contingent on not significantly impacting or delaying the production test schedule, this task plans to gather data from 25 green run engine tests, anticipating the risk that some tests may have issues that are not identified during the test and thus will not produce acceptable data. Honeywell will reduce the analysis results following every test to validate the data, but the production engine tests cannot be delayed while waiting for data validation completion.

The engine rated thrust will be varied in increments from idle to 100 percent MTO per Table 1. The steady-state engine condition will be stabilized at each point for approximately 3 minutes before obtaining the exhaust emissions data

Task 3.3 - Data Reduction and Analysis

Honeywell will reduce and analyze the data following every test to validate that the data set is acceptable.

Task 3.4 - Project Management and Reporting

Honeywell shall manage the program activities and finances in accordance with standard Honeywell practice and provide monthly status reports to MS&T.

Honeywell is proposing completion of this work within 11 months after contract award. Honeywell estimates that it will require four months to procure, install, and check out the required nvPM test equipment before initiating nvPM engine testing.

Current production projections indicate that a sufficient number of AS907-2-1A engines will be produced during the proposed contract period to be able to conduct the 25 planned exhaust emissions tests during planned green runs. Honeywell estimates that this testing will be completed within a four-month period after the nvPM equipment has been cleared for testing.

Following these tests, Honeywell shall compile the data and prepare a draft final report documenting the test results and hold a final briefing to present results to MS&T and FAA representatives. Honeywell shall prepare a limited release draft final report, and make available the nvPM and gaseous emissions data from the engines tested for additional analysis to derive characteristic nvPM mass and number, EIs or any other emissions metrics as needed. Honeywell shall then submit a draft final report to MS&T, and allocate 30 days for review and feedback. Honeywell shall then incorporate the comments and submit the final report to MS&T.

Ref 2 – Presentation poster on Project 2 at the ASCENT Advisory board Meeting in Washington DC, September 2017.

Milestone(s)
Engine testing on 25 engines has been completed – September 2017
Data being reduced analyzed and reviewed – September 2017

Major Accomplishments
With data on 25 engines acquired this project is more than 75% completed.

Publications
None

Outreach Efforts
This work was reported at the ASCENT advisory board meetings held in Washington DC in April and September 2017.

Awards
None

Student Involvement
None

Plans for Next Period
Consult with Honeywell engineers on the interpretation of the data.

Task #4: Ground-Based Nvpm Emissions from an IAE V2527-A5 Engine Burning Four Different Fuel Types
Missouri University of Science and Technology

Objective(s)

1. Measure engine emissions from four different fuel types on the ground using NARS and its ancillary equipment and compare it to the NASA measurement system. Quantify differences
    a. Deploy to Europe
    b. Make measurements and analyze data
2. Contribute to planning the emissions measurements at various altitudes and evaluate cruise nvPM models.

Research Approach

Task 4.1: Contribute to planning the emissions measurements at various altitudes and evaluate cruise nvPM models.
In this task the primary objective of the MS&T team will be to work closely with the ND-MAX principal investigators to plan the logistics and test matrices of the proposed emission measurements at ground level and at altitude including an intercomparison of the NARS data with that acquired with the NASA/DLR deployed nvPM measurement systems. The secondary objective of this task will be to evaluate models predicting cruise nvPM emissions by comparing the model results with the in-situ and ground-based measurements.

Task 4.2: Prepare the NARS and ancillary equipment for deployment to test site in Germany.
In this task the NARS sub-systems will be laboratory tested at Missouri S&T and Aerodyne to assure they meet operational specification as defined in AIR6241/ARP 6320. On completion of laboratory testing the NARS and ancillary equipment will be packaged and shipped to the test site in Germany.

Task 4.3: Deploy to and set up the NARS at an airfield in Germany
In this task the MS&T team will deploy to the test site in Germany and set up the NARS and ancillary equipment and undertake sub-system check-out procedures in preparation for emissions testing.

Task 4.4: Conduct ground-based emissions measurements on four different aviation fuels
In this task the MS&T team will use the NARS and ancillary equipment to characterize the nvPM component of emissions from four separate fuels to be defined by the test matrix established in the work described in task 6.

Task 4.5: Tear-down and ship NARS and ancillary equipment to MS&T
In this task the MS&T team will tear down the NARS and ancillary equipment and package it for return shipment to the US.

Task 4.6: Reduce, analyze and report nvPM data
In this task the raw emissions data acquired during task 3 will be reduced and analyzed using the methods described in AIR6241/ARP 6320. These data will be reported to the FAA and shared with the ND-MAX participants.

Ref 2 – Presentation poster on Project 2 at the ASCENT Advisory board Meeting in Washington DC, September 2017.

Milestone(s)
None during this reporting period

Major Accomplishments
None during this reporting period

Publications
None during this reporting period

Outreach Efforts
None during this reporting period

Awards
None

Student Involvement
No graduate students were employed in this task however four undergraduate research assistants were employed in pre- and post-test activities including individual component testing and calibration and data reduction and interpretation.

Plans for Next Period
Complete the Tasks 4.1through 4.6 described in the research approach for Task 4. The measurement campaign is expected to take place at Ramstein Air Force Base in Germany during the period January 12 through February 4, 2018.

Project 003 Cardiovascular Disease and Aircraft Noise Exposure

Boston University

Project Lead Investigator

Junenette L. Peters
Assistant Professor
Department of Environmental Health
Boston University School of Public Health
715 Albany St., T4W, Boston, MA 02118
617-358-2552
petersj@bu.edu

University Participants

Boston University (BU)

- P.I.(s): Jonathan Levy (University PI); Junenette Peters (Project PI)
- FAA Award Number: 13-C-AJFE-BU-002;
- Period of Performance: October 1, 2016 to September 30, 2017

Tasks:

1. Assign aircraft noise exposures over time to geocoded participant addresses for new cohorts - Nurses' Health Study (NHS), NHSII, NHS3, Health Professional Follow-up Studies (HPFS), and HPFS2.
2. Link aircraft noise exposures to participant data for NHS, NHSII, NHS3, HPFS, and HPFS2.
3. Determine the numbers of CVD-related outcomes of interest available in NHS, NHSII, and HPFS participants living near airports.
4. Develop and execute models for estimating CVD health risks associated with aircraft noise exposure.
5. Determine the number of NHS3/HPFS2 participants residing near airports based on the 2010 and 2015 airport noise data.

Project Funding Level

Total Funding $200,000
Matching: $66,667
Source of Matching:

Matching contribution is in the form of non-federal funds provided to the cohorts studies including the Women's Health Initiative and the Nurses' Health Study and companion Health Professional Follow-up Study in which Boston University and partners are performing noise-health research.

- Nurses'/Health Professional $1.4 M
- Women's Health Initiative $17.5 M
- Total $18.9 M

Investigation Team

Junenette Peters, PI, Boston University

Dr. Peters is responsible for directing all aspects of the proposed study, including study coordination, design and analysis plans, and organizing co-investigator meetings.

Jonathan Levy, Boston University

Dr. Levy will participate in the noise exposure assessment effort and provide expertise in the area of predictive modeling and air pollution.

Francine Laden and Jamie Hart, Harvard University

Dr. Laden is our NHS and HPFS sponsor for this ancillary study. Dr. Jamie Hart's will assign aircraft noise exposures to cohorts' participant geocoded address coordinates. Dr. Laden and Dr. Hart will also assist with documentation of data from the NHS and HPFS based on previous experience working on air pollution and chronic disease outcomes research in these cohorts.

Project Overview

Aircraft noise is a considerable source of stress among near-airport communities. Exposure has been associated with sleep disturbance, physiological responses and psychological reactions, with corresponding effects on blood pressure. However, the extent to which aircraft noise increases the risk of cardiovascular disease (CVD) has not been fully elucidated. Likewise, the role of CVD risk factors in mediating an association between noise and CVD has not been assessed. Additionally, exposure assessment that includes time-varying and spatially resolved noise exposures has not been systematically incorporated into previous epidemiological studies, making it key to receive aircraft noise data over multiple years. FAA PARTNER 44 and ASCENT 03 projects provided the pilot data and collaborations necessary to successfully compete for National Institute of Health (NIH) funding to evaluate noise effects on cardiovascular outcomes in the longitudinal Women's Health Initiative (WHI) cohorts. This study proposes to extend ongoing efforts in the WHI and evaluate the effects of aircraft noise exposure on cardiovascular disease in both women and men in the longitudinal Nurses' Health Studies (NHS, NHSII, and NHS3) and companion Health Professional Follow-up Study (HPFS and HPFS2) cohorts. These studies began with the original cohort (NHS) in 1976 and is currently recruiting the third generation (NHS3), with over 330,000 total participants.

The proposed scope of this research effort would involve multiple years, with activities within Phase I providing the foundation for future activities. The objectives for this year include: 1) Determining noise exposure estimates for study participants; 2) Linking noise exposure estimates to participant data on outcomes (health effects) and other risk factors; 3) Developing and executing models to evaluate cardiovascular effect(s) of noise.

Tasks based on receiving noise data for 90 airports over time in multiple metrics:

- Initially projected timeline for receiving data for 2000, 2005 and 2010 – March 2015
- Also negotiated for noise data for additional years (1995 and 2015)

However, data was modeled by two facilities (Wyle and Volpe) using different methods and assumptions. Data for 37 airports needed to be rerun to harmonize data.

- Requested test rerun of Wyle modeled airports by Volpe for one year (2000) and metric to determine impacts of using differing methods and assumptions on noise estimates assigned to participants. Received test rerun data – February 2017.
- Performed extensive analyses to determine the effect of differing methods and assumptions on noise estimates.
- Rerun negotiated – July 2017.
- Currently projected timeline for receiving data from rerun of 37 airport for key metrics – October 2017.
- Currently projected timeline for receiving data from rerun for remaining metrics – November 2017.

Pre-Tasks

Objective

To gain approval to conduct noise health research in the NHS and HPFS.

Research Approach

BU (Dr. Peters) as an external collaborator will enter into a collaborative agreement with the primary NHS/HPFS investigator (Harvard; Dr. Laden). The BUSPH team will obtain exemption for human subjects research from the Institutional Review

Boards (IRBs) at Boston University Medical Campus and the Harvard team will obtain approvals for human subjects research from the IRB at the Harvard Medical School/Brigham and Women's Hospital.

Milestones

- Receive approval for 'ancillary' noise-health study.
- Execute final Data Use Agreement with Harvard.
- Obtain IRB approvals for human subjects research.

Major Accomplishments

- Submitted and presented proposal to NHS and HPFS for noise-health study and received approvals.
- Obtained IRB exemption at BU and IRB approval at Harvard for human subjects research.
- Executed Data Use Agreement with BU, Harvard and FAA.

Task #1: Assign Aircraft Noise Exposures over Time to Geocoded Participant Addresses

Objective

To intersect geocoded addresses available from 1995 to 2015 with noise surfaces obtained.

Research Approach

We will intersect geocoded addresses with noise contours available from 1995 to 2015. Given the longitudinal nature of this study, noise exposures will be assigned reflecting specific residential addresses over time based on participant address histories. We will estimate the percent of participants across noise exposure categories (e.g., DNL > 55 dB) and assess overall trends in participant noise exposure levels over time.

Milestone

(*Dependent on receiving noise data – originally projected for March 2015; now projected for October/November 2017*)

- Assign aircraft noise exposures – November 2016

Major Accomplishments

- Successfully collaborated to obtain 1995 and 2015 data in all metrics for 90 airports.
- Received aircraft noise data for 53 airports for the years 2000, 2005 and 2010 in May 2016; metrics received include Day-Night Average Sound Level (DNL), Equivalent Sound Level (Leq), Leq Day and Leq Night), Time above Threshold (TA) 65 dB and TA 85 dB.
- Received the data for the above airports and metrics for 1995 and 2015 in April 2017.
- Submitted documentation for need for rerun of data for 37 airports using the same methods and attributes.
- Developed processes for converting noise data into useable formats.
- Received rerun of aircraft noise data in DNL and Leq Night using Volpe methods and attributes for 17 of the 37 Wyle airports in September 2017.
- Linked NHS and HPFS participants to previously obtained 2009 DNL data to get an estimate of the number of participants near airports (within 45 dB contours) (Figures 1 and 2).
    - NHS: 5,666
    - NHS II: 5,802
    - HPFS: 2,952
- Updated penultimate draft of the noise modeling documentation (metadata).

Figure 1. Location of NHS & NHSII participants in relation to airports

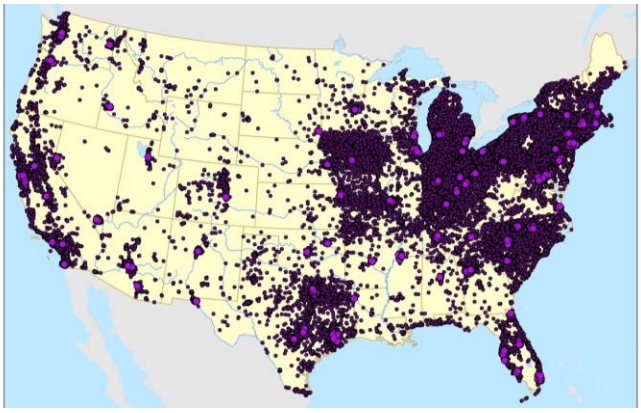

Figure 2. Location of HPFS participants in relation to airports

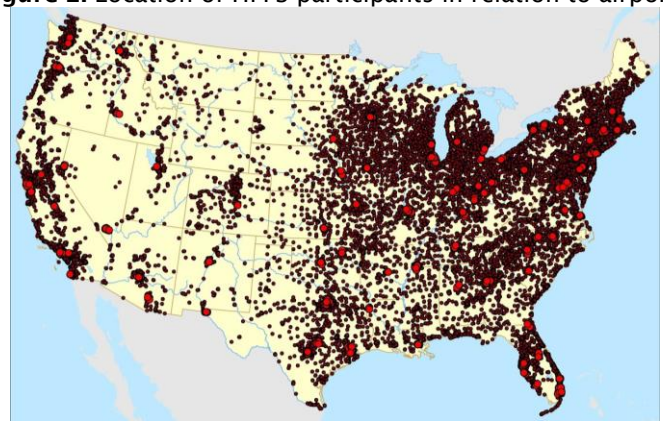

Task #2: Link Aircraft Noise Exposures to Participant Data for NHS, NHSII, NHS3, HPFS, and HPFS2

Objective

To link with the individual level information in NHS and HPFS.

Research Approach

We will link information with the wealth of individual level information on socio-demographics (e.g., age, race/ethnicity, education); lifestyle factors (e.g. physical activity/exercise, diet, smoking, alcohol consumption); and relevant outcomes (e.g., hearing and hearing loss, sleep disturbance, diabetes, CVD and CVD mortality).

Milestone

(*Dependent on receiving noise data – originally projected for March 2015; now projected for October/November 2017*)

- Link aircraft noise exposures to individual data for all cohorts – December 2016

Major Accomplishments

- None (awaiting final noise exposure data).

Task #3: Determine the Numbers of CVD-Related Outcomes of Interest Available In NHS, NHSII, and HPFS Participants Living Near Airports

Objective

To identify all cases of overall and cause-specific incident cardiovascular, cardiovascular mortality and incident hypertension.

Research Approach

We will identify all cases of overall and cause-specific incident CVD, CVD mortality, and incident hypertension among individuals in the NHS, NHSII, and HPFS living within the 45 dB contours. These cohorts have been followed over a long enough period (over two to four decades) to observe health outcomes and participants are of an age when they are at risk for CVD.

Milestones

(*Dependent on receiving noise data – originally projected for March 2015; now projected for October/November 2017*)

- Determine the number of cardiovascular-related outcomes among those living near airports – January 2016
- Determine the number of participants at risk for cardiovascular disease (free of CVD at baseline/earliest time with available noise data [1995]).

Major Accomplishments

- Determined the number of cohort participants alive and free of CVD at baseline (1995). Characteristics of participants provided in Table 1.
    - NHS: 96,000 alive and free of CVD
    - NHSII: 115,000 alive and free of CVD
    - HPFS: 50,000 alive and free of CVD

Table 1. Characteristics of participants alive and free of CVD at baseline (1995)

Characteristics	NHS	NHSII	HPFS
	Mean ± SD or %		
Age (years)	68.6 ± 7.3	46.6 ± 7.0	63.8 ± 10.2
Body mass index (kg/m^2)	25.6 ± 7.5	21.2 ± 3.2	26.6 ± 11.5
Race			
Black	2	2	6
White	94	96	91
Other/Multiple races	6	2	3
Smoking Status			
Never	45	64	40
Former	45	25	41
Current	11	9	6
Family History of MI	32	22	13

Task #4: Develop and Execute Models for Estimating CVD Risk Associated With Noise Exposure in NHS, NHSII, and HPFS

Objective

To develop appropriate measures to evaluate the effects of aircraft noise on cardiovascular outcomes.

Research Approach

The team will develop hazard models for estimating time varying CVD risk associated with noise exposure in the vicinity of each airport. We will also explore methods to account for clustering and spatial correlation between individuals living near each airport. We will then conduct epidemiological analyses to estimate the health effects of noise exposure on each CVD outcome controlling for other risk factors thought to be related to CVD

Milestones

(*Dependent on receiving noise data – originally projected for March 2015; now projected for October/November 2017*)

- Develop models for estimating cardiovascular health risks associated with aircraft noise exposure – January 2016
- Perform analysis of cardiovascular health risks associated with aircraft noise exposure – June 2016

Major Accomplishments

- Submitted, presented and received approval from NHS/HPFS for two manuscript proposals titled:
  - Association of aircraft noise exposure and incident hypertension
  - Association of aircraft noise exposure and prevalent and incident cardiovascular disease
- Developed initial plan for statistical analysis.

Publications
None

Outreach Efforts
None

Awards
None

Student Involvement
None

Plans for Next Period
(October 1, 2017 to September 30, 2018)

- Obtain final metadata on aircraft noise modeling.
- Obtain resolved noise data run with the same assumption and attributes.
- Assign all noise exposure estimates to participants.
- Execute models estimating CVD related risks associated with noise exposure.
- Develop abstracts for presentation at professional conferences.
- Determine the number of newly recruited participants (NHS3/HPFS2) residing near airports from whom survey questions or measurements of noise and sleep disturbance may be obtained.
- Develop suite of survey questions on built environment and noise perception.

Project 005 Noise Emission and Propagation Modeling

Pennsylvania State University
Purdue University

Project Lead Investigator

Victor W. Sparrow
Director and United Technologies Corporation Professor of Acoustics
Graduate Program in Acoustics
Penn State
201 Applied Science Bldg.
University Park, PA 16802
+1 (814) 865-6364
vws1@psu.edu

University Participants

Pennsylvania State University

- P.I.: Victor W. Sparrow, United Technologies Corporation Professor of Acoustics
- FAA Award Number: 13-C-AJFE-PSU, amendments 005, 015, 029
- Period of Performance: August 18, 2014 to December 31, 2017
- Task(s):
    1. Assess applicability of meteorological reanalysis models for possible use in FAA noise tools
    2. Assess measurement data sets for noise propagation model validation

Purdue University

- P.I.(s): Kai Ming Li, Professor of Mechanical Engineering
- FAA Award Number: 13-C-AJFE-PU, amendments 002, 007, 009, 016
- Period of Performance: June 1, 2014 to June 2017
- Task(s):
    3. Extend model for fast moving sources

Project Funding Level

FAA funding to Penn State in 2014-2015 was $132K and in 2015-2016 was $110K. FAA funding to Purdue in 2014-2015 and 2015-2016 was $80K and $90K, respectively.

In-kind cost sharing from Vancouver Airport Authority received in October 2016 was $294,500 to Penn State and $294,500 to Purdue. The point of contact for this cost sharing is Mark Cheng, mark_cheng@yvr.ca. Project support is in the form of aircraft noise and trajectory data, meteorology data, and consulting on those datasets.

Investigation Team

Penn State

Victor W. Sparrow (PI)
Graduate Research Assistant Rachel Romond (meteorological reanalysis data investigation)
Graduate Research Assistant Manasi Biwalkar (measurement data sets for model validation investigation)

Purdue

Kai Ming Li (PI)
Graduate Research Assistant Bao Tong (moving source investigation)
Graduate Research Assistant Yiming Wang (moving source investigation)

Project Overview

The FAA has been funding research efforts in developing enhanced noise emission and propagation capabilities to better support environmental impact studies at both local and national levels. The main emphasis in the near and mid-term is to increase the Research Readiness Level (RRL) of the capabilities so that they can be further matured for implementation into the FAA tools. Validation of the modeling capabilities has been the central focus of the project. Via recent US-EU research collaboration, the field measurement database (BANOERAC) is becoming available for model validation. This database contains acoustic time history of flight events from various types of commercial aircraft during cruise, climb and descent phases of the flight. In addition the DISCOVER/AQ and Vancouver Airport Authority databases have already come on line for use in this and other FAA projects. These datasets make model validation possible. In addition the work will make existing models ready for simulating real weather conditions via proper treatment of the meteorological input parameters and to establish a common basis for comparing US and EU models.

Task #1: Assess Applicability of Meteorological Reanalysis Models for Possible Use in FAA Noise Tools

Completed

Task #2: Assess Measurement Data Sets for Noise Propagation Model Validation

Pennsylvania State University

Objective(s)

The objective of Project 5, Task 1 was to determine if meteorological reanalysis datasets and corresponding input parameters are useful for aircraft noise propagation prediction and whether the same can be integrated into the AEDT noise analysis framework. The objective of Project 5, Task 2 was to begin examination of aircraft measurement databases and ascertain their applicability for validating aircraft noise prediction tools.

Concluding Work

All of the tasks for ASCENT Project 5 has been completed except for one remaining item. Since the beginning of the project, Penn State has been working with ANOTEC Engineering of Motril, Spain to obtain suitable data sharing agreements with the European Aviation Safety Agency (EASA) for the use of the BANOERAC dataset for ASCENT research. BANOERAC stands for “Background noise level and noise levels from en-route aircraft” and that European project concluded in 2009. Specifically, Project 5 had funds budgeted to obtain the BANOERAC flight trajectory data through ANOTEC. ANOTEC had the raw ADS-B data to calculate the flight trajectories, but never produced those trajectories under EASA funding. ASCENT Project 5 was no-cost extended to December 31, 2017 to ensure that a Penn State purchased services agreement to ANOTEC would remain in place so that ANOTEC could provide those flight trajectories.

In early 2017, the data sharing agreements were put into force, and in the spring and summer of 2017 Penn State worked with ANOTEC to establish a purchased services agreement. Currently, ANOTEC is on schedule to deliver the BANOERAC flight trajectory data to Penn State and Purdue by 15 December 2017. Hence, with this data receipt, Project 5 will conclude on time on 31 December 2017. The BANOERAC data will then be available for use in other ASCENT projects at Penn State and Purdue, such as ASCENT Project 40.

All the other accomplishments in Project 5 have previously been reported in the 2015 and 2016 ASCENT annual reports, and ongoing research can be found in the 2017 annual report of Project 40. The final report for Project 5 will be submitted by 31 January 2018.

Milestone(s)

N/A

Major Accomplishments

The BANOERAC data sharing agreement between EASA, Penn State, and Purdue University was established.

Publications
None.

Outreach Efforts
None.

Awards
None.

Student Involvement
None.

Plans for Next Period
Project 5 at both Penn State and Purdue will be completed by 31 December 2017.

References
BANOERAC Project final report, Document ID PA074-5-0, ANOTEC Consulting S.L. (2009).

Task #3: Investigate the Convective Amplification Effects of Fast Moving Sources
Purdue University

At present, we are on the process to formally complete the project by filing appropriate document for record. Nevertheless, the effort of the Purdue team on Project 5 has been integrated to Project 40 as we move on to look into the impact of uncertainties in predicting en-route aircraft noise. More details can be found in the annual report of Project 40.

Milestone(s)
N/A

Major Accomplishments
None.

Publications
None.

Outreach Efforts
None.

Awards
None.

Student Involvement
None.

Plans for Next Period
Project 5 at both Penn State and Purdue will be completed by 31 December 2017.

References
None.

Project 008 Noise Outreach

The Pennsylvania State University

University Members

Penn State Applied Research Laboratory Team Lead	Kathleen Hodgdon
Penn State Institute for Energy and the Environment	Maurie Caitlin Kelly
Penn State Earth & Environmental Systems Institute	Bernd Haupt

Advisory Committee Members

Gulfstream Aerospace Corporation	Robbie Cowart
Port of Portland Sr. Noise Analyst	Jason Schwartz
Volpe National Transportation Systems Center	Juliet Page

Project Lead Investigator

Kathleen Hodgdon
Research Associate
Applied Research Laboratory
The Pennsylvania State University
ARL North Atherton Street
P.O. Box 30 (Mail Stop 2210H)
State College PA 16804-0030
Phone: 814-865-2447
Email: kkh2@psu.edu

University Participants

The Pennsylvania State University

- P.I.: Kathleen Hodgdon, Research Associate
- Researcher: Maurie Caitlin Kelly, Research Associate
- Researcher: Bernd Haupt, Senior Research Associate
- FAA Award No.:13-C-AJFE-PSU Amendment 27
- Period of Performance: July 31, 2016 to July 31, 2017
- Task(s):
  1. Stakeholders Interactions
  2. Content Development
  3. Site Navigation and Infrastructure Enhancement

Project Funding Level

This project supports the Outreach efforts at Penn State with $75K of FAA funds. Matching funds are anticipated to satisfy cost share on all tasks.

Investigation Team

P.I.: Kathleen Hodgdon Research Associate
Researcher: Maurie Caitlin Kelly Research Associate
Researcher: Bernd Haupt Senior Research Associate

Project Overview

Aircraft noise is a predominant aviation environmental concern of the public. Aviation noise issues can be complex and technical, and the NoiseQuest website is designed to mitigate noise concerns through information. Outreach has been implemented through content on the NoiseQuest website and by direct interactions with stakeholders. NoiseQuest, located at www.noisequest.psu.edu, is an international resource that is designed to implement global education on aviation noise topics. The site presents outreach content and aviation noise information on a diverse set of topics. The PSU Outreach team has continued to expand and enhance the NoiseQuest website. The development of the NoiseQuest site provides centralized web based educational outreach for all communities. This supports Outreach efforts for airports too small to have their own outreach programs, and provides additional outreach for airports with an existing outreach program.

Task #8.1: Stakeholders Interactions

The Pennsylvania State University

Objectives

The Outreach project seeks to improve airport and community interactions by providing information and education on aviation noise topics. The objectives of this task include: (1) interactive outreach to identify aviation noise programs; (2) obtain airport noise contour data from airport noise managers; and (3) gather publications and concepts for content to be shared on the NoiseQuest site.

Research Approach

Interactive outreach with airport noise managers and community groups was conducted to identify concerns that could be addressed by expanded content topics and to identify successful programs and initiatives. Efforts to obtain additional GIS noise contour data for the NQ Explorer were not conducted during the site redesign period. The site user statistics are monitored to better inform the site development.

Milestones

We communicated with airport noise managers, stakeholders, and community organizations to identify updates for existing content and opportunities for new content development.

Major Accomplishments

We continue to interact with airport noise managers and community groups to identify topics of interest, successful implementations of outreach, or other approaches taken to resolve aviation noise issues. Jason Schwartz (ASCENT Advisory Committee Member), from the Port of Portland is an active team member. He has provided ideas and content topics as well as offering to interact with other airport noise managers on our behalf.

We interact with the National Organization to Insure a Sound-controlled Environment (N.O.I.S.E.) and they have provided ideas for content and the Spotlight section. Emily Tranter (N.O.I.S.E. National Coordinator) is working with us on identify content topics as well as programs to feature in the Spotlight section. The NoiseQuest site was presented at the National Organization to Ensure a Sound-controlled Environment 2016 Policy Summit and Community Involvement Workshop held in conjunction with the National League of Cities, 2016 City Summit, in Pittsburgh, PA on November 16, 2016.

We continue to encourage stakeholders to link their site to NoiseQuest. We continue to monitor our site statistics to gain insights on site usage (see Appendix A for Site Statistics).

Publications

Contents are published at www.noisequest.psu.edu.

Outreach Efforts

We interact with airport noise managers and community groups from across the country.

Awards
None

Student Involvement
None

Plans for Next Period
We will continue to monitor site statistics to determine site usage patterns. To promote greater site usage, we will work to get additional stakeholders to link to NoiseQuest and to provide recommendations for content.

Task #8.2: Content Development
The Pennsylvania State University

Objectives
This task is focused on identifying and developing content that addresses aviation noise impact and outreach education.

Research Approach
The Outreach team seeks to identify content that presents updates on aviation noise research, addresses noise issues, or meets the educational outreach needs of aviation stakeholders on specific topics.

Milestones
The NoiseQuest team worked with representatives from both the National Organization to Ensure a Sound Controlled Environment (N.O.I.S.E.), and Delta to review the newly organized and reformatted NoiseQuest site. The team maintained existing site areas and added new content.

Major Accomplishments
The content organization was reviewed as part of the restructuring of the site to be accessible across all platforms. Consideration was given to the ease of navigation, ease of adding additional content, the ability to search existing content readily, providing a menu that can respond to changes in viewing size and including video that is easily resizable. The primary content areas for the site include Community Tools, National Airspace, Noise Basics, Sources of Noise, and Noise Effects and Mitigation.

A site review conducted by representatives of the National Organization to Ensure a Sound Controlled Environment (N.O.I.S.E.), Delta, and the Outreach team. A primary recommendation from the site review was to add more graphics and presentations to the site content. General content was expanded and updated, the Noise Research section was expanded, the Spotlight on Noise was updated and content on AEDT, NextGen and Performance-Based Navigation were updated and enhanced.

We are gathering additional materials to expand content on PBN and low boom noise impact. We are working with NASA and the NASA sponsored Waveforms Sonicboom Perception and Response Risk Reduction (WSPRRR) team to develop content on supersonics and low boom noise impact. This NASA sponsored team has developed a test plan for future low boom community field tests. The NASA WSPRRR team includes both ASCENT and NASA researchers, who can team with the NoiseQuest team to identify and develop the low boom content for the NoiseQuest site.

We updated the site to acknowledge contributions from both PARTNER and ASCENT researchers.

Publications
Site developed at www.noisequest.psu.edu

Outreach Efforts
We develop the Outreach content by reaching out to stakeholders for content ideas and development.

Awards
None

Student Involvement
None

Plans for Next Period
The plans for the future included generating enhanced content to further engage the public. The existing site content will be enhanced with content, graphics, videos and presentations. New content topics will be identified and relevant features added to the site. This would include features such as additional videos and images across site, expanded Supersonics low boom content, additional helicopter and rotorcraft noise abatement content, and additional GIS noise contours for NQ Explorer. We plan to add an NQ Explorer tab under Community Tools once we have more contours added to that section of the site. Other topics will be identified based on stakeholder engagement.

Task #8.3: Site Navigation and Architecture Redesign and Development
The Pennsylvania State University

Objectives
Efforts under this task maintain the site architecture and enhance site navigation.

Research Approach
This effort includes website management including backups, updates, and infrastructure enhancement. A review of features on other sites was conducted and the NASA site was identified as a site that utilizes optimized navigation features. The redesign of NoiseQuest used the navigation on the NASA site as a model. To ensure that the site is accessible to the general public, the team works to assure that the information on NoiseQuest is presented in an easily navigated user-friendly format.

Milestones
The entire site was reviewed and updates and new content were posted to the site. During the review, broken links were identified and addressed. Modifications to the NQ Explorer were investigated.

Major Accomplishments
The entire site was reworked, with changes to the navigation features and content areas. To monitor usage of the entire site, website statistics can be viewed using Google Analytics.

NoiseQuest was redesigned to increase the mobile user base. Changes were made to navigational aspects of the site to facilitate the ease of use across multiple platforms. The changes include the following site features. The navigation menu is now persistent at the top of the page and the article links are active from the title, picture and “Read more” links. Images can be dynamically scaled by size and orientation. The redesign afforded a less complex layout to the website, and a larger active zone for the hit box, so that the icon is easier to hit. Both of these are website features that show consideration for the American’s with Disabilities Act. The Search tool uses Google and is displayed within the site, rather than in an exterior page. We resolved the issues related to Google Map’s API within the NQ Mapper in the NQ Explorer.

Publications
None

Outreach Efforts
The team works to ensure that the changes resulted in clarity and ease of navigation across multiple platforms. These actions were taken to facility ease of use on mobile devices so as to increase the mobile user base.

Awards
None

Student Involvement

None

Plans for Next Period

The site is now device agnostic and user-friendly on all platforms simultaneously. The redesign of the site architecture has streamlined the site's usability on a range of hardware (e.g., phones, tablets, touch-enabled laptops, etc.). The team will continue website management which includes backups, updates, and infrastructure enhancement as warranted.

Appendix A NoiseQuest Statistics

September 2016 to September 2017

33,607 Global Sessions
17,866 Sessions across the US

	Country	Sessions	% Sessions
1.	United States	17,866	53.16%
2.	United Kingdom	2,897	8.62%
3.	India	2,221	6.61%
4.	Canada	1,452	4.32%
5.	Australia	993	2.95%
6.	Philippines	752	2.24%
7.	Nigeria	423	1.26%
8.	Pakistan	416	1.24%
9.	Malaysia	415	1.23%
10.	Singapore	350	1.04%

Project 010 Aircraft Technology Modeling and Assessment: Phase I Report

Georgia Institute of Technology, Purdue University, Stanford University

Project Lead Investigators

Dimitri Mavris (PI)
Regents Professor
School of Aerospace Engineering
Georgia Institute of Technology
Mail Stop 0150
Atlanta, GA 30332-0150
Phone: 404-894-1557
Email: dimitri.mavris@ae.gatech.edu

Daniel DeLaurentis (PI)
Professor
School of Aeronautics and Astronautics
Purdue University
701 W. Stadium Ave
West Lafayette, IN 47907-2045
Phone: 765-494-0694
Email: ddelaure@purdue.edu

William Crossley (Co-PI)
Professor
School of Aeronautics and Astronautics
Purdue University
701 W. Stadium Ave
West Lafayette, IN 47907-2045
Phone: 765-496-2872
Email: crossley@purdue.edu

Juan J. Alonso (PI)
Professor
Department of Aeronautics & Astronautics
Stanford University
496 Lomita Mall, Durand Bldg. Room 252
Stanford, CA 94305-4035
Phone: 650-723-9954
Email: jjalonso@stanford.edu

Executive Summary

Georgia Tech, Purdue, and Stanford partnered to investigate the impact of aircraft and vehicle technologies and the future state of demand for aviation on future environmental impacts of aviation. In the context of this research, environmental impacts includes direct CO_2 emissions and noise. The research was conducted as a collaborative effort in order to leverage capabilities and knowledge available from the multiple entities that make up the ASCENT university partners and advisory committee. The primary objective of this research project was to support the Federal Aviation Administration (FAA) in modeling and assessing the potential future evolution of the next generation aircraft fleet. Research under this project consisted of three integrated focus areas: (1) Developing a set of harmonized fleet assumptions for use in future fleet assessments; (2) Modeling advanced aircraft technologies and advanced vehicles expected to enter the fleet through 2050; and (3) Performing vehicle and fleet level assessments based on input from the FAA and the results of (1) and (2).

The team organized a series of virtual workshops to identify and define a standard set of assumptions to use as inputs to aircraft and fleet level modeling tools. A total of four workshops were held with a range of experts from industry, government, and academia. Two of the workshops focused on defining technology impact and development assumptions; the other two workshops focused on identifying and defining the values of factors important to fleet impacts modeling. The outcome of the technology modeling workshops is a series of infographics that provide recommended assumptions that can be used in any aircraft or engine conceptual design tool. Based on the variation in responses, the technology infographics contain minimum, nominal, and maximum estimates of the impact on natural metrics, such as lift-to-drag ratio, or structural efficiency relative to a current day baseline. Estimates are provided for twenty-two key impact areas for technology impact level, maturation rate, current Technology Readiness Level (TRL), applicable subsystems, and applicable vehicle size classes. Estimates are provided for near, medium, and far terms implementation to enable creation of N+1, N+2, and N+3 representative vehicles through modeling and simulation. Minimum, nominal, and maximum estimates of these metrics can be used to provide probabilistic estimates of future vehicle performance.

In order to develop suitable assumptions for the forward looking fleet level analysis incorporating new vehicle technologies, it is necessary to forecast the future. However, most forecasts are extrapolations of the current status quo and trends, which assume an undisturbed continuation of historical and recent developments. In order to enable exploration of this assumption space, the two fleet workshops focused on the development of a standard methodology for capturing potential future states of technology and fleet development. The fleet impact, or the combined impact of multiple aircraft of varying technology levels flying within a given year, is defined broadly though demand and retirement assumptions. Demand is driven by external factors such as Gross Domestic Product (GDP) growth and ticket price. Retirement rates are also dependent on certain external factors. The first fleet workshop defined the external factors that are most important to fleet and technology evolution. A second workshop was held to define quantitative inputs for the defined factors. The outcome is a table of recommended scenarios for use in fleet analysis. The scenarios capture the most pessimistic and optimistic assumptions on technology availability, demand growth, and retirement assumptions. When run as a suite of scenarios, they provide a wide view on the potential future state of noise, fuel burn, and emissions of the fleet.

Georgia Tech and Purdue exercised their respective fleet analysis tools (GREAT and FLEET) applying the technology and fleet scenarios defined through the community workshops. The results show that fleet direct carbon dioxide (CO_2) emissions are unlikely to remain at or below 2005 levels without the addition of significant alternative fuels to offset direct emissions. Given the current state of new technology aircraft and projected introduction rates, it will take until 2030 for technology to have significant impact on direct CO_2 emissions due to the time it takes to turnover existing aircraft. It was also found that the rate of technology maturation and introduction (i.e., new aircraft) is more important to reducing direct fleet CO_2 emissions than reducing demand. Lowered demand certainly helps in reducing fleet CO_2, but inserting technology as soon as possible has the largest impact on achieving carbon-neutral growth and CO_2 emission levels below 2005 by 2050. Both the GREAT and FLEET tools predicted similar impacts for CO_2 emissions. There was more variation between tools in the predicted noise levels of the future fleet, both Purdue and Georgia Tech found significant reductions in noise contour area are possible under a wider range of demand and technology assumptions. However, as is the case with fuel burn, the rate of new technology introduction is the primary driver of reducing noise since noise is a non-linear phenomenon and older, louder aircraft will dominate until retired.

The outcome of this study is intended to provide a glimpse into the future potential states of aviation, but also to provide future researchers with a standard set of assumptions which can be reevaluated and applied in a consistent manner in future years.

Table of Acronyms

AEDT	Aviation Environmental Design Tool
ANGIM	Airport Noise Grid Integration Model
APU	Auxiliary Power Unit
ASPM	Airspace System Performance Metrics
BADA	Base of Aircraft Data
BPR	Bypass Ratio
BTS	Bureau of Transportation Statistics
CAEP	Committee on Aviation Environmental Protection
CLEEN	Continuous Lower Energy, Emissions, and Noise
CMC	Ceramic Matrix Composite
CMO	Current Market Outlook
DNL	Day-Night Level
DOE	Design of Experiments
ECU	Electronic Control Unit
EDS	Environmental Design Space
EIA	Energy Information Administration
EIS	Entry into Service
EPNL	Effective Perceived Noise Level
ETS	Emissions Trading System
EU	European Union
FAA	Federal Aviation Administration
FLOPS	Flight Optimization System
FPR	Fan Pressure Ratio
GDP	Gross Domestic Product
GMF	Global Market Forecast
GREAT	Global and Regional Environmental Analysis Tool
GTF	Geared Turbofan
HPC	High Pressure Compressor
HPCPR	High Pressure Compressor Pressure Ratio
HPT	High Pressure Turbine
HWB	Hybrid Wing Body
ICAO	International Civil Aviation Organization
LPC	Low Pressure Compressor
LPCPR	Low Pressure Compressor Pressure Ratio
LSA	Large Single Aisle
LTA	Large Twin Aisle
MSC	Mission Specification Changes
NEE	Noise Equivalent Energy
NPSS	Numerical Propulsion System Simulation
nvPM	Non-volatile Particulate Matter
OEM	Original Equipment Manufacturer
OPR	Overall Pressure Ratio
PAI	Propulsion Airframe Integration
R&D	Research and Development
RJ	Regional Jet
RPM	Revenue Passenger Miles
SA	Single-Aisle (Includes both SSA and LSA Classes)
SSA	Small Single Aisle
STA	Small Twin Aisle
SUAVE	Stanford University Aerospace Vehicle Environment
TRL	Technology Readiness Level
TSFC	Thrust Specific Fuel Consumption
UHC	Unburned Hydocarbons
USD	U.S. Dollars
VLA	Very Large Aircraft

University Participants

Georgia Institute of Technology
- P.I.(s): Dr. Dimitri Mavris (PI), Dr. Jimmy Tai (Co-PI)
- FAA Award Number: 13-C-AJFE-GIT-006
- Period of Performance: August 1, 2014 – August 31, 2017

Purdue University
- P.I.(s): Dr. Daniel DeLaurentis, Dr. William A. Crossley (Co-PI)
- FAA Award Number: 13-C-AJFE-PU-004
- Period of Performance: August 1, 2014 – May 31, 2017

Stanford University
- P.I.(s): Dr. Juan J. Alonso
- FAA Award Number: 13-C-AJFE-SU-004
- Period of Performance: August 1, 2014 – May 31, 2017

Project Funding Level

The project was funded at the following levels: Georgia Institute of Technology ($985,000); Purdue University ($209,969); Stanford University ($215,000). Cost share details for each university are below:

The Georgia Institute of Technology has agreed to a total of $985,000 in matching funds. This total includes salaries for the project director, research engineers, graduate research assistants and computing, financial and administrative support, including meeting arrangements. The institute has also agreed to provide tuition remission for the students paid for by state funds.

Purdue University provides matching support through salary support of the faculty PIs and through salary support and tuition and fee waivers for one of the graduate research assistants working on this project. While Purdue University provides the majority of the 1:1 cost share for the Aviation Sustainability Center of Excellence (ASCENT) 10-Purdue, an in-kind matching contribution of just under $20,000 comes from a gift of the RDSwin-Pro aircraft design software from Conceptual Research Corp.

Stanford University has met or exceeded its matching funds contribution using a combination of elements. Firstly, Stanford University is cost sharing, through tuition reductions for the students working on this project for the entire period of performance. In addition, our partners at the International Council for Clean Transportation are providing in-kind cost-sharing for the remainder amount though internal and external efforts funded to better understand the impact of cruise speed reduction.

Investigation Team

Georgia Institute of Technology
Principal Investigator: Dimitri Mavris
Co-Investigator: Jimmy Tai
Technology Modeling Technical Lead: Christopher Perullo
Fleet Modeling Technical Lead: Holger Pfaender and Elena Garcia
Students: Matt Reilly, Braven Leung, Marcus Bakke, Ryan Donnan

Purdue University
Principal Investigator: Daniel DeLaurentis
Co-Investigator: William Crossley
Students: Kushal Moolchandani, Parithi Govindaraju, Nithin Kolencherry, Ogunsina Kolawole, Hsun Chao

Stanford University
Principal Investigator: Juan J. Alonso
Aircraft Modeling Technical Lead: Anil Variyar
The team also includes two additional graduate students that have been assisting with the technical work and the development of our aircraft optimization framework, SUAVE, Emilio Botero and Tim MacDonald.

Project Overview

Georgia Tech, Purdue, and Stanford partnered to investigate the impact of aircraft and vehicle technologies on future environmental impacts of aviation. Impacts assessed at the fleet level include direct CO_2 emissions and noise. The research was conducted as a collaborative effort in order to leverage capabilities and knowledge available from the multiple entities that make up the ASCENT university partners and advisory committee. Georgia Tech partnered with Purdue University and Stanford University.

The primary objective of this research project was to support the Federal Aviation Administration (FAA) in modeling and assessing the potential future evolution of the next generation aircraft fleet. Research under this project consisted of three integrated focus areas: (1) Developing a set of harmonized fleet assumptions for use in future fleet assessments; (2) Modeling advanced aircraft technologies and advanced vehicles expected to enter the fleet through 2050; and (3) Performing vehicle and fleet level assessments based on input from the FAA and the results of (1) and (2).

Due to extensive experience assessing the FAA Continuous Lower Energy, Emissions, and Noise project (CLEEN I), Georgia Tech was selected as the lead for all three objectives described above [1]. Stanford and Purdue supported the objectives as shown in Table 1, listing the high-level division of responsibilities amongst the universities.

Table 1: University Contributions

Objectives		Georgia Tech	Stanford	Purdue
1	Harmonize Fleet Assumptions	Lead process, coordinate industry, government participation, provide basis for discussion	Support assumptions definition, provide expert knowledge	Support assumptions definition, provide expert knowledge
2	Advanced Vehicle and Technology Modeling	Use **EDS** for public domain technology modeling, Provide tech models to Stanford and Purdue	Input into public domain technology modeling	Develop cost, fuel burn, block hour values for aircraft models from Georgia Tech
3	Vehicle and Fleet Assessments	Perform vehicle and fleet level assessments using **GREAT** and **ANGIM**	Provide trade factors for mission specification changes using **SUAVE**. Provide tech factors for some tech modeled in (2)	Fleet-level assessments using **FLEET**

EDS – Environmental Design Space
GREAT – Global and Regional Environmental Analysis Tool
ANGIM –Airport Noise Grid Integration Method
SUAVE – Stanford University Aerospace Vehicle Environment
FLEET – Fleet-Level Environmental Evaluation Tool

Georgia Tech led the process of conducting four virtual workshops to collect feedback from industry, academia, and government on potential future scenarios for fleet and technology evolution and evaluation. This work was performed under objective (1) and the outcome is a set of technology and fleet evolution descriptors in a format suitable for use in a wide variety of modeling tools and future analyses. Under objective (2), Georgia Tech used the EDS conceptual modeling tool to create future representative vehicles consistent with the technology evolution scenarios defined under objective (1). Finally, Georgia Tech exercised the GREAT and ANGIM toolsets under objective (3) to assess potential future fleet-wide impacts of aviation.

Stanford provided input based on its experience in applicable public domain technology modeling identified under objective (2) across the entire time horizon contemplated in this work. Stanford has also provided trade factors, resulting from redesign/resizing of all vehicle classes to account for changes in mission specification changes for a public domain mission analysis to be completed under objective (3). This task has helped to define the interfaces between Stanford's expertise with assessing mission specification changes and Georgia Tech and Purdue's expertise with fleet analysis.

Purdue has applied their FLEET tool under objective (3), using a subset of the fleet assumptions defined in objective (1) and public domain vehicle performance generated by Georgia Tech in prior years. This activity has demonstrated the capabilities of FLEET for assessment of fleet-level noise and emissions evolution as a result of new aircraft technologies and distinct operational scenarios.

Major Accomplishments

The following were the major tasks completed under ASCENT Project 10:

Fleet Level Workshop Assumption Setting

Fleet assessment scenarios have been developed by Georgia Tech using input from the project team and virtual workshops comprising industry, university, and government experts. The scenarios are descriptive and are defined through standard future state descriptors such as Gross Domestic Product (GDP) growth, fuel price, and high or low investment in technology. Using these well understood descriptors allows the defined scenarios to be used in a wide range of modeling tools. The defined fleet scenarios are intended to provide bounding cases on future U.S. fleet-wide performance to inform technology development and goal setting.

Technology Level Workshop Assumption Setting

Georgia Tech defined technology development assumptions that are used to drive fleet level predictions of key environmental metrics. These are called technology development roadmaps (or infographics), which provide key information on technology impact, readiness, and estimated development time until entry into service. The technology roadmaps are intended to support future modeling efforts and are tool agnostic.

Evaluation of Impact of Demand and Technology on Future Fleet CO_2 and Noise

Georgia Tech and Purdue used their respective fleet and vehicle simulation models to predict the fleet noise and CO_2 resulting from the defined technology and fleet evolution scenarios. The results indicate that the rate of technology insertion is the major driving factor in reducing fleet wide CO_2 emissions. While CO_2 is a major contributor to the climate, other factors such as particulate matter and contrails were not investigated in the scope of this project. Reducing noise below current levels appears to be achievable even with significant operations growth; however, noise reduction is also dependent on the rate of technology insertion.

Demonstration of FLEET

Purdue used their FLEET modeling tool to simulate a series of future aviation scenarios developed in discussion with the FAA and using public domain Georgia Tech modeled N+1 and N+2 generation aircraft instead of the Purdue modeled aircraft in FLEET. With further studies, Purdue assessed the sensitivity of future aviation emissions to variations in fuel prices, market demand, and the dates of technology availability leveraging the outcomes of the fleet and technology workshops. This demonstration of FLEET capabilities preceded the studies to investigate the scenarios defined for this project.

Vehicle-Level Assessment of Mission Specification Changes

The group at Stanford University has focused on (a) the development of the necessary analysis and optimization capabilities within the Stanford University Aerospace Vehicle Environment (SUAVE) framework, (b) the development and validation (with publicly-available data) of model vehicles in each of the five ICAO/CAEP aircraft classes, and (c) a study of the fuel-burn-reduction opportunities afforded by decreases in cruise Mach number when re-designing (including airframe and engine) these aircraft. All redesigned vehicles have been validated and tested and have been done at current levels of technology and also at more advanced (N+1 and N+2 levels) levels of technology. These improved vehicles have been provided to the rest of the team, so that they can insert such vehicles in the fleet-level analyses done with the Georgia Tech GREAT and Purdue FLEET tools (Task #3 Section). The Stanford team has also supported the team's activities for the preparation and conduct of both the fleet-level and technology workshops.

Task #1: Developing Technology and Fleet Evolution Scenarios

Objective(s)

In order to develop assumptions suitable for a forward looking fleet level analysis that incorporates new vehicle technologies, it is necessary to forecast the future. However, most forecasts are extrapolations of the current status quo and trends, which assume an undisturbed continuation of historical and recent developments. This type of forecasting is necessary and useful, but misses significant changes or disturbances to the current market environment. If one considers changes to the status quo or constraints that might prevent current trends to continue, a possibility space of overwhelming dimensionality opens up. This dimensionality makes it intractable to fully explore all possibilities. This Task focused on the development a standard methodology for capturing potential future states of technology and fleet development. Technology impact is fundamentally captured through the impact of a technology on vehicle performance, emissions, and noise, coupled with the availability of a technology on a given platform within a given timeframe. The fleet impact, or the combined impact of multiple aircraft of varying technology levels flying within a given year, is defined broadly though demand and retirement assumptions. Demand is driven by external factors such as GDP growth and ticket price. Retirement rates are also dependent on certain external factors. This task first conducted virtual workshops to define the external factors that are most important to fleet and technology evolution. A second round of workshops was held to define quantitative inputs to the defined factors.

Summary of Resulting Technology Evolution Scenarios

This section provides a brief overview of the outcomes of the two fleet and technology workshops. A complete description of the data identification, solicitation, and reduction processes for both fleet and technology are described in sections 0 and 0, respectively.

Two fleet workshops were held. The first workshop focused on defining important descriptors and worldviews. The second workshop focused on defining ranges for the selected parameters and defining interesting variations. The team then used the results of both workshops to define a set of scenarios with well-defined parameter settings.

Research Approach

Research Approach Overview

The approach taken was to reduce the overwhelming dimensionality of conventional fleet analysis by selecting a small number of well-defined scenarios. The selected scenarios should encompass future states that are important for specific consideration of significant changes that could occur and also to bind some of the most important future outcomes that could conceivably occur. Therefore, the first goal of the workshop series was to define a range of scenarios to bound aviation's environmental impacts in the future and to examine the effects of aircraft technology on these impacts.

Due to the diverse expertise needed to come to consensus on a set of scenarios, two parallel workshop tracks were undertaken. The first track focused on fleet level trends and assumptions, including future demand and fleet evolution. A second track focused on the state and future of aircraft technologies that reduce fuel burn, emissions, and noise. The information gathered in both these focused workshop tracks was combined to fully define future bounding scenarios and assess the potential of aircraft technology to improve aviation's environmental impact. The fleet level trends and technology trending workshops are discussed in the following sections.

Fleet Workshops

Based on the Fleet Scenario Workshops that were conducted through the summer and fall of 2015, the team created a series of conclusions from the data obtained from the workshop participants. This includes prioritizations of the factors that describe a scenario as well as evaluations of some provided suggested example scenarios and scenarios that the participants were able to customize. This was then used by the team in the first half of 2016 to formulate a number of scenarios through a series of discussions. The final selection stands at twelve scenarios, which are shown in **Table 3**. The specific settings for each of the scenarios are colored by nominal (blue), low (purple), and high (orange). These values were outcomes of the Fleet Workshops and were obtained by analyzing the data that was collected from the participants.

Fleet Workshop One

The goal of the first workshop was to determine what defines a world view or scenario. Therefore, the workshop was designed to gather feedback on the descriptors including variables, ranges of values and importance. Additionally, some initial worldviews were shown to solicit comments from the workshop participants.

This was done in order to define a range of scenarios to bound aviation's environmental impacts in the future and examine effects of aircraft technology on these impacts. The workshop was used to gather feedback on the assumptions for use in future U.S. fleet assessments to 2050 and was composed of the following sections:

- Relative importance of descriptors
- Selection of descriptor ranges (high, medium, low values over next 35 years)
- Selection of descriptor values for worldviews proposed

The initial list of worldview descriptors was down selected and refined by the team in order to focus the workshop on key factors, yet still allow the participants a good amount of room to further refine the list of key descriptors. The descriptors selected to be discussed at the workshop were broken into categories and were then individually presented with background information, a description, the impact on aviation, definition of units, as well as a specific question to answer for selecting a specific numerical answer. These descriptors proposed to the workshop participants are detailed in this section.

Each descriptor was presented to workshop participants on a single slide. An example of a descriptor is shown in **Error! Reference source not found.** for GDP. The idea was to comprehensively present a quick overview of each descriptor that was preselected and introduce the audience to it by showing a brief description and an explanation on how it might impact aviation. Additionally, background information with references was also included. This was then punctuated by specific units and a direct question to answer in the survey to be filled in by the participants.

In order to create the final scenarios, a series of two fleet workshops were held to engage participants from industry, academia, and government and to gather a diversity of opinions and expertise. The first workshop was held on May 14th 2015. Attendees included representatives from: The U.S. Air Force, Airports Council International – North America, Booz Allen Hamilton, Boeing, Department of Transportation Volpe Center, Embraer, FAA Office of Environment and Energy, FAA Office of Aviation Policy & Plans, Georgia Tech, Honeywell, Mitre, NASA, Pratt & Whitney, Purdue, Rolls-Royce, Stanford, Textron Aviation and Virginia Tech. The purpose of this workshop was to decompose the scenario assumptions for the fleet level analysis into high level descriptions of an envisioned future state, which by themselves could include multiple scenarios. Scenarios themselves, however, were intended to be detailed specific descriptions of a future state within a particular worldview.

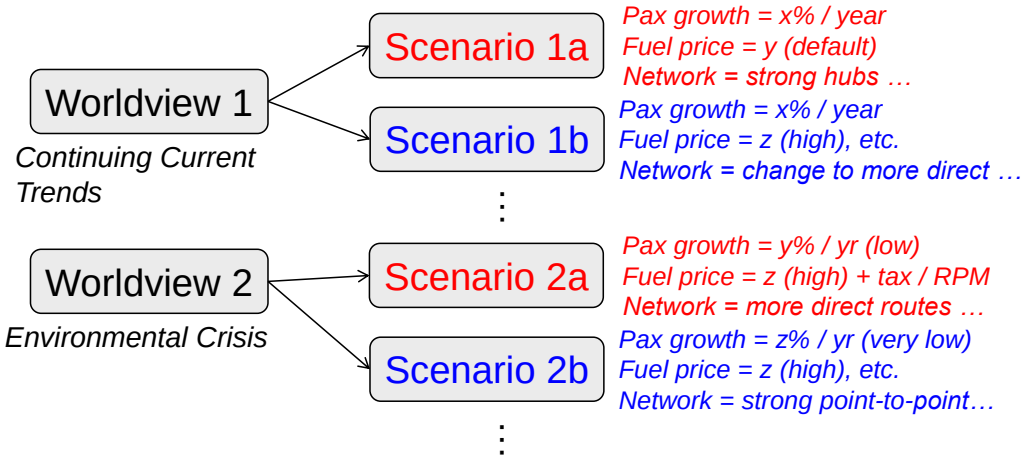

Figure 1: Decomposition of Fleet Assumptions into Worldview and Scenarios

An example of this is shown in Figure 1, where worldviews and scenarios were be used to derive specific assumptions listed on the right. Revenue Passenger Miles (RPM) is a high level metric of aviation demand activity and represents the product of passengers multiplied by miles travelled. The goal of this first workshop was to agree on a variety of worldview and scenario descriptors by asking the attendees about the relative importance of a list of preselected descriptors. Additionally the attendees were given the opportunity to suggest additional descriptors that were not already listed in the survey. Furthermore, the workshops purpose was to define a set of low/medium/high levels for each descriptor. To this end the workshop materials were created with as specific a definition and quantifiable units of each descriptor as possible.

For the purpose of the workshop, the preselected descriptors were grouped into themes that as a whole cover the entire spectrum of assumptions necessary to define future states of aviation. The themes were:

- Economic Factors
- Aviation Industry Factors
- Environmental Factors
- Technological Factors

The potential descriptors were based on existing forecasts. Of those available, the three most commonly used were selected to provide the current trends or values that illustrate the importance of a specific descriptor. These were:

- FAA Aerospace Forecast
- Boeing – Current Market Outlook (CMO)
- Airbus – Global Market Forecast (GMF)

Furthermore, it should be noted that the specific assumptions and predictions contained in these forecasts are subjective and as a result can vary to some degree – in some cases drastically – between them. The following subsections provide in-depth descriptions of each of the descriptor categories listed above.

Economic Factors

Gross Domestic Product (GDP) Growth

The first descriptor is probably one of the most important economic variables: gross domestic product. GDP describes the overall economic development of a specific region or country and is thought to be representative of a nation's wealth. Changes in GDP are primarily due to two components. First is the change in economic activity, when expressed in per capita terms. This introduces the second component such as the change in population. Together, these drive changes in the overall wealth of a country. As shown in Figure 2, aviation trip demand is highly correlated to GDP per capita. Large increases in travel trip demand occur when growing from low levels. Smaller increases in travel demand occur when growing from higher levels. Shown in Figure 3 are the levels of the annual percent growth from the FAA Forecast. Therefore the unit for this descriptor was selected as the percent average annual GDP growth in percent per year. The question asked from attendees was: What is the future annual change of U.S. GDP growth?

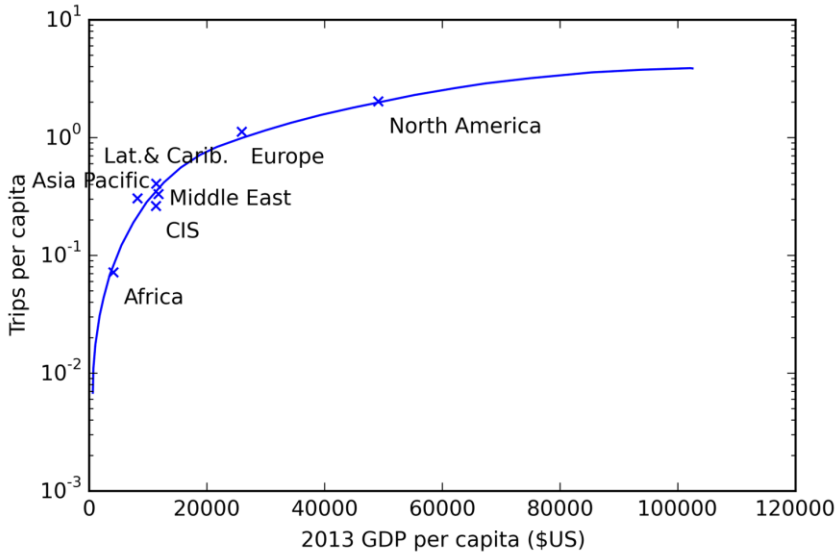

Figure 2: Aviation Demand is Driven by per capita GDP, Adopted from [2]

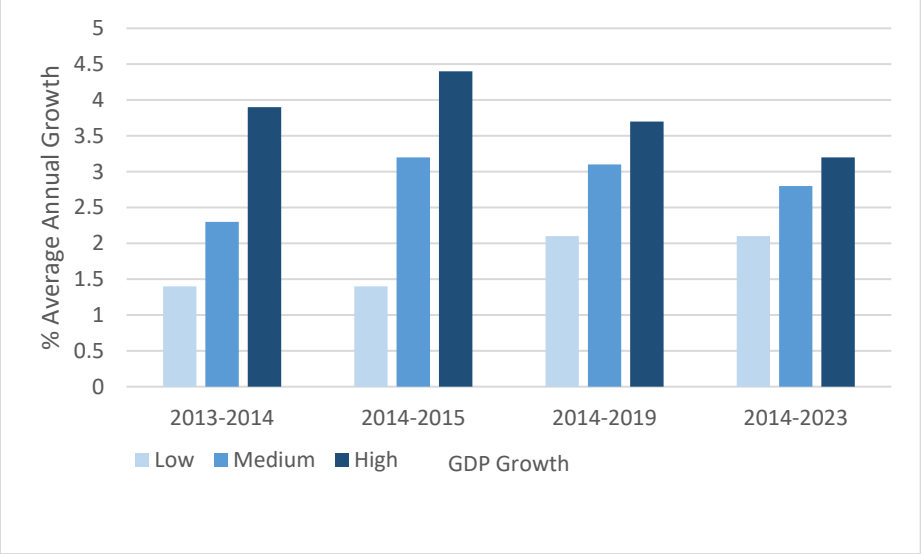

Figure 3: GDP Growth [2]

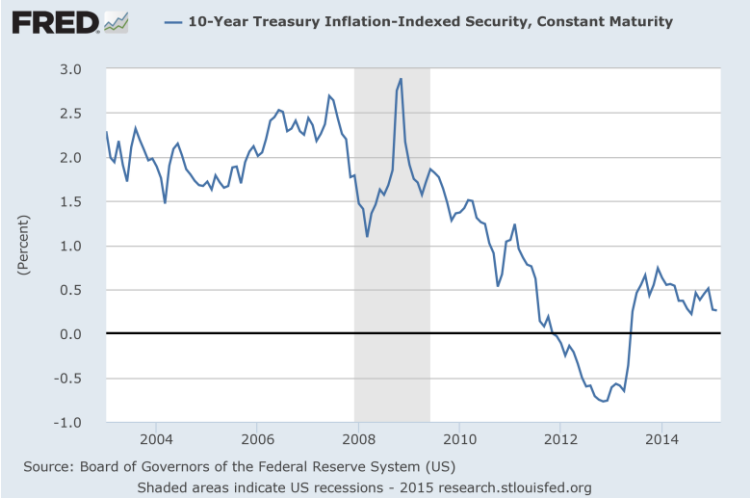

Figure 4: 10 Year Treasury Inflation Indexed Security Interest Rate

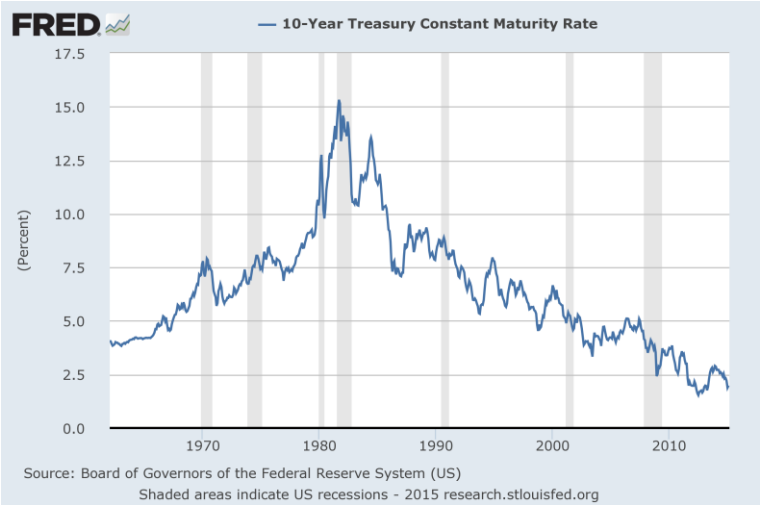

Figure 5: 10 Year Treasury Constant Maturity Interest Rate

Interest Rates

Interest rate is usually the rate at which interest is accrued as a result of borrowing money. The importance for aviation is that it could serve as an important determinant in business decisions regarding whether launching a new aircraft project or purchasing a new aircraft are profitable. The interest rates that firms are offered are usually based on the risk free interest rate plus a risk premium. This is what is usually termed the cost of money, which is the interest rate used in Net-Present-Value or similar valuation approaches for decision making. Therefore, as an example Figure 4 and Figure 5 show the 10-Year Treasury interest rate development over the last decade. They represent as close as possible the risk free interest rate. Changes in this interest rate can have a significant effect on the interest rate charge to firms since it represent the underlying interest rate upon which most other interest rates are based on. The question asked to the workshop participants was: What is the future long term average real risk free interest rate?

Population Growth

Population is another underlying factor that is a large driver of economic activity that can lead to increased passenger traffic. Figure 6 shows the global population growth since 1950, with a forecast to 2050. The question asked attendees was: What is the future average annual U.S. population growth?

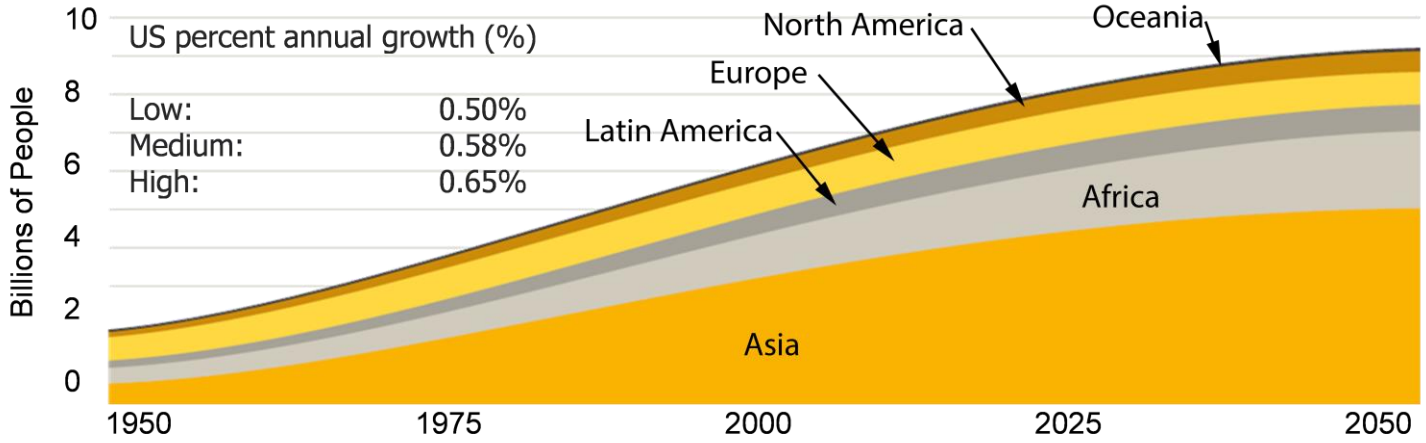

Figure 6: Global Population Growth, Adopted from [2] and U.S. Census 2014 Projections

Labor Force

The labor force composition describes the makeup and the number of people available to work. Some underlying demographics can cause significant long term shifts. The middle age group tends to travel the most with reduced travel demand in early and old age groups being observed. The question asked attendees was: What is the future average participation rate? Figure 7 shows the employment population ratio and the participation rate for the core working age groups. It shows that the participation rate has significantly increased as women entered the labor force. This trend has been reversing itself slightly due to various demographic factors. Also noticeable is the effect of recessions as people leave and re-enter the labor force.

Figure 8 shows the age distribution side of the demographics. These two factors together have an effect on aviation demand with regards to available income as well as travel behavior differences between different age groups.

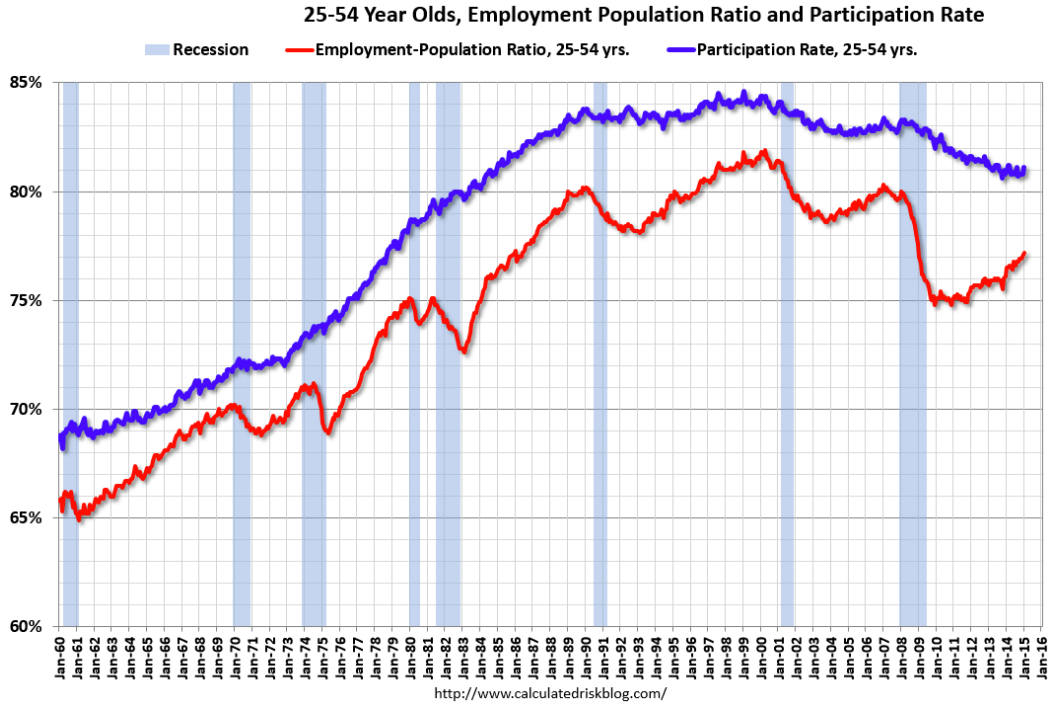

Figure 7: Participation and Employment-Population Ratio [Calculated Risk from BLS Data]

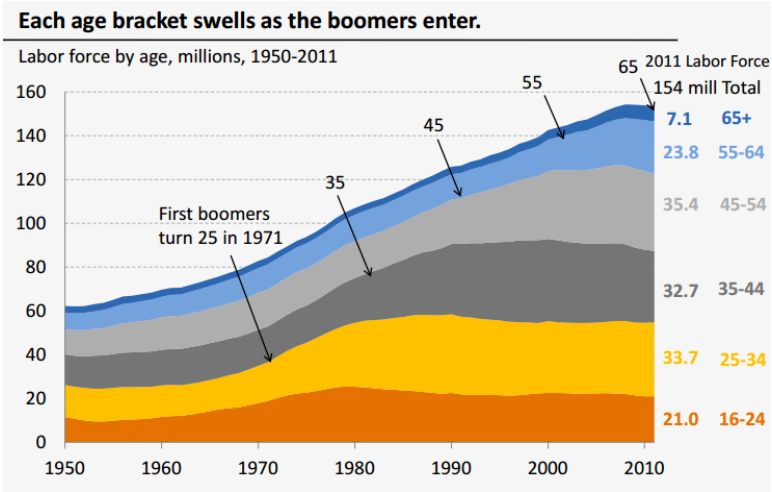

Figure 8: Age Distribution, Adopted from [2]

International Trade

International trade measures the exchange of capital, goods, and services across international borders or territories. It can represent a significant portion of a country's GDP. This portion of GDP is highly influenced by global trade policies, that either represent open border or protectionist policies. Therefore, shown in Figure 9 is the trend of the share of exports to GDP for the U.S. for the last 60 years. What can be observed is a long term trend of increases from very low levels. The last few years showed the share of GDP to be as high as almost 14%. Furthermore, the amount of this trade is influenced by the economic growth outside of the U.S. Therefore, Figure 10 shows the economic growth rates around the world that are

significant for aviation from the latest FAA Forecast. Attendees were asked the following question: What is the future average GDP growth in the major international trade partner regions?

Figure 9: U.S. Share of Exports to GDP

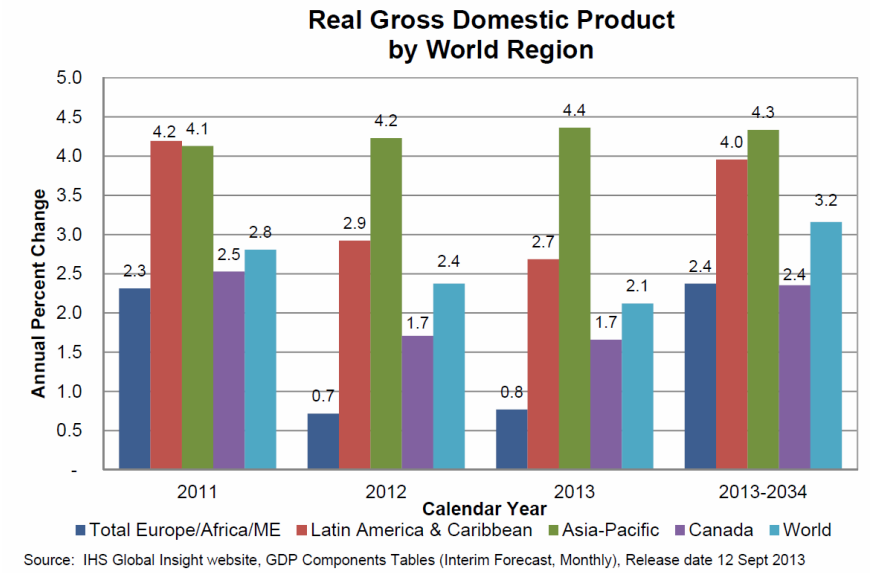

Figure 10: Global GDP Growth Rates [3]

Modal Competition

Competition between various modes of transportation such as airplanes, cars, trains, buses, etc. represent the popularity of each form of travel. Changes in the modal shares depend heavily on travel times and cost. Significant technological advances in different mode of transportation may change the aircraft travel demand. A common mode share determinant is trip distance. Figure 11 and Figure 12 show the total person trip distribution and the percent share for a few select types of transportation. The data used to create these charts is from the 1995 American Travel Survey. The question asked the attendees was: What is the average future aviation mode share trend for the 400-1000mi distance trips?

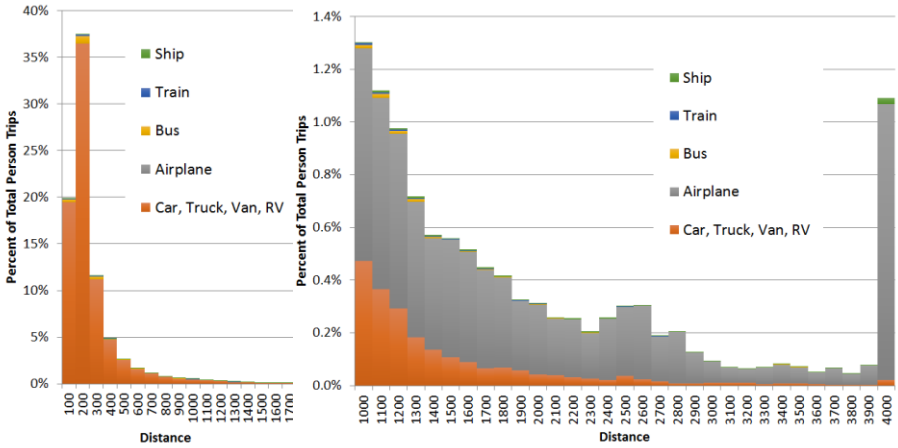

Figure 11: Total person Trip Distribution [5]

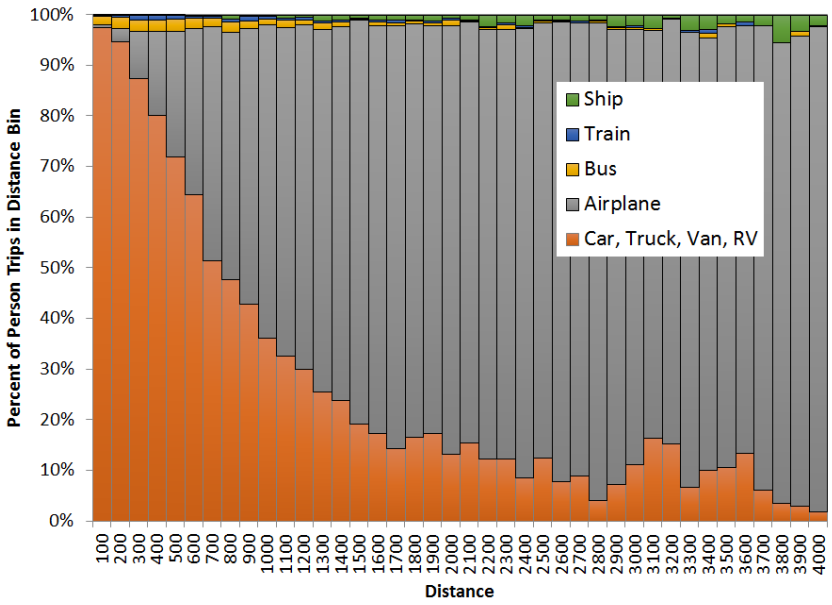

Figure 12: Modal share as a Function of Distance [2]

Energy Price

The price paid for energy, specifically in the case of aviation the price of aviation fuels, is an important factor that determines the cost of travel for aviation. Figure 13 shows the price of oil both in recent decades as well as in the near future. The underlying fundamental factor is the price that refineries charge to produce aviation fuels and pay for the raw crude oil. Therefore, the attendees were asked the following question: What is the future trend of the oil price?

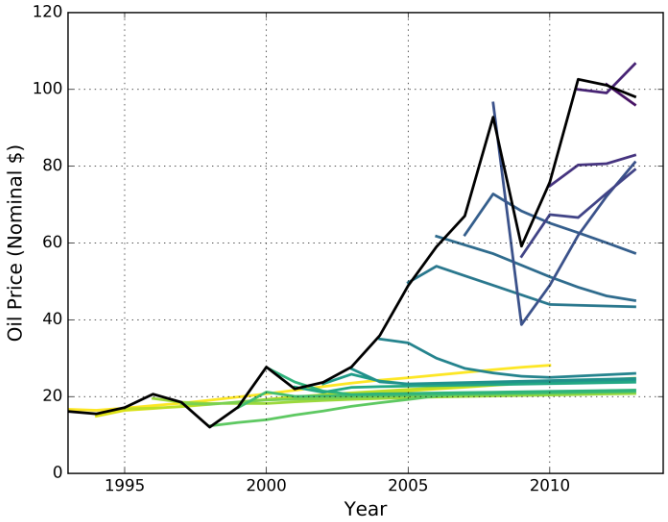

Figure 13: Analysis of EIA Annual Energy Outlook Forecasts [2]

Figure 14 and Figure 15 show the survey questions for the economic factors described in the previous sections.

The following **economic factors** have been selected to describe potential world views. Please rank them in their relative slope/sensitivity of potential impact to describe any potential world views.

	No Impact	Very Low Impact	Significant Impact	Very High Impact	Not Sure
GDP Growth (avg. annual growth)	○	○	○	○	○
Interest Rates (avg. annual growth)	○	○	○	○	○
Population Growth (avg. annual growth)	○	○	○	○	○
Labor Force Composition (participation rate)	○	○	○	○	○
International Trade	○	○	○	○	○
Modal Competition (% share)	○	○	○	○	○
Energy Price ($/bbl)	○	○	○	○	○

Figure 14: Survey Economic Factors Importance

As mentioned previously, the questions related to the values for each major descriptor required quantitative replies, with attendees asked to indicate low, medium, and high values for possible futures.

Descriptor	Units	Disagree?	Low	Medium	High	Explanation
GDP Growth (Domestic)	%/yr	☐	2.1	2.8	3.2	
Interest Rates	%/yr	☐	2.0	8.5	15.0	
Population Growth	%/yr	☐	0.50	0.58	0.65	
Labor Force Composition	%	☐	68.0	76.0	84.0	
GDP Growth: Asia	%/yr	☐	3.6	4.3	5.0	
GDP Growth: Europe	%/yr	☐	0.6	2.4	4.2	
GDP Growth: Latin America	%/yr	☐	2.7	4.0	5.3	
Modal Competition	%	☐	20.0	50.0	80.0	
Energy Price	$/bbl	☐	40	70	150	

Figure 15: Economic Factors Ranges

Environmental Factors

CO_2 Emissions

CO_2 emissions are directly proportional to the amount of fuel consumed. There are concerns about the effects these emissions have on the global climate. Therefore, it is possible that airlines could face some charges for these emissions in the future. The charge in effect currently in Europe is through the European Emissions Trading System (ETS), whose trends are shown in **Figure 16**. It shows the EU ETS annual cap (Cap), annual verified emissions from sources covered by the EU ETS (Emissions), annual offsets surrendered for compliance (Offsets) and average annual future rolling prices (CO_2 price) [7]. Due to variety of charging schemes possible, the question asked the attendees was simplified to: What is the future average cost of CO_2 emissions?

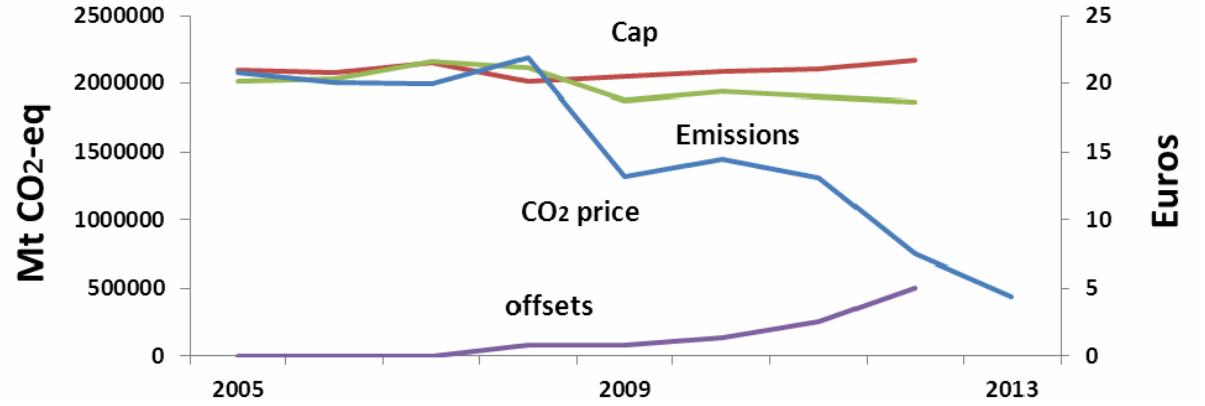

Figure 16: European ETS CO_2, Price and Quantity [2]

NO_x Emissions

NO_x Emissions are of concern due to the effect on the air quality in communities surrounding airports. NO_x emissions are of particular interest as there are existing airport charges related to NO_x emissions and Heathrow recently proposed a significant increase in their NO_x charges [2]. Therefore, concerns about NO_x emissions could result in airline operational charges. The

modeling use would be thorough effects of additional costs on demand, airline decisions, and manufacturer decisions. The question asked the attendees was: What is the future average cost of NO_x emissions at these U.S airports?

Airport Abbreviation	Airport Name
ATL	Hartsfield - Jackson Atlanta Intl
BOS	Boston Logan Intl
BWI	Baltimore/Washington Intl
CLT	Charlotte Douglas Intl
DCA	Ronald Reagan Washington National
DEN	Denver Intl
DFW	Dallas/Fort Worth Intl
DTW	Detroit Metropolitan Wayne County
EWR	Newark Liberty Intl
FLL	Fort Lauderdale/Hollywood Intl
HNL	Honolulu Intl
IAD	Washington Dulles Intl
IAH	George Bush Houston Intercontinental
JFK	New York John F. Kennedy Intl
LAS	Las Vegas McCarran Intl
LAX	Los Angeles Intl
LGA	New York LaGuardia
MCO	Orlando Intl
MDW	Chicago Midway
MEM	Memphis Intl
MIA	Miami Intl
MSP	Minneapolis/St. Paul Intl
ORD	Chicago O`Hare Intl
PHL	Philadelphia Intl
PHX	Phoenix Sky Harbor Intl
SAN	San Diego Intl
SEA	Seattle/Tacoma Intl
SFO	San Francisco Intl
SLC	Salt Lake City Intl
TPA	Tampa Intl

Figure 17: Core 30 U.S. Airports

The additional question was asked: What percent of the Core 30 U.S. airports do you envision will charge for NO_x emissions? A list of Core 30 airports given to the participants is shown in Figure 17. They are the core airports used by the FAA to measure Airspace System Performance Metrics (ASPM) [3].

Non-Volatile Particulate Matter Emissions

The inclusion of non-volatile particulate matter (nvPM) emissions was due to the concern about the effects of these emissions on air quality, which could result in an impact on health and economic considerations such as airline operational charges. Non-volatile particulate matter emissions are the primary pollutant impacting air quality and community health impacts in the vicinity of airports.

The background information presented was limited to mentioning that standards and regulations are currently in development and advances in alternative fuels and combustion designs will help mitigate production of particulate matter. The units suggested for numeric responses were dollars per kg nvPM emissions in (USD/kg). The suggested modeling use was primarily through the effect of additional costs on demand, airline decisions, and manufacturer decisions. The questions asked participants were: Do you think that nvPM emissions will have a cost in the future? If so, what percent of the Core 30 U.S. airports do you envision will charge for nvPM emissions? What is the future average cost of nvPM emissions at these U.S. airports?

Noise

Noise here refers to noise produced by aircraft or its components during various phases of flight. The area around airports exposed to significant noise depends on the number of flight operations, the operational details, and type of the aircraft used. If the number of operations increases, then the noise emissions per aircraft operation have to decrease in order to avoid increasing the relative area. Concern about the effects of airport noise on the health and quality of living could result in airline operational charges. For example, limits on activity and frequency of flights as well as scenarios with more stringent noise constraints could be envisioned. The metric selected in this case for noise limits was defined as the percentage of the core 30 U.S. airports that could have noise limits similar to a quota count system that tries to enforce the maximum noise limits by capping the operations counts that are allowed, depending on the noise levels of the aircraft used. This can be used in modeling by forcing airline and manufacturer decisions through possible operational limits which can then affect aircraft choice. The questions participants were asked to answer were: What percent of the core 30 U.S. airports do you think are currently noise limited? What percent of the core 30 U.S. airports do you envision will be noise limited in the future?

Aviation Industry Factors

Quality of Service

Quality of service represents the quality or service provided by airlines. This includes services such as new nonstop city pairs as well as greater frequency in flights, thus resulting in more flexible flight times for passengers. Various airline operations scenarios can be modeled which would account for changes in airline quality of service. For example, more frequent flights and new nonstop city pair locations could be modeled by changing flight schedules. Figure 18 shows historical data from the BTS sample ticket database that is one attempt to measure how many passengers travelled on connecting flights instead of travelling on direct flights. This does not necessarily mean a direct flight would have been available, but rather that the passenger did have a connecting flight. Therefore modeling use could be achieved by potentially adjusting how passenger Origin-Destination demand is served by airlines with actual flight connections. The metric used here was the ratio of total to only direct tickets. The question participants were asked was: What is this ratio in 2050?

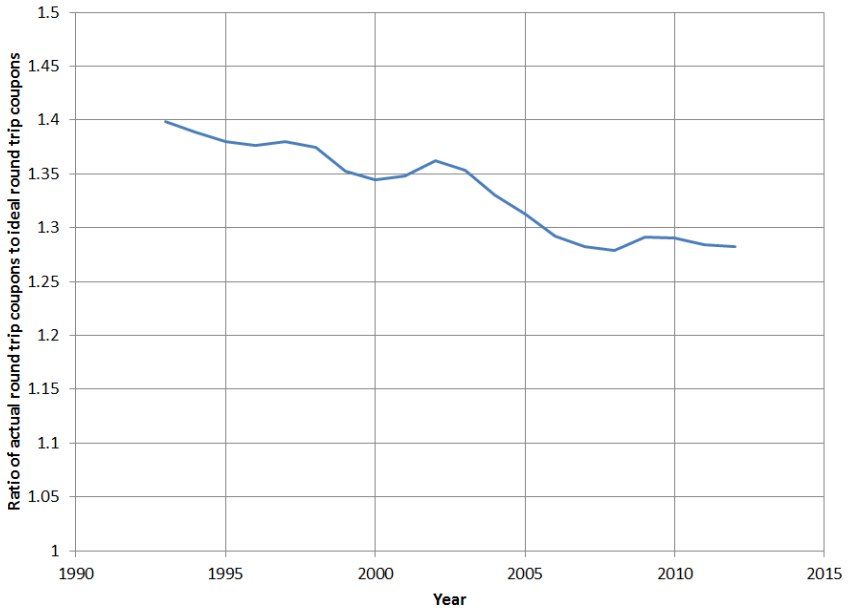

Figure 18: Ratio of Actual to Ideal Round Trip Coupons [4]

Travel Attractiveness

This refers to the amenities provided during travel such as how long it takes to go from leaving home to boarding the plane, how many flights are offered in a given time period, cabin comfort, and seat pitch. Improvements in travel attractiveness could lead to increases in travel demand. The modeling use would be to adjust mode shares relative to competing transportation modes. This means that if more than one mode is available for a traveler, that the relative share given to aviation would be increased or decreased relative to the current status quo. The scale of unit is the relative attractiveness on a scale from 0-100. This is then further defined as relative attractiveness to other modes is compared. Equal 50 means it is even to average competing mode, greater than 50 means better than average competing mode, and less than 50 means worse than average competing mode. The question participants were asked was: What is the future average of the relative attractiveness of aviation?

Industry Competitiveness

This describes the level of competition between airlines as well as the cost structure. Some examples of this are: Number of airline competitors, airline consolidation, and new entrants to airline market. The unit for this factor that were used was: Yield per passenger/seat-mile or revenue per passenger seat-mile. This represents the revenue required to break even, which is strongly related to operating costs and the amount airlines can charge. Industry competition can lead to reduced prices and increased travel demand as a result of airlines competing for customers. The modeling use is to utilize the cost structure of airlines that can impact passenger demand. The question participants were asked was: What is the future average relative required passenger yield for airlines?

Openness of Air Services and Domestic Airline Regulation

This describes the level of flexibility of air services and domestic airline regulations. Reducing regulations – such as slot limits – could give airlines more freedom in planning routes, capacity, and pricing to improve operational efficiency. Some examples of this include: Open Skies Agreements, Lifting Ownership Restrictions, Code Share Agreements, and Gate Slot Assignments. The use in modeling would be through adjusting network structures and capacity. The unit used for this factor are relative normalized levels represent the extremes of open or restrictive with current in the middle. The question asked participants was: What is the future trend of airline regulations?

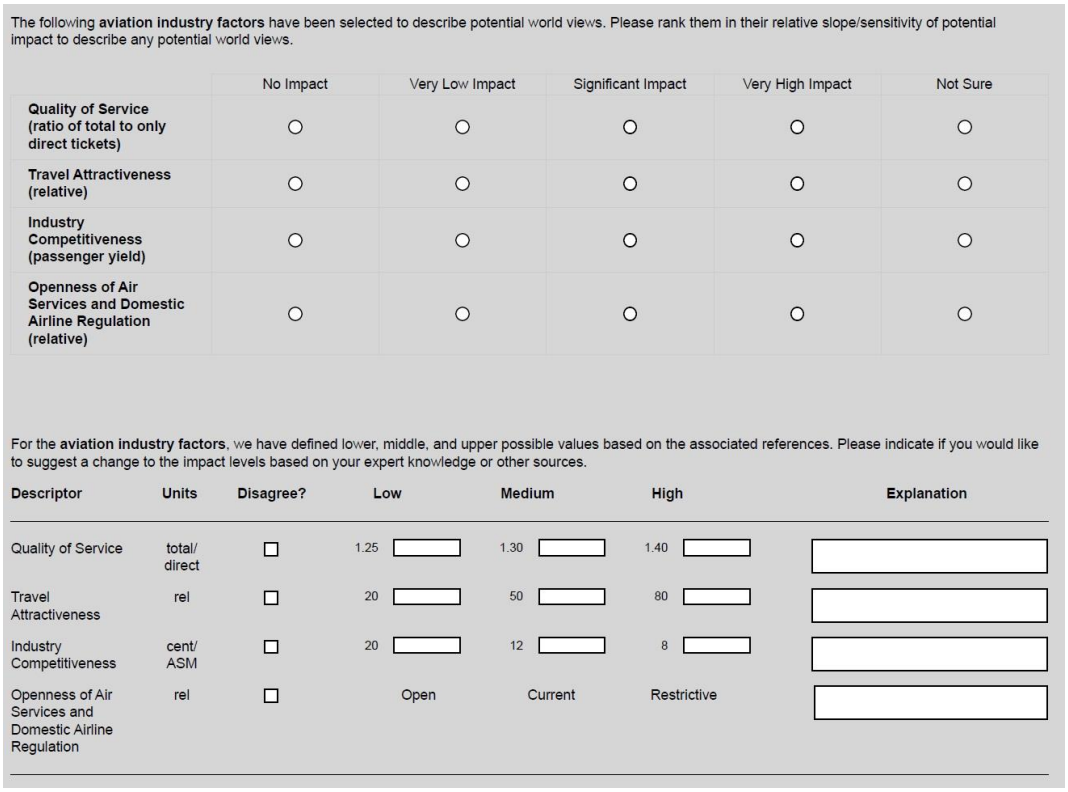

The following **aviation industry factors** have been selected to describe potential world views. Please rank them in their relative slope/sensitivity of potential impact to describe any potential world views.

	No Impact	Very Low Impact	Significant Impact	Very High Impact	Not Sure
Quality of Service (ratio of total to only direct tickets)	○	○	○	○	○
Travel Attractiveness (relative)	○	○	○	○	○
Industry Competitiveness (passenger yield)	○	○	○	○	○
Openness of Air Services and Domestic Airline Regulation (relative)	○	○	○	○	○

For the **aviation industry factors**, we have defined lower, middle, and upper possible values based on the associated references. Please indicate if you would like to suggest a change to the impact levels based on your expert knowledge or other sources.

Descriptor	Units	Disagree?	Low	Medium	High	Explanation
Quality of Service	total/ direct	☐	1.25	1.30	1.40	
Travel Attractiveness	rel	☐	20	50	80	
Industry Competitiveness	cent/ ASM	☐	20	12	8	
Openness of Air Services and Domestic Airline Regulation	rel	☐	Open	Current	Restrictive	

Figure 19: Aviation Industry Factors Section of the Workshop Questionnaire

Figure 19 shows the environmental factors section of the workshop questionnaire that participants were asked to fill out. As mentioned previously, the questions related to the values for each major descriptor required quantitative replies, with attendees asked to indicate low, medium, and high values for possible futures.

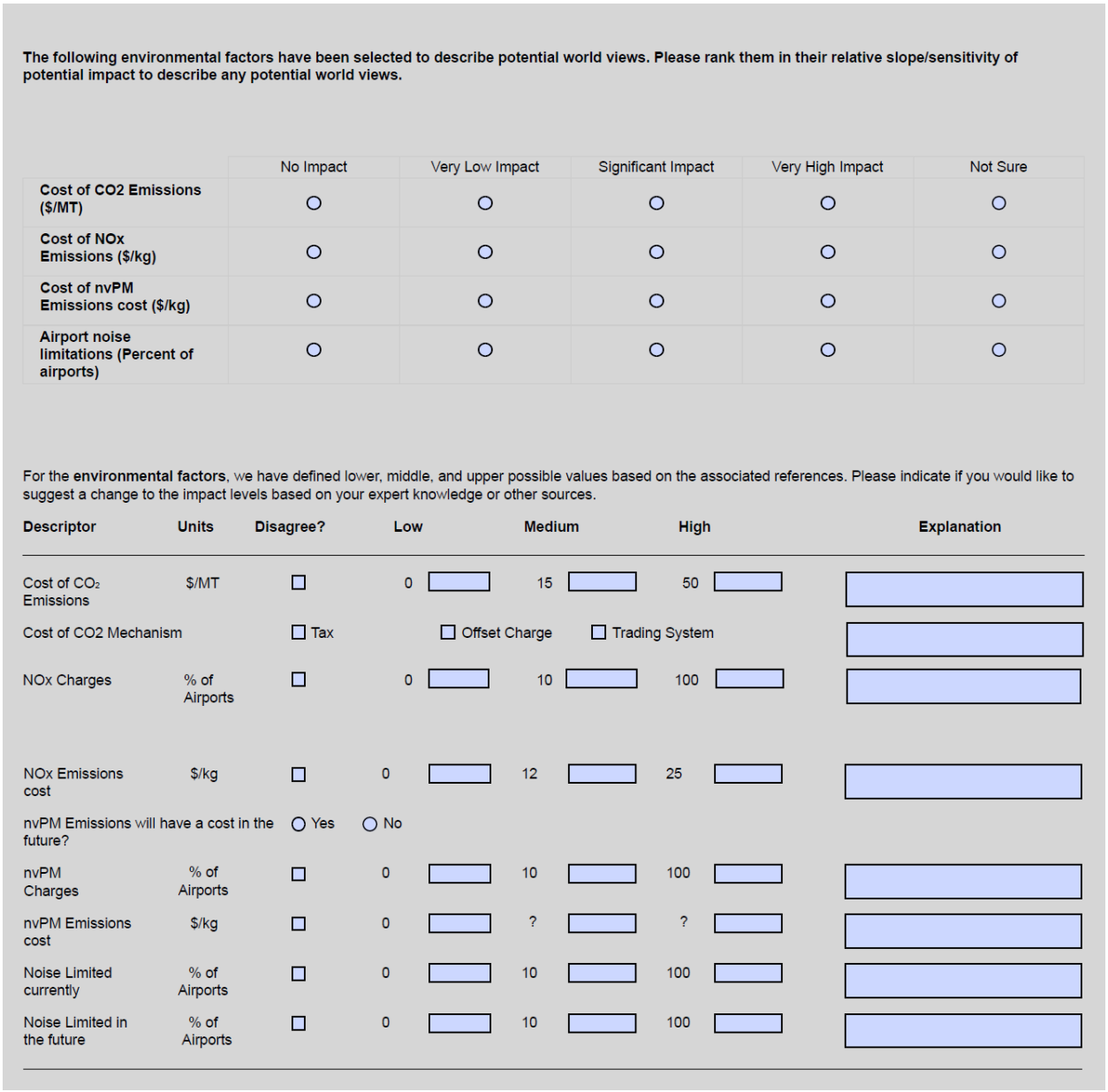

The following environmental factors have been selected to describe potential world views. Please rank them in their relative slope/sensitivity of potential impact to describe any potential world views.

	No Impact	Very Low Impact	Significant Impact	Very High Impact	Not Sure
Cost of CO2 Emissions ($/MT)	○	○	○	○	○
Cost of NOx Emissions ($/kg)	○	○	○	○	○
Cost of nvPM Emissions cost ($/kg)	○	○	○	○	○
Airport noise limitations (Percent of airports)	○	○	○	○	○

For the **environmental factors**, we have defined lower, middle, and upper possible values based on the associated references. Please indicate if you would like to suggest a change to the impact levels based on your expert knowledge or other sources.

Descriptor	Units	Disagree?	Low	Medium	High	Explanation
Cost of CO_2 Emissions	$/MT	☐	0	15	50	
Cost of CO2 Mechanism		☐ Tax		☐ Offset Charge	☐ Trading System	
NOx Charges	% of Airports	☐	0	10	100	
NOx Emissions cost	$/kg	☐	0	12	25	
nvPM Emissions will have a cost in the future?		○ Yes	○ No			
nvPM Charges	% of Airports	☐	0	10	100	
nvPM Emissions cost	$/kg	☐	0	?	?	
Noise Limited currently	% of Airports	☐	0	10	100	
Noise Limited in the future	% of Airports	☐	0	10	100	

Figure 20: Environmental Factors Section of the Workshop Questionnaire

Figure 20 shows the environmental factors section of the workshop questionnaire that participants were asked to fill out. As mentioned previously, the questions related to the values for each major descriptor required quantitative replies, with attendees asked to indicate low, medium, and high values for possible futures.

Technological Factors

Amount and Speed of Technology Research and Development (R&D) Investment

This refers to the level of funding and emphasis placed on aerospace technology research and development. Government R&D investment in technology could reduce the uncertainty of technology performance and accelerate the time at which manufacturers decide to launch new aircraft with the specific technology. The modeling use would be implemented the

through the availability of technology and also aircraft performance impacts. The units are a scalar with settings relative to current levels such as current, high and low. The question asked participants was: What is the future trend of government R&D investments relative to current trends?

Airline Load Factor Development and Limits

This describes limits imposed on the ratio of revenue passenger miles to available seat miles. This can be a measure of an airline's capability to match supply with demand. Improvements in airline load factors could result in reduced prices, increased travel demand, as well as increased industry competition. The modeling use is through airline supply of aircraft flying relative to passenger demand. The units are percent of aircraft seats occupied. Many forecasts currently suggest that this could peak at approximately 85% for the domestic U.S. An example of this is shown in Figure 21. Therefore settings for low/medium/high of 82%/83%/85% were suggested. The question participants were asked was: What is the future load factor limit?

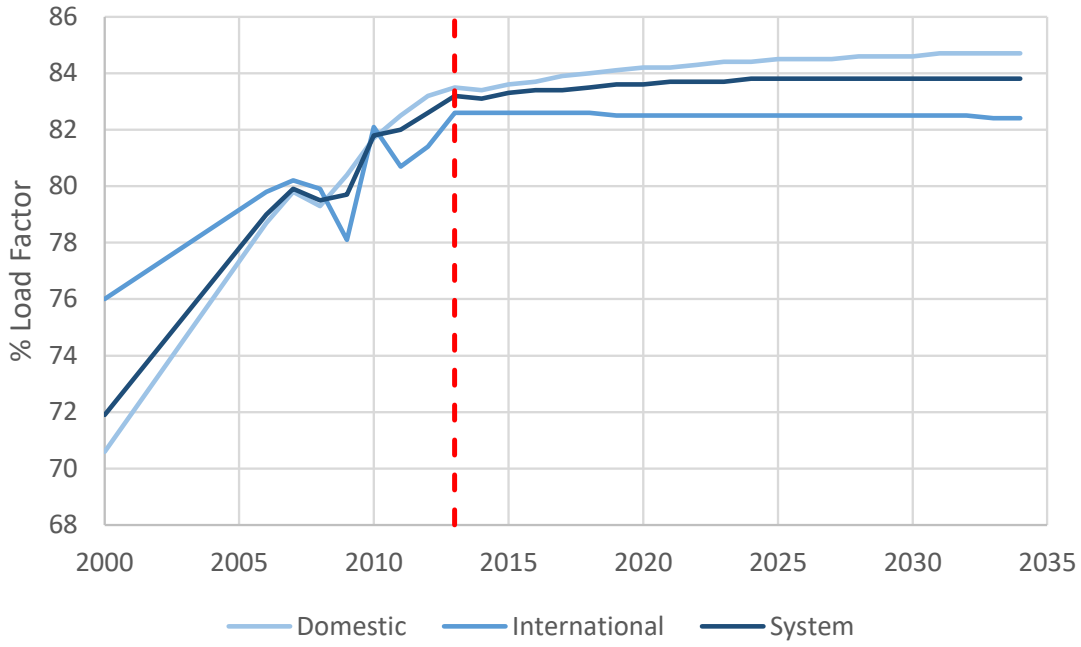

Figure 21: FAA Forecast Load Factor [3]

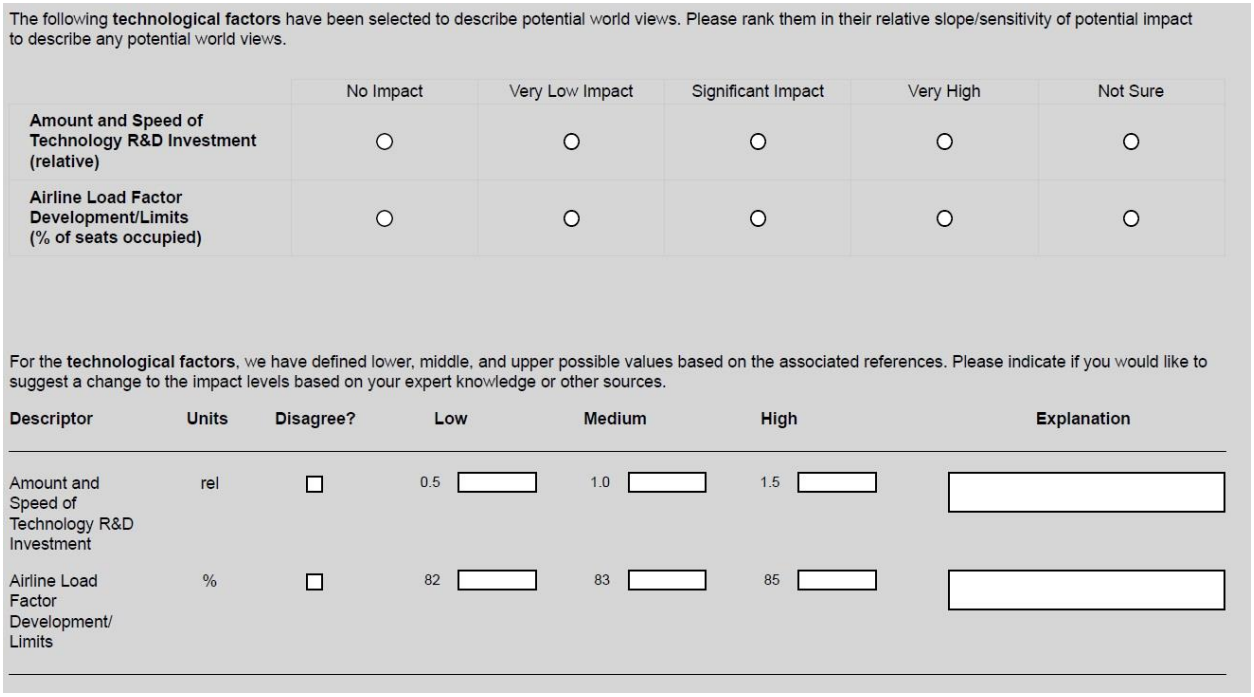

The following **technological factors** have been selected to describe potential world views. Please rank them in their relative slope/sensitivity of potential impact to describe any potential world views.

	No Impact	Very Low Impact	Significant Impact	Very High	Not Sure
Amount and Speed of Technology R&D Investment (relative)	○	○	○	○	○
Airline Load Factor Development/Limits (% of seats occupied)	○	○	○	○	○

For the **technological factors**, we have defined lower, middle, and upper possible values based on the associated references. Please indicate if you would like to suggest a change to the impact levels based on your expert knowledge or other sources.

Descriptor	Units	Disagree?	Low	Medium	High	Explanation
Amount and Speed of Technology R&D Investment	rel	☐	0.5	1.0	1.5	
Airline Load Factor Development/ Limits	%	☐	82	83	85	

Figure 22: Aviation Industry Factors Section of the Workshop Questionnaire

The results of the first workshop were used to generate a ranking of importance of the listed descriptors. **Table 2** shows the eight descriptors ranked by the attendees as the most important in order of decreasing importance.

Table 2: Descriptors in Order of Decreasing Importance

GDP Growth
Energy Price
Cost of CO_2 Emissions
Population Growth
International Trade
Airport Noise Limitations
Industry Competitiveness
Amount and Speed of Technology R&D Investment

This result was used to create the materials for the second workshop, where a number of worldviews were created using variations of each descriptor that came out of the first workshop.

Fleet Workshop Two

The goal of the second workshop was to select specific worldviews and scenarios of interest and define the corresponding values for each descriptor identified in Fleet Workshop One. Furthermore, the relationship between the worldviews defined and technology insertion opportunities and their timing was also explored. The worldviews proposed to the workshop attendees included two reference scenarios, several demand driven scenarios and two scenarios hinging on the level of environmental constraints imposed.

The first reference worldview used demand growth forecasts and considered the environmental effects in 2050 if no new technology was introduced, holding all aircraft at present day in service technology through 2050. This “Frozen Technology”

worldview is not realistic, and is introduced only as a baseline. The second reference worldview is one where "Current Trends" are allowed to continue in all descriptors including technology introduction. This would be considered the most likely scenario with the moderate technology improvement expected without additional government investment.

The workshop participants were also asked to define descriptor values for four worldviews considering different levels of demand. Two of these worldviews saw prosperity driving a high level of demand across the globe and then explored two technology development options. The first sub-scenario considered the environmental impact caused by high demand without additional technology investment. The second sub-scenario examined to what extent accelerated technology investment could alleviate the environmental impact of a demand increase. Conversely, two sub-scenarios were defined probing the different technology investment schedules under a low or stagnated demand worldview. It should be noted that these worldviews were later expanded to include additional very high demand scenarios, and suppressed technology investment scenarios.

Finally, two worldviews were proposed focusing on the application of environmental constraints to reflect the impact of both operational/capacity restrictions and financial disincentives in the form of increased energy costs. This gave rise to an "Environmental Bounds Low" worldview where demand is suppressed, non-compliant aircraft are retired early, and technology investment must be high to meet the environmental constraints. Alternatively, an "Environmental Bounds High" worldview was offered, where demand increased significantly over time, aircraft were retired late and technology investment was not driven by environmental constraints.

Based on the worldviews defined, the workshop participants were asked to identify the importance of each descriptor (GDP, Population growth, etc…) under each worldview. Participants were also asked to set a value for the descriptor (Low/Medium/High) under each scenario proposed. Participants were given the opportunity of defining a custom scenario if they saw a need for it. Figure 23 illustrates a portion of the survey distributed to participants in order to collect descriptor values and importance for each scenario. The questions were presented at the workshop and provided in Excel form as a sheet to be filled out by the participants and returned.

The following columns contain different world views. Fill out each column for each corresponding world view, answering these questions:
What is the value of the descriptor for this world view?
Importance of the descriptor for the specific scenario: + important, - not important
Setting for that particular scenario (High/Medium/Low)

Descriptor	World View 1: High Demand/Prosperity	World View 2: Environmental Constraints	World View 3: Low Demand	Custom World View:
GDP Growth (%/yr)				
Interest Rates (%/yr)				
Population Growth (%/yr)				
Labor Force Composition				
International Trade (as a share of GDP)				
Modal Competition (% share)				
Energy Price ($/bbl)				

Figure 23: Worldview Definition Questionnaire Example

The participant responses were collected, summarized and used to define sub-scenarios within each worldview as illustrated by the Figure 24 below.

Worldviews

- 1) Current Trends
  - Useful as baselines for comparison – what difference is technology making?

Scenarios	GDP Growth (%/year)	Energy Price ($/bbl)	Cost of CO2 Emissions ($/MT)	Population Growth (%/year)	International Trade (%/year Asia)	Airport Noise Limitations (% airports noise limited in future)	Industry Competitiveness (cent/ASM)	Amount and Speed of Technology R&D Investment (relative)
1a: Current Trends Fixed Tech	2.8	77	21	0.58	4.3	25	12	0
1b: Current Trends In-Production Only	2.8	77	21	0.58	4.3	25	12	0
1c: Current Trends	2.8	77	21	0.58	4.3	25	12	1.02

  - Scenario 1a:
    - Current fleet technology and efficiency do not improve any more from current in-service
  - Scenario 1b:
    - Currently out of production aircraft are retired and replaced with in-production vehicles, but no newer technology vehicles are brought into production
  - Scenario 1c: Continuing Current Development
    - Technology improves at historic rates with medium settings for all important descriptors

	Units	Low	Medium	High
GDP Growth	%/year	1.8	2.8	4
Energy Price	$/bbl	41	77	181
Cost of CO2 Emissions	$/MT	0	21	85
Population Growth	%/year	0.45	0.58	0.68
International Trade	%/year Asia	3.3	4.3	5.9
Airport Noise Limitations	% of airports noise limited in the future	4	25	95
Industry Competitiveness	cent/ASM	20	12	8
Amount and Speed of Technology R&D Investment	relative	0.52	1.02	1.71

21

Figure 24: Example Summary of Data Collected from Participants Regarding Each Worldview

Another aspect investigated in this second workshop was fleet evolution, which is a key factor in allowing new technologies to enter the fleet. The workshop participants filled out surveys probing the future of very large and quad engine aircraft, and the likelihood of narrow body vs wide body aircraft development programs being first. Participants also answered questions regarding aircraft development program duration, and the interval between new aircraft or improvement package programs in the future. While these questions helped establish when new aircraft (incorporating the new technologies) are available to enter the fleet, productions rates will affect the rate at which the new aircraft can actually replace previous models. Therefore, workshop participants were also asked to answer questions regarding maximum and minimum production rates for each aircraft type.

The results of the second fleet workshop were compiled and the team had several internal discussions and formulated a final set of scenarios based on the results of the two workshops. These are shown in **Figure 25** as an overview how they align with the different corners of the scenario trade space. A final set of tables containing all scenarios with settings for each are detailed in Table 3 to Table 5.

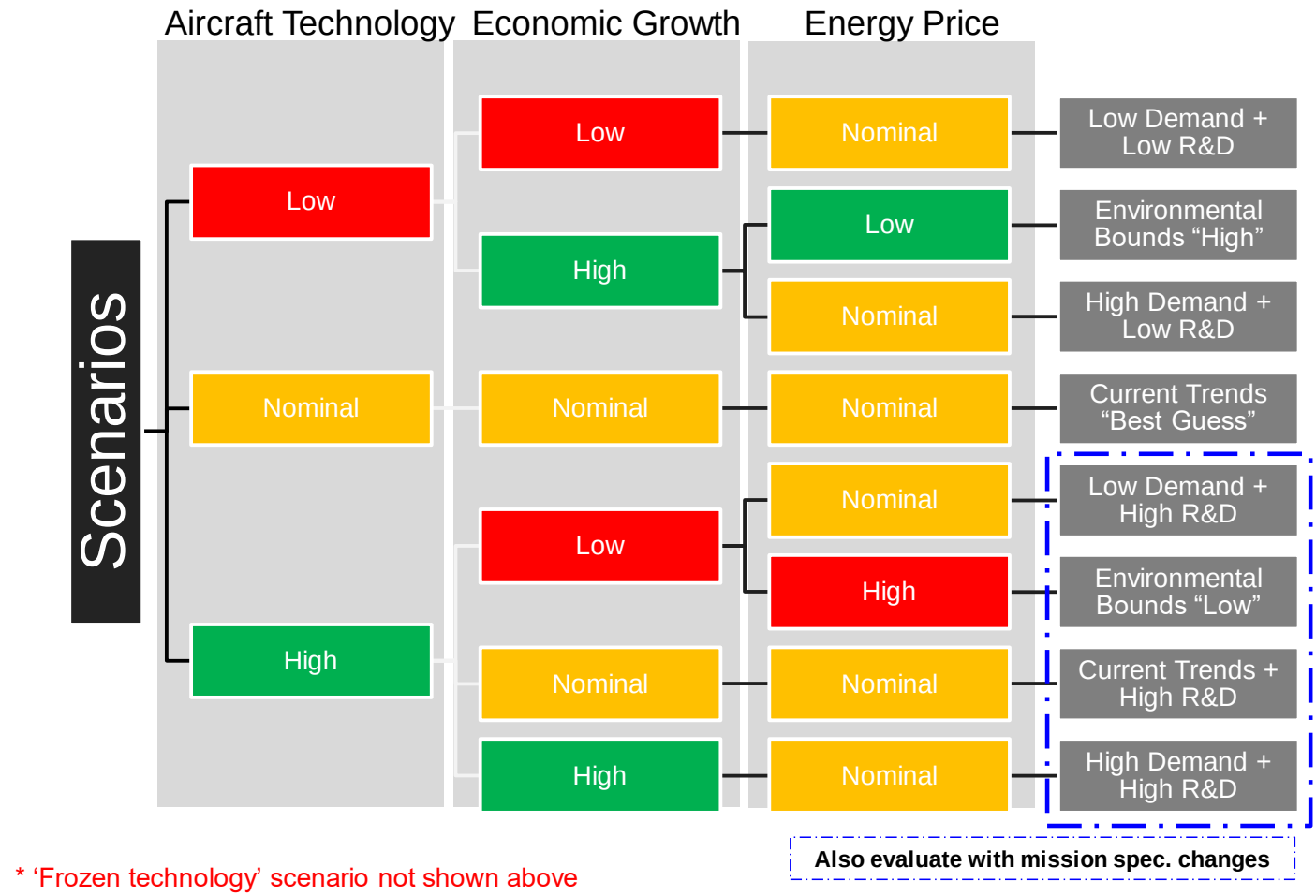

Figure 25: Scenario Tree Overview

Table 3 to Table 5 show the final matrix of scenarios. The scenarios are listed by row, whereas the columns list the final worldview descriptors with specific settings for each scenario. Each cell is colored from low to nominal to high settings.

Table 3: Matrix of Scenarios and Demand and Economic Model Factors

	GDP Growth (%/year)	Energy Price ($/bbl)	Population Growth (%/year)	International Trade (%/year Asia)	Industry Competetiveness (cent/ASM)	Airport Noise Limitations (% airports noise limited in future)	Cost of CO2 Emissions ($/MT)
Current Trends "Best Guess"	2.8	77	0.58	4.3	12	25	21
Current Trends + High R&D	2.8	77	0.58	4.3	12	25	21
Current Trends + High R&D + Mission Spec.	2.8	77	0.58	4.3	12	25	21
Current Trends Frozen Tech - In-Production Only	2.8	77	0.58	4.3	12	25	21
Environmental "Bounds" - Low	1.8	181	0.45	3.3	12	95	85
Environmental "Bounds" - High	4	41	0.68	5.9	12	4	0
High Demand (Including Global) + High R&D	4	77	0.58	5.9	12	25	21
High Demand (Including Global) + Low R&D	4	77	0.58	5.9	12	25	21
Low Demand (Including Global) + High R&D	1.8	77	0.58	3.3	12	25	21
Low Demand (Including Global) + Low R&D	1.8	77	0.58	3.3	12	25	21
Very High Demand with Noise Limits - Low R&D	4	41	0.68	5.9	12	95	0
Very High Demand with Noise Limits - High R&D	4	41	0.68	5.9	12	95	0

High
Nominal
Low

Table 4: Matrix of Scenarios and Fleet Evolution Model Factors

	Fleet Evolution Schedule	Aircraft Retirement	Production Capacity
Current Trends "Best Guess"	Nominal - Twin Aisle First in 2020s	Nominal	No Limits
Current Trends + High R&D	Nominal - Twin Aisle First in 2020s; Adjusted sequence if necessary for first application of new configuration/ architecture/ mission spec. change	Nominal	No Limits
Current Trends + High R&D + Mission Spec.	Nominal - Twin Aisle First in 2020s; Adjusted sequence if necessary for first application of new configuration/ architecture/ mission spec. change	Nominal	No Limits
Current Trends Frozen Tech - In-Production Only	Nominal - Twin Aisle First in 2020s	Nominal	No Limits
Environmental "Bounds" - Low	Nominal - Single Aisle First in 2020s	Early (relative to historical data)	No Limits
Environmental "Bounds" - High	Nominal - Twin Aisle First in 2020s	Late (relative to historical data)	Limits
High Demand (Including Global) + High R&D	Nominal - Twin Aisle First in 2020s	Nominal	No Limits
High Demand (Including Global) + Low R&D	Nominal - Twin Aisle First in 2020s	Nominal	No Limits
Low Demand (Including Global) + High R&D	Nominal - Twin Aisle First in 2020s	Nominal	No Limits
Low Demand (Including Global) + Low R&D	Nominal - Twin Aisle First in 2020s	Nominal	No Limits
Very High Demand with Noise Limits - Low R&D	Nominal - Twin Aisle First in 2020s	Late (relative to historical data)	Limits
Very High Demand with Noise Limits - High R&D	Nominal - Twin Aisle First in 2020s	Late (relative to historical data)	Limits

Table 5: Matrix of Scenarios and Aircraft Technology Model Factors

	Amount and Speed of Technology R&D Investment (relative)	TRL 9 Dates	Benefit Levels	Aircraft Configurations	Engine Architectures	Mission Specification Changes
Current Trends "Best Guess"	1.02	Medium	Medium	"Gen 1" Advanced High AR Wing Type 2035+ (check median gen 1 TRL 9 date response)	"Gen 1" as expected; "Gen 2" Open Rotor Type Benefits 2035+	None
Current Trends + High R&D	1.71	Early - Emphasis over benefit level	High	All 3 generations as responded in surveys, Gen 1 2025+, Gen 2/3 2035+	All 3 generations as responded in surveys, Gen 2/3 2035+	None
Current Trends + High R&D + Mission Spec.	1.71	Early - Emphasis over benefit level	High	All 3 generations as responded in surveys, Gen 1 2025+, Gen 2/3 2035+	All 3 generations as responded in surveys, Gen 2/3 2035+	3 generations. 2nd gen redesign for cruise speed reduction. Include range variants
Current Trends Frozen Tech - In-Production Only	0	N/A	N/A	None	None	None
Environmental "Bounds" - Low	1.71	Early - Emphasis over benefit level	High	All 3 generations as responded in surveys, Gen 1 2025+, Gen 2/3 2035+	All 3 generations as responded in surveys, Gen 2/3 2035+	3 generations. 2nd gen redesign for cruise speed reduction. Include range variants?
Environmental "Bounds" - High	0.52	Late	Low	None	None	None
High Demand (Including Global) + High R&D	1.71	Early - Emphasis over benefit level	High	All 3 generations as responded in surveys, Gen 1 2025+, Gen 2/3 2035+	All 3 generations as responded in surveys, Gen 2/3 2035+	3 generations. 2nd gen redesign for cruise speed reduction. Include range variants
High Demand (Including Global) + Low R&D	0.52	Late	Low	None	None	None
Low Demand (Including Global) + High R&D	1.71	Early - Emphasis over benefit level	High	All 3 generations as responded in surveys, Gen 1 2025+, Gen 2/3 2035+	All 3 generations as responded in surveys, Gen 2/3 2035+	3 generations. 2nd gen redesign for cruise speed reduction. Include range variants
Low Demand (Including Global) + Low R&D	0.52	Late	Low	None	None	None
Very High Demand with Noise Limits - Low R&D	0.52	Late	Low	None	None	None
Very High Demand with Noise Limits - High R&D	1.71	Early - Emphasis over benefit level	High	All 3 generations as responded in surveys, Gen 1 2025+, Gen 2/3 2035+	All 3 generations as responded in surveys, Gen 2/3 2035+	3 generations. 2nd gen redesign for cruise speed reduction. Include range variants

Technology Roadmapping Workshops Overview

The goal of the technology roadmapping workshops was to develop a range of scenarios bounding the possible future of technology, including their impacts and likely entry into service. This information was then used to model advanced aircraft technologies and advanced vehicles expected to enter the fleet through 2050. Technology Workshop 1 was held virtually on June 10th and 11th of 2015 to solicit feedback from government, industry, and academia on a wide range of aircraft technology topic areas. From the results, infographics were created that document the suggested scenarios including technology impact, time to entry into service, and examples of specific technologies. Technology Workshop 2 was followed

up by a virtual workshop held on February 16th of 2016 to evaluate the infographics and get a final consensus on the technology evolution scenarios. In addition to guiding the modelling of advanced aircraft, a publically available document will be prepared from the final infographics.

Attendees to the technology roadmapping workshops included representatives from: The U.S. Air Force, Booz Allen Hamilton, Boeing, Department of Transportation Volpe Center, Embraer, FAA Office of Environment and Energy, Georgia Tech, Honeywell, Lufthansa, Mitre, NASA, Pratt & Whitney, Purdue, Rolls-Royce, Stanford, Textron Aviation and Virginia Tech. The workshop was constructed to ask for information on examples of first, second, and third generation technologies. The first virtual workshop focused on airframe and operational technologies whereas the second focused on engine and operational technologies. Operational technologies were included in both workshops since they affect both aircraft and engine systems. As discussed during the workshop, participants were made aware that the final results of the survey would be published as aggregated data. Specific identifiers would be removed prior to publication other than a general list of organizations that participated. Participants were also made aware of the primary intent to use the data to quantify the potential aircraft and engine technology to meet the FAA's environmental goals.

In order to solicit meaningful feedback without asking for sensitive, proprietary information the Georgia Tech team constructed a survey that solicited information on technologies in the following areas:

Availability – When will the technology be ready for entry into service (EIS)?

Applicability to subsystems and vehicle class – Where on the aircraft/engine can the technology be applied? What sizes of aircraft are applicable? How does this change as technology evolves?

Maturation Rate – How quickly does each generation of a technology mature to technology readiness level (TRL)[1] 9?

Delineation between different generations of a technology – How does the technology evolve as it matures over several product generations?

Primary impact areas – What metrics on the aircraft are impacted by the technology?

Technology Roadmapping Survey 1 Format

A survey format was developed in Microsoft Excel to allow respondents to provide feedback in a structured manner that ensured consistency between responses and reduced the burden of filling out the survey. First, the survey was divided into multiple technology 'topic areas'. Broadly speaking, the technologies were classified into three distinct branches, *engine, airframe, and operational technologies.* Technologies were then further subdivided into technology areas as shown in **Figure 26**. Workshop participants were asked to provide information on three different generations of each technology area at the right-most level of the tree. It was left to workshop participants to define what constitutes a generational change in a technology area; however, as an example, the use of ceramic matrix composite (CMC) technology within an engine can be broken into different generations. A first generation application may involve the use of CMC on the turbine shroud and other static parts outside of the main flow path. Once more experience is gained with CMC; the material may be used in turbine vanes as a second generation application. Further development may enable the use of CMC on highly stressed rotating parts, such as turbine blades. Participants were asked to provide specific examples in each technology area to help baseline their opinion on delineations between technology generations.

[1] "Technology Readiness Levels (TRL) are a type of measurement system used to assess the maturity level of a particular technology. Each technology project is evaluated against the parameters for each technology level and is then assigned a TRL rating based on the projects progress. There are nine technology readiness levels. TRL 1 is the lowest and TRL 9 is the highest." - NASA

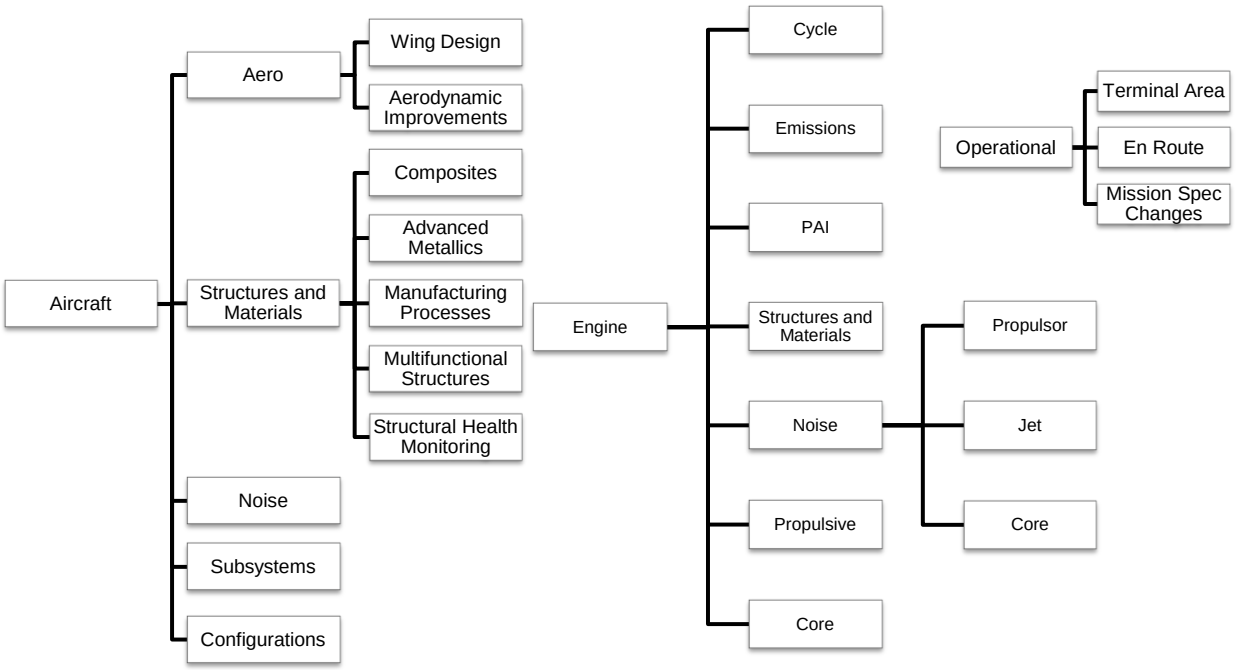

Figure 26: Technology Categorization

There are a few technology categories in Figure 26, which may require further explanation. Engine PAI for example stands for Propulsive Airframe Integration and relates to technologies such as boundary layer ingestion. Many of the technologies that affect Engine Propulsor Noise also affect Engine Jet Noise. Since this survey was mainly focused on turbofan powered aircraft, the major differentiator between the two is that any technology associated with fan noise is related to Engine Propulsor Noise, while technology associated to jet and shock noise is only related to Engine Jet Noise.

For each of the technology categories in Figure 26, a Microsoft Excel survey was constructed. Three generations of each category were placed on a single worksheet, all of which had a consistent structure, shown in Figure 27. The figure shows 1st generation wing design; however, all technology areas had a consistent structure, with the contents of each colored box adjusted accordingly.

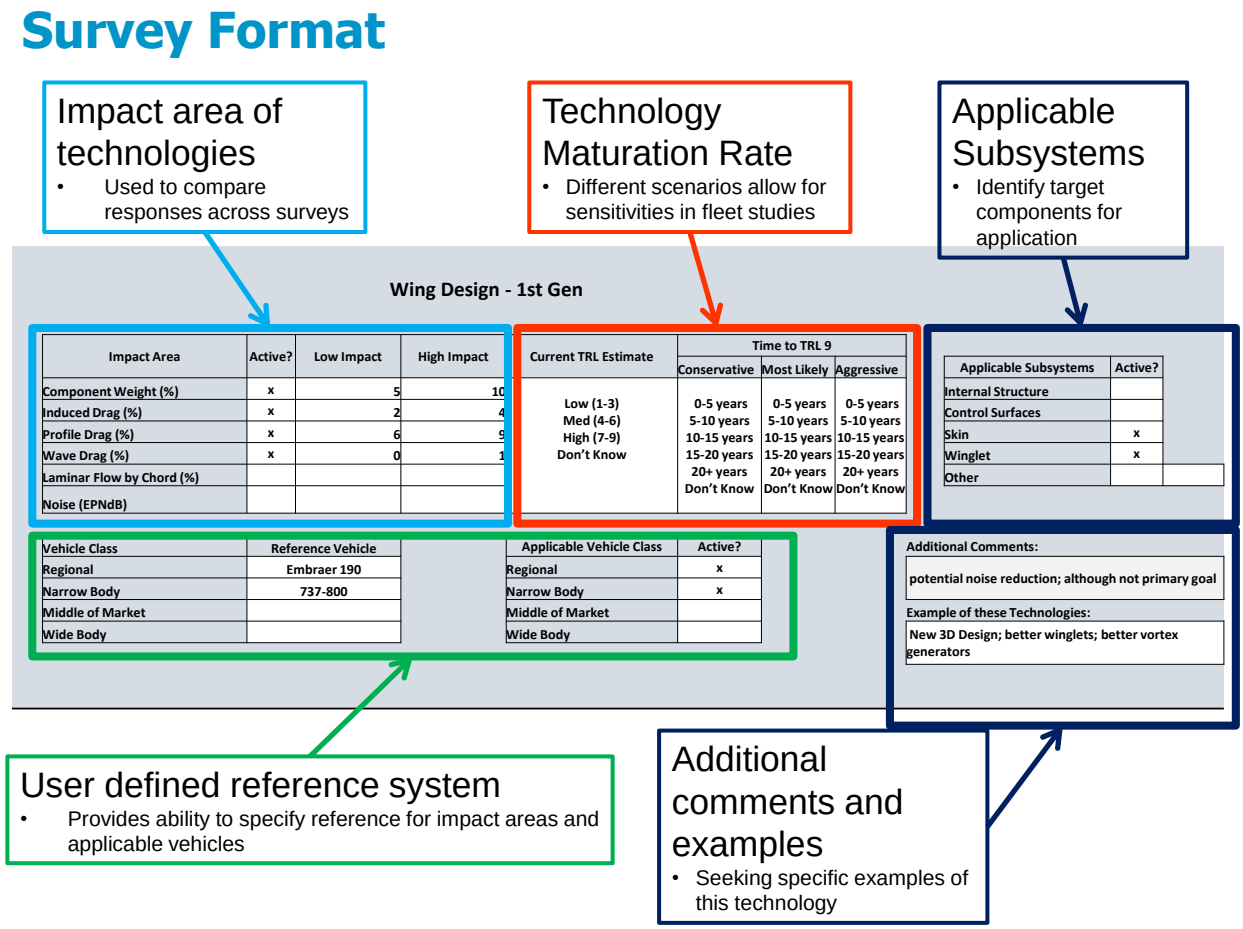

Figure 27: Technology Roadmapping Survey 1 Format

Working clockwise from the upper left of Figure 27 participants were asked for information on the impact of each generation within a technology category. The impact areas were chosen to be at an intermediate level of fidelity, or what has also been referred to as the natural metric. For example, the wing design impacts were solicited as percent reductions from the current state of the art for weight, drag, laminar flow, and noise. Since multiple technologies could be included in a first generation wing design, participants were asked to list the total benefits for all technologies being considered. Moving to the right, the red box asked for the current Technology Readiness Level (TRL) and estimated time to TRL 9. The current TRL estimate was grouped into low (TRL 1-3), medium (TRL 4-6), and high (TRL 7-9). This grouping was selected to allow for multiple technologies to be included in a generation, reduce the possibility of asking for sensitive data, and to account for some level of uncertainty in the technology development process. Under the time to TRL 9, responses were sought for three scenarios: a conservative, most likely, and aggressive technology progression. Possible responses were grouped into 5 year bins up through 20+ years. Moving to the upper right, applicable subsystems were listed for each technology area with check boxes that participants could easily select. On the lower left, participants were asked to provide a reference system which they used to estimate the reductions listed in the impact areas. Vehicle applicability was also requested to identify applicable size classes for the technology. Finally, write-in boxes were provided in the lower right to allow for any comments and concerns in addition to specific examples of technologies that should be classified within the provided technology area and generation.

Table 6 provides a complete listing of the impact areas and applicable subsystems Georgia Tech identified for each technology. Examples of each technology area were also provided to participants in order to help baseline responses.

Table 6: List of Impact Areas and Applicable Subsystems for Each Technology Category

Category	Examples	Impact Areas	Applicable Subsystems
Aircraft Wing Design	Adaptive Trailing Edge Gust/Maneuver Load Alleviation Hybrid Laminar Flow Control Spiroid Winglets	Component Weight (%) Induced Drag (%) Profile Drag (%) Wave Drag (%) Laminar Flow by Chord (%)	Internal Structure Control Surfaces Skin Winglet Design
Aircraft Aerodynamic Improvements	Drag reduction coatings Friction-reducing surface coatings Electro-magnetic technologies for drag reduction in cruise	Induced Drag (%) Profile Drag (%) Wave Drag (%) Laminar Flow by Chord (%)	Fuselage Wing Vertical Tail Horizontal Tail
Aircraft Composites	Damage Arresting Stitched Composites Damage Tolerant Laminates Tow Steered Fiber Composites Hybrid Nanocomposites	Component Weight (%) Reduction in Factor of Safety (%)	Fuselage Wing Vertical Tail Horizontal Tail
Aircraft Advanced Metallics	Functionally Graded Metallics Curvilinear Stiffened Metal Structures Advanced Superalloys Advanced Powder Metallurgy	Component Weight (%) Reduction in Factor of Safety (%)	Fuselage Wing Vertical Tail Horizontal Tail
Aircraft Manufacturing Processes	Ultrasonic Shot Peening Out-of-Autoclave Composite Fabrication Post-buckled Structures	Component Weight (%) Reduction in Factor of Safety (%)	Fuselage Wing Vertical Tail Horizontal Tail
Aircraft Multifunctional Structures	Primary Structure Joining Methodologies Unitized Metallic Structures	Component Weight (%) Reduction in Factor of Safety (%)	Fuselage Wing Vertical Tail Horizontal Tail
Aircraft Structural Health Monitoring	Wireless Integrated Strain Monitoring and Simulation System Fiber-optic Embedded Composites	Component Weight (%) Reduction in Factor of Safety (%)	Fuselage Wing Vertical Tail Horizontal Tail
Aircraft Noise	Continuous Moldline Link for Flaps Slat Inner Surface Acoustic Liner Over the Rotor Acoustic Treatment Landing Gear Integration	Approach Noise (EPNdB) Sideline Noise (EPNdB) Cutback Noise (EPNdB) Source Noise (dB)	Slats Flaps Landing Gear Wing/Tail

Category	Examples	Impact Areas	Applicable Subsystems
Aircraft Subsystems	Solid Oxide Fuel Cell Auxiliary Power Unit Hybrid Wing Ice Protection System Fly-by-Light Systems Lithium Batteries for Secondary Power	Component Weight (%) Fuel Burn (%) Drag (%) On board electrical energy consumption (%) On board pneumatic energy consumption (%) On board hydraulic energy consumption (%)	APU ECU Avionics and Control
Aircraft Configurations	Large-span aircraft (with or without truss- / strut-braced wings) Lifting fuselage (e.g., double bubble fuselage with conventional engine mounting) Integrated propulsion systems (boundary layer ingestion) Blended/Hybrid wing body (HWB)	Emissions (%) Fuel Burn (%) Noise (EPNdB)	Truss Braced Wing Double Bubble Hybrid Wing/Body
Engine Cycle	Direct Drive Cycle Geared Fan Cycle Open Rotor Cycle Hybrid Electric Pulse Detonation Core Engine Variable Core Cycle Technology	TSFC (%) Engine Weight (%) Noise (EPNdB) Emissions (%)	Direct Drive Geared Fan Open Rotor
Engine Emissions	Twin Annular Premixing Swirler (TAPS) Lean Direct Ingestion (LDI) Partially Evaporating Rapid Mixing Combustor (PERM) Lean Premixed Prevaporised Combustor (LPP)	NO_x (%) UHC (%) nvPM (%)	
Engine Propulsion Airframe Integration	Low Interference Nacelle Natural Laminar Flow Fluidic Vaneless Thrust Reversers Short Inlet Engine placement	Interference Drag (%) Nacelle Drag (%) Component Weight (%) Noise Reduction (EPNdB)	Pylon Nacelle
Engine Structures and Material	Ceramic Matrix Composite (CMC) Nozzle Polymer Matrix Composite (PMC) Fan Case High Temperature Corrosion Coatings	Component Weight (%) Reduction in Factor of Safety (%)	Fan Compressor Turbine Nacelle

Category	Examples	Impact Areas	Applicable Subsystems
Engine Propulsor Noise	Fan Vertical Acoustic Splitter Noise Cancelling Stator Fluidic Injection Stator Sweep and Lean Variable Geometry Chevrons	Approach Noise (EPNdB) Sideline Noise (EPNdB) Cutback Noise (EPNdB) Source Noise (dB)	Treated Fan Forward Radiated Noise Treated Fan Aft Radiated Noise
Engine Jet Noise	Fan Vertical Acoustic Splitter Noise Cancelling Stator Fluidic Injection Stator Sweep and Lean Variable Geometry Chevrons	Approach Noise (EPNdB) Sideline Noise (EPNdB) Cutback Noise (EPNdB) Source Noise (dB)	Inner Stream Jet Noise Outer Stream Jet Noise Inner Stream Shock Noise Outer Stream Shock Noise
Engine Core Noise	Compressor Combustor Turbine	Approach Noise (EPNdB) Sideline Noise (EPNdB) Cutback Noise (EPNdB) Source Noise (dB)	Compressor Combustor Turbine
Engine Propulsive Efficiency	Variable Area Nozzle Boundary Layer Ingestion Variable Pitch Fan Ultra High Bypass Ratio Engines Contra-rotating Fan Engines	Propulsive Efficiency (%) Component Weight (%)	Inlet Propulsor Nacelle
Engine Thermal (Core) Efficiency	Tip Injection for Stability Enhancement System Intercooled Engine Heat Exchanger Installation Flow Control by Aspiration Active Tip Clearance Control	Thermal Efficiency (%) Component Weight (%)	Cooling HP Compressor HP Turbine Combustor Subsystems
Operations in the Terminal Area	Taxi Bot Controller Managed Spacing Combined Arrival and Departure Runway Scheduling (CADRS) Runway Configuration Management	Fuel Burn (%) Noise (EPNdB) Emissions (%)	Airport Operations Approach Takeoff/climb
Operations En Route	Operational Airspace Sectorization Integrated System (OASIS) Dynamic Weather Re-routing (DWR) Pair-wise Separation Management (PSM)	Fuel Burn (%) Noise (EPNdB) Emissions (%)	Aircraft in-flight Operation Dynamic Trajectory Re-Routing

Category	Examples	Impact Areas	Applicable Subsystems
Operations Mission Specification Changes	Cruise speed reduction (CSR) Range/payload design characteristics Maximum allowable span (see configurations) Take-off and landing field lengths	Fuel Burn (%) Noise (EPNdB), via weight reduction Emissions (%)	Design Range Design Mach Operational profile

In addition to the requested impact areas and example technologies, Georgia Tech provided examples of what may constitute a first, second, and third generation technology in each technology category. Participants were encouraged to modify according to their own knowledge and experience. A complete listing of the Georgia Tech provided examples of first, second, and third generation technologies in provided in Table 7.

Table 7: Technology Generation Examples

Category	First Generation	Second Generation	Third Generation
Aircraft Wing Design	Winglet designs Variable wing camber designs	Active flow control NLF control HLF control	Active TS control Morphing wing
Aircraft Aerodynamic Improvements	Riblets Excrescence reduction	Shock bumps Active flow control	Discrete roughness elements (DRE)
Aircraft Composites	New composite fibers and matrix Optimized composite design solutions	Pre-form technology Efficient manufacturing processes Joining technologies	Self-reacting (adaptive) structures Nano-technologies
Aircraft Advanced Metallics	New alloys with targeted properties New design solutions	Tailored integral structures Bonding technology	Advanced assembly concepts Self-reacting (self-monitoring) structures
Aircraft Manufacturing Processes	Automated fiber placement layup Autoclave cure Fastener assembly	Advanced structural shapes Co-bonding/Paste bonding assembly 3D printed components	Major Aerostructures 3D Printed Advanced materials, resins, and stitching
Aircraft Multifunctional Structures	Multifunctional coatings	Morphing structures	Self-healing/self-repairing structures
Aircraft Structural Health Monitoring	Off-line sensor systems for maintenance benefits	On-line sensor systems for component weight and maintenance benefits	Fully integrated sensor systems for weight saving and maintenance benefits
Aircraft Noise	Fairing design Slat design Flap design	Flap treatment Slat treatment Landing gear treatment	Active flow control Plasma actuation
Aircraft Subsystems	Advanced fly-by-wire Lithium batteries for secondary power More electric aircraft	Proton exchange member fuel cells Fly-by-light	Solid acids as fuel cell Solid oxide fuel cell
Aircraft Configurations	Large Span / Trussed Braced Wing	Lifting fuselage Conventional engine mounting	Boundary layer ingestion Engines mounted above fuselage

Category	First Generation	Second Generation	Third Generation
Engine Cycle	Geared turbofan Advanced turbofan	Open rotor/unducted fan Counter-rotating fan	Adaptive cycle Pulse detonation Embedded distributed multi-fan
Engine Emissions	Twin annular premixing swirler RWL combustor	Lean direct injection Active combustion control Lightweight CMC liners	Ultra compact low-emission combustor
Engine Propulsion Airframe Integration	Reduced nacelle weight	Buried engines Boundary layer ingestion inlet	Adaptive/active flow control
Engine Structures and Material	CMC nozzle Advanced TBC coatings	Ubiquitous composites Advanced turbine superalloys	Advanced powder metallurgy disk Blisk and Bling concept
Engine Propulsor Noise	Rotor sweep/lean Rotor speed optimization VAN	Zero hub fan Soft vane Active stator	Over-the-rotor treatment Active blade tone control
Engine Jet Noise	Advanced long duct forced mixer Variable geometry chevrons	High frequency excitation Beveled nozzle	Fluidic injection Microjets
Engine Core Noise	Advanced core treatment	Bulk absorber materials 2 DOF/tailored absorbers	Low noise combustor
Engine Propulsive Efficiency	Variable fan nozzle Very high BPR fan Zero hub fan	Ultra high BPR fan Low FPR fan	Active distortion tolerant fan Embedded engines with inlet flow control
Engine Thermal (Core) Efficiency	Advanced combustor Advanced cooling technologies	Variable flow splits Ultra compact low-emission combustor Clearance control	Active film cooling Active flow control
Operations in the Terminal Area	Wake detection and prediction Taxi bot	Parameter driven aircraft separation standards and procedures	Integrated air/ground network for voice and data
Operations En Route	Aircraft-aircraft hazardous weather information sharing	Airborne collision avoidance Synthetic vision systems	Trajectory negotiation 4D Ts Delegated separation digital communications
Operations Mission Specification Changes	CSR on existing aircraft	Aircraft/engines redesigned for CSR Multi-range aircraft variants	Advanced configurations with mission spec changes Very large-span aircraft

Technology Roadmap Infographic Development

Following the first Technology Roadmapping Survey, a large dataset of responses was collected. The results were combed through to identify any logical inconsistencies and gross outliers. For example, it was observed that for one of the respondents there were times when their Generation 2 and 3 impacts were less than their Generation 1 impacts. This respondent was contacted and it was found that they were giving their impacts relative to the previous generation. For example, their Generation 3 impact was the improvement from Generation 2. These responses were adjusted, so that they were all relative to a 1995 baseline aircraft like the other responses.

The aim of the Technology Roadmap infographics was to effectively convey the range of impacts for each generation. An infographic was made for each of the 22 technology areas. Figure 28 provides a diagram of the initial infographic format

that was developed. On each infographic, a bar graph was included for each impact within that technology area. The high and low values from the responses were used to define the technology impact range for each generation. A nominal impact value was also provided. The infographics also included examples of technologies broken into the generation they would be introduced. In addition, they had graphics that showed the range of responses for the "year to TRL 9" and "Current TRL" for each generation. Finally, at the bottom of the infographics was a matrix showing what respondents thought the applicable subsystems for that technology area's impacts were, for a given vehicle class and generation.

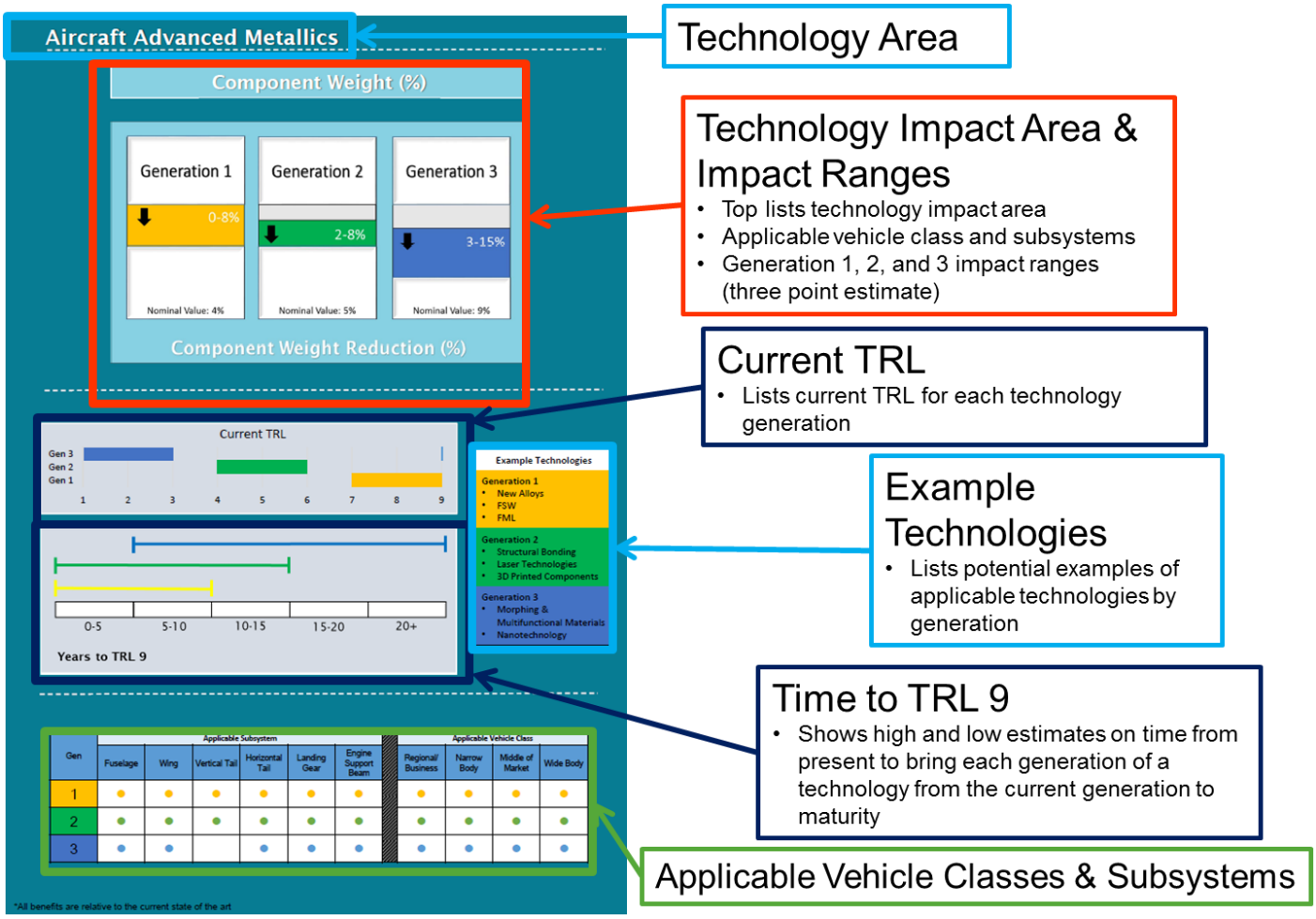

Figure 28: Initial Technology Roadmap Infographic Format Presented at Technology Roadmapping Workshop 2

Technology Roadmapping Survey 2 Format

The goal of the second Technology Roadmapping Workshop was to send participants the infographics to review and provide feedback on the range of responses given in the first workshops. Using the infographics format kept the results anonymous, which helped avoid any bias and ensured participants were viewing the results objectively. As seen in Figure 29, the Technology Roadmapping Survey 2 format was straightforward. For each technology area, participants were asked to review the resulting infographics, one generation at a time. For a given generation, participants were first asked if there were any applicable vehicle classes, applicable subsystems, or example technologies that they thought should be added or removed. Then participants were asked to review the low, nominal, and high technology impact values for that generation. If participants believe an impact value needed to be changed they were asked to explain why. Similarly, for the Current TRL and Time to TRL 9 participants were asked to review the range of values and explain any suggested changes. Throughout

the survey participants were encouraged to leave answers blank if they felt they did not have the background to comment on a particular technology impact area.

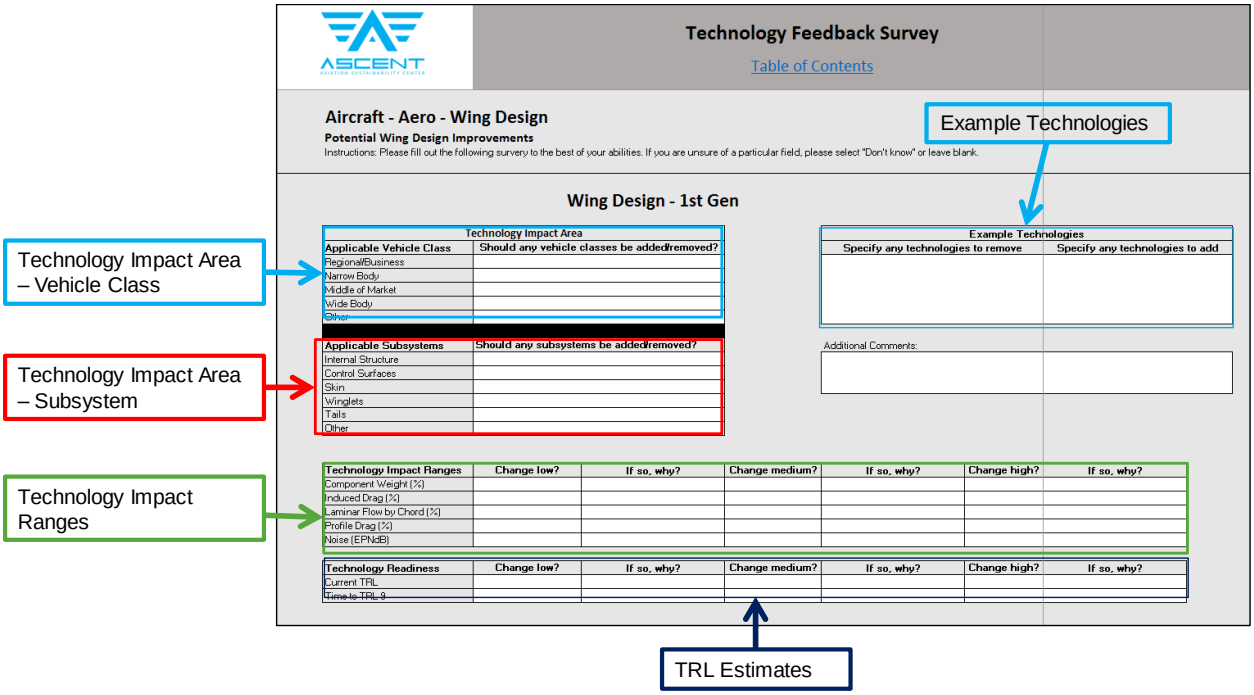

Figure 29: Technology Roadmapping Survey 2 Format

Final Revisions to Technology Roadmap Infographics

Among the responses from the Technology Roadmapping Workshop 2 there was only one technology impact area where respondents felt the impact values should be significantly adjusted, namely Engine Emissions. For both improvement in Particulate Matter and Nitrogen Oxide emissions respondents felt the high values were too extreme and provided justification and noted studies to review for adjusting the values.

Most comments were concerned with the example technologies given on the infographics. Participants either felt that a technology was under the wrong entry-into-service generation, or was not appropriate for the technology area in which it was assigned. For example, additive manufacturing was originally listed as a Generation 1 technology for Engine Emissions. A respondent noted that, while it might be used on test stands, it would mostly not see use in production until Generation 2. Other comments focused on slight adjustments to the "Time to TRL 9" ranges. Overall, the survey feedback was generally showed agreement with the initial infographics. There was some confusion over the matrix at the bottom of the infographics. As seen in Figure 28, in the original infographics, on the left side of the matrix subsystems are listed. A dot was placed to indicate what generations the subsystem would be affected by improvements in the technology area. Separated on the right side of the matrix different vehicles were listed. Similar to the subsystems, a dot was placed to indicate the generations that a vehicle class would be affected by improvements in a technology area. The overwhelming response was that the matrix should really indicate what vehicle and what subsystems on that vehicle were affected by a technology area, instead of separating them. The culmination of these suggestions for the infographics can be seen in Figure 30 to Figure 51. These final infographics will be the basis for a document that will be made publically available on the results of this project.

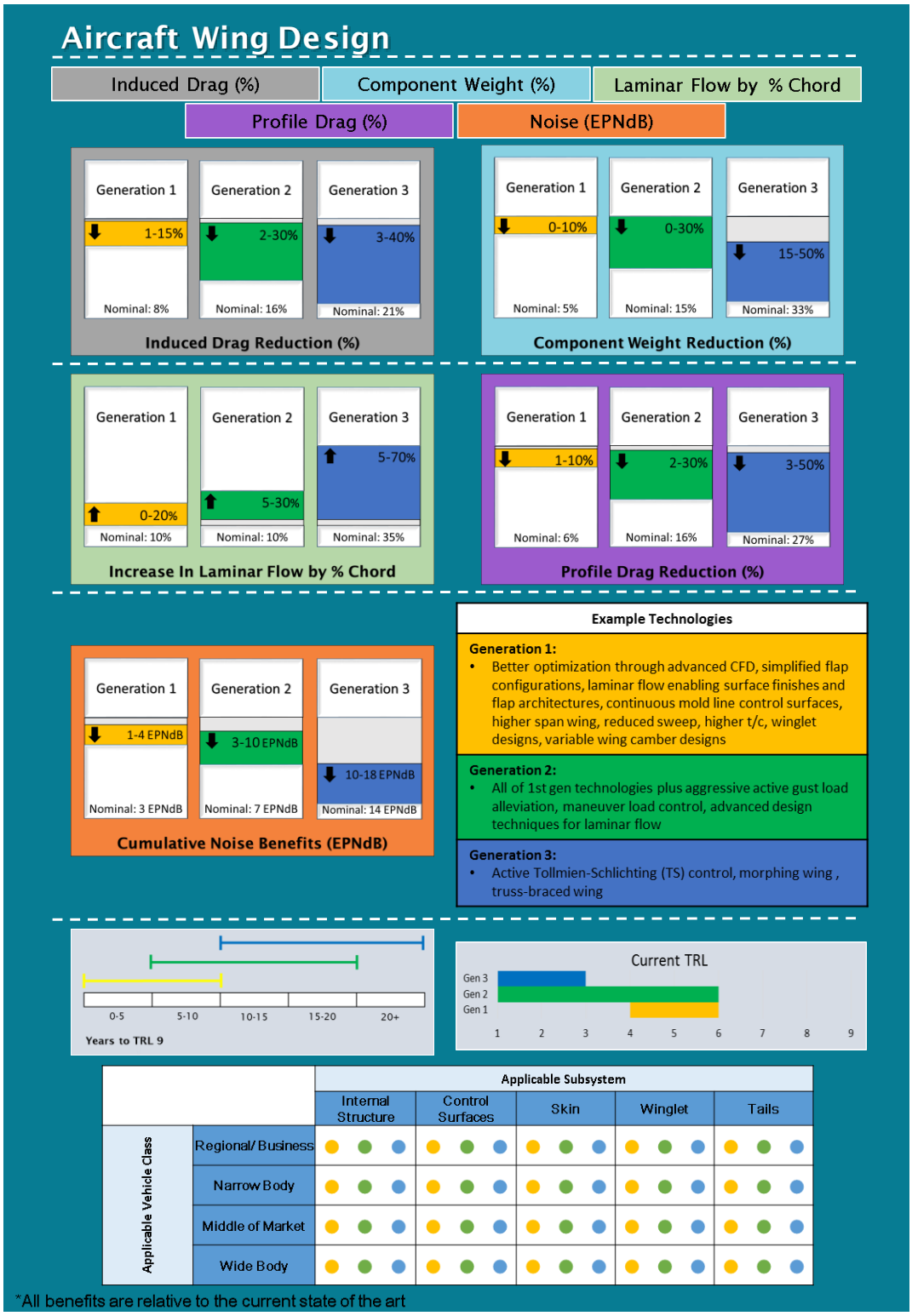

Figure 30: Technology Roadmaps for Aircraft Wing Design

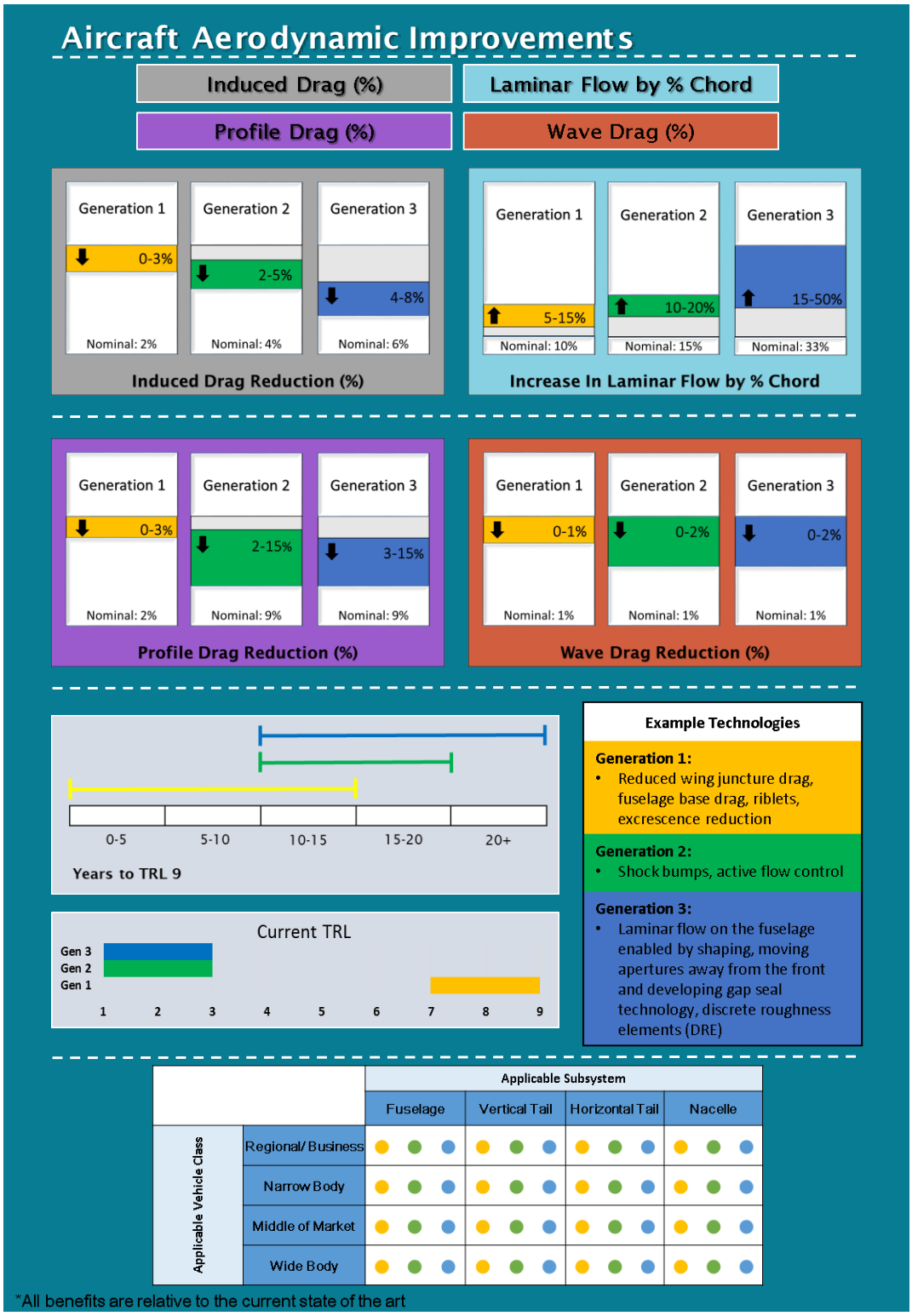

Figure 31: Technology Roadmaps for Aircraft Aerodynamic Improvements

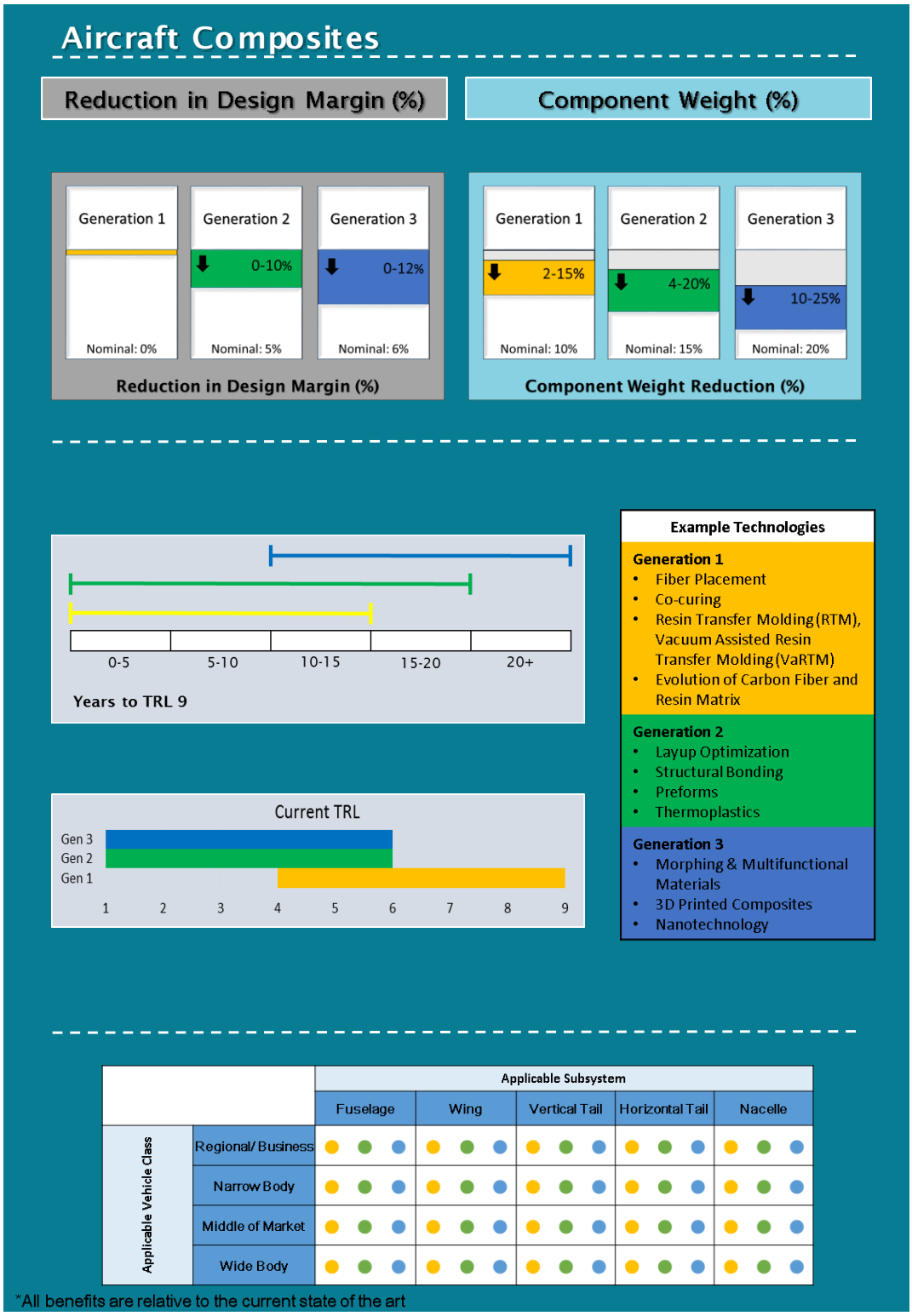

Figure 32: Technology Roadmaps for Aircraft Composites

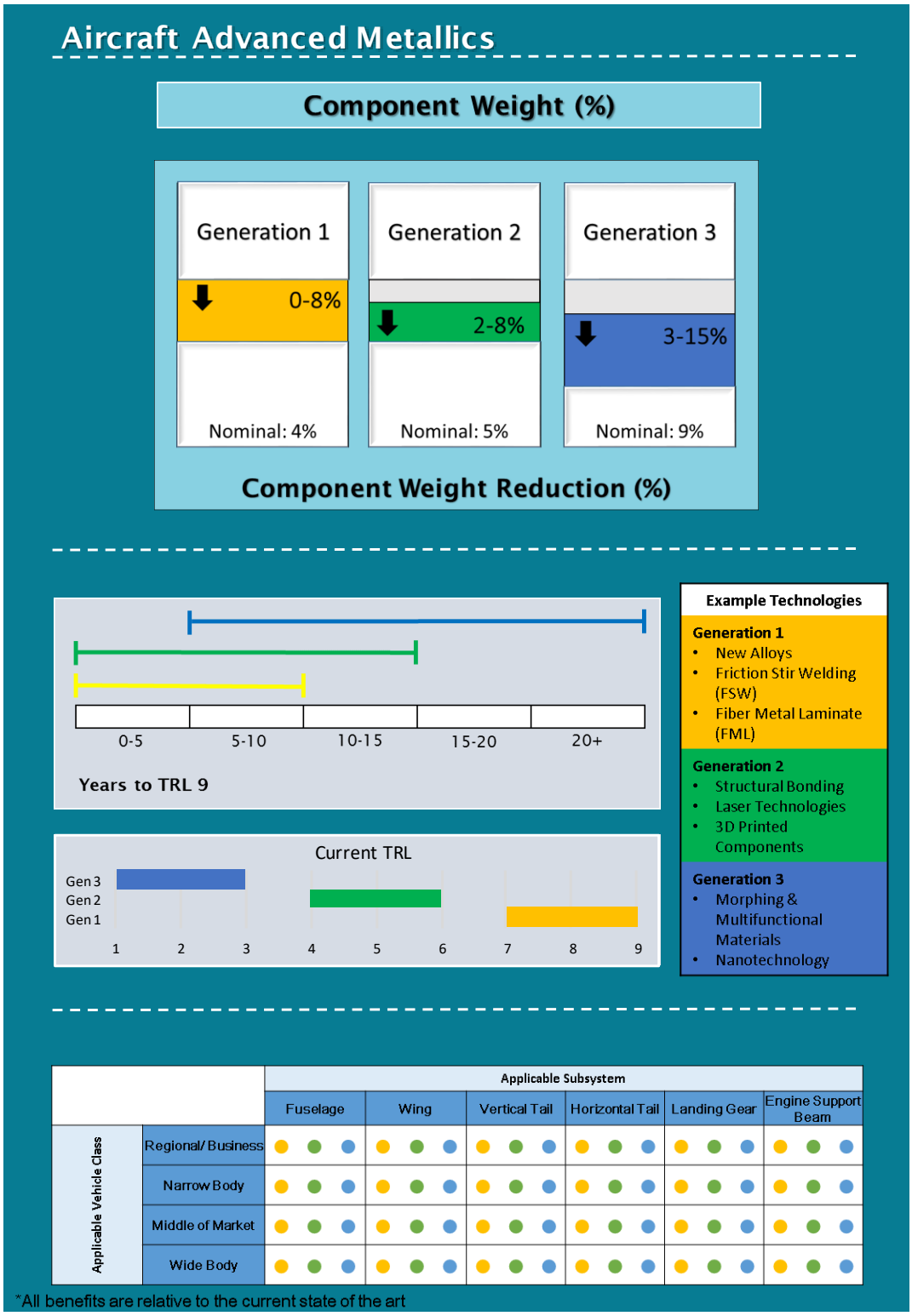

Figure 33: Technology Roadmaps for Aircraft Advanced Metallics

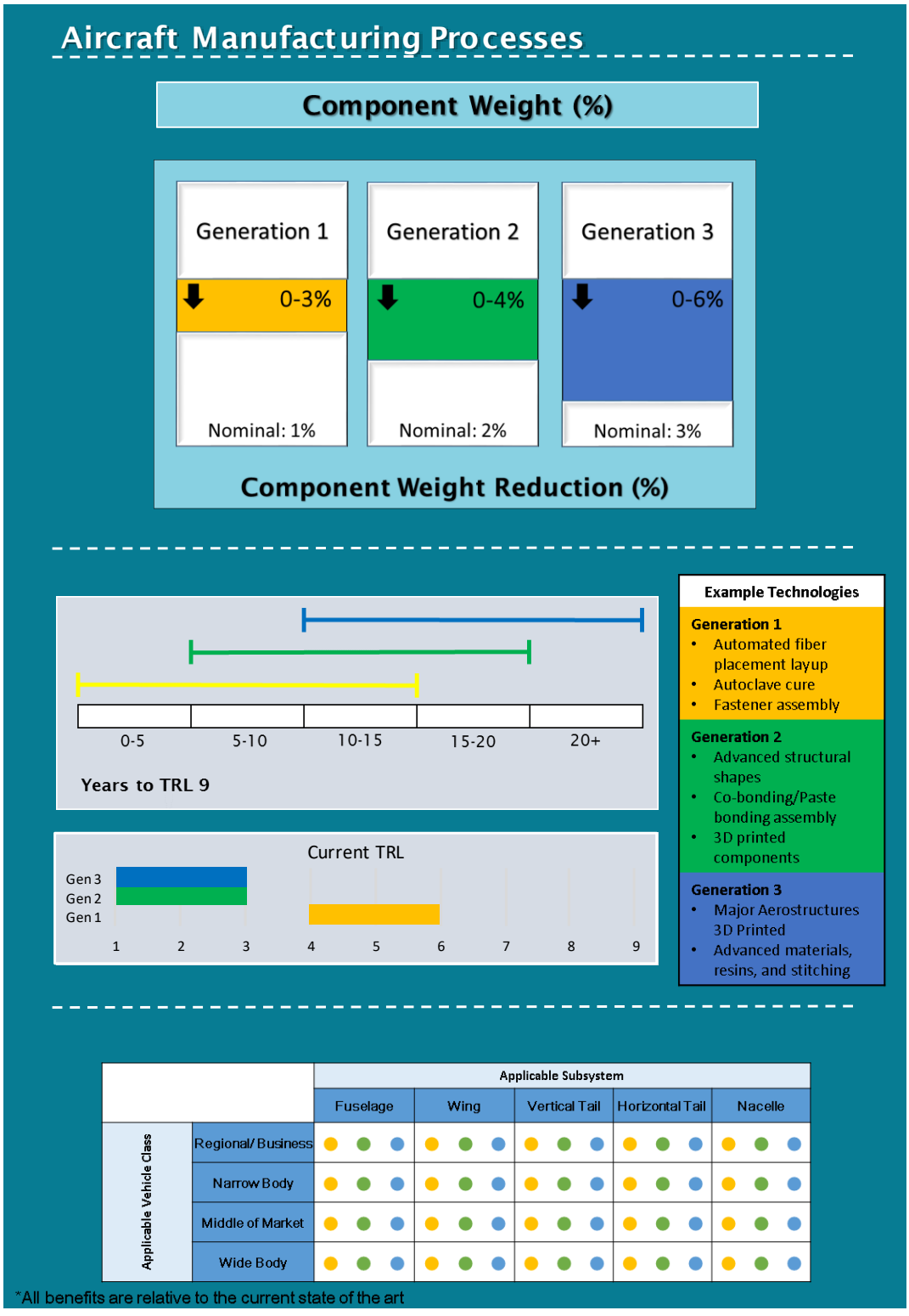

Figure 34: Technology Roadmaps for Aircraft Manufacturing Processes

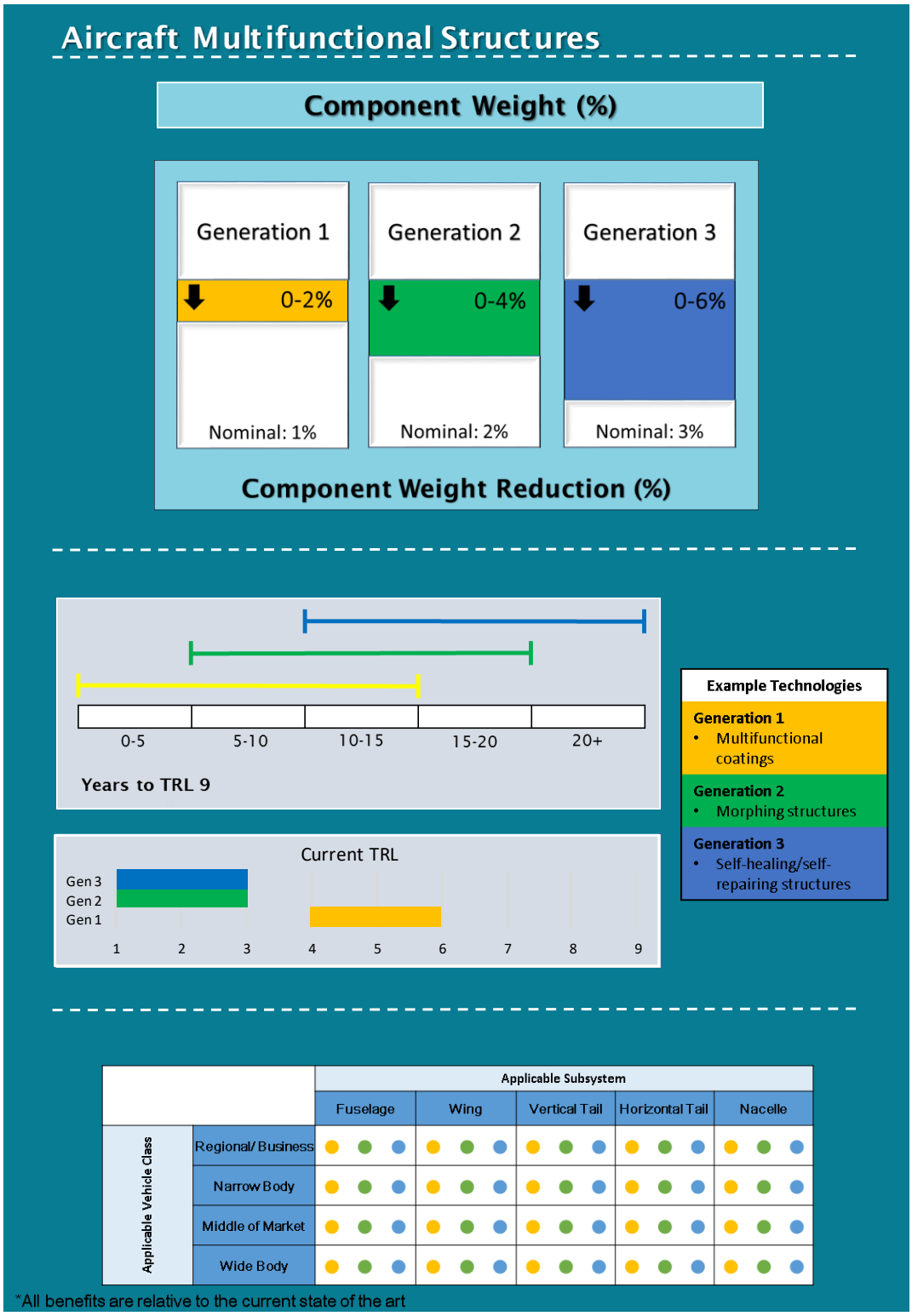

Figure 35: Technology Roadmaps for Aircraft Multifunctioning Structures

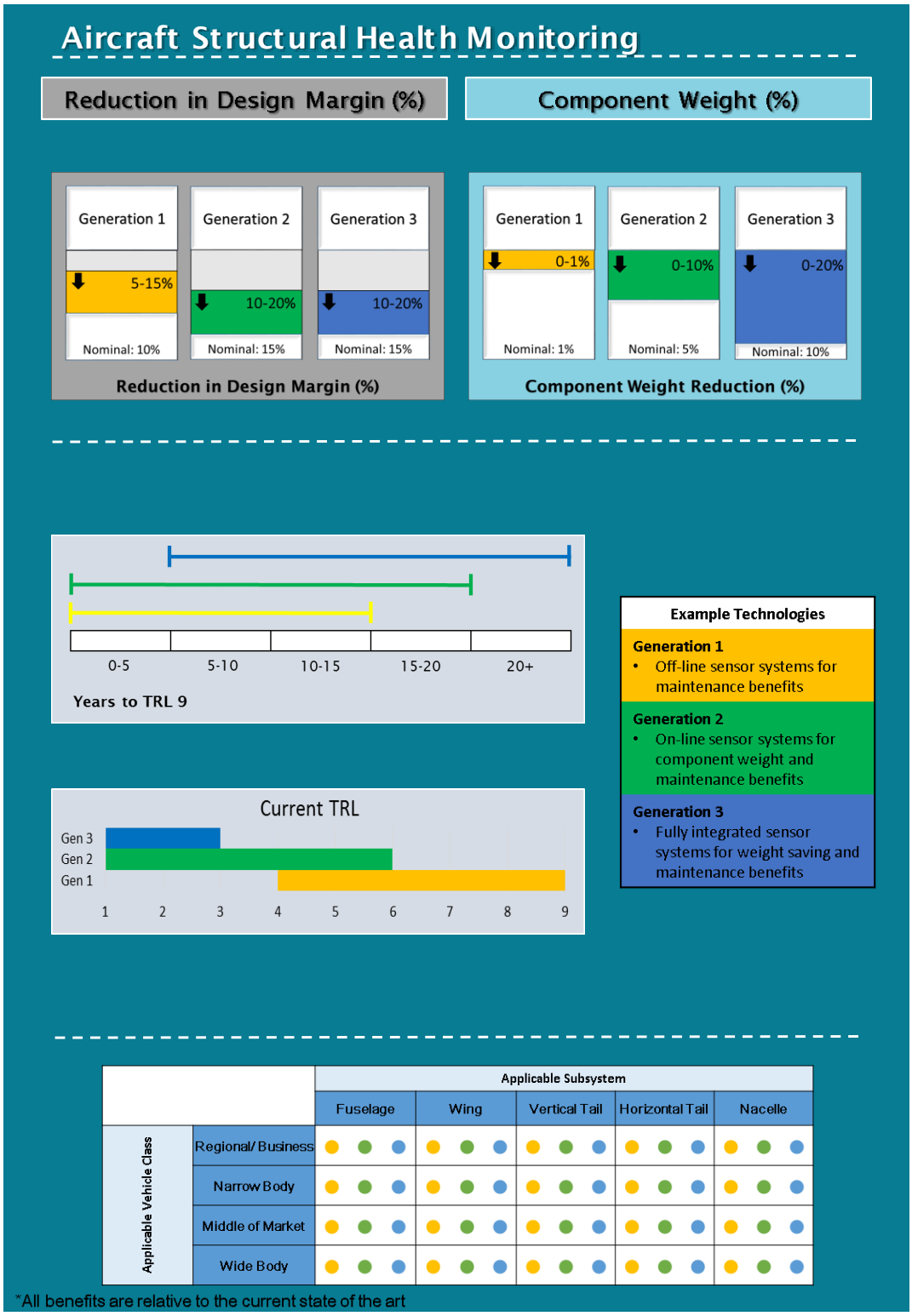

Figure 36: Technology Roadmaps for Aircraft Structural Health Monitoring

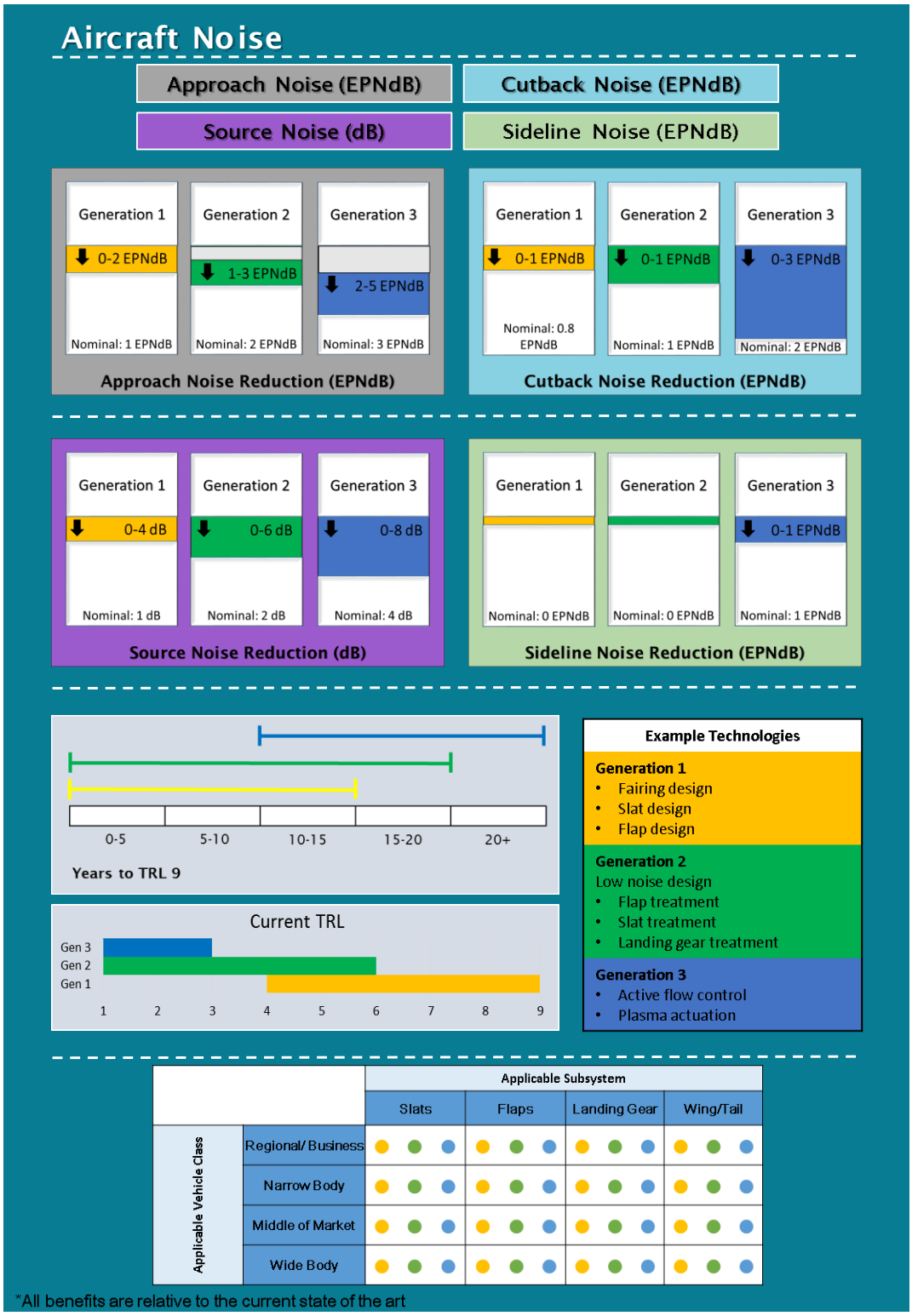

Figure 37: Technology Roadmaps for Aircraft Noise

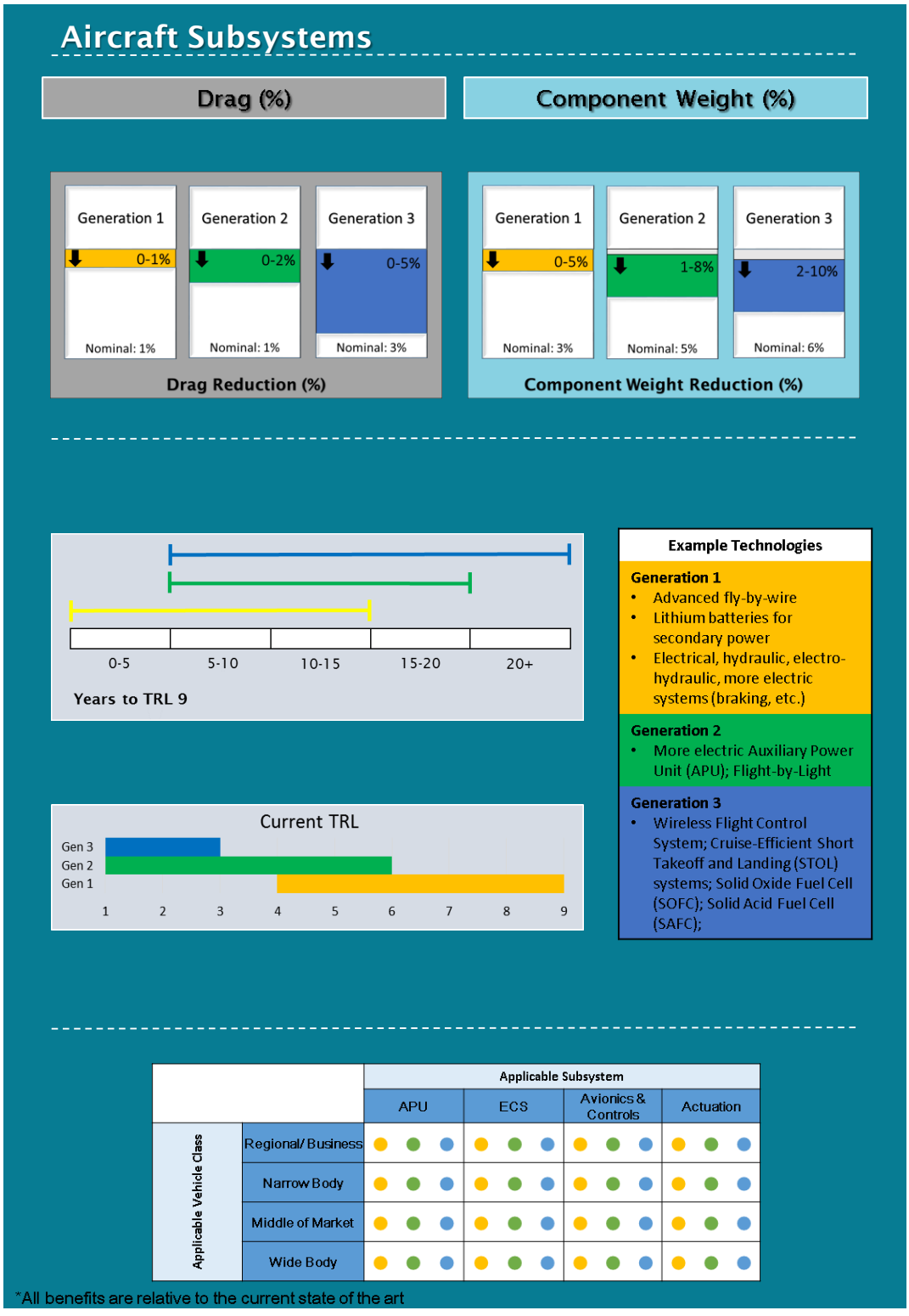

Figure 38: Technology Roadmaps for Aircraft Subsystems

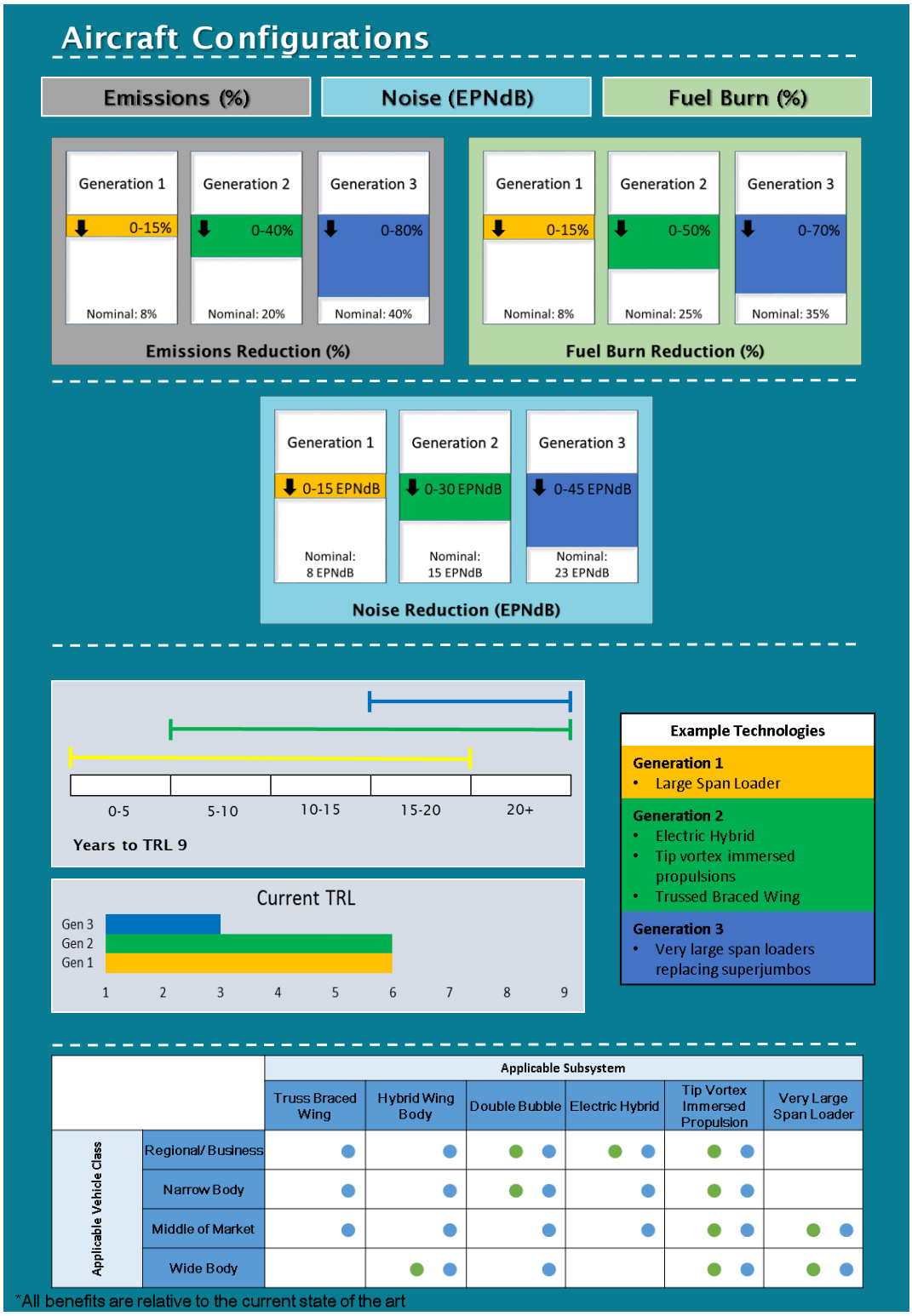

Figure 39: Technology Roadmaps for Aircraft Configurations

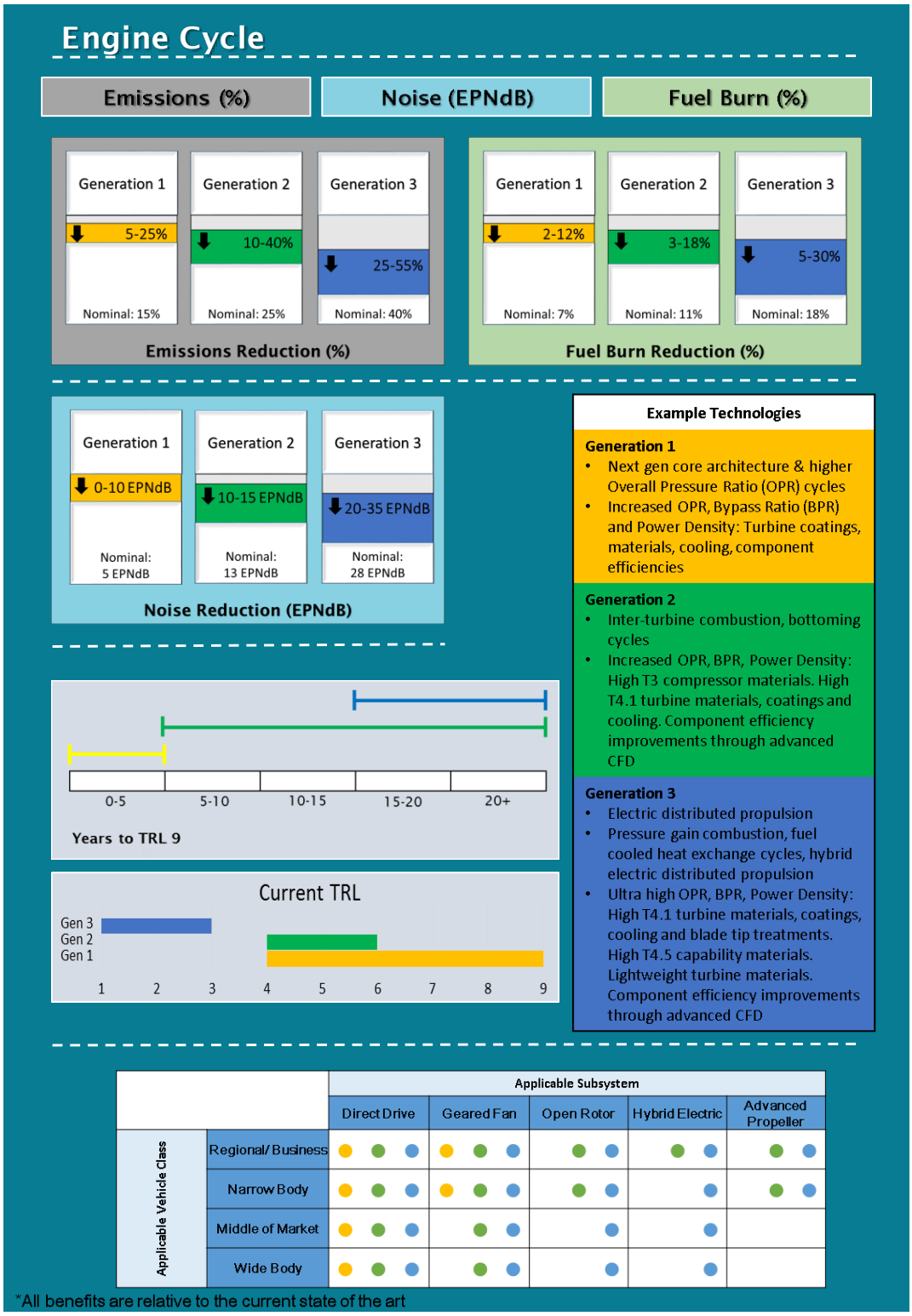

Figure 40: Technology Roadmaps for Engine Cycle

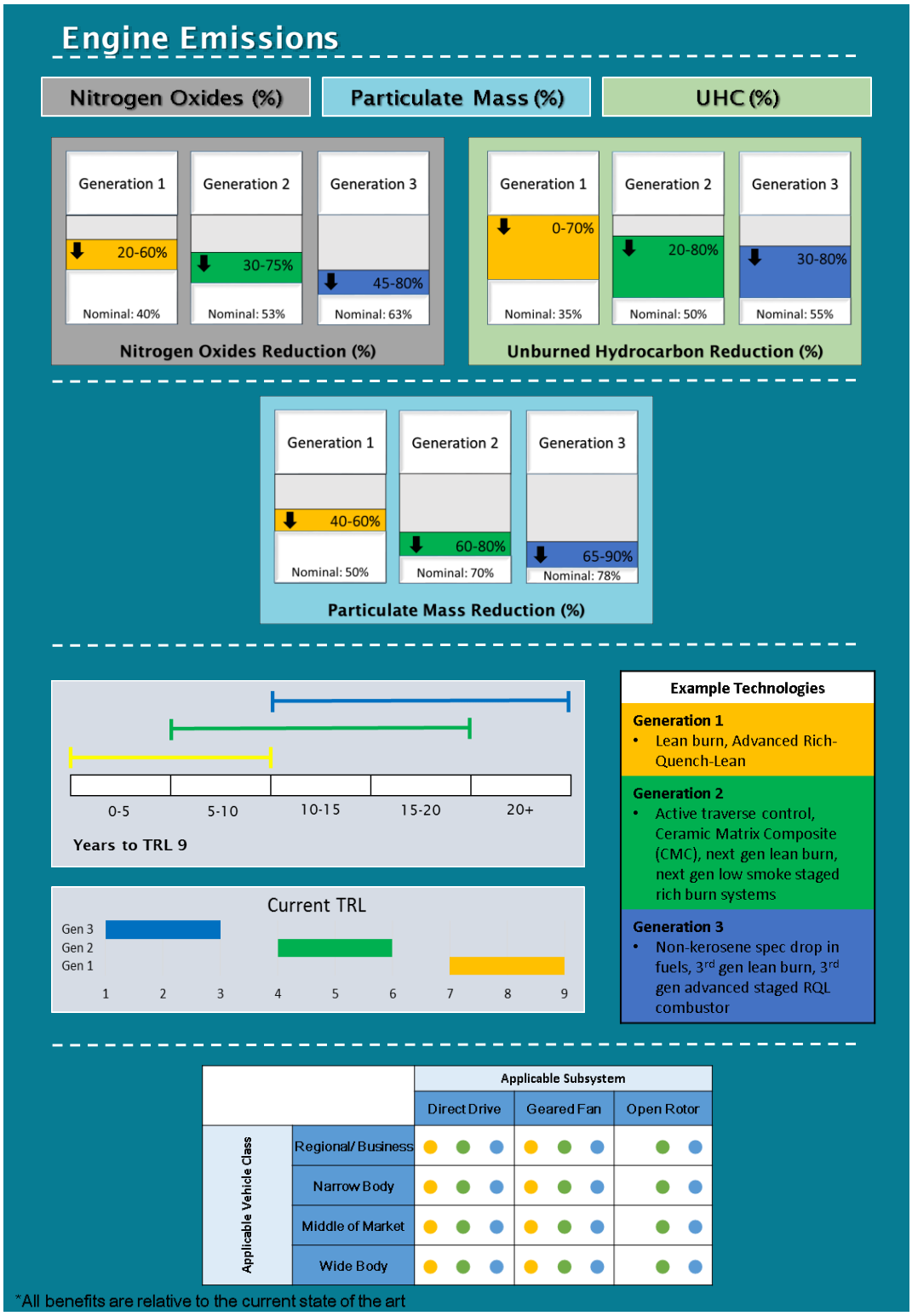

Figure 41: Technology Roadmaps for Engine Emissions

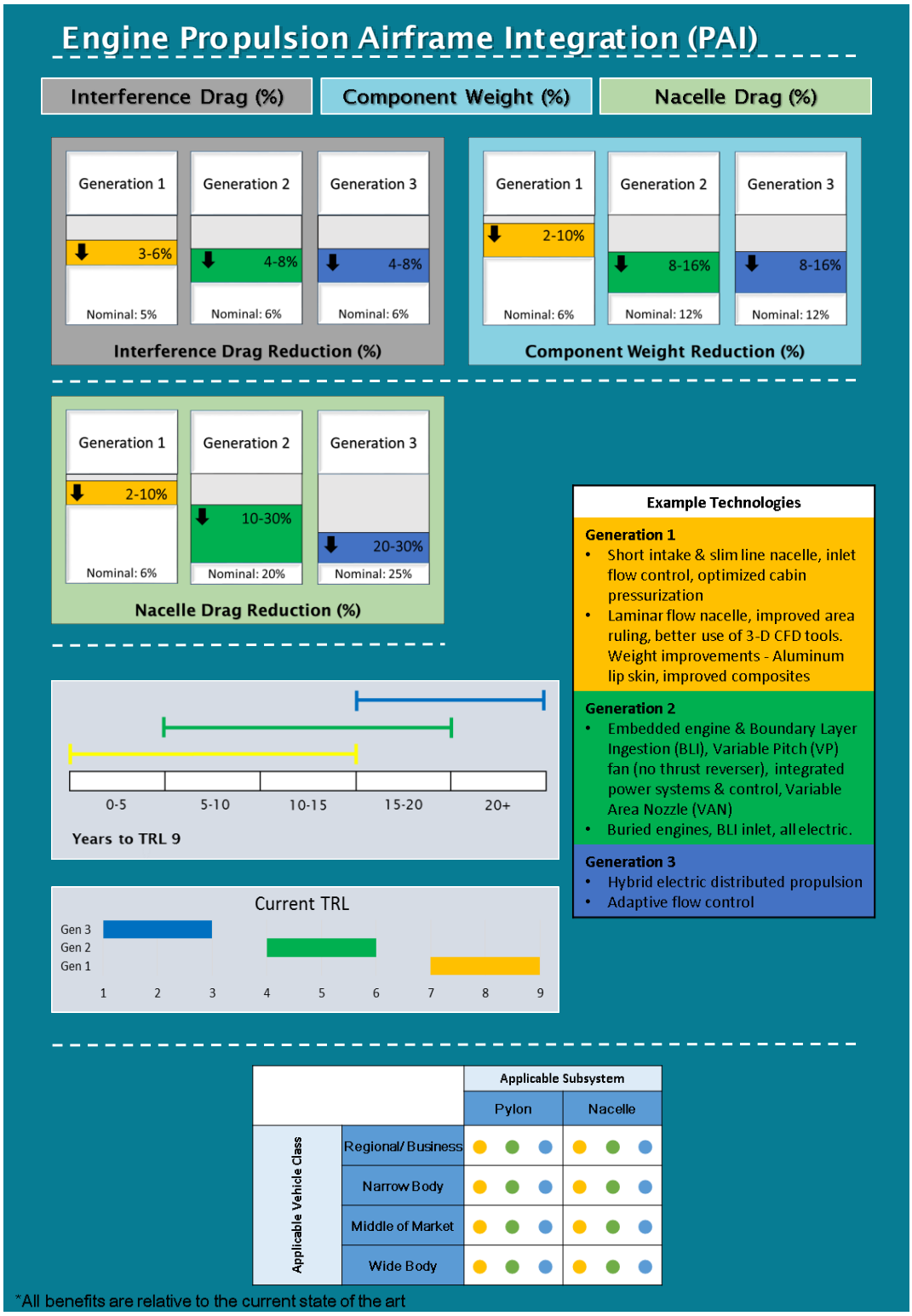

Figure 42: Technology Roadmaps for Engine PAI

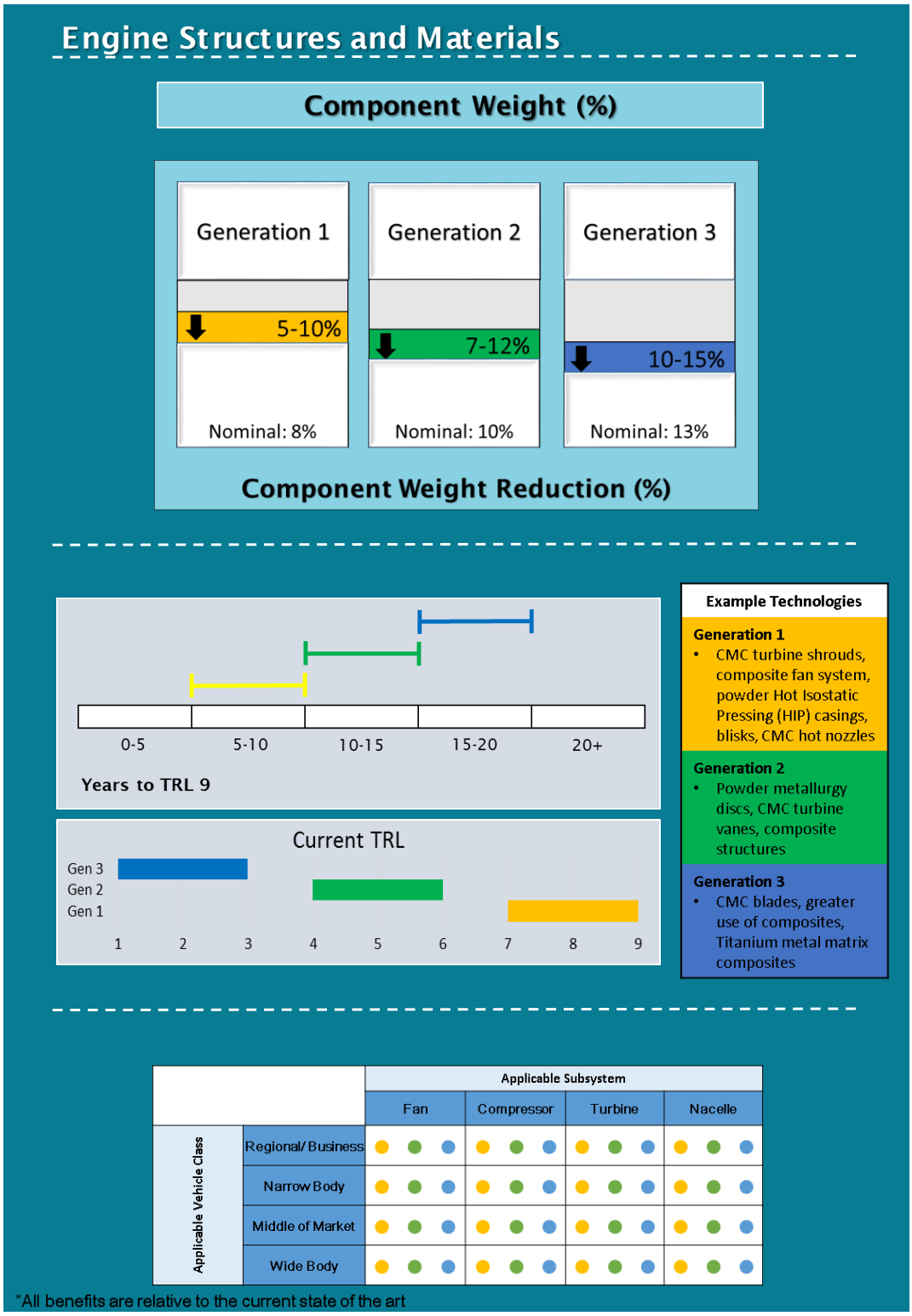

Figure 43: Technology Roadmaps for Engine Structures and Materials

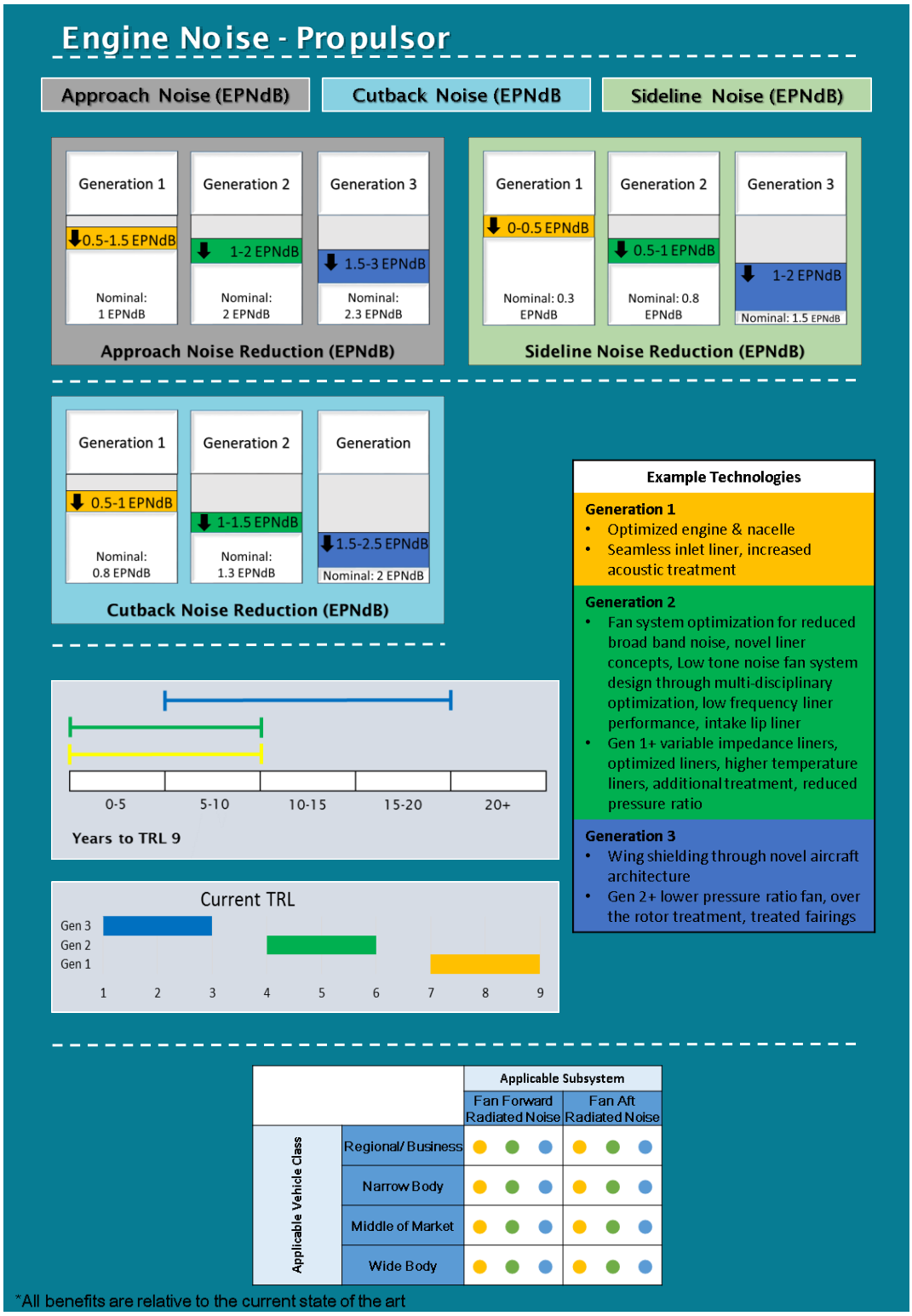

Figure 44: Technology Roadmaps for Engine Noise-Propulsor

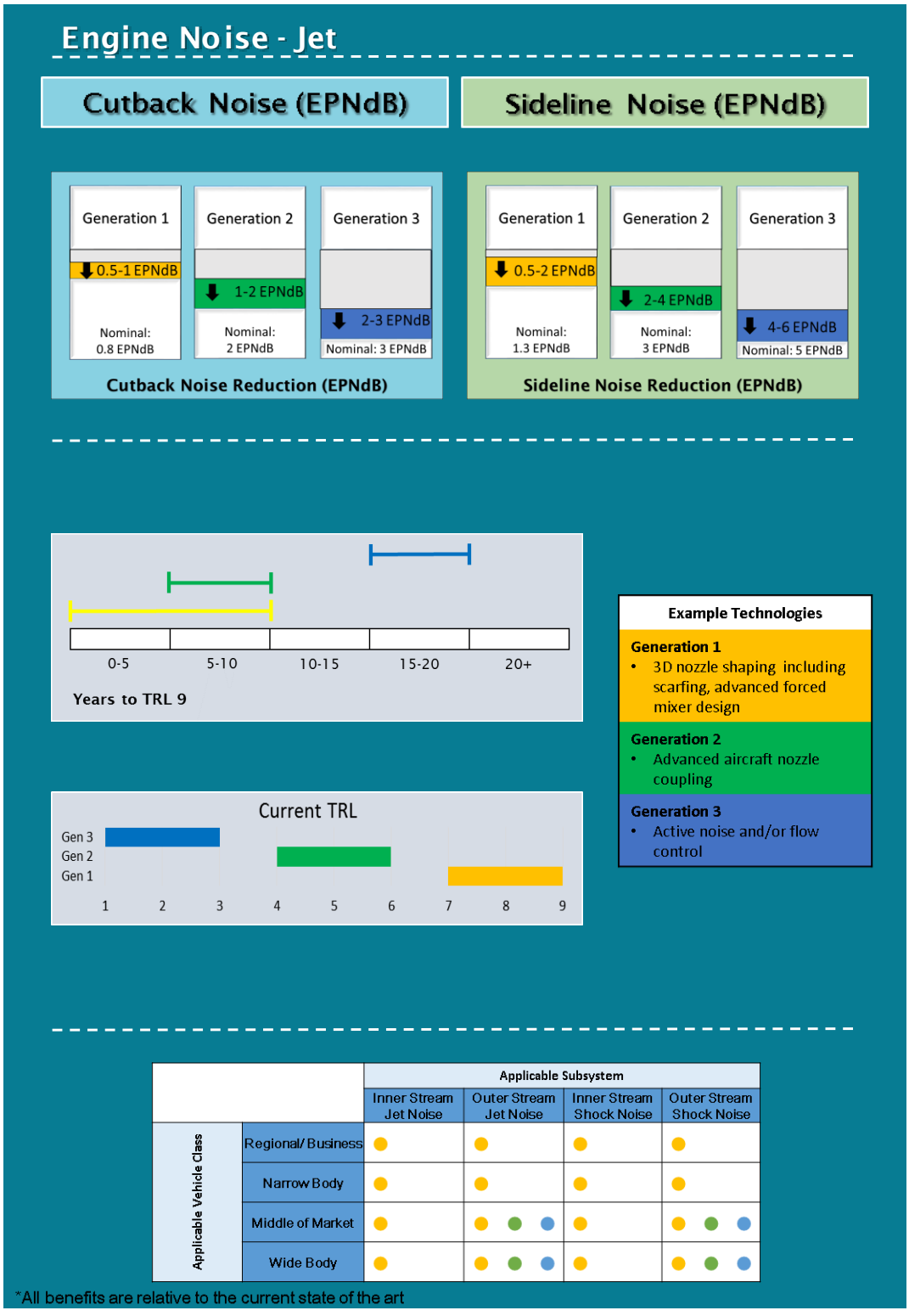

Figure 45: Technology Roadmaps for Engine Noise-Jet

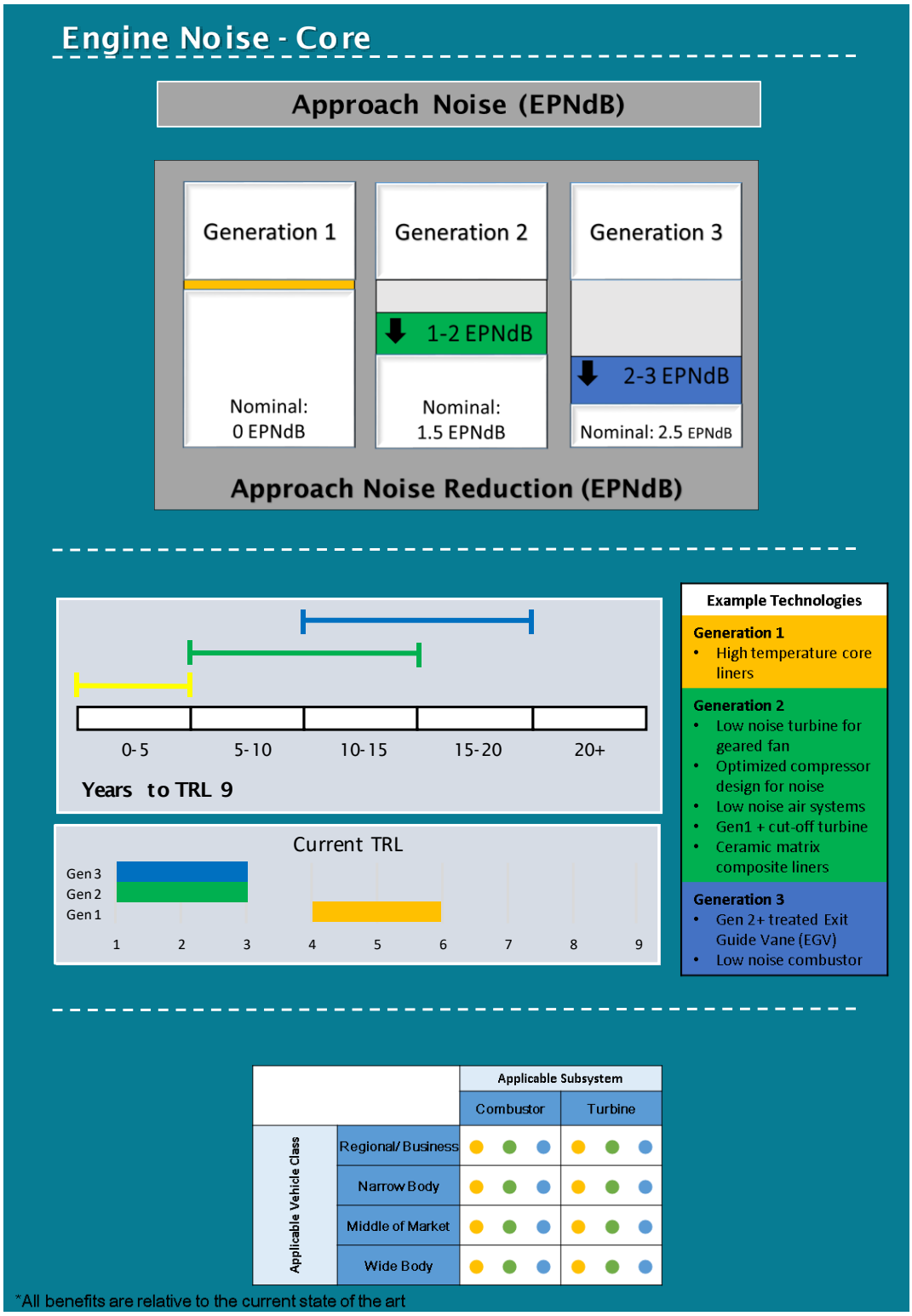

Figure 46: Technology Roadmaps for Engine Noise-Core

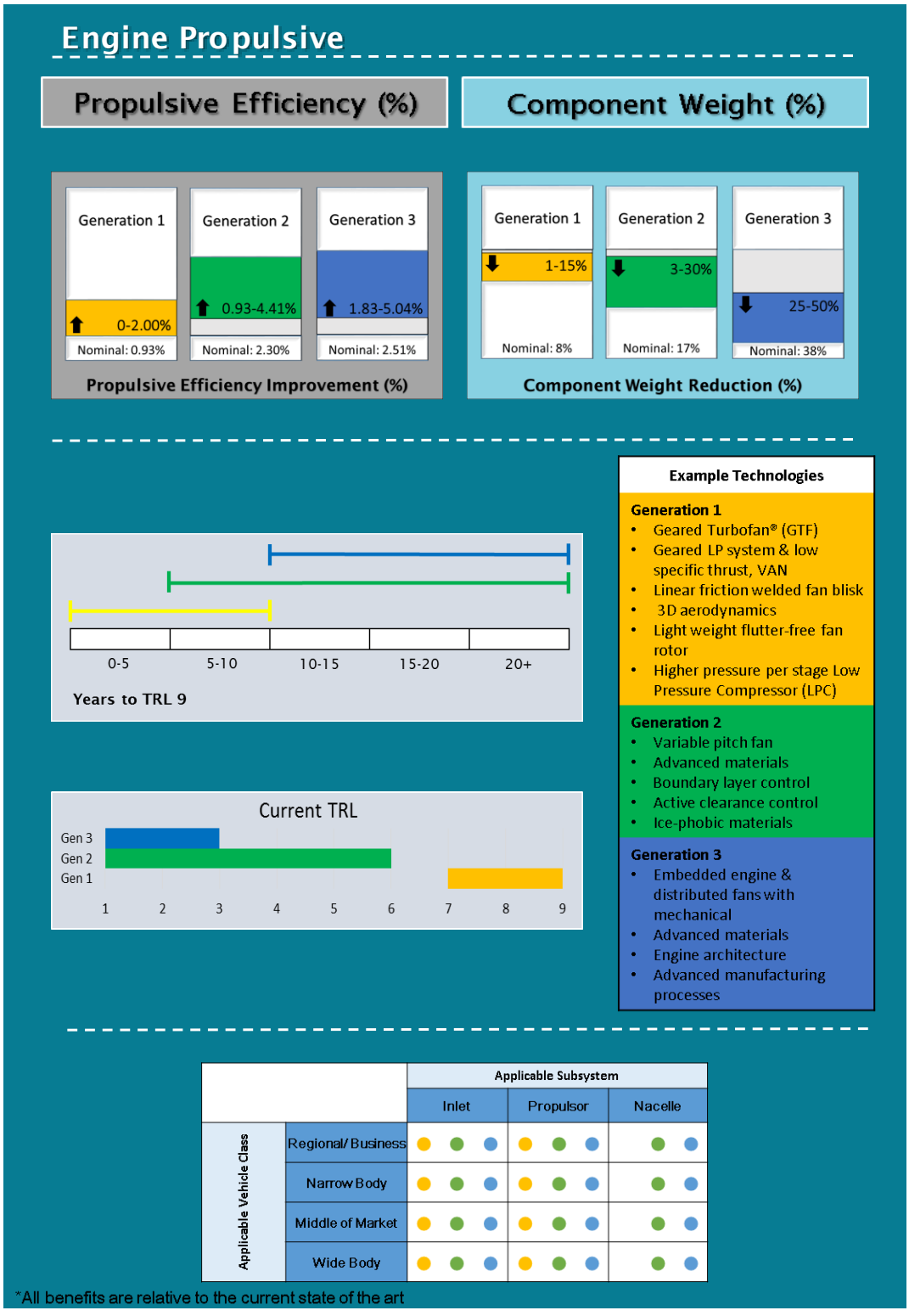

Figure 47: Technology Roadmaps for Engine Propulsive Efficiency Technologies

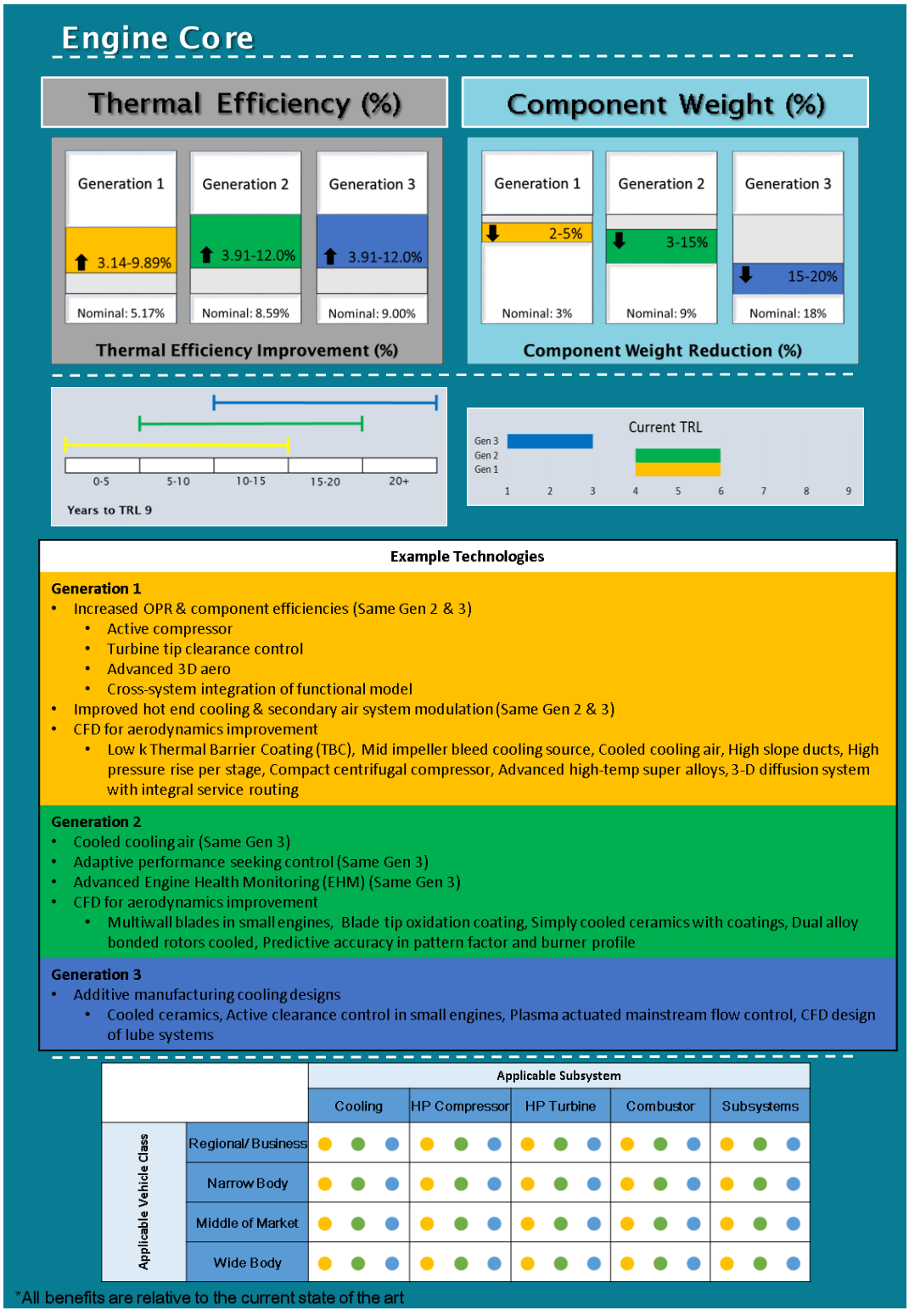

Figure 48: Technology Roadmaps for Engine Core Technologies

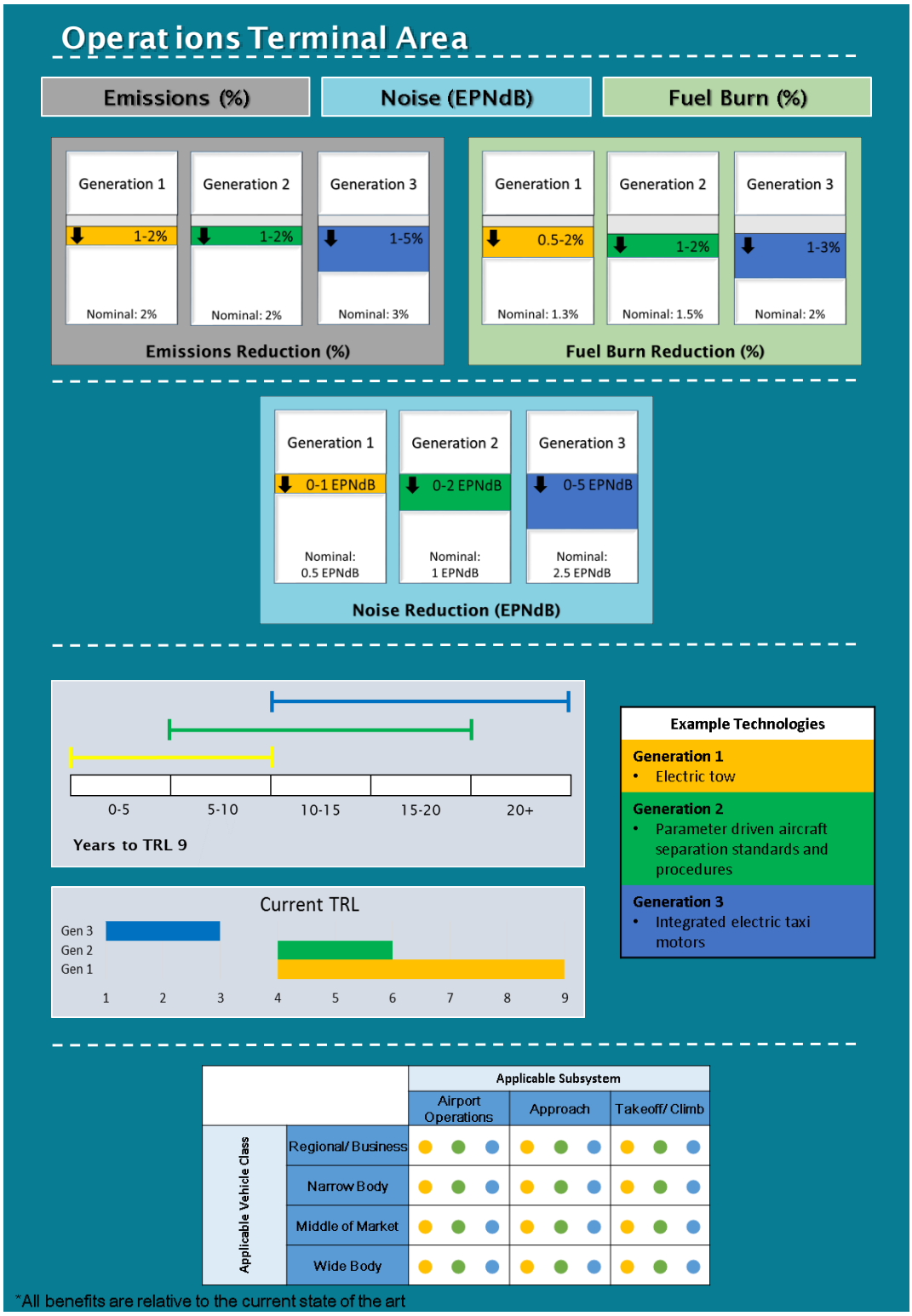

Figure 49: Technology Roadmaps for Operations Terminal Area

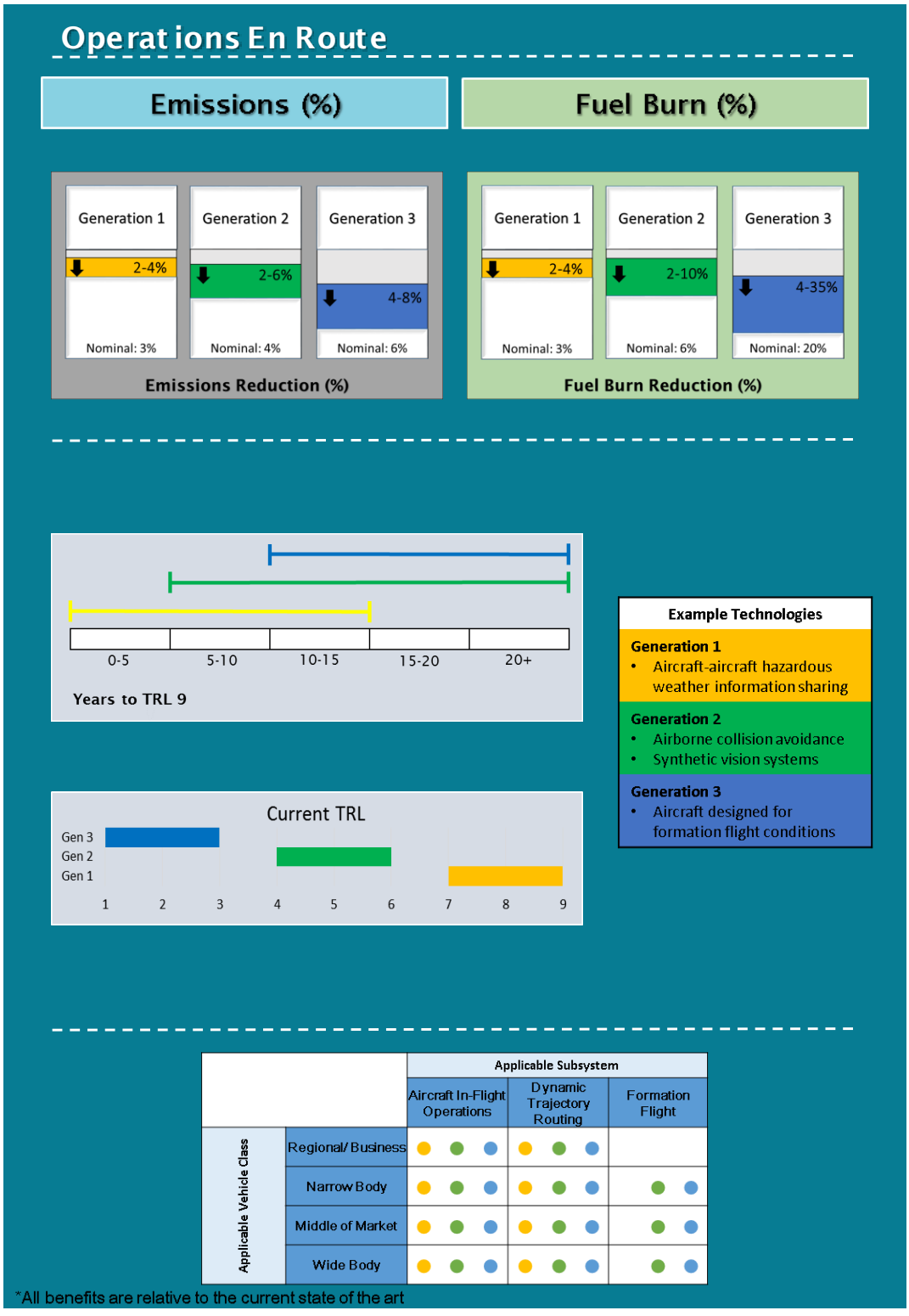

Figure 50: Technology Roadmaps for Operations En Route

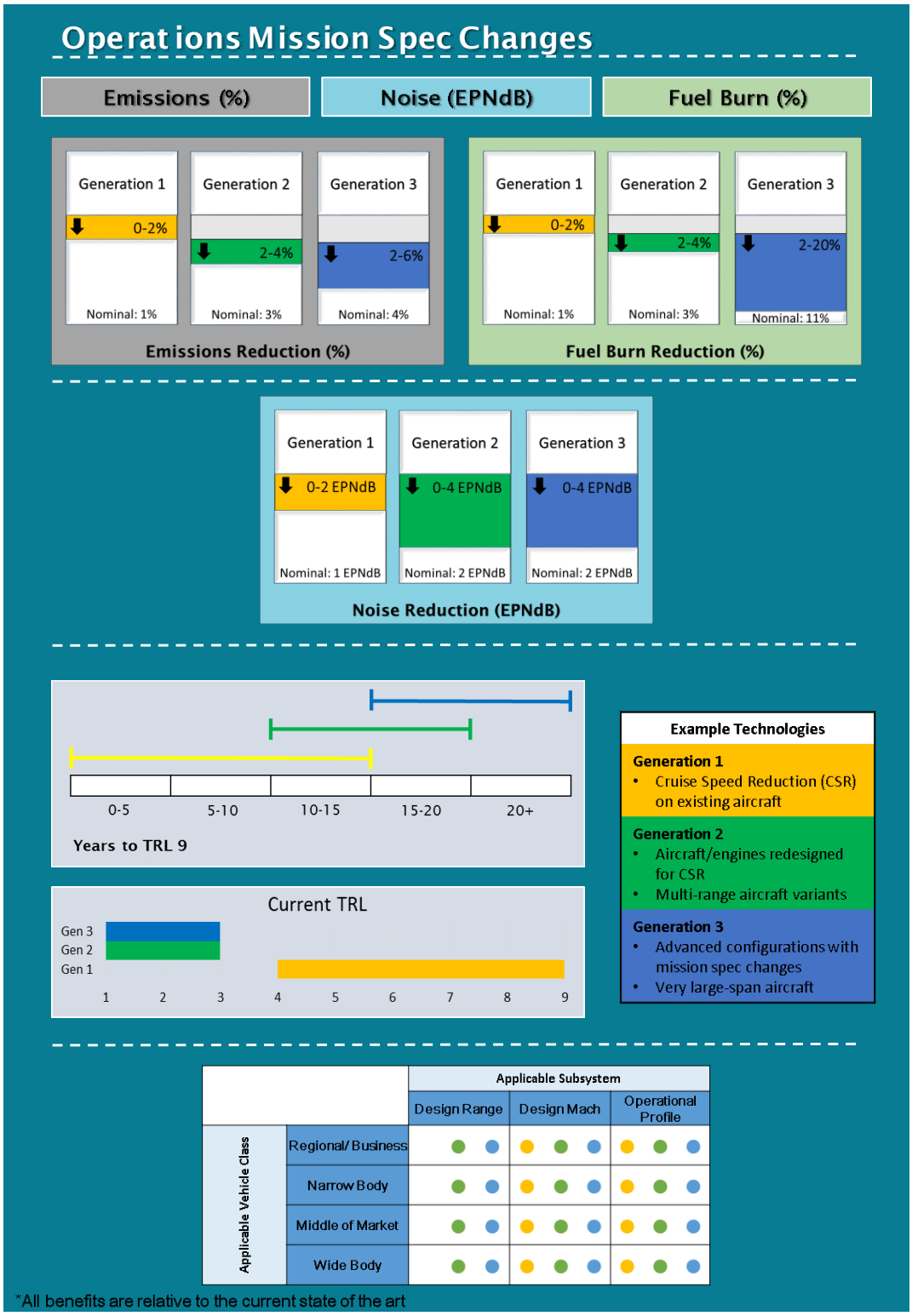

Figure 51: Technology Roadmaps for Operation Mission Spec Changes

Task #2: Vehicle Modeling

Objective: Description of Advanced Vehicles Provided to Purdue and Stanford

In order to allow Stanford to assess the impacts of mission specification changes and for Purdue to exercise their FLEET tool, Georgia Tech provided both universities with a set of public domain Flight Optimization System (FLOPS) aircraft models from the 2014 CLEEN assessments performed under PARTNER Project 36 [4]. More specifically, the vehicles provided were from the assessment scenario named "Aggressive minus CLEEN" or AG-C. This scenario assumed an aggressive introduction of N+1 and N+2 technologies[2], including technologies currently under development or sponsorship of NASA. Since the scenario had all CLEEN technologies removed, Georgia Tech chose to use those models as advanced technology baselines that would allow Stanford and Purdue to carry out their respective tasks with a relatively common set of vehicle performance assumptions. Stanford used the FLOPS models to create corresponding versions in their vehicle modeling tool, SUAVE and Purdue used the FLOPS models directly within their FLEET tool. The FLOPS vehicles in the final set of Purdue's FLEET analysis were consistent with the vehicles described in this section. For more details on the usage of the models in SUAVE and FLEET please see Sections 0 and 0, respectively. For more details on the technologies included in the AG-C vehicle package, please see Reference [4].

Research Approach

Modeling of Technologies and Advanced Configurations Process Overview

The overarching goal was to create models of aircraft that showed improvements from a 1995 baseline vehicle, and matched the values participants had come up with during the Technology Roadmap survey. This was done for five standard vehicle classes, the regional jet (RJ), single aisle (SA), small twin aisle (STA), large twin aisle (LTA), and very large aircraft (VLA). The final vehicle results were used during the fleet analysis by both Georgia Tech and Purdue. Further details on the Technology Roadmap Survey is provided in the Task #1 section. The Environmental Design Space (EDS), developed by Georgia Tech, was used to create these models. First, the variables within EDS that were applicable to the Technology Roadmap impacts were identified. In most cases, there were EDS variables that related directly to impacts, but for some impacts a parametric study had to be performed to identify appropriate modeling inputs (see following sections). A Vehicle Timetable was created from the results of the fleet workshops to identify when improved versions of different vehicle classes would enter the fleet. The spread of the "years to TRL 9" data from the Technology Roadmap survey were mapped to three different R&D levels. For example, the maximum value for "years to TRL 9" for a given technology area generation was treated as a low R&D level scenario. This mapping was used to decide what year the three technology generations for each impact began, for each of the three different R&D levels. Using the Vehicle Timetables in Figure 58 and Figure 59, the technology generations that were active during a vehicle generation could be determined for a given R&D level. This allowed vehicle models to then be created for different scenarios. As noted, these final vehicle models were then used as the basis for both Georgia Tech and Purdue's fleet analysis, described in the Task #3 section.

Identifying Applicable EDS Variables

Once the impact numbers from the Technology Workshop Survey data were finalized, the next step was to translate these impacts to variables native to the Environmental Design Space (EDS). EDS was the environment used by Georgia Tech to develop physics-based models of individual aircraft. Creating these models relied on the user to provide values for a large number of variables that define both the physical and theoretical aspects of the aircraft. The team started with existing models Georgia Tech had previously developed that were representative of 1995 versions of each vehicle class. The variables of these baseline models were then systematically changed to model the effects of the impacts predicted by the Technology Workshop surveys. For each impact, a list of EDS variables was created that could potentially be changed to model that impact. EDS is based off of a number of NASA tools, including Numerical Propulsion System Simulation (NPSS), Weight Analysis of Turbine Engines (WATE++), and FLOPS. The manuals of these tools were also reviewed to identify other variables that could be implemented within EDS that were fixed by default. The final input list consisted of 89 EDS variables. A list of the final EDS variable selections is provided in Table 8 broken down into the impacts for each technology area.

[2] N+1 is indicative of technologies with TRL 4-6 by 2015; N+2 indicates a TRL of 4-6 by 2020.

Table 8: Mapping of Technology Roadmap Impacts to EDS Variables

IMPACT	METHOD FOR MODELING IN EDS
Aircraft Wing Design	
Induced Drag %	Lift dependent drag factor
Component Weight %	Total wing weight
Laminar Flow by % Chord	Percent LF on wing upper and lower surface
Profile Drag %	Lift independent drag factor
Noise EPNdB	Approach, Cutback, and Sideline Noise Suppression Factor on Trailing Edge Wing, Trailing Edge Flap, and Leading Edge Slats
Aircraft Aerodynamic Improvements	
Induced Drag %	Lift dependent drag factor
Laminar Flow by % Chord	Percent LF nacelle, fuselage, vertical tail, and horizontal tail upper and lower surfaces
Profile Drag %	
Wave Drag %	
Aircraft Composites	
Design Margin %	Empty Weight Margin
Component Weight %	Total wing, horizontal tail, vertical tail, and fuselage weight
Aircraft Advanced Metallics	
Component Weight %	Total wing, horizontal tail, vertical tail, fuselage, land gear main, and landing gear nose weight
Aircraft Manufacturing Processes	
Component Weight %	Total wing, horizontal tail, vertical tail, and fuselage weight
Aircraft Multifunctional Structures	
Component Weight %	Total wing, horizontal tail, vertical tail, and fuselage weight
Aircraft Structural Health Monitoring	
Design Margin %	Empty Weight Margin
Component Weight %	Total wing, horizontal tail, vertical tail, and fuselage weight
Aircraft Noise	
Approach Noise EPNdB	
Cutback Noise EPNdB	
Source Noise dB	Approach, Cutback, and Sideline Noise Suppression Factor on Main Landing Gear, Nose Landing Gear, Trailing Edge Horizontal Tail, and Trailing Edge Vertical Tail
Sideline Noise EPNdB	
Aircraft Subsystems	
Drag %	Lift independent drag factor
Component Weight %	Auxiliary power unit, Instrument Group, Hydraulics Group, Electrical Group, and Avionics Group Weight
Aircraft Configurations	
Emissions %	Percent NO_x reduction
Fuel Burn %	
Noise EPNdB	
Engine Cycle	
Emissions %	Percent NO_x reduction
Fuel Burn %	
Noise EPNdB	
Engine Emissions	

Impact	Method For Modeling In EDS
Nitrogen Oxides %	Percent NO_x reduction
Particulate Mass %	
UHC %	
Engine PAI	
Interference Drag %	
Component Weight %	Factor for bare engine weight to engine pod weight
Nacelle Drag %	SWETN
Engine Structures and Materials	
Component Weight %	Fan Containment Material density
Engine Noise - Propulsor	
Engine Approach Noise - Propulsor	Approach Noise Suppression Factor on Inlet and Fan Discharge Noise
Engine Cutback Noise Propulsor	Cutback Noise Suppression Factor on Inlet and Fan Discharge Noise
Engine Sideline Noise - Propulsor	Sideline Noise Suppression Factor on Inlet and Fan Discharge Noise
Engine Noise - Jet	
Cutback Noise EPNdB	Cutback Noise Suppression Factor on Jet Takeoff Noise
Sideline Noise EPNdB	Sideline Noise Suppression Factor on Jet Takeoff Noise
Engine Noise - Core	
Approach Noise EPNdB	Approach Noise Suppression Factor on Fan Discharge Noise
Engine Propulsive	
Propulsive Efficiency %	Improvement modeled adjusting FPR, Extraction ratio at Aero Design Point, HPT chargeable (exit) cooling effectiveness, HPT non-chargeable (inlet) cooling effectiveness, and Maximum T4 (set at Take Off)
Component Weight %	Weight of miscellaneous propulsion systems, Fan Blade Material Density, Fan Stator Material Density, Fan Case Material Density, Inlet Nacelle Material Density and Bypass Nozzle Weight
Engine Core	
Thermal Efficiency %	Improvement modeled adjusting FPR, LPCPR, HPCPR, HPT chargeable (exit) cooling effectiveness, and HPT non-chargeable (inlet) cooling effectiveness
Component Weight %	Material Density of Burner Liner and Blades, Stators, and Disks of HPC, LPC, HPT, and LPT

In a number of cases there were no EDS variables that could be tied directly to an impact. For example, observer effective perceived noise level (EPNL) impacts are not directly related to noise suppression factors. Changes in observer EPNL can only be observed after the model is run. To reconcile this, parametric studies were run to analyze how observer EPNL was impacted by changing noise suppression factors related to wing design, propulsive, jet, and core noise. This is detailed further in the following sections. For Aircraft Noise, source noise impacts were provided in dB, which can be applied directly through noise suppression factors. By applying these suppression factors it was reasoned that the Aircraft Noise impacts for observer EPNL would be accounted for in terms of approach, sideline, and cutback.

Translating Impacts to EDS Variable Ranges

Once appropriate EDS variables had been chosen, the next major task was to determine how the impact values would be applied to the baseline values of the EDS variables. In some cases, it was seen that implementing stated impacts from the technology roadmaps could be done by simply adding, subtracting, or multiplying. In other cases, modeling the impacts required running a parametric study to determine the relationship between the EDS variable and impacts. After analyzing the EDS variables selected, eight different categories of EDS variables were identified as presented in **Table 9**. A detailed description of the Technology Roadmap Design of Experiments (DOE) Aggregator that was created to automate this process is given in the following sections. The Aggregator used the variable type that had been identified for each EDS variable to determine how to apply the impacts.

Table 9: Options for Applying Technology Impact to an EDS Variable

Variable Type	Description	Formula (K# Represents Individual Impact)
Scalar	Multiplicative	=Baseline*((1+K1/100)*(1+K2/100)*(1+K3/100)*…*(1+Ki/100))
Delta	Added together	=Baseline + (K1+K2+K3+…+Ki)
Noise	Combined on decibel scale	=Sum[(1*largest Ki) + (0.75 * 2nd largest Ki) + (0.5 * 3rd largest Ki) + (0.33 * 4th largest Ki)+ (0.16 * 5th largest Ki) + (0.08 * 6th largest Ki)....]
DeltaF	Added together as fraction/decimal	=Baseline + (K1+K2+K3+…+Ki)/100
Switch	Turns on or off from its baseline state if there is an impact	1 or 0
Absolute	Replaces baseline. Chosen based on parametric studies or must be set to zero	

Performing Sensitivity Checks On Benefit Ranges
For scalar and delta type EDS variables, a sensitivity study was run using the one-at-a-time method. This involved applying the Generation 3 maximum impact to a given EDS variable, while keeping all other EDS variables at their baseline values. A case was run for each EDS variable, for all five aircraft class models, to see if the model would run at the limits of this projected future design space.

Results of Sensitivities
In addition to checking if an impact could actually be modeled, the sensitivities helped confirm that the right variable type had been identified for each EDS variable. The only EDS variable that posed a problem was PCT_NO_x, which stands for "Percentage NO_x reduction". The impacts for engine emissions nitic oxides reduction, engine cycle emissions reduction, and aircraft configurations emissions reduction were all mapped to PCT_NO_x. Since PCT_NO_x was a DeltaF type variable, the impacts would typically be added together. Unfortunately, the combination of the maximum values of these three impacts resulted in a NO_x reduction value greater than 100%, which is not possible. It was decided that the largest of these three impacts would be used as representative of all three when modeling the vehicles. This does not mean the same one of these impacts was always dominant. For example, for a vehicle modeled with all Generation 2 impacts, at a high technology level, the impact values for engine emissions engine cycle, and aircraft configurations on PCT_NO_x were 75%, 40%, and 40% respectively, so engine emissions dominated. For a high technology level vehicle with a Generation 2 engine emissions impact, and Generation 3 engine cycle and aircraft configurations impacts, the impact values on PCT_NO_x were 75%, 40%, and 80% respectively, so aircraft configuration dominated instead.

Considerations for Noise and Engine Efficiency
Since observer EPNL and thermal and propulsive efficiency were output metrics of sizing, getting the correct impact values required first understanding the relationship between them and the EDS variables that affect them. This involved a full factorial approach to sensitivity analysis, where the effects of changing the multiple EDS variables together was looked at. The main parameters that could have be modified to improve propulsive efficiency were extraction ratio (Ext_Ratio), fan pressure ratio (FPR), and maximum burner exit temperature (T4max). Thermal efficiency could have been improved by increasing the overall pressure ratio (OPR) and modifying the work split between the low-pressure compressor ratio (LPCPR) and high-pressure compressor ratio (HPCPR). Note that OPR was not a direct EDS variable, but was the product of the EDS variables for LPCPR, HPCPR, and FPR. Both efficiencies could have also have been improved by decreasing the amount of cooling need by the engines using the EDS variables s_HPT_ChargeEff and s_HPT_NonChargeEff. For noise, increasing noise suppression factors could have continued to lower observer EPNL results, but with diminishing returns.

Conducting Parametric Studies for Engine Cycle Variables
As noted in the previous section, the propulsive and thermal efficiency were calculated outputs of EDS, so they could not be directly input. In order to get the impacts reported in the workshop surveys, the engine cycle parameters that affect efficiency were changed. A parametric study was conducted for both thermal efficiency and propulsive efficiency. The goal was to first vary applicable cycle parameters over wide ranges to analyze trends in the efficiencies. From this analysis the team believed

it would then be able to choose cycle parameters values to reach the low, nominal, and high efficiency values for each generation. These studies had to be repeated for each vehicle class, since the baseline models did not all have the same engines. The selected engine cycle parameters were then arranged as a look-up table that could be searched when constructing the EDS cases for the different technology scenarios that were modeled.

Thermal Efficiency Studies

The thermal efficiency sensitivity study was conducted by first increasing OPR by keeping FPR constant and increasing LPCPR and HPCPR, keeping the work split between the LPC and HPC constant. The work split was then modified to see the effects of shifting 20% more of the work to the LPC and then 20% more of the work to the HPC. The results of the first set of sensitivities for the VLA are shown in Figure 52.

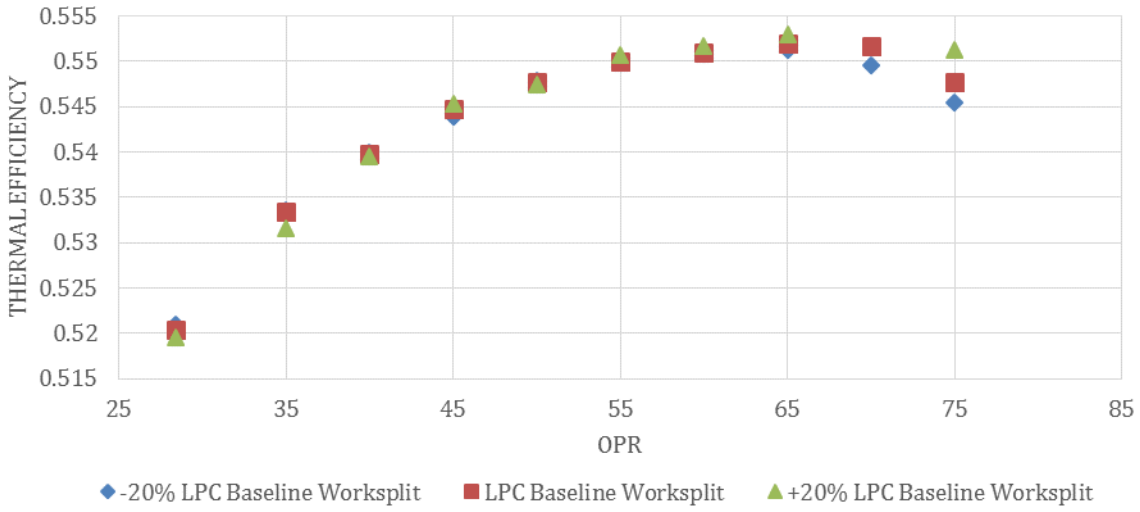

Figure 52: Initial Results of Thermal Efficiency Study for the VLA

As can be seen, the thermal efficiency peaked at 55.2%, which was only a 6.2% relative percent increase from the baseline of 52%. The surveys expected a maximum relative percent increase of 30%, which in the case of the VLA would mean a thermal efficiency of 67.6%. An OPR of 75 was used as an aggressive upper limit for these studies. Note that for an OPR of 75 the theoretical maximum thermal efficiency for a gas turbine was calculated as 70.9%. Similar results were seen for the other four vehicles, where the relative thermal efficiency values were still far away from the projected impacts initially reported in the workshop surveys.

Further studies focused on the LTA and large and small single-aisle (SSA-LSA) aircraft models. The effects of decreasing the amount of cooling required by the high-pressure turbine (HPT) were examined, lowering it until it was nearly zero. The impact of changing FPR was also investigated using the same range of FPR values used during the initial propulsive efficiency studies. As previously noted, these studies used a full factorial approach. Therefore, if the FPR was changed, all cases that had been run with that previous FPR, changing OPR and cooling, were repeated. For the LTA the baseline thermal efficiency was 56.5% and from this process a maximum thermal efficiency of 60.4% was achieved, or a relative percent increase of 6.9%. For the SSA-LSA the baseline thermal efficiency was 49.5% and a maximum thermal efficiency of 54.2% was achieved, which translated to a relative percent change of 9.5%. These efforts began to call into question how reasonable the survey predictions were. As will be detailed further, it should be noted these maximum thermal efficiencies did not correspond the parameters to maximize propulsive efficiency.

Propulsive Efficiency Studies

The propulsive efficiency studies began by decreasing the FPR until it reached a hard lower limit of 1.25. In addition, the extraction ratio was perturbed 20% in either direction of the baseline value. Presented in Figure 53 are the initial results of the study for the SSA-LSA. There was a positive trend in propulsive efficiency between increasing extraction ratio and also decreasing FPR, but clearly there were diminishing returns.

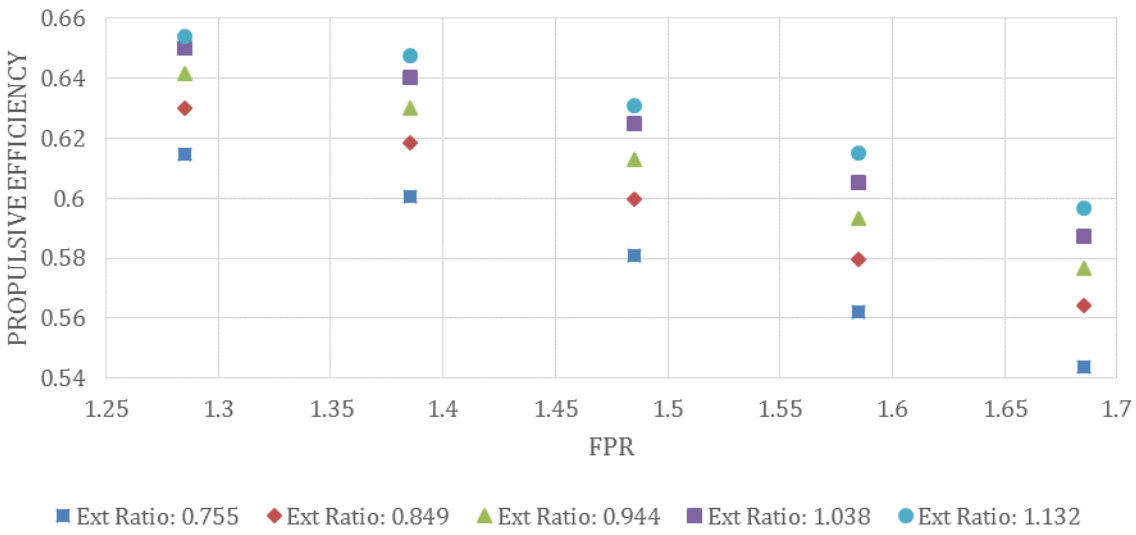

Figure 53: Initial Propulsive Efficiency Sensitivity Study Results for the SSA-LSA

The baseline propulsive efficiency for the SSA-LSA is 57.7% and the maximum propulsive efficiency reached in this study was 65.4%, which was only a relative change of 13.3%. This was below even the Generation 1 maximum impact gathered from the survey of 20%.

For the LTA the maximum propulsive efficiency achieved was 70.6%, which was a relative percent increase of 10.4% from the baseline. A maximum relative percent increase of 18.5% was achieved for the SSA-LSA. It was known that some companies have accounted for propulsive efficiency by dividing out the efficiency of the LPT. Doing this resulted in the maximum relative percentage change from the baseline becoming 11.3% and 18.9% for the LTA and SSA-LSA, respectively. Again these results were below even the maximum Generation 1 impact prediction of a 20% relative percent increase. In addition, the parameters to achieve these maximum propulsive efficiency increases did not correspond with the parameters to maximize thermal efficiency. This concern is best exemplified by Figure 54, which has the thermal efficiency of all the cases run for the LTA plotted against their propulsive efficiency with the LPT efficiency divided out. The figure shows a Pareto frontier, meaning there was a compromise occurring between propulsive and thermal efficiency.

Given the results of this study an alternative solution was proposed. The disparity between the survey and the trade study possibly could have been attributed to the fact that most industry experts spoke of engine improvements in terms of bypass ratio (BPR) and OPR instead of thermal and propulsive efficiency. A literature search was conducted to determine what academia and the aerospace industry believed OPR and BPR values would be over the next three generations for the five different aircraft classes that were modeled. The end goal was to then use those findings as a more credible basis for the engine cycle parameters. The infographics would then be updated based on the final results.

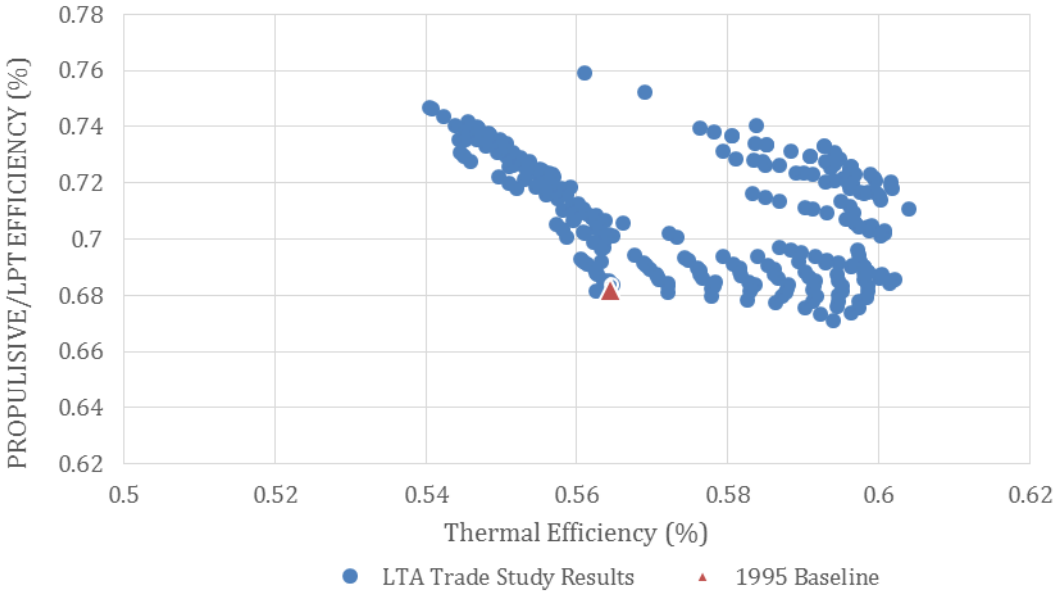

Figure 54: LTA Efficiency Trade Study Results Showing Propulsive Efficiency against Thermal Efficiency

Generation 1 OPR & BPR Research

Generation 1 aircraft were viewed as those entering service in the near term, from 2015 to 2018. The Airbus A320neo, which entered service in January 2016, was a 189 passenger, single aisle jetliner [5]. Neo stands for new engine option, and customers are provided with the choice of either the Pratt & Whitney PW1100G Geared Turbofan (GTF) or the CFM International LEAP-1A turbofan. The A320neo was seen as a fair representation for the LSA. Pratt & Whitney's GTF is reported to have an HPCPR of 16:1 leading to an OPR of 50:1. The engine has a BPR of 12:1. The GE LEAP-1A first saw service on an A320neo in July 2016. It's purported to have a BPR of around 11:1, with a confirmed HPCPR of 22:1 and OPR of 40:1. The LEAP-1C will be powering the Comac C919, which is a narrow-body aircraft that will hold 156-168 seats, making it comparable to the SSA-LSA. The basic engine parameters for the LEAP-1C are the same as the LEAP-1A, it just has a slightly smaller fan causing it to have less thrust.

The Rolls Royce Trent XWB is a three-shaft turbofan currently seeing use on the Airbus A350 XWB, which holds between 250 and 440 passengers depending on the variant [6]. Together they entered commercial service in January 2015. The Trent XWB has a BPR of 9.6:1 and OPR of 50:1. Based on the large seat capacity range the Trent XWB was used as the basis for both LTA and VLA engine cycles.

The GE Passport is a regional and small business jet engine scheduled to first see service in 2018 on the Bombardier Global 7000 [7]. Development of the Passport benefitted greatly from the technology of the CFM International LEAP family of engines. Based on its FAA engine certificate data sheet, the Passport has a BPR of 5.6:1, OPR of 45:1 and HPCPR of 23:1 [8]. Georgia Tech already has Generation 1 regional jet (RJ) model that was used, which has a HPCPR of 22:1 and OPR of 47:1. The HPCPR for the Passport was used as a basis for the Generation 2 RJ engine.

Generation 2 OPR & BPR Research

Research for Generation 2 engine cycles focused on the 2020 to 2030 timeframe. Both the Vision 10 and 20 from Rolls Royce's Future Programmes gave good insight into the progression of turbofan technology [9]. The Advance family is an engine architecture that would enter service after 2020. The Advance3 is the larger three-shaft version seen as the next evolution for Rolls Royce from the Trent XWB, and as a stepping stone towards future geared turbofans. It was chosen to represent the Generation 2 engine for the LTA with a BPR and OPR of over 11:1 and 60:1 respectively. The Advance2 is the two-shaft member of the family that would service aircraft in the 150 passenger market, making it an appropriate representation for the STA and SSA-LSA Generation 2 engines. The Advance2 is targeted to have a HPCPR of 22:1 and a similar BPR to the Advance3. Since the LTA baseline is modeled with a two-shaft engine this HPCPR was also used for the LTA Generation 2 engine cycle.

The Boeing 777X is currently under development with the 777-9 variant slated to hold 400-425 passengers making it a comparable basis for the LTA [10,11]. The 777X will be powered by GE Aviation's GE9X, which is approximated to achieve a BPR of 10:1, HPCPR of 27:1, and OPR of 60:1. Entry into service for the Boeing 777X is targeted for late 2019.

For Generation 2 Regional Jets there was limited quantitative information to be found. Based on historical trends, progress for RJ type aircraft tended to trail behind the larger aircraft classes due to space limitations. With this in mind the GE Passport HPCPR was used, but OPR was increased to be on par with the Trent XWB and BPR was also made more aggressive.

Generation 3 OPR & BPR Research

Rolls Royce's Vision 20 again provided some guidance when looking at Generation 3 engine cycles. The intention of the Advance3 is to be an intermediate step to the three-shaft, geared UltraFan™, as noted in Reference [9]. The current figures for this engine are a bypass ratio greater than 15:1 and OPR greater 70:1, with an entry into service beyond 2025. This engine was viewed as most applicable to the LTA. A large theme in discussions on Generation 3 powerplants was the diminishing gains in efficiency from increasing BPR. Most papers were focused on the implementation of open rotors or even alternative powerplants to gas turbines entirely. Without sufficient information it was decided that the Generation 2 cycle parameters would be reused for the other aircraft.

Identifying Appropriate FPR & Cooling Variables

Since BPR was an output parameter of engine sizing, the next step was to adjust the FPR and cooling required by the HPT to get within the range of the BPR values found, using the OPR and HPCPR values that were identified. After the FPR was found LPCPR was determined by dividing the OPR by the product of FPR and HPCPR. The engine cycle parameters chosen for every vehicle for every vehicle are presented in **Table 10**. The infographics values for propulsive and thermal efficiency were updated using final vehicles for each generation, with all impacts applied as presented in the following sections.

Table 10: Engine Cycle Parameters Chosen for Each Vehicle Class for Every Generation

FPR					
Generation	**RJ**	**SSA-LSA**	**STA**	**LTA**	**VLA**
0	1.629	1.685	1.643	1.58	1.758
1	1.55	1.58	1.54	1.58	1.55
2	1.55	1.58	1.54	1.58	1.55
3	1.55	1.58	1.54	1.28	1.55
OPR					
Generation	**RJ**	**SSA-LSA**	**STA**	**LTA**	**VLA**
0	38.51	30.55	30.63	39.89	28.43
1	47.41	40	40	52	52
2	50	60	60	60	60
3	50	60	60	70	60

Technology Roadmap Design of Experiments (DOE) Aggregator

In order to generate the DOE tables for EDS for any combination of impacts from different generations, an easy to use dashboard interface was created in Excel. Having a DOE Aggregator helped avoid any potential mistakes from manually creating the DOE tables. The DOE Aggregator was also flexible enough to allow new impact values to be input, allowing this

process to be repeated in the future with new surveys. The dashboard was created without the use of macros in order to allow ease of transfer across different organizations and machines.

Overall Layout of Technology Roadmap DOE Aggregator

A diagram of the overall flow of data through the DOE Aggregator is provided in Figure 55. On the Scenario Input sheet each row was a case. The user defined what the case's Technology Level, Vehicle Class, and what the Technology Generation was for each Technology Area. This case information then flowed into the Aggregator sheet, which used the information to look up what the impact values were in the Impact Mapping Sheet. It also found the correct values of the absolute type EDS variables from the Chosen Factors sheet. Impacts were aggregated for each variable according to their variable type. They were then passed on to the Case Construction sheet. The correct baseline EDS values were taken from the Baselines sheet based on what Vehicle Class was given for the case in the Scenario Input sheet. The impacts were then applied to these baselines, according to their variable type, or were replaced entirely if they were absolute type variables. Finally, from the Case Construction sheet cases were filtered into their correct vehicle DOE sheet. The baseline values for the EDS variables that were not modified were taken from the Baselines sheet to complete each DOE.

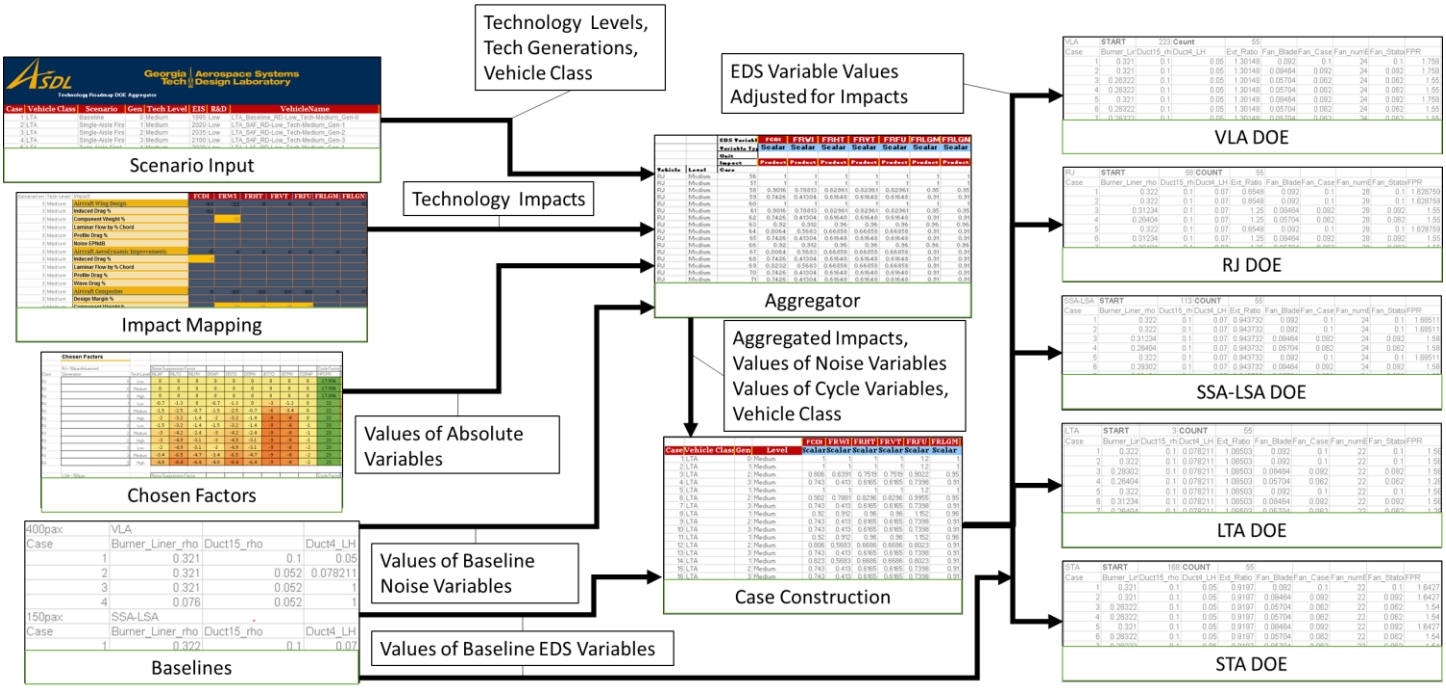

Figure 55: Technology Roadmap DOE Aggregator Data Flow

Scenario Input

The main interface was the Scenario Input sheet, as shown in Figure 56. Each row within the Scenario Input sheet defined a separate case. Cases were created based on the scenario timetables described in the next sections. The scenario timetables provided information specific to each vehicle class. The first column was simply the case number, which was used for tracking purposes throughout the DOE Aggregator. The second column was where the user defined the Vehicle Class for each case, whether it was a VLA, RJ, SSA-LSA, LTA, or STA. The third column contained information on what scenario was being modeled, whether it was the baseline, twin-aisle vehicles entering the market first, or single-aisle vehicles entering the market first. This input did not affect DOE results, but was a reference to which scenario timetable the case was created from. Similarly, the fourth column, which gave the vehicle generation, was also a reference to the timetable. Vehicle generations ranged from 0 to 3. The fifth column was where the user defined the technology level. This referred to how great the technology's impact would turn out to be once it was fully developed. The user had the choice between Low, Medium, and High. Only a single overall technology level was chosen for each case and it effected what values are used from the Impact Mapping sheet. The EIS year for the vehicle was given the sixth column and was a reference from the scenario timetables. The seventh column was the R&D level, which can be Low, Medium, and High. R&D level was not used directly by the DOE Aggregator but was important when creating the cases, as described in the next sections. The technology generation for all 19 technology impact

areas had to be defined in columns 9 through 27. These technology generations were chosen by the user based on the R&D level and "Years to TRL 9". This process is also described in the following sections. Note only three of the 19 impacts are shown Figure 56.

ASDL Georgia Tech Aerospace Systems Design Laboratory

Technology Roadmap DOE Aggregator

Case	Vehicle Class	Scenario	Gen	Tech Level	EIS	R&D	VehicleName	Aircraft Wing Design	Aircraft Aerodynamic Improvements	Aircraft Composites
1	LTA	Baseline	0	Medium	1995	Low	LTA_Baseline_RD-Low_Tech-Medium_Gen-0	0	0	0
2	LTA	Single-Aisle Firs	1	Medium	2020	Low	LTA_SAF_RD-Low_Tech-Medium_Gen-1	0	0	0
3	LTA	Single-Aisle Firs	2	Medium	2035	Low	LTA_SAF_RD-Low_Tech-Medium_Gen-2	2	2	2
4	LTA	Single-Aisle Firs	3	Medium	2100	Low	LTA_SAF_RD-Low_Tech-Medium_Gen-3	3	3	3
5	LTA	Twin-Aisle First	1	Medium	2020	Low	LTA_LAF_RD-Low_Tech-Medium_Gen-1	0	0	0
6	LTA	Twin-Aisle First	2	Medium	2030	Low	LTA_LAF_RD-Low_Tech-Medium_Gen-2	1	1	1
7	LTA	Twin-Aisle First	3	Medium	2045	Low	LTA_LAF_RD-Low_Tech-Medium_Gen-3	3	3	3
8	LTA	Single-Aisle Firs	1	Medium	2020	Medium	LTA_SAF_RD-Medium_Tech-Medium_Gen-1	1	0	0
9	LTA	Single-Aisle Firs	2	Medium	2035	Medium	LTA_SAF_RD-Medium_Tech-Medium_Gen-2	3	3	3

Figure 56: Technology Roadmap DOE Aggregator Scenario Input Tab

Impact Mapping

Impact Mapping was the sheet where the subcategories for all 19 vehicle impacts were mapped in a matrix to their corresponding EDS variables. Each subcategory had a value for all three generations for all three technology levels. The values of the subcategories, like Induced Drag % and Component Weight %, were summed in the rows labeled with the top-level impacts, like Aircraft Wing Design.

Generation	Tech Level	Impact	FCDI	FRWI	FRHT	FRVT	FRFU	FRLGM	FRLGN
3	Medium	Aircraft Wing Design	-21	-33	0	0	0	0	0
3	Medium	Induced Drag %	-21						
3	Medium	Component Weight %		-33					
3	Medium	Laminar Flow by % Chord							
3	Medium	Profile Drag %							
3	Medium	Noise EPNdB							
3	Medium	Aircraft Aerodynamic Improvements	-6	0	0	0	0	0	0
3	Medium	Induced Drag %	-6						
3	Medium	Laminar Flow by % Chord							
3	Medium	Profile Drag %							
3	Medium	Wave Drag %							
3	Medium	Aircraft Composites	0	-20	-20	-20	-20	0	0
3	Medium	Design Margin %							
3	Medium	Component Weight %		-20	-20	-20	-20		
3	Medium	Aircraft Advanced Metallics	0	-9	-9	-9	-9	-9	-9
3	Medium	Component Weight %		-9	-9	-9	-9	-9	-9
3	Medium	Aircraft Manufacturing Processes	0	-3	-3	-3	-3	0	0
3	Medium	Component Weight %		-3	-3	-3	-3		

Figure 57: Impact Mapping Tab in Technology Roadmap DOE Aggregator

Aggregator

The Aggregator sheet was the first step in creating the DOE tables. Each row represented a case from the Scenario Input sheet. For each EDS variable identified, this sheet determined what impacts were related to it. For the subset of impacts related to the variable, the sheet then looked at the Scenario Input sheet to find what the Tech Level for the case was and what the generations were for the impacts in the subset. The sheet then looked at the Impact Mapping sheet for each impact to find the value that was mapped to the EDS variable for that Technology level and Generation. The values for impacts in the subset were then combined based on what variable type the EDS variable was, as explained earlier.

An exception to that process was the EDS variables for the engine cycle related to thermal and propulsive efficiency. As discussed earlier, the values for FPR, Ext_Ratio, LPCPR, HPCPR, s_HPT_ChargeEff, and s_HPT_NonChargeEff were chosen based on a literature search on future engine cycles. Propulsive efficiency was a subcategory of Engine Propulsive and was largely a function of FPR and Ext_Ratio. Thermal Efficiency was a subcategory of Engine Core and was mainly a function of OPR (FPR, LPCPR, and HPCPR). Both were effected by s_HPT_ChargeEff, and s_HPT_NonChargeEff, which were related to the cooling required by the HPT. On the Scenario Input sheet the user had the option to choose different generations for Engine Propulsive and Engine Core. The mixing of engine cycle parameters from different generations though greatly increased the chance of the case failing. To account for this the Aggregator sheet used the lower of the generations between Engine Propulsive and Engine Core and the case's Technology Level and vehicle to look up the engine cycle parameters on the Chosen Factors sheet.

The EDS variables related to Engine Noise for the core, propulsor, and jet were also chosen like the values for the engine cycle, but were based entirely on a parametric study. Different generations were able to be entered for the core, propulsor, and jet engine noise without a problem. The Aggregator sheet then simply grabs the correct values from the Chosen Factors for the provided generation, vehicle and Technology Level. Combining noise variables was more involved than the other EDS variables. The Aggregator sheet had to determine the size order of the impacts, which included treating the baseline value as an impact. With the size order known the values were then combined following the rules in Table 9.

Case Construction
The Case Construction sheet first looked up the baseline value for the cases from the Baselines sheet based on what vehicle the case was using. The combined impacts from the Aggregator sheet were then taken and added to, multiplied by, or simply replaced the baseline value, depending on the EDS variable type. In the case of noise variables the baseline values were already needed by the Aggregator sheet when determining the new noise suppression factors, so these values were able to be put directly into place.

Baseline Vehicles
The Baselines sheet contained the baseline vehicles previously developed by Georgia Tech. For all five vehicles there were four cases. In all instances Case 1 was the baseline used since it represented a vehicle that entered into service in 1995. For future studies though the baseline could easily be transitioned to one of the other cases. The 1995 baseline for the RJ did not have a low pressure compressor (LPC), so the RJ Case 2 was modified to have values appropriate for a 1995 vehicle, but with a LPC. This modified case was then used as the RJ baseline moving forward.

Chosen Factors
The Chosen Factors sheet was where noise suppression factors, from the parametric study, and the engine cycle parameters, based on the literature review, were found. For a given generation and vehicle there was no difference in the engine cycle parameters for different Technology Levels, because there was not enough information found to base that differentiation on.

Vehicle DOEs
A DOE table contained a row for each vehicle case and contained all the information that EDS needed to read in. Creating the DOE tables for each vehicle relied on all the cases for the same vehicle being together on the Scenario Input sheet. For each case the DOE sheet then went through all the EDS variables in the baseline EDS DOE table. If the EDS variable was one of the ones that had been modified, the DOE sheet obtained its new value from the Case Construction sheet. Otherwise it used the baseline value.

Table 11 shows a subset of the final DOE sheet for the VLA, with only six of the over 300 EDS variables in a DOE shown. The “START” number 223 was the row in the Case Construction sheet where the VLA cases started, not the Scenario Input sheet case number. “Count” was the number of VLA cases counted in the Scenario Input sheet. The only manual step for the user was that the row formula had to be dragged down, or rows would be deleted so that the number of cases matched the “Count”.

Table 11: Subset View of Final DOE Table for the VLA from the Technology Roadmap DOE Aggregator

VLA	START	**223**	Count	**55**		
Case	Burner_Liner_rho	Duct15_rho	Duct4_LH	Ext_Ratio	Fan_Blade_rho	Fan_Case_rho
1	0.321	0.1	0.05	1.30148	0.092	0.1
2	0.321	0.1	0.05	1.30148	0.08464	0.092
3	0.26322	0.1	0.05	1.30148	0.05704	0.062
4	0.26322	0.1	0.05	1.30148	0.05704	0.062

Using Technology Roadmap DOE Aggregator
In order to use the Technology Roadmap DOE Aggregator the most probable cases first had to be defined. Defining a case first involved assigning what scenario, vehicle class, and vehicle generation were being used. Using a vehicle replacement

schedule the EIS year for the case vehicle could be determined. An R&D level was then chosen which, along with the "Year to TRL 9" data from the infographics, allowed the EIS year for the three generations of each technology area to be determined. The technology area EIS years were compared to the vehicle EIS year to identify what generation of each technology area was being used for that case. Finally, the case was assigned a technology level, which indicated how great the impacts of the technology areas would end up being. Cases were made for every combination of the two scenarios, five vehicle classes, three vehicle generations, three R&D levels, and three technology levels. Complete case definitions were inserted as a row in the Scenario Input sheet of the DOE Aggregator, which then created five DOEs separated into each vehicle class. These DOEs were then modeled using EDS.

Vehicle Timetable & Scenarios

With the capability provided by the Technology Roadmap DOE Aggregator over 800 billion different technology scenarios were able to be considered. To narrow down to the important ones first a replacement schedule was created. It identified the likely year for introduction of re-engined models, performance improvement packages, and new designs for each vehicle class from 2015 out to 2050. This replacement schedule was then used to assess what the EIS year would be for each vehicle class whether a twin-aisle or single-aisle vehicle was introduced first. The replacement schedule for the single-aisle first vehicle is shown in Figure 58 and the twin-aisle first vehicle is shown in Figure 59. For each of the 19 technology impact categories the "Years to TRL 9" was forecasted for the next three generations assuming a low, medium, or high R&D level, to get EIS dates for that technology. For a given R&D level, the EIS year of the generations for each vehicle was used to determine what the generation each technology impact would be on that vehicle based on the technology EIS years. Technology packages were made for all three vehicle generations for all five vehicles for all three R&D levels for both single-aisle and twin-aisle scenarios. This resulted in 90 cases. In addition, the surveys had provided the information to differentiate levels of technology effectiveness for each generation. Considering the three technology levels resulted in 180 cases worth investigating plus the 5 baselines if technology stayed frozen.

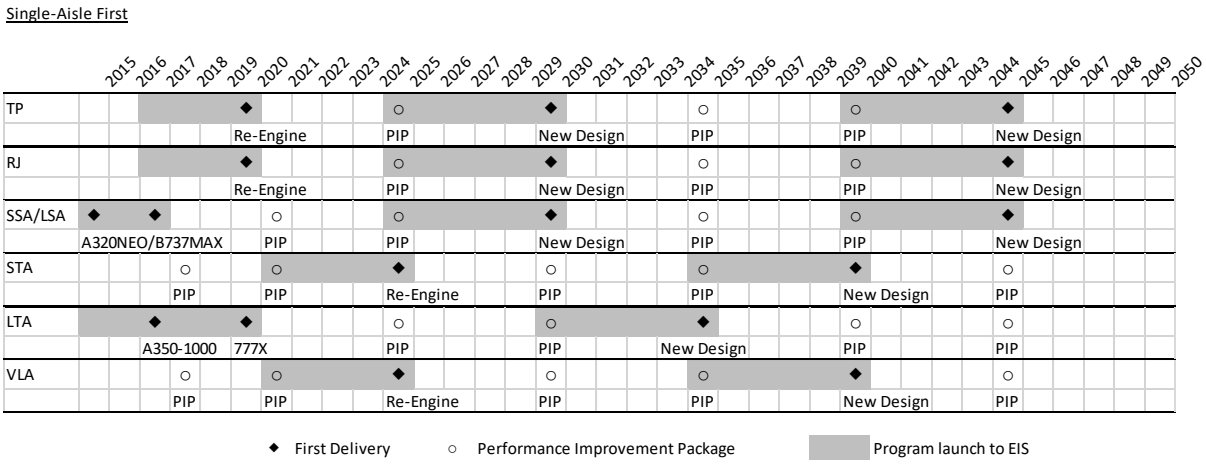

Figure 58: Vehicle Replacement Schedule for Single-Aisle First Assumption

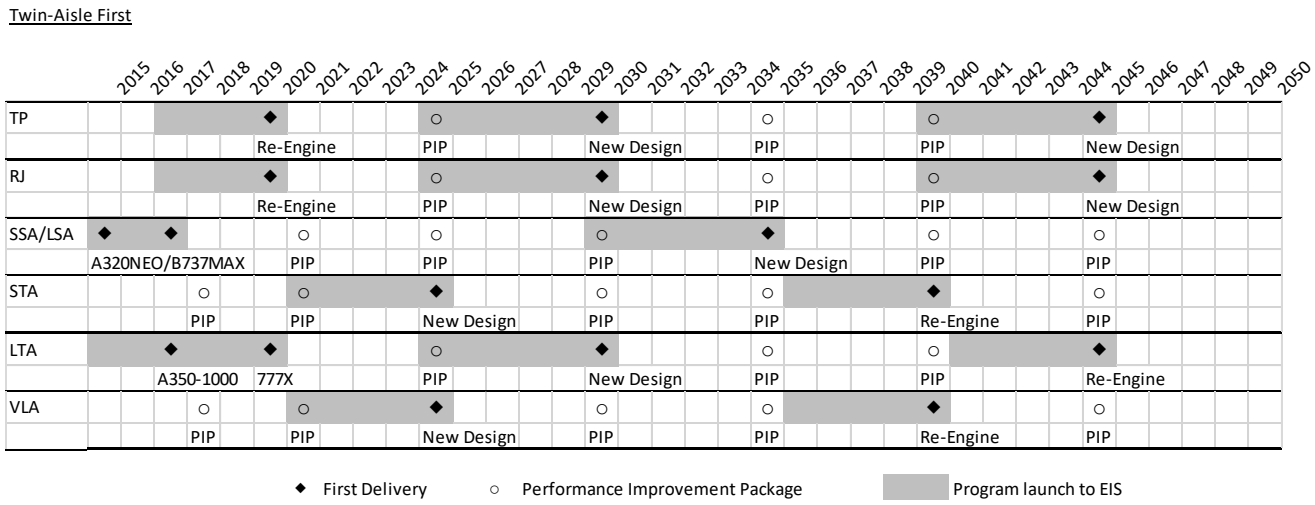

Figure 59: Vehicle Replacement Schedule for Twin-Aisle First Assumption

Vehicle Naming Convention & Identification

Each of the 185 cases were given a name based on its vehicle class, scenario, generation, technology level, and R&D level. The five vehicle size classes under investigation were the RJ, SSA-LSA, and STA, LTA, and VLA. The passenger classes they corresponded to were 50, 150, 210, 300, and 400 passengers, respectively. Keep in mind when looking at the scenarios that the focus of using these five vehicles was on their passenger sizes, not their names. The scenario could be either the baseline, single-aisle first, or twin-aisle first. Single-aisle first and twin-aisle first were shortened to SAF and LAF in the vehicle name. Both the R&D and Technology Level were given intensities of low, medium, or high. The final part of the name was what the vehicle generation was. This generation often varied from the generation of technology impacts on the vehicle. As an example, for a Generation 2 LTA, SAF scenario, with a medium Technology Level and a high R&D Level, the vehicle name was LTA_SAF_RD-High_Tech-Medium_Gen-2.

Importing DOE Tables & Running EDS

Within the file-folder system for EDS were CSV files for each vehicle. The cases and heading were copied from the appropriate DOE sheets in the Technology Roadmap DOE Aggregator and then pasted as values into the CSV files. The 55 cases for each vehicle were then submitted to Condor, which was Georgia Tech's cluster computing network for running cases for different environments like EDS. A script was written to rename the AEDT files output by EDS to match the vehicle naming convention. These AEDT files were used for generating vehicle noise reports and also contained the information for moving forward to fleet level impact analysis. The script also placed the engine deck and flops files for each case in folders using the correct naming convention.

Vehicle Modeling Results

The main metrics from the vehicle results that were analyzed were fuel burn, emissions, and noise. Fuel burn was compared across vehicles by computing the percent reduction in the design block fuel relative to the appropriate baseline. Noise was compared by looking at the noise margin. Noise margin was the difference between the actual aircraft cumulative noise and the Stage 4 noise limit. For emissions only the reduction in nitric oxide relative to the CAEP/6 limit was compared. The CAEP/6 limit was given in terms of D_p/F_∞ , defined as the grams of NOx emitted divided by the thrust in kilo-Newtons, during the LTO-cycle, divided by the thrust rating of the engine. The CAEP/6 limit for an aircraft changed as a function of engine overall pressure ratio. CAEP/6 is shown to facilitate direct comparison to the NASA goals available at the time of this study.

Fuel Burn

The fuel burn results for all the vehicles showed the trends that would be expected, with the same or greater fuel burn reduction as the vehicle generation and R&D level increased. **Figure 60** provides the final results for the Generation 1 vehicles assuming a Single-Aisle First Scenario. Also overlaid on this bar graph were the high and low values for the NASA Subsonic Transport System Level Measures of Success. These were Near Term (2015-2025) desired technology benefits.

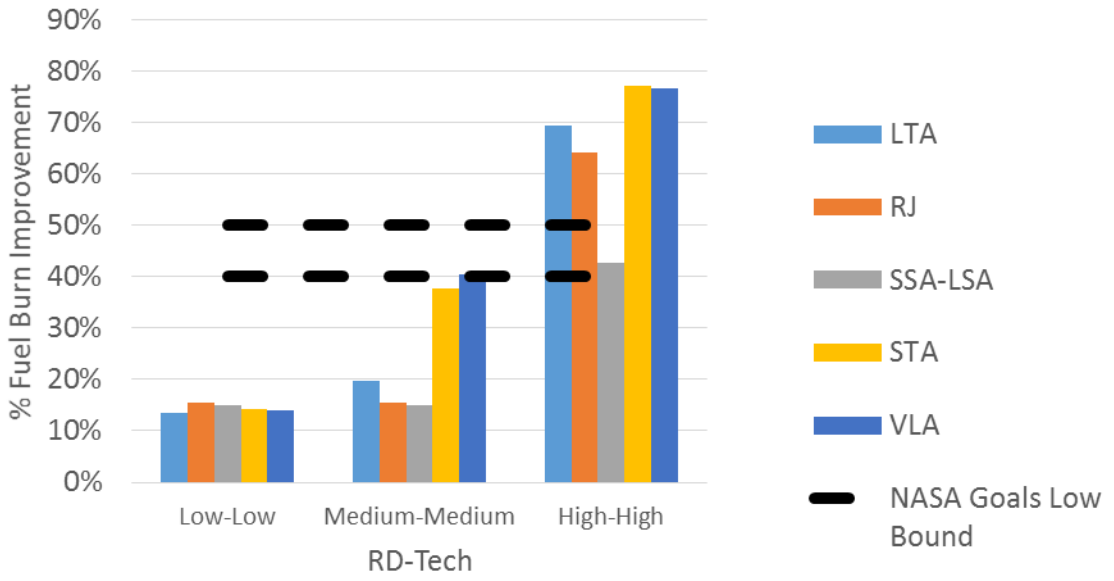

Figure 60: Percent Reduction in Fuel Burn Relative to the Baseline for the Single-Aisle First, Generation 1 Vehicles

Noise Margin

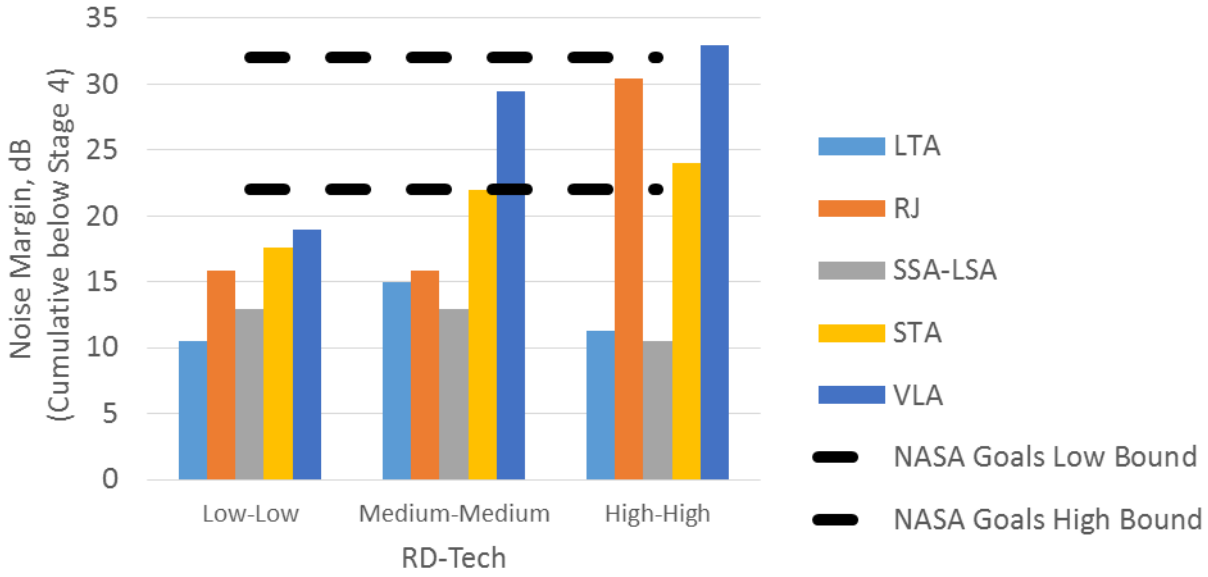

Figure 61: Noise Margin Relative to Stage 4 for Single-Aisle First, Generation 1 Vehicles

Nitric Oxide Emissions

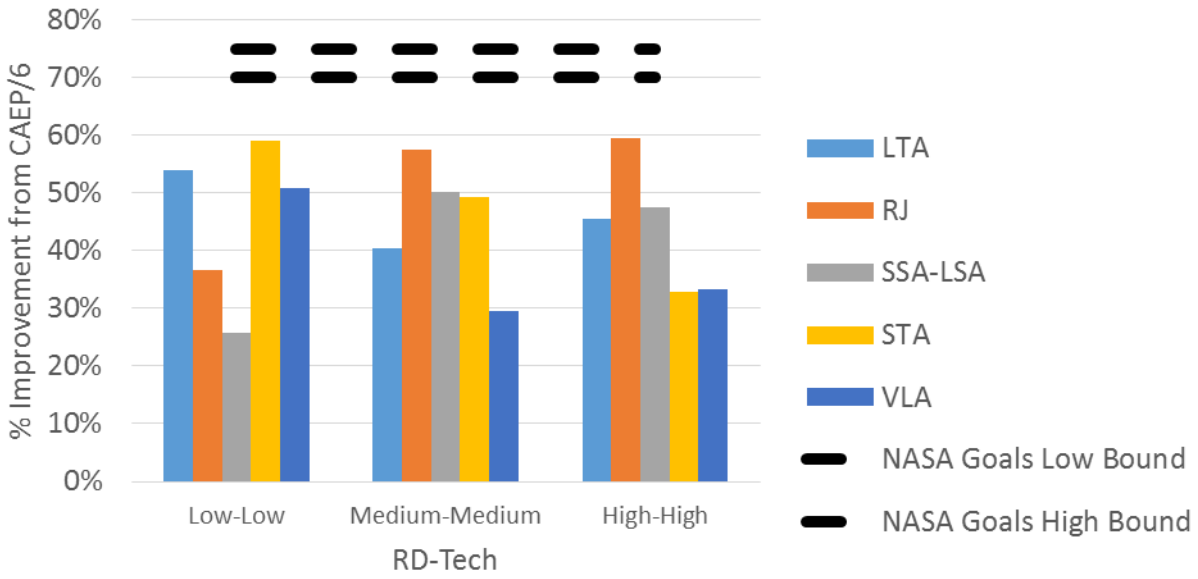

Figure 62: Nitric Oxide Percent Improvement Relative to CAEP/6 for Single-Aisle First, Generation 1 Vehicles

Propulsive Efficiency

In order to update the propulsive efficiency improvement values on the Engine Propulsive infographic, a correlation between BPR and propulsive efficiency was used. The correlation was created by assuming a core velocity of 1660 ft/s and a flight speed of Mach 0.8 at 35,000 ft. It also assumed that, for that core velocity and a given BPR, the optimal jet velocity ratio to maximize propulsive efficiency was able to be achieved. Jet velocity ratio was the ratio between core velocity and bypass velocity. Propulsive efficiency could theoretically be derived as a relationship between bypass ratio, core jet velocity, freestream velocity, and velocity ratio, as given in Equation 1.

$$\eta_p = \frac{\left(u_c + BPR\left(\frac{u_c}{V_{ratio}}\right) - (1+BPR)u_o\right)u_o}{\left(\frac{u_c^2}{2}\right) + BPR\left[\left(\frac{1}{2}\right)\left(\frac{u_c^2}{V_{ratio}^2}\right)\right] - (1+BPR)\left(\frac{u_o^2}{2}\right)}$$

EQUATION 1

Using this relationship, and adjusting the jet velocity ratio to maximize propulsive efficiency, Figure 63 was created which plotted BPR against the theoretical peak propulsive efficiency. The BPR output by EDS for each case was used to determine what its propulsive efficiency would be based on this relation, assuming jet velocity was maximized. The propulsive efficiency for each case was compared to the propulsive efficiency for its respective 1995 baseline to determine what the percent improvement was. The low and high percent improvement values for each vehicle generation were found across all vehicle classes. The nominal values for each vehicle generation were then found as the average of the percent improvement values for that generation across all vehicle classes. The results were used to create the final Engine Propulsive infographic.

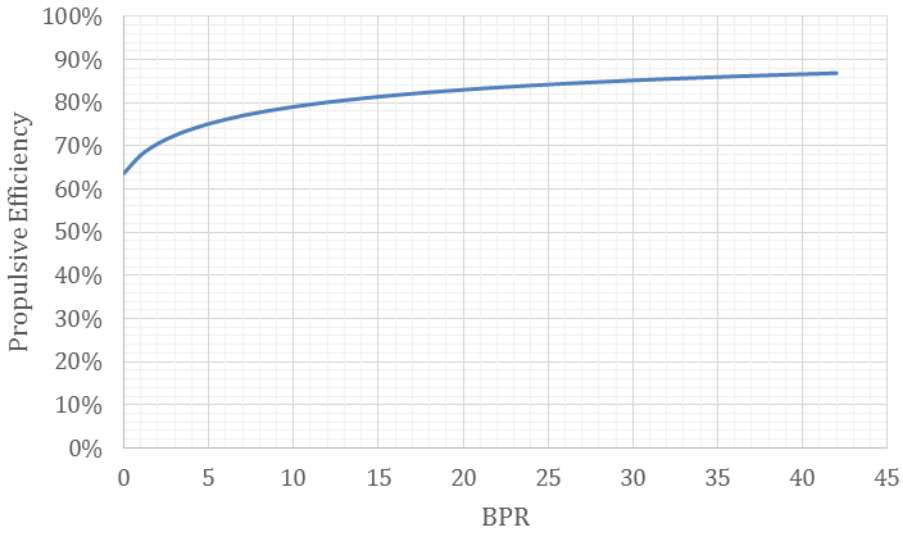

Figure 63: Plot of Correlation between BPR and Propulsive Efficiency

Thermal Efficiency

In order to update the thermal efficiency improvement values on the Engine Core infographic, Equation 2 was used which provides the theoretical thermal efficiency based on OPR and the heat capacity ratio. The thermal efficiency value was calculated for every case using an OPR that was the product of the HPCPR, LPCPR, and FPR values put into the DOE for that case. A heat capacity ratio of 1.4 was assumed. The thermal efficiency for each case was compared to the thermal efficiency for its appropriate 1995 baseline to determine what the percent improvement was. The minimum value for each vehicle generation was found as the lowest percent improvement for that vehicle generation, across all vehicle classes. Similarly, the maximum value was found as the highest value for that vehicle generation, across all vehicle classes. The nominal values were found by taking the average of thermal efficiency improvements for a given vehicle generation. These results were implemented in creating the final Engine Core infographic.

$$\eta_{thermal} = 1 - \frac{T_1}{T_2} = 1 - \frac{1}{OPR^{\frac{\gamma-1}{\gamma}}}$$

EQUATION 2

Mission Specification Change Modeling (Stanford)

Over the past few years, pressure to reduce the overall fuel consumption of the commercial aircraft fleet has been growing steadily. Expenses related to fuel are now one of the largest contributors to an airline's direct operating cost, even if the recent (2015-16) turn of events and global economic slowdown has substantially decreased the cost of fuel. As a result, many technological and operational changes are being considered to alleviate these issues. In this work, the fuel burn impact of varying design mission specifications was investigated, focusing on the cruise Mach number of tube-and-wing aircraft. Thus the Stanford team focused on aircraft and engine redesigns that consider the reduction of the aircraft cruise Mach number, but that leave all other mission requirements (cabin layout, range, payload, take-off and landing field lengths, etc.) unchanged. Representative aircraft from all ICAO (International Civil Aviation Organization) classes are chosen and redesigned for variations in the design cruise Mach number. The effects of improvements in aerodynamic, structural and propulsion technology expected over the next 20 years can also be taken into account in the context of technology scenarios for which the baseline aircraft could be redesigned.

The work is done using a conceptual design environment developed at Stanford from scratch, the SUAVE environment, that represents all aspects of the design (including both the engine and the airframe) using an appropriate level of fidelity. Results from aircraft redesigns indicate that variations in design mission specifications for existing technology aircraft can result in significant reductions in fuel burn, that can then be modeled using one of our team's fleet-level tools.

The following sections describe, in sequence, the improvements that the Stanford team has made to the capabilities and optimization framework in SUAVE under the sponsorship of ASCENT Project 10, the baseline vehicles for the various aircraft classes, the redesign process followed to come up with new vehicles that operate at reduced cruise Mach numbers, and a summary of the results that can be carried forward to fleet-level analyses.

Introduction to SUAVE

SUAVE is a conceptual level aircraft design environment that incorporates multiple information sources to analyze unconventional configurations [12]. Developing the capability of producing credible conceptual level design conclusions for futuristic aircraft with advanced technologies is a primary directive for SUAVE. Many software tools for aircraft conceptual design rely upon empirical correlations and other handbook approximations. SUAVE proposes a way to design aircraft featuring advanced technologies by augmenting relevant correlations with physics-based methods. SUAVE is constructed as a modular set of analysis tools written compactly and evaluated with minimal programming effort. Additional capabilities can be incorporated using extensible interfaces and prototyped with a top-level script. The flexibility of the environment allows the creation of arbitrary mission profiles, unconventional propulsion networks, and right-fidelity at right-time discipline analyses.

To date, SUAVE's analysis capabilities have been used to evaluate a wide variety of configurations including traditional commercial transports (of all sizes and speeds), as well as hybrid-electric commercial transports, supersonic vehicles, and even solar-electric unmanned aerial vehicles (UAVs) among others. Of particular interest to SUAVE is the capability to analyze advanced unconventional aircraft configurations, even if these are not the subject of the investigations in Project 10.

Analysis Capabilities in SUAVE

When determining the inputs to SUAVE, the parts into which the inputs can be broken are: vehicle inputs, mission inputs, vehicle-mission connections, procedure, and variable setup. By determining what inputs are specified and what missions are performed, the engineer will define what type of problem is being analyzed. Part of the code inputs would be the design variables of interest, but others are just the information required to setup SUAVE to run the analyses.

Vehicle: Within the vehicle inputs, the designer must first choose what type or types of configurations SUAVE will study. Does the designer want to optimize a single aisle aircraft for a 1,000 nautical mile (nmi) mission or a family of transoceanic aircraft sharing a common wing where one carries 300 passengers, one carries 350 passengers, and a third aircraft carries 425 passengers? Depending on the type of optimization desired, SUAVE needs to be configured to generate those results. Part of the code inputs is determining what fidelity level or levels will be used to analyze the configurations. A CFD code could

have different inputs than a vortex lattice code or even handbook methods. Making sure the necessary data is provided to SUAVE for the desired analyses is the user's responsibility.

Mission: Beyond just looking at different vehicles over the same mission, SUAVE is used to run the same aircraft through different missions. Instead of optimizing the single aisle aircraft for a 1,000 nmi mission and not considering other missions, one could optimize for a 1,000 nmi mission, but add a constraint that the maximum range of the aircraft be 2,500 nmi. Just as one must specify what parameters would define each vehicle, one must build the missions from the different segments available. For example, in Project 10, in order to ensure that the proper amount of reserve fuel is used, the reserve fuel is calculated by ensuring that the vehicle can fly a separate "reserve" mission at the end of the traditional mission.

Vehicle-Mission Connections: Once the vehicles and the missions the vehicles need to fly have been constructed, the connection between vehicles and missions needs to be specified. This can be done by creating different configurations of the same vehicle, maybe for takeoff and landing, where flaps are deployed, vehicle geometry has been modified, or specifying that only the 300 passenger aircraft will fly 8,200 nmi. This step tells SUAVE have aircraft-1 run missions 1, 2, 3 while aircraft-2 only does missions 1 and 3. It also specifies what results SUAVE will generate when the analysis is completed.

Procedure: The analysis of the problem requires a set of sequential actions to be performed. This is the procedure. A great example of this would be to resize the horizontal tail of the aircraft after a new wing area is selected by the optimization algorithm to keep the horizontal tail volume constant. Additionally, the types of missions are then set here such as a long-range mission and short field takeoff missions. Finally the constraints and objectives that require additional non-standard calculations can be performed as part of the procedure. An example of a non-standard constraint is the fuel margins; which is the fuel volume available in the vehicle minus the fuel used to run the mission.

Optimization using SUAVE

Previous work has shown SUAVE's capability to successfully analyze all these classes of aircraft. However, in order to understand the potential fuel burn reductions of redesigning aircraft with mission specification changes, SUAVE must be used to optimize such aerospace vehicles. During the course of Project 10 at Stanford University, Stanford has conceptualized, developed, implemented, and tested a full optimization environment that works with all of SUAVE's analysis capabilities. In the context of optimization, SUAVE operates as a "black-box" function with multiple inputs and multiple outputs. Several convenient functions are provided to enable connecting the optimization packages to SUAVE more easily. SUAVE's code structure is general enough to be driven from a variety of optimization packages.

In the development of SUAVE, one of the major objectives was to build it to be flexible enough to interface with a multitude of different optimization packages. To adapt SUAVE to all the desired optimization programs, each optimization package must treat SUAVE as a "black-box" where the internal programs run cannot be modified. To formulate SUAVE as a black-box program, the engineer or scientist must specify what inputs need to be defined, how the inputs are connected to the vehicles and missions of interest, how vehicles and missions are connected, and what outputs are going to be returned. In addition, SUAVE allows design parameters, specified by the user, to map to their corresponding parameters inside the code. The general mathematical formulation can be written as a non-linear program:

$$\begin{aligned} \underset{\mathbf{x}}{\text{minimize}} \quad & f(\mathbf{x}) \\ \text{subject to} \quad & g_j(\mathbf{x}) = 0 \quad j \in \{1, ..., l\} \\ & h_k(\mathbf{x}) < 0 \quad k \in \{1, ..., m\} \\ & lb_i \leq x_i \leq ub_i, \; i \in \{1, ..., n\} \\ & \mathbf{x} \in \mathbb{R}^n \end{aligned}$$

where x is a vector containing n design variables x_i which are each bounded by lower and upper bounds lb_i and ub_i. The objective of interest is $f(x)$, typically the fuel burn of the aircraft through an entire mission, including reserves. There are l equality constraints $g_j(x)$ and m inequality constraints $h_k(x)$ that must be satisfied by the re-designed aircraft. The design variables x are typically some subset of the inputs to SUAVE and wrapping functions are provided to enable translation between data dictionaries and design vectors.

Variable Setup: The optimization interface provides a concise way to define several important features of the optimization problem; including variable names (or tags), the initial guess of the variable, the lower and upper bounds, how it should be scaled to yield favorable numerics within the optimizer, and finally its units. Using the information provided in a tabular

structure like the one shown below, accepting input vectors becomes much simpler, enabling SUAVE to pattern across multiple optimization packages.

```
# [ tag , initial, [lb,ub], scaling, units ]
problem.inputs = [
    [ 'aspect_ratio'   ,   10.    , (    5.    ,    20.   ) ,    10.  ,     Units.less],
    [ 'reference_area' ,  125.    , (   70.    ,   200.   ) ,   125.  , Units.meter**2],
    [ 'sweep'          ,   25.    , (    0.    ,    60.   ) ,    25.  ,  Units.degrees],
    [ 'design_thrust'  , 24000.   , ( 10000.   , 35000.   ) , 24000.  ,   Units.newton],
    [ 'wing_thickness' ,    0.11  , (    0.07  ,    0.20  ) ,     .11,     Units.less],
    [ 'MTOW'           , 79000.   , ( 60000.   ,100000.   ) , 79000.  ,      Units.kg],
    [ 'MZFW'           , 59250.   , ( 30000.   ,100000.   ) , 59250.  ,     Units.less],
]
```

Figure 64: Sample Description of Optimization Problem Design Variables, Bounds and Units

Furthermore, within SUAVE the design variables can be defined in any user preferred name and then "aliased" to the internal data structure name. For example, *aspect ratio* above would be an alias of **problem.vehicle.wings.main_wing.aspect_ratio**. SUAVE uses a very verbose methodology, but if the engineer would like to use a different set of variable names, the functionality is in place. Outputs to be used for the objective function, constraints, and output characteristics of interest can also be defined in the same manner. This flexible naming convention also allows multiple parameters inside of SUAVE to be varied as one design variable in the optimization process. This capability reduces the number of variables and constraints since there are no longer multiple variables with constraints requiring that they be equal.

Code Outputs: After all the code inputs have been provided, and the desired vehicle characteristics, mission profiles, vehicle-mission connections and the SUAVE analysis structure are generated, results are produced. Not all of the code outputs are relevant to the optimization of interest. The code outputs might need to be post-processed to generate the actual results of interest for our problem. If one is trying to meet Stage 4 Noise levels, one cares only about generating a cumulative total of 10 dB, not matching certain levels at each condition. The objective function and constraints should be a subset of the final code outputs produced. Once these parameters have been generated, they can be fed to the optimization package for design studies to be completed.

Link to Optimization Packages

With a general interface in place, SUAVE can be incorporated into optimization packages. The flexibility of SUAVE and Python allow optimization with a variety of packages and algorithms. Throughout this section, a variety of optimization packages integrated with SUAVE, as well as various algorithms within these packages that have been applied to various design problems, are discussed.

VyPy[13]: VyPy is a toolbox developed at the Stanford Aerospace Design Lab that exposes useful abstractions for optimization in the context of engineering. Similar to the concept from PyOpt, and serving as an inspiration for the SUAVE data structure, the top level interface is an optimization formulation, with variables, objectives and constraints. Unique to VyPy, these inputs can be defined in a tabular format or in an object oriented format. The problem is then run through a driver or several drivers that each implements an optimization algorithm. At the moment, interfaces for the following algorithms exist: SLSQP, BFGS, COBYLA, and CMA. The interfaces of these drivers have been expanded to permit consistent setup (for example by standardizing the name of common parameters and variable scaling) and consistent data output (like the presentation of the minimized objective and location). Another unique feature is that it handles data based on dictionaries instead of functions, which are especially useful in an engineering context where inputs and outputs are intuitively described with names instead of vector components.

PyOpt[14]: PyOpt is a Python package containing a variety of nonlinear optimizers. The Sparse Nonlinear Optimizer (SNOPT) module, which relies on a Sequential Linear Programming algorithm and quasi-Newton methods, has been used within SUAVE for multiple optimization problems. The Sequence Least Squares Programming (SLSQP) algorithm, which is another quasi-Newton method, has also been used.

There are several more optimization algorithms in the PyOpt package, and all of them can be implemented easily in SUAVE by creating a base interface and attaching them to available SUAVE functions. The exact structure of the interface will depend on the chosen optimization algorithm and can be created based on existing PyOpt documentation.

Dakota[15]: When determining what to expose to outside software and what to only use within SUAVE, Dakota (Design Analysis Kit for Optimization and Terascale Applications) guided this formulation. Dakota is an object-oriented framework developed by Sandia National Laboratories. Designed to work with high performance computers, Dakota together with SUAVE can expand the types of optimization aircraft designers' attempt. Dakota is constructed to connect easily with other "black-box" functions. The user defines the inputs Dakota can change and what results to expect just as the user in SUAVE specifies an input vehicle dictionary and creates an output data set with all the results of the analysis.

Dakota has both gradient and non-gradient based optimization capabilities. Some of the optimization algorithms available in Dakota include, Hasofer-Lind Rackwitz-Fissler (HL-RF), sequential quadratic programming (SQP) from NPSOL, and nonlinear interior-point (NIP) from OPT++.

In addition to optimization capabilities, Dakota combines stochastic expansion methods (such as Stochastic Collocation (SC) and Polynomial Chaos Expansion (PCE)), surrogate models, and Optimization Under Uncertainty (OUU) algorithms to expand the types of problems SUAVE can consider. These methods allow stochastic aircraft defining parameters to be considered as part of the optimization and vehicle analysis. Having the flexibility to deal with uncertainty in certain parameters gives designers the ability to see how certain parameter distributions will propagate through to the final vehicle. With this functionality, Dakota will not only be used as an optimization driver, but also as a tool to trade how certain design inputs can impact the final optimum aircraft.
SciPy[16]: SUAVE is also capable of interfacing with SciPy. In this case, design variables must be inputted via a Python list. SciPy then calls a function designed to return an objective value, which unpacks the variables and interfaces it to a problem set up in SUAVE. Constraints may be handled by either the optimization algorithm, in which case they must be defined in the inputs file, or they must be handled by penalty functions included in the callable SUAVE file. The SciPy optimization package as of the time of writing includes a wide variety of optimization algorithms, including a Nelder-Mead simplex algorithm, SLSQP, and conjugate gradient methods, among others. However, the interface requirements, as well as handling of constraints vary from algorithm to algorithm. As a result, it is up to the user to appropriately ensure that the problem is well formulated.

Several optimization studies have already been pursued. The primary example that has guided our development is the optimization of a Boeing 737-800 aircraft in multiple different scenarios. During the development and verification of the optimization framework, the Stanford team has also worked closely with colleagues at Embraer, who have also conducted their own verification studies (compared with their internal conceptual analysis tools) and who have ensured that the optimization problem formulations include all the necessary realistic constraints to be on par with typical industrial practice. Just as in the analysis capabilities, and beyond the canonical B737-800 problem, the optimization environment is being stress-tested with unconventional configurations on separate projects. The hope is that such additional tests will help our work in Project 10 to ensure that both the capabilities in SUAVE are as developed as possible, but that the robustness of the optimization procedures can allow for repeated redesigns in multiple different scenarios.

Improvements to SUAVE Capabilities as part of ASCENT 10
At Stanford, a considerable amount of effort has been devoted to improve the SUAVE modelling characteristics (particularly in the off-design engine characteristics) and to create, test, and validate the optimization framework within SUAVE that enables the design of new aircraft capabilities with changed mission specifications. As part of this validation effort for this project, five baseline representative aircraft and their technology variants were modelled and their performance parameters like fuel burn were compared with the corresponding aircraft generated by the Georgia Tech team. It was observed that the initial results obtained from SUAVE did not match well enough with the baseline aircraft provided by Georgia Tech (GT) for some of the aircraft. The differences in the performance estimates were traced down to differences in the computation of the drag and the propulsion performance.

Simple changes to the compressibility drag and induced drag prediction routines were made, resulting in aerodynamic predictions better matching the GT results. These changes were fairly minor from the code standpoint.

The major improvement to SUAVE was the addition of multiple propulsion analysis modules to supplement the existing models for prediction of turbofan/turbojet performance. The existing engine model in SUAVE, while predicting accurately

the design performance of the turbofan/turbojet engines, were seen to inaccurately predict the off-design performance of the engine (especially at very low Mach numbers). In order to fix the issue, two new turbofan analysis models were created and integrated into SUAVE.

The first analysis module was based on the off-design analysis methodology described in the propulsion analysis text by Mattingly [17]. Here the off-design residuals for speed matching were computed using functional iteration. No speed/efficiency maps were used and overall component efficiencies were assumed to be constant. While this resulted in improved off-design predictions without significant cost overhead, the level of accuracy required for this effort was not met by the model so the model was not used any further and a more detailed off-design analysis module based on the descriptions in the propulsion analysis course notes (AA283 [18]) by Prof. Brian Cantwell at Stanford and the work in the NASA N+3 Aircraft Concept Designs and Trade studies, Final Report Volume 2[19] was added.

The off-design propulsion analysis model is an extension of the existing engine model in SUAVE. The model solves the 0D flow equations through a turbofan engine, computing the non-dimensional properties at each engine section and the non-dimensional thrust associated with the engine. The mass flow and thrust are then scaled based on the desired thrust at design point. At design point, the mass flows, component speeds, polytropic efficiencies and turbine temperature are known. For off-design analysis, these parameters are treated as unknowns. The mass flows and component speeds and the temperatures are obtained for each evaluation point using Newton/damped Newton iterations. An initial guess for these unknowns is provided (normally the values at design point). During each iteration, the polytropic efficiencies for the components and the speeds are obtained using compressor and fan maps. These maps are generated using the methodology described in the NASA N+3 Aircraft Concept Designs and Trade studies, Final Report Volume 2[19]. However the capability to read in actual component map data and building a surrogate using Gaussian Process Regression is also added to SUAVE. At each iteration, the off-design mass flow residuals (flow/speed matching equations) are computed at the different engine stages and these are driven to zero using Newton iterations. The Jacobians of these residual equations are computed analytically. This is done by symbolically differentiating the propulsion analysis code and analytically computing the required Jacobian terms.

To test and validate the new analysis modules, these are compared with engine performance data provided by Georgia Tech for the different aircraft engines and the results showed reasonable agreement. (**Figure 65**) The thrust and specific fuel consumption predicted by the engine models are compared with the values predicted by GT generated engine data for different throttle settings at the cruise condition (as shown in the plot on the left (**Figure 65**)) and at different Mach numbers and atmospheric conditions at max throttle (as shown in the plot on the right (**Figure 65**)). Comparisons are also ongoing with Embraer to further validate and improve the propulsion model.

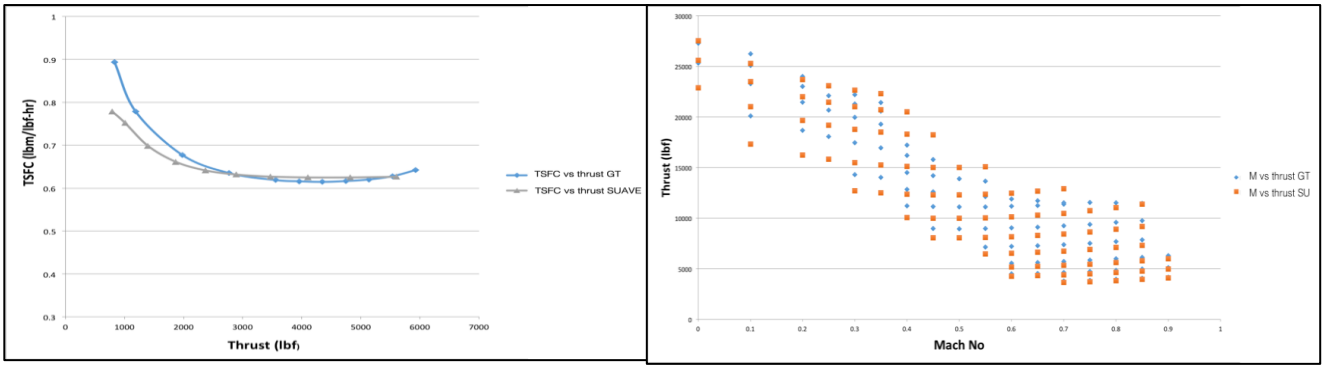

Figure 65: Comparison of Off-Design Propulsion Performance

While the engine models provided fairly good predictions of engine performance, in order to ensure that the any discrepancy associated with engine performance was removed, the capability to use engine decks provided by GT with the SUAVE aircraft models was developed. This was also critical for the inclusion of next gen propulsion technology into the SUAVE models. For this a third engine model was created in order to interface with the EDS engine decks provided by GT. The engine deck file contained the thrust, ram drag, specific fuel consumption and fuel flow rate for a set of Mach numbers, altitudes and throttle

settings. The engine model was capable of reading in the engine deck file and the input parameters are stored as a database. Then using the data from the deck, interpolation models are created for thrust, ram drag and fuel flow rate with respect to the Mach number, altitude and the throttle setting. When queried by the mission solver at different evaluation (atmospheric) conditions, the engine performance estimates are evaluated by interpolating between the given data and the outputs are fed back into the mission solver in SUAVE.

With the addition of these propulsion analysis modules, the baseline aircraft models were seen to match better with the baseline models provided by GT and these were then used for further analysis/design. More details on the baseline aircraft models are described next.

Baseline Aircraft Modelling

To capture the effect of the mission specification changes on the fleet wide fuel burn and emissions, aircraft from all the aircraft classes need to be modelled. For this study the CRJ900 is chosen for the Regional Jet, the B737-800 for the Single Aisle, the B767-300ER for the Small Twin Aisle, the B777-200ER for the Large Twin Aisle, and the B747-400 for the very large aircraft. The baseline aircraft were modelled using SUAVE.

The baseline aircraft modelled in SUAVE were compared with the baseline aircraft modelled by GT. The geometric and propulsion parameters of the aircraft and the performance estimates including fuel burn, design and sea level static thrust are matched to ensure that the fuel burn of the redesigned aircraft computed using SUAVE can be modelled by GT using percentage changes. The fuel burn for a design mission provided by GT and off-design missions are compared. It was observed the baseline fuel burn and the fuel burn variation with mission range match fairly well for the aircraft modelled by GT and Stanford for all aircraft classes. The level of agreement is within the expected differences that would be seen in similar analysis and conceptual design tools.

Reduced Cruise Mach aircraft design (with and without technology)
The next step in this effort is the redesign of the baseline aircraft for mission specification changes. In this effort the Stanford team investigated the effect of cruise Mach reduction i.e. the baseline aircraft are redesigned for a reduced cruise Mach number. This results in aircraft that are significantly more fuel efficient than the baseline aircraft. The aircraft redesign is posed as an optimization problem with the fuel burn for a design mission minimized for a lower cruise Mach number. For this study the optimization framework consists of SUAVE linked up with a gradient based optimizer, SNOPT via PyOPTa python based optimization framework. The design variables used consist of the geometric parameters of the aircraft wing. Initially the engine component pressure ratios and bypass ratio as well as the design thrust (which determines the engine size) were also used as design variables. However the final set of optimizations were run using the engine decks and so the design thrust was the only engine parameter used as a design variable. The cruise altitude of the aircraft is also used as design parameter. The design variables and constraints used for the final set of results are shown below.

DESIGN VARIABLES:
- Main wing aspect ratio
- Main wing reference area
- Main wing sweep
- Main wing thickness to chord ratio
- Engine design thrust
- Cruise altitude

The constraints used for this study are mainly feasibility constraints, a positivity constraint on the fuel burn, constraining the fuel margin (difference in the Takeoff Weight (TOW) and the sum of the Operating Empty Weight (OEW), payload and mission and reserves fuel) to be zero to ensure a feasible mission, a constraint on the wing span to match the baseline aircraft's span and constraining the takeoff field length. Initially the pressure ratio at the combustor inlet and the fan diameter were constrained to be less than equal to the values on the baseline aircraft but the pressure ratio constraint was removed for the engine deck based optimizations. These constraints ensure that the sizing/redesign of the aircraft is realistic and the aircraft is feasible.

CONSTRAINTS:
- Takeoff field length
- Fuel burn (positivity)

Fuel balance: TOW – (OEW+payload+reserves+fuel burn)
Wing span
Fan diameter

Effect of cruise Mach reduction

As expected, redesigning the existing aircraft for reduced cruise Mach numbers resulted in low Mach variants that were more fuel efficient than the existing models. Figure 66 shows the percentage reduction in fuel burn for the baseline technology scenario for all five aircraft classes. It is observed that the percentage reduction in fuel burn is significantly larger (more than 10%) in the larger payload range aircraft (the B777 and B747). The smaller aircraft also show a reduction in fuel burn as cruise Mach number is reduced but the reduction are smaller in magnitude (closer to 5%). Some of the interesting design trends observed during this study are shown in Figure 67.

We see that the redesigned aircraft in all 5 aircraft classes exhibit similar trends. The redesigned aircraft have a lower wing reference area compared to the baseline aircraft. This results in a reduction in wing weight and lower wing drag (parasite) contributing to the improvement in mission performance. The wings are also de-swept as the cruise Mach number is reduced until, for some cases, the lower bound of 5 degrees is met. Similarly the average thickness to chord ratio of the wings increases at lower cruise Mach numbers. These changes are permitted by the reduced effect of compressibility drag at lower cruise Mach numbers. The de-sweeping and increase in wing thickness results in a further reduction in wing weight. The reduction in wing weight and reduced fuel burn due to lower drag results in a reduction in the overall maximum take-off weight (MTOW). This implies a reduction in the required lift and thus a reduction in the lift induced drag. A combination of the effects described above result in the redesigned reduced Mach variants becoming much more efficient than the baseline (Mach) aircraft.

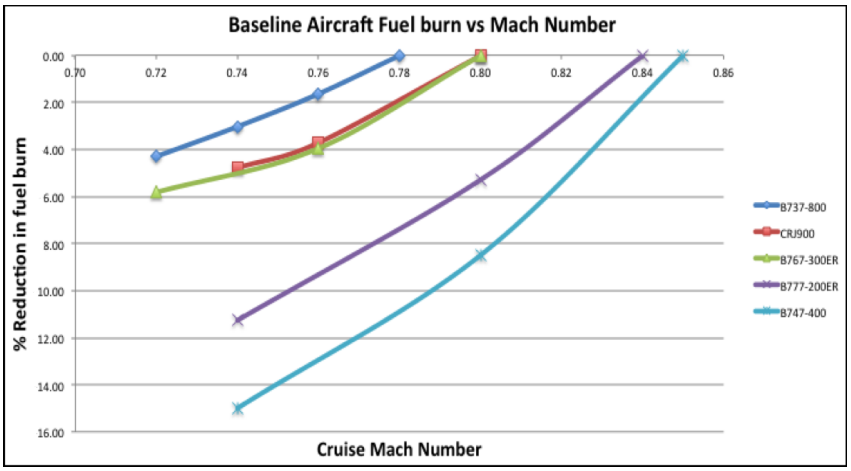

Figure 66: Reduction in Fuel Burn with Cruise Mach Reduction for all Five Aircraft Classes for Baseline Technology

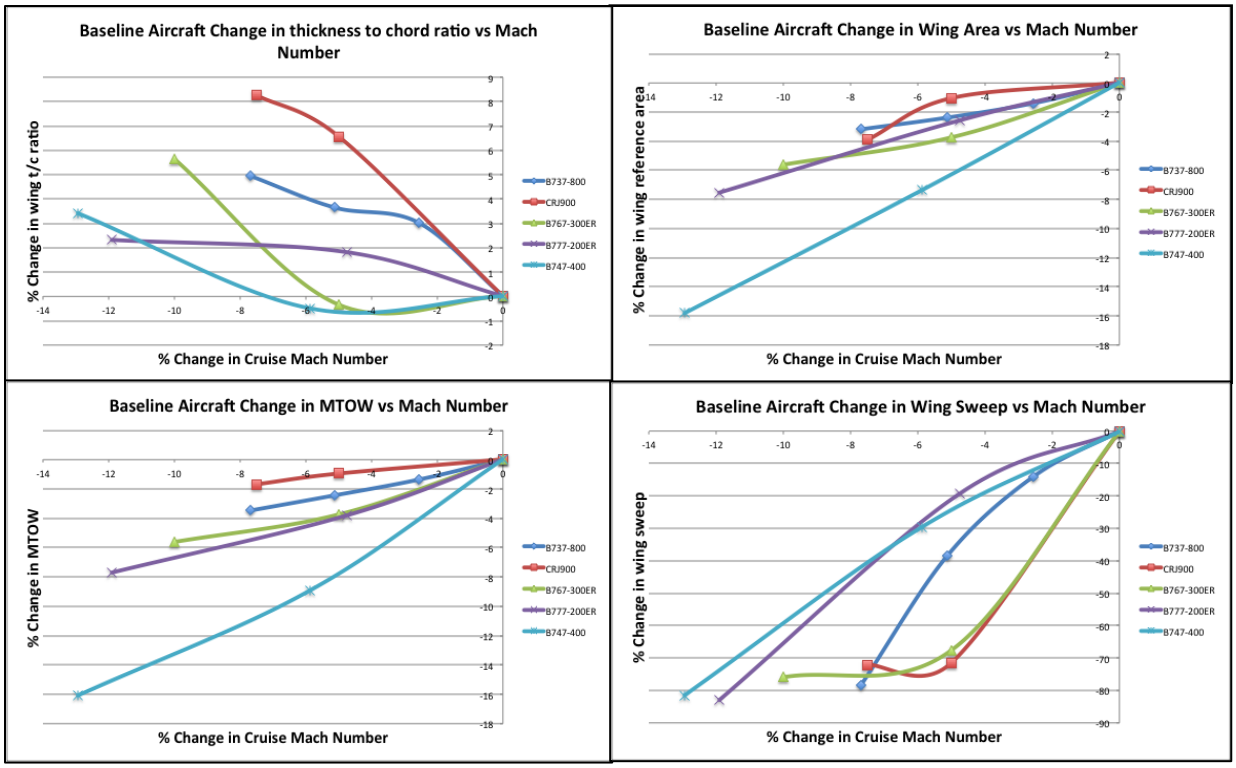

Figure 67: Change in Design Variables with Cruise Mach Reduction

Effect of Technology Variants

The results shown above were for the baseline technology scenario. However it is also important to study how cruise Mach reduction affects the higher technology variants. For this, the technological baselines were modelled in SUAVE based on the corresponding EDS models provided by Georgia Tech. Then these aircraft were redesigned for reduced cruise Mach numbers. **Figure 68** shows the effect of cruise Mach reduction on the fuel burn of the technology variants of the 5 aircraft classes for the baseline and two improved technology levels.

For the higher technology derivatives, the results shown are with respect to the baseline Mach number at the corresponding technology level to isolate the effect of cruise Mach reduction. It is observed that for all 5 aircraft classes, cruise Mach reduction at the higher technology levels is as effective as the for the baseline technology levels. Thus the percentage reductions in the technology 1 and 2 scenarios, can be represented using the same factors associated with the baseline technology scenario if required. The effect of the aircraft class is similar to that observed for the baseline case with the larger aircraft (B777, B747) showing a larger percentage reduction in fuel burn with Mach reduction, while the smaller aircraft classes show a smaller improvement. The trends exhibited by the design parameters mirror those of the baseline technology aircraft presented above and so are not shown again.

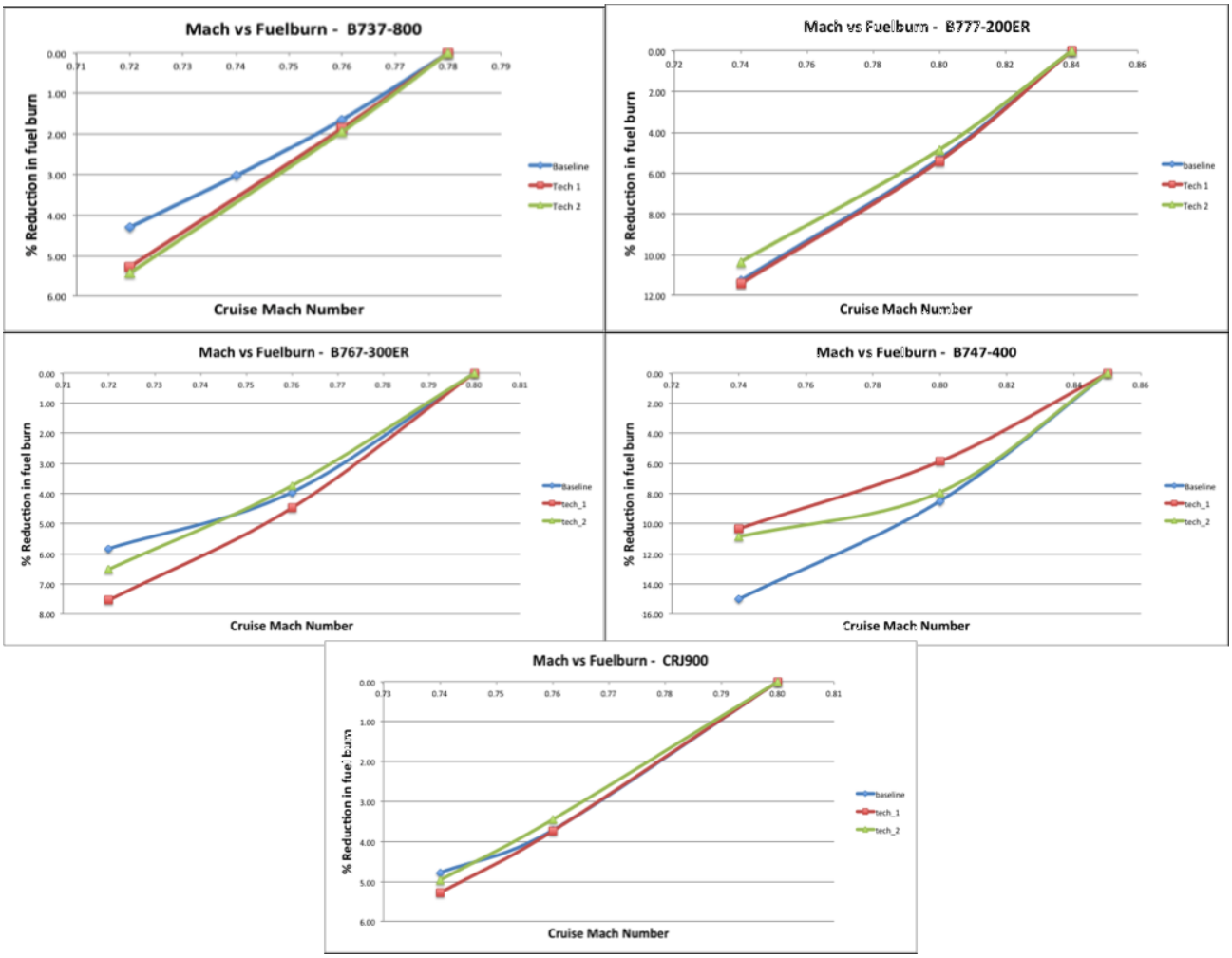

Figure 68: Effect of Cruise Mach Reduction on Technology Variants

Conclusions/Interface with other members of the team/ product of our work

All the percentage reduction values shown above were for the design mission. However, once the aircraft (baseline and higher technology for all 5 classes) were re-designed for cruise Mach reduction, in order for Georgia Tech and Purdue teams to perform fleet level analysis, the re-designed aircraft were flown for a set of off-design missions. The performance (fuel burn) of the aircraft for the off-design missions was compared to the performance of the baseline aircraft also flown for the same off-design missions. The results obtained are shown in Figure 69**.** Except for the second technology scenario for the CRJ900 (CRJ900 tech 2), most the other results show similar trends. The results in general indicate that at ranges significantly lower than the design range, the percentage reductions in fuel burn are not as high as at the higher ranges. However overall, the redesigned aircraft are more fuel efficient than the baseline aircraft for all the off-design missions. For the CRJ900 Tech 2 scenario also the redesigned aircraft are more fuel efficient for the off-design missions than the baseline aircraft. The percentage reductions, however, are different from the other aircraft and from the baseline and the Tech 1 scenario of the CRJ900, too.

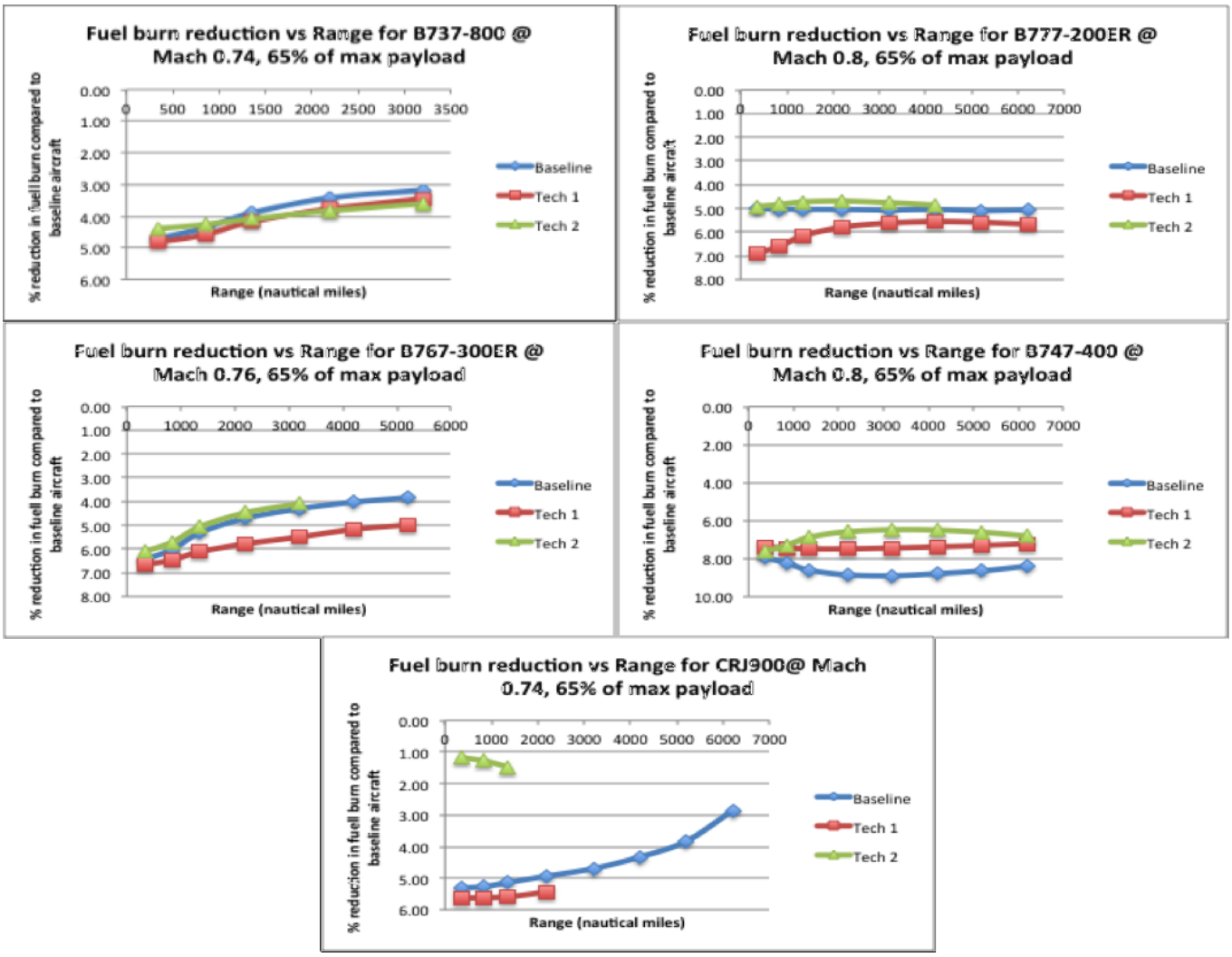

Figure 69: Off-Design Performance Comparison WRT Baselines

All of the results discussed in this section were compiled into the form of a series of improvement factors (multiplicative factors) that could be applied directly to the existing baseline aircraft models in GT's EDS and GREAT tools. Similar comments can be made about the FLEET tool used at Purdue. Using these performance factors for particular aircraft, flown distance, and payload, the actual fuel burn of the reduced cruise Mach number aircraft can be quantified. These fuel burn reductions can then be factored into the fleet-level calculations for the various scenarios.

Task #3: Fleet Level Aircraft Technology Benefits Assessment

Objective: Fleet Level Technology Assessment

The fleet and technology assumptions described in prior sections were assessed using the Georgia Tech GREAT and Purdue FLEET fleet level assessment tools. The following sections provide a brief description of the tools followed by major assumptions and a high level summary of results including comparisons between the two tools. The final subsection provides a detailed summary and analysis of each tool's respective output.

Fleet Analysis Tool Overviews

GREAT (Georgia Tech) Overview

The fleet level aircraft technology benefit assessment at Georgia Tech will be performed using the Global and Regional Environmental Aviation Tradeoff tool (GREAT) and the Airport Noise Interpolation Method (ANGIM), which was developed at Georgia Tech for the purpose of the FAA seeking to complement the AEDT with a lower fidelity screening tool capability that will allow for consideration of a large number of policy scenarios that could be quickly analyzed and reduced to a manageable set of scenarios for more focused, high fidelity analysis in AEDT. Georgia Tech has developed the GREAT tool, which provides a quick means of quantifying the impact of new technologies applied at the aircraft level to assess fleet-wide interdependencies on fuel burn and emissions. Noise and noise exposure are calculated through the ANGIM. Designed to assess the system-wide impacts resulting from the implementation of vehicle-level technology improvements, the GREAT tool synthesizes forecasted operational activity growth, fleet composition evolution, and aircraft-level performance estimates to project fleet-level fuel burn and emissions over time. With its efficient computational algorithm, GREAT can be executed in batch mode to explore multiple scenarios and produce visualizations that highlight the relative contributions of various subsets of the fleet. ANGIM was developed in parallel with GREAT to enable rapid calculation of airport-level DNL contours. By leveraging SAE-AIR-1845 standards to pre-calculate a repository of single-event aircraft grids, ANGIM efficiently pairs airport flight schedules and runway layouts to rapidly produce airport-level DNL decibel grids with runtimes on the order of seconds per airport. Users can plot any contour level desired and measure contour areas and shapes. Population exposure counts can be quickly estimated by overlaying these DNL grids on airport-level population grids derived from 2010 Census-block data using a proportional area-weighted scheme. Recent research efforts have paired ANGIM with GREAT's schedule forecasting to produce similar visualizations of changes in contour areas and population exposure over time. Both GREAT and ANGIM are designed to accept EDS project aircraft as inputs. Both tools maintain flexibility to accept aircraft designs from other vehicle-level design tools as well, provided they adhere to established standards such as those presented in SAE-AIR-1845 and BADA documentation.

FLEET (Purdue) Overview

The Fleet-Level Environmental Evaluation Tool (FLEET) is a computational simulation tool developed to assess how aviation's fleet-level environmental impacts – in the form of CO_2, NO_x emissions and noise – evolve over time. Central to FLEET is an aircraft allocation model that represents airline operations and decision-making. Additionally, the tool has a system dynamics-inspired approach that mimics the economics of airline operations, models the airlines' decisions regarding retirement and acquisition of aircraft, and represents passenger demand growth in response to economic conditions. The overarching objective of FLEET is to enable an understanding of how variation in external factors such as market conditions, policy implementation, and technology availability will affect aviation environmental impacts into the future. The objective in exercising FLEET in this project period was to inform FAA and its partners about the workings of FLEET, its unique inputs and outputs, and a demonstration of its ability to compute estimates of emissions based on fleet level and technology scenarios [20,21,22,23,24,25,26,27].

While several studies exist that investigate either the environmental impact of aviation or the problem of aircraft allocation, these studies do not incorporate a simultaneous assessment of environmental impacts of aviation along with modeling of airline operations and an evolution of passenger demand and airline fleet mix and technology level. FLEET provides the ability to assess the impact of future aircraft concepts and technologies on fleet-wide environmental metrics while also considering economics and operational decisions of airlines and policy implementation. It goes beyond the aircraft-specific technological improvements, and its results reflect relationships between emissions, market demand, ticket prices, and aircraft fleet composition over a period of many years. Given the complexity of studying the aviation industry and the increasing importance being given to its environmental impact, the capabilities provided by FLEET, it is hoped, would help all stakeholders make informed decisions.

FLEET can be used for simulating a number of scenarios defined by setting values for various input parameters. FLEET groups available aircraft in four technology age categories:

Representative-in-class aircraft are the most flown aircraft in 2005 (base year for FLEET)
Best-in-class aircraft are the ones with most recent entry-in-service dates in 2005
New-in-class aircraft are either aircraft currently under development that will enter service in the future or concept aircraft that incorporate technology improvements expected in the future
Future-in-class aircraft are those aircraft expected to include another generation of technology improvements and therefore expected to enter in service a date further in the future

The aircraft within each technology age category further subdivide into six classes, based upon notional or typical seat capacity. These classes represent the mix of aircraft sizes in the airline fleet. For the representative- and best-in-class aircraft, the six FLEET aircraft classes are: 1) Small Regional Jet up to 50 seats (SRJ), 2) Regional Jet, 3) Small Single Aisle, 4) Large Single Aisle, 5) Small Twin Aisle, and 6) Large Twin Aisle. Then, to match the new aircraft models provided by the Georgia Tech team, FLEET uses five new- and future-in-class aircraft classes numbered from 2 to 6 and leaves class 1 empty, recognizing that there are currently (in 2016/2017) no orders for future 50-seat regional jets. The FLEET new- and future-in-class divisions are: 2) Regional Jet (RJ), 3) Single Aisle (SSA-LSA), 4) Small Twin Aisle (STA). 5) Large Twin Aisle (LTA), and 6) Very Large Aircraft (VLA).

FLEET uses a nonlinear relationship to evaluate the demand growth rate in different continents, which is based on the historical data of trips/capita vs. GDP/capita, as shown in **Figure 70**. In other words, if all the continents had the same GDP growth rate, the continents with higher GDP/capita would have a lower trips/capita growth rate.

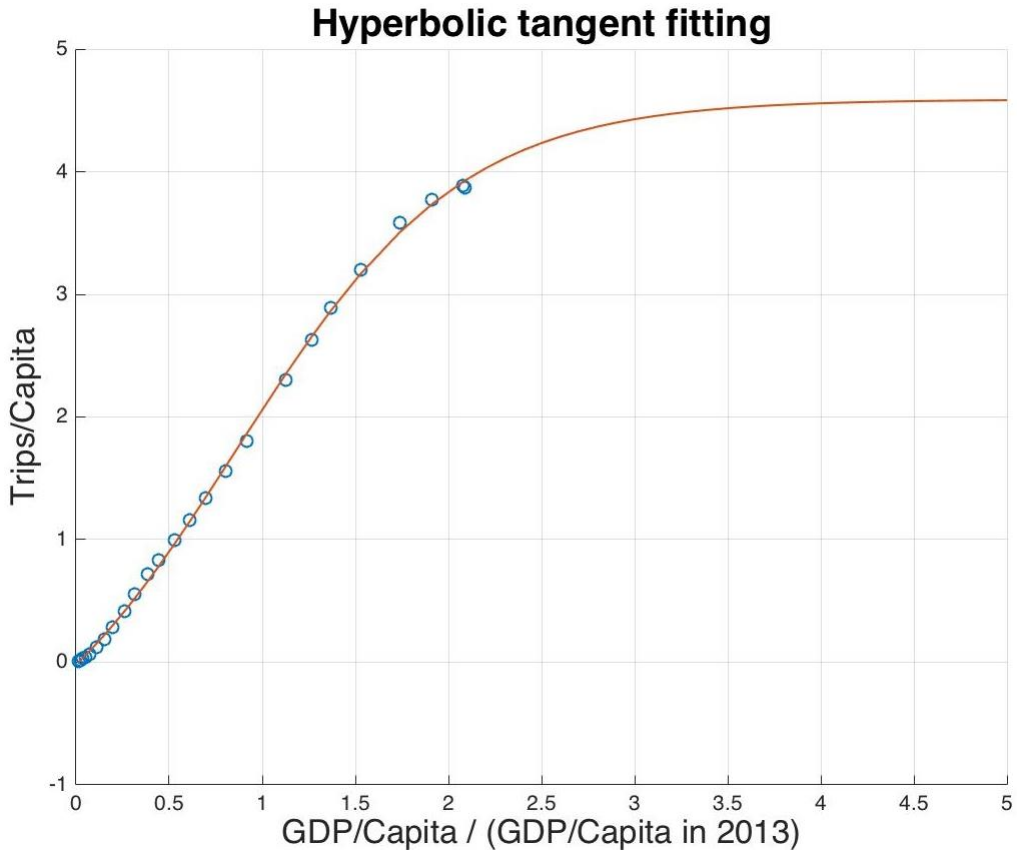

Figure 70: Curve Fitting of Historical Trips Per Capita as a Function of GDP Per Capita

The demand growth rate in each continent in year n can be represented as shown below.

$$Dem_G^n = \frac{f'(GDP_C^n)GDP_C^n}{f(GDP_C^n)} \times \frac{GDP_G^n - Pop_G^n}{Pop_G^n + 1} + Pop_G^n$$

Equation 3

Dem_G^n shows the demand growth rate in year n, while $f(GDP_C^n)$ and $f'(GDP_C^n)$ represent the curve-fitting function and its first derivative, respectively. GDP_C^n and GDP_G^n show GDP per capita and GDP growth rate, while Pop_G^n represent population growth rate. Finally, the model used the GDP and the population in each continent in 2005 from World Bank [28] as initial settings. And, according to the GDP growth rate and population growth rate historical data and predictions, it tracks the demand for each continent from 2005 to 2050 simulation year.

Modeling Assumptions

Since Georgia Tech's GREAT and Purdue's FLEET are different toolsets, the fleet scenarios described in Table 3 to Table 5 had to be interpreted in different ways to be compatible with each toolset. Each of the following subsections describes the Georgia Tech (GREAT) and Purdue (FLEET) approach.

GREAT (Georgia Tech)

Population Growth

One of the important underlying trends for aviation demand is the amount of people wanting to travel by air. This means that the population count is a fundamental underlying factor. As such the population growth given in percent per year was one of the important descriptors with settings from the workshops. **Figure 71** shows the US Census population forecast estimate, which was used a starting point for the time series to be matched to the scenario values.

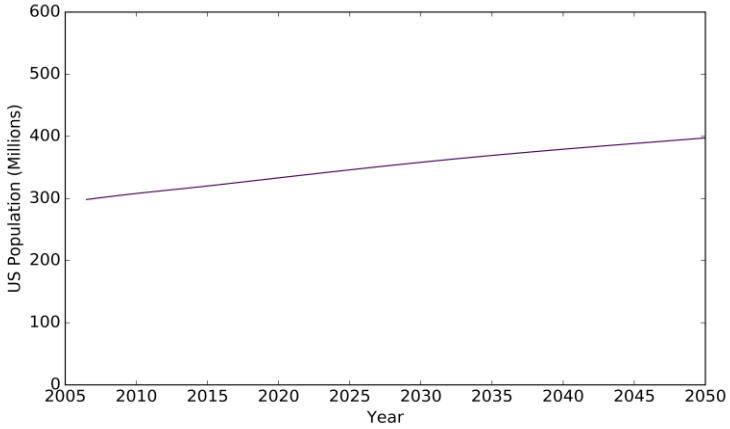

Figure 71: U.S. Population Growth [29]

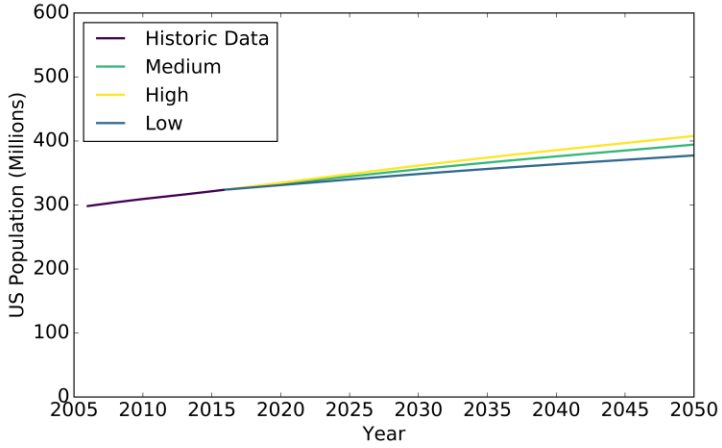

Figure 72: Population Growth Variation

The U.S. Census Bureau population projections, as shown in **Figure 71**, were used as a starting point and then scaled in order to match the values obtained from the workshops for the different scenarios. These range from 0.45 to 0.58 to 0.68 percent per year as the trend to 2050. The adjusted time series are shown in **Figure 72**.

GDP Growth

The next fundamental descriptor of important is the Gross Domestic Product (GDP). The workshop outcomes were defined GDP Growth rates again specified as an average percent per year to 2050. This similarly was applied to and underlying time series by scaling the average of the entire time period in order to achieve the selected values. The three target values in this case were 1.8, 2.8, and 4.0. The underlying time series is the data used by the FAA Aerospace Forecast, shown in Figure 73, which is based on macroeconomic projections by Global Insight [3]. The resulting time series for the low, medium, and high values are shown in Figure 74.

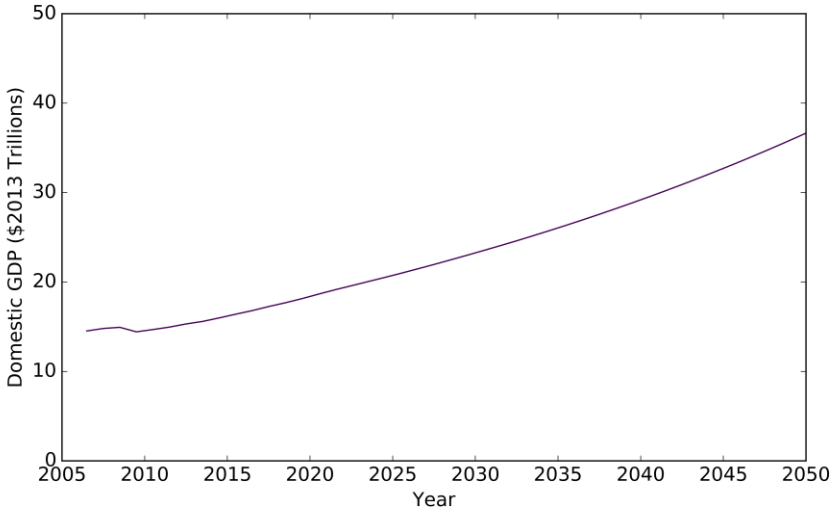

Figure 73: U.S. GDP from FAA Aerospace Forecast [3]

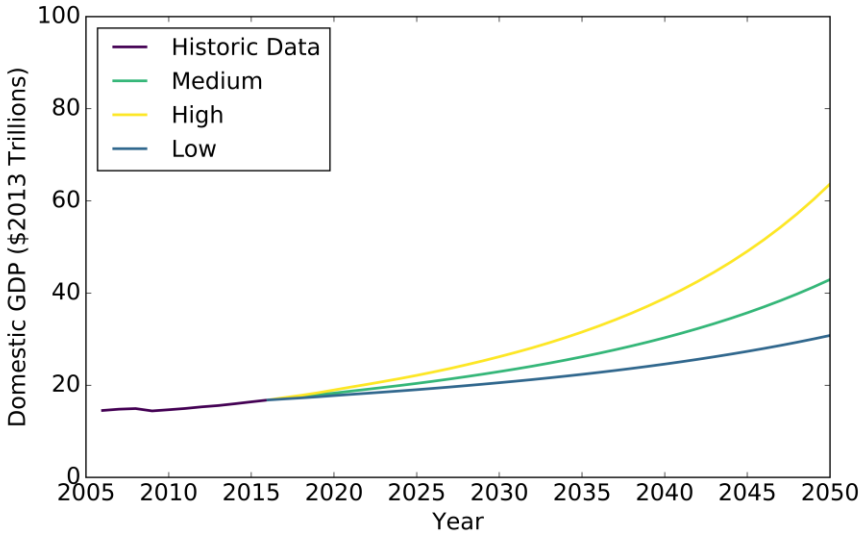

Figure 74: U.S. GDP Variation

The combined GDP and population time series were then combined to compute a GDP per capita time series. The result is a time series that can be used to predict passenger trips per year. The relation is shown in Figure 75.

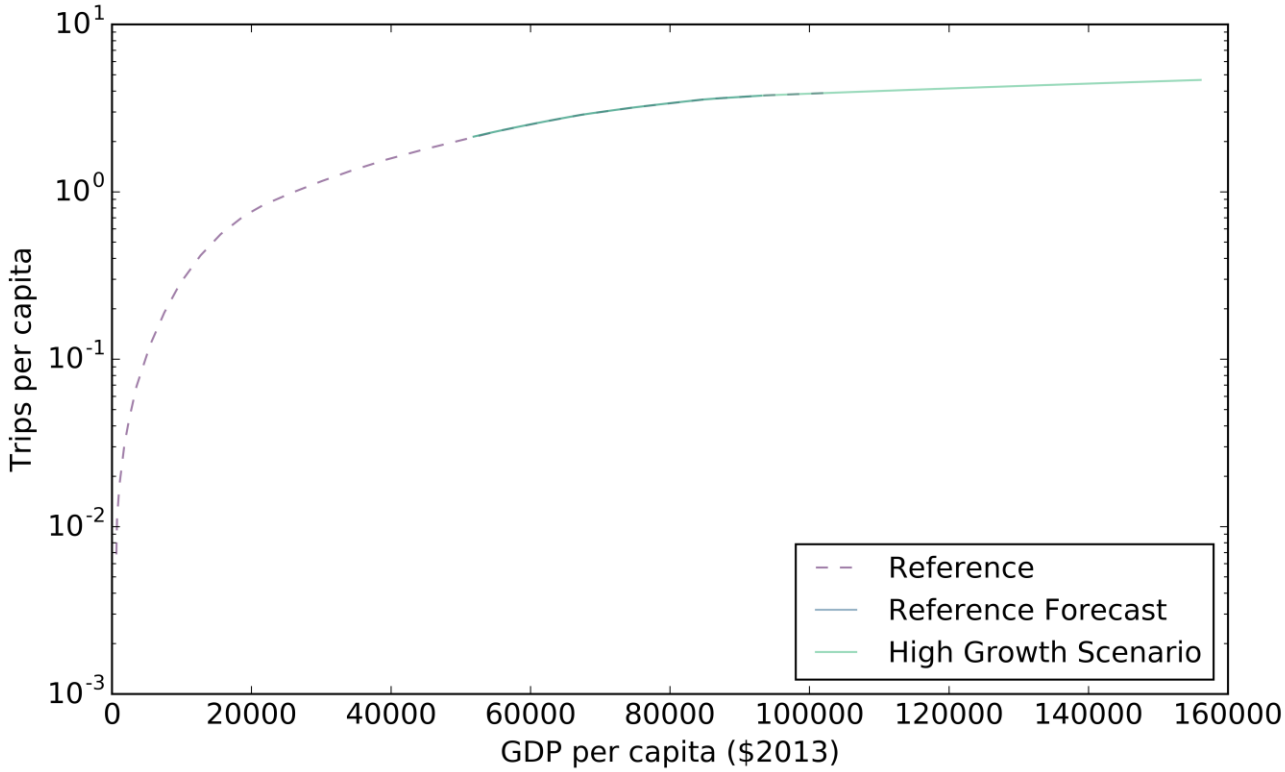

Figure 75: Relation of Trips per Capita per Year to GDP per Capital [29, 30]

The result of this can then be used to compute a scaled demand in revenue passenger miles (RPM) which is the demand input into the model.

International Trade
As a surrogate for international trade the workshops asked for the growth rate in foreign GDP, since changes in GDP in foreign countries can be an indicator of changes in international trade, assuming that the share of international trade for each country changes slowly compared to the absolute change in GDP. Therefore the descriptor that was selected to be most significant was GDP growth in Asia. The values ranged from 3.3, to 4.3, to 5.9 percent per year. These average values were again applied to the international GDP time series provided in the FAA Aerospace Forecast in order to scale these values to the selected value. Additionally, the team decided to also apply similar relative scale factors to the rest of the global GDP growth time series used in the FAA Aerospace Forecast, even though these descriptors were deemed to be of lesser importance by the workshop attendees.

Energy Price
The energy price as defined by the workshops was implemented as a shift of the FAA Aerospace Forecast's jet fuel price time series. Since the workshop results were given in dollars per barrel of oil in 2050, the FAA Aerospace Forecast's refiner's acquisition cost was scaled appropriately. In order to then arrive at a jet fuel price, it is appropriate to look at the ratio of the jet fuel price to the refiner's acquisition cost of oil. This factor, which is known as crack spread, in a competitive environment should be relatively stable. An analysis of various forecasts and historical price data has shown this to be on the order of 1.2, that is that refineries will charge an approximately 20% markup for equal volumes of jet fuel as compared to unrefined oil. This includes many production related efficiencies as well as revenues of other petroleum products as well

as any profit that the market might allow. Therefore, after scaling the refiner's acquisition cost, the resulting jet fuel price is simply scaled by the crack spread to arrive at the future jet fuel price.

Industry Competitiveness
The industry competitiveness was chosen by the workshop participants as a significant descriptor. This descriptor is implemented as a simple value of non-fuel direct operating cost. This will influence the potential ticket price that airline customers would see and therefore shift the demand and supply balance. However, this value was constant for all scenarios.

Airport Noise Limitations
The airport noise limitations were implemented as a reduction factor on the number of allowable aircraft operations. This factor was determined by running the model entirely unconstrained and obtaining the contour area in the base year and for out years of the pertinent aircraft technology insertion scenarios. Once this was obtained, the out year contour areas if they were found to be larger than the base year contour area were used to scale the allowable operations in those out years.

Cost of CO_2 Emissions
The potential cost of CO_2 emissions could manifest itself in a number of ways, depending on the actual implementation of any charging, offsetting, or market scheme. Since the details of any implementation are unknown or uncertain, this cost was implemented as an additional cost to the airline, which acts similar to an implied increase in the price of jet fuel. The unit conversion from metric ton CO_2 to gallon of jet fuel brings each dollar per metric ton CO_2 into roughly the range of a cent increase in jet fuel price per gallon. The values from the workshops were simply used to define a time series ending in 2050 with the specified values. This was implemented as a linear increase to those values starting in 2020.

Fleet Evolution Schedule
The schedule of when new technology aircraft would become available through EIS was defined with the following tables. Depending on the scenario either a single aisle first or twin-aisle first schedule was used. The difference being whether a new design aircraft past 2020 would be focused either on a single aisle size or twin-aisle size aircraft. This means that depending on the scenario the difference becomes what technologies on new aircraft are introduced into actual use depending on the size class of the aircraft.

	2015	2016	2017	2018	2019	2020	2021	2022	2023	2024	2025	2026	2027	2028	2029	2030	2031	2032	2033	2034	2035	2036	2037	2038	2039	2040	2041	2042	2043	2044	2045	2046	2047	2048	2049	2050
TP						◆					○					◆					○					○					◆						
						Re-Engine					PIP					New Design					PIP					PIP					New Design						
RJ						◆					○					◆					○					○					◆						
						Re-Engine					PIP					New Design					PIP					PIP					New Design						
SSA/LSA	◆		◆				○				○					◆					○					○					◆						
	A320NEO/B737MAX						PIP				PIP					New Design					PIP					PIP					New Design						
STA				○			○				◆					○					○					◆					○						
				PIP			PIP				Re-Engine					PIP					PIP					New Design					PIP						
LTA			◆			◆					○					○					◆					○					○						
			A350-1000			777X					PIP					PIP					New Design					PIP					PIP						
VLA				○			○				◆					○					○					◆					○						
				PIP			PIP				Re-Engine					PIP					PIP					New Design					PIP						
							◆	First Delivery					○	Performance Improvement Package													Program launch to EIS										

Figure 76: Single Aisle First Schedule

Aircraft Retirement
The aircraft retirement curves which effectively prescribe what percent or original aircraft sold in a given year are still in operation when they reach a certain age. This analysis uses a nominal (medium) curve that is a clamped sigmoid function with a 50% point of about 30 years, which means that after 30 years only 50% or aircraft originally sold in the same year remain in service. This is based on fleet inventory analysis and represents a rough average of aircraft useful service life in the past decades. The scenario setting of "Early" (Low) corresponds to a curve with a midpoint of 10 years, which is a very aggressive fleet turn over assumption. Conversely, the setting of "Late" (High) corresponds to a curve with a midpoint of 40

years, which would represent an extension of the lifetime compared to historical trends. The specific values are shown in **Figure 77**.

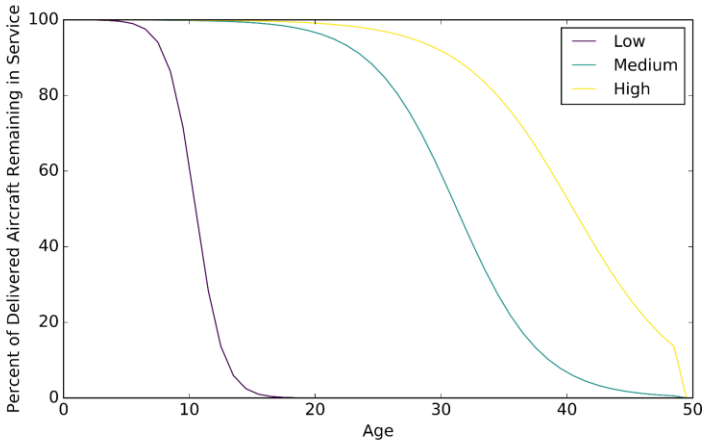

Figure 77: Aircraft Retirement Curves

Production Capacity
Scenarios with production capacity limits were run with a cap imposed on the number of new aircraft being allowed to enter service in a given year. This has the effect of reducing demand somewhat. However, in high or very high demand scenarios this effect is overshadowed by the noise limits that might be increased.

Aircraft Technology
All aircraft technology factors, as defined in the scenarios, are modeled at the vehicle level. In the fleet analysis these factors are represented by different vehicles that are included in the entry into service slots shown in Figure 76.

FLEET (Purdue)

Description of Inherent Demand Model
The market demand model in FLEET is driven by economic growth in each continent and tries to represent two assumptions. First, a higher income per capita results in higher market demand and, second, there is an upper bound for number of trips per person because everyone has only 24 hours per day.

Based on the historical data from Airbus Company, which include trips per capita and GDP per capita in several countries, the model used hyperbolic tangent function to fit the historical data because of two reasons. The hyperbolic tangent function is analytic, and it asymptotically approaches an upper bound.

Description of Exercised Scenario Setups
Purdue ran FLEET with fourteen scenarios that were identified together with the ASCENT 10 Project team and grouped into five categories. This activity also serves to identify enhancements necessary in FLEET to accommodate simulation of all the scenarios examined under ASCENT-10. The fourteen scenarios in five groups examined are:

Current Trend Economic Environment
- Current Trends “Best Guess”
- Current Trends Frozen Technology
- Current Trends High and High Research and Development

High Research and Development (R&D)
- Low Demand and High R&D
- Current Trends High and High R&D
- High Demand and High R&D
- Very High Demand and High R&D with Noise Limits

High Research and Development with Mission Specification Change (MSC)

Low Demand and High R&D with MSC
High Demand and High R&D with MSC
Current Trends High and High R&D with MSC
Very High Demand and High R&D with Noise Limits with MSC
Low Research and Development
Low Demand and Low R&D
High Demand and Low R&D
Very High Demand and Low R&D with Noise Limits
Environmental "Bounds"
Environmental "Bounds" – Low
Environmental "Bounds" – High

The "Current Trend Frozen Technology" scenario setup in FLEET is defined as follows:

- A network of 169 airports including U.S. domestic routes and international routes that have either their origin or destination in the U.S.
- The annual gross domestic product (GDP) grows at a constant value of 4.3% in Asia, 4.2% in Latin America, 2.4% in Europe, and 2.8% for airports in the United States.
- The annual population growth rate at a constant value of 1.1% in Asia, 1.26% in Latin America, 0% in Europe, and 0.58% for the United States.
- Jet fuel prices grow according to the Energy Information Administration (EIA) reference fuel price [29] case and adjusted it to meet the ASCENT survey fuel price, $77.08/bbl, by 2050.
- Carbon emission prices grow linearly from $0/MT in 2020 to $21/MT by 2050.
- Only the Representative-In-Class and Best-in-Class aircraft from **Table 12** are included in the simulation. No New-in-Class or Future-in-Class aircraft are included in this scenario; when the airline needs a new aircraft due to retirement or fleet growth, it acquires an aircraft with the same characteristics as the Best-in-Class aircraft until 2050.

Table 12 shows the various aircraft used in the FLEET simulations. These appear in rows according to the FLEET aircraft class, with the corresponding aircraft labels and, for the new- and future-in-class aircraft, the EIS date used in the study. In Table 12 the aircraft labeled with "GT Gen1 DD" are the Generation 1 aircraft modeled by Georgia Tech with a 'Direct Drive' engine. The Generation 2 aircraft are labeled as "GT Gen2 DD". These include aircraft that belong to the following classes - regional jet (RJ), single aisle (SSA-LSA), small twin aisle (STA), large twin aisle (LTA), and very large aircraft (VLA). Based on the amount and speed of technology incorporated into aircraft, in each of the scenarios, the New-in-Class and Best-in-Class aircraft models will vary. Given the observation that new orders for 50-seat aircraft have diminished to zero, there are no small regional jet (SRJ) aircraft in the new- and future-in-class technology ages.

Table 12: Aircraft Used in Simulation Studies

Aircraft Types in Study				
	Representative-in-Class	Best-in-Class	New-in-Class	Future-in-Class
Class 1	Canadair RJ200/RJ440 [SRJ]	Embraer ERJ145 [SRJ]		
Class 2	Canadair RJ700 [RJ]	Canadair RJ900 [RJ]	GT Gen1 DD RJ (2020)	GT Gen2 DD RJ (2030)
Class 3	Boeing 737-300 [SSA]	Boeing 737-700 [SSA]	GT Gen1 DD SSA-LSA (2017)	GT Gen2 DD SSA-LSA (2035)
Class 4	Boeing 757-200 [LSA]	Boeing 737-800 [LTA]	GT Gen1 DD STA (2025)	GT Gen2 DD STA (2040)
Class 5	Boeing 767-300ER [STA]	Airbus A330-200 [STA]	GT Gen1 DD LTA (2020)	GT Gen2 DD LTA (2030)
Class 6	Boeing 747-400 [LTA]	Boeing 777-200LR [LTA]	GT Gen1 DD VLA (2025)	GT Gen2 DD VLA (2040)

The 'Current Trends "Best Guess"' and 'Current Trends and High R&D' scenarios, in addition to the 'Current Trends Frozen Technology' scenario setup also incorporate the New-in-Class and Future-in-Class aircraft into their fleet mix. The High R&D case has higher speed and amount of technology investments accounted for in their aircraft development than the Best Guess case.

The 'High Demand and High R&D' and 'High Demand and Low R&D' scenarios assume a constant annual GDP growth rate of 5.9% for in Asia, 5.3% for in Latin America, 4.2% for in Europe, and 4.0% for in America. Routes in the FLEET network serving cities in these regions see their inherent demand grow based upon these higher than baseline assumed GDP growth rates. The low R&D case represents a slower rate of change and amount of investments in technology than the Best Guess case.

The 'Low Demand and High R&D' and 'Low Demand and Low R&D' scenarios use a constant annual GDP growth rate of 3.3% in Asia, 2.7% in Latin America, 0.6% in Europe, and 1.8% in the United States. This leads to lower-than-baseline demand growth.

The 'Very High Demand and High R&D with Noise Limits' and 'Very High Demand and Low R&D with Noise Limits' scenarios have the same GDP growth rate setting as 'High Demand' scenarios. But, the fuel prices grow according to the EIA reference fuel price case with a slight adjustment so that the fuel price in 2050 meets the fuel price corresponding to the $41.00/bbl price indicated by the ASCENT survey respondents. These two scenarios do not include carbon emission prices. For these two scenarios, the fleet-level noise area constraint is initiated after 2020. The limitation on the total noise area (based upon the sum of the 65 dB DNL contour area estimates for all U.S. airports in the FLEET network) decreases from no limit in 2020 to 50% of the 2005 total noise area level by 2050. Then, the high R&D and low R&D cases account for the rate of change and amount of investments in technology. **Figure 77** shows the three sets of the adjusted fuel prices based on the EIS reference fuel price scenario and the matching of the ASCENT survey respondents' estimates of 2050 prices.

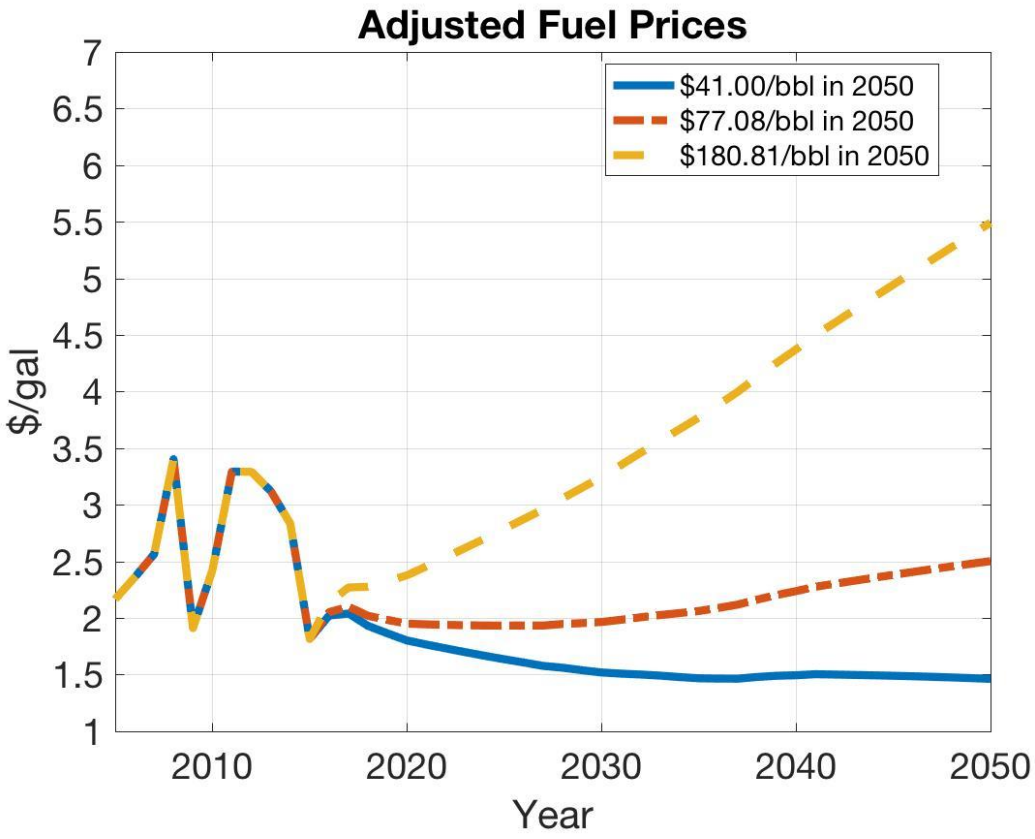

Figure 77: Adjusted Fuel Prices

The 'Mission Specification Change' scenarios assess the environmental impacts of aircraft whose mission profile use slower cruise speed than current aircraft; the Task #2 section above describes the modeling of these aircraft. FLEET captures both the reduced fuel consumption of these aircraft and the impact that the slower-cruising aircraft might have on utilization of these aircraft. These scenarios in the 'MSC' group have the same economic environment and technology development setting as the ones in the 'High R&D' group.

The 'Environmental "Bounds" – High' scenario has the same GDP growth rate, fuel price growth, carbon emission price profile, and aircraft technology improvement rate settings as 'Very High Demand and High R&D with Noise Limits' scenario, but, this 'Environmental "Bounds" – High' scenario has no noise limitations. This scenario seeks to investigate what might occur to lead to a high impact of aviation on the environment.

The 'Environmental "Bounds" – Low' scenario has the same GDP growth rate, carbon emission price profile, and aircraft technology improvement rate settings as 'Low Demand and High R&D' scenario. The fuel prices are adjusted to meet ASCENT survey fuel price, $180.81/bbl, by 2050. The 'Environmental "Bounds" – Low' scenario also initiates the noise constraint to limit total 65dB noise contour area. This scenario seeks to investigate what might occur to lead to a low impact of aviation on the environment.

Description of High R&D Aircraft Models

In the case of the high R&D aircraft models, FLEET allocated the single aisle aircraft (Class 3) on some trans-Atlantic routes, even though the design range was only 2960 nmi. This prompted questions regarding the correct implementation of the FLOPS aircraft models in the scenarios and the implication of using a prescribed load factor when describing the operating missions of the aircraft. The results for the Class 3 aircraft are most striking, but other aircraft classes demonstrate similar behavior under the high R&D assumptions.

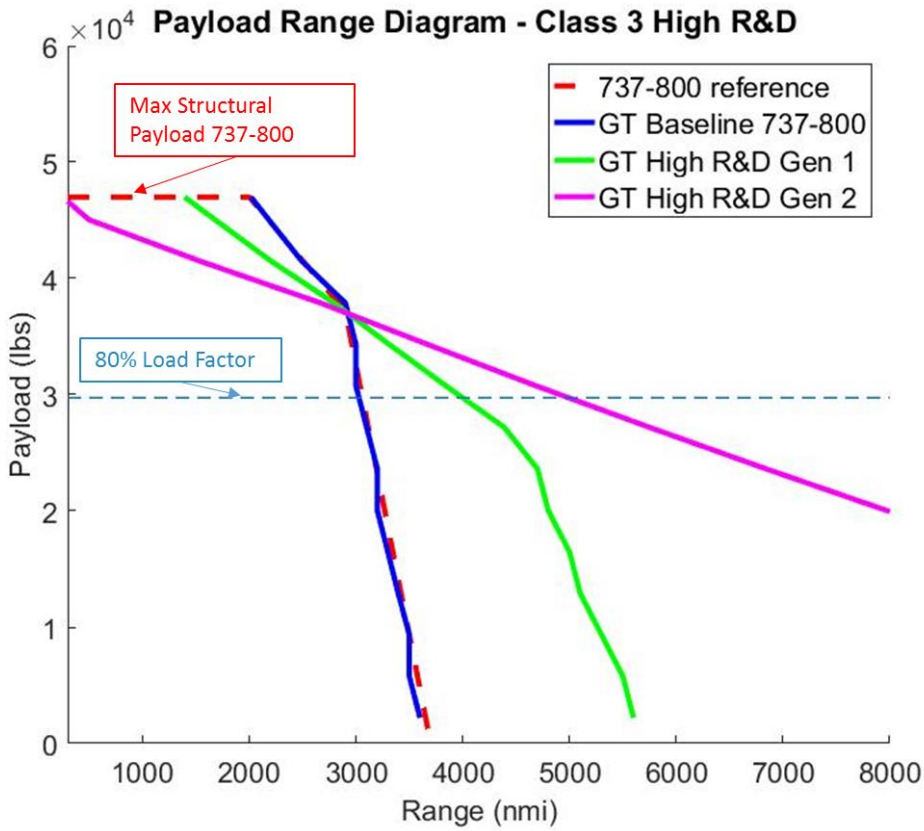

Figure 78: Payload Range Diagram for High R&D Class 3 Aircraft

Figure 78 depicts the payload range diagrams for the three different technology ages of Class 3 aircraft used in FLEET. With the operating mission defined so that the aircraft carries 80% of the passenger load factor, these Class 3 aircraft can operate at a maximum range of 3028 nmi, 3999 nmi, and 4991 nmi, in order of increasing technology age. The reason for the slope change in the payload range diagram for the GT High R&D Gen 1 and GT High R&D Gen 2 aircraft compared to the baseline aircraft has to do with the combination of improved technology and constant fuel volume limit. In the case of the GT High R&D Gen 2 aircraft model, the fuel volume limit is not reached even at an operating range of 8000 nmi because the fuel efficiency of this aircraft is very good. The non-smooth line segments associated with the fuel volume limit are an artifact of the iterative approach with a fairly large tolerance used to determine the range values quickly. Other aircraft classes with this technology level showed similar behavior in aircraft performance.

Based on preliminary studies into limiting the routes for these high R&D aircraft models to their design range, or the maximum range at 80% load factor, the ASCENT-10 project team chose the option where high R&D aircraft were allowed to fly routes limited to the maximum operating range at 80 % load factor. This allowed these 150-seat single aisle aircraft (with High R&D) to operate on several trans-Atlantic routes, which increases the airline profit in the FLEET model. The team feels this has some recent precedents for this with some airlines currently offering trans-Atlantic flights on this class of aircraft with greatly reduced seating capacity.

Description of Noise Constraint Implementation

This section describes how Purdue developed the noise model for FLEET and incorporated the total noise area metric as a constraint for noise-limited scenarios. The constraints setup in FLEET allocation are linear equations in terms of x_{kj}, where x_{kj} is the number of roundtrips of an aircraft type k on a route j. Purdue used a linear equation in terms of x_{kj} to approximate the noise at each airport. The calculated approximate noise area at each airport is determined from the equation below.

$$Area_i = \sum_{k=1}^{24} \left[\begin{Bmatrix} \left(P_k \cdot \delta_i^{TO} + Q_k \cdot \left(1 - \delta_i^{TO}\right)\right) \cdot \left(NEE_k^{TO} \cdot x_{k,i}^{TO}\right) + \cdots \\ \left(P_k \cdot \delta_i^{arr} + Q_k \cdot \left(1 - \delta_i^{arr}\right)\right) \cdot \left(NEE_k^{arr} \cdot x_{k,i}^{arr}\right) \end{Bmatrix} \right] \cdot \frac{1}{10000}$$

Equation 4

where *NEE* is the Noise Energy Equivalent (NEE=$10^{(EPNL/10)-7}$), $x_{k,i}$ is the number of roundtrips by aircraft k at airport index I, *P* is the daytime passenger aircraft regression coefficient, *Q* is the night time passenger aircraft regression coefficient and δ is the day ratio at that airport [30].

FLEET uses the total noise area metric, which is a sum total of the noise areas across all the noise-limited airports in the FLEET network, as a constraint to limit the number of flight operations across all of the noise-limited airports. Because of the manner in which FLEET represents all U.S. domestic flights and all international flights with origin or destination in the U.S., FLEET represents all operations at the U.S. airports and only some of the operations at international airports in the airline network, so only the noise-limited airports are included in this constraint. The noise constraint is given by

$$\sum_{i \epsilon \; noise-limited \; airports} (noise \; area_{2050})_i \leq \Lambda \cdot \sum_{i \epsilon \; noise-limited \; airports} (noise \; area_{2005})_i$$

Equation 5

where Λ is a global FLEET parameter that specifies the limit on the noise area. For scenarios that are noise-limited, the constraint is initiated in the year 2020. The limit on the total noise area decreases linearly from the year 2020 so that in the year 2050, the total noise area across all the noise-limited airports is Λ times that of the total noise area across all the noise-limited airports in 2005.

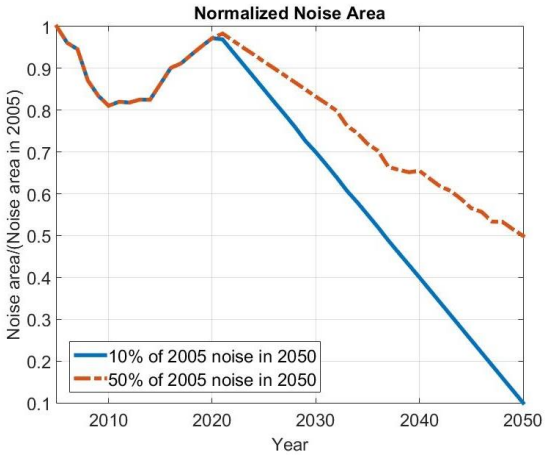

Figure 79: Normalized Noise Area in a Noise-Limited Scenario

Figure 79 shows the evolution of the normalized total noise area across all the noise-limited airports for two cases:

Case 1: Total noise area in the year 2050 is 10 % of the total noise area in 2005.
Case 2: Total noise area in the year 2050 is 50 % of the total noise area in 2005.

As can be seen in Figure 79 the noise constraint is initiated in the year 2020. In case 1, the noise constraint is active all through the simulation for that particular scenario; this is a very noise-restrictive constraint. In order to meet this noise constraint, there is a significant decrease in the demand satisfied over the course of the simulation timeframe

In case 2, the noise constraint is active till 2032 and then resumes being active in 2048. This indicates that the introduction of newer aircraft, which are lighter and use smaller engines leading to lower noise levels, is enough between 2032 and 2048 to have a cumulative noise area lower than the imposed limitations for case 2.

Description of Relief Crew Adjustments

This section describes how Purdue accounted for relief crew members on long haul flights. The Title 14 Code of Federal Regulations (CFR) Part 117 – FLIGHT AND DUTY LIMITATIONS AND REST REQUIREMENTS: FLIGHTCREW MEMBERS (EFF. 1-4-14) [31] determined the number of relief flight crew members required on each flight. FLEET aircraft models have two flight crew members for flights that are eight hours or less, three flight crew members (1 relief flight crew member) for flights over eight hours but less than 13 hours and a flight crew of four members (2 relief crew members) on a flight up to 17 hours. The block time of a particular flight leg alone, determined the number of relief crew members required on the flight leg. In the case of cabin crew members, the following factors affected the number of relief cabin crew members:

Block time of the flight leg,
Whether the flight was a domestic or an international flight,
Number of passenger seats and their split across the different cabin classes.

Based on Title 14 CFR Part 121.467 - Flight attendant duty period limitations and rest requirements: Domestic, flag, and supplemental operations [32], cabin crew members across international and domestic flights were limited to a scheduled duty period of 14 hours per calendar day. For simplicity, each relief crew member was assumed to weigh 200 lbm (to reflect crew member plus their baggage). The relief flight crew was accounted for in the direct operating costs and the relief cabin crew was accounted for in the indirect operating costs.

Modeling Mission Specification Change Scenarios in FLEET

This section describes how Purdue modeled the scenarios that included mission specification changes. The scenarios adjusted for mission specification changes were implemented by adjusting data for the FLOPS aircraft models initialized in FLEET, with block hour and fuel consumption changes based on six different operational ranges provided by Stanford. Upon receiving the percentage change in fuel and block hours between the baseline aircraft and the reduced cruise Mach number aircraft models generated by Stanford's SUAVE tool as described in the Task #2 section. the Purdue team utilized the data to adjust the baseline aircraft model in FLOPS. First, the data from Stanford was curve-fit to facilitate the mapping of the changes in block hours and fuel consumption to the payload-range data tables for the aircraft models in FLOPS. Then, the block hour and fuel consumption data for the feasible segments in the payload-range tables, representing each FLEET baseline aircraft modeled in FLOPS, were adjusted using the factors obtained from the data curve-fit. Next, the adjusted FLOPS block hour table was compared with the original baseline block hour table, and segments in the payload-range tables where the block hours exceeded certain thresholds for relief crew (flight and cabin crew) duty periods were adjusted to accommodate for increased flight and cabin crew per the relevant CFRs. Lastly, FLOPS was re-run to obtain updated payload-range data tables based on the aforementioned adjustments, which represented the aircraft models initialized in FLEET runs for the mission specification change scenarios.

Summary and Comparison of Fleet Benefits Assessment

This section presents combined results from GREAT (Georgia Tech) and FLEET (Purdue) runs for the scenarios defined in Table 3 through Table 5. Focus is placed on macro trends and drivers across the scenarios, namely technology level and demand. Here, it is important to remember that a "high" level of technology assumes a combination of increased technology impact to vehicle performance and rapid introduction of technologies to new vehicles. A "low" technology level assumes both a delayed introduction of new technology and low impact. "Nominal" technology is intended to represent a continuation of current technology trends. In the two following subsections, results from multiple GREAT and FLEET scenarios are combined onto single plots to examine the high level effects of demand and technology on fleet noise and CO_2. All scenarios present noise and fuel burn in the context of U.S. touching operations. More detailed discussions are provided for the GREAT runs and FLEET runs in the following sections.

Fuel Burn and CO_2 Impacts

The first combined result plot, shown in Figure 80, shows the variation in direct CO_2 emissions across both fleet tools and all defined scenarios. Quantile plots are used which show the spread in CO_2 relative to 2005 that is present across all of the scenarios. For example, in 2030, the minimum predicted relative CO_2 is about 60% of 2005 levels for one scenario and as high as 185% of 2005 levels for the worst case scenario. Most of the scenarios predict somewhere between 100% (the same) of 2005 levels and an increase to 140% of 2005. Since there are 12 scenarios with widely varying assumptions, one expects significant variation in the results.

Examining further out years, it appears less likely that direct CO_2 emissions can be held to 2005 levels. To restate, only the direct CO_2 emissions were considered in this study. The impact of alternative fuels would change the results shown proportional to the respective fuels life-cycle impact. Reductions below current CO_2 levels are unlikely until 2035, and in many of the scenarios, the 2050 relative CO_2 level exceeds the 2005 level. Less obvious, but worth noting is the small bump between 2020 and 2030 for the -25%/+75% quantile points. This bump is indicative of the time it takes for new technology to enter the fleet and lower CO_2. Even with new aircraft available immediately, it takes time for older, less efficient aircraft to be retired.

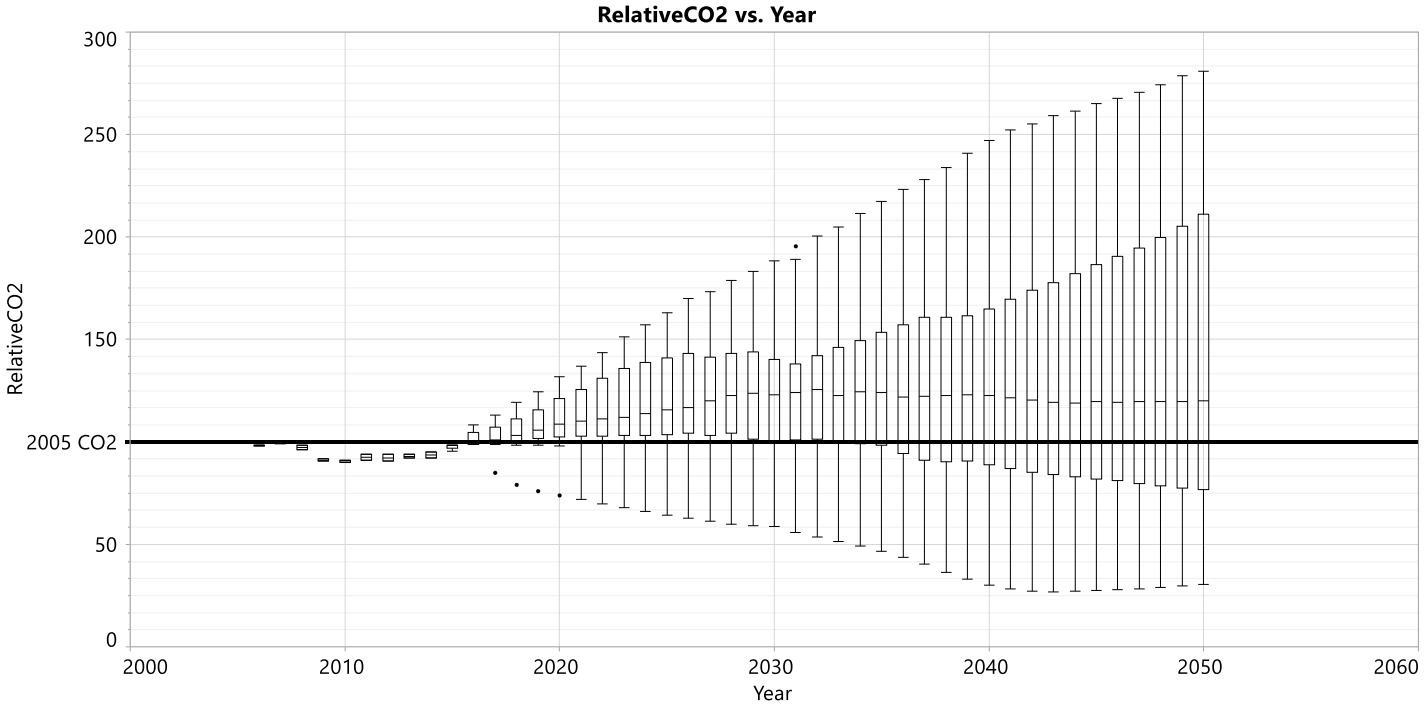

Figure 80: Direct CO_2 Emissions Variation Across All Scenarios

The results shown in Figure 80 can be further decomposed into the major drivers of technology and demand, shown in Figure 81 and Figure 82, respectively. In Figure 81 the variation is due to differences in technology and in Figure 82 the variation is due to variation in demand. The dots that appear in the high technology level scenario are a plotting anomaly due to their large difference from the average trajectory. From the technology level decomposition, it is clear that high technology impacts and rapid insertion are critical to achieving carbon neutral growth. This is true regardless of demand level, which is one of the primary causes of the wide range of outcomes. This is partly by design however, since the scenarios created here were on purpose chosen to show the possible range of outcomes. Breaking down direct CO_2CO_2 emissions by demand shows that low or nominal demand is required to achieve carbon neutral growth for every year between now and 2050. The “very high” demand case in Figure 82 also assumes that operations would be constrained by airport noise. The assumptions were made in GREAT to keep airport noise equal to or less than 2010 contour area and in FLEET to have the contour area at 50% of the 2010 contour area. This shows that high demand may also have an adverse impact on noise contour area, to be further explored later.

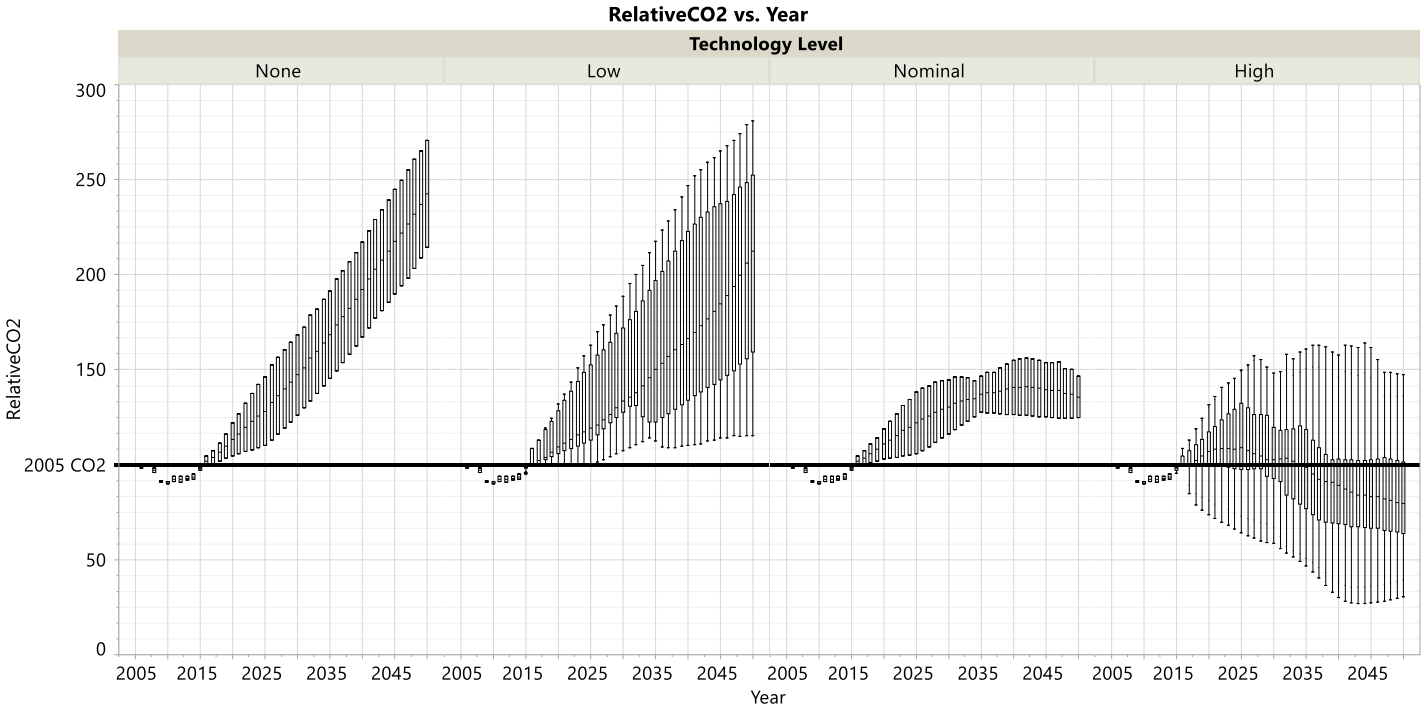

Figure 81: Direct CO_2 Emissions Variation across All Scenarios as Function of Technology Level

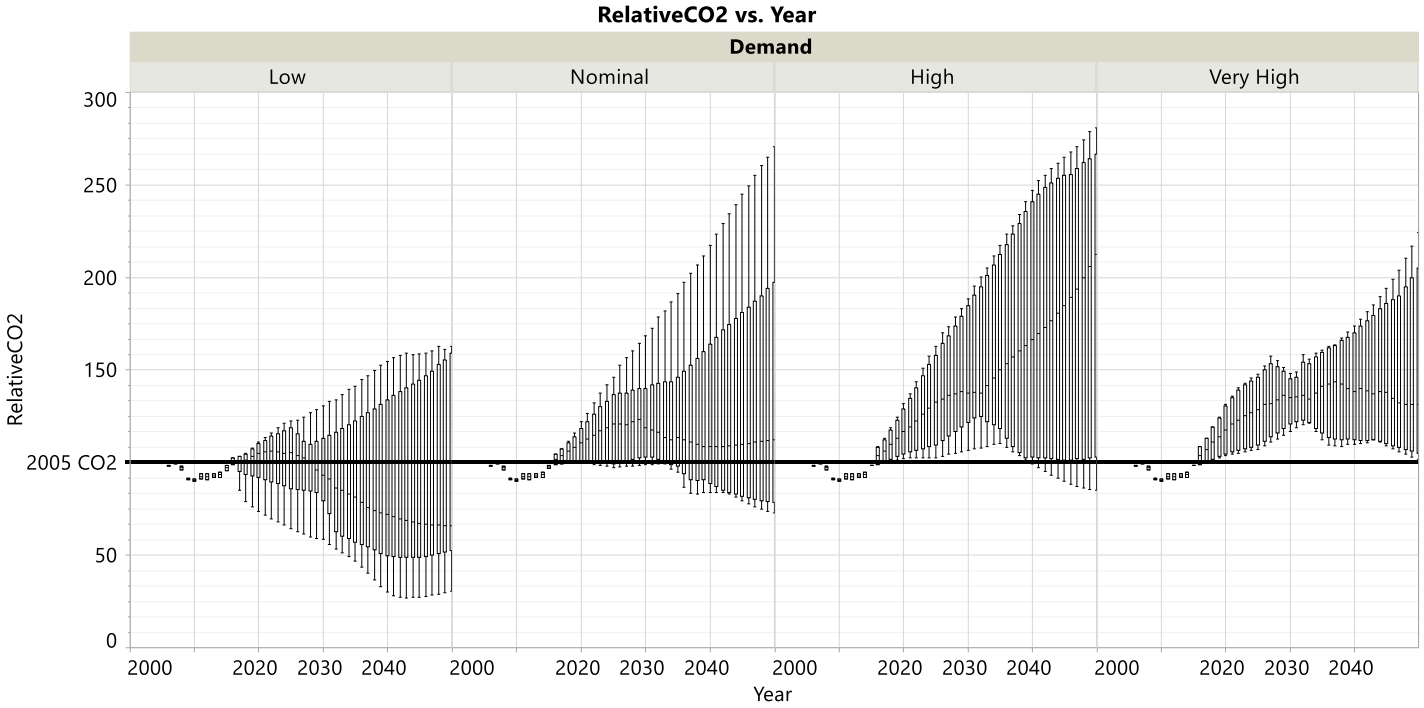

Figure 82: Direct CO2 Emissions Variation Across All Scenarios as Function of Demand

Since future demand is such a large driver of direct CO_2 emissions, it is worth examining the relative predicted operations vs. year, shown in Figure 83. Based on the scenario drivers, demand is expected to increase between 2 and 4 times current operations by 2050. Much is this is driven by an assumption of strong Asian market growth. Even though initially international travel to Asia is not a significant portion of the overall demand, the quite high growth rates become even larger in the high growth in Asia. Additionally, all international travel demand was linked to the scenario assumptions for growth in Asia. This assumption was agreed upon for consistency. Therefore, high demand growth rates for all international demand sustained over several decades then serve to this becoming the dominant factor in future demand for air travel.

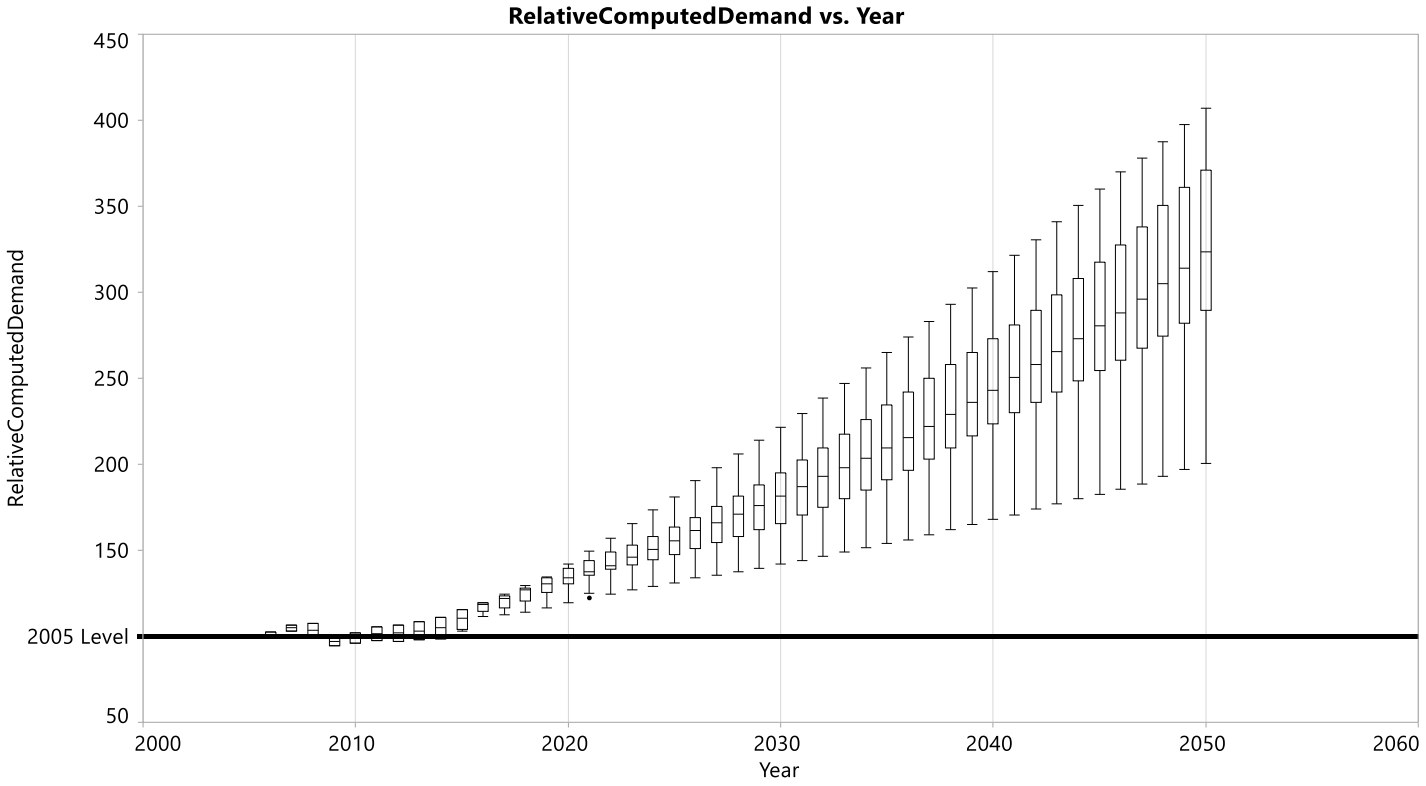

Figure 83: Variation in Future Predicted Demand across All Scenarios

The above figures present combined results from FLEET and GREAT; however, part of the intent of this work was to use two tools, built on different modeling approaches, with similar assumptions in order to corroborate results and predictions. Figure 84 subdivides the results shown in Figure 80 by simulation tool. The plot style has been changed to show trends better. The plot below still shows variation in direct CO_2 emissions across all scenarios; however, darker areas indicate that more of the scenarios go through these areas of the plot. Beyond 2030, three distinct "fingers" emerge. While the absolute CO_2 emissions are slightly different between GREAT and FLEET, the order of magnitude is similar. As expected, the highest direct emissions are produced in the scenarios with the highest demand and lowest technology level. The clustering of scenarios below the 2005 CO_2 levels all include high technology levels. Figure 85 colors the scenarios according to demand. Here, the results are more mixed. While high demand leads to high direct CO_2 emissions, the results of nominal and low demand are more dependent on technology levels. The very high demand case constrains operations to maintain or decrease noise areas below 2010 levels. As a result, one can see that noise constrained operations will have a significant impact on direct CO_2 emissions, but will not reduce them below 2005 levels. In this sense, direct CO_2 emissions are more difficult to achieve than noise area reductions.

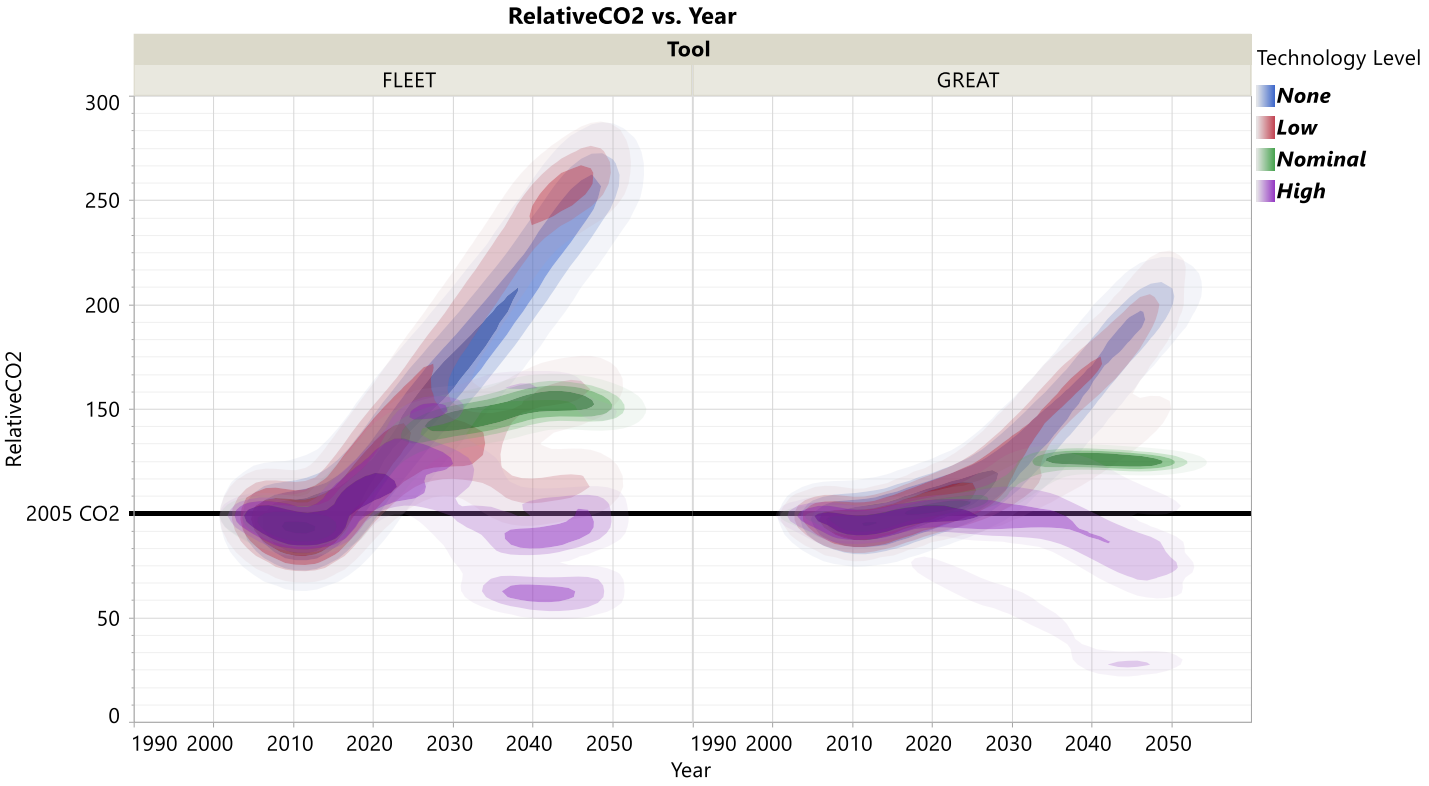

Figure 84: Comparison between FLEET and GREAT Direct CO_2 Emissions Predictions vs. Technology Level

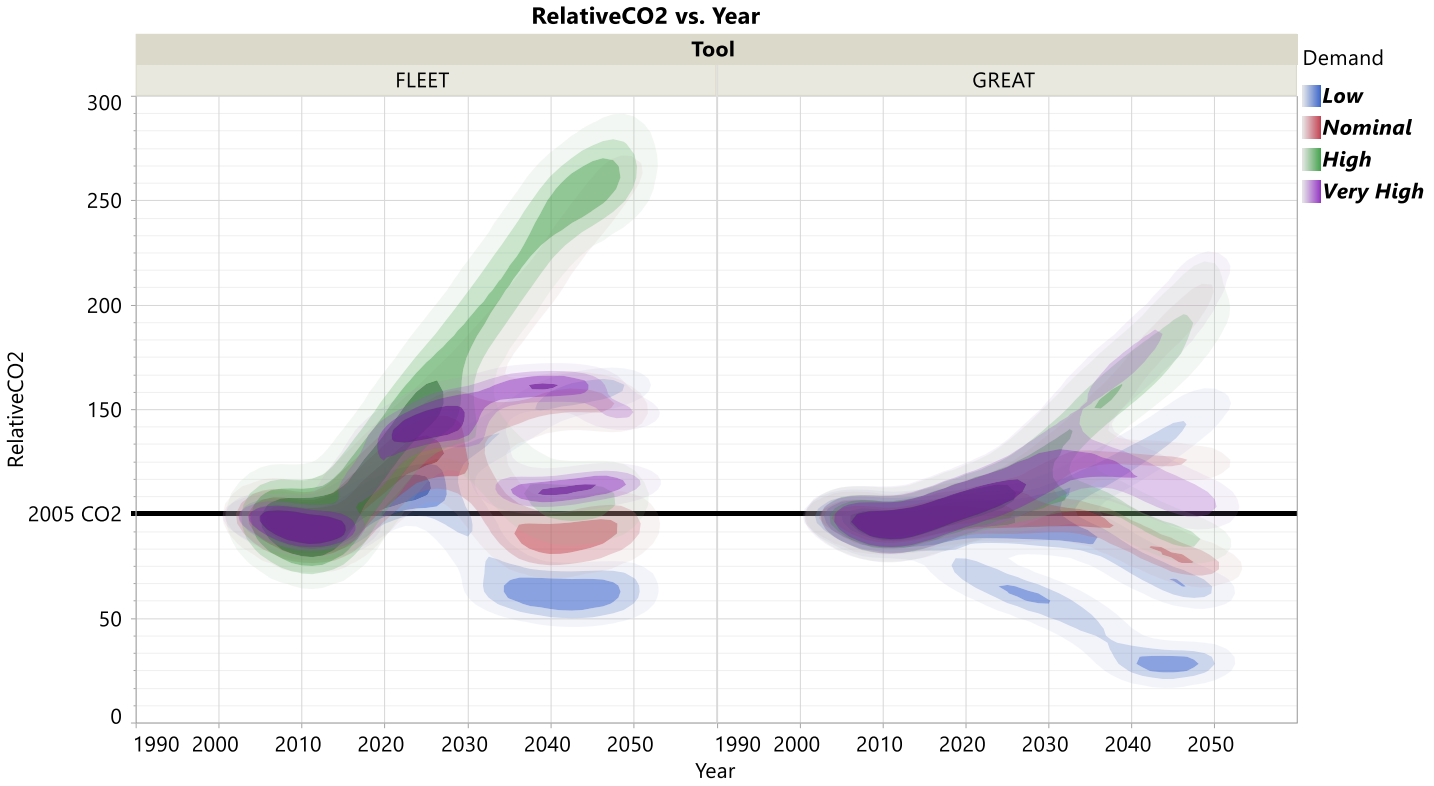

Figure 85: Comparison between FLEET and GREAT Direct CO2 Emission Predictions vs. Demand

Figure 85 further investigates the strong impact of technology as modeled in both fleet-level tools. Recall, a "low" or "high" technology level, as used in the preceding discussion, actually consists of two distinct assumptions, the technology impact on the vehicle, and the rate at which new technology is introduced to the fleet. The rate at which new technology is introduced is heavily dependent on the retirement rate of older aircraft, especially for lower demand scenarios. Figure 86 colors the scenarios according to the aircraft retirement assumptions. Here, it is apparent that early retirement drives fleet turnover and reduces direct CO_2 emissions in out years. This trend holds for both tools.

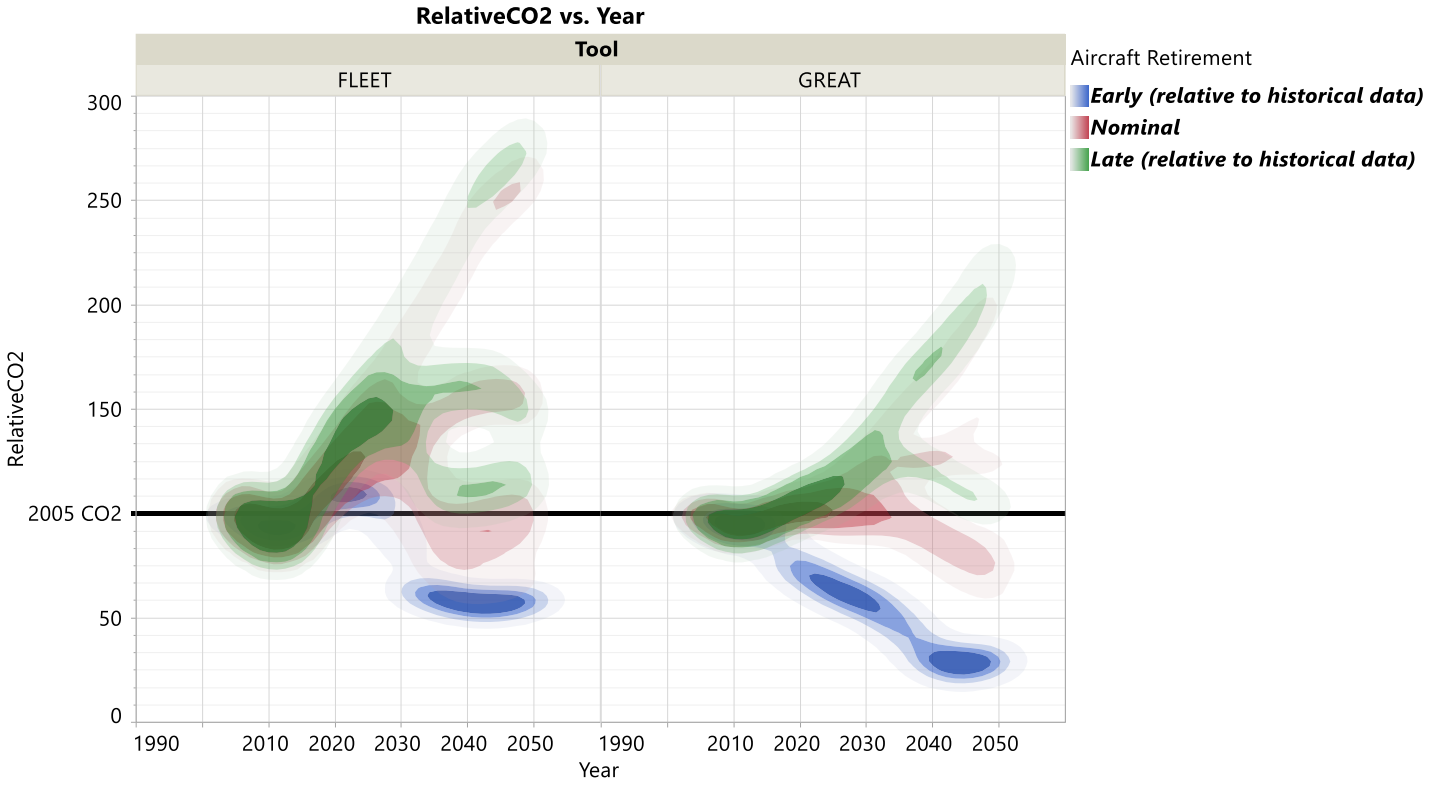

Figure 86: Comparison Between FLEET and GREAT Direct CO2 Emission Predictions vs. Retirement Rates

In summary, with nominal or low demand, which includes a doubling of operations by 2050, carbon neutral growth is achievable only with increased focus on technology maturation and insertion into the fleet. It is critical to get new technologies developed and placed on aircraft as soon as possible, and in a manner that encourages airlines to retire their current fleet in favor of the newer aircraft. Unfortunately, the long life span and development timelines of commercial aircraft make achieving this goal very difficult.

Noise Impacts

Fleet noise can be examined in a similar manner as fuel burn. Figure 87 shows 65 DNL contour area as predicted by GREAT and FLEET. The methodologies for computing noise area are different between the two tools. GREAT uses the aircraft models described in the Task #2 section combined with the predicted operations to perform a noise analysis at a single runway airport. A representative fleet mix is used to calculate contour areas for 2010 through 2050 in 10 year increments. FLEET uses the area equivalency method combined with predicted certification noise values to predict contour area changes at major airports. A simple addition of the contour area at each U.S. airport in FLEET provides a “total area” for the entire airline network; these values appear normalized with respect to the total area in the base year of 2005. FLEET’s noise prediction module runs more quickly; therefore, FLEET has noise prediction results for every year, whereas GREAT predicts in ten year increments.

Immediately obvious in Figure 87 is that GREAT shows a wide spread in potential 2050 65 DNL contour area, but FLEET universally predicts that other than in the frozen technology scenario, that noise will be reduced, regardless of future technology or demand.

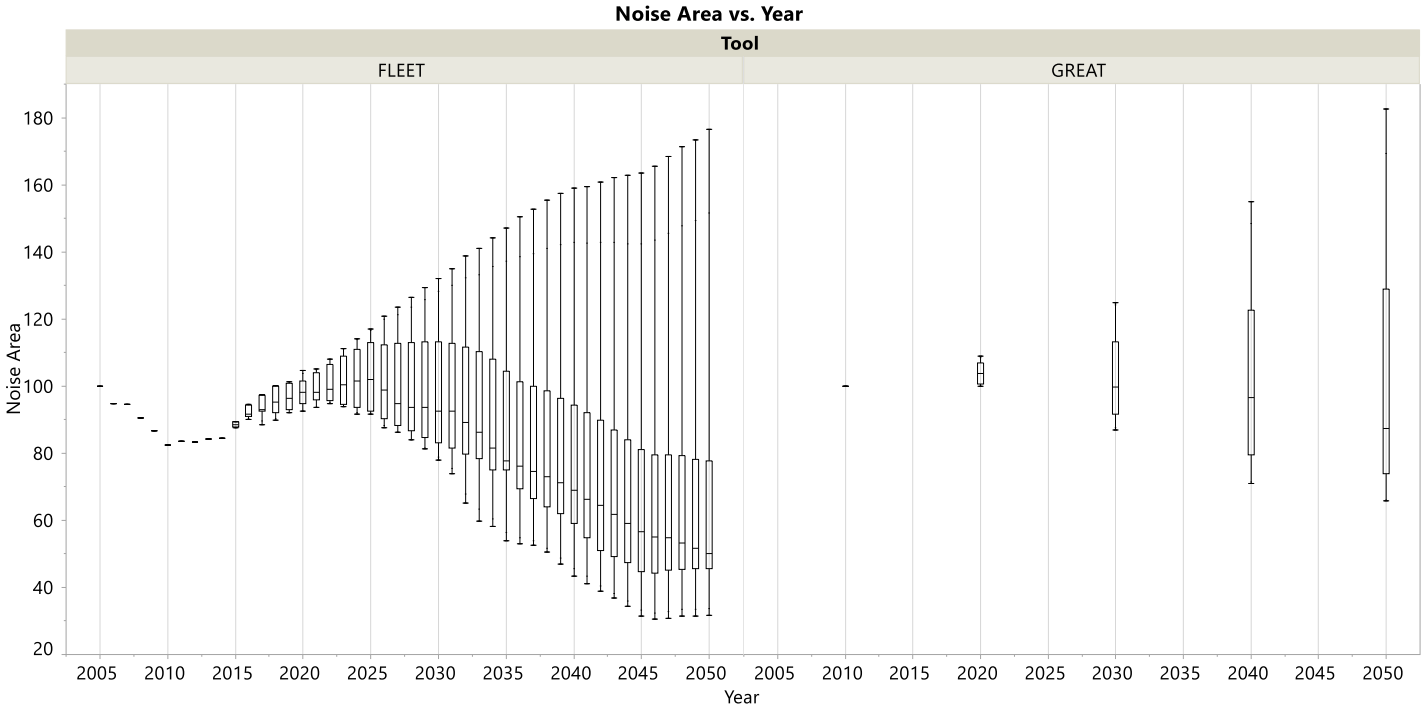

Figure 87: 65 DNL Contour Area Variation Across all Scenarios

GREAT and FLEET Detailed Results

GREAT Fleet Detailed Results

To visualize and observe trends in the fleet over time, noise and fuel burn results from each scenario were aggregated and compared side-by-side in plots, such as the one shown in Figure 89. Noise results are displayed with columns and represent the 65 DNL (day-night average sound level) Noise Area, as calculated using the Airport Noise Grid Interpolation Method (ANGIM) and Global and Regional Environmental Aviation Tradeoff (GREAT) tools. The data for 65 DNL Noise Area is shown for years 2010, 2020, 2030, 2040, 2050. Each noise data point is normalized to year 2010. The 65 DNL Noise Area is a suitable noise exposure metric that helps indicate whether overall noise has increased or decreased through time.

Fuel burn metrics are overlaid on the same plot using the dotted trend lines, and is a direct function of the relative CO_2 emissions. Again, no alternative fuels were assumed in this analysis; however, the life equivalent CO_2 emissions of any given fuel can be used to directly scale the fuel burn results. The fuel burn is shown in the plot for each year over a period spanning 2005 to 2050, alongside noise. Each year for fuel burn is normalized to the year 2005. Each plot displays the trends in noise and fuel burn of several scenarios, with the “Current Trends Frozen Tech” as reference.

A common color scheme was developed for the GREAT results discussion and is shown in **Figure 88**. Grey and black are used to indicate the two baseline cases, frozen technology and the current trends “best guess” which is indicative of a business as usual scenario. Shades of blue are used to indicate increasing demand but with Low Technology R&D Levels. This provides a view of the role of demand in a slow technology development landscape. Green is used to mark the two Environmental Bounds scenarios. Recall, the intention of these two scenarios is to estimate the absolute best and worst case scenarios from an environmental perspective. Finally, shades of red are used to evaluate the impact of demand while holding technology development to a high, rapidly developing level. The following plots compare these sets of scenarios with the goal of isolating impacts to draw general conclusions.

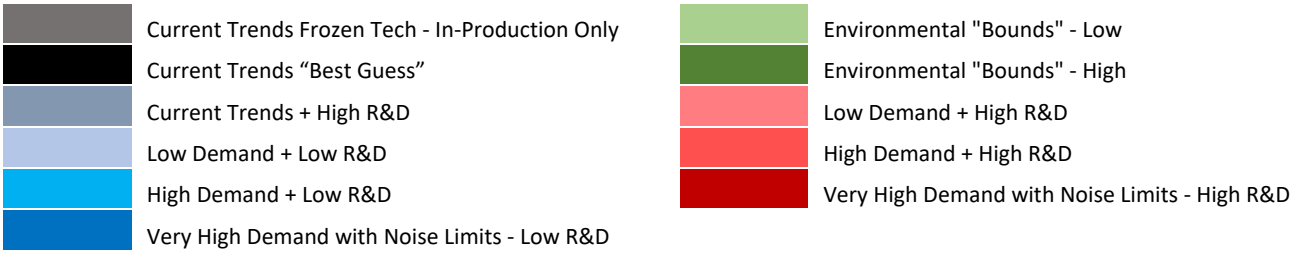

Figure 88: Scenario Color Scheme Legend for Noise & Fuel Burn Plots

Figure 89 shows the three current trends scenario with the frozen technologies, "best guess", and High R&D scenarios. This plot is useful to bound direct CO_2 emissions as a function of technology with current demand levels. The frozen technology scenario is unrealistic, and assumes that the current in production aircraft will be continue to be produced forever, but provides insight into how much current technology trends are already offsetting future CO_2 increases. The High R&D scenario shows that reducing carbon dioxide levels below 2005 are possible with current demand trends, but reaching the current global goals of 50% reductions in 2050 appear to be quite difficult. Recall that the High R&D scenario assumes both a high level of technology impact and more rapid introduction of new technologies into the fleet. It is also apparent that technology has a large impact on contour noise area.

Figure 90 shows variation in demand with low technology R&D. Recall, this means technology impacts are low and the introduction of new technology is slower than historical trends. A few important observations can be made by comparing with the trends just presented in **Figure 89**. First, reducing demand below current levels obviously reduces direct CO_2 emissions, but does not change the fundamental shape of the curve. The 'kink' necessary to bend the curve downward must be introduced through technology infusion, as seen below. The impact of demand on noise is also much smaller than that of technology. These trends are more readily apparent if the reader compares **Figure 90** and **Figure 91**; these two figures both show the impact of varying demand on noise and fuel burn, but **Figure 91** shows the impact at high levels of technology investment. The differences between the two plots are greater than variation in demand, once again indicating technology investment is the primary driver of future fleet emission and noise reductions. It must be restated that even more important than the direct impact of the technology is the rate at which new technology is introduced into the fleet. An aircraft's typical lifespan lies between 15 to 30 years, therefore there is significant lag in new technology having a real world impact.

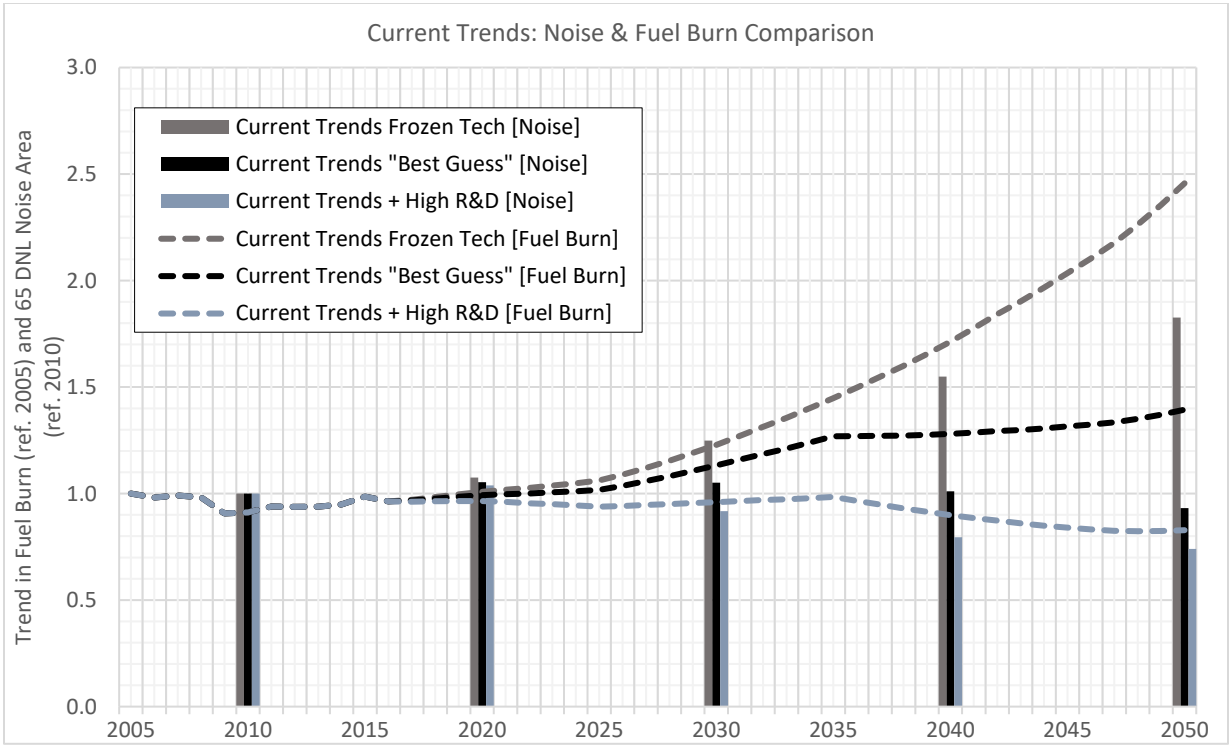

Figure 89: Noise & fuel Burn Comparison – Current Trends

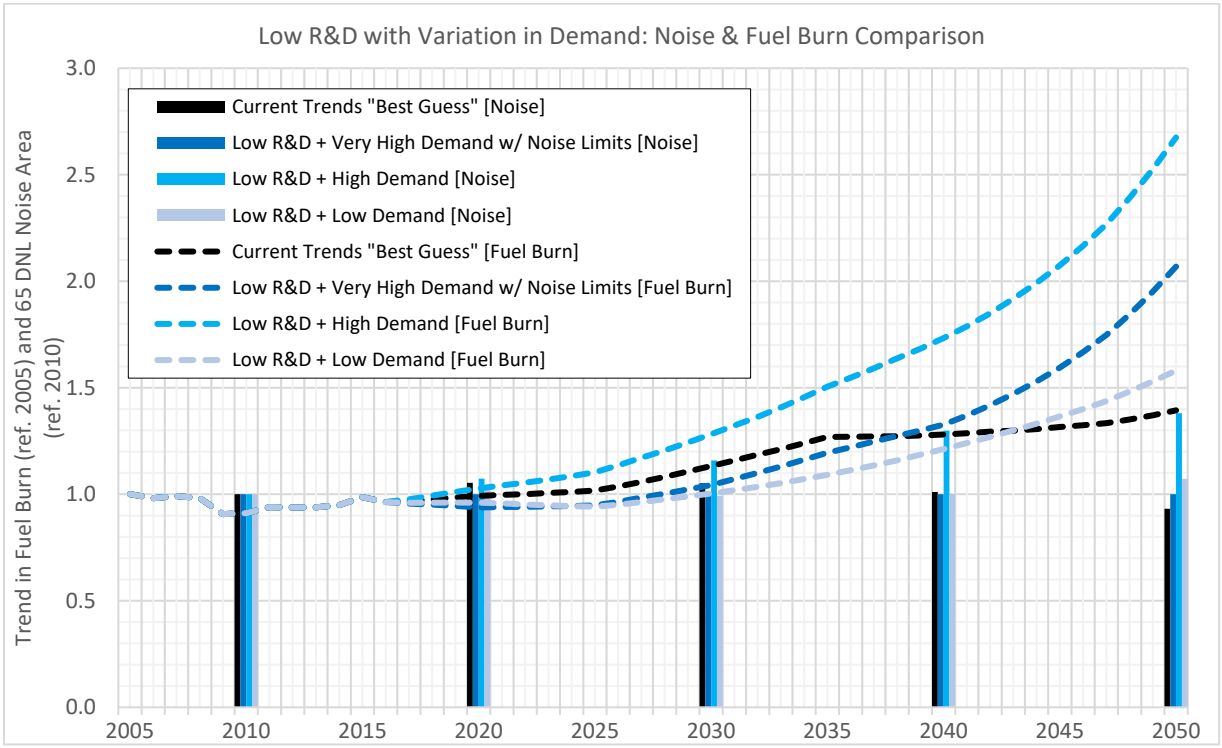

Figure 90: Noise & Fuel Burn Comparison – Low R&D with Variation in Demand

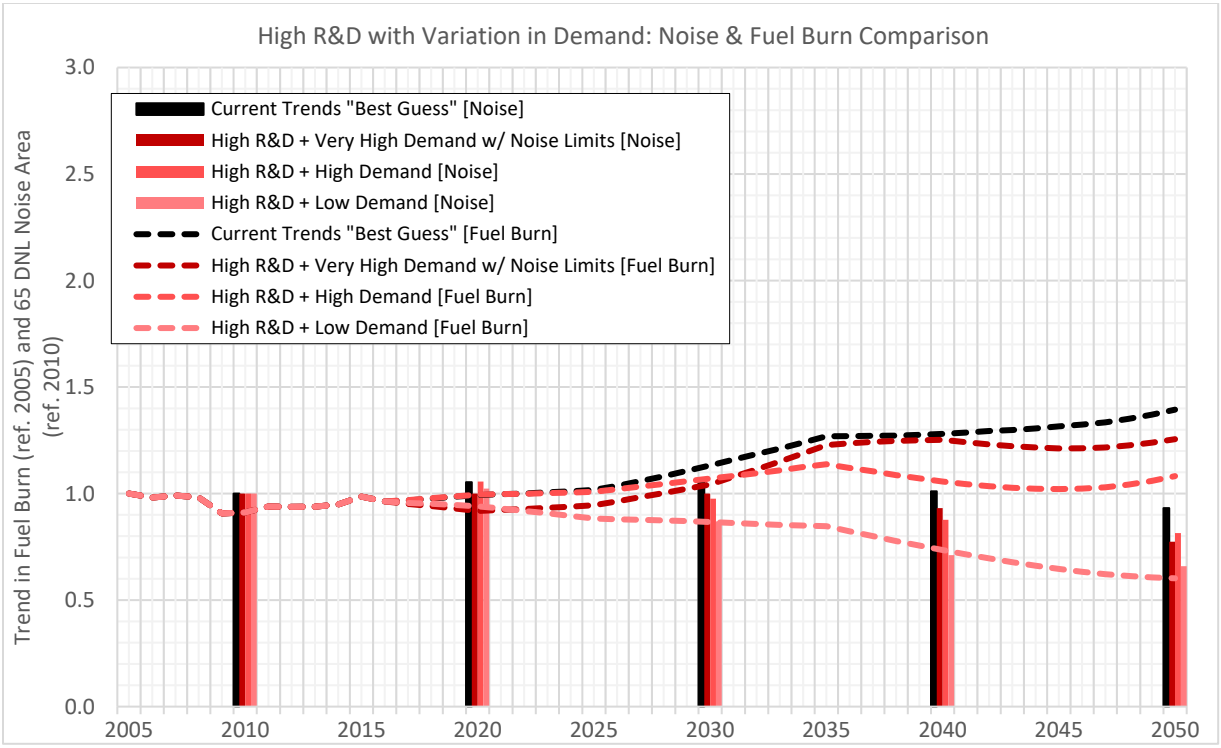

Figure 91: Noise & Fuel Burn Comparison – High R&D with Variation in Demand

Figure 92 shows the two extreme bounding cases on fuel burn and direct CO_2. The best case scenario from an emissions perspective is perhaps an odd and unlikely one from a U.S. economic perspective. In order to achieve the significant reductions shown, GDP growth and airline demand must be stagnant coupled with large increases in technology development, presumably through increases in R&D spending. While unlikely since R&D spending is usually tied to a healthy economy, it shows that significant reductions are achievable under the right circumstances. The upper bounding scenario is more likely and includes a combination of significant economic growth coupled with large airline demand increases and a rate of technology maturation slower than today. While aircraft and engine OEMs tend to pursue R&D to maintain competitive advantage, it is not entirely impossible to have demand increases large enough that the focus is on meeting production rates rather than significant step changes in aircraft performance and noise levels. The trend is exponential and could result in a tripling of direct CO_2 emissions and a 50% increase in contour areas by 2050.

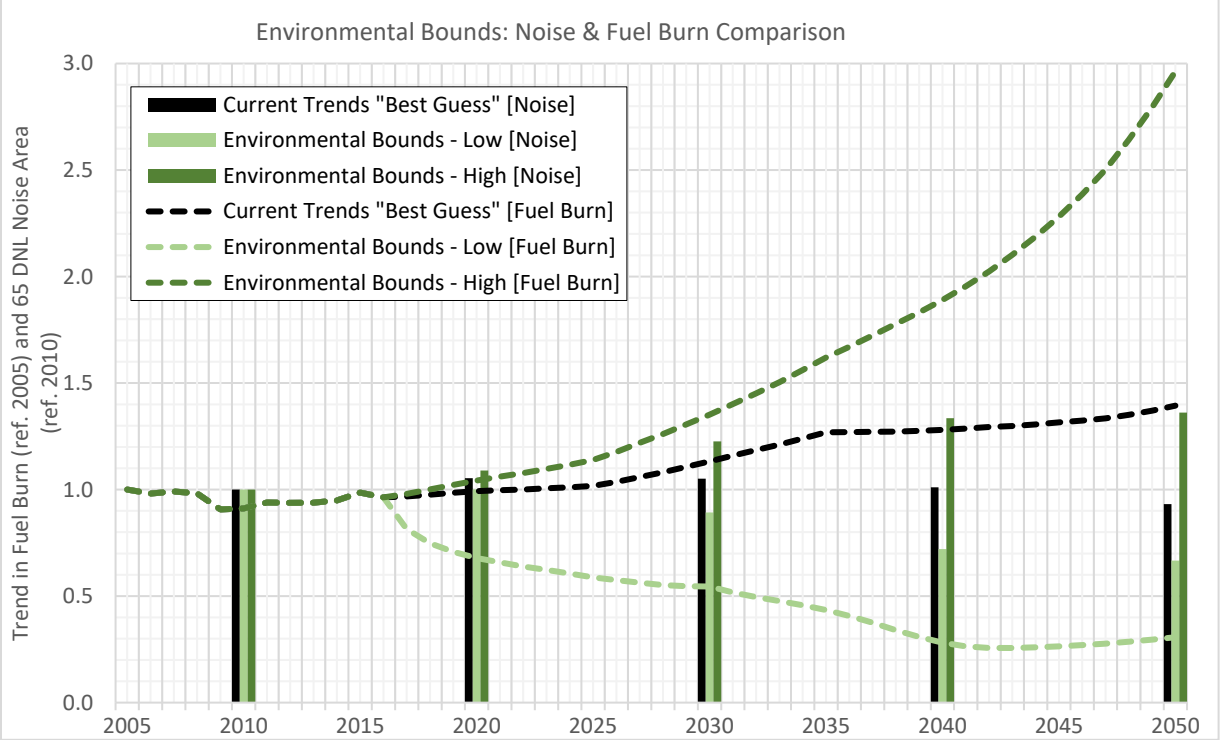

Figure 92: Noise & Fuel Burn Comparison – Environmental Bounds

Finally, Figure 93 and Figure 94 show the impact of varying technology R&D investment against fixed demand. Important to note here is the larger relative impact of technology when demand is high. High demand requires larger numbers of new aircraft. As a result technology is introduced at a more rapid rate than would be the case in a low demand scenario, where aircraft retirement rates are the dominant force in new technology introduction. Nevertheless, from a carbon neutral growth perspective, High R&D is essential regardless of assumed demand increases.

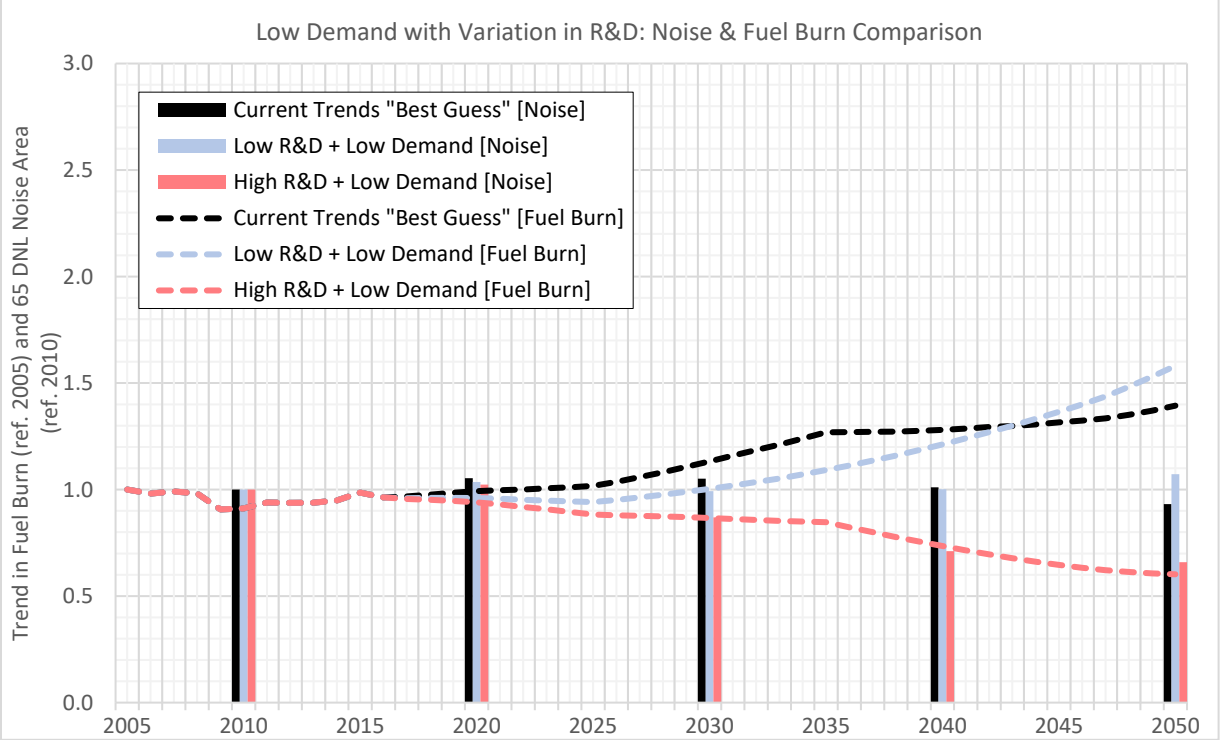

Figure 93: Noise & Fuel Burn Comparison – Low Demand with Variation in R&D

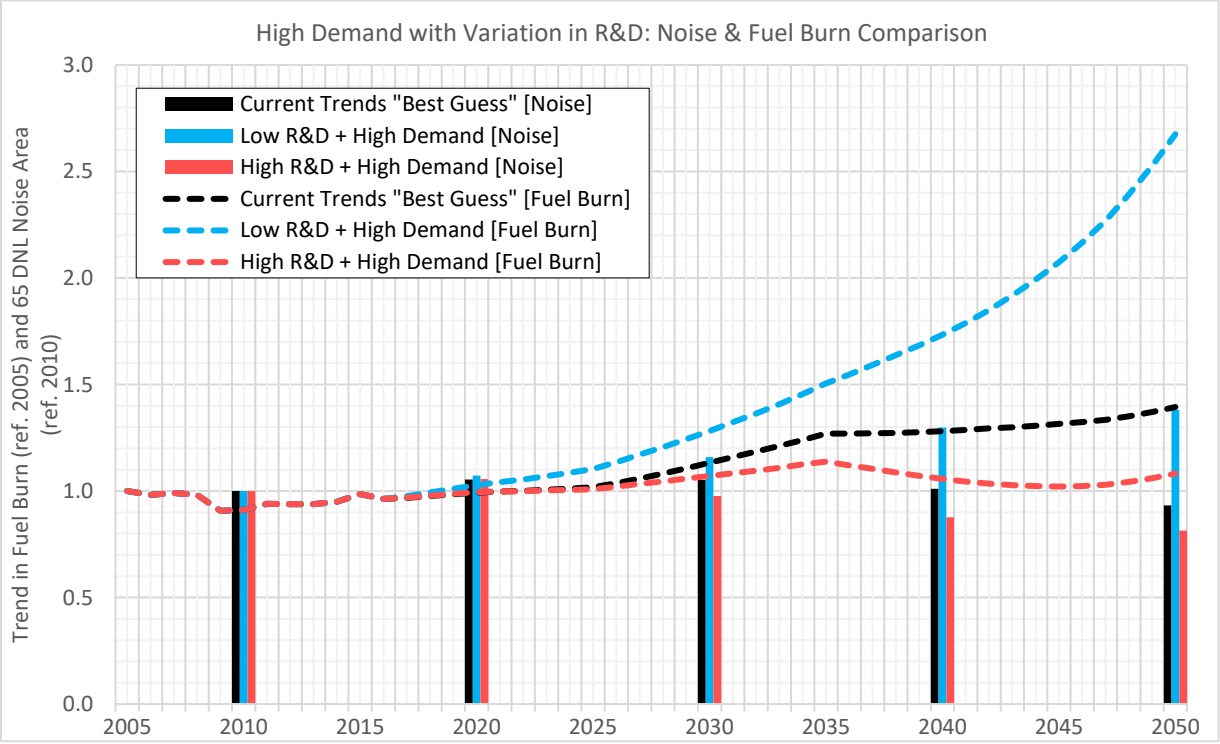

Figure 94: Noise & Fuel Burn Comparison – High Demand with Variation in R&D

FLEET Fleet Detailed Results

The remainder of this section describes Purdue's representation of the "ASCENT 10 Project" scenario simulations using FLEET with the scenario setups aforementioned.

Table 13: Percent GDP Growth Rates for Each Continent Segregated by Demand Scenarios

Scenarios	North America	South America	Europe	Africa	Asia	Oceania
Current Trend	2.8%	4.2%	2.4%	2.8%	4.3%	2.8%
Low Demand	1.8%	2.7%	0.6%	1.8%	3.3%	1.8%
High Demand	4.0%	5.3%	4.2%	4.0%	5.9%	4.0%

Table 13 shows the percent GDP growth rate for each demand scenario type for each continent used in the FLEET model to determine the evolution of the inherent passenger demand growth rate throughout the simulation period. The initial population growth rates for all demand scenarios were set to 0.58%, 1.26%, 0%, 2.6%, 1.10%, and 1.10% for North America, South America, Europe, Africa, Asia, and Oceania respectively. The approach here uses historical demand for trips made between 2005 and 2013, so the yearly GDP growth rates in the table take effect starting after 2013.

Both demand and CO_2 emissions values are normalized to their respective 2005 values. For all scenarios, the demand follows historical data until 2013, when the various trend lines split to demonstrate the predicted future values. **Figure 95** presents the projected demand trends using passenger nautical miles as the measure. Under the current trends assumptions for GDP, the differences in technology levels make some, but little, difference in the demand. The Current Trends + High R&D scenario leads to the highest demand in 2050, because the higher technology aircraft burn less fuel leading to lower operating costs (in fixed year dollars) so that the price elasticity calculation adds some demand on top of the GDP growth rate- and population-driven inherent demand.

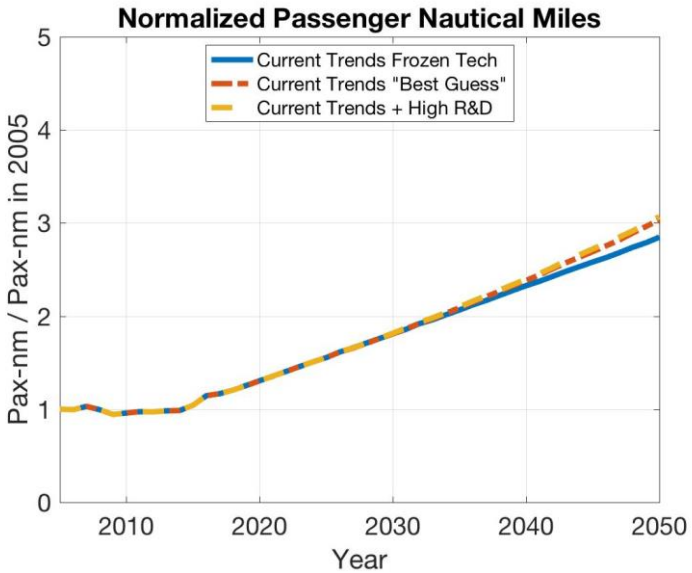

Figure 95: Normalized Passenger Nautical Miles from 2005 to 2050 – Current Trends Scenarios

Figure 96 indicates that CO_2 emissions from U.S.-related airline operations would increase by a factor of about 2.75 from their 2005 level by the year 2050 if no new technology is introduced (this is the "Current Trend Frozen Tech" scenario). This is an unlikely scenario, indicating the upper bound for CO_2 emissions from the current trends assumptions about demand growth. This factor decreases to a factor of 1.45 and 1 in the Current Trend Best Guess and Current Trend High R&D scenarios

respectively, where the new technology aircraft become available over time and the airline retires older aircraft from its fleet. With some of the stated goals for 2050 levels of aviation CO_2 to be at or below the 2005 levels of aviation CO_2, the Current Trends High R&D scenario does show some promise of reducing future CO_2 while serving increasing passenger demand.

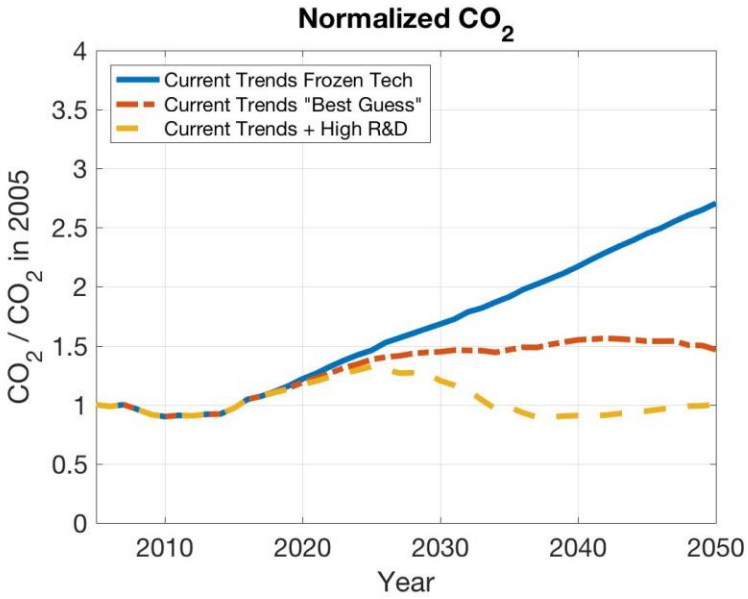

Figure 96: Normalized Fleet-Level Emissions from 2005 to 2050 – Current Trends Scenarios

To help illustrate the role of new technology in the aviation CO_2 predictions, **Figure 97** presents the fleet-wide CO_2 emission intensity (the grams of CO_2 equivalent per passenger mile flown); this value is also normalized using the 2005 level. The Frozen Tech scenario shows a nearly flat trend line from 2014 out to 2050; this scenario assumes that when the airline acquires a "new" aircraft, that aircraft is a "brand new" version of the best-in-class aircraft, so there is no technology advancement. Because of how the airline in FLEET meets future demand, this Frozen Tech trend line shows some deviations as the allocation changes to meet changing demand. In the Current Trend family of scenarios with a best guess at technology introduction and with the high research and development perspective, the fleet-wide CO_2 emission intensities in 2050 relative to 2005 are 0.49 and 0.32, respectively.

The significant change in CO_2 emission intensity trend slopes around the mid-2020s and 2030s in Current Trend High R&D scenario corresponds to the availability of New-in-Class and Future-in-Class aircraft. The High R&D trend line has a clear change in slope in the mid- to late-2030s where there are no "N+3" aircraft to replace the Future-in-Class aircraft, so the airline relies on similar aircraft types to meet the increasing demand.

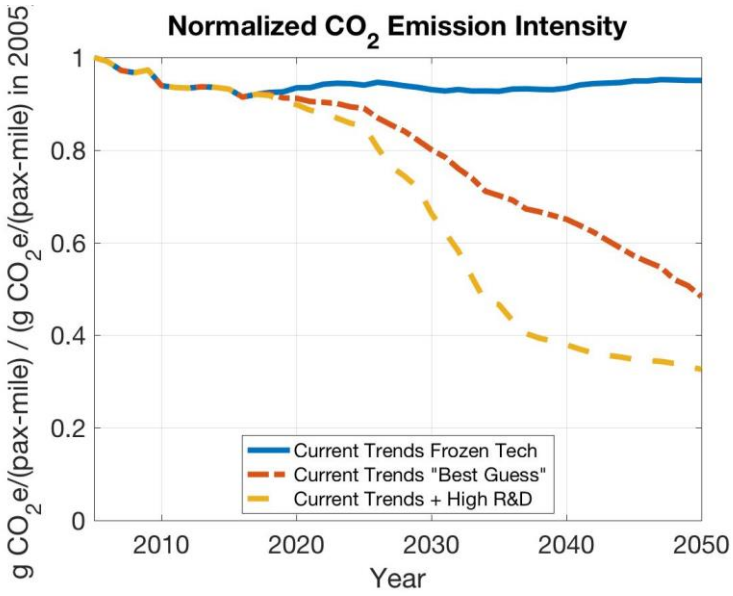

Figure 97: Normalized Fleet-Level CO_2 Emission intensity from 2005 to 2050 – Current Trends Scenarios

Figure 98 displays the relative number of aircraft deployed over time, showing an increasing total number of aircraft in the airline's fleet, while also showing how these aircraft fall into different technology ages or categories. The Frozen Tech scenario shows no New-in-Class or Future-in-Class aircraft; as the airline fleet grows in size, the new aircraft are all Best-in-Class in terms of performance. A small number of representative in class aircraft operate out to their maximum possible age because the small regional jet, in the FLEET model, continues to be profitable on some routes and there is no immediate replacement for these 50-seat jets. In FLEET, the representative-in-class aircraft were still being produced even after their entry in service date, so the last of the representative-in-class aircraft were at most 40 years old. This 40-year maximum possible age matches the maintenance maturity curves used in computing net present value in the retirement model. Also in Figure 98, the "Best Guess" deployed fleet composition shows an increasing airline fleet size, with diminishing numbers of previous technology age aircraft as the next technology age aircraft increase production. The Best-in-Class aircraft make a peak fraction of the fleet around 2025, then the new-in-class peak around 2040, and the future-in-class dominate in 2050 at the end of the scenario. These peaks all occur roughly 20 years after the first of that technology age's aircraft enter service. The fleet size and technology age composition in the High R&D scenario is not strikingly different from the "Best Guess" scenario, even though the High R&D new-in-class and future-in-class aircraft have much lower fuel burn than their counterparts in "Best Guess". This demonstrates that it is difficult for technology improvements to have enough impact on cost to force "earlier" retirement of aircraft already in the airline's fleet.

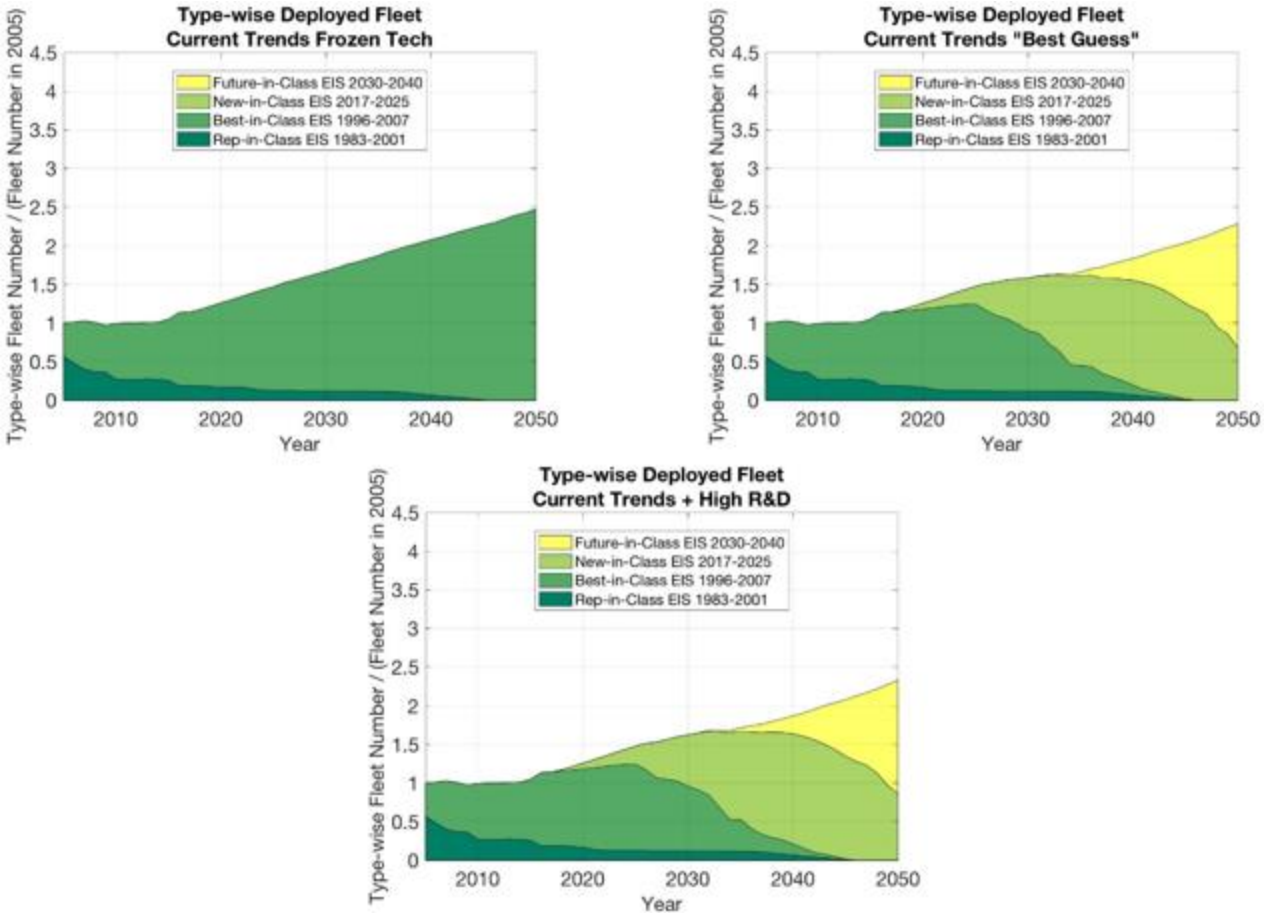

Figure 98: Normalized Deployed Fleet by Type – Current Trends

Figure 99 illustrates the airline fleet growth in a slightly different manner; here, stacked bar charts indicate the deployed fleet by class (or aircraft size) for each year of the scenario. The Best Guess and High R&D scenarios lead the airline to operate a higher fraction of future-in-class single aisle (Class 3) aircraft as this becomes available. The ability of this very efficient aircraft to offer better economic returns, coupled with the retirement of representative- and best-in-class small regional jet (Class 1) aircraft create a need for these aircraft to satisfy the passenger demand, which leads to some up-gauging of the fleet on shorter routes. Further, as mentioned in Section 8.5.4, the High R&D Class 3 aircraft receive notable use on trans-Atlantic routes. Also of interest, the airline flies very few trips using class 5 (Large Twin Aisle – LTA) aircraft, by 2050, in the Current Trend Best Guess and Current Trend High R&D scenarios, primarily due to the technology improvements from the class 6 (VLA) aircraft, which has a capacity of 430 passengers, predominantly serving the few long-range high-demand routes in the FLEET route network. Figure 99 also shows that in the Current Trend Frozen Technology scenario, the airline deploys more classes 4 and 5 aircraft and less class 3 aircraft by 2050 relative to the other Current Trend scenarios. This suggests that the airline operates larger class aircraft in order to remain profitable and reduce emissions, when subjected to increasing passenger demand without aircraft of improved technology.

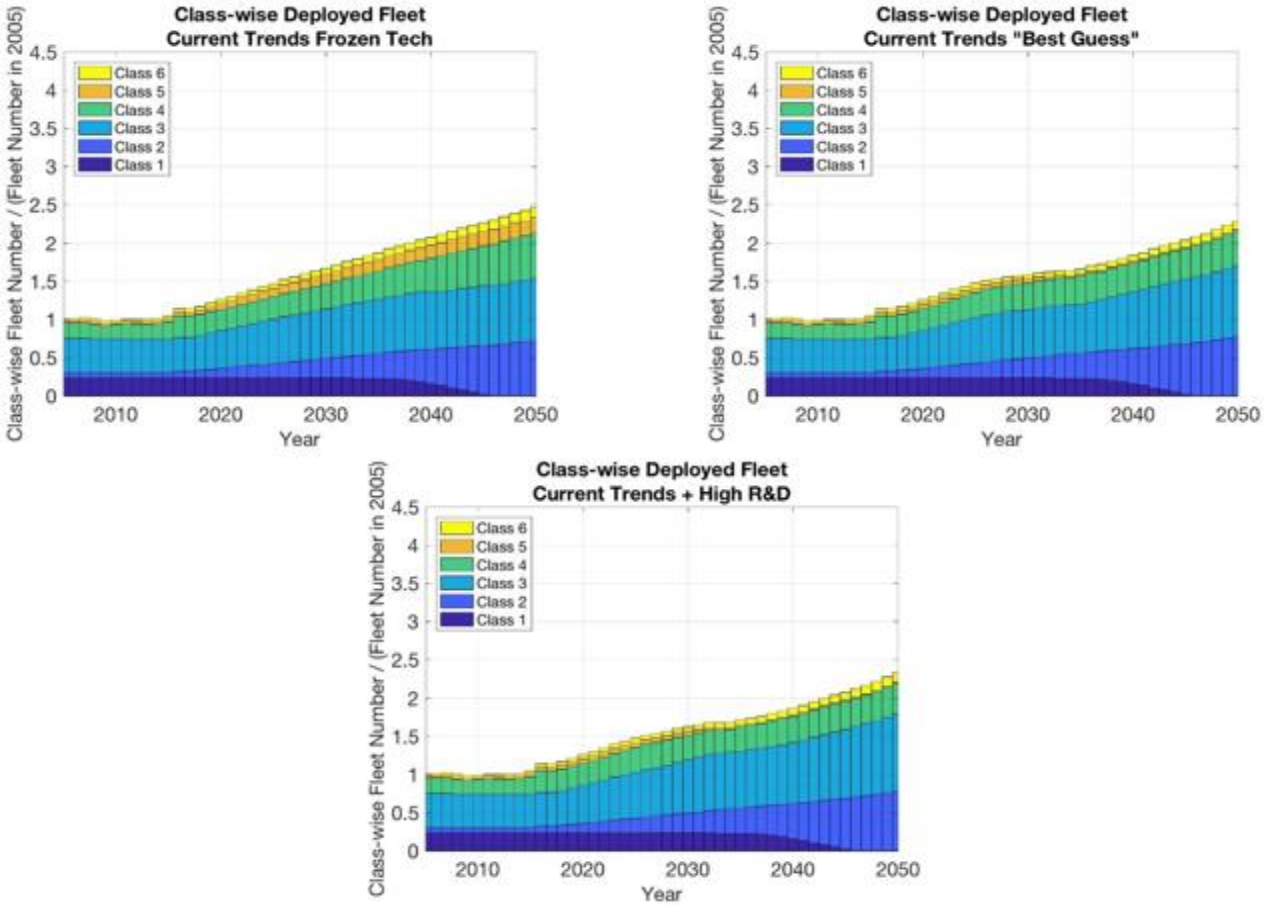

Figure 99: Normalized Deployed Fleet by Class – Current Trends

Figure 100 shows the revenue passenger nautical miles of the airline for the High R&D scenarios throughout the simulation normalized by the value in 2005; the Current Trends Best Guess plot appears along with these High R&D scenarios for reference. The Low Demand High R&D scenario produced the least growth in RPM of about 2.3 times the value in 2005 by 2050. The passenger nautical miles in the High Demand R&D scenario increased to about 4 times respectively of the corresponding values in 2005. Figure 101 shows the fleet-level CO_2 emissions of the High R&D scenarios normalized by the 2005 emission value. The Low Demand High R&D and High Demand High R&D scenarios yielded CO_2 emissions of 75% and 125% respectively of their corresponding 2005 values by 2050. The CO_2 emission intensity normalized by the 2005 value, for the High R&D scenarios throughout the simulation period is presented in Figure 102**.** The emission intensities in the High R&D scenarios by 2050 ranged between 32% and 34% of the corresponding value from each scenario in 2005. Despite the brief period of decreasing CO_2 emissions between the mid-2020s and mid-2030s, indicating that the airline is operating more fuel efficient aircraft, the overall fleet-level emissions show an increasing trend due to the overwhelming demand growth in the scenarios.

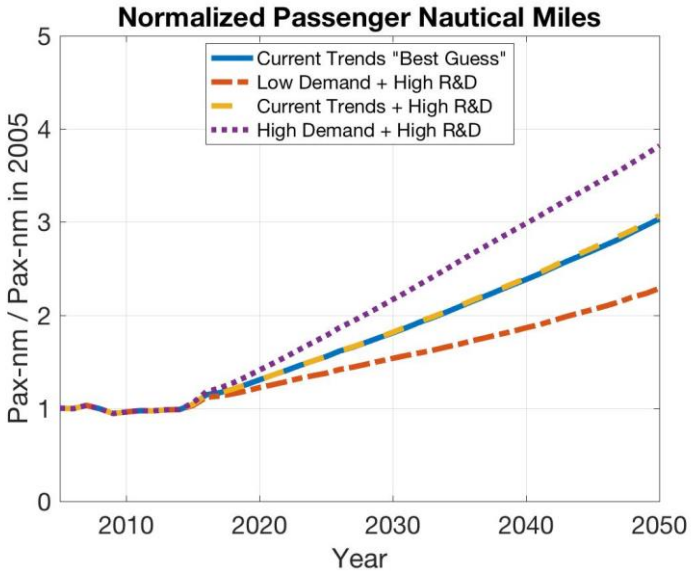

Figure 100: Normalized Passenger Nautical Miles from 2005 to 2050 – High R&D Sciences

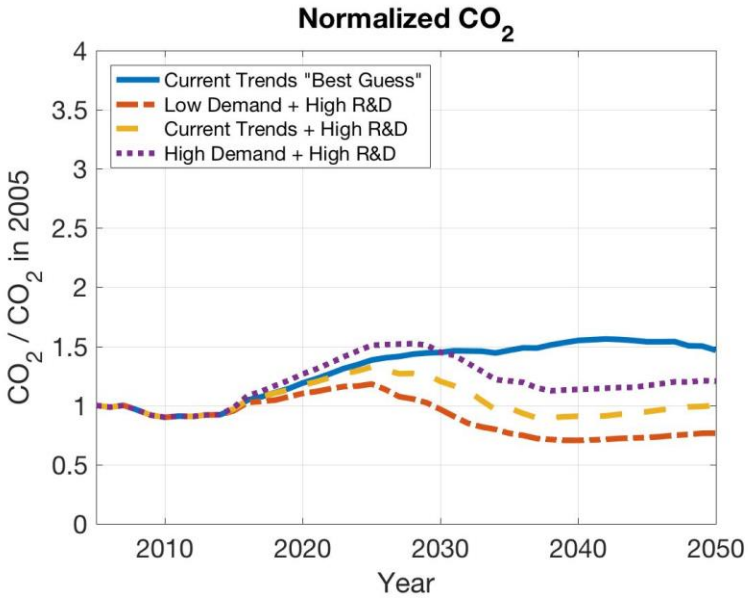

Figure 101: Normalized Fleet-level Emissions from 2005 to 2050 – High R&D Scenarios

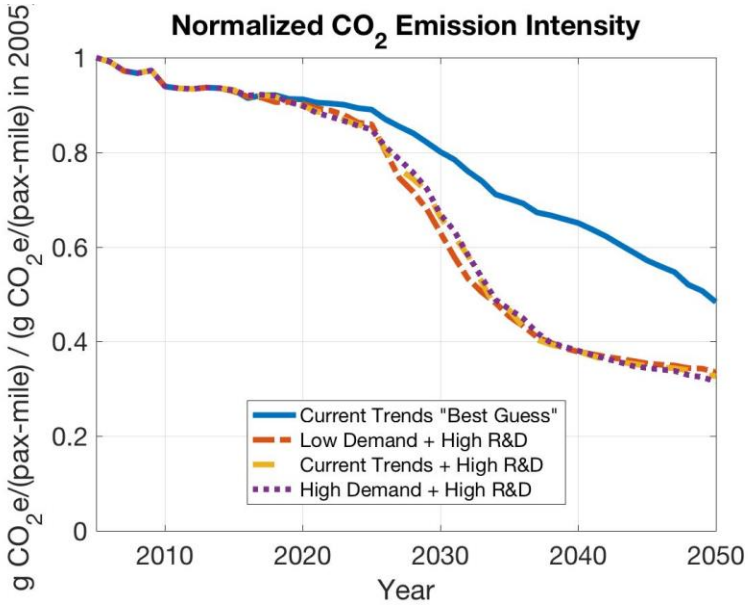

Figure 102: Normalized Fleet-Level CO2 Emissions Intensity from 2005 to 2050 – High R&D Scenarios

Figure 103 and Figure 104 show the deployed fleet by aircraft type and class respectively, normalized by the values in 2005, for High R&D scenarios. The total number of aircraft deployed by the FLEET airline in the Low Demand High R&D and High Demand High R&D scenarios increased by about 75% and 180% of their respective values in 2005 by 2050. Figure 103 reveals the FLEET airline's sensitivity to new technology aircraft due to different variations in demand across the High R&D scenarios. The relatively higher fraction of new-in-class and future-in-class aircraft in the High Demand High R&D scenario suggests that the airline leverages the benefits from next generation aircraft as they become available in order to mitigate carbon emissions due to ever-increasing demand. In the Low Demand scenario, the demand for aircraft to satisfy the increasing passenger demand is lower than that in the other High R&D scenario. Hence, airlines can acquire enough "newer" aircraft to replace their old generation aircraft, which results in a shorter fleet turn-over duration. Figure 104 shows the variation in aircraft fleet by size in the High R&D scenarios. The FLEET airline utilizes a larger fraction of next generation classes 3 and 5 aircraft in the High Demand scenario when compared to the Low Demand, in order to serve demand while reducing CO_2 emissions. The comparison of aircraft types also reveals that the airline retains some older aircraft for a longer duration; for instance, Figure 103 and best-in-class aircraft still operating past 2040.

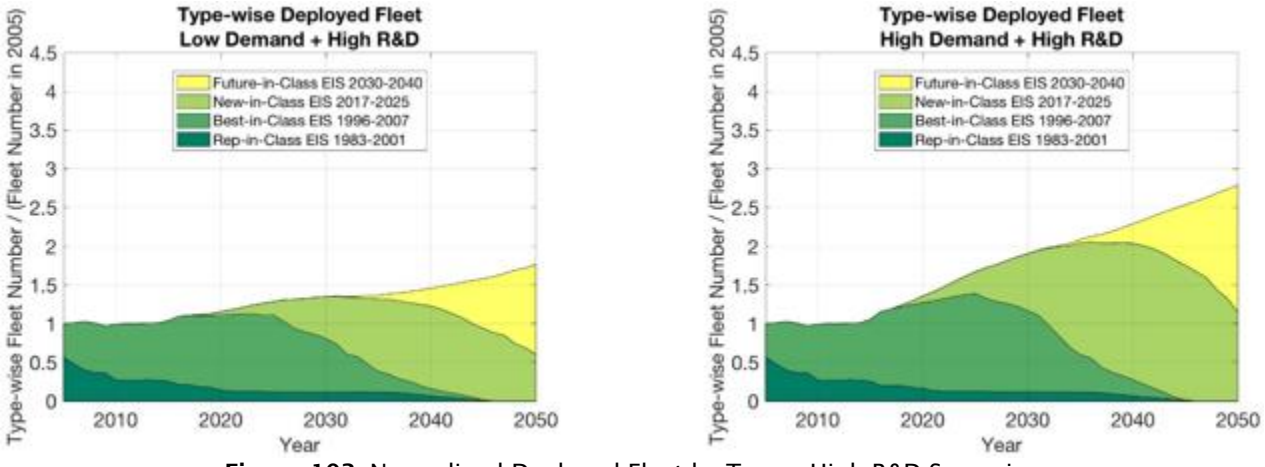

Figure 103: Normalized Deployed Fleet by Type – High R&D Scenarios

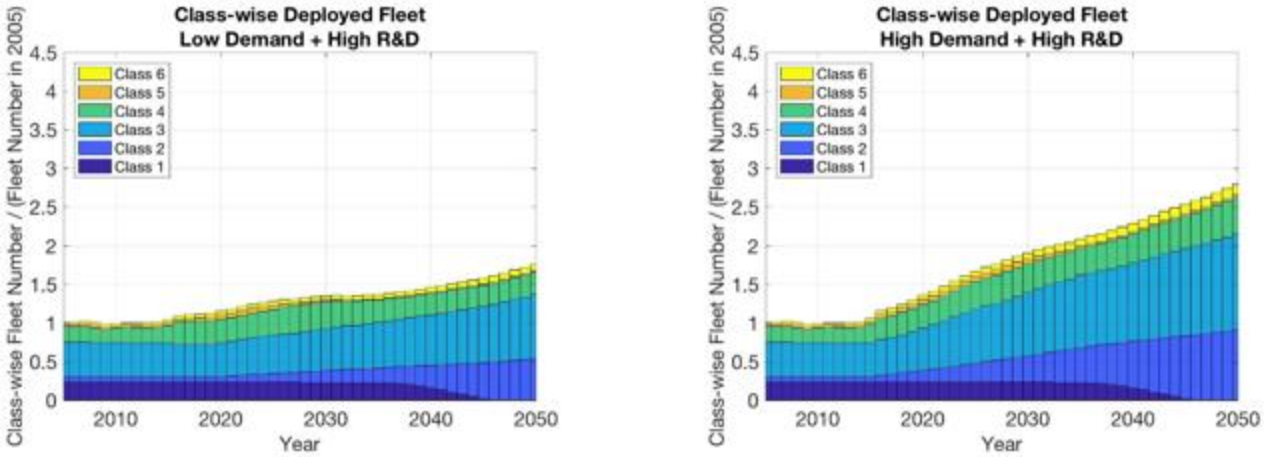

Figure 104: Normalized Deployed Fleet by Class – High R&D Scenarios

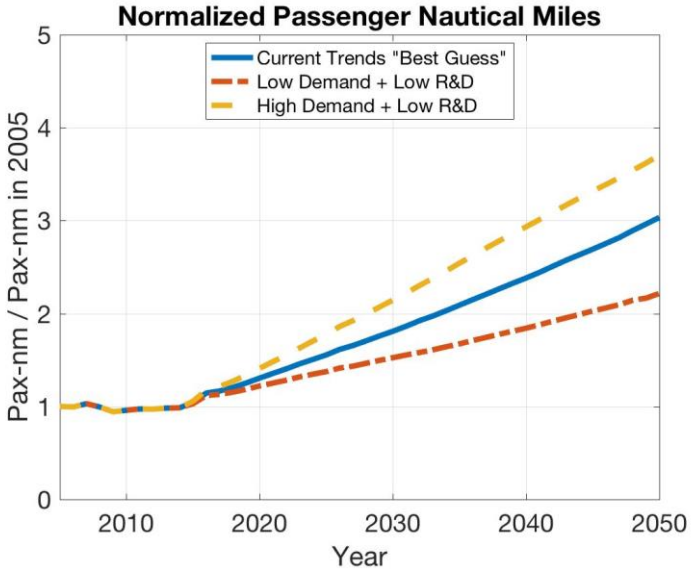

Figure 105: Normalized Passenger Nautical Miles from 2005 to 2050 – Low R&D Scenarios

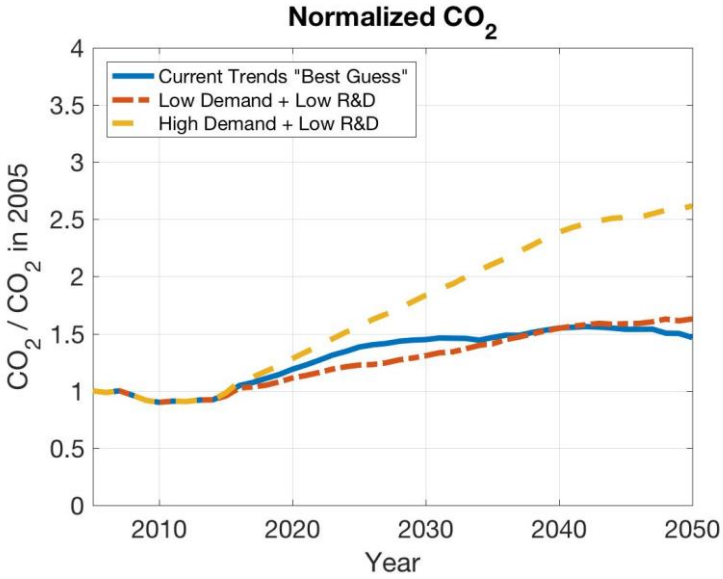

Figure 106: Normalized Fleet-Level Emissions from 2005-2050 – Low R&D Scenarios

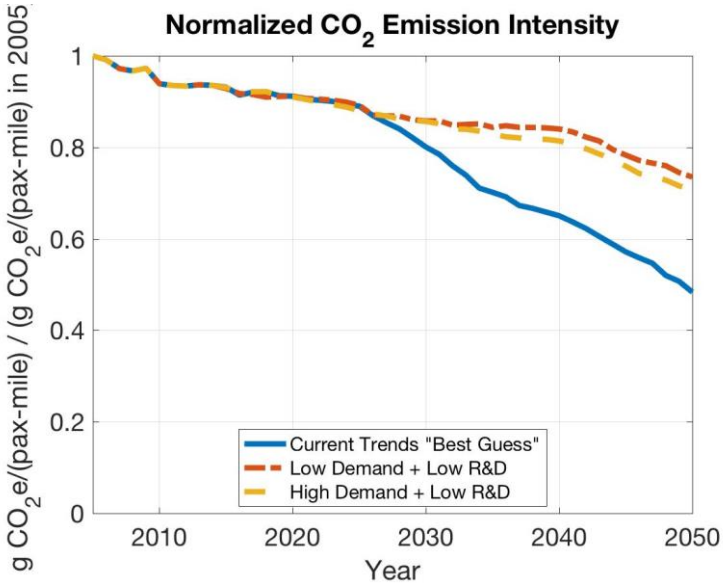

Figure 107: Normalized Fleet-Level CO2 Emission intensity from 2005 to 2050 – Low R7D Scenarios

Figure 105 shows the revenue passenger nautical miles for the Low R&D scenarios throughout the simulation. Similar to other scenarios, the results are normalized by the equivalent values in 2005. As expected, the Low Demand Low R&D scenario produced the lowest growth in RPM of about 2.2 times the value in 2005 by 2050. The passenger nautical miles in the High Demand Low R&D scenario increased to about 280% of the corresponding value in 2005. Figure 105 shows the fleet-level **CO_2** emissions for the Low R&D scenarios normalized by the 2005 emission value. The Low Demand Low R&D scenario yielded about 1.6 times the CO_2 emissions in 2005 by 2050 while the High Demand Low R&D scenario yielded fleet-level CO_2 emissions of about 2.6 times the 2005 value by 2050. The CO_2 emission intensity normalized by the 2005 value, for the Low R&D scenarios throughout the simulation period is represented in Figure 107. Low Demand Low R&D and High Demand Low R&D scenarios decreased to about 73% and 70% respectively of the value in 2005. When compared

to the Current Trend Best Guess scenario, the Low R&D scenarios yielded a significantly higher emission intensity which stems from delayed introduction and access to new technology aircraft.

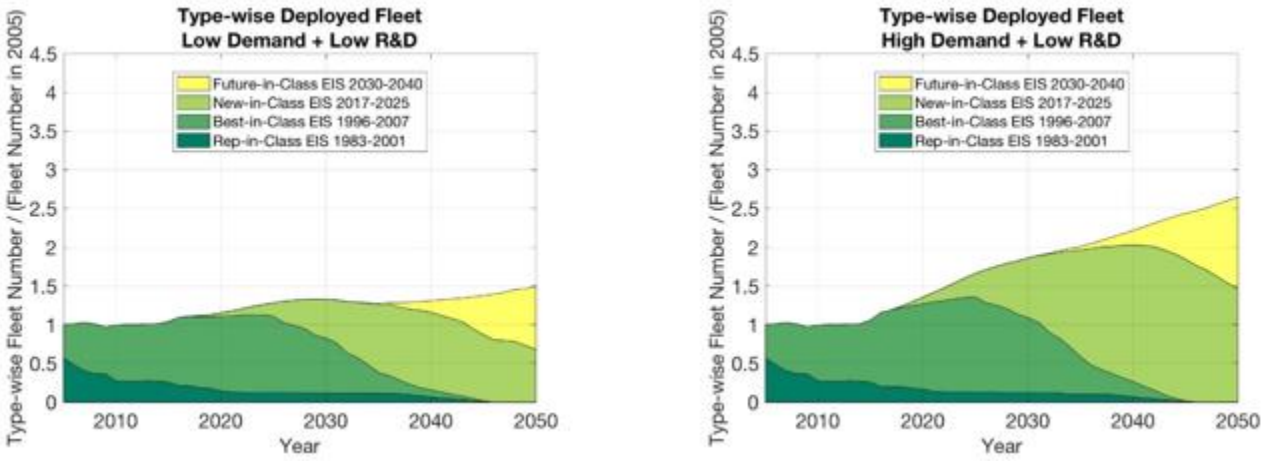

Figure 108: Normalized Deployed Fleet by Type – Low R&D

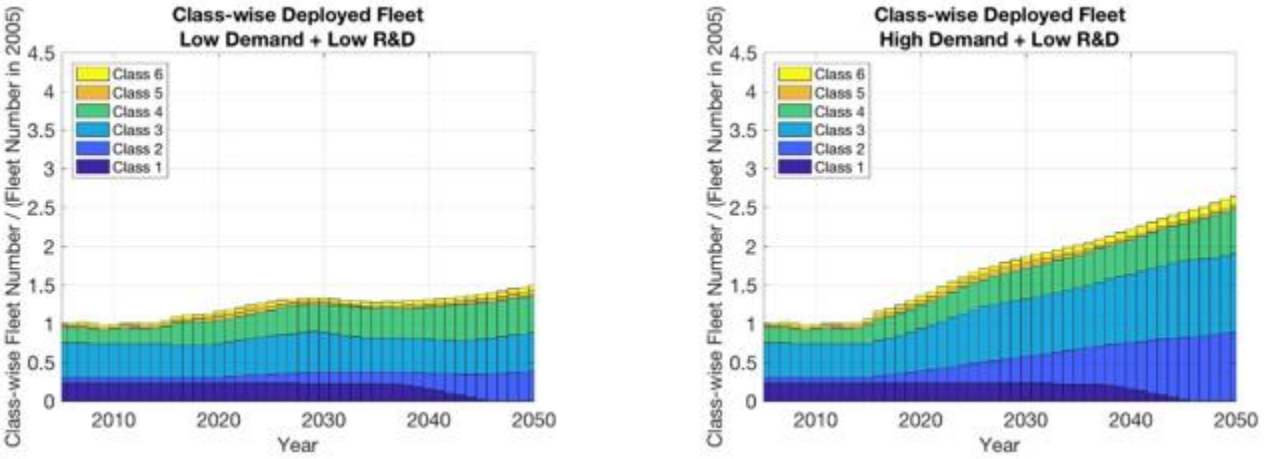

Figure 109: Normalized Deployed Fleet by Class – Low R&D Scenarios

Figure 108 and Figure 109 show the deployed fleet by aircraft type and class respectively for Low R&D scenarios, normalized by the deployed fleet in 2005. The Low Demand Low R&D scenario yielded the least growth in total number of aircraft deployed by the FLEET airline of about 1.5 times the value in 2005 by 2050. The total number of aircraft deployed in the High Demand Low R&D scenario increased to about 2.6 times the number of aircraft deployed in 2005. The significant increase in deployed aircraft in the High Demand scenario, compared to the Low Demand scenario, is due to the difference in demand for air travel between both scenarios.

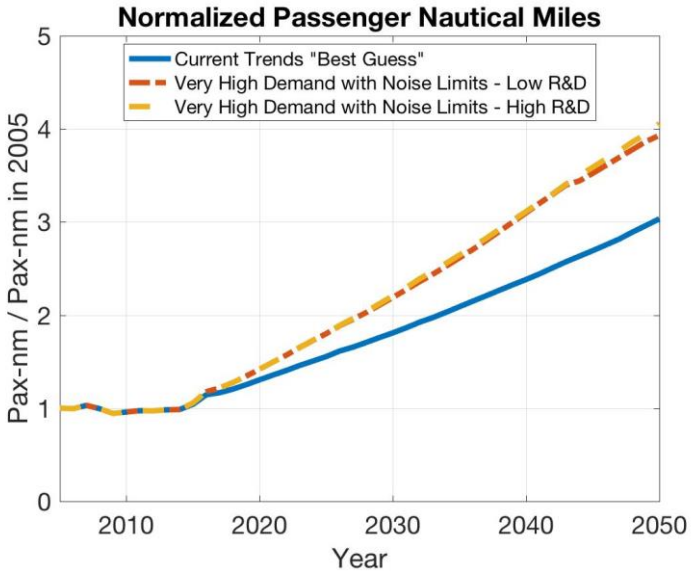

Figure 110: Normalized Passenger Nautical Miles from 2005 to 2050 – Noise Limit Scenarios

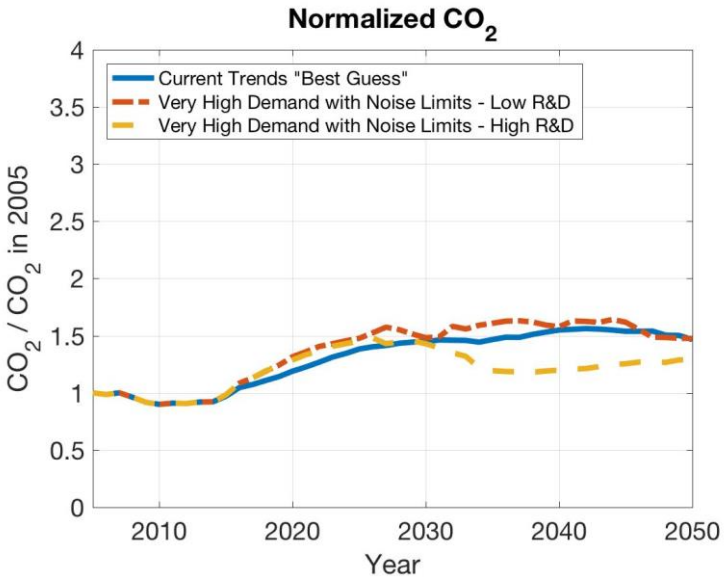

Figure 111: Normalized Fleet-Level Emissions from 2005 to 2050 – Noise Limits Scenarios

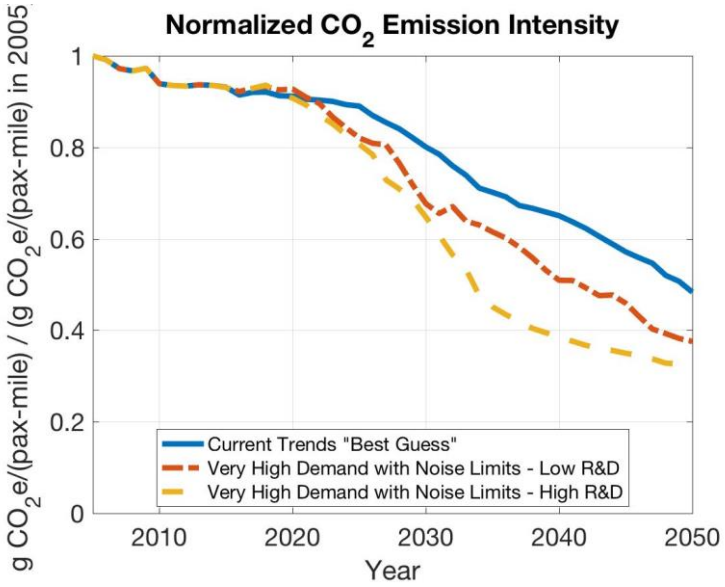

Figure 112: Normalized Fleet-Level CO_2 Emission Intensity from 2005 to 2050 – Noise Limit Scenarios

Figure 110, Figure 111, and Figure 112 show the demand and environmental results for the Very High Demand scenarios with Noise Limits. As with other scenarios, the results are normalized by the equivalent values in 2005. The revenue passenger nautical miles in the Very High Demand scenarios are very close at almost 4 times the 2005 value by 2050, as shown in Figure 110. While there is a significant difference in RPM between the Current Trends Best Guess and the noise-limited Very High Demand scenarios, the 2050 CO_2 emissions are relatively similar amongst all three scenarios as shown in Figure 111. The Current Trends Best Guess and noise-limited Very High Demand Low R&D scenarios yield CO_2 emissions in 2050 of about 1.5 times the 2005 value. The noise-limited Very High Demand High R&D scenario yields in 2050 CO_2 emissions of about 1.3 times the value in 2005. Figure 112 shows the fleet-level CO_2 emission intensity for the noise-limited scenarios normalized by their 2005 emission value. The noise-limited Very High Demand High R&D scenario results in the least emission intensity in 2050 of about 36% of the value in 2005. The difference in CO_2 emissions and intensity between the Low and High R&D scenarios, even though both scenarios have almost similar RPM, is due to the availability of new aircraft technology in the High R&D scenario.

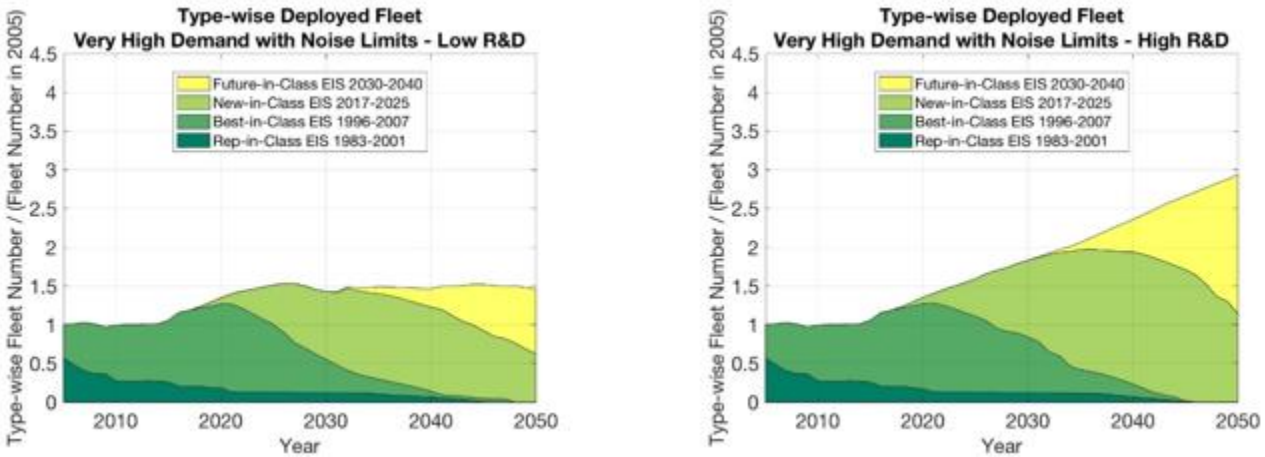

Figure 113: Normalized Deployed Fleet by Type – Noise Limits Scenarios

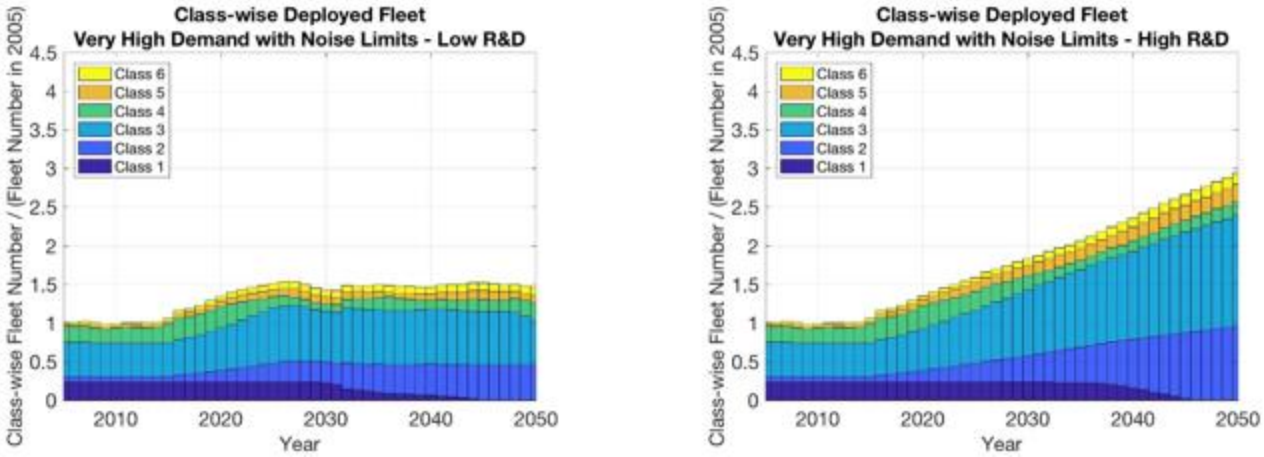

Figure 114: Normalized Deployed Fleet by Class – Noise Limits Scenarios

Figure 113 and Figure 114 show the type-wise and class-wise total number of aircraft deployed by the FLEET airline in the noise-limited Very High Demand scenarios throughout the simulation period, normalized by the total aircraft deployed in 2005. The total number of aircraft deployed by 2050 in the High R&D scenario is almost double the aircraft deployed by the airline in the Low R&D scenario. **Figure 114** shows that the number of next-gen class 3 aircraft deployed by 2050 in the High R&D scenario is significantly more than that deployed in the Low R&D scenario, such that the fairly constant fraction of class 3 aircraft deployed in the Low R&D scenario after 2025 is due to underwhelming demand for air travel.

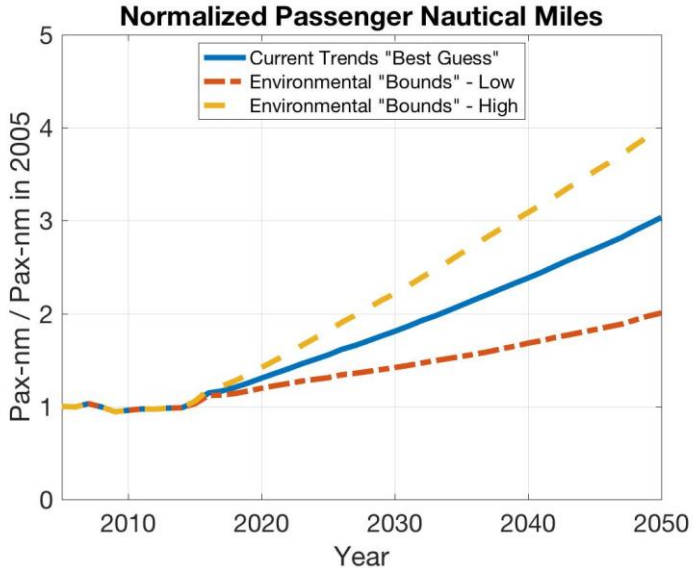

Figure 115: Normalized Passenger Nautical Miles from 2005 to 2050 – Environmental Bounds Scenarios

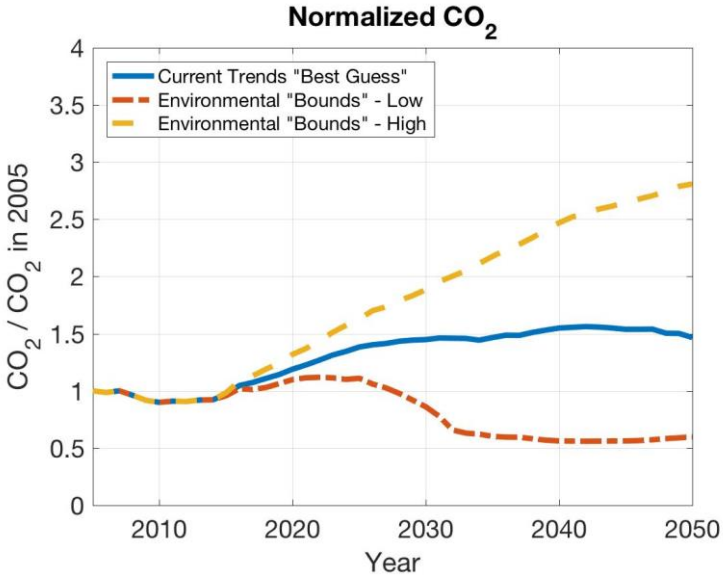

Figure 116: Normalized Fleet-Level Emissions from 2005 to 2050 – Environmental Bounds Scenarios

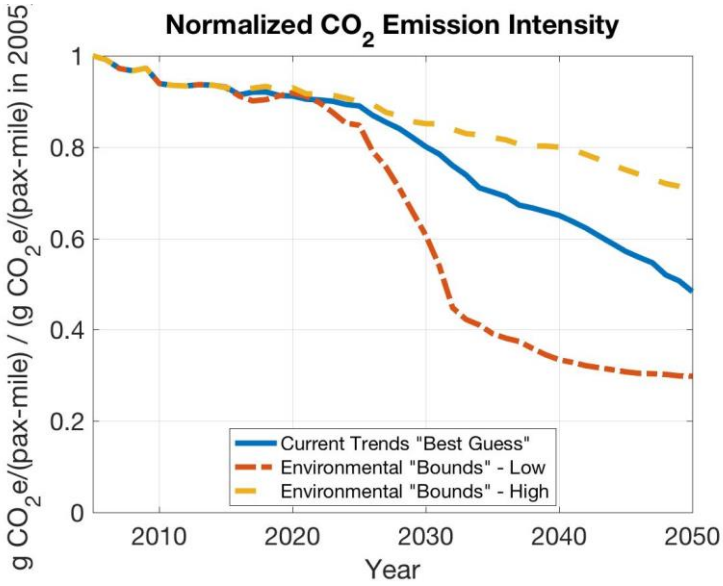

Figure 117: Normalized Fleet-Level CO2 Emission Intensity from 2005 to 2050 – Environmental Bounds Scenarios

The FLEET results, normalized by the 2005 values, from the Environmental Bounds scenario appear in Figure 115 through Figure 117. From Figure 114, the RPM in the Environmental Bounds High scenario by 2050 is almost double (4 times the 2005 RPM value) the corresponding value in the Environmental Bounds Low scenario. Figure 116 shows the fleet-level CO_2 emissions of the airline in the Environmental Bounds scenarios normalized by the 2005 emission value. The Environmental Bounds Low and High scenarios yielded CO_2 emissions of 60% and 260% respectively of their corresponding 2005 values by 2050. The CO_2 emission intensity normalized by the 2005 value, for the Environmental Bounds scenarios throughout the simulation period is presented in Figure 117. The emission intensities in the Environmental Bounds Low and Environmental Bounds High scenario by 2050 are about 30% and 70% of their values in 2005 respectively. The higher RPM, CO_2 emissions and intensity in the Environmental Bounds High scenario is because of higher demand and absence of noise limits when compared to the Environmental Bounds Low scenario.

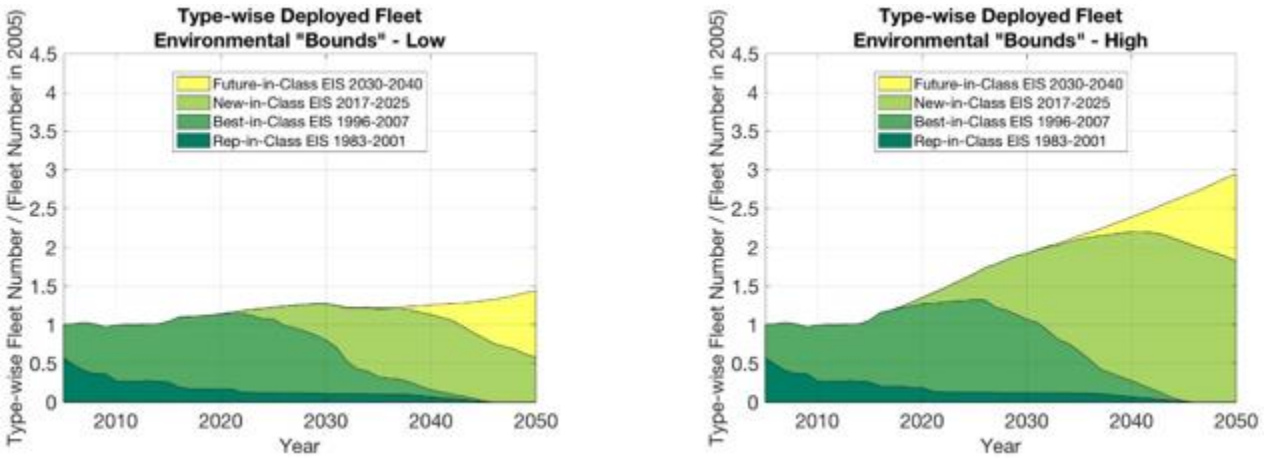

Figure 118: Normalized Deployed Fleet by Type – Environmental Bounds Scenarios

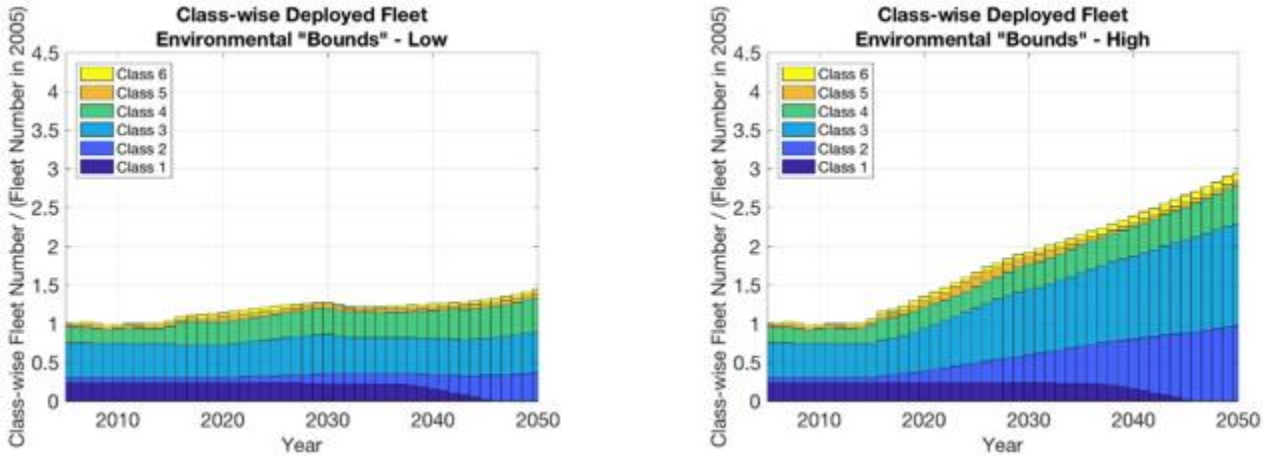

Figure 119: Normalized Deployed Fleet by Class – Environmental Bounds Scenarios

Figure 118 and Figure 119 show the total deployed fleet by aircraft type and class respectively for Environmental Bounds scenarios, normalized by the deployed fleet in 2005. As expected, the Environmental Bounds Low scenario yielded the least growth in total number of aircraft deployed by the FLEET airline of about 1.5 times the value in 2005 by 2050. The total number of aircraft deployed in the Environmental Bounds High scenario increased to about 3 times the number of aircraft deployed in 2005. The significant increase in deployed aircraft in the High Demand scenario, compared to the Environmental Bounds Low scenario, is due to the difference in demand for air travel between both scenarios and noise restriction imposed in the Environmental Bounds Low scenario.

In summary, the GDP growth rates have a positive correlation with CO_2 emissions while R&D levels have a negative correlation with CO_2 emissions, as evidenced by the High Demand Low R&D and Low Demand High R&D scenarios. The technology improvements for airline fleets can reduce emission growths. Moreover, the lower demand and noise-area restrictions can further decrease the number of aircraft operations and reduce emissions even further.

In summary, the Purdue team successfully demonstrated FLEET's capabilities for analyzing the scenarios developed by the largest ASCENT 10 Project team. The demonstrations in the past three years have shown that FLEET is capable of modeling

scenarios developed by ASCENT 10 Project partners and provides some unique features that benefit the FAA in tackling challenging fleet-level emissions forecasting problems.

The results from FLEET help indicate how difficult it may be, in future scenarios with increasing demand for air travel, to reduce CO_2 emissions to levels equal or below the levels in 2005. In some scenarios, the future CO_2 emissions do drop below the 2005 level, but not in all scenarios. The approach of FLEET to use an allocation problem to represent scheduling and assignment decisions of a profit-seeking airline, combined with a retirement model to represent when the airline would remove an existing aircraft from its fleet, also illustrates that having the new, more fuel efficient / less CO_2 emitting aircraft rapidly become a major fraction of the airline's fleet is a challenge.

Publications

T. W. Lukaczyk, A. D. Wendorff, M. Colonno, E. Botero, T. D. Economon, J. J. Alonso, T. H. Orra, and C, Ilario, "SUAVE: An Open-Source Environment for Multi-Fidelity Conceptual Vehicle Design," 16th AIAA/ISSMO Multidisciplinary Analysis and Optimization Conference, doi:10.2514/6.2015-3087, June, 2015.

Ogunsina, K., Chao, H., Kolencherry, N., Moolchandani, K., Crossley, W. A., and DeLaurentis, D. A., "A Model of Aircraft Retirement and Acquisition Decisions Based On Net Present Value Calculations," *17th AIAA Aviation Technology, Integration, and Operations Conference*, 2017.

Outreach Efforts

Multiple interactions with government, industry, and academia have occurred during the course of the fleet and technology assumption setting workshops, described in Sections 0 and 0 of this report.

Awards

None

Student Involvement

Of the Georgia Tech students, Benjamin Bitoun, Marcus Bakke, Ryan Donnan, and Arturo Santa-Ruiz, Marcus Bakke and Ryan Donnan have graduated and have been employed by Boeing and Pratt and Whitney, respectively. Current students include Matt Reilly and Braven Leung.

On the Stanford University side, Anil Variyar, Trent Lukaczyk, Emilio Botero, Tim MacDonald, and Ved Chirayath have participated in the work presented here, and the development of the SUAVE framework. Dr. Lukaczyk has recently completed his doctoral degree and has started a UAV company. Mr. Chirayath is completing his dissertation by the end of the calendar year (2015) and is currently working at the NASA Ames Research Center in the Earth Sciences division.

The Purdue University team has had several students work on the ASCENT 10 effort. Parithi Govindaraju assisted with building the allocation model in FLEET; he has defended his PhD thesis and will graduate in 2017 after deposit of the thesis document. Graduate Research Assistants Nithin Kolencherry, Hsun Chao and Kolawole Ogunsina are all continuing in pursuit of their PhD degrees.

Plans for Next Period

This project initially focused heavily on working with industry, government, and academia to establish a set of agreed upon fleet modeling scenarios for future technology assessments. The outcome of work to date includes a set of recommended future scenarios for use in assessing the impact of aviation on fleet wide fuel burn, emissions, and noise. Prior work focused on subsonic transports and this proposed continuation seeks to extend the modeling and assumption setting processes to assess the impact of introducing supersonic commercial aircraft. As such, the research will be conducted as a collaborative effort in order to leverage capabilities and knowledge available from the multiple entities that make up the ASCENT university partners and advisory committee. Georgia Tech will continue to collaborate with Purdue University from prior work and will focus on the following objectives.

Research under this research thrust will continue to focus on three primary objectives: (1) Defining Fleet Assumptions; (2) Modeling the impact of vehicle technologies; and (3) assessing the combined impact of vehicle technology and fleet demand and growth.

Georgia Tech will continue to be the lead university with Purdue supporting the objectives as shown in Table 1 in the Project Overview, listing the high-level division of responsibilities amongst the universities.

Table 14: University Contributions

Objectives		Georgia Tech	Purdue
1	Fleet Assumptions & Demand Assessment	Identify supersonic demand drivers and supporting airports	Estimate latent demand and flight schedules for supersonic aircraft
2	Preliminary Vehicle Environmental Impact Prediction	Develop estimates of Key Environmental Indicators (KEI) for supersonic aircraft relative to current technology subsonic, Develop estimates of likely operating altitudes (U.S)	Support with expert knowledge
3	AEDT Vehicle Definition	Test current version of AEDT ability to analyze existing supersonic models	N/A
4	Vehicle and Fleet Assessments	Apply GREAT to estimate impact of supersonics in terms of fuel burn, water vapor, and LTO NOx	Apply FLEET to estimate impact of supersonics in terms of fuel burn, water vapor, and LTO NOx

References

1 https://www.faa.gov/about/office_org/headquarters_offices/apl/research/aircraft_technology/cleen/

2 Green Air on line, April 8, 2015

3 The US Core 30 Airports, FAA, accessed July 5,2017, URL:http://aspmhelp.faa.gov/index.php/Core_30

4 Mavris, D., Perullo, C., Pfaender, H., Tai, J., "Project 36, EDS Assessment of CLEEN Technologies: 21st Semiannual PARTNER Technical Status Report."

5 Pratt & Whitney's Geared Turbofan Growth Plan, Aviation Week, 1 July 2013, URL: http://aviationweek.com/awin/pratt-whitney-s-geared-turbofan-growth-plan [cited October 2016].

6 Trent XWB, Rolls-Royce, URL: http://www.rolls-royce.com/products-and-services/civil-aerospace/products/civil-large-engines/trent-xwb.aspx [cited October 2016].

7 GE Passport, GE Aviation, 2015, URL: http://www.geaviation.com/bga/engines/passport [cited October 2016].

8 GE Passport, U.S. Department of Transportation, 29 April 2016, URL: http://rgl.faa.gov/Regulatory_and_Guidance_Library/rgMakeModel.nsf/0/78ad2acef2ea44b986257fb00067591d/$FILE/E00091EN_Rev_0.pdf [cited October 2016].

9 Thomas, M., "Better Power for a Changing World," Royal Aeronautical Society, 11 February 2014, URL: http://aerosociety.com/Assets/Docs/Events/746/GBD_Propulsion_211014_RR_1.pdf [cited October 2016]

10 GE9X Commercial Aircraft Engine, GE Aviation, 2015, URL: http://www.geaviation.com/commercial/engines/ge9x [cited October 2016].

11 Perry, D., "Boeing Advances 777X Service Entry: Sources," FlightGlobal, 11 March 2016, URL: https://www.flightglobal.com/news/articles/boeing-advances-777x-service-entry-sources-423032/ [cited October 2016].

12 Lukaczyk, T. W. et. al., "SUAVE: An Open-Source Environment for Multi-Fidelity Conceptual Design", AIAA 2015-3087, June 2015, Dallas TX

13 Lukaczyk, T. W. , "VyPy : An Optimization Toolbox", https://github.com/aerialgedgehog/VyPy

14 Perez R.E , Jansen, P. W. and Martins, J. R. R. A, "pyOpt: A Python- Based Object –Oriented Framework for Nonlinear Constrained Optimization", Structures and Multidisciplinary Optimization, No 45(1):101-118, 2012

15 Adams, B. M. et al. " Dakota, A Multilevel Parallel Object-Oriented Framework for Design Optimization, Parameters Estimation, Uncertainty Quantification, and Sensitivity Analysis: Version 6.0 User's Manual ," Sandia Technical Report SAND2014-4633, July 2014

16 Jones, E. O., et al. "SciPy: Open Source Scientific Tools for Python",2001-

17 Mattingly, J. D. "Elements of Propulsion: Gas turbines and rockets", Reston Va: AIAA, 2006

18 Cantwell, B. J. "Course Notes – AA 283 Aircraft and Rocket Propulsion",2014

19 Greitzer, E., "N+3 Aircraft Concept Designs and Trade Studies, Final Report," Tech. rep., NASA/CR-2010-216794/Vol2, 2010

20 Tetzloff, I. and Crossley, W., "An Allocation Approach to Investigate New Aircraft Concepts and Technologies on Fleet-Level Metrics," 9th AIAA Aviation Technology, Integration, and Operations Conference (ATIO), Hilton Head, SC, 22 September 2009.

21 Zhao, J., Agusdinata, D.A., DeLaurentis, D., "System Dynamics Fleet Forecasting with Technology, Emission, and Noise Goals," 9th AIAA Aviation Technology, Integration, and Operations Conference (ATIO), Hilton Head, SC, 22 September 2009.

22 Zhao, J., Tetzloff, I.J., Tyagi, A., Dikshit, P., Mane, M., Agusdinata, D.A., Crossley W.A., DeLaurentis, D., "Assessing New Aircraft and Technology Impacts on Fleet-Wide Environmental Metrics Including Future Scenarios", AIAA 48th Aerospace Sciences Meeting, Orlando, Florida, Jan. 4-7, 2010.

23 Mane, M., Agusdinata, D.A., Crossley, W.A., and DeLaurentis, D.A., "Fleet-Wide Environmental Impacts of Future Aircraft Technologies", 10th AIAA Aviation Technology, Integration, and Operations Conference (ATIO), Fort Worth, TX, 18 September 2010.

24 Moolchandani, K. A., Agusdinata, D. B., Mane, M., Crossley, W. A., and DeLaurentis, D. A., "Impact of Development Rates of Future Aircraft Technologies on Fleet-wide Environmental Emissions," 11th AIAA Aviation Technology, Integration, and Operations Conference (ATIO), Virginia Beach, VA, 19 September 2011.

25 Moolchandani, K. A., Agusdinata, D. B., DeLaurentis, D. A., and Crossley, W. A., "Airline Competition in Duopoly Market and its Impact on Environmental Emissions," 12th AIAA Aviation Technology, Integration, and Operations Conference (ATIO), Indianapolis, IN, 17 September 2012.

26 Moolchandani, K. A., Agusdinata, D. B., DeLaurentis, D. A., and Crossley, W. A., "Developing Optimal Airline Fleets Under Environmental and Capacity Constraints," 28th International Congress of the Aeronautical Sciences (ICAS), Brisbane, Australia, 28 September 2012.

27 Moolchandani, K. A., Agusdinata, D. B., DeLaurentis, D. A., and Crossley, W. A., "Assessment of the Effect of Aircraft Technological Advancement on Aviation Environmental Impacts," AIAA 51st Aerospace Sciences Meeting, Grapevine (Dallas/Ft. Worth Region), Texas, Jan. 7-10, 2013.

28 Population Reference Bureau, World Population Data Sheet 0213, 2016, URL: http://www.prb.org/Publications/Datasheets/2013/2013-world-population-data-sheet/world-map.aspx#table/world/population/2013

29 U. S. Energy Information Administration, Annual Energy Outlook 2011, 2011, URL: www.eia.gov/forecasts/aeo/

30 Dikshit, P., "Development of an Airport Noise Model Suitable for Fleet-level Studies", Master of Science Thesis, School of Aeronautics and Astronautics, Purdue University, 2009.

31 FLIGHT AND DUTY LIMITATIONS AND REST REQUIREMENTS: FLIGHTCREW MEMBERS, 14 CFR Ch. I (1-1-13 Edition) Part 117, URL: https://www.gpo.gov/fdsys/pkg/CFR-2013-title14-vol3/pdf/CFR-2013-title14-vol3-part117.pdf

32 Flight attendant duty period limitations and rest requirements: Domestic, flag, and supplemental operations, 14 CFR Ch. I (1-1-13 Edition) Part 121.467, URL: https://www.gpo.gov/fdsys/pkg/CFR-2016-title14-vol3/pdf/CFR-2016-title14-vol3-sec121-467.pdf

Project 011(A) Development of Rapid Fleet-Wide Environmental Assessment Capability Using a Response Surface Modeling Approach

Massachusetts Institute of Technology

Project Lead Investigator

R. John Hansman
T. Wilson Professor of Aeronautics & Astronautics
Department of Aeronautics & Astronautics
MIT
Room 33-303
77 Massachusetts Ave
Cambridge, MA 02139
617-253-2271
rjhans@mit.edu

University Participants

Massachusetts Institute of Technology

- P.I.(s): R. John Hansman
- FAA Award Number: 13-C-AJFE-MIT, Amendment Nos. 006, 011, 014, 023, and 038
- Period of Performance: Aug. 18, 2014 to Aug. 31, 2018 (year 4 as NCE)
- Task(s):
  1. Extend And Enhance Modeling Framework
  2. Extend Fleet Gauge Sample Problem To System Level
  3. Develop Multi-stakeholder Valuation Methods To Enable Comparison And Decisions About Preferred Strategies In The Environmental Output Space
  4. Apply Fast Modeling Framework To Additional Sample Problem

Project Funding Level

$670,000 FAA funding and $670,000 matching funds. Sources of match are approximately $279,000 from MIT, and $231,000 from Byogy Renewables, Inc. and $160,000 from Oliver Wyman Group.

Investigation Team

Prof R. John Hansman (PI)
Greg O'Neill (Post Doctoral Researcher)
Luke Jensen (Graduate Student)
Jacqueline Thomas (Graduate Student)
Alison Yu (Graduate Student)

Project Overview

The objective of the research is to continue development of an analytical framework for evaluating the environmental impact of air transportation and to use that framework on a variety of sample policy and operational problems. This framework will use fast models for aircraft-level performance, noise, and emissions, enabling broad scenario explorations and parametric analyses in environmental studies. Phase I of this research (2014-2015) consisted of general analysis framework development, sample problem selection, and surrogate model development. Phase II of this research (2015-2016) aimed to continue model development while demonstrating the capability of the modeling approach on a specific

multi-dimensional sample problem involving fleet gauge modification. Phase III of this research (2016-2017) aimed to increase the ability to evaluate local noise impacts at the system level and develop additional multi-objective sample problems to demonstrate the flexibility and extensibility of the rapid environmental analysis framework. This phase refined the relationship between local and system-level impacts arising from specific advanced operational procedures and aircraft fleet evolution.

Task #1: Extend and Enhance Modeling Framework

Objective(s)

The modeling framework for rapid environmental impact assessment has been developed to include local and system wide impacts for noise, emissions, and fuel consumption at specific locations based on representative or generic airports. The first two years of this research highlighted the challenge of systematically evaluating local (e.g. noise and LTO emissions) which depend on location-specific elements such as procedure design, fleet mix, population density, etc. with global factors such as emissions and fuel consumption.

This task aimed to develop techniques that can capture key environmental characteristics at a system level that incorporates location-specific characteristics. In order to rapidly analyze individual airport performance, it is necessary to have a generic representation of the operating patterns and flight trajectories. This task leverages work that has been done on statistical clustering methods to identify common operations at individual airports, simplified generic profile definitions for some airports, and detailed procedure modeling for certain classes of advanced operational procedures.

Research Approach

- Expand the modeling framework and architecture developed in the initial phases of the research with greater detail on modules and interfaces to enable implementation of specific sample problems.
- Locate and incorporate data sources for procedure definition, fleet mix, and timetable to enable rapid system-level analysis without requiring extensive manual intervention on an airport-by-airport basis.

Major Accomplishments

- Extended the modeling framework with new simplifying assumptions to allow system wide noise analysis using simplifying straight-in and straight-out procedural assumptions
- Developed data processing architecture and capability for system-level analysis incorporating location-specific procedure definitions

Task #2: Extend Fleet Gauge Sample Problem To System Level

Objective(s)

In Year 2 of this effort, an initial fleet gauge sample problem was evaluated. The objective of this sample problem was to calculate the environmental impact of a 10% upgauge at a single example airport (DCA) using the 2015 operational fleet model. The aggregate noise, emissions, fuel consumption, and NOx impacts were calculated, along with potential effects on passenger throughput. In Year 3, this sample problem will be expanded to a broader system level using the results of Task 1, specifically incorporating local noise analysis at the OEP 35 airports. This allowed for continued development and refinement of the modeling framework, allowing for policy valuation and comparison across multiple stakeholders and impact scales.

Research Approach

- Develop modeling capability at a specific airport (DCA) that is representative of the types of results desired for each airport in a broader system-level analysis.
- Extend the modeling capability developed for the specific airport to a small subset of the NAS to evaluate potential data and analysis implementation challenges.
- Extent modeling capability to full airport sample set of interest (initially the OEP 35 airports)

Major Accomplishments

- Developed operation modeling method using ASPM data for DCA case study that can be applied at any other airport in NAS
- Calculated DNL contours for OEP35 airports using simplified framework
- Compared ASPM runway use results to official FAA runway use assumptions for straight-in and straight-out system level analysis
- Began development of system wide trajectory modeling of RNAV procedures (SIDs and STARs) to capture realistic flight patterns rather than earlier straight-in and straight-out assumption

Task #3: Develop Multi-stakeholder Valuation Methods to Enable Comparison and Decisions about Preferred Strategies in the Environmental Output Space

Objective(s)

Environmental impacts from air transportation activities are felt across multiple stakeholders, geographic scales, and timescales. As a result, different stakeholders have different priorities and perceived valuations of possible policies and procedures. The focus of the first two years in this research effort was to generate system outputs in terms of raw environmental metrics (for noise, emissions, fuel burn, etc.). These metrics do not translate directly to a stakeholder preference structure or an improved understanding of community welfare on local and system wide scales. In this phase of the research effort, multi-stakeholder valuation methods were investigated with specific emphasis placed on an evaluation of different noise metrics to capture annoyance beyond traditional “significant” noise level definitions.

Research Approach

- Evaluate methods and metrics for assessing impact from environmental variables, particularly noise.
- Analyze and compare results using the rapid system-level analysis framework using appropriate metrics of choice.

Major Accomplishments

- Generated fuel results for a sample network using surrogate model version of TASOPT
- Developed fuel burn model for departures to compare effects of speed and configuration modification on fuel/emissions from modified procedures.
- Developed method for rapid population impact analysis in terms of DNL and Nabove noise metrics.

Task #4: Apply Fast Modeling Framework To Additional Sample Problem

Objective(s)

In this task, the fast modeling architecture for local and system wide environmental analysis was applied to an additional sample problem to evaluate system-level applications for location-specific procedural changes. The objective of this task was to exercise modeling capabilities with scenarios that are relevant for multiple stakeholders, including local communities, operators, airports, and regulators.

Research Approach

- Identify methods to model flight operations in the vicinity of airports using representative trajectories based on historical radar data and published procedures
- Integrate schedule, fleet, and runway utilization data from external sources to allow calculation of noise contours at airports of interest
- Analyze noise impacts at a system level that would arise from implementing a specific advanced operational procedure of interest, or modifying procedure design criteria for specific types of PBN procedures.

Major Accomplishments

- Developed concept for additional sample problems at DCA including fleet replacement strategies and minimum-gauge strategies
- Completed analysis on 3 sample problems at DCA, including emissions, fuel, and noise results.
- Develop estimation method for finding noise benefits from advanced operational procedures, including:
  - Shortened final approach segments
  - Steep descents
  - Reduced-speed departures

Publications

"Development of Rapid Fleet-Wide Environmental Assessment Capability," *AIAA AVIATION Forum*, 2017.
DOI: 10.2514/6.2017-3339

Outreach Efforts

1/25/2017: Briefing to FAA Joint University Program research update meeting
4/17/2017: Joint briefing to FAA and MITRE to discuss tool development pathway
4/18/2017: Briefing to ASCENT Advisory Board
6/5/2017: Presentation at AIAA Aviation Conference in Denver, CO.
In-person outreach and collaboration with TASOPT aircraft performance model development team at MIT.
In-person outreach and collaboration with Volpe noise tool development team.

Awards

None

Student Involvement

Graduate students have been involved in all aspects of this research in terms of analysis, documentation, and presentation.

Plans for Next Period

The next phase of this project is a no-cost extension of the Year 3 effort. This Year 4 effort will involve three primary areas of focus:

1. Continued development of a system-level modeling approach with a focus on noise analysis incorporating advanced operational procedures. Specifically, this will involve development of a procedure-based track generation method to supplement straight-in and straight-out procedures at airports with defined SIDs. This will increase the fidelity of noise modeling at airports where straight-in and straight-out assumptions do not capture prevailing traffic flows. This will be accomplished by parsing the FAA Coded Instrument Flight Procedures (CIFP) dataset to automatically generate published ground tracks on a NAS-wide basis and applying a set of standardized climb profiles (altitude/thrust/speed) to the CIFP-derived lateral tracks based on fleet-specific ASDE-X analysis (same method presented in the past).
2. Development of an updated codebase and user interface for noise analysis workflow to simplify analysis flexibility, data sources, and profile assignment and noise contour post-processing workflow.
3. Improved population impact assessment to evaluate sensitivity of system-level noise exposure to specific operational and policy questions such as final approach leg length criteria, final approach intercept angles, and RNAV leg length requirements.

Project 017 Pilot Study on Aircraft Noise and Sleep Disturbance

University of Pennsylvania

Project Lead Investigator

Mathias Basner
Associate Professor of Sleep and Chronobiology
Department of Psychiatry
University of Pennsylvania
1019 Blockley Hall, 423 Guardian Dr.
Philadelphia, PA 19104-6021
215-573-5866
basner@pennmedicine.upenn.edu

University Participants

University of Pennsylvania

- P.I.: Mathias Basner, Associate Professor
- FAA Award Number: 13-C-AJE-UPENN-004
- Period of Performance: October 01, 2016 to September 30, 2017
- Task(s):
    - ATL Pilot Sleep Study: Data collection and analysis

Project Funding Level

The funding amount for this period was $266,001.00. The cost sharing requirement for this project was met by our international collaborators at the German Aerospace Center (DLR).

Investigation Team

- Principal Investigator: Mathias Basner
- Co-Investigator: Sarah McGuire
- Research Assistants: Maryam Witte, Sarah Rocha, Anjana Kallarackal

Project Overview

The long-term goal of this line of research is to derive exposure-response relationships for aircraft noise-induced sleep disturbance that are representative of the exposed U.S. population. As studies will have to investigate samples around multiple airports, it will not be possible to use polysomnography (i.e., simultaneous recording of the electroencephalogram, electromyogram, and electrooculogram) to monitor sleep, as this method requires trained personnel at the measurement site in the evening and in the morning and is thus too costly. An alternative methodology of using a single channel electrocardiogram (ECG) and actigraphy to monitor sleep has been examined. This methodology allows the investigation of larger subject samples at lower cost as individuals can be taught how to apply the electrodes themselves. Also, unlike polysomnography, awakenings can be identified automatically. As part of previous research, an algorithm for identifying EEG arousals (Basner, Griefahn, Müller et al., 2007) based on increases in heart rate was refined in order to only identify those arousals greater than or equal to 15 seconds in duration, which is the most agreed upon indicator of noise-induced sleep disturbance. High agreement between EEG visually scored arousals and arousals identified using the refined ECG based algorithm was obtained. The methodology of using ECG and actigraphy to monitor sleep has been implemented in two pilot field studies to evaluate the quality of data that can be obtained for unattended physiological and noise measurements. Based on lessons learned, the study protocol is being refined in order to inform the design and cost of a potential multi-airport study on the effects of noise on sleep.

Objectives

(1) Finish acquisition and analysis of acoustical and physiological data of the PHL study;
(2) Refine and, to the extent possible, automatize the methodology to identify aircraft noise events and maximum sound pressure levels in complex acoustical signals;
(3) Inform the design and cost of a potential large-scale field study on the effects of aircraft noise on sleep around multiple US airports based on lessons learned from the current field studies;
(4) Continue our collaboration with colleagues at the German Aerospace Center (DLR) to compare, combine, and publish findings from US and German field studies.

Research Approach

Based on lessons learned in the Philadelphia Sleep study, the methodology has been refined and a second pilot study is currently being conducted to evaluate its feasibility. The airport for this study was selected in consultation with the FAA and has relevant amounts of nighttime air traffic and a sufficient population to sample from. To determine the sample regions around the airport, L_{Night} noise contours were provided by the FAA. Additionally, we calculated L_{Night} contours for 84 weekdays based on flight track data. For the study we have 10 sampling regions, 5 east and west of the airport of the following noise categories: < 40 dB (control region), 40-45 dB, 45-50 dB, 50-55 dB, and >55 dB L_{Night}.

To recruit participants for the study, brief surveys were mailed to randomly selected households within each of the 10 sampling frames. The primary purpose of the survey is determining the eligibility of individuals to take part in an in-home sleep study. The survey contains questions on the individual's health, sleep, and noise sensitivity. To increase the response rate to the recruitment survey, different incentives, such as a promised gift card and a pre-paid $2.00 were examined. Additionally, survey length and number of follow-up surveys were varied to determine their effect on response rate. The target number of completed surveys is 200 per 5dB noise category, for a total of 1000 surveys.

In the survey, participants indicate their interest in taking part in the in-home sleep study, which consists of 5 nights of unattended ECG and actigraphy measurements and indoor sound recordings. The equipment is mailed to the participants' homes and instruction manuals and videos on how to setup and use the equipment are provided. Mailing the equipment eliminated the need for staff in the field which significantly reduces the study cost. In addition, mailing the equipment may increase the response rate as staff does not enter the participants' homes. For enrolling in the in-home sleep study, participants received varying amounts of compensation. For survey mailing rounds 1-5, participants received $20 per night in which measurements were completed. Compensation was increased to $30 per night for mailing rounds 6-9, and to $40 per night for rounds 10-17. The purpose of increasing the compensation was to evaluate how response rate changes as compensation increases. This will help determine a cost-effective compensation for a future multiple airport study. The target enrollment for the in-home study is 40 per 5 dB noise category, for a total of 200 participants. The outcomes for this study are to determine the response rates for both the mail and in-home study, assess the feasibility of mailing equipment, and evaluate the quality of data that can be obtained.

Milestones

The following are milestones that were achieved during the past 12 months:
(1) Data collection for the second pilot sleep study began 9/2016 and will be finalized in 11/2017.

Major Accomplishments

The approach for recruiting participants for in-home sleep measurements was refined. This included determining the survey incentive, length of survey, and number of follow-up mailings that maximized the response rate. We have obtained 403 surveys and have completed in-home sleep measurements for 34 participants. The option of providing a hair sample was added to the protocol of the in-home study. The samples will be used to determine cortisol levels, which are a measure of long-term stress. Instructions for the hair collection protocol have been created and all staff has been trained. Data collection is ongoing but will end in 11/2017.

Publications

McGuire, S., Witte, M., Kallarackal, A., Basner, M.: Pilot study examining the effects of aircraft noise on sleep in communities near Philadelphia International airport. Poster at the 31st Anniversary Meeting of the Associated Professional Sleep Societies, Boston, June 11-15, 2016.

Basner, M., McGuire, S.: Pilot study examining the effects of aircraft noise on sleep in communities near Philadelphia International airport. Presentation at the 12th ICBEN Congress on Noise as a Public Health Problem, Zurich, Switzerland, June 18-22, 2017.

Müller, U., Elmenhorst, E.-M., Mendolia, F., Quehl, J., Basner, M., McGuire, S., Aeschbach, D.: A comparison of the effects of night time air traffic noise on sleep at Cologne/Bonn and Frankfurt Airport after the night flight ban. Presentation at the 12th ICBEN Congress on Noise as a Public Health Problem, Zurich, Switzerland, June 18-22, 2017.

McGuire, S., Müller, U., Elmenhorst, E.-M., Mendolia, F., Aeschbach, D., Basner, M.: Cross-country comparison of aircraft noise-induced sleep disturbance. Poster at the 12th ICBEN Congress on Noise as a Public Health Problem, Zurich, Switzerland, June 18-22, 2017.

McGuire, S., Basner, M.: Development of a methodology for field studies on the effects of aircraft noise on sleep. Presentation at the 173rd Meeting of the Acoustical Society of America and the 8th Forum Acusticum, Boston, MA, June 25-29, 2017.

Outreach Efforts

None

Awards

None

Student Involvement

None

Plans for Next Period

Data collection for the in-home sleep study will continue and end in 11/2017. No more surveys will be mailed. The main focus of the next period is to analyze the sound recordings and physiological data of the ATL study. For this analysis we plan to refine and automatize the methodology of identifying aircraft noise events and maximum sound pressure levels in the recordings. The identification of aircraft noise events can be challenging based on indoor sound measurements only due to masking of other noise events (e.g., air conditioning system, snoring). We will continue our collaboration with colleagues at the German Aerospace Center (DLR) to compare findings from US and German field studies

References

Basner M, Griefahn B, Müller U, Plath G, Samel A. An ECG-based algorithm for the automatic identification of autonomic activations associated with cortical arousal. Sleep 2007; 30(10):1349-61.

Project 018 Community Measurements of Aviation Emissions Contribution to Ambient Air Quality

Boston University School of Public Health

Project Lead Investigator

Jonathan I. Levy (through 9/30/17)
Interim Chair and Professor
Department of Environmental Health
Boston University School of Public Health
715 Albany St. T4W, Boston, MA 02118
617-358-2460
jonlevy@bu.edu

Kevin J. Lane (as of 10/1/17)
Assistant Professor
Department of Environmental Health
Boston University School of Public Health
715 Albany St. T4W, Boston, MA 02118
617-414-8457
klane@bu.edu

University Participants

Boston University School of Public Health

- P.I.(s): Jonathan I. Levy, Professor and Associate Chair
- FAA Award Number: 13-C-AJFE-BU, Amendment 7
- Period of Performance: October 1, 2016 – September 30, 2017
- Task(s):
    1. Conduct ambient monitoring of UFP and other pollutants in communities underneath flight paths near Boston Logan International Airport, to determine the locations and atmospheric/flight activity conditions under which exposures could be elevated.
    2. Work with collaborators on ASCENT Projects 19 and 20 to quantify the health implications of modeled aviation-related air pollutant concentrations.

Project Funding Level

$200,000. Matching funds provided by non-federal donor to the Women's Health Initiative (WHI) cohort studies, provided as cost share support to Boston University through Project 3.

Investigation Team

Principal Investigator: Jonathan I. Levy, Sc.D. (Professor of Environmental Health, Department of Environmental Health, Boston University School of Public Health). Dr. Levy is the Boston University PI of ASCENT. He has primary responsibility for the execution of the project and contributes to manuscripts and reports produced.

Faculty member: Kevin J. Lane, Ph.D. (Assistant Professor of Environmental Health, Department of Environmental Health, Boston University School of Public Health). Dr. Lane joined the Project 18 team in July 2017. Dr. Lane has expertise in ultrafine particulate matter exposure assessment, geographic information systems, and statistical modeling of large datasets, along with cardiovascular health outcomes associated with air pollution exposures. He has contributed to study design and data analysis strategies, and as of 10/1/17, has primary responsibility for project execution.

Post-doctoral researcher: Matthew Simon, Ph.D. Dr. Simon joined the Project 18 team in September 2017, and is involved in data analyses, field study design and implementation, and scientific manuscript preparation.

Graduate Student: Chloe Kim, MPH. Ms. Kim is a doctoral student in the Department of Environmental Health at BUSPH. She has taken the lead on organizing and implementing the air pollution monitoring study and will be responsible for the design and execution of related statistical analyses.

Research Assistant: Claire Schollaert. Ms. Schollaert provides field support for the air pollution monitoring study, including design and implementation of monitoring platforms.

Project Overview

The primary goal was to conduct new air pollution monitoring underneath flight paths to and from Boston Logan International Airport, using a protocol specifically designed to answer the question of the magnitude and spatial distribution of ultrafine particulate matter (UFP) in the vicinity of arrival flight paths. Data was collected that would address the question of whether aircraft emissions, and in particular arrival emissions, can contribute significantly to UFP concentrations at appreciable distances from the airport. In addition, Task 2 had the goal of supporting the work of collaborators on Projects 19 and 20, regarding the appropriate concentration-response functions and other datasets to allow atmospheric modeling outputs to be used in health impact assessment calculations.

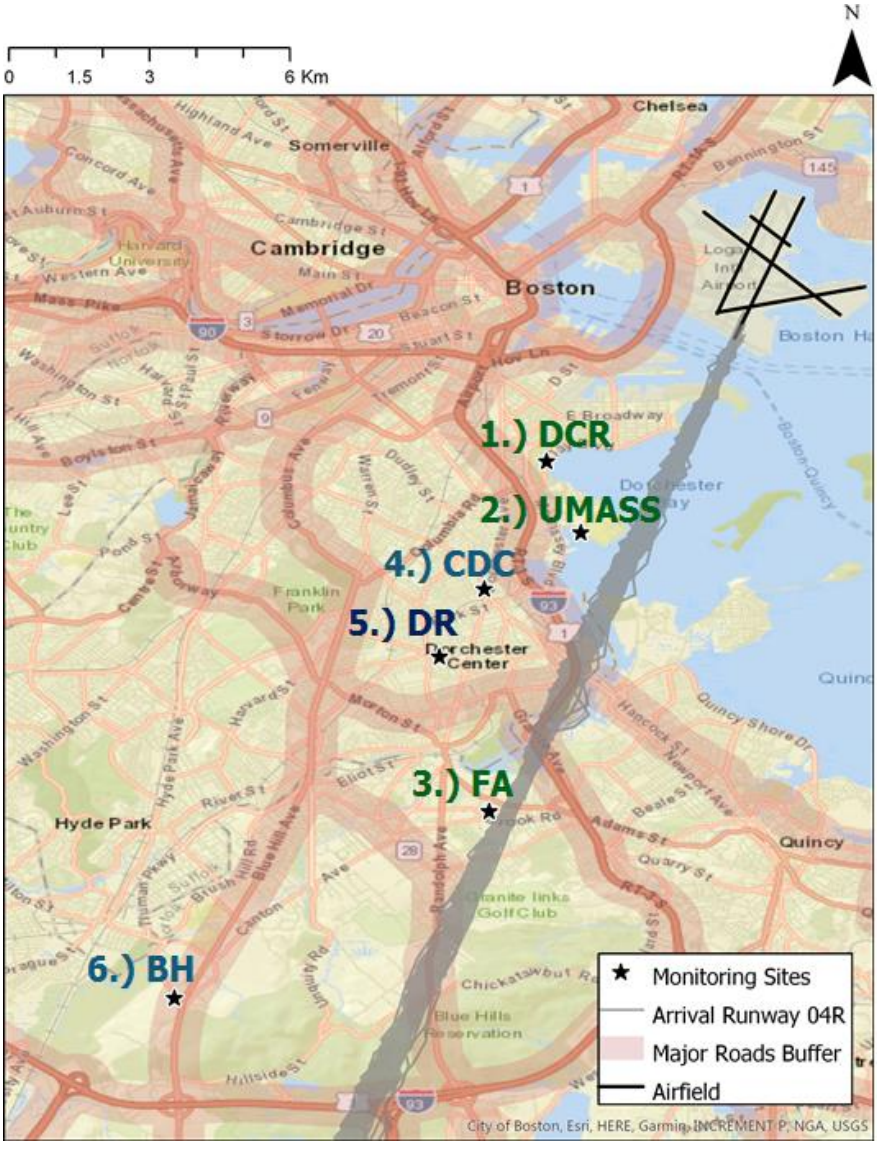

Figure 1. Monitoring sites and runway 4R flight path.

Task #1: Conduct ambient monitoring of UFP and other pollutants in communities underneath flight paths near Boston Logan International Airport, to determine the locations and atmospheric/flight activity conditions under which exposures could be elevated.

Boston University School of Public Health

Objective(s)

Project 18, Task 1 for the 2016-2017 funding cycle focused on designing and implementing an air pollution monitoring study that would allow us to determine contributions from arriving aircraft to ambient air pollution in a near-airport setting. The objective of this task was to address the question of whether aircraft emissions, and in particular arrival emissions, can contribute significantly to ultrafine particulate matter (UFP) concentrations at appreciable distances from the airport.

Research Approach

An air pollution monitoring campaign was conducted at six sites at varying distances from the airport and the arrival flight path to runway 4R (Figure 1). Sites were selected through a systematic process, considering varying distances from the airport and laterally from the 4R flight path, and excluding locations close to major roadways or other significant sources of combustion. These sites were chosen specifically to isolate the contributions of arrival aircraft on runway 4R, which is important for the flight activity source attribution task.

Three sets of particle number concentration (PNC, a proxy for UFP) monitoring instruments were rotated among monitoring sites in a pre-selected scheme to allow for multiple levels of comparison (e.g., sites underneath vs. not underneath flight paths given prevailing winds, sites at varying distances from the airport underneath the same flight path, sites at varying lateral distances underneath the same flight path). PNC was measured with TSI Condensation Particle Counters (Model 3783). In addition, black carbon was measured using AethLabs Microaethalometers (Model AE51), and meteorological data at each site were collected using Davis Vantage Pro2 weather stations. Over 28 million 1-second PNC measurements were collected from April – September of 2017, during one week sampling periods that averaged 63 days of sampling at each site (Table 1). Sites were monitored at each site multiple times under varying meteorological conditions during our campaign.

Milestone(s)

The core milestones articulated in the 2016-2017 Project 18 proposal included:

- Obtain all air pollution monitors and other materials necessary for a field campaign surrounding Logan Airport
- Select candidate monitoring sites and obtain permission to monitor at those sites
- Design field monitoring and site rotation protocols/schedules
- Implement air pollution monitoring protocols, including measurements of meteorological conditions and collection of PDARS data to be used in statistical analyses.
- Develop statistical techniques needed for source attribution given continuous air pollution and flight activity data.
- Complete primary statistical analyses and prepare scientific manuscripts

We obtained air pollution monitors and constructed sampling boxes and field protocols in Fall 2016, as planned. Selection of monitoring sites was successful, and we obtained permission to sample at six sites by Winter 2016-2017. We began collecting field data following our complete protocols in April 2017 with comprehensive data capture throughout the spring and summer, meeting our data collection milestone. As we did not obtain flight activity data until September 2017, given challenges with data access and changes from PDARS to NOP availability, the comprehensive set of statistical analyses were deferred until the subsequent funding year, but all core data collection milestones were easily met.

Major Accomplishments

As described above, the 2017 air pollution field monitoring campaign was conducted from April – September at six sites at varying distances from the airport and the arrival flight path to runway 4R (Figure 1). This met all targets for sample size and data capture, providing a strong foundation for forthcoming statistical analyses.

Table 1. Distribution of PNC at the six monitoring sites

	Site 1	Site 2	Site 3	Site 4	Site 5	Site 6
Sample Size (days)	67	71	57	61	57	62
Sample Size (seconds)	5,262,301	5,301,907	4,126,007	4,363,564	4,233,284	4,661,517
0.1st percentile	800	1,100	1,600	2,500	2,000	1,800
1st percentile	1,000	2,900	2,500	5,100	2,900	2,500
5th percentile	4,300	5,800	4,300	8,200	5,700	4,300
50th percentile	14,100	16, 600	11,600	20,600	17,100	12,000
95th percentile	55,600	63,000	28,000	67,900	47,100	31,400
99th percentile	116,800	119,200	47,400	103,200	70,700	50,500
99.9th percentile	180,200	206,600	87,500	150,800	96,500	95,800

The summary statistics presented in Table 1 cannot provide definitive insight about aviation contributions to measured PNC, but are helpful for hypothesis generation. For example, note that Site 4 has the highest concentrations of all sites through the 95th percentile of the distribution, consistent with its location in an urban neighborhood with traffic sources in relatively close proximity. However, Site 2 has the highest concentrations at the 99th percentile and above. Site 2 does not have nearby traffic (located on a college campus) and is relatively close to the 4R arrival flight path, so the elevated concentrations above the 99th percentile would be consistent with an intermittent contribution from aviation emissions. Similarly, Site 1 also is elevated at the 99th percentile or above and is located closer to the airport and 4R arrival path. However, no formal conclusions can be drawn without statistical analyses that include flight activity and meteorology, and the full set of National Offload Program (NOP) data that were made available on September 22, 2017. Ongoing Project 18 efforts are now focused on linking the NOP data with our PNC second-by-second data and conducting regression analysis.

Prior to conducting statistical analyses, it is important to determine the degree of error in our measurements, to determine whether concentration spikes can be reasonably interpreted. PNC monitoring instruments were tested for agreement during lab and field based co-location. Co-location testing of the three CPCs showed extremely high correlations (R^2=0.98; Figure 2) and similar ability to detect short-term concentration increases. This reinforces that our large sample size will have the statistical power to detect a variety of associations and to construct models with subsets of data if informative (i.e., restricting to specific times of day or meteorological conditions).

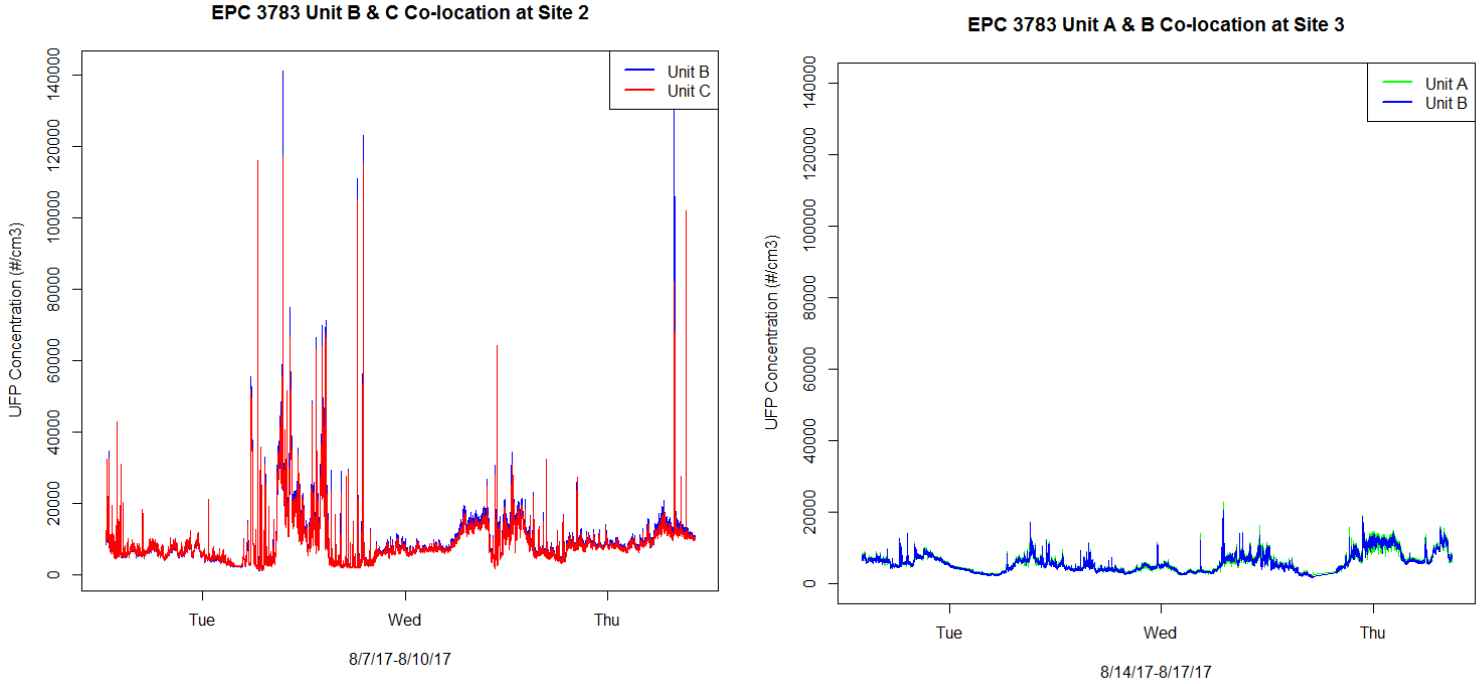

Figure 2. Results from PNC co-location experiments.

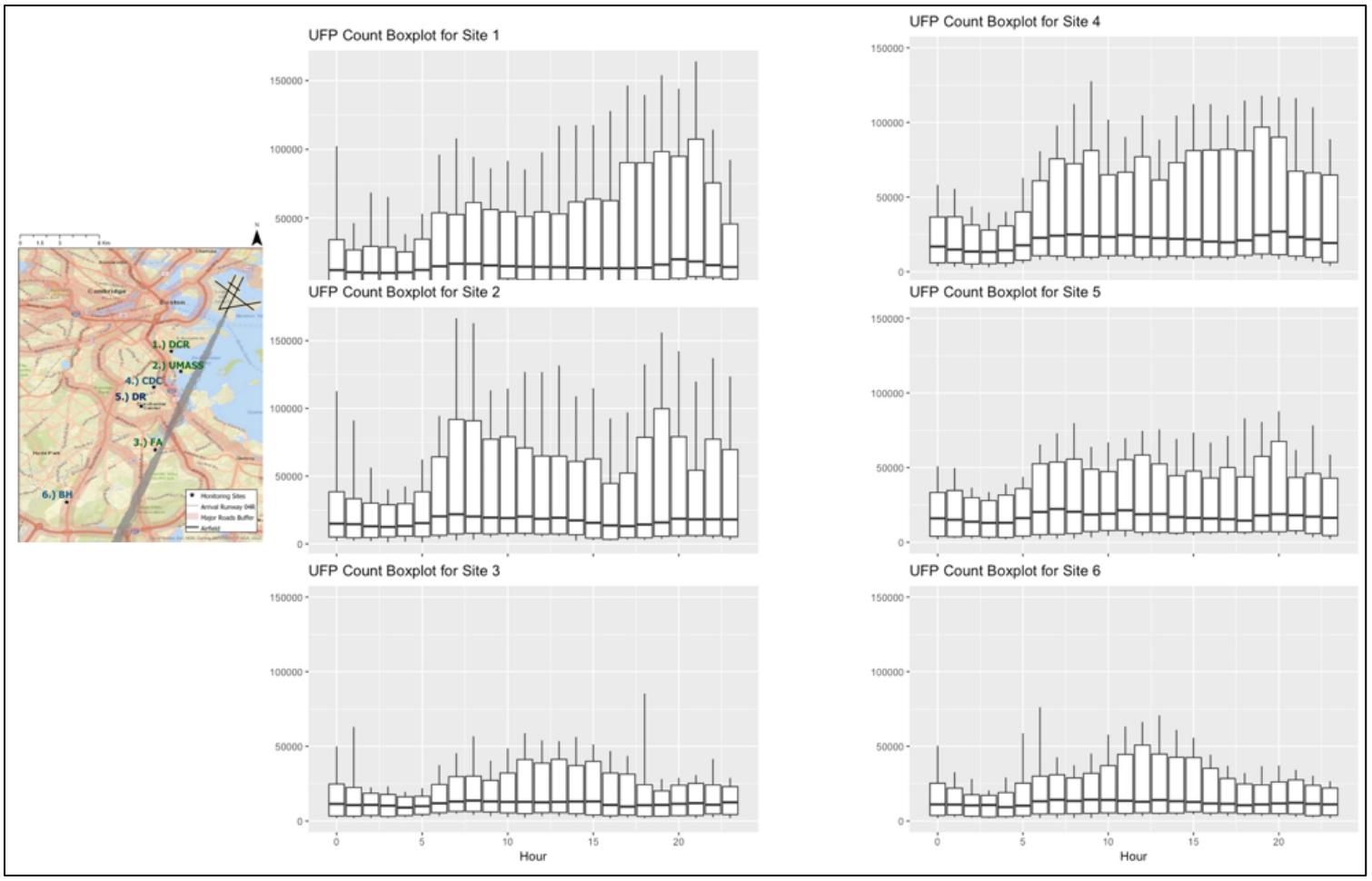

Figure 3. Diurnal boxplots for each monitoring site

Another approach for developing preliminary insights from our monitoring data is to examine diurnal concentration patterns. The diurnal variation of PNC (Figure 3) at each monitoring site allow for continued hypothesis generation. For example, all sites have a similar pattern of increasing concentrations in the early morning hours, which would be consistent with a growing traffic contribution or aviation contributions. Variations in diurnal patterns across sites, coupled with attributes of the sites themselves (i.e., proximity to runways and major roadways), may yield interesting hypotheses for future analyses. For example, elevated concentrations within an hour above the 95th percentile (but not at the median) would be consistent with an intermittent contribution from aviation emissions, versus consistently elevated concentrations at all percentiles. Examining the diurnal patterns, Sites 1 and 2 appear to have greater differences between the median and 95th percentile patterns, which could indicate aviation contributions. In contrast, Sites 4 and 5 have more local traffic and higher altitude flights, and display similar patterns at the median and the 95th percentile. After the NOP data have been linked with the PNC data it will allow for a more robust comparison of the PNC measures to flight path information and inform additional hypotheses with regard to aviation source contributions.

Table 2. PNC distribution by runway 4R being operational or non-operational and wind direction at Sites 2 and 3.

	S2-4R Operational	S2-4R Non-Operational	S2-4R Non-Operational	S3-4R Operational	S3-4R Non-Operational	S3-4R Non-Operational
Date	April 18	July 4	July 10	April 18	July 4	July 21
Sample Size	50,551	59,215	84,097	43,861	35,535	86,400
Wind	NW, N, NE	NE, ENE	SE, SSE	E, NE, NNE	ENE, NE	SW, SSE
0.1st percentile	2,958	8,076	6,913	3,008	11,842	8,504
1st percentile	3,174	10,857	8,267	3,350	12,065	9,039
5th percentile	4,890	13,841	9,335	3,940	12,289	9,460
50th percentile	20,818	20,462	13,923	10,318	14,422	12,519
95th percentile	75,715	41,335	23,362	22,480	21,150	19,094
99th percentile	120,463	54,703	26,008	34,611	25,758	25,768
99.9th percentile	198,934	61,582	37,077	58,117	30,223	30,995

Hypotheses can also be informed by considering concentration patterns by wind direction and by degree of flight activity. During our monitoring campaign, Runway 4R was fully operational for a portion of the period, non-operational for a portion of the period due to runway construction, and partially operational for a portion of the period immediately subsequent to the construction. This provides a natural experiment in which we can examine concentration patterns with varying amounts of flight activity as well as varying meteorology. As shown in Table 2, at Site 2 when 4R was operational and wind direction was from the N/NW/NW (optimal for runway utilization and for dispersion to the monitoring site), concentrations were elevated at the 95th percentile and above, when compared with a day with similar wind conditions when the runway was not operational. Additionally, when 4R was not operational and the winds were from the SE/SSE, the PNC distribution at Site 2 was higher at the lowest percentiles but significantly lower for most of the distribution. At Site 3, located at a greater distance from the airport but along the 4R arrival flight path, concentrations were similarly elevated during an operational day with favorable winds, albeit only at the 99th percentile and above and with a lower magnitude difference with a comparable non-operational day. This is consistent with a small and intermittant but measurable influence of aircraft arrivals at this monitoring site.

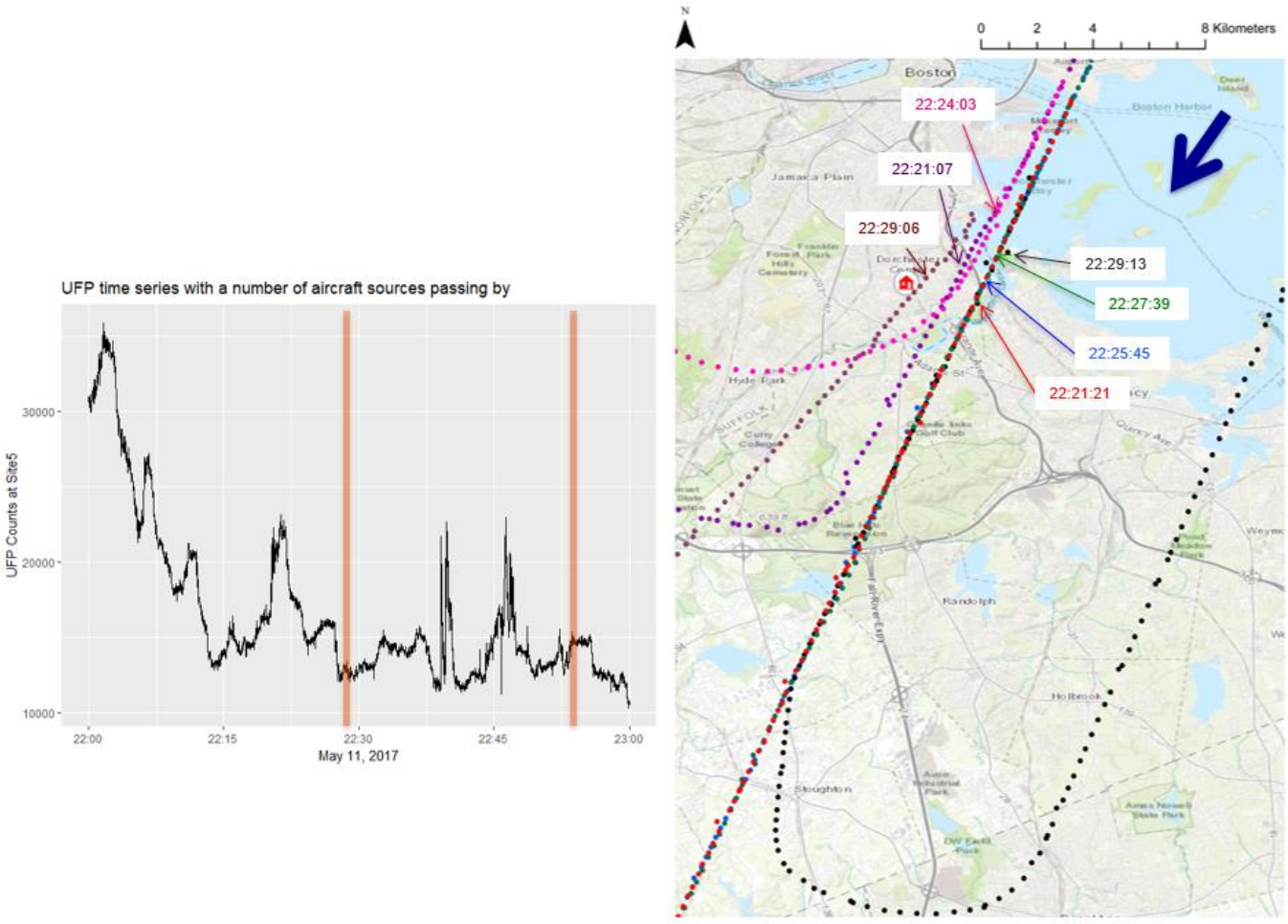

Figure 4. Example of flight activity data and runway PNC temporally linked.

Our regression models will ultimately leverage real-time flight activity data linked with one-second PNC measurements. Illustrating the complexity of these patterns, Figure 4 presents a time-series plot of data from a single hour of measurements at Site 2, with an overlay of flight activity. On a day with winds from the NNE, concentration peaks did occur on or around the times when aircraft were arriving, but peaks also occurred at other time points and the lags between flights and concentration increases were not consistent. This emphasizes the importance of regression modeling that accounts for lags between flight activity and concentrations as well as meteorological conditions, which can appropriately evaluate the incremental contribution of aviation activities.

Publications
None

Outreach Efforts
Dr. Jonathan Levy presented an update of the Project 18 field monitoring and descriptive data analysis at the ASCENT Fall 2017 meeting, along with a poster at the Spring 2017 meeting.

Doctoral student Chloe Seyoung Kim presented an oral presentation on a portion of the major accomplishments of Project 18 at the International Society for Exposure Science annual meeting in October 2017.

Awards
None

Student Involvement
Chloe Seyoung Kim, a doctoral student at BUSPH, was involved with the monitoring of PNC during the field campaign, data compilation and merging as well as statistical analysis.

Plans for Next Period
Four tasks are proposed over the next study period (10/1/17-9/30/18):

Task 1: Construct regression models to determine the contributions of aircraft arrivals to UFP and BC concentrations measured during the 2017 monitoring campaign.
Task 2: Conduct site selection for the 2018 monitoring campaign by analyzing the 2017 measurements and by considering optimal sites to determine multiple types of aviation source contributions.
Task 3: Measure UFP and other air pollutants at sites near Boston Logan International Airport selected under Task 2.
Task 4: Develop platforms that would allow for comparisons between atmospheric dispersion models implemented by collaborators on ASCENT Project 19 and monitored pollutant concentrations from Project 18.

Task 1: Construct regression models to determine the contributions of aircraft arrivals to UFP and BC concentrations measured during the 2017 monitoring campaign.

Utilizing the air pollution data collected during the 2017 monitoring campaign has allowed for an examination of average UFP concentrations on the days when the 4R runway was operational and not operational under all wind conditions, to examine the overall impact of arrival aircraft on ambient UFP concentrations at the study sites. Additionally, an examination of the correlations of simultaneously measured UFPs from multiple study sites to examine the similarities and variations of aircraft impact at different monitoring sites is already underway. The contributions of aircraft to ambient UFP and BC concentrations will be examined by comparing them to the background concentrations as well as by how well UFP and BC measurements correlate.

A few different analytical approaches are being explored to interpret the data collected during the field campaign prior to constructing regression models. Examination of space-time plots of the PNC data will inform if there are distinct patterns of plume movement and potential time lag differences between the sites under specific meteorological conditions. Results from these descriptive analyses will subsequently inform the regression model development process.

For the regression models, the goal is development of multivariate generalized additive models to examine the association between UFP and BC concentrations and real-time flight activity, accounting for aircraft locations in space relative to the monitor including terms for wind speed/direction and temperature. Each study site will be modeled individually to look at location-specific impact of aircraft arrivals along with meteorological and other local environmental conditions, and then combined models will be explored. Each of these regression models will be able to estimate on a short-term and long-term basis the amount of the measured UFP attributable to flight activity, by zeroing out the flight activity terms and determining the predicted concentrations. This would answer the question regarding the spatiotemporal patterns of aviation-related UFP contributions, as well as the relative influence of flight arrivals (and departures where relevant) in different locations.

Task 2: Conduct site selection for the 2018 monitoring campaign by analyzing the 2017 measurements and by considering optimal sites to determine multiple types of aviation source contributions.

The 2017 air pollution monitoring campaign was designed specifically to isolate the contributions of arrival aircraft on runway 4R, which is important for the initial source attribution task, but may not be the optimal sites to determine multiple types of aviation source contributions. A crucial first step in planning the 2018 monitoring campaign will be to evaluate the data obtained during the 2017 monitoring campaign and evaluate the attributes of current and new sites that would allow for additional levels of analysis. For example, new site selection might want to isolate departure contributions as well as arrivals, at varying distances and directions from the airport.

Construction of geospatial layers reflecting key inclusion/exclusion criteria will be used to facilitate site selection. For example, retaining the exclusion criteria that includes proximity to a major roadway or other major local sources of air pollution will help isolate the effects of aircraft within statistical analyses. Mapping key flight paths to determine geographic areas that meet the selection criteria will include both arrivals and departures. A subset of sites from the 2017 monitoring campaign will be selected, to allow for continuity, but choosing a number of new sites to extend the scope of the regression analyses. The length of deployment and the ancillary data collection strategies will also be reassessed to maximize expansion of Task 1 regression model development and future investigations of aviation source contributions. Additionally sites will be prioritized where previously established relationships with individuals or businesses can ensure security and access, to simplify the process of monitor deployment. Also, the new sampling campaign will incorporate additional monitoring equipment to enhance the air pollution analysis to include UFP size distribution and NO/NO_2, which is described in greater detail under Task 3.

Task 3: Measure UFP and other air pollutants at sites near Boston Logan International Airport selected under Task 2.

Given the sites chosen under Task 2, a monitoring campaign in 2018 will be conducted to inform an aviation source attribution analysis to expand upon Task 1 regression model development. Instrumentation and protocol will be similar to the ongoing 2017 monitoring campaign, but with some key enhancements to improve insights regarding aviation source contributions.

Monitoring instruments will include the TSI Model 3783 water-based CPC for UFP, our primary measure of interest, which was used in the 2017 monitoring campaign. The 3783 is intended for long-term deployment and can record 1-second average concentrations, valuable time resolution for capturing short-term concentration spikes. Of note, as the Model 3783 CPC is temperature-sensitive, it needs to be deployed in a conditioned space to protect against extreme heat or cold, allowing for long-term deployment.

To enhance the UFP monitoring campaign a TSI Scanning Mobility Particle Sizer Spectrometer (SMPS) 3938, which is widely used as the standard for measuring airborne particle size distributions, will be integrated into the sampling campaign. The SMPS 3938 connects with the 3783 to provide particle size distribution of short-term concentration spikes. Insight on particle size distributions is crucial information for validating aviation source contributions and connecting with outputs from atmospheric dispersion models for UFP being developed within Project 19. Although obtaining and deploying three SMPS 3938 instruments is beyond the scope of this project, an instrument will be borrowed from collaborators at Tufts University. This instrument will be rotated through the sampling locations.

In addition, the AethLabs model AE51 microaethalometer will be used to measure BC. A number of low-cost NO/NO_2 sensors have recently been developed, and a sensor that gives high-fidelity outputs could allow for future studies with simultaneous real-time measurements at numerous sites. This also provides an additional pollutant for any future comparisons with atmospheric dispersion model outputs, which could help isolate factors that influence predictions of particulate matter vs. gas-phase pollutants.

The local Davis Vantage Pro2 weather stations will be used to capture real-time wind speed/direction and other meteorological conditions. Obtaining flight activity data from FAA for the time periods of sampling will be essential for regression model development, which will include location of each flight as well as basic aircraft characteristics, which could be linked with AEDT to determine aircraft-specific attributes that may be predictive of emissions and corresponding concentrations.

Task 4: Develop platforms that would allow for comparisons between atmospheric dispersion models implemented by collaborators on ASCENT Project 19 and monitored pollutant concentrations from Project 18.

While the primary objective of Tasks 1-3 is to inform aviation source attribution using ambient pollution measurements, the insights from these models could be connected with atmospheric dispersion models applied at the same location and dates. Within Project 19, UNC researchers are implementing CMAQ and other dispersion models to examine the air quality implications of emissions of various air pollutants from aviation, with a current focus on modeling UFP. If in the future Project 19 applies atmospheric dispersion modeling tools focused on locations near Boston Logan International Airport, this would allow for future comparative analyses. The purpose of this Task is to develop data processing systems that would allow for these comparative analyses to be conducted.

To aid these efforts, development of two types of output files under Task 4 will occur. First, the UFP measurements collected during the 2017 monitoring campaign will be processed and provided in a format requested by Project 19. These measurements reflect the contributions from both aviation and other sources, and can be directly compared with all-source dispersion models such as CMAQ. The BU research team will complete QA/QC of the 2017 monitoring data, post-process the data in a form that would be aligned with atmospheric dispersion modeling outputs from Project 19, and make the data available to UNC collaborators. In the second phase, subsequent to the completion of all regression models (Task 2), development of an analogous database with the aviation-attributable UFP concentrations will be processed. This will be calculated by comparing the regression model predictions with the predictions given no aviation sources (i.e., all aviation terms set to zero). This would allow for comparisons with aviation source contribution estimates from atmospheric dispersion models.

Task #2: Work with collaborators on ASCENT Projects 19 and 20 to quantify the health implications of modeled aviation-related air pollutant concentrations.

Boston University School of Public Health

Objective(s)

Multiple tasks within ASCENT Projects 19 and 20 involve estimation of the public health impacts of air pollution exposures associated with aviation sources or potential control strategies. For example, MIT researchers are in the process of developing global adjoint models for ozone, which require globally appropriate concentration-response functions and population datasets. Similarly, UNC researchers are continuing implementation of CMAQ-DDM to examine the air quality implications of changing emissions of various air pollutants from aviation, with corresponding health risk implications. The objective of this task was to support MIT and UNC collaborators on an as-needed basis, conducting new literature review or synthesis as needed.

Research Approach

Other than limited ad hoc consultations, no formal collaboration or input was requested, so there were no defined efforts underneath this task

Milestone(s)

Not applicable

Major Accomplishments

Not applicable

Publications

Penn SL, Boone ST, Harvey BC, Heiger-Bernays W, Tripodis Y, Arunachalam S, Levy JI. Modeling variability in air pollution-related health damages from individual airport emissions. Environ Res 156: 791-800 (2017).

Outreach Efforts

During this funding period, the health damage function work was presented at the Fall 2016 ASCENT meeting and the October 2016 FAA Tools/Analysis Coordination Meeting.

Awards

None

Student Involvement

Stefani Penn and Lindsay Underhill, both doctoral students at BUSPH, were involved in various aspects of developing the health impact assessment modeling platform.

Plans for Next Period

There are no plans to continue any formal consultative engagement on this topic, though we will continue to be available for ad hoc discussions on relevant topics, and collaborative work with Project 19 on health impacts of air pollution will be conducted if appropriate.

Project 019 Development of Aviation Air Quality Tools for Airshed-Specific Impact Assessment: Air Quality Modeling

University of North Carolina at Chapel Hill

Project Lead Investigator

Saravanan Arunachalam, Ph.D.
Research Professor
Institute for the Environment
University of North Carolina at Chapel Hill
100 Europa Drive, Suite 490
Chapel Hill, NC 27517
919-966-2126
sarav@email.unc.edu

University Participants

University of North Carolina at Chapel Hill

- PI: Saravanan Arunachalam, Research Professor
- FAA Award Number: 13-C-AJFE-UNC Amendments 1 - 6
- Period of Performance: January 1, 2017 – October 31, 2017
- Task(s):
    - Perform NAS-wide impact assessment for 2011 and 2015
    - Perform airport-by-airport assessment using CMAQ-DDM
    - Develop generalized gridding tool for AEDT
    - Provide support for High fidelity weather in AEDT
    - Explore collaboration with NAU, Ukraine

Repeat for all participating universities.

Project Funding Level

$212,494 from the FAA

Matching Cost-share provided by Transport Canada

Investigation Team

Prof. Saravanan Arunachalam (UNC) (Principal Investigator) [Tasks 1-5]
Dr. Bok Haeng Baek (UNC) (Co-Investigator) [Task 3]
Dr. Jared Bowden (UNC) (Co-Investigator) [Task 4]
Dr. Carlie Coats (UNC) (Co-Investigator) [Task 3]
Dr. Moniruzzaman Chowdhury (Co-Investigator) [Task 1]
Dr. Jiaoyan Huang (UNC) (Co-Investigator) [Task 1,3]
Ms. Catherine Seppanen (UNC) (Co-Investigator) [Task 3]
Mr. Calvin Arter (UNC) (Graduate Research Assistant) [Task 1,2,3]

Project Overview

With aviation forecasted to grow steadily in upcoming years,[1] a variety of aviation environmental policies will be required to meet emissions reduction goals in aviation-related air quality and health impacts. Tools will be needed to rapidly assess the implications of alternative policies in the context of an evolving population and atmosphere. In the context of the International Civil Aviation Organization (ICAO)'s Committee on Aviation Environmental Protection (CAEP), additional tools are required to understand the implications of global aviation emissions.

The overall objective of this project is to continue to develop and implement tools, both domestically and internationally, to allow for assessment of year-over-year changes in significant health outcomes. These tools will be acceptable to FAA (in the context of Destination 2025) and/or to other decision-makers. They will provide outputs quickly enough to allow for a variety of "what if" analyses and other investigations. While the tools for use within and outside the US (for CAEP) need not be identical, a number of attributes would be ideal to include in both:

- Enable the assessment of premature mortality and morbidity risk due to aviation-attributable $PM_{2.5}$, ozone, and any other pollutants determined to contribute to significant health impacts from aviation emissions;
- Capture airport-specific health impacts at a regional and local scale;
- Account for the impact of non-LTO and LTO emissions, including separation of effects;
- Allow for the assessment of a wide range of aircraft emissions scenarios, including differential growth rates and emissions indices;
- Account for changes in non-aviation emissions and allow for assessing sensitivity to meteorology;
- Provide domestic and global results;
- Have quantified uncertainties and quantified differences from EPA practices, which are to be minimized where scientifically appropriate; and
- Be computationally efficient such that tools can be used in time-sensitive rapid turnaround contexts and for uncertainty quantification.

The overall scope of work is being conducted amongst three collaborating universities – Boston University (BU), Massachusetts Institute of Technology (MIT), and the University of North Carolina at Chapel Hill (UNC). The project is performed as a coordinated effort with extensive interactions among the three institutions and will be evident in the reporting to the three separate projects (ASCENT 18, 19 and 20) by each collaborating university.

The components led by the University of North Carolina at Chapel Hill's Institute for the Environment (UNC-IE) included detailed modeling of air quality using the Community Multiscale Air Quality (CMAQ) model. UNC-IE is collaborating with BU to develop health risk estimates on a national scale using CMAQ outputs and with MIT for inter-comparing against nested GEOS-Chem model applications within the US and to further compare/contrast the forward sensitivity versus the inverse sensitivity (such as adjoint) techniques for source attribution. Our efforts for this project build on previous efforts within Project 16 of PARTNER. This includes detailed air quality modeling and analyses using CMAQ at multiple scales for multiple current and future year scenarios, health risk projection work that successfully characterizes the influence of time-varying emissions, background concentrations, and population patterns on the public health impacts of aviation emissions under a notional future emissions scenario for 2025. Under Project 16, we started to develop a new state-of-the-art base year modeling platform for the US using the latest version of models (CMAQ, WRF, SMOKE) and emissions datasets (AEDT, NEI), and tools (MERRA-2-WRF, CAM-2-CMAQ) to downscale from GCMs being used in Aviation Climate Change Research Initiative (ACCRI). We are continuing to adapt and refine the tools developed from that platform as part of ongoing work in this phase of the project.

In this project, the UNC-IE team is performing research on multiple fronts during the stated period of performance, and we describe them in detail below.

1. Perform NAS-wide impact assessment for 2011 and 2015
2. Perform airport-by-airport assessment using CMAQ-DDM
3. Develop generalized gridding tool for AEDT
4. Provide support for High fidelity weather in AEDT
5. Explore collaboration with NAU, Ukraine

[1] Boeing Commercial Airplane Market Analysis, 2010.

Task #1: Perform NAS-wide Impact Assessment for 2011 and 2015

University of North Carolina at Chapel Hill

Objective(s)

Using the most recent version of the Community Multi-scale Air Quality (CMAQ) model, develop an application for air quality simulation to investigate the trends of aircraft-attributable air pollutant concentrations at the surface for 2005, 2011, and 2015 years.

Research Approach

Introduction

The latest version of CMAQ, v5.2 was released in June 2017. UNC-IE previously used CMAQ v5.0.2 to quantify aircraft emissions impacts on surface air quality for 2005 in previous work. The most stable CMAQ version at the beginning of the year was v5.1. In CMAQv5.1 update from CMAQ v5.0.2, aerosol chemistry, homogeneous/heterogeneous chemistry, and planetary boundary layer scheme are improved (Appel et al., 2017). However, errors in wind-blown dust scheme have been found. Further, lightning NO_x calculation is still based on monthly total flash counts, while v5.2 has an algorithm to leverage the use of hourly data if available, and which we used.

In prior work under PARTNER and ASCENT, Woody et al. (2013) investigated secondary organic aerosols contributions from Atlanta airport (ATL) using CMAQ with three different resolutions (4, 12, and 36km). They concluded that different resolutions lead to different behaviors of organic chemistry. Huang et al. (in preparation) found that when using 36km resolution with CMAQv5.0.2 the 2005, landing and takeoff (LTO) attributable $PM_{2.5}$ is ~0.001 μg m^{-3} for domain average, and the highest increase was located in ATL (0.0029 μg m^{-3}).

Methodology

We modeled year 2011 at a new higher horizontal resolution of 12x12 km to assess aviation-attributable AQ impacts using CMAQ v5.1, meteorology from the Modern Era Retrospective Analysis for Research and Applications (MERRA) downscaled with WRF v3.8.1, background emissions from the National Emission Inventory (NEI) 2011 v6.3 processed through SMOKE v3.7, aircraft emissions from AEDT processed through AEDTProc, lightning NO_x, and inline photolysis.

The initial and boundary condition data for the main meteorology variables (except soil moisture and temperature, sea-surface temperature (SST) and snow height and snow-water equivalent) have been taken from NASA's MERRA data (Reienecker et al., 2011) which has 0.5 x 0.67 degree horizontal resolution with 72 vertical layers from surface to 0.01 hPa. The MERRA was chosen because it is a high resolution 3rd generation reanalysis dataset that includes high vertical and spatial resolution with 6-hourly data for entire globe which can be used in beyond CONUS domain such as northern hemispheric domain. MERRA does not provide soil data required for Weather Research Forecast (WRF) model (Skamarock et al., 2008) simulation. Soil moisture and temperature data for initial and boundary conditions were taken from National Centers for Environmental Prediction (NCEP) FNL (Final) Operational Global Analysis dataset which has 1x1 degree horizontal resolution with 6 hourly data. The sea-surface temperature data for WRF have been taken from the NCEP Environmental Modeling Center (EMC) real-time global SST dataset which has 0.5x0.5 degree resolution (Thiébaux et al., 2003). The snow height and snow water equivalent data have been taken from North American Mesoscale (NAM) model analyses datasets that were developed by the NCEP and obtained from the National Center for Environmental Information (NCEI) formerly known as National Climatic Data Center (NCDC). The model configurations for meteorology has been described in Table 1. The 2011year simulation has been performed using 3 months spin-up time.

We applied the Sparse Matrix Operator Kernel Emissions (SMOKE) v3.7 with the NEI 2011 v6.3 described at: https://www.epa.gov/air-emissions-modeling/2011-version-63-platform to estimate background emissions. We processed 19 emission sectors within 3 emission categories, including point, on-road, and area emissions to generate 2011 background emissions for the Continental United States (CONUS) 12km x 12km data. Biogenic emissions and wind-blown dust are not generated using SMOKE. They are calculated in CMAQ using inline modules. Aircraft emissions were removed in NEI v6.3 and generated using AEDTProc v1. We utilized the AEDT gridding processor called AEDTProc to process segmented aircraft emissions from the FAA's Aviation Environmental Design Tool (AEDT). AEDTProc has been used extensively for FAA in prior work by UNC for the production of regional scale modeling emission inputs like those needed for CMAQ.

We used CMAQ v5.1 to estimate aircraft-attributable ambient $PM_{2.5}$ and O_3 concentrations. CMAQ was built based on CMAQv5.1 with two modules from v5.2 which are windblown dust and lightning NO_x. Table 2 shows the configuration of CMAQ used for 2011 simulations. We updated windblown dust to v5.2 due to the incorrect calculation in v5.1 and lightning NO_x to v5.2 to take advantage of high time resolution of flash strike calculation (from monthly to hourly data). The CB05e51_AE6_AQ chemical mechanism was selected to be consistent with the potential available mechanisms in CMAQ v5.2 DDM. Initial and boundary conditions were downscaled from global MOZART-4/GEOS-5 simulations to 12km x 12km CONUS. After starting day, results from previous day were used as initial conditions. Base and sensitivity scenarios were conducted for 2011 and yearly simulations were trimmed into 4 seasons (Jan-Mar, Apr-Jun, Jul-Sep, and Oct-Dec). For each runtime period, simulations were spun up for a month with 3 months real simulations. Base scenario (base) includes non-aircraft emissions (SMOKE) and sensitivity scenario (sens) includes non-aircraft (from SMOKE) and aircraft emissions (AEDTProc). Aircraft-attributable ambient $PM_{2.5}$ and O_3 concentrations were calculated by subtracting base scenario concentrations from sens scenario.

Results

Meteorological Data (WRF) Processing

The model performance was evaluated with the observation database for winds, temperature, and water mixing ratio from National Oceanic and Atmospheric Administration (NOAA) Earth System Research Laboratory (ESRL) Meteorological Assimilation Data Ingest System (MADIS). The performance metrics used in the evaluation were bias and error for monthly average and diurnal value of 2-m temperature (T2), 2-m water mixing ratio (Q2), 10-m wind speed (WS10) and 10-m wind direction (WD10). Figure 1shows the soccer plot (mean absolute error vs mean bias) for 12 months for a) T2, b) Q2, c) WS10 and d) WD10. For 2-m temperature, there was a cold bias in winter and warm bias in summer shown in Figure 1a. The bias was less than ± 1 K except February when bias was ~ -1.2 K. The 11 months' biases were less (≤ 1.0 K) than the reference benchmark value (within outer rectangle in the figure). The temperature errors for all 12 months were between 1.75 K to 2 K in spring, summer, fall and 2.5 K in winter which were less (≤ 3.0 K) than reference benchmark value (within outer rectangle in the figure). Figure 1b shows the bias and error of 2-m mixing ratio in all 12 months. The biases and errors were within the reference benchmark value (within outer rectangle in the figure). Figure 1c shows the bias and error of 10-m wind speed in all 12 months which were within the reference benchmark value (within outer rectangle in the figure). Figure 1d shows the bias and error of 10-m wind direction in all 12 months which were also within the reference benchmark value (within outer rectangle in the figure).

Background Emission (SMOKE) Processing

Overall, emission data are consistent with the values reported by US EPA (<5% difference). However, some emission sectors showed significant differences, including wildfire, commercial marine vessels, and emissions outside lower 48 states. We confirmed with the US EPA emissions team that these discrepancies were due to the inconsistency of domain sizes.

Aircraft Emission (AEDTProc) Processing

Until recently, we have used AEDTProc for generating emissions at the 36km x 36km grid cell resolution across the CONUS. In the past, we have generated 36km x 36km emissions for the entire 2005 year's worth of AEDT data and January and July AEDT data for the years 2010, 2011, and 2015. We obtained new AEDT data for these recent years (2010, 2011 and 2015) from the U.S. DOT Volpe Center, and tested these new datasets with AEDTProc. We identified a few problems with these datasets and, working with Volpe, we fixed them. We have done extensive testing on the four years' worth of datasets to observe any trends over time and abnormalities in the data. Figures 2 and 3 shows the LTO versus full flight emissions for the three years' worth of data comparing monthly emission totals for January and February and for five different emission species. However, the goal of this task is to update our modeling platform and we have chosen to model at 12km x 12km grid cell resolution for the years 2011 and 2015.

The UNC team performed quality assurance by comparing our January and July 12km x 12km AEDTProc generated emissions to the January and July 36km x 36km generated emissions from the 2011 AEDT data. This comparison is meant to ensure that the overall trends are preserved between the two generated emission sets, while acknowledging that minor differences are unavoidable when gridding at different resolutions. Figures 4 and 5 show the monthly domain-wide total emissions between the two resolutions.

Emission totals are largely the same amongst grid resolutions, with two notable exceptions being POC and PEC species. This is due to the AEDTProc code that was run for the 36km x 36km some time back having a bug for the vertical

allocation of the POC and PEC species. This has since been fixed and is represented correctly in the 12km x 12km grid resolution results.

We then looked at the vertical allocation of the monthly totals (Jan and Jul 2011) for six species across the grid resolutions. The vertical variations of emissions (CO, NO, NO_2, and SO_2) are matching between 12km x 12km and 36km x 36km, but POC and PEC show differences for the same reason explained above. Overall, air pollutant emissions contributed by aircraft in the North America are less than 5% (Table 3) from total emissions. These values are comparable to the numbers reported for Landing and take-off (LTO) 2005 emissions, and LTO aircraft emissions slightly increase (~10% for NO_x and SO_2) from 2005 to 2011, and this is explained by overall growth in aircraft activity.

Chemical Transport Model (CMAQ) Processing

CMAQ evaluations

Overall, the UNC team applied finer resolution and newer CMAQ configuration at 12x12 km for 2011 simulations, and covered full flight rather than LTO activity alone. We plan to run LTO-only next. We used the Atmospheric Model Evaluation Tool (AMET) v1.3 to evaluate CMAQ performance. O_3 error (40-70 % to 25-30%) and bias (40-70% to ~15%) have been significantly decreased for winter, summer and entire year (Table 4). CMAQ $PM_{2.5}$ performances for 2011 and 2005 are similar using these CMAQ configurations and it is worth to note that number of available sites for annual observations is small in 2005 and this could lead the performance bias. In general, errors and biases of most species are comparable with previous studies (Figure 6a) and domain wide annual average chemical composition highly matches between modeled results and field observations (Figure 6b). Based on above information, we conclude CMAQ performance for 2011 simulations is reliable to start to look at aircraft contributions.

Data analysis

Annual domain average of full flight attributable $PM_{2.5}$ is 0.003 ± 0.003 μg m^{-3}, and the contribution of 2005 LTO was ~0.001 μg m^{-3}. The highest impact (0.063 μg m^{-3}) is found in the San Francisco airport (SFO). Figure 7 shows the spatial variation of full flight attributable $PM_{2.5}$, the dark red hot spots are located in the airport grid-cells. There are regional dispersion areas in California Central Valley, Midwest, and Southeast, this regional dispersions have been reported (Woody 2011), secondary $PM_{2.5}$ formed when high NO_x aircraft emissions meet agricultural NH_3 emissions. Although, in 2005 simulations, only LTO was used, the spatial patterns between 2005 and 2011 are similar. Simulations of LTO impact for 2011 are still ongoing. Therefore, based on these evidences, LTO could have a greater impact on surface $PM_{2.5}$ concentrations than cruise emissions. Annual domain average full flight attributable O_3 concentration is 0.05 ± 0.04 ppb. However, in airport grid-cells, surface O_3 concentrations impacted by full flight are always negative due to NO_x titration. Similar to $PM_{2.5}$ hot spots, these O_3 depletion spots are concentrated in the grid-cells near airports (Figure 7). Ultimately, this provides additional evidence that even when full flight emissions are modeled; surface air quality is significantly impacted by aircraft activity during LTO rather than during cruise mode.

Looking into seasonal variation, secondary $PM_{2.5}$ contributions are changing by month (Figure 8). During summertime, the red areas are located in southeast section, whereas, during wintertime, California Central Valley and Midwest are important. Los Angeles Basin is an important full flight attributable secondary $PM_{2.5}$ region. Size of O_3 depletion (due to NO_x titration effects) change with seasons and there are some trajectories matching to regional flights. In general, larger O_3 depletion areas are seen in winter than summer near airports across the North America. These areas shrink in summer and are concentrated near airports (Figure 9). There are two hypotheses to explain this seasonal pattern. Planetary boundary layer is generally lower in winter than summer, which might enhance NO_x concentrations and NO_x titration could be more significant in winter. During summer time, humidity is higher than in winter, and this leads higher NO_3 deposition during nighttime and limits NO_x titration.

Full flight attributable $PM_{2.5}$ concentrations are 0.04, 0.05, and 0.02 μg m^{-3} at ATL, LAX, and ORD, respectively (Figure 10). In this resolution, we are able to separate the $PM_{2.5}$ hot spots between ORD and Midway airport. In LAX, high full flight attributable $PM_{2.5}$ are under the landing trajectories, it extends 3 grid-cells (36km). O_3 depletions at ATL, LAX, and ORD are -0.78, -0.80, and -0.53 ppb, respectively. The O_3 depletion areas are varying at these three airports. In ATL, the depletion area only extends one grid-cell from airports. Inversely, for LAX and ORD, the areas extend to multiple grid-cells. Our conclusion, after looking into full flight contribution in detail, is even when full flight emissions are considered, air quality impacted by aircraft activities is generally limited to near-airport areas with secondary contributions alone dominating at downwind distances.

$PM_{2.5}$ chemical compositions change from airport grid-cell to domain wide average (Figure 9); at top three airports we observed high fraction of elemental carbon, and it decreases to a small fraction for domain average. This is due to the fact that elemental carbon is mostly from direct aircraft emissions as primary aerosols and diluted after dispersion. Figure 11 shows large fraction of NO_3 for domain average which is hypothesized to be due to secondary formation. However, in the top three airports, there are some inconsistencies of full flight attributable chemical compositions. In ATL, high SO_4 but low NO_3 fraction, however, in LAX and ORD, we see a larger fraction of NO_3 than the fraction in ATL. We believe this to be due to changes in local chemical regimes associated with inorganic PM formation.

Table 1– Model configuration for meteorological inputs

Name	Description
WRF model version	WRFv3.8.1(Skamarock et al., 2008)
Simulation period	2011 with 3 month spin-up
Domain	Continental US (CONUS)
Spatial grid size	12X12-km
Number of sigma vertical layers	35 (with top layer at 50 hPa)
Input meteorological data sources	NASA MERRA for most of the variables, NCEP-FNL GFS for soil moisture and temperature, NCEP EMC for SST and NAM for snow
Planetary boundary layer scheme	Asymmetrical Convective Model version 2 (ACM2) (Pleim, 2007)
Cloud microphysics scheme	Morrison 2-moment scheme (Morrison et al., 2009)
Land surface model	NOAH (Mitchell et al., 2001)
Cumulus parameterization	Kain–Fritsch scheme (Ma et al., 2009)
Land use	NLCD40 (NLCD, 2011)
Short wave radiation	RRTMG (Iacono et al., 2008)
Long wave radiation	RRTMG (Iacono et al., 2008)

Table 2 – CMAQ Model Configuration

Options	Description	Note
Mechanism	CB05e51_AE6_AQ v5.1	
CTM_WB_DUST	Windblown dust v5.2	On
CTM_LTNG_NO	Hourly lightning NO_x v5.2	On
CTM_ILDEPV	Inline dry deposition v5.1	On
CTM_MOSAIC	Landuse specific deposition v5.1	On
CTM_ABFLUX	Bidirectional NH3 v5.1	Off
CTM_HGBIDI	Bidirectional Hg v5.1	Off
CTM_SFC_HONO	Surface HONO interaction v5.1	On
CTM_BIOGEMIS	Inline biogenic emission v5.1	On
CTM_PT3DEMIS	Inline plume-rise for point emissions v5.1	Off
CTM_ACAERO	Specific aerosol emissions for aircraft v5.0.2	Off

Table 3 – AEDT-based aircraft emissions in North America

	NO	NO_2	SO_2	Particulate SO4	Elemental carbon	Organic carbon	CO	TOG
2011 Aircraft full flight to total emission contribution (%)	3.6	4.1	0.7	1.3	0.3	<0.1	0.21	<0.1
2011 Aircraft full flight emission (tons)	614,579	72,197	60,713	1,858	1,605	1,444	177,525	29,501
2011 Aircraft LTO to total emission contribution (%)	0.5		<0.1	<0.1			<0.1	<0.1
2011 Aircraft LTO emission (tons)	96,187		7,874	594			56,731	11,397
2005 Aircraft LTO emission (tons)	83,248		7,217	638			62,669	13,841

Table 4 – CMAQ evaluation for 2011

	O_3 (ppb)				$PM_{2.5}$ (µg m^{-3})			
	MEAN OBS	MEAN MOD	NME	NMB	MEAN OBS	MEAN MOD	NME	NMB
Jan_2005	19.1	33.7	75.0	70.7	11.1	12.1	57.1	12.7
Jan_2011 base	23.9	25.6	31.1	2.1	11.6	12.5	53.4	1.6
Jul_2005	34.1	45.9	43.6	36.9	12.8	7.62	49.2	-36.0
Jul_2011 base	34.9	40.5	25.4	15.5	11	5.8	50.4	-43.9
2005	30.4	41.8	45.5	39.2	12.8	11.3	36.7	-10.4
2011_base	31.6	36.4	24.1	12.8	9.87	7.71	47.7	-24.7
2011_sens	31.6	36.5	24.2	13.0	9.87	7.72	47.7	-24.6

OBS: observations, MOD: model results
NME and NMB: Normalized Median Error and Normalized Median Bias

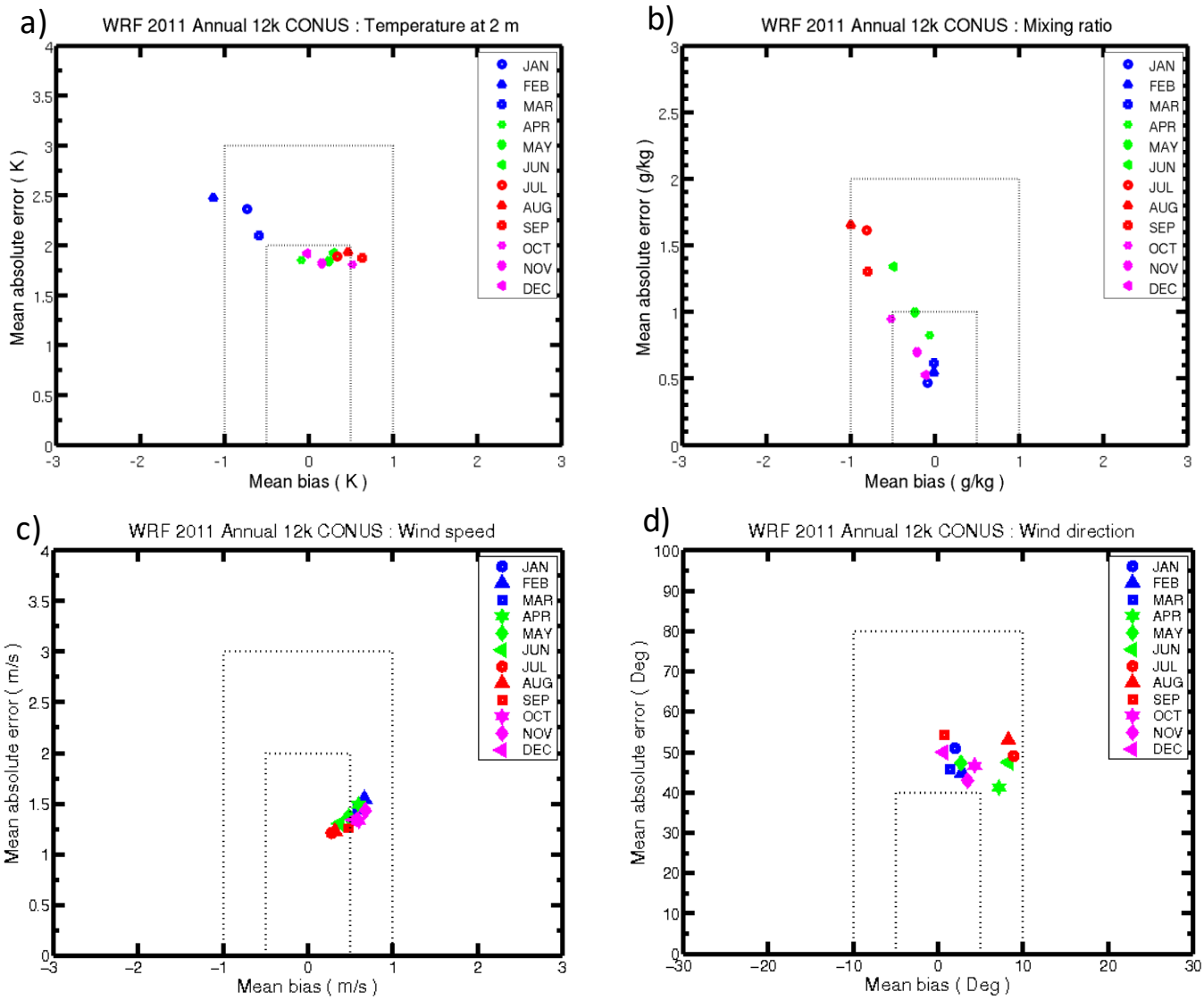

Figure 1 - Soccer plot for error vs bias of a) 2-m mixing ratio, b) 2-m mixing ratio, c) 10-m wind speed and d) 10-m wind direction averaged over the 12-km CONUS domain for all 12 months in 2011 [the inner dotted rectangle is the benchmark value limit for simple model and outer dotted rectangle is the benchmark value limit for the complex model (Moore, 2014)].

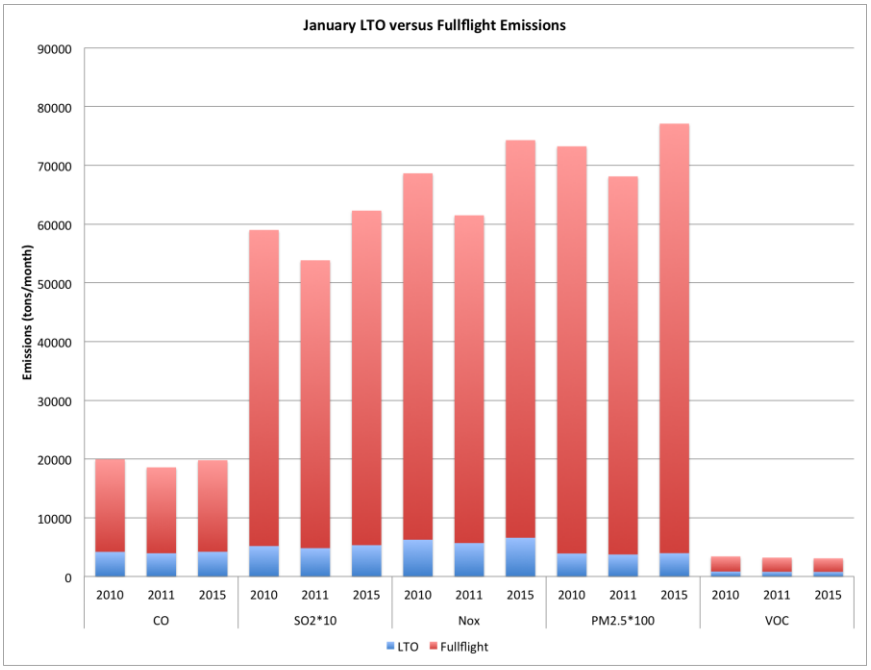

Figure 2 - LTO versus full flight January emission totals for five species across our three years' worth of data

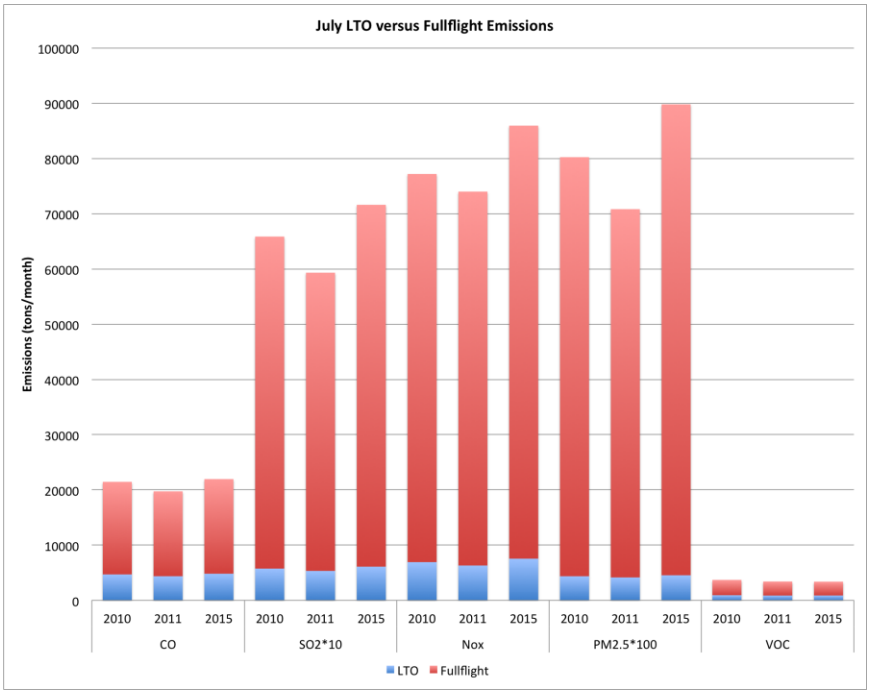

Figure 3 - LTO versus full flight July emission totals for five pollutants from AEDT across our three years' worth of data

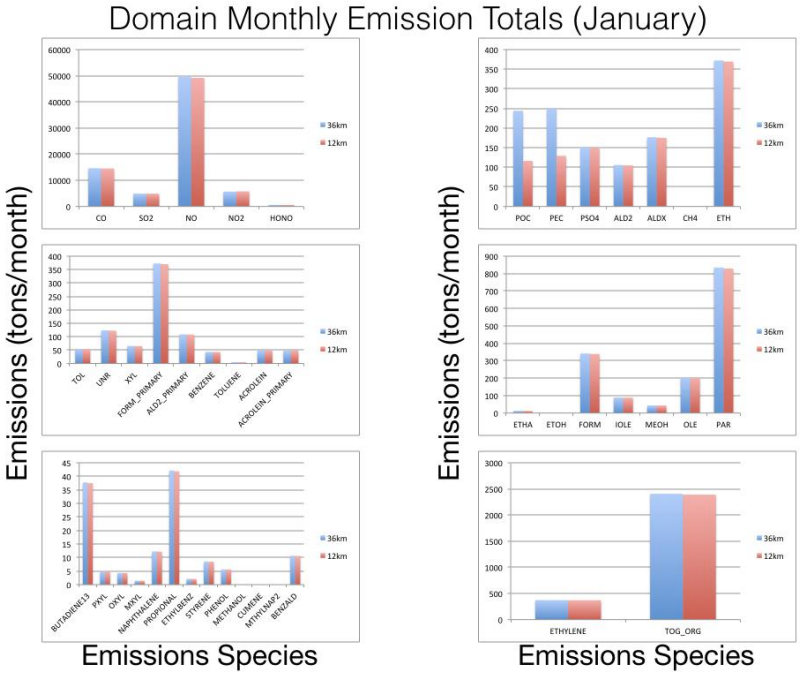

Figure 4 – Domain-wide Monthly Aircraft Emission Totals for January 2011 by model species.

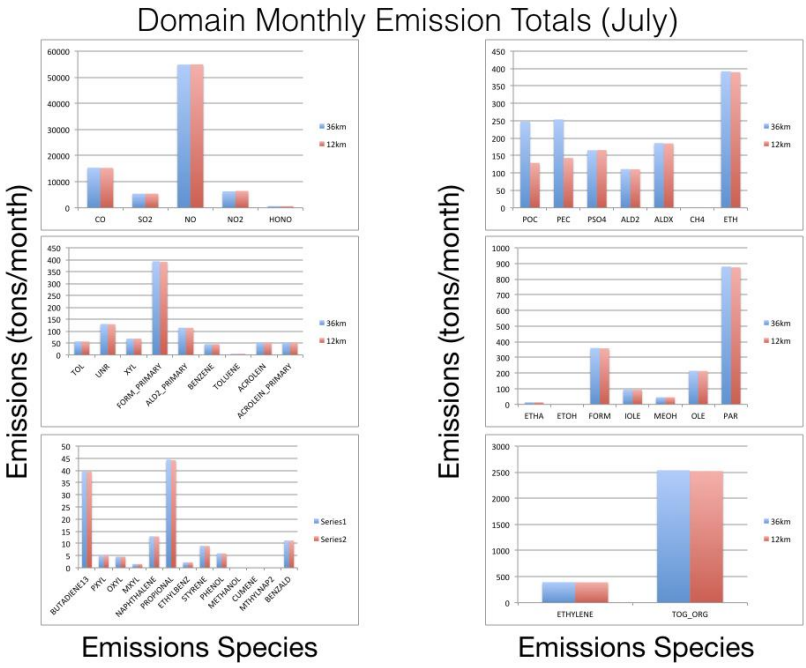

Figure 5 – Domain-wide Monthly Aircraft Emission Totals for July 2011 by model species.

a. Soccer plot for errors and biases by comparing CMAQ outputs with observations in 2011

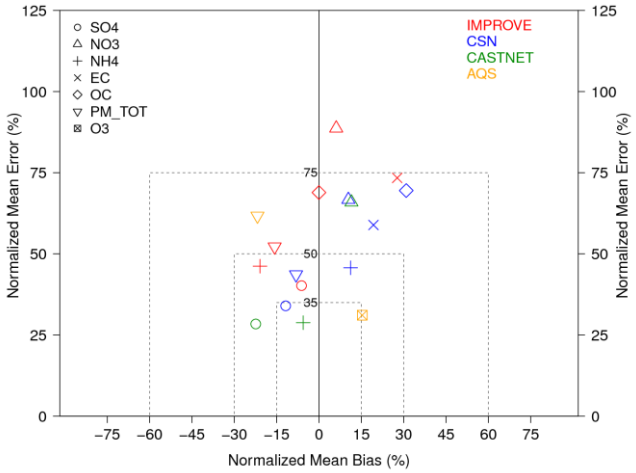

EC: Elemental Carbon
OC: Organic Carbon
PM_TOT: total $PM_{2.5}$
IMPROVE: Interagency Monitoring of Protected Visual Environment
CSN: Chemical Speciation Network
CASTNET: Clean Air Status and Trends Network
AQS: Air Quality System

b. Stacked bar plot for annual domain wide average chemical composition between CMAQ outputs with observations in 2011

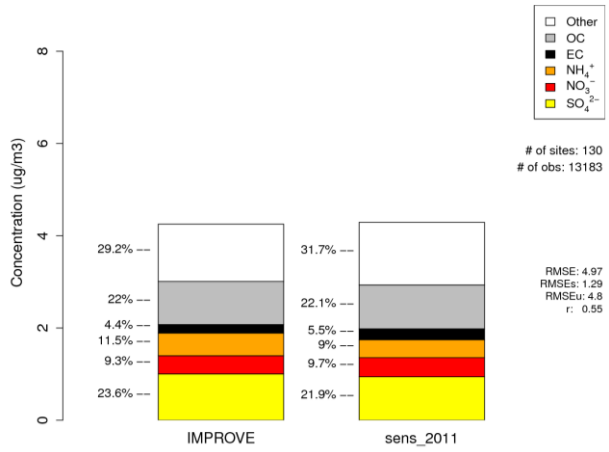

Figure 6 – Performance of CMAQ 2011 platform: a. soccer plot for errors and bias b. stacked bar plot for $PM_{2.5}$ chemical speciation.

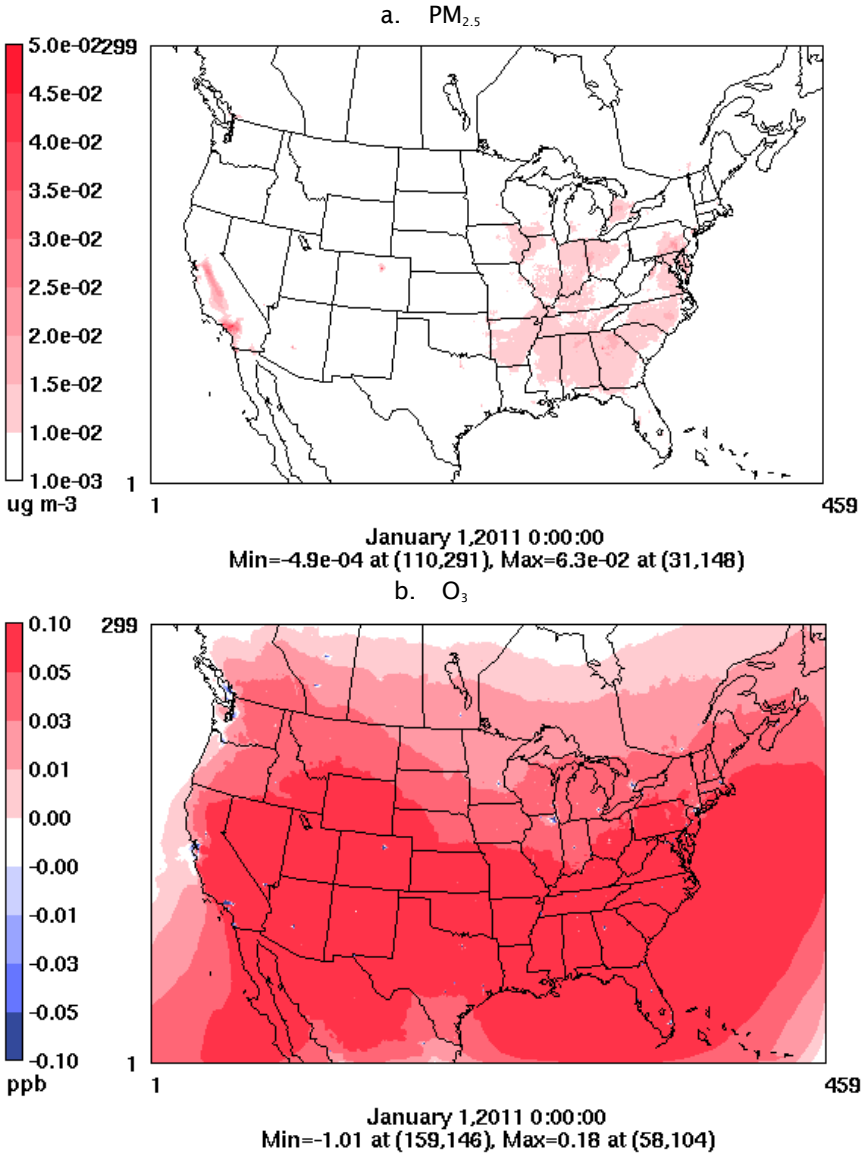

Figure 7 – 2011 Annual-average full flight attributable (a) $PM_{2.}$ and (b) O_3

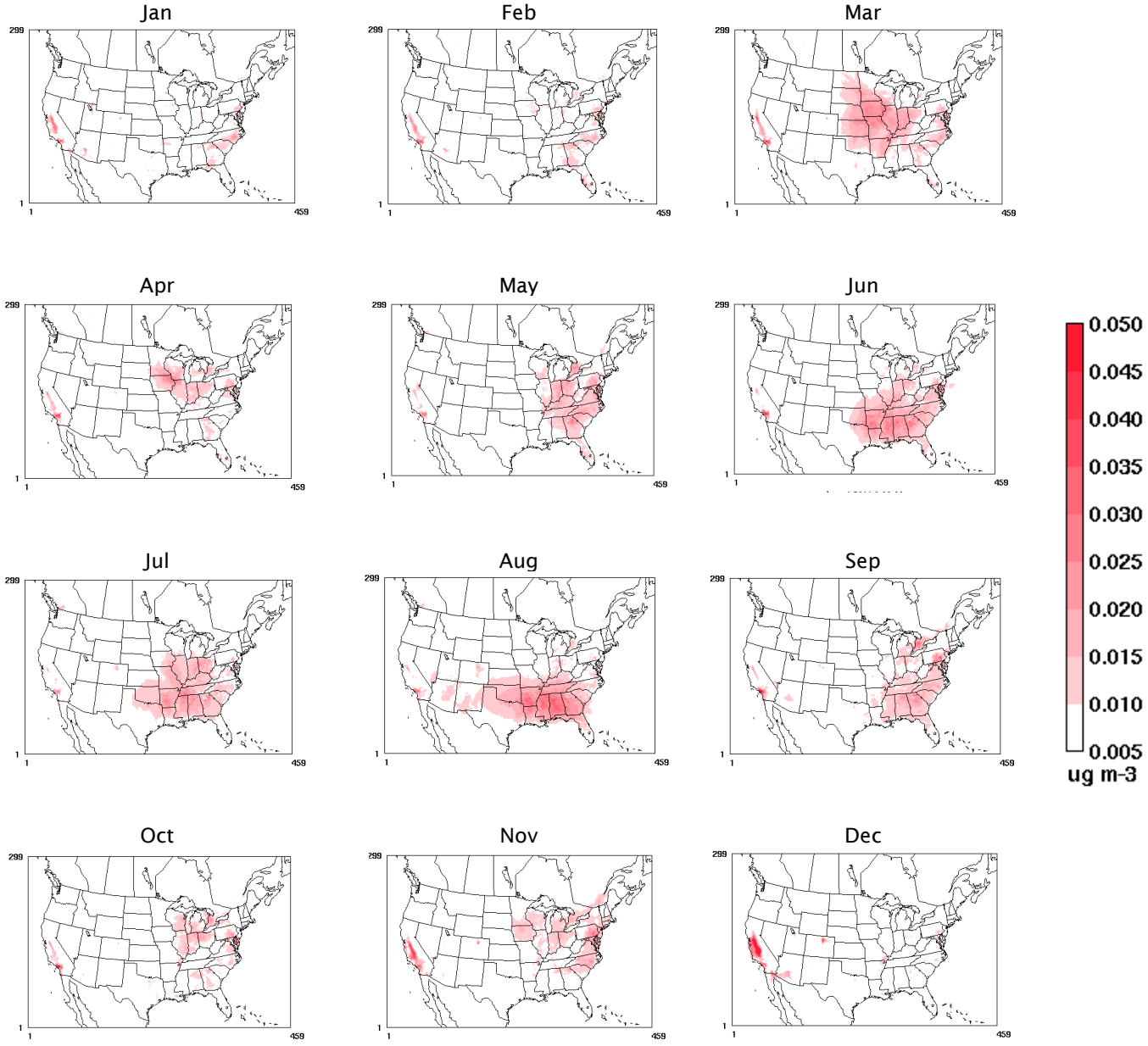

Figure 8 – 2011 Monthly average Spatial patterns of full flight attributable $PM_{2.5}$

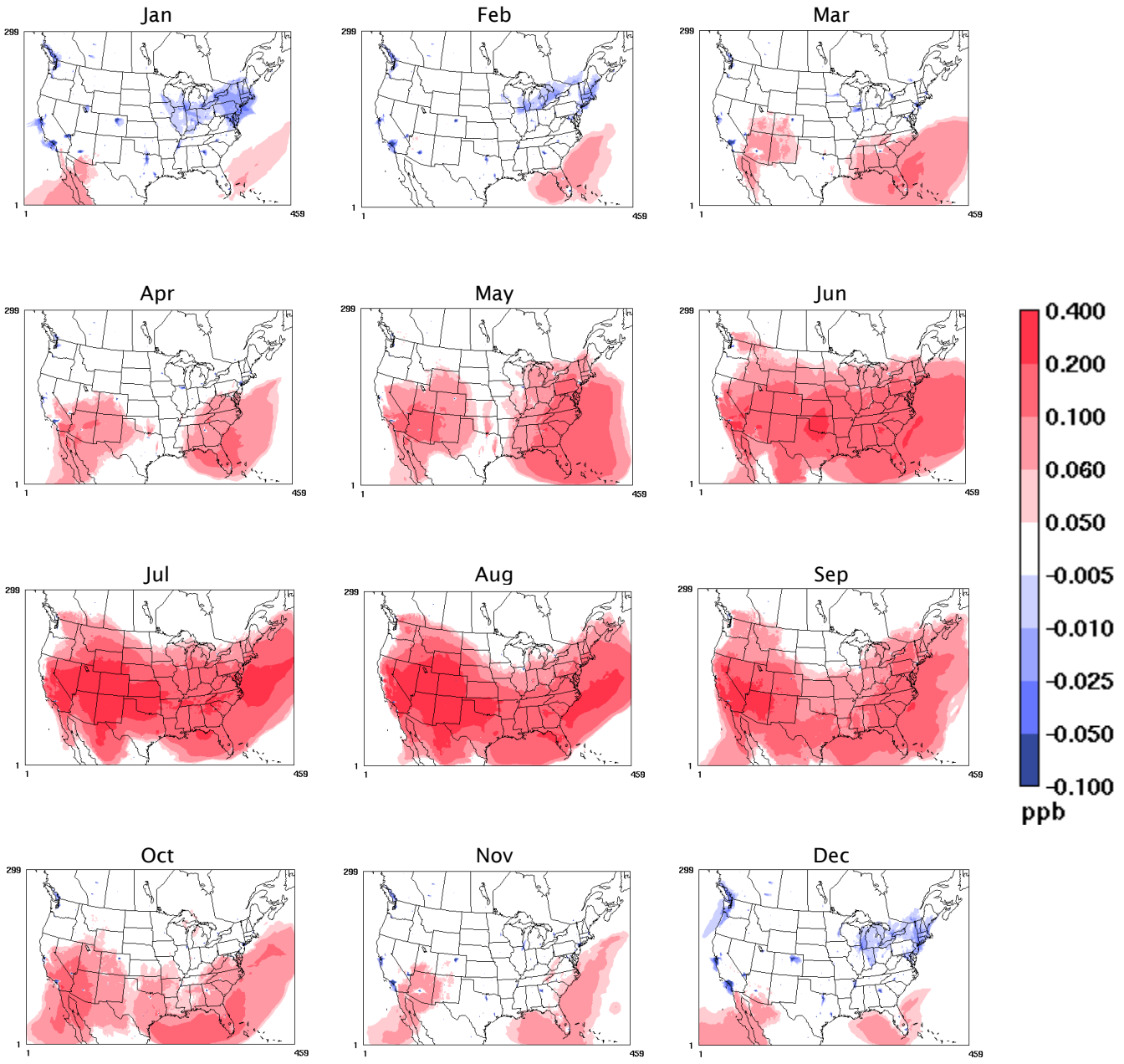

Figure 9 – 2011 Monthly average Spatial patterns of full flight attributable O_3

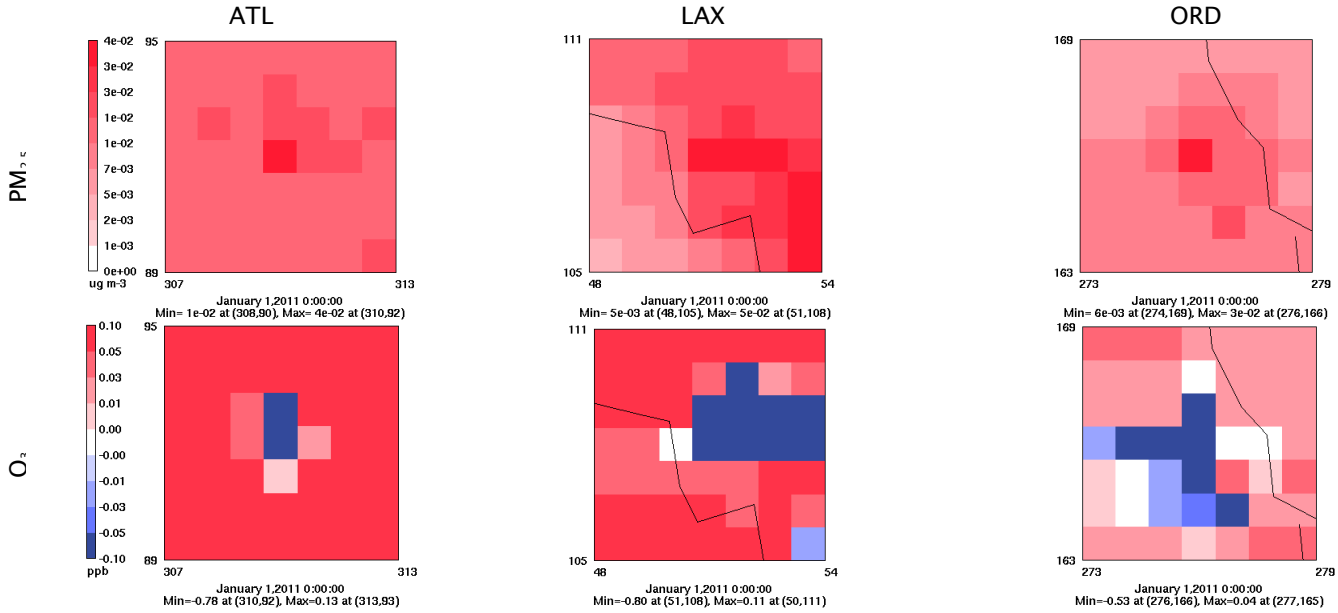

Figure 10 – 2011 Annual average full flight attributable $PM_{2.5}$ and O_3 for top three airports. Each square panel contains 7 × 7 grid-cells (84km × 84km), with airport located in the center of each square.

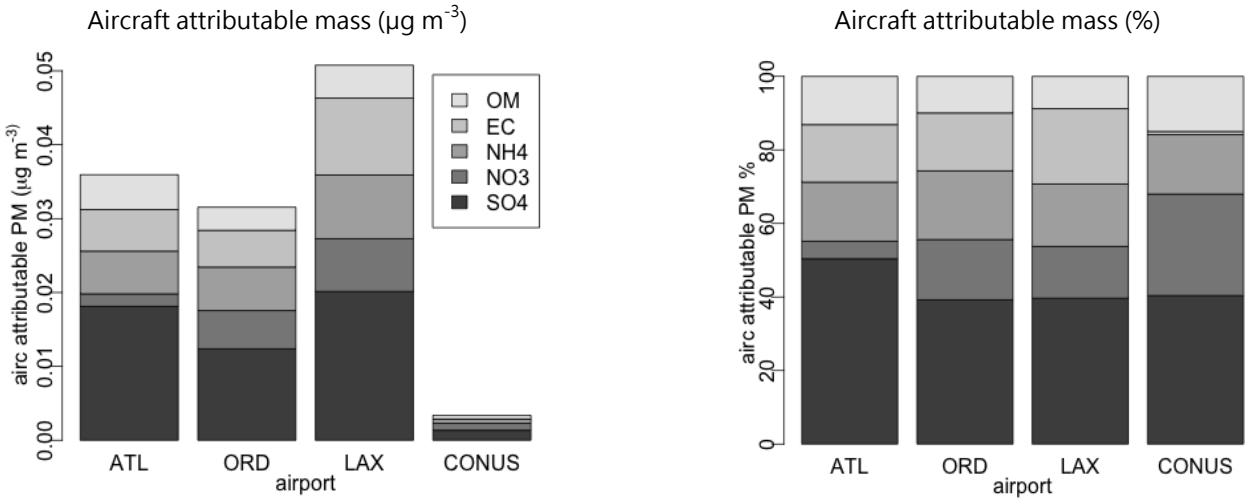

Figure 11 – Chemical composition of $PM_{2.5}$ at top three airports using domain average values.

Milestone(s)

Sep, 2017 – Completed running WRF for the 2011 using the finalized configuration
Sep, 2017 – Completed processing 2011 background emissions and full flight emissions
Sep, 2017 – Completed simulating 2011 base (non-aircraft emissions) scenario with CMAQ
Oct, 2017 – Completed simulating 2011 sensitivity (non-aircraft and aircraft emissions, full flight) scenario with CMAQ
Oct, 2017 – Completed assessment of aircraft-attributable impacts for new 12-km platform

Major Accomplishments

Quantified surface $PM_{2.5}$ and O_3 concentration contributed by full flight emissions for 2011, and performed extensive spatio-temporal analyses.

Publications

None

Outreach Efforts

Presentation at bi-annual ASCENT stakeholder meetings

Awards

None

Student Involvement

Calvin Arter is a Ph.D. student helping AEDT data preparation and evaluating 2011 full flight emissions.

Plans for Next Period

To complete surface air quality impacts from LTO for 2011
To simulate surface air quality impacts from LTO and full flight for 2015

References

Appel, K. W., Napelenok, S. L., Foley, K. M., Pye, H. O. T., Hogrefe, C., Luecken, D. J., Bash, J. O., Roselle, S. J., Pleim, J. E., Foroutan, H., Hutzell, W. T., Pouliot, G. A., Sarwar, G., Fahey, K. M., Gantt, B., Gilliam, R. C., Heath, N. K., Kang, D., Mathur, R., Schwede, D. B., Spero, T. L., Wong, D. C. and Young, J. O., 2017. Description and evaluation of the Community Multiscale Air Quality (CMAQ) modeling system version 5.1, Geoscientific Model Development, Volume 10, pp.1703-1732

Huang, J., Vennam, L. P., Benjamin N. Murphy, B. N., Binkowski, F., and Arunachalam, S., in preparation. A Nation-wide Assessment of Particle Number Concentrations from Commercial Aircraft Emissions in the United States.

Iacono, M.J., Delamere, J.S., Mlawer, E. J., Shepherd, M.W., Clough, S.A., and Collins, W.D., 2008. Radiative forcing by long-lived greenhouse gases: Calculations with AER radiative transfer models. Journal of Geophysical Research, Volume 113, D13103.

Ma, L-M, and Zhe-Min Tan, Z-M., 2009. Improving the behavior of the cumulus parameterization for tropical cyclone prediction: Convection trigger. Atmospheric Research, Volume 92, pp. 190–211.

Mitchell, K. E., and Coauthors, 2001: The Community Noah Land Surface Model (LSM)—user's guide (v2.2). [Available online at http://www.emc.ncep.noaa.gov/mmb/gcp/noahlsm/README_2.2.htm.]

Morrison, H., Thompson, G., and Tatarskii, V., 2009. Impact of Cloud Microphysics on the Development of Trailing Statiform Precipitation in a Simulated Squall Line: Comparison of One- and Two-Moment Schemes. Monthly Weather Review, Volume 137, pp. 991-1007.

Moore, T., 2014. Three-State Air Quality Modeling Study (3SAQS) -- Weather Research Forecast 2011 Meteorological Model Application/Evaluation, Report of Western Regional Air --Partnership c/o CIRA, Colorado State University 1375 Campus Delivery Fort Collins, CO 80523-1375.

National Land Cover Database 2011, http://www.mrlc.gov/nlcd2011.php

Pleim, J. E., 2007. A Combined Local and Nonlocal Closure Model for the Atmospheric Boundary Layer. Part I: Model Description and Testing. Journal of Applied Meteorology and Climatology, Volume 46, pp. 1383–1395.

Rienecker, M. M., Suarez, M. J., Gelaro, R., Todling, R., Bacmeister, J., Liu, E., Woollen, J., 2011. MERRA: NASA's modern-era retrospective analysis for research and applications. Journal of Climate, 24(14), 3624–3648. http://doi.org/10.1175/JCLI-D-11-00015.1.

Skamarock, W.C. and Klemp, J.B., 2008. A time-split nonhydrostatic atmospheric model for weather research and forecasting applications. Journal of Computation Physics, Volume 227, pp. 3465-3485.

Thiébaux, J., Rogers, E., Wang, W., and Katz, B., 2003: A New High-Resolution Blended Real-Time Global Sea Surface Temperature Analysis. Bull. Amer. Meteor. Soc., 84, 645–656, https://doi.org/10.1175/BAMS-84-5-645.

Woody, M.; Haeng, B.; Adelman, Z.; Omary, M.; Fat, Y.; West, J. J.; Arunachalam, S. 2011. An assessment of Aviation' s contribution to current and future fine particulate matter in the United States. Atmos. Environ. Volume 45, pp. 3424–3433.

Woody, M. C.; Arunachalam, S. 2013. Secondary organic aerosol produced from aircraft emissions at the Atlanta Airport: An advanced diagnostic investigation using process analysis. Atmos. Environ. Volume 79, pp. 101–109.

Task #2: Perform Airport-by-Airport Assessment Using CMAQ-DDM

University of North Carolina at Chapel Hill

Objective(s)

In addition to this NAS-wide assessment, to further refine the individual airport-by-airport modeling framework using the CMAQ v5.0.2 enhanced with the Decoupled Direct Method in Three Dimensions (DDM-3D), UNC-IE will use an advanced sensitivity tool to perform seasonal simulations. Previous work used this tool in CMAQ v4.7.1 to compute first order sensitivities. We will enhance this to use second order sensitivities in the latest CMAQ v5.0.2 and use these to perform quantitative analyses to assess the number of airports that will be needed to transition an area in attainment of the U.S. EPA's National Ambient Air Quality Standards (NAAQS) to non-attainment.

Research Approach

Introduction

Sensitivity analysis tools are often used within the air quality modeling framework to evaluate impacts due to changing input parameters in the model such as emission rates, initial conditions, or boundary conditions. These become important for utilizing models as a way to guide emission reduction policies. Sensitivity tools have been limited to finite difference and regression-based methods that often become computationally intractable and are often unable to describe *ad hoc* analyses. Furthermore, to calculate pollutant concentration sensitivities to LTO emissions we use the Decoupled Direct Method (DDM) in CMAQ. DDM methods calculate sensitivity coefficients in a single model run (Russell, 2005; Zhang et al., 2012) allowing for *ad hoc* analyses from changing multiple input parameters at a time. Most importantly, the use of DDM allows for the inline calculation of both first and higher order sensitivity coefficients, which become important for pollutant species that may not be linearly dependent on certain precursors. First order sensitivity calculations will yield information about the change in species concentrations with respect to varying one input parameter. In our case, these calculations will only describe linear changes of concentrations with respect to increasing or decreasing emissions from aircraft. However, some changes in species, such as secondary organic aerosols, do not linearly change with increasing or decreasing precursor emissions and higher order sensitivity coefficients can capture the non-linear change in species concentrations.

Methodology

Higher order DDM was implemented in CMAQ version 5.0.2. DDM becomes an ideal choice for describing aircraft (airport) emissions since the relatively small quantity of emissions emitted by each source can lead to numerical noise with other sensitivity methods that require multiple model runs for each varied parameter (Napelenok, Cohan, Hu, & Russell, 2006).

Our aim for this work was to quantify the amount of emission reductions needed at five individual airports to reduce the concentration of O_3 by 1 ppb and the concentration of $PM_{2.5}$ by 0.1 μg/m^3 at the grid cell containing the airport.

In order to choose the five individual airports, UNC-IE began with a list of all the airports located in the U.S. that are currently located in regions of attainment (nonattainment status of maintenance, marginal, or nonattainment) of the NAAQS for O_3 and PM. We selected from a list all airports that had at least 0.05% of annual passenger boardings designated as being a small hub according to the FAA's Voluntary Airport Low Emissions (VALE) program (FAA 2016). The final selection involved choosing airports across the country that represented the greatest geographic and climatic diversity while servicing major metropolitan areas (MSA population > 1,000,000 people). Table 5 shows the airport hub type (FAA 2016) and its description and Table 6 shows the tier status as defined by Woody et al. 2016, and its description. Figure 12 shows the 17 candidate airports from which we then selected our final five. Table 7 shows the list of 17 airports with various climate, traffic, and pollutant statistics. In consultation with the FAA, we chose Raleigh Durham International Airport (RDU), Boston Logan International Airport (BOS), Kansas City International Airport (MCI), Tucson International Airport (TUS), and Seattle-Tacoma International Airport (SEA) from the list of 17 candidate airports to model with HDDM.

Table 5 - Hub type descriptions

Hub Type	Percentage of Annual Passenger Boardings
Large	1% or more
Medium	At least 0.25%, but less than 1%
Small	At least 0.05%, but less than 0.25%

Table 6 -Tier number descriptions

Tier Number	Number of operations per month
I	Greater than 40,000
II	At least 20,000, but less than 40,000
III	Less than 20,000

Table 7 - List of candidate airports and criteria regarding climate, flight operations, and other pollutant NAAQS

	Size			Attainment Status		Population	Distance	Climate				
	Hub	The Emplaments		CO	SO2	MSA 2016	(km)	Average annual min temp © 1961 to 1990	Average annual max temp © 1961 to 1990	January 2016 Temp © (min, max, ave)	July 2016 Temp © (min, max, ave)	Average annual precipitation (in) 2005 to 2009
MSP	Large	1	16,972,678	Maintenance	Nonattainment/ Maintenance	3,551,036		0.11-2.93	10-15	-11.66, -4.32, -7.94	19.08, 28.87, 23.98	21-35
RDU	Medium	3	4,673,869	Maintenance		1,302,946		8.92-12.46	20-25	-0.84, 8.98, 4.07	22.4, 33.28, 27.76	36-50
MCI	Medium	3	4,982,722			2,104,509		5.86-8.92	15-20	-6.38, 3.80, -1.29	20.83, 30.91, 25.87	36-50
BOS[a]	Large[a]	2[a]	15,507,561[a]	Maintenance[a]		4,794,447[a]		2.93-5.86[a]	15-20[a]	-3.52, 4.18, 0.39[a]	19.69, 29.28, 24.48[a]	51-80[a]
MHT[b]	Small[b]		1,032,964[b]	Maintenance[b]		407,761[b]	72[a-b]	0.11-2.93[b]	10-15[b]	-5.49, 3.75, -1.37[b]	17.7, 30.02, 23.86[b]	51-80[b]
PVD[c]	Small[c]	3	1,764,828[c]			1,614,750[c]	79[a-c]	2.93-5.86[c]	15-20[c]	-4.51, 4.8, 0.15[c]	19.06, 29.8, 24.43[c]	51-80[c]
ABQ[d]	Medium	3[d]	2,354,184[d]	Maintenance[d]		909,906[d]		2.93-5.86[d]	20-25[d]	-3.17, 8.59, 2.71[d]	19.39, 35.37, 27.38[d]	0-20[d]
TUS[e]	Small[e]	3[e]	1,597,247[e]			1,016,205[e]	516[d-e]	8.92-12.46[e]	25-30[e]	3.8, 19.0, 11.4[e]	25.57, 39.16, 32.36[e]	0-20[e]
BUF[f]	Medium	3[f]	2,378,469[f]			1,132,804[f]		0.11-2.93[f]	10-15[f]	-6.65, 1.12, -3.76[f]	18.55, 28.31, 23.38[f]	36-50[f]
ROC[g]	Small[g]	3[g]	1,173,933[g]			1,078,879[g]	88[g-f]	2.93-5.86[g]	10-15[g]	-6.79, 1.76, -2.52[g]	17.64, 29.9, 23.77[g]	21-35[g]
SYR[h]	Small[h]	3[h]	987,169[h]	Maintenance[h]		656,510[h]	126[g-h]	2.93-5.86[h]	10-15[h]	-7.67, 0.96, -3.36[h]	17.22, 28.71, 22.97[h]	36-50[h]
SAT[i]	Medium	3[i]	4,046,856[i]			2,429,609[i]		12.46-19.43[i]	25-30[i]	4.38, 17.56, 11.02[i]	24.85, 36.21, 30.53[i]	21-35[i]
AUS[j]	Medium	3[j]	5,219,982[j]			2,056,405[j]	107[i-j]	12.46-19.43[j]	25-30[j]	2.12, 17.17, 9.64[j]	23.95, 36.53, 30.24[j]	21-35[j]
SEA	Large	2	17,888,880	Maintenance		3,798,902		5.86-8.92	20-25	3.54, 9.47, 6.51	14.24, 24.43, 19.33	36-50
MIA[k]	Large[k]	2[k]	19,471,456[k]							15.78, 23.49, 19.64[k]	35.7, 32.86, 29.28[k]	
FLL[l]	Large[l]	2[l]	12,031,860[l]			6,066,387[l]	34[k-l]	12.46-19.43[l]	25-30[l]	15.67 23.55, 19.61[l]	26.63, 32.5, 29.58[l]	51-80[l]
PBI[m]	Medium	3[m]	2,926,243[m]				68[l-m]			14.15, 23.05, 18.6[m]	28.8, 33.68, 30.13[m]	

Figure 12 - Locations of the 17 candidate airports (MHT and PVD underneath BOS with labels not shown)

CMAQ-DDM simulations instrumented to compute first and second order sensitivities were performed for the five airports for the months of January and July, 2005. Ten day spin-up simulations were performed prior to the start of each month (December and June, respectively). Six precursor species groups (NO_x, SO_2, VOCs, PSO_4, PEC and POC) were designated as sensitivity input parameters. First and second order sensitivities of O_3 and $PM_{2.5}$ to the emissions of these six precursors were calculated. First order sensitivities were of the form:

$$S^{1}_{i,j} = \frac{\partial C_i}{\partial E_j}$$

Eq. 2.1

While second order sensitivities were consisting of two forms:

$$S^{2}_{i,j} = \frac{\partial^2 C_i}{\partial {E_j}^2}$$

Eq. 2.2

$$S^{2}_{i,j,k} = \frac{\partial^2 C_i}{\partial E_j \partial E_k}$$

Eq. 2.3

Eq. 2.2 represents second order sensitivities to one emission species, while Eq. 3 represents second order cross sensitivities to two emission species.

Flight segment data from AEDT (Roof & Fleming, 2007; Wilkerson et al., 2010) were processed into gridded emission rate files using AEDTProc (Baek, B.H., Arunachalam, S., Woody, M., Vennam, L.P., Omary, M., Binkowski, F., Fleming, 2012). Landing and takeoff operations were considered by capping full-flight aircraft emissions at 3,000 feet. Our domain covered the continental United States with 36x36 km horizontal grid resolution and thirty-four time-varying pressure based vertical layers (LTO constrained to the first 17 layers around 3,000 feet or 914 meters). Sensitivities were calculated in the first model layer alone, to reflect where people live and are exposed to air pollution.

Other background anthropogenic emission sources were obtained from EPA's National Emissions Inventories (NEI-2005) and 2005 boundary conditions were derived from global CAM-Chem simulations (Lamarque et al., 2012). Meteorology

conditions for 2005 were obtained from the Weather Research and Forecasting model (WRF) (Skamarock et al., 2008) with outputs downscaled from NASA's Modern-Era Retrospective Analysis for Research and Applications data (MERRA) (Rienecker et al., 2011).

Results

We present spatial plots for one airport (SEA) as an example of the sensitivities we calculated for first and second order with respect to NO_x aircraft emissions. Figure 13 shows the first order (top row) and second order (bottom row) sensitivities of O_3 with respect to NO_x emissions from LTO activity at SEA for the months of January and July. Figure 14 shows the same but for $PM_{2.5}$ sensitivities to NO_x.

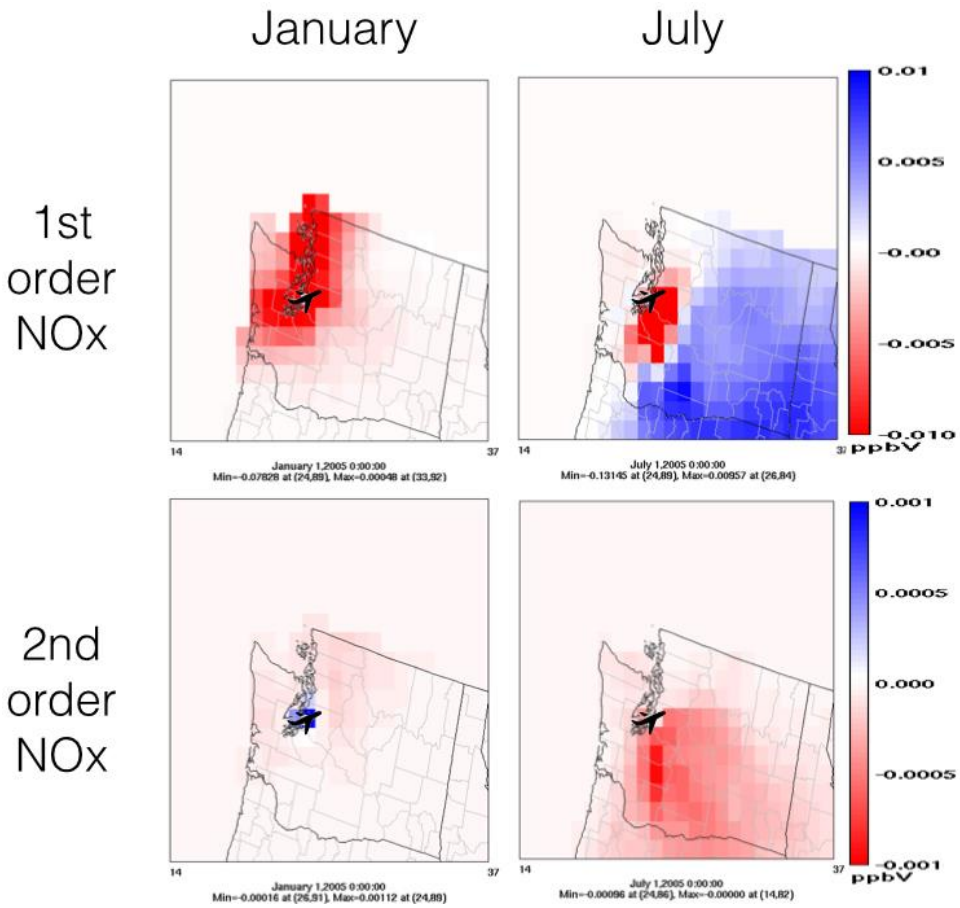

Figure 13 - O_3 first and second order sensitivity coefficients with respect to NO_x emissions at Seattle

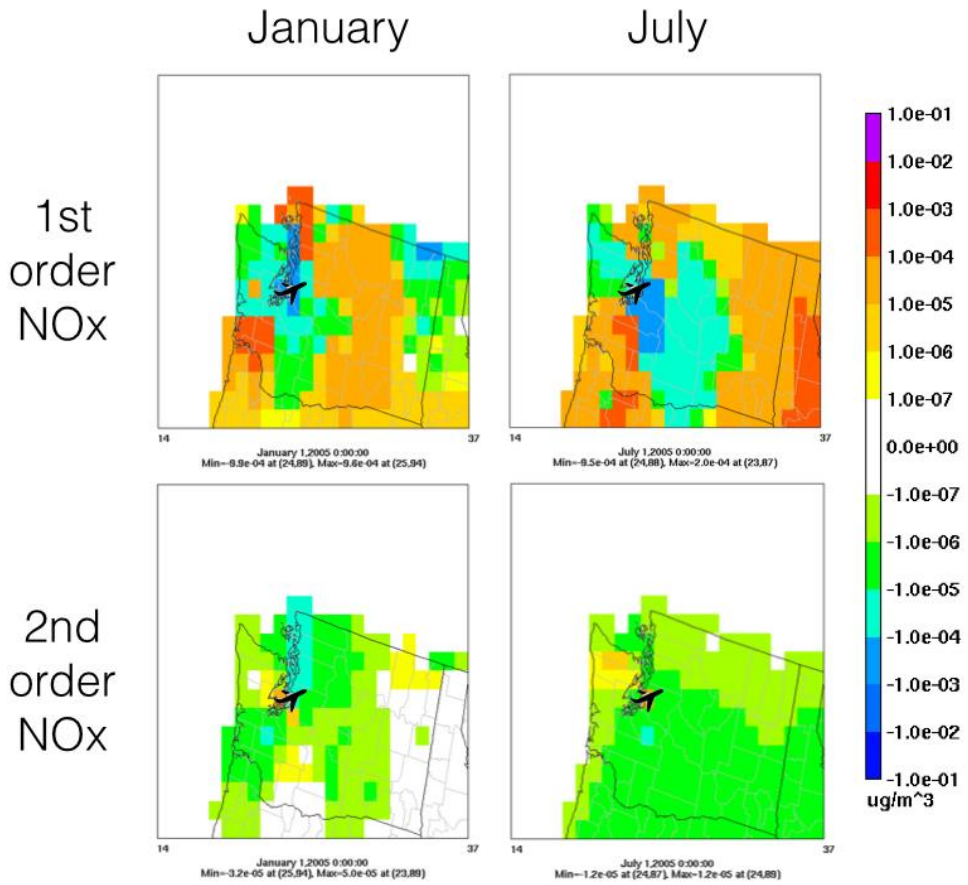

Figure 14 - $PM_{2.5}$ first and second order sensitivity coefficients with respect to NO_x emissions at Seattle

Spatial plots reveal how the emissions at the airport may impact regions downwind with sensitivities calculated at each model grid cell. However for our reduction analysis, we looked at emission reductions in the grid cell containing the airport. Figure 15 shows the pseudo-annual average (January and July averaged) sensitivities of O_3 with respect to NO_x and VOC emissions at each of the five airports. Figure 16 shows the pseudo-annual average sensitivities of $PM_{2.5}$ to NO_x, VOC, SO_2, PSO_4, POC, and PEC emissions at the five airports.

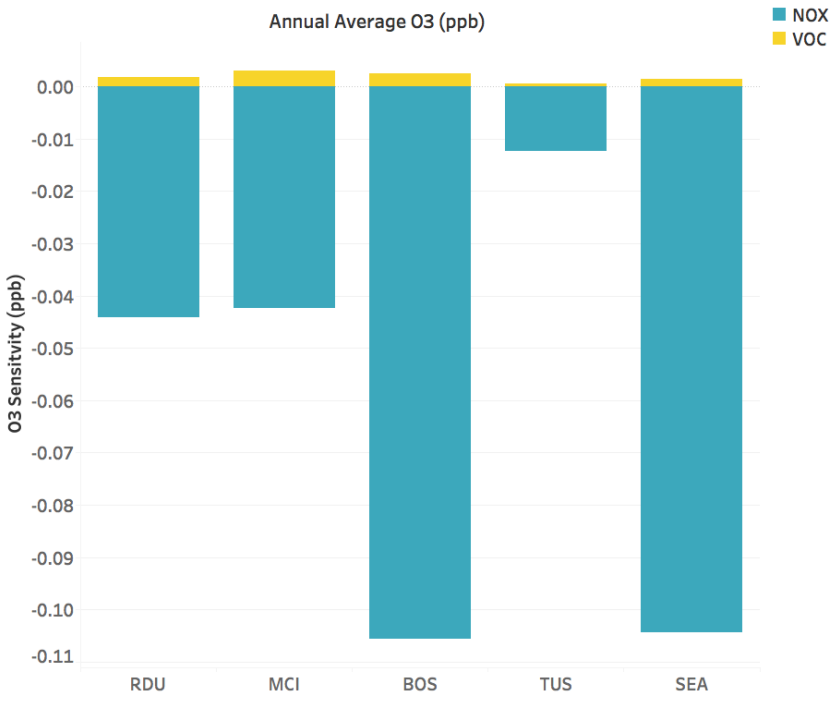

Figure 15 - O_3 sensitivities disaggregated by precursor species at grid cell containing airport

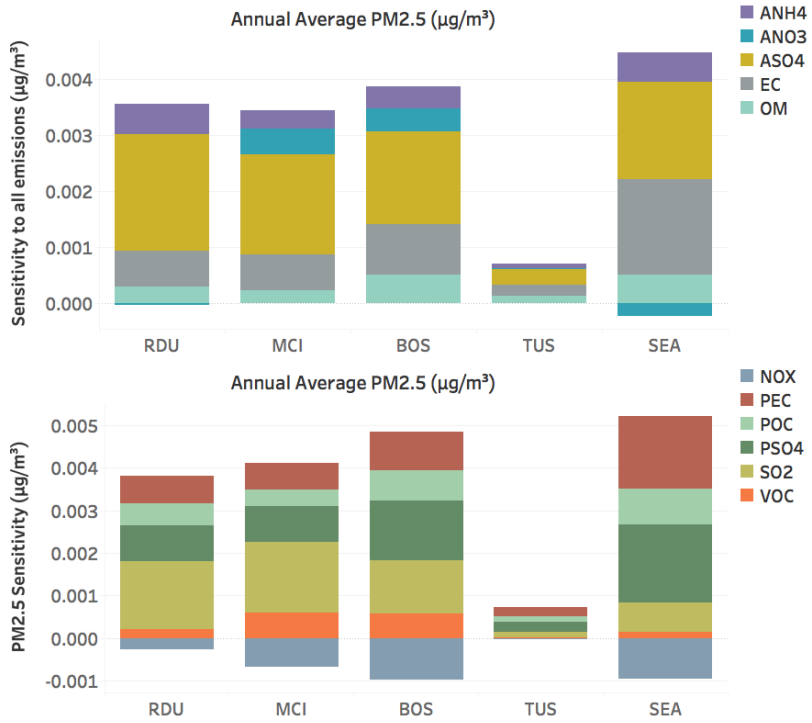

Figure 16 - $PM_{2.5}$ sensitivities disaggregated by output species (top) and precursor species (bottom) at grid cell containing airport

We can utilize Taylor series expansions with only first order sensitivities (Eq. 2.4) and with first and second order sensitivities (Eq. 2.5) to calculate the emission reductions needed to reduce concentrations of O_3 by 1 ppb or $PM_{2.5}$ by 0.1 µg/m³ at the grid cell containing the airport.

$$\sum_{j=1}^{n} C_{\epsilon_j} = C_0 + \Delta\epsilon_j S_j^1 \qquad \text{Eq. 2.4}$$

$$\sum_{k=1}^{n}\sum_{j=1}^{n} C_{\epsilon_j} = C_0 + \Delta\epsilon_j S_j^1 + \frac{\Delta{\epsilon_j}^2}{2} S_j^2 + \Delta\epsilon_j \Delta\epsilon_{j\neq k} S_{j,j\neq k}^2 \qquad \text{Eq. 2.5}$$

(n is the number of precursors, for O_3 $n = 2$, for $PM_{2.5}$ $n = 6$)

Figure 17 shows the emission reductions needed at each airport to reduce the concentration of O_3 at the airport grid cell by 1 ppb. The left side of the figure shows the emission reductions while the right side shows O_3 monitor values for 2005 and 2016 at the monitor closest to the respective airport. The positive reduction values indicate that a large disbenefit is seen in the airport grid cell. This indicates an *increase* in NO_x emissions is needed at the airport to decrease concentrations of O_3 by 1 ppb. Clearly, it is due to the large negative sensitivities at the location of the airport, indicative of a VOC-limited chemical regime in which NO_x emission controls result in more O_3 being produced.

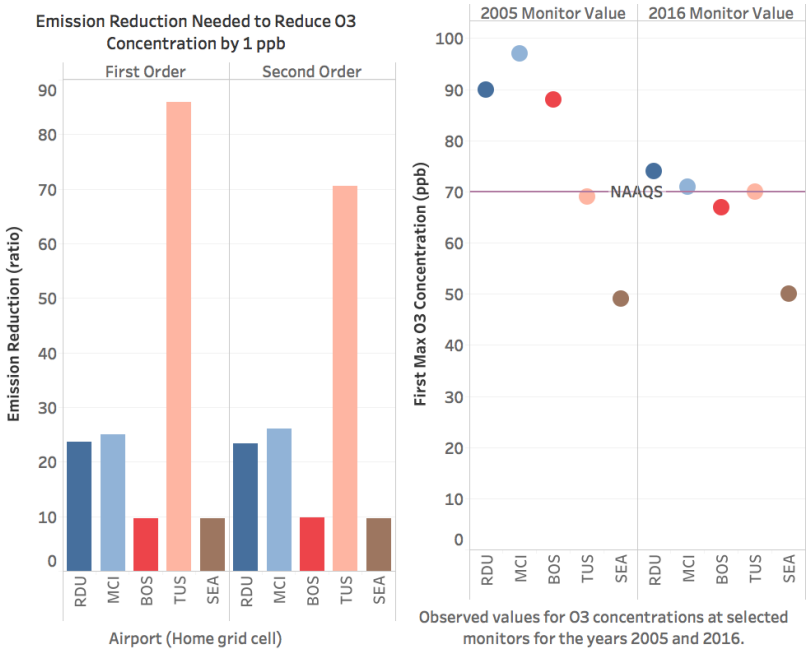

Figure 17 - O_3 reductions analyses (left) and 2005, 2016 observations (right).

Figure 18 shows the emission reductions needed at each airport to reduce the concentration of $PM_{2.5}$ at the airport grid cell by 0.1 µg/m³. As in Figure 17, the right side of the figure shows the emission reductions needed and the right side displays $PM_{2.5}$ monitor values for reference. Negative reduction values indicate that a reduction in precursor emissions at each of the airports will result in a reduction in ambient $PM_{2.5}$. The numbers are scaled relative to the total emissions at each airport with BOS needing for example, approximately 20 times less total emissions at the airport to reduce concentrations of $PM_{2.5}$ by 0.1 µg/m³.

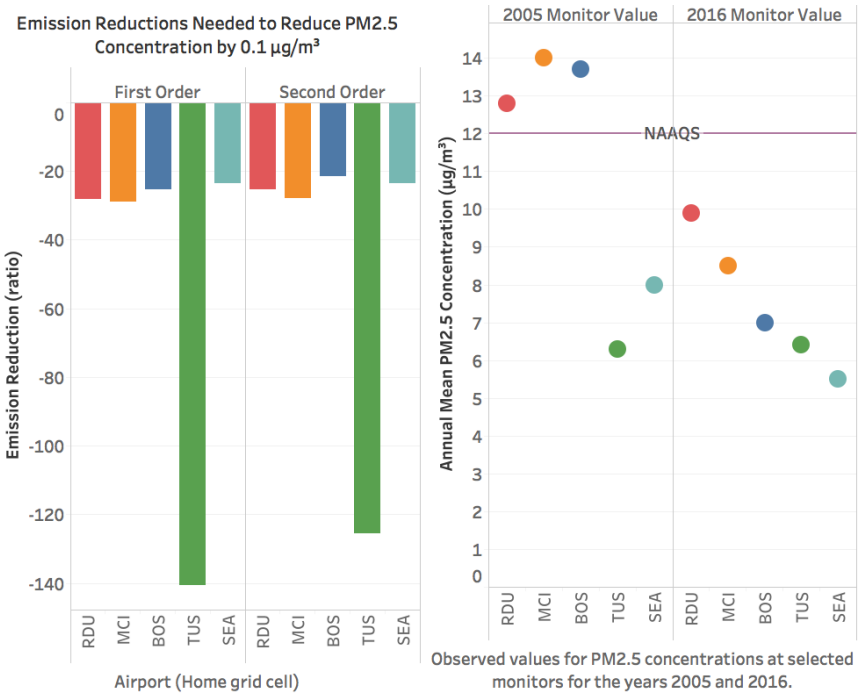

Figure 18 - $PM_{2.5}$ reductions analyses (left) and 2005, 2016 observations (right).

For both O_3 and $PM_{2.5}$ the differences between using only first order sensitivities and using both first and second order sensitivities are very small. The first order sensitivities dominate at the location of the airport and the non-linear chemistry, which the second order sensitivities will help describe, occurs downwind of the airport. We performed an analysis to look at the impact of LTO emissions downwind of Seattle-Tacoma International Airport.

We first looked to define regions where nonlinearity will be important. We utilized a nonlinearity ratio as described in Wang et al. (Wang et al. 2011). The ratio is defined as:

$$R_{C_i} = \frac{|0.5S^2|}{|S^1| + |0.5S^2|}$$

Eq. 2.6

Figure 19 shows the nonlinearity ratio plotted for sensitivities to NO_x emissions. NO_x was the only emission species to show nonlinear response with respect to both O_3 and $PM_{2.5}$ concentrations. The nonlinearity ratio results in a value from 0 to 1 where 1 describes a region that is highly sensitive to nonlinearity. We then selected grid cells with higher values of the nonlinearity ratio (approximately greater than 0.33) as well as the grid cell containing Seattle-Tacoma International Airport. Starting at a hypothetical $PM_{2.5}$ base concentration of 12 µg/m³, we utilized our first and first and second order Taylor series expansions (Eq. 4 and 5, respectively) to calculate the $PM_{2.5}$ response to an approximately 75% increase in NO_x emissions and approximately 50% increase in VOC emissions from Seattle-Tacoma International airport. Figure 20 shows the concentration response at each downwind location as shown in Figure 19 using only first order sensitivities (top) and using both first and second order sensitivities (bottom). It is clear that some locations downwind exhibit a different response when including second order sensitivities; with nonlinearity leading to a decrease in $PM_{2.5}$ from our base value while using only first order sensitivities shows an increase in $PM_{2.5}$ at those same locations.

In addition to the above analyses for airports in attainment areas, we expanded the framework to perform modeling and analyses at four of the largest airports in the nation and that are in non-attainment for O_3 and/or $PM_{2.5}$ - Atlanta (ATL), Chicago O'Hare (ORD), Los Angeles (LAX), New York (JFK) and computed 1st and 2nd order sensitivities for O_3 and $PM_{2.5}$, with the goal to assess changes in emissions needed to reduce O_3 by 1 ppb or $PM_{2.5}$ by 0.1 µg/m³ in the airport grid-cell.

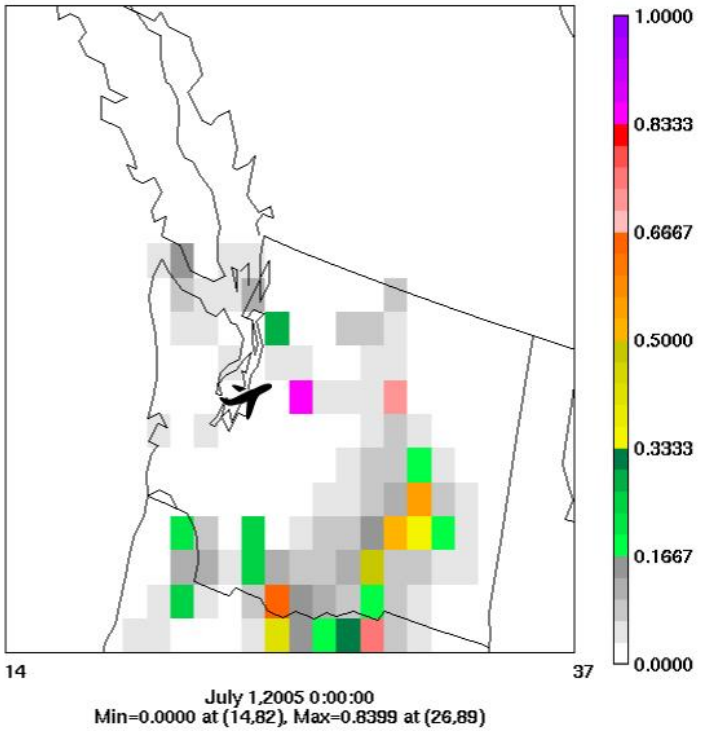

Figure 19 - Nonlinearity ratio plotted for Seattle-Tacoma International airport

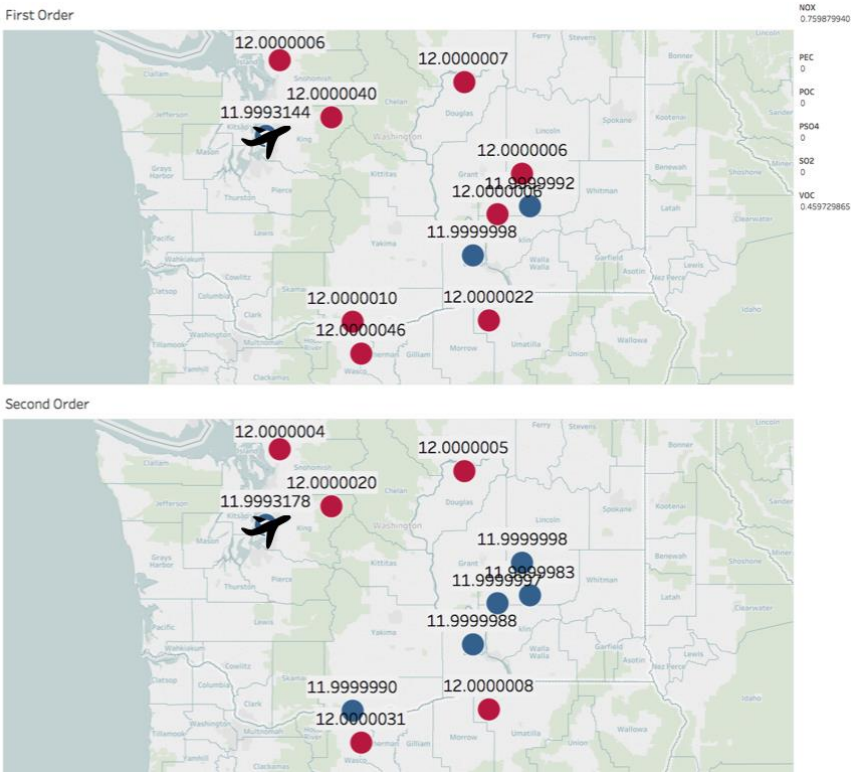

Figure 20 - $PM_{2.5}$ concentration response to increased NO_x and VOC emissions at Seattle-Tacoma International airport

Milestone(s)

Developed candidate short-list of airports for attainment analyses
Computed first and second order sensitivities for O_3 and $PM_{2.5}$ due to 5 airports in attainment areas, for the first time
Expanded framework to look at four additional large airports that are currently in non-attainment areas too.
Developed a novel approach using CMAQ with HDDM to quantify the impacts of airport-specific aircraft emissions on potential O_3 and $PM_{2.5}$ non-attainment.

Major Accomplishments

This is the first use of higher order sensitivities with respect to airport-specific aircraft emissions. We have demonstrated that higher order sensitivities are important for describing nonlinear effects and paint a more accurate picture with regards to the atmospheric chemistry that may be occurring in downwind regions of emission sources. Insights from this novel approach can be used for larger emission sectors to allow for more accurate emission reduction strategies.

In addition to the above 5 airports in attainment areas, we also expanded this work to look at four additional large airports that are in non-attainment areas – Atlanta (ATL), Chicago O'Hare (ORD), Los Angeles (LAX), New York (JFK) to look at 1st and 2nd order sensitivities for O_3 and $PM_{2.5}$.

Publications/Presentations

Arter, C. A. & Arunachalam, S. (2017). *Calculating Second Order Sensitivity Coefficients for Airport Emissions in the Continental U.S. Using CMAQ-HDDM.* Presented at the 2017 ASCENT Advisory Board Meeting, Washington, D.C.
Arter, C. A. & Arunachalam, S. (2017). *Calculating Second Order Sensitivity Coefficients for Airport Emissions in the Continental U.S. Using CMAQ-HDDM.* Poster session presented at the 2017 North Carolina BREATHE Conference, Raleigh, NC.
Arter, C. A. & Arunachalam, S. (2017). *Calculating Second Order Sensitivity Coefficients for Airport Emissions in the Continental U.S. Using CMAQ-HDDM.* Poster session presented at the 2017 University of North Carolina Chapel Hill Climate Change Symposium, Chapel Hill, NC.
Arter, C. A. & Arunachalam, S. (2017). *Using Higher Order Sensitivity Approaches to Assess Aircraft Emissions Impacts on O_3 and $PM_{2.5}$.* Poster session presented at the 2017 Annual CMAS Conference, Chapel Hill, NC.

Outreach Efforts

Presentation at bi-annual ASCENT stakeholder meetings in Spring and Fall 2017, Alexandria, VA.
Presentation to FAA and investigators during monthly Tools telecons
Presentation to New York City Metro Area Energy and Air Quality Data Gaps Workshop, organized by NYSERDA, Columbia University, May 2017

Awards

Calvin Arter – 1st prize ASCENT's Joseph A. Hartman Student Paper Competition 2017

Student Involvement

All of the work in the task has been performed by 2nd year PhD student, Calvin Arter

Plans for Next Period

The next steps for this research will be investigating the chemistry surrounding the second order sensitivities with the goal of explaining the nonlinearities we are seeing. This work will then be incorporated into a manuscript with the goal of publication within the next few months.

The HDDM methods will be used for a new modeling platform with a state of the science model. We will utilize the most recent version of CMAQ (v5.2) with HDDM and a model application for the continental U.S. at a 12km x 12km horizontal grid cell resolution, and using 2011 AEDT emission data.

References

Baek, B.H., Arunachalam, S., Woody, M., Vennam, L.P., Omary, M., Binkowski, F., Fleming, G. (2012). A New Interface to Model Global Commercial Aircraft Emissions from the FAA Aviation Environmental Design Tool (AEDT) in Air Quality

Models.

Boone, S., & Arunachalam, S. (**2014**). Calculation of sensitivity coefficients for individual airport emissions in the continental U.S. using CMAQ-DDM/PM. In *ACM International Conference Proceeding Series*. [10] Association for Computing Machinery. 10.1145/2616498.2616504

Lamarque, J. F., Emmons, L. K., Hess, P. G., Kinnison, D. E., Tilmes, S., Vitt, F., … Tyndall, G. K. (2012). CAM-chem: Description and evaluation of interactive atmospheric chemistry in the Community Earth System Model. *Geoscientific Model Development*, *5*(2), 369–411. http://doi.org/10.5194/gmd-5-369-2012

Napelenok, S. L., Cohan, D. S., Hu, Y., & Russell, A. G. (2006). Decoupled direct 3D sensitivity analysis for particulate matter (DDM-3D / PM), *40*, 6112–6121. http://doi.org/10.1016/j.atmosenv.2006.05.039

Rienecker, M. M., Suarez, M. J., Gelaro, R., Todling, R., Bacmeister, J., Liu, E., … Woollen, J. (2011). MERRA: NASA's modern-era retrospective analysis for research and applications. *Journal of Climate*, *24*(14), 3624–3648. http://doi.org/10.1175/JCLI-D-11-00015.1

Roof, C., & Fleming, G. G. (2007). Aviation Environmental Design Tool (AEDT). *22nd Annual UC Symposium on Aviation Noise and Air Quality*, (March), 1–30.

Russell, A. G. (2005). Nonlinear Response of Ozone to Emissions : Source Apportionment and Sensitivity Analysis, *39*(17), 6739–6748.

Skamarock, W. C., Klemp, J. B., Dudhi, J., Gill, D. O., Barker, D. M., Duda, M. G., … Powers, J. G. (2008). A Description of the Advanced Research WRF Version 3. *Technical Report*, (June), 113. http://doi.org/10.5065/D6DZ069T

Wilkerson, J. T., Jacobson, M. Z., Malwitz, A., Balasubramanian, S., Wayson, R., Fleming, G., … Lele, S. K. (2010). Analysis of emission data from global commercial aviation: 2004 and 2006. *Atmospheric Chemistry and Physics*, *10*(13), 6391–6408. http://doi.org/10.5194/acp-10-6391-2010

Zhang, W., Capps, S. L., Hu, Y., Nenes, A., Napelenok, S. L., & Russell, A. G. (2012). Model Development Development of the high-order decoupled direct method in three dimensions for particulate matter : enabling advanced sensitivity analysis in air quality models, 355–368. http://doi.org/10.5194/gmd-5-355-2012

X. Wang, Y. Zhang, Y. Hu, W. Zhou, L. Zeng, M. Hu, D. S. Cohan, and A. G. Russell, Decoupled direct sensitivity analysis of regional ozone pollution over the Pearl River Delta during the PRIDE- PRD2004 campaign, Atmos. Environ. **45**, 4941 (2011).

M.C. Woody, H.-W. Wong, J.J. West, S. Arunachalam, Multiscale predictions of aviation-attributable PM2.5 for U.S. airports modeled using CMAQ with plume-in-grid and an aircraft-specific 1-D emission model, In Atmospheric Environment, Volume 147, 2016, Pages 384-394, ISSN 1352-2310, https://doi.org/10.1016/j.atmosenv.2016.10.016.

U.S. Federal Aviation Administration. List of Commercial Service Airports in the United States and their Nonattainment and Maintenance Status, 2016

Task #3: Develop Generalized Gridding Tool for AEDT

Objective(s)

The objective of this task is to develop a generalized emissions gridding processor that can take AEDT chorded outputs and create inputs for any global or regional-scale model.

Research Approach

Introduction
The Federal Aviation Administration (FAA)'s Aviation Environmental Design Tool (AEDT) is a software system that dynamically models aircraft performance in space and time to produce fuel burn, emissions and noise. Full flight gate-to-gate analyses are possible for study sizes ranging from a single flight at an airport to scenarios at the regional, national, and global levels. AEDT is currently used by the FAA to consider the interdependencies between aircraft-related fuel burn, noise and emissions. Currently, AEDT outputs are used by multiple regional-scales and additional global air quality and climate models for various purposes. However, the process to take the AEDT outputs and grid them to the model's native resolution is not streamlined. In many cases, different modeling groups develop their own custom approach and "reinvent the wheel" that leads to inconsistency in methods.

To address this concern, the FAA has identified a need to develop a generalized emissions gridding processor that can process the Aviation Environmental Design Tool (AEDT) emissions to meet the needs of multiple models, including and not limited to CMAQ, GEOS-Chem, CAM5, CAMChem, MOZART, GOCART, NASA GISS-E, etc. Ideally, the generalized gridding processor should process the AEDT emissions for uniformly structured as well as unstructured variable grid models. It will process the AEDT segment level aircraft emissions data in dimension of x, y, z, and t, and assign the emissions to any types of modeling grid structures. It has the ability to grid emissions at various spatial resolutions from global to local, to temporally allocate emissions for variable time steps, and to chemically speciate emissions for various modeling platforms. FAA has informed us that the current gridding processor developed by the U.S. DOT's Volpe Center does not meet these specifications, and that it requires many duplicated intermediate output dataset files such as ASCII-formatted segmented aircraft emissions from AEDT Microsoft SQL Databases (DBs) to support various modeling platforms.

Objective
The overall objective of this task is to develop a generalized emissions gridding processor that can support all the specifications desired by FAA without compromising the computational speed and processing efforts. In 2012, UNC-IE developed the AEDT gridding processor called AEDTproc to process the segmented aircraft emissions from AEDT for use in CMAQ, the regional-scale air quality model used in various other FAA projects. AEDTProc has the capability to process emissions only during Landing and Takeoff (LTO), during cruise, etc. for a custom CMAQ modeling domain. UNC-IE will update/enhance the latest AEDTproc program to expand its capabilities beyond current CMAQ modeling needs, and to meet the needs of various regional and global-scale air quality and climate models. The enhancements for AEDTproc for Version 2 (AEDTProc V2 hereafter) include the following:

- Support various modeling projections (i.e., Latitude-Longitude, Polar Stereographic, Lambert Conformal, Mercator, UTM, etc.)
- Support structured (uniform) and variable (non-uniform) modeling grids
- Support altitude-based vertical coordinates layer structure
- Support multiple scale modeling domains (i.e., global, regional, and local scales)
- Support various temporal resolutions (i.e., hourly, daily, weekly, monthly, and so on)
- Support multiple chemical mechanisms (mole-based and mass-based emissions), along with using the FAA/EPA TOG speciation profile
- Support direct access AEDT segment level aircraft emissions from Microsoft SQL server
- Enable to read in the NetCDF format emissions and export the output data in NetCDF Climate and Forecast (CF) compliance format to support various air quality and climate models
- Optimization of AEDTproc to reduce the memory usage as well as the computational time
- Parallelization of AEDTproc Fortran code to take advantage of multiple processors on the servers
- Support of AEDTproc to run on both Linux OS and Windows OS platforms

Approach
To implement all of these capabilities into current AEDTproc, we divided the task into three stages.

Stage 1: First, we implemented the most of technical enhancements, such as multi-scale modeling domains, various map projections, structured/unstructured grids, various chemical mechanisms, various temporal allocations, and optimization and parallelization into the latest Linux-based AEDTproc program.

Stage 2: Second, we implemented the direct accessibility to Microsoft SQL Server on Windows OS into Linux-based AEDTproc to avoid generating any unnecessary intermediate output files from SQL databases prior to the AEDTproc runs.
Stage 3: In the third and final stage, we developed the Windows-based AEDTproc that can directly access MS SQL AEDT DBs on Window OS.

With all three stages completed, FAA or others users can run AEDTproc program on Windows OS machine to generate temporally/chemically/spatially allocated AEDT emissions to support various modeling platforms without generating external segment-level aircraft AEDT emissions files. During each stage of the AEDTproc development, we performed testing with various use cases provided that were identified (which include models with both structured and unstructured grids) along with implementing various QA procedures. The specific use cases we tested were:

- Models with structured grids: e.g. GEOS-Chem for global and CMAQ for regional to hemispheric scales.
- Models with unstructured grids: e.g. Model for Prediction Across Scales (MPAS) [See https://mpas-dev.github.io/ for more information]. The U.S. EPA is developing a Next Generation Model for Air Quality, that will use MPAS as the meteorological driver, and that will provide the horizontal and vertical grid structure.

The latest version of Linux-based AEDTproc has been developed to process only ASCII-formatted segmented AEDT aircraft emissions to create hourly gridded speciated emissions for CMAQ modeling runs. It obtains the modeling grid domain information (x, y, z), and temporal resolution (t) through MCIP (Meteorology-Chemical Interface Processor) meteorology input file for CMAQ model. So, the current version reads the MCIP outputs in NetCDF formats and the text-based AEDT segmented data, and outputs NetCDF format emissions file that can be directly read by CMAQ.

In the following sections, we describe the detailed methods UNC-IE used for the AEDTproc enhancements.

Stage 1: AEDTproc Enhancements on Linux OS
Prior to any development of AEDTproc on direct access to Microsoft SQL Server, UNC focused on implementing all the following specifications into our latest Linux-based AEDTproc program.

1) Various Input/output Format Support

Depending on the formats of three use case emissions input files, we updated AEDTproc program to read accordingly and output the results in NetCDF CF-compliant format to support various modeling platforms other than CMAQ model. Unlike CMAQ, GEOS-Chem, MOZART, and CAM-Chem are global 3-D chemical transport models (CTM) for atmospheric composition driven by meteorological inputs from the Goddard Earth Observing System (GEOS) of the NASA Global Modeling Assimilation Office (GMAO). The GEOS-Chem option will be used for all of the global 3-D models. To create the global CTMs-ready 3-D aircraft emissions file, a user needs to provide the NetCDF-formatted GEOS meteorological input data file to the AEDTPROC program.

2) Various Map Projections Support

Although AEDTproc has been fully tested to support Lambert conformal, Universal Transverse Mercator (UTM), and Latitude/Longitude projections, it has not been applied to other map projections like polar stereographic and Mercator. To support these other projections, UNC-IE obtained polar stereographic and Mercator projection-based CMAQ input file for this update in AEDTproc.

3) Various Output Temporal Resolution Support

As mentioned earlier, current AEDTproc output temporal resolution is based on temporal resolution in MCIP input file. In this update, we updated AEDTproc for users to define their own temporal resolution of output emission values (i.e., hourly, daily, weekly, and so on) to support various modeling platforms.

4) Various Chemical Speciation Allocation Support

We updated AEDTproc to support more than CMAQ-ready chemical speciation profiles (such as Carbon Bond 2005) to support other regional or global-scale models. For CMAQ, the speciation profile is based upon the FAA-EPA Total Organic Gases (TOG) speciation profile developed in 2009 (U.S. EPA, 2009). The tool is now designed to read a specific input list of chemical species and the associated mass fractions as a stand-alone text input file. It then reads the input VOC emissions from AEDT, converts to TOG and then speciates based on the assigned mass fractions, thus providing complete flexibility to the user depending on the modeling system.

5) Unstructured Modeling Grid Support

We implemented this feature into AEDTproc to support unstructured/variable grids, specifically based on the MPAS file structure. This is a significant update to AEDTproc's capability to read and grid unstructured grids, as opposed to uniform grids. The defining features of MPAS are the unstructured Voronoi meshes and C-grid discretization which are used as the basis for many of the model components. The unstructured Voronoi meshes, formally Spherical Centroidal Voronoi Tesselations (SCVTs), allow for both quasi-uniform discretization of the sphere and local refinement. Figure 21 shows an example of horizontal and unstructured grids that are used by CMAQ and MPAS respectively.

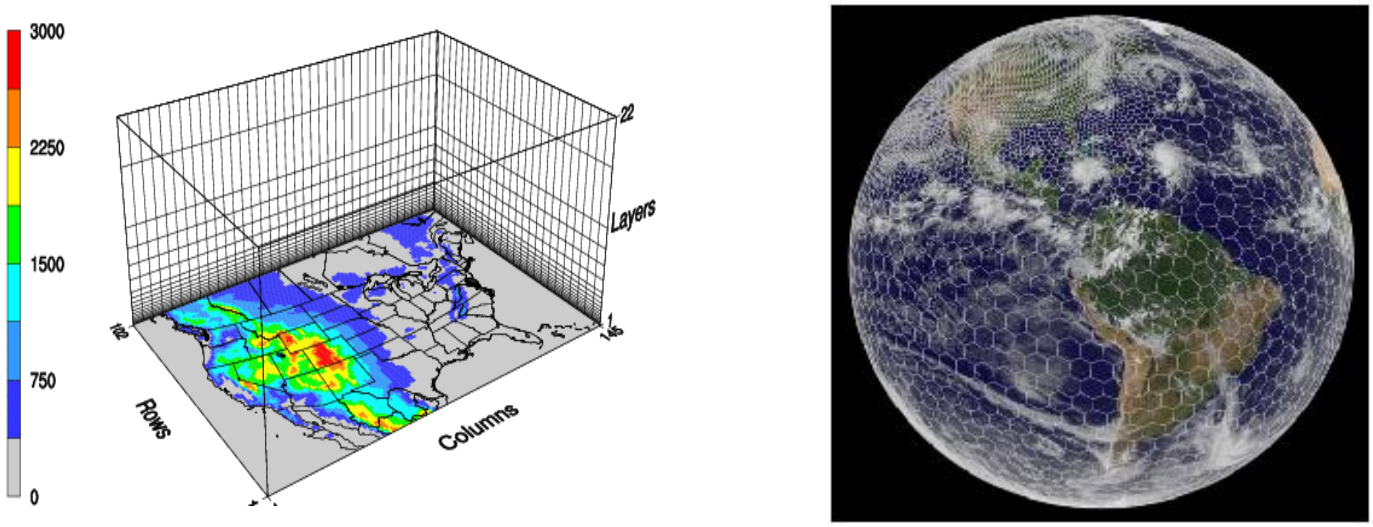

Figure 21 - Uniform horizontal grid structure (left) and unstructured grid structure (right) [Right figure courtesy NCAR]

Stage 2: Linux-based AEDTproc Direct access MS SQL on Windows OS

Once Linux-based AEDTproc development in Stage 1 was completed, UNC added a critical new feature in this task, which allows AEDTproc direct access to Microsoft SQL server to extract AEDT segment-level aircraft emissions directly from the SQL database. This will eliminate the preprocessing steps in current approach, which generates the ASCII-formatted segment-level aircraft emissions AEDT model using the FAA's Power Shell scripts prior to AEDTproc runs. These scripts read the AEDT SQL database, and output ASCII files to be read by AEDTProc.

Because the MS SQL Server that holds AEDT segment-level aircraft emissions is installed on Windows OS, two additional drivers for Fortran-based AEDTproc program are required to directly connect to MS SQL server. Figure 22 shows the schematic of this approach between two different OS (Linux and Windows). First, one needs to install the open source Fortran ODBC driver, called FLIB. FLIB allows Fortran compiled program to directly access standard SQL DBs using ODBC (Open Database Connectivity) which is a standard programming language middleware application programming interface (API). However, since MS SQL Server is not compatible with ODBC, we installed the ODBC driver for MS SQL server on RedHat Linux OS developed by Microsoft. This driver allows FLIB library to directly access MS SQL AEDT DBs through ODBC.

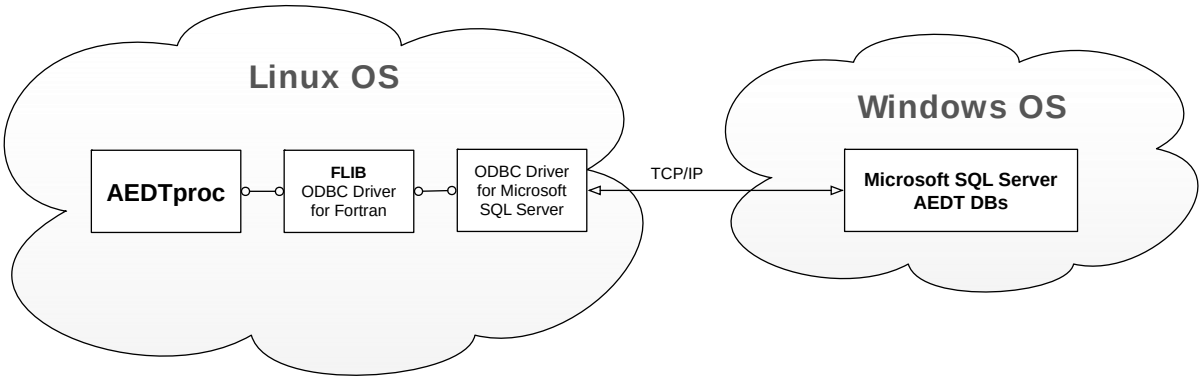

Figure 22 - Schematic of Connectivity between AEDTproc on Linux OS and MS SQL Server on Windows OS

Stage 3: AEDTproc direct access MS SQL on Windows OS
Once the stage 2 work was completed, the UNC team compiled the updated AEDTproc program on Windows OS with windows-based Fortran compiler using Cygwin that provides similar functionalities and environment of Linux on Windows OS. Unlike Stage 2, AEDTproc program now runs on the same Windows OS where MS SQL Server is installed. Based on our testing, we did see some level of computational speed-up due to a faster connectivity between ODBC driver and MS SQL Server.

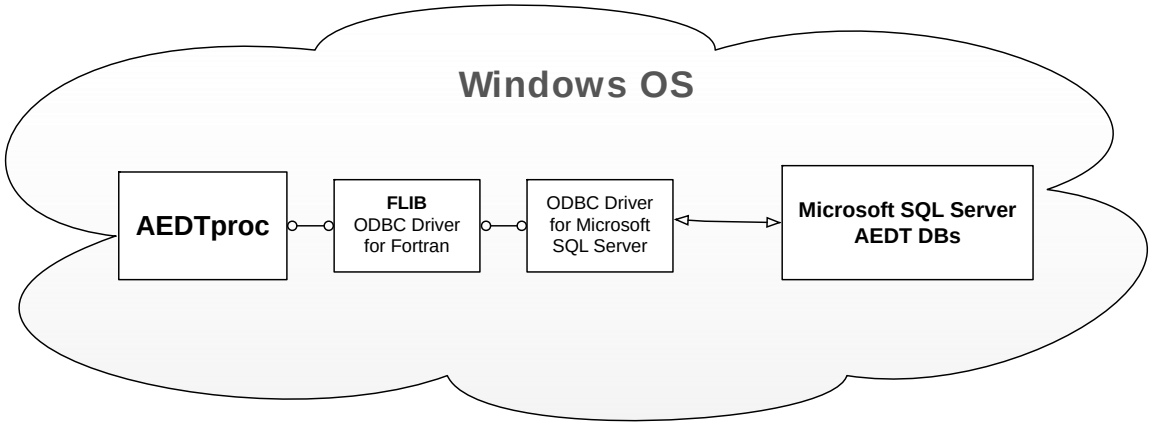

Figure 23 - Schematic of Connectivity between AEDTproc and MS SQL Server on Windows OS

Results

AEDTProc for GEOS-5 gridding
To perform emissions magnitudes QA, UNC-IE first used AEDTProcv2 to grid for a global domain using GEOS-5 meteorology, and then windowed for the continental U.S. We then compared aircraft emissions for a single day in 2011 January 2 generated using AEDTProc v2 with GEOS-5 to the data generated using AEDTProc v2 with MCIP for CONUS total (Table 8). Overall, differences between these two versions are relatively low (up to 11%), and are likely explained by small differences in the domain extents as well as different assumptions in vertical grid structure between the two models.

Table 8 - Differences in CONUS aircraft emissions for 20110102 using GEOS-5 (AEDTProc V2) and MCIP (AEDTProc) V1)

	(AEDTProc V2 for 2011 GOES5 – AEDTProc V1 for 2011 MCIP)/AEDTProc V2 for 2011 MCIP (%)
CO	-11
NO	-3.7
SO2	-8.8
Black carbon	-9.0

AEDTProc for CMAQ gridding: UNC-IE tested AEDTProcv2 versus AEDTProcv1 for one day's worth of AEDT flight data. Domain emission mass totals generated by AEDTProcv2 are comparable to emissions generated from the same day's worth of AEDT data with AEDTProcv1. Figure 24 shows the emissions as a function of model layer for AEDTProcv2 and two different versions of AEDTProcv1 (one version has a correction to the POC/PEC allocation). The results are quite comparable across the two versions.

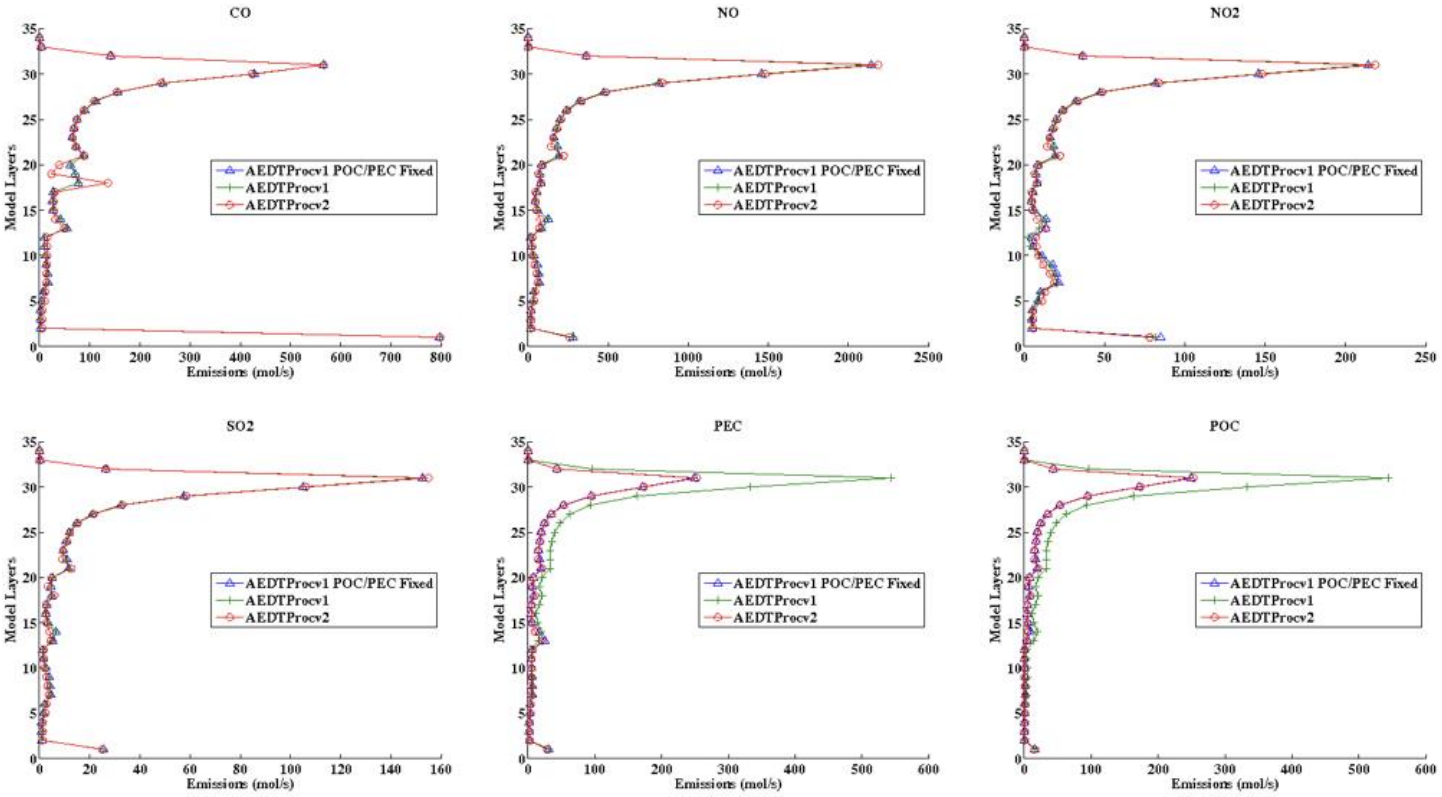

Figure 24 - Vertical profiles for CO, NO, NO_2, SO_2, POC, and PEC emissions from one day's worth of full flight emissions

Milestone(s)
AEDTProcv2 enhanced to support additional features
AEDTProcv2 support now includes both structured and unstructured grids
AEDTProc v2 now can read SQL database directly from AEDT and create gridded emission files for regional-scale and global-scale air quality models.
User's Guide and Demonstration given to the FAA AEE

Major Accomplishments
UNC-IE developed AEDTProc V2 with several substantial enhancements as initially scoped, and delivered tool, user's guide and demonstration to the FAA AEE.

Publications
None

Outreach Efforts
Presentation at bi-annual ASCENT stakeholder meetings in Spring and Fall 2017, Alexandria, VA.

Awards
None

Student Involvement
Calvin Arter, 2nd year Ph.D. student played a key role in testing AEDTProcv2 for CMAQ domain, and performing various QA steps.

Plans for Next Period
None

References
U.S. EPA, 2009. Recommended Best Practice for Quantifying Speciated Organic Gas Emissions from Aircraft Equipped with Turbofan, Turbojet, and Turboprop Engines. EPA-420-R-09-901 and 902.

William C. Skamarock, Joseph B. Klemp, Michael G. Duda, Laura Fowler, Sang-Hun Park, and Todd D. Ringler, 2012. A Multi-scale Nonhydrostatic Atmospheric Model Using Centroidal Voronoi Tesselations and C-Grid Staggering. Monthly Weather Review, 240, 3090-3105, doi:10.1175/MWR-D-11-00215.1

MPAS Home, https://mpas-dev.github.io/ [Last accessed November 18, 2017]

Task #4: Provide Support for High Fidelity Weather in AEDT

Objective(s)
The objectives of this task are to assist U.S. DOT Volpe Center to modify AEDT to use appropriate high fidelity weather data, such as from NASA's MERRA or MERRA-2, and to modify AEDT to directly use outputs from the Weather Research Forecast (WRF) model.

Research Approach
In this continuation task from last year, UNC-IE assisted FAA contractor Volpe Center in the identification, acquisition and implementation of high fidelity weather data from global scale datasets for use in the Aviation Environmental Design Tool (AEDT) for developing aviation emissions inventories. Specifically, we worked with U.S. DOT's Volpe Center (and ATAC) for implementing the Modern Era Retrospective Analyses for Research and Applications (MERRA)2 (Rienecker et al., 2011) dataset to derive meteorological fields in AEDT's calculations. Prior to this, UNC reviewed all available datasets with global coverage and recommended that MERRA be the choice of data for driving AEDT with high fidelity weather. Once we learned that NASA was in the process of migrating from MERRA to MERRA-2 (Bosilovich et al., 2015), we also recommended that

FAA move to MERRA-2. UNC-IE continued to engage with NASA developers as necessary and assisted Volpe in developing and implementing the prototype tool for use in AEDT. In addition to using MERRA-2, we also assisted Volpe to adapt AEDT to process higher resolution meteorological fields from the Weather Research and Forecast (WRF) model. WRF is a limited-area model typically used to prescribe meteorology for CMAQ – the regional scale air quality model that UNC-IE has used for several years in support of FAA's PARTNER and ASCENT COE-related research, and other ongoing activities.

Through these enhancements in AEDT, we aim to achieve the following:

a) Consistent large-scale forcings from MERRA used to drive both global-scale (and sometimes regional-scale) air quality applications and emissions estimation from AEDT
b) Consistent regional-scale forcings from WRF used to drive regional-scale air quality applications and emissions estimation from AEDT.

UNC's assistance to the FAA contractors included the following:

a) Identifying appropriate datasets

b) Developing scripts for data downloads from NASA servers

c) Assist with QA of AEDT processing, and troubleshooting as necessary

d) Assist with evaluation of results

Milestone(s)

AEDT enhanced to process high fidelity weather from MERRA-2
AEDT enhanced to process high fidelity weather from WRF for limited-area regional scale applications.

Major Accomplishments

UNC-IE assisted FAA/Volpe Center to use high fidelity weather from a new global reanalysis product (MERRA-2) or prognostic model (WRF) for the AEDT calculations. This was summarized in two reports that were led by the Volpe Center.

Publications

Volpe Reports 1 and 2 for MERRA and WRF

Outreach Efforts

Presentation at bi-annual ASCENT stakeholder meetings in Spring and Fall 2017, Alexandria, VA.
Presentation to FAA and investigators during monthly Tools telecons.

Awards

None

Student Involvement

None

Plans for Next Period

None

References

Bosilovich, M., Akella, S., Coy, L., Cullather , R., Draper, C., Gelaro, R., Kovach, R., Liu , Q., Molod, A., Norris, P., Wargan, K., Chao, W., Reichle, R., Takacs, L., Vikhliaev, Y., Bloom, S., Collow, A., Firth, S., Labow, G., Partyka, G., Pawson, S., Reale, O., Schubert, S. D., and Suarez, M.: MERRA-2: Initial evaluation of the climate, NASA Tech. Rep. Series on Global Modeling and Data Assimilation, NASA/TM – 2015 - 104606, Vol. 43, 2015.

Rienecker, M. M., Suarez, M. J., Gelaro, R., Todling, R., Bacmeister, J., Liu, E., … Woollen, J. (2011). MERRA: NASA's modern-era retrospective analysis for research and applications. Journal of Climate, 24(14), 3624–3648. http://doi.org/10.1175/JCLI-D-11-00015.1.

Skamarock, W.C., et al. (2008) A Description of the Advanced Research WRF Version 3. NCAR Technical Notes, NCAR/TN-4751STR.

Task #5: Explore Collaboration with NAU, Ukraine

Objective(s)

To explore collaboration with the National Aviation University of Ukraine for local-scale air quality models in support of the nVPM standard.

Research Approach

The National Aviation University of Ukraine in Kyiv has historically performed research related to aviation noise, emissions and operations. FAA identified a need for ASCENT investigators to participate in a technical exchange and reciprocal site visit with NAU. The purpose of the technical exchange and site visit was to continue to discuss the participation of NAU in ASCENT Center of Excellence research, related research, and to assess NAU capabilities.

During a 2.5-day period in July 2017, Dr. Sarav Arunachalam of the University of North Carolina (UNC) and Dr. Vic Sparrow of the Pennsylvania State University (PSU) participated in a technical exchange and site visit with National Aviation University (NAU) of Ukraine in Kyiv. In return, Dr. Kateryna Synylo of NAU visited UNC Chapel Hill during a 10-day visit in October 2017.

From ASCENT 19's perspective, the closest area of interest for collaboration with NAU was the PolEmiCa local-scale dispersion model developed and applied by NAU for several case studies. NAU has applied PolEmiCa for the CAEPport database maintained by the ICAO-CAEP, and submitted model evaluation white papers to the CAEP Modeling and Database Task Force.

PolEmiCa model is based upon OND-86. It has similarities to the AERMOD code in the U.S. However it is antiquated since being first published by Berland in 1987. It is a diffusion equation solution which can determine plume rise, etc. One interesting addition in recent research is to include wing-tip vortices in the distribution of PM. This is a natural methodology for aircraft emissions inventory and it uses a large eddy simulation using the FLUENT CFD code. Recently, NAU conducted a measurement campaign at the Kyiv Borispol airport, and where they compared PolEmiCa output with real airport operations from Ukraine-Germany cooperation (with the University of Wuppertal) during 2012. There they made measurements at moveable stations and found higher NOx at takeoff compared to landing. This is where they noticed a difference in the modeling and experimental data regarding whether they included the wing-tip vortices or not. NAU is planning another field campaign in the Kyiv Zhulyany airport, and UNC-IE provided some inputs for parameters to be measured during this campaign.

During Dr. Arunachala's visit to NAU, he presented a summary of emissions and air quality related research in UNC and ASCENT and toured the NAU facilities which included a fuel testing lab, ICAO training facility for airport operators on safety issues, large hangar with multiple aircraft and helicopters, and worked with NAU researchers to understand the PolEmiCa model and its features.

During Dr. Synylo's visit to UNC, she presented the PolEmiCa model at the 16th Annual CMAS conference in Chapel Hill, and worked with the UNC-IE team to explore how to adapt the PolEmiCa model to apply for the Los Angeles Airport Air Quality Source Apportionment Study (LAX AQSAS). UNC-IE has shared these datasets with NAU.

Milestone(s)

Site visit by UNC to NAU in July 2017
Reciprocal site visit by NAU to UNC in October 2017

Major Accomplishments

Through multiple telecons and the two site visits, UNC has an understanding of the NAU's capabilities in local-scale dispersion modeling.

Publications
None

Outreach Efforts
Presentation at bi-annual ASCENT stakeholder meetings in Spring and Fall 2017, Alexandria, VA.
Presentation at NAU on ASCENT research during site visit in July 2017.

Awards
None

Student Involvement
None

Plans for Next Period
None

References
Zaporozhets O., Synylo K. POLEMICA – tool for air pollution and aircraft engine emission assessment in airport // The Second World Congress "Aviation in the XXI-st century". – Kyiv: National Aviation University, 2005. – P. 4.22–4.28.

Zaporozhets O. Synylo K. New and Improved LAQ Models for Assessment of Aircraft Engine Emissions and Air Pollution in and Around Airports // On board a sustainable future: ICAO Environmental Report 2016, International Civil Aviation Organization 999 University Montreal, QC, Canada H3C 5H7, 2016 – 250p, Pp 82-84

Synylo K. Large Eddy Simulation of wall jet for Airport Local Air Quality // Abstract/ Proceedings. — Athens.: LFME, University of Patras – 2012. – P. 376–383.

LAX Air Quality Source Apportionment Study, 2012. http://www.lawa.org/airQualityStudy.aspx?id=7716 [Last accessed November 18, 2017]

Project 020 Development of NAS wide and Global Rapid Aviation Air Quality Tools

Massachusetts Institute of Technology (MIT)

Project Lead Investigator

Prof. Steven R.H. Barrett
Associate Professor of Aeronautics and Astronautics
Department of Aeronautics & Astronautics
Massachusetts Institute of Technology
77 Massachusetts Ave.
(617) 452-2550
sbarrett@mit.edu

University Participants

Massachusetts Institute of Technology

P.I.: Steven Barrett, Associate Professor of Aeronautics and Astronautics

- FAA Award Number: 13-C-AJFE-MIT, Amendment Nos. 007, 018, 025, and 032.
- Period of Performance: Aug. 19, 2014 to Aug. 31, 2018 (reporting with the exception of funding levels and cost share only for period from October 1, 2016 to September 30, 2017)
- Tasks:
    1) Extend second-order sensitivities to future years
    2) Evaluate sources of uncertainty within the tool
    3) Extend North American nested grid focused to represent Canadian impacts
    4) Develop nested grids for Europe and southeast Asia

Project Funding Level

Project Funding Level: $800,000 FAA funding + $50,000 Transport Canada funding = 850,000 total sponsored funds, with just $800,000 matching funds required. Sources of match are that same $50,000 Transport Canada funding (it constitutes both matching funds itself, as well as being sponsored funds that do not need to be matched), plus approximately $215,000 from MIT, and 3rd party in-kind contributions of $114,000 from Byogy Renewables, Inc. and $421,000 from Oliver Wyman Group.

Investigation Team (all MIT)

Principal Investigator: Prof. Steven Barrett
Co-Principal Investigator: Dr. Raymond L. Speth
Co-Investigator: Dr. Florian Allroggen
Research Scientist: Dr. Sebastian Eastham
Graduate students: Irene Dedoussi, Guillaume Chossière, Kingshuk Dasadhikari

Project Overview

The aim of this project is to develop tools that enable the rapid assessment of the health impacts of aviation emissions. The focus of the project is on aviation-attributable $PM_{2.5}$ and ozone at the NAS-wide and global scales. These tools should allow for rapid policy analysis and scenario comparison. The adjoint method, which the tools are based on, provides a computationally efficient way of calculating the sensitivities of an objective function with respect to multiple model inputs. The project enhances the existing tools in terms of the domains and impacts covered, and in terms of uncertainty quantification. The enhanced tools support the FAA in its strategic vision to reduce the significant health impacts of aviation emissions, and allow for detailed and quantified policy analyses.

Tasks for Current and Next Period

Current Period (AY2016-2017)

- **Task 1:** Extend second-order sensitivities to future years
- **Task 2:** Evaluate sources of uncertainty within the tool
- **Task 3:** Extend North American nested grid focused to represent Canadian impacts
- **Task 4:** Develop nested grids for Europe and southeast Asia

Next Period (AY2017-2018)

- **Task 1:** Continue work on the development of nested domains and provide tool validation
- **Task 2:** Incorporate the nested domains into a single user friendly framework
- **Task 3:** Support and assist the nvPM standard team on consistency-checking input data and interpreting results
- **Task 4:** Finalize and project uncertainty in ammonia emissions onto aviation impact sensitivities
- **Take 5:** Perform scoping of work for developing a multi-scale adjoint tool

Objectives

The aim of the project is to enhance the capabilities of the existing rapid assessment tool. The main objectives of this cycle are aligned with the aforementioned tasks. Specifically:

1. To provide a quantitative estimate of the relationship between aircraft emissions, background emissions and health impacts. By working on second order sensitivities, the impacts of aviation can be understood in the context of the background in which they act, and the relative benefits that can be achieved through policy action on aviation or non-aviation emissions.
2. To quantify the sensitivity of the tool's impact calculations to uncertainties in model inputs. This will ensure that the calculated impacts can be communicated in the context of the known sources of uncertainty, providing a more policy-relevant impact estimate.
3. To provide additional context for North American aviation emissions by incorporating the impacts on additional stakeholders. The ability to simultaneously calculate impacts for Canadian and US residents will allow multiple perspectives on impacts from the same emissions, adding a multinational dimension.
4. To bring high-resolution impact calculations for multiple regions into the net impact calculation. This provides additional validation for the global model results while also allowing high-fidelity estimation of local-scale impacts attributable to aviation for regions beyond the North American domain.

Research Approach

As documented in previous reports, the central tool for this project is the GEOS-Chem adjoint. A major, and unanticipated, focus of this period has been the diagnosis and correction of issues which resulted from an upgrade of the adjoint tool to the most recent version, GEOS-Chem adjoint version 35. Therefore, many of the results presented here are focused on structural improvements, which can be conducted in parallel with the adjoint diagnosis process, or are results which have been produced on a temporary basis using the previous version of the adjoint. Although the majority of the issues with v35 of the adjoint have now been resolved, this has occurred too late in the cycle to permit the production of updated sensitivity maps for this report.

Extension of calculations outside of original time range

The first task for this period of performance was concerned with extending our second-order sensitivity calculations beyond the original domain of interest. Prior sensitivity calculations had been performed almost exclusively using year 2006 meteorology. This resulted in the potential for unacknowledged bias in the results, and excluded the possibility of correctly accounting for the effects of interannual variability on either the model sensitivity or the associated uncertainty. In addition to meteorological variability, there have also been changes in the background emissions which will affect the sensitivity of surface conditions to aviation (the second-order sensitivity).

In response to this, the analysis has been extended to additional years and used to estimate the second order sensitivity of surface air quality to aviation emissions and to changes in background conditions. Formally, this can be expressed as

$$\text{Second order sensitivity} = \frac{\partial^2 J}{\partial E_{av} \partial C_{BG}}$$

where the cost function J is some metric of air quality impact, E_{av} is the rate of aviation emissions at a given point, and C_{BG} is some metric of the background conditions. This is a continuation of results presented previously, which focused on 2011 compared to 2006. With the upgrade to version 35 of the adjoint, sensitivities can be calculated using meteorology generated by the current-generation GEOS-FP output from the GEOS-5 model. This allows the re-calculation of sensitivities on an ongoing basis, up to and including the current day. An early result has been that ~7% of the sensitivity changes between the years of 2006 and 2011are estimated to be the result of changes in meteorology, compared to ~10% changes attributable to changes in population.

Evaluate additional sources of uncertainty within the tool

Following a literature review and feasibility analysis, a key (and, as yet, unquantified) source of uncertainty that has been identified within the current method is the potential impact of uncertainty in ammonia emissions on the sensitivity of air quality to aviation emissions. The rate of near-surface $PM_{2.5}$ formation is known to be highly sensitive to local concentrations of ammonia, which acts to neutralize acidic aerosol and thereby increase the total aerosol mass. However, no study has yet incorporated the known high uncertainty in ammonia emissions into their estimates of health impacts from aviation.

A new strategy has been developed to estimate the impact of uncertainty in ammonia emissions on the sensitivity of average surface-level air quality to aviation emissions. This constitutes an application of the second order sensitivity of aviation's impacts with respect to both aviation emissions and ammonia emissions, making use of the combined power of adjoint sensitivity calculation and forward differencing.

The impact of this uncertainty will be estimated by taking second order sensitivities of population exposure with respect to ammonia emissions, with and without aviation emissions. A typical example is shown in Figure 1, in this case for the sensitivity of surface-level mean $PM_{2.5}$ with respect to ammonia emissions in the baseline environment. These second order sensitivities can then be multiplied with the estimated uncertainty in ammonia emissions to give the impact that uncertainty in ammonia emissions have on aviation's contribution to ground-level $PM_{2.5}$

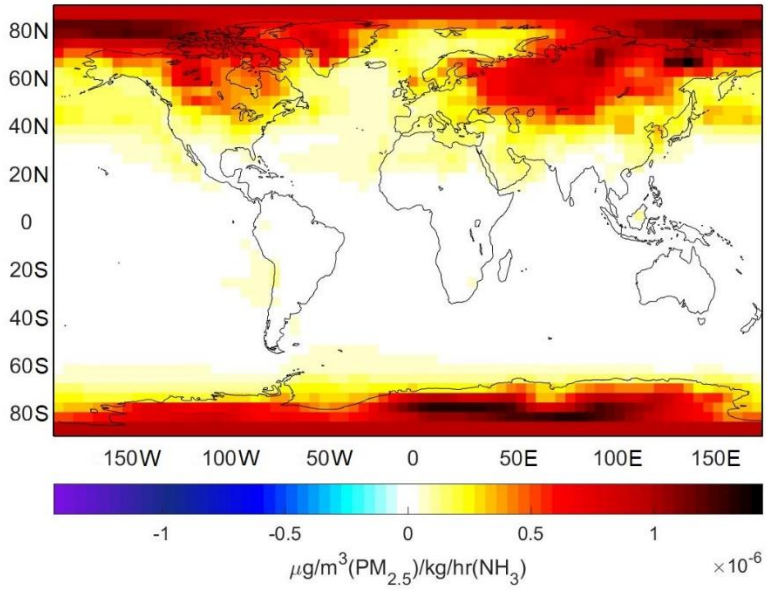

Figure 1: Sensitivities of mean surface-level $PM_{2.5}$ concentration to surface-level emissions of ammonia

In order to obtain the uncertainty in ammonia emissions, a literature review has been conducted to identify previously-derived estimates for the uncertainty, on both a global and regional scales. Thus, values of uncertainty have been obtained across several literature studies. Although some estimates suggest a low level of uncertainty in the overall global ammonia budget, with ~5% uncertainty in global emissions, regional studies have found that the local budgets are much more uncertain, with estimates of ~80% uncertainty for the U.S. (Zhu et al. 2013) and ~50% for China (Zheng et al. 2012, Xu et al. 2016). Multiplying these uncertainty percentages with input ammonia emissions for GEOS-Chem for each domain then gives the emissions uncertainties for post-multiplication with the second order sensitivities.

Incorporation of alternative stakeholders in estimation of North American impacts

All previous estimates of impacts within the North American nested domain had used as their receptor maps either the total population of the contiguous United States, or the total population within the domain. However, this resulted in a loss of nuance with regards to the specific distribution of impacts. While this is to some extent an inevitable result of using adjoint, rather than forward difference, methods, the dimensionality of the analysis can be increased by providing alternative cost functions which take into account the needs of different stakeholders.

To this end, a new receptor region has been implemented for the Canadian portion of GEOS-Chem Adjoint's North American nested grid, including incorporation of the population map for Canada (Figure 2). This enables computation of the sensitivity of average population exposure to $PM_{2.5}$ in Canada to aviation emissions, which can be used to calculate health impacts and costs in Canada attributable to aviation emissions. At present, all structural work necessary for this capability extension has been completed, in addition to the production of preliminary sensitivities for the Canadian nested region. However, full validation of sensitivities to certain emissions species is yet to be completed, pending output from the updated v35 adjoint model.

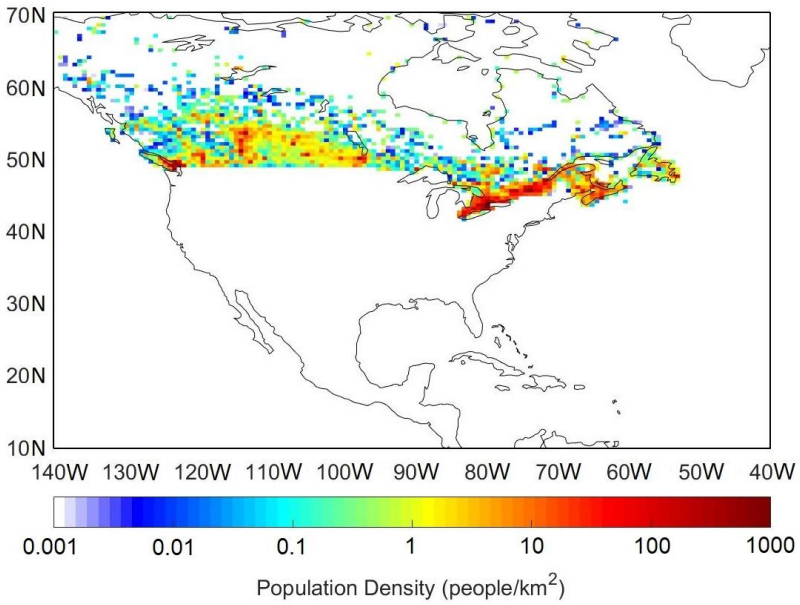

Figure 2: Population distribution used for calculation of sensitivity of Canadian air quality with respect to aviation emissions

Development of additional nested region domains

Given the global nature of aviation, much of the MIT research to date has focused on global impacts using global models with global population maps used to define the receptor regions and weighting. However, investigations using the North American nested domain have revealed that there are significant advantages to higher-resolution simulation over smaller domains. Capture of near-airport impacts is impossible with the coarse (~400 km) resolution at which the global model is run, while the finer (~50 km) resolution of the nested model is sufficient to isolate chemical and dynamical non-linearity associated with urban and coastal regions. This is complemented by further studies, such as Barrett et al (2010) and Eastham et al (2016), which show that the greatest impacts of aviation on surface air quality are incurred not in North America but rather in Western Europe and South Asia.

Accordingly, two additional nested domains have been developed for use with the GEOS-Chem adjoint. The first is the South-East Asia nested domain. This domain, modeled at a resolution of 0.5x0.667 degrees, allows impacts of aviation to be finely resolved throughout India, China, Indonesia, and the rest of the South-East Asian domain. A similar grid has been developed and implemented for Europe.

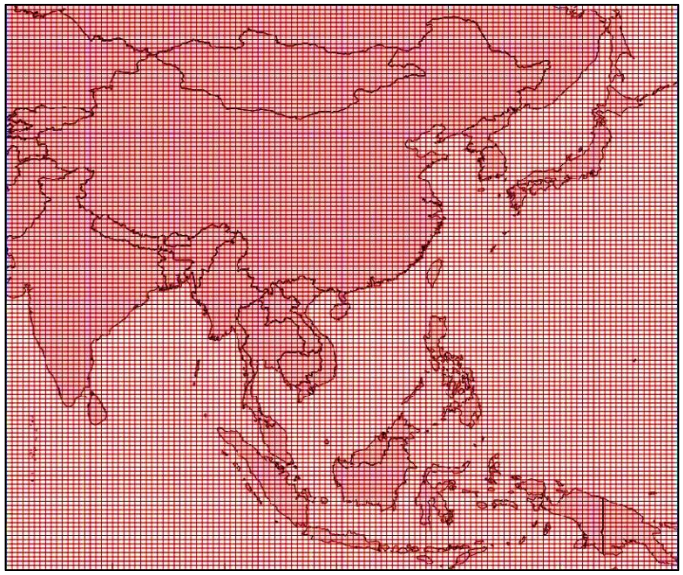

Figure 3: Population distribution used for calculation of sensitivity of Canadian air quality with respect to aviation emissions

These developments are complemented by a focused effort to improve the background emissions in these regions. As mentioned previously, the relative impact of aviation on surface air quality is dictated by the chemical environment encountered by both the LTO and cruise-level emissions, both in the region of production and along the path to their impacts. Although the standard inventories for Europe present in GEOS-Chem are relatively recent (e.g. the European EMEP project), those for China are over a decade old, based on the 2006 estimate by Zhang et al (2009). Use of these emissions would provide a poor representation of the local chemical environment. Accordingly, the most recent version of the EDGAR global anthropogenic emissions inventory (v4.3) has been acquired and implemented, relevant to the base year 2010. Since this is still too old to take into account recent policy, technology, and behavioral changes in the South-East Asian region, an ongoing follow-up project is the production of an updated emissions inventory for this domain using an activity-based updating method.

The calculation of the ozone impacts of aviation emissions required a careful definition of the metric used to measure exposure. On that front, MIT have collaborated with the ASCENT 18 project contributors. Jon Levy and his team suggested an appropriate metric for ozone exposure, and assisted with the choice of the concentration-response function to be used. The one that was chosen ensures consistency with previous FAA work.

The results for ground-level $PM_{2.5}$ from the forward model of this domain using the pre-existing emissions inventories have been validated against observational data from several urban centers in this region, as well as against satellite data for ground-level $PM_{2.5}$, and we are currently awaiting full validation of adjoint sensitivities.

Milestones

- *Extend second-order sensitivities to future years:* Work has continued on evaluating second order sensitivities for years beyond 2006.
- *Evaluate sources of uncertainty within the tool*: an assessment of uncertainty in ammonia emissions, considered to be key to all $PM_{2.5}$ formation, has been performed and will be propagated into impact sensitivities as part of the next project period. Other sources of uncertainty, such as those from variations in emissions and meteorology, have been evaluated and propagated.
- *Extend North American nested grid focused to represent Canadian impacts*: the relevant receptor region has been developed and tested, with final results pending simulation with the frozen, stable adjoint version.
- *Develop nested grids for Europe and southeast Asia:* These grids have been developed, with final validation pending simulation with the frozen, stable adjoint version.

Major Accomplishments

During this period of performance, the adjoint model was upgraded to the recently-released adjoint version 35. This also resulted in an extensive diagnostic effort, identifying, isolating, and resolving multiple unexpected software and data integrity issues present in version 35. An assessment of ammonia emissions uncertainty has been completed, revealing a potentially significant source of uncertainty in all existing estimates of aviation impacts on air quality. Additional nested domains and receptor regions have also been implemented in the adjoint model. Wherever possible, these improvements have been passed back to the adjoint community.

References

Barrett, S. R. H., Britter, R. E., & Waitz, I. A. (2010). Global mortality attributable to aircraft cruise emissions. Environmental Science & Technology, 44(19), 7736–7742.

Eastham, S. D., & Barrett, S. R. H. (2016). Aviation-attributable ozone as a driver for changes in mortality related to air quality and skin cancer. Atmospheric Environment. https://doi.org/10.1016/j.atmosenv.2016.08.040

European Commission Joint Research Centre (JRC) and Netherlands Environmental Assessment Agency (PBL). (2014). Emission Database for Global Atmospheric Research (EDGAR), release EDGARv4.2 FT2012 [Data set]. Retrieved from http://edgar.jrc.ec.europa.eu

Zhang, Q., Streets, D. G., Carmichael, G. R., He, K. B., Huo, H., Kannari, A., … Yao, Z. L. (2009). Asian emissions in 2006 for the NASA INTEX-B mission. Atmospheric Chemistry and Physics, 9(14), 5131–5153.

Outreach Efforts

Presented results at the ASCENT spring and fall meetings.
Presented air quality impacts mechanism at an ECMWF seminar.

Student Involvement

Graduate students involved in this project are: Irene Dedoussi, a PhD candidate in the Department of Aeronautics and Astronautics at MIT and Kingshuk Dasidhakari and Guillaume Chossière, Master's students in the Department of Aeronautics and Astronautics at MIT.

Plans for Next Period

Over the next period of this project (2017-2018), a frozen, stable version of the GEOS-Chem Adjoint rapid policy assessment tool will be generated which can be applied to both the problem of aviation impacts and the broader problems faced by the atmospheric modeling community. This version of the tool will incorporate multiple features not currently available to the community, such as the multiple consistent nested domains discussed above. The tool will also have been fully validated for multiple simulation years. The experience of the past project year has demonstrated the importance of independent validation of the community adjoint model which can be held stable and used for consistent policy analysis.

A key outcome of this testing and validation effort will be the development of a user-friendly framework for rapid policy assessment and analysis using the results from these new grids. A specific development priority will be a MATLAB-based tool which can accept a slate of policy options and return an estimate of impacts. Although previous work has focused on the global and North-American domain, these tools will incorporate results from all three of the now-available nested domains in parallel with the global results, while also incorporating the additional dimensionality of the division between US and Canadian impacts within the same nested domain.

These tools will also incorporate the results of another key task for the next period: the finalization of uncertainty in aviation sensitivities which has been propagated from underlying uncertainty in ammonia emissions. With an initial literature review now complete, significant existing uncertainty in the quantity of ammonia emitted within the target regions has been demonstrated. This will be combined with the existing work on assessing the impacts of background changes in emissions and in meteorology, providing a multidimensional assessment of the sensitivity of aviation impacts to variability and uncertainty.

The next period will see the launch of an ambitious multi-scale adjoint modeling assessment. The primary objective will be to scope out the benefits, requirements, and achievability of different approaches to investigating aviation impacts using adjoint models at multiple scales. Potential avenues of investigation include the use of multiple uncoupled global scales,

internally coupled nested and global models, propagation of sensitivities through nested domain boundary conditions, or even the application of high performance computing techniques which have recently been mooted by the GEOS-Chem adjoint development team. Once this assessment is complete, a viability estimate will be produced for a specific approach to multi-scale adjoint modeling of aviation impact sensitivities.

In addition to these core research efforts, support will be provided for the non-volatile PM (nvPM) standards team, with a specific focus on ensuring consistency of upstream inputs. This will include the validation of gridded emissions data, a priority which intersects well with efforts to update and improve the emissions data within the adjoint model. Assistance will also be provided to the nvPM standard team in results interpretation and policy assessment using the tools described.

Collaboration will continue with the research teams that will be continuing ASCENT projects 18 and 19 to maintain consistency between assumptions and inventories in the rapid assessment tools, health impacts assessments and airport-specific analyses, as has been successfully done in the past with the groups of Prof. Levy at Boston University and Prof. Arunachalam at University of North Carolina. MIT will also continue to assist the teams (e.g. currently ASCENT 48 for the non-volatile PM standard work and ASCENT 39 for the assessment of naphthalene removal from jet fuel) who are either applying or require contributions from the adjoint tool for air quality analyses.

Finally, within the next period a deep refresh of the MIT computing infrastructure will be performed. The GEOS-Chem model is highly computationally intensive, and has become more so over time. Recent versions require significantly more computational power and disk space for the same simulated period. This affects the time taken for a production run but it also slows debugging efforts. The current generation of servers used for this work were purchased in 2010, and are reaching their effective end of life. As such, they will be replaced with a new generation of servers, in addition to higher-capacity network interconnects designed to better cope with the overwhelming data communication burden imposed by the adjoint.

Project 021 Improving Climate Policy Analysis Tools

Massachusetts Institute of Technology

Project Lead Investigator

Steven R. H. Barrett
Raymond L. Bisplinghoff Professor of Aeronautics and Astronautics
Department of Aeronautics and Astronautics
Massachusetts Institute of Technology
77 Massachusetts Avenue
Cambridge, MA 02139
+1 (617) 452-2550
sbarrett@mit.edu

University Participants

Massachusetts Institute of Technology

- P.I.: Steven R. H. Barrett
- FAA Award Number: 13-C-AJFE-MIT, Amendment Nos. 004, 017, 024, and 037
- Period of Performance: Aug. 1, 2014 to Aug. 31, 2018 (reporting with the exception of funding levels and cost share for October 1, 2016 to September 30, 2017 only)
- Tasks:
    1. Development of APMT-Impacts Climate version 24
    2. Investigation of contrail and contrail-cirrus in aviation climate models
    3. Computation of climate metrics indicating the relative importance of short-lived climate forcers
    4. Support knowledge transfer

Project Funding Level

$600,000 FAA funding and $600,000 matching funds. Sources of match are approximately $162,000 from MIT, plus 3rd party in-kind contributions of $114,000 from Byogy Renewables, Inc. and $324,000 from Oliver Wyman Group.

Investigation Team

Dr. Steven R. H. Barrett, Principal Investigator
Dr. Raymond Speth
Dr. Florian Allroggen, Project Management
Dr. Mark Staples
Dr. Philip Wolfe, Tasks 1,3 and 4
Carla Grobler, Tasks 1,3 and 4
Lawrence Wong, Task 2

Project Overview

The objective of ASCENT Project 2014-21 is to facilitate continued development of climate policy analysis tools that will enable climate impact assessments for different policy scenarios at global, zonal and regional scales and will enable FAA to address its strategic vision on sustainable aviation growth. Following this overall objective, the particular objectives of ASCENT 2014-21 are (1) to continue the development of a reduced-order climate model for policy analysis consistent with the latest scientific understanding; and (2) to support FAA analyses of national and global policies as they relate to climate change and environmental impacts.

In the current reporting period, these objectives have been addressed (i) through the development of version 24 of the APMT-Impacts Climate code to replace APMT-Impacts Climate version 23; (ii) by investigating the role of contrail and

contrail-cirrus in aviation climate models through exploring the physical and chemical mechanisms of contrail formation and aviation-induced cloudiness; (iii) through preparing damage ratios which quantify the aviation-induced climate impacts of short-lived climate forcers relative to the impacts of aviation-induced CO_2 emissions; (iv) and by facilitating knowledge transfer to FAA-AEE and other research groups.

Task #1: Development of APMT-Impacts Climate Version 24

Massachusetts Institute of Technology

Objective(s)

During the current reporting period, the ASCENT 21 team focused primarily on developing version 24 of the APMT-Impacts Climate code, in an effort to update the year-2015 operational version of APMT-Impacts Climate (version 23). With the update, APMT-Impacts Climate is supposed to reflect the most recent scientific consensus regarding aviation's impact on climate change. This task comprised 3 main sub-tasks:

1.1 FAA's Aviation Climate Change Research Initiative (ACCRI) Phase II (Brasseur et al., 2016) identified significant climate responses from tropospheric nitrate, which have not been modeled in APMT-Impacts Climate version 23. In APMT-Impacts Climate version 24, this additional climate forcer pathway and its modeling uncertainties are to be considered.

1.2 After evaluating APMT-Impacts Climate with the Office of Management and Budget (OMB), APMT-Impacts Climate is supposed to be amended to produce output consistent with the results from the Interagency Working Group (IAWG)'s Social Cost of Carbon (SCC). Furthermore, the SCC as estimated by APMT-Impacts Climate version 24 are supposed to be compared to the IAWG's SCC estimates.

1.3 In order to bring APMT-Impacts Climate in line with the current consensus regarding the understanding of aviation's climate impacts, parts of the model (e.g. the modelling of atmospheric CO_2 concentrations), some uncertainty distributions (e.g. the underlying climate sensitivity distributions), and some parameter values (e.g. economic growth and inflation) should be updated.

Research Approach and Accomplishments

For policy analyses, fast, efficient, and robust reduced-order tools are needed to effectively model aviation's impact on the climate under numerous future growth scenarios and/or policy scenarios. APMT-Impacts Climate was developed as such a reduced-order tool to probabilistically project aviation's impact on climate using both physical and monetary impact metrics. The APMT-Impacts Climate Module adopts the impulse response function approach (Hasselmann et al., 1997; Sausen and Schumann, 2000; Shine et al., 2005) to model the long-lived CO_2 impacts from aviation emissions. In addition, APMT-Impacts Climate version 23 included the intermediate-lived impact of NO_x on methane (NO_x-CH_4) and its associated primary mode interaction on ozone (NO_x-O_3 long), the short-lived effects of NO_x on ozone (NO_x-O_3 short), the production of aviation induced cloudiness, sulfates, soot, and H_2O. A detailed description of past versions of APMT-Impacts Climate can be found in Marais et al. (2010), Mahashabde et al. (2011) and Wolfe (2012). A summary of the architecture of APMT-Impacts Climate is presented in Fig. 1.

In the current reporting period, APMT-Impacts Climate was updated to reflect the most recent scientific understanding regarding aviation's climate impacts. These updates are outlined in the following subsections. We note that previous modeling methods have been functionally retained in APMT-Impacts Climate version 24.

Improved CO_2 Model

To model CO_2 removal from the atmosphere, APMT-I Climate version 23 uses a linear Impulse Response Function (IRF) approach, which assumes that the removal of (marginal) CO_2 emissions over time is independent of the level of CO_2 background concentrations. However, recent work (e.g. Joos et al, 2013) shows that background CO_2 concentrations alter the CO_2 removal mechanisms from the atmosphere, resulting in non-linear IRFs over time, which vary with assumed background CO_2 concentrations. To reflect this non-linearity in APMT-Impacts Climate, the tool has been updated to consider IRFs for each background CO_2 scenario as defined in the RCP scenarios and for emission pulses in different years. The IRFs applied in APMT-Impacts Climate version 24 were generated by modeling the impact of an emission pulse in a range of years between 2000 and 2500 on atmospheric CO_2 concentrations under different CO_2 background scenarios using the Model for the Assessment of Greenhouse Gas Induced Climate Change (MAGICC6, Meinshausen et al. 2011). The resulting IRFs were then implemented into APMT-Impacts Climate version 24.

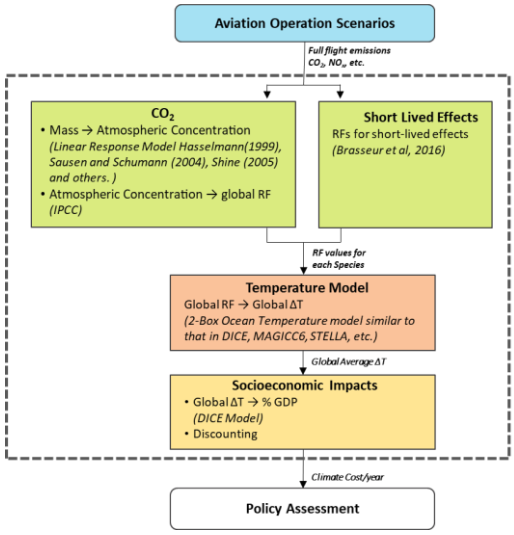

Figure 1: APMT-Impacts Climate Architecture

Equilibrium Climate Sensitivity Distribution

Equilibrium Climate Sensitivity is the expected surface-level temperature response from a doubling of atmospheric CO_2 concentrations relative to the pre-industrial atmospheric CO_2 concentrations. As such, this parameter is one of the key variables, which drives the temperature response in a reduced-order climate model like APMT-Impacts Climate. This parameter still has a large uncertainty. For example, the IPCC's most recent assessment (IPCC, 2013) reports medium confidence that this parameter is between 1.5˚C and 4.5˚C. This parameter is driven primarily by a number of temperature feedback effects and a textbook derivation, using these feedback effects, is presented in Seinfeld and Pandis (2016). Roe and Baker (2007) put forward an uncertainty distribution for Equilibrium Climate Sensitivity based on the uncertainty in the feedback factors. The distribution presented by Roe and Baker (2007) has been used extensively in the literature, for example by the IAWG on the Social Cost of Carbon. To bring APMT-Impacts Climate in closer agreement with the IAWG on SCC approach, the climate sensitivity uncertainty distribution as suggested by Roe and Baker (2007) was implemented into APMT-I Climate version 24.

Improved Background Temperature Model

Previous versions of APMT-I Climate computed background temperature change within APMT-Impacts Climate by using background CO_2 emissions in combination with APMT-Impact Climate's IRF, radiative forcing model, and temperature response model. While this approach captures most of the expected background temperature change, it leads to inconsistencies to the RCP scenarios, as it does not account for (i) the temperature impact of other climate forcers such as methane, nitrous oxide, and aerosols, and (ii) the interdependencies of CO_2 IRFs with background CO_2 emissions as discussed above. To account for the additional impacts and to save computational time, MAGICC6 (Meinshausen et al., 2011) was used to generate background temperature change sequences for each RCP scenario considered in APMT-Impacts Climate. To capture the uncertainties in background temperature change, MAGICC6 was run for different values of the Climate Sensitivity parameter. The resulting look-up table of the background temperature values was then implemented into APMT-I Climate version 24. We note that APMT-Impacts Climate ensures the consistency of the underlying climate sensitivity for the background temperature change and for aviation-attributable temperature change by correlating climate sensitivity parameters to background temperature change under each RCP scenario.

Short-Lived Forcer Distributions

In APMT-I Climate, the climate impacts of short-lived forcers, caused by aviation black carbon (or soot), contrail-cirrus, stratospheric water vapor, sulfates, and nitrates, is modeled based on radiative forcing values presented in the Aviation Climate Change Research Initiative (ACCRI) Phase II report (Brasseur et al. 2016). APMT-I Climate version 23 used triangular uncertainty distributions, which were derived from the set of impact estimates for each forcer as reported in the ACCRI report, to model the uncertainty associated with these impacts. However, given the limited data available in the ACCRI report, consistently using triangular uncertainty distributions might underestimate the uncertainty for some short-lived

forcers. APMT-Impacts Climate consequently uses: (i) a uniform uncertainty distribution if only two radiative forcing estimates are available for a specific short-lived forcer in the ACCRI report; and (ii) a triangular distribution if three or more radiative forcing estimates are published for a specific short-lived forcer in the ACCRI report.

Nitrate Aerosol Pathway
Estimation of aviation-induced climate impacts related to NO_x emissions requires modeling different pathways since NO_x does not follow a well-defined gas cycle model such as the carbon cycle. APMT-Impacts Climate version 23 considered three pathways of aviation NO_x-induced climate impacts: (1) the short-term (1 year) increase in tropospheric ozone concentrations, (2) the longer-term (10-12 year) decrease of methane concentrations, and (3) the longer-term (10-12 year) reduction in ozone concentrations. The Aviation Climate Change Research Initiative (ACCRI) Phase II report (Brasseur et al., 2016) presented evidence for a fourth aviation-induced NO_x pathway, the nitrate aerosols pathway. It is initiated by NO_x emissions reacting with atmospheric hydroxyl radicals to form nitric acid, which reacts with available ammonia to form nitrate aerosols. These aerosols have been found to result in cooling. To reflect the most recent scientific consensus on the aviation-induced climate impacts in APMT-Impacts Climate version 24, the nitrate cooling pathway has been added to the tool. The uncertainties associated with this pathway have been considered using the method as described above.

APMT-I Climate Measure of Inflation
The Shared Socioeconomic Pathway (SSP) scenarios, used by APMT-I Climate for future GDP estimates, are defined in year-2005 USD. To convert monetary values to another year's USD values, APMT-I Climate uses inflation metrics. For this purpose, APMT-I Climate version 23 applied the Consumer Price Index. To not only capture price changes in goods for consumption, APMT-I Climate version 24 uses the GDP deflator.

Comparison to the Interagency Working Group Social Cost of Carbon
Based on feedback obtained from the OMB, APMT-Impacts Climate includes code to compute the climate costs for CO_2 emissions by using the IAWG's Social Cost of Carbon (SCC) values in addition to APMT-I Climate's climate cost estimates. The additional outputs facilitate comparisons and validation for APMT-I Climate as its results can be compared directly to estimates based on the IAWG SCC.

Validation and Verification
Internal validation and verification was performed for each one of the updates, by comparing the APMT-I Climate output before and after the updates. Furthermore, validation included detailed comparisons between the APMT-I Climate Social Cost of Carbon estimates and the IAWG Social cost of carbon.

Documentation
Documentation of APMT-Impacts Climate version 24 was completed using two documents.

1. A presentation outlining the motivation and implementation for all updates was compiled. The slide deck also provides insights into the impact of each update on result metrics.
2. The user documentation describes the version 24 model in the context of previous APMT-I Climate releases.

Together, the documentation and the presentation form the documentation for APMT-I Climate.

Milestone(s)
Under Task 1 of ASCENT-2014-21, the APMT-Impacts Climate version 24 update was to be completed, including validation and verification of the model. The full update was completed by the end of July 2017, with individual update components becoming available earlier during the reporting period. Validation of APMT-I Climate version 24, including the comparison to the SCC published by the IAWG was subsequently completed in August 2017. The documentation and code was made available to the FAA in August 2017.

Publications
Written Reports
Grobler, C., Allroggen, F., Agarwal, A., Speth, R., Staples, M., Barrett, S. (2017). APMT-I Climate version 24 Algorithm Description Document, Laboratory of Aviation and the Environment.

Outreach Efforts

- ASCENT advisory board presentation (Spring 2017 and Fall 2017)
- Presentation of APMT-Impacts version 24 updates to FAA AEE (September 21st, 2017)
- FAA AEE Tools Coordination Meeting (Spring 2017)

Student Involvement

The updates, validation and verification was completed by Carla Grobler (Ph.D. Student, MIT). The documentation was prepared by Carla Grobler, and was based on an APMT literature study by Akshat Agarwal (Ph.D. Student, MIT).

Plans for Next Period

In the next year, the team will further enhance FAA's capabilities to perform rapid environmental policy assessment. In particular, the team aims to:

(1) develop capabilities to quantify the impact of life cycle emissions for different alternative fuels. Production of biofuels often results in methane and nitrous oxide emissions. The climate impacts of these emissions will be considered in APMT-Impacts Climate. As such, the model extension will facilitate comparisons of climate impacts under different alternative fuel scenarios for aviation.

(2) regionalize the damage function used within the APMT-Impacts climate framework. Currently the damage function only provides an estimate of global damages, but does not give an indication of the regional distribution of damages.

(3) assess as to whether regionalized climate sensitivities can be modeled in APMT-Impacts Climate.

References

Brasseur, G. P., Gupta, M., Anderson, B. E., Balasubramanian, S., Barrett, S., Duda, D., ... & Halthore, R. N. (2016). Impact of Aviation on Climate: FAA's Aviation Climate Change Research Initiative (ACCRI) Phase II. *Bulletin of the American Meteorological Society*, *97*(4), 561-583.

Hasselmann, K., Hasselmann, S., Giering, R., Ocana, V., Storch, H. V., Sensitivity Study of Optimal CO_2 Emission Paths Using a Simplified Structural Integrated Assessment Model (SIAM), *Climatic Change*, 37 (2), 345 - 386

Joos, F., Roth, R., Fuglestvedt, J. S., Peters, G. P., Enting, I. G., Bloh, W. V., ... & Friedrich, T. (2013). Carbon dioxide and climate impulse response functions for the computation of greenhouse gas metrics: a multi-model analysis. *Atmospheric Chemistry and Physics*, *13*(5), 2793-2825.

Meinshausen, M., Raper, S. C., & Wigley, T. M. (2011). Emulating coupled atmosphere-ocean and carbon cycle models with a simpler model, MAGICC6–Part 1: Model description and calibration. *Atmospheric Chemistry and Physics*, 11(4), 1417-1456.

RCP Database, 2009, references can be found at: http://tntcat.iiasa.ac.at:8787/RcpDb/dsd?Action=htmlpage&page=about#citation

Roe, G. H., & Baker, M. B. (2007). Why is climate sensitivity so unpredictable?. *Science*, *318*(5850), 629-632.

Sausen, R., Schumann, U. (2000) Estimates of the Climate Response to Aircraft CO_2 and NO_x Emissions Scenarios, *Climatic Change* 44 (1), 27-58.

Shine, K. P., Derwent, R. G., Wuebbles, D. J., & Morcrette, J. J. (1990). Radiative forcing of climate, Climate Change: The IPCC Scientific Assessment, 41–68.

Shine, K. P., Fuglestvedt, J.S., Hailemariam, K., Stuber, N. (2005). Alternatives to the Global Warming Potential for Comparing Climate Impacts of Emissions of Greenhouse Gases. *Climatic Change* 68 (3), 281–302.

World Bank: World Development Indicators (http://data.worldbank.org/indicator/NY.GDP.DEFL.KD.ZG), 2017.

Task #2: Investigation of Contrail and Contrail-Cirrus in Aviation Climate Models

Massachusetts Institute of Technology

Objective(s)

Aviation-induced contrail and contrail-cirrus, referred to as aviation-induced cloudiness (AIC), have been found to potentially be the largest radiative forcing impact of aviation (Lee et al., 2009; Burkhardt and Kärcher, 2011). At the same time, AIC is one of the most uncertain environmental impacts of aviation (Burkhardt et al., 2011). Recent work from ACCRI Phase II has better constrained the current climate-related uncertainty from aviation-induced cloudiness. However, further work is needed to understand the role of AIC on the climate as well as to improve our understanding of the impacts of modeling assumptions on temperature and damage projections. The objective of research under Task 2 of the ASCENT 21 project is to explore the physical and chemical mechanisms of contrail formation and aviation-induced cloudiness. This leads to two sub-tasks for the current reporting period.

2.1 Apply and support the extension of a contrail model, which has been used for the US (Caiazzo et al., 2017) and, more recently, for the global domain.

2.2 Enhance the understanding of contrail impacts from changes in engine technology and alternative fuels.

Research Approach

The ASCENT 21 team is supporting the investigations of the significance of contrail and contrail-cirrus to aviation climate models. More specifically, the Contrail Evolution and Radiation Model (CERM) has been developed at MIT. This is a physically realistic 3D model that can simulate the dynamical and microphysical processes of all stages of a contrail's lifetime from initial formation to the diffusion, advection and growth into a contrail-cirrus (Caiazzo et al., 2017). This model has been and will be used to explore the physical and chemical mechanisms of aviation-induced cloudiness and to understand their impact on the climate.

The ASCENT 21 team has been trained to use CERM and is supporting the extension of CERM from the US domain to the global domain. This model, once validated, can be used to facilitate the development of a reduced-order model to estimate climate impacts from aviation-induced cloudiness on a global scale in the future.

Milestone(s)

Under Task 2 of ASCENT-2014-21, the research team delivered a comprehensive status update on modelling aviation cloudiness and contrails with a particular focus on the impact of fuel properties and engine characteristics in the summer of 2017.

Major Accomplishments

During the reporting period, the team has contributed to three accomplishments.

(1) The ASCENT 21 team is supporting the validation of the CERM code. For this purpose, the team has been working to obtain contrail coverage data for the northern hemisphere, which will be used to compare contrail coverage and microphysical properties between CERM modeled results and satellite observations. This validation will further constrain the uncertainty of contrail- and contrail-cirrus-induced climate impacts.

(2) The global implementation of the contrail model CERM relies on meteorological data which is typically only available on 2° x 2.5° resolution, particularly for future forecasts. This resolution is too coarse for accurately modeling contrails. To solve this problem, research at MIT has set out to develop an approach that attempts to model sub-grid scale variations by statistically analyzing 1 year of fine meteorological data at a 0.25° x 0.3125° resolution. The ASCENT 21 team has supported these efforts and has briefed FAA on progress of these efforts.

(3) Future engine and fuel technologies impact on contrail formation and contrail properties. Biofuels, for example, reduce PM number emissions by more than half thereby decreasing the contrail-related climate impacts, but increase water emissions which leads to an increase in contrail formation. In addition, engines with higher fuel efficiency might reduce CO_2 emissions, but are also more likely to create contrails. The ASCENT 21 team has briefed FAA on current modeling efforts by MIT researchers to analyze these trade-offs.

Outreach Efforts

- ASCENT advisory board presentation (Spring 2017)
- FAA AEE Tools Coordination Meeting (Spring 2017)

Student Involvement

Lawrence Wong (Ph.D. Student, MIT) has supported the development of CERM and has compiled the FAA progress briefing on contrail modeling efforts at MIT. Akshat Agarwal (Ph.D. Student, MIT) and Ines Sanz Morère (Ph.D. Student, MIT) have further supported the team, particularly while briefing the FAA on the effects of alternative fuels and of engine efficiency on contrail-related climate impact.

Plans for Next Period

During the next period, the team aims to support the validation of the contrail modeling efforts at MIT. In particular, a comparison study between observed and simulated contrails is currently being ramped up. This project will compare contrail coverage as modeled using CERM to the satellite data as analyzed by Duda et al. (2013) and a novel computational approach for identifying contrail cirrus from satellite imagery.

Furthermore, the team will observe ongoing research on improving CERM, for example with regards to improving the accuracy of the radiative forcing effects of contrails which overlap with other contrails or with natural cirrus clouds.

References

Burkhardt, U., and Karcher, B. (2011). Global radiative forcing from contrail cirrus. *Nature Clim. Change* 1, 54-58.

Caiazzo, F., Agarwal, A., Speth, R., Barrett, S. (2017). Impact of biofuels on contrail warming. *Environmental Research Letters*, 12(11).

Duda, D. P., Minnis, P., Khlopenkov, K., Chee, T.L., Boeke, R. (2013). Estimation of 2006 Northern Hemisphere contrail coverage using MODIS data. *Geophysical Research Letters*, 40(3), 612-617.

Lee, David S., et al. (2009). Aviation and global climate change in the 21st century. *Atmospheric Environment* 43, 3520-3537.

Task #3: Computation of Climate Metrics Indicating the Relative Importance of Short-lived Climate Forcers

Massachusetts Institute of Technology

Objective(s)

Aircraft emission do not only impact on climate through CO_2-related impacts, but also through short-lived climate forcers such as contrails, sulfates, soot, stratospheric water vapor and other greenhouse gasses or greenhouse gas precursors such as NO_x (Brasseur et al., 2016). The climate impacts resulting from each short-lived forcer differ in magnitude and in the time scale.

To facilitate rapid comparisons of the relative significance of short-lived forcers for the aviation sector, Dorbian et al. (2011) developed a method for estimating the climate impacts of the short-lived forcers relative to the climate impacts of aviation-attributable CO_2 emissions. The results of this approach can also be used to compute the impacts of short-lived forcers on the basis of aviation-attributable climate damage estimates resulting from CO_2 emissions as quantified, for example, with the IAWG SCC.

However, the results in Dorbian et al. (2011) were computed using an earlier version of APMT- Impacts Climate. Since then, APMT-Impacts Climates has undergone multiple update cycles to reflect the most recent scientific understanding of the aviation-induced climate impacts in the tool. Under Task 3 of the ASCENT Project 21, the team aimed to create an updated set of the relative significance metrics of short-lived forcers using APMT-Impacts Climate version 24.

Research Approach

In line with Dorbian et al. (2011), APMT-Impacts Climate is run for a single pulse of aviation emissions in a specific year and the impacts attributable to the emission pulse are captured using metrics such as the Absolute Global Warming Potential (AGWP), integrated Temperature Potential (iTP), and the Net Present Value of damages (NPV). These metrics are then normalized by the CO_2 impact of a unit of fuel burn, which yields the desired output metrics. In order to capture changes in the relative significance of the climate forcers over time, the method is repeated for emissions pulses occurring every 10 years, covering the period between 2015 and 2055.

Milestone(s)
A preliminary set of climate impact ratios were computed using APMT-I Climate version 23, and were shared with the FAA in February 2017. After completing APMT-Impacts Climate version 24 in the summer of 2017, an updated set of metrics has been compiled.

Publications
Written Reports
Grobler, C., Wolfe, P., Allroggen, F., Barrett, S. (2017). Interim Derived Climate Metrics, Laboratory of Aviation and the Environment.

Student Involvement
Carla Grobler (Ph.D. Student, MIT) computed the ratios and documented the results.

Plans for Next Period
During the next period, the team intends to prepare an assessments of the climate cost per unit of emission species, which can guide future first-order assessments of policies and novel technologies which change the composition of aviation emissions.

References
Dorbian, C. S., Wolfe, P. J., & Waitz, I. A. (2011). Estimating the climate and air quality benefits of aviation fuel and emissions reductions. *Atmospheric environment*, *45*(16), 2750-2759.

Task #4: Support Knowledge Transfer
Massachusetts Institute of Technology

Objective(s)
Through transferring APMT-Impacts Climate knowledge to FAA and other research groups, the application of a standardized assessment tool for aviation's climate impacts is encouraged.

Research Approach and Accomplishments
Transferring APMT-Impacts Climate knowledge to FAA and other research groups has been regarded as an enabler for the application of APMT-Impacts Climate for policy analyses.

Milestone(s)
Training has been provided to researchers as needed, including tools training for UIUC to review climate code capabilities (Fall 2017).

Student Involvement
Carla Grobler (Ph.D. Student, MIT), who has been responsible for updating APMT-Impacts Climate to version 24, has transferred APMT-Impacts Climate to FAA and UIUC.

Plans for Next Period
The ASCENT 21 team will provide coaching on APMT-Impacts Climate as requested.

Project 022 Evaluation of FAA Climate Tools: APMT

University of Illinois at Urbana-Champaign

Project Lead Investigator

Dr. Donald Wuebbles (Dr. Robert Rauber has been acting as Principal Investigator while Dr. Wuebbles was on special assignment with the National Science Foundation and the Office of Science and Technology Policy of the Executive Office of the President; we are in process of changing Dr. Wuebbles back to being the PI)
Dept. of Atmospheric Sciences
University of Illinois
105 S. Gregory Street
Urbana, IL 61801
Tel: 217-244-1568
Fax: 217-244-4393
Email: wuebbles@illinois.edu

University Participants

University of Illinois at Urbana-Champaign
P.I.(s): Dr. Donald Wuebbles

- Period of Performance: October 16, 2016 to October 15, 2017
- Task(s):
    1. Evaluate version 23 of APMT
    2. Provide Feedback on plans for APMT version 24
    3. Using the CESM chemistry-climate model, update our earlier analyses of regional effects from aviation based on latitude bands and regions
    4. Evaluate the GTP concept for aviation that is being developed by the CICERO research team

Project Funding Level

Support from the FAA over this time period was $75,000 with an additional $75,000 in matching support, including about $10,000 from the University of Illinois, but also as in-kind support from Reading University.

Investigation Team

Dr. Donald Wuebbles: project oversight
Dr. Arezoo Khodayari (post doc; most recently on subcontract) and Jun Zhang (graduate student): analyses of APMT and 3-D atmospheric climate-chemistry modeling analyses

Project Overview

The primary objective of this project was to evaluate the capabilities of the APMT-I model, particularly the Climate module, to ensure this FAA policy analysis tool uses the current state of climate science. Regional climate impacts of aviation were also evaluated using the 3D atmospheric climate-chemistry model. Findings from these studies were reported at several meetings and in special reports to the FAA.

Task #1: APMT-I Climate Evaluation and Review of Requirements Document

University of Illinois at Urbana-Champaign

Objective(s)

In this project, we act as a resource to FAA for analyses relating to metrics and to model development and evaluation of FAA modeling tools and datasets, with special emphasis on testing the Aviation Environmental Portfolio Tool (APMT) model and the further development and evaluation of its climate component to ensure that the underlying physics of the model is addressed properly. A specific focus of this project is on analyses of zonal and regional effects of aviation on climate and testing the resulting incorporation of such effects within APMT. As such, we want to make sure the APMT linking of aviation emissions with climate impacts and the representation of the various components of the cause-effect chain (i.e., from emissions to climate effect) properly represents the state-of-the-science.

Research Approach

We have focused on (1) evaluating the climate component of the Aviation Environmental Portfolio Tool (APMT) for three main aspects of the model, mainly its treatment of the carbon cycle, short-lived species, and NOx-related impacts, (2) regional climate impacts from aviation using the 3D atmospheric climate-chemistry model. We also test the APMT model following the cause-effect chain from aviation emission to temperature change. The project evaluates the APMT components relative to state-of-the-art modeling that fully considers the physics and chemistry important to the various processes. Our aim is to ensure that the physics and chemistry underlying the treatments in APMT are addressed properly based on our and others published modeling studies.

Milestone(s)

Milestone	Milestone reached
Feedback on plans for APMT version 24	December 15, 2016
Getting started to evaluate the newly developed APMT version 24.	September 30, 2017

Major Accomplishments

Most relevant to this project is the feedback we provided on the plans for development of APMT version 24. Our aim is to ensure that the physics and chemistry underlying the treatments in APMT are addressed properly based on our and others published modeling studies. We recommend that the stratospheric water vapor induced by methane oxidation and nitrates induced by NOx emissions should be included in the model. For the carbon cycle, APMT should couple the impulse response functions (IRF) of atmosphere, ocean and biosphere presented in Joos et al (2013) instead of just using a linear atmospheric IRF. For energy balance model, feedbacks from ocean and temperature need to be considered to get more accurate simulated temperature change under different emission background scenarios. The nonlinearity impacts of the background atmosphere also needs to be taken into account. As a result of making these changes, APMT should be better able to link the various components of aviation emissions with climate impacts relative to the findings from ACCRI.

Publications

Zhang and Wuebbles, Evaluation of FAA Climate Tools: APMT. Report for the FAA, December 2016

Outreach Efforts

ASCENT Advisory Committee Meeting – April 18-19, 2017 (Presentation)
ASCENT Advisory Committee Meeting – September 26-27, 2017 (Presentation)
Bi-weekly meeting with project manager Daniel Jacob

Awards

None

Student Involvement

Graduate Student: Jun Zhang
Ms. Zhang is responsible for the analyses and modeling studies within the project, and leading the initial preparation of the project reports.

Plans for Next Period

Evaluate the new version of APMT (version 24). The following modules of APMT will be tested to evaluate the model performance:
1) the carbon cycle in APMT to simulate the aviation CO2 concentration on different background scenarios;
2) the energy balance model to calculate the temperature change induced by all aviation emissions;
3) the NOx-induced effects and how they are represented in APMT model.

Task #2: Three-Dimensional Atmospheric Climate-Chemistry Modeling Studies for Aviation Regional Effects on Climate

University of Illinois at Urbana-Champaign

Objective(s)

The aim in this work was to have a better understanding of the climate impacts from aviation emissions on a zonal and regional basis. Since the aviation emissions have significant spatial variability in the sign and magnitude of response, the strength of regional effects is highly likely hidden due to the global averaging of climate change. Thus, it is important to look at the impact of aviation emission on climate on a regional scale rather than global scale. We continued using a complex 3-D chemistry-climate model to further our understanding of the chemistry and climate effects from aviation emissions and to do our regional analysis and compare our results with the earlier findings. As part of this effort, we used CAM5-Chem, the atmospheric component of Community Earth System Model (CESM), and did a series of studies to evaluate aviation impact on climate both in 2006 and 2050.

Research Approach

In this study, the chemistry-climate model Community Atmosphere Model (CAM-chem5) is carried out to examine the regional climate effects based on 4 different latitude bands (90°S- 28°S, 28°S-28°N, 28°S-28°N, 60°N-90°N) and regions (contiguous United States, Europe and East Asia). We have completed the studies modeling of aviation effects on global atmospheric composition and on climate we did with FAA support that were published as FAA reports. We have derived the regional effects of NOx-induced species (short-lived O_3, CH_4, long-lived O_3 and stratospheric water vapor) and direct aerosols (black carbon and sulfates) under different latitude bands and regions using CESM.

Milestone(s)

Completed master thesis referenced below. Also made presentations of findings at ASCENT meetings.

Major Accomplishments

We have updated our earlier analyses of regional effects from aviation based emissions on latitude bands and regions using the CESM chemistry-climate model. The short-lived agents are more regionally important than the long-lived species. For NOx-induced effects (including O3-short, CH4, O3-long and Stratospheric water vapor), we found that the short-term O3 forcing is the major contributor to the overall net NOx-induced forcing from aviation. Although the global mean values of net NOx forcing can be very small, forcings over high latitudes in the Northern Hemisphere can be up to 140 mW/m^2 in the future scenarios (shown in Figure 1).

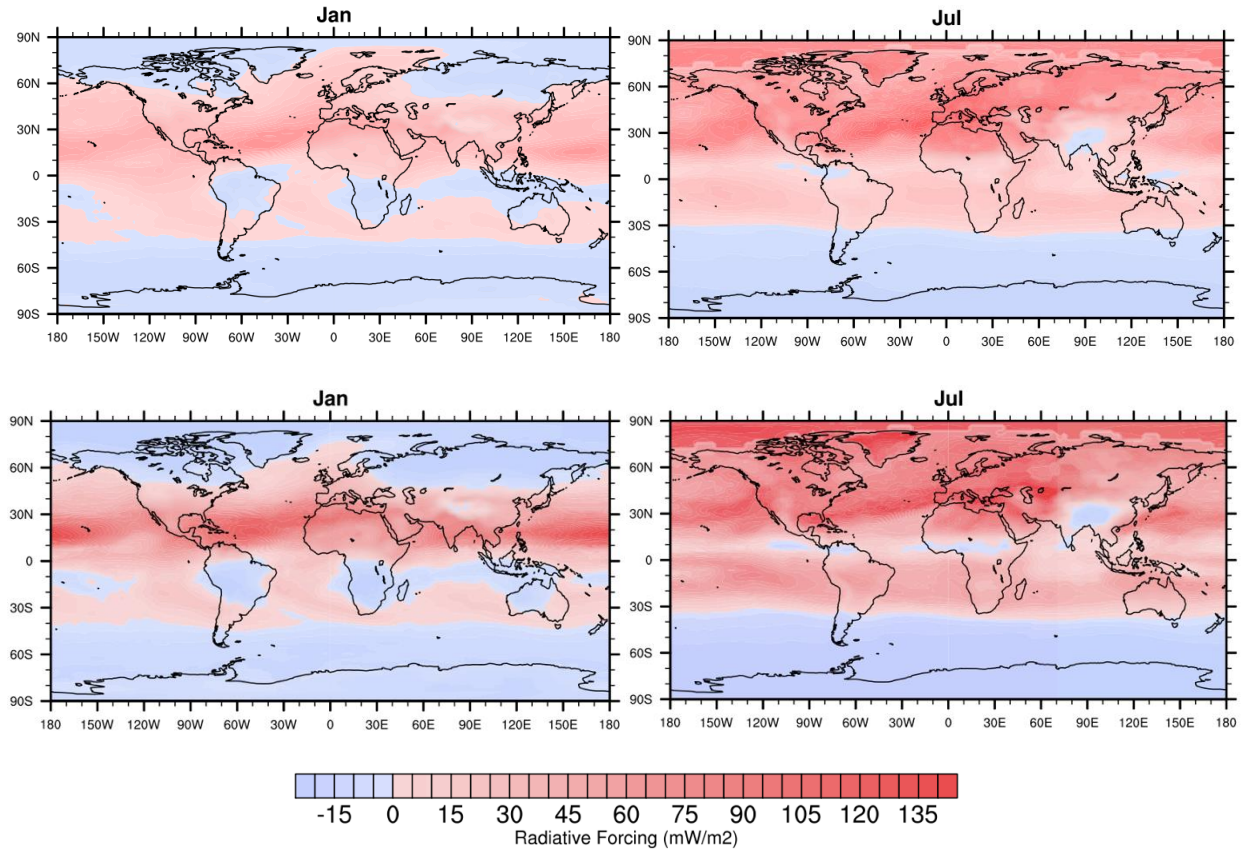

Figure 1. Simulated radiative forcing (mW/m^2) for net radiative forcing (mW/m^2) of aviation NOx emissions for January (left) and July (right). The present-day scenario (2006) is on the top panel and future scenario (2050 S1) is on the bottom. Blue bar indicates negative radiative forcing (cooling effect) while the red bar indicates positive radiative forcing (warming effect).

We also found that the radiative forcings of short-lived agents indicate a large hemispheric asymmetry. Radiative forcings are mainly distributed over the latitude band from 28°N – 60°N where most of aviation emission occurs (Table 1). The radiative forcings for short-lived agents over the United States, Europe and East Asia is approximately 4 times of its corresponding global values. The climate impact over the US has the most information loss and the forcing will be highly underestimated when looking at the climate impacts from aviation emissions using globally-averaged values and ignoring the regional heterogeneity (shown in Table 2).

This regional analysis suggests that the globally-averaged metrics are not able to capture the significant spatial variability induced by aviation emissions since global averaging will lead to cancellations between warming and cooling effects such that the strength of regional impacts is hidden. Thus, the climate impacts from aviation emissions could be much more intense over regional areas than over the globe.

Table 1. Radiative forcing (in mW/m^2) of short-lived species (O_3, BC and sulfates) over different latitude bands compared with global values for the present-day scenario (2006) and future scenarios (2050 S1 and 2050 S2).

2006 Radiative forcing (mW/m^2)	90°S-28°S	28°S-28°N	28°N-60°N	60°N-90°N	Global
O_3	12.6	27.5	67.1	45.6	37.3
BC	0.06	0.14	0.86	0.63	0.3
Sulfate	-1.15	-2.7	-11.37	-7.86	-4.4

2050 S1 Radiative forcing (mW/m^2)	90°S-28°S	28°S-28°N	28°N-60°N	60°N-90°N	Global
O_3	23.4	63.3	82.6	57.5	56.3
BC	0.15	0.22	1.80	1.37	0.6
Sulfate	-4.86	-6.88	-33.2	-25.51	-13

2050 S2 Radiative forcing (mW/m^2)	90°S-28°S	28°S-28°N	28°N-60°N	60°N-90°N	Global
O_3	23.7	65.4	87.2	61.1	58.3
BC	0.07	0.11	0.91	0.67	0.3
Sulfate	-	-	-	-	-

Table 2. As in Table 1, but for different subregions (United States, Europe and East Asia).

2006 Radiative forcing (mW/m^2)	United States	Europe	East Asia	Global
O_3	69.5	68.5	52.7	37.3
BC	0.8	1.1	0.7	0.3
Sulfate	-12.0	-13.2	-8.5	-4.4

2050 S1 Radiative forcing (mW/m^2)	United States	Europe	East Asia	Global
O_3	95	82.7	74.9	56.3
BC	1.6	2.3	1.1	0.6
Sulfate	-31.4	-39.4	-22.1	-13

2050 S1 Radiative forcing (mW/m^2)	United States	Europe	East Asia	Global
O_3	99.5	87.7	78.4	58.5
BC	0.8	1.1	0.6	0.3
Sulfate	-	-	-	-

Publications

Zhang and Wuebbles, Evaluating the regional impact of aircraft emissions on climate and the capabilities of simplified climate model. Master's thesis, University of Illinois, July 2017

Outreach Efforts

Results presented at ASCENT meetings. Journal paper to be prepared.

Awards

None

Student Involvement

Graduate student Jun Zhang is responsible for the analyses and modeling studies within the project, and leading the initial preparation of the project reports.

Plans for Next Period

We will do more analysis of regional climate effects from aviation emissions toward completing these studies for publication. We want to explore the impact of global and regional aviation emissions on global-mean radiative forcing response and the regional radiative forcing response to global and regional aviation emissions. More chemistry-climate runs will be performed as part of this study if needed.

Project 023 Analytical Approach for Quantifying Noise from Advanced Operational Procedures

Massachusetts Institute of Technology

Project Lead Investigator

R. John Hansman
T. Wilson Professor of Aeronautics & Astronautics
Department of Aeronautics & Astronautics
MIT
Room 33-303
77 Massachusetts Ave
Cambridge, MA 02139
617-253-2271
rjhans@mit.edu

University Participants

Massachusetts Institute of Technology

- P.I.(s): R. John Hansman
- FAA Award Number: 13-C-AJFE-MIT, Amendment Nos. 008, 015, 022, and 031
- Period of Performance: Oct. 28, 2014 to Aug. 31, 2018
- Task(s):
    1. Evaluate the noise impacts of flight track concentration or dispersion associated with PBN arrival and departure procedures
    2. Identify the key constraints and opportunities for procedure design and implementation of noise-minimizing advanced operational procedures
    3. Develop concepts for arrival and departure procedures that consider noise impacts in addition to operational feasibility constraints
    4. Analyze location specific approach and departure design procedures in partnership with impacted industry stakeholders
    5. Develop and propose a demonstration plan for new procedure designs through modeling and/or flight testing

Project Funding Level

Project Funding Level: $610,000 FAA funding and $610,000 matching funds. Sources of match are approximately $80,000 from MIT and $530,000 from Massachusetts Port Authority.

Investigation Team

Prof R. John Hansman (PI)
Greg O'Neill (Post-Doctoral Researcher)
Luke Jensen (Graduate Student)
Jacqueline Thomas (Graduate Student)
Alison Yu (Graduate Student)

Project Overview

The objective of this research activity is to evaluate the noise reduction potential from advanced operational procedures in the arrival and departure phases of flight. In particular, the project is intended to address the need and opportunity for noise-driven PBN procedure design utilizing the enhanced flexibility and precision of RNP. Advanced operational procedures change noise exposure near airports in two respects. First, flight track alterations (terminal-area route

changes, concentration, or dispersion) can impact the noise experienced by specific observers or neighborhoods near airports. Second, the source noise generated by engines and aerodynamics are impacted by aircraft speed, thrust, and configuration. Therefore, arrival and departure procedures that impact these variables also impact noise generation. The combined noise impact from these two effects are not well understood or modeled in current environmental analysis tools, presenting an opportunity for further research to facilitate ATM system modernization. This phase of research leverages the analytical tools and approaches developed in prior phases of this project to evaluate noise impacts of variable aircraft speeds and configurations.

Task #1: Evaluate the Noise Impacts of Flight Track Concentration or Dispersion Associated With PBN Arrival and Departure Procedures

Massachusetts Institute of Technology

Objective(s)

This task evaluates the impact of flight track concentration arising from PBN procedure implementation and the potential noise mitigation impact of track dispersion. The effects of track concentration due to PBN procedure implementation have not been fully explored. While the potential benefits of PBN for flight efficiency and predictability are well understood, the resulting environmental impact has caused increased community awareness and concern over the procedure design process. Current methods and noise metrics do not provide adequate information to inform the policy decisions relating to noise concentration or dispersion due to PBN implementation.

In this task, models were used to evaluate noise concentration scenarios using a variety of metrics and procedure design techniques. Noise data from Massport was used to support the simulation effort. The impact of track dispersion was compared to potential community noise reduction through noise-optimal RNP procedure designs that avoid noise-sensitive areas and use background noise masking where possible.

Research Approach

- Evaluate the impact of noise dispersion directly through modeling of a dispersed set of flight tracks in AEDT
- Analyze population exposure impact using multiple metrics, including DNL and Nabove
- Develop alternative rapid dispersion modeling method to reduce computational burden for evaluating operational strategies that impact flight track density

Major Accomplishments

- Developed methodology for rapid dispersion modeling as an alternative to exhaustive flight-by-flight analysis in AEDT/ANOPP.
- Completed development of numerical method for dispersion modeling using a single centerline route rather than individually modeling a representative set of dispersed routes

Task #2: Identify the Key Constraints and Opportunities for Procedure Design and Implementation of Noise-Minimizing Advanced Operational Procedures

Massachusetts Institute of Technology

Objective(s)

Arrival and departure procedure design is subject to physical, regulatory, and workload constraints. Procedures must be flyable by transport-category aircraft using normal, stabilized maneuvers and avionics. The procedures must comply with Terminal Instrument Procedures (TERPS) guidelines for obstacle clearance, climb gradients, and other limitations. The procedures must be chartable and work within the limitations of current Flight Management Systems. Advanced operational procedures must also be compatible with airport and air traffic control operations, avoiding workload saturation for air traffic controllers and pilots.

This task involved evaluating the key constraints impacting advanced operational procedures and opportunities to improve noise performance, identifying those that may impact design and implementation. This process involved collaboration with pilots, air traffic controllers, procedure designers, and community members. The task also considered current research and evidence on physical, psychological and social impacts of aircraft noise as well as emerging issues such as community perceptions of equity and the impact of overflight frequency on noise perception.

Research Approach

- Meet with key stakeholders in the implementation pathway to understand procedure development processes, timeline, and constraints
- Research documentation on regulations and operational standards influencing new flight procedure development
- Consult with stakeholders during candidate advanced operational procedure development to identify potential implementation obstacles

Major Accomplishments

- Met with airport operators and airline technical pilots to discuss potential concepts for advanced operational procedures
- Conducted follow-up meetings with ATC, Massport, FAA representatives, communities, and airline technical pilots to discuss initial procedure concepts
- Identified strong speed dependence on airframe noise that is not captured by NPD-based methods.

Task #3: Develop Concepts for Arrival and Departure Procedures that Consider Noise Impacts in Addition to Operational Feasibility Constraints

Massachusetts Institute of Technology

Objective(s)

This task applied the findings from Task 2 to identify a set of generic constraints and procedures for designing feasible and flyable advanced operational procedures to minimize noise perception as measured by traditional metrics (e.g. 65 dB DNL) and alternate metrics which address noise concentration concerns introduced by PBN procedures and emerging equity issues. Given an understanding of technology capabilities and operational constraints, this task developed potential operational concepts and identified potential implementation pathways for both specific locations and generalizable operational concepts. Some of the approaches considered were;

- Lateral Track Management Approaches (e.g. Dispersion, Parallel Offsets, Equivalent Lateral Spacing Operations, Multiple Transition Points, Vectoring, High Background Noise Tracks, Critical Point Avoidance Tracks, etc.)
- Vertical/Speed Thrust Approaches (e.g. Thrust Tailoring, Steep Approaches, Delayed Deceleration Approaches, etc.)

Research Approach

- Use feedback from Task 2 to identify procedures with noise reduction potential
- Model procedures using AEDT and ANOPP for generic runways to evaluate noise impacts for candidate procedures on a single event and/or integrated basis
- Determine noise impacts based on multiple metrics that are location-agnostic (i.e. contour area) as well as location-specific (i.e. population exposure at specific runways)

Major Accomplishments

- Developed a set of generic approach and departure modifications using PBN and other techniques to take advantage of noise benefits from advanced procedures
- Identified key constraints for lateral, vertical, and speed profile redesign based on ATC operational guidelines and FAA procedure design criteria

Task #4: Analyze Location Specific Approach and Departure Design Procedures in Partnership with Impacted Industry Stakeholders

Massachusetts Institute of Technology

Objective(s)

Advanced operational procedures may be particularly applicable for specific airports based on local geography, population density, operational characteristics, fleet mix, and local support for procedure modernization (among other factors). Specific procedures will be evaluated at a series of representative airports around the US. It is anticipated that this task will involve collaboration with multiple airports and air carriers on potential opportunities at locations which would benefit from advanced PBN procedures.

Research Approach

- Coordinate with a specific airport operator to evaluate procedure design opportunities with noise reduction potential
- Work closely and communicate with impacted stakeholders throughout the procedure evaluation, design, and analysis process to ensure that key constraints and objectives are appropriate for the selected location on a procedure-by-procedure basis

Major Accomplishments

- Established regular meeting and collaboration schedule with Massport and developed an initial set of arrival and departure procedures for analysis at Boston Logan Airport
- Contributed to a joint effort Memorandum of Understanding between the FAA and Massport to identify, analyze, and recommend procedure modifications at Boston Logan Airport
- Performed detailed noise analysis for preliminary arrival and departure procedure concepts, including population impact estimation based on 2010 census data and re-gridding methodology developed for this research
- Assisted with community outreach meetings about noise in the Boston area

Task #5: Develop and Propose a Demonstration Plan for New Procedure Designs through Modeling and/or Flight Testing

Massachusetts Institute of Technology

Objective(s)

The noise impact of advanced operating procedures must be validated in terms of operational acceptability (crew workload, safety, precision, controller workload, etc.) and noise impact. This task involved the generation of a testing plan for high value candidate advanced operational procedures developed in Task 4. Test plans considered included flight simulator studies, noise modeling, initial discussions of flight testing, and noise monitoring plans for newly-implemented procedures.

Research Approach

- Document procedure recommendations thoroughly and unambiguously so that simulator or flight trials are possible
- Meet with airline technical pilots and representatives from aircraft manufacturers to discuss operational constraints and test opportunities
- Develop test plans and protocols for potential flight trials
- Develop test plans and protocols for potential noise measurement campaigns
    - Specific flight test locations
    - Operational field measurements

Major Accomplishments

- Coordinated with airline technical pilots from a major US airline to plan and fly a set of simulator trials of candidate procedures in a Level-D Boeing 767 simulator
- Coordinated with airlines, Massport, and a major aircraft manufacturer to discuss objectives and potential strategies for possible noise measurement campaigns for reduced-speed departure procedures

Publications

"Delayed Deceleration Approach Noise Assessment," *16th AIAA Aviation Technology, Integration, and Operations Conference*, 2016. DOI: 10.2514/6.2016-3907

"Investigation of Aircraft Approach and Departure Velocity Profiles on Community Noise," *23rd AIAA/CEAS Aeroacoustics Conference*, 2017. DOI: 10.2514/6.2017-3188

"Analytical Approach for Quantifying Noise from Advanced Operational Procedures," *12th USA/Europe Air Traffic Management Research and Development Seminar*, 2017.
http://www.atmseminarus.org/seminarContent/seminar12/papers/12th_ATM_RD_Seminar_paper_135.pdf

Outreach Efforts

1/25/2017: Briefing to FAA Joint University Program research update meeting
4/17/2017: Joint briefing to FAA and MITRE to discuss tool development pathway
4/18/2017: Briefing to ASCENT Advisory Board
6/5/2017: Presentation at AIAA Aviation Conference in Denver, CO.
6/29/2017: Presentation at Eurocontrol/FAA ATM R&D Seminar in Seattle, WA.
7/10/2017: Briefing and simulator testing session with a major US-based airline
Numerous community meetings
Numerous briefings to politicians representing Eastern Massachusetts (local, state, and federal)
Briefing to FAA Management Advisory Council
In-person outreach and collaboration with Massport, operator of Boston Logan Airport and ASCENT Advisory Board member
In-person outreach and collaboration with Volpe noise tool development team

Awards

None

Student Involvement

Graduate students have been involved in all aspects of this research in terms of analysis, documentation, and presentation.

Plans for Next Period

The next phase of this project will involve extensive outreach to stakeholders impacted by implementation of advanced operational procedures, including airlines, airports, air traffic controllers, the FAA, and communities. Specific procedures will be evaluated for noise impacts, including a detailed analysis of operational barriers to entry and pathways to implementation for high-benefit options. Procedures will be evaluated in a generic sense as well as at specific airports of interest, including Boston Logan Airport and any other locations agreed upon by the project team and FAA program managers. This procedure evaluation process is expected to inform recommendations to airport operators, airlines, and the FAA to develop noise-mitigating advanced operational procedures at specified locations in the NAS.

Project 024(B) PM Emission Database Compilation, Analysis and Predictive Assessment

The Pennsylvania State University, GE U.S. Aviation

Project Lead Investigator

Randy L. Vander Wal
Professor, Energy and Mineral Engineering, Materials Science and Engineering
John and Willie Leone Family Dept. of Energy and Mineral Engineering
Penn State University 104 Hosler Bldg.
814-865-5813
ruv12@psu.edu

University Participants

The Pennsylvania State University

- P.I.(s): Randy L. Vander Wal, Professor, Energy and Mineral Engineering, Materials Science and Engineering
- FAA Award Number: Grant 12148585, Amendment No. 13-C-AJFE-PSU-019
- Period of Performance: Aug. 1st, 2016, July 31st, 2017
- Task(s):
  1. Test for improved accuracy by separating the temperatures associated with nvPM formation and oxidation. Presently the ImFOX kinetic expression uses one temperature at the exit of the combustor as representing the global temperature. The accuracy of T4 is confirmed by GE cycle deck calculations and consistent with the Brayton thermodynamic cycle for the engine. Yet for RQL style combustors soot formation necessarily occurs near an estimated $\varphi \sim 2$ while oxidation occurs under lean conditions, $\varphi \sim 0.9$. Such differences suggest different temperatures as better representing nvPM formation and oxidation regions.
  2. Assess ACCESS II test procedure upon engine conditions at cruise. A key difference between ground and cruise altitude is the ram effect at cruise and lower (external) pressure. These conditions alter the air-to- fuel ratio and hence while the form of the ImFOX relation is uniform between ground and cruise, different AFR relations may be necessary to capture these effects. With guidance from GE Aviation and their cycle calculations one can assess whether two separate or one unified AFR relations is sufficient – the latter then simplifying ImFOX use.
  3. Evaluate ASAF as the global scaling factor in the ImFOX relation. The ASAF relation was formulated by MIT as an empirical correlation of nvPM across all available engine emissions data. It is based upon aromatic content as the driving parameter for carbon aerosol emission. The MIT consensus is that the ASAF serve as global scaling factor for the ImFOX relation. This will be evaluated by comparison to measured nvPM from JP-8 and blends between conventional and alternative fuels.
  4. Investigate alternative representations to capture fuel composition effects for alternative fuels. Given the limitation of the present ASAF relation a more encompassing metric to capture fuel compositional effects is required. Alternative fuels do not have aromatic content but do have considerable and varying proportions of cyclic and normal paraffins. This introduces a hydrogen variation as well as C/H variation. Blended fuels will contain aromatics as carry-over from the original petroleum component. However naphthalene is currently considered to contribute disproportionately to soot formation with current FAA interest being to remove it from fuels. Such twists necessitate a more encompassing relation than ASAF to represent the different and varying fuel component classes. The fuels used in AAFEX I: JP-8, coal and natural gas based FT fuels and 50:50 blends with JP-8 encompass a range of aromatic and hydrogen contents for which EI(BC) plots are linear in semi-log format. Such data suggests that either or both of these fuel factors may be incorporated into the ImFOX relation in the formation pre-factor. These alternative fuel dependencies will be tested against the field campaign data and compared to the ASAF relation across engine thrusts.
  5. Evaluate the ImFOX relation against the ACCESS II flight data from NASA for nvPM. Presently ground based emission levels are scaled by the Doppelheuer and Lecht (DL) relation to estimate cruise EI(BC). This approach imposes redundancy as the DL relation is a kinetic based expression that then duplicates the kinetic rates explicit in the ImFOX relation. Our remedy is to avoid this scaling step by developing a direct predictive

relation that does not require scaling or correction factors between ground and cruise. Using cycle deck data from GE Aviation, accurate engine conditions of AFR and Tfl are identified and relationships with thrust can be developed. This then permits true evaluation of the ImFOX relation – without skew by inaccuracies in engine operating conditions – an aspect that has plagued and limited prior such efforts.

6. Validate the ImFOX for other engines in the CFM class. As shown by our prior work, with guidance from cycle deck calculations, engine conditions may be accurately modeled known and hence comparison of ImFOX to measured nvPM provides a true assessment of the ImFOX predictive ability. Comparison to the CFM56-3B engine is planned given presently available test data for this engine and with cycle deck calculations provided by our GE partners.

Project Funding Level

FAA funding: $75,000

GE Aviation is the Industrial Partner supplying matching funds, level $75,000, from an original commitment of $1,724895 available to the FAA COE AJFE ASCENT program, administered through Washington State University.

Investigation Team

Professor Randy L. Vander Wal, Penn State EME Dept., with responsibilities for project management, reports, interfacing with FAA program manager, and mentoring the graduate student supported on this project.
Mr. Joseph P. Abrahamson, graduate student. Responsibilities include data assembly, analysis and predictive relation assessment, as integral towards completion of a Ph.D. program.

Project Overview

The recently developed FOX method removes the need for and hence uncertainty associated with (SNs), instead relying upon engine conditions in order to predict BC mass. Using the true engine operating conditions an improved FOX (ImFOX) predictive relation was developed. Necessary for its implementation are its development and validation to estimate cruise emissions and account for the use of alternative jet fuels with reduced aromatic content. Refinement by incorporating separate, independent temperatures for fuel-rich and fuel-lean regions of the combustor will be evaluated against another CFM engine. Comparison to measured nvPM at cruise, to EI(BC) from conventional and alternative fuels across thrust will critically test the ImFOX tool predictive ability with positive results then aiding its adoption for EI(BC) estimates at ground and cruise with varied fuel compositions.

Tasks #1 – 6

The Pennsylvania State University

Objective(s)

1. Develop a predictive relation for nvPM at ground.
2. Develop a predictive relation for nvPM at cruise.
3. Include fuel composition effects for alternative fuels (absent aromatics and naphthalenic compounds) and their blends with conventional fuels.
4. Incorporate thrust dependence into the predictive tool.

Research Approach

Jet engine aircraft exhaust contains combustion byproducts and particulate matter in the form of non-volatile particulate matter (nvPM). Black carbon (BC) is used synonymously for nvPM throughout this paper. Aircraft cruise emissions are the only direct source of anthropogenic BC particles at altitudes above the tropopause.[1] Black carbon aerosols are strong solar radiation absorbers and have long atmospheric lifetimes.[2] Therefore, BC results in positive radiative forcing and is believed to be the second largest contributor to climate change.[3] Additionally, upper troposphere and lower stratosphere BC particles contribute to climate forcing indirectly by acting as ice nucleation sites and cloud activators.[4-6] With regard to human health, a link between cardiopulmonary diseases and carbonaceous black particulate matter has recently been suggested.[7] As concern for human health risks and environmental impacts caused by aviation BC emissions increases, emission reduction strategies will need to be implemented. Predictive tools capable of accurately estimating BC emissions

from the current in-service fleet will be needed for the next decades to quantify atmospheric BC inventory from aviation.

Current models do not accurately predict BC emissions. The First Oder Approximation-3 (FOA3) methodology is used worldwide for estimating BC emissions within the vicinity of airports.[8] The FOA3 was endorsed by the (ICAO)[9] in February 2007 and relies on a measured SN to predict BC emission. Black carbon is most often reported as an emission index of black carbon (EI_{BC}), reported as milligrams of BC emitted per kilogram of fuel combusted. Due to inaccuracies in measuring low SNs produced by modern high bypass ratio engines, the FOA3 and its modifications are unreliable. Recently a kinetic model based on formation and oxidation rates termed the FOX method was reported.[10] The FOX does not require input of a SN, instead the input variables are engine conditions. Hence, the FOX avoids the measurement error built into the FOA3. However, the FOX is fuel independent and cannot be applied to predict EI_{BC} from alternative fuels and alternative fuels blended with conventional jet fuels. Recently, a relation, the Approximation for Soot from Alternative Fuels (ASAF) has been developed to predict BC from alternative fuels relative to conventional fuel BC emissions.[11] Both the FOA3 and the FOX methods are designed to predict EI_{BC} at ground level, which is important for assessing human health concerns at and in the vicinity of airports, however, it is the cruise EI_{BC} that is of the most importance in determining the role aviation BC plays on the Earth's radiative balance. The current practice to arrive at a predicted cruise EI_{BC} is to scale ground values with an additional kinetic type expression, the Dopelheuer and Lecht relation.[12] At the time the Dȍpelheuer and Lecht relation was developed there were limited cruise BC emission measurements. The available data was not representative of real aviation emissions because the aircraft operated at reduced weight and velocities compared to regular operation.[13]

In our prior work, current predictive methods were evaluated for accuracy by comparison to over a decade's worth of field campaign data collected by the National Aeronautics and Space Administration's (NASA) Langley Aerosol Research Group with inclusion of cruise data.[14] An improved semi-empirical method was developed. Accurate engine condition relations were developed based on proprietary engine cycle data for a common rich-quench-lean (RQL) style combustor. In the forthcoming work predictive relations will be developed for alternative fuels and fuel blends as well as a direct cruise prediction. The intent is to provide an improved method to calculate EI_{BC} reductions from the use of alternative fuels.

References

Peck, J.; Oluwayemisi, O; Wong, H; Miake-Lye, R. An algorithm to estimate cruise black carbon emissions for use in developing a cruise emissions inventory. J. Air Waste Manage. Assoc. 2013, 63, 367-375.

Lee, D. S.; Fahey, D. W.; Forster, P. M.; Newton, P. J.; Wit, R. C. N.; Lim, L. L.; Owen, B.; Sausen, R. Aviation and global climate change in the 21st century. Atmos. Environ. 2009, 43, 3520-3537.

Bond, T.; Doherty, S.; Fahey, D.; Forster, P.; Berntsen, T.; DeAngelo, B.; Flanner, M.; Ghan, S.; Karcher, B.; Koch, D.;

Kinne, S.; Kondo, Y.; Quinn, P.; Sarofim, M.; Schultz, M.; Schulz, M.; Venkataraman, C.; Zhang, H.; Zhang, S.; Bellouin, N.; Guttikunda, S.; Hopke, P.; Jacobson, M.; Kaiser, J.; Klimont, Z.; Lohmann, U.; Schwarz, J.; Shindell, D.; Storelvmo, T.; Warren, S.; Zender, C. Bounding the role of black carbon in the climate system: A scientific assessment. J. Geophys. Res.: Atmos. 2013, 118, 5380-5552.

Haywood, J. M.; Shine, K. P. The Effect of Anthropogenic Sulfate and Soot Aerosol on the Clear-Sky Planetary Radiation Budget. Geophys. Res. Lett. 1995, 22, 603-606.

Karcher, B.; Peter, T.; Biermann, U. M. Schumann, U. The Initial Composition of Jet Condensation Trails. J. Atmos. Sci.1996, 53, 3066-3083.

Heymslield, A. J.; Lawson, R. P.; Sachse, G. W. Growth of Ice Crystals in Precipitating Contrail. Geophys. Res. Lett. 1998, 25, 1335-1338.

Pope, C. A.; Dockery, D. W. Health effects of fine particulate air pollution: Lines that connect. J. Air Waste Manage. Assoc. 2006, 56, 709-742.

Wayson, R. L.; Fleming, G. G.; Lovinelli, R. Methodology to estimate particulate matter emissions from certified commercial aircraft engines. J. Air Waste Manage. Assoc. 2009, 59, 91-100.

ICAO. Airport Air Quality Guidance Manual; International Civil Aviation Organization: Montreal, Canada, 2011.

Stettler, M. E. J.; Boise, A. M.; Petzold, A.; Barrett, S. R. H. Global civil aviation black carbon emissions. Environ. Sci. Technol. 2013a, 47, 10397-10404.

Speth, R. L.; Rojo, C.; Malina, R.; Barrett, S. R. H. Black carbon emissions reductions form combustion of alternative fuels. Atmos. Environ. 2015, 105, 37-42.

Döpelheuer, A.; Lecht, M. Influence of engine performance on emission characteristics. In RTO AVT Symposium on Gas Turbine Engine Combustion Emissions and Alternative Fuels; Lisbon, Portugal, 1998; p. RTO MP-14.

Schumann, U.; Arnold, F.; Busen, R.; Curtius, J.; Karcher, B.; Kiendler, A.; Petzold, A.; Schlager, H.; Schröder, F.; Wohlfrom, H. Influence of fuel sulfur on the composition of aircraft exhaust plumes: The experiments SULFUR 1-7. J. Geophys. Res. 2002, 107, 4247.

Moore, R.; Shook, M.; Beyersdorf, A.; Corr, C.; Herndon, S.; Knighton, W.; Miake-Lye, R.; Winstead, S.; Yu, Z.; Ziemba, L.; Anderson, B. Influence of Jet Fuel Composition on Aircraft Engine Emissions: A synthesis of aerosol emissions data from the NASA APEX, AAFEX, and ACCESS missions. Energy Fuels 2015, 29, 2591-2600.

Milestone(s)

Milestone	Planned Due Date
1. Comparison of ImFOX predictions for nvPM at cruise altitude and engine operating conditions to measured values from ACCESS II.	Sept. 30th, 2016
2. Develop a predictive relation for nvPM at cruise.	Dec. 30th, 2016
3. Include fuel composition effects for alternative fuels (absent aromatics and naphthalenic compounds) and their blends with conventional fuels.	March 30th, 2017
4. Incorporate thrust dependence into the predictive tool.	June 30th, 2017
5. Final report	July 30th, 2017

Major Accomplishments

Overview

Aviation black carbon (BC) emissions impact climate and health. Inventory estimates are essential to quantify these effects. These in turn require a means of estimating BC emission indices from jet aircraft. The first order approximation (FOA3) currently employed to estimate BC mass emissions under predicts BC emissions due to inaccuracies in measuring low smoke numbers (SNs) produced by modern high bypass ratio engines. The recently developed Formation and Oxidation (FOX) method removes the need for and hence uncertainty associated with (SNs), instead relying upon engine conditions in order to predict BC mass. Using the true engine operating conditions from proprietary engine cycle data an improved FOX (ImFOX) predictive relation is developed. Still, the current methods are not optimized to estimate cruise emissions or account for the use of alternative jet fuels with reduced aromatic content. Here improved correlations are developed to predict engine conditions and BC mass emissions at ground and cruise altitude. This new ImFOX is paired with a newly developed hydrogen relation to predict emissions from alternative fuels and fuel blends. The ImFOX is designed for rich-quench-lean style combustor technologies employed predominately in the current aviation fleet.

Preface to Task Progress

Given the dependence of task 5 upon the combustor temperature (task 1), AFR, (task 2), evaluation of the ASAF as a global factor for fuel effects (task 3) and evaluation of alternative measures of fuel composition, e.g. C/H ratio (task 4), tasks are reported in order as initial tasks represent key engine condition whose values must be determined prior to assessing the ASAF and C/H ratio methods for incorporating fuel dependence. Last, task 6 is then reported for comparison of ImFOX predictions to nvPM (EI_{BC}) from another RQL style combustor to evaluate the transferability and applicability of the predictive tool for other combustors in the current fleet.

Rationale for a Singular Predictive Tool for EI_{BC} from RQL style combustors – Improved Engine Condition Relations

In this section engine conditions required as inputs for the improved FOX (ImFOX) expression are more accurately provided in the form of predictive relations based on proprietary cycle deck calculations for a common RQL combustor. Aerosol emissions from the NASA campaigns: Aircraft Particle Emissions eXperiments (APEX-I)[1,2]. Alternative Aviation Fuel Experiments I and II (AAFEX-1, AAFEX-II)[3,4]. Alternative-Fuel Effects on Contrails & Cruise EmiSSions I and II (ACCESS-I, ACCESS-II)[5], are from a Douglas DC-8 aircraft equipped with four CFM56-2C turbo fan engines. Although, this engine is an

older design it is a high-bypass engine and serves as the basis for the whole engine family employed by thousands of commercial and military aircraft worldwide. The EI curves from five of the six RQL style combustors tested during APEX-III [6-8] followed a common distorted U-shaped curve[9], with upturns both at low (idle) and high (take-off) thrust levels. (The exception was the Rolls-Royce engine RB211-535E4-B with 40,100 lbs. maximum thrust, which has a BC emission profile peaking at 65% of the maximum thrust and deceased emissions thereafter.) Therefore, it appears the relationships developed here are considered applicable for a majority of rich-burn, quick-quench, lean-burn (RQL) style combustors. Only a select few engine conditions are addressed in this section. This is intentional as the goal is to simplify the calculations needed to predict EI_{BC}. For the relations developed here, the only needed input is the fuel flow rate from which all other engine conditions as input for the ImFOX expression can be calculated.

Task #1: Test for Improved Accuracy by Separating the Temperatures Associated With Nvpm Formation and Oxidation

Flame Temperature, T_{fl}. Flame temperature is arguably the most important variable as it appears in both exponential terms in both the FOX and the Döpelheuer and Lecht scaling relation. Several T_{fl} predictive methods have been developed in addition to the one currently used for the FOX expression, Equation-7. The common practice is to predict a T_{fl} using a linear relationship to T_3. Whereas Equation-7 assumes that 90% of the incoming sensible heat from the hot air leaving the compressor, T_3, adds to a stoichiometric adiabatic flame temperature of 2120 K. A common alternative flame temperature predictor for an RQL style combustor based on T_3 is given in Equation-1.[10]

$$T_{fl}[K] = 0.6T_3 + 1800 \quad [1]$$

This method assumes that 60% of the initial air temperature is converted to flame temperature and that the flame temperature without this addition is that of a fuel rich flame at 1800 K. Considering that the primary zone of an RQL combustor runs fuel rich for flame stabilization, Equation-1 is a more realistic flame temperature predictor to determine the primary zone flame temperature. However, the only variable in either flame temperature predictor is T_3 and since the AFR is a function of thrust the second term should also be variable with relation to AFR, and hence thrust (given flame temperature dependence upon stoichiometry, or AFR). However, since this localized AFR as a function of thrust is proprietary and not readily determined we have elected to use the flame temperature at the back of the combustor (T_4) in place of primary zone flame temperature. Using T_4 for the flame temperature is logical considering that the AFR being used is also from the back of the combustor as a global average of the processes occurring in the formation and oxidation regions of the combustor. Additionally, T_4 is readily calculated by the engine cycle deck, yielding Equation-2.

$$T_4[K] = 490 + 42{,}266FAR \quad [2]$$

There is a strong correlation between T_3 and T_4, the Pearson r correlation value is 0.966. However, it was not selected in the T_4 relation because there is a much stronger correlation between T_4 and fuel-air-ratio (FAR), Pearson r value of 0.995, but more importantly for the fact that an explicit AFR dependence accounts for the expected dependence of T_{fl} upon stoichiometry. Additionally, T_3 is an engine specific parameter that may not be readily available in all cases. Equation-2 accurately predicts T_4 at both ground and cruise. Given the success of this semi-empirical T_4 calculation based on FAR, a thermodynamic basis was evaluated. The thermodynamic Air Standard Brayton Cycle is applied to a jet engine in the SI. Two equations are required to define this cycle. The first is the definition of the polytropic compressor efficiency that is currently used to find combustor inlet temperature, T_3, and the second equation reveals that T_4 is equivalent to exhaust gas temperature (EGT) squared divided by temperature ambient. The NASA campaigns (APEX I-III, AAFEX I & II, and ACCESS I & II) documented both EGT and ambient temperature. Values of T_4 found using the Brayton Cycle compared to values predicted using Equation-2 were slightly higher (~5%), likely because the Brayton Cycle is treated as an idealized adiabatic system. Either relation can be used to find T_4, the benefit of Equation-2 is that only the FAR is needed and Equations-3 and 4 below provide accurate FAR relations.

Task #2: Assess ACCESS II Test Procedure upon Engine Conditions at Cruise

Air-to-Fuel Ratio, AFR. The first condition investigated is AFR, it should be mentioned that AFRs found here are those at the back of the combustor, typically referred to as plane-4, and are not the AFRs in the primary zone or the quench zone. The current method, Equation-5, has been widely accepted. This is partially because an engine manufacture had released

nominal AFR values at 7, 30, 85, and 100 thrust settings.11 Those values were linearly fit to derive the current predictive AFR expression. However, after comparing values using this relation to engine cycle deck data it was evident that the current method results in over prediction of AFR. Two separate equations are needed to accurately calculate AFR. One for ground and another for cruise, equations 3 and 4 respectively.

$$AFR_{grd} = 71 - 35.8\left(\frac{\dot{m}_f}{\dot{m}_{f,max}}\right) \quad [3]$$

$$AFR_{cru} = 55.4 - 30.8\left(\frac{\dot{m}_f}{\dot{m}_{f,max}}\right) \quad [4]$$

As seen from the two AFR equations, at a matching thrust level AFR will be lower at cruise than at ground. This is sensible considering the decreased air density at altitude. However, the cruise cycle deck calculations were case matched to the ACCESS-II campaign and ACCESS-II conditions do not exactly match real conditions. During ACCESS-II the outboard engines were significantly throttled back to maintain an aircraft Mach number of 0.6. This was done so the chase plane could keep up. Therefore, the inboard engines from which the emissions were measured, were burning fuel at a rate typical of a Mach speed of 0.75, the DC-8's nominal cruising speed. It is likely that the AFR would be increased from the ram effect at a higher Mach number, therefore, it is possible that a singular relation (Equation-3) may adequately predict AFR at both ground and cruise.

Task #3: Evaluate ASAF as the Global Scaling Factor in the Imfox Relation

ASAF inclusion. Black carbon emissions from turbo fan jet engines are significantly reduced when conventionally produced (i.e., from petroleum) Jet-A or JP-8 are blended with low aromatic content synthetic blending components as demonstrated in recent measurement campaigns.[5,12-14] Efforts to relate BC emissions from gas turbines to fuel chemistry is a research focus of long-standing interest. A prime motivator is that a decrease in aromatic content results in reduced BC emissions. The ASAF is the first analytical approximation to estimate the BC emission reduction associated with using alternative fuels as compared to conventional jet fuel BC emissions.[15]

$$B = 1 - (1-\lambda\frac{\dot{m}_f}{\dot{m}_{f,max}})(1-\hat{A}) \quad [5]$$

Where B is the relative BC emission reduction, λ is a fitting parameter, and Â is the normalized aromatic content and equal to aromatic content of the fuel over aromatic content of a reference conventional fuel.

The model we have developed uses the FOX16 as the starting point. The FOX is a kinetically balanced relation predicting EI_{BC} by subtracting the rate of soot formation from the rate of soot oxidation. Each global process is represented by a single-step Arrhenius rate. The activation energy (E_a) value in the oxidation step is the well accepted value first proposed by Lee et al.[17] Given the success of this value, no modification to the oxidation step was made, outside of correcting AFR and substituting T_{fl} with T_4. The formation activation energy is that reported by Hall et al.[18] and is their inception E_a based on the formation of polyaromatic hydrocarbons (PAHs). The pre-exponential frequency factor is a function of two and three member PAHs concentration, which in turn is a function of PAH building block molecules; acetylene and benzene. Since there is no practical way to determine these molecular concentrations this pre-exponential factor (also referred to as a formation constant) is fit to C_{BC} data. Using a formation constant value of 356 Settler et al.[16] achieve a coefficient of determination, R^2 , value of 0.8 when fitting to the APEX campaign data. The limitation of this approach is that it does not account for alternative fuels. A different formation constant would be necessary for each fuel composition. A solution encompassing alternative fuels follows.

By combining the ImFOX with the ASAF relation developed by Speth et al.[15] determination of BC emissions from alternative fuels is possible.

$$C_{BC}[\frac{mg}{m^3}] = \dot{m}_f \times B\,(A_{form} \times e^{(-6390/T_4)} - A_{ox} \times AFR \times e^{(-19778/T_4)}) \quad [6]$$

Where B in Equation-6 is the ASAF value found using Equation-5. The fitting parameter λ was found to vary between neat (i.e., 100%) alternative fuel blend components ($\lambda_{alt\text{-}neat}$) and alternative fuel blends ($\lambda_{alt\text{-}blend}$) as follows:

$$\lambda_{alt\text{-}neat} = -0.058 + 0.105\left(\frac{\dot{m}f}{\dot{m}f,max}\right) \quad [7]$$

$$\lambda_{alt\text{-}blend} = -5.3 + 9.6\left(\frac{\dot{m}f}{\dot{m}f,max}\right) - 4.7\left(\frac{\dot{m}f}{\dot{m}f,max}\right)^2 \quad [8]$$

Since the ASAF provides the relative EI_{BC} reduction due to decreased aromatic content, it is ideal as a global correction factor located outside of the ImFOX expression. However, ASAF does not consider naphthenic compounds known to have a higher sooting index[19,20] than that of paraffinic compounds found predominantly in alternative fuels and fuel composition effects more logically belong in the formation constant, rather than as a global correction factor for the ImFOX. Therefore, an alternative approach was developed using hydrogen content in the form of fuel carbon-to-hydrogen (C/H) ratios to determine the formation constants for alternative fuels.

The current version of the FOX over predicts measured values, as displayed in Figure-1. However, the method is promising considering the clear trend between EI_{BC} and thrust.

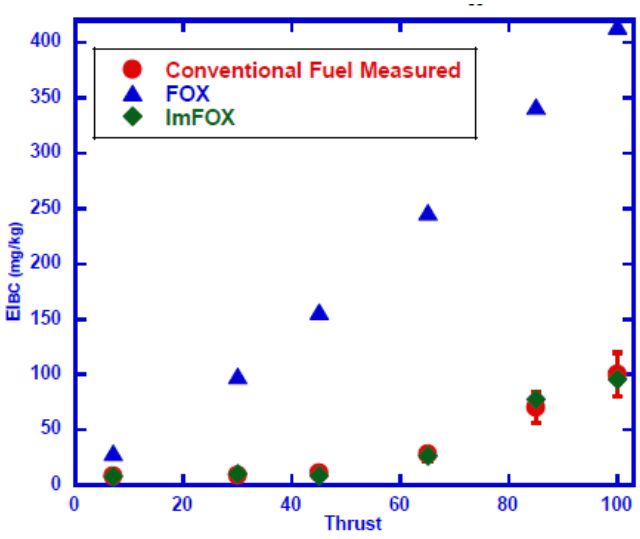

Figure 1. Measured conventional fuel black carbon emission from AAFEX-I (red circles) Shown for comparison are predicted EI_{BC} values from the FOX (blue triangles) and the ImFOX (green diamonds).

As seen in Figure-1 the ImFOX method accurately captures the emissions trend across a full range of thrust settings. The ImFOX method developed subsequently utilizes improved engine condition relations and a thrust dependent formation constant to accurately predict BC emissions from petroleum-based fuel combustion. The agreement represents a vast improvement from the current FOX method given the mean variance is reduced from 400% to less than 10%.

Task #4: Investigate Alternative Representations to Capture Fuel Composition Effects for Alternative Fuels

C/H-ImFOX. An alternative approach was developed using hydrogen content in the form of fuel carbon-to-hydrogen (C/H) ratios to determine the formation constants for alternative fuels. This revised expression is Equation 6 without the ASAF correction (B) and the addition of a variable A_{from} constant. The formation constants have units of (mg×s/kg-fuel×m^3). The

formation constant relation, analogous to the ASAF fitting factor (λ), needs to vary between neat alternative fuels ($A_{form,alt\text{-}neat}$) and alternative fuel blends ($A_{form,alt\text{-}blend}$) as given here:

$$A_{form,alt-neat} = \left(\frac{C}{H} - 0.342\right)T \quad [9]$$

$$A_{form,alt-blend} = \left(\frac{C}{H} - 0.212\right)T \quad [10]$$

Equations 9 and 10 go a step beyond just correcting for C/H ratio, as they relate the formation constant to thrust. The term T, a third order expression, captures the thrust dependent relation and is equal to:

$$T = 1013 - 4802\left(\frac{\dot{m}f}{\dot{m}f,max}\right) + 7730\left(\frac{\dot{m}f}{\dot{m}f,max}\right)^2 - 3776\left(\frac{\dot{m}f}{\dot{m}f,max}\right)^3 \quad [11]$$

For conventional fuels T is the formation constant, without a C/H correction. EI_{BC} was not found to vary between conventional fuels with varying aromatic contents tested during APEX-I, however, the hydrogen content of the fuels tested were nearly equivalent. As part of the Aircraft Particulate Regulatory Instrumentation Demonstration Experiment (A-PRIDE) 7, it was demonstrated by Brem et al.[21] that BC emissions from conventional fuels may vary due to a range of aromatic content and emissions are best predicted based on hydrogen mass content. Therefore, the addition of a C/H term in equation 11 to account for the varying hydrogen content in available conventional fuels may prove to make the relation applicable to a wider range of conventional fuels. However, Equation 11 based on the available NASA data should capture EI_{BC} from the majority of conventional jet fuels. The complex relation between thrust and the formation constant is also evident in the ASAF-ImFOX relation as the λ values already contain thrust terms and are multiplied by an additional thrust term in the ASAF relation, Equation 9. This is sensible considering that PAH building block molecule concentrations will vary with thrust. High-resolution transmission electron microscopy and X-ray photoelectron spectroscopy have been used to demonstrate how the macro, micro, and nano-structure of BC from commercial aircraft vary across thrust settings.[9, 22] Black carbon nanostructure can reflect the species concentrations available for BC formation and growth.[9] As reported by Vander Wal et al.[9] BC emissions vary from amorphous at low power (idle) to graphitic at high power (take off). This observation supports the need for the formation constant to have a complex dependence on thrust.

The C/H dependent fuel effect developed here based on ground data applies equally well at cruise as the emission trend with C/H ratio is the same at both ground and cruise altitude. However, EI_{BC} measured at cruise during the recent ACCESS-II campaign was 264 % higher than ground based measurements when averaged across all observed powers. This is likely due to the decreased AFR at cruise brought on by the reduced air density. The lower AFR or higher equivalence ratio at cruise will give rise to more fuel rich pockets and higher concentrations of BC precursor molecular species. Therefore, the A_{form} needs to be unique between ground and cruise to account for this. During cruise operation thrust settings are typically higher than 30 %, therefore, cruise EI_{BC} emission profiles do not possess the common curve, with upturns both at low (idle) and high (take-off) thrust levels as measured from ground campaigns. From the limited cruise altitude BC measurements, the EI_{BC} increases linearly with thrust, hence complex formation constants, like derived for ground based emissions, are not necessary. A constant formation constant of 295 captures the observed linear trend of increasing EI_{BC} with increased thrust at cruise.

To capture the emission reductions from the use of alternative fuels two variations of the ImFOX were compared: the ASAF-ImFOX and the C/H-ImFOX. Black carbon emissions from a FT fuel measured during AAFEX-I are plotted in Figure 2 with the calculated values from the two versions of the ImFOX expression.

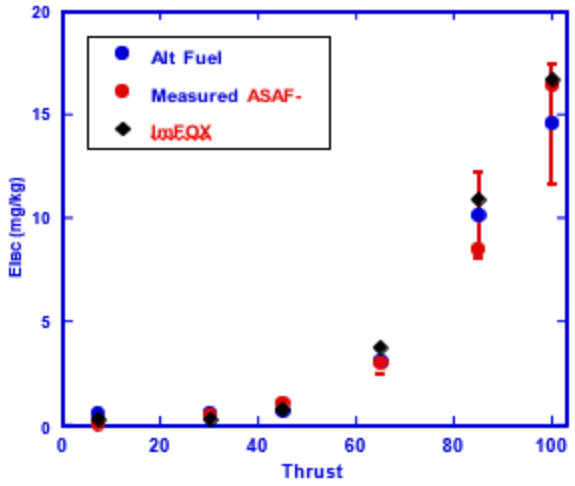

Figure 2. Neat Fischer-Tropsch blend component BC emissions measured during the AAFEX-I campaign. Comparison of the ASAF-ImFOX and C/H-ImFOX methods used for EI_{BC} predictions.

As displayed in Figure 3 both the ASAF-ImFOX and C/H-ImFOX methods capture the emission reductions from the use of a neat Fischer-Tropsch synthetic paraffinic kerosene (SPK) blend component. Due to fuel performance requirements including mass density and wetted-material compatibility SPKs such as the Fischer-Tropsch depicted in this work are approved as alternative fuels only when blended up to a maximum of 50% blend ratio with conventional fuel. Regardless, the SPKs blended up to this limit are still an attractive solution for reducing BC emissions. The ASAF-ImFOX and C/H-ImFOX calculated values are compared to measured BC in Figure 3 for a FT-JP-8 50/50 blend that is within the alternative fuel specification requirements.

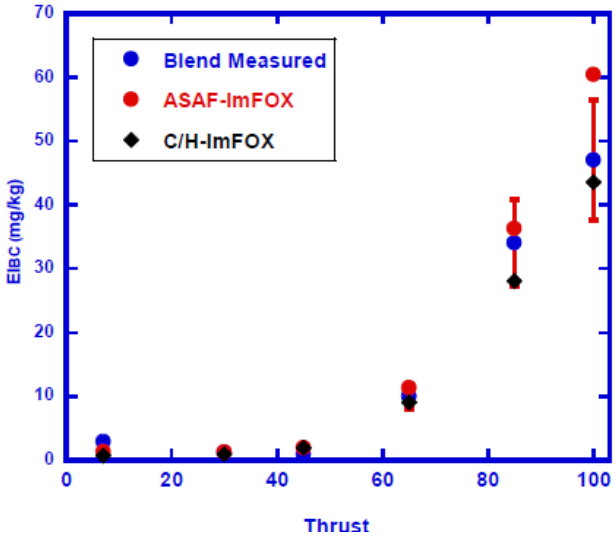

Figure 3. EI_{BC} from a 50/50 blend of Fischer-Tropsch and JP-8 measured during the AAFEX-I campaign. Also shown is a comparison of the ASAF-ImFOX and C/H-ImFOX methods for EI_{BC} predictions of the alternative fuel blend.

As demonstrated in Figure 3 alternative fuel blend emissions are accurately calculated with both expressions except for the ASAF-ImFOX slightly over predicting EI_{BC} at 100% thrust level. This demonstrates that EI_{BC} reductions from alternative fuels can be predicted by correlating the ImFOX with an aromatic or C/H reduction term.

Task #5: Evaluate the Imfox Relation against the ACCESS II Flight Data from NASA for Nvpm

H-ImFOX. As previously mentioned, the pre-exponential frequency factor is a function of two and three member PAH concentration, which in turn is a function of PAH building block molecule concentrations; acetylene, benzene, phenyl radical, and hydrogen. Since there is no practical way to determine these molecular concentrations this pre-exponential factor (also referred to as a formation constant) is fit to C data and given in equation 12.

$$A_{form} = 1013 - 4802\left(\frac{\dot{m}f}{\dot{m}f,max}\right) + 7730\left(\frac{\dot{m}f}{\dot{m}f,max}\right)^2 - 3776\left(\frac{\dot{m}f}{\dot{m}f,max}\right)^3 \quad [12]$$

This 3rd order dependence of the formation constant upon thrust is sensible considering that PAH building block molecule concentrations will vary with thrust. High-resolution transmission electron microscopy and X-ray photoelectron spectroscopy have been used to demonstrate how the macro, micro, and nano-structure of BC from commercial aircraft vary across thrust settings.[9, 22] Black carbon nanostructure can reflect the formation conditions, i.e. species and temperature, of BC.[9] As reported by Vander Wal et al.[35] BC emissions vary from amorphous at low power (idle) to graphitic at high power (take off). This observation supports the need for the formation constant to have a complex dependence on thrust. Black carbon is not an equilibrium product of combustion.[10] Thus, it is difficult to predict its rate of formation and final concentration from kinetics or thermodynamics alone. In practice, the rate of soot formation is strongly impacted by the physical processes of atomization and fuel-air mixing as these processes control the equivalence ratio and resulting flame temperature.[10] This variable, thrust dependent fuel air mixing may be the origin of the complex dependence of A_{from} upon thrust, as expressed in equation 12. This mixing effect would apply across all fuels: conventional, blended, and neat SPK. Therefore, equation 12 developed here for conventional fuel can be used to represent the mixing (combustor) effect across all fuels with a separate fuel term then added explicitly for fuel composition, specifically decreasing EI_{BC} with increasing hydrogen mass content. The new predictive expression is accordingly termed the H-ImFOX, and given in equation 13.

$$C_{BC}\left[\frac{mg}{m^3}\right] = \dot{m}_f \times e^{(13.6-H)}\left(A_{form} \times e^{(-6390/T_4)} - A_{ox} \times AFR \times e^{(-19778/T_4)}\right) \quad [13]$$

The “H” in equation 13 represents hydrogen mass percent and as seen in equation 15 BC emission decays exponentially with increasing hydrogen content. This trend was observed across the previously mentioned NASA campaigns.9 The H-ImFOX will hereafter be referred to as just the ImFOX as the new hydrogen fuel term is universally applied across all fuels and therefore, equation 13 is the ImFOX. A strong correlation between hydrogen content and BC reduction was recently observed during the Aircraft Particulate Regulatory Instrumentation Demonstration Experiment (A-PRIDE) 7. Brem et al.21 found BC emissions from conventional fuels to vary due to a range of aromatic content and concluded that emissions are best predicted based on hydrogen mass content. Additionally, Lobo et al.23 recently reported similar findings by varying the ratio of SPK blending components with conventional fuel.

The hydrogen dependent fuel effect developed here based on ground data applies equally well at cruise as the BC emission trend with hydrogen content is the same at both ground and cruise altitude. However, EI_{BC} measured at cruise during the recent ACCESS-II campaign was 264% higher than ground based measurements when averaged across all observed powers. This is likely due to the decreased AFR at cruise brought on by the reduced air density. The lower AFR or higher equivalence ratio at cruise will give rise to more fuel rich pockets and higher concentrations of BC precursor molecular species. Accordingly, different A_{form} relations are necessary for ground and cruise to account for these differences in mixing. During cruise operation thrust settings are typically higher than 30%, therefore, cruise EI_{BC} emission profiles do not possess the commonly observed emission curve with upturns both at low (idle) and high (take-off) thrust levels as measured in ground campaigns. From the limited cruise altitude BC measurements, the EI_{BC} increases approximately linearly with thrust, hence complex formation constants, like derived for ground based emissions, are not necessary. Although a complex expression for cruise A_{form} may ultimately be needed, however, the limited range of thrust values at cruise presently do not provide justification for such, instead the simplest expression (a constant) was chosen and found

adequate by quality of fit. A A_{form} increased cruise value of 295 captures the observed linear trend of increasing EI_{BC} with increased thrust at cruise.

ImFOX Direct Cruise Prediction.
The litmus test of the ImFOX formalism is whether it captures the range of cruise EI_{BC} values. The ImFOX predictive tool only requires the combustor conditions, AFR and T_4, as input values. If these can be known or otherwise accurately predicted at cruise, then the ImFOX should accurately predict EI_{BC}. Predicted values are compared to measurements made at cruise altitudes during the ACCESS-II campaign for both conventional fuel and an alternative fuel blend, displayed in Figure-4.

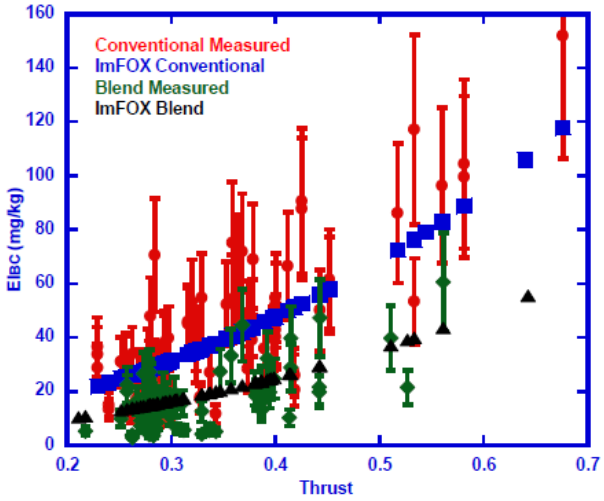

Figure 4. Measured EI_{BC} at cruise altitude burning Jet-A (red circles) and 50/50 blend of Hydrotreated Esters and Fatty Acids (HEFA-SPK) and Jet-A (green diamonds). Shown for comparison are ImFOX predicted values for conventional (blue squares) and blended alternative (black triangles) fuels.

This demonstrates that the ImFOX can be applied to directly predict EI_{BC} values at cruise and will yield accurate results if combustor conditions are known. Predicted values were found using a constant formation constant of 295 and the hydrogen dependent fuel term as described above.

Task #6: Validate the ImFOX for Other Engines in the CFM Class

CFM56-3B. If the form of the ImFOX is correct, it should accurately estimate nvPM emissions from other RQL style combustors. When engine cycle data is not available, the above AFR and T_4 relations can be used. Comparison of the 2C to the 3B is interesting as both are RQL technology and have the same maximum fuel flow rate. Thus, predicted AFR will be the same as dependence is on fuel flow rate with respect to maximum ground fuel flow rate. Predicated T_4 will also be the same as it is dependent on AFR. The ImFOX therefore predicts equivalent emission from the two engines. Evaluating the ImFOX against the 3B is essentially boiled down to comparing emission from the 2C with the expectation of equivalent emissions. Measured nvPM emissions from the NASA APEX campaigns for both engines are provided in Fig. 5. As seen the emission profiles are within the measurement standard deviation. Although within measurement uncertainty, the average emission from three repeated measurements is higher from the 3B as compared to the 2C at higher fuel flow rates. The key difference between these engines is the shape, the 3B has a less rounded bottom by design so it could readily fit under the 737. In doing so, it cut 8 inches off of the front fan blade. Since this was a design restriction and not an engine optimization it may have resulted in a less efficient engine as compared to the 2C. The 2C has a higher pressure ratio and higher maximum thrust. This subtle difference between these two similar engines and the potentially higher emissions from the 3B shows how sensitive emissions are to engine design.

Emission trends from newer combustor technology like the dual staged CFM56-5 and lean burn CFM56-7 are of interest. This is a potential area of collaboration between Penn State and Georgia Institute of Technology as Georgia can provide engine calculations for these engines.

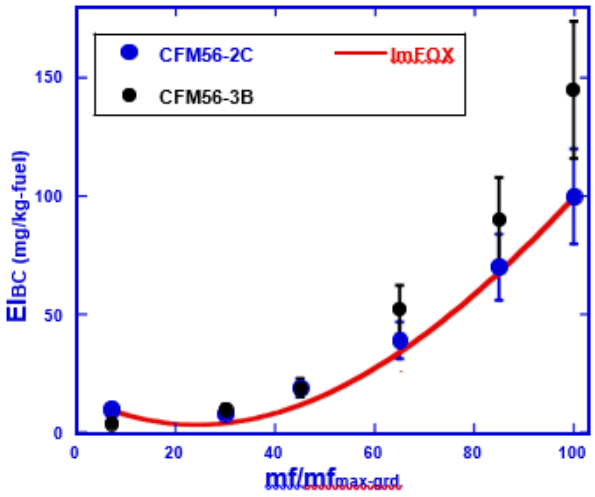

Figure 5. EI_{BC} curves for CFM56- 2C and 3B. Predicted ImFOX values shown for comparison.

References

Wey, C. C.; Anderson, B. E.; Hudgins, C.; Wey, C.; Li-Jones, X.; Winstead, E.; Thornhill, L. K.; Lobo, P.; Hagen, D.; Whitefield, P.; Yevington, P. E.; Herndon, S. C.; Onasch, T. B.; Miake-Lye, P. C.; Wormhoudt, J.; Knighton, W. B.; Howard, R.; Bryant, D.; Corporan, E.; Moses, C.; Holve, D.; Dodds, D. Aircraft Particle Emissions eXperiment (APEX); ARL-TR-3903; NASA Langley Research Center: Hampton, VA, 2006

Wey, C. C.; Anderson, B. E.; Wey, C.; Miake-Lye, R. C.; Whitefield, P.; Howard, R. Overview of aircraft particle emissions experiment. J. Propul. Power 2007, 23, 898-905.

Anderson, B.; Beyersdorf, A.; Hudgins, C.; Plant, J.; Thornhill, K.; Winstead, E.; Ziemba, L.; Howard, R.; Corporan, E.; Miake-Lye, R. Alternative aviation fuel experiment (AAFEX); NASA Langley Research Center: Hampton, VA, 2011

Beyersdorf, A. J.; Timko, M. T.; Ziemba, L. D.; Bulzan, D.; Corporan, E.; Herndon, S. C.; Howard, R.; Miake-Lye, R.; Thornhill, K. L.; Winstead, E.; Wey, C.; Yu, Z.; Anderson, B. E. Reductions in aircraft particulate emissions due to the use of Fischer-Tropsch fuels. Atmos. Chem. Phys. 2014, 14, 11-23.

Moore, R.; Shook, M.; Beyersdorf, A.; Corr, C.; Herndon, S.; Knighton, W.; Miake-Lye, R.; Winstead, S.; Yu, Z.; Ziemba, L.; Anderson, B. Influence of Jet Fuel Composition on Aircraft Engine Emissions: A synthesis of aerosol emissions data from the NASA APEX, AAFEX, and ACCESS missions. Energy Fuels 2015, 29, 2591-2600.

Kinsey, J. S. Characterization of emissions from commercial aircraft engines during the Aircraft Particle Emissions eXperiment (APEX) 1 to 3; EPA-600/R-09/130; Environmental Protection Agency: Washington DC, 2009.

Kinsey, J. S.; Dong, Y.; Williams, D. C.; Logan, R. Physical characterization of the fine particle Emissions form commercial aircraft engines during the Aircraft Particle Emissions eXperiment (APEX) 1-3. Atmos. Environ.2010, 44, 2147-256.

Dong, Y.; Williams, D. C.; Logan, R. Chemical characterization of the fine particle emissions form commercial aircraft engines during the Aircraft Particle Emissions eXperiment (APEX) 1 to 3. Environ. Sci. Technol. 2011, 45, 3415-3421.

Vander Wal, R. L.; Bryg, V. M.; Huang, C.-H. Aircraft engine particulate matter: Macro- mico- and nanostructure by HRTEM and chemistry by XPS. Combust. Flame 2014, 161, 602-611.

Arthur H. Lefebvre; Dilip R. Ballal Gas Turbine Combustion: Alternative Fuels and Emissions; 3rd ed.; CRC Press, 2010; p. 72.

Wayson, R. L.; Fleming, G. G.; Lovinelli, R. Methodology to estimate particulate matter emissions from certified commercial aircraft engines. J. Air Waste Manage. Assoc. 2009, 59, 91-100.

Timko, M. T.; Herndon, S. C.; Blanco, E. R.; Wood, E. C.; Yu, Z.; Miake-Lye, R. C.; Knighton, W. B.; Shafer, L.; DeWitt, M. J.; Corporan, E. Combustion products of petroleum jet fuel, a Fischer–Tropsch synthetic fuel, and a biomass fatty acid methyl ester fuel for a gas turbine engine. Combust. Sci. Technol. 2011, 183, 1039-1068.

Corporan, E.; Dewitt, M. J.; Belovich, V.; Pawlik, R.; Lynch, A. C.; Gord J. R.; Meyer, T. R. Emissions characteristics of a turbine engine and research combustor burning a Fischer–Tropsch jet fuel. Energy Fuels 2007, 21, 2615–2626.

Cain, J.; DeWitt, M.J.; Blunck, D.; Corporan, E.; Striebich, R.; Anneken, D.; Klingshirn, C.; Roquemore, W.; Vander Wal, R. Characterization of gaseous and particulate emissions from a turboshaft engine burning conventional, alternative, and surrogate fuels. Energy Fuels 2013, 27, 2290-2302.

Speth, R. L.; Rojo, C.; Malina, R.; Barrett, S. R. H. Black carbon emissions reductions form combustion of alternative fuels. Atmos. Environ. 2015, 105, 37-42.

Stettler, M. E. J.; Boise, A. M.; Petzold, A.; Barrett, S. R. H. Global civil aviation black carbon emissions. Environ. Sci. Technol. 2013a, 47, 10397-10404.

Lee, K.B; Thring, M.W; Beer, J.M. On the rate of combustion of soot in a laminar soot flame. Combust. Flame 1962, 6, 137–145.

R.J. Hall, M.D. Smooke, M.B. Colket, in Physical and Chemical Aspects of Combustion: A Tribute to Irvine Glassman, F.L. Dryer and R.F. Sawyer (Ed.), Gordon & Breach, 1997, p. 201.

Mensch, A.; Santoro, R. J.; Litzinger, T. A.; Lee, Y.-Y. Sooting characteristics of surrogates for jet fuel. Combust. Flame 2010, 157, 1097-1105.

Yang, Y.; Boehman, A. L.; Santoro, R. J. A study of jet fuel sooting tendency using the threshold sooting index (TSI) model. Combust. Flame 2007, 149 (1−2), 191−205.

Brem, B. T.; Durdina, L.; Siegerist, F.; Beyerle, P.; Bruderer, K.; Rindlisbacher, T.; Rocci-Denis, S.; Andac, M. G.; Zelina, J.; Penanhoat, O.; Wang, J. Effects of fuel aromatic content on nonvolatile particulate emissions of an in-production aircraft gas turbine. Environ. Sci. Technol. 2015, 49, 13149-13157.

Huang, C.-H.; Vander Wal, R. L. Effect of soot structure evolution from commercial jet engine burning petroleum based JP-8 and synthetic HRJ and FT fuels. Energy Fuels 2013, 27, 4946-4958.

Lobo, P.; Christie, S.; Khandelwal, B.; Blakey, S. G.; Raper, D. W. Evaluation of Non-volatile Particulate Matter Emission Characteristics of an Aircraft Auxiliary Power Unit with Varying Alternative Jet Fuel Blend Ratios. Energy Fuels 2015, 29, 7705-7711.

Publications & Presentations

Publication

Abrahamson, J. P., Zelina, J., Andac, M. G., & Vander Wal, R. L. (2016). Predictive Model Development for Aviation Black Carbon Mass Emissions from Alternative and Conventional Fuels at Ground and Cruise. Environmental Science & Technology, 50(21), 12048-12055.

Presentations

Vander Wal, R. L. Abrahamson, J. P., ASCENT Project No. 24B, Emissions data analysis for CLEEN, ACCESS and other tests. FAA Center of excellence for alternative jet fuels and environment. Contractor's workshop. Alexandria, VA. Sept. 27th–28th, 2016.

Abrahamson, J. P., Vander Wal, R. L., PM Emissions Analysis and Predictive Assessment: Update on nvPM predictive modeling from conventional and alternative jet fuels. Aviation Emissions Council (AEC) WEBEX seminar. Feb. 23rd, 2017.

Vander Wal, R. L., Abrahamson, J. P., nvPM Emissions Analysis and Predictive Summary. Poster Presentation. Project 24B Report. FAA Center of Excellence for Alternative Jet Fuels & Environment (FAA COE AJFE). Alexandria, VA April 18th - 19th, 2017.

Abrahamson, J. P., Vander Wal, R. L., (2017). Gas turbine nvPM formation and oxidation semi-empirical model for commercial aviation. Paper 2E19. Topic: Gas Turbine Combustion. 10th US National Meeting of the Combustion Institute, The University of Maryland, College Park, MD April 23rd - 26th, 2017.

Conference Paper

Abrahamson, J. P., Vander Wal, R. L., (2017). Gas turbine nvPM formation and oxidation semi-empirical model for commercial aviation. Paper 2E19. Topic: Gas Turbine Combustion. 10th US National Meeting of the Combustion Institute, The University of Maryland, College Pak, MD April 23rd - 26th, 2017.

Outreach Efforts

Informal discussions with the US EPA regarding variations in nvPM structure and composition dependent upon source.

Awards

None

Student Involvement

The current graduate student, Joseph P. Abrahamson, is conducting data assembly, analysis and predictive relation assessment, towards partial fulfillment of his Ph.D. program in EME, with Fuel Science option.

Plans for Next Period

Options offered:

Possible tasks for this coming year could include,

1. Evaluation of the ImFOX against newer, lean burn engines.
2. Formulation and evaluation of T3, P3 scaling relationships for nvPM (EIbc) between ground and cruise.
3. Testing for correlation between YSI (a lab-based measurement for fuel sooting tendency) and measured EIbc (from jet engines) for JP-8, synthetic fuels and their blends.
4. Develop a number-based predictive relation, including fuel dependence, given forthcoming regulations.

These are described in more detail in the white paper, which was shared with James Hileman and Ralph Iovinelli in April of 2017.

Based on the AEC Roadmap meeting of June 13-15 2017, other needs may be:

1. In our petroleum engineering program, and fuel science courses, we use HYSYS. Aspen HYSYS is the energy industry's leading process simulation software that's used by top oil and gas producers, refineries and engineering companies for process optimization in design and operations. Aspen HYSYS is a process simulation software for the optimization of conceptual design and operations including multiphase flow modeling, gas processing, refining and distillation. We could evaluate necessary refinery operations.
2. Based on Dr. Bruce Anderson's overview of their upcoming contrail/plume measurements this coming year, he stated that extra sampling ports were available on the NASA DC-8, and that other measurements could be accommodated. This would truly be a unique opportunity to collect in situ particulate samples for microscopic analyses, SEM, TEM to benchmark what other aerosol instrumentation is actually measuring, (and insights into the aerosol processing within the plume.)

Project 025 Shock Tube Studies of the Kinetics of Jet Fuels

Stanford University

Project Lead Investigator

Ronald K Hanson
Woodard Professor
Mechanical Engineering Department
Stanford University
452 Escondido Mall
650-723-6850
rkhanson@stanford.edu

University Participants

Stanford University

- P.I.s: Prof. Ronald K Hanson
- FAA Award Number: 13-C-AJFE-SU-008
- Period of Performance: 10/01/2016 to 09/30/2017
- Task: Area #1 – Chemical Kinetics Combustion Experiments

Project Funding Level

$210,000 from FAA with 1-1 matching funding of $210,000 from Stanford University.

Investigation Team

Prof. Ronald K Hanson, Principal Investigator, Research Direction
Dr. David F Davidson, Senior Research Engineer, Research Management
Jiankun Shao, Graduate Student, Research Assistant
Tom C Parise, Graduate Student, Research Assistant
Sarah Johnson, Graduate Student, Research Assistant

Project Overview

Provide shock tube/laser absorption experiments for a fundamental kinetics database for jet fuels. Experiments are expected to continue to reveal the sensitivity of combustion properties to fuel composition for the ultimate use in simplifying the alternative fuel certification process.

Task Area #1: Chemical Kinetics Combustion Experiments

Stanford University

Objective(s)

Experiments provide an extensive fundamental kinetics data for selected jet fuels. These data are used as critical input for Area #2 that seeks to develop a new hybrid and detailed kinetics model for jet fuels (HyChem). These experiments continue to reveal the sensitivity of combustion properties to variations in fuel composition for ultimate use in simplifying the alternative fuel certification process. The team works in close collaboration with Professor Hai Wang, also of Stanford University, the PI for Area #2, who uses the data acquired in our experiments. The data provided will also ensure that the combustion models developed in Area #4 - Combustion Model Development and Validation to model the extinction and ignition processes controlling lean blowout, cold ignition and high altitude relight, are chemically accurate.

Research Approach

The development, refinement and validation of detailed reaction mechanisms describing the pyrolysis and oxidation of fuels require experimental data as targets for kinetics models. Experimentally, the best way to provide these targets at high temperatures and pressures is with shock tube/laser absorption experiments, conducted over a wide range of pressure, temperature, and fuel and oxidizer composition.

Reflected shock wave experiments provide a test environment that does not introduce additional fluid mechanics, turbulence, or heat transfer effects to the target phenomena. This allows isolation of the target phenomena (ignition delay times and species concentration time-histories) in a quiescent high-temperature, high-pressure environment that is very well characterized and hence amenable to modeling. Recent work in our laboratory to develop the Constrained Reaction Volume (CRV) methodology provides an additional tool to provide shock tube data under constant-pressure constraints when needed, to significantly simplify the gasdynamic/thermodymamic models needed to properly simulate reactive reflected shock wave data.

The strength in the Stanford shock tube approach comes with the implementation of laser diagnostics that enable the simultaneous measurement of species time-histories. Using laser absorption, we are able to provide quantitative time-histories during fuel pyrolysis and oxidation of the fuel, including transient radicals (e.g., OH, CH3), stable intermediates (e.g., CH4, C2H4, iso-butene and aromatics), combustion products (including CO, CO2, and H2O), and temperature.

Measurements of the pyrolysis and oxidation systems of real fuels, rather than of surrogates or solvent surrogates, provide a direct link to actual fuel behavior. The combination of high-quality shock tube and flow reactor measurements combined with the HyChem kinetic model based on real fuel decomposition products proposed by Professor Hai Wang is meeting the FAA program objectives.

Shock Tube Experiments

Stanford has the largest and best-equipped shock tube laboratory in the U.S., perhaps in the world, with five shock tubes: three large-diameter (10, 14 and 15 cm I.D.) high-purity shock tubes (see Fig. 1a); one heated high-pressure shock tube (5 cm I.D., capable of achieving 500+ atm); and 10 cm I.D. expansion tube for generating supersonic flows. Additionally, we have unique capability for species measurements using laser absorption (see Fig. 1b) developed over the past 30 years. In these experiments, temperatures from below 500 K to above 3000 K, and pressure from sub-atmospheric (0.2 atm) to 10-500+ atmospheres can be achieved in different carrier gases, such as argon or air, with demonstrated test times up to and exceeding 50 ms at low temperatures.

Three primary types of shock tube experiments are performed.

The first primary shock tube experiments are species concentration time-history measurements obtained during fuel pyrolysis. These data are used to place strong constraints on the reaction mechanism and the individual reaction rates and pathways. Laser absorption techniques, many pioneered at Stanford, are used to measure these species time-histories. The following species time-histories measurements have been acquired and used in the development of the HyChem model: fuel at a wavelength of 3.39 microns, and the stable fuel decomposition products: ethylene, methane, and iso-butene, at wavelengths of 10.53, 3.1754 and 11.3 microns, respectively. We also are able to measure the transient radical OH (in the UV at 306 nm), the combustion products CO, CO2 and H2O (in the IR at 2.7, 4.6 and 2.5 microns, respectively) as well as other product species.

Representative data acquired using these methods are shown in Figures 2a, b, and c. These measurements of the major jet fuel decomposition products during pyrolysis (fuel, ethylene, propene, and isobutene time-histories) were directly applicable to the development of the HyChem Fuel X model by Prof. Hai Wang.

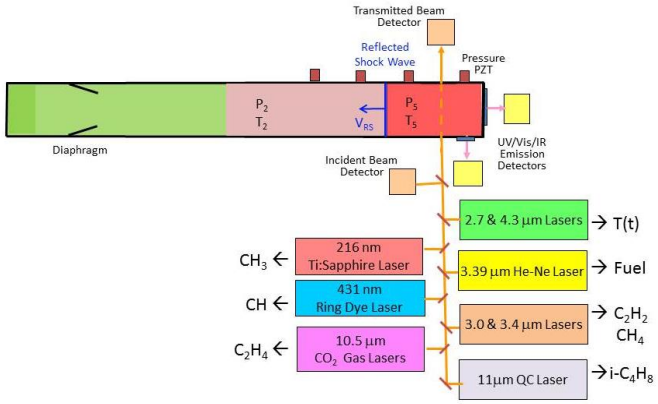

Figure 1a: Stanford 15 cm diameter shock tube. **Figure 1b:** Schematic of shock tube/laser absorption setup. Simultaneous measurement of multiple species time-histories and temperature with microsecond time resolution are enabled using this arrangement. Only a partial list of accessible species is indicated.

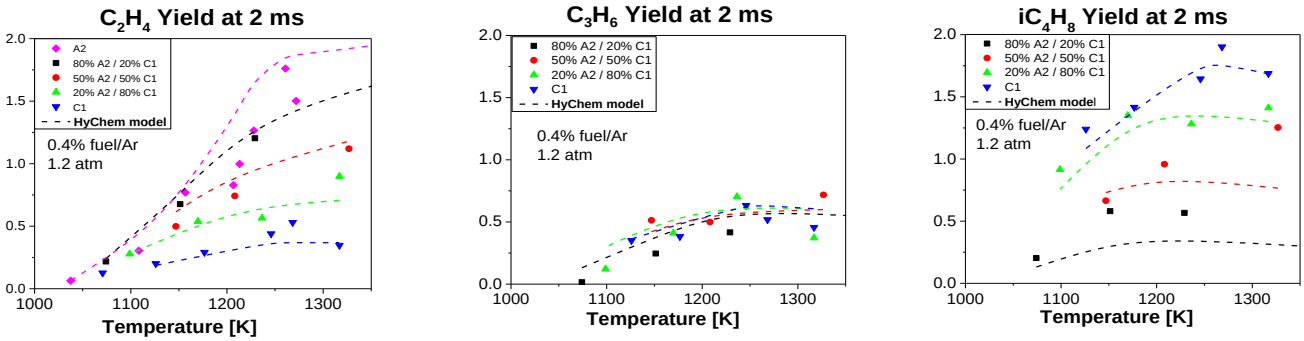

Figure 2a, b, & c: C2H4 C3H6 and iC4H8 yields acquired during the pyrolysis of blends of FAA fuels A1 & C1.

Milestones

Major milestones included regular reporting of experimental results and analysis at monthly meetings for both the Kinetics Working Group and the Steering Working Group, as well as reporting at FAA Quarterly and ASCENT annual meetings.

Major Accomplishments

During this third year of this program, we made advances in several areas.

We have developed infrared laser diagnostics schemes for propene at 10.975 microns and for fuel at 3.41 microns. These diagnostics provide quantitative, sensitive, low-noise detection of key species involved in the combustion of jet fuels.

Using these new diagnostics schemes and our existing systems for ethylene, methane and isobutene, we have acquired refined multi-species data for Cat A and C1 fuels using a six-IR-wavelength strategy.

In the analysis of this multi-species/multi-wavelength approach we have also assessed the role of minor interfering species (e.g. 1-butene, 2-butene, and allene) on the measured iso-butene and propene pyrolysis yields.

In separate experiments we measured ignition delay times (IDT) of a series of jet fuels with varying cetane number and showed the variation of IDT with CN.

We have also performed IDT measurements of a series of Air Force jet fuels from geographically varying locations to investigate the range of commercially available jet fuel performance.

Finally, we are currently developing a diagnostic scheme to measure aromatics yields during fuel pyrolysis. These measurements will enable us to close the carbon balance of jet fuel pyrolysis products.

Publications

Peer-reviewed journal publications

D. F. Davidson, Y. Zhu, J. Shao, R. K. Hanson, "Ignition Delay Time Correlations for Distillate Fuels," Fuel 187 26–32 (2017).

Published conference proceedings

R. Xu, D. Chen, K. Wang, Y. Tao, J.K. Shao, T. Parise, Y. Zhe, S. Wang, R. Zhao, D.J. Lee, F.N. Egolfopoulos, D.F. Davidson, R.K. Hanson, C.T. Bowman and H. Wang, "HyChem Model for Petroleum-Derived Jet Fuels," 10th U. S. National Combustion Meeting, April 23-26, 2017, College Park, Maryland.

R. Xu, H. Wang, D.F. Davidson, R.K. Hanson, C.T. Bowman, F.N. Egolfopoulos, "Evidence Supporting a Simplified Approach to Modeling High-Temperature Combustion Chemistry," 10th U. S. National Combustion Meeting, April 23-26, 2017, College Park, Maryland.

J.K. Shao, D.F. Davidson and R.K. Hanson, "Shock Tube Study of Jet Fuel Pyrolysis and Ignition at Elevated Pressure," 10th U. S. National Combustion Meeting, April 23-26, 2017, College Park, Maryland.

K. Wang, R. Xu, T. Parise, J.K. Shao, D.F. Davidson, R.K. Hanson, H. Wang, C.T. Bowman, "Evaluation of a Hybrid Chemistry Approach for Combustion of Blended Petroleum and Bio-derived Jet Fuels," 10th U. S. National Combustion Meeting, April 23-26, 2017, College Park, Maryland.

K. Wang, R. Xu, T. Parise, J.K. Shao, D.J. Lee, A. Movaghar, D.F. Davidson, R.K. Hanson, H. Wang, C.T. Bowman and F.N. Egolfopoulos, "Combustion Kinetics of Conventional and Alternative Jet Fuels using a Hybrid Chemistry (HyChem) Approach," 10th U. S. National Combustion Meeting, April 23-26, 2017, College Park, Maryland.

Outreach Efforts

Ignition delay time measurements of a series of jet fuels with varying cetane number from the Army Research Laboratory (ARL) providing fuel characterization data of use to both the FAA and the ARL.

Ignition delay time measurements of a series of jet fuels from geographically varying locations from the Air Force/Wright Patterson Airbase providing fuel characterization data of use to both the FAA and the AFOSR.

Awards

None

Student Involvement

Graduate students are actively involved in the acquisition and analysis of all experimental data. Tom C. Parise is preparing to defend his Ph.D. thesis based on work performed under this contract.

Plans for Next Period

Advances in the HyChem model development based on the experimental and theoretical work so far indicate that there are several important issues that should be addressed as the model is further developed and validated. 1) The HyChem model will be tested on a wide range of jet fuel types to establish temperature and pressure boundaries for the validity of the HyChem modeling approach. 2) Efforts will be made to update the foundational fuel chemistry, paying particular attention to the i-C4H8 sub-mechanism, that is the basis of the oxidation sub-mechanism of HyChem. 3) Shock tube/laser absorption measurements will be used to investigate the relationship of Cetane Number (CN) and ethylene yields during pyrolysis. 4) Efforts will also be made to completely characterize jet fuel using shock tube/laser absorption measurements by completing the carbon balance of fuel pyrolysis products.

Project 027(A) National Jet Fuels Combustion Program – Area #3: Advanced Combustion Tests (Year III)

Georgia Institute of Technology, Oregon State University, University of Illinois[3]

*this report covers portion of University of Illinois

Project Lead Investigator

Tonghun Lee
Associate Professor
Mechanical Science & Engineering
University of Illinois at Urbana-Champaign
1206 W. Green St.
Urbana IL 61801
517-290-8005
tonghun@illinois.edu

University Participants

University of Illinois at Urbana-Champaign

- P.I.(s): Tonghun Lee, Associate Professor
- FAA Award Number: 13-C-AJFE-UI-016
- Period of Performance: 10/1/2016 to 9/30/2017
- Task(s):
    1. Conduct high altitude relight ignition probability measurements in the modified sector rig at ARL.
    2. Conduct ignition delay measurements of the targeted cetane number fuels in the RCM at UIUC.

Project Funding Level

Funding Level: $200,000
Cost Share: In-kind academic time of the PI, cost share provided by software support from Convergent Sciences Inc.

Investigation Team

- Eric Mayhew (Graduate Student, University of Illinois at Urbana-Champaign): Execution of laser and optical diagnostics at ARL.
- Kyungwook Min (Graduate Student, University of Illinois at Urbana-Champaign): Rapid Compression Machine testing of fuels.
- Brendan McGann (Graduate Student, University of Illinois at Urbana-Champaign): Execution of laser and optical diagnostics at ARL.
- Constandinos Mitsingas (Graduate Student, University of Illinois at Urbana-Champaign): Execution of laser and optical diagnostics at ARL.

Project Overview

The objective of this project is to support measurements of ignition probability at high altitude conditions and fundamental ignition delay measurements as a part of the FAA COE ASCENT's combustion program. The effort will strive to meet two critical targets. The first is to make measurements of ignition probabilities of jet fuels at altitudes between 10,000 and 30,000 ft. in a sector rig with key geometry matching the NJFCP referee rig at Wright-Patterson Air Force Base. The second goal is to make measurements of ignition delay for targeted cetane number fuels in a rapid compression machine at UIUC

to enhance our understanding of the importance of cetane number in low-temperature autoignition experiments and how it relates to lean blowout (strongest correlating parameter to lean blowout). The success of this program will substantially accelerate the efforts of the FAA and the OEMs to certify alternative, fit for purpose fuels.

Task #1: Measure Ignition Probability for Various Fuels at High Altitude Conditions and Implement High-Speed Imaging to Visualize Ignition Process

University of Illinois at Urbana-Champaign

Objective(s)

The objectives in this project are to work with ARL in the design, setup, and implementation of ignition experiments in the high-altitude chamber at Army Research Laboratory at Aberdeen Proving Ground:

- Design and set up sector rig in high altitude chamber at Army Research Laboratory at Aberdeen Proving Ground.
- Conduct measurements of ignition probability at high altitude conditions (low temperature, low pressure).
- Implement high-repetition rate broadband and OH* imaging to visualize ignition kernel and flame kernel propagation.

Research Approach

The process of developing and approving new jet fuels derived from alternative feedstocks requires certifying that those fuels, whether neat or blended with conventional fuels, can be used in current engines without hardware modification. Understanding how these new fuels perform in extreme combustion regimes is important to ensuring that the fuels can be used as drop-in replacements. One regime in which it is essential that new fuels perform as well as conventional fuels is in a scenario where an engine needs to be relit at high altitude. The lower temperatures and pressures seen at high altitudes result in a lower probability of spark kernel ignition and flame stabilization when compared to sea level conditions. A few of the causes of this reduced probability include slower chemistry, poorer atomization due to the higher fuel viscosity, slower evaporation due to the reduced vapor pressure of the fuel, and shorter spark kernel lifetime due to the entrainment of the lower temperature air. To study the effects of fuel differences in this high altitude relight scenario, a gas turbine combustor sector rig was designed and built. The sector rig is operated inside of a high-altitude chamber with the chamber conditions varying as shown in Table 1, with 30,000 ft being the highest altitude that the chamber is capable of simulating.

Table 1 Chamber air temperature and pressure as a function of altitude

Altitude (ft)	T_{air} (K)	P_{air} (kPa)
0	288	101.3
10,000	268	69.6
20,000	249	46.6
25,000	239	37.7
30,000	229	30.2

Ignition probabilities for alternative and conventional jet fuels are measured in a gas turbine sector rig inside of a high-altitude chamber as shown in Figure 1. Experiments are designed to simulate combustor relight at high altitude conditions. Initial relight experiments were conducted at conditions representative of ambient air at 10,000 feet with an air mass flow rate of 0.3lbm/s. This air flow mass flow rate resulted in a pressure drop across the swirler of 3.87%. The fuel is chilled by placing the fuel holding vessel in the inlet air flow path, resulting in an average fuel injection temperature of -15°C. The equivalence ratio is varied by changing the inlet fuel pressure, and fuel flow rates could be varied to achieve equivalence ratios from 0.6 and 1.0. This range of equivalence ratios was sufficient to span from no ignition to always igniting.

A single test begins with the opening of a solenoid valve just upstream of the nozzle, allowing fuel flow at the desired equivalence ratio. After two seconds in which the fuel flow rate is allowed to stabilize, a 24 VDC voltage is supplied to an ignition exciter (Champion CH305050), which supplies high voltage to an igniter from a General Electric T700 at a frequency of 3.7 Hz. The igniter is allowed to spark for 10 seconds, after which the voltage and fuel supply are stopped. The sparks and flame are monitored with a photo diode as well as a high-speed camera (Photron SA-Z) coupled to a high-speed intensifier (LaVision IRO), fitted with a bandpass filter centered at 320 nm, with a full-width, half-max of 20 nm. A sample photodiode trace is shown in Figure 3. The spark emission events are shown as the sharp peaks, and the flame is observed as the slight increase in photodiode signal above the baseline between the sharp peaks.

Figure 1 High altitude chamber at the Army Research Laboratory at Aberdeen Proving Ground

A total of 5 fuels were tested, all from the National Jet Fuel Combustion Program. Three conventional fuels, designated A-1 (JP-8), A-2 (Jet A), and A-3 (JP-5), represent current petroleum-derived fuels that are used in modern aircraft engines. Two category C fuels were tested as well, designated C-1 and C-3. The C-1 fuel is Gevo alcohol-to-jet; its notable properties are a low derived cetane number (~16) and a relatively low temperature boiling curve. C-3 is notable for its high viscosity, a parameter that is particularly important for atomization at these low temperatures.

For each test, a photo diode trace like the one shown in Figure 3 is obtained. A flame is considered to have stabilized when the ratio of the absolute value of the integrated negative signal to the integrated positive signal is less than 1% for two consecutive periods between sparks. The number of sparks that do not result in a stable flame are counted along with the one spark that resulted in the stable flame. The ignition probability for a single equivalence ratio for a single fuel is the number of successful sparks divided by the total number of sparks. The ignition probability for all of the fuels and equivalence ratios tested are shown in Figure 1 as well as the binomial regression fits calculated from the ignition probabilities. Defining the 'best' fuel case as the fuel that has the highest ignition probability for each equivalence ratio, the preliminary analysis yielded a fuel ordering, from best to worst of: A-1, C-1, A-2 and A-3 about equal, and then C-3. More complete analysis of the images and ignition probabilities is ongoing; however, the parameters that appear to be most important in determining ignition probability are viscosity and vapor pressure at the temperatures measured in the rig. Further analysis of the video will provide a better qualitative understanding of the process in which a spark kernel leads to a flame kernel, eventually resulting in stabilization of the flame in the combustor. Further testing is required and planned to obtain lower uncertainties in the probability curves as well as to obtain data for more fuels and at more altitudes.

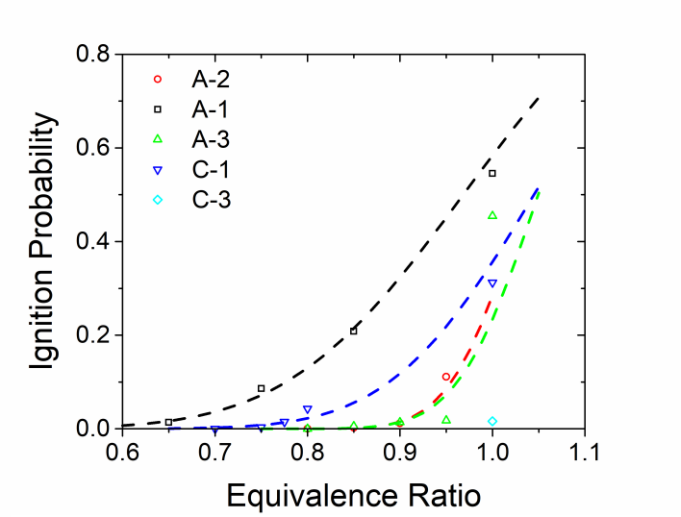

Figure 2 Ignition Probability versus equivalence ratio for the 3 category A fuels and 2 category C fuels at 10,000 ft.

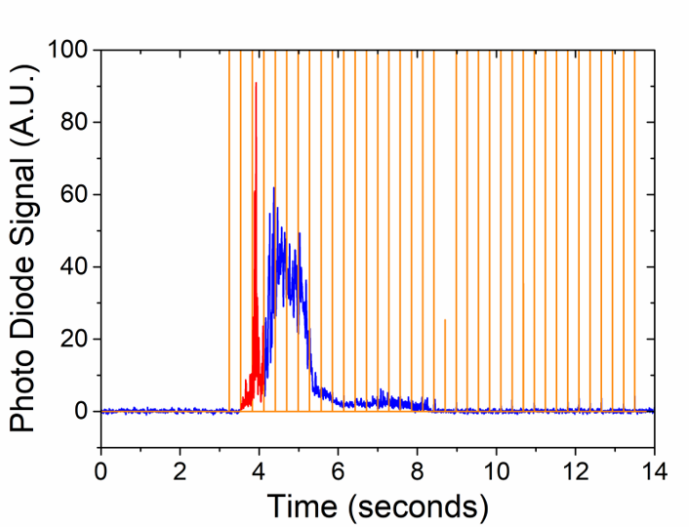

Figure 3 Example photodiode trace of sparks and a successful ignition

Task #2: Measure Ignition Delay at Low Temperature Conditions for Fuels with Targeted Cetane Numbers

University of Illinois at Urbana-Champaign

Objective(s)

The objectives in this project are to make measurements of ignition delay of targeted cetane number fuels developed by ARL cetane number has shown a strong correlation to lean blow out equivalence ratio.

Varied cetane number army research fuels

Six different fuels have been tested to measure the ignition delay time in the RCM. These fuels are blended to match a targeted cetane number between 30 and 55. CN 50 appears to be the base fuel used prior to the inclusion of cetane inhibitors /improvers. Isododecane (pentamethylheptane) is used as the cetane inhibitor, as well as naphthalene in the CN 30. Inclusion of higher n-alkanes (C14 - C16) is used as the cetane improver for CN 55. Navy Fuel Composition and Screening Tool (FCAST) have been used to classify detailed chemical group composition of the fuels as in Table 2. Contents of isoalkanes and aromatics are higher for low cetane number fuels, whereas higher cetane number fuels tend to contain more normal alkanes.

Table 2 Compisition of the Army research fuels tested

mass %	Jet A-30CN	Jet A-35CN	Jet A-40CN	Jet A-45CN	Jet A-50CN	Jet A-55CN
Normal Alkanes	16.02	16.48	21.83	19.54	36.50	54.10
Isoalkanes	54.80	58.22	41.41	48.14	34.14	28.33
Cyclocalkanes	3.85	1.21	3.22	10.94	12.18	6.08
Aromatics	25.32	24.08	33.53	21.41	17.18	11.46

Ignition delay of varied cetane number fuels

Ignition delay time measurements have been conducted for compressed pressures of P_c=20 bar, at equivalence ratios (φ) of 1.0, 0.5, and 0.25. Compressed temperature T_c varies by compression ratio: 615K to 725K. Figure 4 shows measured ignition delay time at P_c=20 bar.

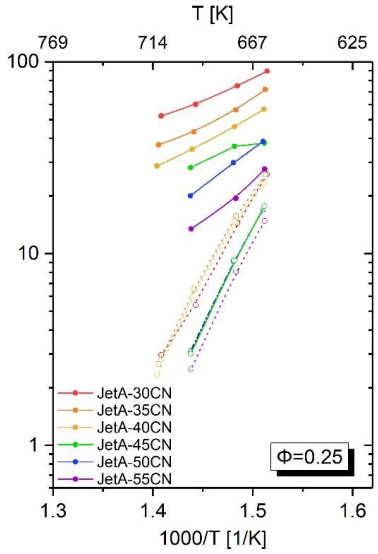

Figure 4 First and overall ignition delay time results at φ=0.25

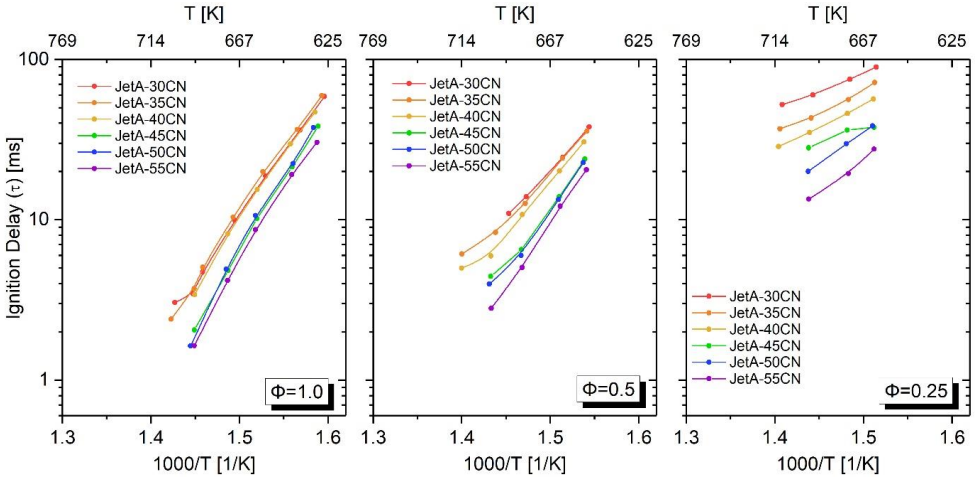

Figure 5 Ignition delay times of Jet A fuels with varied cetane numbers at Pc=20 bar, varied temperatures, and equivalence ratios

As expected, fuel with lower cetane number results in longer ignition delay, and the tendency is more prominent at leaner conditions. In the φ=1 case, some of the ignition delay time results do not exactly follow the cetane number ordering. No negative temperature coefficient (NTC) behavior is observed in these tests. Further analysis of the φ=0.25 case is illustrated in Figure 5, where dotted lines are separated first stage ignition delay time. The difference in first stage ignition delay time by fuels are much less than difference in overall ignition delay time. In other words, the second stage ignition delay constitutes nearly all of the differences in the overall delay time. Additional ignition delay time measurements will be conducted at lower compressed pressure, P_c=10 bar. Further analysis on multistage ignition will be investigated using CHEMKIN, chemical kinetics simulation results.

Milestones

Proposed (3 Month): At the 3 month mark, we should have shipped the sector rig to ARL to begin setting it up in the high altitude chamber.
Achieved: Army Research Combustor-L1 shipped to ARL, and preparations for high altitude relight campaign have begun.

Proposed (6 Month): At the 6 month mark, we should have purchased peripheral components for the high altitude relight campaign, and a test matrix should have been decided on.
Achieved: The designs have been finalized and drawings sent to the machine shop. Materials for the rig have been ordered.

Proposed (9 Month): At the 9 month mark, we should have completed the high altitude ignition probability test matrix set out in the previous period. The ignition delay measurements in the RCM should have been completed.
Achieved: High altitude relight measurements at 10,000 ft, and hardware upgrades for future campaigns have been planned. Ignition delay measurements have been completed.

Proposed (12 Month): At the 12 month mark, we should have finished analyzing the ignition probability data and RCM ignition delay data.
Achieved: Preliminary analysis of the ignition probability data and RCM data has been completed

Major Accomplishments

High Altitude Relight Combustor
Design and fabrication of a high altitude relight rig, replicating the key geometry and flow features of the referee rig has been completed. The sector rig was set up in the high-altitude chamber, and modifications to the chamber and fuel delivery system were made. Measurements of ignition probability for 5 fuels across a range of equivalence ratios at ambient pressure and temperature conditions that correspond to 10,000 ft. Further data is needed at higher altitudes to gain a better understanding of the fuel properties that drive ignition behavior at these conditions.

Target Cetane Number Ignition Delays
Ignition delay measurements for targeted cetane number fuels, with cetane numbers varying from 30 to 55, were made in a rapid compression machine at the University of Illinois at Urbana-Champaign. Higher cetane number correlated strongly with shorter ignition delay at low temperature. The results warrant further investigation into the targeted cetane number fuels in the NTC region to gain a better understanding of how the cetane number drives autoignition delay time in this regime.

Publications

E. Mayhew, C. Mitsingas, B. McGann, T. Lee, T. Hendershott, S. Stouffer, P. Wrzesinski, A. Caswell, Spray Characteristics and Flame Structure of Jet A and Alternative Jet Fuels, AIAA SciTech, AIAA-2017-0148, 2017

I. Chterev, N. Rock, H. Ek, B. Emerson, J. Seitzman, T. Lieuwen, D. Noble, E. Mayhew, T. Lee, Simultaneous High Speed (5 kHz) Fuel-PLIE, OH-PLIF and Stereo PIV Imaging of Pressurized Swirl-Stabilized Flames using Liquid Fuels, AIAA SciTech, AIAA-2017-0152, 2017

Outreach Efforts

None

Awards

I. Chterev, N. Rock, H. Ek, B. Emerson, J. Seitzman, T. Lieuwen, D. Noble, E. Mayhew, T. Lee, Simultaneous High Speed (5 kHz) Fuel-PLIE, OH-PLIF and Stereo PIV Imaging of Pressurized Swirl-Stabilized Flames using Liquid Fuels, AIAA SciTech, AIAA-2017-0152, 2017
(winner of the ***The Walter R. Lempert Student Paper Award in Diagnostics for Fluid Mechanics, Plasma Physics, and Energy Transfer***)

Student Involvement

Four graduate students (listed above) have participated in this project on a rotational basis to address various aspects of the project. Two students (Brendan McGann, and Eric Mayhew) made trips to ARL to deliver and set up the Army Research Combustor-L1 in preparation for the high altitude experiments. Three students executed (Brendan McGann, Constandinos Mitsingas, and Eric Mayhew) set up and executed the high altitude relight experiments outlined in Task 1. Kyungwook Min conducted the ignition delay measurements in RCM at UIUC.

Plans for Next Period

In year IV of the NJFCP, the main focus of our efforts will be to continue the execution of high altitude ignition experiments at the Army Research laboratory. The test conditions will be worked out with OEM input based on the data already collected, and the work will also be coordinated with the ongoing ignition work at GATech. We will continue to support AFRL in any diagnostics efforts required in the referee rig combustor. Looking into the future, we anticipate either PIV or PDPA measurements will be required in the sector rig a ARL to obtain flow field information. We have already designed the required hardware for this effort and will look for an opportunity to implement them with support from ARL and AFRL.

Project 027(B) Advanced Combustion (Area #3)

Georgia Institute of Technology
Oregon State University

Project Lead Investigator

Tim Lieuwen
Professor
Aerospace Engineering
Georgia Institute of Technology
270 Ferst Drive, G3363 (M/C 0150)
Atlanta, GA 30332-0150
404-894-3041
tim.lieuwen@ae.gatech.edu

University Participants

Georgia Institute of Technology

- P.I.(s):
  - Professor Tim Lieuwen
  - Professor Jerry Seitzman
  - Professor Wenting Sun
- FAA Award Number: 13-C-AJFE-GIT-008
- Period of Performance: 12/1/2016 to 11/30/2017
- Task(s):
  - Task #1 - Lean Blowout. This task measures the lean blowout characteristics of alternative jet fuels and compares them to the lean blowout characteristics of jet A.
  - Task #2 - Ignition. This task measures the ignition probabilities of alternative jet fuels and compares them to the ignition probabilities of jet A.

Oregon State University

- P.I.(s): David Blunck
- FAA Award Number: 13-C-AJFE-OSU-02
- Period of Performance: 12/1/2016 to 11/30/2017
- Tasks:
  - Task #3 - Turbulent Flame Speed. This task measures the turbulent flame speeds of alternative jet fuels and compares them to the turbulent flame speeds of jet A.

Project Funding Level

Georgia Institute of Technology
FAA Funding: $300,000
Cost Share: $300,000 provided by Georgia Institute of Technology

Oregon State University
FAA Funding: $80,000
Cost Share: $80,000 provided by Oregon State University

Investigation Team

Tim Lieuwen (Georgia Institute of Technology): Principal Investigator. Professor Lieuwen is the PI overseeing all tasks, and is manager of Task 1. Lean Blowout
Jerry Seitzman (Georgia Institute of Technology): Co-Principal Investigator. Professor Seitzman is the manager of Task 2. Ignition
David Blunck (Oregon State University): Co-Principal Investigator. Professor Blunck is the manager of Task 3. Turbulent Flame Speed
Wenting Sun (Georgia Institute of Technology): Co-Principal Investigator. Professor Sun is acting as an internal expert consultant on kinetic mechanisms
Tonghun Lee (University of Illinois Champaign): Co-Principal Investigator. Professor Lee is the lead diagnostic expert.
Benjamin Emerson (Georgia Institute of Technology): Research Engineer. Dr. Emerson is responsible for designing and maintaining experimental facilities, as well as experimental operations and management & safety of graduate students. He is also acting as the administrative coordinator for all three tasks.
David Wu (Georgia Institute of Technology): Research Engineer. Mr. Wu is responsible for designing and maintaining experimental facilities, as well as experimental operations and management & safety of graduate students.
Brandon Sforzo (Georgia Institute of Technology): Postdoctoral Fellow. Dr. Sforzo is the lead experimentalist in the ignition task. Dr. Sforzo left Georgia Tech during year 3.
Glenda Duncan (Georgia Institute of Technology): Administrative Staff. Mrs. Duncan provides administrative support.
Tiwanna Williams (Georgia Institute of Technology): Administrative Staff. Mrs. Williams provides administrative support.
Seth Hutchins (Georgia Institute of Technology): Lab Coordinator. Mr. Hutchins maintains the core lab facilities and provides technician services.
Machine Shop Staff (Georgia Institute of Technology). The Aerospace Engineering machine shop provides machining services for experimental facility maintenance/construction
Nick Rock (Georgia Institute of Technology): Graduate Student. Mr. Rock is leading the lean blowout task.
Ianko Chterev (Georgia Institute of Technology): Graduate Student. Dr. Chterev assisted with the diagnostics for the lean blowout task. Dr. Chterev graduated during year 3.
Hanna Ek (Georgia Institute of Technology): Graduate Student. Ms. Ek is the lead data analyst for the lean blowout task.
Sheng Wei (Georgia Institute of Technology): Graduate Student. Mr. Wei currently leads the ignition task.
Aaron Fillo (Oregon State University): Graduate Student. Mr. Fillo was the lead grad student experimentalist on the turbulent flame speed task. He is no longer working on this project.
Jonathan Bonebrake (Oregon State University): Graduate Student. Mr. Bonebrake is currently the lead grad student experimentalist on the turbulent flame speed task.
Nathan Schorn (Oregon State University): Graduate Student. Mr. Schorn recently started and has transitioned to leading the effort to operate the burner and collect and analyze data
Eric Mayhew (Graduate Student, University of Illinois at Urbana-Champaign): Graduate Student. Mr. Mayhew leads the execution of laser and optical diagnostics at ARFL.
Rajavasanth Rajasegar (Graduate Student, University of Illinois at Urbana-Champaign): Graduate Student. Mr. Rajasegar led the optimization of laser diagnostics during year 1.
Brendan McGann (Graduate Student, University of Illinois at Urbana-Champaign): Graduate student. Mr. McGann executed the laser and optical diagnostics at GATech during year 1.

Project Overview

The objective of this project was to provide advanced combustion testing of alternative jet fuels. We performed this advanced combustion testing to accomplish two goals. The first goal was to rank the lean blowout boundaries, ignition probabilities, and turbulent flame speeds of alternative fuels relative to conventional Jet A. The second goal was to produce data that could support the modeling and simulation tasks of other teams. For this second goal, data were measured as needed and as requested by the other teams. These data typically consisted of velocity field measurements, high speed flame images, and test rig boundary conditions.

During this program we tested fifteen different pure fuels, known to the program as: A1, A2, A3, C1, C2, C3, C4, C5, S1, S2, high TSI, C7, C8, C9, and n-dodecane. The A1, A2, and A3 fuels represent the range of conventional jet-A fuels. The other fuels have different physical and/or chemical properties. We have also tested two different sets of blends: A2/C1 blends and A2/C5 blends. These fuels have been tested under three different tasks, which are summarized next and which are detailed in the rest of this report.

(1): The first task consisted of lean blowout measurements. The highest priority lean blowout measurement was fuel screening, where the blowout boundaries of various fuels were compared to the blowout boundary of jet A. This task also included measurements of the combustor velocity field, the spatio-temporal evolution of the flame position, and several thermodynamic rig boundary conditions. Thermodynamic boundary conditions included measurements such as air flow rates, surface temperatures, gas temperatures, and gas pressures.

(2): The second task consisted of forced ignition measurements. Like the blowout task, the highest priority forced ignition measurement was fuel screening. In the case of the forced ignition task, the fuel screening activity measured the ignition probabilities of various fuels and compared them to the ignition probability of Jet A. Ignition probability is a common measure of combustor ignitability. It was measured by sparking the igniter hundreds of times and measuring the fraction of spark events that successfully ignited the combustor. This task included a modeling component which began to develop predictive capability for ignition probability. Such a predictive capability would take combustor conditions (pressure, temperature, and fuel-air ratio) in addition to key fuel properties (vaporization and chemical kinetic properties) as inputs and would produce an ignition probability as the output. To support this modeling effort, the forced ignition task produced measurements of detailed ignition physics. These detailed measurements captured fuel spray images, ignition kernel images, and flame images.

(3): The third task consisted of turbulent flame speed measurements. Like the other two tasks, the high priority measurement was fuel screening. For this task, fuel screening compared the turbulent flame speeds of various fuels to the turbulent flame speed of Jet A. This task additionally had a significant rig development aspect. The rig development added sub-atmospheric pressure capability.

These tasks were designed to address critical needs of the larger program. These needs are the rapid screening of alternative fuels and detailed measurements to support the modeling teams. The rest of this report details the specific activities that have been conducted under each of these tasks to address these important needs.

Task #1: Lean Blowout

Georgia Institute of Technology

Objective(s)

The objective of this task was to obtain two types of measurements in a combustor rig operating near lean blowout. The two types of measurements were fuel screening and detailed diagnostics. The objective of the fuel screening was to rank the blowout boundaries of each fuel relative to the blowout boundary of Jet-A. The objective of the detailed diagnostics was to produce data that could support the modeling teams. These data would support the modeling teams by developing physical insight and by providing important simulation boundary conditions. To summarize, the objectives of this task were to obtain fuel screening data and detailed diagnostic measurements.

Research Approach

This task was performed with a combustor rig, shown in Figure 1. The rig was a high pressure, swirl-stabilized spray combustor with OEM-relevant hardware. The combustor was configured similarly to the referee rig at the Air Force Research Lab. The difference between the Georgia Tech rig and the referee rig was their dome and liner cooling arrangements. The referee rig had a greater level of complexity of these components, providing a closer simulation of a real combustor. However, the reduced complexity of the Georgia Tech rig enabled a greater rate of data generation. The reduced complexity of the Georgia Tech rig also enabled laser-based diagnostics that were not possible in the referee rig.

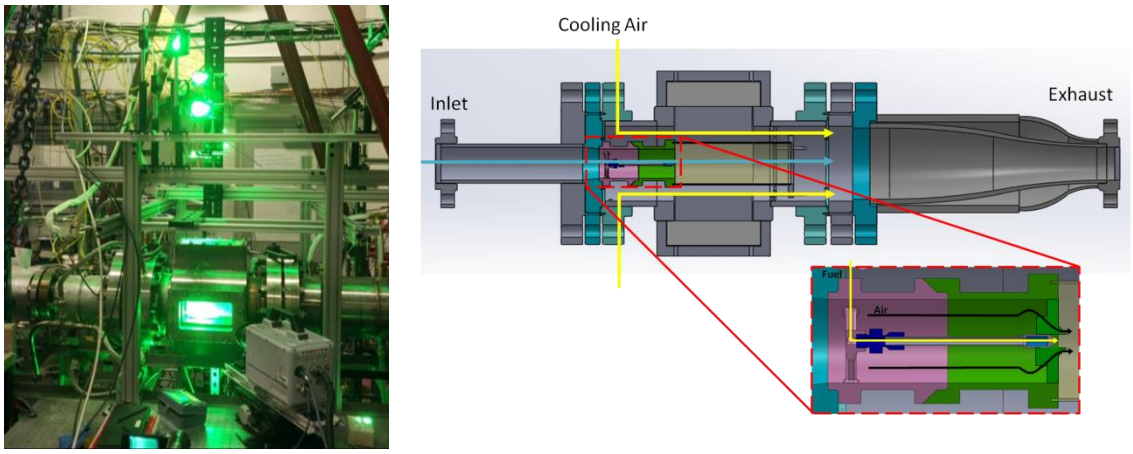

Figure 1. High shear swirl combustor, showing a) pressure vessel instrumented for high speed stereo PIV and OH PLIF, and b) a cross section with generic swirler holder/injector for illustrative purposes

The research approach consisted of four major activities. The first of these activities was to collaboratively select the test conditions. This activity was conducted through the LBO working group. Thus, test condition selection included input from the OEMS as well as other stakeholders such as the referee rig team and the modeling teams. Together, these teams selected one combustor pressure and three air preheat temperatures for lean blowout testing. These were designed to simulate idle and altitude conditions where lean blowout poses the greatest risk. The selected combustor pressure was 3 atmospheres and the selected air preheat temperatures were 300 K, 450 K, and 550 K.

The second activity was to acquire screening data. This was accomplished by outfitting the combustor test rig with an advanced fuel cart. The fuel cart had ten different fuel tanks, each of which could hold a different fuel. The cart could rapidly switch between these fuels, which enabled the lean blowout testing of ten different fuels in a single sitting. The testing of many fuels in one sitting was advantageous because it promoted repeatability by eliminating the potential for uncontrolled variations in test conditions between test days. Fuel screening was conducted by igniting the combustor and intentionally leaning it to the lean blowout limit. Conditions where the combustor blew out were recorded, and the process was repeated until the first fuel tank was empty. This repetition process typically produced 20-30 blowout points for a single fuel. This was then repeated for the fuels in the other nine tanks.

The third activity was detailed data acquisition. This activity produced data to support the modeling groups, and it also produced data to improve the program's understanding of the physics of lean blowout. In support of the modeling groups, the lean blowout team performed detailed laser-based measurements. These measurements were delivered to the modeling groups to help them refine and validate their simulations. The measurements incorporated several different laser-based techniques that were synchronized together at 5,000 frames per second. These diagnostics included:

- Stereoscopic particle image velocimetry (s-PIV) to obtain planar measurements of the three-component velocity field
- Planar laser-induced fluorescence of the OH molecule (OH PLIF) to obtain measurements of the flame position
- Planar laser-induced fluorescence of the liquid fuel (fuel PLIF) to obtain measurements of the liquid fuel spray location

The third activity also produced high speed chemiluminescence images. These measurements were easier to perform and analyze than the laser-based diagnostics outlined above. Therefore, the advantage of the chemiluminescence imaging was that it was faster to implement. Because it was faster to implement, it was applied for more fuels and test conditions than the laser-based techniques. The chemiluminescence images helped reveal the qualitative burning characteristics near lean blowout. The chemiluminescence images also produced data to help the program determine the roles of ignition and extinction in the lean blowout process. Area 3 and area 7 have both been analyzing these data to try to make such a determination. In addition to these optical measurements, the third activity also produced measurements of combustor boundary conditions. The measured boundary conditions included air flow rates, air and fuel temperatures, combustor pressure, and surface temperatures.

The fourth activity was data analysis. This activity was very important because it converted the raw measured data into useful data. In the case of screening data, analysis was performed on the combustor operational data to identify lean blowout events and their associated operating points. Analysis of screening data also included uncertainty analysis. The uncertainty analysis was necessary in order to determine the statistical significance of the results, and in some cases it motivated the lean blowout group to take additional data in order to tighten the uncertainty. In the case of detailed data, analysis was performed in two steps: pre-processing and post-processing. Pre-processing was applied to the velocity field measurements, and consisted of an intensive cross-correlation algorithm to convert raw images into velocity fields. This was extremely time consuming and was the most difficult data analysis step. Post-processing was conducted to produce the time-averaged velocity field, to produce the rms velocity field, and to extract key vortical flow features. These post-processed data were the deliverable to the modeling teams.

Milestone(s)

1. **Boundary condition measurements.** All requested boundary condition measurements have been produced and delivered to modeling teams.
2. **Detailed diagnostic measurements.** All detailed diagnostic imaging that was planned for year 3 has been completed and is being analyzed to extract physical insight.
3. **Screening data.** This has been completed for all planned cases and is being analyzed and disseminated to all project participants.
4. **Analysis.** Substantial data analysis has been completed this year and has delivered insight into the importance of the cetane number as well as the dynamics of lean blowout.

Major Accomplishments

1. To date, we have expanded our screening dataset which consists of several thousand lean blowout measurements.
2. We have demonstrated that the cetane number nicely captures the lean blowout risk of a given fuel (see Figure 2), especially at higher temperatures.
3. We have demonstrated an intermittent burning stage that occurs on the approach to lean blowout. This provides an important qualitative picture for blowout simulations (see Figure 3 for a sample chemiluminescence image from this diagnostic).

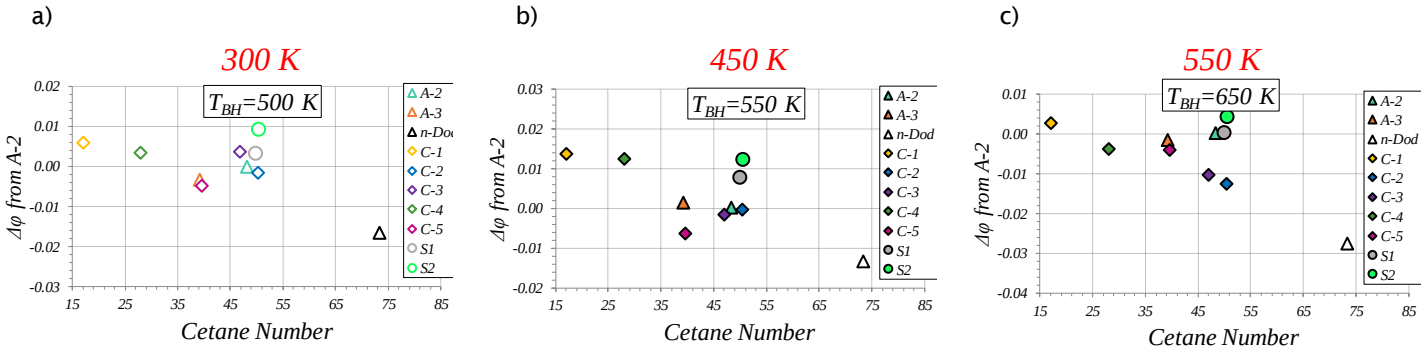

Figure 2. Sample of year 3 screening data at three different preheat temperatures and three different bulkhead temperatures, demonstrating the strong correlation of lean blowout with the cetane number

Figure 3. Sample flame chemiluminescence image from n-dodecane burning at 300 K air preheat temperature.

Publications

Chterev, I., Rock, N., Ek, H., Emerson B., Seitzman J., Jiang, N., Roy, S., Lee, T., Gord, T., and Lieuwen, T. 2017. Simultaneous Imaging of Fuel, OH, and Three Component Velocity Fields in High Pressure, Liquid Fueled, Swirl Stabilized Flames at 5 kHz. Combustion and Flame. 186, pp. 150-165.

Rock, N., Chterev, I., Smith, T., Ek, H., Emerson, B., Noble, D., Seitzman, J. and Lieuwen, T., 2016, June. Reacting Pressurized Spray Combustor Dynamics: Part 1—Fuel Sensitivities and Blowoff Characterization. In *ASME Turbo Expo 2016: Turbomachinery Technical Conference and Exposition* (pp. V04AT04A021-V04AT04A021). American Society of Mechanical Engineers.

Chterev, I., Rock, N., Ek, H., Smith, T., Emerson, B., Noble, D.R., Mayhew, E., Lee, T., Jiang, N., Roy, S. and Seitzman, J.M., 2016, June. Reacting Pressurized Spray Combustor Dynamics: Part 2—High Speed Planar Measurements. In *ASME Turbo Expo 2016: Turbomachinery Technical Conference and Exposition* (pp. V04AT04A020-V04AT04A020). American Society of Mechanical Engineers.

Outreach Efforts

We have provided research opportunities to undergraduate students and a high school student with this program. We have submitted a paper for the 2018 ASME Turbo Expo which will give a graduate student the opportunity to attend the conference.

Awards

Graduate student Nick Rock was awarded ASCENT student of the year in April 2017.

Student Involvement

- Nick Rock has been actively involved in the lean blowout experimental effort for all years. Nick was the PhD student responsible for operating the experimental facility. He led the screening measurements and operated the facility for the detailed diagnostic efforts, and has also performed the analysis of the screening data.
- Ianko Chterev was also actively involved in the lean blowout experimental effort. His primary responsibility was the design of experimental procedures and support of detailed diagnostic measurements.
- Hanna Ek was involved in the lean blowout effort as a data analysist. Hanna has been responsible for processing and analyzing the large volume of detailed data produced by the PIV, PLIF, and Mie scattering measurements.

Plans for Next Period

Four new activities are planned for the next period. These activities are very closely related to the current period's activities. The first of these activities is the analysis of the year 3 chemiluminescence data. Early analysis of the chemiluminescence data showed clear evidence of both ignition and extinction as the combustor approached lean blowout. Evidence of extinction and ignition were most pronounced for the n-dodecane fuel, which had a vastly different cetane number than the other fuels. This is especially interesting, since this program has strongly hypothesized that the cetane number is the most important fuel property for assessment of lean blowout risk. Therefore, we see strong potential for the chemiluminescence data to support this hypothesis. Since the chemiluminescence data are relatively new, much of their analysis has been qualitative. Therefore, analysis efforts in the next period will quantify the rate of extinction and ignition during lean blowout. This will be repeated for all fuels so that the extinction and ignition rates can be correlated to the cetane number. This correlation will test the hypothesis that the cetane number is an important fuel property for assessment of blowout risk. We also hope that this activity will help us answer four important questions that the community has asked about the blowout process:

- What is the primary mode of flame anchoring near blowout?
- How broad in equivalence ratio is the extinction/ignition stage, and is this fuel-dependent?
- Are the statistics (extinction event arrival rates, durations, etc.) of this intermittent burning stage fuel-dependent?
- Does it make more sense to correlate fuel properties with the onset of the intermittent burning stage than with the terminal blowout event?

The analysis task outlined above will need additional data to answer those four questions. Therefore, the second activity will generate additional data to answer those questions. These two activities (analysis and measurement) are anticipated to occur iteratively to fine-tune the measurements. For example, preliminary analysis of the detailed data have shown that we will need some high repetition rate chemiluminescence images to answer the flame anchoring physics question, and analysis of photomultiplier tube (PMT) data have shown that we will need longer PMT records, particularly at higher air preheat temperatures. Therefore, we have included a task to measure improved datasets based on the results of year 3 data analysis.

The third activity will be additional fuel screening. The goal of this additional screening will be to address the inter-correlation of fuel properties. The inter-correlation of fuel properties has historically been a challenge for this program, because fuels that have one extreme property tend to have many extreme properties. For example, fuels with especially low T10 boiling points tend to also have low flash points, low aromatic content, and high cetane numbers. This makes it difficult to determine which property causes the blowout risk. In year 3, the program started to address this through the introduction of neat n-dodecane, which has an extremely high cetane number but which does not have other extreme property values. This demonstrated the value of fuels that have been carefully selected or engineered to possess targeted physical or chemical properties. These targeted properties can be selected in order to break the inter-correlation of fuel properties. The program has developed several new fuels to accomplish this. Some of these fuels have already arrived at Georgia Tech. The year 4 screening activity will therefore test these new fuels to expand the fuel screening database. This expanded database will help determine which fuel properties are truly correlated to lean blowout risk.

The fourth activity will be measurements of additional boundary conditions as needed by modeling groups. This potentially has very large scope, and thus will be limited to the available resources of year 4. However, we acknowledge that this will be an important activity and will make every attempt to characterize additional wall temperatures, exhaust temperatures, spray behavior, or other items which may not yet be characterized but which may be needed to refine the models.

Task #2: Ignition

Georgia Institute of Technology

Objective(s)

The ignition task had three objectives. The first objective was to analyze the prior year's data to better understand the kernel ignition process. This is important for the development of ignition models. The second objective was to acquire and analyze ignition probability data for liquid fuel sprays (in prior years we investigated only pre-vaporized fuels). This is important, because ignition poses the greatest risk at conditions where the fuel does not vaporize. The third objective was to develop a chiller to enable ignition testing of cold fuels. This is important because ignition is an even greater challenge with cold fuels.

Research Approach

During its third year, the ignition task approached its goals through three activities. The first activity was analysis of the prior year's detailed diagnostic imaging data. The detailed imaging included data from three high speed, synchronized diagnostic methods: Schlieren, planar laser-induced fluorescence (PLIF), and chemiluminescence. The acquisition rate was 10 kHz. Three pre-vaporized fuels were investigated with these techniques: A2, C1, and C5. Figure 4a presents an example of the raw data. The top row of Figure 4a shows an example of the chemiluminescence data, and the middle row of Figure 4a presents an example of the PLIF data. These measurements show that chemical reactions occur in the highly mixed regions of the vortical kernel structure. The PLIF measurement indicates that chemical reactions occur within tens of microseconds of the ignition kernel interaction with the fuel/air mixture. The bottom row of Figure 4a presents an example of the Schlieren images. These are useful for assessment of the plasma development. The images show the initial rapid volumetric growth of the hot plasma kernel after it is ejected from the igniter. The rapid growth is due to the mixing of the high temperature kernel gases with surrounding fluid. This entrainment of cold surrounding fluid results in a rapid reduction of the kernel's temperature. Consequently, the chemically active region of the kernel decays substantially after 400-500 μs. In cases where there is successful ignition (as seen in Figure 4a), these kernels eventually grow and transition into a self-sustaining flame (as verified by PLIF and chemiluminescence images from later times). This competition between cooling/entrainment and chemical heat release determines the outcome of an ignition event.

The chemiluminescence images also provide insight into the temporal development of the ignition kernel intensity. Figure 4b presents these results for successful ignition events. The results show an initial decrease in intensity (due to early air entrainment and cooling) followed by an increase in intensity (due to chemical heat release). The time at which the minimum intensity is observed indicates when flame growth becomes dominant. Interestingly, C1 exhibited the longest delay until flame growth dominated. This is interesting because C1 also had the lowest ignition probability in earlier screening studies. This correlation between long delay times and low ignition probabilities suggests the importance of early chemistry. This provides important guidance to the chemical kinetics community, since the early chemistry for this problem is classified as high temperature chemistry. Therefore, successful ignition modeling will likely require accurate high temperature chemistry models.

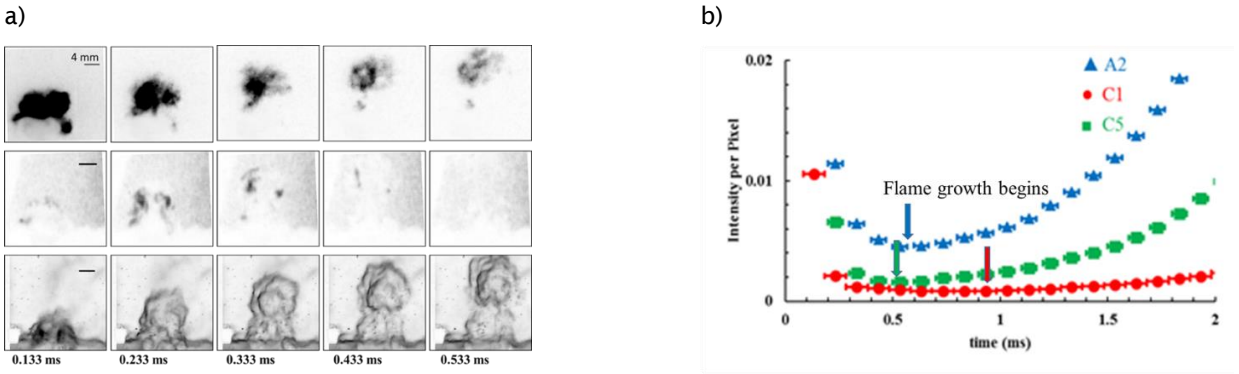

Figure 4. a) High-speed diagnostic imaging of a successful ignition event in pre-vaporized A2. Top row shows chemiluminescence images; middle row shows PLIF images; bottom row shows Schlieren images. Images from each row are spatially registered and temporally synchronized. Spark discharge occurs at $t = 0$ ms. b) Spatially integrated chemiluminescence for successful ignition events with fuels A2, C1, and C5. The points with lowest intensity are defined to be markers for the start of flame growth.

The second activity in the ignition task was to test ignition probabilities of liquid sprays. This began with modification of the test facility. The fuel delivery system was modified to provide liquid sprays rather than pre-vaporized fuels. The most important fuel system modification was the installation of a solid cone pressure atomizer (a fuel injector) near the entrance to the test section. Also, the splitter plate was removed from the test rig to provide a single fresh air stream. The fuel injector location was selected to produce ignition probabilities in the range of 1-10%. The injector location was also fine-tuned to prevent fuel droplet impingement on the igniter. Therefore, the injector positioning was selected empirically. This empirical process used a HeNe laser-based Mie scattering measurement to monitor the spray trajectory. Figure 5a shows an example of the spray imaging.

Liquid fuel testing was conducted with a crossflow air velocity of 10 m/s and an equivalence ratio of φ=0.55. The crossflow air temperature was 80 ˚F and its pressure was 1 atmosphere. Ignition probabilities were measured for eleven different fuels: A1, A2, A3, C1, C2, C3, C4, C5, S1, S2, and n-dodecane. Each of these fuels was tested as a liquid spray. The ignition probabilities of each fuel relative to A2 are shown in Figure 5b. For comparison, the figure also includes the results from earlier testing of pre-vaporized fuels. There are several noteworthy differences between the ignition probabilities of liquid versus pre-vaporized fuels. One of these noteworthy differences is a change in the ranking of ignition probabilities. For example, the ignition probabilities of A3, C2, and C3 are reduced when tested as liquid sprays. Another noteworthy difference is the reduction of fuel sensitivity.

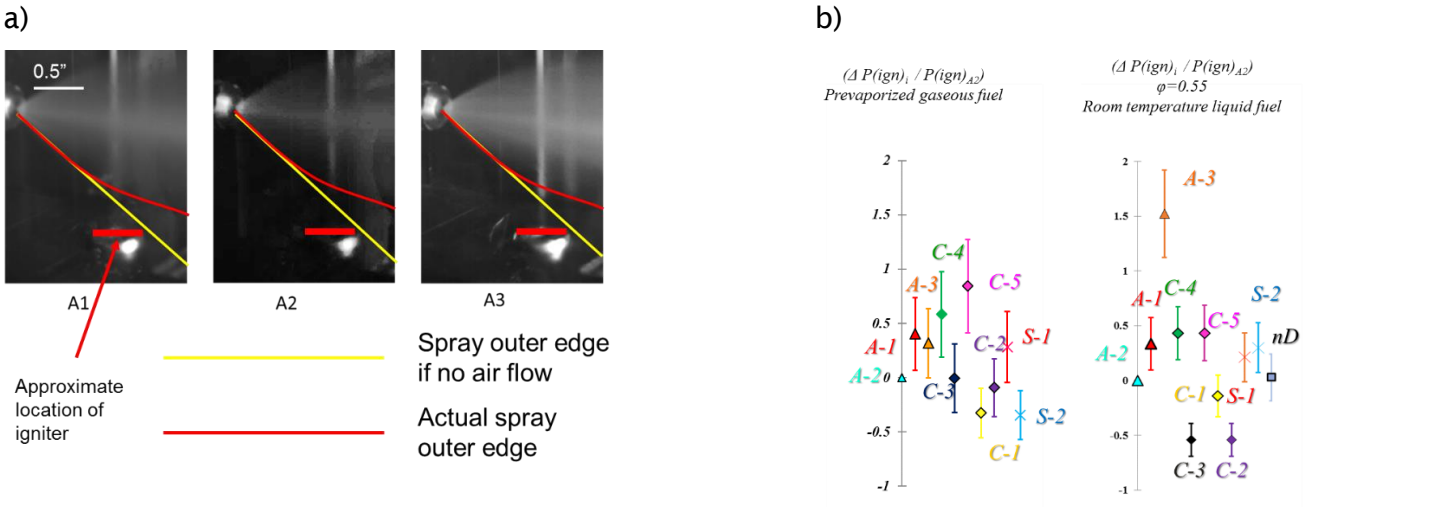

Figure 5. a) Spray pattern of fuels A1, A2, and A3 under broadband scattering. b) Relative ignition probability from pre-vaporized tests (left) and room temperature spray test (right).

The differences in the ignition probabilities of liquid sprays versus pre-vaporized fuels provide some important insight. For example, the rate-limiting properties of pre-vaporized fuels should be the chemical properties. This is because the physical properties govern the vaporization process, which has been bypassed by pre-vaporization. However, the rate-limiting properties for liquid sprays may include physical properties in addition to chemical properties. Therefore, the differences in ignition probability demonstrate the important role of physical properties (such as viscosity, boiling points, etc.) for ignition of liquid fuel sprays. Currently, this activity is trying to correlate ignition probability to physical properties. Special attention has been paid to properties that govern vaporization (recovery temperature, vapor pressure) and atomization (viscosity). An example from this work is shown in Figure 6a. Pearson correlation results (Figure 6b) indicated strong correlations to vaporization and atomization properties, and they indicated weaker correlations to chemical properties such as auto-ignition delay time and aromatic concentration.

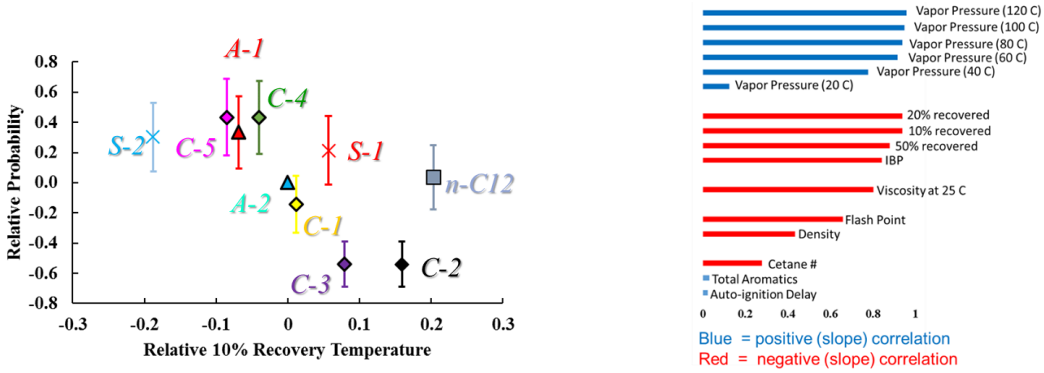

Figure 6. a) Ignition probabilities as a function of the 10% recovery temperature. b) Pearson correlation results for ignition probability versus fuel properties.

The third activity in the ignition task was to develop a fuel chiller. The fuel chiller system is shown schematically in Figure 7. The chiller uses a mixture of propylene glycol and water to control the fuel temperature. This is accomplished by submerging dry ice in the mixture. Since the dry ice is colder than the freezing point of the mixture, this begins to freeze the mixture. The mixture remains at its freezing point throughout the freezing process. In this way, the phase change (freezing) of the mixture is used to control the mixture temperature. This maintains a mixture temperature of -50 F. Fuel is routed through a heat exchanger that is submerged in the -50 ˚F mixture. By the time the fuel reaches the fuel injector, its temperature is -19 ˚F. This low temperature capability is important, because viscosities (and therefore atomization characteristics) are very different at low temperatures versus room temperature.

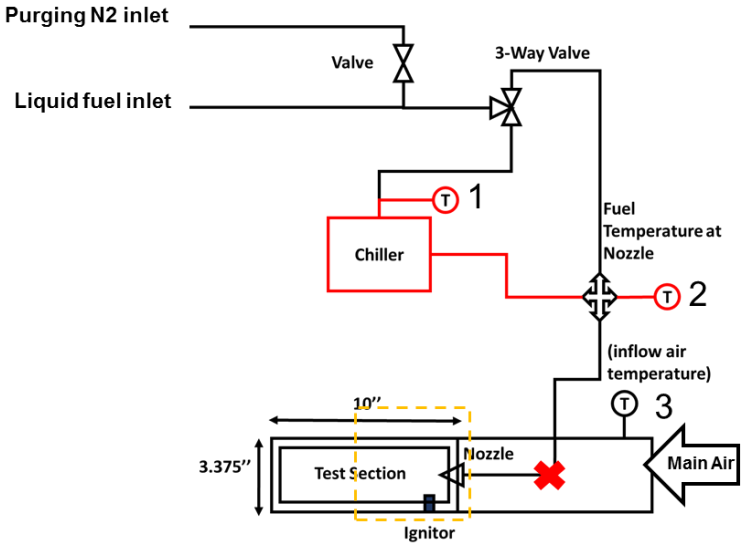

Figure 7. Schematic of fuel spray test setup with fuel chiller system.

Milestone(s)

- Achieve repeatable liquid fuel testing procedures. This milestone was completed early in the year when we began testing liquid sprays.
- Post-process year 2 detailed data. This has been completed, and significant understanding of ignition in stratified flow fields was gained.
- Ignition probability data for room temperature fuel spray. Ignition probability data were acquired for A1, A2, A3, C1, C2, C3, C4, C5, two surrogate fuels (S1 and S2) and n-dodecane.
- Probability data analysis. This has been completed.

- Final data archiving. The final data were uploaded to KSN.

Major Accomplishments

- Entrainment cooling and local chemical reactions were observed with high speed imaging. This enabled reduced order modeling by confirming the competition between entrainment cooling and chemical heat release during ignition.
- Room temperature liquid fuel ignition probability data were measured. The data show strong positive correlation to properties controlling vaporization and atomization, and only weak correlation was found among ignition probabilities and chemical properties.
- A fuel chiller was developed. The chiller can deliver fuels to the rig at -19 ˚F.

Publications

Wei, S., Sforzo, B., and Seitzman, J., 2017, "High Speed Imaging of Forced Ignition Kernels in Non-Uniform Jet Fuel/Air Mixtures," *ASME Turbo Expo 2017: Turbomachinery Technical Conference and Exposition*, Charlotte, NC, USA

Sforzo, B., Wei, S., and Seitzman, J., 2017, "Non-premixed Ignition of Alternative Jet Fuels," AIAA SciTech Forum, Grapevine, Texas, USA

Outreach Efforts

Conference presentation at ASME Turbo Expo 2017, Charlotte, NC, USA
Conference presentation at AIAA SciTech Forum 2017, Grapevine, Texas, USA

Awards

ASME Young Engineer Turbo Expo Participation Award

Student Involvement

- Sheng Wei has been actively involved in the Task 2 detailed diagnostic effort. Sheng supported the ignition probability measurement collection and was the primary student responsible in fuel spray ignition probability data. Sheng is also the lead student involved in design and modification of rig.
- Jared Delrose has been actively involved in ignition probability data acquisition and rig design.
- Daniel Cox has been actively involved in rig design and modification.

Plans for Next Period

Four activities are planned for the next period. The first activity will be to obtain data for the chilled liquid fuel. This will implement the new fuel chiller that was developed during the current period. The second activity will be to characterize the fuel spray. This characterization will be performed for room temperature fuel and chilled fuel. These spray characterizations will be compared to confirm the impact of fuel temperature on fuel atomization. The third activity will be to produce a reduced order model of ignition probabilities of liquid sprays. In prior years the ignition task has had good success with the development of such models for pre-vaporized fuels. In the next period, we will use the data from the first two activities to expand these models for liquid sprays. The fourth activity will be to perform additional ignition probability screening as required by the program. Several new fuels have already been designed by the program, and some of these have been delivered to Georgia Tech. Therefore, this activity will test the new fuels.

Task #3: Turbulent Flame Speed

Oregon State University

Objective(s)

This task had three objectives. The first objective was to measure and identify the sensitivity of the turbulent flame speed to fuel composition. This objective spanned a range of jet fuels and test conditions (including atmospheric and sub-atmospheric pressures). The second objective was to build a database of turbulent flame speeds for pre-vaporized jet fuels. The third objective was to measure the sensitivity of turbulent flames to local extinction.

Research Approach

Two activities were conducted under the turbulent flame speed task. The first activity was experimental testing. Experimental testing was conducted in a laboratory test rig. The test rig was designed to produce turbulent flames. The rig featured a pre-vaporizer based on designs developed by the Air Force Research Lab, and a burner based on designs developed by Lieuwen and colleagues. The experimental setup consisted of fuel and air metering systems that delivered pre-vaporized jet fuel and air to the burner. Fuel was vaporized using a series of heaters, and elevated to a temperature near 200 ºC. The air/fuel mixture flowed through an adjustable turbulence generator which produced turbulence intensities ranging from 10% to 20% of the bulk flow velocity. Turbulence intensity (TI) is independent of bulk flow velocity. A premixed methane pilot flame was used for ignition and to stabilize the Bunsen burner flame.

Data were collected for each three fuels (A2, C1 and C5). Test conditions included a range of Reynolds numbers ($5{,}000<Re<10{,}000$), a range of equivalence ratios ($0.75 \leq \Phi \leq 1.0$), and a range of turbulence intensities ($10\% \leq TI \leq 20\%$). The test data consisted of chemiluminescence imaging. Chemiluminescence imaging was conducted using a 16-bit intensified charge-coupled device (ICCD) camera with a 1024 x 1024 pixel resolution and a 25 mm f/4.0 UV camera lens. For each flow condition (Re, Φ, and TI), data were collected over a 3 minute period at 2 Hz.

The most important accomplishment of this activity was sub-atmospheric pressure testing. Measurements of turbulent flame speeds at sub-atmospheric conditions were enabled by the design and fabrication of a pressure vessel and vacuum system. The vessel can currently operate down to 0.6 atm, although lower pressures are anticipated in the future. Figure **8** shows a photograph of the rig operating at sub-atmospheric conditions.

Figure 8. Picture of flame operating in pressure vessel at sub-atmospheric conditions.

The second activity was data analysis. Data analysis was conducted to determine the time-averaged flame position. To accomplish this, the line-of-sight images were first time-averaged and then background-subtracted. Next, the images were checked to verify symmetry and they were median filtered. Finally, a three-point Abel deconvolution was applied. The results of this process were subjected to an edge detection algorithm. The output of the edge detection algorithm was defined as the time-averaged flame position. The height of this time-averaged flame position determines the turbulent flame speed. This process is illustrated by the sequence of images in Figure 9. Its estimated uncertainty is 1%-2% [1]. An example of turbulent flame speed results for several fuels is presented in Figure 10.

.

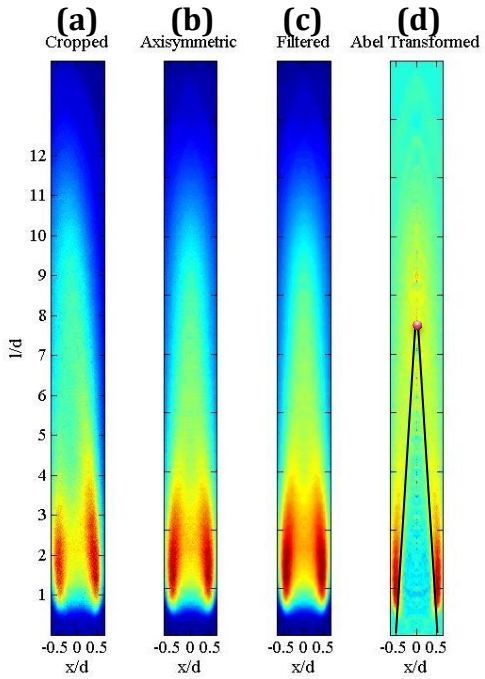

Figure 9. Step-by-step summary of image processing approach, showing (a) time-averaged and background subtraction (b) axi-symmetry verification (c) 2-D median filtering (d) Abel deconvolution with time-averaged flame position drawn.

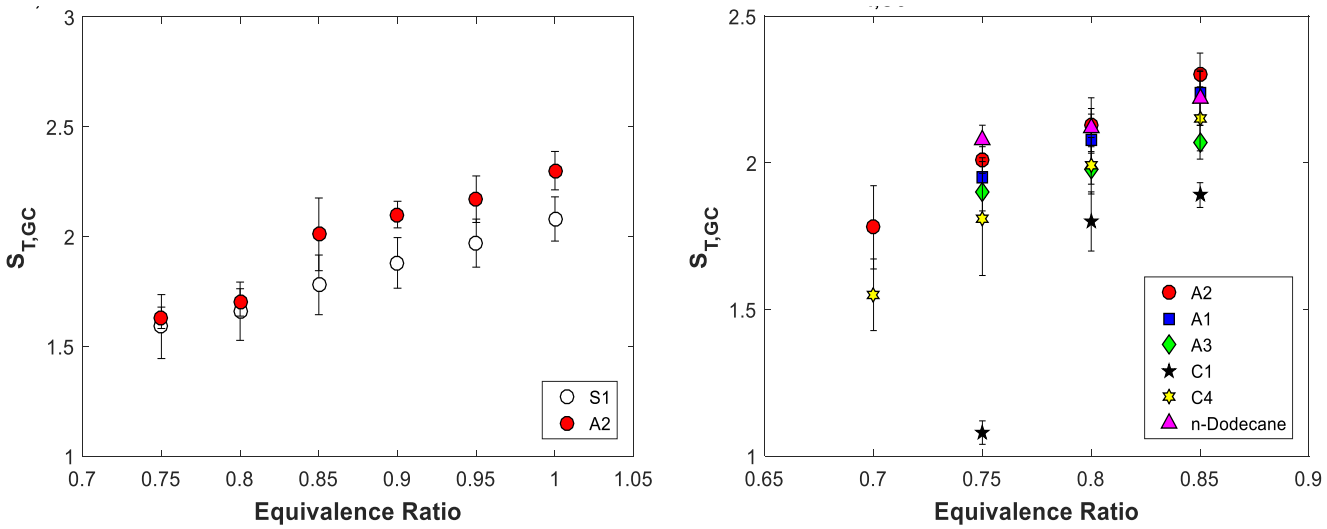

Figure 10. Turbulent consumption speeds for A2 and S1 (left panel) and a variety of other fuels (right panel). Data shown in the right panel were used to identify sensitivities to local extinction. The lowest equivalence ratio shown was the last equivalence ratio prior to local extinction being identified.

Milestone(s)

- An initial test campaign evaluating local extinction events was completed.
- Turbulent flame speeds for conventional and surrogate fuels were determined.

Major Accomplishments

- We have made the observation that the turbulent flame speeds of Jet-A and the surrogate fuels are similar.
- We have made the observation that flame extinction is sensitive to fuel composition. This will be important for the program's lean blowout tasks, which aim to understand how ignition and extinction influence the lean blowout process.

Publications

N. Schorn, **D. Blunck**, "Flame Stability of Turbulent Premixed Jet Flames of Large Hydrocarbon Fuels," *Western States Section of the Combustion Institute Meeting*, Laramie, WY (2017).

A. Fillo, J. Bonebrake, **D. Blunck**, "Impact of Fuel Chemistry and Stretch Rate on the Global Consumption Speed of Large Hydrocarbon Fuel/Air Flames," *10th US Combustion Meeting,* College Park, ME (2017).

Fillo, Aaron, M.S., Thesis, "The Global Consumption Speeds of Premixed Large- Hydrocarbon Fuel/Air Turbulent Bunsen Flames," Oregon State University.

Outreach Efforts

None

Awards

Fillo, Aaron, M.S., Thesis, "The Global Consumption Speeds of Premixed Large- Hydrocarbon Fuel/Air Turbulent Bunsen Flames," received a 2017 OSU Distinguished Master's Thesis Award.

Student Involvement

- Jonathan Bonebrake, a PhD student, has helped to collect and analyze data. He also designed and built the sub-atmospheric pressure vessel and vacuum system.
- Aaron Fillo, a PhD student, has worked tangentially on this project to analyze results and further investigate scientific phenomena.
- Nathan Schorn, a MS student, has recently started and has transitioned to leading the effort to operate the burner and collect and analyze data.
- Multiple undergraduate students, including underrepresented students have worked with the graduate students to operate the burner and collect data. This has provided a significant opportunity for the students to experience research.

Plans for Next Period

Two activities are planned for the next period. The first activity will be additional measurements of turbulent flame speeds. This activity will utilize the recently developed sub-atmospheric testing capability. This activity will also focus on the fuels that the program determines to be of interest. The second activity will be analysis of the flame extinction observations. For example, flame extinction behavior will be compared to the lean blowout data from Georgia Tech. The results of this activity will determine if turbulent flame speed testing can provide early insight into the risk of lean blowout.

References

Venkateswaran, P., Marshall, A., Shin, D. H., Noble, D., Seitzman, J., and Lieuwen, T. "Measurements and Analysis of Turbulent Consumption Speeds of H2/CO Mixtures" *Combustion and Flame* 158, no. 8 (2011):

Project 028 Combustion Model Development and Evaluation

Georgia Institute of Technology, University of Connecticut

Project Lead Investigator

Suresh Menon
Hightower Professor of Engineering
School of Aerospace Engineering
Georgia Institute of Technology
270 Ferst Drive, Atlanta, GA 30327
404-894-9126
suresh.menon@ae.gatech.edu

University Participants

Georgia Institute of Technology

- P.I.(s): Suresh Menon, Professor; Wenting Sun, Associate Professor
- FAA Award Number: 13-C-AJFE-GIT-018
- Period of Performance: Oct. 1, 2016-Sept. 30, 2017
- Task(s):
    1. Travel to NJFCP meeting. Funds only for travel (S. Menon, PI)
    2. Development of dynamic adaptive chemistry solver and demonstrate the algorithm in different flame configurations, travel to meeting (W. Sun)

University of Connecticut

- P.I.(s): Tianfeng Lu, Associate Professor
- FAA Award Number: 13-C-AJFE-GIT-018
- Period of Performance: October 1, 2016 - September 30, 2017
    3. The task of UCONN in the NJFCP program is to develop reduced chemical kinetic models for jet fuels that can be employed in efficient large eddy simulations.
    4. The technical aspects of the UCONN task is to cover the travel expenses of the UCONN team to present the results from the NJFCP program in the conferences and program review meetings.

Project Funding Level

The Georgia Tech award is $6000 for S. Menon (PI), FY 2017 for travel
The Georgia Tech award is $39,999 for W. Sun, FY 2017 for travel and partial student support.
The UCONN subaward is $5000 for FY2017 for travel support

Investigation Team

The Georgia Tech team includes: Suresh Menon (PI) (travel funds only),
Wenting Sun (co-PI), Suo Yang (graduate student), Xiang Gao (graduate student)
Tianfeng Lu (co-PI, UCONN), Yang Gao (graduate student), and Ji-Woong Park (graduate student)

Project Overview

This project is developing computational tools to evaluate alternate fuel combustion in a spray combustion system. Reduced reaction kinetics from UCONN is being used for LES of reacting flows to investigate performance of various fuel mixtures. Funding for PI and Co-PIs are for travel to FAA meetings. One of the co-PI (W. Sun) has some additional funds to support a graduate student.

Task #1: Development of Reduced Kinetics For NJFCP Fuels

University of Connecticut

Only travel funds are provided to attend NJFCP program reviews in May and December 2017. All research is funded by a NASA NRA.

Task #2: Network Modeling and Kinetics Acceleration

Georgia Institute of Technology

Travel funds are provided to attend NJFCP program reviews in May and December 2017. Some additional funds provided for student.

Task #3: LES of Spray Combustion In NJFCP Test Facilities

Georgia Institute of Technology

Only travel funds are provided to attend NJFCP program reviews in May and December 2017. All research is funded by a NASA NRA.

Objective(s)

The primary objective for PI and Co-PI is to provide funds to travel to NJFCP and ASCENT project reviews and also to allow students to attend these reviews. The objective of the research for one of the co-PI (W. Sun) is to develop a Dynamic Adaptive Chemistry (DAC) Algorithm to employ different reduced kinetic models at different grid points to reduce the computation time in LES and DNS.

Research Approach

Primarily travel funds for all PI.

W. Sun: Research Description: Due to the increasing demand for combustion-based energy and concerns on its environmental impacts, high-fidelity simulation of turbulent combustion becomes a highly-important tool for combustor design. For any practical simulation method, the key is to provide quantitative solutions with minimal empirical constants. Large-eddy simulation (LES) has drawn significant attention during the past three decades, and its predictive capability is continuously increasing. In LES, the energy-containing large-eddy motions are resolved with sufficient grid resolution, while motions of scales smaller than the grid sizes, i.e. subgrid-scale (SGS) motions, are modeled. The chemical reaction rates are highly-nonlinear functions of species concentrations and temperature, which heavily depend on the turbulent mixing. On the other hand, chemical reactions also release heat and subsequently affect species concentrations and temperature, which in turn change the turbulent mixing. Chemical reactions occurring at different time scales may interact with eddies of different length/time scales, which further complicates the physiochemical processes. Therefore, turbulence/chemistry interaction is considered the most challenging problem in turbulent combustion modeling.

The turbulent combustion models that have been developed for LES can be classified into two major categories: the finite-rate chemistry (FRC) models, and the flamelet generated manifold (FGM) models. The FRC models category includes the laminar chemistry model, the perfectly-stirred reactor (PSR) model, the partially-stirred reactor (PaSR) model, the linear-eddy model (LEM), the Monte Carlo method for Lagrangian filtered probability density function (FDF) transport equations, and the thickened flame model (TFM). The FGM models category includes the steady laminar flamelet model, the Lagrangian flamelet model, and the flamelet/progress-variable (FPV) model. Among FGM models, the steady laminar flamelet model provides the advantages of easy implementation and low computational cost. There are, however,

limitations associated with this model. First, the mixture fraction essentially does not carry information about the chemical states. The model uses the filtered dissipation rate of mixture fraction as an additional parameter to account for the flame stretching effect. The dissipation rate, however, does not provide a unique mapping from mixture fraction to the corresponding reaction state. In order to overcome the drawbacks of the steady laminar flamelet model, the FPV model was proposed to incorporate a transport equation to track a progress variable. This model has been developed to account for low-level of extinction, re-ignition, and unsteady mixing effect to some extent. It, however, cannot handle multiple-feed streams unless adding a third parameter, which makes the look-up table very difficult to handle due to the large computer memory requirement and time to build up the table. In addition, the higher-dimension look-up table results in a more complicated data retrieval process and coarser table grid, which could introduce higher interpolation errors. Compared to the FGM models, the detailed chemical kinetics in the FRC models are computationally prohibitive for LES applications due to the large number of species and the stiffness resulting from a broad range of chemical time scales. In the present work, DAC is incorporated into a preconditioning scheme to allow an Eulerian FRC-LES approach in a fully-compressible flow CFD solver. The established FRC-LES framework is then used to investigate a low-Mach partially premixed turbulent flame (Sandia Flame D) as a benchmark case.

Milestone(s)

Attend FAA mid-year meeting in May and annual meeting in Dec 2017 as required

Major Accomplishments

UCONN team:

Reduced kinetic models for five jet fuels, namely Cat A1, A2, A3, C1 and C5, have been developed from Version 2 of the detailed HyChem models and validated for ignition delay, stirred reactor extinction, flame speed, and extinction of premixed and non-premixed counterflow flames. The reduced models have been delivered to the NJFCP numerical simulation teams. Note this work was done under NASA funding but provided to other researchers in this program.

Georgia Tech team:

Travel to ASCENT and NJFCP meetings to present progress (on work funded by NASA).

For W. Sun, additional funding from the ASCENT program has allowed to get the DAC implemented into Sandia Flame D. We developed a 20-species and 84-reactions methane/air kinetics model reduced from the GRI-3.0 as a kinetic model in computation since Sandia Flame D is a methane/air flame. Results shows that the DAC method provides effective local mechanism reduction with negligible computational overhead. In FRC-LES, the techniques of ODEPIM and DAC provide an acceleration of 8.6 times for chemistry, and 6.4 times for the total computation. This work laid the foundation in the application of DAC in more complicated problem such as gas turbine combustor simulation.

Publications

None

Outreach Efforts

None

Awards

None

Student Involvement

UCONN team:

Two graduate students (Yang Gao and Ji-Woong Park) are involved in the NJFCP project. The students are responsible for the development and validation of reduced jet fuel models and the compilation of a package to help integrating the reduced models to large eddy simulations. Yang Gao has graduated in October 2017.

Georgia Team:

S. Menon: Achyut Panchal (funded by NASA) and Dr. Reetesh Ranjan, Research Engineer will be attending the NJFCP review.

W. Sun: Two graduate students (Suo Yang and Xiang Gao) are involved in the NJFCP project. The students are responsible for the development of reduced kinetic models and conduct LES simulation with DAC for Sandia Flame D.

Plans for Next Period

Funds for FY 18 are being provided for the PI to travel to NJFCP meeting only at this time.

Project 029(A) National Jet Fuels Combustion Program – Area #5: Atomization Test and Models

Purdue University

Project Lead Investigator

Robert P. Lucht
Ralph and Bettye Bailey Distinguished Professor of Combustion
School of Mechanical Engineering
Purdue University
West Lafayette, IN 47907-2088
765-714-6020 (Cell)
Lucht@purdue.edu

University Participants

Purdue University

- P.I.(s): Robert P. Lucht, Jay P. Gore, Paul E. Sojka, and Scott E. Meyer
- FAA Award Number: COE-2014-29A , 401321
- Period of Performance: 10/1/2016-9/30/2017
- Tasks:
  1. Obtain PDA data across one plane in the VAPS test rig operated with the Referee Rig nozzle and for numerous fuels at near-lean blowout (LBO) conditions and for cold fuel/cold air flow conditions approximating ground light off (GLO) and high-altitude relight (HAR) conditions
  2. Extend PDA measurements to obtain data across multiple planes for evaluation of Detailed Combustor Simulations (DeCS) by Suresh Menon, Vaidya Sankaran, and Matthias Ihme,
  3. Obtain PDA and/or Malvern measurements for selected operating conditions either in the VAPS test rig to provide data for the spray correlation analysis of Nader Rizk,
  4. Perform PDA measurements for fuel blends including Fuel X and/or another blend designed for testing differences in atomization characteristics to examine the sensitivity of correlations and computations to changes in fuel properties,
  5. Ensure quality of data with repetition tests at Purdue and comparisons with spray measurements at P&W, UDRI/AFRL, and UIUC.

Project Funding Level

The funding level from the FAA was $250,000 for Year 3. Purdue University provided cost sharing funds in the amount of $250,000.

Investigation Team

PI Dr. Robert Lucht, Bailey Distinguished Professor of Mechanical Engineering is responsible for the oversight of the entire project here at Purdue University. He is also responsible for mentoring one of the graduate students, coordinating activities with Stanford and will work with all parties for appropriate results and reporting as required.

Co-PI Dr. Jay Gore, Reilly Professor of Mechanical works closely with the PI for all deliverables of Purdue University, and also oversees the work performed by one of the graduate students that he is mentoring.

Co-PI Dr. Paul Sojka, Professor of Mechanical Engineering is responsible for mentoring one of the graduate student and is responsible for supervising the PDPA measurements.

Co-PI Scott Meyer, Managing Director of the Maurice J. Zucrow Laboratories is responsible for coordinating facility upgrades and for facility design reviews.

Senior Research Scientist Dr. Sameer V. Naik is responsible for direct supervision of the two graduate students involved in the project.

Graduate students Andrew Bokhart and Daniel Shin are responsible for performing the PDPA measurements and for modifying the RTS test rig for operation at near-lean-blow-out (LBO) conditions.

Project Overview

The objectives of this task as stated in the Invitation for ASCENT COE Notice of Intent (COE-2014-29) are to "measure the spray characteristics of the nozzles used in the Referee Combustor used in Area 6 tests and to develop models for characterizing the atomization and vaporization of the reference fuels." We are the experimental part of a joint experimental and modeling effort to achieve these objectives. The experimental tasks will be performed at Purdue University and the modeling tasks will be performed by Prof. Matthias Ihme's group at Stanford University, Prof. Suresh Menon's group at Georgia Tech, and by Vaidya Sankaran at UTRC. Nader Rizk will also develop spray correlations based on our measurements.

Purdue University has very capable test rig facilities for measuring spray characteristics over very wide ranges of pressure, inlet air temperature, and fuel temperature. The experimental diagnostics that are applied include both phase Doppler anemometry (PDA) as well as high-frame-rate shadowgraphy. The atomization and spray dynamics for multiple reference and candidate alternative fuels have been characterized for the referee rig nozzle operated at near lean blowout (LBO) conditions. In the future these same sorts of measurements will be performed for many of these same fuels at operating conditions characteristic of ground lightoff (GLO) and high-altitude relight (HAR).

Task #1: National Jet Fuels Combustion Program Area #5 - Measurement of Spray Characteristics at Near Lean Blowout and Chilled Fuel Conditions

Purdue University

Objective(s)

The objectives of this research program are to visualize and measure the characteristics including drop size distributions, axial, and radial velocity components of the sprays generated by a nozzle being used in the Referee combustor rig in the Area 6 tests. The resulting data will be used for the development of spray correlations by consultant Nader Rizk and for the purpose of submodel development for detailed computer simulations being performed by Matthias Ihme (Stanford University), Suresh Menon (Georgia Tech), and Vaidya Sankaran (UTRC). The experimental tasks are performed at Purdue University and the resulting data will be shared with FAA team members developing modeling, simulations, and engineering correlation based tools.

The upgraded Variable Ambient Pressure Spray (VAPS) test rig at Purdue University is used for measuring spray characteristics over the ranges of pressure, inlet air temperature, and fuel temperature. Our work during the first year allowed us to identify the challenges associated with making reliable and repeatable spray measurements while keeping the windows of the rig clean. Phase Doppler Anemometry (PDA) has emerged as a technique of choice for obtaining fundamental drop size distribution and axial and radial velocity data for comparison with numerical simulations. The VAPS facility has been upgraded to allow us to test over the entire range of fuel and air temperatures and air pressures of interest. We will be able to directly compare reacting and non-reacting spray data by collaborating with the UIUC/UDRI/AFRL Area 6 team.

The experimental data will support continued development and evaluation of engineering spray correlations including the dependence of Sauter Mean Diameter (SMD), spray cone angle, and particle number density per unit volume on the fuel properties at fuel and air temperatures of interest. The experimental data will provide detailed statistical measurements for comparisons with high-fidelity numerical simulations of mixing and combustion processes. The prediction of the spatial distribution of the liquid fuel and resulting vapor and breakdown components from the liquid fuels critically affects the ignition, flame-stabilization, and pollutant formation processes.

The project objectives are summarized as:

(a) Obtain PDA data across one plane in the VAPS test rig operated with the Referee Rig nozzle and for numerous fuels at near-lean blowout (LBO) conditions and for cold fuel/cold air flow conditions approximating ground light off (GLO) and high-altitude relight (HAR) conditions
(b) Extend PDA measurements to obtain data across multiple planes for evaluation of Detailed Combustor Simulations (DeCS) by Suresh Menon, Vaidya Sankaran, and Matthias Ihme,
(c) Obtain PDA and/or Malvern measurements for selected operating conditions either in the VAPS test rig to provide data for the spray correlation analysis of Nader Rizk,
(d) Perform PDA measurements for fuel blends including Fuel X and/or another blend designed for testing differences in atomization characteristics to examine the sensitivity of correlations and computations to changes in fuel properties,
(e) Ensure quality of data with repetition tests at Purdue and comparisons with spray measurements at P&W, UDRI/AFRL, and UIUC.

Research Approach

The Purdue University test rig facilities are designed for measuring spray characteristics over very wide ranges of pressure, inlet air temperature, and fuel temperature. An atmospheric pressure spray test rig facility was extensively used in year 1 of the project to establish the differences in spray properties of the different fuels at multiple fuel temperatures, fuel pressures, and swirler pressure drops. The second facility is the VAPS test rig which allows measurements under high and low pressure conditions relevant to the aviation applications and was being reactivated during the last part of year 1 activities and the first part of year 2 activities.

The operating system for the atmospheric pressure spray facility and the instrument positioning and atomization systems have been upgraded over the first year to allow high repeatability for PDA drop size and velocity measurements. The PDA system itself was repaired and refurbished near the end of Year 2, beginning of Year 3. A high speed camera with backlighting has yielded significant insights into the structure of the liquid fuels flowing out of the nozzle with and without the swirling co-flow through the injector. An optical patternator was also used for rapid analysis of spray distribution patterns.

Liquid fuels can be supplied to the test rigs by multiple systems. A facility-integrated system draws fuel from one of two certified flame-shield fuel containments for testing standard aviation fuels as well as other alternative blends. A mobile fuel cart, developed under the combustion rules and tools (CRATCAF) program and redeployed during the first year of the NJFCP program is being utilized for further control of additional injector circuits or for running alternative fuel blends. Both systems were designed with two independently controlled and metered circuits to supply fuel to pilot and main injector channels of the test injector. The mass flow rates of both supplies are measured with Micro Motion Elite® Coriolis flow meters. A nitrogen sparge and blanket ullage system is used to reduce the dissolved oxygen content of the fuel, which is monitored with a sensor just upstream of the fuel control circuits. High pressure gear pumps provide fuel at up to 300 kg/hr, supplied to the control circuits at a 10 MPa regulated line pressure. The mobile fuel cart was built with two onboard heat exchangers and a chilling unit controls the temperature of the fuel over a range of 233 K to 600 K (-40ºF to 600ºF).

Milestone(s)

The tasks that were performed in FY2017 are listed below:

Quarter 1

1. Collaborated with area 4 and 6 groups, and with the Area 5 subcommittee, for development of experimental test matrix for FY2017.
2. Returned Dantec PDA system to Denmark for repair and refurbishment.
3. Designed system for mixing of liquid and gaseous nitrogen to produce gaseous nitrogen at temperatures down to 230 K.

Quarter 2

1. Received the refurbished fiber-based color separator from Dantec and installed it in the PDA system. We then demonstrated excellent performance of the PDA system in the 1D PDA configuration.
2. Presented AIAA SciTech Conference paper describing the PDA spray measurements for near LBO conditions at the AIAA SciTech Conference in Grapevine, TX, 9-13 January 2017.
3. Performed extensive 1D PDA measurements of droplet size and axial velocity for A2 and C1 fuels over a wide range of near-LBO operating conditions.
4. Tested successfully operation of the variable ambient pressure spray (VAPS) test rig for low fuel temperatures of -30F.

Quarter 3

1. Continued 1-D fiber PDA measurements of droplet size and axial velocity over a wide range of near-LBO conditions for A2, C1, and C5 fuels. Performed repeatability tests, especially for A2 at near-LBO conditions. In particular, the pressure drop across the swirler and the pilot fuel pressure drop were varied over significant ranges.
2. Performed 1-D fiber PDA measurements of droplet size and axial velocity over a wide range of near-LBO conditions for the Fuel-X fuels C7, C8, and C9.
3. Performed PDA measurements of droplet size and axial velocity for A2, A3, and C3 fuels over a wide range of operating conditions with fuel temperatures of -30F, airbox nitrogen temperature of 40F, and at an absolute pressure of 15 psia.
4. Hosted the NJFCP Midyear Meeting on 19-23 June, 2017.

Quarter 4

1. Continued 1-D fiber PDA measurements of droplet size and axial velocity over a wide range of near-LBO conditions for A2, C1, and C5 fuels. Performed numerous repeatability tests, for near-LBO conditions. Characterized the uncertainties associated with our measurements of droplet size (Sauter mean diameter) and axial velocity.
2. Performed PDA measurements for near-LBO conditions at planes both closer and further way from the nozzle exit than the 1-inch plane for which we have taken most of our measurements. These measurements will be of great interest to the modelers, including Vaidya Sankaran of UTRC, who is working on a detailed spray model and is using our measured downstream conditions to project back up to the nozzle exit.
3. Installed a liquid nitrogen line for injection of liquid nitrogen into the supply line for our airbox flow.

Major Accomplishments

The work described in this section is a part of the Purdue contributions to the larger FAA-funded effort, the National Jet Fuels Combustion Program (NJFCP). The major objective of the work at Purdue is to perform measurements of spray properties (droplet size, droplet velocity, spray cone angle) for a variety of jet fuels and candidate jet fuels under a wide range of conditions, including lean blowout (LBO), Ground Lift Off (GLO), and high altitude relight (HAR). Representative measurements of spray properties for LBO and chilled fuel conditions are presented in the rest of this section. The Purdue Variable Ambient Pressure Spray (VAPS) test rig is discussed along with modifications needed for the LBO measurements. A generic hybrid airblast pressure-swirl injector is used and we have investigated the spray characteristics of eight different fuels. The spray data is being used as initial conditions for computational models of the combustion process in a Referee rig developed by the NJFCP team.

Experimental Systems

The Purdue Variable Ambient Pressure Spray (VAPS) rig has three main components: the airbox assembly, the pressure vessel, and the fuel cart. The airbox assembly includes a length of pipe which is housed within the vessel. The hybrid pressure swirl airblast atomizer assembly is mounted on one end of the pipe and nitrogen enters through the other end. The airbox isolates the nitrogen flow traveling through the swirler from the flow within the vessel, allowing the creation of a higher pressure environment within the airbox compared to the pressure of the vessel. The airbox allows a pressure differential to be created across the swirler component of the injector, which results in the airblast component of the atomization process to occur. The airbox can be vertically traversed to allow spray measurements at different distances from the injector exit.

The vessel houses the airbox and injector assemblies and allows the variation of different ambient pressure into which the fuel is being injected. The vessel is rated to withstand 4.14 MPa (600 psi) at 648.9˚C (1200˚F). The pressure within the

vessel is controlled by a butterfly valve downstream of the test section which can be partially closed to increase pressure and opened to vent pressure or operate at ambient pressures. The vessel has four windows in the same horizontal plane, which allows laser diagnostic measurements to be performed within the test section. Two windows have a diameter of 127 mm (5 inches) and the other two windows have a diameter of 76.2 mm (3 inches). The 76.2 mm windows are both at a 60° angle from one of the 127 mm windows, with one of the 76.2 mm windows located on either side of the 127 mm window. There are two nitrogen flows entering the vessel: the sweeping flow and the window purge flow. These two flows are supplied by the same regulated line, which is split with one line going to the top of the vessel for the sweeping flow and the other traveling to two manifolds that supply the window purge flow. The purpose of these flows is to mitigate the recirculation and collection of fuel drops and vapors on the vessel windows, and thereby avoid obscuration for laser diagnostic measurements. These two flow are also used to build pressure within the vessel. A diagram depicting these two nitrogen flows as well as the airbox co-flow is shown in Fig. 1(a) and a picture of the VAPS vessel is shown in Fig. 1(b).

The fuel cart is a mobile fuel supply system that was designed for the Combustion Rules and Tools (CRATCAF) program. The fuel cart uses an IMO CIG Lip Seal and Weep Hole Design gear pump, which is used to supply pressurized fuel to the injector mounted on the airbox. There are two independently controlled and metered fuel lines on the fuel cart, which are used to supply fuel to the pilot and main orifices on the pressure swirl injector in the hybrid design.

The measurement system used in this study is a DANTEC DANAMICS Phase Doppler Particle Anemometry (PDPA). The alignment of the system relative to the VAPS vessel is shown in Fig. 2. The PDPA probe and receiver are mounted on Zaber translation stages to move the system to measurement locations throughout the spray along the horizontal axis shown in Fig. 2. The center of the spray on the horizontal axis is defined as the zero location for the radial locations. Positive radial locations denote locations on the left side of spray in Fig. 2 while negative radial locations denote locations on the right side. The positive and negative definitions for the radial locations was a result of the values communicated to the Zaber stages. Positive inputs moved the PDPA system to the left away from the motor while negative inputs moved the system to the right toward the motor. Measurements were taken along the negative radial locations for all conditions.

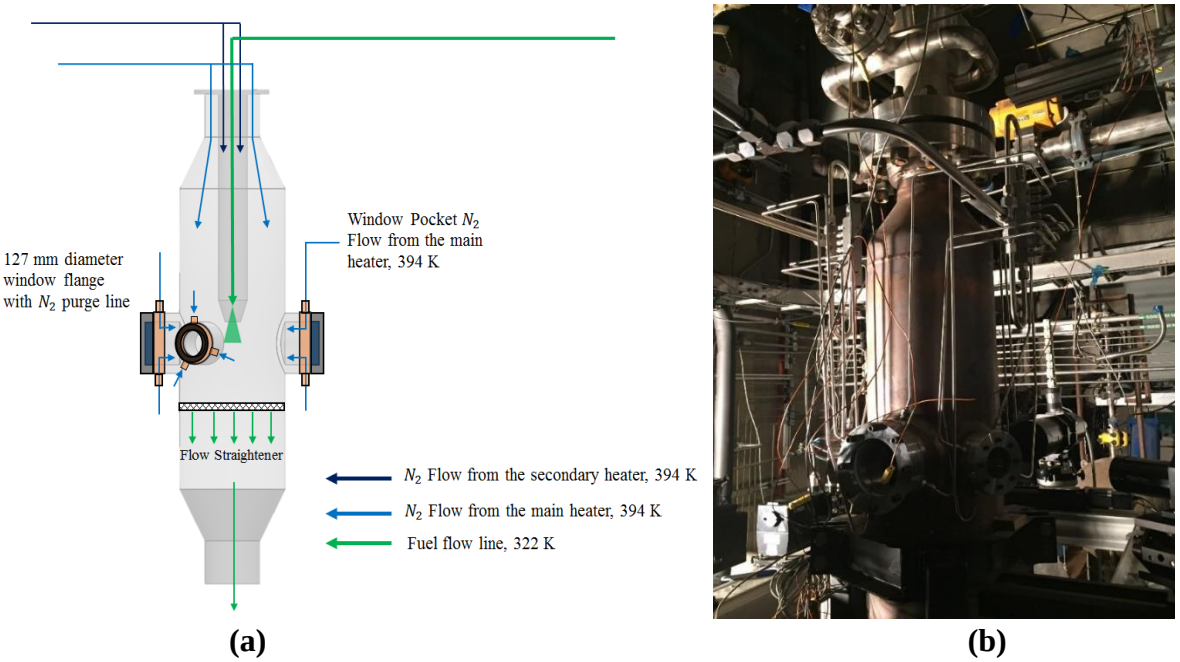

Figure 1: (a) diagram showing the three nitrogen flows within the VAPS vessel, (b) image of the VAPS rig

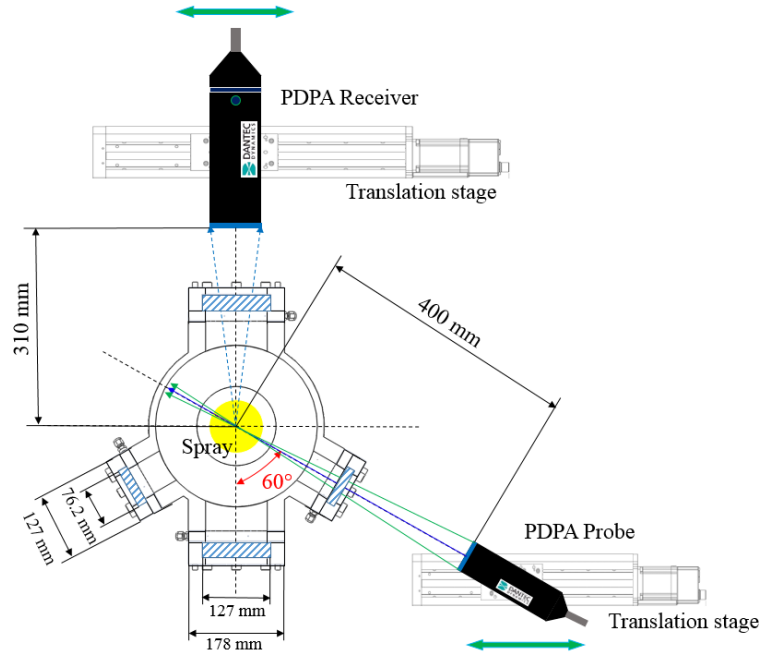

Figure 2: PDPA alignment relative to the VAPS test rig

Experimental Results: PDPA Measurements

Spray measurements at LBO operating conditions have been performed in the VAPS rig for six different fuels: A-2, C-1, C-5, C-7, C-8, and C-9. The LBO operating conditions are at an ambient pressure of 2.07 bars (30 psia), an air box nitrogen temperature of 394 K (250^{0}F), a pilot fuel temperature of 322 K (120^{0}F), a pilot fuel mass flow rate of 9.22 kg/hr (2.56 g/s), and a pressure drop of 3% across the swirler. All six fuels were investigated at a distance of 25.4 mm (1 inch) downstream from the exit of the injector swirler. Figure 3a shows the comparison of the D_{32} measurements for all six fuels while Figure 3b shows a comparison of the measured axial velocities for each fuel.

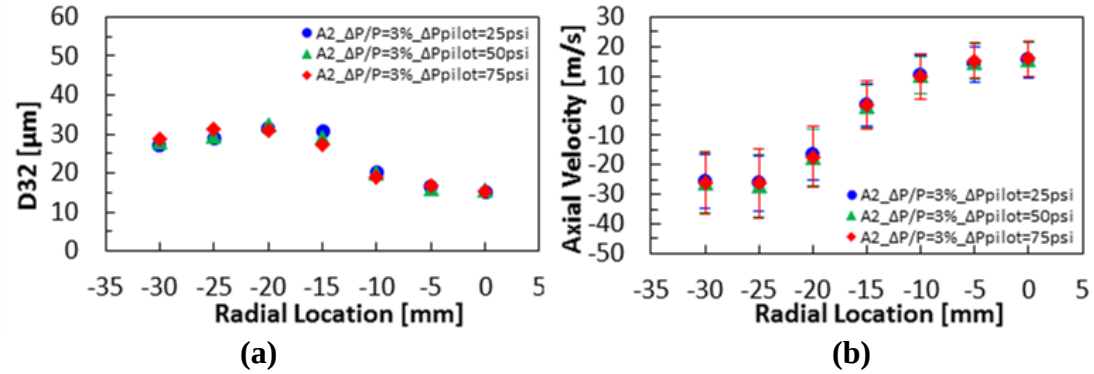

Figure 3: D_{32} and axial velocity for A-2 at near LBO condition with varied $\Delta P_{pilot.}$ Vertical bars on velocity represent RMS.

The injection pressure differential (ΔP_{pilot}) was varied for investigations of A-2, C-1, and C-5 at LBO conditions on the 25.4 mm plane. Injection pressure differentials investigated were: 25, 50, and 75 psid. Figure 4a shows the comparison of D_{32} measurements for A-2 for each injection pressure differential investigated while Fig 4b shows the axial velocity comparison. The pressure drop ($\Delta P/P$) was varied for each of the six fuels studied at LBO conditions on the 25.4 mm plane. The pressure drops investigated were: 2, 3, and 4%. Figure 4a show the comparison of D_{32} measurements for A-2 for each pressure drop investigated while Fig. 4b shows the axial velocity comparison.

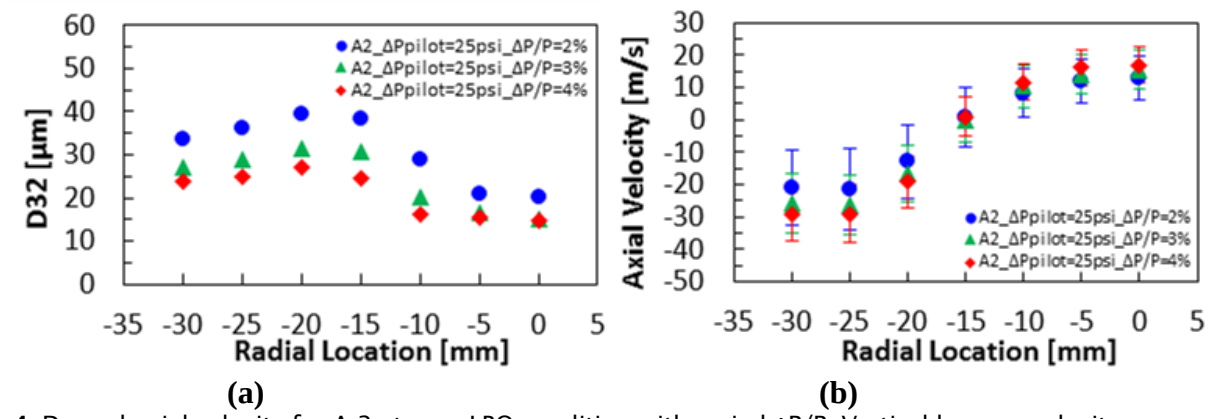

(a) **(b)**

Figure 4: D_{32} and axial velocity for A-2 at near LBO condition with varied $\Delta P/P$. Vertical bars on velocity represent RMS

A-2, C-1, and C-5 were also investigated at different distances away from the injector exit. The measurement planes investigated were 12.7, 25.4, and 38.1 mm (0.5,1.0, and 1.5 inches). Investigations of pressure drop variations (2, 3, and 4%) were performed for all three fuels at each of the three measurement planes. The injection pressure variation (25, 50, and 75 psid) has only been additionally investigated for C-1 on the 38.1 mm plane. Figure 5a shows the comparison of D_{32} measurements for A-2 at multiple measurement planes while Fig. 5b shows the axial velocity comparison.

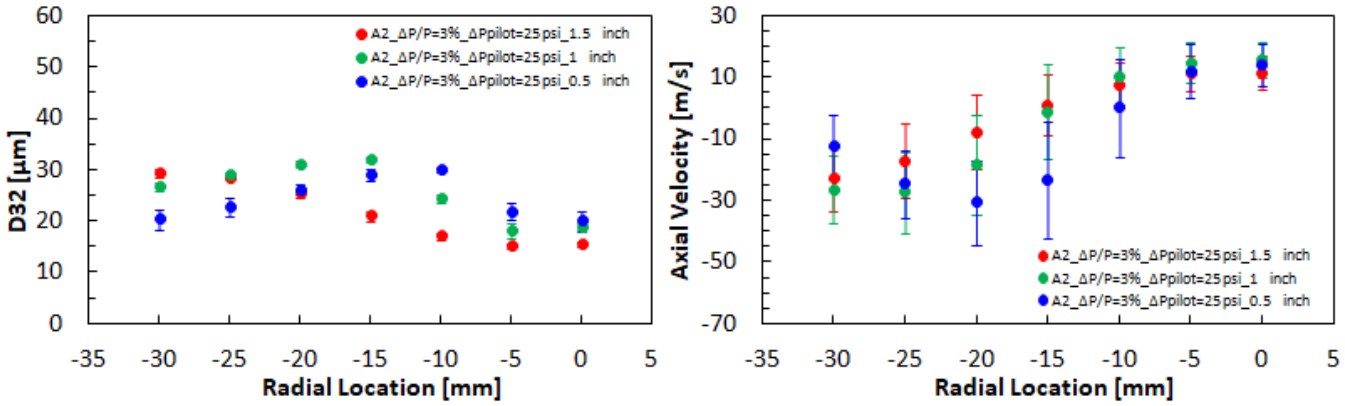

(a) **(b)**

Figure 5: D_{32} and axial velocity for A-2 at near LBO condition for different measurement planes. Vertical bars on the D_{32} plot represents uncertainty from repeatability standard deviation. Vertical bars on velocity represent RMS.

Three fuels were chilled to 239 K (-30˚F) and investigated in the VAPS test rig. The three fuels were: A-2, A-3, and C-3. The pressure drop ($\Delta P/P$) and injection pressure differential (ΔP_{pilot}) were varied using the same values as the LBO investigation. All measurements for the chilled fuel conditions were performed at the 25.4 mm (1 inch) plane. The nominal operating

conditions for the chilled investigation are an ambient pressure of 1.01 bars (14.7 psia), an air box nitrogen temperature of 279 K (42^{0}F), a pilot fuel temperature of 239 K (-30^{0}F), a pilot fuel mass flow rate of 9.22 kg/hr (2.56 g/s), and a pressure drop of 3% across the swirler. Figure 6a shows the D_{32} comparison of all three fuels at the nominal operating condition while Fig. 6b shows the axial velocity comparison. Figure 7a shows the D_{32} comparison for A-2 for an investigation of $\Delta P/P$ variation while Fig. 7b shows the axial velocity comparison. Figure 8a shows the D_{32} comparison for A-2 for the ΔP_{pilot} variation for chilled fuel while Fig. 8b shows the axial velocity comparison.

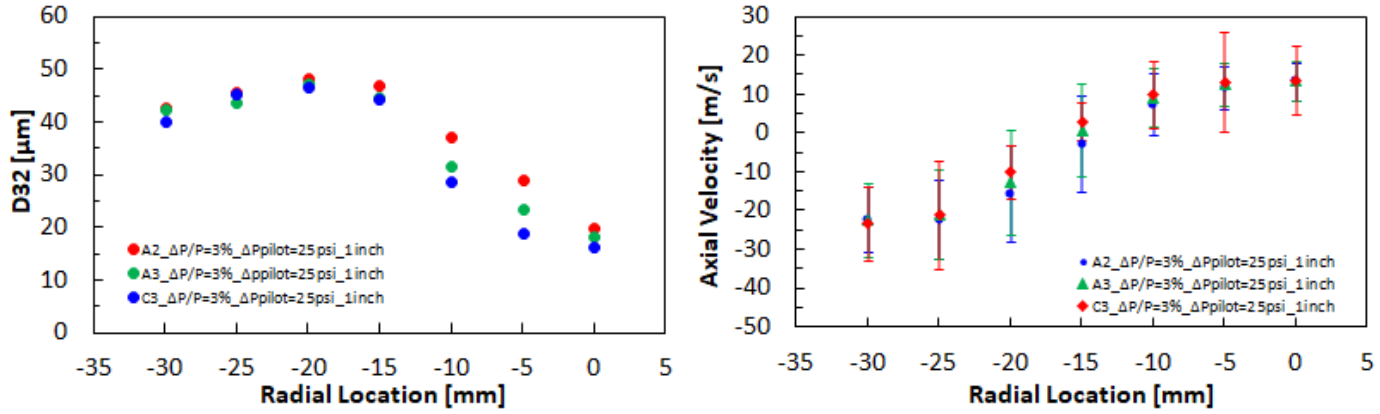

(a) **(b)**

Figure 6: D_{32} and axial velocity plots for fuel variation at chilled fuel conditions. Vertical bars on velocity represent RMS

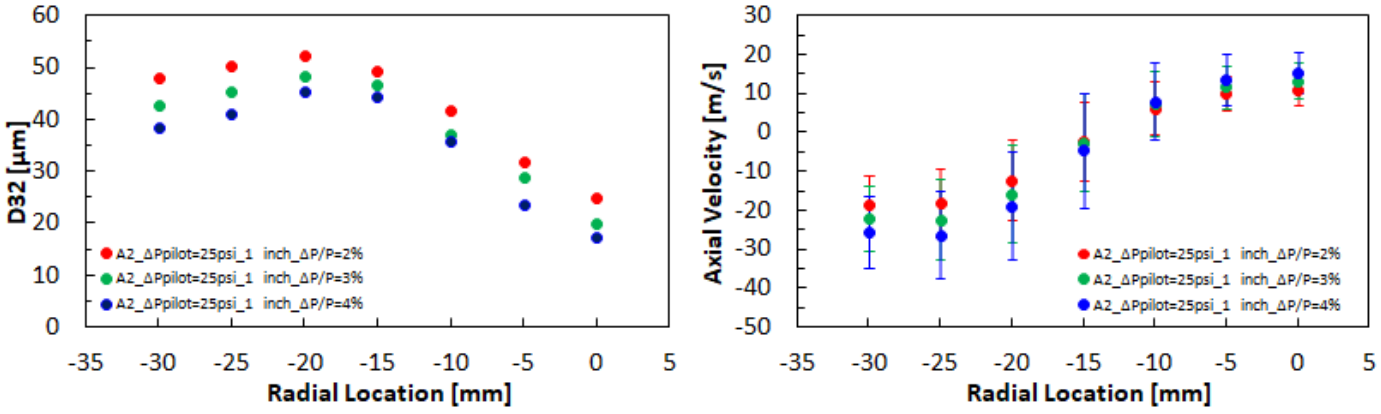

(a) **(b)**

Figure 7: D_{32} and axial velocity plots for A-2 at chilled fuel condition with varied $\Delta P/P$. Vertical bars on velocity represent RMS

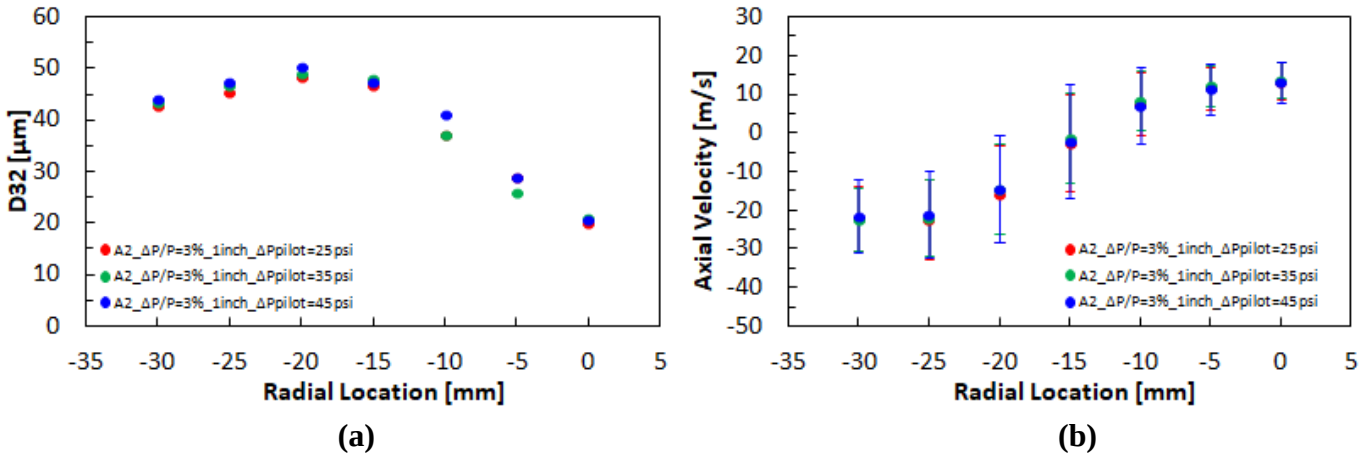

Figure 8: D_{32} and axial velocity plots for A-2 at chilled fuel conditions with varied $\Delta P_{pilot.}$ Vertical bars on velocity represent RMS

Publications

- "Effect of Aviation Fuel Type and Fuel Injection Conditions on Non-Reacting Spray Characteristics of Hybrid Air Blast Fuel Injector," Timo Buschhagen, Robert Z. Zhang, Sameer V. Naik, Carson D. Slabaugh, Scott E. Meyer, Jay P. Gore, and Robert P. Lucht, presented at the 2016 AIAA SciTech Meeting, San Diego, CA, 4-8 January 2016, Paper Number AIAA 2016-1154.
- "Large-Eddy Simulations of Fuel Injection and Atomization of a Hybrid Air-Blast Atomizer," P. C. May, M. B. Nik, S. E. Carbajal, S. Naik, J. P. Gore, R. P. Lucht, and M. Ihme, presented at the 2016 AIAA SciTech Meeting, San Diego, CA, 4-8 January 2016, Paper Number AIAA 2016-1393.
- "Spray Measurements at Elevated Pressures and Temperatures Using Phase Doppler Anemometry," A. J. Bokhart, D. Shin, R. Gejji, T. Buschhagen, S. V. Naik, R. P. Lucht, J. P. Gore, P. E. Sojka, and S. E. Meyer, presented at the 2017 AIAA SciTech Meeting, Grapevine, TX, 8-13 January 2017, Paper Number AIAA-2017-0828,.
- "Spray Characteristics at Lean Blowout and Cold Start Conditions using Phase Doppler Anemometry," A. J. Bokhart, D. Shin, N. Rodrigues, S. V. Naik, R. P. Lucht, J. P. Gore, P. E. Sojka, and S. E. Meyer, to be presented at the 2018 AIAA SciTech Meeting, Kissimmee, Florida, 8-12 January 2018.

Outreach Efforts

- "Effect of Aviation Fuel Type and Fuel Injection Conditions on Non-Reacting Spray Characteristics of Hybrid Air Blast Fuel Injector," Timo Buschhagen, Robert Z. Zhang, Sameer V. Naik, Carson D. Slabaugh, Scott E. Meyer, Jay P. Gore, and Robert P. Lucht, presented at the 2017 AIAA SciTech Meeting, San Diego, CA, 4-8 January 2016
- "Large-Eddy Simulations of Fuel Injection and Atomization of a Hybrid Air-Blast Atomizer," P. C. May, M. B. Nik, S. E. Carbajal, S. Naik, J. P. Gore, R. P. Lucht, and M. Ihme, presented at the 2016 AIAA SciTech Meeting, San Diego, CA, 4-8 January 2016.
- "Spray Measurements at Elevated Pressures and Temperatures Using Phase Doppler Anemometry," A. J. Bokhart, D. Shin, R. Gejji, T. Buschhagen, S. V. Naik, R. P. Lucht, J. P. Gore, P. E. Sojka, and S. E. Meyer, presented at the 2017 AIAA SciTech Meeting, Grapevine, TX, 8-13 January 2017, Paper Number AIAA-2017-0828,.
- "Spray Characteristics at Lean Blowout and Cold Start Conditions using Phase Doppler Anemometry," A. J. Bokhart, D. Shin, N. Rodrigues, S. V. Naik, R. P. Lucht, J. P. Gore, P. E. Sojka, and S. E. Meyer, to be presented at the 2018 AIAA SciTech Meeting, Kissimmee, Florida, 8-12 January 2018.

Awards
None.

Student Involvement
MS students Andrew Bokhart and Daniel Shin are primarily responsible for performing the PDPA measurements and for modifying the RTS test rig for first LBO and then HAR/GLO measurements. PhD students Neil Rodrigues and Timo Buschhagen and postdoctoral research associate Rohan Gejji assist with the project when their expertise is required.

Plans for Next Period
The proposed deliverables and tasks for FY2018 and Quarter 1 of FY2019 are listed below:

Year 4 Deliverables
The Year 4 deliverables for Area #5, Project 29A are as follows:
1. Move variable ambient pressure spray (VAPS) test rig to the new test facility.
2. Continue measurements with chilled fuel (-30F)/chilled nitrogen (-30F)
3. Make the ejector on the test rig functional; verify subatmospheric operation for the VAPS test rig.
4. Begin measurements with chilled fuel (-30F)/chilled nitrogen (-30F) measurements at subatmospheric ambient pressure (down to 4 psia), coordinate with Nader Rizk and Area 6 on exact operating conditions to investigate.
5. Collaborate with Andrew Corber at NRC on SLIPI imaging measurements in the VAPS test rig.
6. Continue interactions with the three CFD groups (Ihme, Vaidya and Menon).
7. Investigate spray structure for sprays with very low levels of pressure drop across the swirler or with the swirler removed.
8. Investigate the structure with the pilot+main spray and/or the main without pilot spray.

The tasks to be performed for FY2018 and Quarter 1 of FY2019 are listed below:

Quarter 1 FY2018
1. Collaborate with Area 4 and Area 6 members, and with the spray subcommittee, for development of experimental test matrix for the remainder of Year 3.
2. Perform PDPA measurements at near-LBO conditions at axial planes 0.5 in and 1.5 in downstream of the nozzle exit. Continue measurements with chilled fuel.
3. Develop and demonstrate the chilled nitrogen system for obtaining airbox flow temperatures down to -30F. Begin measurements with chilled fuel and chilled nitrogen.
4. Plan the move of the VAPS rig to the new High Pressure Combustion Laboratory.
5. Share boundary, initial, and operating conditions and resulting experimental data with correlations and modeling team (Rizk, Ihme, Menon, and Sankaran).

Quarter 2 FY2018
1. Collaborate with Area 4 and Area 6 members, and with the spray subcommittee, for development of experimental test matrix for Year 4.
2. Move the VAPS rig to the new High Pressure Combustion Laboratory.
3. Make the VAPS test rig operational again.

Quarter 3 FY2018
1. Continue extensive characterization of sprays with chilled fuel and chilled N_2.
2. Share boundary, initial, and operating conditions and resulting experimental data with correlations and modeling team (Rizk, Ihme, Menon, and Sankaran).
3. Make the ejector operational in preparation form subatmospheric operation of the VAPS rig.

Quarter 4 FY2018
1. Collaborate with Andrew Corber at NRC on SLIPI imaging measurements in the VAPS test rig.

2. Perform measurements with chilled fuel and chilled N_2 at subatmospheric pressure.
3. Share boundary, initial, and operating conditions and resulting experimental data with correlations and modeling team (Rizk, Ihme, Menon, and Sankaran).

Quarter 1 FY2019

1. Investigate spray structure for sprays with very low levels of pressure drop across the swirler or with the swirler removed.
2. Investigate the structure with the pilot+main spray and/or the main without pilot spray.
3. Share boundary, initial, and operating conditions and resulting experimental data with correlations and modeling team (Rizk, Ihme, Menon, and Sankaran).

Project 31(A) Alternative Jet Fuel Test and Evaluation

University of Dayton Research Institute

Project Lead Investigator

Steven Zabarnick, Ph.D.
Division Head
Energy & Environmental Engineering Division
University of Dayton Research Institute
300 College Park, Dayton, OH 45469-0043
937-255-3549
Steven.Zabarnick@udri.udayton.edu

University Participants

University of Dayton Research Institute

- P.I.(s): Steven Zabarnick, Division Head
- FAA Award Number: 13-C-AJFE-UD
- Overall Period of Performance: April 8, 2015 to August 31, 2019
- Period of Performance: April 8, 2015 to March 14, 2016 – Amendment No. 006
  1. Evaluate candidate alternative fuels for their performance via the ASTM D4054 approval process
- Period of Performance: August 13, 2015 to August 31, 2016 – Amendment No. 007
  2. Evaluate candidate alternative fuels for their performance via the ASTM D4054 approval process
- Period of Performance: August 5, 2016 to August 31, 2017 – Amendment No. 012
  3. Management of Evaluation and Testing of Candidate Alternative Fuels
- Period of Performance: July 31, 2017 to August 31, 2019 – Amendment No. 016
  4. Management of Evaluation and Testing of Candidate Alternative Fuels

Project Funding Level

Amendment No. 006 $309,885
Amendment No. 007 $99,739
Amendment No. 012 $693,928
Amendment No. 016 $999,512

In-kind cost share has been obtained from:
LanzaTech $55,801 (2015)
LanzaTech $381,451 (2016)
Neste $327,000
Boeing $2,365,338

Investigation Team

Steven Zabarnick, PI, new candidate fuel qualification and certification
Richard Striebich, Researcher, fuel chemical analysis and composition
Linda Shafer, Researcher, fuel chemical analysis and composition
John Graham, Researcher, fuel seal swell and materials compatibility
Zachary West, Researcher, fuel property evaluations

Project Overview

Alternative jet fuels offer potential benefits of reducing global environmental impacts, achieving national energy security, and stabilizing fuel costs for the aviation industry. The Federal Aviation Administration is committed to the advancement of "drop in" alternative fuels and has set the aspirational goal of enabling the use of 1 billion gallons annually by 2018. Successful adoption of alternative fuels requires approval for use of the fuel by the aviation community followed by large scale production of a fuel that is cost competitive and meets safety standards of conventional jet fuel. Alternative jet fuels must undergo rigorous testing in order to become qualified for use and incorporated into ASTM International Specifications.

Cost effective and coordinated performance testing capability (in accordance with ASTM D4054) to support evaluation of promising alternative jet fuels is needed. The objective of this project is to provide capability to conduct the necessary work to support alternative jet fuel evaluation of either a) to-be-determined fuel(s) that will be selected in coordination with the FAA, or b) a fuel test and evaluation project with a specific fuel(s) in mind.
The proposed program should provide the following capabilities:

- Identify alternative jet fuels (which may include blends with conventional jet fuel) to be tested and that have the potential to be economically viable and support FAA's NextGen environmental goals.
- Perform engine, component, rig, or laboratory tests, or any combination thereof, to evaluate the performance of an alternative jet fuel in accordance with ASTM International standard practice D4054.
- Identify and conduct unique testing beyond that defined in ASTM International standard practice D4054 necessary to support evaluation of alternative jet fuels for inclusion in ASTM International jet fuel specifications.
- Obtain data for baseline and alternative jet fuels to demonstrate any effects of the alternative jet fuel on aircraft performance, maintenance requirements, and reliability.
- Coordinate effort with activities sponsored by Department of Defense and/or other government parties that may be supporting relevant work.
- Report relevant performance data of the alternative fuels tested including a quantification of the effects of the alternative fuel on aircraft and/or engine performance and on air quality emissions relative to conventional jet fuel. Reported data will be shared with both the FAA (NJFCP) and the broader community (e.g. ASTM International) and with ASCENT COE Program 33 "Alternative Fuels Test Database Library."

Tasks #1 & #2: Evaluate Candidate Alternative Fuels for their Performance via the ASTM D4054 Approval Process and Management of Evaluation and Testing of Candidate Alternative Fuels

University of Dayton Research Institute

Objective(s)

Cost effective and coordinated performance testing capability (in accordance with ASTM D4054) to support evaluation of promising alternative jet fuels is needed. The objective of this project is to provide capability to conduct the necessary work to support alternative jet fuel evaluation of either a) to-be-determined fuel(s) that will be selected in coordination with the FAA, or b) a fuel test and evaluation project with a specific fuel(s) in mind.

Research Approach

The intent of this program is to provide the capability of performing specification and fit-for-purpose (FFP) evaluations of candidate alternative fuels towards providing a pathway forward through the ASTM D4054 approval process. The UDRI team possesses the capability of performing a large of number of these evaluations, and we are prepared to work with other organizations such as SwRI and engine OEM's, as needed, for their unique test capabilities. These include additional engine, APU, component, and rig evaluations. The UDRI testing capabilities cover our efforts at the laboratories of the Fuels Branch of AFRL and at our campus laboratory facilities.

The following are examples of the evaluations that UDRI is able to provide:

Tier I
1. Thermal Stability (Quartz Crystal Microbalance)
2. Freeze Point (ASTM D5972)
3. Distillation (ASTM D 86)
4. Hydrocarbon Range (ASTM D6379 & D2425)
5. Heat of Combustion (ASTM D 4809)
6. Density, API Gravity (ASTM D 4052)
7. Flash Point (ASTM D 93)
8. Aromatics (ASTM D 1319)

Tier II
1. Color, Saybolt (ASTM D 156 or D 6045)
2. Total acid number (ASTM D 3242)
3. Aromatics, (ASTM D 1319 & ASTM D 6379)
4. Sulfur (ASTM D 2622)
5. Sulfur mercaptan (ASTM D 3227)
6. Distillation temperature (ASTM D 86)
7. Flash point (ASTM D 56, D 93, or D 3828)
8. Density (ASTM D 1298 or D 4052)
9. Freezing point (ASTM D 2386, D 5972, D 7153, or d 7154)
10. Viscosity, at -20˚C, (ASTM D 445)
11. Net heat of combustion (ASTM D 4809)
12. Hydrogen content (ASTM D 3343 or D 3701)
13. Smoke point (ASTM D 1322)
14. Naphthalenes (ASTM D 1840)
15. Calculated cetane index (ASTM D 976 or D4737)
16. Copper strip corrosion (ASTM D 130)
17. Existent gum (ASTM D 381)
18. Particulate matter (ASTM D 2276 or D 5452)
19. Filtration time (MIL-DTL-83133F Appendix B)
20. Water reaction interface rating (ASTM D 1094)
21. Electrical conductivity (ASTM D 2624)
22. Standard Test Method for Thermal Oxidation Stability of Aviation Turbine Fuels (ASTM D3241)

Extended Physical and Chemical Characterization
1. Lubricity Evaluation- BOCLE test (ASTM D 5001)
2. Low Temperature Properties – Scanning Brookfield Viscosity
3. Detect, quantify, and/or identify polar species - Analyze as necessary
4. Detect, quantify and/or identify dissolved metals - Analyze as necessary
5. Initial Material Compatibility Evaluation – Perform optical dilatometry and Partition Coefficient Measurements to determine the fuel-effected swell and the fuel solvency in 3 O-ring materials (nitrile, fluorosilicone and fluorocarbon) and up to 2 additional fuel system materials
6. Experimental Thermal Stability Evaluation – Quartz Crystal Microbalance – Measure thermal deposit tendencies and oxidation profile at elevated temperatures
7. Viscosity versus Temperature – (ASTM D 445) determination of the fuels viscosity at 40˚C and -40˚C to assess the fuel's viscosity's variation with temperature

In addition to the above physical and chemical fuel evaluation capabilities, UDRI also has extensive experience in evaluation of microbial growth in petroleum-derived and alternative fuels. These evaluations include standard lab culturing and colony counting methods, as well as advanced techniques such as quantitative polymerase chain reaction (QPCR) and metagenomic sequencing. These methods allow the quantitative measurement of microbial growth rates in candidate alternative fuels in comparison with petroleum fuels.

UDRI also has extensive experience in evaluation of elastomer degradation upon exposure to candidate alternative fuels. Various methods are used to evaluate seal swell and o-ring fixture leakage, including: optical dilatometry, measurement of sealing pressure, fuel partitioning into elastomer, and a pressurized temperature controlled o-ring test device.

UDRI is also able to perform fuel-material compatibility testing using the D4054 procedures for fuel soak testing, post-exposure non-metallic and metal materials tests, and surface and microstructural evaluation. Testing of both 68 "short-list" materials and the complete 255 materials list can be performed.

Milestone(s)
The schedule for this project is dependent upon receipt of alternative fuel candidates for testing. As candidate fuels are received a schedule of testing will be coordinated with the FAA and collaborators. Our existing relationships with these organizations will help expedite this process.

Major Accomplishments
The Phase I Research Report for the LanzaTech/PNNL Ethanol-to-Jet (LT/PNNL ATJ) Synthetic Paraffinic Kerosene Fuels and Blends has been completed and submitted to the OEM's for approval. The Boeing/Neste HFP-HEFA research report has been completed and is in the process of Phase I review by the OEM's. We are awaiting arrival of the Shell IH2 and IHI Bb Oil fuels for Phase 1 evaluations.

Publications
"Evaluation of LanzaTech/PNNL Ethanol-to-Jet (LT/PNNL ATJ) Synthetic Paraffinic Kerosene Fuels and Blends Phase 1 Research Report," 2016.

"Evaluation of High Freeze Point HEFA as Blending Component for Aviation Jet Fuels," ASTM Research Report Version 1.1, 2017.

Outreach Efforts
Presentations were given at the April and Sept 2017 ASCENT meeting and meetings were held with European D4054 Clearinghouse initiators at the Rome IASH meeting in September. Meetings were held in Dayton with IHI, a Japanese company interested in entering their algae fuel in the D4054 process. We also continue to speak with Shell on their soon to be submitted IH2 fuel.

Awards
None

Student Involvement
None

Plans for Next Period
We plan to attend the ASTM December meeting in Houston and hold an OEM meeting with fuel producers in a separate session prior to the main ASTM meeting as in the past. We expect to receive the first shipment of the Shell IH2 fuel and begin the process of testing the fuel for Tier 1 and 2 evaluations. We expect to receive the first shipment of the IHI Bb oil algae fuel near the end of 2018.

Tasks #3 & #4: Management of Evaluation and Testing of Candidate Alternative Fuels
University of Dayton Research Institute

Objective(s)
The objective of this work is to manage the evaluation and testing of candidate alternative jet fuels conducted in accordance with ASTM International standard practice D4054 (see Figure 1).

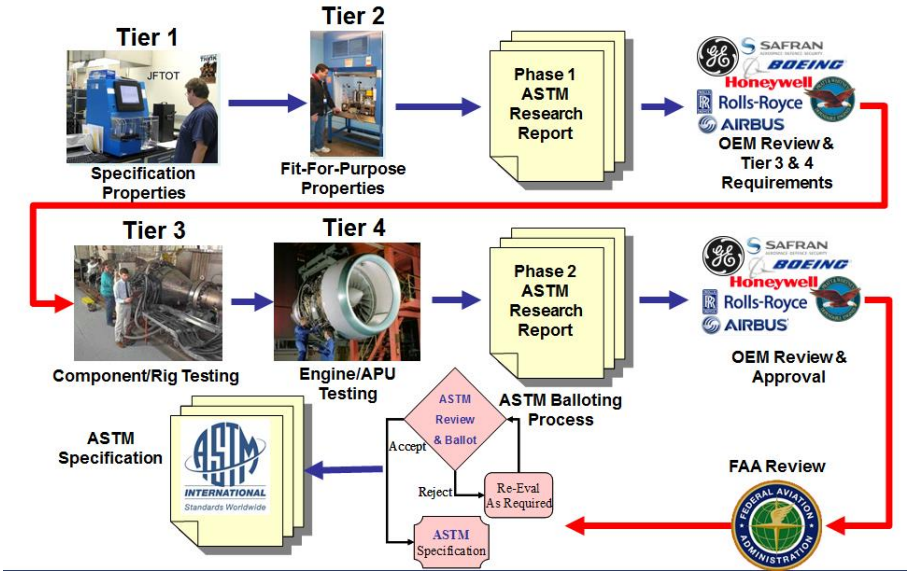

Figure 1. ASTM D4054 Qualification Process

Research Approach

UDRI will subcontract with other research organizations and/or test laboratories or OEMs to carry out the following tasks in support of evaluation and ASTM specification development for AJFs. The purpose of the project is to manage and coordinate the D4054 evaluation process shown in Figure 2 to facilitate transition of alternative fuels to commercial use.

Subtask 1: General Support

- Develop and make available a D4054 process guide that describes logistics procedures for handling of test fuels, documentation requirements, test report issuance and delivery, and contact information. This is intended to provide clear instructions to candidate fuel producers for entering into the ASTM D4054 process.

Subtask 2: Phase 1 Support

- Coordinate the handling of the Phase 1 candidate test fuel samples for Tier 1 and 2 testing.
- Review process description provided by the fuel producer for acceptability for incorporation into the Phase 1 research report.
- Review test data from Tier 1 and 2 testing for acceptability for incorporation into the Phase 1 research report.
- Issue and deliver a Phase 1 research report to the OEMs.
- In conjunction with the fuel producer, review and respond to comments to Phase 1 Research Report submitted by the OEMs.
- Conduct additional Tier 1 or 2 testing in response to OEM comments as required.
- Review and consolidate OEM requirements for D4054 Tier 3 & 4 testing submitted by the OEMs.
- Deliver consolidated D4054 Tier 3 & 4 testing requirements to the fuel producer.

Subtask 3: Phase 2 Support

- Coordinate the funding and scheduling of D4054 Tier 3 & 4 testing with OEMs and other test facilities.
- Coordinate the handling of the Phase 2 candidate test fuel samples for Tier 3 and 4 testing.
- Review test data from Tier 3 and 4 testing for acceptability for incorporation into the Phase 2 research report.
- Issue and deliver the Phase 2 research report to the OEMs.
- In conjunction with the fuel producer, review and respond to comments to the Phase 2 Research Report submitted by the OEMs.
- Conduct additional Tier 3 or 4 testing in response to OEM comments as required.
- Issue and deliver Phase 2 research report addendums reporting the additional Tier 3 or 4 test results as required.

Subtask 4: OEM Review Meetings

- Schedule periodic OEM Review Meetings to review the status of testing and research report review.
- Identify suitable meeting venues and support equipment.
- Develop agendas and coordinate with attendees for participating in the meeting.
- Record meeting minutes, including agreements, commitments, and other action items.

- Issue and distribute the meeting minutes to all attendees.

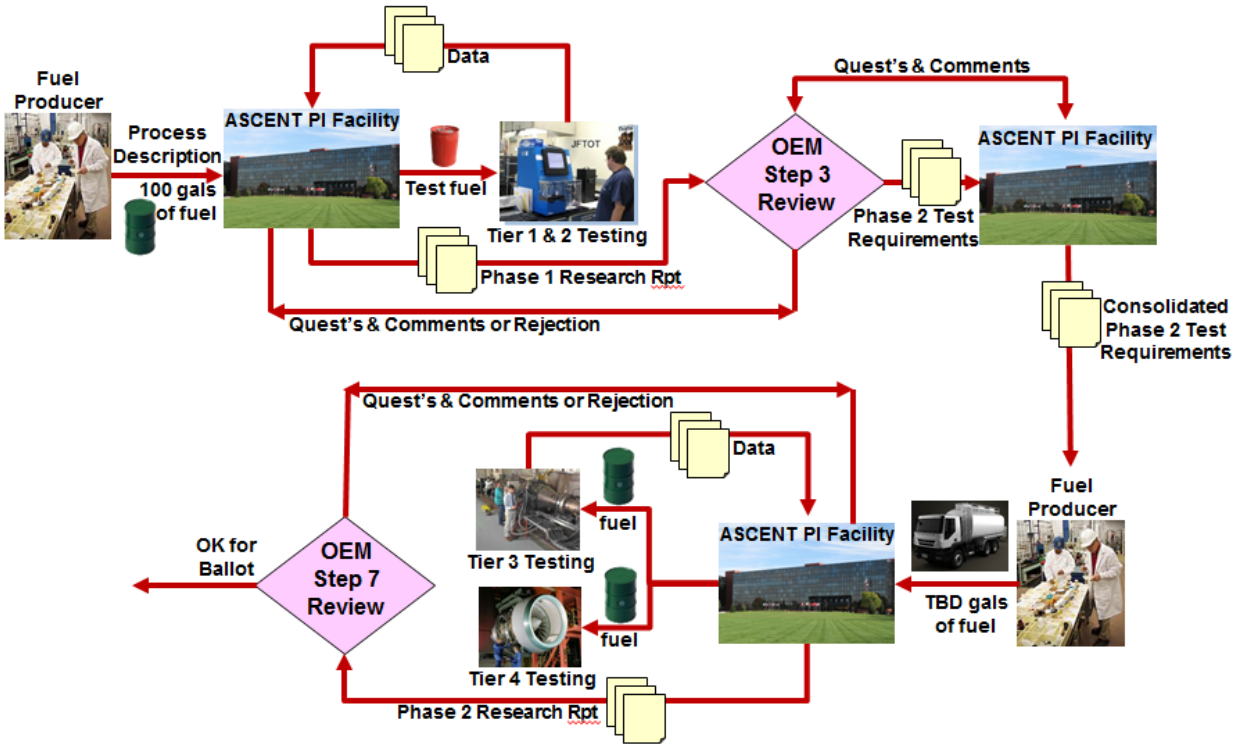

Figure 2. D4054 Evaluation Process

Milestone(s)

The schedule for this project is dependent upon receipt of alternative fuel candidates for testing. As candidate fuels are received a schedule of testing will be coordinated with the FAA and collaborators. Our existing relationships with these organizations will help expedite this process.

Major Accomplishments

The Phase I Research Report for the LanzaTech/PNNL Ethanol-to-Jet (LT/PNNL ATJ) Synthetic Paraffinic Kerosene Fuels and Blends has been completed and submitted to the OEM's for approval. The Boeing/Neste HFP-HEFA research report has been completed and is in the process of Phase I review by the OEM's. We are awaiting arrival of the Shell IH2 and IHI Bb Oil fuels for Phase 1 evaluations.

A number of major activities occurred during the period. We attended the ASTM OEM meeting (Dec 2016 in Orlando) with engine and airframe OEMs to review progress on ASTM research report reviews. We gave a presentation on the chemical analysis of heteroatomic polars for development of a generic annex for alternative fuel certification. We presented the results of the on-going project at the April 2017 ASCENT meeting in Alexandria. We also attended the AFC meeting in London and discussed alternative fuel qualification and certification with the FAA and OEMs. Discussions with alternative fuel candidate producers also occurred at each of these meetings.

In addition, we presented a poster on the project at the Sept 2017 ASCENT meeting in Alexandria VA. We also attended the IASH meeting in Rome Italy and met with a European group that wishes to start a European version of the D4054 Clearinghouse. We advised this group on how the Clearinghouse is structured and will continue to work with them to

identify entities in the EU that can perform the necessary evaluations for D4054 certification. We also met with representatives from IHI, a Japanese company that wishes to certify their algae feedstock product via a modification to the HEFA annex of D7566. In addition, a Gantt chart showing the status of new fuels in the D4054 process was generated and sent to the fuel producers and OEM's. This Gantt chart is being continuously updated and provided to the FAA, fuel producers, and the OEM's. We have finally finished getting all six of the original engine and airframe OEM's on subcontract for the research report review process. We have also begun the process of funding AirBus for an initial amount for research report reviews.

Publications

"Evaluation of LanzaTech/PNNL Ethanol-to-Jet (LT/PNNL ATJ) Synthetic Paraffinic Kerosene Fuels and Blends Phase 1 Research Report," 2016.

"Evaluation of High Freeze Point HEFA as Blending Component for Aviation Jet Fuels," ASTM Research Report Version 1.1, 2017.

Outreach Efforts

Presentations were given at the April and Sept 2017 ASCENT meeting and meetings were held with European D4054 Clearinghouse initiators at the Rome IASH meeting in September. Meetings were held in Dayton with IHI, a Japanese company interested in entering their algae fuel in the D4054 process. We also continue to speak with Shell on their soon to be submitted IH2 fuel.

Awards

None

Student Involvement

None

Plans for Next Period

We plan to attend the ASTM December meeting in Houston and hold an OEM meeting with fuel producers in a separate session prior to the main ASTM meeting as in the past. We expect to receive the first shipment of the Shell IH2 fuel and begin the process of testing the fuel for Tier 1 and 2 evaluations. We expect to receive the first shipment of the IHI Bb oil algae fuel near the end of 2018.

Project 031(B) Methods for the Fast Quantification of Oxygenated Compounds in Alternative Jet Fuels

Washington State University

Project Lead Investigator

Manuel Garcia-Perez
Associate Professor
Biological Systems Engineering
Washington State University
LJ Smith, Room 205, PO Box 646120
Pullman, WA 99164-6120
509-335-7758
Email: mgarcia-perez@wsu.edu

University Participants

Washington State University

- P.I.(s): Manuel Garcia-Perez
- FAA Award Number: 13-C-AJFE-WaSU-008
- Period of Performance Reported: September 1st, 2016 to August 31st, 2017.
- Task(s):
    1. Literature review
    2. Improving the method for quantification of independent oxygenated compounds in AJFs
    3. Development of methods for the fast quantification of oxygenated compounds in jet fuels

Project Funding Level

Washington State University: Amount of funding from the FAA ($ 50,963), Matching funds ($51,130), Source: State Funds to support one graduate student (from Dr. Wolcott's state funded program) and Dr. Garcia-Perez's salary.

Investigation Team

Yinglei Han (PhD student): Improving the methods for quantification of independent oxygenated compounds in AJFs

Mainali Kalidas (MSc student): Literature review and development of methods for the fast quantification of oxygenated compounds in jet fuels

Manuel Garcia-Perez (Associate Professor): Principal Investigator, project management and reporting

Project Overview

This project has confirmed that the chemical compositions of the alternative jet fuels under the ASTM consideration (SK and SAK from Virent, Kior, Gevo, Amyris, and ARA; HEFA from UOP; FT from Sasol and Syntroleum) range from fuels comprised of single molecules to fuels with thousands of molecules with a wide range of molecular weights and functionalities. These fuels have contents of trace oxygenated molecules similar to commercial jet fuels, but the types of oxygen groups are fuel dependent. UV Fluorescence methods for the fast identification and quantification of oxygenated compounds for quality control in distribution and blending points were studied.

Task #1: Literature Review

Washington State University

Objective(s)

To conduct a literature review on the methods for the quantification of oxygenated compounds in alternative jet fuels.

Research Approach

We concluded a literature review on methods for the quantification of oxygenated compounds in alternative jet fuels. The main goal of this task was to review the methods available for the quantification of total functional groups (acids, carbonyl, phenols) and the methods for the quantification of independent compounds in alternative jet fuels. We also reviewed methods that can be potentially used for the quantification of targeted oxygenated compounds in organic matrices.

Milestone(s)

We concluded the literature review early this year and this literature review will be part of the MSc thesis that Mainali Kalidas will defend in the spring 2018.

Major Accomplishments

The literature review on the methods for the quantification of oxygenated compounds was completed.

Publications

None

Outreach Efforts

None

Awards

None

Student Involvement

A MSc student (Mainali Kalidas) conducted this literature review and is expected to graduate in spring 2018.

Plans for Next Period

None

Task #2: Improving the Method for Quantification of Independent Oxygenated Compounds in AJFs

Washington State University

Objective(s)

Validation of Balster's method (Balster et al 2006) for the quantification of oxygenated compounds in AJFs.

Research Approach

We quantified the content of individual oxygenated compounds by the method described by Balster et al. (2006). The polar molecules were concentrated through Solid phase Extraction (SPE) using a 6 mL Agilent SampliQ silica SPE cartridge. 10 mL sample of jet fuel was analyzed per run. A volume of 12 mL hexane was used to rinse the cartridge and after that 11 mL of methanol eluted to polar species. The samples collected from SPE were then analyzed by GC/MS. Both internal and external standards were used for the analysis. Both methods were validated with new standards.

Milestone(s)
We conducted several tests, varying jet fuel/methanol ratios, with jet fuels doped with several phenols. Our results confirmed the reliability of the experimental method tested. Almost 100 % of the phenol doped was in fact detected.

Major Accomplishments
This task was completed early this year.

Publications
Pires APP, Han Y, Kramlich J, Garcia-Perez M: Chemical Composition and Fuel Properties of Alternative Jet Fuels. Submitted to *Bioresources*, **2018**

Outreach Efforts
None

Awards
None

Student Involvement
Two graduate students (Yinglei Han and Kalidas Mainali) worked in this task. Yinglei Han is still working in his PhD program and is expected to graduate next year. Kalidas Mainali will complete his MSc program in the Spring 2018.

Plans for Next Period
None

Task #3: Development of Methods for the Fast Quantification of Oxygenated Compounds in Jet Fuels
Washington State University

Objective(s)
Develop a method for the fast quantification of oxygenated functional groups in alternative jet fuels

Research Approach
The third task consists of studies to develop methods for the fast quantification of oxygenated functional groups in alternative jet fuels (E411 2012, Christiensen et al. 2011). The goal is to develop fast detection kits that can be used in field conditions. We focused on the development of kits for the analysis of total phenols by UV-Fluorescence spectroscopic that can be easily miniaturized (Kauffman 1998, Qian et al 2008, Galuszka et al 2013, Novakova and Vickova 2009, Saito et al 2002, Tobiszewski et al 2009).

Milestone(s)
This task was completed in September 2017.

Major Accomplishments
A new method for the fast determination of oxygenated functional groups based on UV florescence was developed and tested. This method is helpful because it allows the fast quantification of mono and oligo-phenols in jet fuels.

Publications
A research paper with the results of this study will be submitted in the summer 2018.

Outreach Efforts
None

Awards
None

Student Involvement
This task was conducted by our MSc student Mainali Kalidas and our PhD student Yinglei Han. Kalidas will graduate in the spring 2018. Yinglei is planning to defend his PhD dissertation in 2019.

Plans for Next Period
None

References

Balster, LM., Zabarnick S, Striebich RC, Shafer LM, West ZJ. Analysis of Polar Species in Jet Fuel and Determination of Their Role in Autoxidative Deposit Formation. *Energy & Fuels*, 2006, 2564–71.

Christensen ED, Chupka GM, Luecke J, Smurthwaite T, Alleman TL, Iisa K, Franz JA, Elliott DC, McCormick RL: Analysis of Oxygenated Compounds in Hydrotreated Biomass Fast pyrolysis Oil Distillate Fractions. *Energy Fuels* 2011, 25, 5462 - 5471

Galuszka A, Migaszewski Z, Namiesnik J: The 12 principles of green analytical chemistry and the SIGNIFICANCE mnemonic of green analytical practices. TrAC *Trends in Analytical Chemisytry*, Vol. 50, 2013, 78 - 84

E411, ASTM. 2012. "Standard Test Method for Trace Quantities of Carbonyl Compounds with 2 ,4 - ."

Kauffman RE: Rapid, Potable Voltammetric Techniques for Performing Antiocidant, Total Acid Number (TAN) and Total Base Number (TBN) Measurements. *Lubrication Engineering* 54.1 (1998), 39

Novakova L, Vickova H: A review of current trends and advances in modern bio - analytical methods: Chromatography and sample preparation. *Analytical Chimica Acta*. Vol. 656, Issues 1 - 2, December 2009, pages 8 - 35

Qian K, Edwards KE, Deschert GJ, Jaffe SB, Green LA, Olmstead WN: Measuremnt of Total Acid Number (TAN) and TAN Boiling Point Distribution in Petroleum Products by electrospray Ionization Mass Spectrimetry. *Analytical Chem*. 2008, 80 (3), pp. 849 - 855

Saito Y, Kawazoe M, Imaizumi M, Morishima Y, Nakao K, Hayashida M, Jinno K: Miniaturized Sample Preparation and Separation Methods for Environmental and Drug Analyses. *Analytical Sciences*. Vol. 18 (2002) No 1, pp. 7 - 17

Tobiszewski M, Mechlinska A, Zygmut B, Namiesnik J: Green analytical in sample preparation for determination of trace organic pollutants. TrAC *Trends in Analytical Chemistry*, Vol. 28, 8, 2009, 943 - 951

Project 033 Alternative Fuels Test Database Library (Year III)

University of Dayton Research Institute, University of Illinois

*this report covers portion of University of Illinois

Project Lead Investigator

Tonghun Lee
Associate Professor
Mechanical Science & Engineering
University of Illinois at Urbana-Champaign
1206 W. Green St.
Urbana IL 61801
517-290-8005
tonghun@illinois.edu

University Participants

University of Illinois at Urbana-Champaign

- P.I.(s): Tonghun Lee, Associate Professor
- FAA Award Number: 13-C-AJFE-UI-009
- Period of Performance: 8/15/2016 to 8/14/2017
- Task(s):
    1. Development of an alternative fuels test database

Project Funding Level

Funding Level: $120K
Cost Share: Software license support from Reaction Design (ANSYS)

Investigation Team

- Kyungwook Min (Graduate Student, University of Illinois at Urbana-Champaign): Compilation of fuel test data.
- Anna Oldani (Graduate Student, University of Illinois at Urbana-Champaign): Compilation of fuel test data and development of database.

Project Overview

This study seeks to create a comprehensive, foundational database of current and emerging alternative jet fuels by integrating relevant pre-existing jet fuel data into a common archive which can provide guidelines for design and certification of new jet fuels in our future as well as aid federal work including fuel certification. Thus far, the effort has focused on the integration and analysis of pre-existing jet fuel data from various government agencies and individual research groups with oversight from the Federal Aviation Administration (FAA). We hope that the database will one day serve as 'the comprehensive and centralized knowledgebase' shared by the academic, government, and industrial communities in fuels research and policy, possibly facilitated on a cyber-based infrastructure. With ongoing prolific diversification of new jet fuels, this effort to integrate dispersed information is critical in providing the FAA with an overview of the latest developments and to support many other tangential fields of research in government, industry, and academia impacted by integration of new alternative jet fuels.

Task #1: Development of an Alternative Fuels Test Database

University of Illinois at Urbana-Champaign

Objective(s)

The main objective of this study is to establish a ***foundational database*** of current and newly emerging alternative jet fuels by integrating all relevant pre-existing jet fuel data into a common archive which can provide guidelines for design and certification of new jet fuels in our future as well as aid and shorten fuel certification relevant work. This proposal outlines the year II efforts under this mandate. The vision is to institute a database that can be utilized for the design and optimization of new propulsion and energy systems including development of next-generation engines, fuel delivery systems, as well as pollution mitigation technologies. Furthermore, it can provide data for screening and certification of newly emerging fuels and thereby impacting legislative measures and national policy. In so doing, the goals of this project are as follows:

- Survey current pre-existing data and analyze information
- Prioritize current data and compile into centralized logical structure
- Analyze the obtained information into chronological order and regroup into relevant groups
- Obtain information on detailed test platforms and test conditions
- Develop a controlled web portal for access to the information
- Develop and implement a database/web portal infrastructure and methodology
- Integrate available alternative fuel test data into the database in organized format
- (Future Work) Integrate FAA ASCENT and NJFCP Data

Research Approach

Development Strategy of a Successful Fuels Test Database (Long Term Plan)

- **Phase I:** Integrate Current Pre-Existing Data: Preliminary survey and integration of all pre-existing database and data (including raw data) on jet fuels from universities, national laboratories, government archives, and private industry (i.e., existing database from Sandia, NIST, DoD Labs, ASTM research reports, government technical reports etc. is part of the year I efforts and will be used to initially seed the basic infrastructure of the fuels database proposed in this study). Year II efforts continued to assemble information and annex a prioritized set into the web portal/database. In year II, we focused our efforts on obtaining relevant fuel property specification test data for the certification process.
- **Phase II:** Analysis of Preliminary Data: Conduct comprehensive analysis of the initial data to categorize all relevant physical and chemical characteristics of the fuels and relevant testing conditions. Effort will be made to determine insufficient areas for further investigation. In year II, we have significantly expanded our efforts to the analysis of information into chronological order and in incorporating detailed test platform and test condition data. An effort will be made to re-categorize the data according to different testing groups and performance. A preliminary effort will be made to vet some of the data according to test conditions as required (future efforts will more fully address vetting and analysis of data).
- **Phase III:** Establish Web Portal/Database Infrastructure and Methodology: A basic web portal has been established during the year I efforts. In year II, based on the analysis of pre-existing data, we will work with national laboratories to establish a flexible and accessible database structure and data access protocols both for retrieval of current data and also for integration of new information in the future. This will be integrated into the web portal. We anticipate increased functionality in the web portal to conduct advanced searches and user feedback on each data item (community based vetting system).
- **Phase III-b:** Integration of FAA ASCENT and NJFCP Data: New data generated from both the FAA ASCENT and the NJFCP will be integrated into the database according to the pre-defined infrastructure. This will be coordinated with Area #7 of the NJFCP program.
- **Phase IV:** Integrate with Current and Future Research: Disseminate and integrate new database to relevant research groups in universities, national laboratories, government, and industry. Formulate partnerships for stewardship, preservation, and continued development of the alternative jet fuel database to include emerging analysis methods (e.g. GCxGC fuel analysis).
- **Phase V:** Continued Development: Continue development of the database after the initial integration and distribution phase into a more widely distributed community based infrastructure (potentially cyber-based). Link and expand the database to encompass pre-existing data from other countries as well as interlink with efforts such as Europe's JETSCREEN program.

Milestone(s)

Milestone 1 (up to 10/1/2016)

Proposed: The first milestone of this reporting period was to complete the technical development of the database site housed at the University of Illinois with user registration and other additional requested features including refinement of the search results and data categorization. We will also continue to visit AFRL to obtain fuel test data for inclusion on the site as well as other relevant fuel reports and publications.

Achieved: We finalized the design and organization of the website housing the Alternative Jet Fuels Test Database Library. We are confident that this final structure achieves the needs and features identified by the jet fuel community. Additional data retrievals were completed during this period to obtain testing data for approved alternative jet fuels that have been annexed under ASTM D7566 including FT, HEFA, SKA, SIP, and ATJ.

Milestone 2 (up to 12/1/2016)

Proposed: For our second planned milestone, we will determine the feasibility of including the chemometric analysis software developed by NRL, FCAST, into the database. This will involve an evaluation of the software and its potential usefulness for alternative jet fuel development partners. We also plan to reach out to link in additional related programs dealing with aviation industry such as CLEEN, CAAFI, and NJFCP.

Achieved: We obtained a license from NRL to use the FCAST software at the University of Illinois to evaluate its potential use within the database. With this access, we ran sample alternative jet fuel data to determine how well the FCAST software performed in its fuel property predictions. It performs a Partial Least Squares (PLS) regression to establish correlations between measured fuel chemical components and observed fuel properties from a test dataset. It then uses these correlations to provide fuel property predictions of relevant aviation fuel specifications. We also tested the blending feature of the software, which allows users to blend the GCxMS data of two fuels in 10% increments. After analyzing the software, we determined it could be implemented at some future point into the database if there is enough support to fund such a project. However, in its current state, FCAST is a standalone software that would require modification to be integrated into an online portal such as the database. Regarding additional related programs, we continued conversations with groups involved in the NJFCP program to assess if the AJFTD site could serve their needs. We agreed to function as data and documentation dissemination site as specified under the Data Management Plan for the NJFCP program. Further discussions will be ongoing to determine the appropriate timing and release of data.

Milestone 3 (up to 12/31/2016)

Proposed: To wrap up 2016, we will conduct an initial survey of alternative fuel properties taken from the AFRL fuels database maintained at Wright-Patterson Air Force Base in Dayton, OH. This survey will help identify data still needed across the various alternative jet fuel categories. We will also discuss with our AFRL collaborators useful next steps to take regarding data collection and analysis.

Achieved: After examining the initial retrievals of fuel test data (primarily from AFRL), we decided to task ourselves with collecting additional fuel data for the HEFA and ATJ fuel categories. We also began discussions regarding future directions of fuel analysis, specifically potential improvements to current testing methods. This also began our discussions with project collaborators dealing with the ASTM Generic Annex proposal to evaluate how the AJFTD site can support the goals to streamline the certification process for new alternative fuels.

Milestone 4 (up to 3/31/2017)

Proposed: For the first quarter of 2017, we will begin to develop a statistical analysis of fuel variation data taken from reports such as the World Fuel Survey and alternative fuel approval reports. From these data sources, we will evaluate property-temperature relations for properties including density, viscosity, isentropic bulk modulus, and surface tension. We hope to determine whether significant variance exists in property temperature dependence between conventional and alternative jet fuels.

Achieved: Following our discussions with project collaborators at the NJFCP meeting, we obtained fit for purpose fuel property data that allowed us to analyze the variance of the aforementioned properties with regard to temperature. From this analysis, we concluded that across all properties, several alternative fuel categories show significant variance from conventional fuels.

Milestone 5 (up to 5/31/2017)

Proposed: For the next milestone, we will work to evaluate the implication of the variance observed in the alternative jet fuels. We will seek to determine if the significant variability of alternative fuels from conventional fuels poses additional considerations for the ASTM Generic Annex. To accomplish this, we will develop expected fuel property ranges from the fuel variance data and then compare these expected ranges with specification requirements.

Achieved: Using the fuel variability data, we generated 95% confidence intervals to provide expected fuel property ranges to evaluate if, given their variability, the alternative fuels remain within specification requirements. We concluded that, for all properties evaluated, the alternative fuels remain with specification requirements as outlined in ASTM D7566. This provided us with the assurance that alternative fuel variability does not present an additional concern for meeting fuel specifications.

Milestone 6 (up to 8/14/2017)
Proposed: For the final milestone of this reporting period, we will evaluate whether FCAST can be used to support the proposed requirements under the ASTM Generic Annex. Specifically, the Generic Annex seeks to introduce new alternative fuels at low blending ratios of 10%. To provide justification for this blending level, we will test the blending capability of FCAST by comparing the fuel blend tool with actual blended fuel results. Following this, we can determine the accuracy of FCAST in computing fuel blend properties using solely fuel blend-stock data without utilizing actual blended fuel data.
Achieved: We worked with FCAST to test blends of A1 (JP8) and C1 (Gevo) fuels in in varying ratios. We evaluated the FCAST blending tool by providing GCxMS data for the neat components and blending within the tool to then predict property values. We compared these blend predictions with actual blends of A1 and C1 that were prepared and run through our GCxMS facility. The data from these actual blends was then provided to FCAST to compute predicted properties. In comparing the predicted properties for the computed blend and the actual blend, we found less than a 5% difference across most properties for all the fuel blends. From this, we concluded that the FCAST blending tool does an accurate job at predicting blended fuel properties, and thus, can be potentially used to evaluate fuel blends for the ASTM Generic Annex.

Major Accomplishments

The Alternative Jet Fuels Test Database, established through the coordinated efforts of members at the University of Illinois, continued to grow with additional jet fuel test data, which was utilized for a statistical analysis of fuel variability during year III. Improvements over the years include the development of basic and advanced search functionalities and enhanced search algorithms to return more robust search results. There are public access areas including general information regarding the mission and goals of the database project, funding agencies of the program, a directory of members involved in the work, and links to partner institutions participating in the larger FAA ASCENT database project, links to relevant updates regarding alternative jet fuel, and links to contact site administrators. There are also site features accessible only to registered users that include links to the advanced and basic search features of the database, access to the database file dropdown feature, and descriptive information of the various areas under the NJFCP program which will include NJFCP data in the future. To register, users must request access and be approved by site administrators. Registered users can also submit data directly to the site, which is reviewed and categorized by site.

Users have two methods to access data on the site: a basic or advanced search which allow users to search by terms of interest (e.g. authors, title, DOI, year of publication, data type, and keywords) and file folder dropdown structure that gives users access to all the categorized documents without requiring users to input a specific search term. Users can download original file formats as well as any tabular data that has been converted into .XLSX files for improved accessibility. The site will also house data from the National Jet Fuel Combustion Program (NJFCP) Areas 1 through 6. Discussions are ongoing as how to best to include data from this multi-group collaborative effort. Once further guidelines have been discussed and approved regarding which data to include, this section of the site will be expanded.

In year III, the data contained within the database was analyzed for variability of thermophysical properties. This work was done to provide a more thorough understanding of the variation present in alternative jet fuels. A statistical analysis of conventional fuels and alternative fuels approved via annexation to the ASTM D7566 Standard Specification for Aviation Turbine Fuel Containing Synthesized Hydrocarbons found significant variance in property-temperature relations for alternative fuels as compared to World Fuel Survey conventional fuel averages and is summarized in Table 1. The full results for slope and intercept results with slope statistical analysis results are shown in Table *2* for the alternative fuel categories as compared to conventional fuels. Bolded results indicate properties that are significantly different from conventional fuels (WFS) while statistical tests were not done on pure hydrocarbons (HCs, HCs1, HCs2) or CRC handbook properties (CRC).

Table 1: Summary of property-temperature relation variance

Fuel Property	*Fuels with Significant Variance*
Density	SKA
Isentropic Bulk Modulus	HEFA, FT
Specific Heat	FT, FSJF
Speed of Sound	HEFA
Viscosity	SKA, HEFA

Table 2: Property-temperature relation variance results

Density	*Slope*	*Intercept*	*T-test*
WFS	-0.7216	815.49	
WFS w. light+heavy	-0.7225	815.53	
FT	-0.7376	777.68	0.0778
SKA	-0.7439	796.76	**0.0239**
Renewable	-0.7419	796.87	0.1694
HCs 1	-0.8881	826.87	
HCs 2	-0.8651	825.48	
CRC	-0.7723	817.66	

Specific Heat	*Slope*	*Intercept*	*T-test*
WFS	0.0036	1.5597	
FT	0.0030	1.7845	**0.0466**
FT 2	0.0032	1.7732	0.0763
FSJF	0.0018	1.5797	**4.7E-06**
HEFA	0.0037	2.0513	0.4214
2nd Gen	0.0037	1.8663	0.8462
HCs	0.0042	1.7836	
CRC	0.0035	1.7233	

Speed of Sound	*Slope*	*Intercept*	*T-test*
WFS	-4.113	1403.7	
FT	-3.974	1399.4	0.0686
HEFA	-2.748	1371.4	**0.0010**
HCs	-3.641	1339.6	

Viscosity	*m*	*b*	*T-test*
WFS	0.9750	2.8487	
FT	0.9758	2.9994	0.7989
SKA	0.9815	3.0912	**0.0015**
HEFA	0.9777	2.8944	**0.0137**
2nd Gen	0.9708	3.2623	0.3013
HCs	0.9890	1.8502	

Where: $y=bm^{x}$

Surface Tension	*Slope*	*Intercept*	*T-test*
WFS	-0.0751	27.407	
FT & HEFA	-0.0741	25.921	0.8581
SPK	-0.0800	25.873	0.2261
Renewables	-0.0771	26.687	0.4125
CRC	-0.0443	15.971	

To evaluate the impact of this variance, 95% confidence intervals were constructed from the fuel data to provide expected property value ranges for the various properties evaluated including density, isentropic bulk modulus, specific heat, speed of sound, and viscosity. It was important to assess whether the significant variance as identified from **Table *2*** would result in property values that do not meet specification requirements. From these property value bounds, it was concluded that the fuels remain within specification requirements for the properties under consideration. Averaged property-temperature relations were also produced for the examined fuel categories and are shown in **Table *3***. These averaged relations can be used to provide property ranges for the various fuels categories, useful for determining property values that can be reasonably expected for each respective fuel category. When evaluating fuel blends for the ASTM Generic Annex, similar property-temperature relations can be constructed to provide the bounds for possible fuel properties. These relations can then be analyzed as blend ratios vary, to determine the magnitude of the impact of blend ratios on resulting fuel properties, specifically properties identified under fuel specification requirements.

Table 3: Averaged property-temperature relations

Density	*Equation*
WFS	y=-0.7216x +815.5
WFS w. light+heavy	y=-0.7225x +815.5
FT	y=-0.7376x +777.7
SKA	y=-0.7439x +796.8
Renewable	y=-0.7419x +796.9
HCs 1	y=-0.8881x +826.9
HCs 2	y=-0.8651x +825.5
CRC	y=-0.7723x +817.7

Specific Heat	*Equation*
WFS	y=0.0036x +1.560
FT	y=0.0030x +1.784
FT 2	y=0.0032x +1.773
FSJF	y=0.0018x +1.580
HEFA	y=0.0037x +2.051
2nd Gen	y=0.0037x +1.866
HCs	y=0.0042x +1.784
CRC	y=0.0035x +1.723

Isentropic Bulk Modulus	*Equation*
WFS	y=-10.715x +1629
Boeing HEFA	y=-7.957x +1720
FT	y=-9.864x +1603

Speed of Sound	*Equation*
WFS	y=-4.113x +1403.7
FT	y=-3.974x +1399.4
HEFA	y=-2.748x +1371.4
HCs	y=-3.641x +1339.6

Surface Tension	*Equation*
WFS	y=-0.0751x +27.4
FT & HEFA	y=-0.0741x +25.9
SPK	y=-0.0800x +25.9
Renewables	y=-0.0771x +26.7
CRC	y=-0.0443x +16.0

Thermal Conductivity	*Equation*
Renewables	y=-1.43E-04x +1.16E-01
FT	y=-4.72E-05x +1.34E-01
FSJF	y=-3.11E-07x +2.98E-04
HEFA	y=-8.52E-05x +1.05E-01

Viscosity	*Equation*
FT	y=2.999*0.9758x
SKA	y=3.091*0.9815x
HEFA	y=2.894*0.9777x
WFS	y=2.849*0.9750x
2nd Gen	y=3.262*0.9708x
HCs	y=1.850*0.9890x

Finally, work was also completed in collaboration with NRL and their fuel chemometric analysis program, FCAST. This software performs a Partial Least Squares regression analysis to correlate fuel composition to expected specification properties. Using a training set of data, these correlations can then be applied to new GCxMS data provided to the program, resulting in predicted properties for jet fuel relevant specifications. We were granted access to this software, allowing us to evaluate its performance for alternative aviation fuels. We also employed the fuel blending tool to assess the potential for its use to support the ASTM Generic Annex approach of introducing new alternative fuels at lower blending ratios of around 10%. To evaluate the blending capability, fuel samples of A1 (JP8) and C1 (Gevo) fuels were prepared as neat samples and blended mixtures of varying ratios. **Figure *1*** shows the results of a 50:50 A1:C1 fuel blend as calculated by the FCAST blending tool and as prepared in the lab. When the predicted fuel properties of the calculated blend and actual blend are compared, generally a 5% or less difference is observed for all properties at the varying blend ratios. We believe that this tool can support the plans within the Generic Annex to provide control of conventional and alternative fuel blends through limited alternative fuel blending levels. Additionally, if there is interest in the future to integrate an FCAST type tool on the AJFTD site, modifications can be made to its current form to allow for online accessibility.

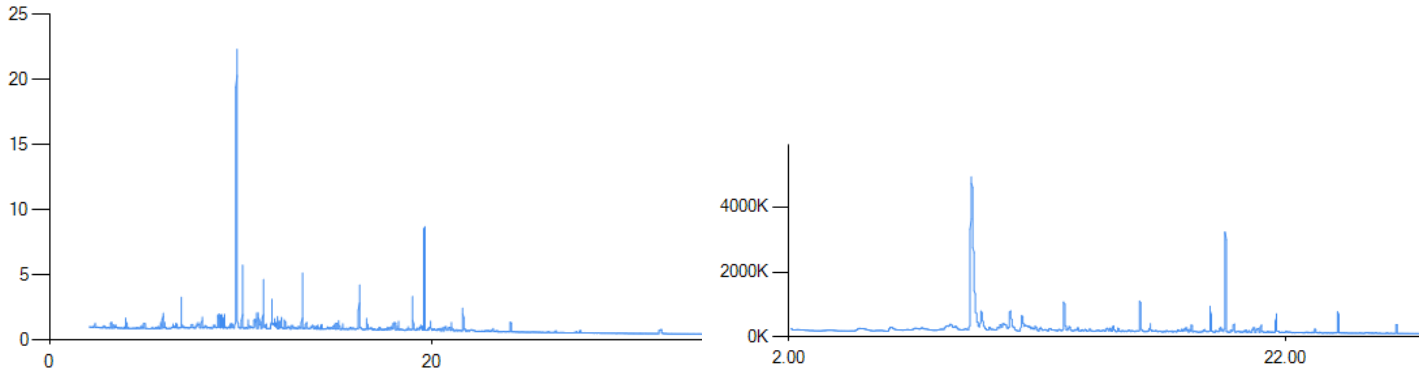

Figure 1: 50:50 A1:C1 blend - calculated TIC (L), actual TIC (R)

Publications

(In Progress) Oldani, Anna. "Alternative Jet Fuel Variation and Certification Considerations." 2017.

Outreach Efforts

None

Awards

Anna Oldani (Graduate Student): Society of Women in Engineering (SWE) Award for Research Excellence

Student Involvement

Two graduate students (listed above) have participated in this project on a rotational basis to address various aspects of the project. They have surveyed the data, interacted with the data sources and created strategies to integrate the data into the database. They developed the web-based portal for the actual implementation of the web interface. They have also conducted a statistical analysis of the available data to evaluate property variance. They continue efforts to update the database with relevant alternative jet fuel test data as it is made available.

Plans for Next Period: Start of Analysis

Year IV for the database project will see continued evaluation of the data contained within the database as well as an assessment of emerging fuel analysis methods such as GCxGC. Several key efforts are planned and are currently underway. They include:

- Evaluation of GCxGC procedures and data processing methods
- Inclusion of available GCxGC data for approved alternative jet fuels to the database site
- Data analysis of fuel blending ratios to support ASTM General Annex effort for fuel certification to determine additional correlation work to link fuel properties to the overall evaluation
- Inclusion of NJFCP data: put up vetted and organized NJFCP data on the database
- Integration of efforts with European JETSCREEN program to collaborate fuel screening and property evaluation under NJFCP program

Project 034 Overall Integration and Coordination

University of Dayton

Project Lead Investigator

Joshua Heyne
Assistant Professor
Mechanical Engineering
University of Dayton
300 College Park
Dayton, OH 45458
937 229-5319
Jheyne1@udayton.edu

University Participants

University of Dayton

- P.I.(s): Joshua Heyne, Scott Stouffer, and Alejandro Briones
- FAA Award Number: 13-C-AJFE-UD (Amendment Nos. 9, 10, 13, & 17)
- Period of Performance: September, 18 2015 to December, 31 2017
- Task(s):
    1. Overall NJFCP integration and coordination
    2. Well-Stirred Reactor experiments on LBO and Speciation
    3. Cross-experiment analysis
    4. Common format routine software and model development
    5. Spray modeling of Area 3 (GT P&W pressure atomizer)
    6. Cold ignition experiments in the Referee Rig of alternative fuel blends

Project Funding Level

Amendment No. 9: $134,999.00 (September, 18 2015 to February, 28 2017)
Amendment No. 10: $249,330.00 (July, 7 2016 to December, 31 2017)
Amendment No. 13: $386,035.00 (August, 30 2016 to December, 31 2017)
Amendment No. 17: $192,997.00 (August, 3 2017 to September, 30 2018)

Cost share is provided by GE Aviation ($135,000.00), DLR Germany ($512,924.00), United Technologies Research Center ($150,000.00), ANSYS/FLUENT ($175,000.00), and the University of Dayton ($53,887.00) in to form of in-kind research at GE Aviation, DLR Germany, and United Technologies, direct financial support at the University of Dayton, and reduced software license fees at ANSYS/FLUENT.

Investigation Team

- Joshua Heyne (University of Dayton) is the Project Lead Investigator for coordinating all NJFCP teams (both ASCENT and non-ASCENT efforts), Well-Stirred Reactor experiments, procuring additional geometrical configurations, and leading studies across experimental platforms within the NJFCP.
- Scott Stouffer (University of Dayton Research Institute) is conducting ignition testing of NJFCP fuels in the Referee Rig.
- Alejandro Briones (University of Dayton Research Institute) is the P.I. responsible for leading the common format routine software development.
- Vaidya Sankaran (UTRC) is sub-contracted to conduct the spray modeling of the Area 3 pressure atomizing spray injector.

- Bob Olding (University of Dayton Research Institute) is part of the team managed by Alejandro Briones to develop the common format routine software. Mr. Olding's main task is on Scheme GUI/TUI programing for later use by OEM CFD teams.
- Mike Hanchak (University of Dayton Research Institute) is part of the team managed by Alejandro Briones to develop the common format routine software. Mr. Hanchak's main task is on CFD and combustion programing for later use by OEM CFD teams.
- Tyler Hendershott (University of Dayton Research Institute) is part of the team working on the ignition of conventional and alternative jet fuels in the Referee Rig.
- Jeffery Monfort (University of Dayton Research Institute) is part of the team working on the ignition of conventional and alternative jet fuels in the Referee Rig.
- Robert Stachler (University of Dayton) is a Ph.D. student conducting the Lean Blowout and emissions measurements in the Well-Stirred Reactor.
- Erin Peiffer (University of Dayton) is a Master's student linking experimental results across ASCENT and non-ASCENT teams.
- Jeremy Carson (University of Dayton) was a Master's student linking experimental results across ASCENT and non-ASCENT teams. Jeremy has since graduated and is now employed full time at UDRI.
- Sherri Alexander (University of Dayton) is an administrative assistant aiding in the compilation of meeting minutes and setting up teleconference times.
- Katherine Opacich (University of Dayton) is an undergraduate research assistant working to document NJFCP activities.

Project Overview

In total, the NJFCP is composed of more than two dozen member institutions contributing information and data as diverse as expert advice from gas turbine Original Equipment Manufacturers (OEMs), federal agencies, other ASCENT universities and corroborating experiments at DLR Germany, NRC Canada and other international partners etc. The project is tasked to coordinate and integrate amongst these diverse program stakeholders, academic Principle Investigators (PIs) and etc., cross-analyze results from other NJFCP areas, collect data for modeling and fuel comparison purposes in a Well-Stirred Reactor (WSR), conduct Large Eddy Simulations (LES) of sprays for the Area 3 High Sheer Rig, and procure additional swirler geometries for the NJFCP Areas and Allied Partners while developing interface of NJFCP modeling capabilities with OEM requirements. Work under this program consists of, but is not limited to:

- meetings with member institutions to facilitate the consistency of testing and modeling,
- coordinate timely completion of program milestones,
- documentation of results and procedures,
- creation of documents critical for program process (e.g. fuel down selection criteria)
- solicit and incorporate program feedback from OEMs,
- reporting and presenting on behalf of the NJFCP at meetings and technical conferences,
- integrate the state-of-the-art combustion and spray models into user-defined-functions (UDFs),
- WSR testing of NJFCP Category A, Category C, and Surrogate fuels,
- LES of sprays for A2, C1, and C5 fuels using the Area 3 High Sheer Rig Pratt & Whitney swirler and air blast atomizer,
- facilitate travel for University of Cape Town student,
- and advise the program Steering Committee.

Task #1: Integration and Coordination of NJFCP Teams

University of Dayton

Objective(s)

The objective of this task is to integrate and coordinate all ASCENT and non-ASCENT team efforts via facilitation of meetings, summarizing results, presenting results external to the NJFCP, communicating on a regular basis with the Steering Committee, and other related activities.

Research Approach

The NJFCP is integrated and coordinate via two main techniques: 1) the structural lumping of various teams into 6 Topic areas and 2) routine meeting and discussion both internal and external to individual Topic areas. The Topic areas are distinguished by the dominant physics associated with them (Topics I and IV), the culmination of all relevant combustion physics (Topics II, III, V), and wrapping all work into a singular OEM GUI package (Topic VI). These 6 Topic areas are:

Topic I. Chemical Kinetics: Foundational to any combustion model is a chemical kinetic model and the validation data anchoring modeling predictions.
Topic II. Lean Blow Off (LBO): This Topic covers data, screening, and validation at relevant conditions to statistically and theoretically anticipate fuel property effects on this FOM.
Topic III. Ignition: Similar to the LBO topic, the focus here is experimental screening and validation data for statistical and theoretical predictions.
Topic IV. Sprays: Historically, the dominant effect of fuel FOM behavior has been the spray character of the fuel relative to others. Experimentalists in this Topic area focus on measuring the fuel property effects on spray behavior. In analogy to Topic I, the spray behavior is not a FOM like Topic II and III, although it is critical to bound the physical property effects on combustion behavior relative to other processes, i.e. chemical kinetics.
Topic V. Computational Fluid Dynamics (CFD) Modeling: Complementary to the empirical Topics II, III, and IV, the CFD Modeling Topic focuses on the theoretical prediction of measured data and facilitates the development of theoretical modeling approaches.
Topic VI. User Defined Function (UDF) Development: Once the theoretical modeling approaches matured in Topic V are validated. UDFs are developed for OEM evaluation of fuel performance in proprietary rigs.

These topic area teams meet and coordinate on a regular basis. At minimum, NJFCP wide meetings are held monthly with Topic area meetings occurring typically every 2-3 weeks.

Milestone(s)

NJFCP Mid-Year Meeting 2017
NJFCP Year-End Meeting 2017, in preparation.

Major Accomplishments

Presentations at CRC Aviation Meeting, AIAA SciTech Meeting Paper and Presentation, NJFCP December 2016 and June 2017 meetings, JetScreen kick-off meeting, and ASCENT Spring and Fall presentations 2017.

Publications

Peer-Reviewed Journal Publications:

Colket, Meredith B., Joshua S. Heyne, Mark Rumizen, James T. Edwards, Mohan Gupta, William M. Roquemore, Jeffrey P. Moder, Julian M. Tishkoff, and Chiping Li. 2017. “An Overview of the National Jet Fuels Combustion Program.” AIAA Journal, https://doi.org/10.2514/1.J055361.

Published conference proceedings:

Heyne, Joshua S., Colket, Meredith B., , Rumizen, Mark, Edwards, James T., Gupta, Mohan, Roquemore, William M., Moder, Jeffrey P., and Li, Chiping. 2017. “Year 2 of the National Jet Fuels Combustion Program: Moving Towards a Streamlined Alternative Jet Fuels Qualification and Certification Process. Grapevine, TX: American Institute of Aeronautics and Astronautics. (AIAA 2017-0145) https://doi.org/10.2514/6.2017-0145.

Outreach Efforts

Presentations at CRC Aviation Meeting, AIAA SciTech Meeting Paper and Presentation, ASCENT Spring and Fall presentations 2017, and DESS ASME conference.

Awards

Jeremy Carson – Best presentation DESS 2016, Best presentation DCASS 2017.

Student Involvement

Jeremy Carson, Graduate Research Assistant, January 2015 – May 2017 (graduated), now at UDRI.
Erin Peiffer, Graduate Research Assistant, June 2017 - present.

Jennifer Colborn, Undergraduate Research Assistant, August 2016 – August 2017, now at UDRI.
Katherine Opacich, Undergraduate Research Assistant, November – 2017 – present.

Plans for Next Period

Continue to perform all relevant coordination and integration related tasks, .

Task #2: Testing of NJFCP in a Well-Stirred Reactor

University of Dayton

Objective(s)

We aim to measure the Lean Blowout (LBO) limit and emissions/speciation characteristics for NJFCP fuels within the program.

Research Approach

In response to legislative orders, industrial and governmental organizations are actively pursuing strategies to promote alternative energy fuels in gas turbine combustors, and to reduce pollutant emissions. Emissions tend to be of importance because of the adverse effects they have on air quality, health and the environment. Gaseous emissions of interest include nitrogen oxides (NO and NO_2), sulfur oxides (SO_x), carbon monoxide (CO), carbon dioxide (CO_2) and unburned hydrocarbons (UHC). The International Civil Aviation Organization (ICAO) currently regulates the total amount of UHC among NO_x, CO, and particulate (smoke number) emissions for aircraft, but the concentration of these emissions, whether unburned hydrocarbons or carbon monoxide, etc., have seen to have a local effect on areas around airports or flight lines (Anneken et al. 2014; D. L. Blunck et al. 2015; FAA 2012; Colket et al. 2016). Because of these effects and these initiatives, it is important to understand the emissions footprints of fuels for aviation for not only a sustainable future, but for better aircraft performance towards a carbon neutral future.

The National Jet Fuels Combustion Program (NJFCP) aims in streamlining the alternative jet fuel research and evaluation process, which is a major R&D directive covered in the Federal Alternative Jet Fuels Research and Development Strategy(AJF-IWG 2016; Colket et al. 2016). Use of specialized laboratory scale rigs are used in this program to determine fuel performance of a candidate alternative jet fuel while minimizing the use of multiple combustor rig tests. These rigs evaluate the impact of engine operability Figures of Merit (FOMs) such as lean blow off (LBO, high altitude relight, and cold start. These FOMs chosen indicate a strong impact on aircraft safety or engine hardware and are likely due fuel variation, whether due to the physical or chemical effects of the fuel. Performance and operability are also studied via emissions, combustor fuel coking and effects of temperature through pattern factors, radiation, and flame structure, all of which are secondary FOMs (Colket et al. 2016). It is imperative to investigate and pursue novel strategies and balance the combustor design characteristics with emissions reduction. Understanding performance and emissions with varying fuel composition provides the opportunity for use of potential alternative fuels in legacy and future aircraft and guidance to the quality and quantity of aircraft emissions produced.

Well-Stirred Reactor (WSR) experiments provide a simplified combustion environment to investigate chemical kinetic effects, among other parameters, such as combustion efficiency and LBO in the absence of physical property effects from the fuels. The lean premixed, prevaporized fuel and air mixtures used in these experiments remove physical effects such as droplet injection, evaporation, and atomization in addition to molecular mixing and transient and chemistry interaction of which is seen in typical gas-turbine combustors. With removing these physical effects, we also eliminate the physical complications native to modeling practical diffusion flame combustors such as, multi-dimensional flow, multi-phase fuel, and transient fluid dynamic and chemistry interactions. Use of this fundamental combustor experiment provides insight into LBO and emissions, a primary and secondary FOM in the NJFCP program, respectively, under relevant residence times and temperatures typically seen in practical gas-turbine-combustor environments(Colket et al. 2016).

We report the investigation of emissions and LBO of surrogate, conventional, and alternative fuel mixtures as lean combustion limits are approached in the WSR as funded by the FAA in relation the NJFCP. The WSR has provided considerable

knowledge toward understanding lean and rich blow off limits, pollutant and particulate formation, kinetics of gaseous and liquid fuel combustion and combustion stability (D. Blunck et al. 2012; J. Blust, Ballal, and Sturgess 1997; S. D. Stouffer et al. 2005; J. W. Blust, Ballal, and Sturgess 1999; S Stouffer et al. 2002; Manzello et al. 2007; Vijlee 2014; Scott Stouffer et al. 2007; Nenniger et al. 1984; Zelina 1995; Karalus 2013; D. L. Blunck et al. 2015). Knowledge of the emissions and LBO provides the opportunity to investigate the controlling chemical kinetics and relating chemical properties among the fuels. Here we report a statistically significant correlation between LBO, derived cetane number, and radical index, yielding insight to the controlling chemical effects experienced in typical gas turbine combustors near LBO.

I. Experimental Details and Methodology

Well-Stirred Reactor

LBO and emissions experiments were performed in the well-stirred reactor (WSR) facility at the Air Force Research Laboratory in Dayton, OH. The toroidal WSR design was derived from the work of Nenniger et al.(Nenniger et al. 1984), Zelina (Zelina 1995), and Stouffer (S Stouffer et al. 2002) and approximates a zero-dimensional perfectly stirred reactor, *i.e.*, homogeneous in both space and time. The reactor, shown during operation in Fig. 1 a and b, comprises an Inconel jet ring, upper and lower ceramic reactor hemispheres, flow straightener, and exhaust stack. A representative cross section drawing of the reactor is shown in Fig. 1b. Premixed prevaporized fuel and air enter the jet ring through two opposed inlets to ensure equal flow around the reactor.

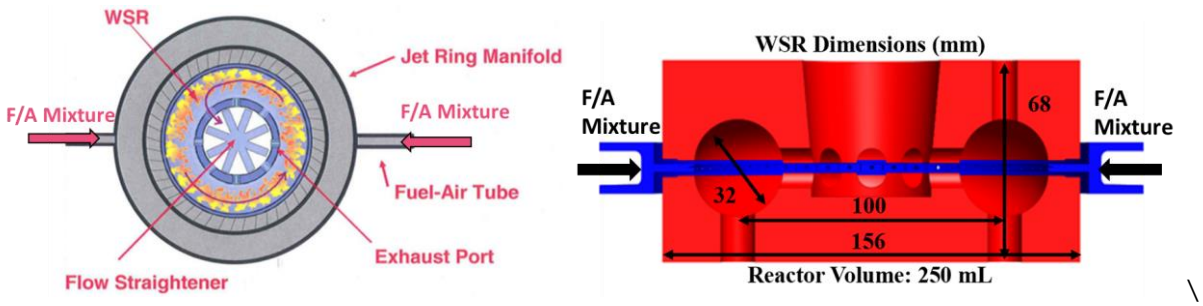

(a) (b)

Figure 1. (a) Cross-section of the WSR, top view (S. D. Stouffer et al. 2005; Scott Stouffer et al. 2007). Premixed, prevaporized fuel and air enters the jet ring via the two opposed inlets. The angled jets (20 degrees from the radius of the torus) inject the mixture into the reactor, where bulk recirculation and flow occurs around the reactor. Burned products exit towards the inner diameter of the toroid through the exhaust ports, the flow straightener, and exhaust stack. (b) Cross-section of the WSR, side view. Fuel an air enter the toroidal reactor through the jet ring in blue.

In the current work, a fused silica reactor (Rescor 750, SiO_2) was utilized and sealed using spring loaded sections.(S Stouffer et al. 2002; D. Blunck et al. 2012) This reactor material was chosen due to its low thermal conductivity, resistance to thermal cracking from fast transients, and reduction in the active cooling necessary around the reactor yielding reduced heat loss. An Inconel jet ring with 48 fuel/air jets at 1mm diameter was sealed between the reactor components. A ceramic paper gasket seal (Cotronics 390, 1/8" thickness) was placed between the upper reactor halve and jet ring while a mica gasket (0.064" thickness) was placed between the jet ring and bottom half to seal the reactor under fuel-lean operating conditions. Figure 1 highlights the construction of the WSR with the ceramic components in red and the jet ring in blue.

The feed jets in the jet ring inject the premixed fuel/air at an angle 20 degrees off the radius of the torus causing the bulk flow to move circumferentially around the reactor (S. D. Stouffer et al. 2005; S Stouffer et al. 2002; Vijlee 2014; Scott Stouffer et al. 2007; Nenniger et al. 1984). The sonic velocity and angle from the jets provides for recirculation zones around the upper and lower half of the toroid in addition to around the toroid. The high rate of continuous mixing between the unburned reactants and burned products is an additional characteristic that separates the WSR from other premixed combustions systems (Briones et al. 2008; D. L. Blunck et al. 2015; D. Blunck et al. 2012; S. D. Stouffer et al. 2005; Scott Stouffer et al. 2007). Previous work using numerical modeling has been performed to show that the WSR operates in the well-stirred turbulent regime (Briones et al. 2008). Products from combustion exit the reactor via 8 radial ports at the toroid inner diameter and through a 5-cm-diameter ceramic stack above the WSR. In this region, recirculation zones and bulk flow are reduced via the use of an alumina flow straightener, rested at the end of the exhaust and base of the stack(D. L. Blunck et al. 2015).

Liquid fuel is delivered to the vaporizer by two syringe pumps (Isco 500 D) operated in continuous flow mode. The piston flow meter accuracy is +/- 0.5%. The liquid fuel passes through a swirler and enters a heat exchanger, where the fuel reaches a temperature of 473 K at the inlet of the vaporizer. Heated fuel is introduced in the vaporizer with 10-20% of the total combustion air via an air-swirled atomizer nozzle containing heated air at 400 K and mass flow of 60 standard liters per minute (slpm). Remaining air at 489 K and mass flow of 440 slpm is added in the vaporizer as a coaxial stream(Scott Stouffer et al. 2007). Prior to entering the vaporizer, the airlines are filtered and monitored along with being controlled using two mass flow controllers, one rated at 1000 slpm and one rated at 75 slpm (Brooks Instruments) (S Stouffer et al. 2002). The accuracy for the mass flow controllers is rated at +/- 1% full scale and a repeatability of 0.25% of the flow rate. The flow controllers were measured and calibrated using sonic nozzles to allow for a more accurate measurement of the air flow rate. Electric, PID-controlled heaters preheat the incoming fuel and air streams. Flow rates of the fuel and air, paired with the temperature control of each, are used to control the incoming fuel-air mixture to the reactor. These flow rates ensure turbulent mixing and sonic velocities from the jets into the reactor (Vijlee 2014). The vaporizer used for the atmospheric WSR has been used in previous tests and was shown to safely and successfully mix the fuel with the air(S. D. Stouffer et al. 2005; Scott Stouffer et al. 2007). This strategy, using premixed and pre-vaporized fuel, eliminated physical complications associated with droplet combustion and established an ideal premixed combustion environment without physical complication.

A fixed custom spark igniter within the reactor initiates combustion. When testing with liquid fuel, the reactor was first brought to a stable thermal condition using a gaseous fuel (usually ethylene). Gaseous fuel flowrate into the WSR was controlled with a series of pressure regulators, to slowly reduce pressure, and mass flow controllers (Brooks Instruments). Introducing gaseous fuel before the liquid fuel allowed the reactor to effectively preheat for prevention of fuel condensation within the small jet ring passages. After operational temperatures were reached, the fuel was transitioned smoothly from the gaseous fuel to the given liquid fuel (Scott Stouffer et al. 2007).

B. Fuels

Four fuels tested in the current work are part of the National Jet Fuels Combustion Program (NJFCP). The NJFCP focus is to streamline the certification process for alternative jet fuels. Here the focus is to study the fundamental fuel kinetics and investigate the impact of alternative fuels on engine operability FOMs relative to reference fuels (Colket et al. 2016), enabling the process to be streamlined. FOMs such as cold start, altitude relight and LBO are key parameters considered in these fuels studies (Colket et al. 2016). The WSR is aimed to focus on the LBO FOM of engine operability in addition to determining the emissions footprint of the fuels in similar gas turbine combustor environments. The test fuels and their properties are shown in Table 1. These test fuels were characterized from the Combustion Rules and Tools for the Characterization of Alternative Fuels (CRATCAF) program and defined previously by OEMs (Colket et al. 2016). The category A fuels are intended to represent current jet fuels over a range of properties seen in current practice. Previous work has shown that flash point, aromatic content, and viscosity are of most impact for combustion behavior (Colket et al. 2016). A-2 and A-3 are fuels which exhibit 'average'/'worst' physical and chemical properties such as flash point, viscosity, aromatics, density, and derived cetane number respectively, giving an expectation envelope for conventional fuel combustion properties as they map to combustion behavior. C-1 and C-5 are alternative test fuels down selected by the NJFCP committee in 2015 from a total of six alternative jet fuel solvents (Colket et al. 2016). These fuel blends were selected to have properties near or exceed the limits acceptable jet fuels (i.e. viscosity, distillation curve, and chemical composition) (Colket et al. 2016). C-1 is composed of highly branched iso-paraffinic molecules with 12 and 16 carbon atoms, which have a low reactivity as exhibited by a derived cetane number of 17.1 (Colket et al. 2016). C-5 is a test fuel composed of two components, an isoparaffinic 10 carbon molecule and 1,3,5 trimethyl-benzene, which results in a flat boiling temperature/distillation curve (Colket et al. 2016). These two test fuels, C-1 and C-5, were intended to investigate effects of low cetane and narrow vaporization range of fuels on these combustor FOMs (Colket et al. 2016).

Table 1. Properties of the NJFCP Fuels Used for Testing in the WSR.

Fuel ID	A-2	A-3	C-1	C-5
POSF	10325	10289	12368	12345
Empirical Formula	$C_{11.4}H_{22.1}$	$C_{11.9}H_{22.6}$	$C_{12.6}H_{27.2}$	$C_{9.7}H_{18.7}$
AMW (g/mole)*	159	166	178	135
H/C Ratio	1.939	1.899	2.159	1.928
Stoichiometric Fuel/Air	0.0685	0.0687	0.0671	0.0686
Heat of Combustion (MJ/kg)	43.3	43	43.9	42.8
Density (g/cc)**	0.803	0.827	0.759	0.770
Derived Cetane Number (DCN)***	48.3	48.8	17.1	39.6

*Average molecular weight (AMW) measured using GCxGC
**Density measured using ASTM 4052, 15˚C (kg/L)
***DCN measured using ASTM D5890(Colket et al. 2016)

Additional fuel surrogates were studied to investigate the effects of chemical structure on combustion performance and emissions and compared against current conventional fuels and fuel solvents. The surrogate fuels were chosen from the Strategic Environmental Research and Development Program (SERDP) aimed at studying the science of emissions of alternative fuels. *n*-Dodecane was used as a base fuel, and commonly used as a second generation fuel surrogate, emulating JP-8 flame speed. This surrogate provides a better representation of the n-alkane content in jet fuels. *m*-Xylene was chosen as an additive to the base surrogate fuel to study the effects of aromatic content, and was chosen as 25% by volume to emulate the aromatic limit of JP-8. Molar carbon for the additive was kept constant to the aromatic content in the *n*-dodecane mixture, establishing a baseline for comparing surrogate performance. This fuel surrogate represents the *iso*-alkane hydrocarbon structure in jet fuels, and typically found in gas-to-liquid and FT fuels. Methylcyclohexane is used as the fuel surrogate for the cycloparaffins found in coal derived fuels. *n*-heptane is a straight chained hydrocarbon that mimics the light hydrocarbons in jet fuel and represents straight chain alkanes for a gasoline fuel surrogate. All surrogate mixtures in this paper were formulated to preserve the same carbon mole fraction as the *m*-xylene additive. Table 2 contains a list of relevant fuel properties pertaining to the WSR. Derived cetane number (DCN) for S-1, S-2, S-4, and S-5 were measured using the same ASTM standard as the NJFCP fuels. The DCN for S-3 was calculated using the summation of the volume fraction of the given fuel multiplied by its corresponding cetane number(Yanowitz et al. 2004).

Table 2. Properties of the Surrogate Fuels Used for Testing in the WSR.

Surrogate Blends	*n*-dodecane (61.8 mol%) / *m*-Xylene (38.2 mol%)	*n*-dodecane (61.8 mol %) / *iso*-Octane (38.2 mol%)	*n*-dodecane	*n*-dodecane (58.6 mol%) / Methyl-cyclohexane (41.4 mol%)	*n*-dodecane (58.6 mol%) / *n*-heptane (41.4 mol%)
Fuel ID	S-1	S-2	S-3	S-4	S-5
Empirical Formula	$C_{10.47}H_{19.9}$	$C_{10.49}H_{22.98}$	$C_{12}H_{26}$	$C_{9.93}H_{21.03}$	$C_{9.93}H_{21.86}$
H/C Ratio	1.900	2.191	2.167	2.118	2.201
Stoichiometric Fuel/air	0.0687	0.0669	0.0670	0.0673	0.0668
MW	145.84	149.12	170.31	140.45	141.28
Density (g/cc)	0.778	0.737	0.750	0.758	0.734
Derived Cetane* Number (DCN)	57.47	60.91	78.5	54.05	67.46

*DCN for S-1, S-2, S-4, S-5 measured using ASTM D5890(Colket et al. 2016)

C. Emissions and Instrumentation

A bare, linear-tracking, custom, type-B thermocouple (0.2mm diameter, platinum – 6% rhodium, platinum – 30% rhodium) without coating was used to measure reactor temperature. Measurements for temperature were taken at 0.25" from the outer wall of the reactor and were not corrected for radiation and other heat losses. Therefore, the gas temperature readings may not be accurate in an absolute sense, yielding lower temperatures than expected, but enable relative comparisons between conditions. The thermocouple location is within the uniform temperature region in the WSR and the temperature can therefore be taken as the average temperature in the reactor. A 0–5 psia pressure transducer was used to monitor the slight pressure increase in the reactor during operation. A maximum pressure of 5.5 kPa above ambient conditions was experienced during testing.

Exhaust samples were extracted using an oil-cooled probe (420 K) through a 1.4-mm-diameter orifice. The samples were passed through the probe which quenches the reactions, similar to quenching in a typical combustor (D. Blunck et al. 2012). The probe rested 5 mm above the wall of the lower toroid and is 90 degrees around the axis of the toroid from the thermocouple. Temperatures of the oil were kept constant at 420 K while sampling to minimize condensation in the sampling line.

Gaseous emissions were transported through a heated line containing a pump, filter and oven before entering the Fourier Transform Infrared (FTIR) analyzer. The heated lines and oven were maintained at 420 K by PID controllers. Flow entered and exited the FTIR at a constant temperature of 463 K where it was exhausted or sampled via charcoal tubes and gas bags. A sketch of the sampling methodology is shown in Fig. 3.

The FTIR system utilized in the current work was a MKS 2030 High Speed (5Hz) gas analyzer with a gas cell path length of 5.11 m and was used to measure the emissions from the WSR. This FTIR system allows major gaseous species to be detected online, while saving the spectra for later detailed investigation. The Gasoline Ethanol method, within the MKS software package, was employed to analyze the IR spectra and calculate emission concentration values. Measurement accuracy using this FTIR is +/- 2%. Carbon monoxide (CO), carbon dioxide (CO_2), water (H_2O), nitrogen oxide (NO), nitrogen dioxide (NO2), acetylene (C_2H_2), ethylene (C_2H_4), and formaldehyde (CH_2O) are among the many emissions that absorb infrared radiation and can be quantified using the method employed in the FTIR.

Following the FTIR was a valve to capture bag samples and enable offline measurement of C1–C12 species, primarily for C1–C4 hydrocarbons. An Agilent 6890/5973 GC-FID-MS (Gas Chromatography-Flame Ionization Detector-Mass Spectrometry) and Gas Pro Column was utilized to analyze emissions from the extracted samples. Capturing exhaust emissions through charcoal tubes was also employed as a sampling technique to obtain heavy hydrocarbon species, generally above C4 species.

Another valve following the FTIR was used to draw these samples. A pump drew 1-liter exhaust emission samples at a rate of 1 liter per minute. Remaining gases pulled through the pump were exhausted through the hood where the WSR operates. Previous work has been performed using this method to extract hydrocarbons from jet-fuel emissions (Anneken et al. 2014). The tube was later extracted with carbon disulfide and the mass of each component was measured using an Agilent 7890 GC-FID and Gas Pro Column.

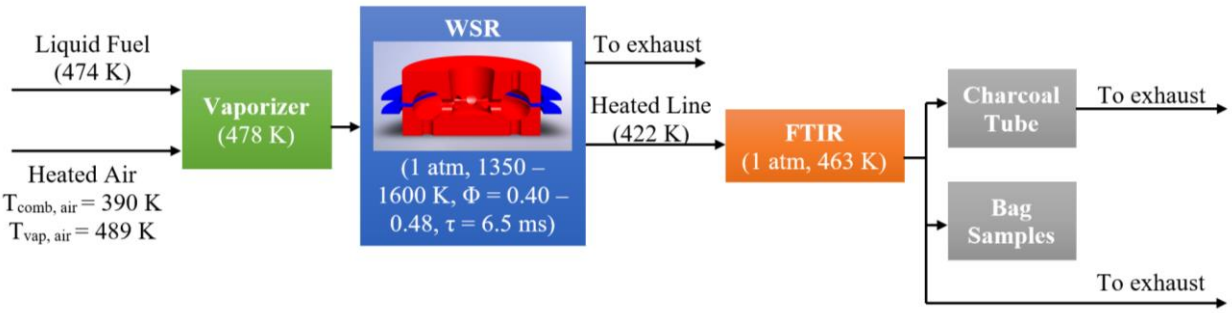

Figure 2. Experimental Schematic for WSR Emission Studies. A heated line takes the sample from the reaction region in the WSR to the FTIR. Charcoal tube and bag samples are taken after the FTIR before being exhausted.

During testing, online concentration measurements of various species were made using an FTIR. Roughly 95% of the carbon containing species were recovered by the FTIR at the higher equivalence ratios, reducing to roughly 92% near LBO as shown in Figure 3. The ~5% carbon deficit can be attributed primarily to FTIR measurement uncertainties. In addition, insufficient quenching during extractive sampling from the WSR can contribute to the uncertainty as sampled could react in the sampling lines and measurements are not representative of the actual combusting environment. The high percent of carbon recovered provides confidence as to the quantitative fidelity of species measured and the relative species concentration between fuels.

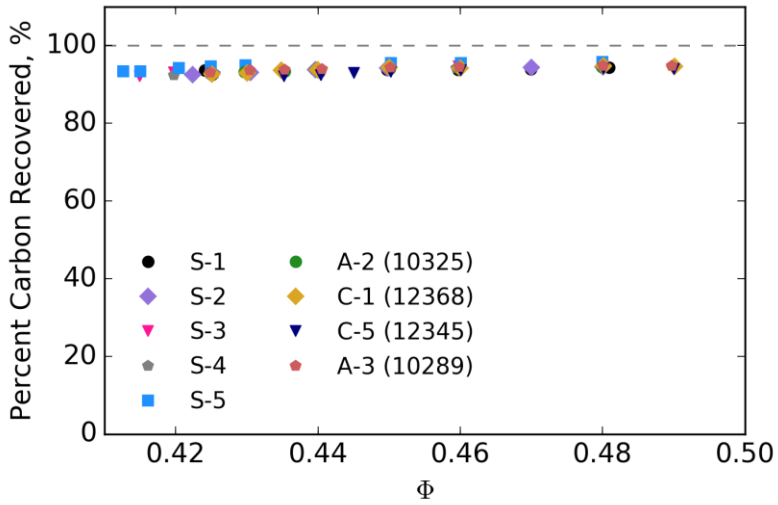

Figure 3. Carbon recovery from the species captured via online FTIR sampling. A decrease in percent carbon recovered is seen as equivalence ratio (Φ) is decreased. This signifies that intermediate species are produced and some are not recovered using this emissions measurement technique. The high percentage of carbon recovered provides confidence that this method captures emissions adequately to yield quantitative results.

II. Experimental Conditions

The equivalence ratio was set by varying fuel flow rate. Each LBO measurement was initiated at an equivalence ratio of >0.48 where formaldehyde levels dropped below the detection limit (≈0 ppm). Equivalence ratios were reduced by keeping air constant and decreasing fuel flow until LBO where the flame extinguished. Heat loss at LBO conditions becomes too large and combustion is unstable and is not sustained. A drop in reactor temperature and change in noise generated by the reactor corresponded to a LBO(Scott Stouffer et al. 2007).

Temperatures at these conditions were well below the maximum operating temperature of the ceramic. This enabled durability for testing with a single build of the reactor and prevented cracking. Premixed fuel and air coming into the jet ring was held at a constant temperature of 460 K, which is in the typical combustor range of 200–900 K (McAllister, Chen, and Fernandez-Pello 2011; Colket et al. 2016). Reactor temperatures during the test varied between 1350 K and 1500 K based on the heat of combustion of each fuel and heat loss from the system. The heat loss from the system was estimated at 5% using the ceramic reactor (J. Blust, Ballal, and Sturgess 1997). The health of the ceramic reactor was monitored by measuring the temperature of the jet ring. When a cracked formed, a large asymmetric temperature profile was observed in the jet ring. Towards leaner conditions, the jet ring temperature profile varied a maximum of approximately 2% (10 K) peak-to-peak, indicating the ceramic reactor remained free from cracks.

Global reacting residence time for the experiments was 6-7 ms. Bulk residence time was calculated using the volume of the reactor, the flow rates of the fuel and air, and the density of the mixture under reacting conditions. Variations in residence time were primarily a result of changes in reactor temperature and fuel mass flow since change in reactor pressure and molecular weight are small(Scott Stouffer et al. 2007). At most points throughout each experiment, the reactor was allowed to reach a thermal steady state and then held at constant flow and thermal conditions for more than 12 minutes. Non-emission data was captured from a running average of approximately 12 seconds every 3 minutes.

FTIR measurements, recorded continuously at 5 Hz, were averaged over the 12 second running average period for each sample, while gas bags and charcoal tubes were taken at the last point of the sampling process for each equivalence ratio. This holistic sampling process captured major and minor species throughout the duration of the experiment, while ensuring steady state conditions for the bag and charcoal tube samples.

For points at or near LBO, the reactor could not be held constant for 12 minutes because of the tendency to blow off. At these near-LBO conditions, a non-steady-state condition between the wall and gas temperatures may be responsible for some scatter in the WSR temperature data. Once blow off occurred, the reactor was re-ignited by reducing air and fuel flow rates. Once steady state conditions were reached at the start of the blow off test, a second test was conducted in a similar fashion. As experienced in previous experiments, hysteresis does exist in approaching LBO if there is insufficient time for the reactor to reach a steady-state temperature at each condition. Leaner conditions can be reached if the reactor walls are relatively hot, resulting from a rapid decrease in equivalence ratio. If LBO is approached more slowly, the walls have sufficient time to cool to the local gas temperature and, therefore, LBO is experienced at higher equivalence ratios(Vijlee 2014). Increments were small while decreasing the fuel flow, thus reducing the chance for hysteresis. Previous literature showed variance in blow off temperature of +/- 50 K(Vijlee 2014) and uncertainty of blow off equivalence ratio near 2% (D. L. Blunck et al. 2015). Based on the sonic nozzle calibration and the self-consistency between the two or more LBO tests per fuel, the uncertainty in equivalence ratio was estimated as Φ +/- ~0.0025. The primary parameter controlling the uncertainty was the repeatability of the air mass flow controllers based on the operating conditions.

Table 3. Operating conditions using the WSR

Pressure (atm)	**1**
Inlet Temperature (K)	460
Reactor Temperature (K)	1350 – 1600
Bulk Residence Time (ms)	6 – 7
Mass Flow Air (g/min)	600
Equivalence Ratio	0.425 – 0.49

III. Results and Discussion

D. LBO

LBO occurs when the flame cannot be sustained because of either fluid dynamic or chemical processes. In the WSR, LBO is most sensitive to chemical processes associated with heat release, and ideally insensitive to mixing and fluid processes. Experimental results are shown in the figures below for the four NJFCP fuels and the five surrogate mixtures. Figure 4 shows the effect of lowering the fuel flow, hence lowering the equivalence ratio. The reactor trends to decrease linearly with leaner conditions. C-1 shows to have the least resistance to LBO, having the highest Φ at LBO, while the S-3 and S-5 straight chained alkane surrogates trended to have the most resistance to LBO. LBO occurs at the lowest recorded equivalence ratio of roughly 0.414, In contrast, the C-1 fuel exhibits LBO at the highest recorded equivalence ratio.

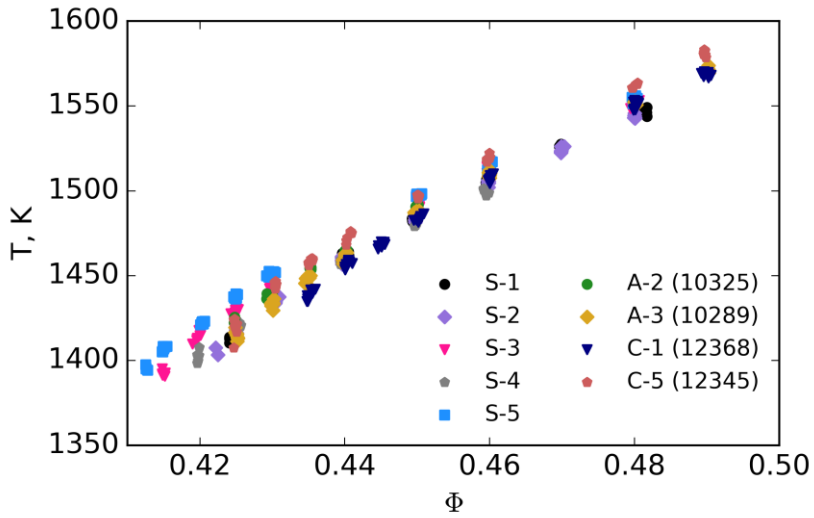

Figure 4. Reactor temperature (K) as a function of Φ for the fuels. Points represent the samples taken at each equivalence ratio tested. As leaner conditions are approached, the reactor temperature lowers linearly to the point where combustion cannot be sustained, corresponding to LBO. C-1 has the least resistance to LBO, having the highest Φ at LBO, while S-3 and S-5, straight chain alkane blends, trended to have the most resistance to LBO.

Since the WSR is operating in a lean, premixed, prevaporized combustion environment, the combustion property targets (CPTs) can be investigated as it relates to LBO. These CPTs, H/C ratio, MW, Threshold Sooting Index (TSI), and derived cetane number (DCN), have shown to sufficiently match combustion behaviors in pre-vaporized environments for petroleum-derived and synthetic jet fuels(Won, Veloo, Santner, Ju, Dryer, et al., n.d.). H/C ratio is used as it relates energy density of a particular fuel, as well as describes the composition and the distribution of radicals produced form combustion processes.(Won, Veloo, Santner, Ju, Dryer, et al., n.d.) LBO is shown below in Figure 7 as a function of H/C ratio. For each fuel, the last sampled condition immediately preceding LBO was averaged for both runs. If LBO occurred during sampling, the mean LBO was calculated using the average of those samples with the previous full sample preceding LBO. The uncertainty bars represent the uncertainty based on the air and mass flow rates. Towards the left of Fig. 5, mean LBO was nearly identical at ~0.425. This is a result of the roughly 0.005 (~1%) step size in equivalence ratio, used to obtain stable points for emissions capture near LBO. The mean Φ represents roughly the last point captured for emissions data before blow off occurs. However, based on the given fuels and their LBO conditions, there exists a distribution of fuels which lie outside the bounds of the uncertainty estimated and are statistically significant. Based on the current distribution of data, there doesn't exist a correlation of LBO for the given fuels with varying H/C ratios. Molecular weight was also plotted as a function of Φ for the fuels. This property corresponds to the reactivity of the fuel via the normal and branched alkanes in the fuel and also does not trend to correlate, shown in Figure 6.

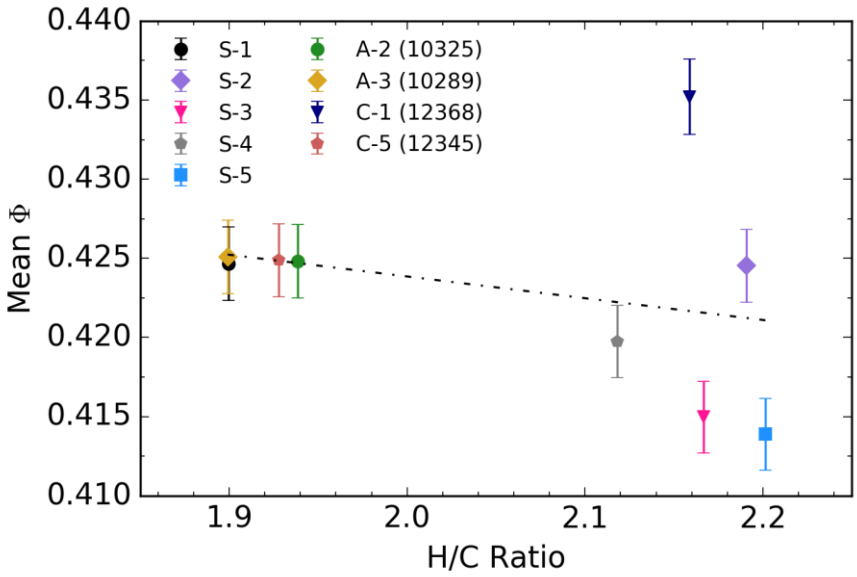

Figure 5. Mean Φ as a function of H/C Ratio. Points represent the average of the data at each equivalence ratio, while the error bars represent the uncertainty of the measured and averaged Φ. (Eq. -0.01374x+0.45134 = y, R^2 = 0.0849).

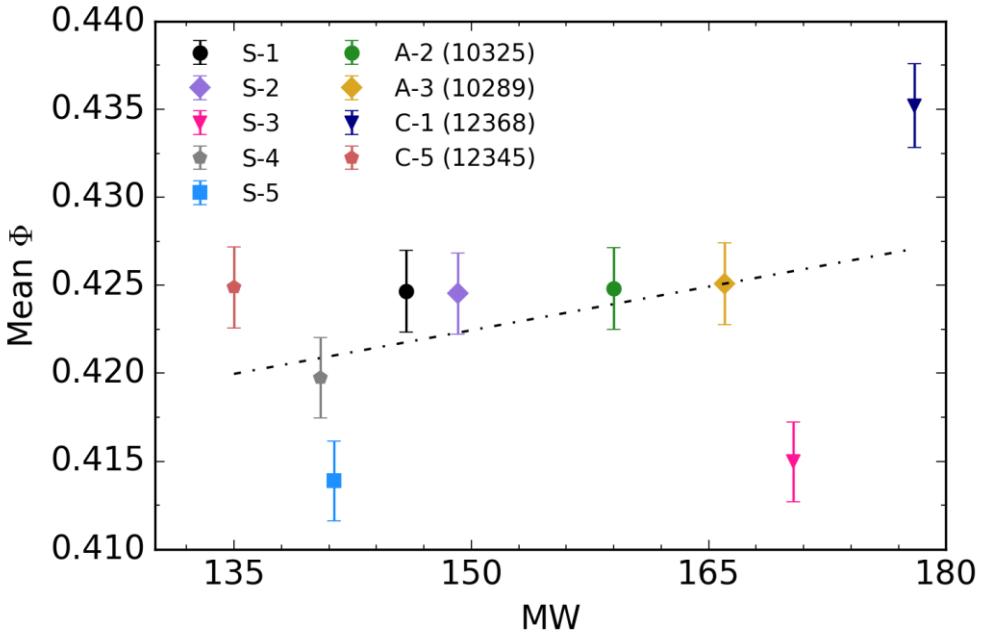

Figure 6. Mean Φ as a function of molecular weight. Points represent the average of the data at each equivalence ratio, while the error bars represent the uncertainty of the measured and averaged Φ. (Eq. 1.652E-04x+0.0.3977 = y, R^2 = 0.1527).

TSI, another CPT, correlates the competition of aromatic molecules and highly-branched alkanes with the radical pool and is important as it describes the sooting tendency of a fuel(Won, Veloo, Santner, Ju, Dryer, et al., n.d.). This correlation of reactivity of a fuel varies inversely with TSI, using this methodology(Won, Veloo, Santner, Ju, Dryer, et al., n.d.). Values were

estimated for the given surrogate fuels using linear combination of each mole percent of components by their corresponding TSI.(Mensch 2009) Based on Fig. 9 below, there doesn't exist to show a correlation among the TSI and LBO. Although there is no apparent correlation, the effect of aromatic content in S-1 shows to have an effect on increasing the TSI, where further investigation on determining the TSI of the conventional and alternative fuels would be useful.

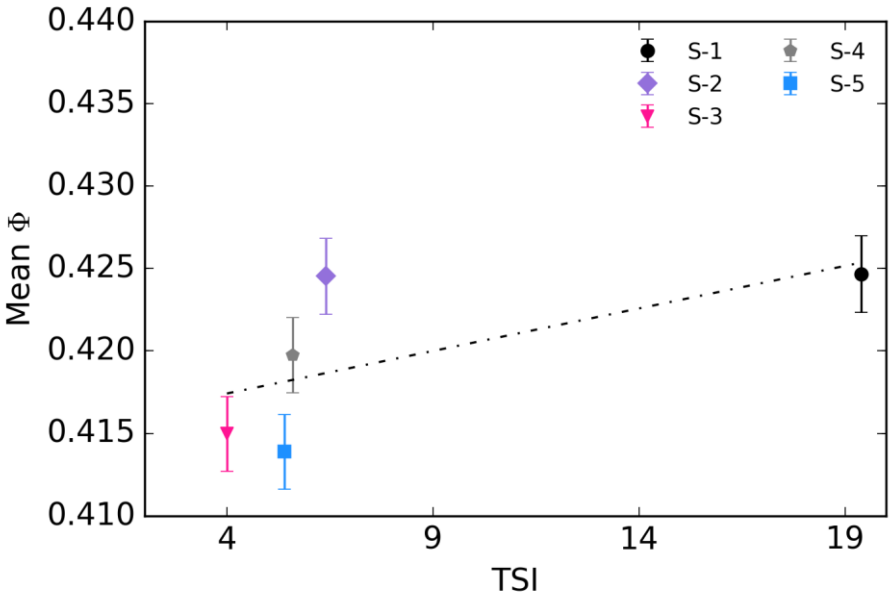

Figure 7. Mean Φ as a function of TSI. Points represent the average of the data at each equivalence ratio, while the error bars represent the uncertainty of the measured and averaged Φ. (Eq. 5.158E-04x+0.41536= y, R^2 = 0.41134).

Figures 8 and 9 display the effects of LBO with DCN and radical index, respectively. Based on the given data set and Fig. 8 below, there appears to be a functional dependence on cetane number of the fuel when comparing to LBO. Low derived cetane numbers correspond to a longer ignition delay, which is a potential attribute to the LBO difference seen in the given fuels set. This trend can yield understand towards this parameter and potential implications in gas turbine combustors. Also, the tested data only contains two emissions profiles per fuel, yielding some additional uncertainty.

Radical indices were approximated from literature (Won, Veloo, Santner, Ju, and Dryer, n.d.; Won, Dooley, et al., n.d.). S-1 and S-2 were estimated using the radical indices of the surrogate mixture components multiplied by the corresponding mole percentage. The radical index for *m*-xylene was approximated between toluene and 135TMB assuming a linear correlation(Won, Dooley, et al., n.d.). S-3 and S-5 mixture was approximated at 1, being of n-paraffinic structure, where A-2 and C-1 were assumed to be similar to JP-8 and IPK, respectively(Won, Veloo, Santner, Ju, and Dryer, n.d.). A-3 was assumed to be of JP8(Won, Veloo, Santner, Ju, and Dryer, n.d.), even though A-3 contains more iso-paraffins. The radical indices for *iso*-octane and JP8 were near identical and used as a rough estimate to investigate potential correlations of LBO with radical index. A radical index for m-xylene was approximated between the values of toluene and 135TMB, assuming a linear relationship between the values. These preliminary approximations show a correlation with LBO as seen in Fig. 8. The higher radical index indicates a larger radical pool in which the radicals aid in sustaining combustion, tending to blow out at leaner conditions. Towards the left portion of Fig. 6, C-1 trends to blow out at a higher equivalence ratio, where it has the lowest assumed radical index. Behavior experienced in Figure 8 and 9 show a similar trend with LBO and indicate dependence on DCN and on radical index. This knowledge, along with the ability to create surrogates to vary one of the characteristics (DCN or RI), can assist in further understanding the extinction and LBO behavior of a given fuel.

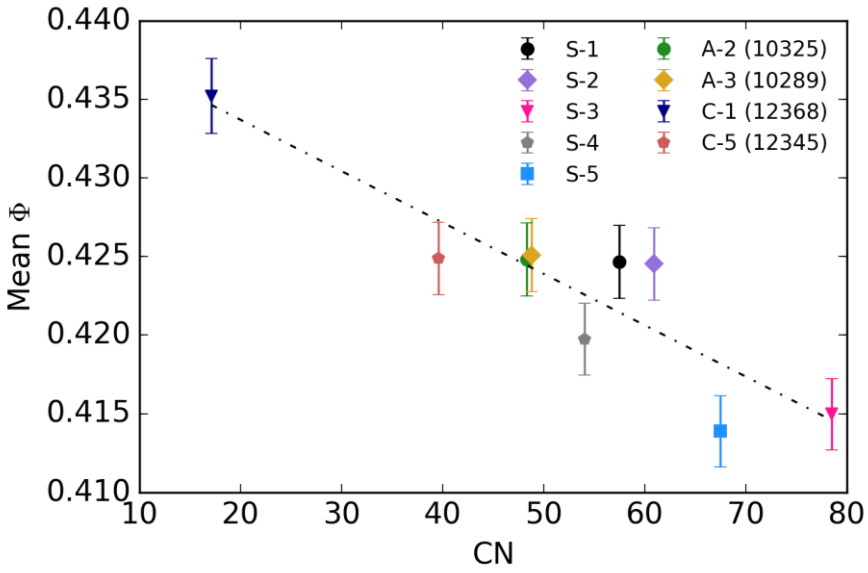

Figure 8. Mean Φ as a function of DCN. Points represent the average of the data at each equivalence ratio, while the error bars represent the uncertainty of the measured and averaged Φ. (Eq. -3.268E-4x+0.44023 = y, R^2 = 0.8097). Percent Difference in Φ from S-5 to C-1 is ~5%.

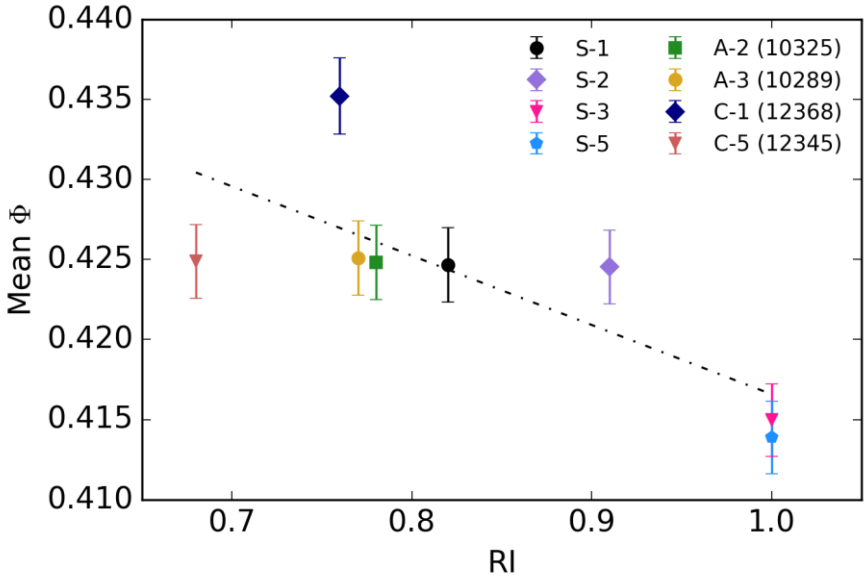

Figure 9. Mean Φ as a function of Radical Index. Points represent the average of the data at each equivalence ratio, while the error bars represent the uncertainty of the measured and averaged Φ. (Eq. -0.04328x+0.4599= y, R^2 = 0.585)

E. Emissions Profile

As described in the previous section, the fuel chemistry can play an important role in LBO. For instance, surrogate fuels may have a similar heat of combustion and derived cetane number, S-1 and S-2, but different radical index, 0.82 and 0.91 respectively. This difference in radical index can be caused by the presence of radical-promoting reactions and/or radical-trapping reactions that occur as a result of the fuel chemistry, in this case aromatic or iso-alkane content. The WSR is specifically designed to provide relevant information on the effects of fuel chemistry on combustion emissions and stability

under conditions similar to those in typical combustors, specifically the primary and secondary zones. This approach enables fuel-specific emissions fingerprints to be generated while approaching LBO. The species produced under these conditions are highly sensitive to the specific fuel chemistry and, therefore, provide a sensitive metric for developing reduced-order chemical mechanisms. These emissions profiles can also be utilized along with the DCN, radical index, H/C ratio, MW, and TSI to determine the chemical property dependencies driving LBO in various experimental arrangements.

Figure 10 shows the major carbon-containing combustion products, as a function of equivalence ratio, produced during testing of the WSR. CO and CO_2 compose approximately 99.9% and 99% of the total carbon count in the sampled emissions at the areas of higher equivalence ratios and towards the leanest conditions, respectively. As the fuel rate decreases to leaner conditions, less CO_2 is produced allowing for intermediate species to be formed as a result of incomplete combustion and thus incomplete conversion to CO_2. As observed in Figure 10(a), CO_2 produced from the C-1 fuel and the S-2 surrogate mixture are similar yet follow a distinctly different curve towards LBO relative to the other fuels, although C-1 LBO occurs at a higher equivalence ratio. In contrast, CO is increased as LBO is approached for all fuels. The two bounding fuels are S-5 which produced the most CO_2 and least CO and C-1 which produced the least CO_2 and most CO for a given equivalence ratio.

Although the carbon deficit in the CO_2 production between C-1 and S-5 was primarily recovered in the form of CO, the total carbon count for the six largest carbon containing species is shown in Figure 11. It is clear that at $\Phi = 0.435$, C-1 produces an order of magnitude more formaldehyde than any other fuel, in addition to increased concentrations of ethylene, acetylene, methane, and isobutene.

Formaldehyde production as a function of equivalence ratio is displayed in Figure 12 for all fuels. This species is particularly important as it is a key intermediate species in the oxidation of hydrocarbons and can significantly shorten the ignition delay time of fuel/air mixtures. Specifically, previous work has shown that many hydrocarbon species can be linearly related to formaldehyde production, regardless of fuel type(D. L. Blunck et al. 2015), although C-1 tends to be the outlier. Methane recorded from the FTIR is seen to exhibit that linear relationship as a function of formaldehyde, as observed in the same figure. For this reason, species production in all subsequent figures are plotted against both equivalence ratio and formaldehyde.

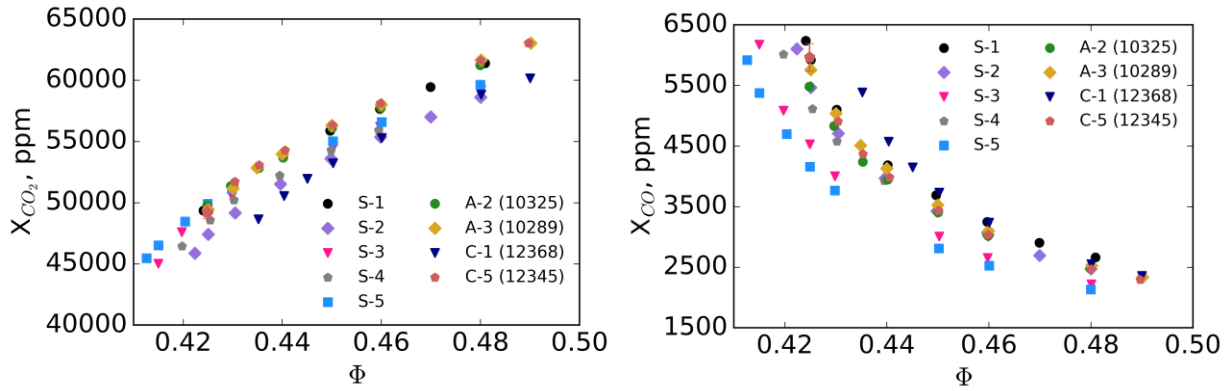

(a) (b)

Figure 10. CO_2 (a) and CO (b) as a function of equivalence ratio (Φ). Points represent the average of the data at each equivalence ratio, while the error bars represent one standard deviation. Trends in decreasing CO_2 and increasing CO while approaching leaner conditions is expected, signifying losses in combustion efficiency towards LBO.

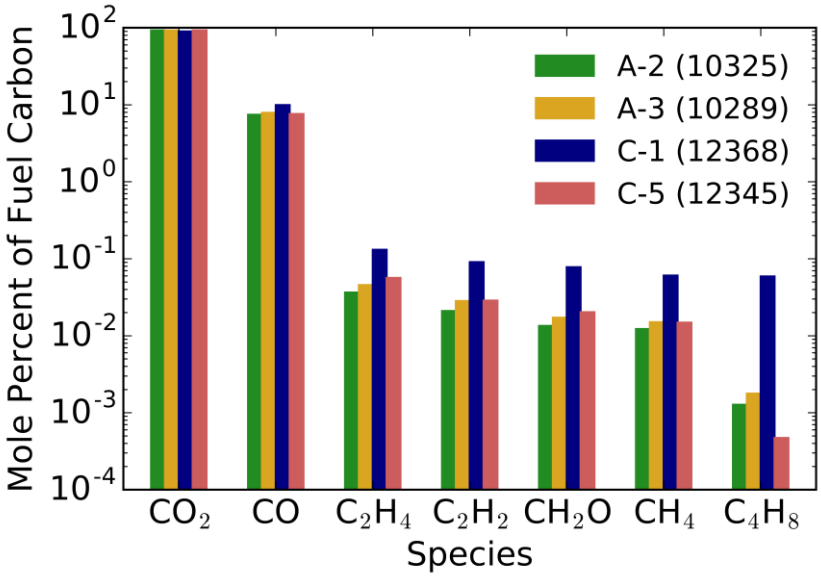

Figure 11. Mole percent of fuel carbon on the given species at Φ = 0.435. C-1 appears to be most distinguished, as it is at the leanest condition before LBO, producing more intermediate species.

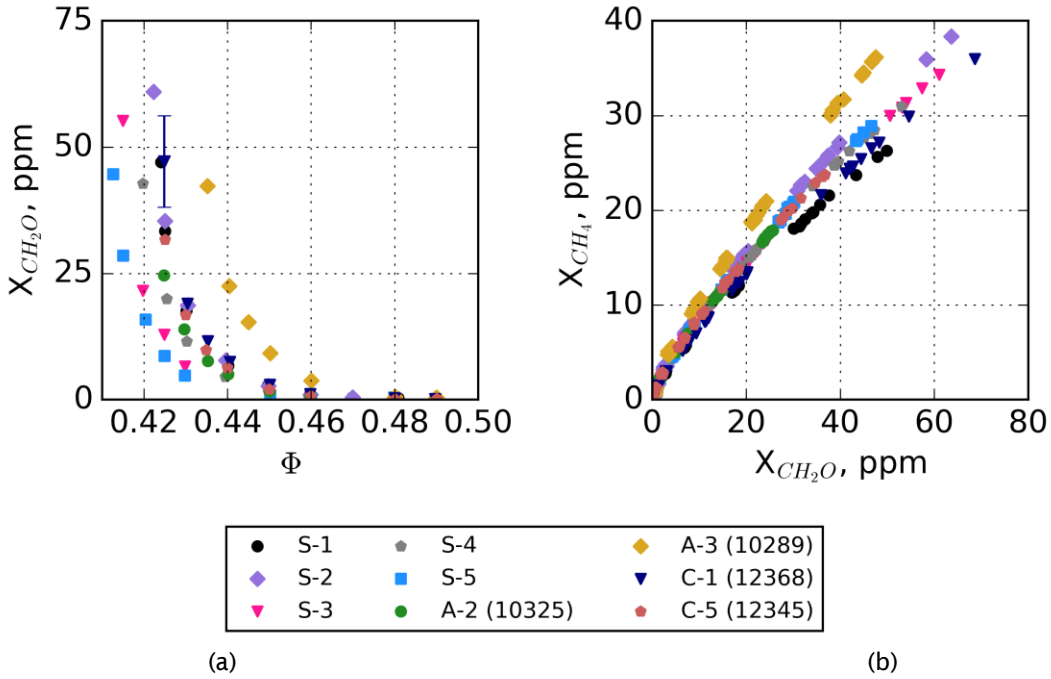

Figure 12. Formaldehyde (CH_2O) as a function of equivalence ratio (Φ) and methane (CH_4) as a function of formaldhyde production. Points represent the average of the data at each equivalence ratio, while the error bars represent the maximum standard deviation in the reported set.

Figure 13 and 14 displays ethylene and acetylene production towards lean low off conditions using the online FTIR method, respectively. Figures 17 and 18 show the isobutene production using both the FTIR and charcoal tube methodologies of capturing emissions.

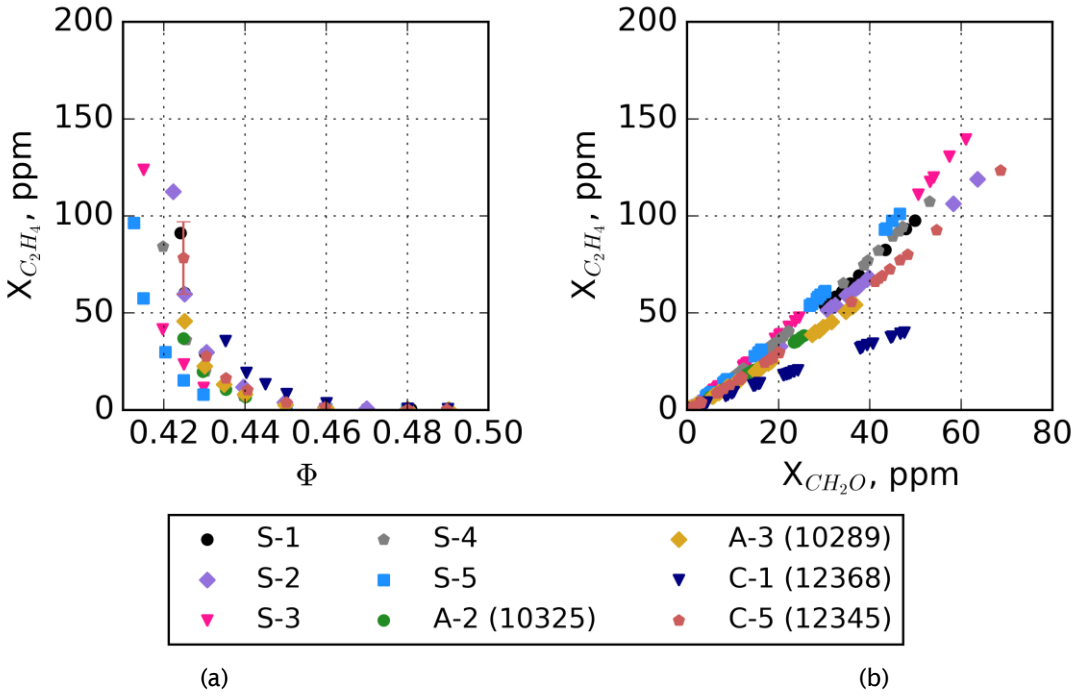

Figure 13. Ethylene (C_2H_4) as a function of equivalence ratio (Φ) sampled from the FTIR. (a) Points represent the average of the data at each equivalence ratio, while the error bars represent the maximum standard deviation in the reported set. (b) Points represent the all the sampled data as a function of formaldehyde.

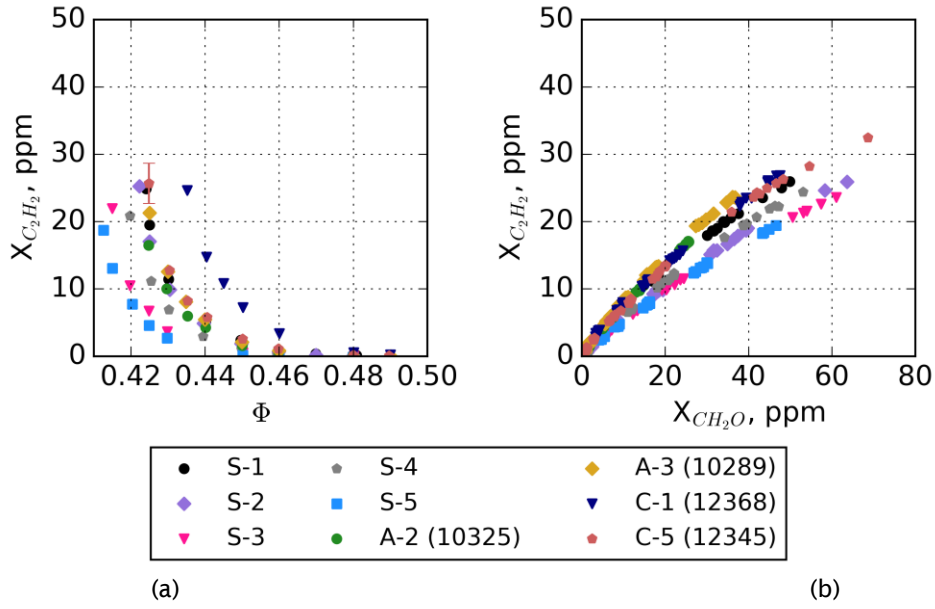

Figure 14. Acetylene (C_2H_2) as a function of equivalence ratio (Φ) sampled from the FTIR. (a) Points represent the average of the data at each equivalence ratio, while the error bars represent the maximum standard deviation in the reported set. (b) Points represent the all the sampled data as a function of formaldehyde.

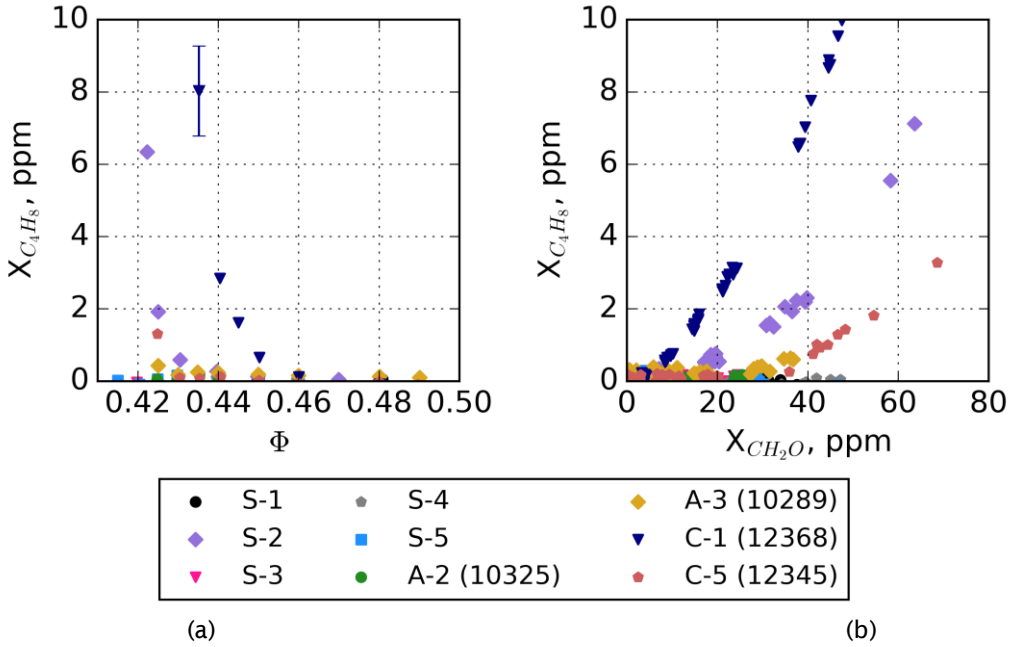

Figure 15. Isobutene (C_4H_8) as a function of equivalence ratio (Φ) sampled from the FTIR. (a) Points represent the average of the data at each equivalence ratio, while the error bars represent the maximum standard deviation in the reported set. (b) Points represent the all the sampled data as a function of formaldehyde.

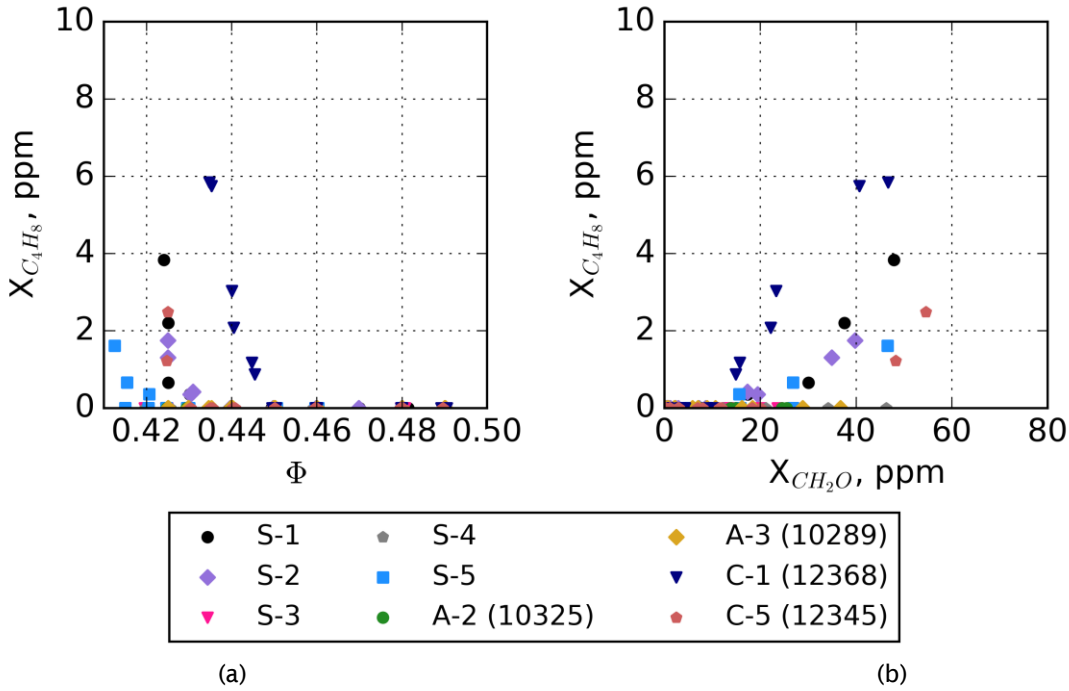

Figure 16. Isobutene (C_4H_8) as a function of equivalence ratio (Φ) from the charcoal tube methodology. (a) Points and samples taken during testing at the end of each condition as a function of equivalence ratio. (b) Points and samples taken during testing at the end of each condition as a function of formaldehyde.

Additional efforts were made with the Well-Stirred Reactor to refine the LBO measurements. The previous procedure towards LBO provided the ability to obtain steady state emissions measurements within the WSR approaching LBO. A new technique was integrated into the data acquisition system to decrease the fuel flow rate automatically, keeping the air flow rate constant, as in previous experiments. This procedure allows for multiple LBO measurements to be made within a single test run per fuel. The fuels tested with this new approach were selected to stress-test the DCN hypothesis.

Table 4: Fuels tested in the WSR using the new LBO procedure (*S-1 from Won, et. al. 2017).

Name	DCN	Nomenclature
Dodecane (n-C12)	74	C_{12}
Surrogate Fuel 1*	50.4	S-1
NJFCP A-2	48.3	A-2
NJFCP C-4	28	C-4
75.5% 135 TMB, 24.5% n-C12	19.08	J-1
NJFCP C-1	17.1	C-1

Dodecane was selected on the upper bound of the DCN that was tested, where C-1 was the lower bound to the DCN. Additional fuels tested as part of the NJFCP program include A-2 and C-4. A surrogate fuel to emulate the characteristics of

NJFCP A-2 and given combustion property targets was additionally selected, named S-1 (Won, et. al., 2017). An additional fuel, J-1, comprised of 1,3,5 trimethylbenzene (135 TMB) and dodecane, was added to investigate the effect of radical index at a lower DCN to investigate radical pooling effects towards extinction, as previously discussed. Number of ramp rates performed with LBO testing was 13 for the fuels except Dodecane (5 samples for Dodecane). A lean equivalence ratio usually around 0.45, above the extinction limit, was established before decreasing the equivalence ratio 0.001 (~0.05 mL/min using the Isco pumps for the fuel) every 4 seconds. This ramp rate was chosen to reduce wall effects on LBO that are around the outer surface of the reactor and to establish a steady decrease in reactor temperature as minimizing transient effects are optimal. LBO is reached when there exists a significant temperature drop from the previous value. The tradeoff with this approach is that emissions sampling was reduced to only the FTIR online sampling, as the duration of capturing the emissions using the gas bags and charcoal tube measurements takes longer than the ramp rate utilized in the experiment. Data acquisition from the 5Hz online MKS 2030 HS gas analyzer was averaged and matched to the time histories of the other experimental data captured (0.5 Hz). The gas analyzer was the same as previously used in the other experiments.

LBO and emissions towards LBO are presented in the figures below. Fig. 17 shows the linear correlation between the LBO and DCN of the corresponding fuels. Error bars on the figure represent the standard deviation of the LBO J-1 and C-1 both yield similar LBO values, although the chemical compositions are vastly different, and their radical index is different. High percentages of aromatics as seen in the J-1 fuel also decreases the resistance to LBO, whereas the C-1 fuel is comprised of the iso-paraffinic compounds. S-1 and A-2 have been observed to have similar LBO values, as expected. Dodecane is also seen to have the lowest LBO value and having the highest DCN value. Emissions profiles for ethylene and isobutene are plotted as functions of equivalence ratio and formaldehyde. An exponential increase in emissions is seen similarly to the other experiment performed in the WSR. As leaner conditions are approached towards LBO, there is a reduction in combustion efficiency, where incomplete reactions are occurring, not converting the fuel to the CO2 and H2O and is seen in the figures. S-1 emissions trends yield similarity to A-2, further establishing similarity between a surrogate fuel mixture comprised of 3 compounds to a jet-fuel comprised of multiple components. Emissions as a function of formaldehyde has been presented as formaldehyde is a marker for the incomplete combustion and for other pollutant emissions to be generated. Non-linearity is presented towards higher amounts of formaldehyde production and shows the instability towards the extinction process.

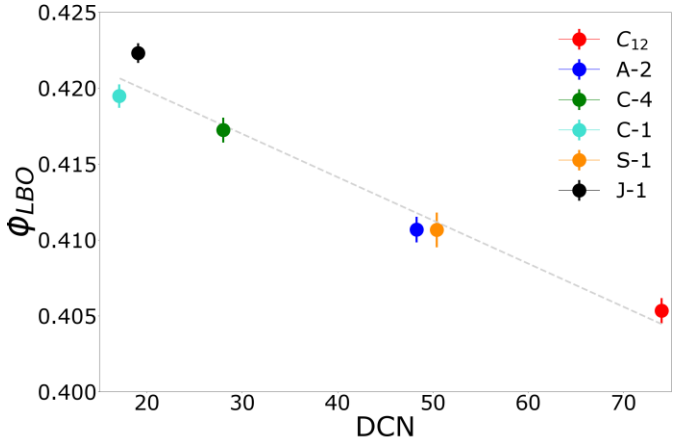

Figure 17: LBO as a function of DCN. The R^2 value based off a linear fit is 0.9581 (-2.8466E-04*DCN + 0.42552 = ϕ_{LBO}).

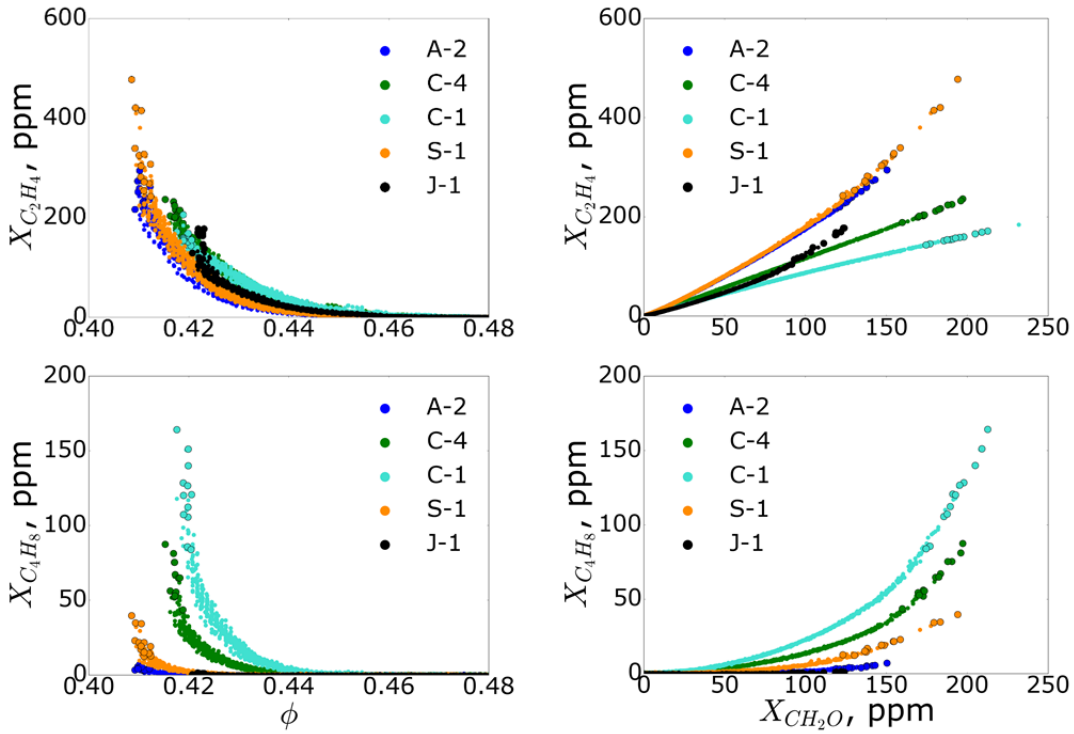

Figure 18: Emissions v. ϕ_{LBO} for the WSR. (R side) Emissions v. CH_2O for the WSR. A-2 and S-1 data trends similarly with each other.

IV. Conclusions

A WSR operating under fuel-lean conditions was utilized to measure performance and gaseous emissions characteristics of conventional and alternative aviation fuels. LBO was also explored under the same loading condition to determine the difference in LBO with different fuels. The experiment showed:

1. Recovery of carbon captured is favorable from the FTIR and can provide encouraging results with the current species captured.
2. The C-1 test fuel is least resistant to LBO as the conditions for which it occurs happens at a higher equivalence ratio and at a higher reactor temperature than the other tested fuels.
3. LBO shows a strong correlation with derived cetane number, which describes a need for investigating fuel dependency on combustor design.
4. As conditions approach LBO, intermediate species are produced that have a correlation between formaldehyde productions. These conditions towards LBO signify decreased combustion efficiency as more intermediate species are seen.
5. S-1 yielded similar performance characteristics in the WSR as A-2.

Continued analysis will enable investigation of chemical kinetic pathways specific to each fuel, which then establishes an understanding of the chemical effects in a lean, premixed, prevaporized environment, a relevant area of interest for future gas turbine combustor design. The WSR represents an ideal, premixed, pre-vaporized combustor. It is used to study fuel chemistry effects on emissions and LBO. Thus, we believe the knowledge gained from the fuel effects in our LBO and emissions studies have relevance to current and future combustion systems.

References

AJF-IWG. 2016. "Federal Alternative Jet Fuels Research and Development Strategy." OSTP.

Anneken, David, Richard Striebich, Matthew J. DeWitt, Christopher Klingshirn, and Edwin Corporan. 2014. "Development of Methodologies for Identification and Quantification of Hazardous Air Pollutants from Turbine Engine Emissions." Journal of the Air & Waste Management Association 65 (3): 336–46. doi:10.1080/10962247.2014.991855.

Blunck, D, J Cain, Rc Striebich, Sz Vijlee, Sd Stouffer, and Wm Roquemore. 2012. "Fuel-Rich Combustion Products from a Well-Stirred Reactor Operated Using Traditional and Alternative Fuels." Central States Combustion Meeting, 1–8.

Blunck, David L., Steven Zeppieri, Justin T. Gross, Scott Stouffer, and Meredith B. Colket. 2015. "Hydrocarbon Emissions from a WSR Near Lean Blow-Off." In 53rd AIAA Aerospace Sciences Meeting, 1–12. Kissimmee, FL: American Institute of Aeronautics and Astronautics. doi:10.2514/6.2015-0415.

Blust, J., D. Ballal, and G. Sturgess. 1997. "Emissions Characteristics of Liquid Hydrocarbons in a Well Stirred Reactor." In 33rd AIAA/ASME/SAE/ASEE Joint Propulsion Conference & Exhibit, 1–18. Seattle, WA: AIAA. doi:10.2514/6.1997-2710.

Blust, J. W., D R Ballal, and G J Sturgess. 1999. "Fuel Effects on Lean Blowout and Emissions from a Well-Stirred Reactor." Journal of Propulsion and Power 15 (2): 216–23. doi:10.2514/2.5444.

Briones, AM, B Sekar, J Zelina, R Pawlik, and SD Stouffer. 2008. "Numerical Modeling of Combustion Performance for a Well-Stirred Reactor for Aviation Hydrocarbon Fuels (AIAA-2008-4565)." In 44th AIAA/ASME/SAE/ASEE Joint Propulsion Conference & Exhibit, 1–19. Hartford, CT: AIAA. doi:doi:10.2514/6.2008-4565.

Colket, Meredith B., Joshua S. Heyne, Mark Rumizen, James T. Edwards, Mohan Gupta, William M. Roquemore, Jeffrey P. Moder, Julian M. Tishkoff, and Chiping Li. 2016. "An Overview of the National Jet Fuels Combustion Program." In AIAA SciTech. AIAA SciTech. San Diego, CA: American Institute of Aeronautics and Astronautics. doi:doi:10.2514/6.2016-0177.

FAA. 2012. "U.S. Aviation Greenhouse Gas Emissions Reduction Plan," no. June: 1–16.

Karalus, Megan. 2013. "An Investigation of Lean Blowout of Gaseous Fuel Alternatives to Natural Gas." University of Washington.

Manzello, Samuel L., David B. Lenhert, Ahmet Yozgatligil, Michael T. Donovan, George W. Mulholland, Michael R. Zachariah, and Wing Tsang. 2007. "Soot Particle Size Distributions in a Well-Stirred Reactor/plug Flow Reactor." Proceedings of the Combustion Institute 31 (1): 675–83. doi:10.1016/j.proci.2006.07.013.

McAllister, Sara, Jyh-Yuan Chen, and A. Carlos Fernandez-Pello. 2011. Fundamentals of Combustion Processes. Mechanical Engineering Series. New York, NY: Springer New York. doi:10.1007/978-1-4419-7943-8.

Mensch, Amy. 2009. "A Study on the Sooting Tendency of Jet Fuel Surrogates Using the Threshold Soot Index." M.S. Thesis. The Pennsylvania State University.

Nenniger, J.E., A. Kridiotis, J. Chomiak, J.P. Longwell, and A.F. Sarofim. 1984. "Characterization of a Toroidal Well Stirred Reactor." Twentieth Symposium (International) on Combustion. The Combustion Institute, 473–79.

Stouffer, S, R C Striebich, C W Frayne, and J Zelina. 2002. "Combustion Particulates Mitigation Investigation Using a Well-Stirred Reactor." In 38th AIAA/ASME/SAE/ASEE Joint Propulsion Conference and Exhibit, 1–11. Indianapolis, IN: American Institute of Aeronautics and Astronautics. doi:10.2514/6.2002-3723.

Stouffer, Scott D, Dilip R Ballal, Joseph Zelina, Dale T Shouse, Robert D Hancock, and Hukam C Mongia. 2005. "Development and Combustion Performance of High Pressure WSR and TAPS Combustor." In 43rd AIAA Aerospace Sciences Meeting and Exhibit, 1–9. Reno, NV: American Institute of Aeronautics and Astronautics. doi:10.2514/6.2005-1416.

Stouffer, Scott, Robert Pawlik, Garth Justinger, Joshua Heyne, Joseph Zelina, and Dilip Ballal. 2007. "Combustion Performance and Emissions Characteristics for a Well Stirred Reactor for Low Volatility Hydrocarbon Fuels." In 43rd AIAA/ASME/SAE/ASEE Joint Propulsion Conference and Exhibit, 1–12. Cincinnati, OH: American Institute of Aeronautics and Astronautics. doi:10.2514/6.2007-5663.

Vijlee, Shazib Z. 2014. "Effects of Fuel Composition on Combustion Stability and NOX Emissions for Traditional and Alternative Jet Fuels." University of Washington.

Won, Sang Hee, Stephen Dooley, Frederick L Dryer, and Yiguang Ju. n.d. "Radical Index on Extinction Limits of Diffusion Flames for Large Hydrocabon Fuels." doi:10.2514/6.2011-318.

Won, Sang Hee, Peter S Veloo, Jeffrey Santner, Yiguang Ju, and Frederick L Dryer. n.d. "Comparative Evaluation of Global Combustion Properties of Alternative Jet Fuels." doi:10.2514/6.2013-156.

Won, Sang Hee, Peter S Veloo, Jeffrey Santner, Yiguang Ju, Frederick L Dryer, and Stephen Dooley. n.d. "Characterization of Global Combustion Properties with Simple Fuel Property Measurements for Alternative Jet Fuels." doi:10.2514/6.2014-3469.

Won, S. H., Haas, F. M., Dooley, S., Edwards, T., and Dryer, F. L., "Reconstruction of chemical structure of real fuel by surrogate formulation based upon combustion property targets," Combustion and Flame, vol. 183, Sep. 2017, pp. 39–49.

Wordland, Justin. 2015. "What to Know About the Historic 'Paris Agreement' on Climate Change."

Yanowitz, J, Ecoengineering M A Ratcliff, R L Mccormick, J D Taylor, and M J Murphy. 2004. "Compendium of Experimental Cetane Numbers."

Zelina, Joseph. 1995. "Combustion Studies in a Well-Stirred Reactor." University of Dayton.

Milestone(s)

Measured LBO, a Figure of Merit in the NJFCP, for 4 fuels. Results are consistent with the more complicated Area 6 Referee Rig.

Major Accomplishments

Reporting LBO equivalence ratios for four NJFCP fuels.

Publications

Peer-reviewed Publications:

None. (One publication is in preparation.)

Conference Proceedings:

Stachler, Robert D., Joshua S. Heyne, Scott D. Stouffer, Joseph D. Miller, and William M. Roquemore. 2017. "Investigation of Combustion Emissions from Conventional and Alternative Aviation Fuels in a Well-Stirred Reactor." In 55th AIAA Aerospace Sciences Meeting. Grapevine, TX: American Institute of Aeronautics and Astronautics.

Outreach Efforts

Conference presentations:

Stachler, Robert D., Joshua S. Heyne, Scott D. Stouffer, Joseph D. Miller, and William M. Roquemore. 2017. "Investigation of Combustion Emissions from Conventional and Alternative Aviation Fuels in a Well-Stirred Reactor." 55th AIAA Aerospace Sciences Meeting. Grapevine, TX: American Institute of Aeronautics and Astronautics.

Stachler, Robert D., Joshua S. Heyne, Scott D. Stouffer, Joseph D. Miller, and William M. Roquemore. 2016. "Investigation of Combustion Emissions from Conventional and Alternative Aviation Fuels in a Well-Stirred Reactor." 12th Annual Dayton Engineering Sciences Symposium. Dayton, OH: ASME.

Awards

Joshua Heyne – SOCHE Faculty Excellence Award

Robert Stachler – ASME Outstanding Young Engineer

Student Involvement

Robert Stachler, Ph.D. student, leads this effort.

Plans for Next Period

It is planned to continue with additional LBO tests for the remaining NJFCP fuels (i.e. the remaining category A and C fuels as well as the fuel blends and surrogate blends).

Task #3: Cross-Experiment Analysis

University of Dayton

Objective(s)

The objective of this task is to link low cost fundamental experiments to larger cost more complicated experiments internal to the NJFCP.

Research Approach

Our current approach is linking experiments within the NJFCP via Random Forest Regression Analysis. This regression technique is advantageous for several reasons: 1) it can handle diverse sets of data with both qualitative and quantitative information, 2) it is a relatively unbiased regression technique, 3) the regression is a white-box approach, and 4) the regression can output the relative importance of various fuel and experimental features. More details regarding Random Forest Regression Analysis can be found elsewhere e.g., (Hastie, Tibshirani, and Friedman 2009).

Initial Results

We have been able to compile the data from Area 3 and 6 as well as the data from the WSR studies on LBO. Lean Blowout (LBO) is typically defined as the lower limit equivalence ratio that a geometry at a given condition can sustain a flame. This limit is of particular interest in relation to alternative fuel certification, as it represents an engine operability limit. If an aircraft that is designed to operate with conventional Jet-A fails to hold a flame under similar conditions with an alternative

Table 5: Summary of LBO rigs with fuels tested reported. Additional data, beyond that of LBO ϕs, was taken for the rigs and fuels below. These additional data and results can be gleamed from companion papers (Chtev et al. 2017; S. D. Stouffer et al. 2017; Stachler et al. 2017).

Rig Name	Geometry type (injector/swirler)	T_{air}	T_{fuel}	P	Institution
PA-GT	Pressure atomizer/ Pratt & Whitney Swirler	550, 450, 300 K	445-460 K	3.4 atm	Georgia Tech
AB-GT	Air blast atomizer/ Pratt & Whitney Swirler	450 K	445-460 K	3.4 atm	Georgia Tech
PA-HW	Pressure atomizer/ toroidal	324, 525, 557, 562, 394 K	288 K	1, 1.3, 1.4, 3.3, 5.7, 2 atm	Honeywell
PA-RR	Pressure atomizer/ High-Swirl (P03)	400 K	320 K	2 atm	AFRL/UDRI
PV-WSR	Prevaporized/ toroidal	450 K	450 K	1 atm	AFRL/UDRI
LDI-NASA	Lean Direct Injection	575, 645, 730, 830 K		6.8, 10.9, 17 atm	NASA
PA-SH	Pressure atomizer/ swirler stabilized	280, 310, 340 K			Sheffield
PA-OSU	Pressure atomizer/ swirler stabilized	470 K		1 atm	Oregon State
PA-CAM	Pressure in bluff-body/swirler stabilized	340 K	300 K	1 atm	Cambridge
UTRC		555, 494 K		8.64, 5.6 atm	UTRC
DLR	Pressure atomizer/ swirl stabilized	323, 373 K		1 atm	DLR Germany

*Future analysis of GT data is only for the 450 K testing.

fuel, thrust and/or power would be lost to important aircraft functions and potentially pose a safety risk. LBO is identified as a FOM for this reason, and the NJFCP has multiple works documenting LBO results (Chtev et al. 2017; S. D. Stouffer et al. 2017; Stachler et al. 2017; Khandelwal 2017; Sidney, Allison, and Mastorakos 2017; Allison, Sidney, and Mastorakos 2017; Podboy, Chang, and Moder 2017). Figure 1 shows the various inlet pressures and temperatures that have been tested for LBO while a brief description of the conditions and experimental configurations of the source data presented in this paper are outlined in Table 5.

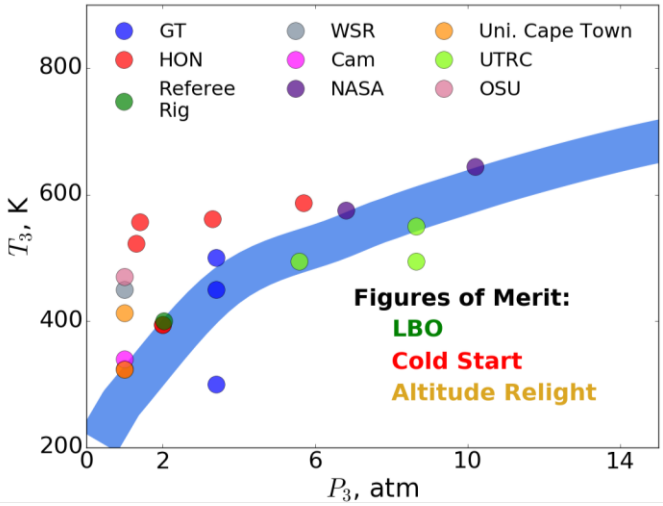

Figure 19. P3-T3 graphically displaying the rig conditions tested to measure the Figures of Merit (FOM), specifically for LBO tests for Georgia Tech (GT), Honeywell (HW), Referee Rig, Well-Stirred Reactor (WSR), Cambridge (Cam), NASA, University of Cape Town, UTRC, and Oregon State University (OSU).

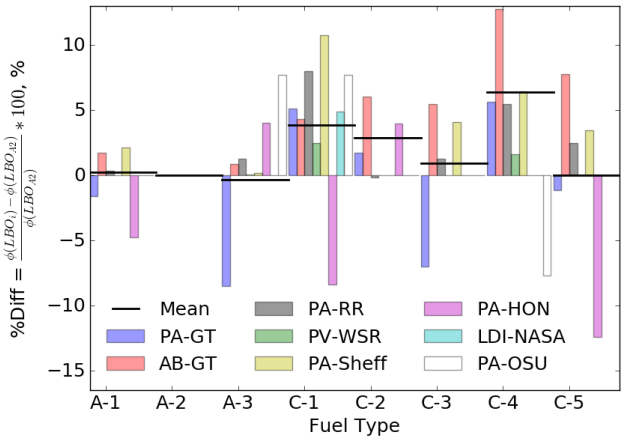

Figure 20: Nominal percent difference for Pressure Atomizer (PA), Lean Direct Injection (LDI), Air Blast (AB), and Prevaporized (PV) atomization/evaporation configurations using the Georgia Tech (GT), Referee Rig (RR), Well-Stirred Reactor (WSR), Sheffield (Sheff), Honeywell (HON), NASA, and Oregon State University (OSU) geometries versus A-2. The solid horizontal black line is the average for all tested fuels. C-1, C-2, and C-4 fuels are observed to be nominally different vs. A-2 for each experimental configuration. A-1, A-3, C-3, and C-5 are observed to blow off at equivalence ratios both leaner and richer than A-2 depending on the geometrical configuration. PA-GT bulk head temperatures are less than 550 K.

Year 3 of the program focused on the screening of NJFCP fuels in each experimental rig. Figure reports a box and whiskers plot illustrating the percent difference between A-2 and the various NJFCP fuels. The results are reported as a percent

difference from A-2 as the rigs display diverse ϕs at LBO, i.e. typical (overall) LBO ϕs for the Referee Rig are an order of magnitude more dilute than the Well-Stirred Reactor, since much of the air in an aero combustor is added subsequent to main combustion for liner cooling and dilution. The box and whisker plot shows significant scatter in the data for several fuels and rigs. The scatter in the data are not necessarily indicative of experimental shortcomings but are characteristic of the stochastic nature of limit phenomena and changing semi-controlled experimental conditions in the case of the Georgia Tech (GT) rig, as incremental bulk head temperatures/boundary conditions effect LBO. Finally, most fuels are found to have statistically similar LBO character, i.e. the whiskers overlap across fuels for a given geometrical configuration.

Significant systematic differences are observed across geometries as illustrated with Figure 6, which plots a geometry's root-mean-square (RMS) value across the fuels tested. The RMS value for a geometry is the variance the geometry produces for the variances in the NJFCP fuels. Geometries with relatively high RMS values are more sensitive to fuel variations, and conversely geometries with relatively small RMS values are less fuel sensitive.

To analyze the results collectively, a Random Forest regression analysis is performed on all the LBO data presented in this paper. For the analysis, the average percent difference for each fuel and configuration relative to the LBO ϕ of A-2 at similar conditions is evaluated relative to the chemical and physical properties of each fuel. It should be noted that some of these chemical and physical properties, when unavailable, are estimated via the methods described in Ref. (Bell et al. 2017). The regression results yielded results differing from previous reports and publications, e.g. Ref. (Lefebvre 1983),

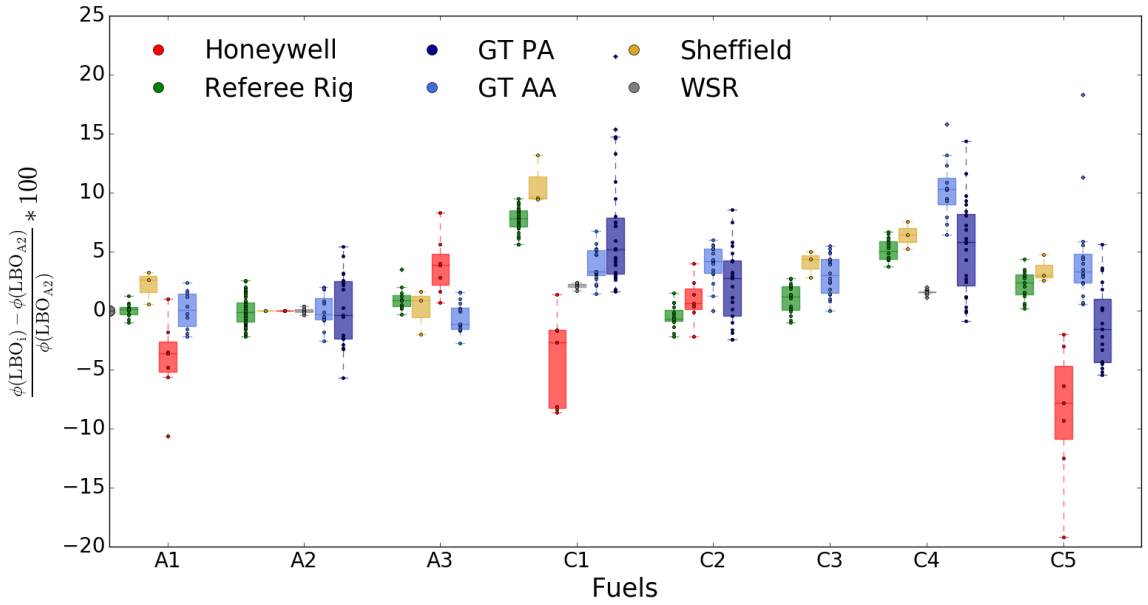

Figure 21: Box plot of percent difference LBO from A-2 for six NJFCP experimental configurations and eight fuels within the program. The circles represent individual observations, boxes represent the upper and lower 75 and 25 percentiles with the horizontal bar illustrating the median, the 'x' is the mean LBO value, the upper and lower bars are the first and fourth quartiles respectively, and data outside the quartiles are outliers. Experimental repeatability is greater than LBO differences between fuels. Fuel C-1 is observed to blow off at the richest equivalence ratios **relative to A-2.**

which implied stronger correlations to physical property effects versus the chemical property effect of DCN observed here. Beyond the reactivity effect of DCN on LBO, there is significant rig and atomizer geometry influence observed on the relative LBO of the fuels. The effect of fuel property effects and the aiding of the development of CFD models will be an area of continued investigation moving into Year 4 of the NJFCP. Finally, it should be noted that these regression techniques are in no way comprehensive in predicting LBO. The predictive capability of the current reported technique returns a R^2 value of approximately 0.85 for test data.

In Year 3 of the NJFCP, similar data analysis techniques were used to evaluate ignition results from different rigs throughout the program. Ignition at cold start and altitude relight conditions were stressed as both of these are also FOM

for the program. Figure 23 shows inlet temperature and pressure conditions tested for ignition while Table 3 outlines the various ignition test conditions and configurations used in the program to date.

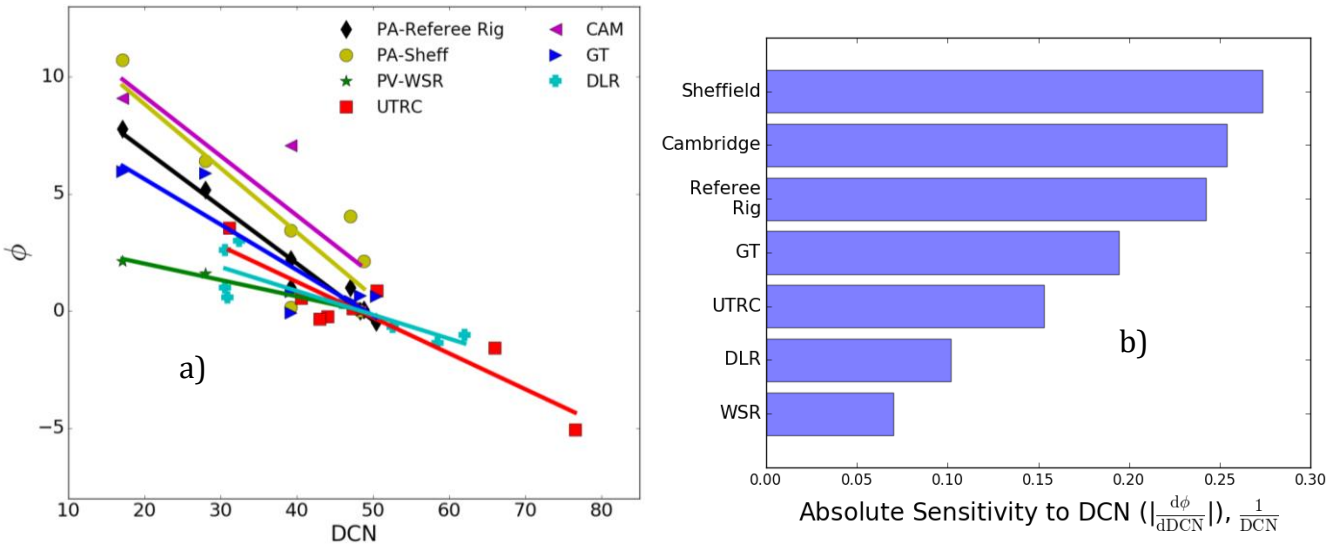

Figure 22: a) LBO Rig sensitivity to Derived Cetane Number (DCN) for seven NJFCP rigs. Whereas last year only three of the NJFCP rigs were shown to have a strong correlation with DCN for LBO, this year eight of the nine NJFCP rigs show this sensitivity (only seven shown here). The one rig that does not show this sensitivity is the Honeywell rig, the only rig that is not swirl stabilized. b) The bar graph on the left shows the Sheffield rig as being the most sensitive to DCN and the well-stirred reactor (WSR) as being the least sensitive. Note that ϕ represents percent difference LBO from A-2 for the category A and category C fuels.

Similar to LBO, Random Forest regressions were used as a way to determine feature importance from the chemical and physical properties, along with test conditions, when available in determining the ignition limit. Results have shown strong correlations to distillate properties and test conditions for the Honeywell rig, similar to what was found for LBO, while Georgia Tech prevaporized ignition tests have shown strong dependence primarily on test conditions. While the results for LBO over the last several years of the program were helpful in determining new properties that should be part of the alternative fuels certification process, ignition results so far have not presented any major new findings. As more ignition data is collected over the next year, more analysis will be done to gain better insight.

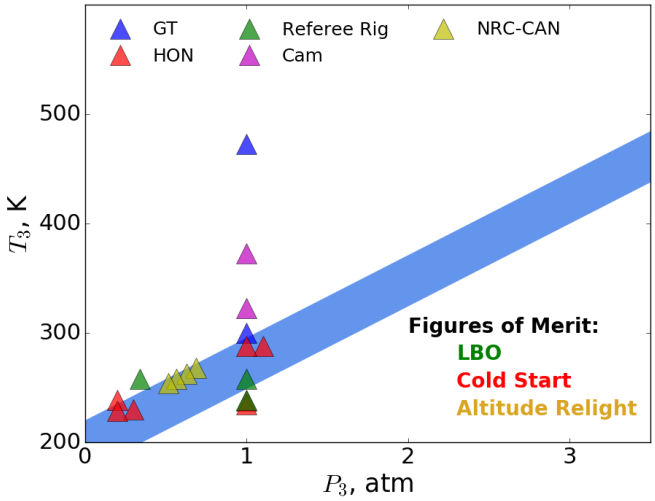

Figure 23: Ignition inlet pressure (P_3) and temperature (T_3) tested in Georgia Tech (GT), Honeywell (HON), Referee Rig, Cambridge (CAM), and NRC-Canada rigs. Ignition cold start and altitude relight were identified as two of the three FOM to be stressed in the program.

Table 6: Summary of Ignition rigs.

Rig Name	Rig Description	Ignition Source	T_{air}	T_{fuel}	P	Institution
NRC-CAN	Pressure atomizer in a small gas turbine engine (TRS-18)	Discharge	254 to 268 K	254 to 268 K	10-17 kft	NRC-CAN
Honeywell	Pressure Atomizer in APU	Discharge	230 to 317 K	236 and 288 K	0.2 to 1.1 atm	Honeywell
Cambridge	Partially Prevaporized flow Rig	Laser (YAG)	323 to 373 K		1 atm	Cambridge
GT – PV	Prevaporized fuel/air flow split from air coflow	Discharge	478 K	470 K	0.96 atm	Georgia Tech
AFRL/UDRI	Pressure atomizer, high swirl	Discharge	394 and 233 K	322 and 233 K	2 atm	AFRL/UDRI
GT - Spray	Pressure atomizer injected into air coflow	Discharge	293 to 478 K	470 K	0.96 atm	Georgia Tech

Milestone(s)
Presentation at the NJFCP Year-End Meeting. Contributing to the upcoming AIAA paper and presentation.

Major Accomplishments
We have shown strong evidence that LBO is most strongly predicted by the chemical property DCN across four experimental platforms in the NJFCP. This could potentially aid in developing blending rules for fuels to proceed through the ASTM approval process.

Publications
None.

Outreach Efforts

Oral presentations:

Carson, Jeremy, Joshua S. Heyne, Scott D. Stouffer, and Tyler Hendershott. 2016. "On the Relative Importance of Fuel Properties on LBO Behavior." 12th Annual Dayton Engineering Sciences Symposium. Dayton, OH: ASME.

Carson, Jeremy and Joshua S. Heyne. 2017. "Updates on the Relative Importance of Fuel Properties on LBO Behavior." 42nd Dayton-Cincinnati Aerospace Sciences Symposium. Dayton, OH: AIAA.

Peiffer, Erin, Joshua S. Heyne. 2017. "LBO, Ignition, and Spray Feature Importances from Year 3 of the National Jet Fuels Combustion Program." 13th Annual Dayton Engineering Sciences Symposium. Dayton, Ohio: ASME.

Awards
Jeremy Carson – Best presentation DESS 2016, Best presentation DCASS 2017.

Student Involvement
Jeremy Carson, Graduate Research Assistant, January 2015 – May 2017 (graduated), now at UDRI.
Erin Peiffer, Graduate Research Assistant, June 2017 - present.

Jennifer Colborn, Undergraduate Research Assistant, August 2016 – August 2017, now at UDRI.
Katherine Opacich, Undergraduate Research Assistant, November – 2017 – present.

Plans for Next Period
We plan to continue our current research technique incorporating greater depth into our results and incorporating additional data (i.e. spray) into our work.

Task #4: Common Format Routine Software Development
Alejandro Briones
Bob Olding
Mike Hanchak
Joshua Heyne

Objective(s)
We aim to develop a software package in which the OEMs can utilize the state of the art models being developed by the other NJFCP modeling teams.

Research Approach
This work is motivated for the imperative necessity of expediting combustor rig evaluation process for ASTM D4054 through improved combustion modeling capabilities. This fuel certification entails three main figures of merit, viz., lean blowout, ignition, and cold relight. Current fuel certification requires expensive and time-consuming experimental testing in gas turbine engines. State-of-the-art combustion models that could expedite this process are not readily available for original engine manufacturers (OEMs). The main objective of this work is to bridge the gap between state-of-the-art academic combustion models and industrial software. The second aspect of this project is to speed up the academic codes

for reaching industrial grade software category. The third aspect of this project involves verification and validation of this common format routine (CFR) software.

Modeling and simulation of complex fuels in gas turbine combustors is not trivial. Gas turbine combustors are intricate devices with characteristic length scales varying from the sub-millimeter laminar flamelet thickness to the large centimeter-size dilution holes. Therefore, the mesh resolution for gas turbines combustors is in the order of millions to even hundreds of million cells. The time scales associated with combustion and turbulence in the combustor vary from microseconds for the Kolmogorov turbulent length scales and species reaction rates to milliseconds associated with the flow through-time of the combustor. The time steps and mesh requirements for modeling and simulating a combustor are nearly prohibited. In order to mitigate some of the challenges associated with modeling and simulation of gas turbine combustors, the lower-dimensional manifold combustion (LDMC) models decouple the chemistry and chemistry-turbulence interaction from the complex turbulence computational fluid dynamics (CFD) calculations. The chemistry is computed *a priori* from one-dimensional stagnation flow equations and/or equilibrium calculation. The chemistry-turbulence interaction is computed by presuming probability density functions (PDFs). Transport equations for the moments of the mixture fraction (Z) and progress variable (C) are solved in the physical space. Then, these values are used to interpolate and to extract the thermo-chemical and transport information of the pre-tabulated table.

Commercial software such as Fluent [1,2] and Star-CCM+ already have built-in LDMC models. However, there are always limitations in terms of implementation. For instance, Fluent [1,2] pre-tabulates the table in a mixture fraction space directly. Hence, it does not solve for the one-dimensional equations. On the other hand, the CFR software presented in this paper uses a modified Cantera 2.3 [1] package. The CFR pre-tabulates chemical-turbulence interaction in the one-dimensional physical space. This allows the user to vary the transport coefficient formulation and investigated such effects on numerical predictions. Another difference between Fluent [1,2] and the CFR is that the latter can compute the three branches of the combustion phenomenon. Moreover, the CFR is more flexible because molecular properties are directly interpolated from the table. On the contrary, Fluent [1,2] does not offer this capability. Other commercial software package such as Chemkin [1] offers flamelet calculations that include the three branches of combustion. This software is very robust, but does not offer the turbulence-chemistry convolution capability needed for computing turbulent flames. To the best of our knowledge there is no standalone software that offers the capability of performing turbulence-chemistry convolution of a flamelet library. In addition, the CFR software is designed in a manner that more modules and capability can be easily annexed providing more flexibility to the user.

The purpose of this paper are to document the development of the CFR as well as to prove that such software has been verified and validated. Subsequently, the software is introduced. Important definitions are formulations are illustrated and discussed. Then, the verification and validation tests are presented.

Common Format Routine (Cfr) Software

In short, the CFR software can be sub-divided into two components, viz., the pretabulator and the flamelet-based software, which is illustrated in Appendix Figure 1. The pretabulator is capable of tabulating thermo-chemical and transport data for laminar and turbulent flames. The pretabulator is based on a modified version of Cantera 2.3 [3]. Cantera is written in C++ and Python wrappers/codes were developed in order to include new capabilities in Cantera. This Python codes also interact with a C# GUI. This can currently tabulate flamelet prolongation of the intrinsic low-dimensional manifold (FPI) and flamelet progress variable (FPV). The flamelet-based software can attach the pretabulated turbulence-chemistry interaction table to a CFD code. In this case the flamelet-based software was attached to Fluent [1,2]. The flamelet-based software machinery can perform bilinear, trilinear and tetralinear interpolation of this thermochemical table. This software is written in C and its GUI is written using C#. Now detailed description of the software is provided next.

A. Mixture Fraction Definition

Mixture fraction is a conserved scalar. This means that mixture fraction cannot be created or destroyed. Because atomic elements and enthalpy cannot be created or destroyed, mixture fractions is typically defined in this context. Here the mixture fraction is defined in terms of atomic elements and any combination of atomic elements is valid. However, the atomic composition needs to be chosen so that mixture fraction varies between zero and unity.

$$\mathrm{Z} = \sum_{i=1}^{N_{atomic\ selection}} \sum_{n=1}^{N_{species}} \frac{MW_i}{MW_n} Y_n \qquad (1)$$

The user selection of the mixture fraction definition is given by Appendix Figure A 2.

B. Progress Variable Definition

The progress variable provides quantitative information of the combustion efficiency. The latter is equal to zero when the flame blows out and combustion efficiency is zero. The maximum value of the progress variable is a real number less than unity. The progress variable is defined in terms of species mass fractions. The equation below indicates that the mixture fraction is the summation of species mass fractions. Typically in the literature CO and CO_2 are selected to indicate the level of completeness of the combustion process. In addition, CO, CO_2, H_2 and H_2O are also chosen species to indicate the combustion efficiency (or completeness of the combustion process).

$$\mathrm{C} = \sum_{n=1}^{N_{species\ selected}} Y_n \qquad (2)$$

The user selection of the mixture fraction definition is given by Appendix Figure A 3.

C. Progress Parameter Definition

For premixed and diffusion flamelets, the progress variable defined by Eq. (2) varies in the spatial direction. For a premixed flamelet C increases monotonically from the unburned reactants from zero to a maximum value downstream the flame front. For diffusion flamelets the behavior is non-monotonic and the maximum value of C occurs near stoichiometry and then its value decreases to zero towards the reactant inlets. Therefore, the progress variable definition is a function of mixture fraction, i.e. $C = \mathrm{C}(\mathrm{Z})$. Thereby, the progress parameter Λ is defined as a bijective, unique identifier that can be used to sort each flamelet. This definition is given below.

$$\Lambda = f(C, Z) \qquad (3)$$

This definition is particularly useful for modeling diffusion flamelets and has been implemented in the current software. In the CFR this conversion can be enable or disable.

D. Convoluted Thermochemical and Transport Variables

Once state relationships have been computed between thermochemical and transport properties and the lower dimensional manifold variables (i.e., Z and □) these quantities need to be convoluted for the turbulence-chemistry interaction using the equation below. The probability density functions (PDF) in this equation reads as "the probability density function of Z as a function of $\tilde{Z}$ and $\widetilde{Z''^2}$." Then, all thermochemical and transport properties (ϕ) such as density (□), molecular weight (MW), temperature (T), specific heat capacity (c_p), dynamic viscosity (□), thermal conductivity (k), species mass fractions (Y_i) and species reaction rates ($\dot{\omega}_i$) are a function of the transported lower-dimensional manifold variables ($\tilde{Z}, \widetilde{Z''^2}, \tilde{\Lambda}$ and $\widetilde{\Lambda''^2}$).

$$\widetilde{\phi}(\tilde{Z}, \widetilde{Z''^2}, \tilde{\Lambda}, \widetilde{\Lambda''^2}) = \int_0^1 \int_0^1 \phi(Z, \frac{\Lambda}{\Lambda_{max}})\, PDF(Z; \tilde{Z}, \widetilde{Z''^2}) PDF(\frac{\Lambda}{\Lambda_{max}}; \tilde{\Lambda}, \widetilde{\Lambda''^2})\, dZ d\Lambda \qquad (4)$$

Importantly to note is that the above equation, the progress parameter requires normalization before integration.

E. Lower Dimensional Manifold Transported Variables For Laminar Flows

Equations (5) and (6) are mixture fraction (Z) and progress variable (C) transported equations. When solving for laminar flows convolutions such as that represented by (4) are not necessary. Both equations here contain a transient, a convective and a diffusive term. However, the progress variable in addition contains a source term $\dot{\Omega}_C$.

$$\frac{\partial(\rho Z)}{\partial t}+\frac{\partial(\rho Z u_j)}{\partial x_j}=\frac{\partial}{\partial x_j}\left(\frac{\lambda}{c_p}\frac{\partial Z}{\partial x_j}\right) \quad (5)$$

$$\frac{\partial(\rho C)}{\partial t}+\frac{\partial(\rho C u_j)}{\partial x_j}=\frac{\partial}{\partial x_j}\left(\frac{\lambda}{c_p}\frac{\partial C}{\partial x_j}\right)+\dot{\Omega}_C \quad (6)$$

The source term ($\dot{\Omega}_C$) is computed as follows,

$$\dot{\Omega}_C=\sum_{i=1}^{N_{species\ selected}}\dot{\Omega}_i \quad (7)$$

Hence, the definition of Eq. (7) has to be consistent with the definition of Eq. (2). Then, all thermochemical and transport properties such as density (□), molecular weight (MW), temperature (T), specific heat capacity (c_p), dynamic viscosity (□), thermal conductivity (k), species mass fractions (Y_i) and species reaction rates ($\dot{\omega}_i$) are a function of the transported lower-dimensional manifold variables. The progress parameter can be obtained via Eq. (3).

F. Lower Dimensional Manifold Transported Variables For Turbulent Flows

The transport equations for the lower-dimensional manifold variables (i.e., mixture fraction ($\tilde{Z}$), mixture fraction variance ($\widetilde{Z''^2}$), and progress variable ($\tilde{C}$) are illustrated by equations (8)-(10)) in tensor notation (and in conservative form) in the context of either the unsteady Reynolds-Averaged Navier Stokes (URANS) or Large-eddy simulation (LES) turbulence model formulations. For the former formulation the dependent variable represents the Favre-weighted time-averaged variable whereas for the latter the dependent variable represents the Favre-weighted filtered variable. Equations (8) through (10), respectively, correspond to the mixture fraction ($\tilde{Z}$), mixture fraction variance ($\widetilde{Z''^2}$), and progress variable ($\tilde{C}$).

1. Transport Equations

The transported equations of the lower-dimensional manifold variables contain at least three terms, viz., transient, convection and diffusion. The mixture fraction variance in addition contains a destruction and production of $\widetilde{Z''^2}$ represented by the last two terms of Eq. (9), respectively. The progress variable transport equation also contains a source term represented by the last term of Eq. (10).

$$\frac{\partial(\bar{\rho}\tilde{Z})}{\partial t}+\frac{\partial(\bar{\rho}\tilde{Z}\tilde{u}_j)}{\partial x_j}=\frac{\partial}{\partial x_j}\left(\left(\frac{\lambda}{c_p}+D_t\right)\frac{\partial\tilde{Z}}{\partial x_j}\right) \quad (8)$$

$$\frac{\partial\left(\bar{\rho}\widetilde{Z''^2}\right)}{\partial t}+\frac{\partial\left(\bar{\rho}\widetilde{Z''^2}\tilde{u}_j\right)}{\partial x_j}=\frac{\partial}{\partial x_j}\left(\left(\frac{\lambda}{c_p}+D_t\right)\frac{\partial\widetilde{Z''^2}}{\partial x_j}\right)-\bar{\rho}\widetilde{\chi_Z}+2\bar{\rho}D_t\left(\frac{\partial\tilde{Z}}{\partial x_j}\right)^2 \quad (9)$$

$$\frac{\partial(\bar{\rho}\tilde{C})}{\partial t}+\frac{\partial(\bar{\rho}\tilde{C}\tilde{u}_j)}{\partial x_j}=\frac{\partial}{\partial x_j}\left(\left(\frac{\lambda}{c_p}+D_t\right)\frac{\partial\tilde{C}}{\partial x_j}\right)+\bar{\rho}\overline{\dot{\omega}_C} \quad (10)$$

2. Closure Models

For RANS, SAS, DES and LES models the scalar dissipation rate associated with the progress variable (C) is as computed as follows [5].

$$\widetilde{\chi_C}=\gamma_C\frac{\widetilde{Z''^2}}{\widetilde{C''^2}}\widetilde{\chi_Z} \quad (11)$$

The closure models for the RANS-based lower-dimensional manifold transported variable equations are given by the following equations [5].

$$D_t=\frac{\mu_t}{Sc_t} \quad (12)$$

$$\widetilde{\chi_Z}=2.0\frac{\varepsilon}{k}\widetilde{Z''^2} \quad (13)$$

The turbulent Schmidt number (Sc_t) is a constant that is typically chosen to be equal to 0.9. The closure models for the LES-based lower-dimensional manifold transported variable equations are given by the following equations [5].

$$D_t = C_\phi \Delta^2 |S| \quad (14)$$

$$\widetilde{\chi_Z} = 2.0 \frac{\mu_t}{Sc_t} \frac{1}{\Delta^2} \widetilde{Z''^2} \quad (15)$$

The constant C_ϕ is typically chosen to be equal to 0.4.

G. Low-Dimensional Manifold Combustion Models

The flamelet prolongation of ILDM (FPI) and the flamelet/progress variable (FPV) model utilize the one-dimensional stagnation flow equations for computing freely-propagating premixed flames and counterflow diffusion flames, respectively. The freely-propagating premixed flamelets of the FPI model are computed in the physical space and each flamelet is converted to the progress variable space (C) using Eq. (2). In turn, each premixed flamelet correspond to a mixture fraction (Z), which is directly related to an equivalence ratio. On the other hand, FPV model invokes the calculation of multiple diffusion flames. Each flame is computed in the physical space as well. The physical space can be converted to a mixture fraction state relationship (Z) following Eq. (1). Each flamelet correspond to a progress parameter (Λ). Therefore, calculations of multiple premixed and diffusion flamelets lead to a tabulation of thermochemical and transport properties as a function of mixture fraction (Z) and progress variable (C).

1. Transport Equations

The one-dimensional stagnation flow equations are presented above from Eqs. (16)-(21). In ascending order these equations represent the continuity, radial momentum, pressure curvature or strain rate eigenvalue, energy, species and a one-point or two-point dummy differential equation. The equations on the left of the table represent the original equations in Cantera 2.3 [3] for which the pressure curvature is the eigenvalue. The equations on the right represent the optional equations in a modified Cantera 2.3 in which strain rate (a) replaces the pressure curvature as the eigenvalue. The species and temperature equations are not modified. However, an additional dummy Eq. () was added to the governing equations for when the flame control methods are activated.

Table 7. Original and modified Cantera governing equations.

Equation	Cantera	Modified Cantera	
Continuity	$\frac{\partial \rho u}{\partial z} + 2\rho V = 0,\ V = \frac{v}{r}$	$\frac{\partial \rho u}{\partial z} + a\rho V = 0\ ,\ V = \frac{v}{v_e}$	(16)
Radial Momentum	$\rho u \frac{\partial V}{\partial z} + \rho V^2 = -\Xi + \frac{\partial}{\partial z}\left(\mu \frac{\partial V}{\partial z}\right)$	$\rho u \frac{\partial V}{\partial z} = \frac{\partial}{\partial z}\left(\mu \frac{\partial V}{\partial z}\right) + \Xi(\rho_F - \rho V^2)$	(17)
Pressure Curvature/Strain Rate	$\frac{d\Xi}{dz} = 0,\ \Xi = \frac{1}{r}\frac{\mathrm{dP}}{dr}$	$\frac{d\Xi}{dz} = 0,\ \Xi = a$	(16)
Energy	$\rho u c_p \frac{\partial T}{\partial z} = \frac{\partial}{\partial z}\left(\lambda \frac{\partial T}{\partial z}\right) - \sum_k j_k c_{p,k} \frac{\partial T}{\partial z} - \sum_k h_k W_k \dot{\omega}_k$		(1917)
Species	$\rho u \frac{\partial Y_k}{\partial z} = -\frac{\partial j_k}{\partial z} + W_k \dot{\omega}_k$		(20)
One- or Two-point Control	$\frac{\mathrm{du}_O}{dz} = 0$		(21)

2. Flamelet Prolongation of ILDM (FPI)

The FPI model computes premixed flamelets for each mixture fraction (Z). When the calculations do not converge because either the flamelets have exceeded the flammability limits or because the maximum temperature of the flamelet is higher than that of equilibrium, equilibrium calculations replace the freely-propagating premixed flamelets. The transport equations for the freely-propagating flamelets are given by Eqs. (22) – (26). The boundary conditions associated with the freely-propagating flamelets are shown in Table 8.

Table 8. Premixed flame boundary conditions.

Equation	Fuel Inlet	Oxidizer Inlet	
Continuity	-----	$\rho u = (\rho u)_O$	(22)
Radial Momentum	$V = V_F$	$V = V_O$	(23)
Pressure Curvature/ Strain Rate	$\rho u = (\rho u)_F$	-----	(24)
Energy	$T = T_F$	$T = T_O$	(25)
Species	$\rho u Y_k + \rho Y_k V_k = (\rho u Y_k)_F$	$\rho u Y_k + \rho Y_k V_k = (\rho u Y_k)_O$	(26)

3. Flamelet Progress/Variable

The FPV model computes diffusion flamelets for each progress parameter (Λ) along the S-curve. Multiple diffusion flamelets are necessary to build a table of thermochemical and transport properties. The first flamelet is computed at $\Lambda_{max}|Z$ and then the strain rate is increased by either increasing the inlet velocities, reducing the distance between the opposing jets, or by either the one-point or two point continuation. The computation of diffusion flamelets as a function of strain rates leads to the calculation of the S-curve containing two stable branches (strong and weak) and one unstable (middle) branch. Special continuations techniques are needed to compute the S-curve associated with the diffusion flamelets. This will be discussed in subsequent chapters. The boundary conditions associated with the counterflow flamelets are shown in Table 9.

Table 9. Nonpremixed flamelet boundary conditions.

Equation	Inlet B.C.	Internal B.C.	Outflow B.C.	
Continuity	-----	$T_{j=specified} = T_{fixed,specified}$	------	(18)
Radial Momentum	$V = V_0$	--------	$\frac{dV}{dz} = 0$	(19)
Pressure Curvature/ Strain Rate	$\Xi = 0$	--------	-----	(20)
Energy	$T = T_0$	--------	$\frac{dT}{dz} = 0$	(21)
Species	$\rho u Y_k + \rho Y_k V_k = (\rho u Y_k)_0$	--------	$\frac{dY_k}{dz} = 0$	(22)

H. Continuation Methods

Continuation techniques are now presented, viz., zero-order, scaling rules, arc-length, and one- and two-point continuation techniques are presented. The zero-order continuation technique is used for FPI, whereas hybrid continuation techniques of zero-order, scaling rules, some features of arc-length continuation, and one- and two-point continuation techniques are used for the FPV model. The arc-length continuation technique was, however, fully utilized for perfectly-stirred reactors (PSRs) in order to progressively attain the now-used continuation technique for the FPV model. The arc-length continuation for PSR is only available in Python scripts and not through the GUI.

1. Zero Order Continuation

Zero-order continuation techniques can be applied to any flamelets. This technique only supposes that the previous solution is the initial solution to the current solution. This can be represented as $\boldsymbol{x}^* = \boldsymbol{x_0}$, where $\boldsymbol{x}$ refer to a vector solution with M grids points times N equations. This continuation methods can be applied to both FPI and FPV methods. For the former this is the only method available for continuation. For the latter the number of zero-order continuation can be selected from the Flame Control tab as illustrated in Appendix Figure 4.

Figure A 4

2. Scaling Rules

The scaling rules are ideal for computing the upper branch of S-curve. The scale factor proposed by Fiala and Sattelmayer [2] are suitable for the FPV model. These scaling factors are $u{\sim}a^{-1/2}$, $V{\sim}a$, $\dot{m}''{\sim}a^{1/2}$, and $\Lambda{\sim}a^2$. The strain factor, which is the ratio of two sequential flame strain rates, can be entered by the user as illustrated in Appendix Figure 4.

3. Arc-Length Continuation

The system of nonlinear ODEs is represented by $\boldsymbol{F}(\boldsymbol{x}) = 0$. The solution is given by the vector $\boldsymbol{x}$**.** The results of these equations depend on the parameter λ. The extended solution is represented by $\boldsymbol{F}(\boldsymbol{x}(\lambda), \lambda) = 0$. The arc-length continuation [3] is a predictor-corrector continuation technique.

1. Predictor:

One such predictor is the forward Euler predictor given by:

$$\boldsymbol{x}^* = \boldsymbol{x_0} + \frac{\boldsymbol{dx}}{\boldsymbol{ds}} ds \qquad (16)$$

The gradient $\boldsymbol{dx/dF}$ can be either a tangent or a secant gradient. Here the former is used. The predicted solution $\boldsymbol{x}^*$ is the initial guess for computing the new flame. The solution vector $\boldsymbol{x}$ that lies on the path depends on the parameter λ and this, in turn, depends on arclength s.

2. *Corrector:*

The plane equation parameterized as a function of arclength, s, needs to correct the initial guess $\boldsymbol{x}^*$.

$$N\left(\boldsymbol{x}(\lambda(s)), \lambda(s)\right) \equiv \left\|\frac{\partial \boldsymbol{x}}{\partial s}\right\|_2^2 + \left(\frac{\partial \lambda}{\partial s}\right)^2 - 1 = 0 \qquad (17)$$

Now the augmented systems of equations is given by:

$$\begin{vmatrix} \boldsymbol{F}\left(\boldsymbol{x}(\lambda(s)), \lambda(s)\right) \\ N\left(\boldsymbol{x}(\lambda(s)), \lambda(s)\right) \end{vmatrix} = \begin{vmatrix} 0 \\ 0 \end{vmatrix} \qquad (18)$$

This new vector can also be written as $\mathrm{G(F(y),N(y))} = 0$. The augmented solution vector is given by $\mathrm{y} = \big(\mathrm{x(\lambda(s)),\lambda(s)}\big)$. The Jacobian matrix for the augmented system is represented by the following equation.

$$\boldsymbol{J} = \begin{vmatrix} \frac{\partial F}{\partial x} & \frac{\partial F}{\partial \lambda} \\ \frac{\partial N}{\partial x} & \frac{\partial N}{\partial \lambda} \end{vmatrix} \tag{19}$$

The partial derivative of the plane equations needs to be determined from the plane equation:

$$N\left(\boldsymbol{x}(\lambda(s)),\lambda(s)\right) \equiv \left\|\frac{\partial \boldsymbol{x}}{\partial s}\right\| d\boldsymbol{x} + \frac{\partial \lambda}{\partial s} d\lambda - ds = 0 \tag{20}$$

$$\frac{\partial N}{\partial x} = \left|\frac{\partial \boldsymbol{x}}{\partial s}\right|^T \tag{23}$$

$$\frac{\partial N}{\partial \lambda} = \frac{\partial \lambda}{\partial s} \tag{22}$$

After substituting the equations above into the Jacobian, the augmented Jacobian is now given by:

$$\boldsymbol{J} = \begin{vmatrix} \frac{\partial F}{\partial x} & \frac{\partial F}{\partial \lambda} \\ \left|\frac{\partial \boldsymbol{x}}{\partial s}\right|^T & \frac{\partial \lambda}{\partial s} \end{vmatrix} \tag{23}$$

The augmented Jacobian and the residual equations are used in a Newton-Raphson type solver. The previous k solution is used to compute the new solution k+1.

$$\boldsymbol{y_{k+1}} = \boldsymbol{y_k} - \boldsymbol{J^{-1}G} \tag{24}$$

The Newton-Raphson solver proceeds in this way. It computes the new change in the solution vector, $\Delta \boldsymbol{y_k}$. This change is added to the solution vector of the previous iteration. Note that k=0 the values of $y_0[0{:}\,N_{eqs}-2]$ are equal to the values of $\boldsymbol{x}^*$.

$$\boldsymbol{J}\Delta \boldsymbol{y_k} = -\boldsymbol{G} \tag{25}$$

$$\boldsymbol{y_{k+1}} = \boldsymbol{y_k} + \Delta \boldsymbol{y_k} \tag{26}$$

$$if\ \Delta \boldsymbol{y_k} < \varepsilon\ \rightarrow \boldsymbol{y_n} = \boldsymbol{y_{k+1}} \tag{27}$$

3. *Step-size Control:*

The user specifies an initial step size ds that is very large at first and the simulation proceeds. Near the turning points (bifurcations) the step size needs to become smaller in order to resolve the curve and avoid divergence of the Newton solver. Once the solution has passed the turning point the step size ds needs to increase again towards the other turning point. This is accomplished using the following step size control method.

$$\delta = N_{opt}/i_{Newton} \tag{28}$$

$$if\ \delta < 0.5\ \rightarrow \delta = 0.5 \tag{29}$$

$$if\ \delta > 2.0\ \rightarrow \delta = 2.0 \tag{30}$$

$$ds = \delta\ \cdot ds \tag{31}$$

This step size control technique works by allowing the user to specify the optimum number of Newton iterations, N_{opt}. If the number of Newton iterations i_{Newton} is below or above the N_{opt} the step size will increase or decrease, respectively. The multiplication factor δ is bounded between 0.5 and 2.0 in order to

avoid very small step size or very large step sizes that would either get the simulation stagnant or diverging. The step size control can be accessed through the Flame Control tab as illustrated in Figure A 55.

Some verification calculations are shown in Figure 24 through Figure 26 with numerical results available in the literature. There is nearly perfect match between previously computed S-curve for perfectly-stirred reactors (PSRs) and those computed here. This demonstrates that homotopic calculations and step size control are appropriately programmed for later used in the FPV tabulation procedure.

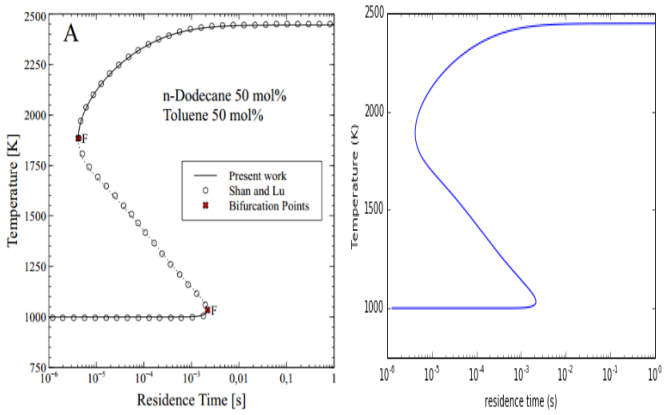

Figure 24. Comparison between Acampora and Marra [7] and in-house arc-length continuation for perfectly-stirred reactor (PSR). The inlet mass flow rate is the independent variable. Both temperature and residence time are output of the PSR. Reprinted from Computers and Chemical Engineering, 85, Acampora, L., Marra, F.S., A general study of counterflow diffusion flames at subcritical and supercritical conditions: Oxygen/hydrogen mixtures, with Permission from Elsevier

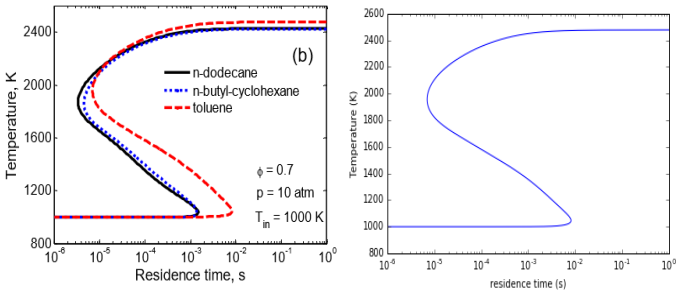

Figure 25. Comparison between Shan and Lu [1] and in-house arc-length continuation for perfectly-stirred reactor (PSR) burning Toluene. The inlet mixture temperature is the independent variable.

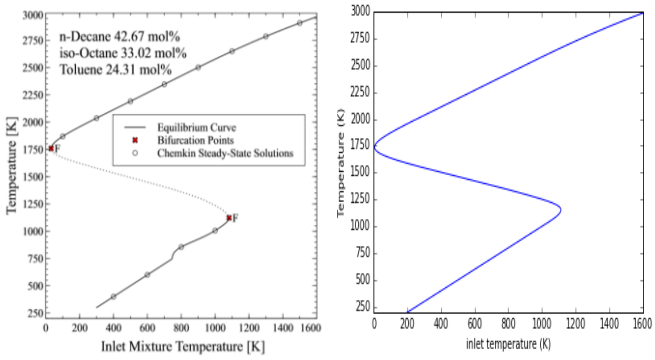

Figure 26. Comparison between Acampora and Marra [8] and in-house arc-length continuation for perfectly-stirred reactor (PSR). The inlet mixture temperature is the independent variable. Reprinted from Computers and Chemical Engineering, 85, Acampora, L., Marra, F.S., A general study of counterflow diffusion flames at subcritical and supercritical conditions: Oxygen/hydrogen mixtures, with Permission from Elsevier.

4. Flame Control Methods: One- and Two-Point

When the zero-order continuation and the scaling rules fail a flame control can be used to continue the bifurcation path of the S-curve. In the CFR this is automatically activated. The one- and two-point boundary conditions are based on the work of Nishioka et al. [8]. The boundary conditions for the pressure curvature or strain rate eigenvalue (Eq. (24)) is removed and replaced with an internal boundary condition (Eq. (24)) for the one-point continuation method. For the two-point continuation method the continuity equation boundary condition (Eq. (22)) is removed and a new internal boundary condition is added (Eq. (25)). For the one-point control method the oxidizer flux is specified as well as a fixed temperature on the fuel side. For the two-point control method neither the fuel nor the oxidizer flux are specified, but instead two fixed temperature location for the consecutive flamelet calculation at each side of the stagnation plane are prescribed.

Table 10. One- and two-point control boundary conditions.

Equation	Fuel Inlet	Internal B.C.	Internal B.C.	Oxid Inlet	
Pressure Curvature/ Strain Rate	-----	$T(j_{F,specified}) = T_{F,specified}$	-----	-----	(24)
Two-Point Control	------	-----	$T(j_{O,specified}) = T_{o,specified}$		(25)

Figure 24 clearly shows that upper and middle branches can be successfully calculated with the CFR at low and high pressure conditions. Figure 5 illustrates the effect of transport model on the S-curve. There is a slight change on the S-curve for hydrogen-oxygen combustion. This is important because it suggests that the inexpensive unity Lewis number computation is sufficient for PSR without having to invoke more computationally-expensive calculations such as mixture-averaged diffusivity. Figure demonstrates that effect of varying the detailed chemistry. The same fuel-air composition is used with two different chemistry sets, but there is substantial change in the extinction strain rate.

Figure 27 shows the calculation of the S-curve for a more practical fuel used in gas turbine combustors.

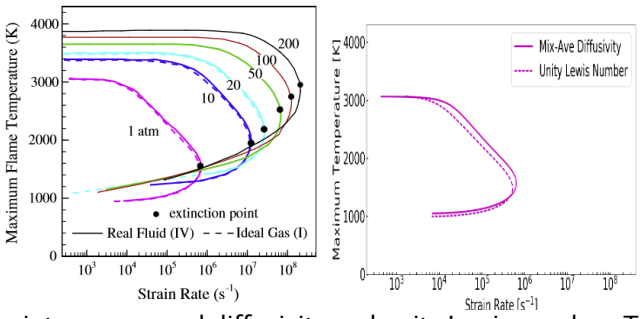

Figure 23. Comparison between mixture-averaged diffusivity and unity Lewis number. The mechanism used here is that of Burke et al. [13] Reprinted from Combustion and Flame, 161, Huo, H., Wang, X., Yang, V., A general study of counterflow diffusion flames at subcritical and supercritical conditions: Oxygen/hydrogen mixtures, with Permission from Elsevier.

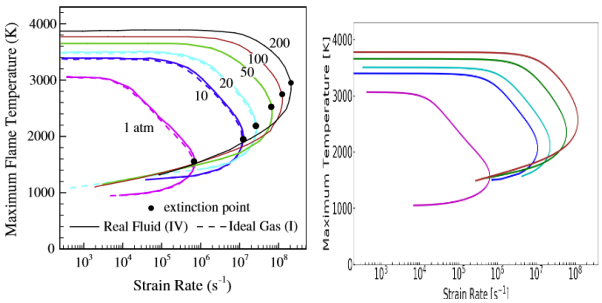

Figure 24. Comparison of strain rate vs. maximum flame temperature between Wang et al. [11] (left) and the in-house model (right). Wang et al. uses Li et al. [12] mechanism, whereas the in-house model uses Burke et al. [13] *Reprinted from Combustion and Flame, 161, Huo, H., Wang, X., Yang, V., A general study of counterflow diffusion flames at subcritical and supercritical conditions: Oxygen/hydrogen mixtures, with Permission from Elsevier.*

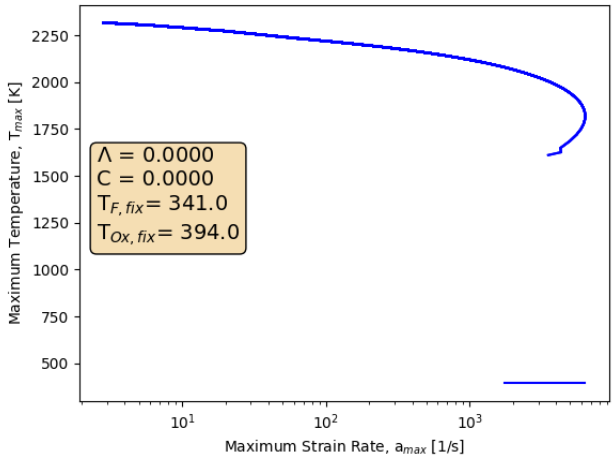

Figure 5. POSF10325-air diffusion flame s-curve.

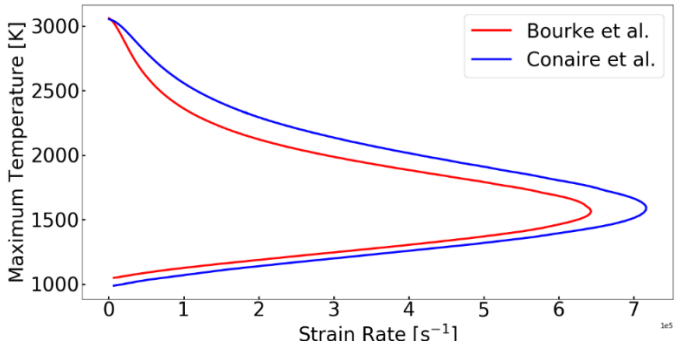

Figure 29. Comparison between Bourke et al. and Conaire et al. mechanisms for the H_2-O_2 flame at 1 atm and inlet temperatures of 300K.

I. Probability Density Functions

Here the Dirac-delta and Beta probability density functions (PDFs) are discussed here. These PDFs could be applied to either the lower-dimensional manifold variables. However, it has been proven that the Beta PDF is more suitable for mixture fraction (Z), whereas Dirac-delta or Beta PDF can be used for progress parameter (Λ).

1. Dirac Delta

The Dirac-delta probability density function is given by the equation below. Dirac-delta could be used for the progress parameter. Hence the x in the equation can be substituted by Λ.

$$\delta(x - x_0) = \begin{cases} 0, & x \neq x_0 \\ 1, & x = x_0 \end{cases} \tag{32}$$

2. Beta

The Beta probability density function is given by the equations below. The probability density function is appropriate for the mixture fraction (Z). Hence, the x in the equation can be substituted for the Z. This PDF could also be utilized to model the progress parameter and the x below would be substituted by Λ.

$$\beta\left(x;\tilde{x},\widetilde{x''^2}\right) = \frac{\Gamma(a+b)}{\Gamma(a)\Gamma(b)} x^{a-1}(1-x)^{b-1} \quad (33)$$

$$a = \frac{\tilde{x}\left(\tilde{x}-\tilde{x}^2-\widetilde{x''^2}\right)}{\widetilde{x''^2}} \quad (34)$$

$$b = \frac{(1-\tilde{x})\left(\tilde{x}-\tilde{x}^2-\widetilde{x''^2}\right)}{\widetilde{x''^2}} \quad (35)$$

The demonstration of these convolutions are shown in Figure. The images correspond to a convoluted methane-air diffusion flame. Dirac-delta PDF was used for the progress variable. Note that the effect of turbulence-chemistry interaction represented by the variance of the mixture fraction (in this case) is to weaken the flame by lowering the peak temperature from ~2050 K to ~1750K. Similar the peak progress variable source term drops from ~500 to ~100 ks/m^{3}s^{-1}.

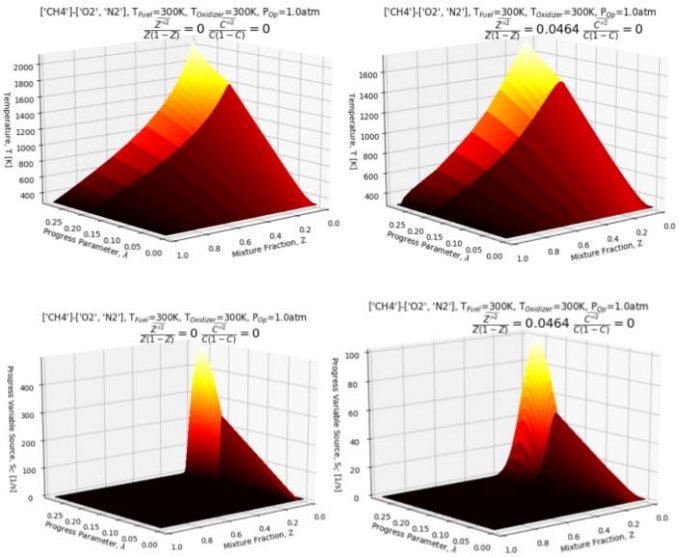

Figure 30. Sample images of a tabulated thermochemical transport tables for a CH_4-air diffusion flame. The top and bottom images illustrate temperature and progress variable source, respectively. The left images show the tabulated variables when both mixture fraction and progress variables are zero. The right images show the tabulated variables when the mixture fraction variance is non-zero.

J. Verification Tests

There are several verification and validation tests. A canonical laminar triple flame was computed using FPI or FPV models. The Sandia D piloted flame was also simulated using RANS/FPV and LES/FPV model. Finally, a single cup combustor rig was simulated using the LES/FPV model.

A. Simulations of a Canonical Triple Flame

Here is the verification test for the laminar formulation for the FPI model. Figure indicates that both calculations are very similar in terms of temperature and CO mass fraction contours. Subtle difference can be attributed to the fact that Wu et al. [9] used FlameMaster solver [10], which computes the flamelets in mixture fraction space directly.

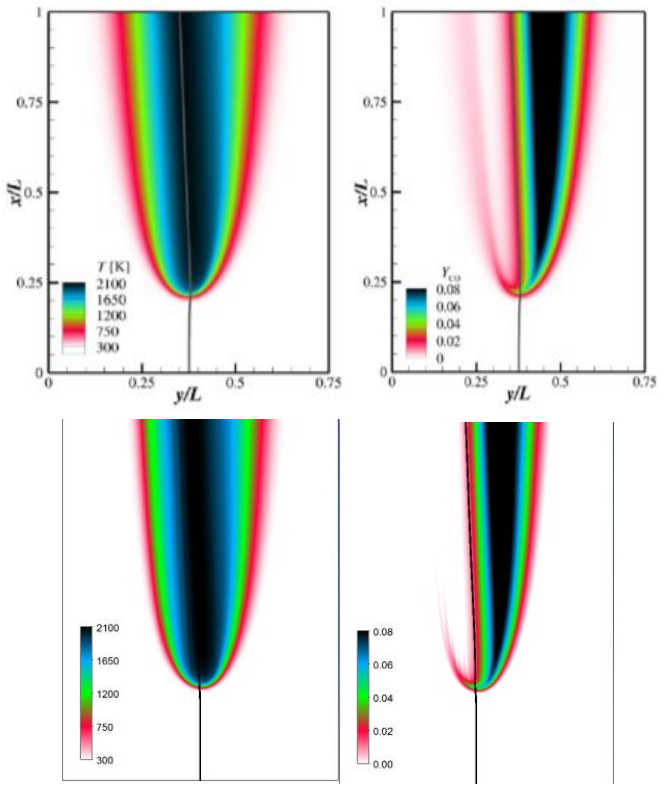

Figure 31. Comparison between (top) Wu et al. [15] and (bottom) CFR results of a laminar triple flame using FPI in terms of (left) temperature and (right) CO mass fractions.

B. Laminar Fpv Simulations For A Canonical Triple Flame

Here is the verification test for the laminar formulation for the FPV model. Figure illustrates the verification step for computing the laminar version of the FPV combustion model of the CFR software.

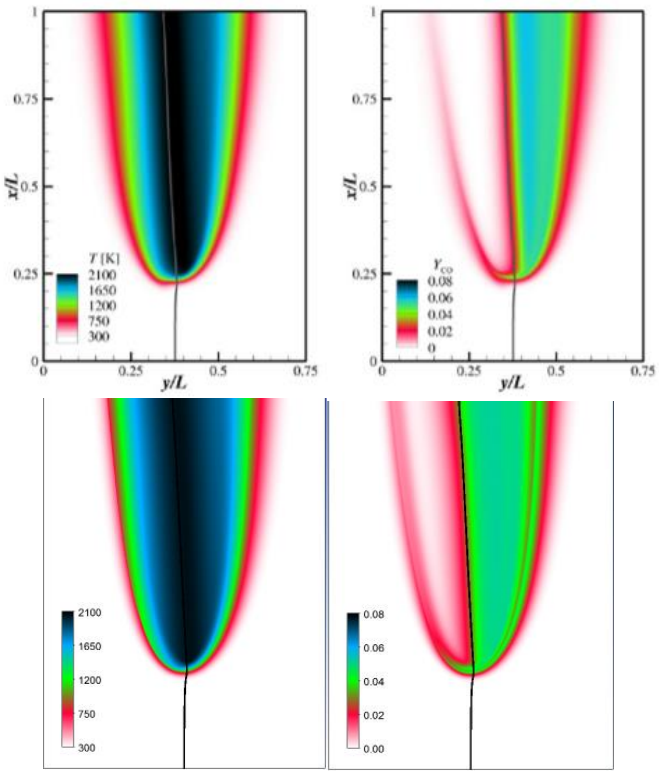

Figure 32. Comparison between (top) Wu et al. [15] and (bottom) CFR results of a laminar triple flame using FPV in terms of (left) temperature and (right) CO mass fractions.

C. Turbulent Simulations of Sandia D Flame

Here are the verification and validation tests for turbulent formulation of the FPV model. Figure 33 presents the experimental measurements against numerical predictions. Numerical simulations were performed only with Fluent [1,2] and with Fluent+CFR software. The k-ε and k-ω RANS version of FPV model were utilized. The Beta PDF is used for mixture fraction and Dirac-delta is used for progress variable. Generally, both the Fluent and Fluent+CFR results compared well with the experimental measurements in terms of temperature and species mass fractions. However, the Fluent+CFR outperforms the Fluent results, specifically, in terms of CO mass fraction. Both Fluent and Fluent+CFR results, nonetheless, underpredict the mixture fraction variance. In terms of RANS model, the k-ω better approximates the measurements.

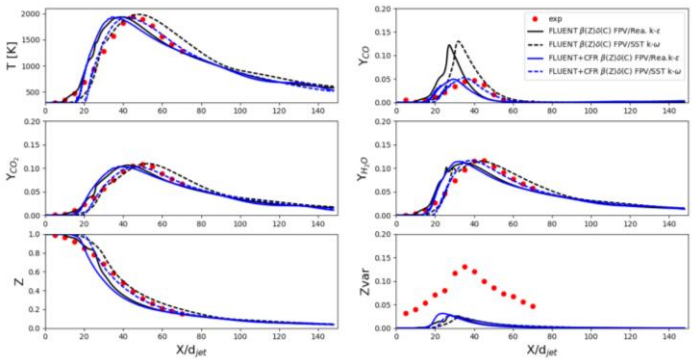

Figure 33. Centerline comparison between experiments and RANS simulations of the Sandia D turbulent flame.

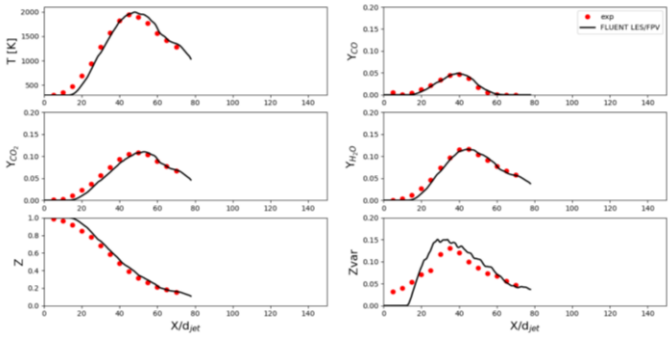

Figure 34. Centerline comparison between experiments and LES simulations of the Sandia D turbulent flame.

Conclusions

A common format routine (CFR) software for modeling combustion problems have been developed. This software is sub-divided into a thermochemical transport property pretabulator software and a flamelet-based software. The former can be used to create flamelet prolongation of the ILDM (FPI) or flamelet/progress variable (FPV) tables for either laminar or turbulent flames. The pretabulator allows for turbulence-chemistry interaction through either Beta or Dirac-delta probability density function (PDF) of the independent variables. The flamelet-based software can read, search and interpolate the table to extract thermochemical and transport composition based on lower-dimensional manifold transport variables (i.e., mixture fraction, mixture fraction variance and progress parameter). The k-□ and k-□ RANS, SAS, DES and LES turbulence model were coupled with the flamelet-based combustion models. A multiphase spray model successfully couples with the gas phase by exchanging mass. The CFR software was positively compared against laminar and turbulent flames in canonical configurations as well as in more practical single-swirler combustor rig. The developed software is reliable for modeling and simulation of complex combustion phenomena.

References

Ansys Inc., Fluent User's Guide, v18.0.

Ansys Inc., Fluent Theory Guide, v18.0.

Goodwin, D.G., Moffat, H.K., Speth, R.L., Cantera: An object – oriented software toolkit for chemical kinetics, thermodynamics, and transport properties," http://www.cantera.org, 2017, Version 2.3.0. doi:10.5281/zenodo.170284

ANSYS 18.0, Chemkin-Pro Theory Manual, ANSYS, Inc.: San Diego, 2017.

Ihme, M., Pitsch, H., "Prediction of extinction and reignition in nonpremixed turbulent flames using flamelet/progress variable model: 2. Application in LES of Sandia flames D and E," Combustion and Flame, 155, (1-2), pp. 90-107, 2008.

Fiala, T., Sattelmayer, T., "Nonpremixed Counterflow Flames: Scaling Rules for Batch Simulations," Journal of Combustion, 2014, 484372.

H. B. Keller, in Applications of bifurcation Theory, P. Rabinowithz, Ed. (Academic Press, New York, 1977).

Luigi Acampora and Francesco S. Marra, "Numerical Strategies for the Bifurcation Analysis of Perfectly Stirred Reactors with Detailed Combustion Mechanisms," Computers and Chemical Engineering 82 (2015) 273-282.

Ruiqin Shan, Tianfeng Lu, Effects of Surrogate Jet-Fuel Composition on Ignition and Extinction in High Temperature Applications, 8th U. S. National Combustion Meeting Organized by the Western States Section of the Combustion Institute and hosted by the University of Utah May 19-22, 2013.

Nishioka, M., Law, C., Takeno, T., "A flame controlling continuation method for generating S-curve responses with detailed chemistry," Combust. Flame 104 (3):328-342

Huo, H., Wang, X., Yang, V., "A general study of counterflow diffusion flames at subcritical and supercritical conditions: Oxygen/hydrogen mixtures," Combustion and Flames, 161, 2014.

J. Li, Z. Zhao, A. Kazakov, F.L. Dryer, "An updated comprehensive kinetic model of hydrogen combustion," Int. J. Chem. Kinetics, 36, 2004, 566-575.

Burke, M.P., Chaos, M., Ju, Y., Dryer, F.L., Klippenstein, S.J., "Comprehensive H2/O2 Kinetic Model for High-Pressure Combustion," Int. J. Chem. Kinet. (2011).

Connaire, M. O., Curran, H J., Simmie, J. M., Pitz, W. J. and Westbrook, C.K., "A Comprehensive Modeling Study of Hydrogen Oxidation", International Journal of Chemical Kinetics, 36:603-622, 2004.

Wu, H., See, Y.C., Wang, Q., and Ihme, M., "A Pareto-efficient combustion framework with submodel assignment for predicting complex flame configurations," 162(1), 2015, 4208-4230.

Pitsch, H., FlameMaster v3.1, "A C++ computer program for 0D combustion and 1D laminar flame calculations," 1998.

Milestone(s)

Development of a stand-alone CFR.
OEMs have used the CFR internally.

Major Accomplishments

Developed and delivered to OEMs a stand-alone common format routine incorporating the latest theory from academic teams.

Publications

Nothing to report. A paper is in preparation.

Outreach Efforts

None.

Awards

Joshua Heyne – SOCHE Faculty Excellence Award, 2016.

Student Involvement

None.

Plans for Next Period

We plan to continue our current path with OEM participation continuing to increase with collaborations on simulating the Referee Rig with the developed CFR.

CFR APPENDIX

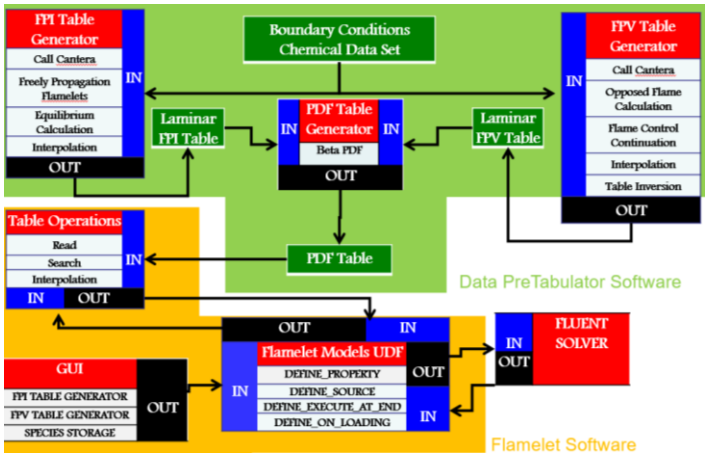

Figure A 1. Schematic of the Common Format Routine (CFR) software. All the components with the green background correspond to the thermochemical and transport data pretabulator. All the components with the amber background corresponds to the flamelet-based software.

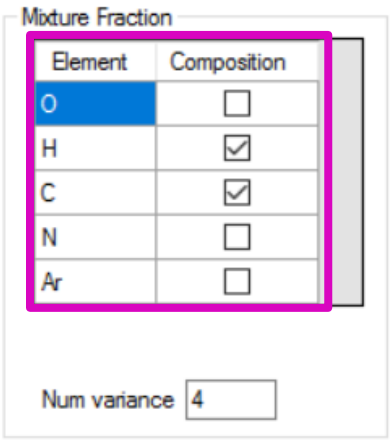

Figure A 2. Pretabulator software selection of user's mixture fraction definition is indicated within the magenta-line box.

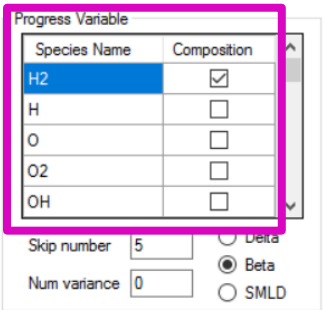

Figure A 3. Pretabulator software selection of user's progress variable definition is indicated within the magenta line box.

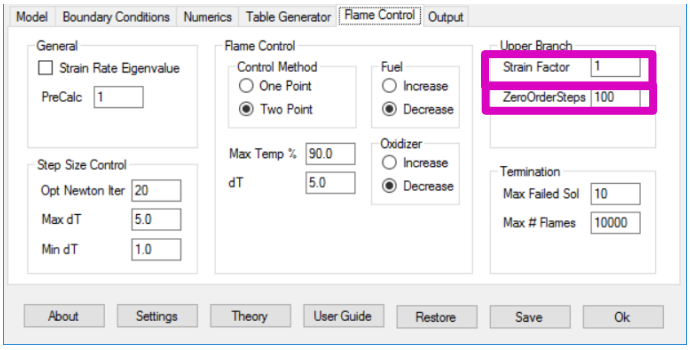

Figure A 4. Pretabulator software selection of zero order continuation steps and strain factor are indicated in the magenta boxes.

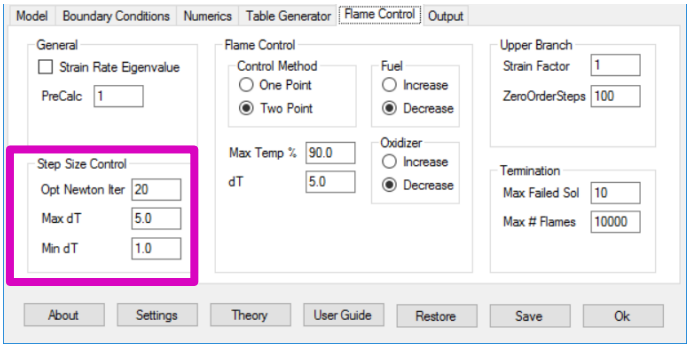

Figure A 5. Pretabulator software selection of step size control is indicated in the magenta box.

Task #5: Spray Modeling of Area 3 Pressure Atomized Spray Injector

Joshua Heyne
Vaidya Sankaran

Objective(s)

The objective of this task is to simulate the Area 3 High Sheer Rig pressure blast spray atomizer. Simulations of NJFCP experiments in the Area 3 High Sheer Rig will be done to explore the relative performance of simulations versus experiments and the relative spray and combustor character between the A-2, C-1, and C-5 fuels. These computational results will also illuminate the relative impact of a Pratt & Whitney swirler-injector geometry as compared to the other geometries in the program.

Research Approach

Large Eddy Simulations of the Area-3 Georgia Tech High Shear Rig have been conducted. As an initial step to validate the grid resolutions, boundary conditions, numerical and physical model used in the simulation, non-reacting calculations are performed. Figure 35 shows the mean axial velocity contours, and Figure 38 a)is a series of line plots which are in very good agreement with experimental data.

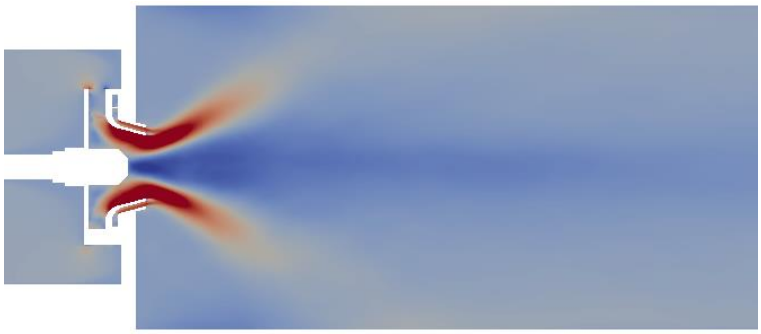

Figure 35: Mean axial velocity contours for Area 3 rig. Good prediction of the central & corner recirculation zones due to swirling flow-field Wall models are needed for resolving swirler walls which are not used here.

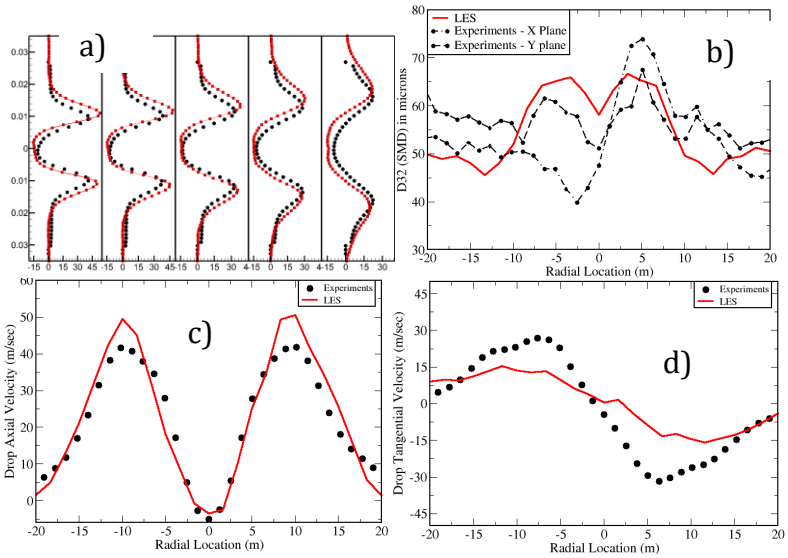

Figure 36: Line plot comparing a) mean axial velocity profiles, b) spray size, c) spray axial velocity, and d) spray tang, velocity for Georgia Tech data (solid circles) and UTRC simulations (red line). The simulations mimic the Georgia Tech data well by matching maximums, minimums, and overall maximums.

Since spray boundary conditions play a key role in reacting simulations, we also have performed another intermediate simulation were the measured spray data at a downstream location was projected back to the injector face and used as spray boundary conditions. Results from that simulations were then compared with measured data at downstream location to ascertain the validity of this approach. As shown in the line plots Figure 38, b) SMD, c) mean droplet axial velocity, and d) mean tangential velocities were predicted very well in this approach. As a final step, reacting simulations were performed with the A2 and C1 fuels using the previously validated models. The images of instantaneous and time-averaged temperature contours and mean reaction rate contours are shown in Figures 39 and 40 below.

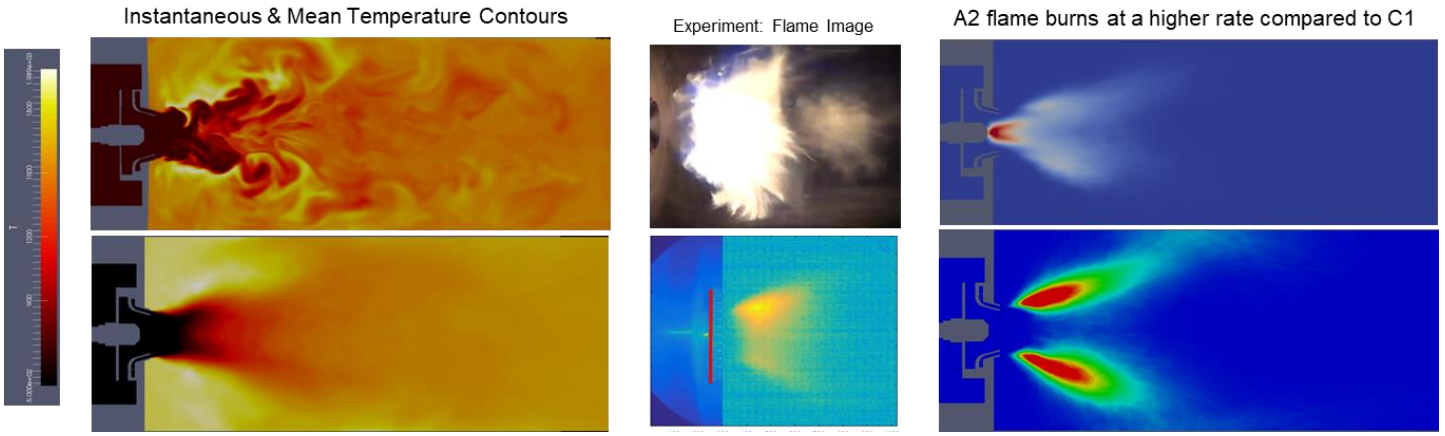

Figure 37: Comparisons of instantaneous (top) and mean (bottom) temperature (far left images) and heat release rates (far right images) for the nominal jet fuel (A-2). The middle images show a comparison of predicted vs. experimental results.

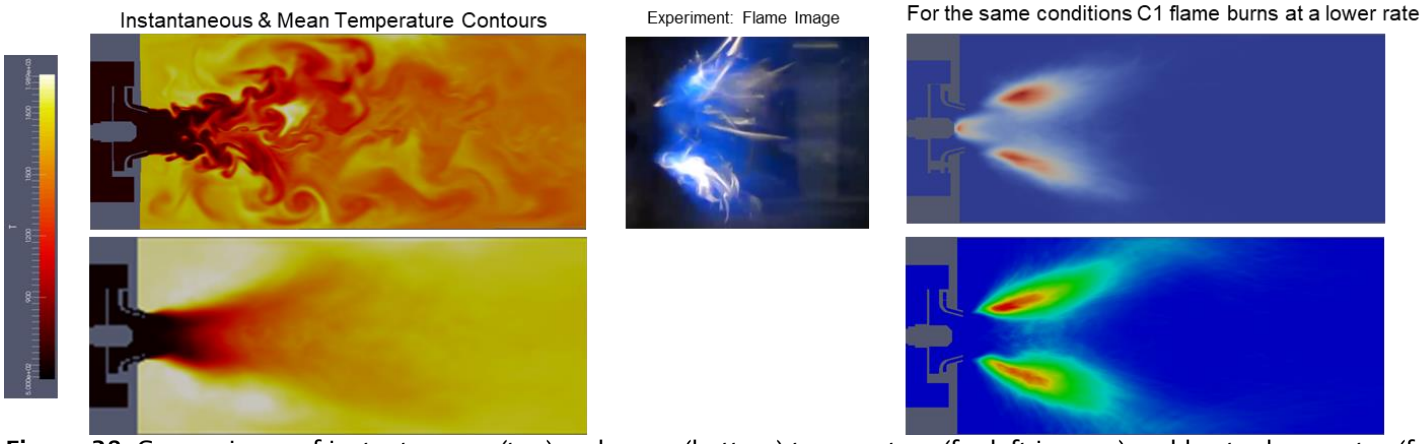

Figure 38: Comparisons of instantaneous (top) and mean (bottom) temperature (far left images) and heat release rates (far right images) for an alternative jet fuel (C-1).

While the temperature contours do not show significant differences between the two fuels, the reaction rate contours show that the C-1 flame is weaker than the A-2 flame, an initial marker of LBO. This is qualitatively consistent with the observed LBO behavior.

Milestone(s)

Execution of sub-contract.
Simulation of multiple fuels for the swirler and nozzle configuration at Georgia Tech.

Major Accomplishments

Comparisons of experiments and simulation results.

Publications

Nothing to report.

Outreach Efforts

Nothing to report.

Awards
Joshua Heyne – SOCHE Faculty Excellence Award, 2016.

Student Involvement
None.

Plans for Next Period
LBO simulations are being conducted to assess the impact of fuel on the LBO phenomena. UTRC to deliver final report on Area 3 spray simulations in Spring 2018.

Task #6: Procure Additional Geometries for Testing at Various NJFCP Facilities
Joshua Heyne
Scott Stouffer

Objective(s)
As seen earlier in this report, combustor geometry is an important sensitivity parameter in alt. jet fuel certification. For this reason, the NJFCP is interested in additional geometries for testing and constraining expectations from alt. fuels. Here we will procure these additional geometries for testing at various NJFCP facilities.

Research Approach
We have contacted a vendor capable of manufacturing the necessary hardware.

Milestone(s)
Nothing to report.

Major Accomplishments
Nothing to report.

Publications
Nothing to report.

Outreach Efforts
Nothing to report.

Awards
Joshua Heyne – SOCHE Faculty Excellence Award

Student Involvement
None.

Plans for Next Period
Order and acquire additional geometries from vendors.

Task #7: Ignition Testing of Conventional and Alternative Jet Fuels

Joshua Heyne
Scott Stouffer
Tyler Hendershott
Jeffery Monfort

Objective(s)

The objective of this task is to measure the ignition probabilities of alternative and conventional jet fuels. The result of these tests are used to inform OEMs on the controlling physics in the Referee Rig at relevant conditions.

Research Approach

The Referee Rig is designed to mimic some of the most fuel sensitive engine combustor configurations while maintaining a relatively low cost size and operation. Previously, this rig has been used to test Lean Blowout (LBO) characteristics for various alternative and conventional jet fuels in the NJFCP and other programs. Here ignition probabilities are reported for the Referee Rig for a best, nominal, and worst case conventional fuel as well as one alternative fuel that was shown to have deleterious LBO behavior, see Figure and Figure .

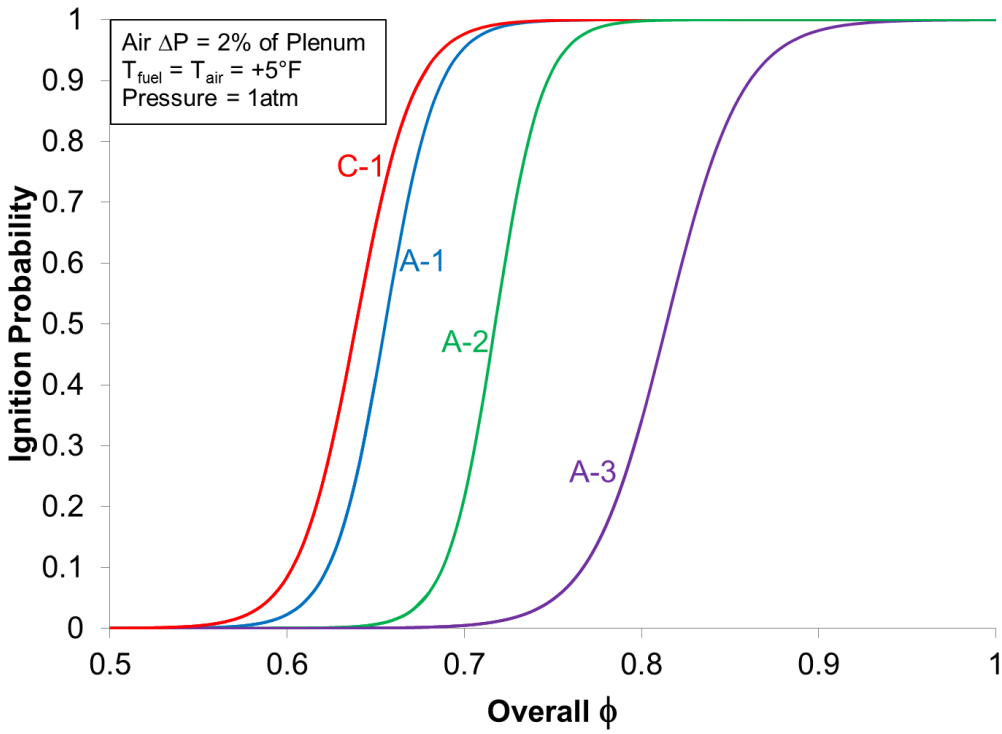

Figure 39: Ignition probabilities for the three conventional fuels as well as C-1, the alternative fuel with the worst LBO performance, at ΔP = 2%, T_{fuel}/T_{air} = 5 F, and P=1 atm. Significantly different ignition probabilities were observed for the conventional fuels. The alternative fuel C-1 is observed to have better ignition behavior than all the conventional fuels.

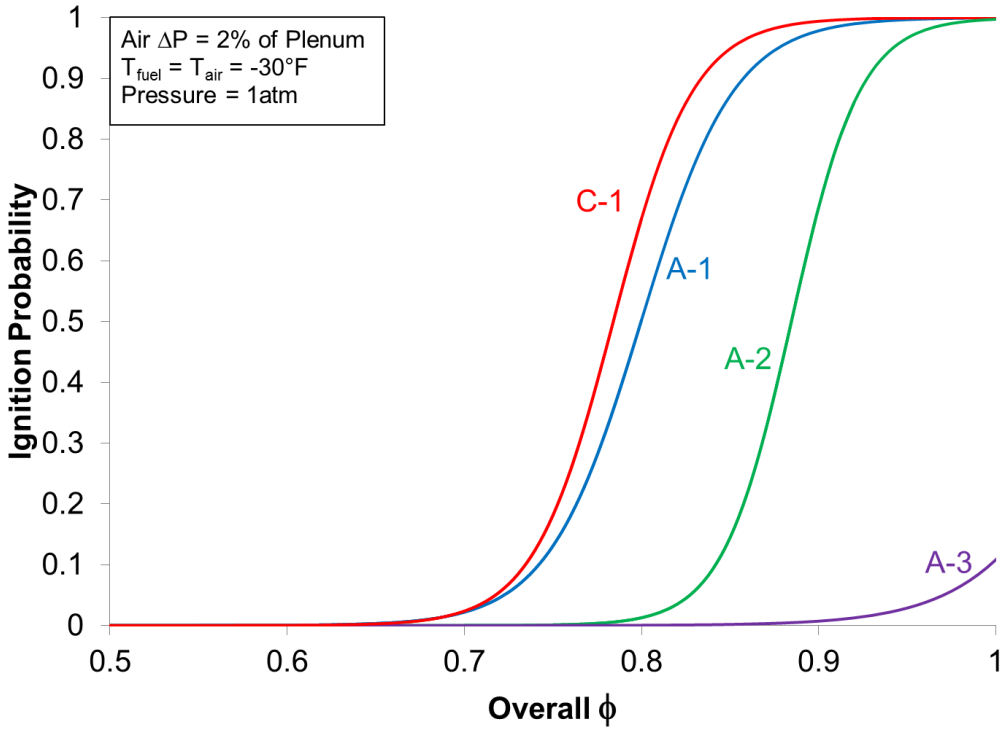

Figure 40: Ignition probabilities for the three conventional fuels as well as C-1, the alternative fuel with the worst LBO performance, at ΔP = 2%, T_{fuel}/T_{air} = -30 F, and P=1 atm. The overall ϕ required for an equivalent ignition probability for this temperature condition is significantly larger. Additionally, the fuel sensitivity is increased at the lower temperatures.

These data show that significant differences in ignition probabilities exist for conventional fuels. Where as in LBO, conventional fuels showed very similar LBO limits. Further, the fuel effects, i.e. the relative differences between fuels, is greater at lower temperatures. This implies a temperature dependent variable such as viscosity is driving the differences between fuels.

Milestone(s)
The generation of cumulative distribution functions for the various conventional and alternative jet fuels in the Referee Rig at cold conditions.

Major Accomplishments
Demonstrating significant fuel sensitivity in ignition probability for various fuels.

Publications
None.

Outreach Efforts
Presentation and poster at ASCENT Fall 2017.

Awards
None.

Student Involvement
None.

Plans for Next Period

We plan to pursue additional Referee Rig ignition studies via:

1. Further ignition experiments at fuel/air temperatures down to -30 ℉ at atmospheric pressure,
2. Ignition experiments at pressures as low as 0.3 atm, and
3. Implementation of advanced optical diagnostics.

Project 036 Parametric Uncertainty Assessment for Aviation Environmental Design Tool (AEDT)

Georgia Institute of Technology

Project Lead Investigator

Principal Investigator:
Professor Dimitri N. Mavris
Director
Aerospace Systems Design Laboratory
School of Aerospace Engineering
Georgia Institute of Technology
Phone: (404) 894-1557
Fax: (404) 894-6596
Email: dimitri.mavris@ae.gatech.edu

Co-Principal Investigator:
Dr. Dongwook Lim
Chief, Air Transportation Economics Branch Aerospace Systems Design Laboratory
School of Aerospace Engineering
Georgia Institute of Technology
Phone: (404) 894-7509
Fax: (404) 894-6596
Email: dongwook.lim@ae.gatech.edu

- FAA Award Number: 13-C-AJFE-GIT, Amendment 019, 29, and 30
- Period of Performance: January 1, 2017 – August 31, 2018
- Task(s):
    1. AEDT 2b Uncertainty Quantification Closeout Study
    2. Validation and Verification of BADA4 Implementation
    3. Capability Demonstration and Validation of AEDT 2c and 2d Functionality

Project Funding Level

According to the original project plan, the funding from the FAA is $175,000 for 12 months. The Georgia Institute of Technology has agreed to a total of $175,000 in matching funds. The project was augmented for the period for 12/1/2016 to 3/31/2017 to add additional tasks. The augmented funding from the FAA is $80,000 for 4 months. The Georgia Institute of Technology has agreed to additional $80,000 in matching funds. The next augmentation was for $300,000 for the period of performance of 4/1/2017 to 8/31/2018. The Georgia Institute of Technology has agreed to additional $300,000 in matching funds.

Investigation Team

Prof. Dimitri Mavris, Dr. Michelle Kirby, Dr. Dongwook Lim, Dr. Yongchang Li, Dr. Matthew Levine, Junghyun Kim (Graduate student), Ameya Behere (Graduate student), and Evanthia (Eva) Kallou (Graduate student) with consultation/support by research staff Dr. Holger Pfaender.

Project Overview

The Federal Aviation Administration's Office of Environment and Energy (FAA/AEE) has developed a comprehensive suite of software tools that allow for a thorough assessment of the environmental effects of aviation, in particular the ability to assess the interdependencies between aviation-related noise and emissions, performance, and cost. At the heart of this

tool suite is the high fidelity Aviation Environmental Design Tool (AEDT). AEDT is a software system that models aircraft performance in space and time to estimate fuel consumption, emissions, noise, and air quality consequences. This software has been developed by the FAA Office of Environment and Energy for public release. It is the next generation FAA environmental consequence tool. AEDT satisfies the need to consider the interdependencies between aircraft-related fuel consumption, emissions, and noise. AEDT 2 has been released in four phases. The first version, AEDT 2a, was released in March 2012 [1, 2]. The second version of AEDT 2b was released in May 2015 [3], the third version of AEDT 2c was released in September 2016, and the fourth version of AEDT 2d was released in September 2017. A new series AEDT 3 will be released which have major updates including Base of Aircraft Data 4 (BADA4) performance model for fuel consumption, emissions and noise, and implementation of ASCENT Project 45 findings.

This uncertainty quantification comprehensively assesses the accuracy, functionality, and capabilities of AEDT during the development process. The major purposes of this effort are to:

- Contribute to the external understanding of AEDT
- Build confidence in AEDT's capability and fidelity (ability to represent reality)
- Help users of AEDT to understand the sensitivities of output response to the variation of input parameters/assumptions
- Identify gaps in functionality
- Identify high-priority areas for further research and development

The uncertainty quantification consists of verification and validation, capability demonstrations, and parametric uncertainty/sensitivity analysis.

Task #1: AEDT 2b Uncertainty Quantification Closeout Study

Georgia Institute of Technology

Objective(s)

Aviation Environmental Design Tool (AEDT) is a software system that models aircraft performance in space and time to estimate fuel consumption, emissions, noise, and air quality impacts. This software, developed by the FAA Office of Environment and Energy (AEE), is the next generation FAA environmental consequence tool. In order to ensure the accuracy, functionality, and capabilities of AEDT 2b during the development process, Uncertainty Quantification (UQ) analyses were conducted to assess AEDT 2b's capability and fidelity [3]. Additional objectives of the UQ analysis also include contributing to the external understanding of AEDT 2b, helping users of AEDT 2b to understand sensitivities of output response to variation in input parameters/assumptions, identifying gaps in functionality, and identifying high-priority areas for further research and development [4, 5].

Since AEDT 2b replaces legacy software tools (e.g., Integrated Noise Model (INM), Emissions and Dispersion Modeling System (EDMS), and AEDT 2a), the UQ analyses were designed as a verification/validation of the capability of AEDT 2b. For noise, fuel consumption and emissions modeling, UQ analyses were conducted by evaluating AEDT 2b against INM, EDMS and other legacy tools. The comparison shows that there are relatively large differences in noise, fuel consumption, emission inventory and emission dispersion between AEDT and the legacy tools. Thus, a further investigation was performed to assess and understand the causes that lead to the differences. This section presents the studies for investigating a number of factors that may have impacts on the noise and emissions results produced by AEDT and the legacy tools. The findings and recommendations about the uncertainty quantification analysis for AEDT on noise and emissions were also presented and discussed.

Research Approach

To understand and validate the capability of AEDT 2b, further analysis is conducted to investigate the causes that lead to the differences in noise, fuel burn, emission inventory and emission dispersion between AEDT 2b and the legacy codes. For emissions analysis, since the differences in emission inventory mainly result from the aircraft and other sources like GSE, APU and stationary sources' contributions to the differences can be neglected, the investigation is focused on the differences produced only by aircraft.

The investigations of the difference between AEDT and the legacy tools focus on evaluating the assumptions, methods, and implementation for noise and emissions calculations. Thus, the technical manuals of AEDT and legacy tools were reviewed to understand the assumptions and methods used, and the factors that have impact on the noise and emissions

calculation were identified. Additional studies were designed and performed to further validate the metric results, and findings and recommendations were discussed.

Investigation of the Differences in Emissions Inventory and Dispersion between AEDT and EDMS

To evaluate AEDT 2b's capability in modeling fuel consumption, emission inventory and emission dispersion, a NEPA/CAA analysis was used to provide a verification and validation of AEDT 2b functionality and a comparison to EDMS. This analysis utilized a single airport study for testing the functionality and comparing the results to EDMS [3]. The comparison results show that for emission inventory analysis of the aircraft sources, the difference in fuel consumption, CO2, H2O, and SOx is about 14~15% between AEDT 2b and EDMS. The differences in HC, TOC, VOC, and NMHC aircraft emissions are about -3%, and the difference in NOx is about 15%. PM features the largest difference between AEDT 2b and EDMS, ranging from -17% to -26%. In addition, for air quality analysis, the difference in pollutant concentration can be as large as 76% (e.g. CO 1 HR concentration) between AEDT and EDMS. Thus, the goal of this task was to investigate the causes that lead to the difference between AEDT and EDMS by comparing factors

- Weather
- Engine Emission Databank (EDB) coefficients
- ANP coefficients, flight procedure and trajectory
- Taxi time
- Aircraft and operation type
- Operation modes
- Fuel burn and emissions calculation methods
- Flight track
- Spatial assignment of emissions for dispersion modeling
- Aircraft operation

Investigation for Fuel Consumption and Emission Inventory Modeling

The causes that led to the differences in fuel consumption and emission inventory between AEDT and EDMS are investigated [3, 4, 6, 7]. The factors that were investigated include weather, engine emission databank coefficients, ANP coefficients, flight procedure and trajectory, taxi time, aircraft and operation type, operation modes, and fuel burn and emissions calculation methods.

Weather

This analysis was performed to make sure both AEDT and EDMS use the same weather profile when calculating fuel burn and emissions since weather can have a significant impact on the results. It was found that AEDT uses different temperature, pressure, sea level pressure, relative humidity and wind speed values than EDMS. To enable an apples-to-apples comparison, the weather in AEDT was edited to match the weather in EDMS. AEDT was then re-run and the results show that for aircraft sources, the difference in fuel burn and all emissions except for NOx improved slightly.

Engine Emission Databank (EDB) Coefficients

Both AEDT and EDMS use Emission Indices (EIs) to calculate emission inventory for aircraft and non-aircraft sources. EI is the emissions produced per unit fuel consumed which are available in the ICAO engine emission certification databank (EDB). The EDB is a living DB and the data is continuously updated as new data becomes available. EIs have direct impact on the emission inventory results and it is necessary to compare the EDB coefficients (EIs) between AEDT and EDMS. For each engine, the AEDT Fleet database contains the EIs and fuel flow values corresponding to the standard landing-and-takeoff (LTO) cycle modes, including takeoff, climbout, approach, and idle. The EDB coefficients of AEDT and EDMS were compared. The comparison showed that, for most of the engines the EI values were the same. For some of the engines, however, AEDT and EDMS use very different EIs. This indicates that the difference in EIs contribute to the difference in emissions results produced by AEDT and EDMS.

ANP Coefficients, Flight Profile and Trajectory

Additional AEDT and EDMS assumptions and inputs were also compared, including ANP coefficients and flight profile. Both AEDT and EDMS use the STANDARD flight departure procedure and same ANP coefficients for all the aircraft. The flight trajectories generated by AEDT and EDMS were compared to investigate possible differences in the APM used by AEDT and EDMS. It should be noted that EDMS does not store trajectory information, but EDMS uses the same APM module as INM. Therefore, the trajectory was actually generated by INM when conducting the comparison. The comparison shows that the trajectories were almost identical except that AEDT calculates more segments. This implies that there is no major

difference in the APM between AEDT and EDMS. Thus, ANP coefficients, flight profile and APM did not contribute to the difference in fuel burn and emissions for AEDT and EDMS.

Taxi Time

In the LTO operations, taxi in/out segments are important since these segments contribute approximately 30% of the terminal area fuel consumption. The fuel burn for a taxi segment is calculated by multiplying the taxi time by the fuel flow. In order to compare the fuel burn and emission between AEDT and EDMS, one must make sure both tools use the same taxi time. To investigate the impact of taxi time, one small study was built consisting of six aircraft selected from the study and run through AEDT and EDMS respectively. Identical taxi times were assigned to the operations of the six aircraft, with taxi out time as 19 minutes and taxi in time as 7 minutes. The results showed that even with the same taxi time, for most of the aircraft, the fuel burn and emission results produced by AEDT and EDMS still have large difference which makes it necessary to look into other factors which will be discussed in the following sections.

Aircraft and Operation Type

Another observation that can be drawn from the analysis conducted using the study presented in previous section is that Boeing aircraft showed better agreement in fuel burn and emissions than Airbus aircraft. In addition, fuel burn and emissions calculated for departure operations showed much better agreement than those calculated for arrival operations by AEDT and EDMS. It is shown that the difference in fuel burn and NOx between AEDT and EDMS is very small for Boeing aircraft, especially, for the Boeing 737-300 (2%, 1% for fuel burn and NOx, respectively).

Operation Mode

The aircraft level study discussed in previous section shows that the Airbus 320-200 featured the biggest difference in fuel burn and NOx among the six aircraft. In this analysis a further investigation was conducted to better understand the causes. A single A320-200 flight study was built, consisting of a departure and arrival operation. The study was run in AEDT and EDMS, and the fuel burn results were compared by mode. It was found that AEDT produced much more fuel burn for climb out and approach modes, while EDMS produced more fuel burn for taxi modes. In order to verify this finding, another single flight study was built using Boeing 737-700, and the fuel burn results was compared by mode. The comparison also indicate the same trend as found in the A320-200 single flight study.

Fuel Burn and Emissions Calculation Methods

Based on the analysis in previous section, it can be seen that AEDT and EDMS produce very different fuel burn for each LTO mode. Further investigation was done by reviewing the AEDT and EDMS manuals to understand the methods used for calculating fuel burn and emissions. The methods are summarized in Table 1. It can be seen that except fuel burn, both AEDT and EDMS use the same methods to calculate the emissions (for PM, they both used FOA 3a). AEDT can use three different models for fuel consumption, and EDMS only uses Boeing Fuel Flow Method 2 (BFFM2). Based on the AEDT technical manual, for terminal area modeling, AEDT uses:

- Senzig-Fleming-Iovinelli (SFI) fuel burn model when the proper coefficients are available;
- BADA fuel burn model when coefficients for the SFI fuel burn model are not available;
- BFFM2 when other sources for fuel consumption data are not available or when thrust is not a parameter in the aircraft's performance profile.

.

Table 1: Fuel Burn and Emission Methods Used by AEDT and EDMS

Fuel Burn/Emissions	AEDT	EDMS
Fuel Burn	Senzig-Fleming-Iovinelli (SFI)	BFFM2
	BADA fuel burn model	
	BFFM2	
NOx, HC, and CO	BFFM2	BFFM2
PM	FOA 3.0	FOA 3.0 - Non-US airport
	FOA 3a	FOA 3a - US airport
SOx, CO2	Fuel composition-based factors	Fuel composition-based factors
NMHC, VOC, TOG	Derivative factors	Derivative factors

The mathematical equations of these three methods can be found in the AEDT technical manual [3]. For this study. SFI coefficients were available for all the aircraft, therefore AEDT used the SFI method to calculate the fuel consumption, while EDMS used BFFM2 to calculate the fuel consumption. The use of different fuel consumption models is the main cause that led to the difference in fuel burn between AEDT and EDMS, which sequentially caused the difference in emissions calculated via EIs operating on the per segment fuel consumption.

In AEDT 2b, the thrust setting type, rather than pounds of thrust, is recognized as 'other', and the aircraft that use such thrust setting in AEDT are denoted as TTO aircraft. To further verify this conclusion, a TTO aircraft emission analysis study was conducted. This is a single airport (DULLES airport) study consisting of 119 TTO aircraft, mainly military aircraft. Originally, the fuel burn difference between AEDT and EDMS was found to be about -51%. After the weather, emission indices, ANP coefficients, flight procedure, flight trajectory, and taxi time were matched between the AEDT and EDMS studies, the fuel difference reduced to -5%, as shown in Table 2. Since the study is for TTO aircraft, AEDT uses the same fuel consumption model as EDMS uses – BFFM2. This implies that with all the assumptions and inputs matched, AEDT and EDMS show good agreement on fuel burn and emissions result if they use the same fuel burn methods. It can be seen from Table 2 that the difference in PM results are still big, which is mainly due to that AEDT 2b used FOA3.0 method while EDMS used FOA3.0a method for calculating PM, as indicated in Table 1.

Table 2: Fuel Burn and Emission Comparison with Same Fuel Consumption Method

	Fuel (lb)	CO (lb)	HC (lb)	TOG (lb)	VOC (lb)	NMHC (lb)	NOx (lb)	CO2 (lb)	SOx (lb)	PM 2·5 (lb)	PM 10 (lb)
AEDT 2b	278449	9788	5909	6829	6790	6826	2335	878507	326	77	77
EDMS 5.1.4	293438	10323	6213	7181	7141	7179	2532	925796	379	320	320
Diff	-5.11%	-5.18%	-4.89%	-4.91%	-4.92%	-4.92%	-7.79%	-5.11%	-13.98%	-76.01%	-76.01%

Investigation for Air Quality Modeling

In this section, the causes that led to the differences in emission dispersion between AEDT and EDMS will be investigated. The factors that were investigated include flight tracks, AREA source, and aircraft operations.

Flight Tracks

Different flight tracks can have significant impact on the hourly emission rate and how the emissions are allocated spatially and temporally. Based on the EDMS technical manual, the aircraft flies straight-in and straight-out. Upon investigation of the flight tracks, it was determined that AEDT also uses straight-in/straight-out tracks for the PVD airport in this study. Thus, flight track definition does not contribute to the observed differences in emission concentrations between AEDT and EDMS in this case.

Spatial assignment of emissions

American Meteorological Society (AMS)/United States Environmental Protection Agency (EPA) Regulatory Model (AERMOD) is the module integrated in AEDT that handles the emission dispersion analysis. One of the basic inputs to AERMOD is the source information, such as the source location, size, orientation, etc. The emissions from the AERMOD sources are assigned spatially and temporally, and the respective hourly emissions rates are input to AERMOD for emissions dispersion calculations. Each aircraft operation is associated with respective aircraft movements and consists of a set of the flight segments. The EDMS distributes a flight segment's emissions between one or more rectangular AERMOD area sources while AEDT assigns them typically to square shaped sources. Since the difference in emission dispersion is mainly from aircraft operation, the investigation shifted focus to the spatial assignment of emissions.

After comparing the emissions source assignment data between AEDT and EDMS, it was further found that the area sources are constructed differently in these two tools. In AEDT, the size of ground source and airborne source are defined as 20(m)x20(m) and 200(m)x200(m) respectively, and the orientation angle for these sources are 0 (i.e. the sources align with the X (east) and Y (north) directions). On the other hand, in EDMS the size and orientation of the ground source and airborne source depend on the runways.

The differences in emissions source assignments in AEDT and EDMS lead to the different emission allocation, which is a major contributor to the differences in emission dispersion. Figure 1 shows an example of concentration comparison between AEDT and EDMS at each receptor location. It is the 2nd highest 1-HR average concentration for CO from all sources. It can be seen that the difference in area source definition between AEDT and EDMS has a big impact on the concentration value of the receptors.

In addition, the differences in emissions resulting from the differences in emissions methods, as shown in Table 1, also contribute to these differences in modeled concentrations. Especially the fuel consumption models are different between AEDT and EDMS, as discussed in the Fuel Burn and Emissions Calculation Methods section, and consequently this will contribute to the differences in emissions and emission concentration results.

Aircraft Operation Schedule

The aircraft operation schedule has a big impact on the emission dispersion as well. In this study, both AEDT and EDMS use a fixed random seed value to develop the pseudo-schedule based on the predefined operation profiles. Because of the difference in how flights are handled computationally, AEDT 2b and EDMS do not generate the same exact pseudo-schedule. The number of operations and aircraft types are both the same in the EDMS and AEDT 2b airport studies, but the times at which those aircraft operate will vary between the two models due to the way the random generator for the pseudo-schedule is applied. It is important to note that the overall schedule will follow the assigned operational profiles in AEDT 2b. In addition, due to the differences in the generation of the pseudo-schedule, aircraft operations may take different taxi-paths as well as take-off and land on different runways in the two models. These all are major contributors to the difference in the emission concentrations between AEDT and EDMS.

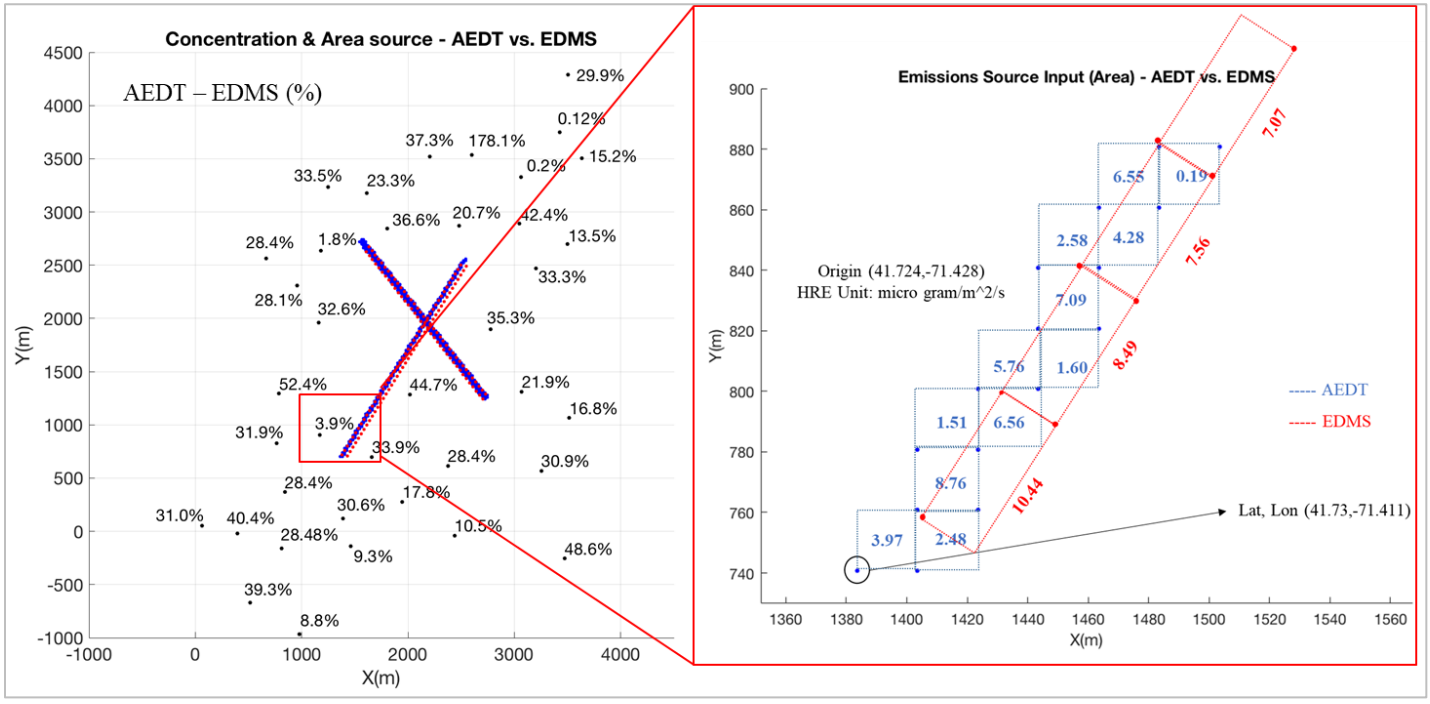

Figure 1: Concentration Comparison between AEDT and EDMS at Each Receptor

The comparison of emissions inventory results showed that there are differences. The differences associated with the emissions inventories are mainly attributed to aircraft sources. The main reason for differences between the aircraft sources is due to the fact that AEDT and EDMS use different fuel consumption models. In addition, there is some difference in the APM that may be causing some additional difference as well. Previous testing and comparisons of AEDT 2b to EDMS at the flight and segment level have shown that AEDT 2b produces higher fuel burn, specifically at climb-out and approach modes. This is aircraft-dependent and is the primary reason why fuel burn, CO2, H2O, SOx, and NOx emissions are higher for AEDT 2b than EDMS. Overall, the fuel burn, CO2, H2O, SOx, NOx, CO, HC, VOC, NMHC, and TOG emissions inventories comparison between AEDT 2b and EDMS show a certain degree of differences given the differences in the fuel burn models used by the two tools. The big difference in PM results mainly from the fact that AEDT doesn't have SN for some engines while EDMS does.

There are also differences between the pollutant concentrations reported by AEDT 2b and EDMS associated with air quality dispersion modeling. Dispersion results vary between EDMS and AEDT 2b due to the different fuel consumption calculated by the two models. Also, the area source size and orientations differ between the two models for ground and airborne sources. The different area sources in AEDT and EDMS lead to the difference in emission assignments for these two tools. Most importantly, operational profiles are utilized to distribute aircraft operations annually on a quarter-hour, daily, and monthly basis. However, due to the difference in how flights are handled computationally compared to EDMS, AEDT 2b and EDMS do not generate the same exact pseudo-schedule. Due to the differences in the generation of the pseudo-schedule, aircraft operations may take different taxi-paths as well as take-off and land on different runways in the two models.

With the exception of PM10 and PM2.5, the differences in pollutant concentrations of CO and NOx between AEDT 2b and EDMS are within an acceptable range. This indicates that the air quality dispersion functionality is operating as intended. The primary cause of any differences in the pollutant concentration results of AEDT 2b and EDMS are associated with fuel consumption models. The PM2.5 and PM10 concentrations mirror what was observed in the emissions inventory. AEDT 2b PM2.5 and PM10 concentrations are consistently lower than the EDMS results, which is partially due to PM values produced by AEDT are lower than EDMS since they used different method. AEDT uses FOA3.0 while EDMS uses FOA3.0a method to calculate PM. An additional analysis was conducted and showed that AEDT and EDMS produced similar PM results when they used the same PM calculation method (FOA3.0).

Comparison of INM and AEDT 2b for Noise Computation Functionality
The purpose of this Use study is to evaluate the capability in AEDT 2b to perform a Part 150 airport noise analysis, and to test other aircraft noise modeling functionality in AEDT 2b. Historically, Part 150 analyses were performed with the legacy INM tool. Since a key requirement for AEDT 2b was to sunset INM, Use Case D includes detailed comparisons between INM 7.0d su1 (the final version of INM) and AEDT 2b, to confirm that AEDT 2b performs as expected for Part 150 studies.

Additional noise-related functionality included in AEDT and INM, but not necessarily used for Part 150 analyses, was also evaluated. Several different airport studies were compared, in order to focus on different noise functionalities in the tools. A comparison of the AEDT 2b and INM 7.0d showed that the models have comparable noise results in most cases, although some differences were noted. GT's role in this study was to investigate the cause of the differences and communicate the findings back to the FAA and the AEDT development team. Each of the following subsections discusses the key causes of differences between INM.

Airport Weather
The default weather data used in AEDT resides in the airport database. Even when an INM study, with user-defined weather data (or even INM default weather data), is imported into AEDT, the AEDT data is utilized unless explicitly edited by the user in AEDT after the importation. Differences in weather data can result in differences in noise levels, even if default atmospheric absorption is used (SAE-AIR-1845). Of particular note is the headwind. INM assumes a default 8 kts headwind, whereas AEDT uses airport-specific headwind data.

One of the Part 150 like studies conducted for the ANC airport revealed the different noise results due to the differences in the weather. ANC was run in both INM 7.0d su1 and AEDT 2b.

Table 3 provides the DNL 55 to 85 dB contour areas from INM and AEDT. For the ANC study with bank angle turned on, the differences between the AEDT 2b and INM DNL contour area results were less than 6.3% for the contour areas of interest (with the difference for the DNL 65 dB DNL contour being 4.5%). A visual comparison of the contour plots in Figure 2 showed that the AEDT 2b and INM contours had similar shapes. At higher noise levels that produce smaller contour areas (e.g., 85 dB DNL), the differences became greater than 10%, but this is attributed to differences in contouring methods and contour resolution.

The observed differences in the noise results between INM and AEDT are caused by a combination of updates to the APM module, airport weather data, aircraft performance data, and different noise grid locations. The average temperature at ANC used in AEDT is much colder than the standard weather used in INM as shown in
Table 4. The ANC study was rerun after modifying the AEDT weather to match the standard weather used in INM. The noise results in Table 5 show much better agreement in DNL contour areas between INM and AEDT with a 1.66% difference for DNL 65 dB.

Table 3. ANC – DNL with Bank Angle Testing Results

Level (dB)	INM (sq km)	AEDT (sq km)	Diff [INM -AEDT] (sq km)	Diff (%)
55	268.233	278.475	-10.242	3.6
60	94.780	101.163	-6.383	6.3
65	43.234	45.291	-2.057	4.5
70	20.246	20.992	-0.746	3.6
75	8.993	9.284	-0.291	3.1
80	3.919	4.069	-0.150	3.7
85	1.295	0.358	0.937	N/A[1]

[1] At higher noise levels that produce smaller contour areas (e.g., 85 dB DNL), the differences between AEDT and INM contours often becomes large (greater than 10-20%). This is attributed to differences in contouring methods and contour resolution. In addition, AEDT does not plot contours that intersect the study boundary, which can be problematic when

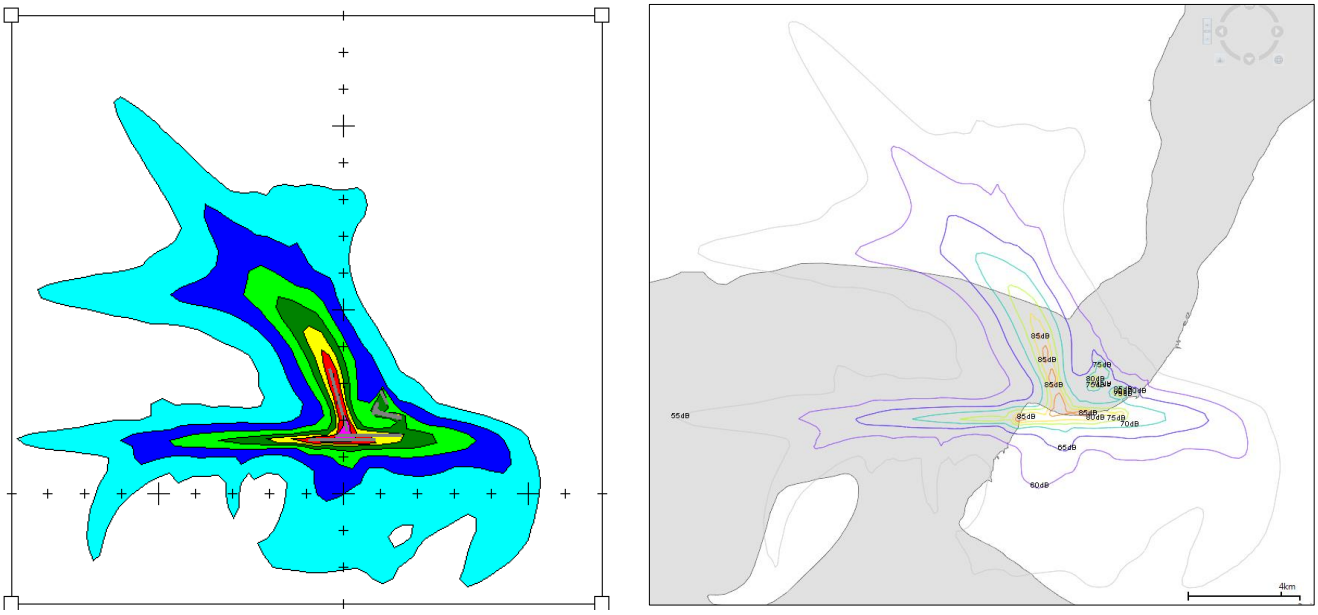

Figure 2. Comparison of the DNL Contours of the ANC Airport between INM (left) and AEDT 2b (right)

Table 4. ANC Annual Average Weather in AEDT 2b vs the Standard Weather in INM

Parameters	AEDT 2b	INM 7.0
Temperature(˚F)	36	59
Pressure (millibars)	1003.05	1013.2
Head Wind (knots)	6.34	8

Table 5. ANC – DNL with Bank Angle Testing Results after Matching the Airport Weather

Level (dB)	INM (sq km)	AEDT (sq km)	Diff [INM -AEDT] (sq km)	Diff (%)
55	268.233	266.021	2.212	-0.83
60	94.78	97.914	-3.134	3.20
65	43.234	43.965	-0.731	1.66
70	20.246	20.257	-0.011	0.05
75	8.993	8.989	0.004	-0.04
80	3.919	3.939	-0.02	0.51

comparing large contour areas (e.g., 55 dB DNL). When these differences became greater than 50%, they were not included in this analysis, and they were earmarked to be revisited in the future, through an investigation of contour/grid resolution.

Contouring Algorithm

JFK was run in both INM 7.0d su1 and AEDT 2b with and without bank angle. All the results with the bank angle are presented in Table 6. For the JFK study with bank angle turned on, the difference between the AEDT 2b and INM DNL contour area results were less than 9.3% for the contour areas of interest (with the difference for the DNL 65 dB contour being 9.3%). However, several contours in AEDT 2b were unrealistically small (DNL 70 and 80 dB). After an investigation, it was found that the unrealistically small contours were caused by a bug in AEDT's contouring algorithm. The AEDT's contouring algorithm was found to work properly most of the time when the contour shapes are relatively simple. However, when contour shapes become complex due to multiple runways and turning tracks, the contouring algorithm could fail to capture all the features of a complex contour such as contour holes and islands. This bug was fixed for the AEDT 2c release.

Table 6. JFK – DNL with Bank Angle Testing Results

Level (dB)	INM (sq km)	AEDT (sq km)	Diff [INM -AEDT] (sq km)	Diff (%)
55	329.804	316.054	13.750	-4.4
60	140.853	140.707	0.146	-0.1
65	49.602	54.670	-5.068	9.3
70	20.426	0.011	20.415	N/A
75	9.644	9.905	-0.261	2.6
80	4.630	0.099	4.531	N/A
85	1.885	1.887	-0.002	0.1

Noise Grid Point Positions

AEDT and INM use slightly different methods for assigning grid point positions in a study. In both INM and AEDT, a set of fixed grids is created by defining the numbers of points being generated to X and Y directions from a reference point and the spaces among the points. The set of generated points forms a flat planar surface, and they are projected down to the Earth's surface to assign the latitude and longitude coordinates to each of the grid points. The X-Y plane of the grids and the Earth's surface make contact at a point, used as the projection origin. INM and AEDT use different projection origins to create this map projection. INM uses the airport origin as the projection origin, whereas AEDT uses the grid origin (the south-west corner of the X-Y plane). This can result in different coordinate locations for what is supposed to represent the same grid point, even if a grid is imported from INM. The differences in the grid coordinate locations don't necessarily impact noise contours as long as the grid resolutions are fine enough. However, care must be made when noise results are compared on a receptor point-by-receptor point basis. An update to AEDT 2c was made to use the airport reference point as the projection origin.

Impact of Enhancement in the APM Module to Noise Results

The flight path segmentation in AEDT and some additional functionalities in the APM are different from the segmentation and performance methods used in INM. This can result in small changes to flight path segment geometry, speed and thrust, which in turn can have small effects on noise levels. Please see Figure 5 in the next section for more details.

Engine Installation Locations

AEDT and INM calculate the directivity in lateral attenuation of noise accounting for engine installation locations for jet aircraft. In INM, the engine installation location values are associated with the spectral class database. Since separate spectral classes were used for approach and departure operations for any given aircraft, there existed the possibility that an aircraft could (incorrectly) have different engine installation directivity adjustments for approach and departure operations. This issue was resolved in AEDT with decoupling of engine installation location and spectral class. Therefore, only a single engine installation location is referenced for each aircraft, and therefore the same engine installation directivity adjustment is guaranteed to be used for approach and departure operations in AEDT 2b. However, this means that engine installation location value for several aircraft in the test cases used in this study are not consistent between AEDT and INM. Implications of the differences in engine installation locations are discussed in this section.

The different engine installation directivity adjustments are presented in Figure 3. Since separate spectral classes were used for approach and departure operations for any given aircraft, there existed the possibility that an aircraft could

(incorrectly) have different engine installation directivity adjustments for approach and departure operations. If the incorrect engine installation location was assigned to an aircraft, the result could be a noise level difference of up to 1.9 dB, depending on the elevation angle.

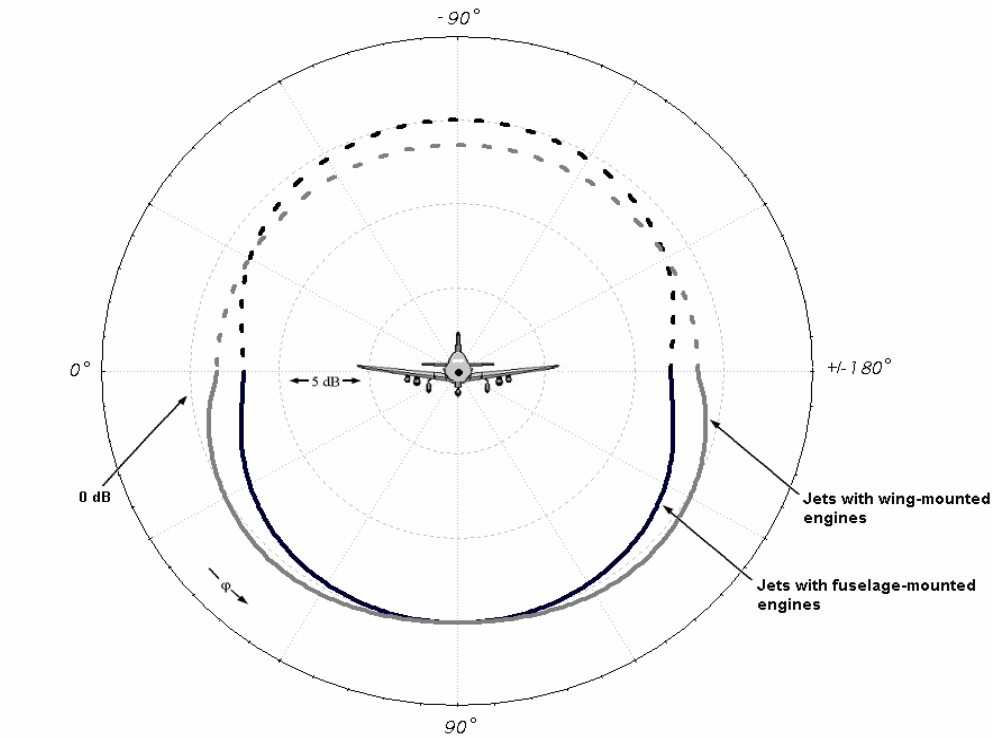

Figure 3. Illustration of Engine-Installation Effects for Jet-Powered Airplanes

This issue was resolved in AEDT with the decoupling of engine installation location and spectral class. Therefore, only a single engine installation location is referenced for each aircraft, and therefore the same engine installation directivity adjustment is guaranteed to be used for approach and departure operations in AEDT 2b. However, this means that several aircraft in the test cases used for AEDT UQ Use Case D do exhibit this issue. Those aircraft are listed in Table 7. As listed in the table, 26 INM aircraft types had different engine locations from the corresponding AEDT aircraft for either or both departures and arrivals. While AEDT corrected the inconsistent engine installation locations of the INM aircraft, the process also introduced errors in AEDT engine installation locations for some aircraft. INM aircraft 727100, 727EM1, 727Q15, 727Q7, and 727QF are Boeing 727-100 and 727-200 with various engine models. In INM, the engine locations of all of the Boeing 727s are correctly assigned as fuselage mounted. However, in AEDT, the engines of the corresponding aircraft types are incorrectly assigned as wing mounted.

Table 7. Aircraft with Engine Installation Location Differences in INM vs. AEDT

INM AIRCRAFT ID	AIRCRAFT DESCRIPTION	INM Eng. Location for Arrivals	INM Eng. Location for Departures	AEDT Eng. Location	Is AEDT Correct?
737	Boeing 737/JT8D-9	Fuselage	Wing	Wing	YES
717200	Boeing 717-200/BR 715	Wing	Fuselage	Fuselage	YES
727100	Boeing 727-100/JT8D-7	Fuselage	Fuselage	Wing	NO
727EM1	FEDX 727-100/JT8D-7	Fuselage	Fuselage	Wing	NO
727Q15	Boeing 727-200/JT8D-15QN	Fuselage	Fuselage	Wing	NO
727Q7	Boeing 727-100/JT8D-7QN	Fuselage	Fuselage	Wing	NO
727QF	UPS 727100 22C 25C	Fuselage	Fuselage	Wing	NO
737D17	Boeing 737-200/JT8D-17	Fuselage	Wing	Wing	YES
737QN	Boeing 737/JT8D-9QN	Fuselage	Wing	Wing	YES
CNA510	Cessna Mustang Model 510 / PW615F	Wing	Fuselage	Fuselage	YES
CNA55B	Cessna 550 Citation Bravo / PW530A	Wing	Fuselage	Fuselage	YES
CNA750	Citation X / Rolls Royce Allison AE3007C	Wing	Fuselage	Fuselage	YES
ECLIPSE500	Eclipse 500 / PW610F	Fuselage	Wing	Fuselage	YES
EMB170	ERJ170-100	Fuselage	Fuselage	Wing	YES
EMB175	ERJ170-200	Fuselage	Fuselage	Wing	YES
FAL20	FALCON 20/CF700-2D-2	Wing	Fuselage	Fuselage	YES
GIV	Gulfstream GIV-SP/TAY 611-8	Wing	Fuselage	Fuselage	YES
GV	Gulfstream GV/BR 710	Wing	Fuselage	Fuselage	YES
LEAR25	LEAR 25/CJ610-8	Wing	Fuselage	Fuselage	YES
MD81	MD-81/JT8D-217	Wing	Fuselage	Fuselage	YES
MD82	MD-82/JT8D-217A	Wing	Fuselage	Fuselage	YES
MD83	MD-83/JT8D-219	Wing	Fuselage	Fuselage	YES
MD9025	MD-90/V2525-D5	Wing	Fuselage	Fuselage	YES
MD9028	MD-90/V2528-D5	Wing	Fuselage	Fuselage	YES
MU3001	MU300-10/JT15D-5	Wing	Fuselage	Fuselage	YES
SABR80	NA SABRELINER 80	Wing	Fuselage	Fuselage	YES

In order to assess the noise impacts due to the changes in engine installation locations from INM to AEDT, SEL contour areas from single flight operations of a couple of aircraft types were compared. Five aircraft types of 737QN, MD81, SABR80, 727Q15, and 727Q7 were flown individually at the SFO airport in both INM and AEDT. For 737QN, MD81, and SABR80, the engine locations for the arrivals were incorrectly assigned in INM and were fixed in AEDT. Table 8, Table 9, and Table 10 provide comparisons of SEL contour areas of these three aircraft types between INM and AEDT. For 737QN, MD81, and SABR80, the differences in SEL contour areas were small for most dB levels. The tests showed that changes in engine installation locations for these three aircraft did not have a significant impact on noise results.

Table 8. SEL Contour Areas at SFO from a Single 737QN Arrival Flight

Level (dB)	INM (sq km)	AEDT (sq km)	Diff [INM -AEDT] (sq km)	Diff (%)
75	25.869	25.805	0.064	0.25
80	11.859	11.793	0.066	0.56
85	4.335	4.253	0.082	1.93
90	1.141	1.051	0.09	8.56

Table 9. SEL Contour Areas at SFO from a Single MD81 Arrival Flight

Level (dB)	INM (sq km)	AEDT (sq km)	Diff [INM -AEDT] (sq km)	Diff (%)
75	14.593	14.461	0.132	0.91
80	4.092	4.005	0.087	2.17
85	0.87	0.911	-0.041	-4.50
90	0.326	0.296	0.03	10.14

Table 10. SEL Contour Areas at SFO from a Single SABR80 Arrival Flight

Level (dB)	INM (sq km)	AEDT (sq km)	Diff [INM -AEDT] (sq km)	Diff (%)
75	18.095	18.062	0.033	0.18
80	8.886	9.02	-0.134	-1.49
85	4.276	4.291	-0.015	-0.35
90	1.63	1.604	0.026	1.62

On the other hand, the test results for 727Q15 in for an arrival and in Table 12 for a departure flight showed from 12% up to 20% differences in SEL contour areas. For both the departure and arrival cases, AEDT showed greater contour areas for all dB levels. Table 13 and Table 14 provide the LAMAX contour areas from a 727Q15 arrival and a departure flight at SFO. Similar to the SEL results, AEDT had about 13% greater contour areas for all dB levels. Figure 4 shows the SEL noise contours from a 727Q15 arrival at SFO calculated from INM and AEDT. Visual inspection of the contours from 70 to 95 dB reveals that the contours from AEDT (red) are larger than the contours from INM (blue), while the general shapes are very similar.

Table 11. SEL Contour Areas at SFO from a Single 727Q15 Arrival Flight

Level (dB)	INM (sq km)	AEDT (sq km)	Diff [INM -AEDT] (sq km)	Diff (%)
75	34.33	40.59	-6.26	-15.42
80	16.15	19.14	-2.99	-15.62
85	7.08	8.59	-1.51	-17.58
90	2.86	3.57	-0.71	-19.89

Table 12. SEL Contour Areas at SFO from a Single 727Q15 Departure Flight

Level (dB)	INM (sq km)	AEDT (sq km)	Diff [INM -AEDT] (sq km)	Diff (%)
75	304.91	346.36	-41.45	-11.97
80	194.32	223.75	-29.42	-13.15
85	96.81	114.96	-18.15	-15.79
90	39.44	46.99	-7.55	-16.07

Table 13. LAMAX Contour Areas at SFO from a Single 727Q15 Arrival Flight

Level (dB)	INM (sq km)	AEDT (sq km)	Diff [INM -AEDT] (sq km)	Diff (%)
75	8.4	9.71	-6.26	-13.49
80	4.36	5.06	-2.99	-13.83
85	2.06	2.4	-1.51	-14.17
90	0.92	1.07	-0.71	-14.02
95	0.4	0.46	-0.21	-13.04

Table 14. LAMAX Contour Areas at SFO from a Single 727Q15 Departure Flight

Level (dB)	INM (sq km)	AEDT (sq km)	Diff [INM -AEDT] (sq km)	Diff (%)
75	74.41	85.6	-6.26	-13.07
80	36.16	41.86	-2.99	-13.62
85	17.32	20.03	-1.51	-13.53
90	9.41	10.85	-0.71	-13.27
95	5.76	6.64	-0.21	-13.25

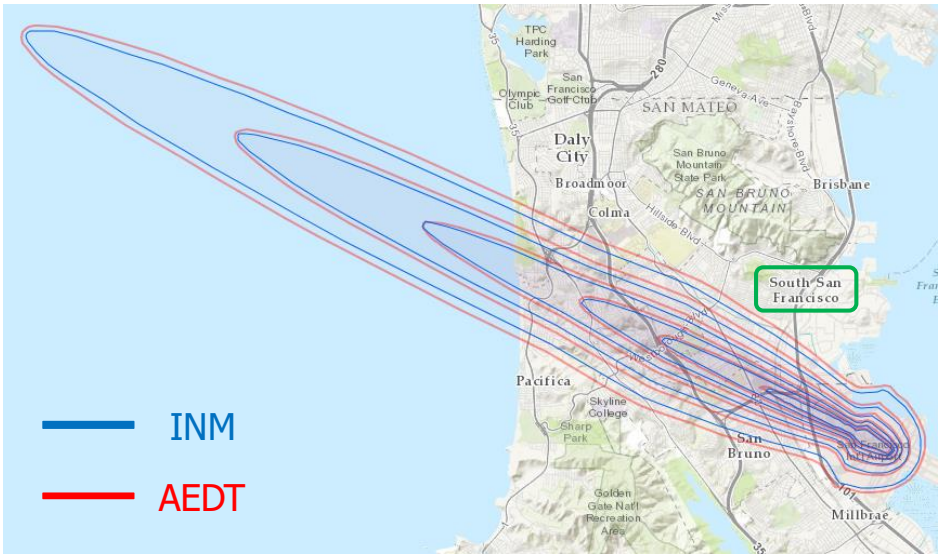

Figure 4. SEL Contour Comparisons for a 727Q15 Single Arrival Flight

To confirm that the differences in noise results are due to the different engine installation locations, a series of investigations were conducted. First, all the ANP coefficients of 727Q15 including aircraft performance characteristics, departure procedures, and NPD curves were compared and confirmed that they were all exactly the same. The INM and AEDT studies were set up at the SFO airport using the same airport weather, runway, flight track, and noise grid definitions. To see if differences in the APM were responsible for differences in the noise results, flight tracks from INM and AEDT were compared as well. Figure 5 shows comparisons of flight trajectories and thrust profiles from INM and AEDT. Both the altitude and thrust against ground distance profiles from INM and AEDT show a very close match to each other. The AEDT flight path had slightly more segments than the flight path from INM, which can improve accuracy of noise calculations. However, the differences in noise results due to the increased number of flight segments are less than 1%. Finally, the engine installation location of 727Q15 was temporarily corrected in AEDT's fleet database to accurately model the installation effect. After changing the engine location from wing to fuselage for 727Q15 in AEDT, the arrival and departure SEL 70 to 90 dB contour areas matched the INM results with less than 0.5% differences for all dB levels. This series of tests confirmed that the differences in noise results between 727Q15 between INM and AEDT were driven by the different engine installation locations.

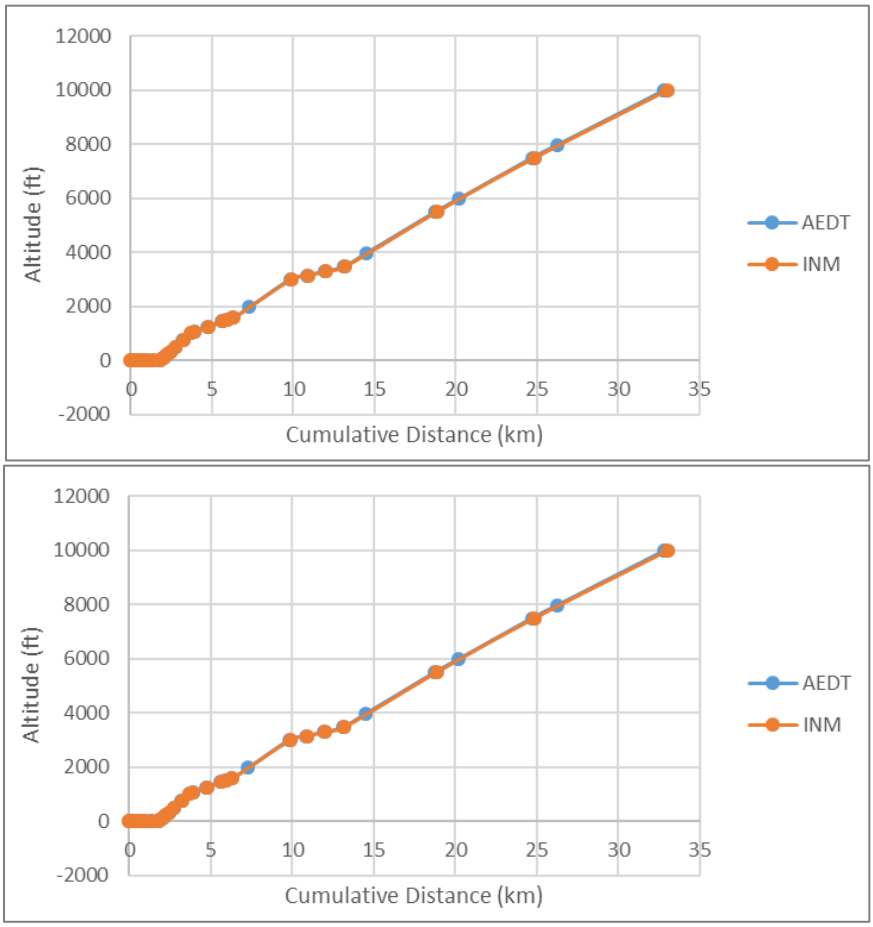

Figure 5. Comparison of Flight Trajectories and Thrust Profiles of a 727Q15 Departure from INM and AEDT

An additional test result is provided here to show the differences in the noise results when the engine locations between INM and AEDT are the same. 727D17 and 727Q9 are other Boeing 727 aircraft with different engine models than the 727Q15. For these two ANP aircraft, the engine locations are correctly assigned as fuselage in both INM and AEDT. Figure 6 depicts the SEL 70 to 95 dB contours for a 727D17 arrival from INM and AEDT. Table 15 compares the contour areas for the corresponding contours. The test results show that a model of 727-200 with consistent engine location can produce very similar noise results between INM and AEDT with less than 1% difference for all the SEL levels compared. The incorrect engine installation locations found in AEDT 2b have been fixed in the AEDT 2d release.

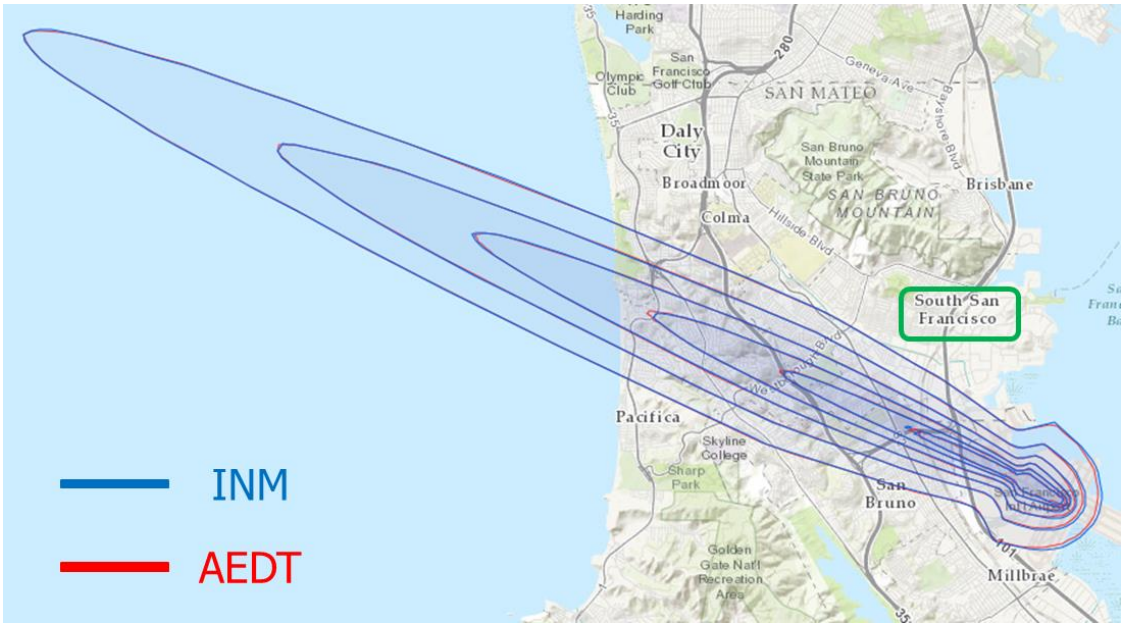

Figure 6. SEL Contour Comparisons for a 727D17 Single Arrival Flight

Table 15. SEL Contour Comparisons for a 727D17 Single Arrival Flight

Level (dB)	INM (sq km)	AEDT (sq km)	Diff [INM -AEDT] (sq km)	Diff (%)
70	71.387	70.972	0.415	0.58
75	36.644	36.431	0.213	0.58
80	18.023	17.905	0.118	0.66
85	7.881	7.882	-0.001	-0.01
90	2.983	2.957	0.026	0.88
95	0.87	0.862	0.008	0.93

Update to AEDT's Aircraft Performance and Noise Database (FLEET DB)

Updates to AEDT's aircraft performance and noise database can lead to different noise results. The AEDT's fleet database are constantly updated in order to incorporate the best available information. Since the INM database does not receive the same updates, improvements in the AEDT database can lead to differences in aircraft performance data (ANP coefficients) and noise data (NPD curves) between AEDT and INM.

Noise from Helicopter Taxi Operation

UCD-Helis is a simple airport study with helicopter operations that includes taxi operations. The study was run in both INM 7.0d su1 and AEDT 2b with bank angle. It should be noted that although UCD-Helis focuses on modeling helicopter operations, not all helicopters nor all helicopter profiles in the AEDT Fleet database were included in this analysis. This analysis is meant to check the noise computation functionality related to helicopters in AEDT, and not specifically review the contents of the AEDT 2b databases. The DNL noise results from INM and AEDT are compared in Table **16**.

Table 16. UCD-Helis – DNL with Bank Angle Phase 2 Testing Results

Level (dB)	INM (sq km)	AEDT (sq km)	Diff [INM -AEDT] (sq km)	Diff (%)
55	175.579	176.575	-0.996	0.6
60	81.555	82.447	-0.892	1.1
65	4.278	5.008	-0.730	14.6
70	0.585	0.583	0.002	-0.3
75	0.237	0.237	0.000	-0.2
80	0.097	0.101	-0.004	4.0
85	0.036	0.033	0.003	-8.3

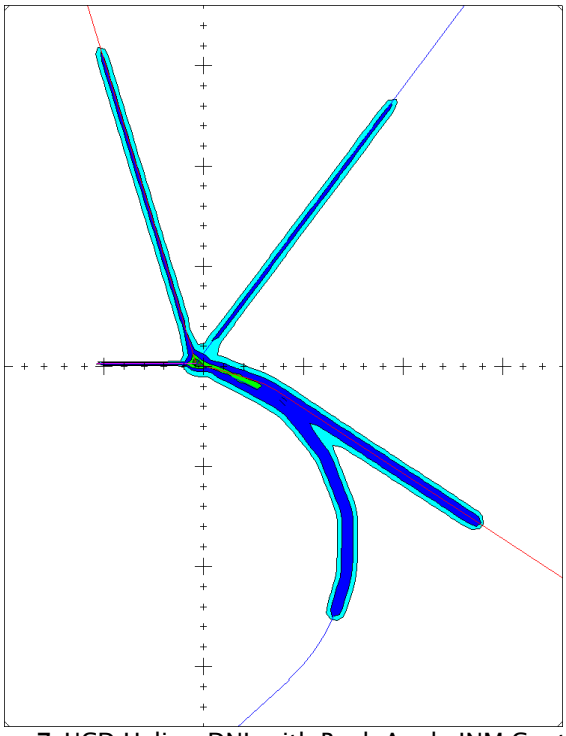

Figure 7. UCD-Helis – DNL with Bank Angle INM Contours

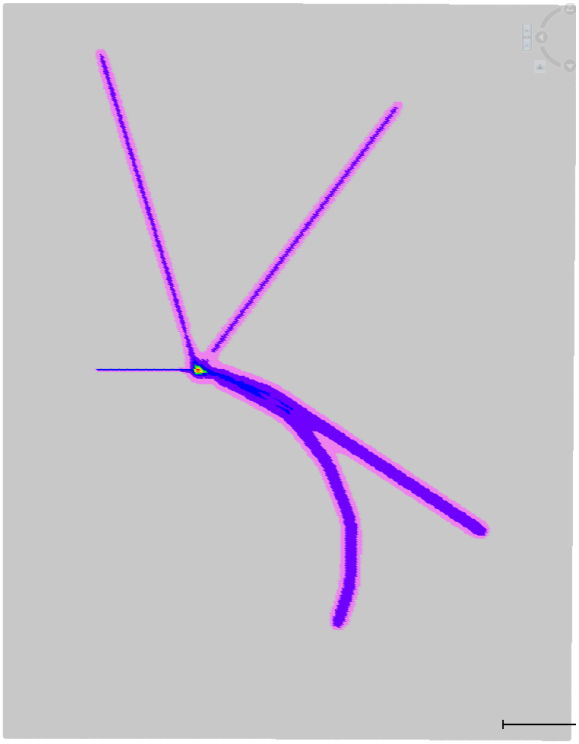

Figure 8. UCD-Helis – DNL with Bank Angle AEDT 2b Contours

For UCD-Helis, the differences between the AEDT 2b and INM DNL contour area results were less than 14.6% for the contour areas of interest. The 65 dB DNL contour results showed a difference of 14.6% between INM and AEDT 2b, and shows the largest contour area difference for this study. A visual comparison of the contour plots showed that the AEDT 2b and INM contours have similar shapes except for one small 65 dB DNL contour island.

After an investigation, a couple of reasons were identified to have caused the differences in the noise results. First, the update to the AEDT airport weather database caused differences in the results. While INM used the standard atmosphere, AEDT used the annual average weather at the Central Wisconsin airport. The annual average temperature at the Central Wisconsin airport was 43 degrees Fahrenheit. In addition, the differences in the noise grid locations combined with insufficient grid resolution have also contributed to the differences in the noise results. As mentioned in a previous section, differences in noise grid location due to different grid map projection methods in INM and AEDT 2b do not necessarily cause differences in contour areas as long as the grid resolution is fine enough. The spacing of the grid points used in the initial analysis was 0.8 nm, which is sufficient for a typical airport noise study. However, since the UCD study had a small number of helicopter operations, a finer resolution was necessary. Therefore, the study was rerun after updating the airport weather in INM and decreasing the grid spacing to 0.2 nm from 0.8 nm. The updated results are presented in Table 17. The differences in contour areas decreased after rerunning the study except for 70 and 75 dB. Visual inspection of the updated contour plots showed that differences in the small westerly contour lobe caused these contour areas differences. Figure 9 provides comparisons of the westerly lobe between INM and AEDT. This westerly lobe is due to a taxi operation of a Bell 212 helicopter. INM correctly modeled this taxi operation using a taxi track and a taxi procedure. However, AEDT modeled this operation as a departure operation while using the same taxi track. Assigning an incorrect operation type in AEDT caused the Bell 212 to use the maximum takeoff thrust instead of the idle thrust for this taxi operation. This bug in AEDT caused greater DNL 70 and 75 dB areas. This issue was reported to the AEDT development team and was resolved in the AEDT 2d release.

Table 17. UCD-Helis – DNL with Bank Angle Phase 2 Testing Results after matching the Weather and increasing Grid Resolution

Level (dB)	INM (sq km)	AEDT (sq km)	Diff [INM -AEDT] (sq km)	Diff (%)
55	176.509	176.264	0.245	-0.1
60	83.432	83.336	0.096	-0.1
65	5.959	5.889	0.07	-1.2
70	1.033	1.097	-0.064	5.8
75	0.248	0.449	-0.201	44.8
80	0.108	0.105	0.003	-2.9
85	0.047	0.045	0.002	-4.4

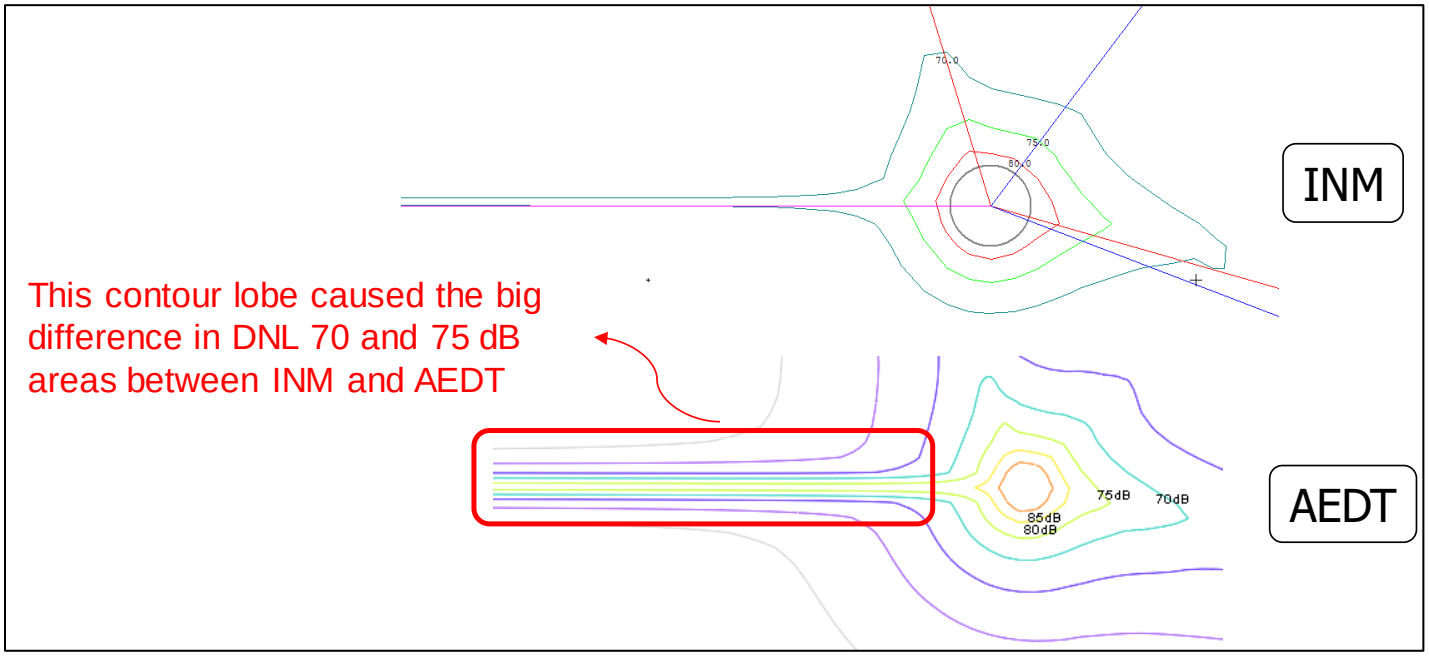

Figure 9. UCD-Helis – DNL with Bank Angle AEDT 2b Contours

Task #2: Validation and Verification of BADA4 Implementation

Georgia Institute of Technology

Objective(s)

The FAA has incorporated BADA4 as part of the AEDT Fleet DB. This task focuses on a fleet wide environmental V&V effort to assess the implications of BADA4 from the historical Fleet DB. GT will ensure that the BADA4 algorithm and associated data are properly incorporated into AEDT by performing investigation at flight segment, entire flight, and airport level tests. The BADA4 performance results will be compared to the results using ANP model for terminal area operations. The

BADA4 performance results will be compared to the results using BADA3 for en-route operations. The environmental impacts that is fuel burn, emission, and noise results, using BADA4 will be compared to the results from using BADA3, ANP, and Senzig-Fleming-Iovinelli (SFI) methods.

Research Approach

Sensor Path Flight in BADA4

Base of Aircraft Data Family 3 (BADA3) method has been widely used for aircraft performance and fuel consumption in AEDT. Although BADA3 works well in the cruise region, it is well known that BADA3 is not optimized for terminal area operations. For this reason, AEDT uses BADA3 for an altitude above 10,000 feet and Aircraft Noise and Performance (ANP) method for an altitude below 10,000 feet.

In order to address the drawbacks of BADA3 in the terminal area, the high fidelity Base of Aircraft Data Family 4 (BADA4) has been developed. Currently in AEDT, BADA4 model only works for the sensor-path flights which is based on trajectory-driven flight performance. To understand how AEDT models sensor path flights, AEDT related documents were reviewed to determine how to create a sensor-path flight study in AEDT by the method shown in Figure 10.

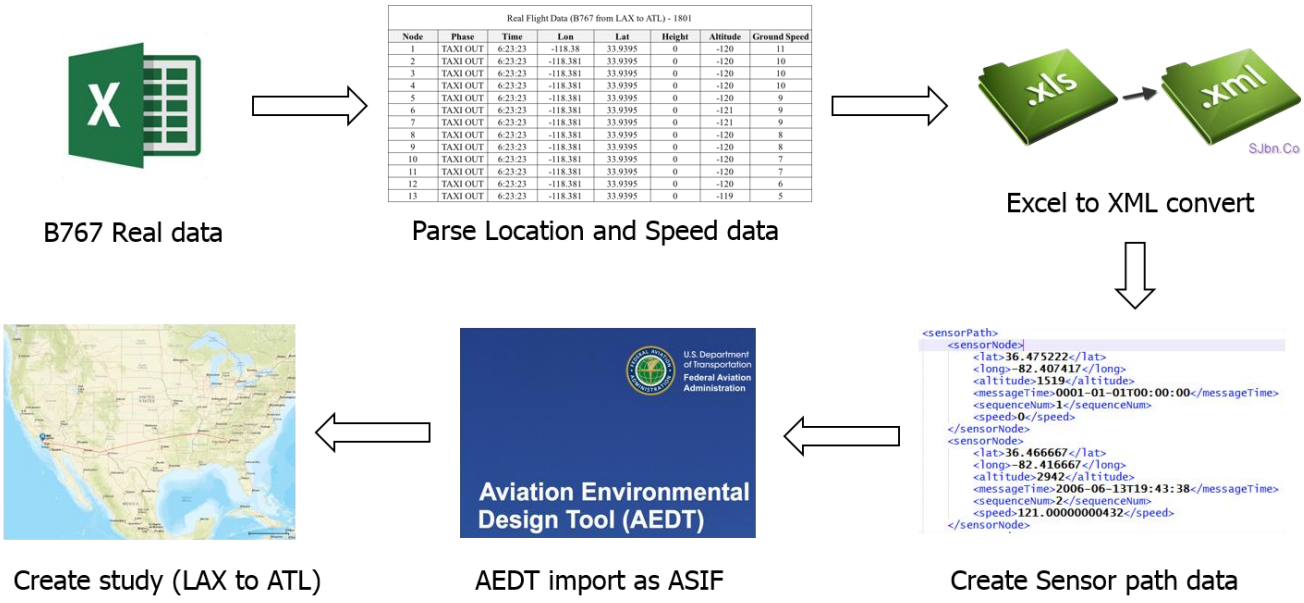

Figure 10: Pre-processing for ASIF import into AEDT

As can be seen in Figure 10, a few important parameters for creating a sensor path in AEDT from a flight data recorder (FDR) data of B767 were parsed as the first step. Using those parameters, a table in Excel was generated and converted into an XML file. The sensor nodes created from the table were combined into the sensor path for the case study. For the next step, the sensor path file was imported into AEDT with ASIF import option. Finally, a study was created in AEDT which was a flight from Los Angeles International Airport (LAX) to Hartsfield-Jackson Atlanta International Airport (ATL). In terms of the runway assignment defined in the sensor path, the location information from the FDR data was investigated to assign a proper runway for both departure and arrival. After the flight track was created in AEDT, the ANP 767300 aircraft was chosen to compare with FDR data with respect to fuel consumption.

In order to model the study as exact as possible, the take-off weight for AEDT was changed to match with the FDR data. Additionally, the Modern-Era Retrospective analysis for Research and Application version 2 (MERRA-2) was used as AEDT's high-fidelity weather model. Lastly, smoothing and filtering of the data was performed to create the sensor path.

Investigation of BADA4 APM (by comparing with BADA3 and FDR data)

In this task, a validation and verification study was conducted to investigate the implementation of BADA4 performance model in AEDT. The BADA4 results were compared against FDR data tabulated as below. In order to protect the flight identity, the exact aircraft variant and day of the flight are not included. Four different cases were created in order to estimate important factors for accurate simulation results. For example, case 4 represents the result for the simulation setup which used SPI tool for data smoothing and filtering, MERRA-2 as high-fidelity weather, and real takeoff weight to reduce the gap between FDR and AEDT data. In terms of the results of fuel burn, AEDT provided the results for all test cases and fuel burn for FDR was calculated from the FDR fuel burn data. For case 4, as can be seen, the difference between FDR and BADA4 implementation on AEDT is 7.6%. This comparison shows the importance of data filtering, takeoff weight, and hi-fidelity weather required for accurate fuel consumption prediction in AEDT.

Table 18: Fuel consumption comparison (BADA4 vs. FDR)

	SPI	Weight	MERRA-2	Fuel Burn (kg)	Difference
FDR				19,182	N/A
Case 1				18,576	- 3.2 %
Case 2	Y			18,547	- 3.3 %
Case 3	Y	Y		21,393	11.5 %
Case 4	Y	Y	Y	20,642	7.6 %

In order to compare the FDR thrust data with AEDT, the location data with latitude and longitude was converted into a distance because the FDR data didn't have cumulative distance information. The result of the comparison between BADA3, BADA4, and FDR with respect to net corrected thrust versus cumulative distance is shown below.

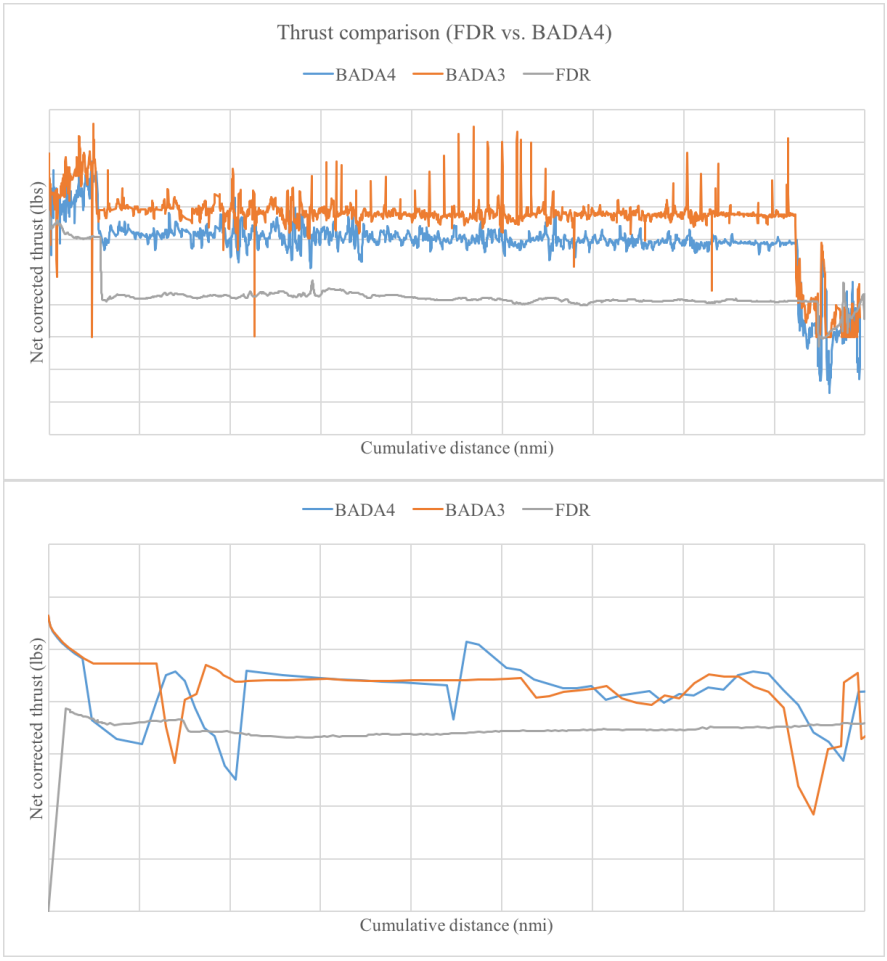

Figure 11: Net corrected thrust (per engine) vs. Cumulative distance (BADA3 vs. BADA4 vs. FDR)

In Figure 11, BADA4 was more exact than BADA3 compared to the FDR data under same conditions such as same flight track and aircraft. However, it was also found that the terminal area for both departure and arrival was quite different between BADA and FDR data. The reason why there was a discrepancy will be further investigated by using high fidelity validation data in the near future.

Thrust vs N1 Analysis

In order to compare the results of AEDT with real world data, FDR data was obtained. This data is available in a tabular format and contained detailed information from the aircraft's sensors including the phase of the flight, time, position, engine parameters, aircraft control inputs, wind and weather data. The time resolution of the data is once per second. The only information available is the aircraft type and the origin-destination airports.

Although the FDR data includes a lot of detailed parameters, it does not include any direct measure of thrust. Thrust is one of the most important parameters that affects noise and emissions. When comparing BADA3 or BADA4 to FDR data, matching the thrust is imperative to ensure a match of real world emissions and noise footprint. Therefore, methods for obtaining thrust from the available parameters in the FDR data were investigated. The available engine parameters are fuel flow and fan rotation speed for each engine.

A method to estimate thrust from corrected fan speed, altitude and temperature is included in INM 7.0 Technical Manual. The formulation, known as the General Thrust equation is given as

$$\frac{F_n}{\delta} = E + FV_c + G_aA + G_bA^2 + HT + K_2(N1_c) + K_3(N1_c)^2 \quad (1)$$

$$N1_c = \frac{N1}{\sqrt{\theta}}$$

Where

$N1$ is proportional to the engine's fan rotation speed and is measured in percentage
θ is the temperature ratio
$N1_c$ is the corrected measure of the engine's fan rotation speed in percentage
$\frac{F_n}{\delta}$ is the net corrected thrust
V_c is the speed of the airplane
A is the altitude
T is the temperature
$E, F, G_a, G_b, H, K_2, K_3$ are all engine/aircraft specific coefficients

Given the coefficients and the operating conditions, the net corrected thrust was obtained using the formulations above. The INM manual includes the coefficients for 27 aircraft. A comparative visualization of the thrust dependence on engine fan speed is shown in Figure 12. It was observed that the dependence is mostly linear ($R^2 = 99.5\%$) with all aircraft reaching full thrust at 100% fan speed as expected. The different coefficients for each aircraft lead to different slopes. It is important to note that Figure 12 is based on sea-level and static conditions. For each of the aircraft, $V_c = 0$ and $A = 0$ in the formulation above.

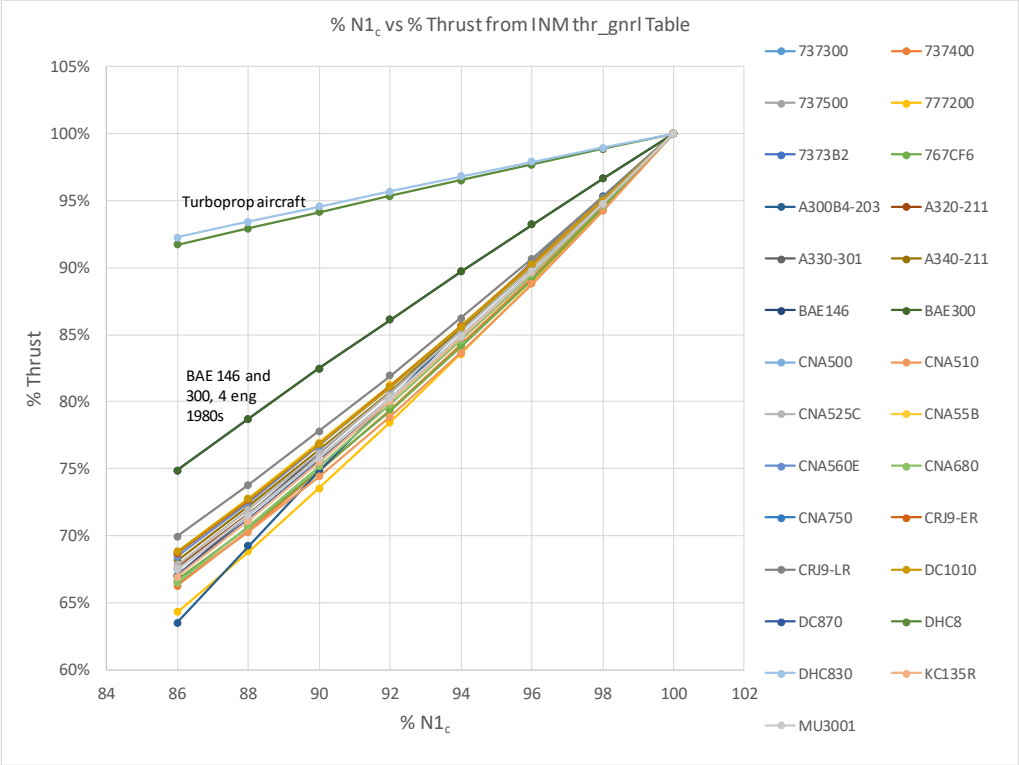

Figure 12: Thrust dependence on engine fan rotational speed, sea-level static conditions

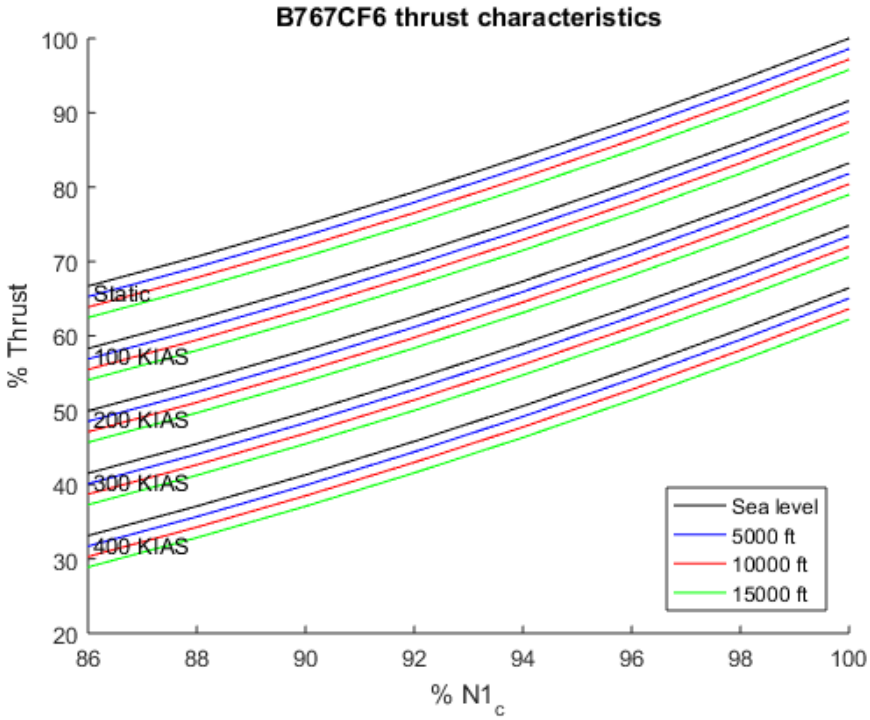

Figure 13: Thrust dependence on fan rotational speed, varying speed and altitude

In order to study the dependency on altitude and speed, the same formulation was applied to a single aircraft (B767CF6 in the ANP database) with a number of combinations of speed and altitude. The results are depicted in Figure 13. It was observed that the general shape of the curve remains the same. The effect of speed and altitude is to shift the curve up or down. Each color represents a particular altitude. The five distinct sets of 4 lines represent different airspeeds measured in KIAS (Knots, Indicated Air Speed). In order to estimate the net corrected thrust, we need to identify the aircraft's indicated airspeed and the altitude it is flying at. An increase in either altitude or speed shifts the curve downwards. This indicates a lower thrust for the same fan rotation speed if the speed or altitude is higher which is as expected.

Since the FDR has altitude and speed data included, the formula to calculate the thrust could be directly used for each engine at every point in the flight. For comparison, the average of the thrust from the two engines was used.

In this situation, coefficients were readily available for the aircraft in question. This may not always be the case and a more general method to estimate thrust may be required in the future. One way to work around this is to exploit the linearity of the thrust dependence. Eliminating the outliers and fitting a linear model across all jet aircraft types in Figure 12 one can obtain a method to estimate the thrust for any modern jet aircraft at a sea level static condition. The results are shown in Figure 14. While this model only holds for a sea-level static condition, it can be extended in a similar way to include varying speed and altitude conditions as well.

There is a limitation to this formulation. The technical manual for INM 7.0 states that the General Thrust coefficients should be valid up to 16,000 ft. The same coefficients have been used throughout the flight and hence the calculated thrust may not be valid at higher altitudes, particularly for cruise.

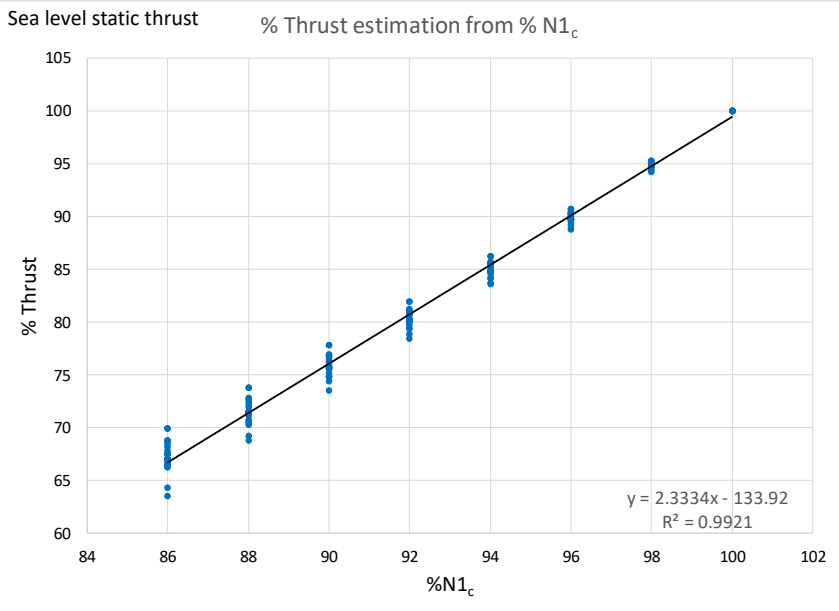

Figure 14: Linear model of thrust dependence on engine fan rotational speed, sea-level static condition

Task #3: Capability Demonstration and Validation of AEDT 2c and 2d Functionality

Georgia Institute of Technology

Objective(s)

For each of the AEDT 2c and 2d service pack releases, the scope of the UQ effort identifying the key changes to the AEDT versions from the previous releases was formulated. Depending on the type of updates incorporated, it would be necessary to identify the key sources of uncertainties and the best approach to conduct V&V and parametric uncertainty analysis. Depending on the analysis scope of the V&V, Parametric UQ can be optional. The outcome of this task is the definition of analysis scope, required tools, required data, V&V method, Parametric UQ method, and a list of input parameters to vary and their uncertainty bounds. Due to the dynamic nature of the agile AEDT development process, it is important that the research team remains flexible in the choice of the V&V approach and the work scope. The best available methods and data will be used in order to ensure accuracy and functionalities of future AEDT versions based on the discussion with the FAA/AEE.

A V&V and capability demonstration was conducted of the newly released AEDT versions. The analysis in this task can take a couple of different approaches depending on the type of updates and data availability. In the past UQ efforts, one of the most important methods of ensuring confidence in the tool capability was to conduct a use case(s) using both legacy tools and the new AEDT release and compare the results. This method would be the most appropriate way whenever a legacy tool has the same or similar functionalities and a validated use case has been modeled in that legacy tool. When the new functionality of AEDT does not exist in the legacy tools, the V&V exercise should use direct comparisons to the results generated by the mathematical algorithms behind the newly added functionality and/or real world data whichever available.

Research Approach

In order to provide the best possible environmental impacts modeling capabilities, the FAA/AEE continues to develop AEDT by improving existing modeling methods and data and adding new functionalities. The AEDT development team led by Volpe has been exercising the agile development process, as shown in Figure 15, where minor updates are released in a new Sprint version every three weeks. Major updates and/or new functionalities are incorporated as new service packs or

feature packs in about a three months cycles as shown in Figure 15. An AEDT development cycle includes rigorous testing of all levels of software functionality from the individual modules to the overall system. However, the FAA/AEE seeks a robust uncertainty quantification effort in addition to this test program.

Figure 15: The Agile Methodology [Source: http://www.screenmedia.co.uk]

Table 19: AEDT Development and Public Release Schedule

Dates	Milestones
5/1/2016	Project Start
6/13/2016	AEDT 2b SP3 Release
9/12/2016	AEDT 2c Release
12/5/2016	AEDT 2c SP1 Release
3/13/2017	AEDT 2c SP2 Release
9/27/2017	AEDT 2d Release
3/2018	AEDT 2e Release
7/30/2018	Project End

For each of the AEDT version and service pack releases, GT reviewed the AEDT requirement documents and AEDT release notes to identify the key features and functionalities that need to be tested. During the period of January 2017 to October 2017, two public version of AEDT were released – including AEDT 2c SP2, and AEDT 2d, as listed in Table 19.

The main features/capabilities that were added to AEDT during the period include the following:

- Enhanced nvPM
- VALE Reporting with MOVES
- Runup Operation of Military Aircraft
- Open Contours
- Vector Tracks
- Track Dispersion
- Contour Combination
- Dynamic Grid
- Detailed Noise
- Bulk Operation Creation

The V&V and capability demonstration of the new features listed above are either completed or in progress.
Starting from January 2017, all the new AEDT sprint releases including Sprints from 80 to 94 have been tested. Sprints 80 – 94 included two public releases of AEDT, namely AEDT 2c SP2, and AEDT 2d. Fifteen sprint releases of AEDT focusing on new features and capabilities added have also been tested. Some of the new features/capabilities were minor updates to

the GUI, bug fixes or data updates. Major updates included enhanced nvPM, VALE reporting with MOVES, runup operation of military aircraft, open contours, vector tracks, track dispersion, contour combination, dynamic grid, detailed noise and bulk operation creation.

In order to understand the background of new AEDT features, the relevant documents were reviewed including the software requirement documents, Database Design Documents (DDD), AEDT sprint release notes, updated technical manual [8, 9], user manual [10, 11], and research papers/reports [12-15]. Basic testing of all the new AEDT versions to confirm its functionality have been performed. While some of the tests are in progress, the next subsections discuss the current progress and findings in more details.

Enhanced nvPM

Currently, the enhanced nvPM is a hidden feature that needs to be activated in the debug mode or using a hash key. In the enhanced nvPM capability implemented for AEDT 2c and 2d, the correlation options are implemented for estimating nvPM mass and number. And a new modeling methodology for estimating cruise nvPM mass and number is utilized based on CAEP's guidance. In addition, the nvPM system loss correction method for assessing particle losses that occur in the sampling system that measures the nvPM mass and number at the end of the sampling system is also implemented as one part of the enhanced nvPM features.

In the current implementation, there are four enhanced nvPM methods in AEDT including full-flight aerodyne-only, full-flight smoke number, full-flight emission index, and full-flight smoke number-aerodyne hybrid methods. The two correlation options SCOPE11 and FOA3 are only available for the full-flight smoke number and full-flight emission index methods. And the system loss correction method is only applicable to the correlation method of SCOPE11.

Since the enhanced nvPM function is not included in the public released version, a special version of AEDT needs to be used to demonstrate and test this feature. The special version (92.0.6001.1) was obtained by the research team and a test study to conduct the UQ analysis on the enhanced nvPM capability. The features related to this capability that were tested include correlation option, altitude adjustment, system loss correction factor, and other nvPM methods. And the tests utilized the system requirements document agreed by AEE on 8/3/2017 as a guideline.

Correlation Option

Based on the system requirements document, correlation options are enabled for Full-Flight Smoke Number and Full-Flight Emission Index method. This was tested and it worked as expected. There is a minor issue that when a user copies a metric with SCOPE11 correlation option, the option is not correctly copied, instead, FOA3 is copied. The two correlation options were further tested for nvPM mass and number, and Table 20 shows the nvPM results. It can be seen that regardless the nvPM methods used, the nvPM results are identical for the same correlation option, which might be a bug and is currently being investigated. Comparing SCOPE11 and FOA3, the difference in nvPM mass is huge, however nvPM number calculated by these two methods have same magnitude. Further investigation found that the unit for SCOPE11 is micro gram instead of gram which will be corrected.

Table 20: AEDT Development and Public Release Schedule

Mode	nvPM Mass (g)				nvPM Number			
	SN+FOA3	EI+FOA3	SN+SCOPE11	EI+SCOPE11	SN+FOA3	EI+FOA3	SN+SCOPE11	EI+SCOPE11
Climb Taxi	0.07	0.07	70.66	70.66	8.37E+15	8.37E+15	7.96E+15	7.96E+15
Climb Ground	28.28	28.28	34576.27	34576.27	1.76E+17	1.76E+17	2.34E+17	2.34E+17
Climb Below 1000	43.22	43.22	49904.31	49904.31	2.65E+17	2.65E+17	3.54E+17	3.54E+17
Climb Below Mixing Height	91.51	91.51	87080.45	87080.45	1.47E+18	1.47E+18	7.05E+17	7.05E+17
Climb Below 10000	104.86	104.86	120353.22	120353.22	2.10E+18	2.10E+18	1.24E+18	1.24E+18
Above 10000	1588.26	1588.26	916740.08	916740.08	7.90E+18	7.90E+18	1.15E+19	1.15E+19
Descend Below 10000	7.88	7.88	6987.69	6987.69	7.36E+17	7.36E+17	6.94E+17	6.94E+17
Descend Below Mixing Height	5.33	5.33	4548.47	4548.47	4.48E+17	4.48E+17	4.17E+17	4.17E+17
Descend Below 1000	2.77	2.77	2474.14	2474.14	1.59E+17	1.59E+17	1.77E+17	1.77E+17
Descend Ground	0.46	0.46	427.78	427.78	4.96E+16	4.96E+16	4.82E+16	4.82E+16
Descend Taxi	0.09	0.09	89.46	89.46	1.06E+16	1.06E+16	1.01E+16	1.01E+16
Full Flight	1701	1701	1044080.99	1044080.99	1.07E+19	1.07E+19	1.35E+19	1.35E+19

Altitude Adjustment

The enhanced nvPM capability allows the user to enable/disable altitude adjustment for flights below 3000 feet above ground level (AGL). This feature is tested for the SCOPE11 correlation method. However, the results show that SCOPE11 method produced the exactly same results for the cases with and without altitude adjustment. Further tests were conducted using FOA3 method. The results show that with altitude adjustment, FOA3 method produced more nvPM mass and number for most of the modes. One issue is that for two of the modes, even FOA3 method with altitude adjustment generated more nvPM mass, however, the nvPM number is less than the case without altitude adjustment. This is an issue that will be investigated and fixed.

System Loss Correction Factor

Based on the system requirements document, the system loss correction factor can be enabled/disabled for SCOPE11, and should not be available for FOA3 method. However, it was found that the following issues exist in this feature and will be fixed in the future:

- When the emission report is generated for a metric with "SCOPE11" option, the system loss correction box will be enabled for all emission report, and vice versa
- And for the metric with "FOA3" option, check the system loss correction box will double the nvPM results in emission report
- The "Apply System loss correction factors to nvPM results" checkbox is correlated between different emission reports
- System loss is not unselected by default if it was selected in a metric previously

Other Methods

To fully test the enhanced nvPM capability, other nvPM methods including full-flight Aerodyne-only and full-flight smoke number-Aerodyne hybrid methods were also tested. The results show that the hybrid methods generate reasonable results for nvPM mass and number. However, for full-flight aerodyne method, negative values were generated for nvPM mass for some of the modes, which is most likely due to the interpolation algorithm and will be fixed.

MOVES and AEDT Integration, and VALE Reporting

The Environmental Protection Agency (EPA) Motor Vehicle Emissions Simulator (MOVES) model is used to generate emissions inventories and/or AERMOD input files for on-road or off-road mobile sources. Although MOVES is not integrated in AEDT, a feedback mechanism is established through the AEDT Graphical User Interface (GUI). This mechanism provides the user an ability to feed the required link-based inputs needed by MOVES. The MOVES modeled link-based and aggregated emissions can then be fed back to AEDT. Link-based MOVES inputs are provided in AEDT GUI through the mobile-source layout components: roadways, parking facilities, and construction zones, in the Airport Layout.

Design and Export MOVES Links

To model roadway, parking facilities and construction zones using MOVES, users can create mobile-source layout components by using the Airport Layout Design feature in AEDT and then export the link-based inputs to MOVES for further modeling. After the MOVES link-based inputs are imported into MOVES, users can use MOVES to conduct project-level analysis, thus, mobile-source emissions inventory can be generated for the imported links. Once the MOVES emissions output for each link are obtained or the aggregated emissions by category, they can then be imported back into AEDT for integrating with other analysis.

The design of MOVES links was tested using the airport layout design feature in AEDT. This function works properly. Users can design MOVES links for roadway, parking facility, and construction zone. After the links were designed, they can be exported in the selected airport layout as MOVES links.

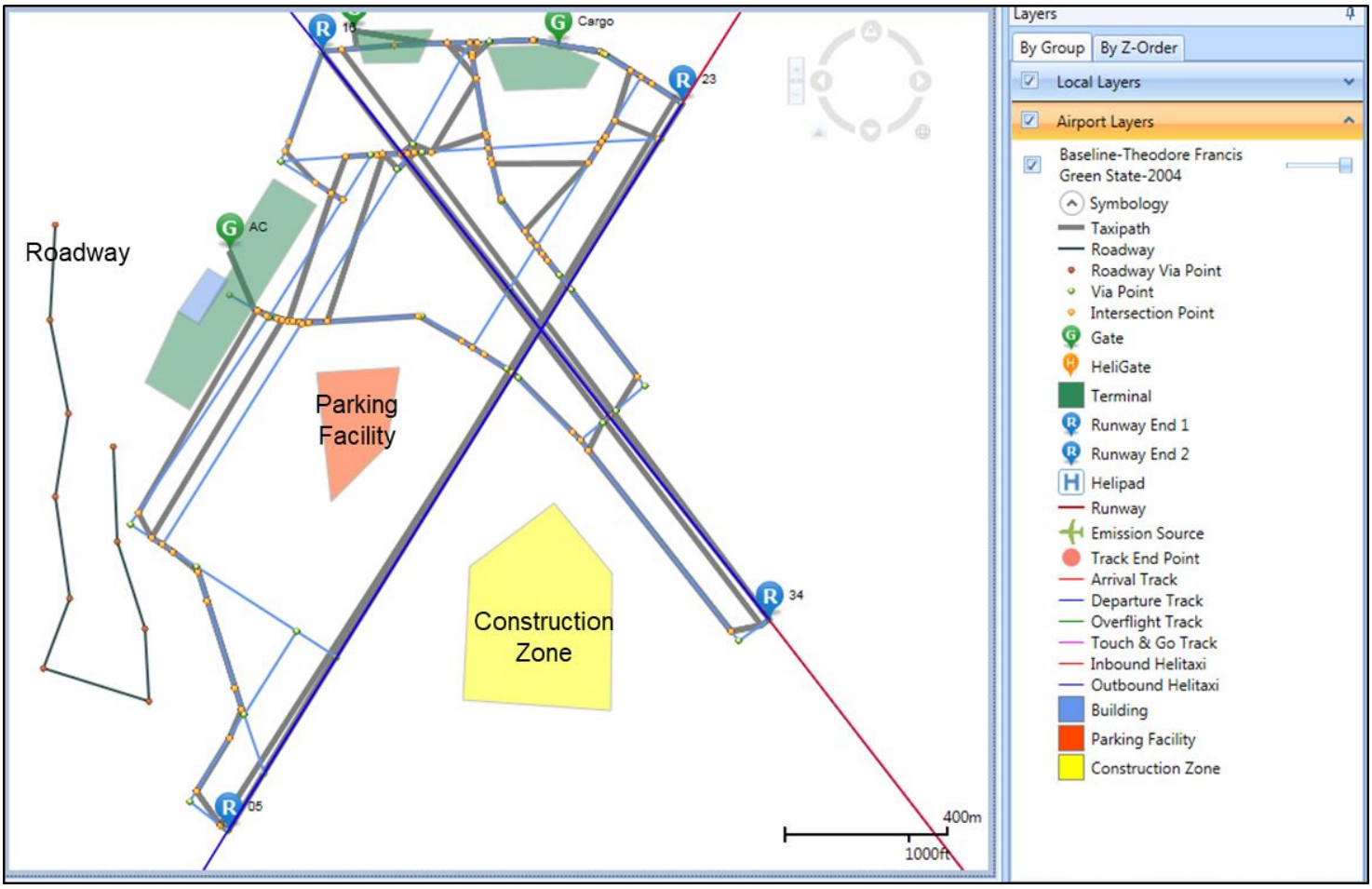

Figure 16: Design Roadway, Parking Facility and Construction Zone in AEDT for MOVES Modeling

VALE Reporting with MOVES

After the roadway, parking facilities, and/or construction operations emissions inventory was calculated externally by the MOVES tool, the emissions inventory results can be imported to AEDT and included in the emissions report for all metric results. To integrate the MOVES inventory scenario with an emissions metric result, one needs to specify the MOVES inventory file in the definitions tab of AEDT. After the MOVES emissions inventory was imported, one can define an emissions metric and select the MOVES inventory scenario in the step of set processing options. Once the metric result is run, one can generate the emissions report which will include the MOVES emissions inventory.

The integration of MOVES emissions inventory was tested with the Voluntary Airport Low Emissions (VALE) report. A VALE reduction report shows net differences in emissions between a baseline and an alternative (VALE) metric result for a single analysis year. The baseline scenario simulates existing conditions while the alternative scenario conveys hypothetical equipment replacements. A test study was used and the VALE report with MOVES emissions inventory was generated. This feature works properly with minor issues which will be fixed. A sample VALE report is shown in Table 21.

Table 21: A Sample VALE Report

VALE Report 45_48

Print Preview

Baseline (Source): Base_2010

Alternative (Destination): VALE_2010

Pollutant (Unit): Grams

No.	Year	Scenario	Source Group	CO	VOC	NOx	SOx	PM-10	PM-2.5
1	2016	Base_2010							
			Baseline_FuelOilBoiler1 (Stationary Sources)	17,280.000	7,320.000	109,440.000	1,615,680.000	16,992.000	12,444.840
			Baseline_FuelOilBoiler2 (Stationary Sources)	18,432.000	1,808.470	89,088.000	179,712.000	3,686.400	884.740
			Baseline_GasolineEmergencyGenerator (Stationary Sources)	3,071,923.200	134,073.680	77,184.000	14,356.220	4,137.060	4,137.060
			Baseline_GasolineAircraftTractor1 (GSE Population)	828,951.840	23,257.070	34,287.040	5,567.220	298.530	274.650
			Baseline_GasolineAircraftTractor2 (GSE Population)	828,951.840	23,257.070	34,287.040	5,567.220	298.530	274.650
			Baseline_DieselAirCond-DieselLavatory (GSE Population)	8,945.850	942.490	23,721.340	10.580	1,493.480	1,448.680
			Baseline_TrackOps_LightDay_Jan2010	627,167.380	69,971.610	4,756,336.720	313,149.450	113,029.700	113,029.700
			Baseline_TrackOps_LightDay_Jan2010 (GSE LTO)	902,221.160	29,920.290	83,852.180	4,002.450	3,842.070	3,635.710
			Baseline_TrackOps_LightDay_Jan2010 (APU)	173,473.630	12,694.600	157,025.770	21,228.860	19,366.070	19,366.070
			Baseline_TrackOps_HeavyDay_Jan2010	1,537,954.680	163,929.750	5,120,136.660	354,735.790	129,741.250	129,741.250
			Baseline_TrackOps_HeavyDay_Jan2010 (GSE LTO)	1,156,498.830	38,577.360	109,169.520	5,028.130	4,878.290	4,617.870
			Baseline_TrackOps_HeavyDay_Jan2010 (APU)	55,166.920	3,887.520	41,839.430	5,878.940	5,869.530	5,869.530
			Base_2010 Total	**9,226,967.330**	**509,639.910**	**10,636,367.700**	**2,524,916.860**	**303,632.910**	**295,724.750**
		VALE_2010							
			VALE_NaturalGaseBoiler_1_2 (Stationary Sources)	33,331.200	26,331.130	133,324.800	595.200	2,856.960	2,856.960
			VALE_DieselEmergencyGenerator (Stationary Sources)	46,773.500	15,063.850	216,115.200	14,356.220	15,405.930	15,405.930
			VALE_DieselAircraftTractor (GSE Population)	17,651.370	1,292.330	44,641.030	20.420	3,140.950	3,046.730
			VALE_DieselAirCond-DieselLavatory (GSE Population)	8,945.850	942.490	23,721.340	10.580	1,493.480	1,448.680
			VALE_TrackOps_LightDay_Jan2010	627,167.380	69,971.610	4,756,336.720	313,149.450	113,029.700	113,029.700
			VALE_TrackOps_LightDay_Jan2010 (GSE LTO)	116,302.270	7,355.740	34,906.850	480.850	1,940.560	1,872.930
			VALE_TrackOps_LightDay_Jan2010 (APU)	173,473.630	12,694.600	157,025.770	21,228.860	19,366.070	19,366.070
			VALE_TrackOps_HeavyDay_Jan2010	1,537,954.680	163,929.750	5,120,136.660	354,735.790	129,741.250	129,741.250
			VALE_TrackOps_HeavyDay_Jan2010 (GSE LTO)	279,579.070	12,963.330	52,087.290	1,085.300	2,629.500	2,527.830
			VALE_TrackOps_HeavyDay_Jan2010 (APU)	55,166.920	3,887.520	41,839.430	5,878.940	5,869.530	5,869.530
			VALE_2010 Total	**2,896,345.870**	**314,432.350**	**10,580,135.090**	**711,541.610**	**295,473.930**	**295,165.610**
			2016 Net ER	***-6,330,621.460***	***-195,207.560***	***-56,232.610***	***-1,813,375.250***	***-8,158.980***	***-559.140***

Runup Operations for Military Aircraft

Runup operations only generate noise results. In addition, runup operations are only applicable for fixed-wing aircraft and not for helicopters, and they are not associated with tracks. Runup operations for military aircraft was not working properly in AEDT 2b when the AEDT 2b UQ analysis was conducted. The purpose of this task is to test if runup operations for military aircraft are fully supported in AEDT 2c.

To test this function, a runup operation of military aircraft was created. In the process of defining runup operation, one of the key parameters in runup details step needs to be specified. It was found that this parameter can be different for different aircraft, such as power lever angle, percent corrected rotor speed, engine pressure ratio, percent propeller or compressor RPM. The defined runup operation can be edited, copied and deleted.

Several runup operations were created for military aircraft and verified that the function is working properly. The only issue is that, when the runup operation is defined, the key parameter that needs to be specified in runup details can be assigned any value, which can generate infeasible runup operation and noise results. Figure 17 shows that AEDT can generate noise contour for a military aircraft runup operation with the percent corrected rotor speed being 80 and 200. And there is no limit on the percent corrected rotor speed and can go even higher. This generated infeasible noise results, and this issue will be fixed in the future.

Percent CRS: 80

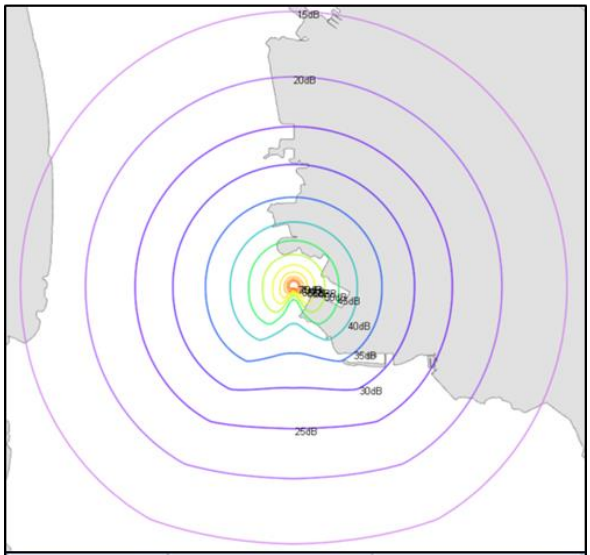

Contour (dB)	Shape Length (m)	Shape Area (sq m)
60	3923.55707926759	922806.707464999
65	2510.83041613241	409819.699880011
70	1802.01598072552	212079.346630353
75	1265.20359103488	105313.671700045

Percent CRS: 200

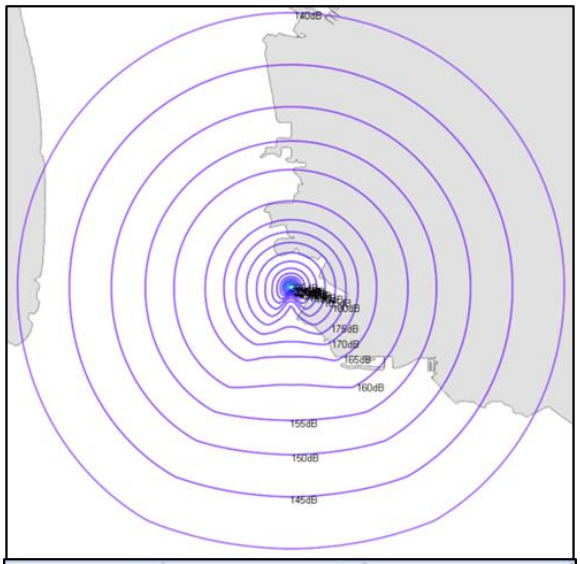

Contour (dB)	Shape Length (m)	Shape Area (sq m)
140	69411.8048936481	382759685.418234
145	56235.1105796719	251027282.314551
150	45559.4662166852	164558704.650389
155	36914.1416486244	107815739.902844

Figure 17: Noise Contours for Runup Operations of Military Aircraft with Different Percent CRS

Emission Dispersion Open Contour

Emission Dispersion Open Contour requires AEDT to be able to generate contour for emission depression analysis. Contour generation requires the grid receptor with a smaller range compared with the noise receptor grid. It is typical to use the spacing for 0.5 nautical mile (926 meter) for noise grid; however, emissions dispersion needs 100 to 200 meter spacing to create a reasonable contour. That is, the emission dispersion contours are generated using grids in meter unit in AEDT. The emission dispersion contours are shown in two scales – linear and log scale in Figure 18.

Emissions can be transported and dispersed over very large distances. Although the focus of most emissions dispersion analyses generated using AEDT will be on receptors close to the airport, there is frequently the need to visualize emission contour lines which are open ended. These open-ended contours could be closed by extending the receptor grid over a very large distance which could be computationally prohibitive. In order for those contours to be accurately represented visually, AEDT was updated to allow for these open-ended contours to be displayed.

To test the emission dispersion open contour function, a study was created and tested. After the study was run, the emission dispersion contours were generated, including open contour lines, as shown in Figure 18. The test showed that AEDT can successfully generate open contours for emission dispersion analysis, and the contours can be displayed in

linear or log scales. In addition, AEDT is able to calculate contour area for contours in log scale. One suggestion for this function is that it will be helpful if AEDT can calculate contour area for linear scale as well.

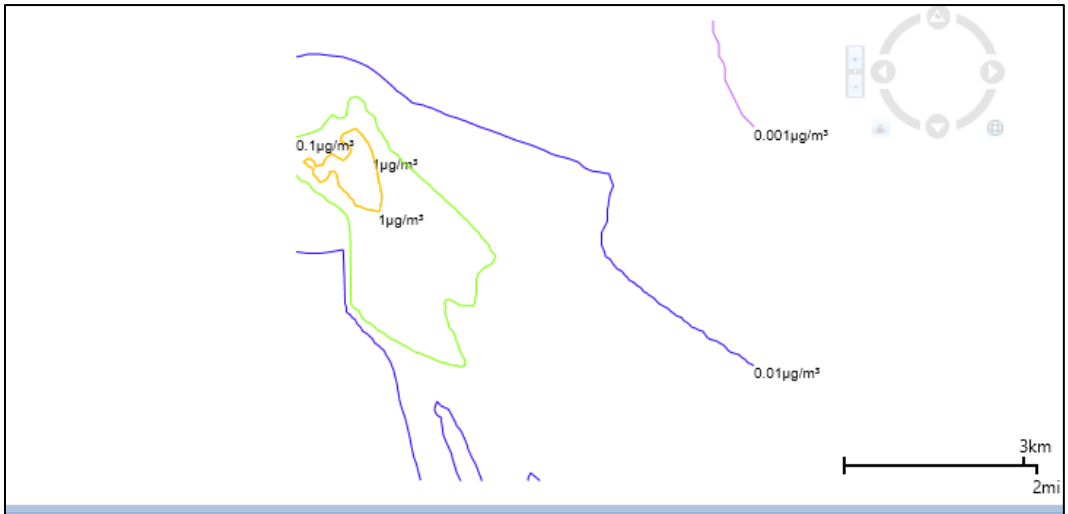

butes

CO_J1_ALL_8-HR_2ND_Log10_Lines × CO_J1_ALL_8-HR_2ND_Log10_Contour ×

Drag a column header and drop it here to group by that column

Object ID	Concentration	Shape Length (m)	Group	Average	Rank	ScalingMethod	Concentration (µg/m³)
1	-3	2003.95387407548	ALL	8-HR	2ND	Log10	0.001
4	-2	10511.2352957615	ALL	8-HR	2ND	Log10	0.01
5	-2	5105.35510890311	ALL	8-HR	2ND	Log10	0.01
6	-2	3062.16282110275	ALL	8-HR	2ND	Log10	0.01
7	-2	352.524468860242	ALL	8-HR	2ND	Log10	0.01
3	-1	12759.6213057087	ALL	8-HR	2ND	Log10	0.1
2	0	5251.3206938891	ALL	8-HR	2ND	Log10	1

Figure 18: Emission Dispersion Open Contours

Vector Track

One of the functionalities implemented in AEDT was to input vector track geometry via the GUI by adding a series of track segments. In this capability, the user can select the following types of vector track segments: straight, left turn, and right turn with a proper angle. For a verification purpose, the vector track was created to compare both emission and noise results with a point track and flew one aircraft with the vector track. Once the simulation was completed, both latitude and longitude information were parsed from performance results in order to generate a point track. For example, as can be seen in Figure 19, a single-aisle aircraft was flown from San Diego International Airport and both vector and point tracks were created. In terms of the vector track, the blue line was supposed to be the vector track for departure and it was created by the GUI. On the other hand, the red line referred to the flight for arrival to the airport. Using the results from the vector track, the red dot points were used to create the point track.

Both fuel burn and noise results were compared for the arrival and departure cases between the vector and point track as tabulated below. For fuel consumption comparison, aircraft was flown with both arrival and departure procedures using either vector or point track. As a result, they were almost identical. For noise contour area comparison, 65, 70, and 75 SEL

levels were chosen in order to compare the results between vector and point track. As a result, the difference between them was less than one percent.

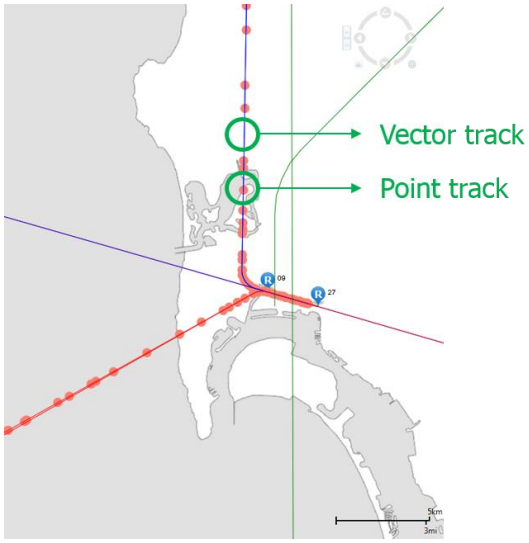

Figure 19. Vector vs. Point Track

Table 22. Fuel burn comparison (Vector vs. Point Track)

	Arrival FB (kg)	Departure FB (kg)
Vector track	281.43	643.24
Point track	281.41	643.77

Table 23. Noise (SEL) comparison (Vector vs. Point track)

SEL Area (km2)	Vector Track	Point Track	Difference (%)
65	269.17	271.25	0.8
70	169.96	170.94	0.6
75	92.27	92.56	0.3

Track Dispersion

One of the key features added to AEDT is the capability of track dispersion. Users have the ability to edit or modify an existing ground track with dispersion through the AEDT GUI environment. Since the track dispersion is designed only for a point track at this point, GT created a point track and made dispersion with the track. For a verification purpose, a case study was defined with nine dispersion sub-tracks and one hundred operations as shown in Figure 20.

In Figure 20, one departure point track was at first defined at San Diego International Airport. And then, the blue line, which was a point track for departure operation, was dispersed with the capability. With the dispersion, eight sub-tracks were generated with different distances. All blue lines shown in Figure 20 represent the dispersed tracks.

In order to see the dispersion effect, DNL contour area was compared between dispersed and undispersed tracks. As a result, the difference of DNL areas between dispersed and undispersed track was increased as the DNL level was increased.

It does make sense because dispersed track would be having more impacts on the noise area than undispersed track. The DNL results are tabulated in Table 24, which shows from 50 to 80 DNL levels.

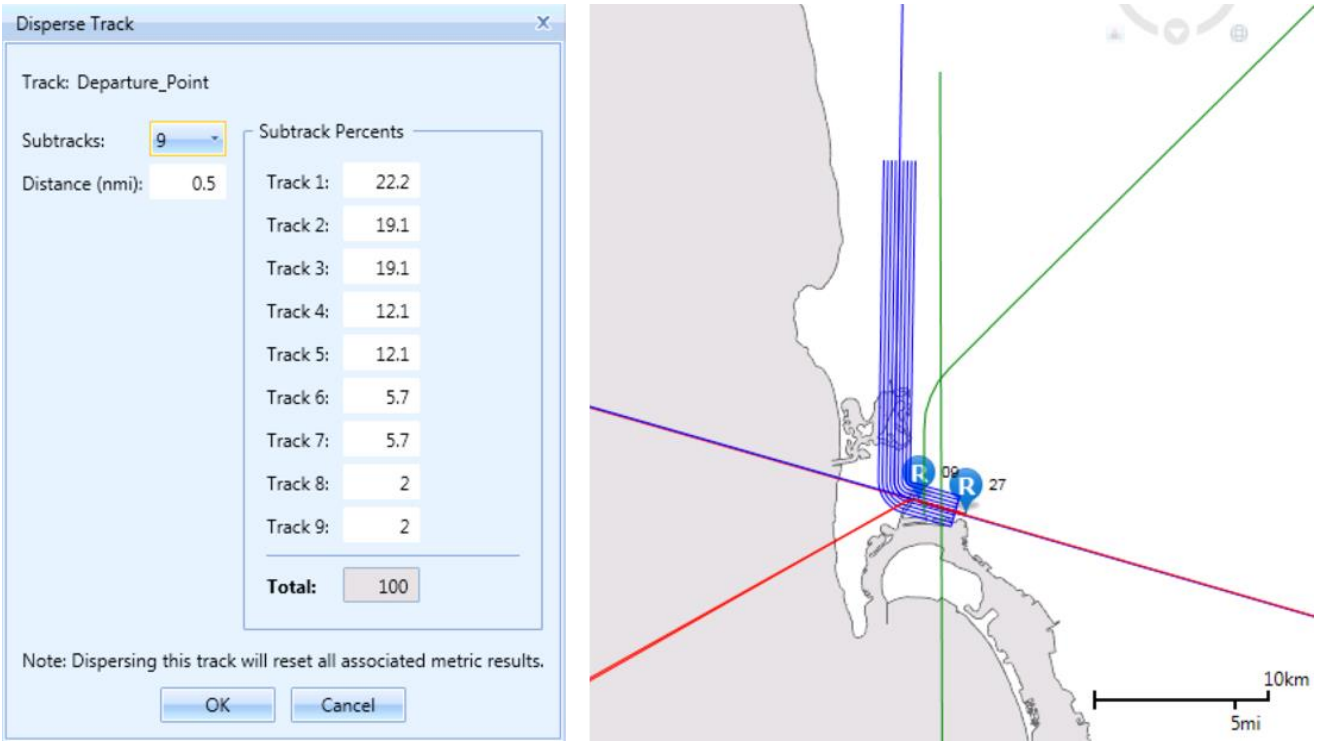

Figure 20: Case study setup for dispersion test

Table 24: DNL comparison (Dispersed vs. Undispersed track)

DNL Area (km^2)	Dispersed track	Undispersed track	Difference (%)
50	183.51	181.95	0.9
60	41.70	40.57	2.8
70	8.58	6.51	31.8
80	1.30	0.89	46.1

Contour Combination

One of the capabilities implemented in AEDT is to enable users to import grids from other noise models and to combine grids. In terms of contour combination, users are even able to combine more than two grids. For a verification purpose, the capability was tested with two cases: 1) Using the grid from other noise model and 2) Using multiple grids created by GT in AEDT. First, two different grids were successfully imported to AEDT and combined with each other. Second, the capability was tested by creating a new study which included three different grid spacing in AEDT as shown in Figure 21.

In Figure 21, three different grid types were created with different grid spacing. For example, the first grid so-called as coarse grid was created with 1.0 nautical mile grid spacing. The second grid so-called as medium grid was created with 0.5 grid spacing. For this reason, an area of the medium grid is less than the one of coarse grid. Finally, the fine grid with grid spacing 0.25 was created. As expected, it was successfully merged which is shown in the bottom of Figure 21. Also, the results were successfully obtained from the combined grid as expected.

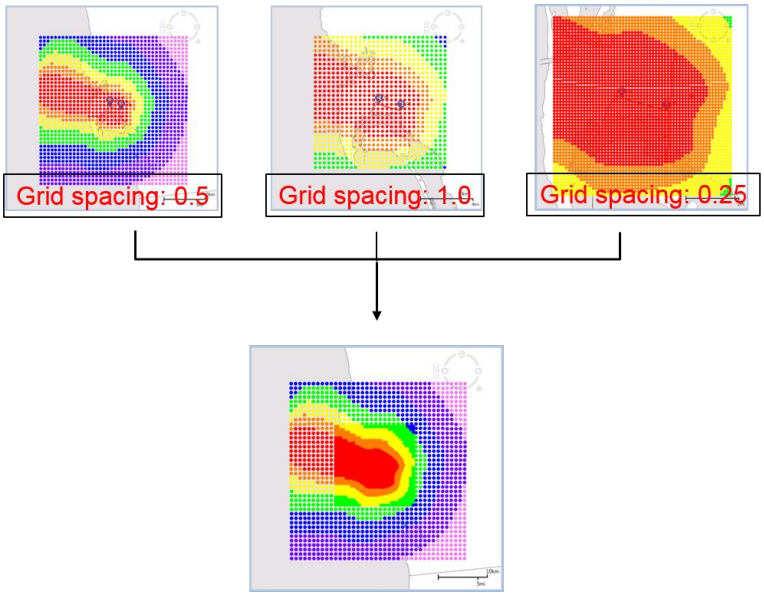

Figure 21: Three different grids with consistency

Dynamic Grid

In AEDT, noise contours are usually calculated from a grid receptor with equally spaced contour grid, namely fixed grid. Dynamic grid, which is variably spaced contour grid, was implemented as one of capabilities in AEDT. The dynamic grid method would start with small grids and expand outward until the desired contour level is closed. To be more specific, noise levels are first computed for the starting receptor grid and are compared to the specified expansion level. If any noise level exceeds the minimum expansion level, the grid expands in that direction by adding a new grid. This is done for all four sides of the starting grid and the process continues until no noise levels on the edges of the grids exceed the expansion level and the contour is closed.

In order for a verification purpose, two studies were created to evaluate the functionality of dynamic grid for both dB and non-dB metrics. In terms of the test for dB metric, the SEL metric was chosen and defined 55dB as the minimum expansion level for the dynamic grid test. As a result, the noise contour between fixed and dynamic grids was almost identical.

In Figure 22, the fixed grids described in the left hand side were defined around KBHB airport and a single-aisle aircraft was flown to south-east direction. As expected, the fixed grids were all used to compute noise levels. On the other hand, when dynamic grid was turned on from the option, it seemed that AEDT calculated grids less than the fixed grids. In the meantime, the noise contours for both fixed and dynamic grids were almost identical.

In terms of the test for non-dB metric, TAUD was selected as a non-dB metric and defined one minute as the minimum expansion level. Although the dynamic grid worked well for TAUD, it was found that there was an error for generating contour area with respect to the TAUD metric. However, the issue had been resolved since it was reported to the development team and was retested it again to make sure that the contouring algorithm works well. Finally, it was found that it worked successfully without any contour algorithm problems.

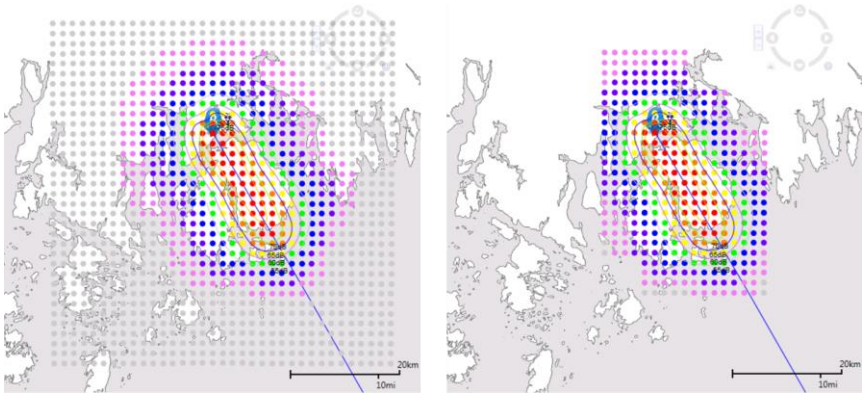

Fixed Grid Dynamic Grid

Figure 22: Fixed vs. Dynamic grid (SEL)

In Figure 23, the dynamic grids used less grid points than a fixed grid. Although the dynamic grid method used less grid points, the contour areas generated by the dynamic grid were almost identical compared to the fixed grid. For each colored line, it represented the level of contour areas.

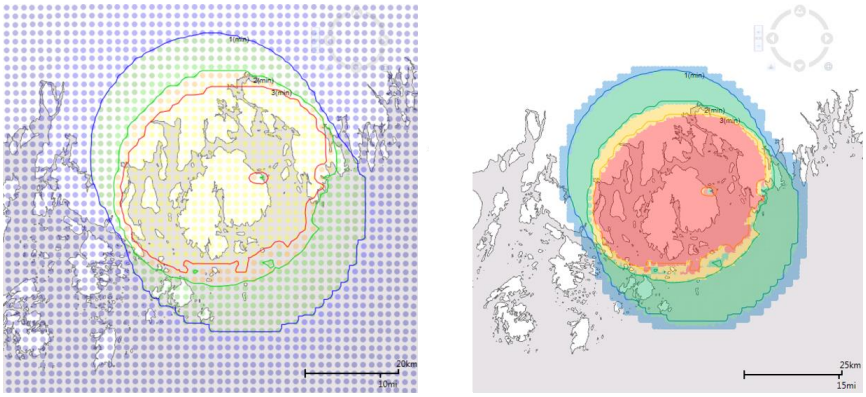

Fixed Grid Dynamic Grid

Figure 23: Fixed vs. Dynamic grid (TAUD)

Detailed Noise

INM had a capability to store noise results from a flight segment of each of the flights when detailed grid option was used. For AEDT, a capability to set up and view the detailed noise report through the GUI was implemented. Therefore, users were able to obtain the detailed noise results from each grid point as well as every combination of aircraft, profile, and track.

Three different cases were tested to evaluate the functionality of detailed noise implemented in AEDT. The test case one was supposed to be single arrival flight with standard option. The option was chosen to compare it with the test case two which was also supposed to be a single arrival flight but with detailed noise option. Lastly, the test case three was defined to verify if the detailed noise functionality was also working with multi-flights. From all the tests defined, the detailed noise functionality worked well as intended.

Noise Exposure Report 2

Altitude (ft)	Distance (ft)	Speed (knots)	Corrected Net Thrust Per Engine	Thrust Type	Elevation Angle at CPA	Equivalent Operations	Metric Value All	Metric Value One
427.37	6255.37	130.42	3863.59	Pounds	3.92	5.0000	70.02	63.03
989.16	11950.52	130.42	3942.36	Pounds	4.75	5.0000	63.98	56.99
1550.95	17646.57	143.72	3187.46	Pounds	5.04	5.0000	60.03	53.04
2913.73	15916.08	163.14	1493.71	Pounds	10.55	5.0000	60.42	53.43
427.37	6255.37	135.86	9475.86	Pounds	3.92	5.0000	70.06	63.07
989.16	11950.52	135.86	9684.20	Pounds	4.75	5.0000	64.50	57.51
1550.95	17646.57	135.86	9892.55	Pounds	5.04	5.0000	62.67	55.68
2913.73	15916.08	146.38	1860.82	Pounds	10.55	5.0000	63.61	56.62

Figure 24: Detailed noise example generated in AEDT

In Figure 24, the table was created in AEDT by choosing the detailed noise option. The table included a lot of information such as noise level, speed, distance, and elevation angle at Closed-Point-Approach (CPA). To manage the data size, the results were stored for a Closed-Point-of-Approach (CPA), which is the closest point to the receptor, to the receptors and were compared under the same conditions. From the comparison, the thrust values from AEDT were about 3.45 times greater than those of INM in Sprint 82. This was because there was a bug in terms of calculating equivalent operations. However, in Sprint 88, the difference between INM and AEDT with respect to the thrust values was only 0.4%.

Bulk Operation Creation

One of the most enhanced functionalities in AEDT was to implement bulk operation. In the bulk operation, the user could choose multiple equipment at the same time. In addition, the user could specify stage length for each equipment and choose multiple flight tracks. For example, if users selected three different aircraft and two flight tracks, then AEDT would provide users to six combinations of aircraft operations. Six different aircraft were selected at the same time in the operation tab, as depicted in Figure 25 to test this functionality. However, a few minor issues were found that users could not delete multiple operations at the same time. Although the user could choose multiple operations, the operations could not be deleted simultaneously. In addition, there was another minor issue that a user could not select multiple equipment when the filter option was used to find out different equipment in a sequence. These minor issues are investigated under development team members.

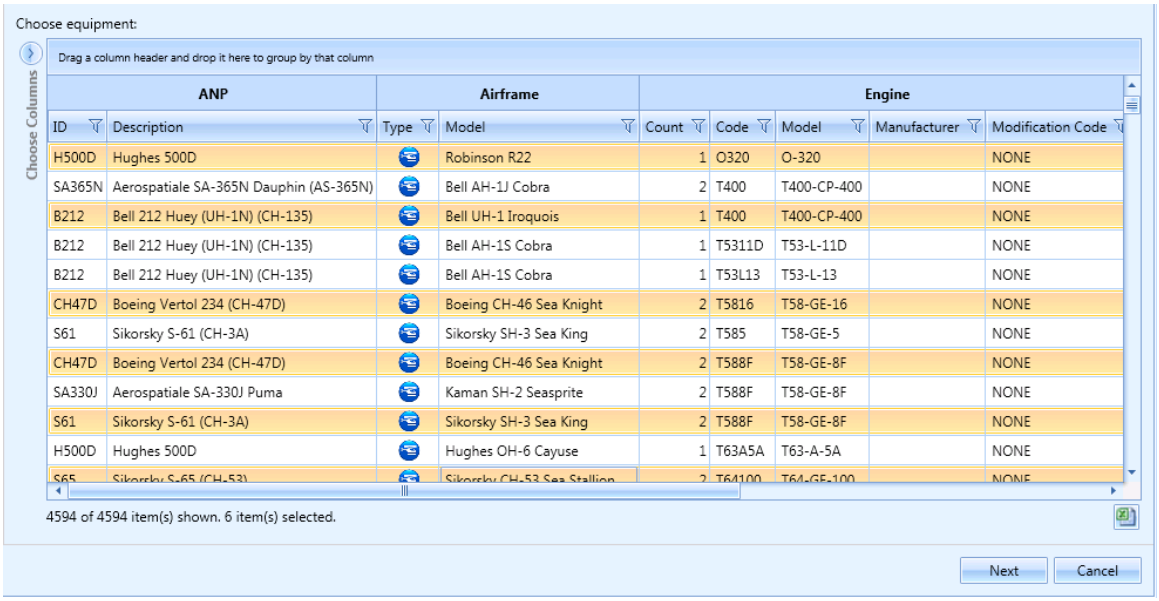

Figure 25: Bulk operation example

Milestone(s)

Milestone	Due Date	Estimated Date of Completion	Actual Completion Date	Status	Comments (Problems & Brief Resolution Plan)
A36 Kickoff Meeting	5/3/2016	5/3/2016	5/3/2016	Completed	
Quarterly Report (Aug)	7/31/2016	7/31/2016	7/31/2016	Completed	
ASCENT Meeting	9/27-28/2016	9/27-28/2016	9/27-28/2016	Completed	
Quarterly Report (Nov)	10/31/2016	10/31/2016	10/31/2016	Completed	
Annual Report	1/18/2017	1/18/2017	1/13/2017	Completed	
Quarterly Report (Jan)	1/31/2017	1/31/2017	1.27/2017	Completed	
Quarterly Report (March)	3/31/2017	3/31/2017	3/31/2017	Completed	
ASCENT Meeting	4/18/2017	4/18/2017	4/18/2017	Completed	
Quarterly Report (June)	6/30/2017	6/30/2017	6/30/2017	Completed	
ASCENT Meeting	9/26/2017	9/26/2017	9/26/2017	Completed	
Quarterly Report (Oct)	10/30/2017	10/30/2017	10/30/2017	Completed	
Annual Report	11/30/2017	11/30/2017	11/30/2017	In Progress	

Major Accomplishments

Starting from January 2017, all the new AEDT sprint releases including Sprints from 80 to 94 have been tested. Sprints 80 – 94 included two public releases of AEDTs, namely AEDT 2c SP2, and AEDT 2d.. Fifteen versions of AEDT have been tested focusing on new features and capabilities added. Some of the new features/capabilities were minor updates to the GUI, bug fixes, or data updates. Major updates included enhanced nvPM, VALE reporting with MOVES, runup operation of military aircraft, open contour, vector track, track dispersion, contour combination, dynamic grid, detailed noise and bulk operation creation. In order to understand the background of new AEDT features, all the relevant documents were reviewed including the software requirement documents, Database Design Document, AEDT sprint release notes, updated technical manual, user manual, and research papers/reports. Basic testing of all the new AEDT versions and service packs was completed to confirm its functionality and a number of minor and major bugs and reported them to the FAA and the development team via bi-weekly ASCENT project telecons and weekly AEDT development-leads calls. Through the on-line system named Team Foundation Server (TFS), identified issues and follow-up actions taken by the developers were documented and shared. The TFS also allows for reporting any potential areas of improvements in AEDT algorithms and user-friendliness.

Finally, further analysis was conducted to investigate the differences in noise, fuel consumption, emission inventory and emission dispersion between AEDT and the legacy tools reported in the original AEDT 2b report. Studies were performed for Use Case B&C, Use Case D, and Use Case E to investigate the differences in emissions and noise between AEDT, EDMS and INM. The investigations of the differences between AEDT and the legacy tools focuses on evaluating the assumptions, methods, and implementation for noise and emissions calculations. Thus, technical manual of AEDT and legacy tools were reviewed to understand the assumptions and methods used by different tools, and the factors that have impact on the noise and emissions calculation were identified. Additional studies were designed and performed to further validate the metric results, and findings and recommendations were reported.

Publications

Yongchang Li, Don Lim, Michelle Kirby, Dimitri Mavris, George Noel, Uncertainty Quantification Analysis of the Aviation Environmental Design Tool in Emission Inventory and Air Quality Modeling, Submitted to AVIATION 2018 conference.

Dongwook, Lim, Yongchang Li, Matthew J Levine, Michelle R Kirby, Dimitri, Mavris, Parametric Uncertainty Quantification of Aviation Environmental Design Tool, Submitted to AVIATION 2018 conference.

Junghyun Kim, Dongwook Lim, Yongchang Yi, Michelle Kirby, and Dimitri Mavris, Parametric Study of Noise Impact on the Airspace over the Acadia National Park using Time-Audible metric in AEDT, Submitted to AVIATION 2018 conference.

Outreach Efforts

None

Awards

None

Student Involvement

Junghyun (Andy) Kim is a third year PhD student who started in fall 2015. Mr. Kim has conducted a literature review on UQ methods, and performed tests for newly release AEDT features. Mr. Kim is being trained on related tools such as INM, AEDT Tester, AEDT2c and AEDT 2d.

Ameya Behere is a second year PhD student who started in fall 2016. Mr. Behere has conducted a literature review on UQ methods, and performed tests for newly release AEDT features. Mr. Behere is being trained on related tools such as INM, AEDT Tester, AEDT2c and AEDT 2d.

Evanthia (Eva) Kallou is a third year PhD student who started in fall 2015. As a Graduate Research Assistance, Ms. Kallou has conducted a literature review on UQ methods. Ms. Kallou is being trained on related tools such as EDMS, AEDT Tester, AEDT2c and AEDT 2d.

Plans for Next Period

GT will continue uncertainty quantification tasks for new AEDT 2d releases. AEDT 2e is planned to be released in mid-March 2018. GT will perform the validation and verification tasks for the preliminary versions of AEDT 2d to identify any issues that need to be addressed by the development team.

Task 1. Proper Definition of AEDT Input Parameter Uncertainty
The first step in the UQ effort is to properly define the problem. For each of the AEDT service pack releases, GT will define the scope of the UQ effort identifying the key changes to the AEDT versions from the previous releases. Depending on the type of updates incorporated, it would be required to identify the key sources of uncertainties and properly define the uncertainties for the input parameters if it is necessary.

Task 2. Verification and Validation plus Capability Demonstrations
GT will continue to conduct V&V and capability demonstrations of the newly released AEDT versions. The V&V analysis can take a couple of different approaches depending on the type of updates and data availability. In the past UQ efforts, one of the most important methods of ensuring confidence in the tool capability was to conduct a use case(s) using both legacy tools and the new AEDT release and compare the results. This method would be the most appropriate way whenever a legacy tool has the same or similar functionalities and a validated use case has been modeled in that legacy tool. When the new functionality of AEDT does not exist in the legacy tools, the V&V exercise should use direct comparisons to the results generated by the mathematical algorithms behind the newly added functionality and/or real world data whichever available.

Task 3. Identification of Important Output to Input Relationships (Optional)
This optional task may not be performed for every AEDT service pack releases. Instead, this task will be performed when a major feature is added to the AEDT, and if potential sources of uncertainties remain through the analysis of previous two tasks. The outcome of this task will be the identification of the key input drivers across multiple vehicle types to multiple

AEDT metric outputs. This can provide a comprehensive insight to the uncertainty associated with AEDT outputs and the joint-distribution of Fleet DB coefficients. Various uncertainty quantification techniques will be used depending on the metric of interest. This may include, but not limited to the following techniques: Analysis of Variance (ANOVA), Multivariate Analysis of Variance (MANOVA), Monte Carlo Simulation, Copula Techniques, or Global Sensitivity Analysis. The specific techniques will be proposed by GT and reviewed by the FAA for concurrence.[i]

Task 4. Guidelines for Future Tool Research
In this task, each of the prior tasks will culminate into a summary document of the data assumptions, techniques utilized, the resulting observations and findings to help guide the FAA to further research the areas of AEDT development to improve its supporting data structure and algorithms. In addition, the document will build confidence in AEDT's capability and fidelity and help users to understand the sensitivities of output response to the variation of input parameters/assumptions.

References

[1] US FAA, AEDT 2a UQ Report, 2014

[2] US FAA, AEDT 2a SP2 UQ Supplemental Report, 2014

[3] US FAA, AEDT 2b UQ Report, 2016

[4] US FAA, AEDT 2b Technical Manual, 2015

[5] US FAA, AEDT 2b User Manual, 2016

[6] CSSI, Inc., "Emissions and Dispersion Modeling System (EDMS) Version 5", FAA-AEE-07-07, Rev.5, June 2014

[7] CSSI, Inc., "Emissions and Dispersion Modeling System (EDMS) User's Manual", FAA-AEE-07-01, Rev. 10, June 2013

[8] US FAA, AEDT 2c User Manual, 2016

[9] US FAA, AEDT 2d Technical Manual, 2017

[10] US FAA, AEDT 2c Technical Manual, 2016

[11] US FAA, AEDT 2d User Manual, 2017

[12] Noel, George, "AEDT Uncertainty Quantification", presented in FAA/AEE Tools Review, December 2010

[13] Willcox, "Tools Uncertainty Quantification", presented in FAA/AEE Tools Colloquium, December 2010

[14] Allaire and Willcox, "Surrogate Modeling for Uncertainty Assessment with Application to Aviation Environmental System Models", AIAA Journal, 2010

[15] EUROCONTROL, Base of Aircraft Data (BADA) Aircraft Performance Modeling Report, EEC Technical/Scientific Report No. 2009-009, March 2009

Project 037 CLEEN II System Level Assessment

Georgia Institute of Technology

Project Lead Investigator

Dimitri Mavris (PI)
Regents Professor
School of Aerospace Engineering
Georgia Institute of Technology
Mail Stop 0150
Atlanta, GA 30332-0150
Phone: 404-894-1557
Email: dimitri.mavris@ae.gatech.edu

University Participants

Georgia Institute of Technology

P.I.(s): Dr. Dimitri Mavris (PI), Mr. Christopher Perullo (Co-PI), Dr. Jimmy Tai (Co-PI)
FAA Award Number: 13-C-AJFE-GIT-013
Period of Performance: August 31, 2016 – August 31, 2017

Project Funding Level

The project is funded at the following levels: Georgia Institute of Technology ($170,000).

The Georgia Institute of Technology has agreed to a total of $170,000 in matching funds. This total includes salaries for the project director, research engineers, graduate research assistants and computing, financial and administrative support, including meeting arrangements. The institute has also agreed to provide tuition remission for any students paid for by state funds.

Investigation Team

Georgia Institute of Technology
Principal Investigator: Dimitri Mavris
Co-Investigators: Christopher Perullo, Jimmy Tai
Fleet Modeling Technical Lead: Holger Pfaender
Noise Modeling Technical Lead: Greg Busch

Project Overview

The objective of this research project is to support the FAA by independently modeling and assessing the technologies that will be developed under the CLEEN II program. This will involve direct coordination and data sharing with companies developing technologies under CLEEN II, in order to accurately model the environmental benefits of these technologies at the vehicle and fleet levels.

Georgia Tech (GT) was previously selected to perform all of the system level assessments for the CLEEN program under PARTNER project 36 and ASCENT project 10. As a result, Georgia Tech has a unique position from both a technical and programmatic standpoint to continue the system level assessments for CLEEN II. From a technical perspective, GT has significantly enhanced the Environmental Design Space (EDS) over the last 5 years to incorporate advanced, adaptive, and operational technologies targeting fuel burn, noise, and emissions. EDS was successfully applied to all CLEEN I contractor technologies including: GE open rotor, TAPS II combustor, FMS-Engine and FMS-Airframe; Pratt & Whitney geared fan; Boeing adaptive trailing edge and CMC nozzle; Honeywell hot section cooling and materials; and Rolls-Royce turbine cooling technologies. GT also gained significant experience in communicating system level modeling requirements to industry engineers and translating the impacts to fleet level fuel burn, noise, and emissions assessments. This broad

technical knowledge base covering both detailed aircraft and engine design and high level benefits assessments puts GT in a unique position to assess CLEEN II technologies.

As the ultimate goal of this work is to conduct fleet level assessments for aircraft representative of future 'in-service' systems, GT will need to create system level EDS models using a combination of both CLEEN II and other public domain N+1 and N+2 technologies. The outcomes of the technology and fleet assumptions setting workshops conducted under ASCENT Project 10 will be heavily leveraged for this effort. Non-CLEEN II technologies for consideration along with potential future fleet scenarios will help to bound the impact of CLEEN II on future fleet fuel burn, emissions, and noise. In the first year, non-disclosure agreements have already been signed with all of the CLEEN II contractors.

Since the FAA will also be performing a portion of the EDS technology modeling work, EDS training has been provided to the FAA in 2016 under the ASCENT Project 10. The training has provided the requisite skill set required to use EDS.
In the prior year of this project, Georgia Tech began modeling activities with Aurora, Pratt and Whitney, and GE. This modeling process included validation of underlying EDS models, information and data exchange necessary to model the individual technologies, and related EDS modeling activities. In addition, Georgia Tech has assisted the FAA with in-house modeling of Delta/MDS and GE technologies. This process has increased the FAAs use of FAA personnel for EDS system level assessment modeling.

More specifically, this year has focused on modeling and assessment of Aurora, Delta/MDS, Pratt & Whitney, and GE technologies. Georgia Tech and the FAA have collaborated on the modeling and assessment of the GE FMS and Delta/MDS technologies. The GE FMS system improves vehicle performance through more intelligent operations and flight path planning. The Delta/MDS technology uses a coating to reduce erosion rates on the fan blade leading to improved performance retention. Both of these technologies have been modeled within EDS. The modeling work for Delta/MDS is complete and the modeling work for GE FMS is currently in iteration with GE. Erosion maps were implemented into the EDS software to simulate the degradation with and without the Delta / MDS fan blade coatings. The erosion maps were provided by a CFD analysis study that Delta had conducted in the spring of 2016. Direct changes of fan efficiency retention were modeled in EDS from the CFD data. The level of fuel burn benefit is dependent on other technology assumptions.

In addition, Georgia Tech has completed modeling assessments for Aurora on the D8 aircraft concept. Benefits have been shared with Aurora and the FAA. While specific benefits are proprietary under the terms of the nondisclosure agreement between GT and Aurora, the benefits predictions match to within 1.5% difference. Georgia Tech has is also in the middle of modeling and assumptions setting discussions for the GE MESTANG more electric aircraft power systems technology.

Major Accomplishments

- GT has signed non-disclosure agreements with all CLEEN II contractors
- Delta/MDS Modeling Complete
- Aurora Modeling Complete
- Pratt & Whitney modeling started
- Modeling and data exchange underway for GE FMS
- Modeling and data exchange underway for GE MESTANG
- Discussions on modeling process held with all contractors

Publications

None.

Outreach Efforts

None.

Awards

None

Student Involvement

Students will be involved later in the period of performance once specific modeling work begins.

Plans for Next Period

GT will continue to model and assess CLEEN II technologies. Specifically, EDS models will be created for the UTAS Integrated Nacelle including fuel burn, noise, and emissions sub-models where appropriate. GT will work with UTAS to verify EDS models before adding to the CLEEN II assessment. GT will also work with Boeing to model the Compact Nacelle technology including any fuel burn and acoustics impacts. Additional EDS modules developed under this effort will be made available to the FAA by GT in the event they are based on public domain information. Proprietary data developed by, or in collaboration with, CLEEN II contractors will need to be obtained by the FAA directly from the respective contractor. This work will also support attendance at CLEEN consortium meetings and contractor preliminary and detailed design reviews to identify any updates required to technology models developed in prior years.

References

None

Project 038 Rotorcraft Noise Abatement Procedures Development

The Pennsylvania State University/Continuum Dynamics, Inc. / Sikorsky Aircraft Corporation/AHS International

Project Lead Investigator

Kenneth S. Brentner
Professor of Aerospace Engineering]
Department of Aerospace Engineering
The Pennsylvania State University
233 Hammond Building, University Park, PA
(814)865-6433
ksbrentner@psu.edu

University Participants

The Pennsylvania State University

- P.I.: Kenneth S. Brentner, Professor of Aerospace Engineering
- FAA Award Number: 13-C_AJFE-PSU-038, Amendment No. 22
- Period of Performance: September 2016 to August 2017
- Task(s): (during this period)
  5. Development and evaluation of noise procedure
  6. Analyze noise abatement procedures and assist in flight test planning
  7. Compare flight test data with prediction
  8. Evaluate flight test data

Project Funding Level

FAA: $150,000; In-Kind Match: (Continuum Dynamics, Inc.: $75,000 to PSU; Sikorsky Aircraft Corporation: $37,500; AHS International: $37,500)

Investigation Team

Kenneth S. Brentner, PI, The Pennsylvania State University; acoustics predictions lead on all tasks.
Joseph F. Horn, Co-PI, The Pennsylvania State University; flight simulation lead supporting all tasks
Daniel A Wachspress, Co-PI, Continuum Dynamics, Inc.; responsible for rotor loads and wake integration, and CHARM coupling.
Mrunali Botre, Graduate Research Assistant, The Pennsylvania State University; primary responsibility for setting up new aircraft models, developing simulations with new helicopter types, acoustic predictions and development of flight abatement procedures, involved in all tasks.
Eric Jacobs, Industrial Partner, Sikorsky Aircraft Corporation; primary responsibility for flight test plan development, provide feedback on all aspects of project, especially related to flight test.
Paul Schaaf, Industrial Partner, AHS International; pilot and operator experience, provides guidance on abatement procedure development.

Project Overview

Rotorcraft noise consists of several components including rotor noise, engine noise, gearbox and transmission noise, etc. Rotor noise is typically the dominant component of rotorcraft noise that is heard by the community upon takeoff, landing, and along the flight path of the helicopter. Rotor noise consists of several different noise sources including thickness noise and loading noise (together typically referred to as rotational noise), blade-vortex-interaction (BVI) noise, high-speed-impulsive (HSI) noise, and broadband noise – with each noise source having its own unique directivity pattern around the

helicopter. Furthermore, any aerodynamic interaction between rotors, interaction of the airframe wake and a rotor, or unsteady, time-dependent loading generated during maneuvers typically results in significant increases in loading noise. The combination of all the potential rotor noise sources makes prediction of rotorcraft noise quite complex, even though not all of the noise sources are present at any given time in the flight (e.g., BVI noise usually occurs during descent and HSI noise only occurs in high-speed forward flight).

In ASCENT Project 6, "Rotorcraft Noise Abatement Operating Conditions Modeling", the project team coupled a MatLab based flight simulation code with CHARM and PSU-WOPWOP to preform rotorcraft noise predictions. This noise prediction system was used for developing noise abatement procedures through computational and analytical modeling. Although this noise prediction system does not contain engine noise or HSI noise prediction capability, it was thoroughly validated by comparing predicted noise levels for a Bell 430 aircraft with flight test data (Ref. 19) for several observer positions and operating conditions.

In the previous year's work in ASCENT Project 38, representative helicopters for noise abatement procedure development were recommended. These helicopters were selected to determine if it is feasible to develop noise abatement procedures for categories of helicopters, (i.e., 2 blade light, 4 blade light, 2 blade medium, etc.) or if aircraft specific design considerations will be required in the development of noise abatement procedures.

Objectives

The objective of this project is to utilize computational and analytical modeling to develop noise abatement procedures for various helicopters for various phases of flight. An extension of the project also includes predictions to support flight test planning and abatement procedure development for the flight testing.

The research team will recommend representative helicopters for which noise abatement procedures will be developed. The helicopters will be selected to determine if it is feasible to develop noise abatement procedures for categories of helicopters, (i.e., 2 blade light, 4 blade light, 2 blade medium, etc.) or if aircraft specific design considerations will be required in the development of noise abatement procedures. Noise abatement procedures will be compared to representative baseline operations. Comparisons will be made using various noise metrics (SEL, DNL, EPNL, etc.) along with the acoustic pressure time history and acoustic spectrum plots (which will be used primarily to explain what is impacting the metrics).

Note: The FAA/NASA flight test occurred late in this year (August and October 2017), so some of the activities reflect this unanticipated change in schedule.

Task #5: Development and Evaluation Of Noise Abatement Procedures

The Pennsylvania State University

Objective(s)

The object of this task is to continue the development various noise abatement procedures and to determine the noise the procedures common across various helicopter categories (weight, number of main rotor blades, tail rotor configuration, technology generation, etc.). This will help to determine the fidelity required for designing the abatement procedure. The helicopters used for flight test will be used to do the analysis and consequently will design the flight procedure.

Research Approach

For this effort, the noise prediction system developed in ASCENT Project 38 will be used and updated as necessary. The PSU-WOPWOP code will be used for noise prediction, and will be coupled with a MatLab flight simulator and CHARM (Comprehensive Hierarchical Aeromechanics Rotorcraft Model) to form a rotorcraft noise prediction system. Limited validation of the system through comparison with the NASA/Bell flight test has demonstrated that the system is reasonably accurate with very reasonable computational cost. The initial procedure considered is a decelerating decent case, which should reduce or eliminate BVI noise during decent. Other flight procedures will be considered after that, including turns and descending turns – which often occur in urban settings. The noise abatement procedures will be compared to standard procedures through comparison of several different acoustic metrics.

Milestone(s)

Evaluation of noise abatement flight procedures for a variety of helicopter categories.

Major Accomplishments

While evaluating noise prediction of unsteady aircraft motion (like decelerating decent) an error was found in the noise prediction system. This error was related to the reconstruction of the rotor wake in the Charm rotor module that is done to provide high-resolution airloads for the noise prediction. In particular, after the high-resolution airloads were output, the module restores the wake geometry to its original low resolution and then continues the flight simulation until the next time when high-resolution airloads need to be saved. The process of restoration added a small error that accumulated after several reconstruction/restoration cycles. To debug this problem, the code was run multiple times with only reconstruction (no restoration), but the code was run to different times. Once the source of the problem was identified, it was fixed and computations of decelerating flight were resumed.

Another accomplishment during this task, is related to validation of the noise prediction system. For more direct comparisons with flight test data, a tool was written that takes the acoustic pressure measure in the flight test and puts it into a format that PSU-WOPWOP can read. In this way, noise predictions and flight test data are post processed in exactly the same manner – both using the post processing procedures in PSU-WOPWOP.

One of the accomplishments of this task is the simulation of different flight conditions and comparing the noise with flight test data. The validation of the noise prediction system in both level flight and a blade-vortex-interaction flight conditions is a significant achievement for the project. The agreement between the predicted and measured results is quite reasonable for fidelity of these tools and it demonstrates that the tools are able to predict the significant physical noise sources that must be modified to achieve noise abatement. This validation enables the noise prediction system to be used for the other tasks in the project with a degree of confidence. Figure 1 shows the prediction for a 95 kts level flight case. The noise components and total noise are shown in terms of OASPL and A-weighted OASPL as a function of the helicopter time (0 sec. is the time with the helicopter is overhead). Note that the flight test data (black line) includes a ground reflection on a hard ground. The noise predictions labeled "Total …. – No Wall" are free-field noise prediction, while the "Total … - Wall in" include the effect of a hard ground; hence, the "wall in" prediction should be compared with the flight test data (Run 273126). In Fig. 2, the predicted noise for a 0.05g deceleration along 6 deg. descent is shown. During this flight procedure, the aircraft velocity reduces from 100 kts to approximately 68 kts.

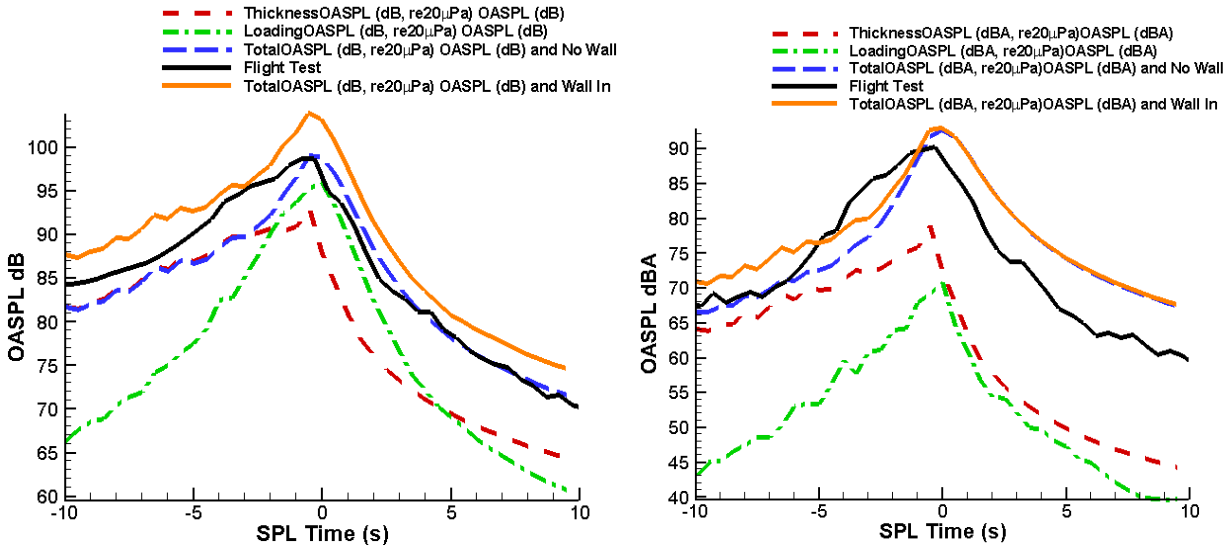

(a) OASPL, dB (b) A-weighted OASPL, dBA

Figure 1- OASPL and A-weighted OASPL levels for Bell 430 in 94.7 kts level flight, compared with flight test data (Run 273126).

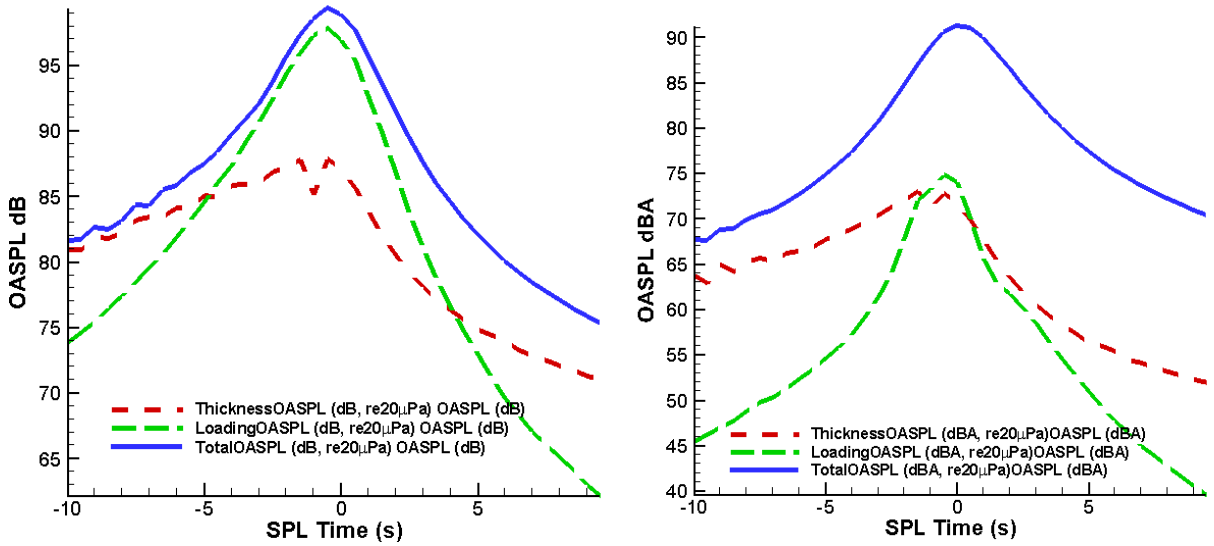

(a) OASPL, dB (b) A-weighted OASPL, dBA

Figure 2 - OASPL and A-weighted OASPL levels for Bell 430 in deaccelerating descent flight.

Publications
None

Outreach Efforts
None

Awards
None

Student Involvement
Mrunali Botre, graduate assistant currently working toward her Ph.D. at Penn State, performed the acoustic predictions and worked on debugging the problem with the error introduced by the reconstruction/restoration process.

Plans for Next Period
Validation of the system with the FAA/NASA flight test data will be an ongoing process, that will be done in parallel to "understanding" what was likely the reasons for changes in noise in the flight tests. The flight test data does not have any details about blade loadings, specific BVI information, etc., but the predictions can suggest which noise components were dominant in different parts of the flyover and at different directivity angles. For example, the predictions show that the broadband noise is dominant when the aircraft is overhead and downrange – so the broadband noise model can be validated for the different aircraft during this part of the flight profile.

Task #6: Analyze Noise Abatement Procedures and Assist In Flight Test Planning
The Pennsylvania State University

Objective(s)

This task will develop and analyze of rotorcraft noise abatement flight procedures for the aircraft used in flight test. The procedures will be used to plan flight test and the data will be used to validate the tools.

Research Approach

In support of an FAA/NASA flight test, the helicopters used in the flight test were modeled and the noise from the anticipated flight procedures (baseline and noise abatement procedures) were predicted. The aircraft selected for the flight test originally included the Sikorsky S-76C and S-76D models, but ultimately Sikorsky decided not to provide the aircraft for the flight test, so the final group of helicopters were: Robinson R-44 and R-66 (piston and turbine engines respectively); Bell 206L and 407 (2 and 4-bladed main rotors, different generation of similar aircraft); and Airbus AS 350 and EC130 (standard tail rotor and Fenestron).

While these aircraft are all generally smaller, there are subtle differences that can be compared. The research approach is to determine if the approximate modeling using in the predictions is sufficient to distinguish between the aircraft, and to determine if the difference between aircraft result in significant noise differences between related models and other manufacturers models.

- Robinson Helicopters: R44 and R66 (similar size, but R44 has piston engine, while R66 has turbine engine and different main rotor).

- Bell Helicopter Textron, Inc.: 206L and 407 (similar weight and size, but 2-bladed vs 4-bladed main rotor; 407 is newer generation).

- Airbus Helicopter: AS 350 and EC 130 (different anti-torque technology, tail rotor vs. Fenestron; 3-bladed main rotors).

Figure 3 - Helicopters used in FAA/NASA flight test and modeled in PSU predictions.

Milestone(s)

Computational models for all the flight test aircraft need were developed. Predictions on a hemisphere, 100 ft radius, were computed for all steady flight conditions in the flight test and for segments of the abatement procedures. These noise hemispheres were provided to Volpe for their noise prediction activity to explore more rapidly various noise abatement procedures.

Major Accomplishments

Prediction of the SEL contours for several of the flight conditions were performed to compare the different flight procedures to determine which procedures had the lowest noise. Much of the focus was on descent, when BVI noise can occur – and should be avoided as part of a noise abatement strategy. To show the subtle differences between aircraft that are nearly the same, Figs. 4 and 5 compare the SEL contours on the ground for 3 and 6 deg descents for the Robinson R-44 and R-66 aircraft for 3 flight speed (60, 80, and 100 kts). The size and weight of the two Robinson aircraft is nearly the same, but the engine in the R-44 is a piston engine, while the R-66 has a turbine engine. The main rotor blade on the R-66 has a different chord and twist distribution as compared to the R-44 as well, but these differences are not readily identifiable by a cursory visual inspection.

These figures show a couple of different trends, visible at both descent angles. First, flying at higher speeds in the descent tends to take the helicopter out of the BVI noise condition and the noise levels are lower. Although not shown, a steeper descent angle or deceleration can also achieve this result. A secondary observation is that although the differences in the helicopter configuration are relatively small, there are noticeable difference in the noise levels and directivity on the ground plane. A more detailed investigation is needed to determine if these small differences are significant, and when they might be significant.

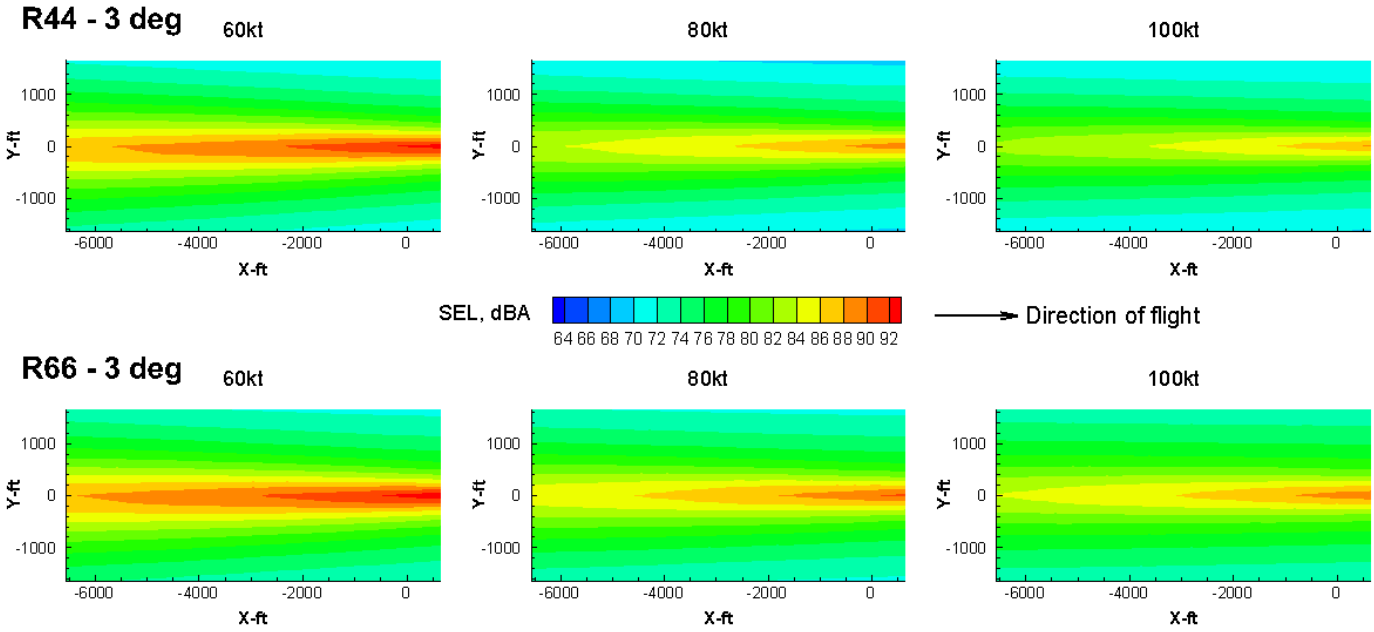

Figure 4 - Predicted SEL contours: 3 deg steady descent for different flight speeds.

Publications

None

Outreach Efforts

None

Awards

None

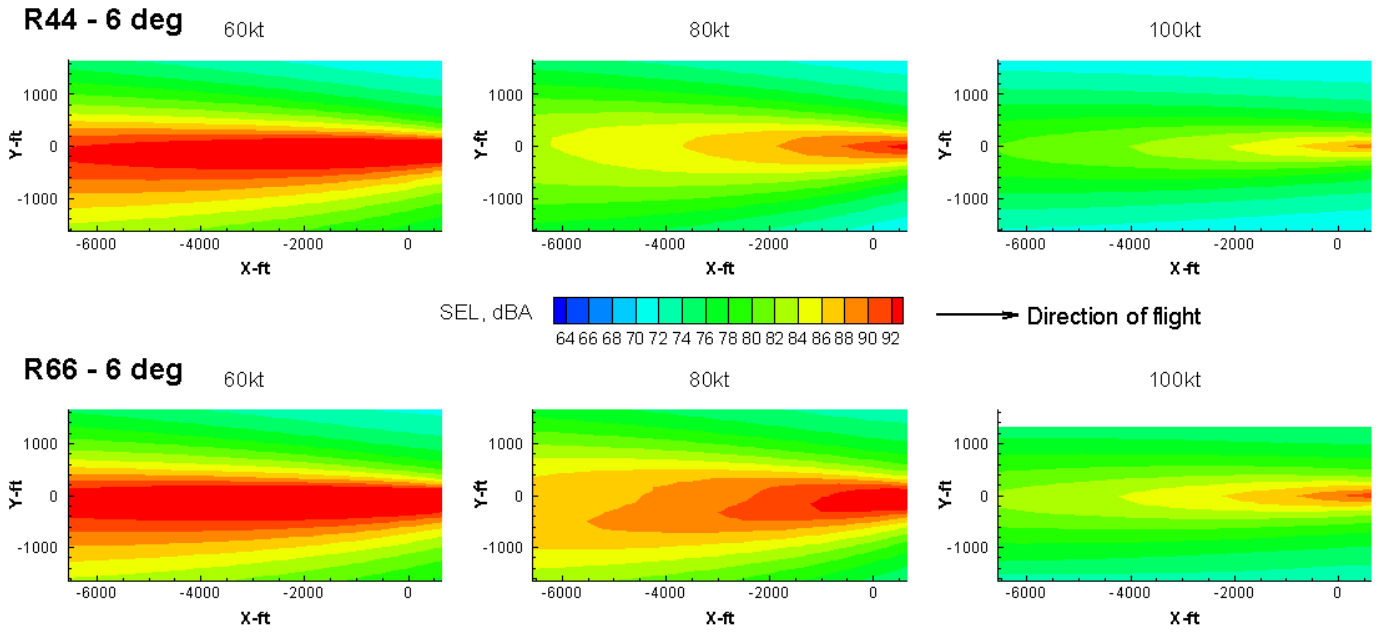

Figure 5 - Predicted SEL contours: 6 deg steady descent for different flight speeds.

Student Involvement

Mrunali Botre, graduate assistant currently working toward her Ph.D. at Penn State, led the noise prediction effort, including development of the flight test aircraft models (with the help of Dan Wachspress and the rest of the team). She performed a large number of noise predictions in a short period of time leading up to the flight test.

Plans for Next Period

The primary noise abatement procedures (or procedure element) for the flight test will be predicted with the noise prediction system. The aircraft models for the anticipated flight test aircraft will be developed.

References

None

Task #7: Compare Flight Test Noise Results with Predicted Results for the Same Aircraft for Validation and Assessment of the Noise Prediction System

The Pennsylvania State University

Objective(s)

The objective is to compare the flight test data with predicted noise levels to validate the effectiveness of the noise abatement procedures.

Research Approach

In this task, acoustic data from the flight test will compared with the noise predictions. This comparison will have two primary goals: 1) to assess and validate the effectiveness of the prediction system and to determine the significance of noise sources not currently modeled (i.e., engine noise); and 2) to evaluate and verify the effectiveness of noise abatement flight procedures. Although the flight test did not occur as early as anticipated, some preliminary flight test data was available for comparison – in the form of data extrapolated by Volpe (i.e., based on measured data). This allows comparison of predicted and interpolated/extrapolated flight test data for a few cases for the R-44 helicopter. It should be noted that the extrapolation is not thought to be accurate at distant sideline observers because the microphone array data used to form an acoustic data hemisphere for the Volpe extrapolation does not have any data near the rotor plane (zero elevation angle) because that would require very distant microphones on the ground.

Milestone(s)

Sound exposure levels for interpolated/extrapolated data and predictions have been compared for two flight conditions for the Robinson R-44 aircraft: 3 deg descent at 60 kt forward speed and 6 deg descent at 80 kt forward speed. In the flight test, the aircraft does not fly all the way down to a hover at a touchdown point and in the predictions, the simulation is stopped when aircraft reaches a minimum altitude.

Major Accomplishments

The Robinson R-44 helicopter was modeled and flown in several different flight conditions. In particular, two descent conditions, 3 deg descent at 60 kts and 6 deg descent at 80 kts were compared with flight test data. The predictions included both main rotor and tail rotor noise sources, including thickness noise, loading noise, and broadband noise. Engine noise was not modeled in the simulation. The ground reflection was included in the discrete frequency noise sources (thickness and loading), but the noise prediction system is not currently able to model ground reflection for broadband noise. The ground reflection model is for a perfectly hard ground, which is not completely representative of the flight test. Atmospheric attenuation of the noise was also modeled, but the specific relative humidity was not used in these preliminary comparisons. It should be noted that the flight test data interpolation/extrapolation is thought to be representative of the flight test over the region where microphones were placed on the ground (± 0.5 SELdBA), but once the flight test is complete, the data processing needs to be reviewed to ensure that the data is correct. Then refinements to the predictions can also be considered.

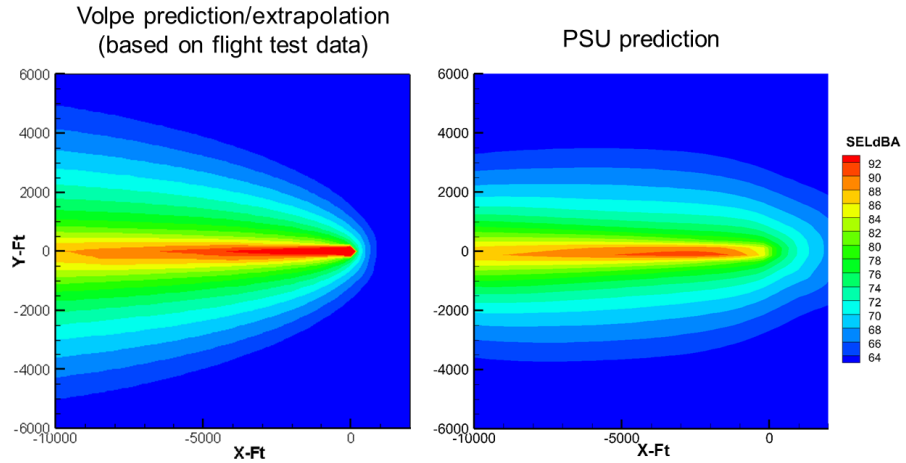

Figure 6 - Comparison of SEL flight test data (interpolation/extrapolation) with PSU prediction for Robinson R-44 helicopter in 3 deg descent at 60 kt.

In Fig. 6, the helicopter flight path is from left to right along the y axis. The target touchdown point is at x = 0 ft. The SEL values along the flightpath and within the first 1500 ft to each side are very similar to those of the flight test. For a more direct comparison, without the interpolation and extrapolation of the flight test data, comparison of the SELdBA values were made at three microphone locations at x = -1900 ft, along the flight path and 400 ft to either side. The measure data and predicted values are shown in Table 1. At this location, the SELdBA value is within 0.5 SELdBA along the flightpath and

3 SELdBA on each side. Further investigation is needed to understand if this agreement can be improved and if there is a reason why the levels at the sideline locations are too low (although not accounting for ground reflection of the broadband noise is likely to raise all the levels by a few SELdBA).

In Fig. 7, a similar comparison of flight test data and PSU prediction is made for the Robinson R-44 for a 6 deg descent at 80kt. There the prediction seems to predict higher SEL values farther away from the target touchdown point. It is not clear if there this has something to do with an actual difference in the flight path angle (intended vs. what was flow, or due winds), but this difference will need to be investigated further. Nonetheless, at x = - 1900 ft where the actual data is compared with the prediction, the SELdBA values are all within 2 SELdBA or less, as shown in Table 1.

Table 1. Comparison of measured and predicted SEL values at 3 locations; 6 deg descent at 80 kt.

Location	Measured #156 (SELdBA)	PSU prediction (SELdBA)
X= - 1900 ft, Y = 400 ft	82.4	80.0
X = -1900 ft, Y = 0 ft	87.4	88.8
X = -1900 ft, Y = -400 ft	83.3	81.1

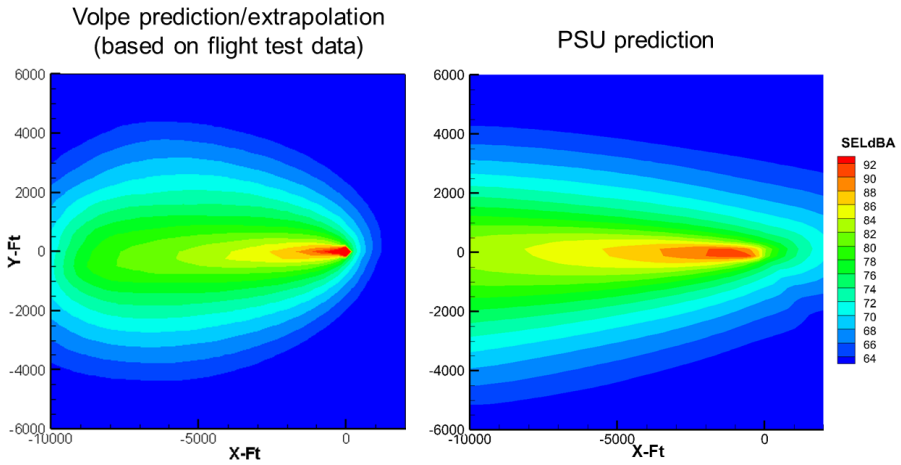

Figure 7 - Comparison of SEL flight test data (interpolation/extrapolation) with PSU prediction for Robinson R-44 helicopter in 6 deg descent at 80 kt.

Publications

None

Outreach Efforts

None

Awards

None

Student Involvement
Mrunali Botre, graduate assistant currently working toward her Ph.D. at Penn State, has performed the comparison of predicted results with flight test data.

Plans for Next Period
Many more flight conditions will be considered for the various aircraft flown in the FAA/NASA flight test. Investigation into the details of different comparisons can be made to understand more deeply the differences between the predictions and flight test data. In particular, it will be important to determine if the prediction is uniformly accurate for all aircraft classes or is better for some more than others. This information will be important in considering the noise abatement procedure predictions.

References
None

Task #8: Assist In Initial Evaluation of Flight Test Data to Determine Effectiveness of Noise Abatement Procedures
The Pennsylvania State University

Objective(s)
This task will support the flight test team to determine the effectiveness of the noise abatement procedures.

Research Approach
This task for this extended project is to provide assistance in the initial evaluation of the flight test data and the effectiveness of various noise abatement procedures. This will involve evaluation of the flight test data and examination and comparison of measured and predicted results to help explain any significant unexpected noise measurement. This evaluation can also identify which noise sources are the primary and secondary noise sources involved in a flight procedure and provide understanding about how the noise abatement was achieved (which can lead to generalizing the procedure to other helicopter categories, weights, etc.).

Milestone(s)
The flight test has just been completed at two different sites. The PI attended the R-66 testing at Eglin AFB and was able to review some of that data as the test was taking place, but most of the data has not been received by Penn State yet.

Major Accomplishments
This task has just begun looking at the limited flight test data available. Based on the flight test, some work has begun on developing better ways to generate noise abatement procedures and an abstract for a paper has been prepared for the 2018 AHS Forum Acoustics Session. Once the data becomes available, which is expected in before the end of the calendar year 2017, and then more work can be done on this task.

Publications
None

Outreach Efforts
None

Awards
None

Student Involvement
Mrunali Botre, graduate assistant currently working toward her Ph.D. at Penn State, will assist in this effort.

Plans for Next Period

During the next period analysis of the flight test data for each of the 6 aircraft will be performed and analysis of the abatement procedures will begin. Comparisons with predicted results will also be used to guide the analysis.

References

None

Project 039 Naphthalene Removal Assessment

Massachusetts Institute of Technology

Project Lead Investigator

Prof. Steven Barrett
Leonardo Associate Professor of Aeronautics and Astronautics
Department of Aeronautics and Astronautics
Massachusetts Institute of Technology
77 Massachusetts Avenue – Bldg. 33-316
Cambridge, MA 02139
(617)-452-2550
sbarrett@mit.edu

University Participants

Massachusetts Institute of Technology

- P.I.(s): Prof. Steven Barrett & Dr. Raymond Speth
- FAA Award Number: 13-C-AJFE-MIT, Amendment Nos. 026 and 034
- Period of Performance: July 8, 2016 to Aug. 31, 2018 (With the exception of funding and cost share information, this report covers the period from October 1st, 2016 to September 30th, 2017)
- Task(s):
    1. Preliminary screening of refinery processes for naphthalene removal
    2. Kinetic model of PAD formation with fuel-composition effects
    3. Calculation of process requirements and fuel composition effects for selected refining processes

Project Funding Level

Project Funding Level: $490,000 FAA funding and $490,000 matching funds. Sources of match are approximately $129,000 from MIT, plus 3rd party in-kind contributions of $361,000 from Oliver Wyman Group.

Investigation Team

Prof. Steven Barrett (MIT) serves as principal investigator for the A39 project as head for the Laboratory for Aviation and the Environment. Prof. Barrett coordinates both internal research efforts and maintains communication between investigators in the various MIT research teams mentioned below.

Dr. Raymond Speth (MIT) serves as co-principal investigator for the A39 project. Dr. Speth directly advises student research in the Laboratory for Aviation and the Environment focused on assessment of naphthalene removal refinery options, climate and air quality modelling, and fuel alteration life-cycle analysis. Dr. Speth also coordinates communication with FAA counterparts.

Prof. William Green (MIT) serves as a co-investigator for the A39 project as a head of the Green Research Group. Prof. Green advises student work in the Green Research Group focused on computer-aided chemical kinetic modeling of PAH formation.

Mr. Randall Field (MIT) is the Executive Director of the MIT Energy Initiative, and a co-investigator of the A39 project. Drawing upon his experiences as a business consulting director at Aspen Technology Inc., Mr. Randall provides mentorship to student researchers in selection and assessment of naphthalene removal refining option, and process engineering at-large.

Mr. Drew Weibel (MIT) is a graduate student researcher in the Laboratory for Aviation and the Environment. Mr. Weibel is responsible for conducting selection and assessment of naphthalene removal refining options, calculation of refinery process requirements and fuel composition effects from selected processes, relating PAH formation to aircraft PM

emissions, estimating capital and operating costs of naphthalene removal, air quality and climate modelling, and an integrated cost-benefit analysis.

Mr. Max Liu (MIT) is a Ph.D. candidate researcher in the Green Research Group. Mr. Liu is responsible for development and analysis of a chemical kinetic model of PAH formation with fuel-composition effects and supporting development of a relationship between PAH formation and aircraft PM emissions.

Project Overview

Aircraft emissions impact the environment by perturbing the climate and reducing air quality, which leads to adverse health impacts, including increased risk of premature mortality. As a result, understanding how different fuel components can influence pollutant emissions, as well as the resulting impacts and damages to human health and the environment, is of importance to leading future research aims and policy. Recent emissions measurements have shown that removal of naphthalenes, while keeping total aromatic content unchanged, can dramatically reduce emissions of particulate matter (Brem et al., 2015, Moore et al., 2015). The objective of this research is to determine the benefits, costs, and feasibility of removing naphthalenes from jet fuel, in regards to the refiner, the public, air quality, and the environment. Specific goals of this research include:

- Assessment and selection of candidate refining processes for the removal of naphthalenes from conventional jet fuel, including details of required technology, steady-state public cost, and changing life-cycle emissions impacts at the refinery.
- Development of a chemical kinetics model to better understand the link between fuel aromatic composition resulting PM emissions due to jet fuel combustion.
- Assessment of the intrinsic climate and air quality impacts associated with naphthalene reduction and/or removal from jet fuel.
- Development of a succinct life-cycle analysis of the relative costs of removing naphthalene from jet fuel and the associated benefits due to avoided premature mortalities and climate damages for a range of possible scenarios.

Task #1: Preliminary Screening of Naphthalene Removal Refining Processes

Massachusetts Institute of Technology

Objective(s)

Naphthalene is present in varying levels in straight-run crude oil distillation cuts used to produce jet fuel, and is currently not targeted for removal in treatments used to meet industry standard fuel specifications. As a result, reducing the naphthalenic content in jet fuel entails the introduction of an additional refinery treatment process. The objective of this task is to identify suitable refinery processes that can be used to remove or convert naphthalenes. Once identified, data for key refining process parameters will be collected to inform future cost estimation of applying the selected processes for jet fuel naphthalene removal.

Research Approach

Introduction

Refining processes, and chemical processes at large, are focused on subjecting chemical species to various environments to allow for conversion, combination, separation, etc., in order to produce useful, increased value products. When considering removal of a chemical component from a mixture, say naphthalenic species from a kerosene feed, a process designer must consider unique properties shared by the chemical component that allow for its conversion, combination, separation, etc. without affecting the underlying mixture.

While naphthalenes are not currently targeted for removal to meet industry standards, there are several mature refining technologies that, once tuned, can complete this reduction/removal with high efficiency. In AY 2016/2017, we will select suitable, readily accessible refining technologies for the removal of naphthalenes from the U.S. jet fuel pool. Our focus is on technologies currently used in industry, in order to provide possible policies that could be implemented in the near term.

Methods

In order to select a number of refining processes for the large-scale removal of naphthalenes from the U.S jet fuel pool, we will complete a literature review of current technologies, qualitative evaluation of those technologies in terms of their applicability of naphthalene removal, the scope of economic and process data available, and the level of naphthalene removal achievable. Particular attention will be given to preserving non-naphthalenic aromatics, since reducing the amount of these components would limit the capacity to blend paraffinic alternative jet fuels while still meeting minimum requirements for aromatics.

In order to evaluate each candidate process, we will leverage existing literature to estimate the utility (process fuel, electricity, hydrogen, etc.) requirements for each process, the effect on the composition of the resulting jet fuel, and the capital costs of new refinery equipment required. We will include the effects of any pre-processing that may be required. We will then compare processes side-by-side in order to demonstrate the trade-offs associated with naphthalene removal at the refinery.

As a by-product of analyzing a range of different refining pathways, we will be able to assess the tradeoffs associated with different levels of naphthalene removal. Combined with later work in development of a relationship between jet fuel composition and PAH formation, we will be able to assess the level of severity in which naphthalene's should be removed, in order to optimize costs and benefits.

Results

AY 2016/2017 Task 1 was concluded with the selection of extractive distillation and selective hydro-treating as candidate refinery processes for the large-scale removal of naphthalenes from the U.S. jet fuel pool.

Naphthalenes are unsaturated, double ring aromatic species which may contain alkylated or impurity groups. They are most readily removed via conversion to mono-aromatic or saturated species – via hydrogen addition or carbon removal – or separated on the basis of polarity. A desired refinery process would remove naphthalenic species with high efficiency, not affect the remaining aromatic content, produce minimal changes to other fuel properties, and produce limited emissions and economic impact; removal of other impurities (sulfur, nitrogen, etc.) is an added bonus. A list of potential refining processes is listed below (Gary et al., 2007). Description of each process, and associated pros and cons can be found in the AY 2016/2017 deliverable 1 presentation.

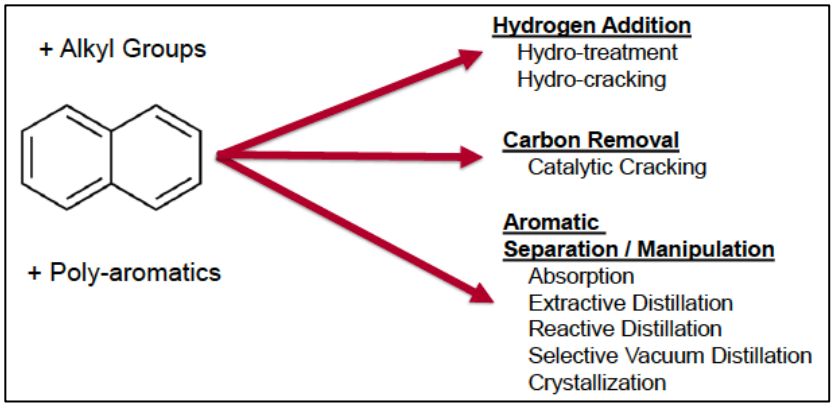

Figure 1

As noted in Figure 1, there are three families of processes pertinent to the removal of naphthalenes; conversion by hydrogen addition (saturation), conversion by carbon removal (cracking), or aromatic separation. Hydrogen addition and aromatic separation are often used as finishing processes, and can operate under mild conditions. Carbon removal, on the other hand, is often associated with molecular cracking, has the potential to radically convert the feed, is associated with the production of olefins, and often cannot break apart stable aromatic rings. As a result, only hydro-conversion and aromatic separation processes were considered.

Hydro-conversion processes are a family of refining units that react a petroleum feed with gaseous hydrogen at elevated temperatures and pressures in order to saturate – and in severe processes, crack – hydrocarbon molecules. Hydro-treating is a mild hydro-conversion finishing process used to remove impurities and saturate olefin and aromatic species. Selective hydro-treating for the conversion of naphthalenes is a viable process candidate because the second ring of naphthalenic species will tend to be fully saturated prior to the saturation of mono-aromatic species. Due to the relative selectivity of fuel components, we also expect desulfurization and di-nitrogenation to occur. As a result, with a robust catalyst selection and finely tuned process parameters, we expect a selective hydro-treating process could reduce/remove naphthalenes by converting them to mono-aromatics with little change to the overall aromatic content and other fuel characteristics, and with reasonable hydrogen requirements (Fahim, 2010).

Separation processes provided a separation of mixture components about some defining species characteristic, such as weight, size, polarity, etc. Extractive distillation provides a separation of petroleum components based on polarity, by introducing a heavy, high-boiling point polar solvent to the feed. Highly polar component (including all aromatic and impurity containing species), will bind to the solvent and be separated from other species based on weight. The solvent is then separated using by simple distillation. Finally, mono-aromatic and naphthalene species can be roughly separated in a second distillation step, the prior cut being returned to the feed. Extractive distillation, while less common for feed mixture separations, was identified as a second candidate for naphthalene removal from the U.S. jet fuel pool (Meyers, 2004).

After selection of extractive distillation and selective hydro-treating as candidate refining processes for the removal/reduction of naphthalene from the U.S. jet fuel pool, further details were collected on each process to define their offsite needs and fuel composition impacts. A table of relevant process requirements and fuel effects is given below.

Table 1

Process Name	Hydro-Treatment	Extractive Distillation
Description	Naphthalenes are hydrogenated to mono-aromatic and cyclo-paraffinic components.	All aromatics are separated via a polar solvent. Mono-aromatics are separated from naphthalenes via distillation and blended back into the jet fuel product
Process Type	Conversion (H_2 addition)	Aromatic Separation
Existing Uses	Desulfurization, impurity removal, aromatic hydrogenation	Separation of polar feed components, BTX separation
Removal of Naphthalenes	Assumed 95% efficient	Assumed 95% efficient
Effect on Mono-Aromatics	Limited (<10%) hydrogenation	Fully separated; fraction returned to product can be controlled
Impurity Removal	S, N removal to <50 ppm	Small removal of S, N impurities
Supporting Processes Req'd	Hydrogen production, Sulfur gas removal, sulfur post-treatment, steam generation and cooling facilities	Naphthalene / mono-aromatic post distillation, steam generation and cooling facilities
Process Innovation Req'd	Minimal required. Very similar to existing units	Efficient solvent with impurity (S,N) resiliency

Milestone(s)

This work was completed in February 2017, and is described in the deliverable 1 presentation provided to the FAA on February 28th, 2017.

Major Accomplishments
During this period, two refining processes – selective hydro-treating and extractive distillation – were chosen as suitable candidates for large-scale naphthalene removal from the U.S. jet fuel pool. A summary of this work is contained in the deliverable 1 presentation provided to the FAA on February 28th, 2017.

Publications
None

Outreach Efforts
None

Awards
None

Student Involvement
Drew Weibel, Master's student in the Laboratory for Aviation and the Environment is working directly with Prof. Steven Barrett and Dr. Raymond Speth to conduct the research objectives of Task 1. Mr. Weibel is a 2nd year graduate student, and will serve on the research team through the remainder of the A39 project timeline.

Plans for Next Period
The work completed in Task 1 has informed the calculation of process requirements and fuel composition effects for hydro-treating and extractive distillation systems in AY 2016/2017 Task 3, as describe below. In AY 2017/2018, an economic model for the cost of naphthalene removal via selective hydro-treating and extractive distillation will be assembled and tested to determine the societal net present value of such a policy change. This "cost" will ultimately be applied to a Cost-Benefit Analysis in order to assess the realized benefits of naphthalene removal.

Task #2: Kinetic Model of PAH formation with fuel-composition effects
Massachusetts Institute of Technology

Objective(s)
The formation of black carbon (soot) from hydrocarbon fuels can be considered as taking place in two stages. First, fuel components and combustion intermediates react to form polycyclic aromatic hydrocarbons (PAHs). Large PAHs then act as soot nuclei, which grow as they absorb both PAH and other species, coagulate through collisions with other soot particles, carbonize, and partially oxidize (Richter and Howard, 2000). The details of fuel composition mainly affect the first step of this process, the formation of PAHs. In this project, we will use the Reaction Mechanism Generator (RMG) to develop a detailed chemical kinetic mechanism for jet fuel combustion that includes the formation of PAH (Gao et al., 2016).

The objective of AY2016/2017 Task 2 is to update the RMG algorithm in order to handle aromatic species, and to include aromatic reactions up to three-ring species, which will be used as identifiers for soot precursors in later models. The updates to RMG will also undergo preliminary validation using experimental results from shock-tube pyrolysis and co-pyrolysis studies.

Research Approach

Introduction
RMG (http://rmg.mit.edu) is an automatic chemical reaction mechanism generator that constructs kinetic models composed of elementary chemical reaction steps using a general understanding of how molecules react. This tool provides a powerful method to identify reaction mechanisms computationally, and ensure full coverage of pertinent species and reactions based on the current literature. RMG has previously been used to analyze various fuels including JP-10 and di-isopropyl ketone combustion and pyrolysis (Gao et al., 2015; Allen et al., 2014).

In AY 2016/2017, we will add updates to the RMG algorithm in order to accurately handle aromatic species, and to include aromatic reactions up to three-ring species, which will be used as identifiers for soot precursors in later models.

Method

Previously, RMG was unable to robustly represent aromatic structures. The algorithm depended primarily on representation using Kekulé structures, which resulted in incorrectly treating them like aliphatic species. In order to correctly represent aromatic species, RMG was updated to generate the Clar structure representation of PAHs. As result, aromatic species are more clearly differentiated from aliphatic species, and the number of different representations has been reduced in many cases. An example of the reduced representations for a phenanthrene radical is shown below.

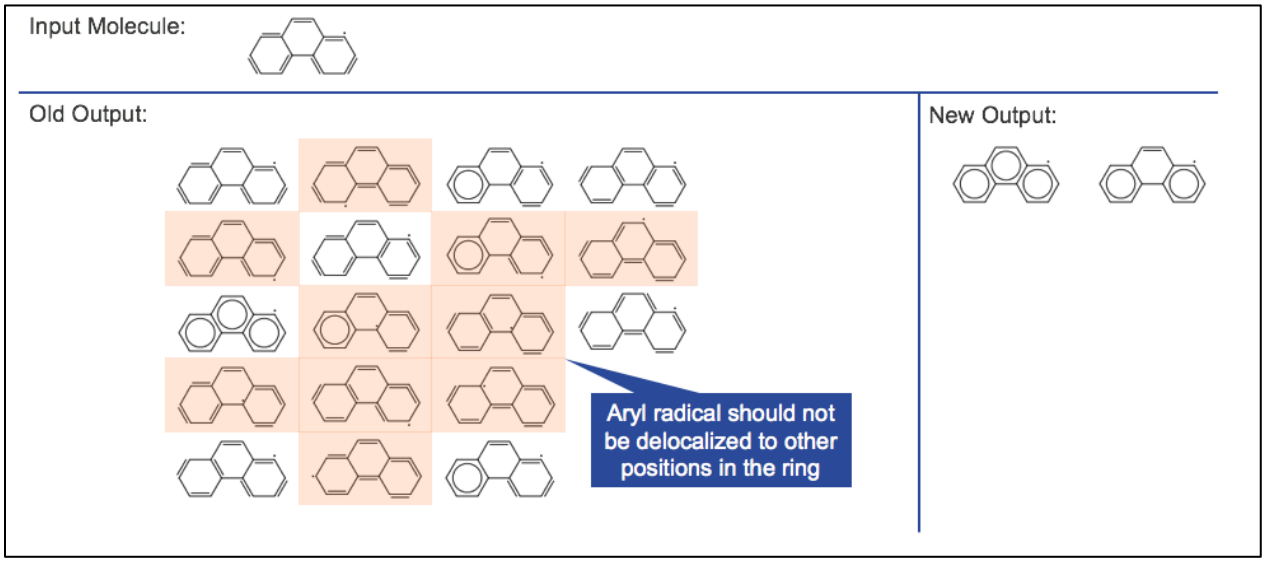

Figure 2

Other changes were made to further improve reaction rate predictions. An algorithmically challenging task of allowing aromatic bond types was completed after implementing a custom kekulization algorithm. This allows rate rules for aromatic species to be specified separately from those for aliphatic species. Also, ring perception was implemented for rate rules to allow separation of rates for linear versus cyclic species.

In order to validate updates described previously, the RMG model was tested against experimental shock-tube pyrolysis data (Lifshitz et al., 2009). Additional co-pyrolysis models were also generated, although without experimental comparisons.

Results

The improvements described above successfully enabled RMG to handle aromatic species. Prior to the updates, program crashes were inevitable when modeling any aromatic system. To support the algorithm changes, new literature data for aromatic thermochemistry and kinetics were also added to the database.

For preliminary validation, a model was generated for pyrolysis of 1-iodonaphthalene and acetylene for comparison to shock-tube data. The model predictions for the major products, acenaphthalene and naphthalene matched well with the experimental data (see figure shown below). The RMG model predicted a higher yield of 1-ethynyl naphthalene than the literature model, although none was observed in the experiment. The RMG model also predicted smaller side products such as vinylacetylene and 1,3-butadiene, which were not reported in the experiment, although the authors do note that small molecule products from acetylene reactions were assumed to be negligible.

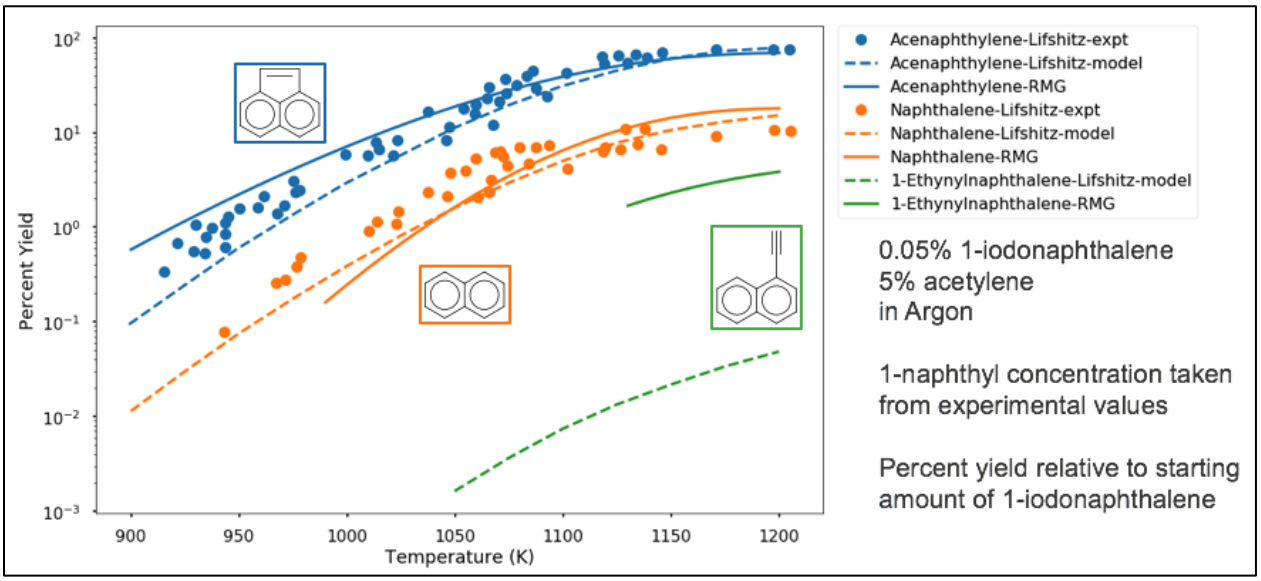

Figure 3

Co-pyrolysis models for equimolar naphthalene or tetralin with acetylene were also generated to get an initial view at whether RMG could capture the differences in reactivity. For naphthalene and acetylene, RMG predicted the major products to be acenaphthalene and hydrogen, which was initially surprising, since other PAHs such as anthracene or phenanthrene were also expected. However, these observations were corroborated by Parker et al. (2015), who also saw that acenaphthalene was the main product in contrast with generally accepted HACA mechanism for PAH growth. The model for tetralin and acetylene displayed markedly different behavior, as expected. Major products were hydrogen, naphthalene, methane, and ethene. No three ring aromatics were formed, possibly because of the overall higher hydrogen/carbon ratio.

Overall, these modeling results are very promising, and show that RMG is now much better at modeling aromatics.

Milestone(s)

This work was completed in June 2017, and is contained in the deliverable 2 presentation provided on Jun 30th, 2017.

Major Accomplishments

During this period, the RMG algorithm was successfully updated to handle aromatic species and kinetics data was added for aromatic species. These updates also underwent preliminary validation when compared to experimental shock-tube pyrolysis data. A summary of this work is contained in the deliverable 2 presentation provided to the FAA on June 30th, 2017.

Publications

Presentations

Going Bigger: Capturing PAH Chemistry in RMG *May 23, 2017*
Mengjie Liu, Kehang Han, William H. Green
Overview of RMG developments to improve thermochemistry estimation for polycyclic species and general handling of aromaticity for kinetics. International Conference on Chemical Kinetics.
Presentation, manuscript in preparation. FAA support was acknowledged.

Outreach Efforts

None

Awards
None

Student Involvement
Mengjie (Max) Liu, PhD student in the Green Research Group in MIT's Department of Chemical Engineering completed the majority of the updates to the RMG. Mengjie will be continuing work to further validate and refine the RMG models, as well as provide comparison of the kinetic model to LFP/PIMS experimental data during AY 2017/2018.

Plans for Next Period
During the next period, the work completed in Task 2 will be used to inform development of a relationships between fuel naphthalene content and aviation PM emissions. The updated RMG code is now capable of development of reaction mechanisms with aromatic species up to three rings. A reaction mechanism will be constructed to represent aviation jet fuel, and the intermediate and product species of combustion. This reaction mechanisms will then be tested in simple combustion structure models to estimate the relative production of PM precursors (three-ring aromatics) per each reactant species. As a result, the relative production of PM from naphthalenes versus mono-aromatic, cyclo-paraffinic, and paraffinic will be assessed.

Task #3: Calculation of Process Requirements and Fuel Composition Effects for Selected Refining Processes
Massachusetts Institute of Technology

Objective(s)
In AY2016/2017 Task 1, selective hydro-treating and extractive distillation were selected as candidate refinery process for large-scale reduction or removal of naphthalene from the U.S. jet fuel pool. In addition, data was collected regarding the offsite (or the supporting process) requirements and fuel composition effects of each process.

The objective of AY2016/2017 Task 3 is to continue quantitative analysis of both processes in order to develop simplified estimation models of process requirements and fuel composition effects. The result of this task will be the cost estimation for individual selective hydro-treating and extractive distillation refinery units, modelled as brown-field additions to existing refinery operations.

Research Approach

Methods
Based on the collection of process parameters as part of AY2016/2017 Task 1, utility requirements and capital cost data were collected for distillate hydro treating, extractive distillation, and their supporting processes. The supporting processes of selective hydro-treating are steam methane reforming for hydrogen production, amine separation for hydrogen sulfide separation from off-gasses, and the Claus process for sulfur recovery. Because these supporting processes are often connected to several units at a refinery, they are costed based on both the size of the modelled refinery and the capacity of the modelled hydro-treatment unit. The sole supporting process for extractive distillation is post-distillation.

In order to calculate the net present value of an added refinery finishing process for the reduction/removal of naphthalene from jet fuel, the methods described by Gary et al., 2007 are adopted. Fixed capital investment was estimated from the desired process capacities and the collected cost data. Operating cost was calculated as a function of the fixed costs, and as a function of the utility requirements and estimated utility costs (shown in the figure below) Catalyst/Solvent and process water utility costs are assumed constant (Gary et al. 2007, Peters et al., 2003). Historical and predicted natural gas and electricity prices, by U.S. census region, are taken from the U.S. Energy Information Administration. Using an auto-regressive – moving average (ARMA) model, calibrated to the predicted trend and historical price variations, natural gas and electricity prices are estimated stochastically. The net present value is then calculated using a Discounted Cash Flow Rate of Return (DCFRoR) model over the lifetime of the process unit. A discount factor of 2.74%, based on the 20 year constant maturity rate, is used for the estimated cost to society.

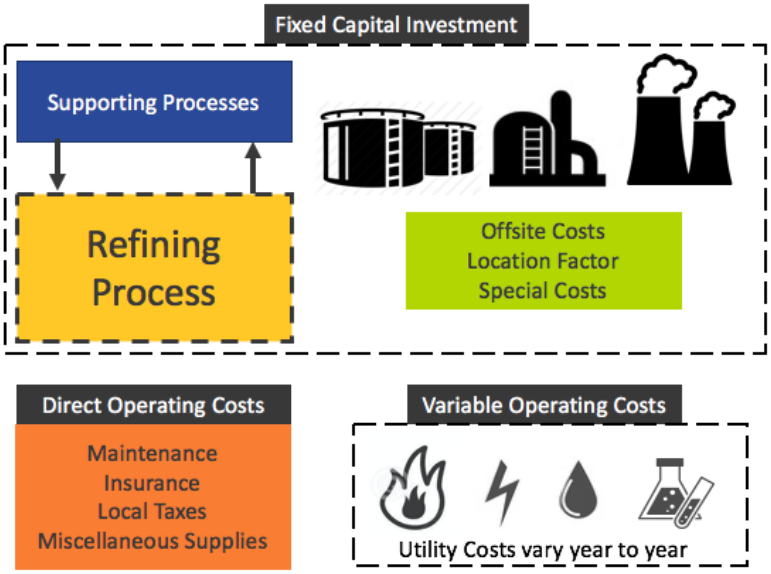

Figure 4

Results
The model successfully estimates the cost of the reduction or removal of naphthalene from U.S. jet fuel pool via operation of an additional finishing process (either selective hydro-treating or extractive distillation) at U.S. refineries. Preliminary cost data is presented in the deliverable 3 presentation provided to the FAA on August 31st, 2017.

Milestone(s)
This work was completed in August 2017, and is contained in the deliverable 3 presentation provided on August 31st, 2017.

Major Accomplishments
During this period, a simplified model was created for the purpose of cost estimation of individual selective hydro-treating and extractive distillation process units. This included effects on fuel composition, utility requirements, and estimated costs over the lifetime of the unit. Results collected from the discounted cash flow model are presented as the net present value of the unit over its life-time. A summary of this work is contained in the deliverable 3 presentation provided to the FAA on August 31st, 2017.

Publications
None

Outreach Efforts
None

Awards
None

Student Involvement
Drew Weibel, Master's student in the Laboratory for Aviation and the Environment is working directly with Prof. Steven Barrett and Dr. Ray Speth to conduct the research objectives of Task 3. Mr. Weibel is a 2nd year graduate student, and will serve on the research team through the remainder of the A39 project timeline.

Plans for Next Period

During the AY2017/2018 period, the process unit cost estimation model will be expanded to stochastically estimate the cost of removal across all U.S. refineries. This net present value estimate will be used as the "cost" the overarching cost-benefit analysis carried out in order to assess the societal benefits realized by possible naphthalene-free or -reduced jet fuel policy.

References

Allen, J. W.; Scheer, A. M.; Gao, C. W.; Merchant, S. S.; Vasu, S. S.; Welz, O.; Savee, J. D.; Osborn, D. L.; Lee, C.; Vranckx, S.; Wang, Z.; Qi, F.; Fernandes, R. X.; Green, W. H.; Hadi, M. Z.; Taatjes, C. A. Combust. Flame 2014, 161 (3), 711–724.

Brem, Benjamin T., et al. "Effects of Fuel Aromatic Content on Nonvolatile Particulate Emissions of an In-Production Aircraft Gas Turbine." *Environmental Science & Technology*, vol. 49, no. 22, Nov. 2015, pp. 13149–57. *ACS Publications*, doi:10.1021/acs.est.5b04167.

Energy Information Administration, https://www.eia.gov.

Fahim, M. A. *Fundamentals of Petroleum Refining. [Electronic Resource]*. Amsterdam ; London : Elsevier Science, c2010., 2010.

Gao, C. W.; Allen, J. W.; Green, W. H.; West, R. H. Comput. Phys. Commun. 2016, 203, 212–225.

Gao, C. W.; Vandeputte, A. G.; Yee, N. W.; Green, W. H.; Bonomi, R. E.; Magoon, G. R.; Wong, H.-W.; Oluwole, O. O.; Lewis, D. K.; Vandewiele, N. M.; Van Geem, K. M. Combust. Flame 2015, 162 (8), 3115–3129.

Gary, James H., et al. *Petroleum Refining: Technology and Economics, Fifth Edition*. CRC Press, 2007.

Lifshitz, A.; Tamburu, C.; Dubnikova, F. J. Phys. Chem. A 2009, 113 (39), 10446–10451.

Meyers, Robert. *Handbook of Petroleum Refining Processes*. 3rd ed., McGraw-Hill, 2004.

Moore, Richard H., et al. "Influence of Jet Fuel Composition on Aircraft Engine Emissions: A Synthesis of Aerosol Emissions Data from the NASA APEX, AAFEX, and ACCESS Missions." *Energy & Fuels*, vol. 29, no. 4, Apr. 2015, pp. 2591–600. *ACS Publications*, doi:10.1021/ef502618w.

Parker, D. S. N.; Kaiser, R. I.; Bandyopadhyay, B.; Kostko, O.; Troy, T. P.; Ahmed, M. Angew. Chemie Int. Ed. 2015, 54 (18), 5421–5424.

Peters, Max, et al. *Plant Design and Economics for Chemical Engineers*. 5th ed., McGraw-Hill, 2003.

Project 040 Quantifying Uncertainties in Predicting Aircraft Noise in Real-world Scenarios

Pennsylvania State University
Purdue University

Project Lead Investigator

Victor W. Sparrow
Director and United Technologies Corporation Professor of Acoustics
Graduate Program in Acoustics
Penn State
201 Applied Science Bldg.
University Park, PA 16802
+1 (814) 865-6364
vws1@psu.edu

University Participants

Pennsylvania State University

- P.I.: Victor W. Sparrow, United Technologies Corporation Professor of Acoustics
- Co-PI: Philip J. Morris, Boeing/A.D. Welliver Professor of Aerospace Engineering
- FAA Award Number: 13-C-AJFE-PSU, amendment 023.
- Period of Performance: June 28, 2016 to December 31, 2017.
- Task(s):
    1. Assess meteorological and acoustic measurement data sets for noise propagation model validation
    2. Assess influence of aircraft noise sources on uncertainty in noise modeling
    3. Assess overall modeling uncertainty for aircraft noise prediction
    4. Assess usefulness of SILENCE-R dataset

Purdue University

- P.I.(s): Kai Ming Li, Professor of Mechanical Engineering
- FAA Award Number: 13-C-AJFE-PU, amendment 14
- Period of Performance: August 1, 2016 – December 31, 2017
    5. Assess DISCOVER-AQ Acoustics data for model validation
    6. Assess the uncertainty due to the ground effect and source directivity for en-route aircraft

Project Funding Level

FAA funding to Penn State in 2016-2017 is $128K. FAA funding to Purdue in 2016-2017 is $90K.

In-kind cost sharing from Vancouver Airport Authority was received for ASCENT Project 5, and additional cost sharing is likely in Project 40. The point of contact for this cost sharing is Mark Cheng, mark_cheng@yvr.ca. Project support is in the form of aircraft noise and trajectory data, meteorology data, and consulting on those datasets.

Additional cost sharing from ANOTEC Engineering, Motril, Spain is likely in the future for ASCENT Project 40 regarding the BANOERAC data set. The point of contact for this cost sharing is Nico van Oosten, nico@anotecengineering.com.

Further cost sharing from National Aviation University of Ukraine (and Airbus) is possible in the future for ASCENT Project 40 regarding the SILENCE-R data set. The point of contact for this cost sharing is Sasha Zaporozhets, zap@nau.edu.ua.

Investigation Team

Penn State

Victor W. Sparrow (PI)
Philip J. Morris (Co-PI)
Graduate Research Assistant Manasi Biwalkar (measurement data sets for noise propagation model validation)
Graduate Research Assistant Harshal Patankar (uncertainty modeling for aircraft noise propagation)

Purdue

Kai Ming Li (PI)
Graduate Research Assistant Yiming Wang (moving source investigation)

Project Overview

To assess the uncertainties in aircraft noise prediction, an integrated approach will be used to understand uncertainties in the aircraft state and resulting noise levels and directivity (source), the atmospheric and meteorological conditions (propagation), and ground impedance and terrain model (receiver). This approach will include all predominant uncertainties between source and receiver. The primary focus in the current year is in validating the propagation uncertainty. In addition, a new collaborative initiative with National Aviation University of Ukraine is underway.

Reporting will be provided for tasks 1-4 of Penn State and tasks 5-6 of Purdue collectively instead of separately.

Task #1: Assess Meteorological and Acoustic Measurement Data Sets for Noise Propagation Model Validation
Task #2: Assess Influence of Aircraft Noise Sources on Uncertainty in Noise Modeling
Task #3: Assess Overall Modeling Uncertainty for Aircraft Noise Prediction"
Task #4: Assess Usefulness of SILENCE-R Dataset

The Pennsylvania State University

Objective(s)

This research seeks to validate current FAA/Volpe noise modeling capabilities by comparing with measurement dataand to quantify uncertainties of both model prediction and measurement in trying to predict aircraft noise (or patterns or changes) in real world situations, particularly when meteorological conditions over various different time periods may affect prediction output.

The research will focus on four areas: (1) review and analyze available field measurement data for patterns that are influenced by the (change of) meteorological conditions; (2) identify sets of field data for specific scenarios that contain proper parameters/quality input values to validate the enhanced modeling capabilities; (3) use the enhanced modeling capabilities to understand the patterns identified in the field measurement data that are influenced by the (change of) meteorological conditions and (4) quantify uncertainties in predicting aircraft noise in real-world situations.
In addition, a new collaborative initiative on aircraft noise propagation model validation will be begin with National Aviation University, Kiev, Ukraine.

Research Approach

Introduction

It is a challenging task to include the influences of atmospheric conditions and ground properties for the prediction of aircraft noise. However, the accuracy of these inputs are critical for the predictions. In the past three years, the research performed by Penn State and Purdue through FAA ASCENT Center research grants has informed FAA regarding the limitations of existing noise tools and helped advance the state-of-the-art in aircraft noise modeling. Appropriate models were enhanced and developed to account for the effects of meteorological conditions, atmospheric absorption, and the Doppler effect due to source motions on the propagation of aircraft noise. Field data obtained from Discover/AQ[1] are currently used to validate these numerical models. At the same time, Penn State and Purdue sought support from Vancouver Airport Authority[2], which has kept a comprehensive set of measured terminal area noise data around the Vancouver Airport. There are plans to use this database, and other databases, to improve the accuracy of the AEDT and quantify the sensitivities in the predicted noise levels due to the variation in atmospheric conditions and ground properties. It is possible that additional data available at National Aviation University of Ukraine may be helpful for the work. In Project 40, Penn State and Purdue will continue their efforts and extend them to quantify noise prediction uncertainties, now beginning to include the effects of the noise source.

In the first few months of Project 40, documented in last year's annual report, a survey of available datasets was provided. These datasets have not changed, so the focus here will be on the dataset that was explored in detail at Penn State during the period October 1, 2016 to September 30, 2017. This is the aircraft noise and meteorology data made available by the Vancouver (Canada) airport authority. That airport was chosen because of its availability and similarity to large U.S. airports in both number of operations and aircraft fleet mix. Vancouver had available radar data, noise monitor data, and meteorology. Penn State would like to particularly thank Mark Cheng and Rachel Min from Vancouver Airport Authority for their help with and suggestions about these data.

Thesis of Biwalkar

The work described in the next sections is summarized from the Masters of Science Thesis by Ms. Manasi Biwalkar.[1] The thesis was completed in November 2017, just after the completion of the project period. That thesis will be available online in early 2018 from the website: https://etda.libraries.psu.edu . It is suggested to search by author using the keyword "Biwalkar".

NORD2000 noise model

In addition to a simplified in-house model accounting only for spherical spreading and atmospheric absorption, the project team elected to use the NORD2000 sound propagation model as it can also include the effects of atmospheric refraction in the case of simplified sound speed profiles. Including atmospheric refraction is important in the propagation of aircraft noise as the aircraft noise can be bent toward or away from the ground due to the effects of both temperature and wind variations. NORD2000 uses the effective sound speed approximation, i.e., assumes only the horizontal wind component is additive or subtractive with the temperature-dependent sound speed. The program also assumes the effective sound speed is a log-linear function of height (as an approximation) so NORD2000 uses analytical curved. This type of modeling seems sufficient for a comparison with the Vancouver Airport Authority noise data, as it provides the simplest model to include refraction in a robust and consistent way. The NORD2000 Matlab model utilized was provided by Delta (a company in Denmark), and the project team appreciates the use of their code.

Data processing

The different data types needed to be processed in various ways to lead to comparisons between noise monitor terminal (NMT) measured data and predicted noise levels. First, the radar data from individual flight events at Vancouver airport needed to be analyzed and processed. It took a substantial amount of time for the project team to decipher the radar data and turn it into useable flight trajectory information to ascertain the position of an individual aircraft. Once accomplished, then the processed flight tracks needed to be sorted with respect to the positions of the NMTs, see Fig. 1. Criteria were established to ascertain if NMT acoustic events corresponded to nearby aircraft. The NMTs react to all environmental sounds, so sorting which events were likely due to aviation activity was important. Once this was established, it made sense to only use aircraft flight tracks that corresponded to recordings at multiple NMTs. As an example three arrival flight tracks where multiple NMTs were involved is shown in Fig. 2 for one of the runways.

Calculation methodology

An initial attempt to model each aircraft as a moving omnidirectional source with a fixed sound power level eventually did not agree very well with the NMT recorded events. Ultimately what worked better was to use the databases available in the Aviation Environmental Design Tool (AEDT), and carry out similar calculations as are performed in that program.[3] The details of this processing are described in detail in the thesis of Biwalkar.[1] In summary, it was necessary to know the aircraft type for each event, use the corresponding information for that type of aircraft in AEDT's Fleet Database, particularly both its noise power distance (NPD) information and its spectral class. These adjustments were made identically, to the best of the Project team's ability, to the way they are done in AEDT. Numerous suggestions from E. Boeker of the Volpe National Transportation Systems Center and H. He of the FAA were very helpful in correcting the levels of the spectral information for the aircraft source noise. This tremendously improved the comparisons between the measured and predicted noise levels. Another thing that was found to improve the agreement was to include the effects of refraction. To do this, atmospheric conditions needed to be taken into account. In this investigation weather data from both Environment Canada and the Climate Forecast Systems Reanalysis (CFSR) were utilized. Details on the processing and use of that information are available in Biwalkar's thesis. The temperature and horizontal wind information, corresponding to the day or evening of the aircraft flights, were used as inputs to develop the sound speed profiles that were used in the NORD2000 calculations.

Overall results

In summary it was determined that including both the atmospheric data and corresponding curved-ray modeling of NORD2000 gave better agreement for these aircraft single events, compared to simply using a straight-ray model. As mentioned previously, using the correct spectrum for each individual aircraft was absolutely required, as a minimum. These results are displayed in Fig. 3. One further observation is that the predictions for takeoffs were not as good as for landings. Not having additional data to assume otherwise, the presumption was that each takeoff would be at maximum thrust. This was very likely not the case for most of the aircraft departure events, but it was assumed to provide consistency across the analysis. Additional details are available in Biwalkar's thesis.[1] A short overview of these analyses and results was presented at the Acoustics '17 meeting in Boston, MA, USA in June 2017.[5]

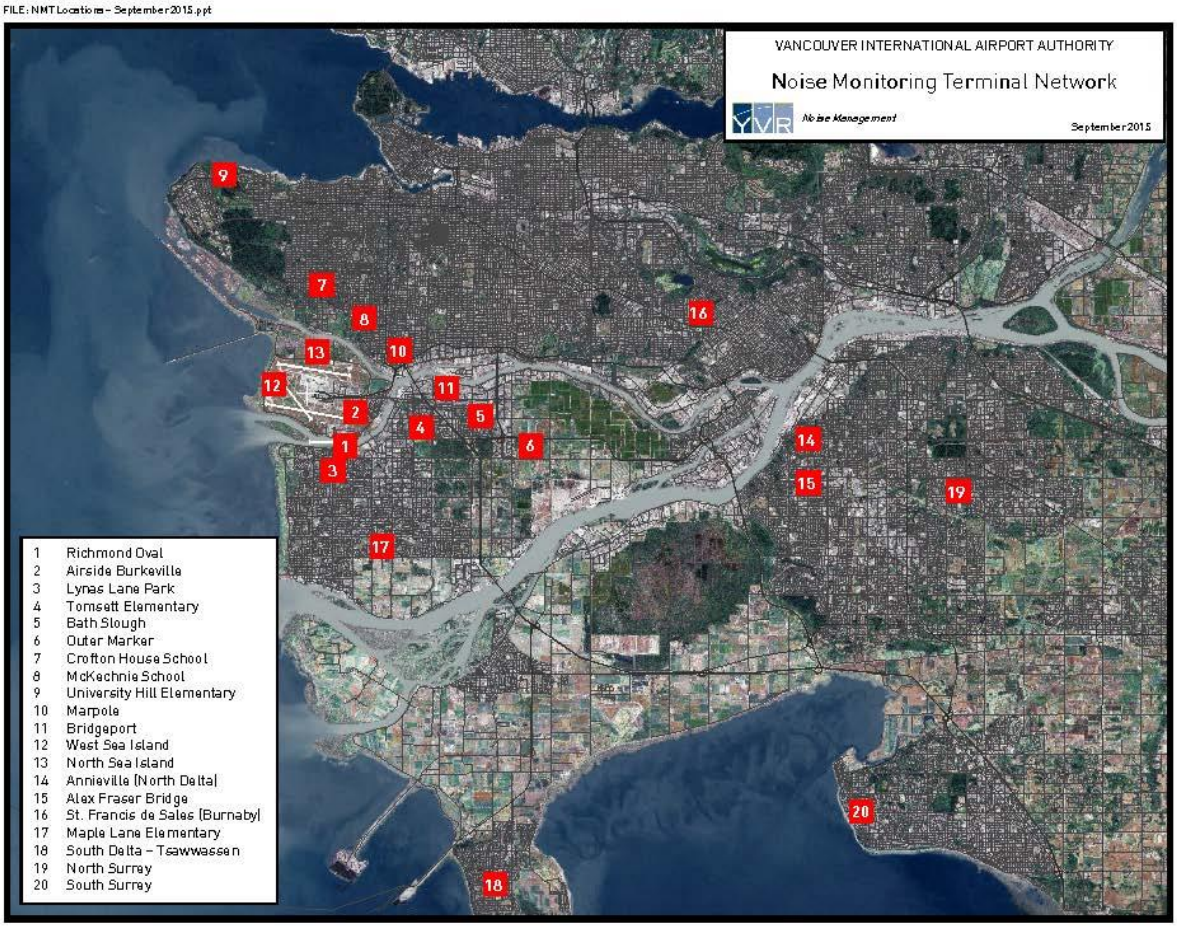

Figure 1: Overview of Vancouver International Airport and the surrounding noise monitors.

Figure 2: Three arrival flight tracks that activated multiple noise monitors. The red asterisk indicates the position of the Vancouver airport's map reference coordinate used for the radar.

Input spectrum	Input atmosphere	NMT Vs. prediction
Overall SWL Back-calculated from NMT SEL	Const Temp & No wind = Homogeneous $c(z)$	Poor agreement
1/3rd octave SPL Correct aircraft i/p spectrum from AEDT database	Const Temp & No wind = Homogeneous $c(z)$	Satisfactory agreement
	Temp gradient & Wind data = Log-Lin $c(z)$	Overall Better Agreement

Figure 3: Overall results for single events at Vancouver International Airport. SWL is an abbreviation for sound power level, and SPL is an abbreviation for sound pressure level. NMT SEL stands for noise monitor terminal sound exposure level. *c(z)* is the speed of sound profile as a function of height *z*. The best overall agreement occurs when both the correct aircraft spectrum and the temperature and wind information are incorporated in the predictions.

Uncertainty in aircraft noise source models
To assess the overall uncertainty in an aircraft noise prediction it is necessary to understand the uncertainties in the aircraft noise sources. This is an additional task in progress at Penn State under the direction of Boeing/Welliver Professor Philip Morris. During the reporting period, two sources of aircraft noise source uncertainty were considered. The first examined issues with the prediction of fan noise and identified the effects of inaccuracies in the specification of engine conditions on the noise source predictions. Secondly, the issues related to slat noise, which is an important component of airframe noise on approach were examined. The various parameters and dimensions that are important for noise prediction of the component were identified and the relative effect of errors in them were examined.

Silence(R) dataset and international cooperation
This year was very productive in beginning a discussion with National Aviation University (NAU) of Ukraine, located in Kiev, Ukraine. Dr. Sasha Zaporozhets of NAU attended both the Fall 2016 and Spring 2017 ASCENT Advisory Committee Meetings in the USA, and Dr. Victor Sparrow of Penn State visited NAU in July 2017. Each of these meetings was productive regarding a number of technical discussions related to the prediction of aircraft noise. Some of the discussions focused on the SILENCE(R) dataset, from a large aircraft noise reduction program funded by the European commission.[8] Particularly the part of the dataset which focused on the certification of Airbus aircraft, the data seems potentially very useful for validation of FAA and university noise tools. Hence, discussions will continue in the next project year to see if data sharing agreements can be established between Airbus/Xnoise and both Penn State and Purdue.

Milestone(s)
Completed initial analysis of Vancouver International Airport data set.

Major Accomplishments
Comparisons between Vancouver airport data and predictions confirm the importance of including correct aircraft noise source spectra as well as accounting for atmospheric effects such as wind and temperature gradients. Hence, it is confirmed that including atmospheric refraction effects is a required element to improve aircraft noise prediction. For the Vancouver airport data set, the research team has met the objectives of the project to analyze field data and to determine those aspects important for validating existing modeling capabilities. The both the aircraft noise source spectra and the time-dependent meteorological conditions are important.

Publications
M.S. thesis of Manasi Biwalkar.
Acoustics ’17 abstract.

Outreach Efforts
None

Awards
None.

Student Involvement
Graduate Research Assistant Manasi Biwalkar has been the primary person working on this task. She will receive her M.S. in Acoustics degree from Penn State in December 2017. A new Graduate Research Assistant Harshal Patankar started working on the project in August 2017.

Plans for Next Period
Now that the utility and limitations of the Vancouver Airport Authority’s data has been assessed, the project team will focus on some of the newer approaches for including uncertainty in the propagation of aircraft noise. Graduate Research Assistant Harshal Patankar already replicated a portion of the results for ground-to-ground sound propagation presented by Wilson, et al.[6] This approach should yield important tools that may be applicable for aircraft noise prediction. At the same time an additional dataset will be considered, BANOERAC,[7] which may be useful in further assessment of aircraft

noise models. Further, a complementary effort will generate a realistic noise source model in the form of a set of time dependent sound source spheres. These will serve as the starting point for the subsequent prediction of propagation effects on the uncertainty of the predicted noise at the ground.

References

[1] M. Biwalkar, "Single event comparisons of predicted and measured sound at Vancouver International Airport," M.S. Thesis (Graduate Program in Acoustics, Pennsylvania State University, University Park, PA, 2017).

[2] M. Cheng, *et al.,* Vancouver Airport Authority [Private Communication] (2016).

[3] M. Ahearn, *et al.,* "Aviation environmental design tool (AEDT): Technical manual, Version 2c," (U.S. Dept. of Transportation Volpe National Transportation Systems Center, 2016).

[4] B. Plovsing, "NORD2000: Comprehensive Outdoor Sound Propagation Model, Part 2: Propagation in an atmosphere with refraction," (Delta, Denmark, 2006).

[5] M. Biwalkar and V. Sparrow, "Quantifying uncertainties in predicting aircraft noise in real-world situations," J. Acoust. Soc. Am. **141** (5, Pt. 2) 3878 (2017). This is an abstract in the program of the Acoustics '17 meeting, Boston, MA, USA.

[6] D. K. Wilson, C. L. Pettit, V. E. Ostashev, and S. N Vecherin, "Description and quantification of uncertainty in outdoor sound propagation calculations," J. Acoust. Soc. Am. **136**(3) 1013-1028 (2014).

[7] BANOERAC Project final report, Document ID PA074-5-0, ANOTEC Consulting S.L. (2009).

[8] SILENCE(R) dataset. See https://www.xnoise.eu/index.php?id=85.

Task #5: Assess DISCOVER-AQ Acoustics Data for Model Validation
Task #6: Assess the Uncertainty Due to the Ground Effect and Source Directivity for En-Route Aircraft

Purdue University

Research Approach

Background

There are significant impacts of atmospheric conditions and ground properties on accurate predictions of aircraft noise. It is well known that the accuracy of these inputs are critical for the predictions. The research performed by Penn State and Purdue through FAA ASCENT Center research grants has informed FAA regarding the limitations of existing noise tools and helped advance the state-of-the-art in aircraft noise modeling. Appropriate models were enhanced and developed to account for the effects of meteorological conditions, atmospheric absorption, and the Doppler effect due to source motions on the propagation of aircraft noise.

The Purdue project team has identified the key drivers for quantifying uncertainties in predicting aircraft noise. To assess these uncertainties, an integrated approach will be used to understand uncertainties in (a) the aircraft state and resulting noise levels and directivity (source), (b) the atmospheric and meteorological conditions (propagation), and, (c) the ground impedance and terrain model (receiver). This integrated approach will include all predominant uncertainties between the source and receiver. One of the main motivations of the current project is to guide these recent advancements for reaching a sufficient Research Readiness Level (RRL) that leads to a possible implementation in AEDT in near future.

Results

In the recent years, the project team has obtained measurement data from NASA/VOLPE,[1] and Vancouver Airport Authority.[2] Two more datasets: BANOERAC[3] and SILENCE(R)[4] will become available this year. These 4 datasets will form a vital part in the assessment of uncertainties in predicting aircraft noise at various atmospheric, typographic and ground conditions.

For the Purdue effort, there are 4 tasks listed below:

A. Assess experimental datasets for use in validating noise tools (propagation).

B. Assess the influence of aircraft noise source modeling (source).
C. Assess the impacts of geometric locations of source and receiver, the effective surface impedance and the ground topography on the accurate prediction of aircraft noise (receiver).
D. Assess the overall uncertainty in the noise prediction (propagation+source+receiver)

Three of these 4 tasks (A, B and D) are comparable to the effort of the PSU team. Nevertheless, the Purdue team has been tasked to investigate the influence of ground effect on predicting aircraft noise (Task C). On the other hand, the PSU team has been invited to maintain an international link with National Aviation University of Ukraine for the possible use of SILENCE(R) dataset and other collaborations. Through PSU's effort, the Purdue team will be able to interact with the Ukraine team and access the relevant dataset. The achievements for each of the 4 tasks will be explained in the following sections.

Task A
In the past year, the Purdue team has concentrated on the analysis of the DISCOVER-AQ dataset. The full details of the scope of the DISCOVER-AQ acoustic research effort and its measured results can be found in Ref. 1. After an initial study, the Purdue team has identified that the maneuvers of Lockheed P-3B Orion (see Figure 4) contains the most relevant acoustic datasets for detail investigations. Lockheed P-3B Orion is a four-engine turboprop aircraft with a maximum gross take-off weight of 135,000 lbs. The propeller blades were manufactured by Hamilton Standard. Each of the propeller blades was driven by an Allison T56-A-14 turboprop engine delivering 4,100 shp.

Figure 4: Lockheed P-3B Orion 4-engine turboprop aircraft used in the experiment

A typical source spectrum of the noise radiated from Lockheed P-3B Orion is shown in Figure 5. For this type of propeller-driven aircraft, it is apparent that the low-frequency tonal components dominate the sound fields which is quite different from the noise spectrum for a typical jet-engine aircraft. Noise radiated from turboprop engines can travel a longer distance to the ground because the rate of atmospheric absorption of sound is typically much smaller in the low frequency regime. For ground-based receivers, it is most likely that en-route noise from turboprop aircraft is more noticeable than a jet-driven aircraft.

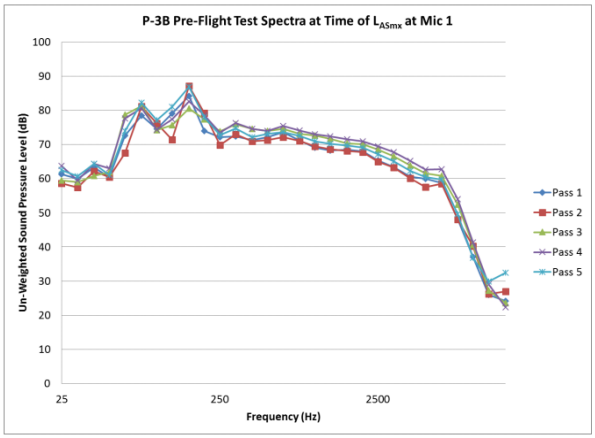

Figure 5: Typical Spectrum of a Lockheed P-3B Orion turboprop aircraft

From the DISCOVER-AQ dataset, event 34 was chosen to illustrate the flight trajectory of the test aircraft (see Fig. 6) and the measured time histories of A-weighted noise levels at different octave-band frequencies from 63 to 500 Hz (see Fig. 7). In Fig.7, the aircraft locations at the beginning and end points are marked. In addition, the aircraft locations at the peaks of the measured sound pressure levels (SPL) are also shown for frequencies at 63 and 500 Hz only.

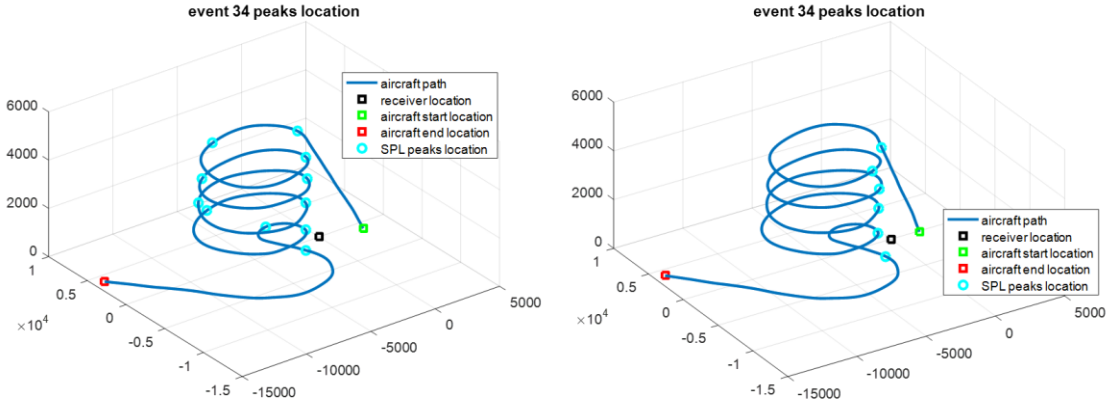

Figure 6: Flight trajectories of the test aircraft. Aircraft locations at the beginning and end points and also at the peak SPL are marked. Left plot: 63 Hz. Right plot: 500 Hz

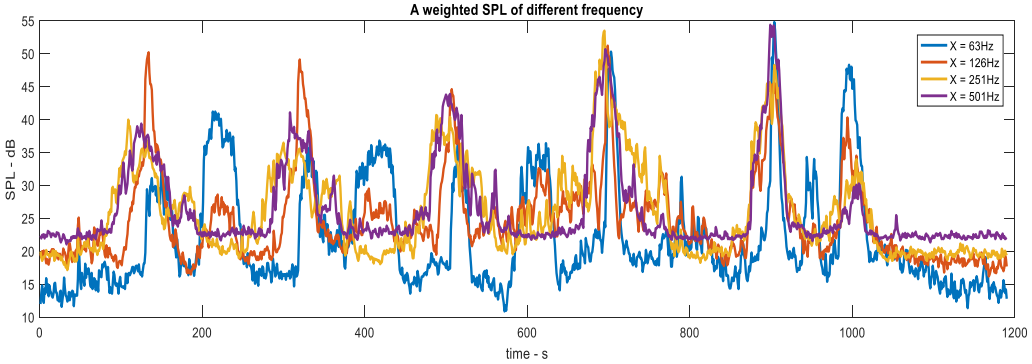

Figure 7: Measured time-histories of the A-weighted SPL for different frequencies

For clarity and completeness, an aerial view (taken from the goggle map) of the test site and photographs of microphone locations are shown in Fig. 8. In the aerial view, the flight paths of Event 33 and 34 are shown with the test aircraft moving in 5 downward spiral loops and the average diameter of about 4 km.

During the test flights, temperature and wind profiles were recorded. These profiles have been presented in Fig. 9 in terms of sound speed and wind speed profiles. A close examination of Fig. 9 suggests that the sound speed gradient

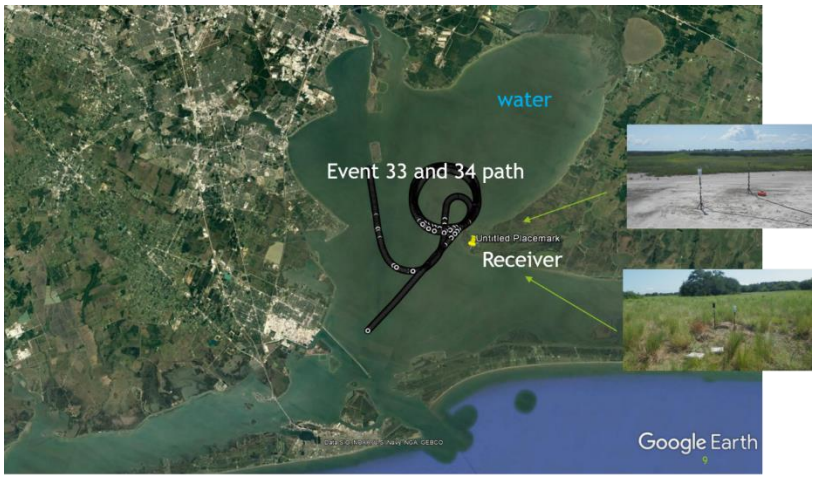

Figure 8: Aerial view of the test site, trajectory of the test aircraft and receiver locations.

was about 4 m/s per 1 km and the largest wind speed gradient was about 8 m/s per 1 km. Thus, the highest effective sound speed gradient should not be more than 12 m/s per 1 km. Given this weak effective sound speed gradient, the atmosphere may be treated as homogeneous throughout the measurement period for Lockheed P-3B Orion.

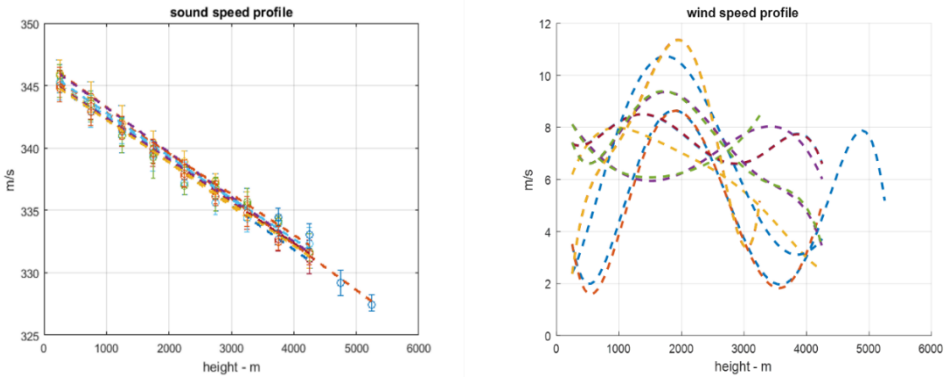

Fig. 9: Sound speed and wind speed profiles for Events 33 and 34

Task B

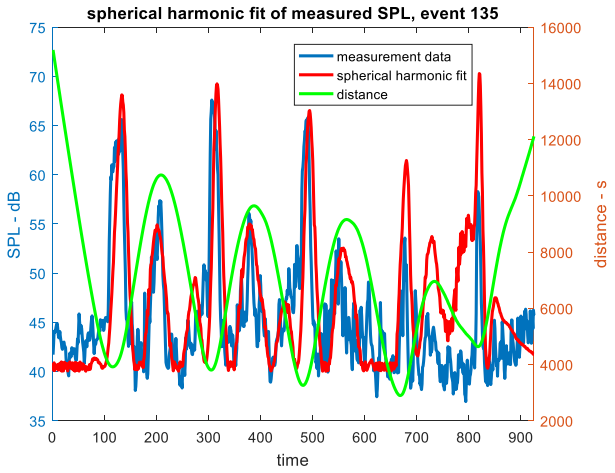

Fig. 10: Comparison of measured and predicted time histories of A-weighted noise level of the test aircraft at the frequency 63 Hz.

Measured results from DISCOVER-AQ dataset indicate that the test aircraft (noise source) has a strong directivity pattern. This is illustrated in the time history measurements at different frequencies shown in Fig. 7. Because of the effect of the source directivity, the measured peak levels for different frequencies occurred at different times. A simple assumption of an omni-directional moving source will not be adequate to model the pass-by noise levels of the test aircraft especially for the frequency below 125 Hz. Currently, the Purdue team has developed an empirical model (based on a spherical harmonic function) to estimate the directivity patterns of the test aircraft. Essentially, the measured noise levels from Event 33 were used to deduce the directivity patterns of the test aircraft. This directivity pattern was then applied to predict the time histories of other events. Figure 10 shows a comparison of the predicted and measured time histories of Event 135 for the source frequency at 63 Hz. Generally speaking, the agreement between the measured results and predictions are reasonably well.

Task C

In the past year, the Purdue team has examined theoretically the uncertainties in the prediction of aircraft noise due to the ground effect. In essence, the ground effect of the predicted/measured sound fields is caused by the interference of the direct and reflected waves arriving at the receivers. The intrinsic variability in the predictions depends on a host of factors including the source/receiver geometry, source frequency, atmospheric turbulence, acoustic characteristics of the ground surface, and, terrain profile. Figure 11 shows a comparison of the predicted attenuation due to the ground effects for source frequencies of 250 and 500 Hz. The prediction according to the AEDT model is shown in 'gold' solid line. The predicted attenuation at different sideline distances are shown for snow-covered (blue) and grass-covered (red) grounds with frequencies at 250 Hz (solid line) and 500 Hz (dashed line). The Delaney and Bazley (D-B) model[5] is used to predict the effective impedance of the ground surface in Fig. 11. We can see that the discrepancy in predicting the attenuation can be as high as 6 dB between the AEDT and (D-B) models.

In fact, the D-B model has been used in the predictions showed in Fig.10 that lead to a better agreement between the measured data and numerical prediction except for the region towards the end of the event. This apparent disagreement may be explained by the fact that the test aircraft was very close to the ground during this period of measurements. In this situation, the effects of ground impedance, shielding by obstacles and ground typography may play an important role that introduce uncertainties in predicting the aircraft noise. The development of a more accurate model to account for these uncertainties will be explored in our next stage of study.

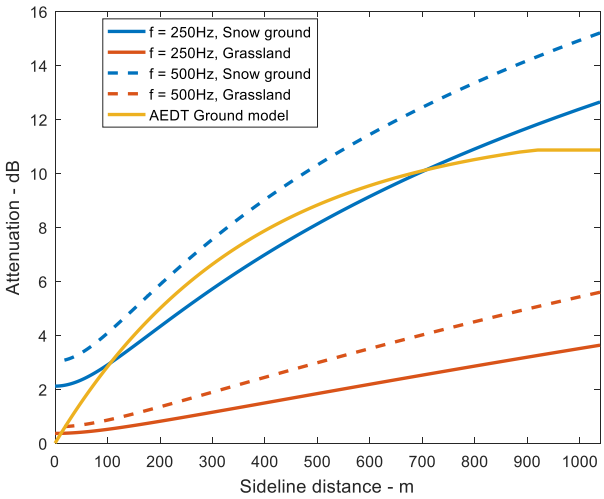

Fig. 11: Comparison of AEDT ground model with a more precise ground impedance model

Task D

The Purdue team has conducted an initial analysis on the overall uncertainties on the DISCOVER-AQ data set. Event 33 was chosen for illustration here. Figure 12 shows the improvement on the prediction of the A-weighted sound pressure level (SPL). The agreement between the field data and our current prediction scheme using a better directivity pattern (gold) is much better than the prediction using the monopole model (red), especially, at the location of the first peak.

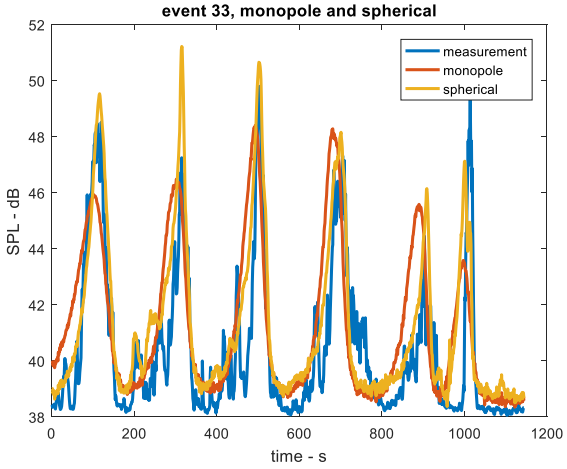

Fig. 12: Comparison of predictions and field data for A-weighted SPL for event 33

Figure 13 shows that the errors of the prediction with directivity model decreased obviously, however, lager error still exists when the distance is short and elevation angle is small. Future work should focus on the analysis of ground effects since most measurement sites are located not far away from forest and many aircraft paths are above water-covered region.

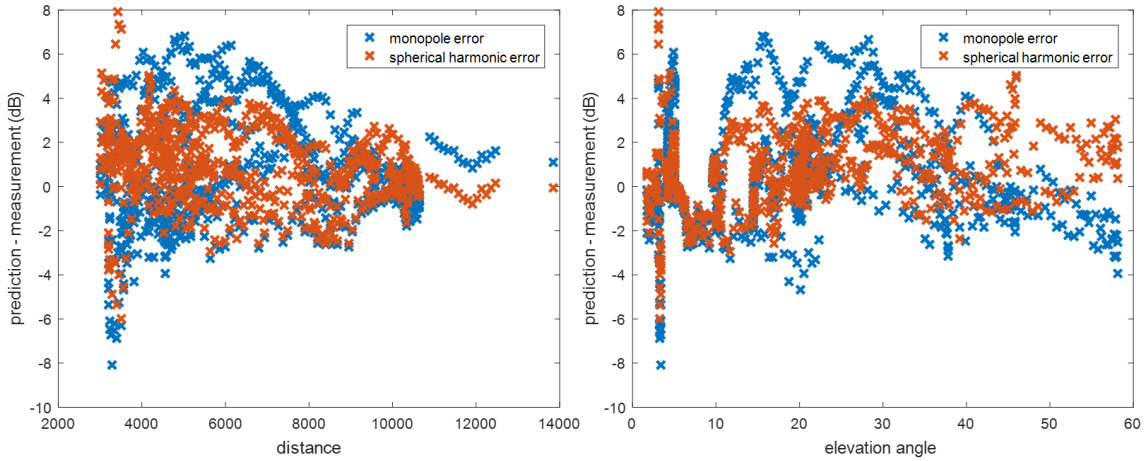

Fig. 13: Discrepancies between measurement data and predictions for Event 33.

Milestone(s)

Several Discover-AQ acoustic events were reviewed and analyzed. The current models, which have been used in AEDT, have been used to compare with the measured data. Particularly, the uncertainty due to the ground effect for an en-route aircraft has been assessed. An empirical model for evaluating the source directivity of a propeller-driven aircraft (P3-Orion) has been developed and used to assess a fly-by aircraft.

Major Accomplishments

In coordination with Penn State University, the Purdue research team has focused on the analysis of the experimental data retrieved from the Discover-AQ dataset. The quality of field data, which offers real world situations, allows the uncertainties of both model prediction and measurement in predicting aircraft noise to be identified and quantified. It has been shown that the source directivity has played an important role in predicting aircraft noise. The uncertainty in the ground vegetation can lead to significant variations in the measured aircraft noise levels. Enhanced model capabilities have been used to investigate the difference in the noise levels due to an approaching and a receding aircraft.

Publications

Acoustics ’17 abstract.

Outreach Efforts
None

Awards
None.

Student Involvement
Graduate Research Assistant Yiming Wang has been the primary person working on this task.

Plans for Next Period
Continue the current work, particularly, we shall examine,
- The impact of Doppler-shift in source frequency on the overall A-weighted noise levels
- The shielding effects due to ground vegetation.
- The uncertainties in predicting the noise levels in upward refracting medium where the receiver is located at the shadow boundaries.

References
[1] E. Boeker et al. Discover-AQ Acoustics Measurement and Data Report,"DOT-VNTSC-FAA-15-09 (2015).

[2] M. Cheng, *et al.,* Vancouver Airport Authority [Private Communication] (2016).

[3] BANOERAC Project final report, Document ID PA074-5-0, ANOTEC Consulting S.L. (2009).

[4] SAE-AIR-5662 "Method for Predicting Lateral Attenuation of Airplane Noise" (2012).

[5] K. Attenborough, K.M. Li, and K. Horoshenkov. *Predicting Outdoor Sound*. Taylor & Francis, 2007.

[6] C. G. Fleming, J. Burstein, A. S. Rapoza, D. A. Senzig, and J. M. Guilding. "Ground effects in FAA's integrated noise model," Noise Control Engineering Journal **48**, 16-24.

[7] C. Hobbs, Interim Report on ACRP 02-52: Improving AEDT noise modeling of ground surfaces (2016).

Project 041 Identification of Noise Acceptance Onset for Noise Certification Standards of Supersonic Airplanes

The Pennsylvania State University

University Members

Penn State Acoustics Program	Principal Investigator	Victor W. Sparrow
Penn State Applied Research Laboratory	Co-Principal Investigator	Kathleen K. Hodgdon

Advisory Committee Members

AERION: Jason Matisheck, Peter Sturdza, *et al.*
Boeing: Hao Shen, Bob Welge, *et al.*
Gulfstream: Robbie Cowart, Matthew Colmar, Brian Cook, Joe Gavin, *et al.*
Lockheed Martin: John Morgenstern, Tony Pilon, *et al.*
Volpe-The National Transportation Systems Center: Juliet Page, Bob Samiljan, et.al.
Wyle: Kevin Bradley, Chris Hobbs, *et al.*

Project Lead Investigator

Victor W. Sparrow
Director and United Technologies Corporation Professor of Acoustics
Graduate Program in Acoustics
Penn State
201 Applied Science Bldg.
University Park, PA 16802
+1 (814) 865-6364
vws1@psu.edu

University Participants

The Pennsylvania State University

- P.I.: Vic Sparrow, United Technologies Corporation Professor and Director, Graduate Program in Acoustics
- Researcher: Kathleen Hodgdon, Research Associate
- FAA Award No.: 13-C-AJFE-PSU Amendment 21, 33
- Period of Performance: Amendment 21: June 28, 2016 to December 31, 2017
- Period of Performance: Amendment 33: August 7, 2017 to December 31, 2018
- Task(s):
  1. Obtaining confidence in signatures, assessing metrics sensitivity, and adjusting for reference day conditions

The Pennsylvania State University Applied Research Laboratory

- P.I.: Kathleen Hodgdon Research Associate
- Researcher: John Morgan R&D Engineer
- Researcher: Bernard Kozykowski
- FAA Award No.: 13-C-AJFE-PSU Amendment 25,
- Period of Performance: Amendment 25: July 21, 2016 to December 31, 2017
- Period of Performance: Amendment 35: August 7, 2017 to July 31, 2018
- Task(s):
  2. Community Impact and Acoustic Acceptability

Project Funding Level

This project supports the identification of noise acceptance onset for noise certification standards of supersonic airplanes through research conducted on multiple tasks at the Penn State University. FAA funding to Penn State in 2016-2017 was $160K comprised of $50K to Task 1 and $110K to Task 2. The FAA funding to Penn State in 2017 -2018 was $221K comprised of $150K to Task 1 and $71K to Task 2. Matching funds are expected to meet cost share on both Tasks.

Investigation Team

For 2016-2017 the investigation team includes:

The Pennsylvania State University
Victor W. Sparrow (Co-PI) (Task 1)
Kathleen K. Hodgdon (Co-PI) (Task 2)
Researcher: John Morgan R&D Engineer (Task 2)
Researcher: Bernard Kozykowski R&D Engineer (Task 2)
ARL Graduate Research Assistant Will Doebler (Task 1: Signatures and metrics investigation)
ARL Eric Walker Graduate Assistant: Annelise Hagedorn (Task 2: Community Monitoring)
College of Engineering Graduate Research Assistant Janet Xu (Task 1: Signatures and metrics investigation)

Project Overview

FAA participation continues in International Civil Aviation Organization, Committee on Aviation Environmental Protection (ICAO CAEP) efforts to formulate a new civil, supersonic aircraft sonic boom (noise) certification standard. This research investigates elements related to the potential approval of supersonic flight over land for low boom aircraft. The efforts include investigating certification standards, assessment of community noise impact and methods to assess public acceptability of low boom signatures. The proposed research will support NASA in the collaborative planning and execution of human response studies that gather the data to correlate human annoyance with low level sonic boom noise. As the research progresses, this may involve the support of testing, data acquisition and analyses, of field demonstrations, laboratory experiments or theoretical studies.

Task #1: Obtaining Confidence in Signatures, Assessing Metrics Sensitivity, and Adjusting For Reference Day Conditions

The Pennsylvania State University

Objective

As national aviation authorities move forward to develop noise certification standards for low-boom supersonic airplanes, several research gaps exist in the areas of signature fidelity, metrics, metrics sensitivity to real-world atmospheric effects, adjustments for reference-conditions, etc. Research support is needed by FAA and international partners in these areas to progress toward standards.

The objective of this activity is to continue research at The Pennsylvania State University in the ASCENT COE to complement the sonic boom standards development ongoing within the Committee for Aviation Environmental Protection's (CAEP) Working Group 1 (Noise Technical), Supersonics Standards Task Group (SSTG). This research will ensure that the behavior of the sonic boom metrics considered in the SSTG discussions are well-understood, and account for sonic boom variability effects, to move forward with sonic boom noise certification standards development and consideration of subsequent rulemaking.

Task 1 in ASCENT Project 41 focuses on several, but not all, research initiatives needed to move forward toward the development of a low-boom supersonic en-route noise certification standard. In addition, this project supports the travel of V. Sparrow so that he can serve as co-rapporteur of the CAEP Impacts and Science Group (ISG).

Research Approach

Background
A review of previous work over the last few years was presented in the 2015-2016 annual report for ASCENT Project 41. Last year focused on the topics of removing the turbulence[4] in sonic boom signatures that have propagated through the atmosphere, establishing that the de-propagation technique does not work for sonic booms, and evaluating a number of sonic boom metrics regarding their stability due to turbulence effects. The latter work showed that B-weighted sound exposure level was the most robust with regard to the influences of atmospheric turbulence, among a number of metrics regarded as candidates for use in certification. This work has resulted in a new Journal of the Acoustical Society of America Express Letters paper this year.[5]

Appropriate placement and number of microphones for certification measurements
The major effort over the period October 1, 2016 to September 30, 2017 in Project 41 (Task 1) has centered on efforts to assess the minimal number of microphones that can be used for supersonic cruise certification. Because of atmospheric turbulence, each microphone in a linear array will record a slightly different pressure versus time signature. However, the effort to make such measurements is painstaking, and minimizing the number of measurement microphones will make such certification measurements easier. It is unlikely that applicants for certification will have the resources to deploy upwards of 100 microphones in the field. How many microphones are enough?

Penn State Graduate Research Assistant William Doebler worked on this problem, initially funded by ASCENT Project 41, and then as a NASA AS&ASTAR Fellowship recipient. His work was reported at a CAEP/WG1/SSTG Workshop in February 2017, at the Acoustics '17 meeting[2] in Boston, MA, USA in June 2017, and then in his M.S. thesis. The research is now summarized from the Masters of Science thesis by Ms. William Doebler.[1] The thesis was completed in November 2017, just after the completion of the project period. That thesis will be available online in early 2018 from the website: https://etda.libraries.psu.edu . It is suggested to search by author using the keyword "Doebler".

The goal was to somewhat mimic the current subsonic aircraft certification procedure by establishing 90% confidence intervals. The available dataset that was utilized was the recordings of steady supersonic flights along linear microphone arrays from NASA's SCAMP field test.[3] W. Doebler considered this a helpful dataset as SCAMP used 81 microphones spaced at 38.1 m intervals along a 3 km linear array, substantially more than the number of microphones that would likely be available in a certification measurement.

Figure 1 shows an example result showing two plots. The left plot depicts the mean PLdB obtained as a function of the number of microphones used, as well as the confidence intervals above and below that mean, computed using the student's t-distribution. The distance between the mean and the +10% confidence interval, the "confidence radius" is then plotted on the right to show the diminishing utility of adding more microphones. For the case depicted here, one observes that perhaps 7 microphones are all that are needed to establish a confidence interval with a minimal number of microphones.

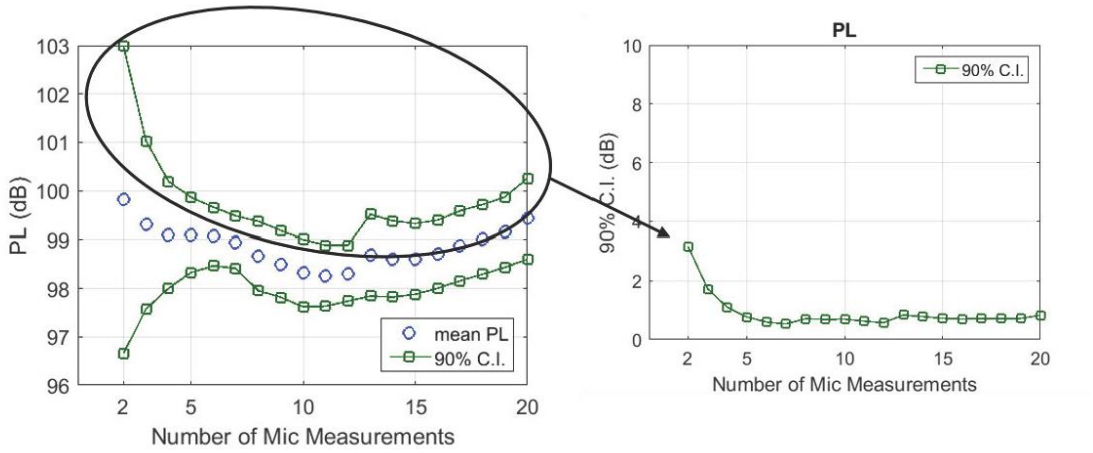

Fig. 1. The positive confidence intervals for the PL metric on the left are extracted onto the plot on the right. For this particular case, it is seen that about 7 microphones provides a minimal 90% confidence interval, and additional microphones are unneeded.

W. Doebler selected the microphones a number of different ways, including examining (1.) random placement of microphones, (2.) adjacent groups of microphones, and (3.) down-sampling across the entire microphone array. The results did not depend on which of these microphone selection methods employed. Overall, it was determined that 10 microphones were sufficient to provide a minimal confidence interval for certification. 20 microphones is more than needed, and any additional microphones do not increase the quality of the data. Further details on the processing methods used, more results, and checks on the results are available in Doebler's M.S. thesis.

Milestone(s)
A minimal number of microphones was established for future certification measurements of sonic boom noise.

Major Accomplishments
A minimal number of microphones was established for future certification measurements of sonic boom noise.

Publications
Acoustics '17 abstract.
M.S. thesis of William Doebler.
JASA Express Letters paper by Doebler/Sparrow on metric stability.

Outreach Efforts
None.

Awards
None.

Student Involvement
William Doebler is the graduate research assistant supported by the Applied Research Laboratory on Project 41 in 2016. In 2017 Doebler was supported by a NASA AS&ASTAR Fellowship. He is pursuing his Ph.D. in the Penn State Graduate Program in Acoustics. Toward the end of the report period, a new student Graduate Research Assistant Janet Xu started working on the project.

Plans for Next Period

In general, the work will continue to support CAEP WG1, SSTG, and ISG. Specifically, Graduate Research Assistant Janet Xu will be applying new signal processing techniques, such as audio fingerprinting, in an attempt to develop new methods to remove turbulence from sonic boom signals.

References

[1]W. Doebler, "The minimum number of ground measurements required for narrow sonic boom metric 90% confidence intervals," M.S. Thesis (Graduate Program in Acoustics, Pennsylvania State University, 2017).

[2]W. Doebler and V. Sparrow, "The minimum number of ground measurements required for narrow sonic boom metric confidence intervals," J. Acoust. Soc. Am. **141** (5, Pt. 2) 3625 (2017). Presented at Acoustics '17, Boston, MA, USA.

[3]J. Page, C. Hobbs, E. Haering, D. Maglieri, R. Shupe, C. Hunting, J. Giannakis, S. Wiley, F. Houtas, "SCAMP: Focused sonic boom experiment execution and measurement data acquisition," AIAA paper 2013-0933, 51st AIAA Aerospace Sciences Meeting, Grapevine, TX, January 2013.

[4]D. Maglieri, *et al*., *Sonic Boom: Six Decades of Research* (NASA SP-2014-622, 2014), pp. 51-52.

[5]W. Doebler and V. Sparrow, "Stability of sonic boom metrics regarding signature distortions from atmospheric turbulence," J. Acoust. Soc. Am. **141** (6) EL592 (2017).

Task #2: Community Impact and Acoustic Acceptability

The Pennsylvania State University Applied Research Laboratory

Objective

This is part of a series of research efforts that were designed to provide data to help answer the question: "What is needed from a standard to reconsider 14 CFR part 91.817, which currently prohibits civil supersonic flight over land?" Supersonic flight over land is currently restricted in the U.S. and many other countries because sonic booms from *non-low-boom* aircraft create shock waves that disturb people on the ground and can potentially damage private property. This research effort supports research on the human perception of *low level* sonic booms and the assessment of community impact in noise field tests.

The research supports the regulatory standard development process and the identification of noise acceptance onset. The tasks are proposed in support of NASA in the planning and execution of human response studies, and in the development of protocols, methods and planning for Community Response Testing.

Research Approach

This research encompassed several topics that were investigated in support of future field tests to assess community noise impact and public acceptability of low boom signatures. Community noise impact research requires gathering noise data as well as community response data. This effort is finalizing the design of low cost noise monitors (LCNM) that could be used as a rapid deploy monitor to augment the use of standard higher fidelity instrumentation to gather noise data. Community response data can be gathered through formal survey methods or gleaned through observations using social media monitoring tools as a means to observe public domain comments on noise within the field test community. The evaluation of social media monitoring (SMM) tools as a means to observe the response of the general community to the noise impact was finalized. A new task was initiated to conduct a review of differences in perception between urban, suburban and rural environments to better understand the potential impact that masking has on noise field test results for human impact.

Milestone(s)

This research was conducted in support of future NASA-sponsored *low boom* noise community impact field tests. The LCNM design is being finalized. PSU researchers are teaming with researchers from Volpe, The National Transportation Systems Center on this effort. The LCNM monitor design will be shared with Volpe for further testing and development. The investigation of social media monitoring tools as a means to observe social dynamics and to provide insights into

community perceptions of noise impact during the field tests was finalized. The literature review of urban vs. rural aviation noise impact is ongoing to assess the role of environmental background noise and identify methods to address it.

Major Accomplishments

The Low Cost Noise Monitor and Social Media Monitoring tasks are being finalized. These two tasks were conducted in support of efforts to gather both objective measurements and subjective observations in test communities. The literature review of the impact of environmental background noise on community noise impact is ongoing. The review of environmental masking was initiated to understand the potential impact that masking has on noise field test results for human impact. Accomplishments on each of these tasks follow.

Low Cost Noise Monitor (LCNM) Design

A report that provides an overview of the design for the Low Cost Noise Monitors (See Figure 2 and Table 1) is in development. The design will be shared with Volpe for further development and testing. The LCNM was designed as a prototype with the potential for project specific modifications when building future monitors. The evaluation of LCNM is in progress assessing the applicability of commercial off the shelf (COTS) instrumentation for this effort. Design selection was contingent on the availability of low cost parts.

Fig. 2: LCNM prototype

Table 1: LCNM Components

LCNM Components
2 Microphones
GPS Sensor
Environmental Sensor
Accelerometer Sensor
Single Board Computer (SBC)

The noise monitoring is provided through a single board computer, microphones, and batteries. The design includes two microphone channels that can be set with different dynamic ranges. This affords the ability to capture low level signals with integrity, and affords a second microphone channel set with a higher dynamic range. The monitor also includes temperature and humidity sensors as well as an accelerometer channel to provide greater applicability for a range of noise monitoring projects. The monitor will require the development of software to facilitate the ability to readily download the field data.

Social Media Monitoring Tools
The monitoring of social media was explored as a supplemental means to observe the impact of the noise field testing on the community, by observing the publicly available comments that are posted to social media. By monitoring online discussions, researchers have the opportunity to identify concerns within the community related to the noise impact.

Social media monitoring tools include the capability to use a defined geographic-based search of keywords used in social media comments during a noise field tests. A review of the comments could potentially identify unanticipated locations of concern for greater noise impact. An increase in social media comments in a specific geographic region could indicate a potential sound channel due to topography, urban canyons or environmental variability or community concerns related to the field test. Being made aware of such issue would be of valuable in helping to explain secondary influences on the primary data. The observations would be gathered from public domain information only and are not viewed as formal response data. Two commercially available social media monitoring tools were considered, GeoFeedia and EchoSec. Tests of EchoSec were conducted to assess its applicability to this effort. The observations would primarily allow the team to engage the community with targeted news releases or Outreach materials that address issues observed on posts to social media. The observations could also identify if community members have mistaken the impulsive boom noise to be an explosion, prompting the team to issue a media release to alleviate these concerns. While noise monitors will be located across the boom carpet, there is the potential that a combination of wind and terrain could produce a sound channel. The observations may indicate a “noise pocket” that could prompt stationing a noise monitor in that area. Monitoring social media provides the opportunity to identify concerns within the community related to the low boom field test.

The review of SMM tools was shared with the Waveforms Sonicboom Perception and Response (WSPRRR) team that is designing the low boom community noise risk reduction field test sponsored by NASA. The team is currently working with NASA Public Affairs on a field research design for community engagement that includes elements related to education, Outreach and potential monitoring of community response. It is likely that NASA Public Affairs will use their Facebook page as a form of education and outreach. NASA currently uses Sysomos for social media monitoring on Facebook. Sysomos is a suite of social data tools that affords the ability to monitor social trends and keywords on social media platforms. This form of observing the community response to the noise impact will most likely be utilized. The team recognizes the value of social media monitoring to proactively identify areas of concern to the community, and to afford the opportunity for engaged Outreach.

Environmental Masking (urban vs suburban/rural) Literature Review and Survey Development
This task includes a review of concepts and available literature of noise studies related to the role masking plays on the perception of noise. Masking is the extent that one noise source “covers” or masks another noise source. The *low boom* noise has been described as sounding like distant thunder, or two car door slams in quick succession. In urban areas, a car door slam may not be noticed, due to other noise sources. The same car door slam would be more clearly noticed in a quiet rural environment. The noise impact is measured by both objective noise metrics and subjective human response. The task will initially review and compile information on urban vs. rural impact of aviation noise. While the preferred noise source to investigate is aviation noise, data gathered on analysis methods for other noise sources may also prove to be relevant. A review of noise impact and analysis methods for various noise sources and environments could further identify patterns in noise impact and response, and provide a more informed approach to illuminate those patterns in future data sets. An attempt is being made to include a range of publications such as The Journal of the Acoustical Society of America, Journal of Sound and Vibration, Journal of Environmental Psychology, and Environment and Behavior. The literature review is intended to further understanding of potential differences in noise impact between such communities that could inform future research efforts. The results of this study should provide insight into the influence of background noise on the annoyance rating of aviation noise.

Publications
None

Outreach Efforts
This research task supports NASA activities on supersonics and sonic boom research. The team has provided information to the NASA sponsored Waveforms Sonicboom Perception and Response Risk Reduction (WSPRRR) team. This NASA sponsored team consists of ASCENT Project 41 team members from Penn State, Volpe, Wyle and Gulfstream working with NASA team lead APS to formulate a test plan for future low boom community field tests.

Awards
None

Student Involvement
Annelise Hagedorn has just started on this effort as an Eric Walker Graduate student, looking at aviation environmental impacts on urban vs rural communities. She is a doctoral candidate in Agricultural Economics, Sociology and Education. She is conducting a literature review of aviation noise studies to document methods, analyses and findings for aviation noise impact research conducted in different types of communities.

Plans for Next Period
The LCNM instrumentation task is being finalized. The outcome is the development of noise monitoring technology that can be used to supplement existing noise measurement methods for greater quantification of coverage at lower cost and complexity. Such technology could be used as intermediate measures among the standard higher fidelity instrumentation to confirm and interpolate data.

The literature review will be continued on noise studies related to the role masking plays on the potential low boom noise impact in differing background noise for urban, suburban or rural noise environments. The findings of the Environmental Masking literature review will facilitate interpreting noise field test results and masking due to environmental surrounding (community density), and the relevance masking has on low boom noise for such varying background environments.

References
Babisch, W., Houthuijs, D., Pershagen, G., Cadum, E., Katsouyanni, K., Velonakis, M., . . . HYENA Consortium. (2009). Annoyance due to aircraft noise has increased over the years—Results of the HYENA study. Environment International, 35(8), 1169-1176. doi:10.1016/j.envint.2009.07.012

Fields, J. M. (1993). Effect of personal and situational variables on noise annoyance in residential areas. The Journal of the Acoustical Society of America, 93(5), 2753. doi:10.1121/1.405851

Job, R. F. S. (1988). Community response to noise: A review of factors influencing the relationship between noise exposure and reaction. Journal of the Acoustical Society of America, 83(3), 991-1001. doi:10.1121/1.396524

Kroesen, M., Molin, E. J. E., Miedema, H. M. E., Vos, H., Janssen, S. A., & van Wee, B. (2010). Estimation of the effects of aircraft noise on residential satisfaction. Transportation Research Part D, 15(3), 144-153. doi:10.1016/j.trd.2009.12.005

Quehl, J., & Basner, M. (2006). Annoyance from nocturnal aircraft noise exposure: Laboratory and field-specific dose-response curves. Journal of Environmental Psychology, 26(2), 127-140. doi:10.1016/j.jenvp.2006.05.006

Ruths, D., and J. Pfeffer. "Social Media for Large Studies of Behavior." Science 346.6213 (2014): 1063-064. 28 Nov. 2014. Web. 10 Feb. 2015.

Rylander, R., Björkman, M., Åhrlin, U., Sörensen, S., & Berglund, K. (1980). Aircraft noise annoyance contours: Importance of overflight frequency and noise level. Journal of Sound & Vibration, 69(4), 583-595. doi:10.1016/0022-460X(80)90627-6

Staples, S. L., Cornelius, R. R., & Gibbs, M. S. (1999). Noise disturbance from a developing airport: Perceived risk or general annoyance? Environment and Behavior, 31(5), 692-710. doi:10.1177/00139169921972308

Project 042 Acoustical Model of Mach Cut-off Flight

Pennsylvania State University
University of Washington
Georgia Institute of Technology
Volpe National Transportation Systems Center (non-University IAA)

Project Lead Investigator

Victor W. Sparrow
Director and Professor of Acoustics
Graduate Program in Acoustics
Penn State
201 Applied Science Bldg.
University Park, PA 16802
+1 (814) 865-6364
vws1@psu.edu

University Participants

Pennsylvania State University

- P.I.(s): Dr. Victor W. Sparrow (PI), Dr. Michelle C. Vigeant (Co-PI)
- FAA Award Number: 13-C-AJFE-PSU-020
- Period of Performance: June 28, 2016 - December 31, 2017
- Task(s):
    1. Assess and extend modeling capability for Mach Cut-off events (a.k.a. Task 1A)
    2. Study human perception of Mach Cut-off sounds

University of Washington

- P.I.(s): Dr. Michael Bailey (PI)
- FAA Award Number: 13-C-AJFE-UW-005
- Period of Performance: June 27, 2016 – December 31, 2017
- Task(s):
    3. Develop a test plan for laboratory experiments for Mach cut-off that might be possible in the future

Georgia Institute of Technology

- P.I.(s): Dr. Dimitri Mavris (PI), Dr. Jimmy Tai (Co-PI)
- FAA Award Number: 13-C-AJFE-GIT-023
- Period of Performance: June 28, 2016 – August 14, 2017
- Task(s):
    4. Sensitivity study of Mach Cut-off flight
    5. Evaluate technologies to enable Mach cut-off flight

Volpe National Transportation Systems Center (non-University, Interagency Agreement)

- P.I.(s): Juliet Page
- Volpe Project Number: FA5JCT
- Period of Performance: execution date – December 31, 2017
- Task(s):
    6. ASCENT Project 42 support

Project Funding Level

FAA funds were distributed at the following levels:
$170K, The Pennsylvania State University
$15K, University of Washington
$70K, Georgia Institute of Technology
$15K, Volpe National Transportation Systems Center

Aerion Corporation is providing cost-share matching funds to Penn State and U. Washington. Our point of contact at Aerion is Jason Matishek, jrmatisheck@aerioncorp.com. Aerion is providing the necessary near-field CFD data and other relevant information to help guide the project team make accurate predictions of the Mach cut-off sonic boom signatures that may be produced by Aerion's future supersonic aircraft.

Investigation Team

Pennsylvania State University
Principal Investigator: Victor W. Sparrow
Co-Investigator: Michelle C. Vigeant
Graduate Research Assistant Zhendong Huang (assessment and extension of Mach cut-off models)
Graduate Research Assistant Nick Ortega (human perception of Mach cut-off sounds)

University of Washington
Principal Investigator: Michael R. Bailey PhD, University of Washington
Wayne Kreider, PhD, source characterization, University of Washington
Oleg A. Sapozhnikov, DSc, atmospheric stratification, University of Washington
Vera a. Khokhlova, DSc, numerical simulation, University of Washington
Barbrina Dunmire MS, gel layer fabrication, University of Washington
Julianna Simon PhD, postdoc, University of Washington

Georgia Institute of Technology
Principal Investigator: Dimitri Mavris
Co-Investigator: Jimmy Tai
Research Faculty: Greg Busch
Graduate Research Assistant: Ruxandra Duca
Graduate Research Assistant: Ratheesvar Mohan

Volpe National Transportation Systems Center
Principal Investigator: Juliet Page

Project Overview

ASCENT Project 42 brings together resources to provide preliminary information to the FAA regarding the noise exposure of supersonic aircraft flying under Mach cut-off conditions. Studies in the 1970s showed that Mach cut-off supersonic flight was possible, but there is currently no data establishing the frequency and extent of noise exposures and no guidelines for managing such exposures. Penn State will lead a team of investigators from Penn State, University of Washington, Georgia Tech, and Volpe—each bringing unique contributions to shed light on the Mach cut-off phenomena.

Aerion Corporation and many others believe that Mach cut-off supersonic flight is both viable [Plotkin, et al., 2008] and very likely to be acceptable to the public. But there is a lack of data to back up this assertion. Thus, research needs to be conducted to provide a technical basis for rulemaking regarding Mach cut-off operations.

The basic concept of Mach cut-off relies on the fact that the ambient temperature is substantially colder at flight altitudes than on the ground. Hence, the speed of sound is substantially slower at flight altitudes than at the ground. As illustrated in Figure 1, it is possible to fly in a range of Mach numbers (perhaps between Mach 1.0 and Mach 1.15) while having the sonic boom noise refract (bend) upwards such that the rays never reach the ground. However, the reader should be aware

that this picture is over-simplified since the temperature profile in the atmosphere is never a smooth, linear function as depicted here. For higher Mach numbers, the sonic boom will impact the ground before refracting upward.

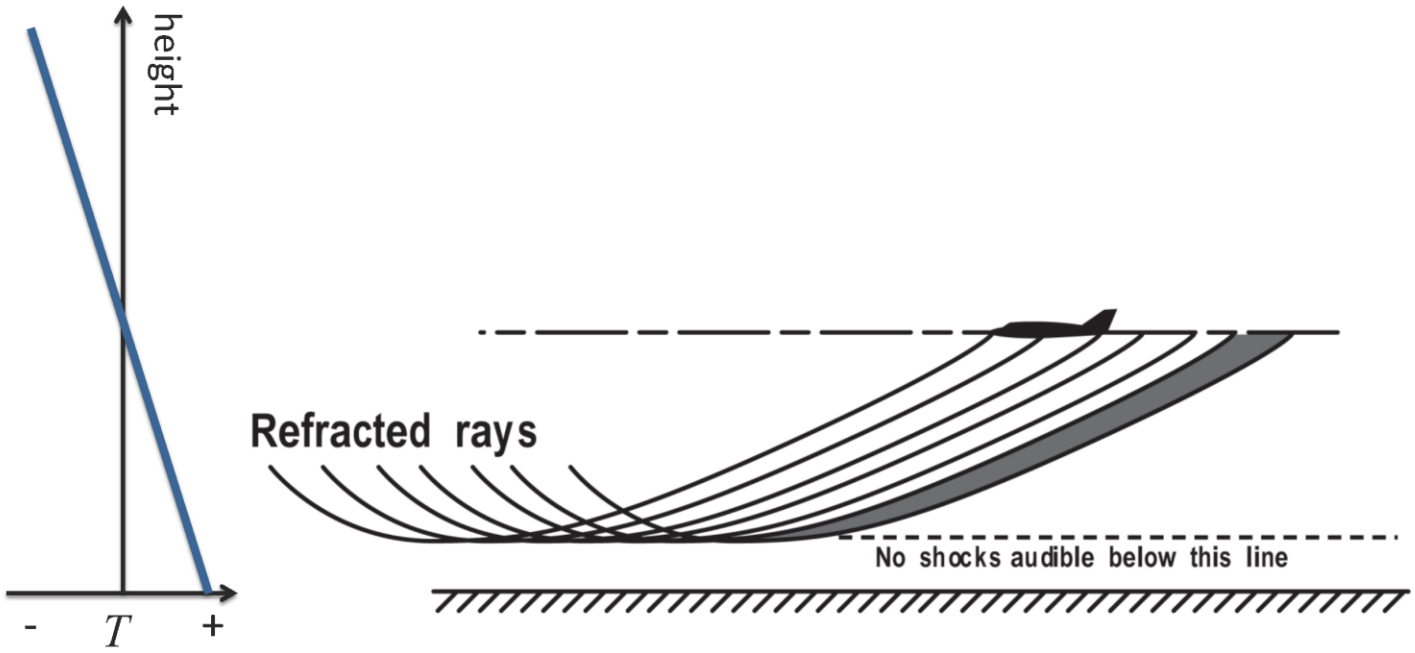

Figure 1 - Simplified view of Mach cut-off where sonic boom noise does not reach the ground surface. Left: ambient temperature versus height. [Sparrow] Right: aircraft and ray diagram showing refraction of sonic boom [NASA].

Little is known about the noise impact of Mach cut-off operations for future supersonic aircraft. The concept of Mach cut-off was introduced by Lockheed engineers in the mid-1960s [Shurcliff, 1970]. NASA conducted some field experiments in the early 1970s, focusing on other speed regimes of flight, validating some of the Mach cut-off theory for some of the sound field. This research was conducted in Nevada with a 466 m (1,529 ft) tower [Haglund and Kane, 1973]. Then to more directly address the Mach cut-off issue, a theoretical and experimental study was conducted in the mid-1970s with FAA support. The studies estimated altitudes and Mach number regimes to ensure the focus boom does not reach the ground. That field campaign used fighter jets flying out of Langley AFB to a test area in the Atlantic Ocean off Wallops Island, Virginia [Perley, 1977]. Using the available instrumentation, the study concluded that Mach cut-off flight was feasible.

In none of those studies were any recordings made of sufficient quality to assess human response to the Mach cut-off noise. The theoretical studies estimating the altitude and Mach number restrictions for focus boom avoidance assumed a simple atmospheric model (linear sound speed profile), and did not include real-world atmospheric effects. Hence the 1960s-1970s work was very good, but is only a start to determining appropriate flight conditions for routine Mach cut-off supersonic flights over the continental United States.

ASCENT Project 42 is a joint effort between the participants. Georgia Tech is responsible for Tasks 4 & 5 and the final report-out for these tasks are detailed in this report.

NOTE: As Georgia Tech, the University of Washington, and Volpe are concluding their efforts in ASCENT Project 42, those task reports are given first. The tasks at Penn State, which are continuing, are provided last.

Task #4: Sensitivity Study of Mach Cut-off Flight

Georgia Institute of Technology

Objective(s)

Georgia Tech's primary task for the ASCENT 42 project is to perform a sensitivity study on the acoustical model for Mach cut-off flight. This task aims to identify the major variables that can impact a supersonic aircraft's ability to fly (and maintain) Mach cut-off and determine the sensitivity of Mach cut-off flight to these variables. This will be determined by assessing both atmospheric variability and flight condition variability. This task is performed for both a standard vehicle model (the F-18 input model in PCBoom), as well as a model representative of Aerion Corporation's AS2 vehicle. Aerion's vehicle is assessed using computational data provided by Aerion under ASCENT 42. Through studying the sensitivity of Mach cut-off flight to atmospheric conditions, the ASCENT 42 team aims to provide insight on the degree of robustness for Mach cut-off flight as it pertains to a supersonic business jet. The goal of this task is to help provide Aerion (and other supersonic aircraft developers), the FAA, and the aerospace community at large, a better understanding of how feasible Mach cut-off flight could be and to assist in guiding policy regarding supersonic flight using Mach cut-off.

Research Approach

Introduction

The research approach for task 4 was heavily dependent on data, advice, and research provided by the other members of the ASCENT 42 team. Throughout the first year of the ASCENT Project 42, the various members had a lot of interaction and shared opinions and insights into each other's work – which has worked very well for this effort. Project 42, as a whole, has been very collaborative and GT acknowledges and thanks the other team members for their continued assistance and enthusiasm. The Acoustical Model for Mach Cut-off Flight project has thrived in this collaborative environment.

The preliminary step of the research performed by Georgia Tech for the sensitivity study was to select a tool for the analysis. Since NASA's PCBoom (v6.7) was made available to the Project 42 and Juliet Page of Volpe was brought in as a participant in the project, PCBoom was decided to be the primary method in which Georgia Tech assessed the sensitivity of Mach cut-off flight. This required Georgia Tech to understand the mechanics and operating procedures of NASA's PCBoom. This involved running test cases, analyzing results, and understanding the data required to input into PCBoom as well as breaking down the output and understanding what the program was calculating and how it was preforming the analyses. This preliminary step in the research approach took approximately one month, which was expedited primarily due to the help and guidance from Juliet Page in instructing the Georgia Tech researchers and students on intricacies of PCBoom and how to properly run a sonic boom analysis using the software.

The preliminary sensitivity study using PCBoom and the provided F-18 geometry was performed to understand the code and determine if the results made physical sense. This was done by running the F-18 model through PCBoom at various flight conditions (steady-level flight, acceleration, and a handful of maneuvers) to determine if Georgia Tech had a good handle on the PCBoom settings required to accurately generate results. This model was run through various atmospheric conditions. The results of this preliminary study was shared with the ASCENT 42 participants to gather their opinions, advice, and suggestions regarding the execution of PCBoom. After a few iterations, the GT team developed a comfortable level of knowledge of PCBoom and was able to produce results for both Mach cut-on and cut-off flight.

After the analysis tool was selected and learned, the Georgia Tech team laid out a plan for the research approach for Task 4. This plan included four step for the sensitivity study of Mach Cut-off Flight:

- PCBoom Wrapper – Develop a capability to run large amounts of analyses automatically and rapidly
- Atmospheric Profiles – Create / Gather a large library of both "standard" and "realistic" temperature profiles (include temperature, relative humidity, and horizontal winds)
- Sensitivity Study: Standard Profiles – Perform study for both F-18 signature and Aerion AS2 signature for various flight conditions in standard atmospheric profiles
- Sensitivity Study: Realistic Profiles - Perform study for both F-18 signature and Aerion AS2 signature for various flight conditions in realistic atmospheric profiles

The research plan allows Georgia Tech to show how sensitive Mach cut-off flight is to both flight conditions and a wide range of atmospheric profiles, and assess the robustness supersonic Mach cut-off flight. Georgia Tech's goal was also to

determine the key factors that drive the sensitivity. Through the results, Georgia Tech seeks to assist other participants in Project 42, the FAA, and the supersonic industry in understanding Mach cut-off and assessing its feasibility as a method of over-land supersonic flight. The details of each phase of the research plan are described in the following sections as well as the results of Task 4: Sensitivity Study of Mach Cut-off Flight.

PCBoom Wrapper

To facilitate the execution of Task 4, Georgia Tech decided to develop a capability to easily and rapidly execute PCBoom to generate large amounts of data for analysis. The effects of atmospheric variables and flight conditions on sonic boom metrics and cut-off conditions were investigated through sensitivity studies. The variables – temperature, humidity, and wind – were systematically modified to produce various atmospheric profile combinations, or "cases". The near-field noise signature was then propagated through these profiles and the results were recorded for further analysis. The computational tool used to obtain the results – PCBoomv6.7 – had several executable programs that required numerous inputs and produced various output files. To efficiently run all the cases, the process was automated by creating a wrapper in a different tool – Matlab. The wrapper's purpose was to read a table of cases (created a priori in Excel), go through each of them, create all the required input files, run the relevant executable programs, parse the output files, and record the metrics of interest in an Excel sheet.

To propagate a noise signature, PCBoom required a main input file, a trajectory file and an atmospheric file. These were produced by copying templates created as part of the pre-processing stage and replacing specific portions with data from the table of cases. After the program was run, the cut-off conditions, noise metrics, and the noise signature at the ground were read from various output files and recorded in a table of results. All files generated for each case were saved for archiving purposes. The process is illustrated in the following figure:

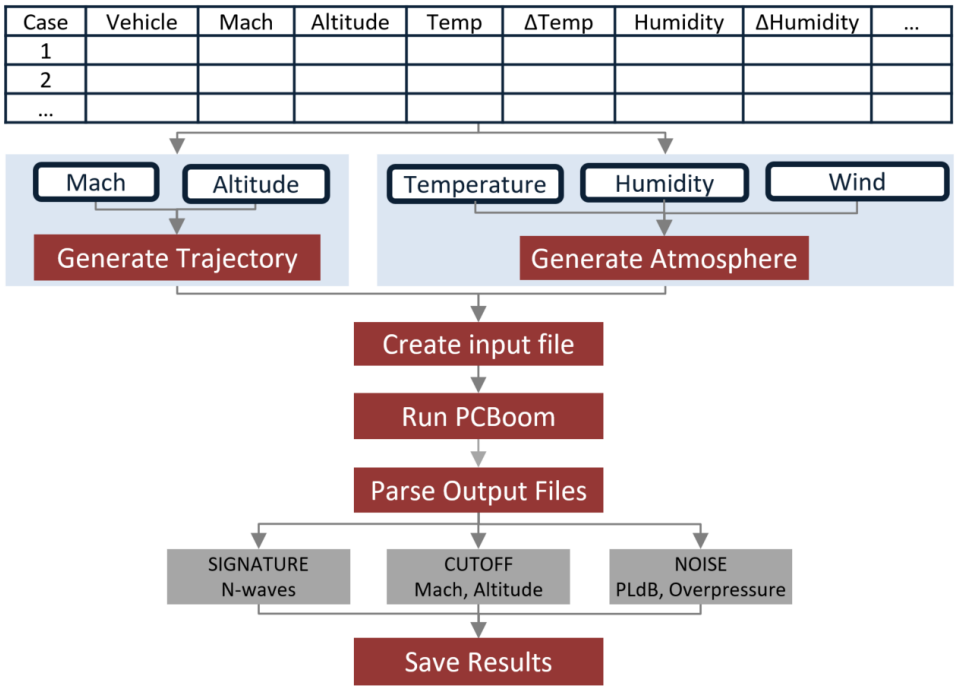

Figure 2 - PCBoom Wrapper Flowchart

Inputs – Trajectory File

For the purpose of this project, only steady, level, un-accelerated flight was considered. This was decided upon through consensus with the entire Project 42 team in an effort to scope the project to accomplishable tasks for the first year. Thus, a point trajectory was sufficient, where only the flight altitude and Mach number were specified. Based on the flight conditions read from the table of cases, the wrapper created a trajectory file by replacing placeholders in a template file with the desired Mach and altitude of the aircraft.

Inputs – Atmospheric File

Two main types of atmospheric profiles were analyzed for this project: standard and realistic. The standard profiles were mathematical descriptions of the variable profiles as functions of altitude. The realistic ones involved real weather data from various locations in the United States. To generate the atmospheric file required by PCBoom, several operations were needed as described further. Note: this section will detail the generation of the standard atmospheric profiles in the PCBoom Wrapper and how the wrapper uses the profiles. A more detailed description of the realistic atmospheric profiles and reasoning behind various standard atmospheric profiles are enumerated in the Atmospheric Profiles phase following the complete description of the PCBoom Wrapper.

Standard profiles

The standard profile used in PCBoomv6.7 is the U.S. Standard Atmosphere, No Winds, ANSI S1.26 Annex C. The first step in creating varying standard profiles was to specify the type of profile desired. The options are shown in the following table.

Table 1: Reference profile types for standard atmospheres

Temperature	**Humidity**	**Wind**
Linear	Standard	Constant
Constant	Constant	No wind
Concave	No humidity	
Convex		

For each of the temperature options, the tropopause temperature was set to -56.5˚C and the variation was created with mathematical formulae based on the ground temperature, as specified in the table. The following figure illustrates how a ground temperature of -7˚C and one of 49˚C result in different profiles.

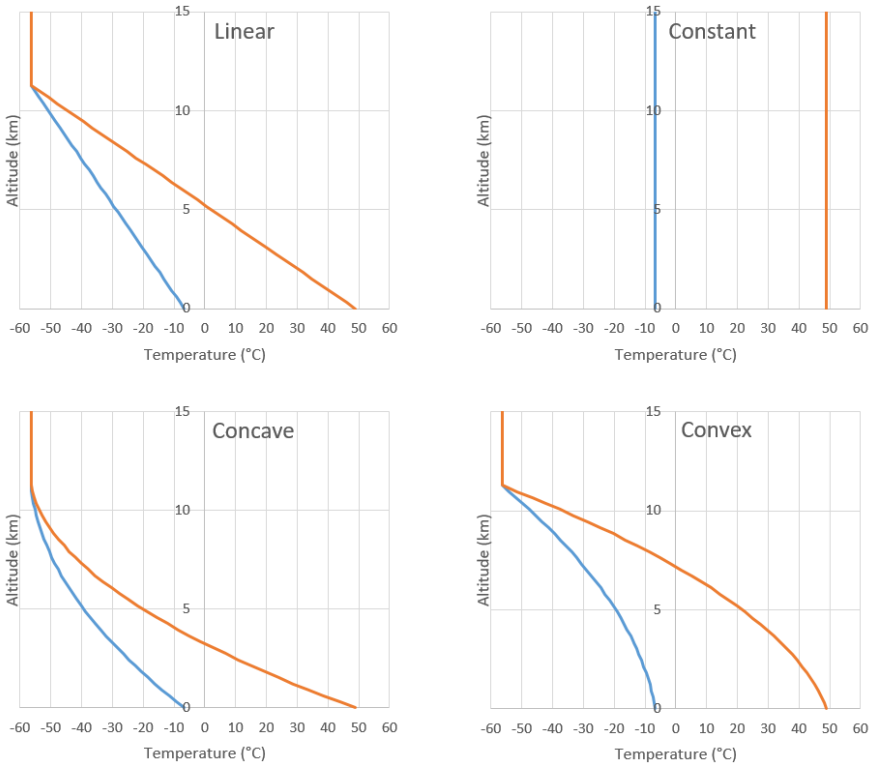

Figure 3 - Variation of Temperature Profiles: Linear, Constant, Concave, Convex

For humidity, the standard profile (which was the US standard ANSI 1976 atmosphere) was varied by shifting the entire curve by a value specified in the table, without going outside of the range 0-100%. The constant humidity profile was simply set to the value specified at all altitudes, while no humidity meant 0% for all altitudes. The only available wind profiles were no wind or constant wind in various directions. For the latter, the magnitude and direction read from the table were used to calculate the x and y components of the wind at each altitude. The resulting curves for temperature, humidity, and wind in both x and y directions were written in the atmospheric file following the format required by PCBoom. This process was repeated for each case.

Realistic profiles

The second type of atmospheric files was based one real weather data gathered a priori (The details of the gathering and creation of these profiles is detailed in the next phase of Task 4). Five locations were chosen to be representative of the following combinations of temperature and humidity: humid and hot, humid and cold, arid and hot, arid and average temperature, and finally arid and cold. Five templates with this data were created. Then, the wrapper picked the corresponding profiles from the templates and shifted them based on the specifications of each case. A new atmospheric file was generated for each case. An example of this would be: humid/cold reference profile where the temperature is shifted by +10˚C, the humidity by -10%, and the wind by +40 m/s in magnitude and -10˚ in direction.

Inputs - Main File

Once the auxiliary files – the trajectory and the atmosphere – were generated, the main input file was created. To do this, the wrapper made a copy of a template file and replaced placeholders with the following data:

- Vehicle, as specified in table (Aerion AS2 or generic supersonic aircraft available in the PCBoom library)
- Format of near-field signature and propagation mode (done automatically based on the vehicle type)
- Angle where noise metrics are to be recorded (such as 0˚ for directly undertrack)

Running PCBoom

Two executable programs were of interest in this project: FOBoom and PCBurg. FOBoom was the main boom calculation program and its outputs included ray paths and ray tube areas to be used by PCBurg, as well as cut-off conditions: maximum Mach to maintain cut-off flight at current altitude and minimum altitude to maintain cut-off flight at current Mach. This executable, however, did not account for the effects of humidity and temperature. Thus, PCBurg was subsequently used to consider the added effects of molecular relaxation on sonic boom signature evolution. This tool propagated the near field signature in increments of 304.8 m, all the way down to the ground (if cut-off did not occur) through the atmospheric profiles specified in the input files. To propagate the signature, the wrapper read the following options for PCBurg from the table

- Sampling rate (available options were 10000, 25600, 512000, and 102400 Hz)
- Activation of the anti-Gibbs filter
- Angle for the desired ray (which matched the one in the input file)

The wrapper ran each case in batch mode and placed all the generated files in various folders for storage. The following table shows an example of the required "table of cases". It contains all the data necessary to create the required input files described previously and to run the program.

Table 2 - Inputs in the table of cases to be used by the PCBoom wrapper

	Flight Conditions			Atmospheric Conditions							Run Conditions		
Case	Vehicle	Mach Number	Altitude (m)	Temperature Profile	Temperature Delta from 15 (°C)	Humidity Profile	Humidity Delta (%RH)	Wind Profile	Wind Magnitude Delta (ft/s)	Wind Direction Delta (deg)	PHI	SR	Gibbs
1	F-18	1.4	13716	Linear	-61.7	Standard	0	No Wind	0	0	0	1	1
2	F-18	1.4	13716	Linear	-58.9	Standard	0	No Wind	0	0	0	1	1
3	F-18	1.4	13716	Linear	-56.1	Standard	0	No Wind	0	0	0	1	1
4	F-18	1.4	13716	Linear	-53.3	Standard	0	No Wind	0	0	0	1	1
5	F-18	1.4	13716	Linear	-50.6	Standard	0	No Wind	0	0	0	1	1
6	F-18	1.4	13716	Linear	-47.8	Standard	0	No Wind	0	0	0	1	1
7	F-18	1.4	13716	Linear	-45	Standard	0	No Wind	0	0	0	1	1
8	F-18	1.4	13716	Linear	-42.2	Standard	0	No Wind	0	0	0	1	1
9	F-18	1.4	13716	Linear	-39.4	Standard	0	No Wind	0	0	0	1	1
10	F-18	1.4	13716	Linear	-36.7	Standard	0	No Wind	0	0	0	1	1

Parsing the outputs

The cut-off conditions, namely the maximum Mach to maintain cut-off flight at current altitude and minimum altitude to maintain cut-off flight at current Mach, were obtained from a text file outputted by FOBoom. Then, if the given case was not cut-off, PCBurg produced several noise metrics including the loudness (in PLdB), the maximum overpressure (in psf) and A- and C- weighted sound exposure levels (in PLdB). The noise signature at the ground was also an output of PCBurg. All these values as well as the corresponding input values were recorded in a Matlab file for easy manipulation and post-processing. The wrapper also generated an Excel spreadsheet with all the resulting data (with the exception of noise signatures which are saved in a separate Matlab file). The following table shows the columns of outputs that are appended to the table of inputs cases described in Table 2:

Table 3: Outputs of the PCBoom Wrapper

Max Overpressure (Pa)	Loudness (PLdB)	ESEL	CSEL	ASEL	Max Mach for Cut-off	Min Altitude for Cut-off
44.529	95.34	114.18	102.11	80.38	1.0618	0
45.007	95.34	114.19	102.28	80.15	1.0678	0
45.486	95.69	114.23	102.5	80.65	1.0738	0
45.965	96.28	114.24	102.7	81.54	1.0798	0
46.444	96.98	114.25	102.87	82.58	1.0857	0
46.444	97.71	114.25	103.01	83.63	1.0916	0
46.444	98.39	114.25	103.1	84.57	1.0974	0
46.444	98.88	114.26	103.18	85.29	1.1033	0
46.444	99.26	114.25	103.19	85.67	1.1091	0
45.965	99.39	114.24	103.19	85.91	1.1148	0

Data Visualization Graphical User Interface

Developing the wrapper capability ultimately allowed for fast evaluation of thousands of cases by automatically creating all the required files and recording all desired outputs, without any intervention from the user. Because the computational time was significantly reduced, more focus was put on post processing the data and understanding the results. To visualize the vast amount of data generated, a data visualization capability in the form of a graphical user interface (GUI) was developed, as seen in the figure below. In the top left corner, the user must select among the various options which types of cases to investigate. The bottom half shows two plots of maximum overpressure and loudness. In the top right corner, a plot shows a superposition of all the pressure signatures from all the cases satisfying the options in the top left.

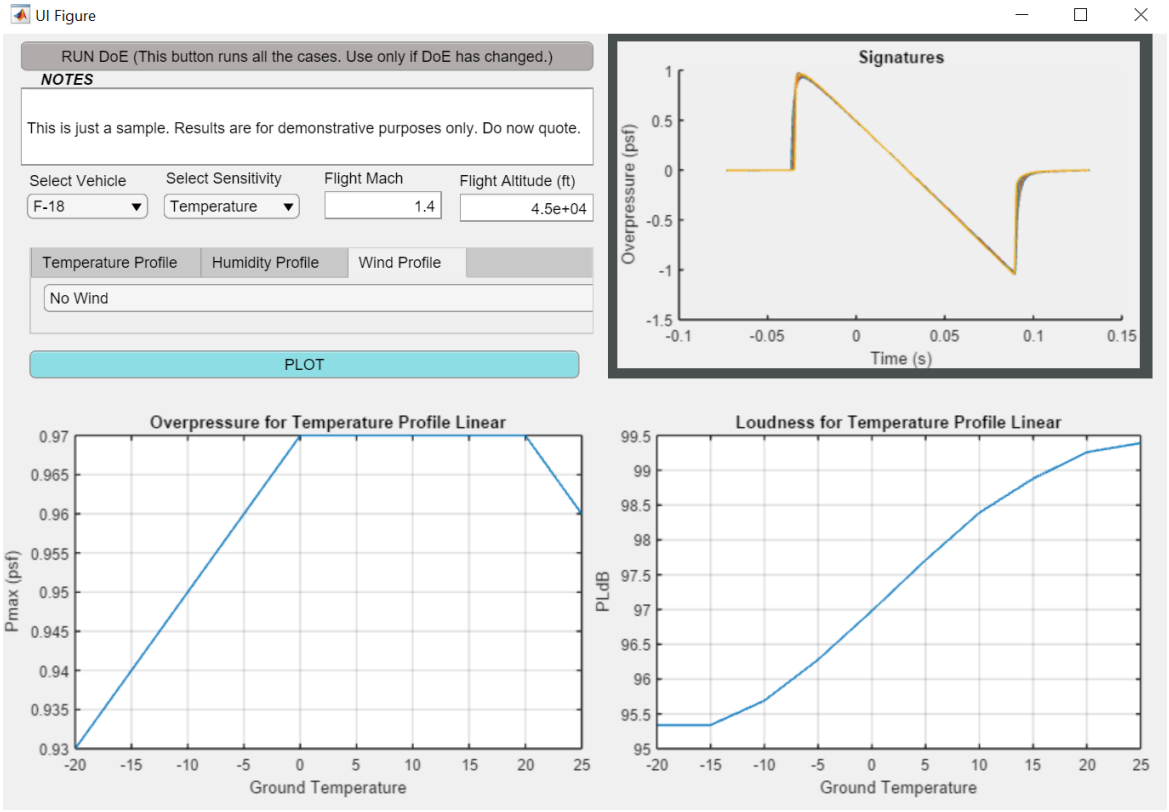

Figure 4 - General View of the Data Visualization GUI

Once the wrapper finished running all the cases, it also saved the results in a MATLAB specific “Table” format which allows for easy manipulation. The GUI uses this table to generate various plots: maximum overpressure and loudness versus changes in either temperature, humidity, or wind magnitude or direction. To successfully generate them, the user must input a number of options. Because two airplanes were investigated in this study, a dropdown menu allows the user to select the vehicle (either F-18 from the PCBoom library or Aerion AS-2). Then, the user must select the type of sensitivity desired for the plots, which will modify the x-axes of the plots accordingly. The options are the four atmospheric parameters analyzed in this study: temperature, humidity, and wind magnitude and direction. The user must also specify the desired flight conditions. The following figure illustrates some of these options:

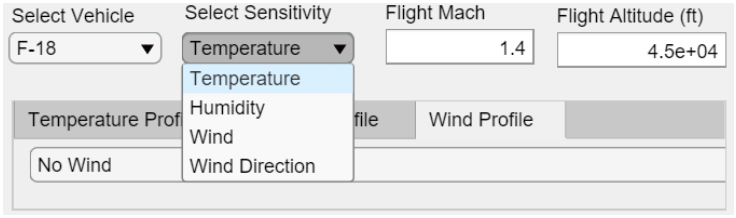

Figure 5 - Various Options Available for User Selection in GUI

For each of the atmospheric parameters, various profiles were investigated. Thus, the user must go through the three tabs ("Temperature Profile", "Humidity Profile", and "Wind Profile") and select the desired case for each of them. The following figures illustrates the concept:

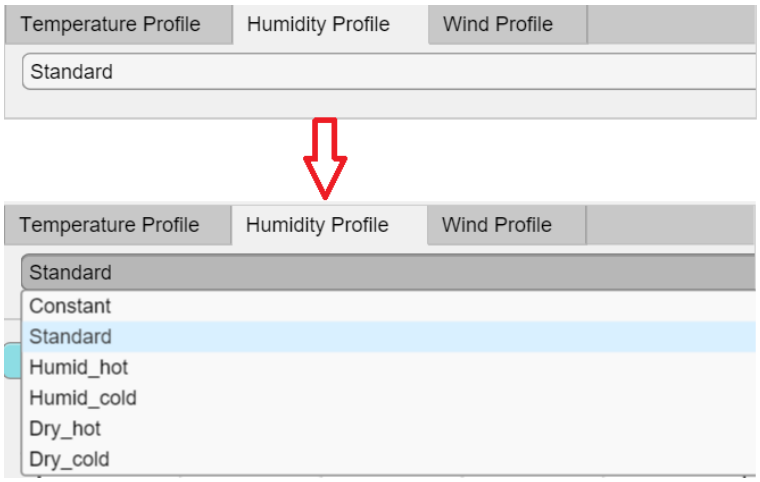

Figure 6 - Dropdown Options for Atmospheric Parameter Profiles

These options are predicated on the fact that the combinations selected by the user were present in the table of input cases and have been run by the wrapper. If the combination required does not exist, the plots will simply not show any curves. The GUI allows the user to make new selections and click on the button "Plot" to repopulate the graphs. Every time this button is pressed, the corresponding cases are selected and sorted from all the outputs. There is also a button called "Run DOE" that allows the user to run an entirely new batch of cases directly from the GUI. This graphical user interface capability allows for fast sorting through large amounts of data and automated plotting. By being able to quickly change the options, the user can rapidly visualize very different types of cases and assess general trends, without spending time on processing the data and generating graphs. Thus, more focus can be placed on understanding the results.

Atmospheric Conditions

In an effort to perform the sensitivity study of Mach cut-off flight as extensively as possible, the Georgia Tech team strived to create a large library of atmospheric profiles to capture large amount of variation in the atmospheric parameters used by PCBoom. The atmospheric parameters the user has the ability to alter include temperature, relative humidity, and horizontal winds (both in the lateral and longitudinal directions). Mach cut-off conditions are sensitive to all three of these parameters and also vertical winds, as shown in Penn State's tasks for Project 42. However, vertical winds are currently not within the capabilities of PCBoomv6.7 so Georgia Tech decided to only develop profiles to include temperature, relative humidity, and horizontal winds – but adding in vertical winds to the profiles and atmosphere file generator in the PCBoom Wrapper can be easily done.

The Georgia Tech research team decided to split the atmosphere profiles studied into two groups. The first being "standard" atmospheric profiles and the second being "realistic" atmospheric profiles. The term "standard" profiles indicates that the atmospheric profiles are deviations from the standard US atmosphere profile, but maintain continuity and have no inversions. The reason for investigation of both types of atmospheric profiles was to identify sensitivities in both ideal and non-ideal conditions. By assessing the Mach cut-off conditions in realistic profiles and comparing those

results to the Mach cut-off conditions in standard profiles, Georgia Tech was able to determine the impact of varying temperature gradients and temperature inversions on the Mach cut-off altitude and Mach number.

Standard Profiles

The standard temperature profiles generated and used in this study are based on the standard profile used in PCBoomv6.7, the U.S. Standard Atmosphere, No Winds, ANSI S1.26 Annex C, with the ability to add in horizontal winds. Georgia Tech created four "types" of standard profiles for temperature, two for relative humidity, and three for wind. The temperature profiles created fall into four different categories: Linear, Constant, Concave, and Convex. In the linear set of temperature profiles, the US standard atmosphere is used as the baseline and then the ground temperature is shifted while maintaining the tropopause temperature (-56.5ºC). This provides different slopes to the temperature profile are the sound propagated from altitude down to the ground. A sample of the linear temperature profiles is given in Figure 7 below.

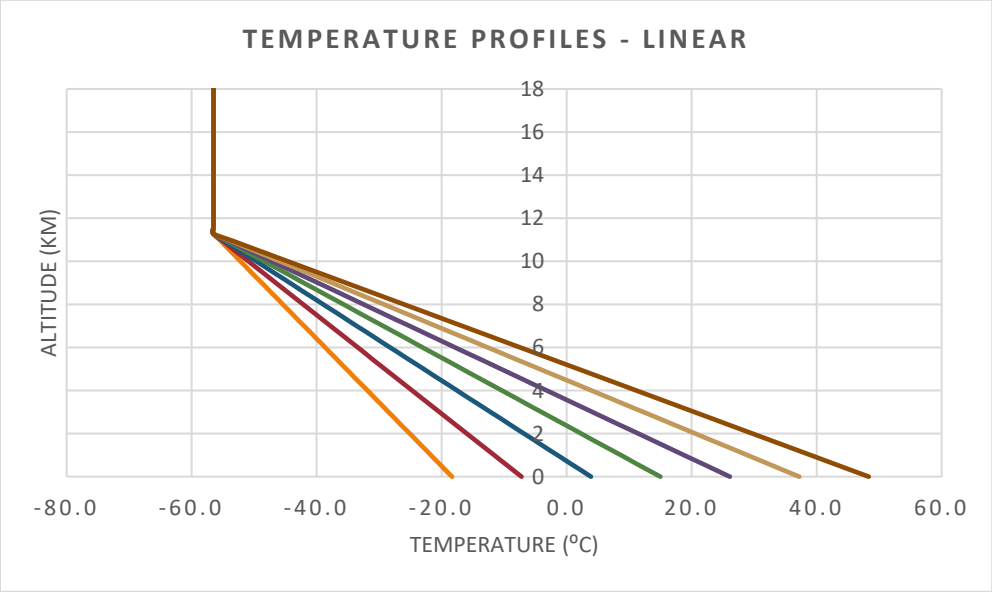

Figure 7: Standard Profiles: Linear Temperature

The next type of temperature profiles created were constant temperature profiles. These temperature profiles are constant temperature from the ground up to altitude. These profiles were not used extensively, but rather as a way to determine what PCBoom would predict as the Mach cut-off conditions if the speed of sound at altitude and at ground level were equal. The third and fourth types of temperature profiles are concave and convex profiles. These follow the same basic function as the linear profiles in changing the ground temperature, but in these profiles the temperature gradient is non-constant. An example of these profiles can be seen in Figure 8.

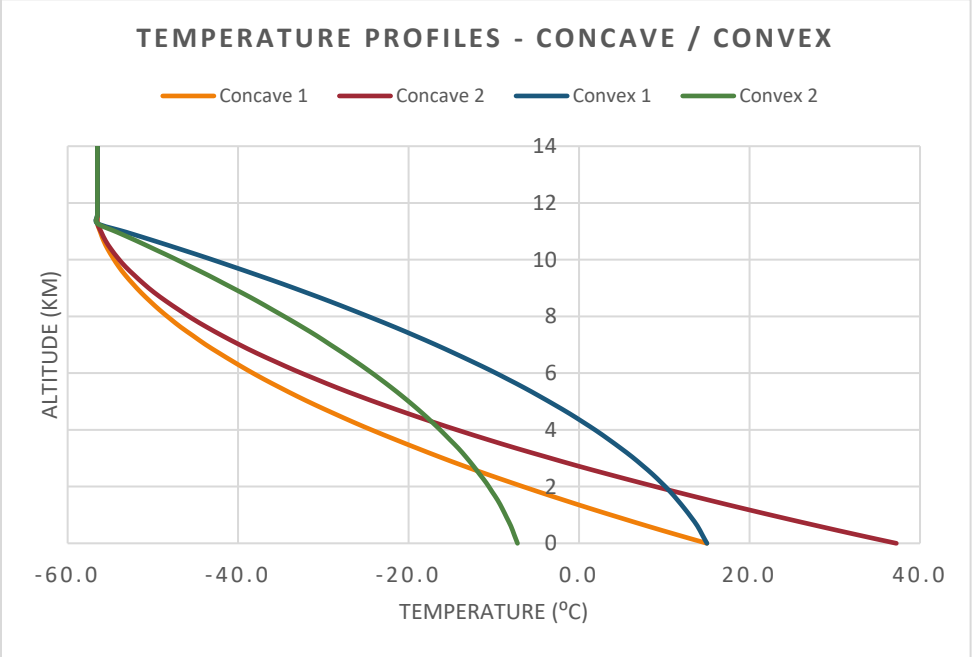

Figure 8: Standard Profiles: Concave and Convex Temperature

The humidity and wind are also included in the standard atmosphere profiles. For relative humidity, there are two options. The first is a constant relative humidity throughout the entire profile, which can be set from anywhere from 0 to 100% relative humidity. The second humidity profile is the U.S. standard atmosphere humidity profile, which can be shifted by a constant percentage throughout the profile. An example of these profiles can be seen in Figure 9.

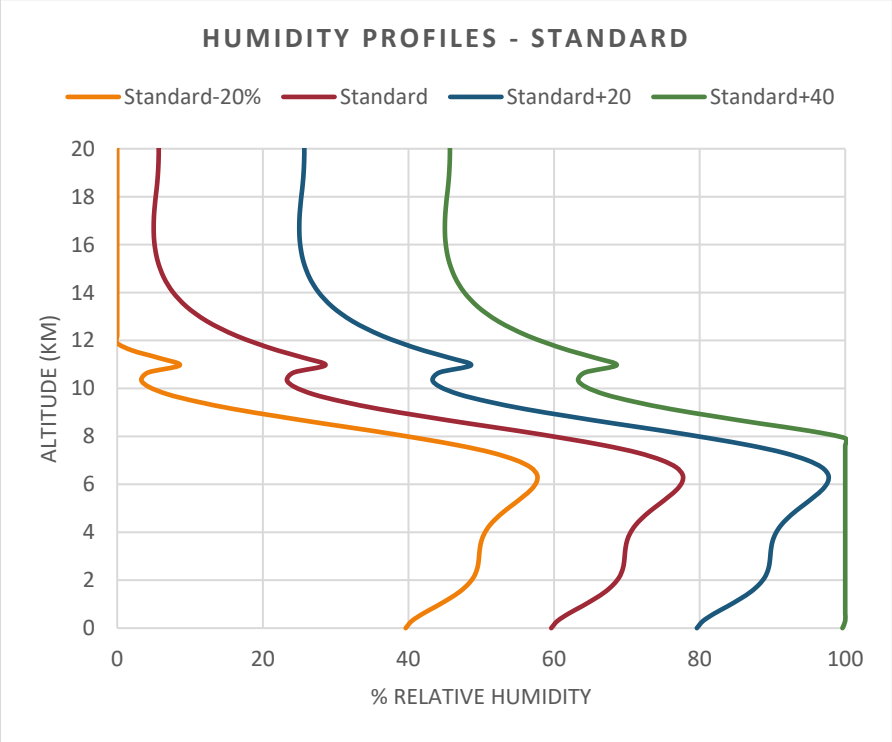

Figure 9: Standard Profiles: Relative Humidity

The remaining attribute in the standard profiles is the horizontal wind. Horizontal winds are set to zero in the standard atmosphere file for PCBoom 6.7, but can be altered easily. Using GT's PCBoom Wrapper, the user can create any wind profile desired by giving discrete wind information at every altitude station in the profile. The other option is to choose a constant wind profile with a given magnitude and direction. The PCBoom Wrapper then takes this information and splits the horizontal wind into x and y components for the atmospheric input file. The wind direction is defined for the remainder of this task as shown in Figure 10 – where 0º is a tailwind and 180º is a headwind.

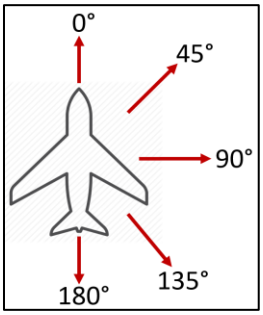

Figure 10: Wind Directions Definitions

The combination of temperature, relative humidity, and horizontal winds completely defines the atmospheric profile in PCBoom. Through the use of the atmospheric file generator developed for the PCBoom Wrapper, the Georgia Tech Research team has created over 10,000 unique atmospheric profiles for case analyses in PCBoom. However, many of these atmospheric profiles are idealistic and don't actually represent what an aircraft would experience in real-world flight. This led the Georgia Tech team to develop "realistic" atmospheric profiles from publically available data.

Realistic Profiles

The Georgia Tech team developed a set of realistic atmospheric profiles to study the sensitivity of Mach cut-off flight in real-world conditions. The purpose of studying these profiles and shifting the temperatures within these profiles, was to capture the impact of temperature fluctuations and inversions as well as variable horizontal winds on the Mach cut-off conditions. The Georgia Tech team decided to investigate these impacts in four distinct climates (Temperature/Rel. Humidity):

- Hot/Humid: Miami, FL, USA
- Hot/Arid: Tucson, AZ, USA
- Cold/Humid: Minneapolis, MN, USA
- Cold/Arid: Denver, CO, USA
- Average/Average: Oakland, CA, USA

These realistic atmospheric profiles were generated from radiosonde data from the Department of Atmospheric Sciences at the University of Wyoming [http://weather.uwyo.edu/upperair/sounding.html]. The data tracked included altitude relative humidity, temperature, and wind magnitude and direction. The Georgia Tech team used this data and translated it to a format for input to PCBoom using the PCBoom Wrapper. The profiles gathered were from cities that represented extremes on both the temperature and humidity ranges and an average city: Miami, FL, Tucson, AZ, Minneapolis, MN, Denver, CO, and Oakland, CA. The realistic temperature profiles are shown in Figure 11, the humidity profiles are shown in Figure 12, and the wind profiles are shown in Figure 13.

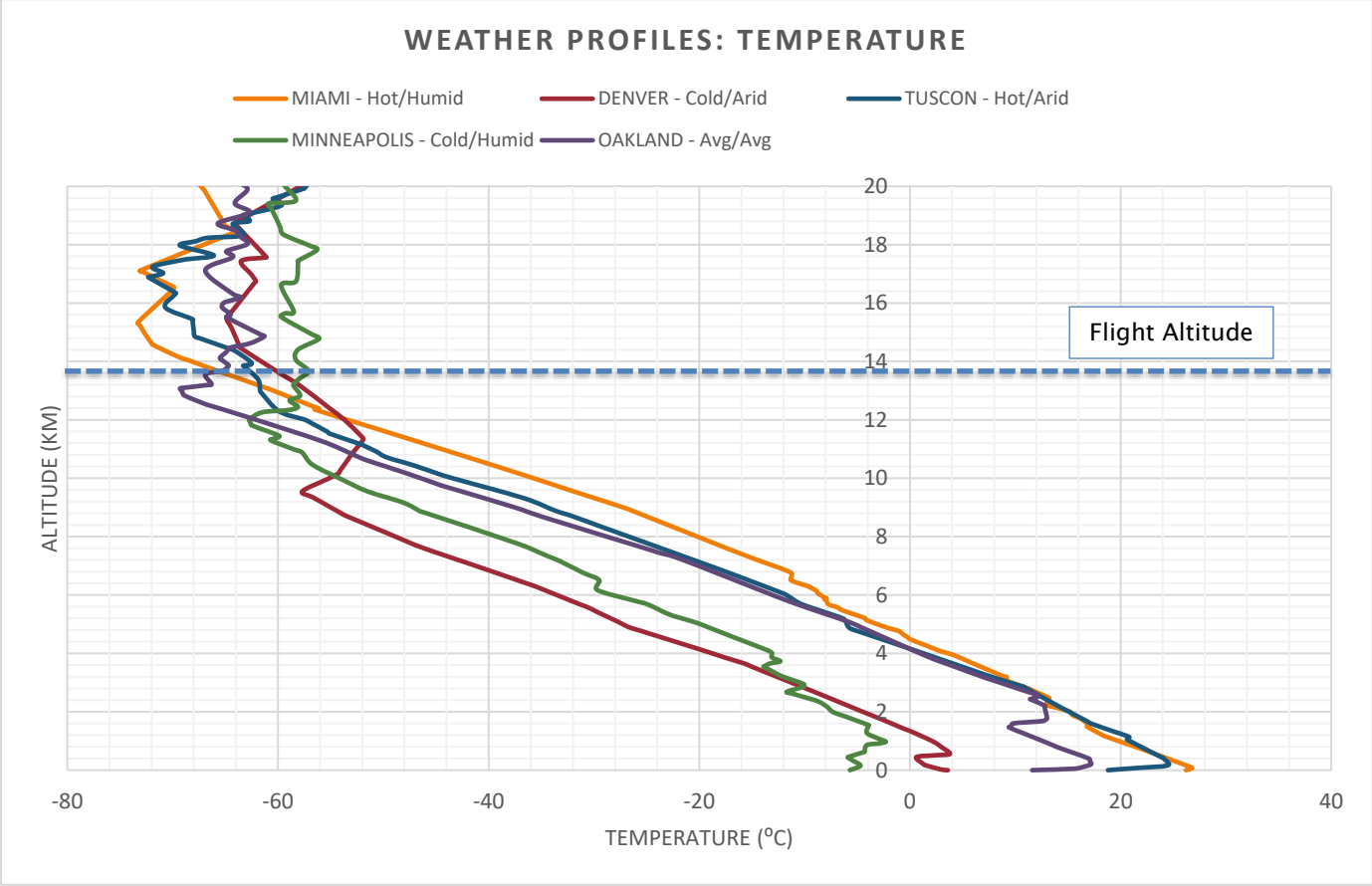

Figure 11: Realistic Profiles: Temperature

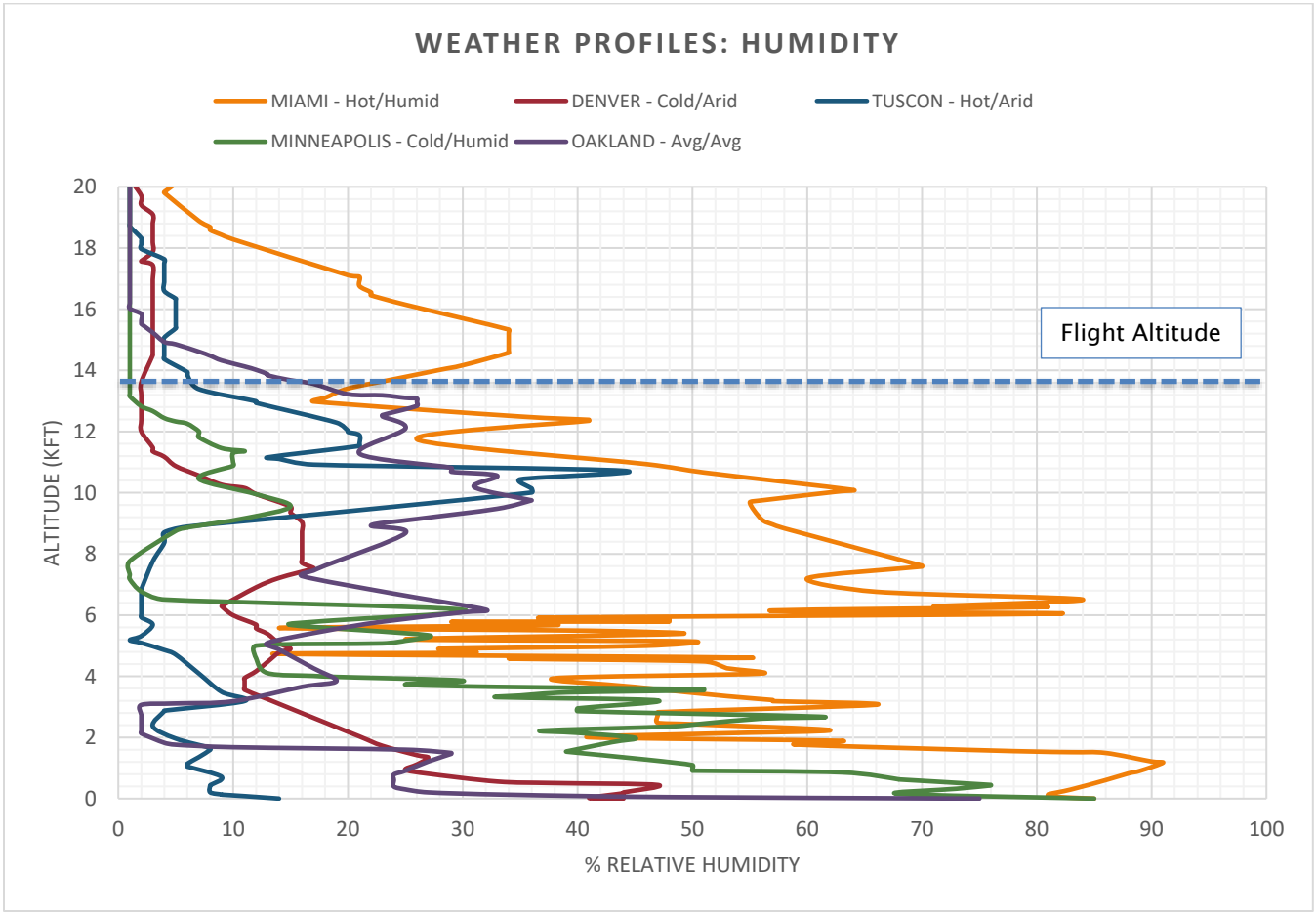

Figure 12: Realistic Profiles: Relative Humidity

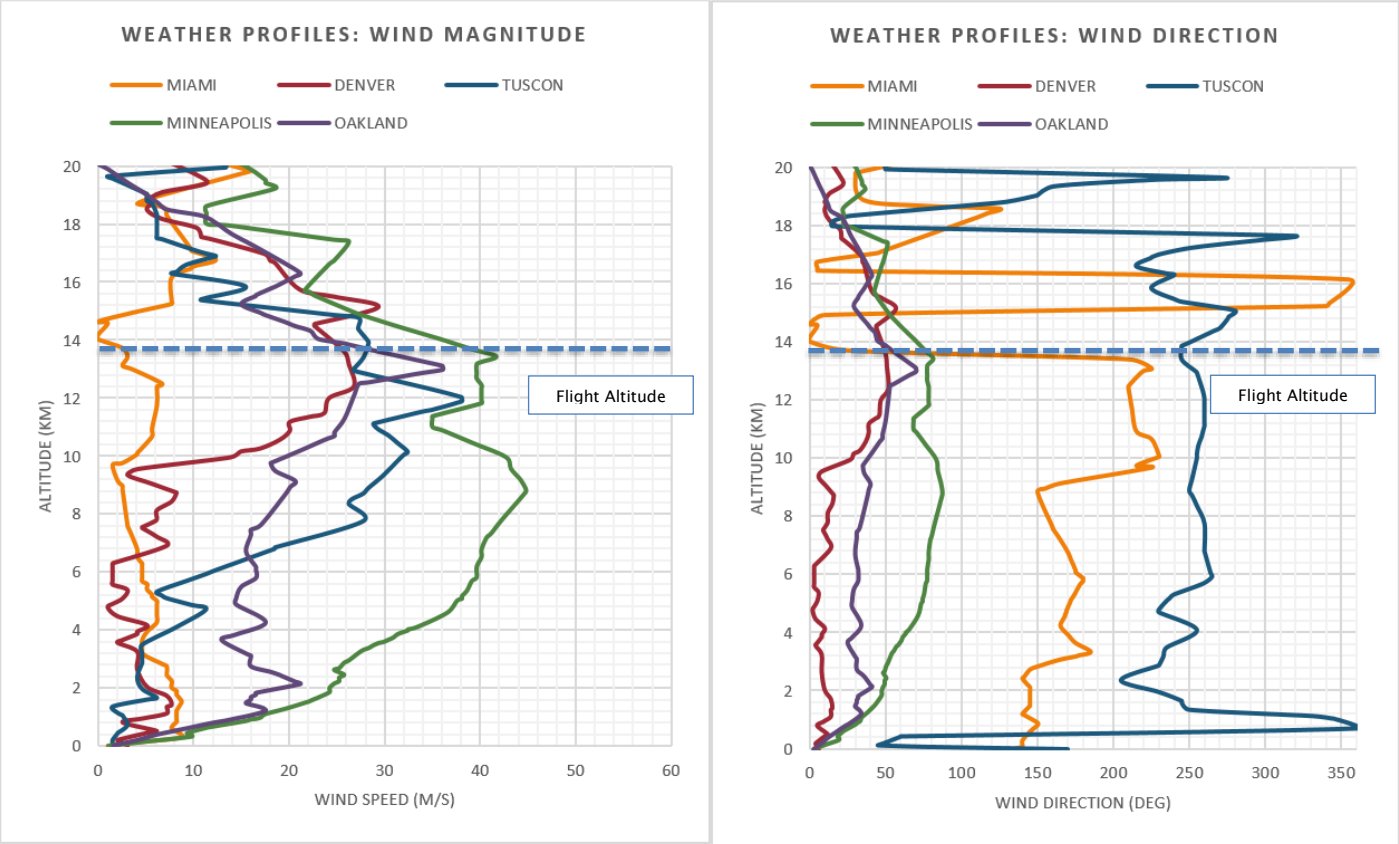

Figure 13: Realistic Profiles: Wind Magnitude and Direction

The five realistic atmospheric profiles were integrated into the PCBoom Wrapper to allow for use in large designs of experiments. This allowed for the altering of the profiles from the baseline profiles generated from data. This enabled the Georgia Tech team to study the sensitivity of certain aspects of each atmospheric profile to Mach cut-off conditions. The sensitivity study performed during the first year of Project 42 was accomplished through shifting and altering the temperatures of both the realistic and standard atmospheric profiles. The results of the sensitivity study are presented in the following section.

Sensitivity Study & Results

Introduction

The main sensitivity study performed for Task 4 was performed in three stages. The first stage consisted of benchmarking the results and generating baseline results using PCBoom to study the sensitivity of Mach *cut-on* results to atmospheric conditions. Through studying what happens to the cut-on sonic boom metrics (such as overpressure and Loudness at the ground), Georgia tech hoped to gain insight on the physics of the sonic boom propagation through different atmospheres. The second stage of the study was performed for Mach cut-off conditions through standard atmospheric profiles. This provided Georgia Tech a controlled response to set temperature gradients that could be studied and easily obtain a sensitivity of Mach cut-off conditions to variations in the standard atmospheric profiles. The third stage of the sensitivity study was performed for Mach cut-off conditions under realistic atmospheric profiles. The goal of this stage was to observe how non-standard profiles impact Mach cut-off conditions and how abnormalities (such as temperature inversions) impact an aircraft's ability to maintain Mach cut-off flight. The results of these three stages of the sensitivity study are presented in this section. It is important to note that all three stages were performed with Aerion's AS2 nearfield sonic boom signature and Georgia Tech would like to extend it's gratitude to Aerion Corporation for making the data available to the

participants of Project 42. The results presented in this report do not detail Aerion's near field pressure signal, only the propagated PCBoom results and cut-off conditions.

Benchmarking & Mach Cut-On

The benchmarking stage of the results was done with Mach cut-on conditions. For this study, Georgia Tech used a flight altitude of 13.7km (45,000ft) at a flight Mach number of 1.4. This consistently produces signatures on the ground. In order to observe the impact of the atmosphere on the resulting noise levels, the GT team chose to run the Mach cut-on conditions through both standard and realistic atmosphere profiles. The first sensitivity investigated was ground boom strength to atmospheric temperature. This was done by observing the changes in both loudness (PLdB) and maximum overpressure (Pa) to changes in humidity and wind for various temperature profiles.

Humidity/Temperature Sensitivity - Loudness

The sensitivity of loudness to changes in relative humidity are shown in Figures 14-17, Figure 14 displays the sensitivity under linear temperature profiles, Figure 15 displays the sensitivity under constant temperature profiles, Figure 16 displays the sensitivity under concave temperature profiles, and Figure 17 displays the sensitivity under convex temperature profiles.

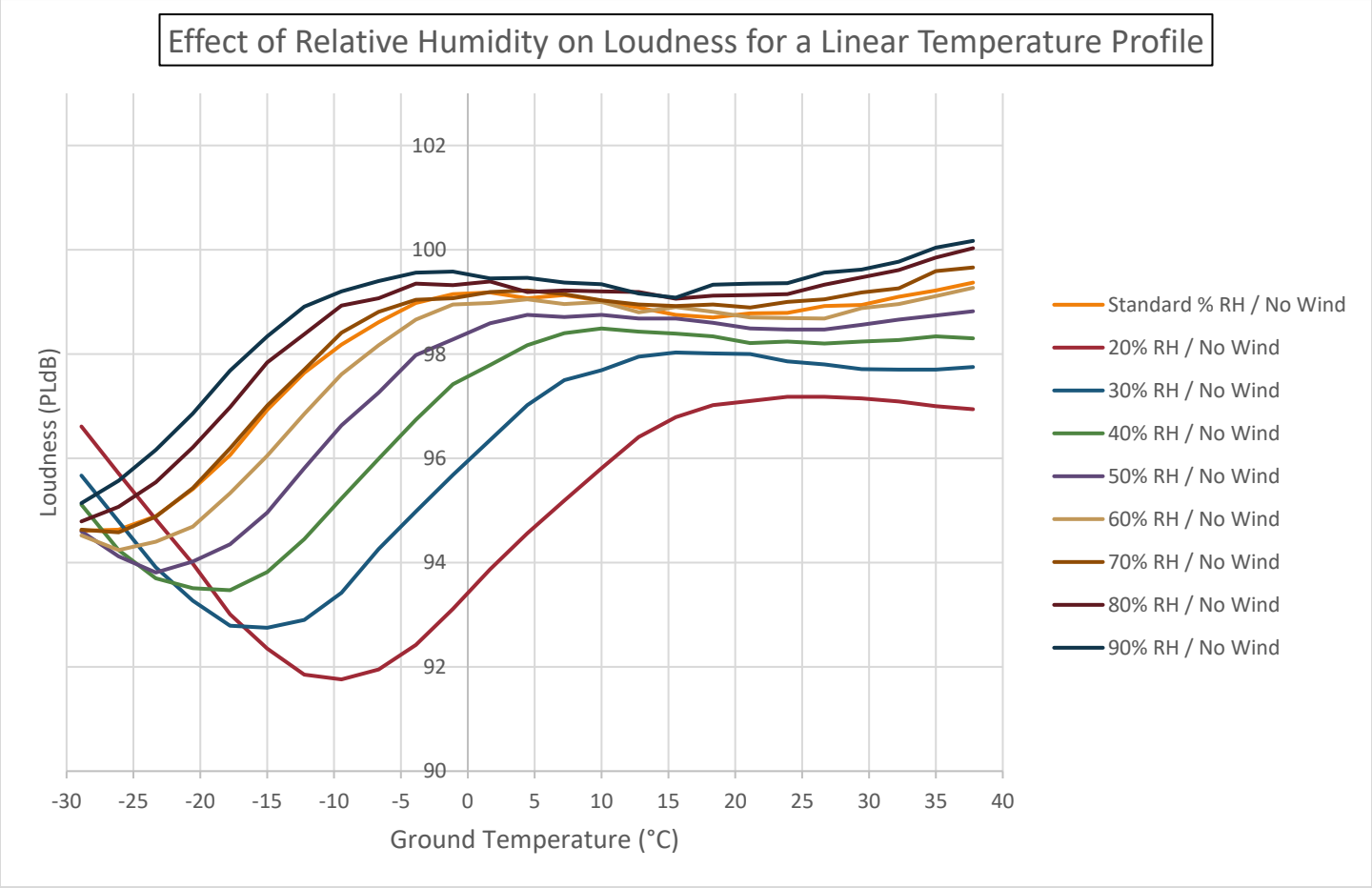

Figure 14: Loudness Sensitivity to Humidity - Linear Temperature Profiles

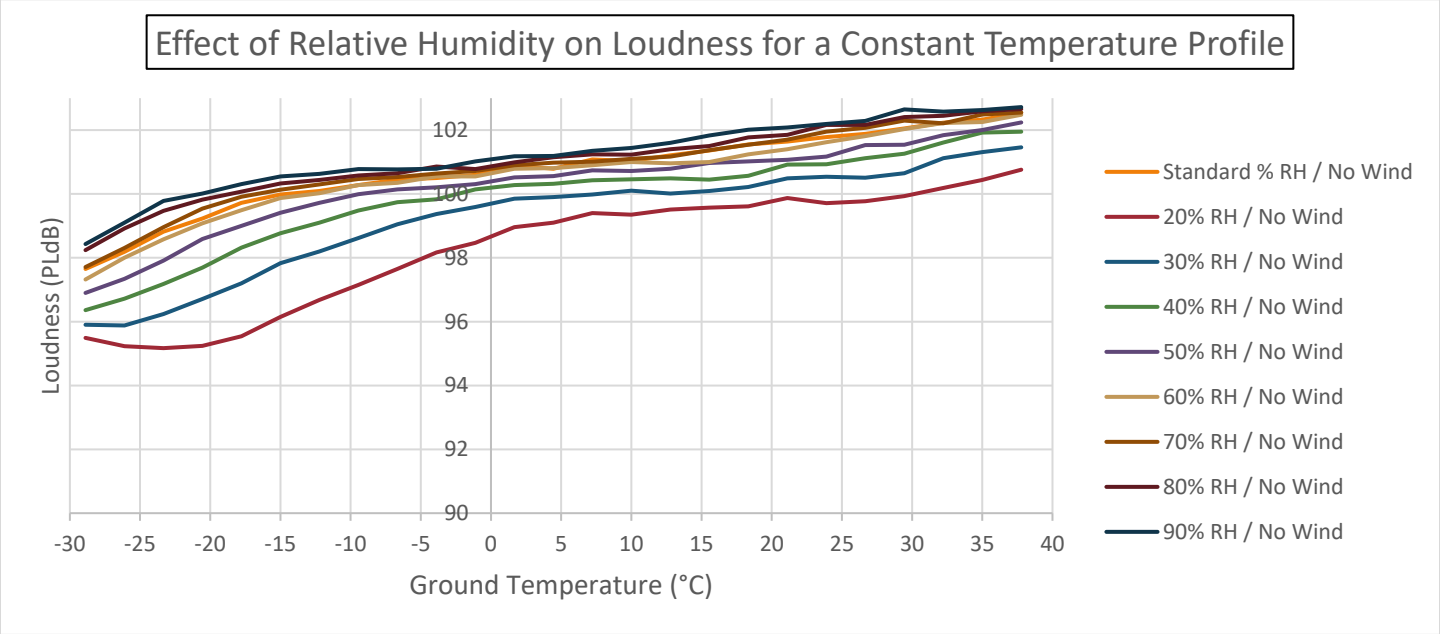

Figure 15: Loudness Sensitivity to Humidity - Constant Temperature Profiles

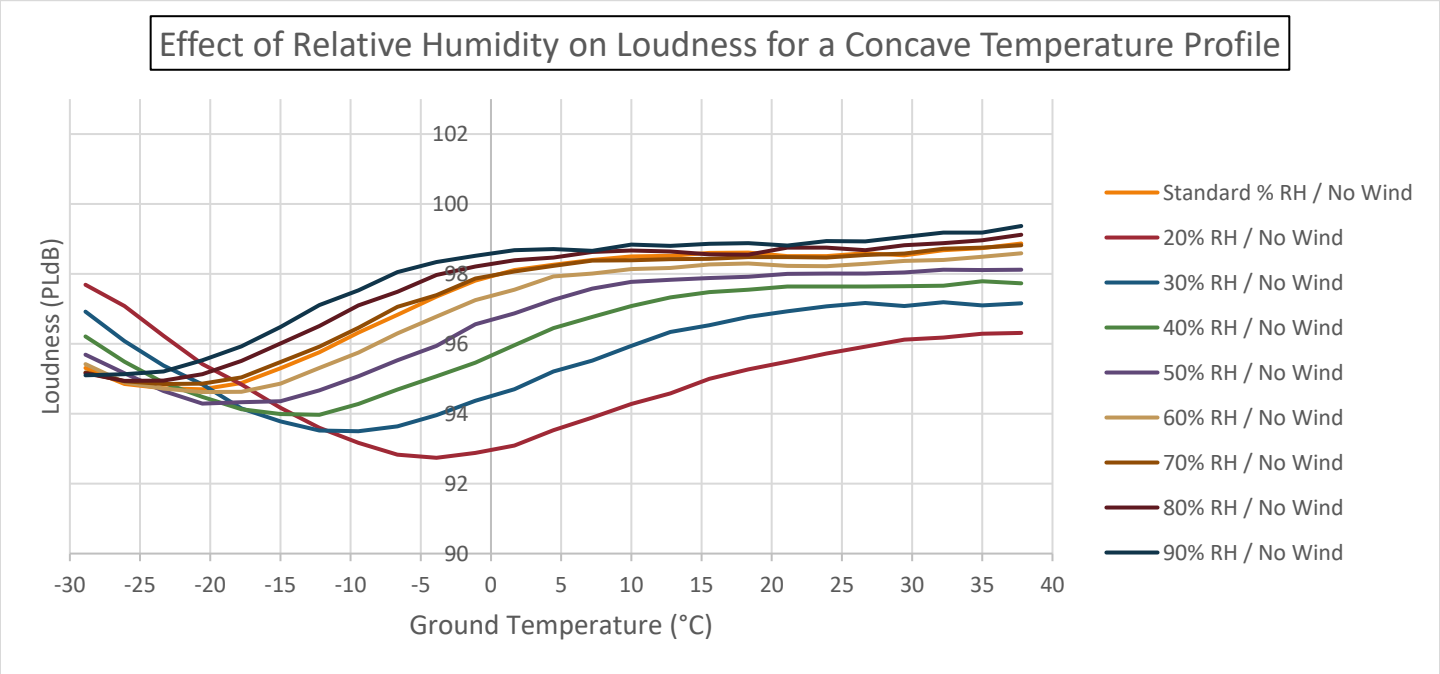

Figure 16: Loudness Sensitivity to Humidity - Concave Temperature Profiles

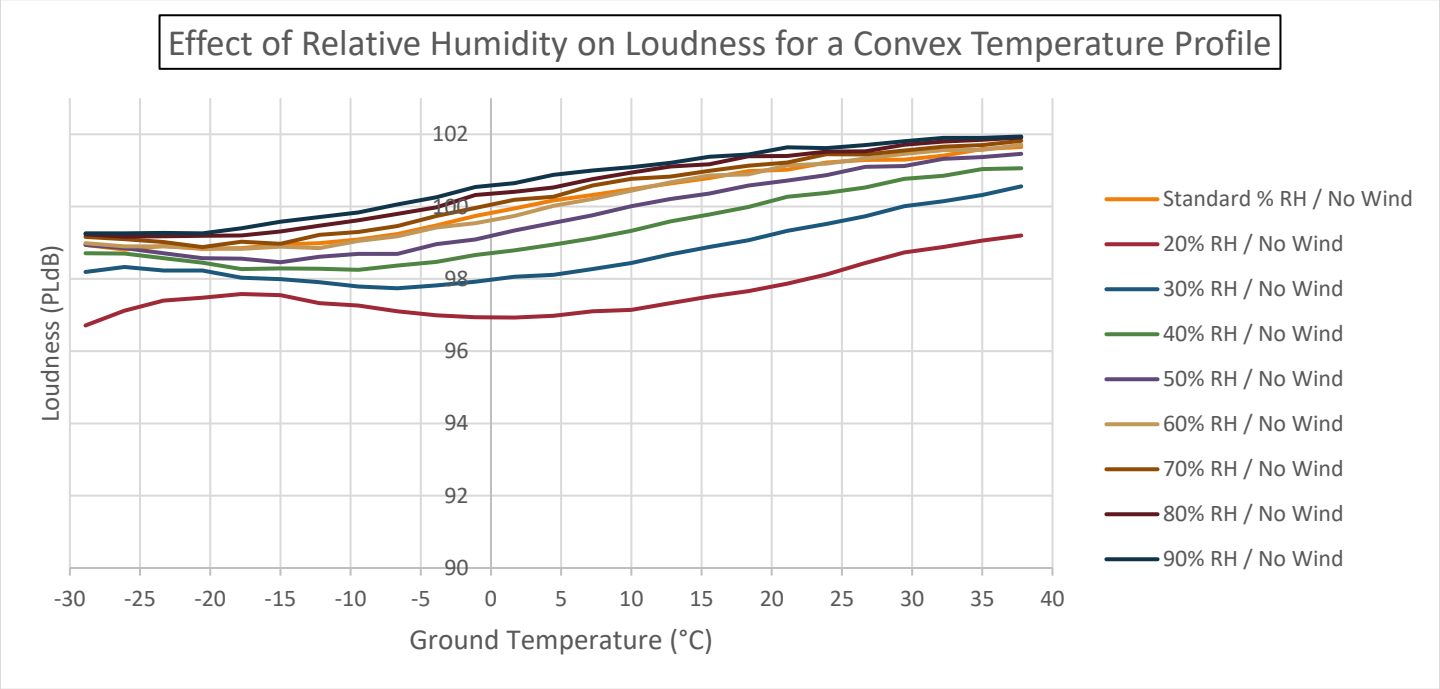

Figure 17: Loudness Sensitivity to Humidity - Convex Temperature Profiles

The above results show that the relative humidity impact on loudness is sensitive to absolute ground temperature, temperature gradient, and relative humidity. As shown in Figure 15, the impact of absolute ground temperature on loudness is almost linear. In general, as constant atmospheric temperature increases, the loudness of the ground boom increases roughly 4-5 PLdB going from -30 C to +40 C. The only exception happens in the extreme cold region for low humidity; when the air is arid and cold, the loudness seems to asymptote to a low value of 95PLdB. For varying temperature gradient, the sensitivity becomes non-linear as you alter the gradients within the propagation path. In general, it seems that the convex temperature profiles produce a higher loudness on the ground than linear profiles and concave profiles produce the quietest ground booms. This appears to be the case regardless of relative humidity or wind. The impact of humidity on ground boom follows the general trend that if the atmosphere has more humidity, the loudness on the ground will increase. The exception to this trend appears in Figures 14 and 16, when the ground temperature gets extremely cold and a low humidity causes a much louder ground boom. The Georgia Tech team is investigating this behavior to determine if this is a physical phenomenon or if it is a result of reaching the limitation of PCBoom and is a computational error.

Humidity/Temperature Sensitivity – Max Overpressure

The sensitivity of maximum overpressure (Pa) to changes in relative humidity are shown in Figures 18-21, Figure 18 displays the sensitivity under linear temperature profiles, Figure 19 displays the sensitivity under constant temperature profiles, Figure 20 displays the sensitivity under concave temperature profiles, and Figure 21 displays the sensitivity under convex temperature profiles.

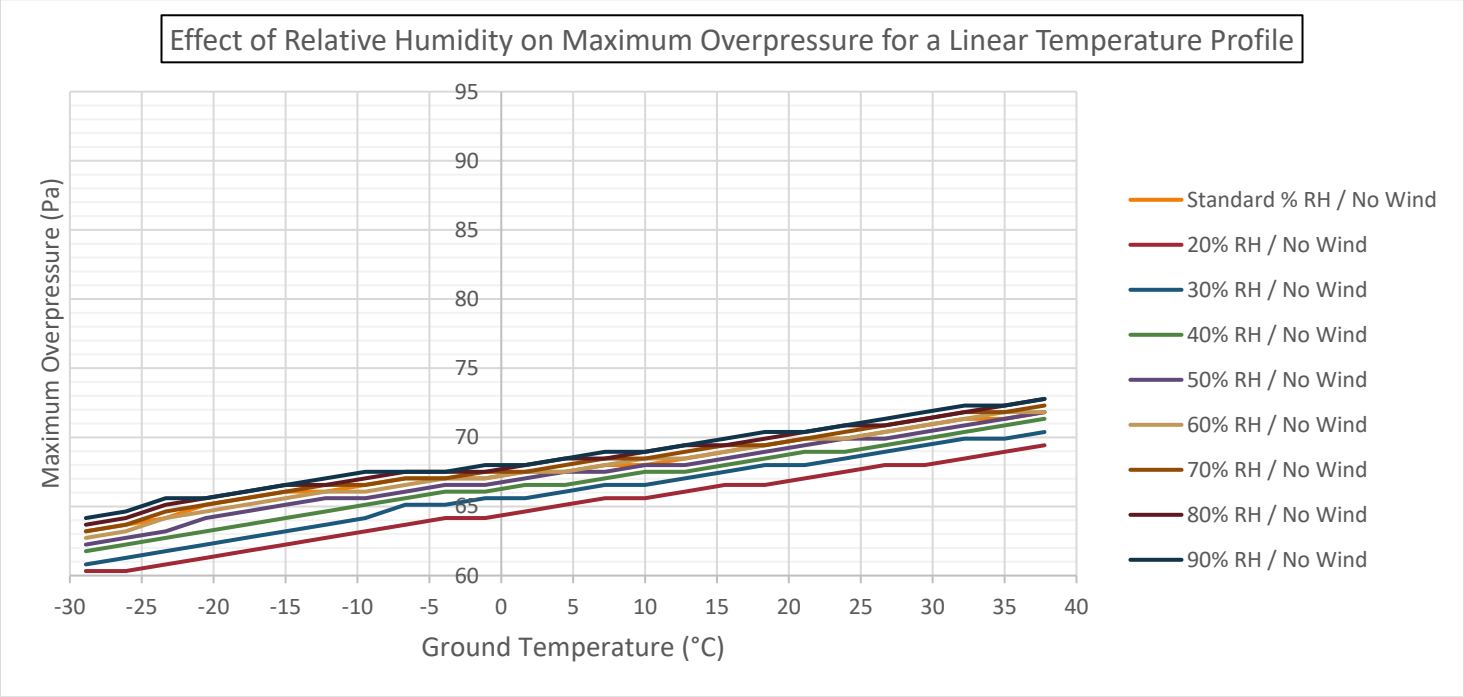

Figure 18: Max Overpressure Sensitivity to Humidity - Linear Temperature Profiles

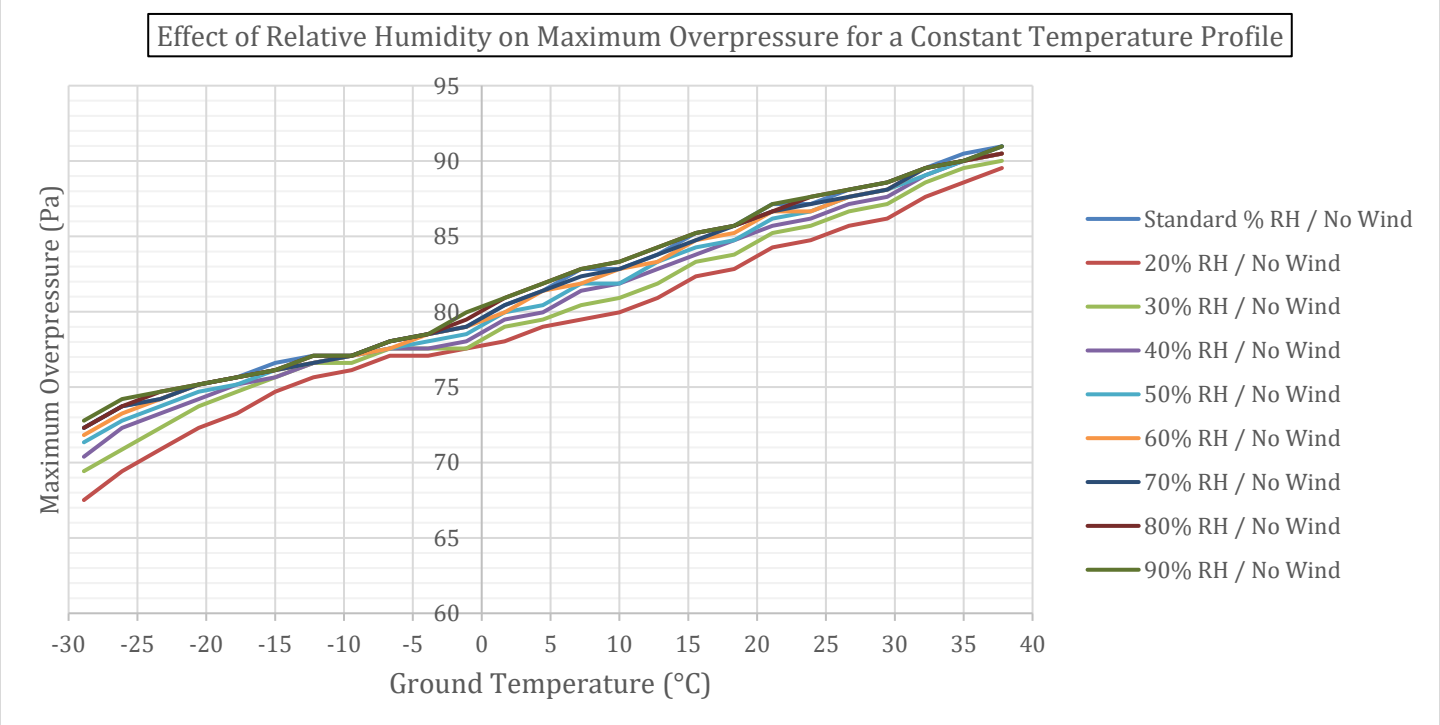

Figure 19: Max Overpressure Sensitivity to Humidity - Constant Temperature Profiles

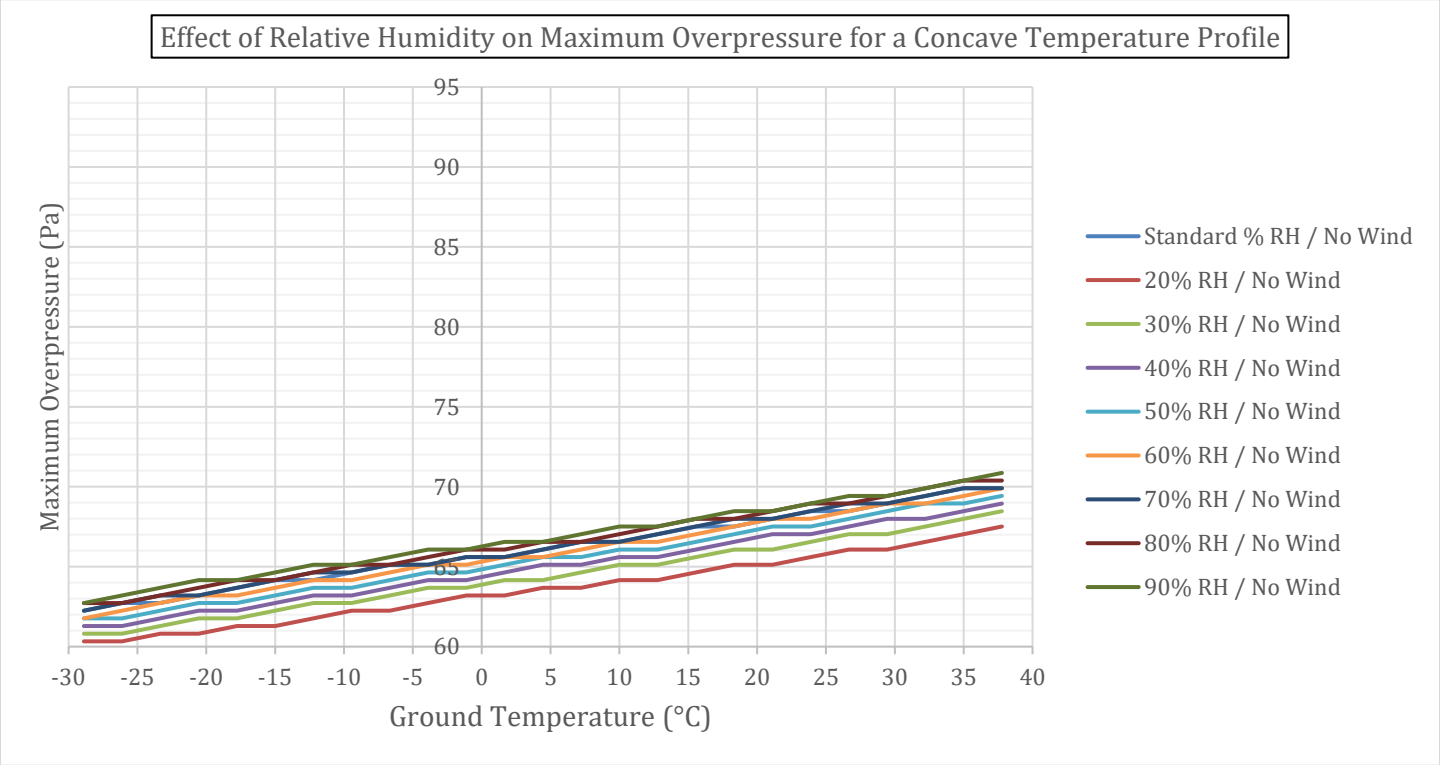

Figure 20: Max Overpressure Sensitivity to Humidity - Concave Temperature Profiles

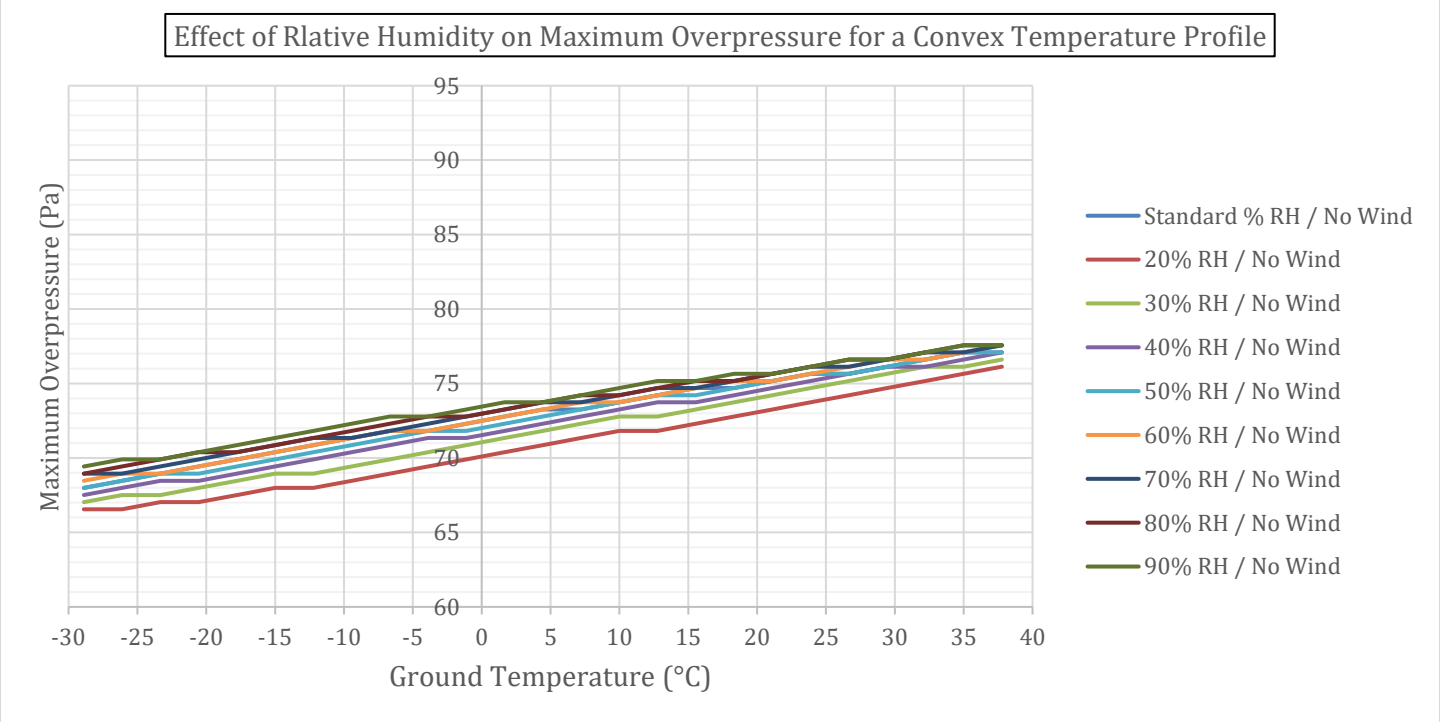

Figure 21: Max Overpressure Sensitivity to Humidity - Convex Temperature Profiles

The impact of humidity and temperature on max overpressure is more linear than the impact on loudness, most likely because loudness has a frequency dependency to it while max overpressure does not. For all standard temperature profiles, constant, linear, concave, and convex, the higher the relative humidity, the higher the max overpressure of the ground boom. It also appears that linear and concave temperature profiles are more sensitive to changes in relative humidity than constant temperature profiles – most likely because in a constant temperature profile atmosphere the propagation path does little to no bending as it travels down through the atmosphere.

Wind/Temperature Sensitivity – Loudness

The sensitivity of loudness (PLdB) to changes in wind direction and magnitude are shown in Figures 22-25. The wind direction was varied from a pure tailwind (0º) to a pure crosswind, to a pure headwind (180º). The magnitude of the wind was taken at both 12.2 m/s and 24.4 m/s. For the wind sensitivity studies, the relative humidity was set to 0% (even though this is un-realistic) in an attempt to isolate the impact of horizontal winds. Figure 22 displays the sensitivity under linear temperature profiles, Figure 23 displays the sensitivity under constant temperature profiles, Figure 24 displays the sensitivity under concave temperature profiles, and Figure 25 displays the sensitivity under convex temperature profiles.

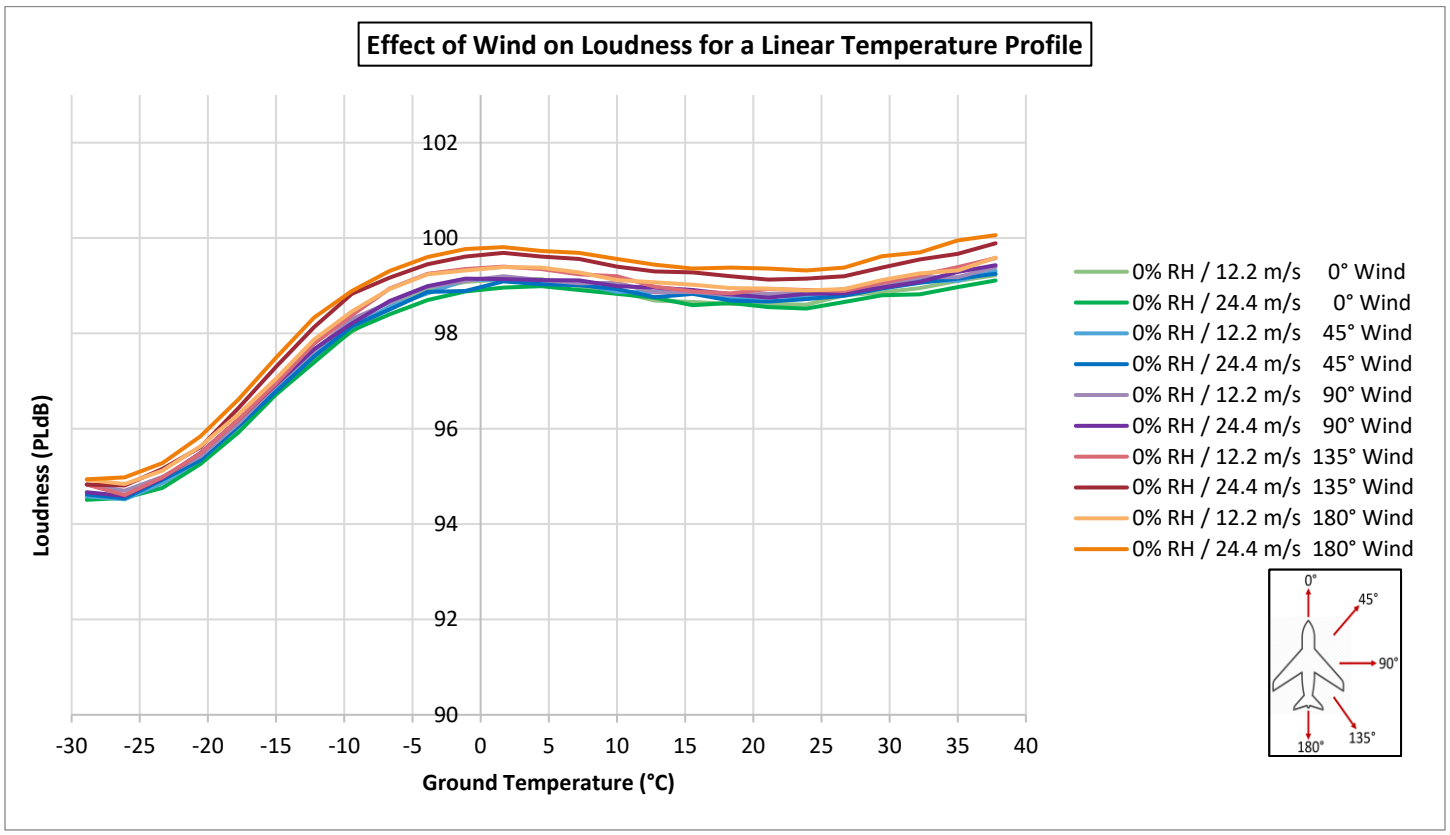

Figure 22: Loudness Sensitivity to Wind - Linear Temperature Profiles

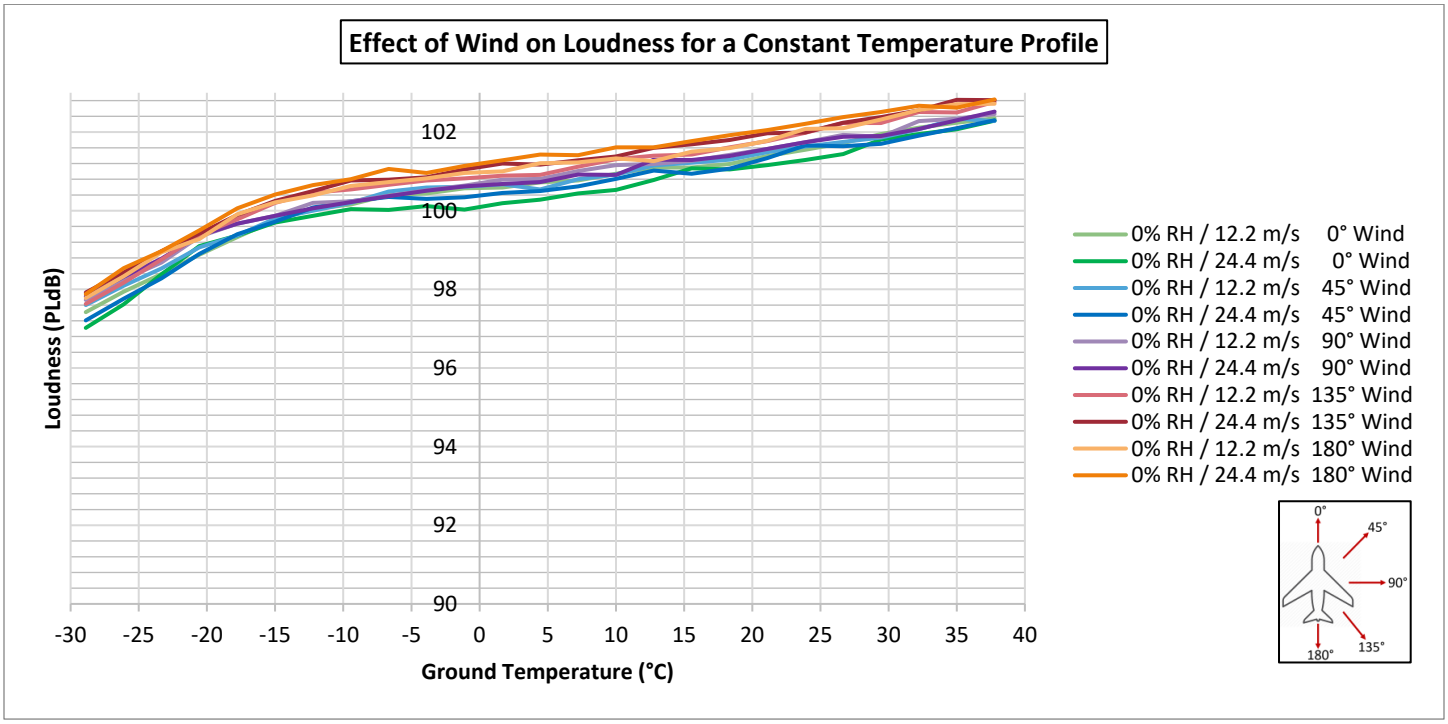

Figure 23: Loudness Sensitivity to Wind - Constant Temperature Profiles

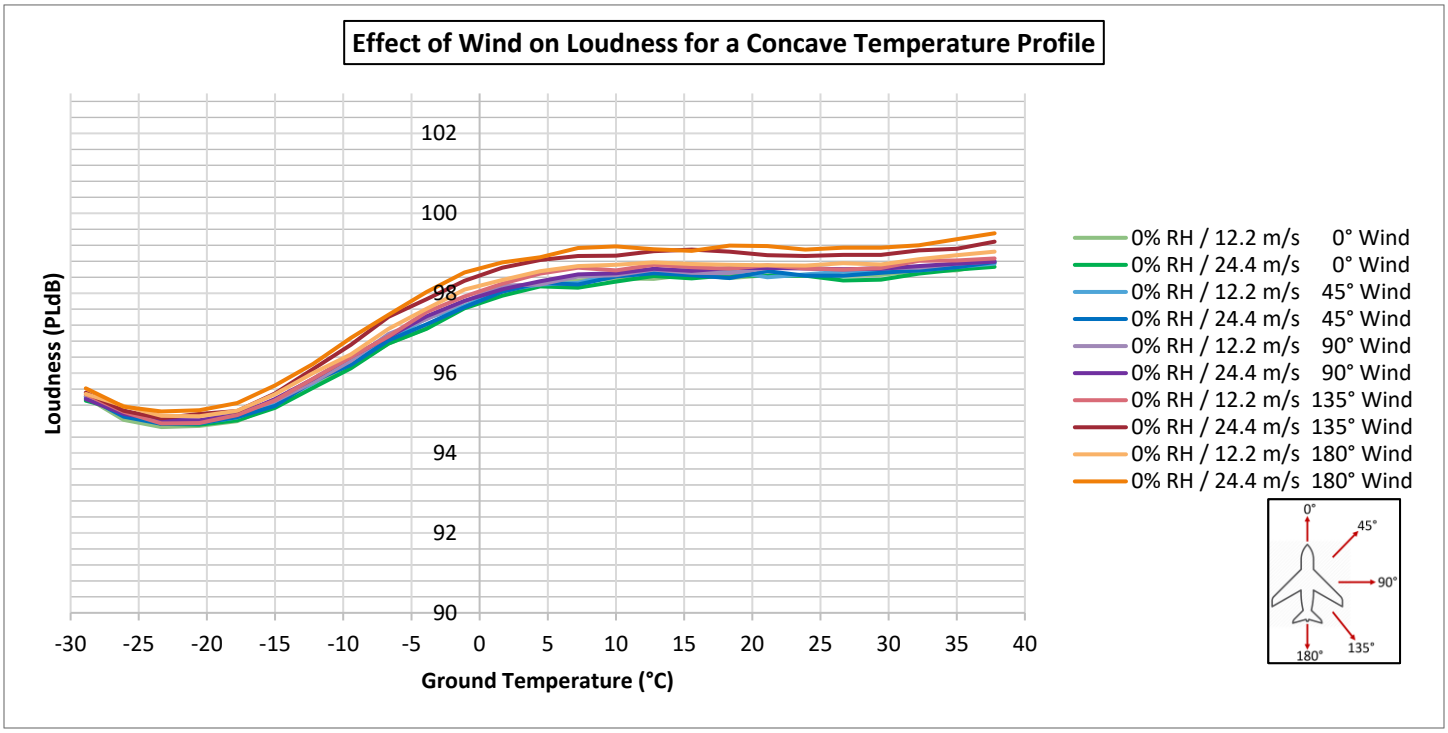

Figure 24: Loudness Sensitivity to Wind - Concave Temperature Profiles

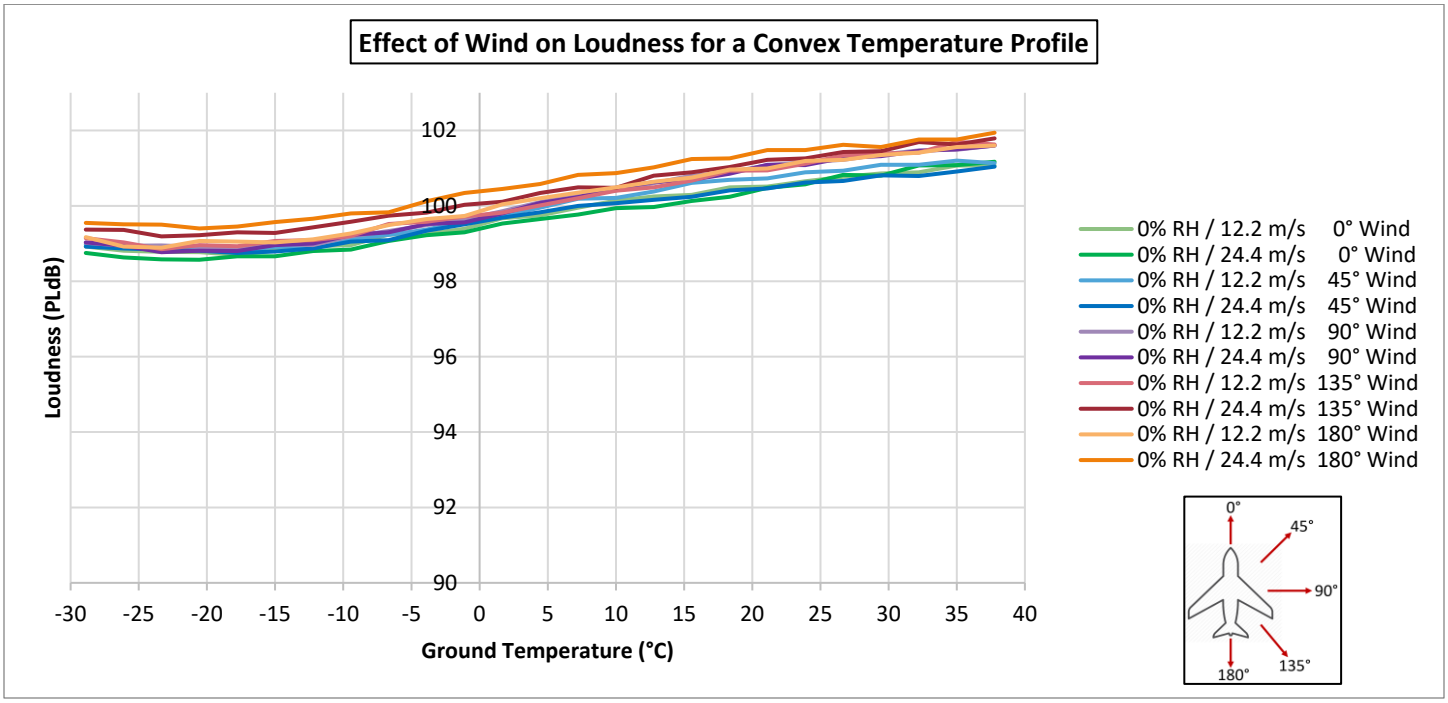

Figure 25: Loudness Sensitivity to Wind - Convex Temperature Profiles

The sensitivity of the loudness of ground booms in Mach cut-on conditions to wind direction and magnitude is consistent for constant, linear, and concave, and convex temperature profiles. Pure tailwinds result in the quietest ground booms while pure headwinds result in the loudest ground booms. This is consistent with what the Penn State team has shown in their horizontal wind studies. The variation in PLdB due to wind is smaller than that dues to changes in relative humidity. The difference between a strong headwind and a strong tailwind is only about 1-1.5 PLdB. The differences seen in the loudness due to changing ground temperatures are consistent with the humidity/temperature studies implying that impact of temperature profiles are primarily independent of wind and humidity (the one exception might be at colder temperatures with low humidity).

Wind/Temperature Sensitivity – Max Overpressure

The sensitivity max overpressure (Pa) to changes in wind direction and magnitude are shown in Figures 26-29 The wind direction was varied from a pure tailwind (0º) to a pure crosswind, to a pure headwind (180º). The magnitude of the wind was taken at both 12.2 m/s and 24.4 m/s. For the wind sensitivity studies, the relative humidity was set to 0% (even though this is un-realistic) in an attempt to isolate the impact of horizontal winds. Figure 26 displays the sensitivity under linear temperature profiles, Figure 27 displays the sensitivity under constant temperature profiles, Figure 28 displays the sensitivity under concave temperature profiles, and Figure 29 displays the sensitivity under convex temperature profiles.

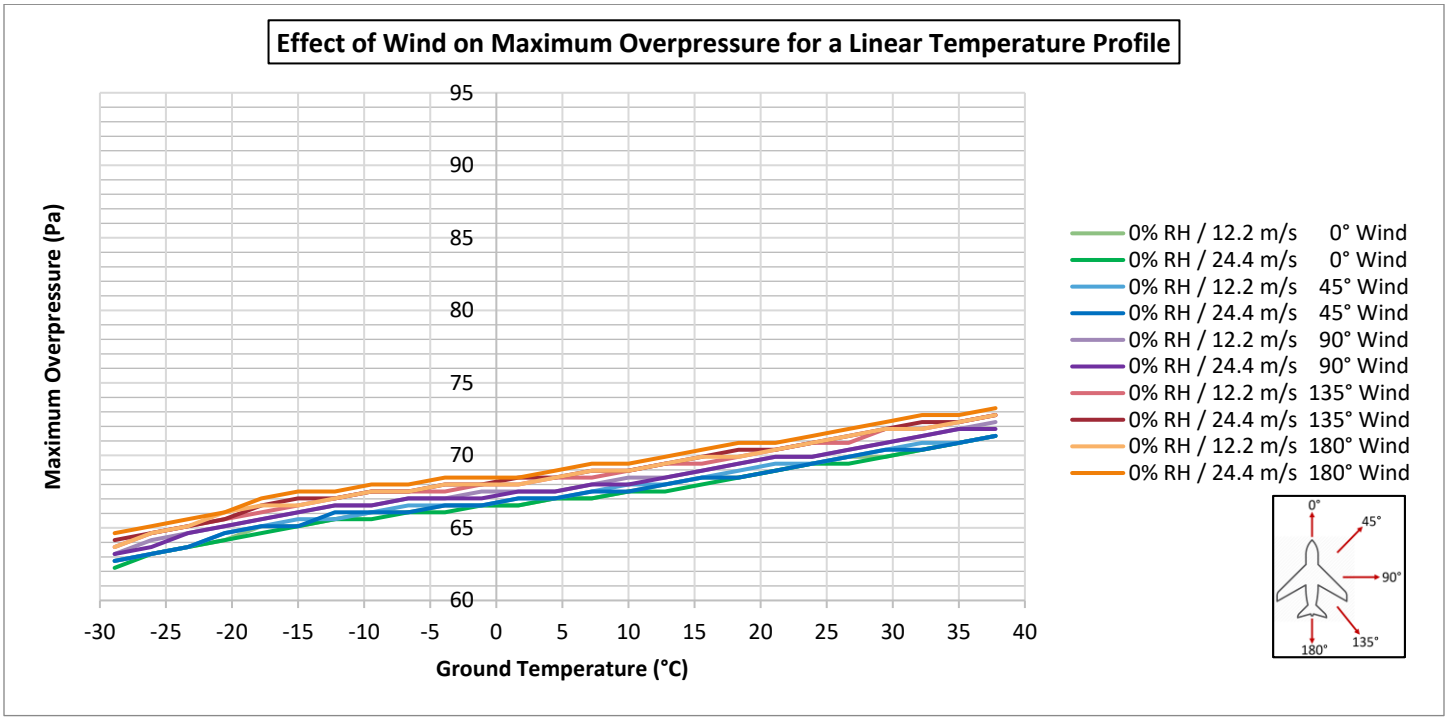

Figure 26: Max Overpressure Sensitivity to Wind - Linear Temperature Profiles

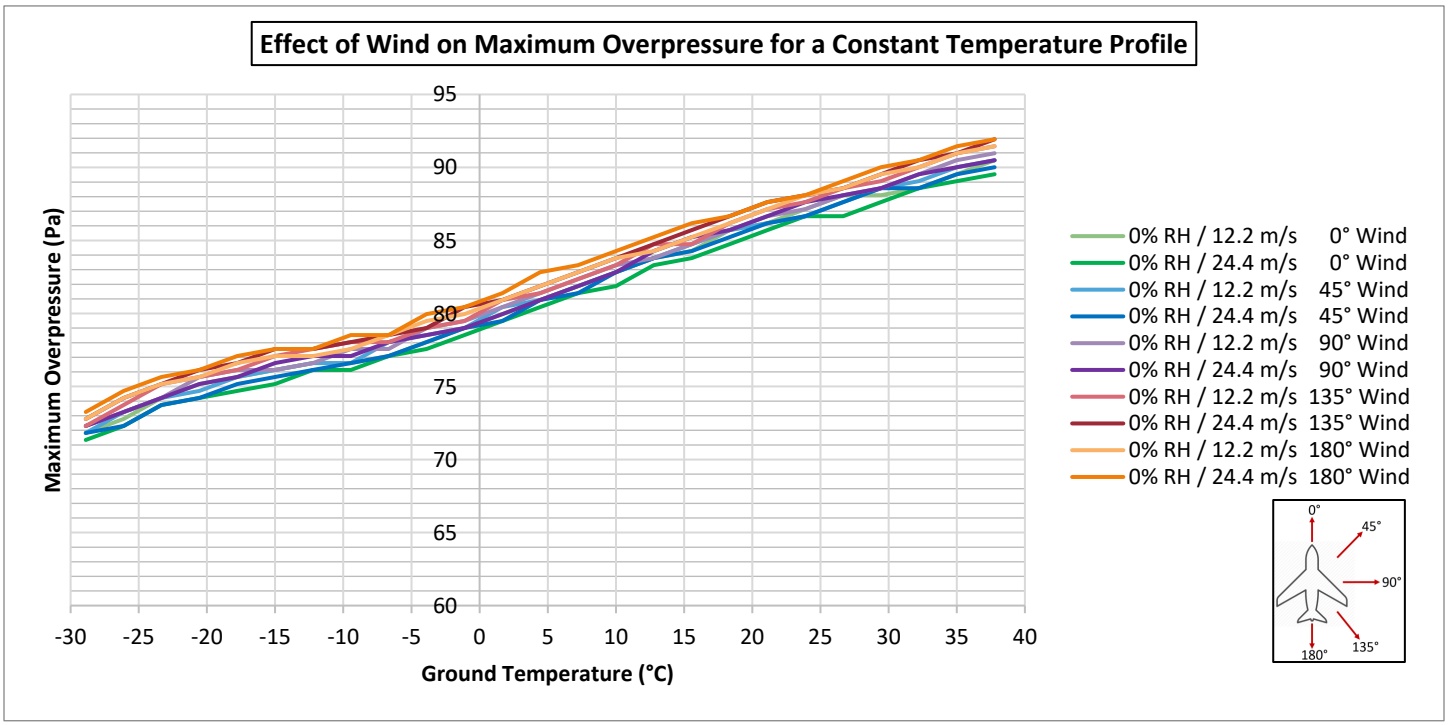

Figure 27: Max Overpressure Sensitivity to Wind - Constant Temperature Profiles

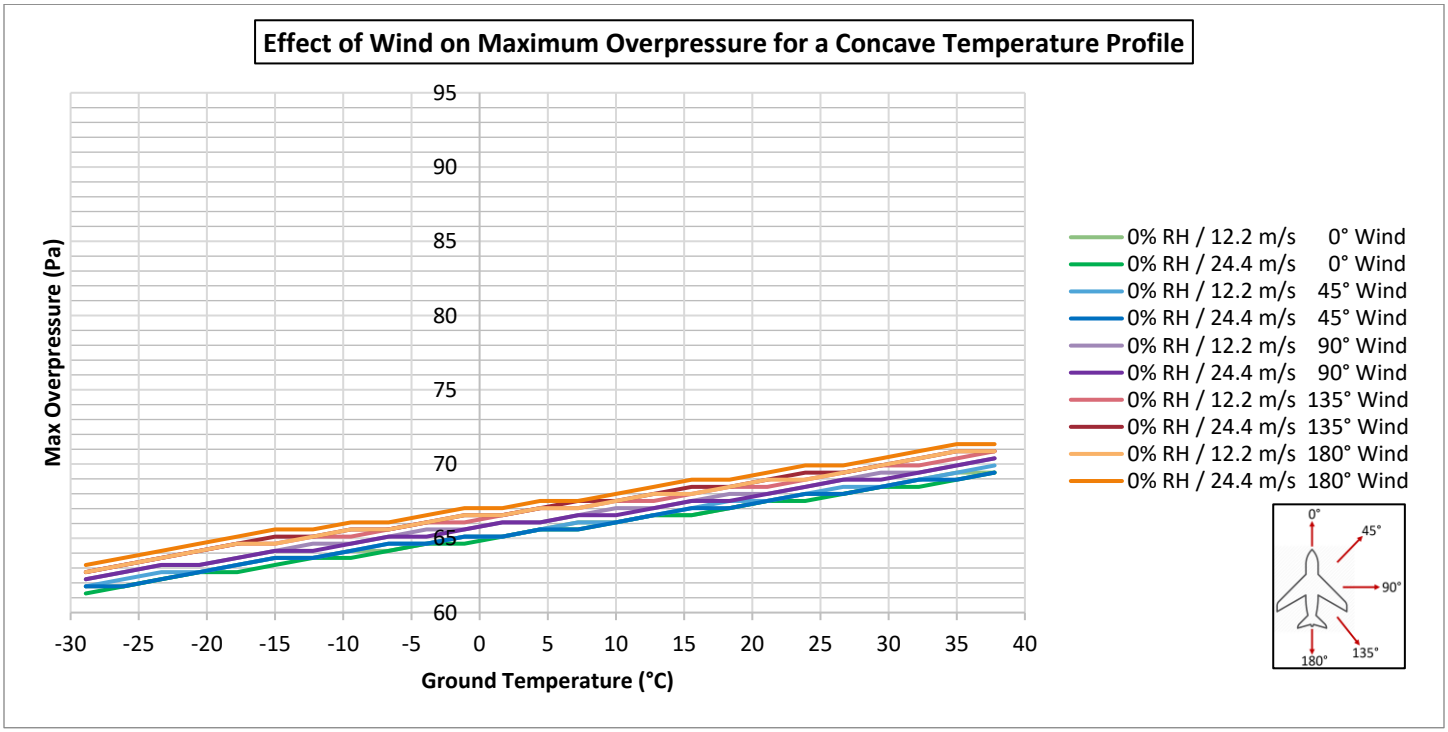

Figure 28: Max Overpressure Sensitivity to Wind - Concave Temperature Profiles

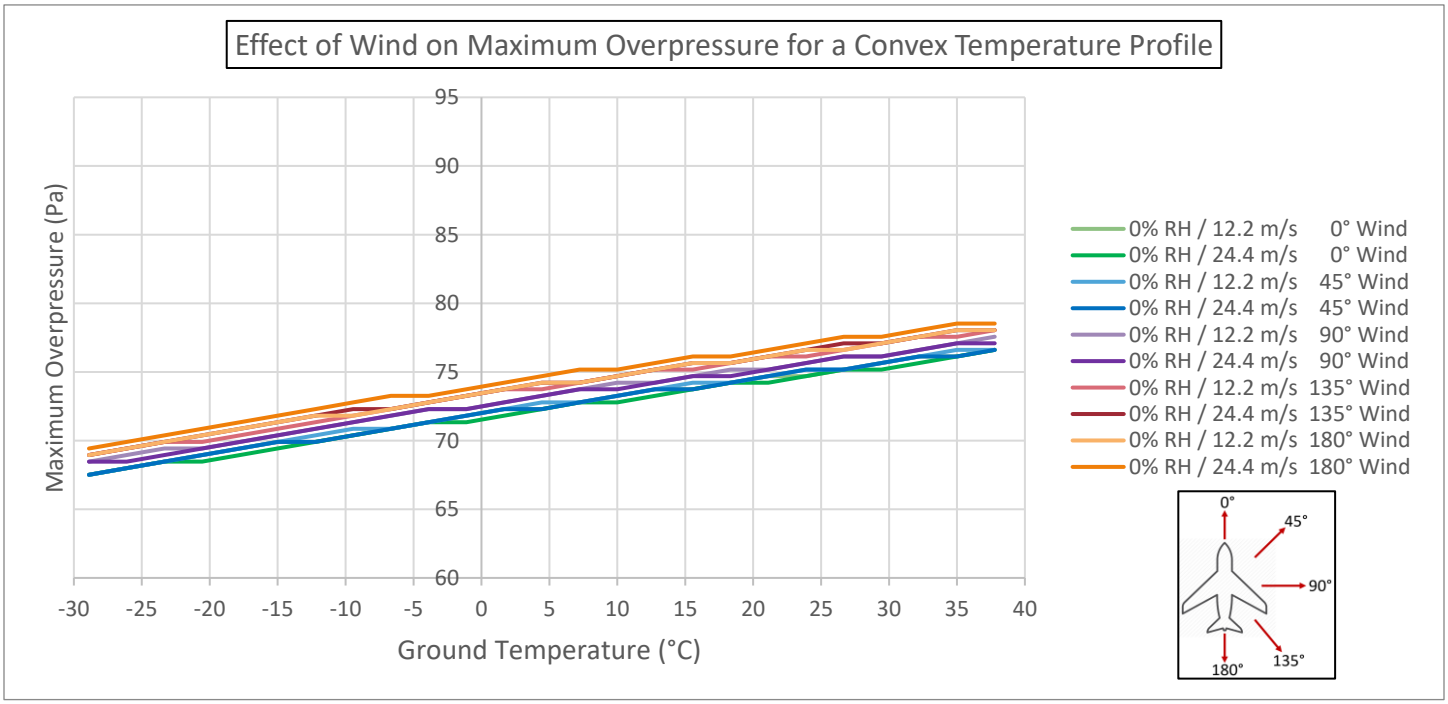

Figure 29: Max Overpressure Sensitivity to Wind - Convex Temperature Profiles

The sensitivity of the max overpressure of ground booms in Mach cut-on conditions to wind direction and magnitude is consistent for constant, linear, and concave, and convex temperature profiles, and follows the same general trends as loudness. Pure tailwinds result in lower max overpressure ground booms while pure headwinds result in higher max overpressure ground booms. The difference between a strong headwind and a strong tailwind is about 2-3 Pa, and is the roughly the same regardless of the temperature profile.

Realistic Profiles

Mach cut-on conditions were also studied for the realistic temperature profiles in order to ascertain the impact of changing the temperature profile on these atmospheres. The realistic temperature profiles contain real data for temperature, wind, and humidity. The sensitivity study was run by shifting the temperature profiles by a constant temperature to see the impact of flying over these locations in during different seasons. This study was also done to benchmark the realistic profiles before performing the Mach cut-off studies. The sensitivity of loudness to temperature changes in the realistic profiles is shown in Figure 30. The sensitivity of max overpressure to temperature changes in realistic profiles is shown in Figure 31.

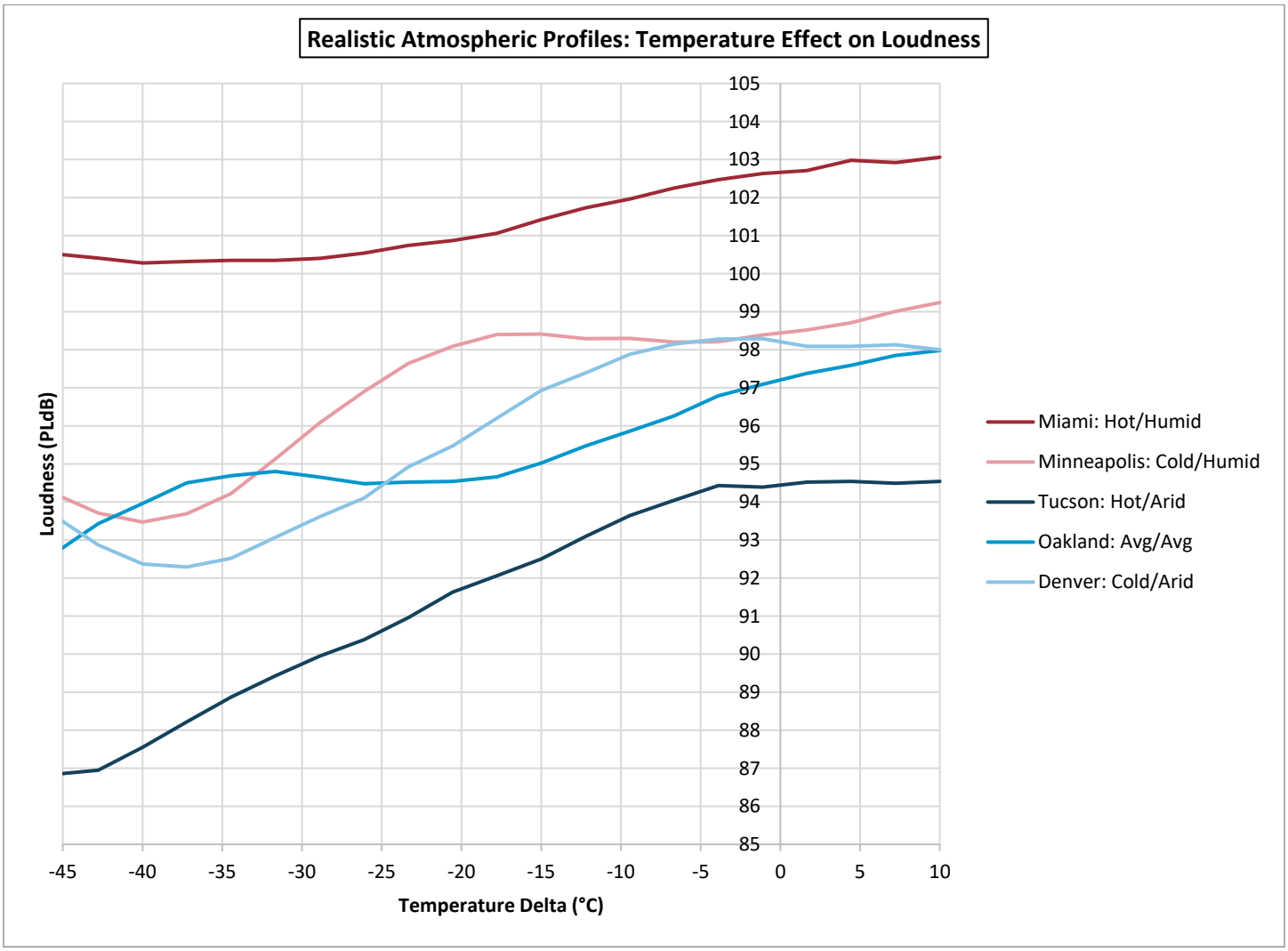

Figure 30: Loudness Sensitivity to Temperature - Realistic Profiles

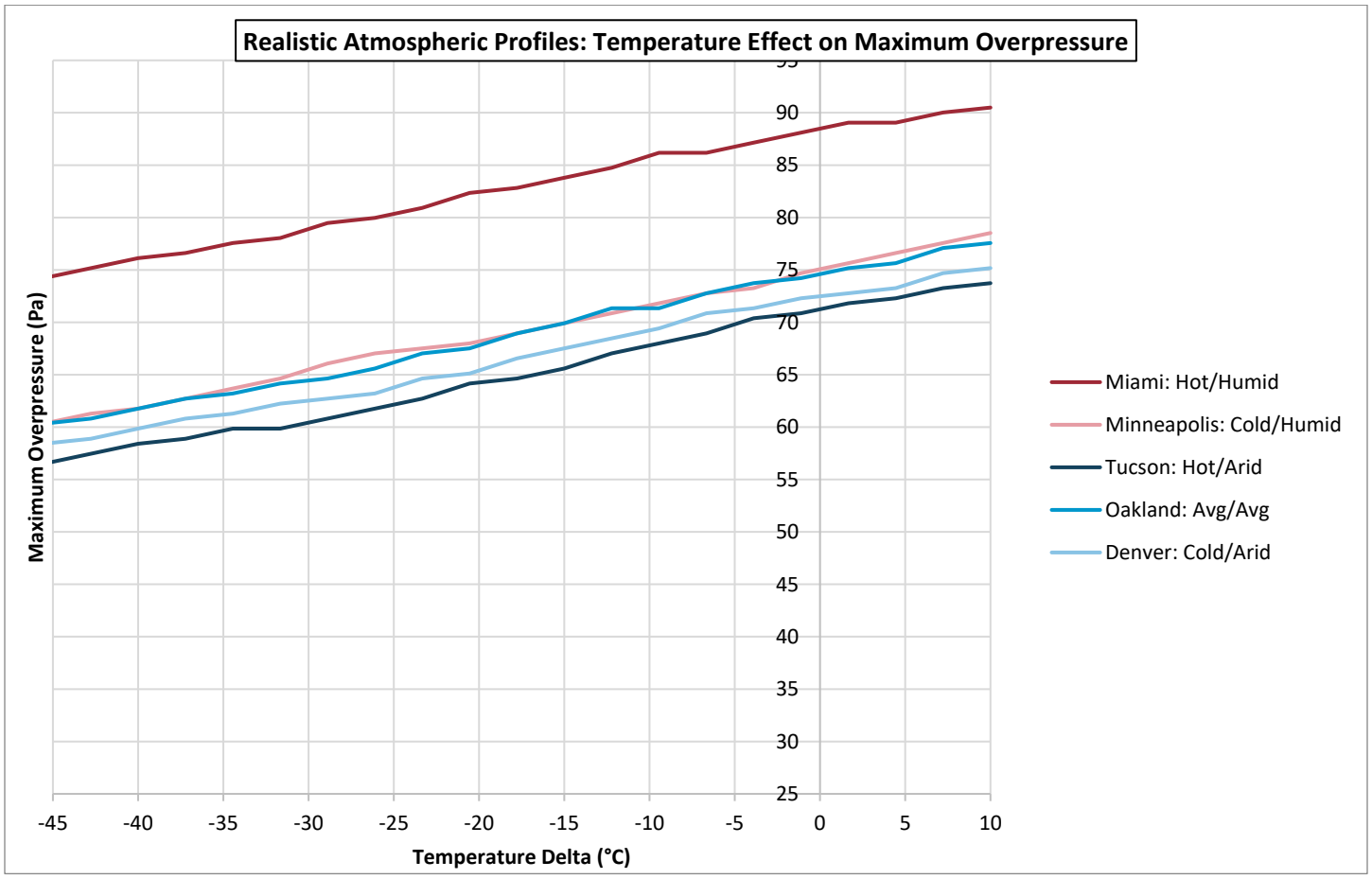

Figure 31: Max Overpressure Sensitivity to Temperature - Realistic Profiles

As can be seen in the above results, the impact of shifting the temperatures in the realistic profiles mimics that show in the standard profiles. As the overall temperature in the atmosphere increases, both the loudness and the max overpressure of the ground boom increases. This trend is much more linear in the max overpressure results than the loudness results. For loudness, there is a more non-linear relationship for colder atmospheres. Most likely due to the frequency dependency of the loudness metric. Another interesting observation from this study is that humidity has a large influence on the loudness and max overpressure, almost more than temperature. Both the humid climates (regardless of hot or cold) have higher max overpressures and loudness results for ground boom. For example, even Miami on a very cold day would have a louder ground boom than Tucson on a very hot day due to the difference in relative humidity. These results were important to gather to help benchmark the realistic profiles going into the Mach cut-off study.

Mach Cut-Off Results: Standard Profiles

The primary goal of Task 4 was to study the impact of atmospheric changes on Mach cut-off conditions. This was done through using PCBoom and using the near-field pressure signature for Aerion's AS2 vehicle. The conditions run for Mach cut-off flight were a flight speed of Mach 1.1 at an altitude of 13.7km (45,000ft). The metrics tracked in this study were Mach cut-off Mach number and Mach cut-off altitude. Mach cut-off Mach number indicates the *fastest* speed at which the aircraft could fly at 13.7km (45,000ft) and still maintain cut-off. Flying at any speed faster than the Mach cut-off Mach number will result in a ground boom. Mach cut-off altitude indicates the *lowest* altitude at which the aircraft could fly a Mach 1.1 and still maintain Mach cut-off. Flying at any altitude lower than the Mach cut-off altitude at Mach 1.1 will results in a ground boom. The first Mach cut-off study performed was for the standard profiles. Initially, this was done for humidity, wind, and temperature variations. However, it was discovered that the PCBoom calculations for Mach cut-off conditions do not consider humidity. The calculations do consider horizontal winds (not vertical winds), but the Georgia

Tech team initially only created constant wind speed changes which did not impact the Mach cut-off results. Studying Mach cut-off sensitivity to varying horizontal winds could potentially be a task for future research, although Penn State has done much of this in Task 1A: Assess and Extend Modeling Capabilities for Mach Cut-off Events. Georgia Tech decided to focus primarily on the impact of varying temperature gradients on Mach cut-off flight conditions. Both realistic and standard temperature profiles were examined, and the results are presented below.

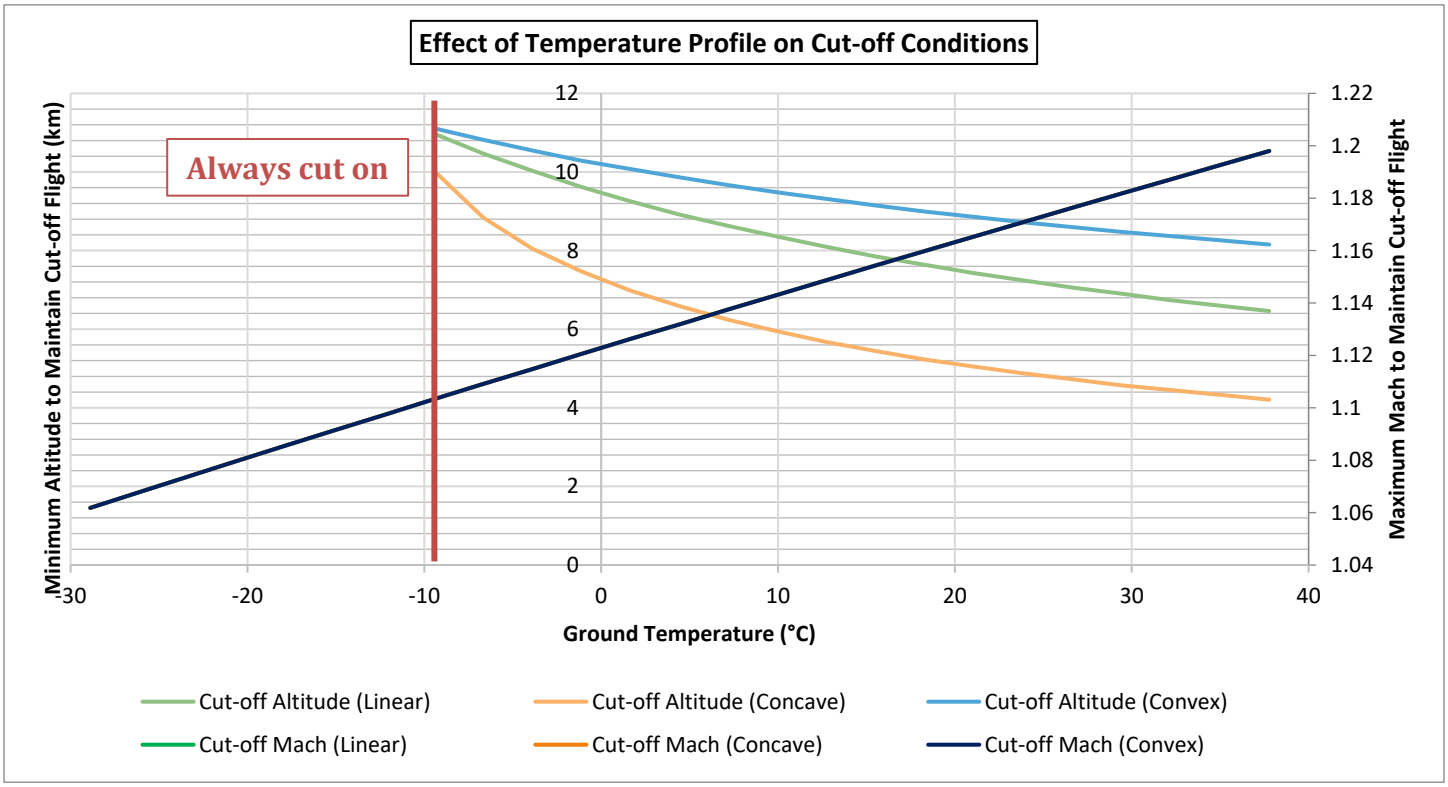

Figure 32: Mach Cut-off Conditions for Variations in Standard Profiles

Figure 32 displays the sensitivity of Mach cut-off conditions to changes in temperature gradients of standard atmospheric profiles. The first observation made pertains to the Mach cut-off Mach number. It was discovered that the Mach cut-off Mach number is independent of changes in the temperature profiles gradients, if flying at a fixed altitude. The only temperatures that impact the Mach cut-off Mach number are the temperature at altitude and the ground temperature; the temperature profile in-between these points do not impact the results. This is because the speed of sound at altitude and the ground are the only parameters that vary Mach cut-off conditions. Therefore, this implies that phenomena such as temperature inversions do not impact the Mach cut-off Mach number. The insensitivity to temperature gradients is logical since PCBoom utilizes Snell's law to map the propagation path through the atmosphere and the refraction is directly proportional to the change in speed of sound (temperature). It was observed, for all temperature profiles, as the ground temperature increases the maximum Mach cut-off flight Mach number increases monotonically. This implies that if a supersonic aircraft is flying at a constant altitude and Mach number it will be more likely for the aircraft to produce a ground boom as it flies over colder locations.

The sensitivity of Mach cut-off flight to temperature gradients is also observed in the Mach cut-off altitude. The Mach cut-off altitude differs from the trends seen for Mach cut-off Mach number as the shape of the temperature profile does impact the Mach cut-off altitude. Using a linear temperature profile as a reference point, a convex temperature profile will result in a higher Mach cut-off altitude and a concave temperature profile will result in a lower Mach cut-off altitude. This is a result of the temperature enabling Mach cut-off flight being located at different altitude for the different profile shapes. This is shown in Figure 33. For flight at 13.7km and Mach 1.1, the cut-off altitude is a function of where the "cut-off temperature"

is located in the atmosphere. This temperature is located at a higher altitude in the convex temperature profile than the linear and concave temperature profiles.

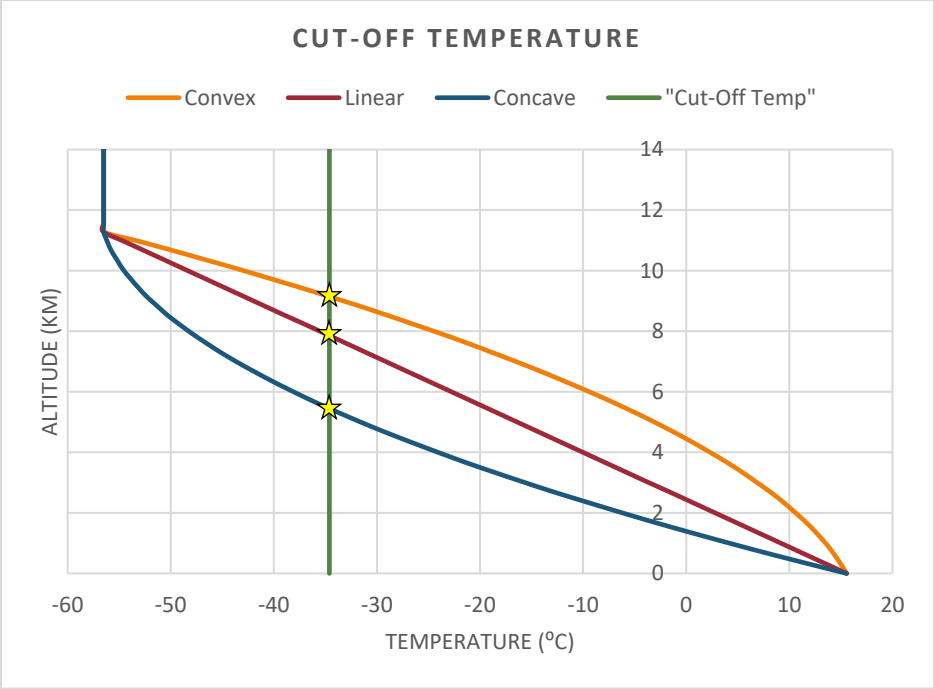

Figure 33: Mach Cut-off Altitudes Resulting from Different Temperature Profiles

The other observation made during this study was, for the same temperature profile shape, as the ground temperature increases the Mach cut-off altitude decreases. This implies that as the ground temperature increases, a supersonic aircraft flying at constant Mach number would need to lower its flight altitude in order to maintain Mach cut-off flight. It was also observed that as the ground temperature decreases past a certain point, the boom will always be cut-on for a fixed flight velocity. This is because the tropopause temperature (which does not change) and the ground temperature do not provide a large enough difference in temperature to allow for Mach cut-off conditions. All the results from the standard temperature profile sensitivity study provided insight to the Georgia Tech team and the other Project 42 participants.

Mach Cut-off Results: Realistic Profiles

The final part of Task 4 was to study the sensitivity of Mach cut-off flight conditions under realistic atmospheric conditions. This was done using the same five atmospheric profiles utilized in the Mach cut-on benchmarking exercise: Hot/humid, hot/arid, cold/humid, cold/arid, and average/average. It should be noted that for this study the Georgia Tech team maintained the wind and relative-humidity profiles and shifted the temperature profiles by constant deltas. The goal of this study was observed that changes in both Mach cut-off altitude and Mach cut-off Mach number as the temperatures in the realistic profile changed. The sensitivity of Mach cut-off altitude is shown in Figure 34 and the sensitivity of Mach cut-off Mach number is shown in Figure 35. The data represented in red corresponds to humid climates and the data represented in blue corresponds to climates with lower humidity. The results were divided in this way because the largest difference in observed behavior seemed to correlate to relative humidity.

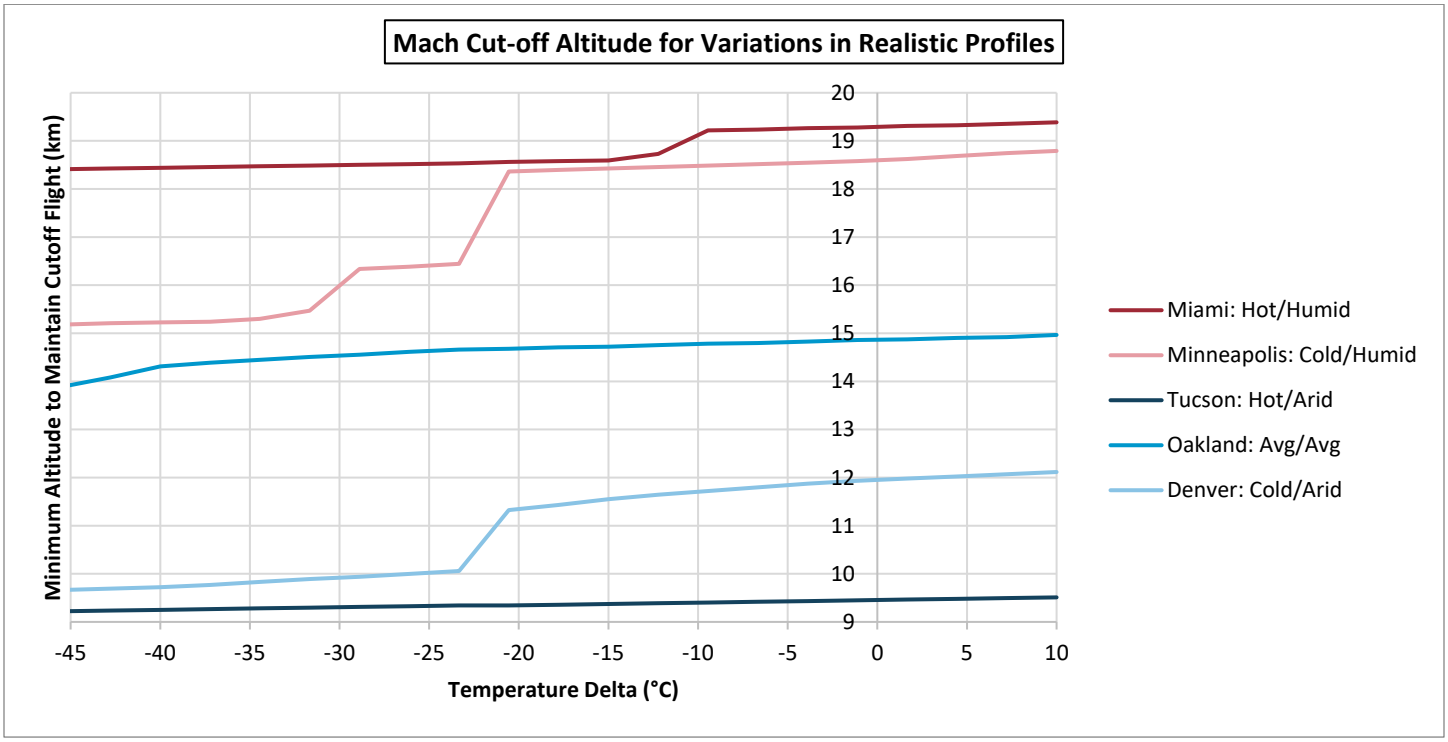

Figure 34: Mach Cut-off Altitude for Variations in Realistic Profiles

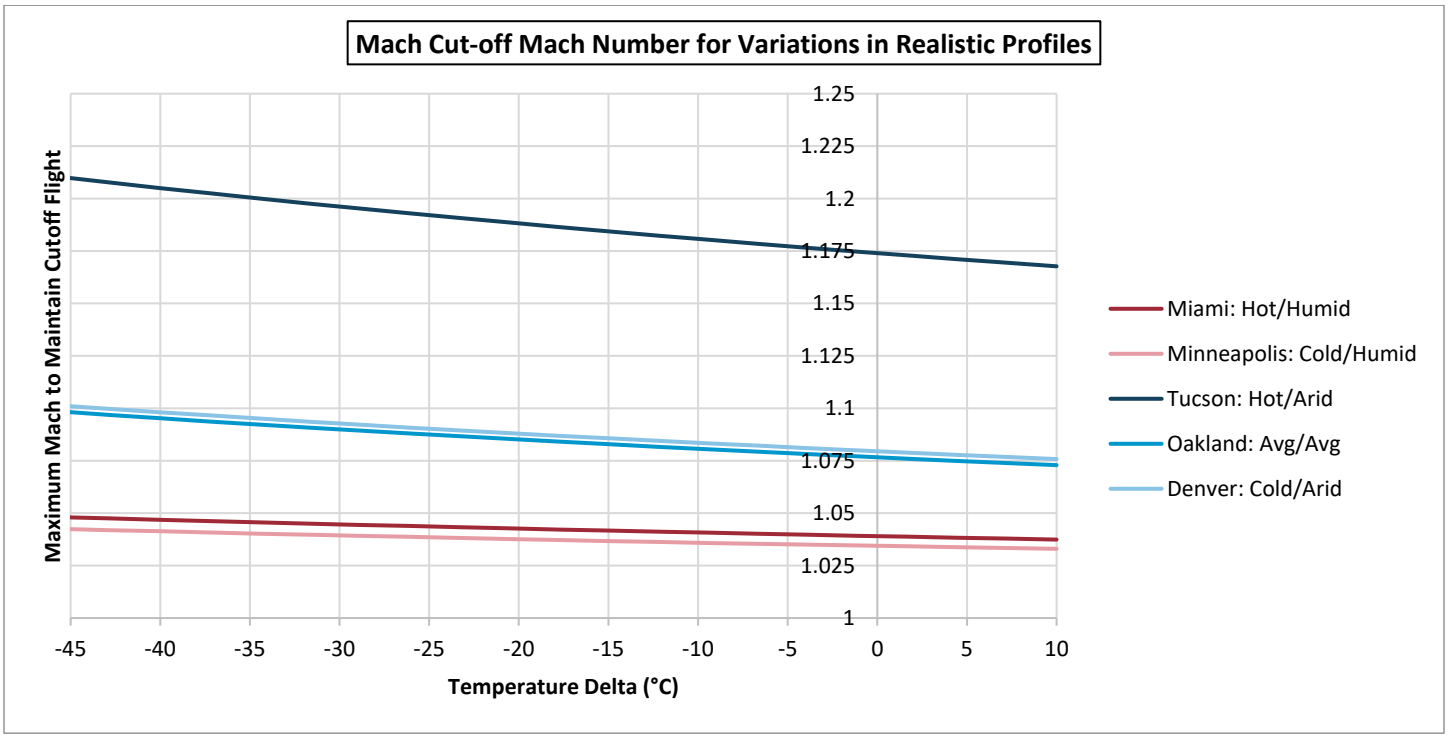

Figure 35: Mach Cut-off Mach Number for Variations in Realistic Profiles

The sensitivity observed for Mach cut-off altitude to constant shifts in the entire temperature profile for the realistic atmospheres is that as the temperature increases the Mach cut-off altitude increases (for a constant flight Mach number). This highlights the difference between changing the temperature gradient (as was done for the standard profiles) and shifting the temperature profile. As the entire atmosphere gets warmer the Mach cut-off altitude increases, whereas if only the ground temperature increases, the Mach cut-off altitude decreases. As can be seen in Figure 34, the Georgia Tech team also observed large jumps in the Mach cut-off altitude for both the Denver and Minneapolis atmospheres. This was traced back to a combination impact of both the location/altitude of the temperature required to maintain Mach cut-off flight and large changes in wind direction and magnitude. If the Mach cut-off temperature is located at an altitude around which there is large variations in horizontal winds, small changes in the temperature can significantly impact the Mach cut-off altitude.

The sensitivity for Mach cut-off Mach number to constant shifts in the entire temperature profile for realistic atmosphere is as the temperature in the entire atmosphere increases, the Mach cut-off Mach number decreases (for a constant flight altitude). This is also a different behavior than the observed sensitivity for changing the temperature gradient (ground temperature). It was also observed that in climates with more humidity, the sensitivity to temperature was less than climates with lower atmospheric relative humidity. The results of the Mach cut-off sensitivity study show that in terms of atmospheric conditions, the gradients tend to produce greater alterations to Mach cut-off conditions than absolute shifts. This confirms that the propagation path of sonic booms is heavily dependent on the refraction through the atmosphere and less dependent on the absolute conditions.

Conclusions

The research performed for Task 4: Sensitivity Study of Mach Cut-off Flight provided interesting results that shine light on the behavior of Mach cut-off flight and the conditions which enable it. Important observations were made in the sensitivity of Mach cut-off flight to temperature, and minor observations were made relative to wind and humidity. With further expansion of sonic boom propagation tools, the sensitivity to wind and humidity could be studied more completely. An important aspect of this is capturing the impact of vertical winds on Mach cut-off flight, as being actively pursued by the Penn State research team. A large benefit of the research done through this task was Georgia Tech's development of the PCBoom Wrapper. This tool will help facilitate any future studies using PCBoom to quickly assess a large amount of cases, whether it be for different atmospheric parameters, flight conditions, or aircraft.

Georgia Tech also concluded that the initial boom signature at flight altitude does not impact the propagation path for Mach cut-off flight. The only factors that Mach cut-off flight is sensitive to are the speed and altitude at which the aircraft is flying at as well as the atmospheric profile. The implications of this are that a large supersonic cruiser, such as the Concorde, will have the same Mach cut-off restriction as a small supersonic business jet. This results from the fact that the propagation path of sound is not a function of amplitude or frequency of the sound; only the initial angle of propagation and the changes in the atmospheric speed of sound. A lot was learned about Mach cut-off flight through this task; however, this is just the beginning of the effort to fully understand Mach cut-off flight.

Milestone(s)

- Finished development of PCBoom Wrapper
- Gathered atmospheric data for realistic profiles
- Completed initial benchmarking Mach cut-on study for standard profiles
- Completed initial benchmarking Mach cut-on study for realistic profiles
- Completed Mach cut-off study for standard profiles
- Completed Mach cut-off study for realistic profiles
- Completed Task 4

Major Accomplishments

Georgia Tech has completed the research plan for this task. Georgia Tech has also acquired both the source code and executable for PCBoomv6.7. PCBoomv6.7 was used to perform the sensitivity analysis on the acoustical model provided by Aerion, Volpe, and Penn State University. Georgia Tech completed the initial benchmarking study for the sensitivity of Mach cut-off flight on a standard sonic boom signature (F-18 geometry provided with the executable). Georgia Tech assessed the sensitivity of the resultant ground boom strength and shape of the F-18 model with variations in atmospheric temperature and humidity as well as various flight Mach numbers. A tool to help facilitate the execution of task 4, the PCBoom wrapper,

was developed and utilized. The Aerion AS2 model was successfully incorporated into the study and the sensitivity of the model was assessed for both Mach cut-on and Mach cut-off conditions. The sensitivity study was performed and completed for various temperatures, winds, and relative humidity in both standard atmospheric profiles and realistic atmospheric profiles. The results of the study were compiled and presented in this report.

Publications

Gregory Busch, Jimmy Tai, Dimitri Mavris, Ruxandra Duca, and Ratheesvar Mohan, "Sensitivity analysis of supersonic Mach cut-off flight," J. Acoust. Soc. Am.,Vol. 141, No. 5, Pt. 2, 3565 (2017).

Outreach Efforts

Conference Presentations:

- Autumn ASCENT COE Meeting 2016: Alexandria, Virginia – Sept. 27-29, 2017
- Spring ASCENT COE Meeting 2017: Alexandria, Virginia – April 18-20, 2017
- ASA Acoustics 2017: Boston, Massachusetts – June 24-27, 2017
- Autumn ASCENT Meeting 2017 & ASCENT Noise Working Group: Alexandria, Virginia – Sept. 26-28, 2017

Awards

None

Student Involvement

Ruxandra Duca and Ratheesvar Mohan both preformed significant work under Task 4 and Task 5. Both students were integral parts of the Georgia Tech research team and worked diligently in researching technologies pertaining to Mach cut-off flight as well as learning how to operate PCBoom, generate results, and analyze the output/results. Ruxandra and Ratheesvar attended weekly research meetings and provided deliverables to the Georgia Tech ASCENT 42 research team. Ruxandra is currently still a Graduate Research Assistant and student at Goergia Tech and recently passed her PhD qualifying exams. Rathessvar graduated with his Master's degree in Aerospace Engineering in May 2017 and is currently working in industry.

Plans for Next Period

Task 4 is not continuing for the next research period.

Task #5: Evaluation of Technologies to Facilitate Mach Cut-off Flight

Georgia Institute of Technology

Objective(s)

The objective of this task is to identify and evaluate technologies that could be utilized to facilitate Mach cut-off flight. This task will primarily focus on nearer-term technologies that could be utilized by supersonic business jets. Most of these potential technologies will be external to the aircraft or technologies that can be placed on an aircraft with minimal to no change in the design. However, Georgia Tech also investigated more long-term technologies that could be integrated into future aircraft designs and could potentially be applicable to larger supersonic aircraft.

Research Approach

Georgia Tech's research approach in this task was primarily through literature review and solicitation of opinions from experts in the fields of aerospace, policy making, meteorology, and manufacturing. Georgia Tech performed this task in a phased approach. The first phase was performing an initial literature survey to identify potential technologies that would benefit Mach cut-off flight. Based on the team's initial knowledge and understanding of Mach cut-off flight, the first phase of literature review targeted technologies that could make it easier for operators of supersonic business jets to identify or predict atmospheric conditions. These technologies were studied using a cost-benefit type of evaluation to identify both the strengths and potential weakness of each technology.

The second phase of this task was done after the sensitivity study from Task 4 has been completed. With the knowledge and insight gained through performing Task 4, the ASCENT 42 research team had a better understanding on how flight conditions and atmospheric conditions impact the capability of a supersonic aircraft to fly at Mach cut-off. This allowed the

Georgia Tech team to identify any additional technologies that were overlooked during the initial phases of this task. The result of both of these phases was a portfolio of technologies that the Georgia Tech team hopes will be able to guide investment in technologies to facilitate Mach cut-off flight.

Mach cut-off flight is a phenomenon that occurs when the sonic boom rays of an airplane refract above the ground. This results in the absence of a sonic boom at the ground; only subsonic, evanescent waves reach the ground. This type of flight allows aircraft to fly at supersonic speeds while avoiding sonic booms that can be perceived by humans at the ground. This phenomenon is caused by changes in the local sound propagation speed, which is in turn a function of the local atmospheric properties. PCBOOM was used to investigate the sensitivity of Mach cut-off flight to various parameters, and it was discovered that the noise signature thereof is sensitive to the following factors:

- Temperature
- Wind speed
- Wind direction
- Relative Humidity
- Flight Mach number

Since it is evident that local weather conditions affect Mach cut-off flight, research was done into technologies that could be leveraged to accurately detect and/or predict weather ahead of an aircraft both in and out of its flight path. This would allow pilots to adjust the flight path and/or the flight speed such that the aircraft could operate in cutoff conditions as much as possible. The subsequent section summarizes the technologies identified.

Weather Sensing Technologies

List of Technologies Investigated

A. Dual Polarization Doppler Weather Radar
B. Wind Cube
C. WVSS-II
D. WSI Total Turbulence
E. Portable Scanning LIDAR for Profiling the Lower Troposphere
F. Honeywell Intuvue
G. Rockwell Collins MultiScan ThreatTrack

A. **Name:** Dual Polarization Doppler Weather Radar
Source: NOAA/NWS [http://www.nssl.noaa.gov/tools/radar/dualpol/]
Highlights:
- Determines composition and intensity of rain using electromagnetic pulses on water droplets.

Benefits:
- Clearly distinguishes between weather types (rain, snow, or hail) and even non-weather features (smoke, dust).
- Can detect aviation hazards such as birds.
- Can detect aircraft icing condition.

Drawbacks:
- On ground, cannot be installed on aircraft.
- Analyzes specific points of interest rather than entire areas.
- Cannot predict weather.

Features/Description:
- Location of the rain area can be determined from the time taken by the echoes returning back to the radar. For rainfall intensity, in general, stronger echoes (reflectivity) indicate heavier rainfall.
- Unlike traditional single polarization radar, the new radar can transmit and receive electromagnetic pulses from both of the horizontal and vertical polarizations.
- The two polarized waves give rise to echoes of varying characteristics when reflected by water droplets of different sizes or by different ice shapes.
- These characteristics can be analyzed to determine the composition of rain areas as well as the rainfall intensity.

Maturity Date: In service currently.
Adaptation: This system cannot be installed on an aircraft. It can only be used on the ground.

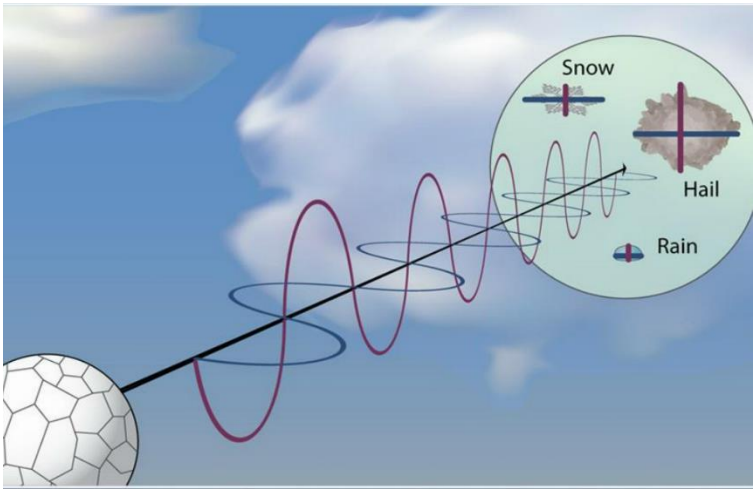

Figure 36: Dual Polarization Doppler Weather Radar

B. **Name:** Wind Cube
Source: NRG Systems [https://www.nrgsystems.com/products/lidar/detail/windcube-v2-lidar]
Highlights:
- Wind and Aerosol 3D Scanning (using Doppler LIDAR).

Benefits:
- Real-time wind, cloud layers, and aerosol (ice, ash, dust, smoke) layers measurements.
- Any scanning geometry up to 10km.
- Monitors height of the Planetary Boundary Layer (PBL).

Drawbacks:
- Dimensions: 1m x 1.3m. Therefore, it cannot be installed on an aircraft.

Features/Description:
- Based on optical fiber technology, WINDCUBE Scanning LIDARs are designed to run unattended and meet extreme operational requirements.
- Incorporates a fast endless rotation scanner head that enables capture of highly turbulent local phenomena or scans of a wide area at a high frequency.

Maturity Date: In service.
Adaptation: It is too large to be installed on an aircraft.

Figure 37: Wind Cube

C. **Name:** WVSS-II
Source: SpectraSensors/SWA [https://www.spectrasensors.com/wvss/]
Highlights:
- Water Vapor Sensing System: monitors moisture distribution and evolution in the atmosphere.

Benefits:
- Mounted on fuselage.
- Data collection in real-time.
- Good prediction capabilities.

Drawbacks:
- Data forwarded to US National Weather Service in near real-time.

Features/Description:
- Measures the amount of atmospheric water vapor in a sample of air continuously drawn from outside the aircraft.
- Sensor consists of:
  - Air Sampler
  - Connecting Hoses
  - Analyzer System Electronics Box (SEB)
- The SEB uses Tunable Diode Laser Absorption Spectroscopy to accurately measure the amount of water vapor in the atmosphere.
- Laser selected to be at wavelength corresponding to absorption wavelength of water.
- Absorption of laser light is proportional to the amount of water in the sampled air.

Maturity Date: In service currently.
Adaptation: Can be mounted on the fuselage of the aircraft.

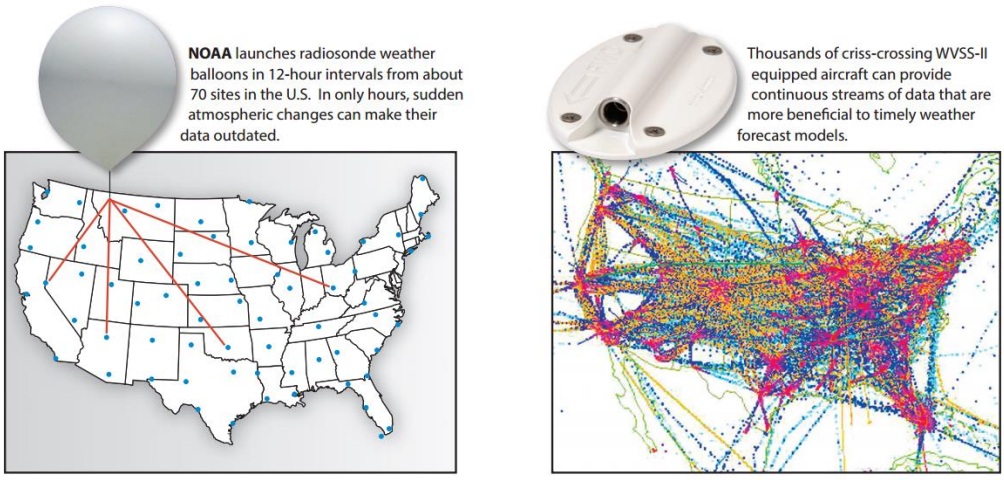

Figure 38: WWVS-II

D. Name: Total Turbulence
Source: WSI Corp [https://business.weather.com/products/total-turbulence]
Highlights:
- Real-time turbulence detection technology and reporting system.

Benefits:
- Delivers precise forecasts of turbulence for the next 24 hours.
- Delivers actionable turbulence alerts throughout all phases of flight.

Drawbacks:
- Crowdsourced data; only near real-time.
- Has to be incorporated in Aircraft Condition Monitoring System (ACSM).
- Coverage only in North America and East Asia.

Features/Description:
- State-of-the-art software monitors every bump and even measures the exact force of the turbulent air outside the plane.
- Automates the reporting of aircraft encounters with significant turbulence and severe loads based on certain g- load thresholds
- All of this data is instantly relayed to the ground where it is mapped and combined with the latest weather reports from aviation meteorologists.
- Combined, this vital information provides a detailed map of the world's turbulence which can then be beamed to pilots in the area, helping them to pick clean air.
- Some 700 aircraft worldwide are currently fitted with the system.

Maturity Date: In service currently.
Adaptation: This system can be installed directly on the aircraft.

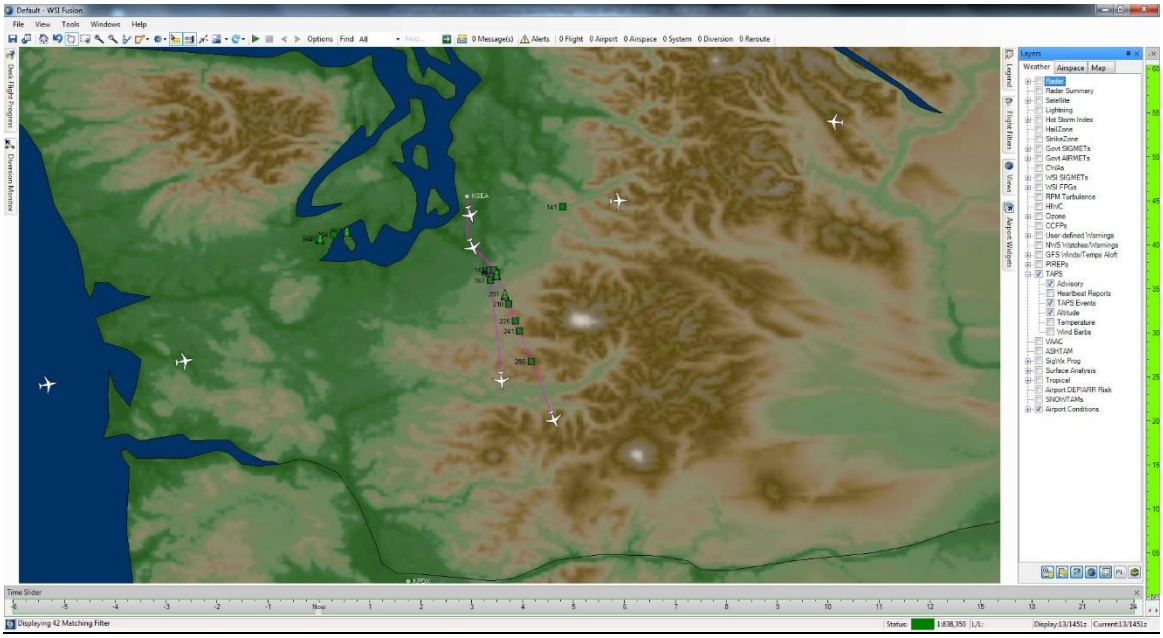

Figure 39: Total Turbulence

E. **Name:** Portable Scanning LIDAR for Profiling the Lower Troposphere
Source: [https://www.geosci-instrum-method-data-syst.net/4/35/2015/]
Highlights:
- Real-time measurement of atmospheric aerosols, clouds, and trace gases

Benefits:
- 3D
- Small size, light weight. This makes it suitable for installation in various vehicles.
- Real-time.
- Monitors atmospheric variables (aerosol, cloud, temperature, water vapor, optical depth of particulate matter, etc.) and meteorological processes (boundary-layer growth, aerosol and cloud layering, etc.).
- Horizontal coverage of 8-10km while scanning.
- In zenith mode good quality backscattered signals can be from 20 km away.

Drawbacks:
- Not fully developed yet.

Features/Description:
- Uses LIDAR (laser radar), which is based on the principle of light spectroscopy.
- The atmospheric species are sensitive to different wavelengths. Thus a multi-wavelength laser arrangement is used.
- The optical power measured with LIDAR is proportional to the signal backscattered by the atmospheric particles and molecules.
- The system includes:
  - The laser as a transmitter.
  - A Schmidt-Cassegrain telescope as a receiver.
  - Photomultiplier tube as a detector.
  - Real-time data acquisition and signal processing unit.
- Components are mounted on a vibration-isolated platform in an aluminum framework for good structural stability.
- All the hardware sections of the LIDAR system are controlled automatically via a computer with the Microsoft Windows platform with a user-friendly GUI.

Maturity Date: Unknown; system is not fully developed yet.
Adaptation: This system can be installed directly on a wide variety of aircraft, owing to its small size and light weight.

F. **Name:** Intuvue
Source: Honeywell [https://aerospace.honeywell.com/en/products/safety-and-connectivity/intuvue]
Highlights:
- Captures 'all' weather from -80 to +80 degrees in front of aircraft, up to 320 nm ahead of aircraft, and from 0 to 60,000 ft.
- Allows vertical scanning with high resolution.
- Can distinguish between types of convective weather.
- Features advanced turbulence detection capability (FAA certified) out to 40nm.

Benefits:
- 3D volumetric scanner is not limited to 2D scanning like most current systems.
- AUTO mode allows for scanning of both on-path and off-path weather.
- Capable of scanning vertical development of storms in 1000 ft increments.
- Internal terrain database removes ground clutter; corrects for Earth's curvature.

Drawbacks:
- Definition of 'all' weather is unclear. Literature provided by the manufacturer fails to clarify this.
- Cost is unknown; appears to be very expensive. A quote would have to be requested from the manufacturer to determine the exact cost of purchasing and installing the system on an aircraft.

Features/Description:
- Key technological enhancements of the system are volumetric 3D scanning and pulse compression technologies, which vastly improve weather detection and predictive hazard warnings, compared to conventional 2D radar.
- Continuously and automatically scans all the weather in front of the aircraft and stores data in a 3D buffer, creating a three-dimensional image of the weather and terrain; eliminates the need for manual tilt control.
- Pulse compression increases long-range detection and resolution; utilizes fact that energy of pulse (P*T) is constant – results in pulses of shorter duration with much higher power (917W vs. 150W).
- Uses Maximum Reflectivity Indication (MRI) technology to display both weather in flight path and secondary weather below 25,000 ft.
- In MAP mode, plan-view map is generated continuously, and simultaneously with weather de-clutter based on the internal terrain database. Reflectivity data that is considered ground clutter is the basis for the Ground Map.
- Detects turbulence at lower signal-to-noise ratio, enhancing performance at lower reflectivity levels, and at greater distances. This enables better correlation to predicted aircraft turbulence response.

Maturity Date: In service on A320, A330, B737NG, B737Max, B777, E-170/175/190/195/E2, F5X, F7X, F8X and G650 aircraft.
Adaptation: This system is designed to be installed directly on the aircraft without requiring special adaptation.

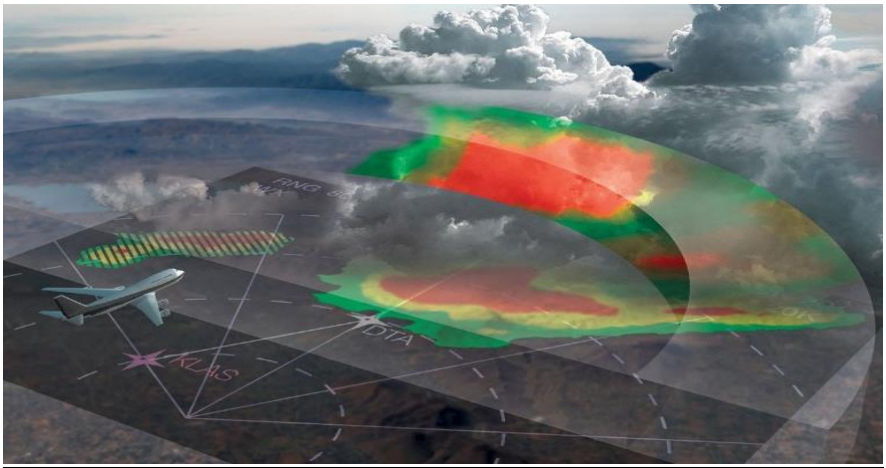

Figure 40: Honeywell Intuvue

G. **Name:** MultiScan ThreatTrack
Source: Rockwell Collins
[https://www.rockwellcollins.com/Products_and_Services/Commercial_Aviation/Flight_Deck/Surveillance/Weather-Radar/WXR-2100_MultiScan_Threat_Track_weather_radar.aspx]
Highlights:
- Optimized weather detection from 0 to 320 NM and all altitudes.
- Variable temperature based gain.
- Two-level enhanced turbulence detection - certified turbulence display plus "ride quality" turbulence display.
- Advanced ground clutter suppression at all ranges.
- Fully automatic operation.

Benefits:
- OverFlight™ Protection (prevents inadvertent thunderstorm top penetration).
- Geographic weather correlation using a database of historical data to augment algorithms.

Drawbacks:
- Seems to focus mostly on detection of thunderstorms; it is unclear what other types of weather phenomena it can detect.

Features/Description:
- Patented track-while-scan technology prioritizes weather threats out to 320 nm by performing dedicated horizontal and vertical scans on developed or fast-growing convective cells that pose an actual threat.
- Predictive OverFlight™ protection tracks thunderstorm cells ahead and below the aircraft, measures growth rate, predicts bow-wave turbulence and indicates potential threats in the aircraft's flight path.
- Two-level enhanced turbulence detection detects severe and ride-quality turbulence up to 40 nm ahead of the aircraft.

Maturity Date: In service on B737NG and B777 aircraft.
Adaptation: This system is designed to be installed directly on the aircraft without requiring special adaptation.

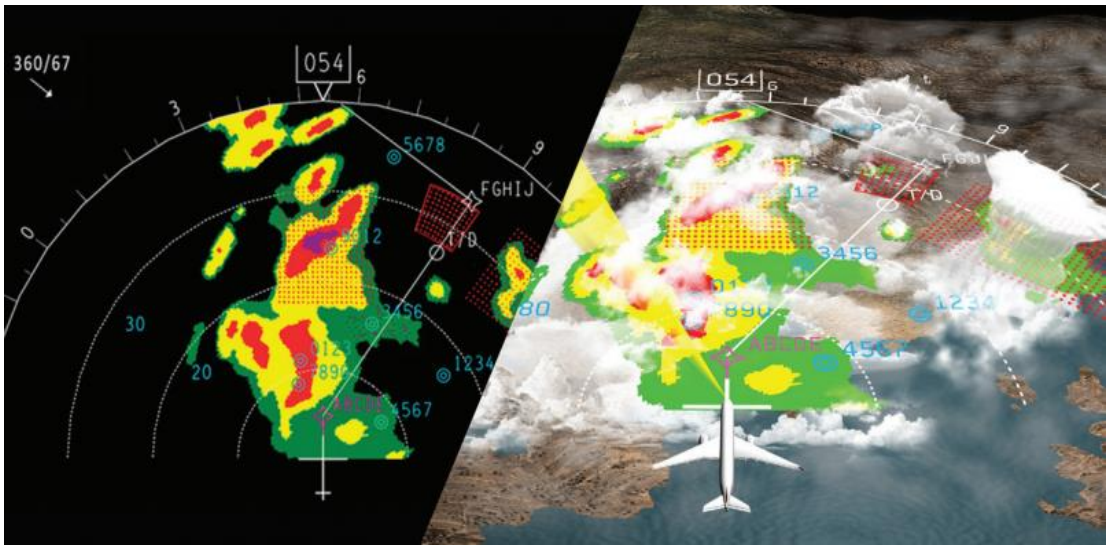

Figure 41: Rockwell Collins MultiScan ThreatTrack

H. **Name:** Cockpit Interactive Sonic Boom Display Avionics (CISBoomDA)
Source: NASA [https://www.nasa.gov/centers/armstrong/Features/CISBoomDA_software.html]
Highlights:
- Software that allows pilots the ability to physically see their sonic footprint on a map as the boom occurred.

Benefits:
- Pilots can identify where they need to fly to avoid sonic booms reaching the ground.
- Geographic weather correlation using a database of historical data to augment algorithms.

Drawbacks:
- This technology currently only provides descriptive data, not predictive data.
- The cost is unknown. Until development is finished, it is difficult to estimate the final price of installing this system on an aircraft.

Features/Description:
- Honeywell and Rockwell Collins are currently developing displays, using the same underlying algorithm, with predictive displays. These displays would allow identification of sonic booms on a proposed flight path. The flight path could then be modified to avoid sonic booms over populated areas.

Maturity Date: Currently in development. Estimated entry into service is unknown.
Adaptation: This system is being designed to be installed directly on aircraft, integrated with the aircraft's avionics.

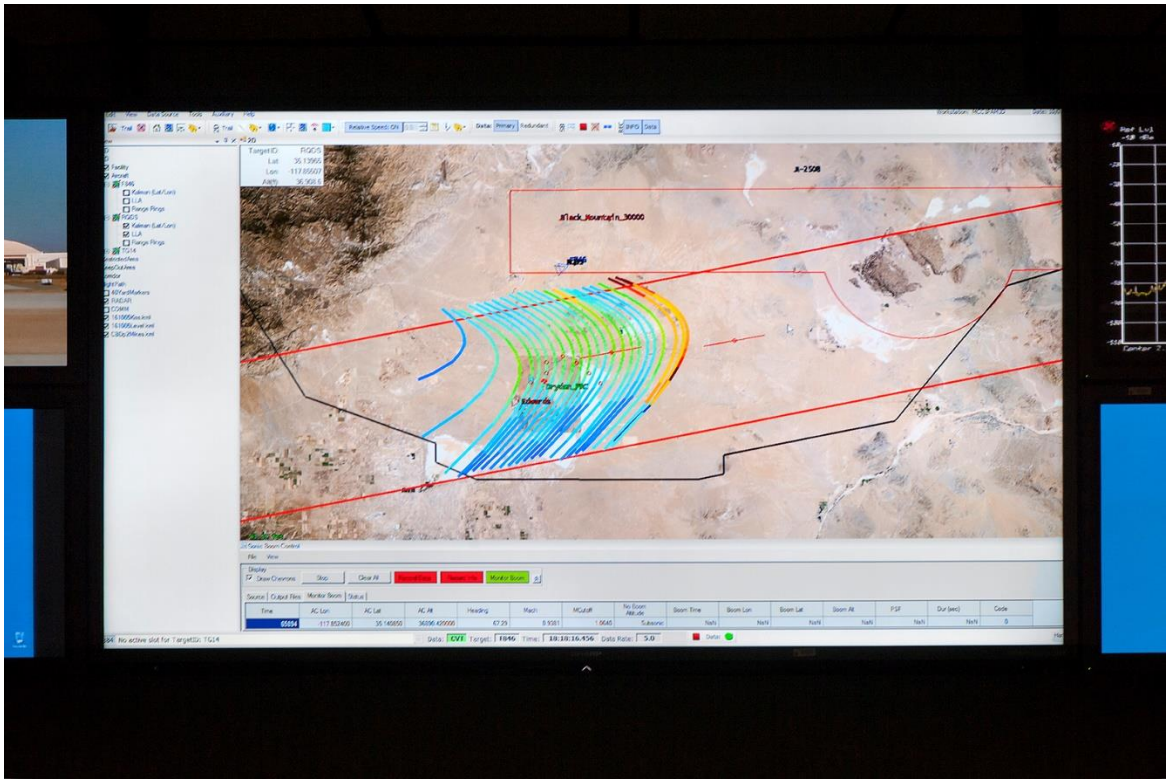

Figure 42: NASA CISBoomDA

Summary of Task 5

Various technologies were researched for Task 5. These technologies were discovered through extensive research in publicly available literature as well as recommendation from experts. Georgia Tech's presence at the Acoustics 2017 conference in Boston, MA was very helpful to gathering additional technologies as researchers and scientist there provided additional resources for this task. It was found through Task 4, that atmospheric conditions can greatly impact the ability to maintain Mach cut-off flight and being able to assess the atmosphere accurately and quickly will be crucial in avoiding any unwanted ground booms. Georgia Tech sees promise in accomplishing this task with the current state of technology, especially in NASA's CISBoomDA, but the technologies will need to mature further to make their way onto aircraft without causing a detriment to vehicle performance. A system for sensing the atmospheric profile will need to be compact and lightweight. The best answer for a technology that will help enable Mach cut-off flight is most likely not any singular technology presented here, but a combination of the best aspects of many different technologies.

Milestone(s)

- Initial technology information gathering completed
- Input from experts and researchers received
- Expansion of technology portfolio completed
- Identification of most promising technology completed and presented
- Task 5 completed

Major Accomplishments

Task 5 was completed through extensive research into various technologies that could help enable Mach cut-off flight. Insight on many of the technologies was solicited from scientists and researcher in the atmospheric sciences. The most promising technologies were investigated further, and a summary of those technologies is presented in this report.

Publications

None.

Outreach Efforts

Conference Presentations:

- Autumn ASCENT COE Meeting 2016: Alexandria, Virginia – Sept. 27-29, 2017
- Spring ASCENT COE Meeting 2017: Alexandria, Virginia – April 18-20, 2017
- Autumn ASCENT Meeting 2017 & ASCENT Noise Working Group: Alexandria, Virginia – Sept. 26-28, 2017

Awards

None.

Student Involvement

Ruxandra Duca and Ratheesvar Mohan both preformed significant work under Task 4 and Task 5. Both students were integral parts of the Georgia Tech research team and worked diligently in researching technologies pertaining to Mach cut-off flight as well as learning how to operate PCBoom, generate results, and analyze the output/results. Ruxandra and Ratheesvar attended weekly research meetings and provided deliverables to the Georgia Tech ASCENT 42 research team. Ruxandra is currently still a Graduate Research Assistant and student at Goergia Tech and recently passed her PhD qualifying exams. Rathessvar graduated with his Master's degree in Aerospace Engineering in May 2017 and is currently working in industry.

Plans for Next Period

Task 5 is not continuing for the next research period.

Task #3: Develop a Test Plan for Laboratory Experiments

University of Washington

Objective(s)

The University of Washington's Center for Industrial and Medical Ultrasound endeavored to develop a test plan for laboratory experiments for Mach cut-off that might be possible in the future.

Research Approach

A test plan for laboratory experiments for Mach cut-off that might be possible in the future was developed. A scaling argument was developed. The components of the design were characterized. And the design vetted in presentations.

In summary the design was to build a stratified atmosphere from layers of gel phantom of slightly varying sound speed. The sonic boom source was a collimated unfocused shock wave from a shock wave lithotripter. The speed of the aircraft was simulated by the angle of the shock wave axis. A 3D sound field was recorded by acoustic holography using a hydrophone. Modeling was to be accomplished with nonlinear acoustic wave propagation numerical models based on the KZK and Westervelt equations. All components were carefully characterized. Work was conducted in a tank < 1.5 m long in a laboratory setting. The simulated atmosphere was robust and did not change over time but could be reconfigured to simulate other atmospheres.

Milestone(s)

The design was completed by July 2017.

Major Accomplishments

A laboratory scale model for sonic boom tests was designed, characterized and developed. The original goal was to save cost and complexity of flight measurements and build a testbed for rapid more controlled but flexible measurements for comparison to rigorous numerical simulations. This was delivered.

Publications

MR Bailey, W Kreider, B Dunmire, VA Khokhlova, OA Sapozhnikov, JC Simon, VW Sparrow, "Laboratory test bed for sonic boom propagation," J. Acoust. Soc. Am. **141** (5, Pt. 2) 3565 (2017).

Outreach Efforts

The UW team has participated in monthly telecons with the ASCENT 42 team and presented at an ASCENT semi-annual meeting with the ASCENT 42 team.

Awards

None.

Student Involvement

Julianna Simon PhD graduated from UW and continued on as a post-doc funded by NASA. Julianna worked on the project at UW until she was hired at Penn State as an Assistant Professor where she continued in a consulting role.

Plans for Next Period

The project has been completed.

Task #6: Support Development of Acoustical Model of Mach Cut-off Flight

Volpe National Transportation Systems Center

Objectives

Volpe will provide guidance to the Project 42 team on using suitable CFD-solutions as source inputs to PCBoom. Configuration analysis and development of near field pressure characteristics from CFD will be provided to Volpe. Volpe support may also include a PCBoom web-based training session for team members. Volpe will provide insight to team members on the appropriate use of PCBoom so that team members can conduct sonic boom ray tracing and Mach cut-off analysis using PCBoom for a variety of environmental, flight operation and vehicle source conditions. Volpe will support team activities investigating the addition of supplemental operational parameters into the sonic boom analysis. Volpe will support the evaluation of the applicability of early Mach Cut-off theories under realistic atmospheric conditions by providing information relative to PCBoom capabilities and fundamental formulations.

Background

PCBoom is a full ray trace sonic boom program that calculates sonic boom footprints and signatures from flight vehicles performing arbitrary maneuvers. The PCBoom model has been developed [Plotkin & Cantril, 1975], refined [Plotkin, 1998; Page, Plotkin and Wilmer, 2010] and validated [Page *et al.*, 2010] over many decades with investments from NASA, the US Air Force and other entities. PCBoom computes detailed ground signature shapes starting from a variety of near-field signature definitions. It has its roots in the NASA sonic boom program written by Thomas [1972] in the early 1970s. Initial development consisted of adding focus boom prediction capability [Plotkin & Cantril, 1975]. Further development, through a series of versions extended the original code (which computed boom on a single ray for a single flight condition) to handle full maneuvers and a variety of aircraft source inputs. There have been improvements to the algorithms, such that boom aging is now handled by waveform steepening and shock fitting, rather than Thomas's waveform parameter method. Three dimensional ray tracing algorithms [Schulten, 1997] have replaced Thomas's original flat earth layered ray equations, although Thomas' original ray equations are present as an option.
PCBoom6 has the following capabilities:

- Specification of the vehicle as an F-function, a data line of $\Delta p/p$, via data from a CFD solution [Page & Plotkin, 1991; Plotkin & Page, 2002], as a simple form from a library of aircraft, or as a blunt hypersonic body. There is a launch vehicle mode, which includes the effect of the vehicle itself plus the effect of an underexpanded rocket plume.
- Ray tracing through a 3-D stratified atmosphere over either flat earth or over a WGS-84 ellipsoidal earth.
- Specification of arbitrary maneuvers in either local Cartesian coordinates or in geographic latitude and longitude.
- Calculation of superboom signatures at focal zones, and also the secondary post-boom signatures a distance away from the geometric focus.
- Calculation of booms along particular rays, or across the full width of the primary sonic boom carpet.
- Calculation of secondary booms including tracing of "Over the Top" complex 3D ray paths and computation of secondary sonic boom signatures [Plotkin *et al.*, 2007].
- Calculation of shock structures, either as a simple Taylor structure or via molecular relaxation and absorption processes [Burgers, 1939].
- Calculation of spectra and a variety of loudness metrics for ground booms.
- Calculation of the effect of finite ground impedance on boom signatures.
- Effect of turbulence on sonic boom ground signatures [Crow, 1969; Plotkin, Maglieri & Sullivan, 2002; Locey, 2008]
- Effects of wind and terrain [Rachami & Page, 2010] on boom propagation.
- Penetration of sonic booms and propagation underwater [Sparrow & Ferguson, 1997; Sawyers, 1968; Cook, 1970; Cheng *et al.,* 1996; Garrelick, 2002]

Major Accomplishments

Task 1: Volpe provided sonic boom modeling guidance on using suitable sonic boom configuration inputs including CFD-solutions for supersonic aircraft configurations as source characteristic inputs for PCBoom. Web-based training was provided to the team regarding configuration analysis and development of near field pressure characteristics suitable for sonic boom analysis.

Volpe interacted with the Aerion team to ensure the CFD analysis yielded suitable off body pressure results for sonic boom assessment. The resultant CFD pressure data for the Aerion vehicle was provided to Volpe and the other team members. Volpe supported the CFD analysis by processing the data and creating a complete set of input and output files and conducted a PCBoom web-based training session for Project 42 participants on the use of CFD data for sonic boom modeling. The analysis stream included capability to consider different atmospheres and environmental parameters, varying flight conditions and computation of footprints or single ray metrics using the Burgers' solver in the PCBurg module.

Task 2: Volpe provided insight on the appropriate use of PCBoom for conducting sonic boom ray tracing and Mach cut-off analysis for a variety of environmental, flight operation and vehicle source conditions. Volpe assisted with the investigation of supplemental operational parameters in the sonic boom analysis including fine tuning of ray tracing parameters within the main propagation module FOBoom. Guidance was provided to the team regarding shock structure as controlled by a combination of nonlinear steepening and molecular relaxation processes, and computed by solution of the Burgers equation solver (PCBurg). Web-based training included operation of FOBoom, PCBurg and the batch solver to support calculation of sonic boom metrics. Volpe also worked directly with Georgia Tech to fine tune PCBoom model parameters in support of their temperature sensitivity analysis examining Mach cut-off flight under both standard and real-world atmospheric conditions.

Task 3: Volpe supported evaluation of the applicability of early Mach cut-off theories under realistic atmospheric conditions by providing information relative to PCBoom capabilities, limitations and fundamental formulations. A set of benchmark condition results from PCBoom was provided to the team for curved ray calculations using PCBoom's horizontally stratified atmosphere with winds. An assessment of Concorde signatures was conducted using standard PCBoom source characteristics to support Aerion comparisons. Example files for the calculation of sonic boom over varying terrain was also provided to the ASCENT team (though it was not demonstrated in the online training). A ground terrain file for the Continental US was provided for use with PCBoom along with a set of example analysis files based on an earlier NASA NextGen study [Rachami & Page, 2010].

As part of all three tasks, Volpe provided PCBoom guidance and training to PSU, Georgia Tech and Aerion both as a group and individually as needed via email and phone. Two structured online training classes for PCBoom analysis were conducted. These classes used specific test cases by example and all PCBoom files were provided to the participants. The team independently acquired the PCBoom code directly from NASA using established protocols. The online training was recorded by Penn State and made available to the ASCENT team for supplemental review. Sample analysis covered during the two online PCBoom training classes with example input and output files distributed to ASCENT 42 participants included the following:

- Level flight from an F-18 using the simple Carlson source model
- Assessing Mach and lateral cutoff
- CFD pressure distribution inputs using the NASA LM1021 publicly available dataset[1]
- Burgers loudness propagation applying molecular relaxation
- Calculation of sonic boom signatures from the Concorde using built-in source data
- Complex maneuvering flight analysis involving an F18 executing a low-boom dive maneuver
- Analysis of the Aerion RL3 configuration starting with CFD data
- Ground metric calculations accounting for molecular relaxation using the LM1021 dataset and the Burgers solver module PCBurg
- Batch mode execution of FOBoom and PCBurg using the updated NASA batch executable.

References

Burgers, J.M., 1939. "Mathematical Examples Illustrating Relations Occurring in the Theory of Turbulent Fluid Motion", *Trans. Roy. Neth. Acad. Sci.,* Amsterdam, **17**,pp. 1-53.

Cheng, H.K., C.J. Lee, M.M. Hafez, and W.H. Guo, 1996. "Sonic boom propagation and submarine impact: a study of computational and theoretical issues," AIAA-96-0755.

Cook, R.K., 1970. "Penetration of a sonic boom into water," *J. Acoustic Soc. Am.,* **47**(5, pt2), pp.1430-1436.

[1] NASA Sonic Boom Prediction Workshop: https://lbpw.larc.nasa.gov/

Crow, S.C., 1969. "Distortion of Sonic Bangs by Atmospheric Turbulence", *J.Fluid Mech.,* **37**, 529-563: also, NPL Aero Report 1260.

Garrelick, J., 2002. "The effect of a coastline on the underwater penetration of sonic booms," *J. Acoust. Soc. Am.*, **111** (1), Pt. 2, January, pp.610-613.

Locey, L.L., 2008. "Sonic boom post processing functions to simulate atmospheric turbulence effects," Ph.D. dissertation, (Grad. Program in Acoustics, The Pennsylvania State University).

Page, J.A., and K.J. Plotkin, 1991. "An Efficient Method for Incorporating Computational Fluid Dynamics Into Sonic Boom Prediction", AIAA-91-3275, September.

Page, J.A., K.J. Plotkin, and C. Wilmer, 2010. "PCBoom Version 6.6 Technical Reference and User Manual", NASA Contract No. NNL10AB94T, Wyle Research Report WR 10-10, December.

Page, Juliet A., Christopher M. Hobbs, Kenneth J. Plotkin, Domenic J. Maglieri, 2010. "PCBoom Model Prediction Comparisons with Flight Test Measurement Data," NASA Contract No. NNL05AA04Z, Wyle Technical Note TN 10-01, March.

Plotkin, Kenneth J., and Jerry M. Cantril, 1975. "Prediction of Sonic Boom at a Focus", Wyle Research Report 75-7, October.

Plotkin, Kenneth J., 1998. "PCBoom3 Sonic Boom Prediction Model – Version 1.0e", Wyle Research Report WR 95-22E, October.

Plotkin, K.J., and J. Page, 2002. "Extrapolation of sonic boom signatures from CFD solutions," AIAA paper 2002-0922, 40th Aerospace Sciences Meeting, Reno, NV, January.

Plotkin, K.J., D.M. Maglieri, B. Sullivan, 2002. "Measured Effects of Turbulence on the Loudness and Waveforms of Conventional and Shaped Minimized Sonic Booms", AIAA 2005-2949, May.

Plotkin, K.J., J.A. Page, and E.A. Haering, Jr., 2007. "Extension of PCBoom to Over-The-Top Booms, Ellipsoidal Earth, and Full 3-D Ray Tracing," AIAA 2007-3677, May.

Rachami, J., Page, J., 2010. "Sonic Boom Modeling of Advanced Supersonic Business Jets in NextGen," AIAA 2010-1385, January.

Sawyers, K.N., 1968. "Underwater sound pressure from sonic booms," *J. Acoust. Soc. Am.,* **44**(2), pp. 523-524.

Schulten, J.B.H.M., 1997. "Computation of aircraft noise propagation through the atmospheric boundary layer," NLR TP 97374, December.

Sparrow, V.W., and T.J. Ferguson, 1997. "Penetration of Shaped Sonic Boom Noise into a Flat Ocean," AIAA Paper 97-0486.

Thomas, C.L., 1972. "Extrapolation of Sonic Boom Pressure Signatures by the Waveform Parameter Method," NASA TN D-6832, June.

Task #1A: Propagation Modeling with Enhanced Ray-tracing Capabilities

The Pennsylvania State University

Objective(s)

For Task 1A, the original propagation theory [Nicholls, 1971] will be retraced for extensibility and to incorporate the operational parameters proposed by Aerion. Ray calculations will be made to assess the back-of-the-envelope predictions for Mach cut-off operations that were known to the FAA in the 1970s. This research will help to provide a technical basis for rulemaking regarding Mach cut-off operations, which includes estimating the altitude and Mach number restrictions for focus boom avoidance including real-world atmospheric effects.

Research Approach

Methodology

The original propagation theory [Nichols, 1971] has been retraced for extensibility. In that theory, the atmosphere is assumed to have only vertical variations of temperature and horizontal wind. In reality, however, for sonic boom propagation

over a large distance, the horizontal variations of the atmospheric temperature and wind speed can be important for Mach cut-off, which are not included in Nicholls' theory.

Mach cut-off depends on the refraction of sound in the atmosphere. In Nicholls' theory, this has been described by one form of the sound refraction law which specifies the direction of the wavefront normal. By arguing the sonic boom would not reach the ground as long as the wavefront normal of the sound becomes parallel to the ground aloft, the "safe altitude" for Mach cut-off flight is determined. This is only true in the absence of vertical winds. When the vertical winds becomes non-negligible, ray-tracing is a more accurate tool to predict the cut-off Mach number and the "safe altitude" [Ostashev, 2001].

Besides that, in Nicholls' theory, by calculating the cut-off Mach number based on the atmospheric conditions only at the flight and ground levels, the impact of the detailed realistic atmospheric profile in between those two levels on the cut-off Mach number hasn't been taken into account.

In order to build an acoustical model that can lead to more accurate estimates of the safe cut-off altitude and Mach number for Mach cut-off flight, 2-D ray tracing equations have been examined [Pierce, 1989]. Based on which, a 4th order Runge-Kutta integration ray tracing scheme has been developed, which takes into account realistic atmospheric conditions including arbitrary speed of sound variations and arbitrary two-dimensional winds with a vertical wind component. In this version of the algorithm, the effect of the cross-wind is not included.

For ray calculations, the same atmospheric temperature profile has been used based on the 1976 U.S. Standard Atmosphere, and different wind speed profiles has been tested. To incorporate the Mach cut-off operational parameters proposed by Aerion Corporation, a flight altitude of 12.5 km, which corresponds to 41010 ft, has been consistently used, and results are given for flight Mach numbers from 1.01 up to 1.20.

Results

To assess the robustness of the theory, the results of which have been benchmarked with NASA's PCBoom code using the same 1976 U.S. standard atmosphere with no wind and with a linear tailwind of a gradient of 4 (m/s)/km, respectively, for both the Mach 1.15 and Mach 1.20 cases.

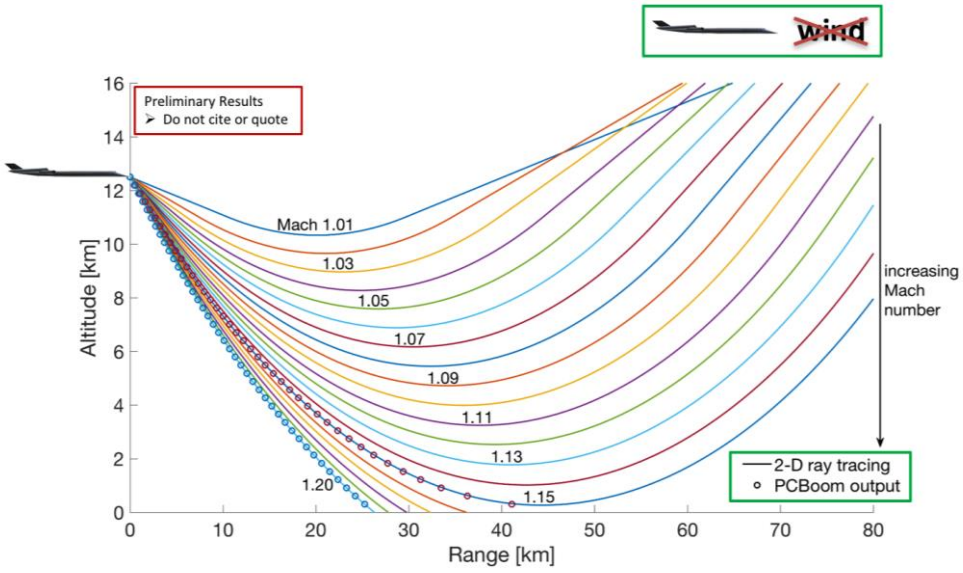

Fig. 43: 2-D Ray Tracing for Different Mach Numbers Using the 1976 U.S. Standard Atmosphere with No Wind.

As shown in Figure 43, when the flight Mach number increases, the sound rays get closer to the ground. The ray calculation by the 2-D ray-tracing algorithm for a standard atmosphere and no wind case matches the results from NASA's PCBoom very well. The predicted cut-off Mach number of 1.15 for the no wind case also agrees with the results from an earlier technical

report [Onyeonwu, 1971]. A linear headwind case and a linear tailwind case which both have the same wind speed gradient of 1 (m/s)/km are examined (see Figures 44 and 45). It shows that the wind direction matters. Linear horizontal winds can affect the Mach cut-off operations. A linear tailwind contributes to a downward refraction of the sonic boom so that a higher "safe altitude" is needed, while a linear headwind leads to a stronger upward sound refraction so that a higher cut-off Mach number can be achieved.

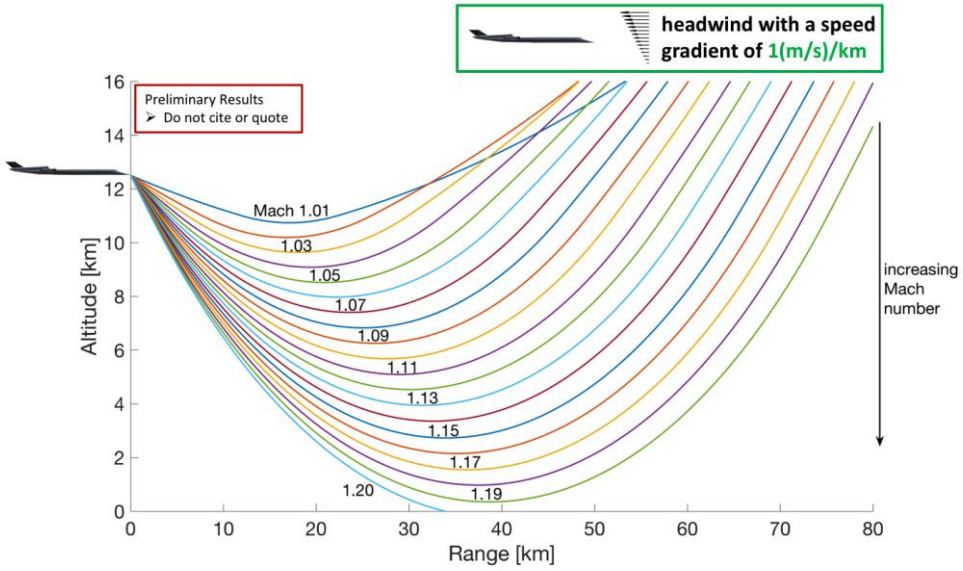

Fig. 44: 2-D Ray Tracing for Different Mach Numbers Using 1976 U.S. STD Atmosphere. and a Linear Headwind with a Wind Speed Gradient of 1 (m/s)/km

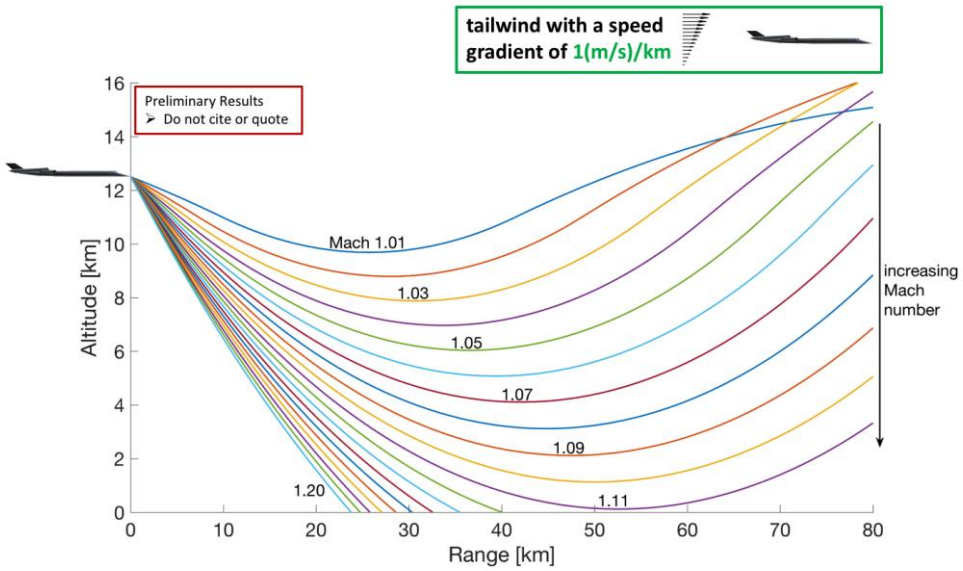

Fig. 45: 2-D Ray Tracing for Different Mach Numbers Using 1976 U.S. STD Atmosphere and a Linear Tailwind with a Wind Speed Gradient of 1 (m/s)/km

One limitation of earlier Mach cut-off theories (including Nicholls') and existing tools (e.g., PCBoom) is that vertical winds are not included. In a realistic atmosphere, however, a noticeable vertical wind can sometime exist. A sea breeze is a wind

that blows from sea to land, which normally occurs along coasts during daytime (see Figure 46). This is driven by the pressure gradients in the air due to the differences in the heat capacities of sea water and dry land, that introduce temperature contrasts, which can often include a return flow from land back to sea aloft [Wallace, 2006].

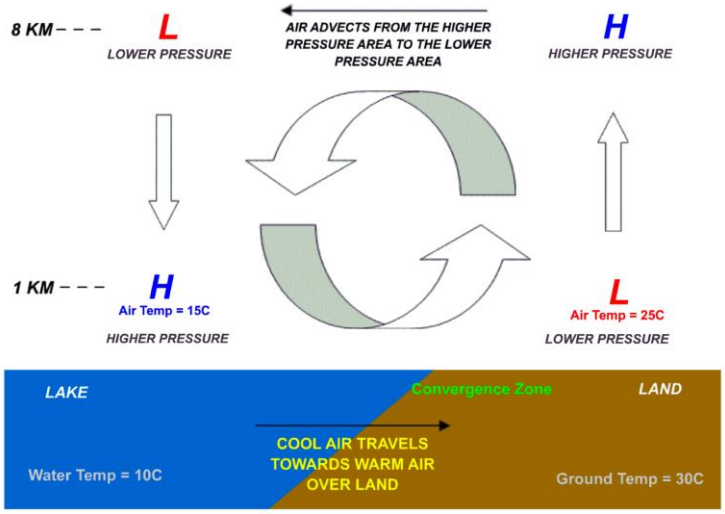

Fig. 46: A Sea Breeze Circulation. Adopted from https://en.wikipedia.org/wiki/Sea_breeze

In order to model a sea breeze circulation, a simple convective wind profile has been developed, in which a vertical wind component is included, and the size of the cell has been chosen so that it extends from the ground up to an altitude of 16 km for demonstration, as shown in Figure 47. Numerical results are given in Figures 48 and 49 for clockwise and counterclockwise convection cells respectively, in both of which, the maximum horizontal wind speeds are 8 m/s, and the vertical wind component can be seen which has a maximum value of 1.6 m/s.

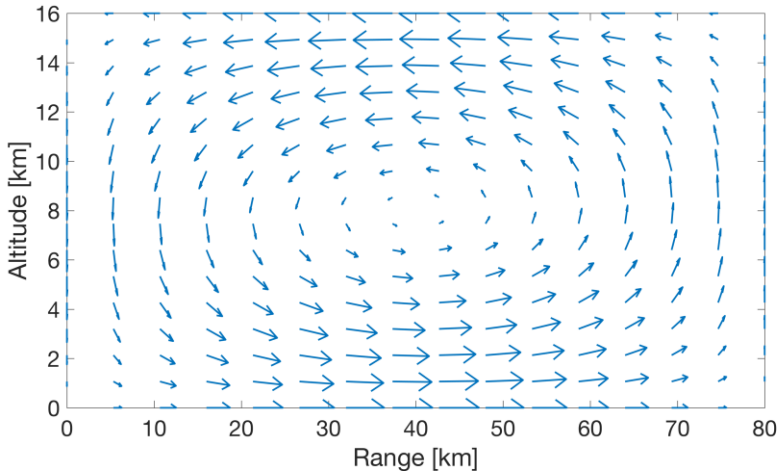

Fig. 47: Wind Speed Profile of a Counterclockwise Convection Cell

The direction of the wind circulation has been very important to the sonic boom refraction and thus the Mach cut-off operation. Depending on the flight direction, a clockwise wind circulation contributes to a downward refraction of the sonic boom similar to that of a linear tailwind, while a counterclockwise cell leads to a higher cut-off Mach number. Including vertical winds in sonic boom predictions seems very important to ascertain "safe altitudes" for Mach cut-off operations.

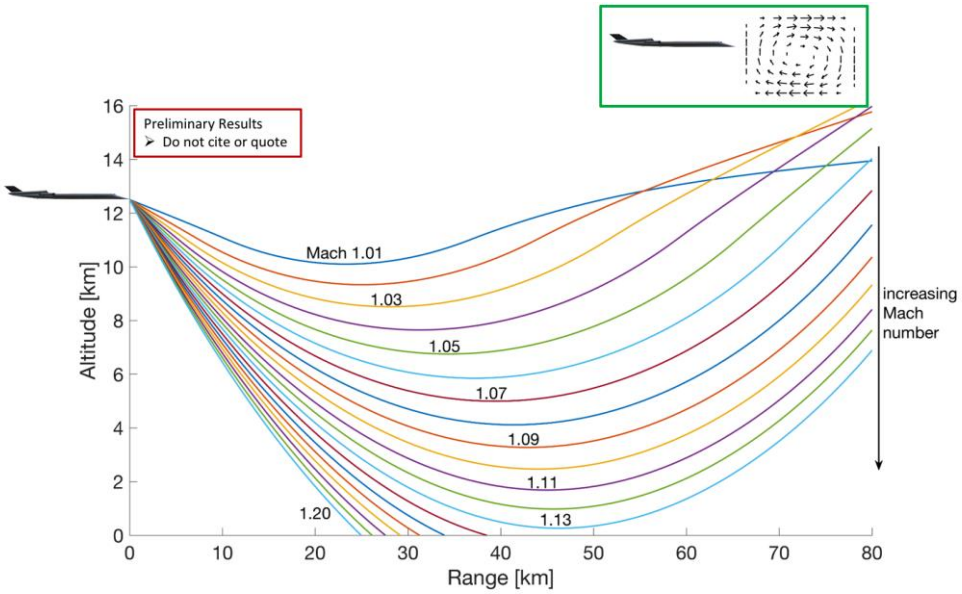

Fig. 48: 2-D Ray Tracing for Different Mach Numbers Using 1976 U.S. STD Atmosphere and a Clockwise Convection Cell

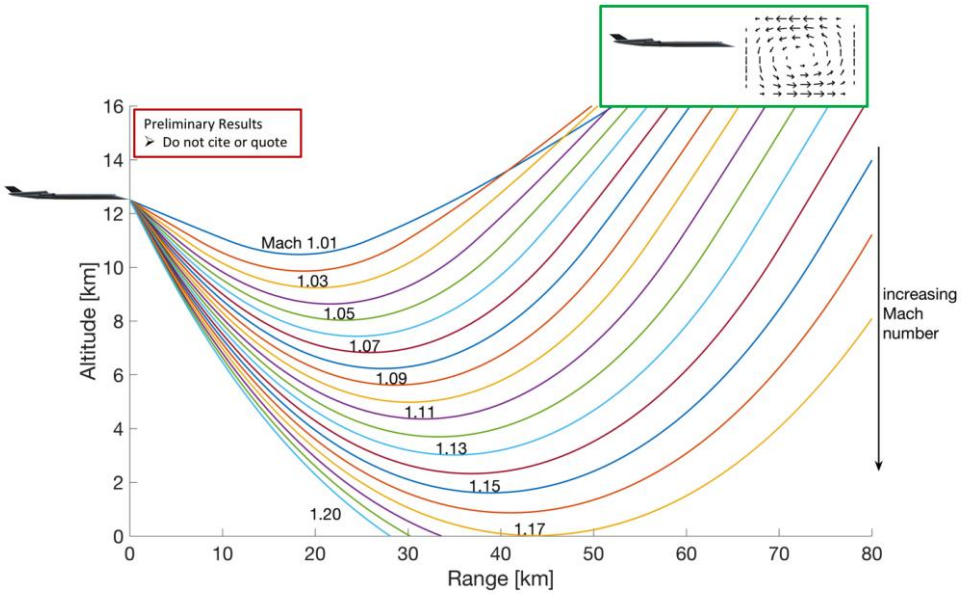

Fig. 49: 2-D Ray Tracing for Different Mach Numbers Using 1976 U.S. STD Atmosphere and a Counterclockwise Convection Cell

Results of each individual wind speed profile given above include the contribution from different Mach numbers. Since a caustic is formed aloft when the rays become parallel to the ground, which corresponds to a loud sound energy, to ascertain "safe altitudes" for Mach cut-off operations, ray calculations along a flight path at a fixed flight Mach number can also be useful. From Figure 50 to 52, it shows that the magnitude of the wind (or the gradient of the wind speed) affects Mach cut-off operations. When the wind speed gradient of the linear tailwind increases from 0 (m/s)/km (that corresponds to the no

wind case) through 1 (m/s)/km up to 2 (m/s)/km, the caustic line gets closer to the ground surface, and eventually reaches the ground.

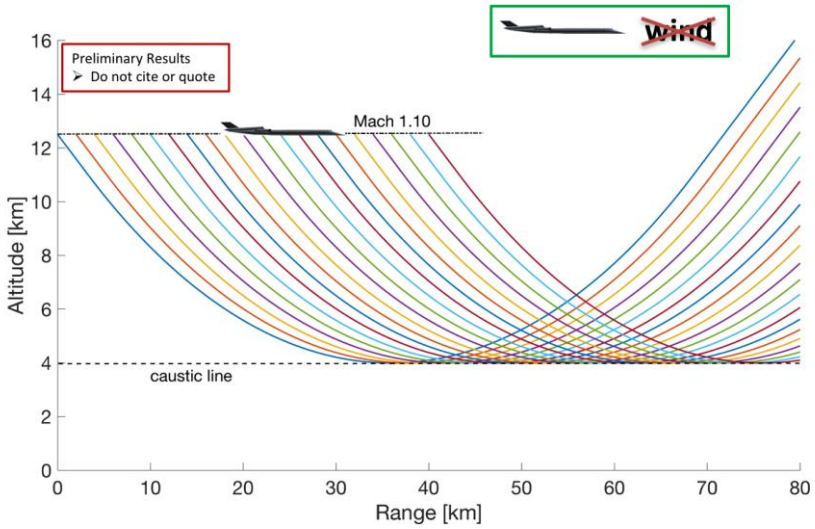

Fig. 50: 2-D Ray Tracing for Mach 1.10 Using 1976 U.S. STD Atmosphere and No Wind

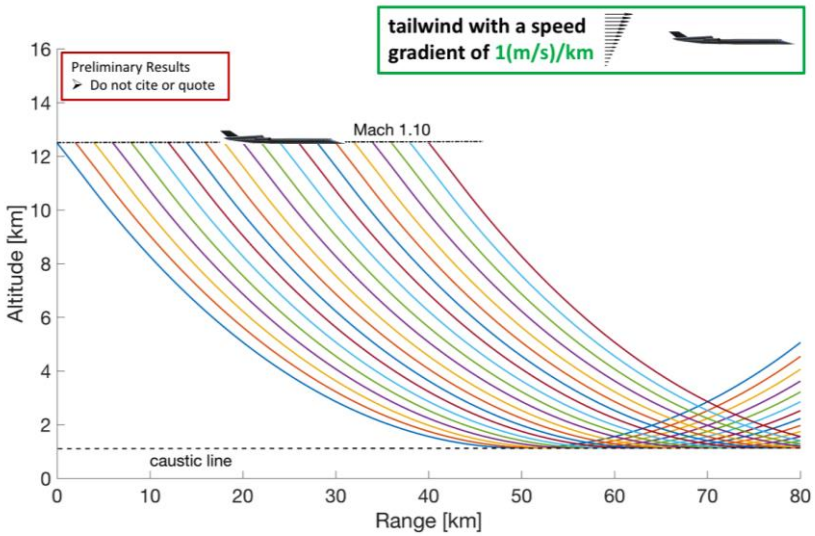

Fig. 51: 2-D Ray Tracing for Mach 1.10 Using 1976 U.S. STD Atmosphere and a Linear Tailwind with a Wind Speed Gradient of 1 (m/s)/km

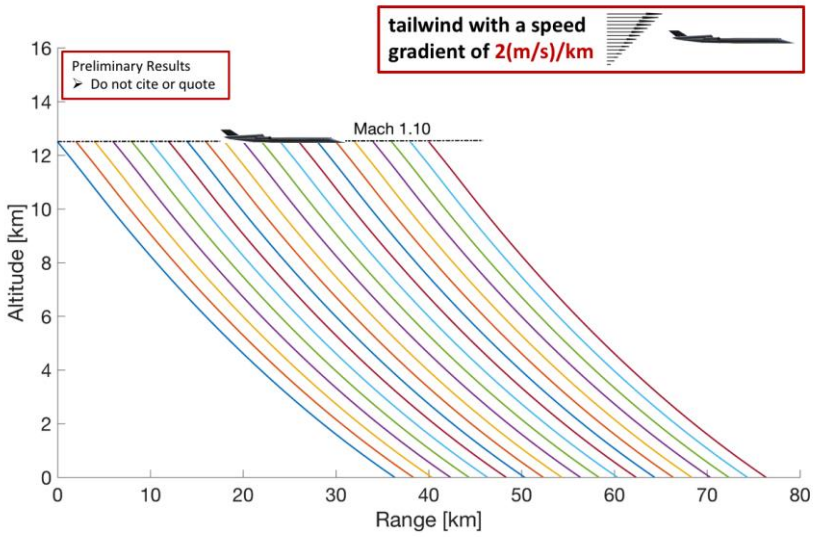

Fig. 52: 2-D Ray Tracing for Mach 1.10 Using 1976 U.S. STD Atmosphere and a Linear Tailwind with a Wind Speed Gradient of 2 (m/s)/km

Results of similar calculations for a clockwise convection cell shows a different caustic line pattern, in which the caustic line is not parallel to the ground (Figure 53), and people at some places on the ground that's closer to the caustic line over heads may hear a louder noise. This is because, for a circulative wind profile, the wind speed can also vary horizontally. Thus, accounting for realistic winds including the horizontal variations of the wind are important.

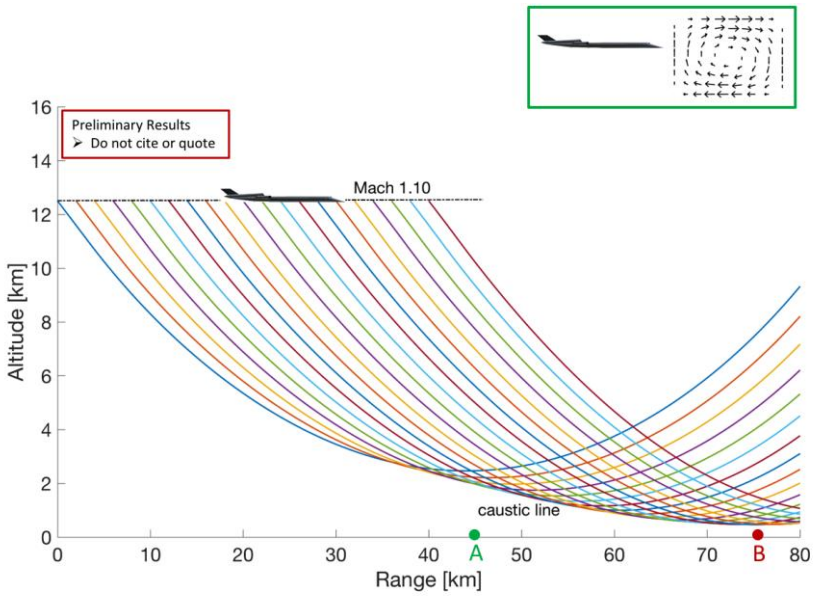

Fig. 53: 2-D Ray Tracing for Mach 1.10 Using 1976 U.S. STD Atmosphere and a Clockwise Convection Cell

Milestone(s)

Milestone	Date Finished
Nicholls' Mach cut-off theory has been examined, and it has been determined that there are some questionable assumptions in the Nicholls' formulation. The limitations of Nicholls' theory have also been identified.	6 mo. = February 1, 2017
A 2-D ray-tracing algorithm has been developed, and ray calculations of Mach cut-off parameter space are performed and benchmarked to the output from NASA's PCBoom code.	12 mo. = July 31, 2017

Major Accomplishments

In this research, a 2-D ray-tracing algorithm has been developed and validated for the acoustical model of Mach cut-off flight, which takes into account realistic atmospheric conditions including arbitrary speed of sound variations and arbitrary two-dimensional winds with a vertical wind component. Based on the 1976 U.S. standard atmosphere, the effects from the vertical wind speed and the horizontal variations of the wind on the "safe altitudes" for Mach cut-off operations have been examined.

Publications

Acoustics '17 abstract.

Outreach Efforts

Z. Huang and V. W. Sparrow, "Preliminary assessment and extension of an existing Mach cut-off model," Poster for the Penn State Center for Acoustics and Vibration (CAV) Spring Workshop, University Park, PA, April 25-26, 2017.

Awards

None.

Student Involvement

Zhendong Huang is the graduate research assistant supported by Project 42 at Penn State on this task. He is pursuing his Ph.D. in the Penn State Graduate Program in Acoustics.

Plans for Next Period

The project team is developing an improved Mach cut-off model using a 3-D ray tracing method so that both a 3-D atmosphere and arbitrary 3-D winds are accounted for correctly. Using measured atmospheric data provided by the Integrated Global Radiosonde Archive (IGRA), a radiosonde dataset from the National Centers for Environmental Information (NCEI) consisting of radiosonde and pilot balloon observations, as input, to perform ray calculations for certain busy air routes in the United States, and to examine the influence of realistic atmospheric profiles and flight conditions on the Mach cut-off operations.

References

G. Haglund and E. Kane, "Flight test measurements and analysis of sonic boom phenomena near the shock wave extremity," NASA Report CR-2167 (1973).

Z. Huang and V. W. Sparrow, "Preliminary assessment and extension of an existing Mach cut-off model," Invited paper for Acoustics '17, the 3rd Joint Meeting of the Acoustical Society of America and the European Acoustics Association, Boston, MA, June 25-29, 2017. Paper 2aNSb2 for special session: Sonic Boom Noise II: Mach Cutoff, Turbulence, Etc., *J. Acoust. Soc. Am.*, **141**(5, Pt. 2), 3564 (2017).

J. Nicholls, "A note on the calculation of 'cut-off' Mach number, " Meteorological Mag. 100 33-46 (1971).

W. Shurcliff, "S/S/T and sonic boom handbook," (Ballentime, 1970), p. 63.

R. O. Onyeonwu, "The effects of wind and temperature gradients on sonic boom corridors, "UTIAS Technical Note No. 168. AFOSR-TR-71-3087. University of Toronto (1971).

V. E. Ostashev, D. Hohenwarter, K. Attenborough, P. Blanc-Benon, D. Juvé, & G. H. Goedecke, "On the refraction law for a sound ray in a moving medium, " Acta Acustica united with Acustica, 87(3), 303-306 (2001).

A. Pierce, "Acoustics: An Introduction to its Physical Principles and Applications, " Acoustical Soc. Am., New York (1989).

J. M. Wallace and P. V. Hobbs, "Atmospheric science: an introductory survey, " Vol. 92. Academic press (2006).

Task #2: Subjective Study on Annoyance, Metrics, and Descriptors

The Pennsylvania State University

Objective(s)

- Develop a set of descriptors suitable for describing Mach-cutoff ground signatures to identify the key perceptual attributes of Mach cutoff signals.
- Determine how these attributes are correlated with annoyance ratings of these signals.
- Identify a metric appropriate for predicting annoyance due to Mach-cutoff ground signatures.

Research Approach

Introduction

The research to be conducted in this task will be the seminal work in the perception of Mach cut-off. The overall objective is to identify a metric that corresponds to annoyance due to Mach-cutoff flights. Subjective data from listening tests will inform this identification. Mach-cutoff ground signatures are unique sounds, the likes of which are not part of day-to-day experience. They are perceived differently from traditional sonic booms. As such, a new set of vocabulary will also be developed as a prerequisite to running an annoyance study.

The task was subdivided into three stages: subjective (listening) test design, stimulus selection, and testing preparations. The first stage included designing a descriptor study that will feed into a multi-factor annoyance study. Stimuli were selected from NASA's FaINT dataset [1] through careful listening tests. Test preparations included improving the low-frequency output of an existing sound-field reproduction facility at Penn State and all subjective testing preparations. Each stage is explained in more detail in the sections below.

Design of the Subjective Listening Tests

General subjective impressions, such as annoyance and preference, are often studied using factor analysis. This type of test requires that attributes be selected as potential factors of the broader impression. Ratings on each attribute and on the broad impression are then analyzed to find which of the attributes most factor into the impression. However, these attributes must be named before this type of study can be done.

When developing a set of vocabulary, care must be taken to ensure that the descriptors chosen will represent words common to the general population. To this end, three test methods were considered: Free-Choice Profiling (FCP) [2], Flash profiling (Flash) [3], and Individual Vocabulary Profiling (IVP) [4]. Each method involves descriptor selection on an individual basis followed by rating stimuli on these developed descriptor scales. The main differences between the methods lie in the rating step. In FCP, subjects rate each stimulus individually on their own set of descriptors. In Flash, subjects rate each stimulus individually on a pooled set of descriptors. This method is disadvantageous, as it requires each participant to complete two testing sessions, where the second session cannot take place until all subjects have finished developing descriptors. In IVP, subjects rate stimuli simultaneously on comparative scales based on their own set of descriptors. This method is disadvantageous because the comparative scale limits the number of stimuli that can be included for rating. Given these disadvantages, FCP was deemed the most appropriate method for this study. Similar procedures have been used in the fields of virtual acoustics [4] and concert hall acoustics [5].

The procedure for each subject in the vocabulary development test is as follows:

1. Each subject listens to a set of 12 stimuli. Once a participant has listened to all 12 of the signals, they are required to provide their own words to describe the sounds they heard (descriptors) and a definition for each of these words. Subjects are allowed to listen to each stimulus as many times as they want in this part of the testing session, even after they have started providing descriptors. For example, a subject listens to the twelve stimuli. He or she might then choose to describe these stimuli using the word "rumble". He or she would write down the word "rumble" with an appropriate definition, such as "like the sound rocks make tumbling down a hill".
2. After this first part of the test, the test administrator meets with the participant to discuss the developed descriptors, refine provided definitions, and narrow down their list. The interview ensures each descriptor is appropriate for a rating scale and removes words that describe the same aspect of the sounds. Continuing the example, the subject might have provided the word "thunder-like" in addition to the word "rumble". In the interview process, if these two words were determined to mean the same thing, then only one would be selected for use in rating.
3. For the last part of the testing session, each subject rates the stimuli based on their descriptor list. For each descriptor, the subject listens to each stimulus one at a time and are asked to rate the "presence" of that descriptor in the given stimulus. For example, a subject who used the word "rumble" to describe these stimuli would then rate how present the "rumble" is in each stimulus.

The statistical analysis technique used to analyze this type of data is the Generalized Procrustes Analysis, which is a type of factor analysis. This method rotates each subject's rating space, finding alignment between attributes, which results in a list of descriptors that represent all major perceptual attributes of the stimuli. This final list will be used for the annoyance study, in which subjects will rate stimuli on the final descriptor list and annoyance.

Stimulus Selection

For the first part of this study, stimuli were taken from Mach-cutoff ground signatures recorded in NASA's "Farfield Investigation of No-boom Thresholds" (FaINT) field measurements [1]. These measurements produced a large database with 36 total Mach-cutoff flyovers recorded on more than 120 microphones, which were divided into two arrays: (1) a 60-microphone linear array and (2) a 62-microphone spiral array, as shown in Figure 54. Only sounds recorded by microphones in the linear array were considered for producing stimuli because the spiral array used microphones that were not ideal for capturing the low-frequency energy of Mach-cutoff sonic booms.

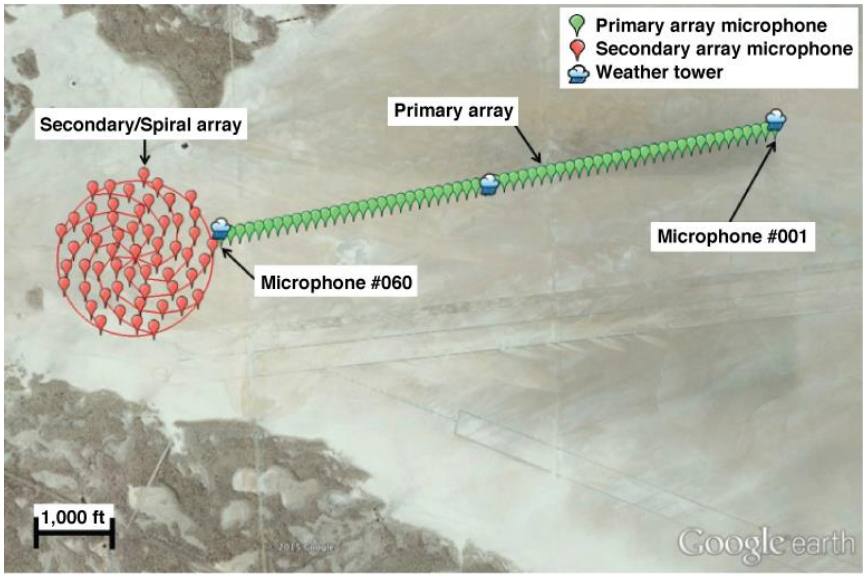

Fig. 54: FaINT microphone arrays. The descriptor study will use recordings made on the primary array (the linear array). Image reproduced from [1].

The 36 flyovers by 60 recordings were assumed to be a good sampling of all possible Mach-cutoff ground signatures. For this study, it was thus helpful to sample the database so that the final stimulus set represented the variety within the database. Stimulus categorization was first attempted through clustering then through methodical listening.

For the objective approach to categorize the signals, the method of K-means clustering was run on the time-domain signals in an attempt. Each time series was first normalized to its maximum amplitude and time shifted to maximize correlation. While the method did produce clusters that were related analytically, the raw time-series data did not produce clusters that were perceptually similar. Additionally, repeated runs of the clustering algorithm did not agree well with one another. These findings support the need for metrics that do correspond to perception.

Since the method of clustering the signals did not turn out to be a viable method to categorize the signals, a qualitative approach was used. Specifically, the set of signals were then categorized based on critically listening, which was broken into the following steps:

1. Before listening to any of the stimuli, any passes that did not result in successful Mach-cutoff ground signatures, as indicated by the FaINT researchers' notes and listening to the recordings, were discarded, which was a total of 7 passes.

2. With these passes eliminated, that still left a total of approximately 1700 (29 passes X 60 microphones) possible signals to use in the study. In order to listen to a representative sample of recordings, signals from several microphones along the array were evaluate to determine the amount of perceptual variation along the flight path each signature had. This qualitative analysis revealed that the most perceptually different signals for a given flight pass occurred between the two endpoints of the arrays, which thus reduced the possible number of stimuli to 58 recordings. Each of these signals were then perceptually evaluated to identify if there were any problems with the recordings, such as excessive wind noise, and if so they were eliminated from the set of possible stimuli for the study.

3. During the previous step, it was noted that the perceptual differences between recordings were much more apparent between passes as opposed to between microphones for a given pass. As a result, critical listening was carried out for one signal from each pass to develop a set of appropriate categories with which to organize the recordings. In the end, the stimuli were divided into four categories by Ortega. With the signals now organized into groups, 5 to 7 passes were chosen from each category and finally recordings from two microphones for a given flight pass were selected to form a reduced set of 48 stimuli.

4. With this reduced set of stimuli, both Vigeant and Ortega blindly listened to and categorized all 48 stimuli, which were given random identifiers (from 1 through 48) to disguise their related nature while evaluating the recordings. The process also resulted in only four categories, which were relatively similar across the two raters. In broad terms, the categories were “rumble”, “surge / surging rumble” (where the signal got louder over time), “thumps (not distinct booms)”, and “waving/hitting sheet metal”.

Finally, a set of 24 recordings were selected for use in the subjective study, where 5 to 7 representative signals were identified for each of the four categories as shown in Table 4. This set of 24 signals represents the variety of Mach-cutoff ground signatures recorded during the FaINT field test measurements. The 12 most distinctive signals were then selected for the development of descriptors for the first part of the formal subjective test, while all 24 will be used in the rating portion of the test.

Table 4: Selected stimuli from NASA's FaINT data sets with subjective descriptions, as described by Ortega and Vigeant. The last two columns indicate which recordings will be used in each part of the listening test.

	FaINT Recording Information				Inclusion in Subjective Study	
Category	**Flight**	**Pass**	**Mic**	**Description From Pilot Study**	**Part 1 - Descriptor Development**	**Part 2 - Ratings**
1 Rumble	1392	1	10	Rumble (like distant thunder)	X	X
	1392	3	46	Rumble	X	X
	1389	4	32	Rumble		X
	1391	4	58	Rumble (lower amplitude)		X
	1391	7	52	Rumble (lower amplitude)		X
	1392	2	36	Rumble		X
	1393	1	5	Rumble		X
2 Surge / surging rumble	1388	5	52	Surge (like water rushing upwards)	X	X
	1389	3	8	Surging rumble	X	X
	1393	4	17	Surging rumble	X	X
	1388	2	60	Surging rumble		X
	1390	1	3	Surge		X
	1390	4	43	Surge		X
	1390	6	3	Surging rumble		X
3 Thumps (not distinct booms)	1388	3	32	Thumps followed by surge	X	X
	1391	5	27	Thump followed by surge	X	X
	1388	4	5	Thumps followed by surge		X
	1389	6	5	Thump followed by surge		X
	1392	6	51	Sharper thump followed by surge		X
4 Waving / hitting sheet metal	1389	1	6	Hitting sheet metal	X	X
	1389	5	26	Waving sheet metal or surge	X	X
	1390	2	24	Hitting sheet metal or surge	X	X
	1392	4	50	Waving sheet metal or rumble	X	X
	1393	3	37	Waving sheet metal	X	X

Subjective Listening Test Preparations

The listening tests will be conducted in the AUralization Reproduction of Acoustic Sound-fields (AURAS) facility at Penn State, shown in Figure 55. The facility originally consisted of 30 custom loudspeakers installed in an anechoic chamber, but now also has two subwoofers that were designed and constructed for this study. Sound fields are reproduced using third-order Ambisonics.

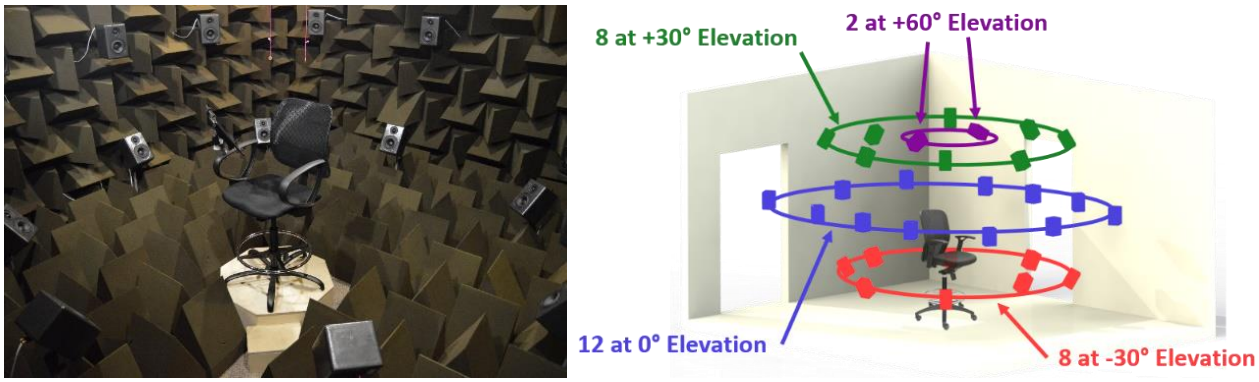

Fig. 55: The AURAS facility at Penn State, where the subjective listening tests will take place. This facility can be used to reproduce a range of sound fields, including interior aircraft noise and office environments.

To prepare for the listening tests, the low-frequency output of the existing AURAS facility needed to be increased. The existing 30 loudspeakers were designed to have a flat frequency response extending down to 60 Hz. While such a response is suitable for reproducing room-acoustics stimuli, Mach-cutoff signals have significant energy well below the audible cutoff of 20 Hz. In order to reproduce the signals, a pair of large subwoofers was designed and built, where each houses a Dayton Ultimax 18" driver in a 3'x2'x1.25' closed plywood box. A Crown K2 power amplifier supplies 800 W of power to each subwoofer. The boxes needed to be custom constructed to fit the existing chamber. The resulting frequency responses achieved for each of the subwoofers as installed in the anechoic chamber are shown in Figure 56. Note that the anechoic chamber in which the reproduction system is housed has a low-frequency room mode around 63 Hz. This results in the significant notch in the frequency response of Subwoofer 1. The subwoofer was positioned in the room to minimize this effect, but the effect could not be eliminated without affecting the distribution of sound. Also note the steep roll-off below 20 Hz. Both of these factors prompted the design of digital filters that would boost the low-frequency output and reduce the effect of the room mode.

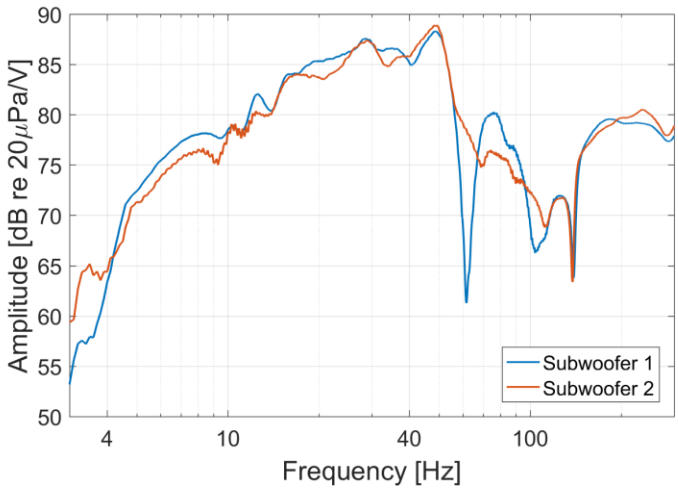

Fig. 56: Frequency response of constructed subwoofers. The two subwoofers are needed to produce the low frequency energy present in Mach-cutoff ground signatures.

Because of the significant low-frequency energy in the Mach-cutoff signals (see blue line in Figure 57), digital filters were designed to boost the low-frequency output of the subwoofers. In order to allow power output equal to the original signal levels across most frequencies, a 6 dB/octave roll-off was necessary below 20 Hz. Recordings of signals produced using these filters show faithful reproduction of the original signals, as seen in Figure 57.

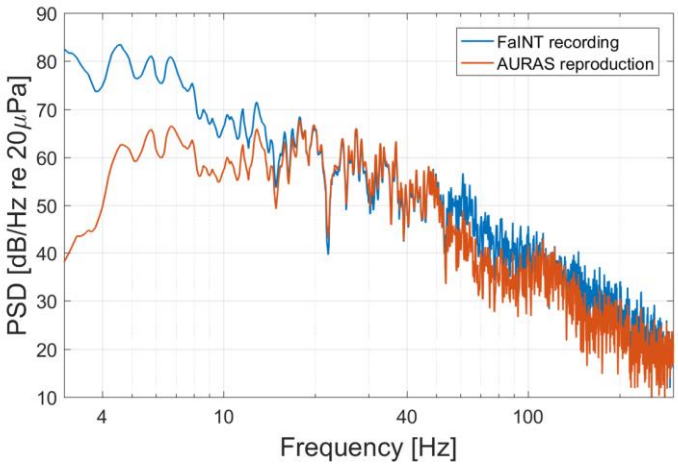

Fig. 57: Example Mach-cutoff ground signature, as recorded by FaINT and as reproduced in the AURAS facility

With a suitable sound system in place, the next step was to decide which direction the signals should appear to be coming from. Despite the fact that the majority of the energy is these signals is contained within the low frequencies, which radiate in a uniform (omnidirectional) manner, there is enough high-frequency content for listeners to identify a source location. Three possible locations were identified: from the front, overhead, and 60 degrees forward of vertical. Ortega, Vigeant, and Sparrow individually listened to each case and determined that the overhead sounds were the most natural and realistic.

In order to subjectively validate the quality of the reproductions of the Mach cutoff signals, Sparrow was asked to compare reproductions of post sonic boom noise, which have a similar character to Mach cutoff signals are sounds that he is very familiar with, to the Mach cutoff reproductions. An interface was developed which allowed for instantaneous switching between each of the signals to make it straightforward to easily do an A/B comparison of the presented pairs of signals. Switching between the post-boom signals and the Mach-cutoff signals, he determined they sounded similar. He also felt the post-boom noise sounded realistic and that the Mach-cutoff booms matched descriptions from other researchers.

User interfaces required for testing were developed in Cycling '74's Max programming environment. Max is a visual programming language that allows for easy audio interface and quick user interface setup. It was selected as the best environment based on the need to control 32 channels of audio. Two interfaces were created – one for entering descriptors and one for rating stimuli. The descriptor interface (Figure 58) allows the subject to play all 12 of the first set of stimuli, one-at-a-time in an order of their choosing. The circles adjacent to the 'play' buttons are used to indicate which signal is being played at any given moment and if they have already listened to that signal. Once subjects have listened to all stimuli, they can enter descriptors and accompanying definitions.

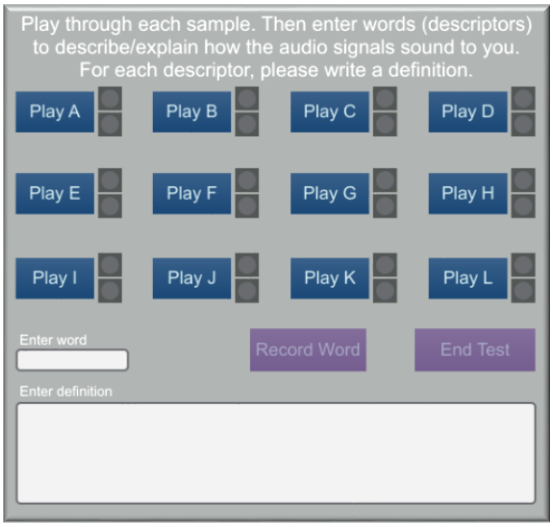

Fig. 58: User interface for descriptor entry. This interface allows test subjects to enter their own descriptors for Mach-cutoff stimuli along with accompanying definitions.

For the second part of the listening test, participants will use the rating interface shown in Figure 59. Participants will be asked to rate each of the 24 stimuli individually for three or four of the descriptors they developed. The stimuli will be played in random order and they will only rate one descriptor at a time to reduce the potential for rating bias that might occur if they were asked to rate multiple attributes at the same time. For example, if they had terms "loud" and "rumble" and were rating both of these terms at the same time, they might tend to give similar ratings for both attributes when rating both at the same time, which may or may not be an accurate representation of the relationship between the attributes.

Fig. 59: User interface for stimulus rating. This interface allows subjects to rate stimuli on their own descriptors. During testing, a subject's descriptor will replace the label "DESCRIPTOR 1".

All procedures and testing material were reviewed and approved by Penn State's Human Subjects Institutional Review Board (IRB). Prior to receiving the award, a preliminary protocol and supporting documentation was submitted to the IRB for approval, but significant modifications were needed based on the work carried out in the past year to fully develop the upcoming listening study. The main document which describes the proposed study, known as the protocol, underwent

significant revisions, wherein the details about the recruitment process, process of obtaining consent, testing procedure, data storage protocol, potential risks, and safeguards against those risks, were all updated. In addition, the supporting documentation and testing materials were also updated, which included: subject information forms, a tutorial slideshow, a noise sensitivity questionnaire, recruitment advertisement text and flyer, an informed consent form, and images and descriptions of the user interfaces.

Milestone(s)

Milestone	Planned Due Date	Status
Report on assessment of FaINT data for subjective tests	February, 2017	Complete
Report on pilot subjective test and initial metrics assessment	July 31, 2017	In progress
Report on initial metrics assessment	July 31, 2017	In progress

Major Accomplishments

- Descriptor study was designed: several different test methods were reviewed and the method of Free Choice Profiling was determined to be the most suitable for this research task. The results from the upcoming subjective study will provide a set of descriptors useful in describing Mach cut-off, which will then be used in a subsequent test to study annoyance due to this signals, which will then be used to propose metrics to predict public acceptance of these types of sounds.
- FaINT dataset characterized – Methodical listening was used to sort the FaINT recordings into four categories. This categorization made it possible to select a suitable subset of flight passes for use in the listening test and will helpful in later stages when comparing quantities of different metrics across signals
- Frequency range of existing testing facility extended Subwoofers constructed – A pair of subwoofers were designed and constructed to extend low-frequency output of Penn State's sound-field-reproduction facility, which was necessarily in order to accurately reproduce of the Mach-cutoff signals from the FaINT recordings.
- Descriptor study preparations completed – Administrative approvals were obtained and testing instruments (e.g. user interfaces, questionnaires) were developed. Subjective data collection will begin in November 2017.

Publications

Acoustics '17 abstract.

Outreach Efforts

CAV Workshop 2018 – Poster presentation: This consisted of one poster outlining the listening test design and preparation.

Awards

None.

Student Involvement

Nicholas Ortega was primarily responsible for test design, stimulus selection, test preparations, and presentation preparations. He also presented the poster at the CAV workshop and the talk at the ASA / EAA Conference. He will continue to work on this task during the following period.

Plans for Next Period

Over the next period, the work will be focused on obtaining subjective data and analyzing how this data relates to existing metrics. First the descriptor study will be administered and is projected to be completed by mid-January. Results from the descriptor study will then be analyzed and attributes will be selected for inclusion in the annoyance study, which will be run in early 2018. The results from this second study will be used to determine which attributes factor into annoyance. Calculated metrics will then be analyzed for correlation with the given ratings, and a metric or group of metrics will be proposed that may be useful in predicting response to Mach cut-off by April-May 2018.

References

L. J. Cliatt II; M. A. Hill; E.A. Haering Jr., "Mach cutoff analysis and results from NASA's Farfield Investigation of No-boom Thresholds", 22nd AIAA/CEAS Aeroacoustics Conference, AIAA 2016-3011 (2016).

A. A. Williams; S. P. Langron, "The Use of Free-choice Profiling for the Evalueation of Commercial Ports", J. Sci. Food Agri., Vol. 35, pp. 558-568, (1984).

V. Dairou; J.-M. Sieffermann, "A Comparison of 14 Jams Characterized by Conventional Profile and a Quick Original Method, the Flash Profile", J. of Food Sci., Vol. 67, no. 2, pp. 826-834, (2002).

L. Gaëtan, ""Individual Vocabulary Profiling of Spatial Enhancement Systems for Stereo Headphone Reproduction", Audio Engineering Society Convention 119, paper 6629, (2005).

T. Lokki; J. Pätynen; Antti Kuusinen, *et al.,* "Concert hall acoustics assessment with individually elicited attributes", J. Acousti. Soc. Am., Vol. 130, no. 2, pp. 835-849, (2011).

M. Gerzon, "Periphony: With-Height Sound Reproduction," J. Audio Eng. Soc., Vol. 21, no. 1, pp. 2-10, (1973).

N. D. Ortega, M. C. Vigeant, and V. W. Sparrow, "Subjective study on attributes related to Mach cut-off sonic booms," J. Acoust. Soc. Am. Vol. **141** (5, Pt. 2) 3565 (2017). Presentation at Acoustics '17 in Boston, MA, USA in June 2017.

Project 043 Noise Power Distance Re-Evaluation

Georgia Institute of Technology

Project Lead Investigator

Dimitri Mavris (PI)
Regents Professor
School of Aerospace Engineering
Georgia Institute of Technology
Mail Stop 0150
Atlanta, GA 30332-0150
Phone: 404-894-1557
Email: dimitri.mavris@ae.gatech.edu

University Participants

Georgia Institute of Technology
P.I.(s): Dr. Dimitri Mavris (PI), Mr. Christopher Perullo (Co-PI)
FAA Award Number: 13-C-AJFE-GIT-021
Period of Performance: June 28, 2016 – August 14, 2017

Project Funding Level

The project is funded at the following levels: Georgia Institute of Technology ($150,000). Cost share details are below:

The Georgia Institute of Technology has agreed to a total of $150,000 in matching funds. This total includes salaries for the project director, research engineers, graduate research assistants and computing, financial and administrative support, including meeting arrangements. The institute has also agreed to provide tuition remission for the students paid for by state funds.

Investigation Team

Georgia Institute of Technology
Principal Investigator: Dimitri Mavris
Co-Investigator: Christopher Perullo
Research Faculty: Matthew LeVine, Greg Busch, Holger Pfaender, Michelle Kirby
Students: Arturo Santa-Ruiz, Kenneth Decker

Project Overview

The standard technique for evaluating fleet noise from flight procedures estimates source noise using Noise Power Distance (NPD) curves. Noise calculations within the Aviation Environmental Design Tool (AEDT) rely on NPD curves derived from aircraft certification data, provided by aircraft manufacturers. This dataset reflects representative aircraft families at set power levels and aircraft configurations. Noise levels are obtained as a function of observer distance via spherical spreading through a standard atmosphere. Other correction factors are applied to obtain the desired sound field metrics at the location of the receiver. The current NPD model does not take into account the aircraft configuration (e.g., flap settings) or alternative flight procedures being implemented. This is important as the noise characteristics of an aircraft depend on thrust, aircraft speed and airframe configuration, among other contributing factors such as ambient conditions. The outcome of this research is a suggested NPD + configuration (NPD+C) format that enables more accurate noise prediction due to aircraft configuration and speed changes.

Georgia Tech leveraged domain expertise in aircraft and engine design and analysis to evaluate gaps in the current NPD curve generation and subsequent prediction process as it relates to fleet noise prediction changes from aircraft configuration and approach speed. The team used EDS physics based modeling capabilities to conduct a sensitivity analysis to identify additional parameters to be included in the NPD+C (NPD + Configuration) curve format.

This study assumes that the aircraft procedure is unchanged. The sensitivity studies provided are indicative of changes due solely to changes in the source noise characteristics and propagation effects due to use of the NPD+C. A coupled study of changes in trajectories using NPD+C vs. the traditional NPD is recommended as a follow on effort.

NPD and NPD+C Modeling and Prediction Overview

The current method use to obtain an airport (DNL) contour is outlined in Figure 1. First, the NPD data is obtained either through testing and certification or analytically. In this project, Georgia Tech used NASA's ANOPP software to predict aircraft source noise. A traditional NPD assumes limited variation in engine and airframe noise for a limited number of configurations. Typically an approach and departure NPD are generated, each of which assumes a fixed configuration as described later in Table 5. This data is currently acquired or calculated for a vehicle flying at a reference speed of a 160 kts. Noise prediction is then coupled with aircraft performance analysis to compute the SEL contour area for each stage length. DNL contours can then be generated using an assumed operations mix. For this study, only SEL contour areas were examined to simplify examination of the results. Historically, an 80 dB SEL contour area is representative of a 65 DNL contour area; therefore, the 80 db SEL is used in this study to calculate representative changes in contour area.

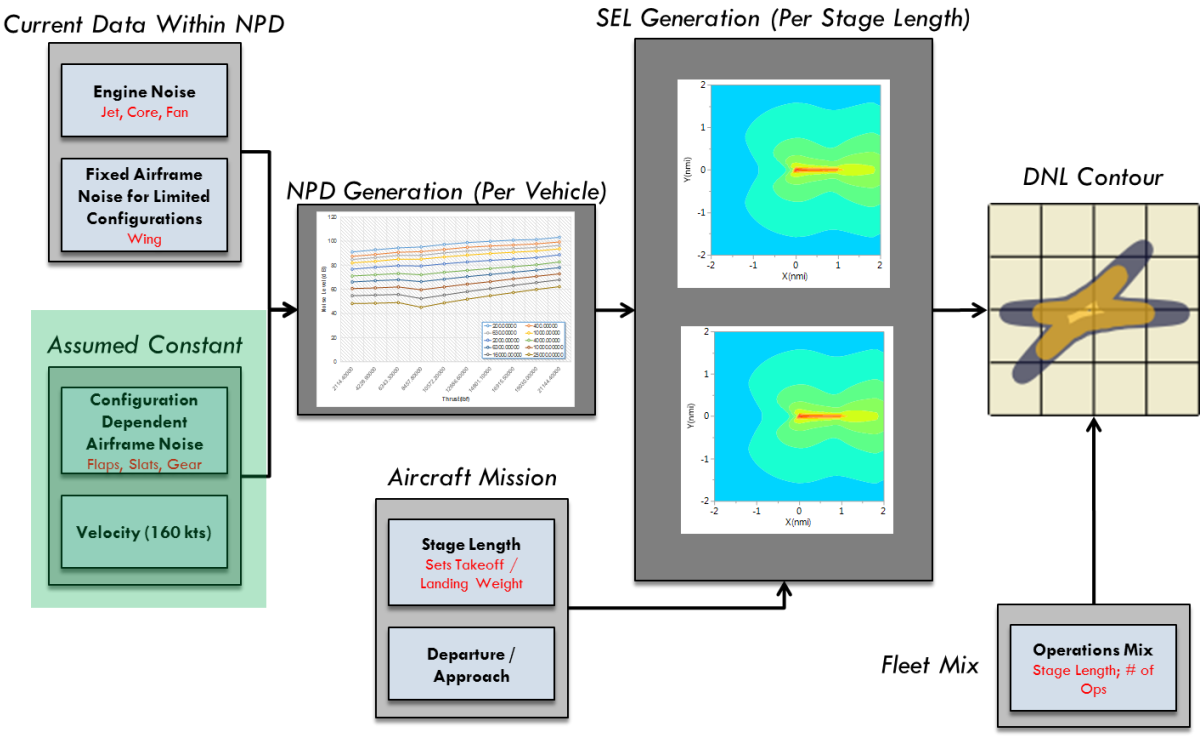

Figure 1. Noise contour analysis process

It is evident from the described approach that the final noise signature computed relies significantly on the physics based corrections present in the algorithm. Furthermore, a high-fidelity analysis of missions considerably deviating from the baseline procedures becomes strenuous. Consequently, the Georgia Tech team pursued two main objectives:

- Understand the sensitivity of including aircraft configuration changes and speed in NPDs, developing thus NPD+Cs on resulting noise contours
- Provide physics-based recommendations on format of NPD + Configuration (NPD+C) curves for use in AEDT

The research is broken down into three distinct phases. First, a sensitivity study is performed on the generation of NPDs to understand the dimensions required to accurately assess each vehicle class. This step is detailed within the Task 1 section of the report. The second step is to generate the NPD+Cs (superset of 12 NPDs) and research the impact of including aircraft configuration (gear and flap-slat settings) at a range of reference velocities (130 – 190 kts) on the resulting 80 dB SEL noise contour. In order to perform this task, a thorough understanding of the acoustic computation process within AEDT is obtained. AEDT's relevant algorithm sections regarding procedures, performance and acoustic analyses were modified to properly assess the input XML vehicles. The Task 2 section of the report details the process, modifications of the adjustments to the source algorithm. The AEDT NPD+C studies section includes results and analyses. The last phase, the Task 3 section, highlights the steps taken to validate Georgia Tech's approach and confirm the reproducibility of results. Furthermore, the analysis provides an intuitive understanding of each segment's contribution to the total noise contour shape.

Task #1: Perform Sensitivity Study on NPD+C Curve Generation and Prediction

Georgia Institute of Technology

Objectives

The first task of this study is to determine which airframe configuration parameters to include in the subsequent sensitivity analysis. It is possible to consider contour area sensitivity with respect to gear setting (up or down), speed, flap angle, and slat angle. Statistical analysis is performed with respect to each of these parameters to determine the appropriate resolution required in each dimension when constructing the NPD+C. Reduction of resolution is desirable since this will be less computationally expensive and will ultimately require fewer experimental runs if this information is to be generated experimentally. In addition, each dimension (speed, flap angle, slat angle, gear up/down) will be analyzed to determine which parameters, if any, do not significantly contribute to the overall variability of the source noise characteristics.

Before sensitivity analyses can be performed, careful consideration must be given to determining appropriate methods for modeling the effects of configuration parameters on vehicle source noise. Typically, vehicle manufacturers experimentally generate Noise Power Distance (NPD) curves for each vehicle as part of the noise certification process. These NPD curves are then provided to AEDT to predict SEL contours. In this study, the effects of configuration parameters are modeled by extending traditional NPD data to include additional dimensions for configuration parameters. These expanded data sets will be referred to as Noise Power Distance plus Configuration (NPD+C) curves and will enable sensitivity analysis with respect to vehicle configuration. While NPD+Cs are a key enabler for noise power distance re-evaluation, manufacturers do not typically provide data in the form of an NPD+C. Due to the expense of experimental testing, limited experimental data is available beyond that which is required for official certification. Due to the absence of experimental or historical data, NPD+C data must be generated for this using physics-based computational modeling methods. NASA's ANOPP tool was used to generate configuration specific noise information. The specific procedures used to generate NPD+Cs in ANOPP are discussed in further detail in the following sections.

To accurately analyze a mission in AEDT, NPD+C information must be available for every point in the takeoff or landing trajectory. Whereas a normal NPD is applicable to all points in the departure or approach trajectories, since the configuration behind the NPD is fixed, the NPD+C is speed and configuration dependent. This means that there is conceivably a NPD+C unique to every segment in the trajectory. To generate these unique NPD+C signatures, it is possible to use ANOPP to generate NPD+C data for each point in the AEDT trajectory. While this method is more accurate when considering a few standard mission profiles, it lacks generality. Any time a new mission is considered, a new set of NPD+Cs would have to be generated for each segment, which can be time consuming and computationally expensive. Furthermore, the cost of experimentally obtaining enough NPD information to analyze any arbitrary mission profile may be cost prohibitive for manufacturers. Therefore, the NPD+Cs must be generated in a way that is general enough to be applicable to a variety of mission profiles while minimizing the information that must be obtained from either experimental data or modeling and simulation tools. To achieve this, NPD+Cs will be generated using a polynomial interpolate model with respect to each configuration dimension (flap/slat, gear setting, and speed). Once it is determined which of these dimensions are to be considered, a sensitivity analysis is conducted to determine the regression order to

be used and the number of model fit points necessary to accurately predict noise levels with respect to each configuration dimension. AEDT is then modified to perform this interpolation prior to its analysis based on a superset of NPD+C data generated from ANOPP. This method is advantageous because it can be applied to any mission profile or parameters so long as the settings lie within the ranges of data generated for the interpolate model. Moreover, by performing a sensitivity analysis to determine the appropriate polynomial orders and grid densities for each dimension, it is possible to minimize the number of model fit points that are required to generate the interpolate model, which will reduce computational cost and/or experimental effort.

Research Approach

ANOPP NPD Generation

The first phase of research for this task is to generate the vehicle-level NPD curves using non-standard configurations for various vehicle class models. Georgia Tech used NASA's Aircraft Noise Prediction Program (ANOPP) to simulate the noise generated by individual sources on board the aircraft. ANOPP has the capability to generate NPD tables (which can be plotted to produce NPD curves) for a specific aircraft model. NPD tables include four noise metrics (as a function of power setting and altitude): sound exposure level (SEL); effective perceived noise level (EPNL); maximum A-weighted sound pressure level (max SPL); and maximum tone-corrected perceived noise level (max PNLT). The input variables in the NPD prediction method include airframe geometry, engine geometry and performance, aerodynamic performance, flight path and configuration parameters.

AEDT currently requires specific standard settings for NPD generation. As a result, ANOPP's NPD prediction module has corresponding pre-set defaults for many of the flight path and configuration parameters. It is necessary to alter ANOPP to account for non-standard configuration settings. This includes flap deployment angle, slat deployment angle, landing gear setting, and flight velocity. Flap/slat deployment angles and landing gear settings are classified as configuration parameters while aircraft flight velocity is a flight path parameter. However, for the sake of simplicity, flight velocity will also be referred to as a configuration parameter in this report. This is required because as the flight velocity changes, the source noise levels will also change drastically. Once the parameters to be altered are identified in the ANOPP model, a new set of flight path library files must be generated for each configuration (using a separate ANOPP module). These flight path library files are then used by source prediction and propagation modules that comprise the rest of the ANOPP model to generate NPD curves for the aircraft. This process is repeated for each distinct configuration of the aircraft model used in the sensitivity analysis. The results of the sensitivity analysis will then determine the number of executions of ANOPP are necessary for the NPD superset generation for each vehicle class being assessed.

NPD Sensitivity Analysis

A sensitivity analysis was performed to determine the effect that each configuration parameter has on the sound exposure level (SEL) generated by the vehicle at a given distance and thrust setting. This study is repeated for EPNL and max PNLT, showing similar results. To perform the sensitivity analysis, ANOPP was used to generate NPD curves for the 150 passenger class (150pax) vehicle model by sweeping through a range of flap angles, slat angles and speeds for both the gear up and gear down configurations. The 150pax model is used as the baseline vehicle to indicate sensitivity to these factors because the model has gone through extensive calibration and verification in previous studies to emulate the performance a Boeing 737-800. It is important to note that a sensitivity analysis of each vehicle can be time consuming due to program set up and run times; however, the trends are expected to be similar across different vehicle size classes. These results will be used to infer sensitivity of SEL to configuration parameters for other vehicle size classes.

Ultimately, ANOPP data will be used to interpolate noise level with respect to configuration parameters. To avoid extrapolation, the maximum possible ranges of each configuration parameter are considered.

Table 1. Variable ranges for sensitivity analysis

Variable	Min	Baseline	Max	Units
Flap angle	0	15	30	deg
Slat angle	0	10	30	deg
Speed	130	160	200	kts

Table 1 shows the ranges of values considered for each configuration parameter. It is important to note that the flap and slat angle values tested in this study correspond to the actual angles of the devices on the vehicle, not the flap setting that a pilot sets. The mapping of flap setting set by the pilot to the actual flap and slat angle of the vehicle is vehicle dependent and not relevant to the goal of this study, but could be included in future work. Each variable sweep is performed individually with other remaining parameters held fixed at their baseline values. Flap angles are modified in 5 degree increments while speed is varied in ~12 knot increments. It was ultimately determined that flap angle and speed are the dominant variables.

NPD Superset Generation

When performing analysis in AEDT, a superset of NPD+C curves will be imported that comprise of a set of NPD curves, one each for a different vehicle configuration, including speed. Each vehicle configuration has its own NPD curve that can be used to interpolate noise level based on distance and thrust setting (as AEDT does already). By considering configuration, multiple dimensions are being added to the noise model and AEDT must be able to interpolate noise with respect to each of these dimensions. The solution to this problem is to generate a grid of NPD curves, or superset, which contains enough points needed to interpolate with respect to each configuration dimension. These curve fits are then evaluated to interpolate noise level along each dimension. A study was performed to determine the appropriate order of interpolation in each dimension and the appropriate number of points needed to produce these curves.

After running the study the appropriate dimensions for configuration parameters are to be accounted for in AEDT analysis by importing a superset of NPD relationships that vary in each new dimension. Flap angle is accounted for by importing 3 sets of NPD curves at 3 flap settings at each set of parameters and interpolating between them using parabolic fits. Speed is accounted for by importing two NPD curves for each set of parameters and linearly interpolating between them. Each case will also need to be run for gear up and gear down cases. The result is 12 NPD curves (3 flap settings x 2 speed settings x 2 gear settings) that must be imported into AEDT to fully map the space of configuration parameters.

Table 2. NPD+C superset values for 150 passenger class

Run	Gear	Speed (kts)	Flap (deg)
1	Up	130	0
2	Up	130	15
3	Up	130	40
4	Up	190	0
5	Up	190	15
6	Up	190	40
7	Down	130	0
8	Down	130	15
9	Down	130	40
10	Down	190	0
11	Down	190	15
12	Down	190	40

Table 2 shows a breakdown of the 12 NPD simulations that must be run in ANOPP, compiled into an NPD+C, and then imported into AEDT. It is important to note that while particular values and ranges may change from vehicle to vehicle, it is expected that the same interpolation method should be valid for each vehicle in the fleet. The 150pax class model provides a valuable case study due to the availability of calibration and verification data from previous studies that can be used to validate the method. Now that the method has been validated, the next step is to apply it to all other vehicle size classes.

Task #2: NPD+C Generation, AEDT Modifications and SEL Sensitivity Study

Georgia Institute of Technology

Objectives

With the ANOPP NPD+C's superset-generation-procedure completed, the team at Georgia Tech used it and EDS to generate the input vehicles with the respective NPD+C curves for different aircraft size classes. **Table 3** lists the EDS vehicles that have been used in the analysis. NPD+C curves are generated for vehicles in each size class to ensure the resulting format is appropriate and representative across the fleet. GT and the FAA coordinated on the appropriate vehicles of interest to carry forward in the research. EDS and ANOPP are used to parametrically vary vehicle low-speed configuration, speed, and ambient conditions. The outcome of this parametric study is a series of NPD curves that represent varying configurations, speeds, and ambient conditions. A sensitivity study is performed to identify the quantitative impact of changing vehicle characteristics on both the resulting NPD and on the resulting fleet noise. Finally, the results of the sensitivity study are used to recommend a format for the NPD+C tables. The format includes both the additional parameters that should be included (i.e., flap angle, gear setting, vehicle speed), and the number of additional conditions at which NPD data must be provided (e.g., 3 coupled flap/slat settings and 2 flight speeds). The outcome of Task 2 is a detailed comparison of differences in predicted noise when using the AEDT database NPDs, EDS baseline vehicle NPDs, and the NPD+C curves generated in this task.

To perform the analysis, a detailed research of AEDT acoustic process and source code was required. The Task 2 section synthesizes the solution modifications for NPD+C implementation. Several approaches were considered in integrating the capability to assess multidimensional noise power distance curves. This process is explained in the Task 2 section., which also contains more detail about the types of different analysis performed. Study I contained the main effect analysis; study II was performed to analyze the impacts of cross term effects, and study IV researches the impact of adding more accurate approach and departure procedures for all of the discussed dimensions.

Table 3: Existing EDS baseline vehicles

AIRCRAFT SIZE	EDS REPRESENTATIVE AIRCRAFT
50 PAX	CRJ900
100 PAX	737-700
150 PAX	737-800
210 PAX	767-300ER
300 PAX	777-200ER
400 PAX	747-400

Research Approach

Including the vehicle's varying low-speed configuration and reference velocity for the complete flight will lead to differences in predicted contour area. In order to generate these contours to evaluate the impact of aircraft configuration on contour area, representative NPD+C curves are required. These curves are acquired through an interpolation of the NPD supersets, which are described in more detail in the Task 1 section of the report. For the first iteration, each superset contains a grid of NPDs for a combination of the three following parameters: coupled flap and slat setting (0°, 15°, & 40°); aircraft airspeed (133.35 knots & 190 knots); and gear setting (up & down). Furthermore, each individual NPD superset, from the 12 simulated in ANOPP, is composed of 12 NPD curves. A curve describes the uncorrected noise metric (SEL or LAmax) for a specified slant distance for increasing thrust settings. Figure 2 depicts a notional NPD supersets library. The NPD superset is collectively referred to as an NPD+C.

For the computation of an SEL grid, AEDT currently assumes a fixed reference speed of 160 knots and flight trajectory information that is discretized into segments. The segment's data can be expanded to include instantaneous reference speed and the vehicle's configuration. By increasing the data used in the acoustic computation algorithm, an interpolated NPD (NPD+C) is obtained corresponding to a higher fidelity description of the segmented vehicle parameters. This description is to be propagated in AEDT to appropriately obtain the noise characteristics for the complete flight envelope.

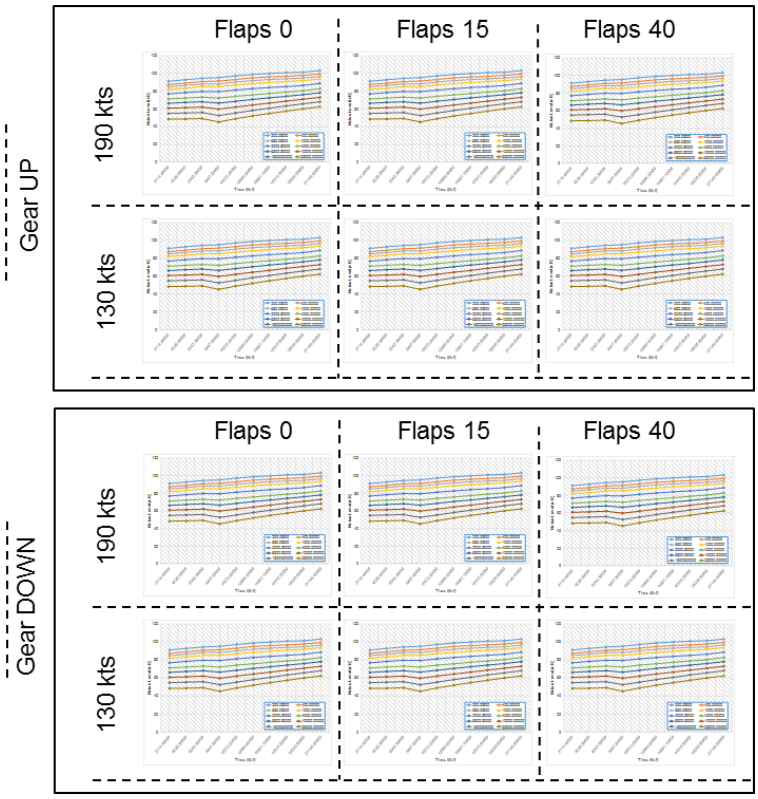

Figure 2. In-house developed NPD supersets library

NPD+C Integration Approaches with AEDT

In order to integrate the NPD+C supersets into AEDT, three approaches were initially considered. The first option involved running each NPD from the superset one-at-a-time through the AEDT algorithm in order to extract the custom noise metric results describing the flight procedure. This method was discarded due to the prohibitive computational expense incurred for a fleet of vehicles. A normal procedure result for a single aircraft is computed on the order of minutes. An analysis including 12 different combinations of a vehicle configuration and reference speed amounts for several hours in a fleet analysis. Furthermore, by following this process, a more intensive modification of the source code would be required because segment-to-segment information would need to be post-processed. The parameters required to properly assess the noise adjustments would complicate the procedure as each computation would include its native configurations and reference velocities.

A variation to this approach requiring the analysis of all the NPD supersets was deliberated as well. In this case, the custom SEL grid was to be used in the ANGIM tool available to Georgia Tech in order to superimpose the necessary segmented grids to portray the mission. This methodology suffered from the same weaknesses as the aforementioned practice. Figure 3 further portrays the discarded methods. It is important to note that Figure 3 does not reflect the NPD's currently used. Slat angle and flap angle were found to be correlated in the algorithm and are considered in the same vehicle configuration.

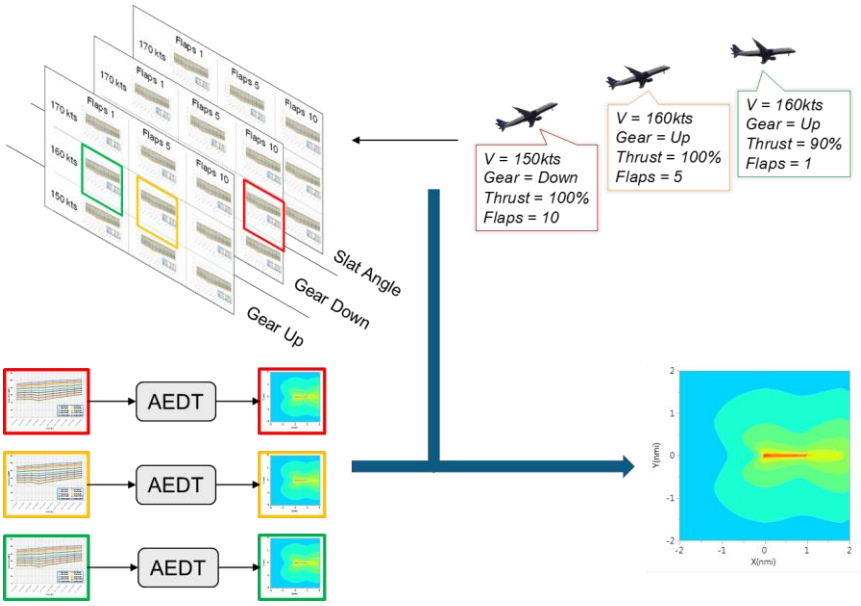

Figure 3. Discarded methods for the integration of the NPD library

The third, and subsequently selected, approach was to assemble a custom NPD+C representing the flight procedure input to AEDT. This approach uses vehicle flight segment and trajectory information (velocity, configuration) to interpolate amongst the 12 NPD+C input curves. In this approach a single NPD is essentially created for each segment that contains a noise signature specific to the vehicle configuration and velocity at that segment. The segment-to-segment part of the acoustic computation process is then expanded to contain an interpolation algorithm for each specific point required within the 12 NPD supersets. The detailed process description is available upon request from the authors. Using this approach does not increase the computational expense as significantly as the two other solutions considered. The required alterations to AEDT's source code, even though significant, are considered to have less potential alterations and be more computationally efficient due to the potential inclusion of the interpolation algorithm within the segmented information. The parameters describing the mission profile are available, and the NPD+C interpolation of the LAMAX and SEL metrics need to be computed only once through the profile (for the initial grid point considered) and are then utilized for the complete grid. Modifications were made within AEDT to read in the higher fidelity NPD+C data. A description of these modifications is available upon request from the authors.

AEDT NPD+C Studies

Dimension specific procedures

With the interpolation scheme implemented in AEDT and the superset of NPD+C data generated using ANOPP, the modified version of AEDT is used to analyze the effects of configuration on noise contours. For each vehicle, 80 dB SEL contours are generated and compared to those generated from the unmodified version of AEDT using the baseline vehicle configuration.

Table 4. Study I & II

Grouping	Study	Parameters
Baseline	0	Baseline NPD
Main Effects	I.A	Include only reference speed
	I.B	Include only flaps-slats setting
	I.C	Include only gear setting
Cross Terms	II.A	Speed + Gear
	II.B	Speed + Flaps
	II.C	Gear + Flaps
	II.D	Speed + Gear + Flaps

Table 4 outlines the sensitivity analyses to be performed in this study. Currently, NPD data only contains the ability to predict aircraft SEL as a function of engine power and aircraft distance. NPD+C data now adds the capability to predict aircraft noise as a function of flap angle, speed, and gear setting. Sensitivity analyses must be performed to determine which of these configuration parameters has the most significant effect on contour area. This could influence future recommendations to OEMS about which dimensions should be included when gathering empirical data. In Study I, all aspects of the baseline vehicle are held constant except for NPD+C data in the dimension being studied. This allows the effect of each configuration parameter to be isolated and assessed. In Study II, multiple configuration parameters are allowed to vary in a single study. This is achieved by holding each aspect of the original baseline constant except for NPD+C data in the dimensions being studied. Study II is performed to reveal whether the interactions between multiple configuration dimensions are significant with respect to the main effects. Furthermore, by examining each possible combination of configuration parameters, it is possible to determine if any of the given parameters have a dominant effect on aircraft noise.

Table 5. Standard Configuration Parameters

Noise Curve Generation		*V_{ref}*	*Flaps/Slats*	*Gear Setting*
Baseline	Approach	160 kts	15	Down
	Departure	160kts	15	Up
NPD+C	Approach	130 - 190 kts	0 → 15	Up → Down
	Departure	130 - 190kts	5 → 1 → 0	Down → Up

Table 5 shows the configuration that is used for both the baseline vehicle and the NPD+C vehicle during standard approach and departure procedures. The 80 dB SEL contour for each sensitivity study is compared to the baseline to graphically show the effects that changes in NPD data have on contour size and shape. Furthermore, the area, length, and maximum width of the contours are computed and compared to quantify NPD+C effects. A standard mission profile is performed for each study. This eliminates variability in contour dimensions due to mission profile variations to isolate the effects of NPD data. The speed, distance, and flap angle of the vehicle at each segment is computed by AEDT based on standard approach and departure procedures. In this study, landing gear considered to be deployed when flaps are deployed and retracted when flaps are retracted.

Before generating contours accounting for variations in each configuration dimension, it is of interest to analyze the effect of each configuration dimension individually. Isolating each configuration parameter is important to determine the relative contribution each parameter makes to the overall variability of contour dimensions.

Table 6. Main Effect Study Parameters

Noise Curve Generation		*V_{ref}*	*Flap/Slat Setting*	*Gear Setting*
Speed Sensitivity	Approach	130-190 kts	15	Down
	Departure	130-190 kts	15	Up
Flap Sensitivity	Approach	160 kts	0 → 15	Down
	Departure	160 kts	5 → 1 → 0	Up
Gear Sensitivity	Approach	160 kts	15	Up → Down
	Departure	160 kts	15	Down → Up

Table 6 shows the vehicle configurations for the main effect sensitivity analyses. The goal of these studies is to isolate the effects of each configuration variable individually. In speed sensitivity study, NPD data is only changed as speed changes during the mission profile. NPD data is interpolated for speeds between 130 and 190 kts with zero velocity correction. For speeds above below 130 kts or above 190 kts, velocity corrections are applied as previously described. Flap and gear settings are kept identical to the baseline in the speed sensitivity. Likewise, in the flap sensitivity, NPD data is only allowed to change when flaps are deployed or retracted in the mission profile. NPD data is interpolated from ANOPP data at flaps 0, 15, and 40 as described previously. Speed and gear settings are kept identical to the baseline configuration in the flap sensitivity. Finally, in the gear setting, NPD data only changes when landing gears are deployed or retracted during the mission. Speed and flap settings are kept identical to the baseline configuration in the gear sensitivity.

Table 7. Cross-Effect Study Parameters

Noise Curve Generation		*V_{ref}*	*Flap/Slat Setting*	*Gear Setting*
Speed + Gear	Approach	130-190 kts	15	Up → Down
	Departure	130-190 kts	15	Down → Up
Speed + Flap	Approach	130-190 kts	0 → 15	Down
	Departure	130-190 kts	5 → 1 → 0	Up
Flap + Gear	Approach	160 kts	0 → 15	Up → Down
	Departure	160 kts	5 → 1 → 0	Down → Up
Speed + Flap + Gear	Approach	130-190 kts	0 → 15	Up → Down
	Departure	130-190 kts	5 → 1 → 0	Down → Up

Once the main effect studies are performed, sensitivity analysis are conducted using each possible combination of variation using each of the three configuration parameters. Table 7 shows all combinations that are analyzed with the respective configuration parameter ranges. These cross-term studies are of particular interest since they allow the relative significance of each configuration parameter to be directly quantified. By comparing the results of the cross-term studies with the main effect studies, it is possible to identify which configuration variables make the most significant contribution to the overall variability of contour dimensions.

Finally, once sensitivity analyses are performed for each combination of configuration parameters, modifications are made to the flap/slat settings in the mission profile. Table 7 shows the modified flap/slat settings during the profile that are to be examined. It is important to note that no changes are made to aerodynamic performance in AEDT; only the noise related to flap/slat setting pertaining to source noise prediction is changed. This allows the mission profile to remain constant so that only changes in NPD data are considered. Changing the flap setting causes the modified version of AEDT to interpolate new NPDs based on ANOPP generated data, which does account for variations in flap lift coefficients as flap setting changes as described previously.

The following analysis is performed for each vehicle in each proposed study. Both approach and departure operations are considered. The process enables the build-up analysis of the given total SEL for the relevant segment and grid-point pair,

- Output graphs of ground track, velocity profile, trajectory, thrust profile, and 80 dB SEL segment contours (representative of 65 DNL contours) are obtained.
- SEL & LAMAX NPD curves are shown for both the baseline, and the NPD+C cases.
- Velocity correction, noise fraction, and interpolated SEL & LAMAX dB values are calculated for each segment, and each grid-point.
- Normalized noise power contribution of each segment to the relevant grid point is computed.

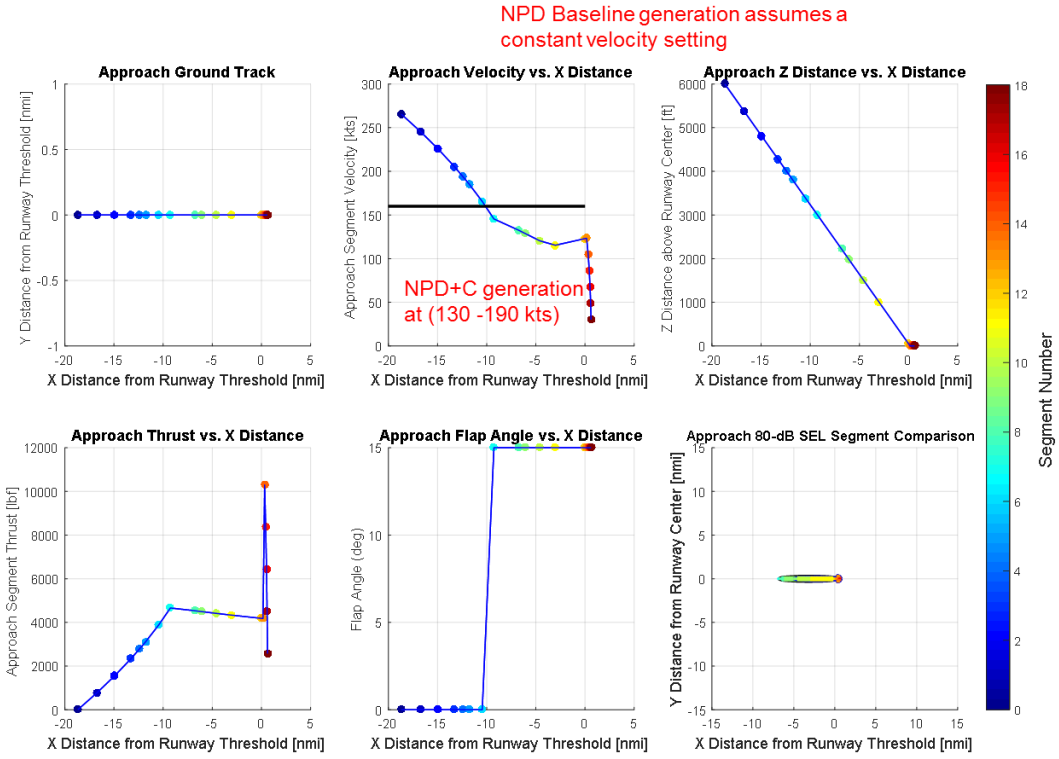

Figure 4. Vehicle specific analysis 100 PAX, I.A - 1

The contour shown is expanded upon, to clearly see the differences between the baseline and the main effect of speed for the case of Figure 4. Once the major differences in the contour are associated to the maximum contributing segment of the aircraft's flight procedure, Figure 5 is plotted. It is important to note that the representative figures shown for this section correspond to the analysis of including a range of speeds (130 kts – 190 kts) as a main effect, for the 100-passenger class vehicle. This example shows the complete procedure and analysis performed for each study and each specific aircraft. Any vehicle-study could have been chosen as an example (all the material shown in this section is available for all of the classes); however, the 100 PAX main effect analysis allows the reader to follow the effect with relative ease.

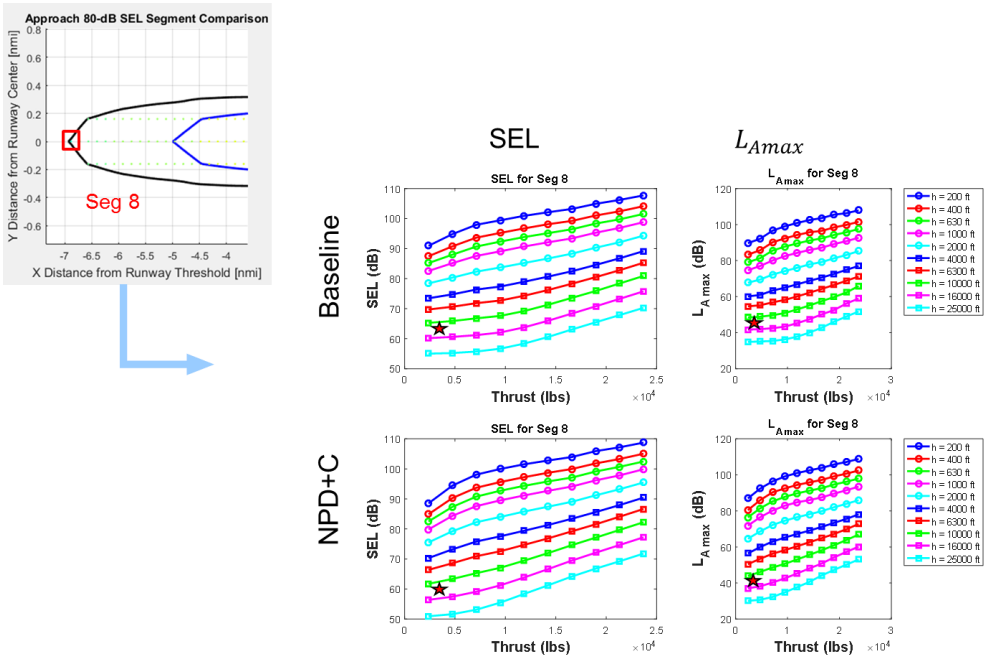

Figure 5. Vehicle specific analysis 100 PAX, I.A -2

With this information at hand, three grid points are studied for a higher fidelity analysis in order to understand the trends. Figure 6 depicts the contribution of the grid points located at the maximum difference between the baseline and the sensitivity contours. The ANOPP generated metrics, which are interpolated for both the NPD+C and the baseline, are tabulated with a corresponding velocity correction (duration adjustment) and noise fraction for the flown segment.

(X = -7.04 nmi, Y = 0 nmi, seg 8)

	Baseline	NPD+C
Distance (ft)	13842	13842
Thrust (lbs)	4651	4651
NPD Value (SEL dB)	62.2	59.2
LA max (dB)	44.1	40.6
Noise Fraction	0.787	0.828
Velocity Correction	0.6055	0
Contour Area (nmi^2)	4.0134	2.2715
Total SEL	79.88	77.76

(X = -6.88 nmi, Y = 0 nmi, seg 8)

	Baseline	NPD+C
Distance (ft)	14793	14793
Thrust (lbs)	4651	4651
NPD Value (SEL dB)	61.5	58.4
LA max (dB)	43.1	39.5
Noise Fraction	0.577	0.594
Velocity Correction	0.6055	0
Contour Area (nmi^2)	4.0134	2.2715
Total SEL	80.05	77.84

(X = -6.72 nmi, Y = 0 nmi, seg 9)

	Baseline	NPD+C
Distance (ft)	2292	2292
Thrust (lbs)	4527	4527
NPD Value (SEL dB)	79.1	77.3
LA max (dB)	67.7	66.2
Noise Fraction	0.646	0.709
Velocity Correction	0.8695	0
Contour Area (nmi^2)	4.0134	2.2715
Total SEL	80.31	77.98

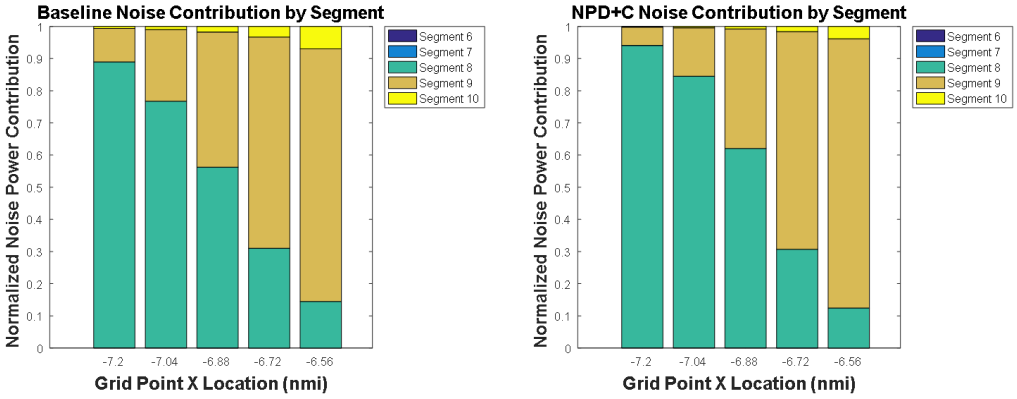

Figure 6. Vehicle Specific Analysis 100 PAX, I.A – 3

The method allows for a detailed research of the effects of including each dimension by itself (Study I), or a combination of expanded dimensions (Study II) and their combined impact on the noise contour created for the single runway analyzed.

A detailed research of the 100 PAX aircraft at an approach procedure, shows that the smaller contour generated by the AEDT NPD+C is explained by a combination of the velocity corrections and the noise metrics obtained at a lower reference velocity. The SEL and LAMAX values used for the interpolation correspond (in the case of the most contributing segment) to a velocity of 145.47 kts. It is evident that they will consequently yield lower noise results. Segment 7 for the specific case contributes to approximately 80% of the total SEL metric at the studied grid-points.

The aforementioned approach was taken for all vehicle sizes and studies. Figures **Figure 7** 8, & 9 depict the result for a departure operation for the same representative vehicle (100 PAX). The AEDT NPD+C Studies section analyzes the full results.

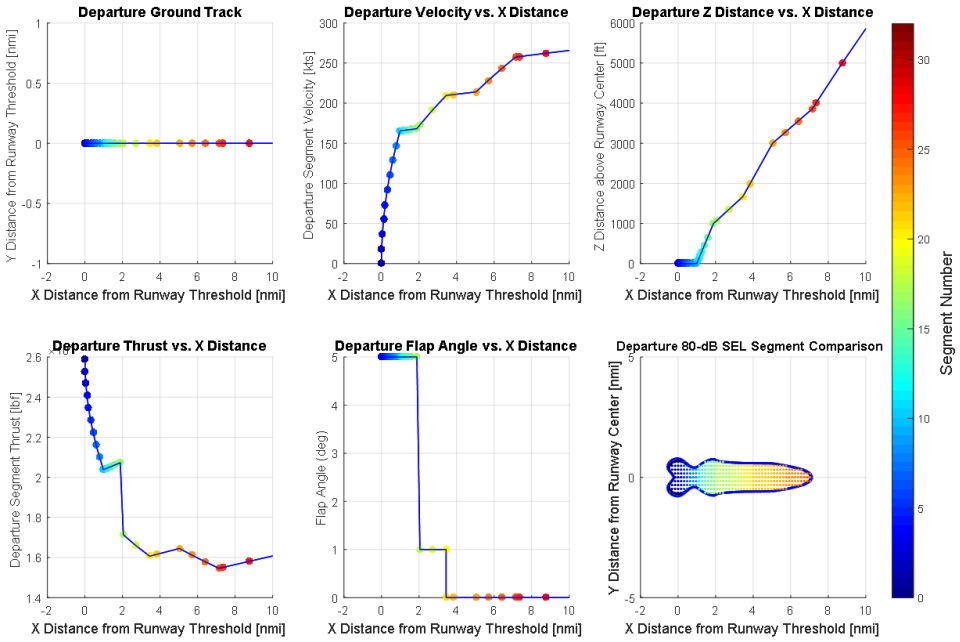

Figure 7. Departure trajectory - zoomed in

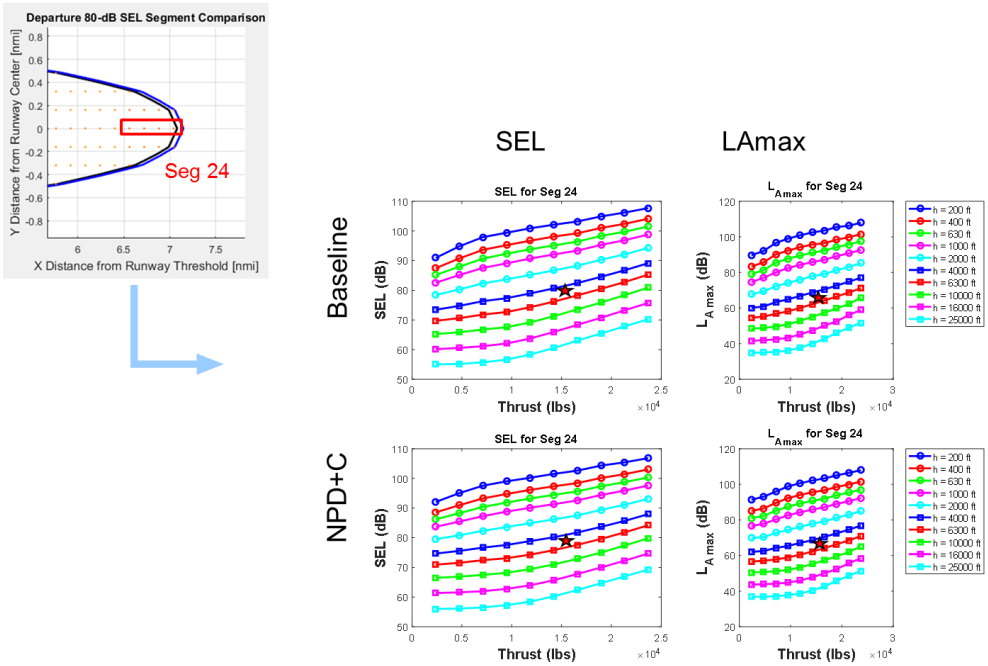

Figure 8. Segment NPD+C vs. NPD data

(X = 6.88 nmi, Y = 0 nmi)

	Baseline	NPD+C
Distance (ft)	4610	4610
Thrust (lbs)	15793	15793
NPD Value (SEL dB)	80.5	79.9
LA max (dB)	68	67.9
Noise Fraction	0.777	0.760
Velocity Correction	-1.9436	-1.2065
Contour Area (nmi^2)	8.1854	8.5523
Total SEL	80.40	80.52

(X = 7.04 nmi, Y = 0 nmi)

	Baseline	NPD+C
Distance (ft)	5283	5283
Thrust (lbs)	15793	15793
NPD Value (SEL dB)	79.2	78.6
LA max (dB)	66.1	66
Noise Fraction	0.662	0.648
Velocity Correction	-1.9436	-1.2065
Contour Area (nmi^2)	8.1854	8.5523
Total SEL	80.08	80.20

(X = 7.20 nmi, Y = 0 nmi)

	Baseline	NPD+C
Distance (ft)	6038	6038
Thrust (lbs)	15793	15793
NPD Value (SEL dB)	78	77.4
LA max (dB)	64.2	64.1
Noise Fraction	0.452	0.450
Velocity Correction	-1.9436	-1.2065
Contour Area (nmi^2)	8.1854	8.5523
Total SEL	79.76	79.90

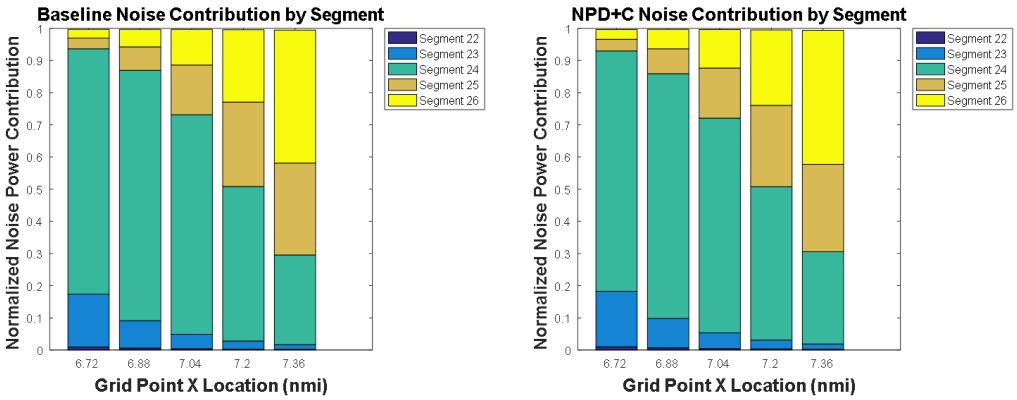

Figure 9. Analysis and noise contribution - 100 PAX I.A Departure

Main effects

Study I.A

As explained in the Dimension specific procedures section, the 100 PAX vehicle was chosen as an example because the reader is able to follow the analysis presented before encountering the effects of further increases in NPD dimensions. Any vehicle could have taken its place (the material, plots, and tables are available). For the case of the speed sensitivity analysis (I.A) presented in Table 4, the interpolated SEL & LAMAX NPD+C values are lower because of the lesser reference speed at which the aircraft noise metrics were acquired. Furthermore, the NPD baseline metrics generated at 160 kts are corrected (duration adjustment = +0.6049), while NPD+C generated metrics interpolated to the aircraft velocity of 145.47 kts at segment 7 have no correction applied. The velocity correction for this type of aircraft is found to have a significant contribution to the total SEL value differences. From the lower part of Figure 6, it is evident that the normalized noise contribution is larger for segment 7 in the NPD+C case, as the segment 8 noise metrics are obtained at a 132.93 kts reference velocity. For the 100 PAX in study I.A, it is concluded that the overall contour is smaller due to the effect of the velocity corrections and the lower noise metrics at the most contributing segments.

The contour area, length and width is plotted as a bar chart for the nominal results of the NPD+C case vs. the baseline outputs. With this information, the percent change is graphed for all of the case studies. Study I.A results -which researches the main effect of including speed as the expanded dimension for ranges 130 -190 kts- are depicted in Figure 16. Two interesting main trends are observed: first, the percent change in area is negative, then, there is a linear trend from the smaller sized vehicles to the largest.

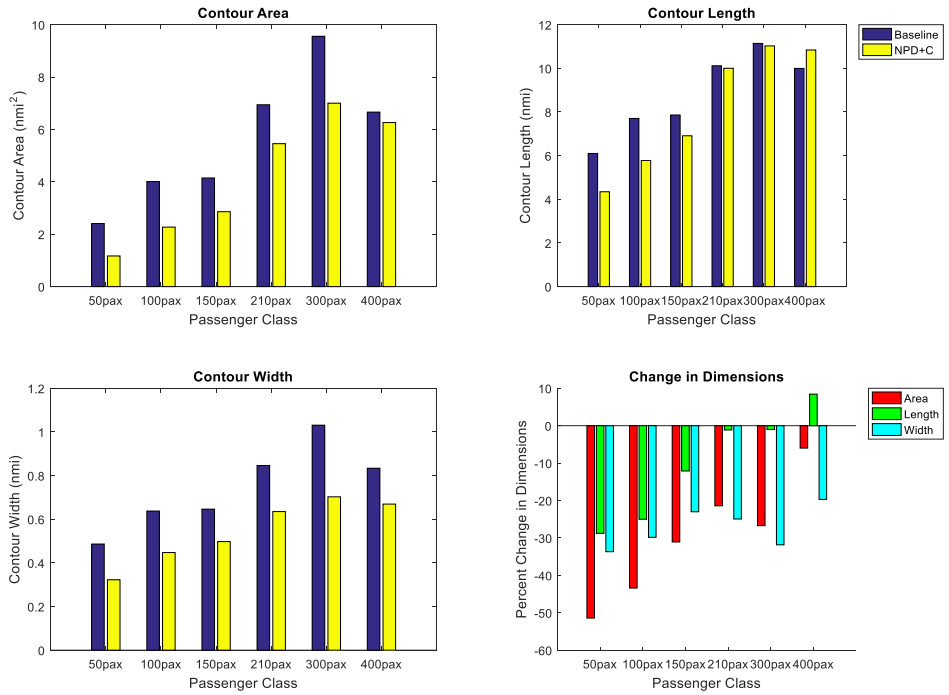

Figure 10. Study I.A Approach

As explained at the beginning of the current section, the duration adjustment has a large effect when including the speed dimension. This correction will either be negative if the reference velocity is higher than 190 kts, or positive should it be less than 130 kts. No correction is applied if the reference speed, during the operation, falls within the interpolation ranges as noise data is directly obtained within the bounds. This computation is explained physically by the fact that when the aircraft flies a given segment in less time, the segment contributes less to the overall total noise metric; same is true vice versa. Another factor important for the research is that the noise metrics (SEL & LAMAX)

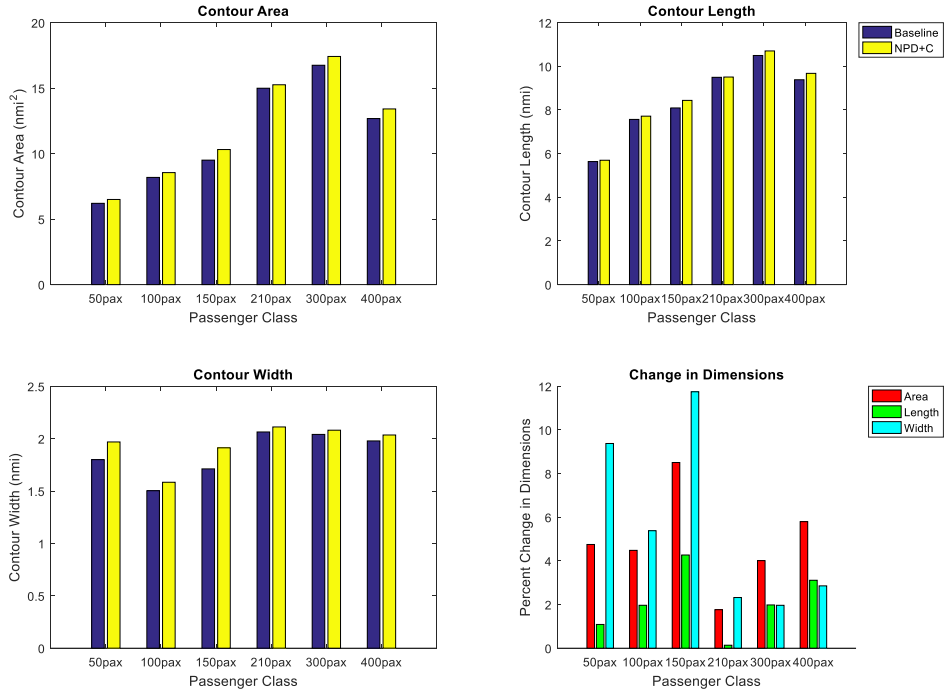

Figure 11. I.A Departure

In contrast to the approach procedure, departure operations present smaller change in magnitude between vehicles as the jet source noise has the largest effect on the contours. Figure 11 researches the effect of including the aircraft speed in the NPD+C AEDT output noise contour. The noise power distance curves have been obtained for constantly higher reference speeds thus increasing the total SEL value for each of the grid points.

Study I.B

Study I.B researches the impact of including control surfaces as part of the noise signature. For this case, the flap-slat combination setting (AEDT treats both settings in the same dimension) follows the procedure the aircraft is flying at approach and departure. As explained in the Task 1 section, the baseline noise SEL and LAMAX noise metrics are obtained at a flap-slat deflection of 15 ° with a constant reference speed of 160 knots. Study I.B interpolates from the superset of 12 NPD+Cs to obtain a metric specific to the flight procedure. At approach the mission follows a clean configuration to a deflection of 15 degrees; whilst on departure, the initial flap-slat configuration is set to 5°, which is then retracted to 1° during rotation, following a clean configuration for the rest of the procedure.

The results for the analysis match what's expected (explained further in detail below) from the understanding of the effect of control surface interference with the airflow. The sound exposure levels associated with a more/less deflected state, increase/decrease respectively as sound pressure levels change appropriately. The output noise contours for all of the vehicles during approach (Figure 21 top) now includes metrics corresponding to a descending clean configuration for the initial 7 segments of the path (on average). The percentage change is more pronounced for the 400 PAX because

it includes double-slotted, double-flap configuration. The percentage change in area associated with the departure profile (Figure 21, bottom) is rationalized with similar logic. The baseline NPDs correspond to a 15° deflection which are then corrected, whilst the SEL and LAMAX inputs to AEDT – for the current study - are associated to the 5, 1, 0 setting. The percentage change is less pronounced than in approach because the engine source noise dominates the trend. Figure 22 is plotted from the algorithm's results and graphically shows the differences between the NPD and NPD+C for the most contributing segments.

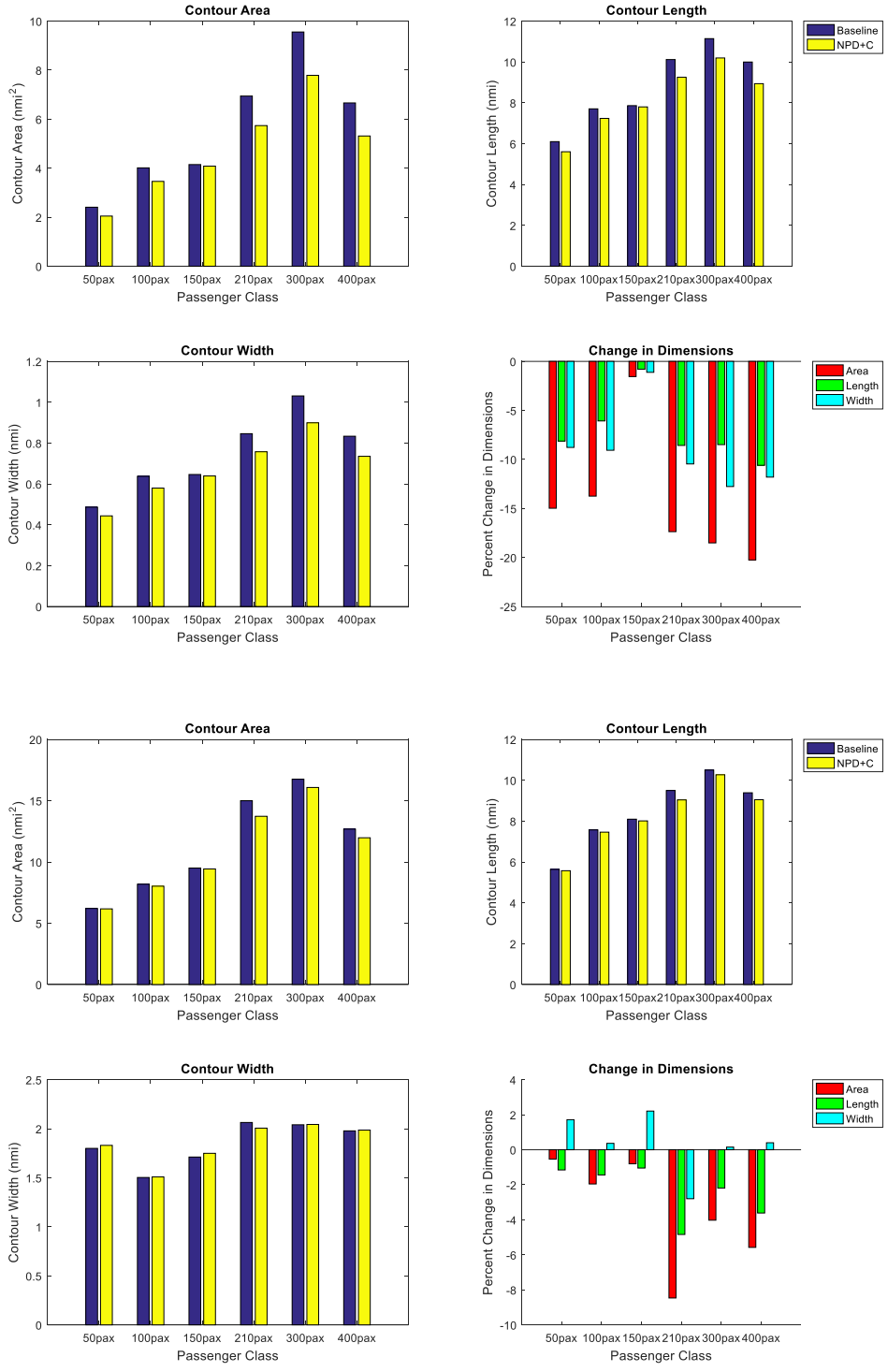

Figure 12. Study I.B Approach (Top) & Departure (Bottom) procedures

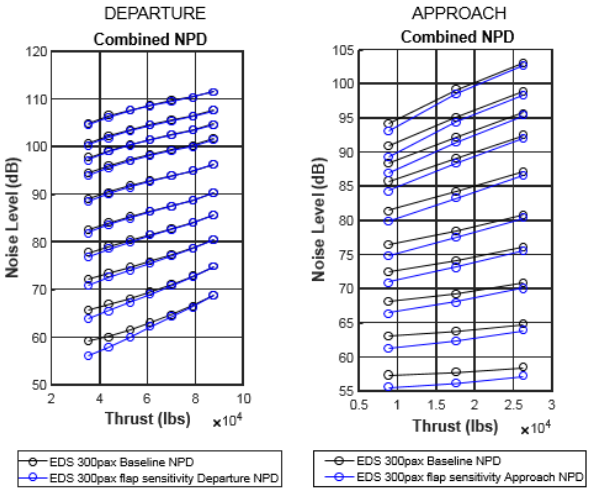

Figure 13. NPD vs. NPD+C most contributing segment. I.B

Study I.C

I.C researches the effect of including the gear setting as part of the NPD+C's interpolation procedure. The gear configuration includes two unique settings: gear-up and gear-down, which had to be defined in the acoustic computation process of AEDT as the initial source code did not include a parameter to analyze the differences with respect to this dimension. Gear-up is associated with a clean configuration and a flap-slat deflection of 1°, while the gear down setting is included to account for deflections at $5°, 10°, 15°, 30°$ & $40°$. Figure 14 & Figure 15 highlight the percentage change in dimensions for approach and departure respectively.

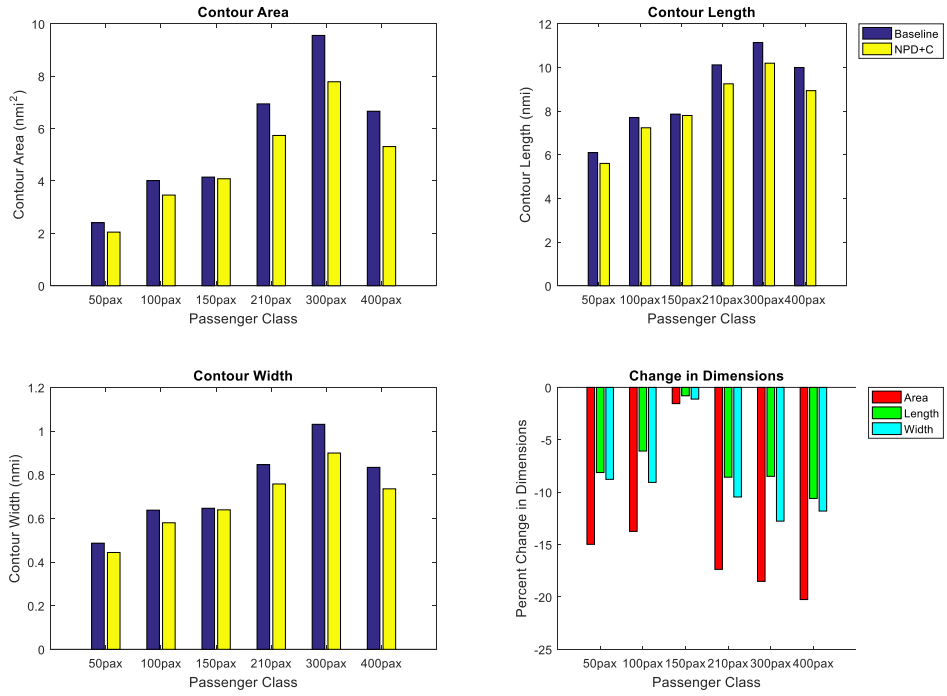

Figure 14. Study I.C Approach

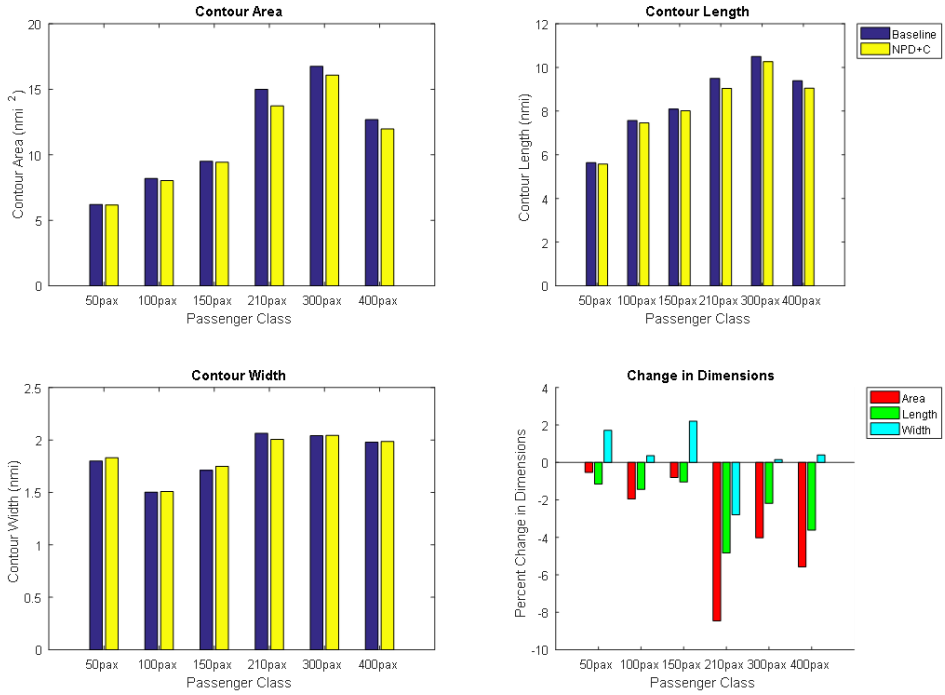

Figure 15. Study I.C Departure

By further analyzing the results, the Georgia Tech team observed that the percentage differences between including the flap setting or the gear setting as main effects were minimal for smaller sized vehicles during approach. This outcome is explained with the fact that for a single grid-point in the contour, the total SEL is computed by summing the noise exposure of the flown segments. There are, on average, 2 segments that contribute about 99% to the total SEL. In studies I.C, the smaller vehicle classes (50 – 100 – 150 PAX) had their respective total SEL maximum noise contribution from segments in which the parameters were equal (i.e. flap-slats at 15°, gear-down). The Pareto plot depicted in the Task 3 section, along with the vehicle-specific-impact (studies I & II) plots, and the detail research in the AEDT NPD+C Studies section of the report contain further detail.

$$E_{seg} = 10\text{^}\left[\frac{L_{E,NPD+C,ADJ} + NF_{ADJ} + DUR_{ADJ} - LA_{ADJ} + TR_{ADJ} + DIR_{ADJ}}{10}\right]$$

$$SEL = 10 * \log_{10}\left[\sum_{i=1}^{n_{seg}} E_{seg(i)}\right]$$

Cross-term combinations' impact

The AEDT NPD+ C Studies section provides the results and insights obtained from the investigation. Each study's main findings are explained after which summary plots are included following the same study order.

Study II.A

This research section analyzes the impact of including a combination of reference-speed-dimension-expansion and the finite gear setting. In order to properly analyze the impact of the combination, a comparison is performed against the results obtained from including the speed dimension only (I.A). There are two distinct behaviors between approach and departure procedures. At departure, the same logic applies as the one encountered in the comparison case. The jet source noise has the most significant impact on the noise signature. The higher reference speed range associated with the higher thrust setting yield larger values of the noise metrics acquired from the NPD+C (SEL & LAMAX). This factor overcomes the impact of the airflow noise created by the gear-down setting. The maximum contributing segments correspond to the same configuration between I.A and II.A, which is at a gear-down setting. The difference is minimal in this respect and the trend can be observed in yellow in Figure 16 which is provided as a reference for the percent area change between studies. In contrast, the approach procedure presents noticeable differences to I.A. The clean configuration for the initial segments, which is now adopted in the NPD+C interpolation yield a larger magnitude in percent reduction when juxtaposed to the baseline. The baseline approach procedure assumes a gear-down setting for all the segments. This is not the case in study II.A; therefore, the decrease in the 80-dB noise contour area matches the physical behavior. The complete results of study II are presented at the end of this section.

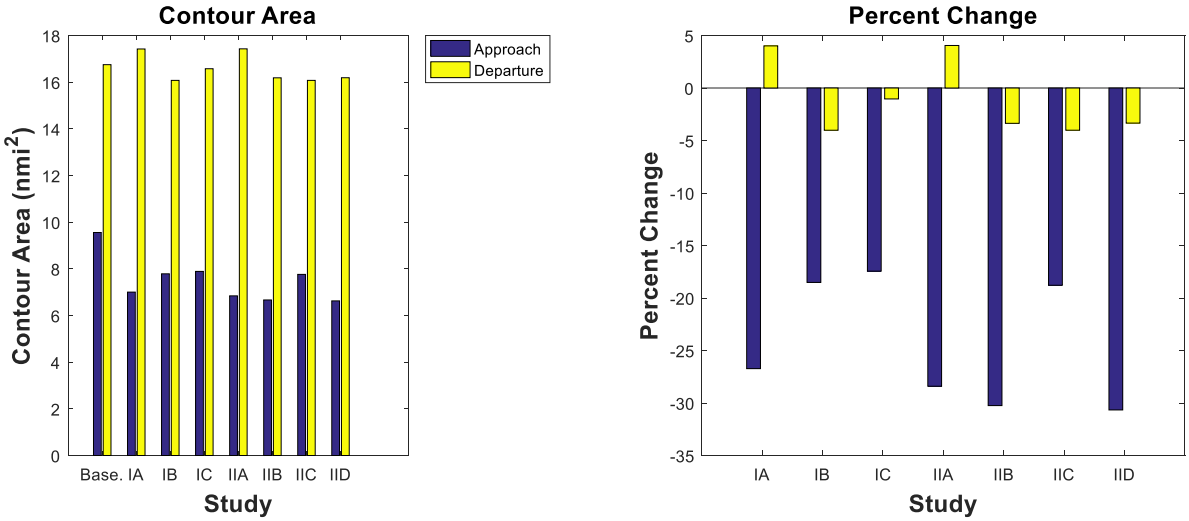

Figure 16. Aircraft-specific impact for studies I & II. 300 PAX

Study II.B

Having studied the effect of II.A, this research section analyzes the impact of including a combination of reference-speed-dimension-expansion and the flap-slat deflection. To follow the same line of analysis, the results are contrasted to the effect of including only speed as the extra-dimension, and to the previous study (II.A). Important to note is that by including the flap setting, the departure-operation noise-contour-change is now negative. This is expected, as in the baseline operation, the noise metrics are corrected from a flaps-slat deflection of 15°; whilst this is not the case for study II.B. The metrics are directly interpolated in AEDT NPD+C for the 5° → 1° → 0° settings. Nonetheless, the decrease of the contour is still less in magnitude than the effect observed during approach. This led the team to confirm that for departure paths, the effect of jet source noise dominates the response. Interestingly, by including the effect of speed with surfaces deflection instead of gear setting, a more substantial decrease in the total SEL contour is observed during approach (blue bars in Figure 16). Therefore, the effect of a 15-degree flap deflection is larger than a gear-down configuration in the AEDT algorithm. The vehicle specific studies are presented for all the aircrafts in the Task 2 section. The 300 PAX bar plot is shown as reference; however, there are slight differences in the trends encountered in each passenger class. The 50 – 100 – 150 PAX show insubstantial differences between studies II.A & II.B at approach. It is important to iterate that an exhaustive research of this tendency is given in the validation section (Task 3) of the report.

Study II.C
This research section analyzes the effect of an aircraft's variable configuration. The combination of flap-slat deflection with the gear setting provides a definition of the vehicle's configuration. I.B and I.C depict each dimension's impact by itself. It is interesting to note that the most substantial decreases for both the approach and departure procedures are accumulated in I.C. The reasoning behind the decrease lies in the procedure and surface interference with the airflow producing noise. This is explained in larger detail for the previous cases; thus, the reader is referred to those sections for the specifics of percentage area change with respect to each dimension. A salient feature form the study is that the combined effect of configuration settings is nonetheless less consequential than speed.

Study II.D
Study II.D is of essential importance to the goals specified in this research project. It is the initial study analyzing the complete effect of including the NPD+C superset while keeping trajectories constant with respect to the baseline. In II.D, the flap-slat deflection, gear setting, and reference speed, vary according to approach and/or departure. The specific procedures are explained further in detail in Task 2 section. With a validation and detail research of the results, the effect of changing trajectories within AEDT NPD+C to reflect more realist paths can be examined. Specific results for the 300 PAX study II.D are shown in Figure 17, Figure 18, and

Figure **19.**

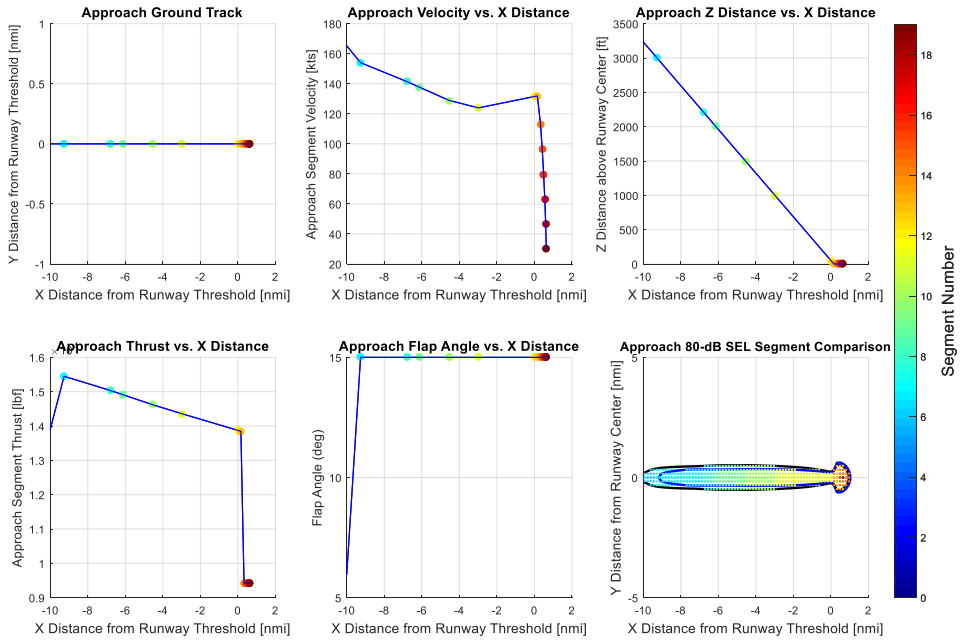

Figure 17. 300 PAX Study II.D – 1

The outcome of the modified AEDT which includes a NPD+C superset for all of the dimension follows the tendency expected as a result from all of the buildup-studies performed. It is evident that the speed impact is most substantial in the superset while keeping the trajectory constant with respect to the baseline. Both departure and approach procedure decrease in contour area magnitude, and a higher fidelity analysis with respect to the noise metrics acquired and the calculated corrections is performed.

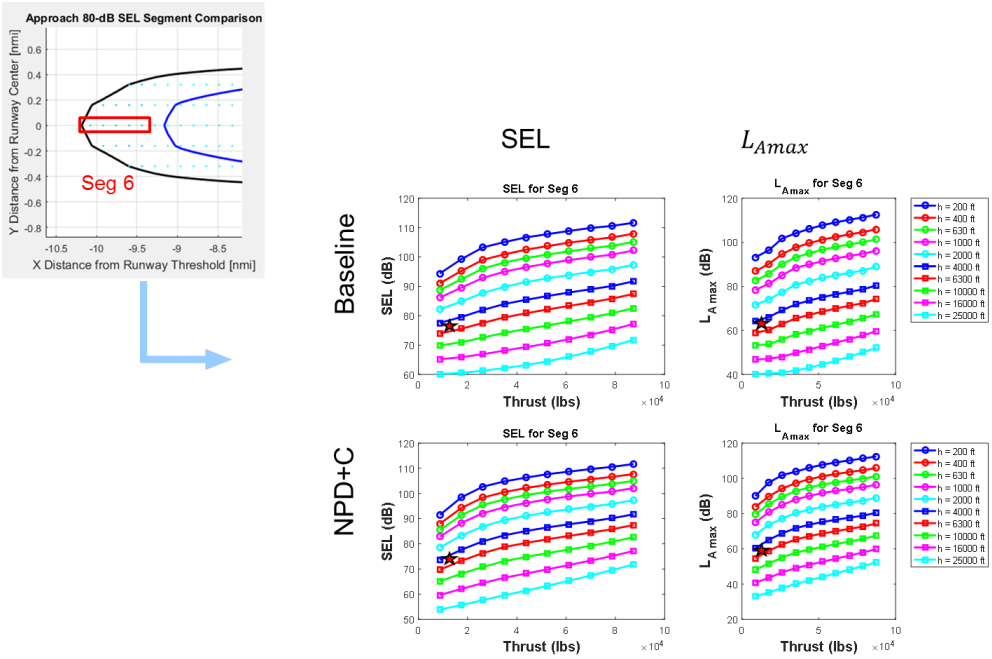

Figure 18. 300 PAX Study II.D – 2

(X = -10.24 nmi, Y = 0 nmi)

	Baseline	NPD+C
Distance (ft)	3706	3706
Thrust (lbs)	12875	12875
NPD Value (SEL dB)	79.1	76.1
LA max (dB)	66	63.5
Noise Fraction	0.760	0.788
Velocity Correction	-0.0895	0
Contour Area (nmi^2)	9.5576	6.6271
Total SEL	79.92	77.58

(X = -10.08 nmi, Y = 0 nmi)

	Baseline	NPD+C
Distance (ft)	4195	4195
Thrust (lbs)	12875	12875
NPD Value (SEL dB)	78.1	75.1
LA max (dB)	64.5	62
Noise Fraction	0.841	0.870
Velocity Correction	-0.0895	0
Contour Area (nmi^2)	9.5576	6.6271
Total SEL	80.17	77.82

(X = -9.92 nmi, Y = 0 nmi, seg 7)

	Baseline	NPD+C
Distance (ft)	4832	4832
Thrust (lbs)	12875	12875
NPD Value (SEL dB)	76.9	73.8
LA max (dB)	62.8	60.1
Noise Fraction	0.871	0.900
Velocity Correction	-0.0895	0
Contour Area (nmi^2)	9.5576	6.6271
Total SEL	80.40	78.07

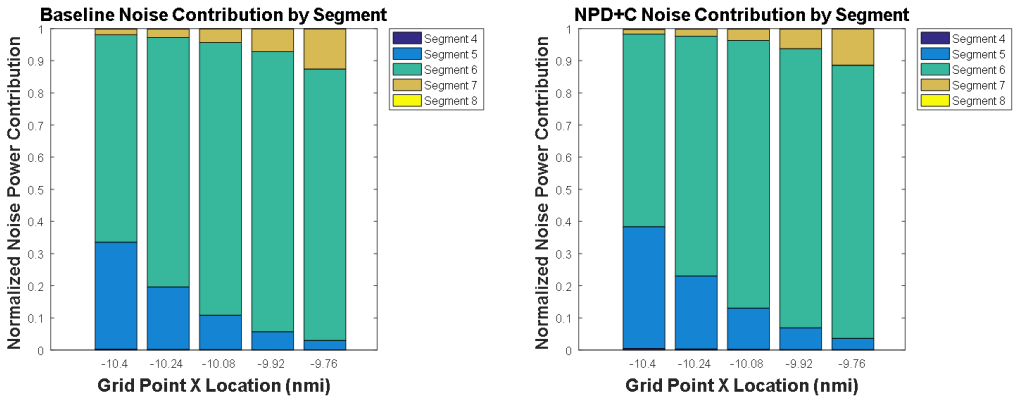

Figure 19. 300 PAX Study II.D – 3

Study II.A summary plots

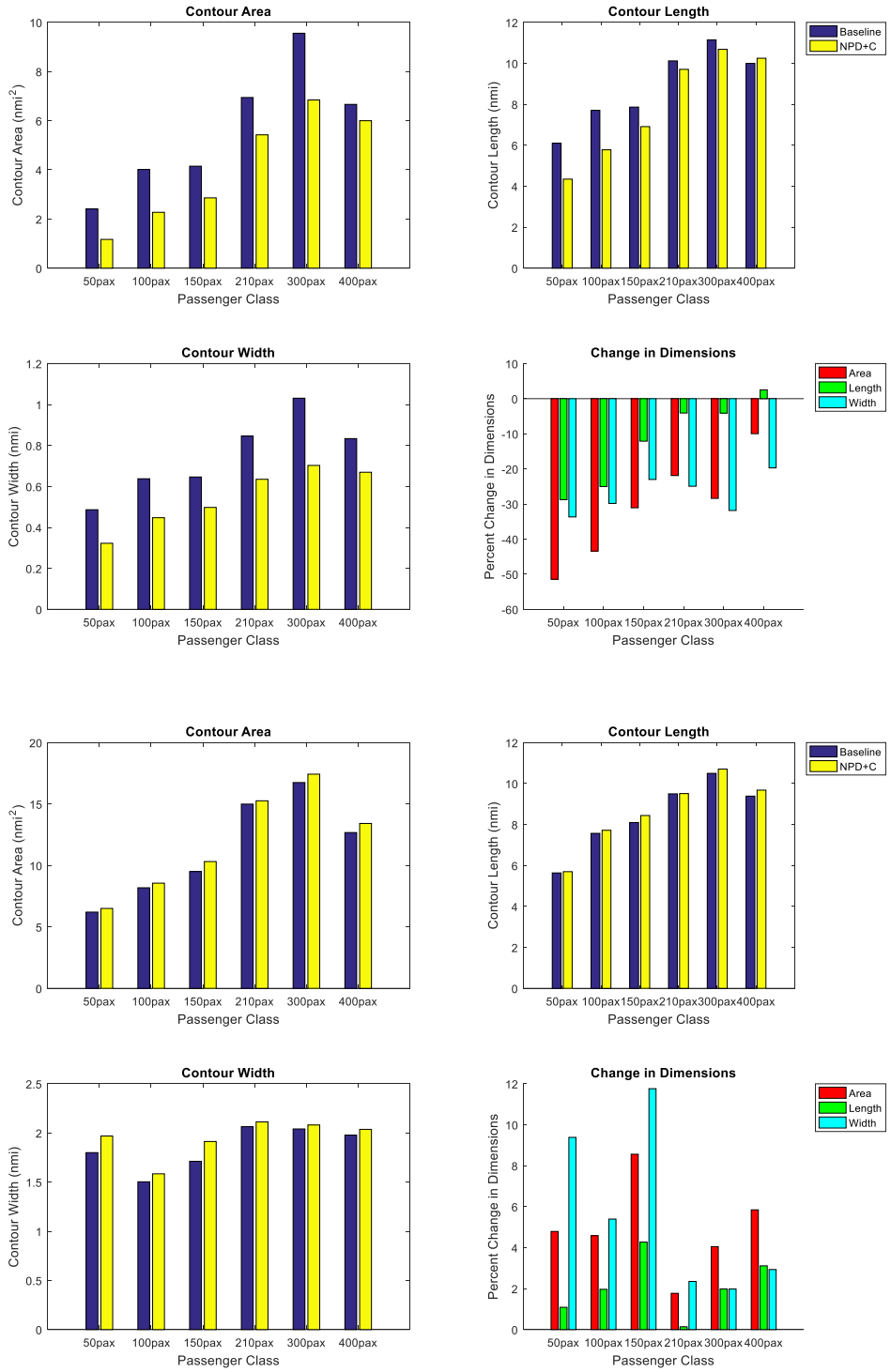

Figure 20. Study II.A Approach (top) – Departure (bottom)

Study II.B summary plots

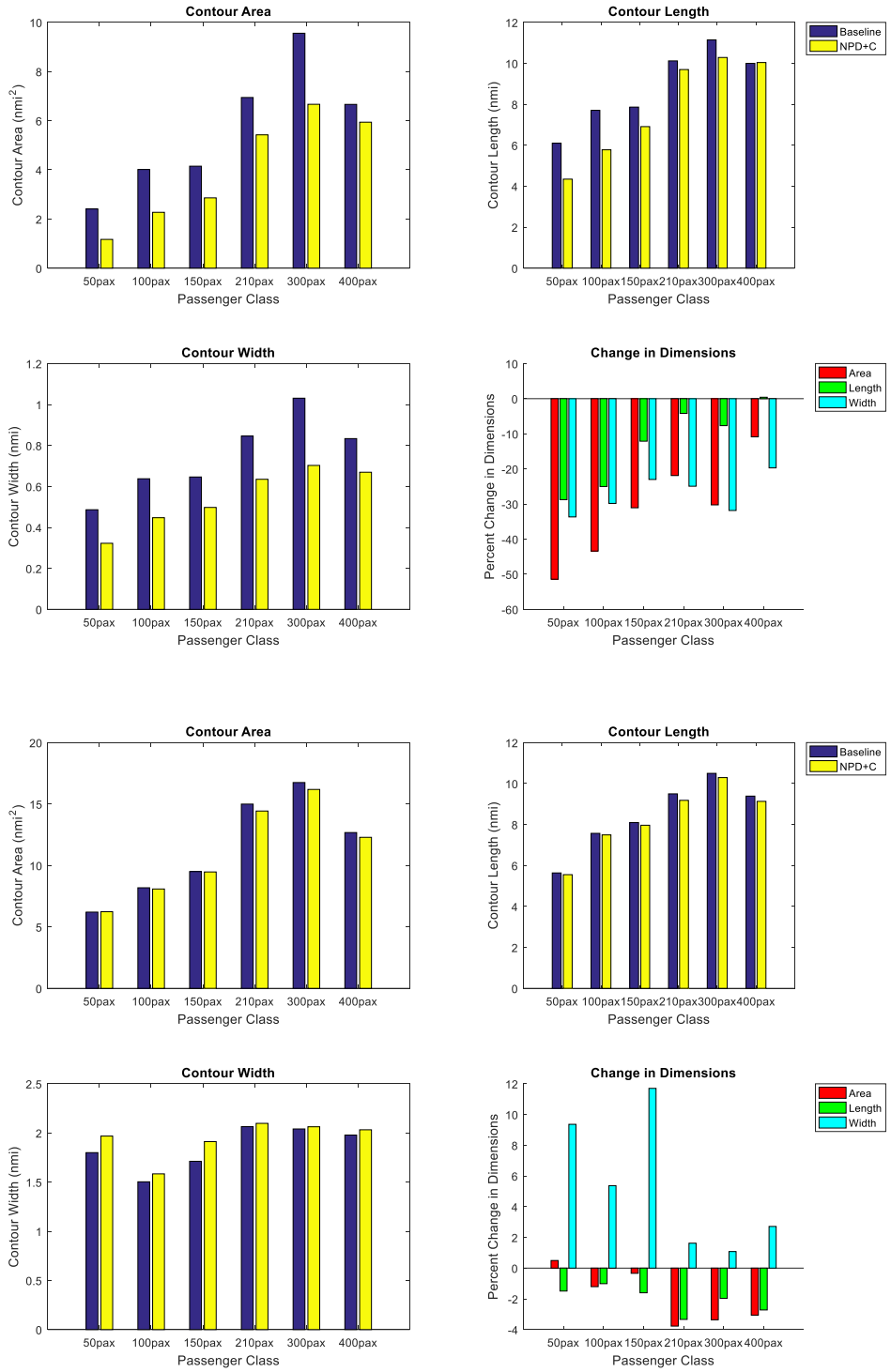

Figure 21. Study II.B Approach (top) – Departure (bottom)

Study II.C summary plots

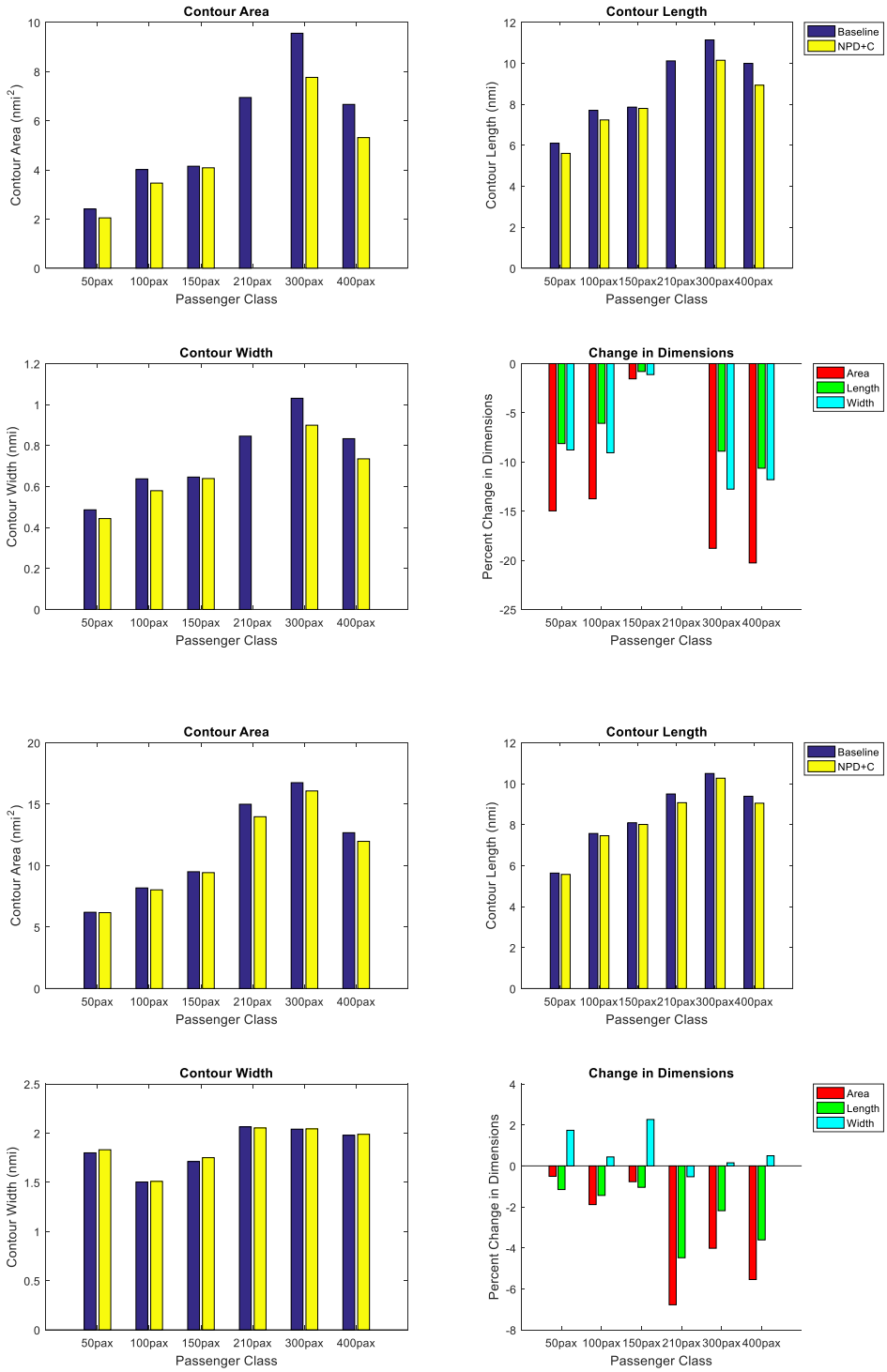

Figure 22. Study II.C Approach (top) – Departure (bottom)

Study II.D summary plots

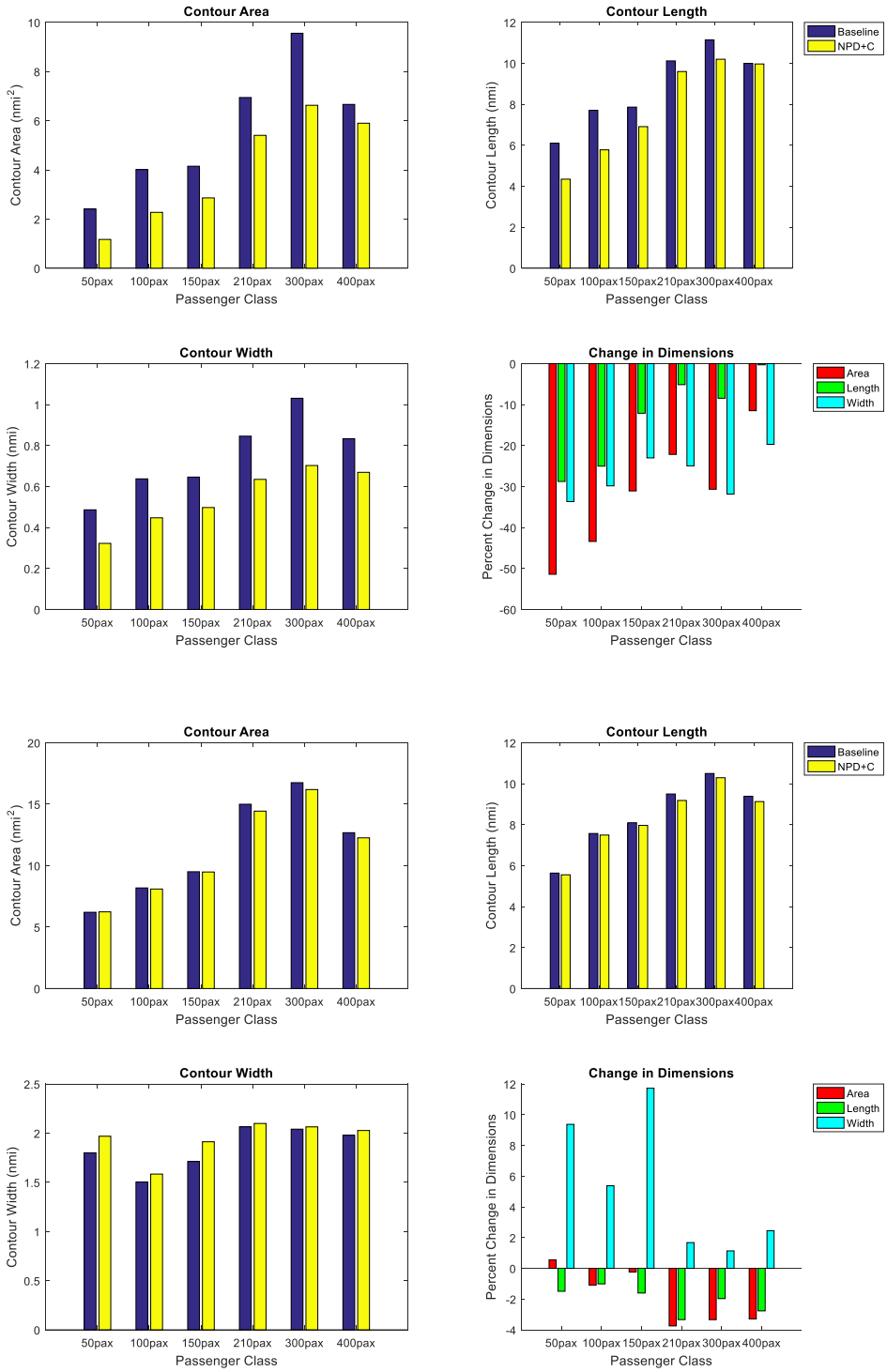

Figure 23. Study II.D Approach (top) - Departure (bottom)

Summary of results

Figure 24 includes a bar plot with a synthesis of the results obtained for the complete studies of I & II. The range of aircraft size classes is included with a quantile description of the mean, max and min values corresponding to the percent area change. These results are evident from the flight procedure which more closely corresponds to the noise procedure. At approach the clean configuration decreases the noise impact around the airport, while in departure, gear contributes to a larger contour. These results are analyzed in more detailed in Figure 25 & Figure 26. Both of these figures describe the area change for small & large size vehicles respectively. Recommendations from the combined findings are then explained in the NPD+C Recommendations section.

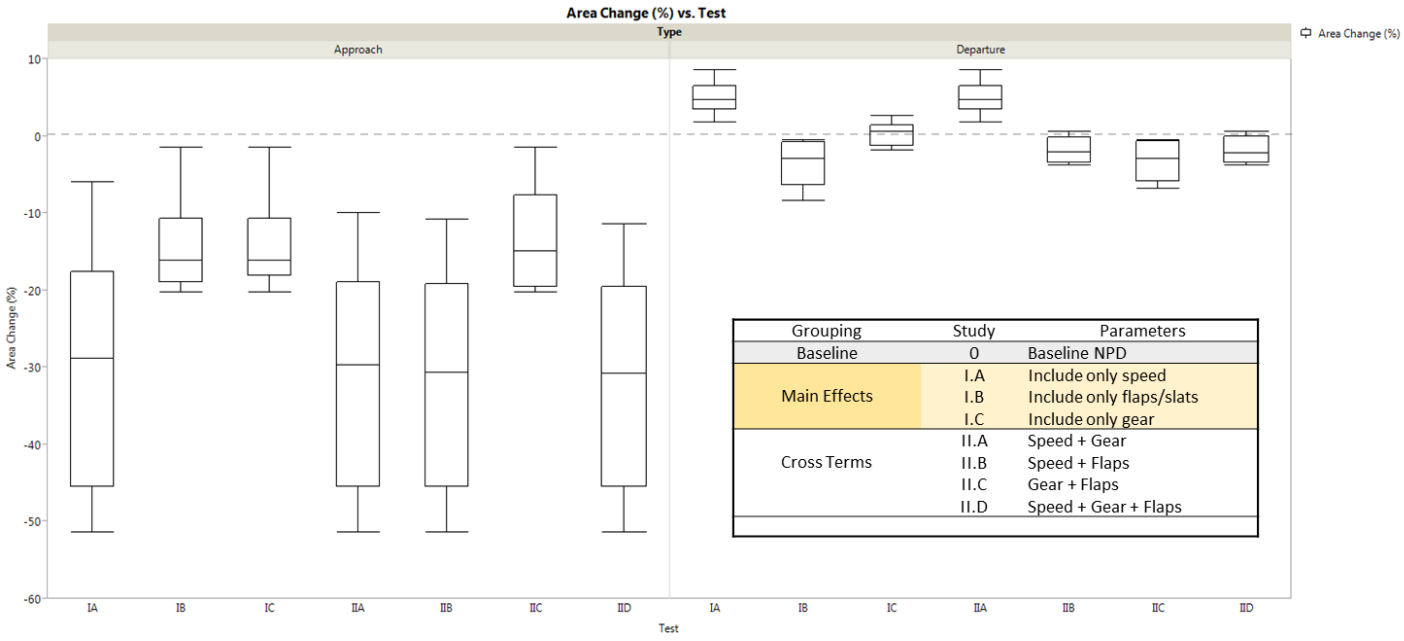

Figure 24. Noise contour area change (%) for all of the studies

The presence of the speed dimension in the NPD+C curves has the most significant impact in the overall noise contour obtained from running the modified AEDT environment for studies I & II. It is evident from the figure that departure procedures are less affected by the modifications. These impacts are observed to be explained by the following facts:

- Jet source noise is more relevant than airframe-configuration source noise, consequently explaining the configuration-dimension's lower impact
- Velocity corrections (duration adjustments) at higher reference speeds are negative, thus decreasing the total SEL value for the grid points obtained from higher noise metrics interpolated from the NPD+C
- Noise fraction adjustment show a similar behavior with respect to reference velocity and SEL vs LAMAX differences
- Impact of including the studies is mostly an area decrease during approach procedures due to:
- The initial procedures obtained at more deflected configurations
- The velocity corrections having a great impact in the final total SEL value for the given grid point
- The higher noise metrics with regards to the speed pertain to segment points further away from the observer

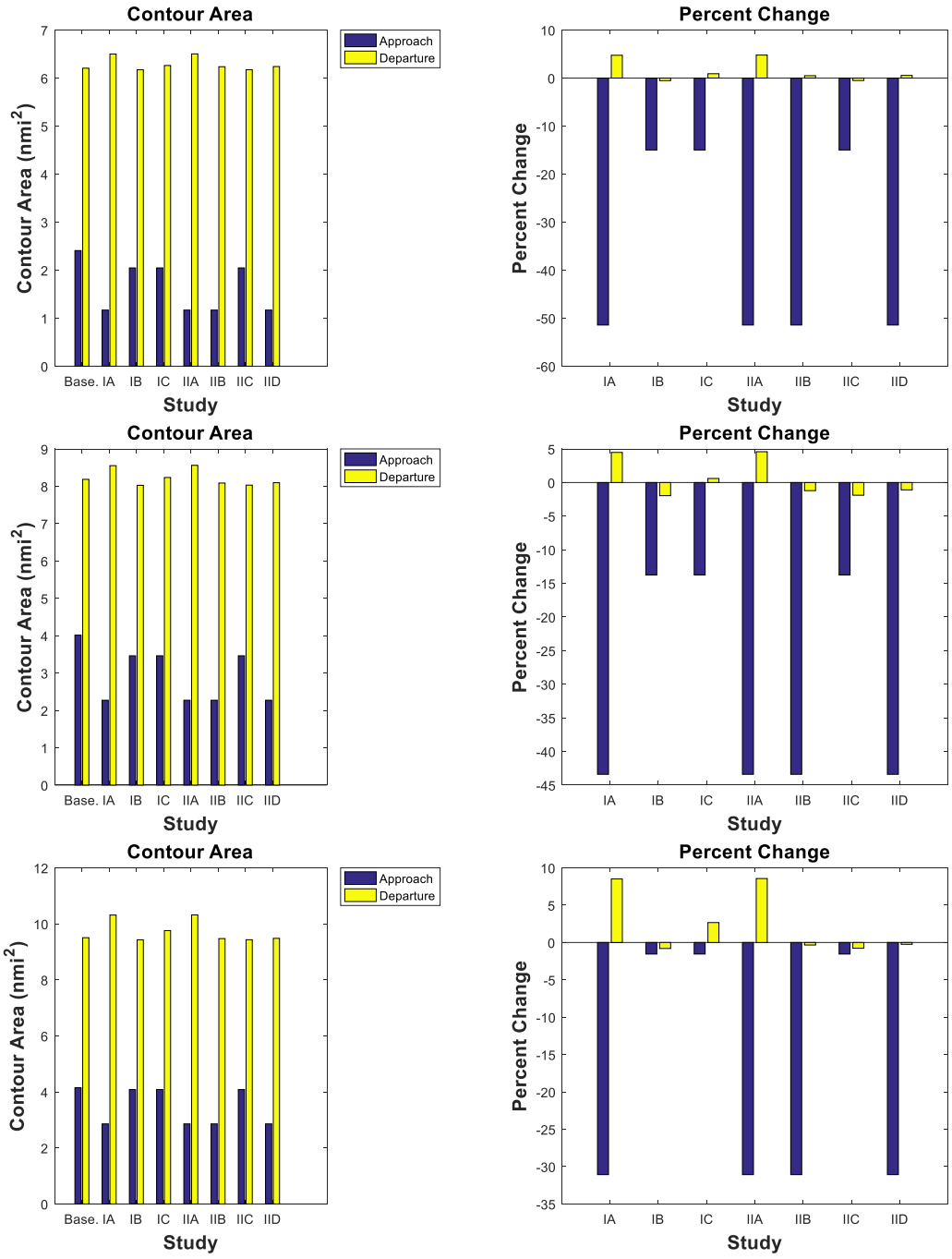

Figure 25. 50 – 100 – 150 PAX. Study I & II

Vehicle specific impacts - studies I & II – large sized aircrafts

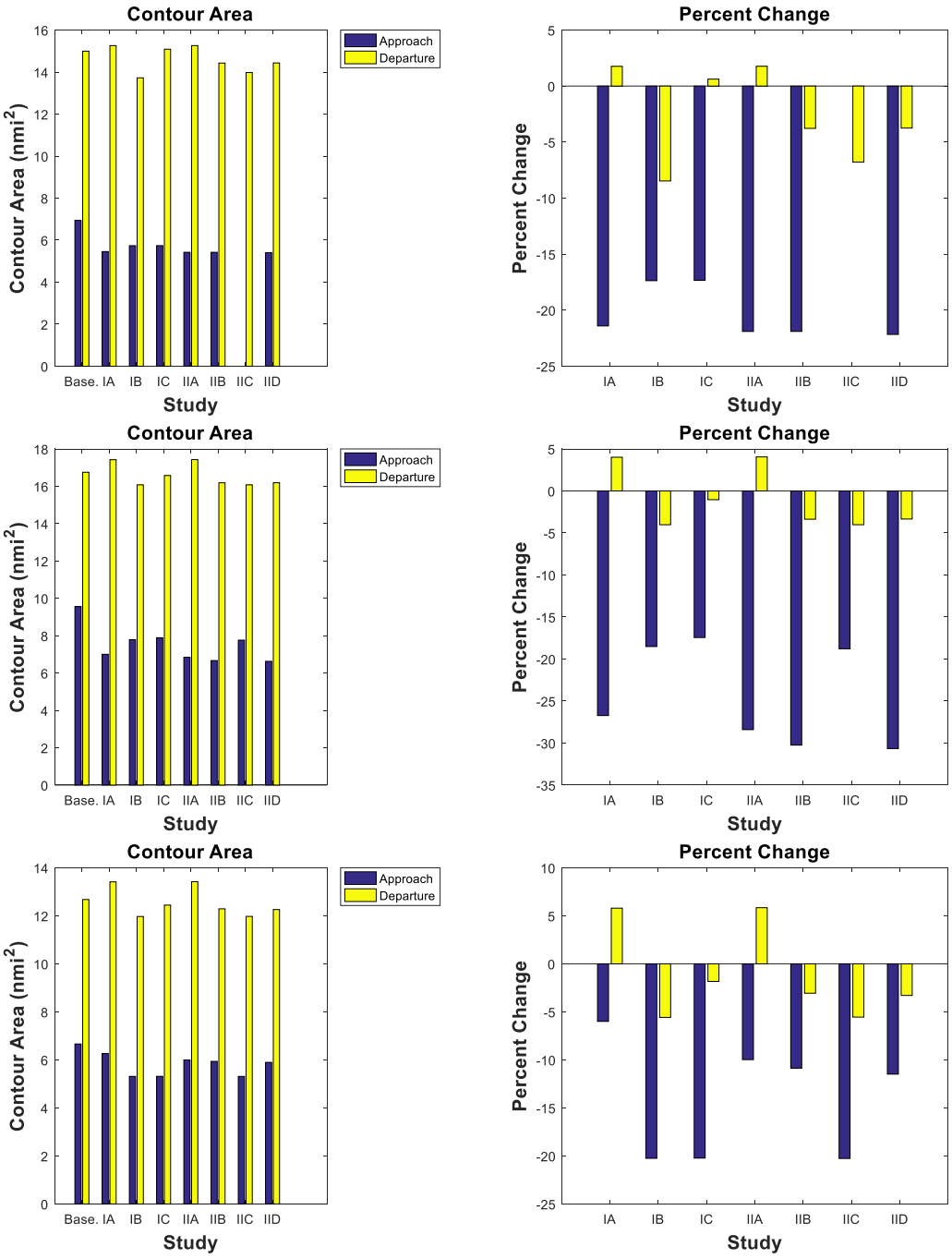

Figure 26. 210 – 300 – 400 PAX. Study I & II

NPD+C Recommendations

Figure 25 and Figure 26 provide insight into which dimensions should be expanded for a higher fidelity of the noise contours outputted by the AEDT NPD+C. Both the smaller and larger sized aircrafts demonstrate a large sensitivity to the reference velocity range 130 – 190 kts. A substantial percent area decrease for approach operations (-25% to -50% area) and a significant increase in departure procedures (5% to 10%) is observed when the expanded range of reference velocities is included in the NPD+C input XML vehicle. Consequently, Georgia Tech recommends an increase in the NPD+C data which initially includes the velocity dimension. This initial consideration would require the minimum effort as there will be a maximum of 2 NPD sets.

The aircraft configuration, however, becomes increasingly relevant for the larger sized vehicles. A minor difference is observed between the gear and flap-slat setting effect, with the control surfaces having a more considerable impact. The optimum second expansion would be to include flap-slat setting noise metrics in the NPD+C superset data; nonetheless, this consideration would require the most effort. Accordingly, the second reasonable expansion is to acquire data with respect to gear-setting. Ultimately, both recommendations increase the NPD from a single set to a 4 set NPD+C input vehicle.

Task #3: Implementation Validation

Georgia Institute of Technology

Baseline vehicles validation

To validate the modifications made to AEDT, the noise contours generated by the modified version of AEDT must be compared to those generated by the unmodified version of AEDT using the original baseline vehicle. To allow for interpolation, the modified version of AEDT must be run using 12 sets of NPD+C data corresponding to the test matrix discussed previously. These results must be compared to the original version of AEDT, which only allows for one set of NPD data. To produce comparable results, the original baseline vehicle for each class is run using the original unmodified version of AEDT. This vehicle is referred to as the "Baseline" vehicle. To compare this with the modified version of AEDT, a new vehicle is defined using 12 sets of NPD+C data that are each identical to the single set of NPD data from the Baseline vehicle. This vehicle is referred to as "singleNPD1." By defining an NPD+C vehicle with all NPD information identical to the original baseline, it is possible to compare the results generated by the original and modified versions of AEDT. The results should be identical, since the interpolation scheme in the modified version of AEDT should always generate the baseline NPD data based on the 12 identical NPD+Cs. This simple validation test is performed to ensure that none of the modifications made to AEDT in this study have any effect on how AEDT is performing analysis, but is instead only affecting the NPD information that AEDT is provided at each segment.

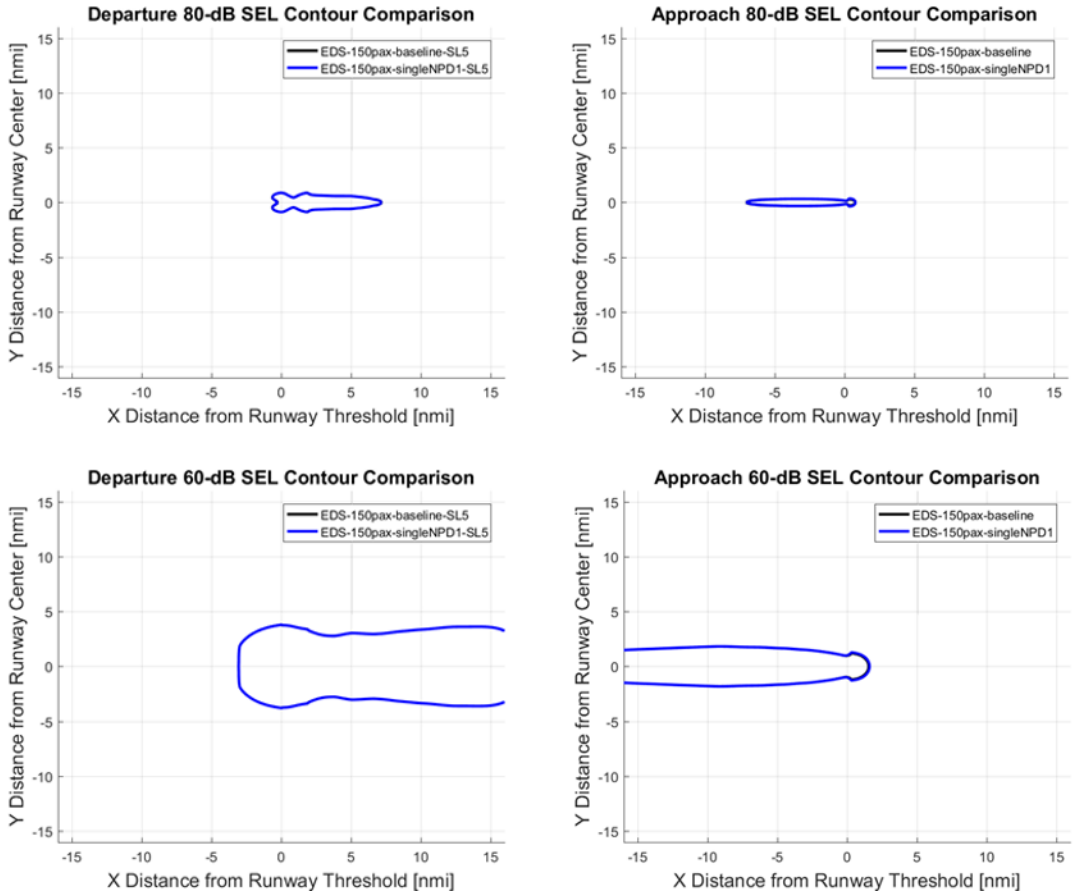

Figure 27. Validation Results for 150 PAX Vehicle Class

Figure 27 show the SEL contours of the validation study for approach and departure at both 60 and 80 dB. In each case, the contours generated by both the Baseline and singleNPD1 match identically. This shows that the modified version of AEDT developed in this study produces identical analysis to the original version of AEDT when provided identical NPD+C information. This study confirms that the modifications made to AEDT only work to change the NPD data that AEDT uses to perform analysis for each segment without changing any of the analysis methods.

Segment-wise contribution build-up

The ability to analyze segment-wise noise contribution was instrumental to validate results obtained from the modified AEDT algorithm developed for the NPD+C studies. The build-up analysis enabled as well the assessment of the minor amount of cases with unintuitive behavior.

This was the case for a subset of the smaller-sized vehicles (50 – 100 – 150 PAX), which portray a similarity in the noise contour impact between gear-setting and flap-slat-configuration main-effect analyses. Specifically, the approach procedure 80 dB contours (for both studies - studies I.B & I.C are available through requesting from the authors) shared identical changes in the total SEL values for grid-points showing the largest difference with respect to the reference baseline. Figure 29. Segment-wise contribution – APPROACH 150 PAX depicts the graphical explanation of this behavior and Table 8 help explain the differences in the flight path characteristics. The graph's orange line represents the difference between the baseline value and the flap sensitivity output; the blue line represents the difference between the baseline value and the gear sensitivity output; and the gray line is the difference between the flap-slat and the gear sensitivity outputs.

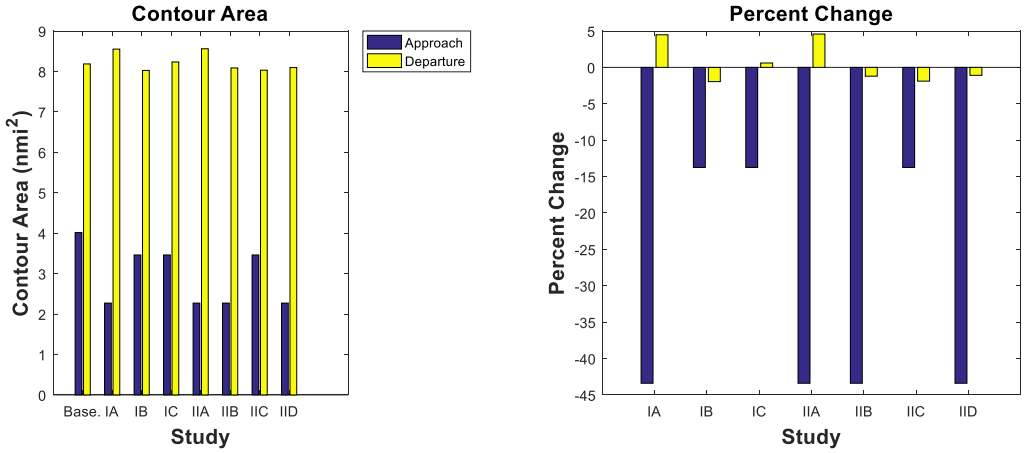

Figure 28. 100 PAX Studies I & II

As explained in Task 2 section, the changes in NPD+C's at approach lies in the initial segments having a clean configuration, gear-up setting. These differences are reflected until segment 7. Afterwards, the segment-wise noise metric values with regard to the baseline should be zero (due to the instantaneous configurations being the same); however, it was then realized that the discrepancies were due to the rounded lift coefficient value ($C_l = 0.355$ for the baseline, $C_l = 0.354$ for the studies) in the 150 PAX case. Both gear and flap sensitivity studies converge to the same dB difference to the baseline, which is the expected behavior. The blue trend differs significantly from the orange trend during the initial segments (as expected due to the differences in aircraft configuration); nonetheless, these SEL values contribute very little to the total SEL value for the studied grid-point. As highlighted in the plot, segment 7 and 8 contribute 99.2% of the noise value (Figure 30. Pareto plot for an NPD+C notional departure that can better describe the differences in contribution). For these segments, both gear and flap analyses converge to the same value as seen in the gray trend. Consequently, the detailed research performed explained the similarities in the calculated values.

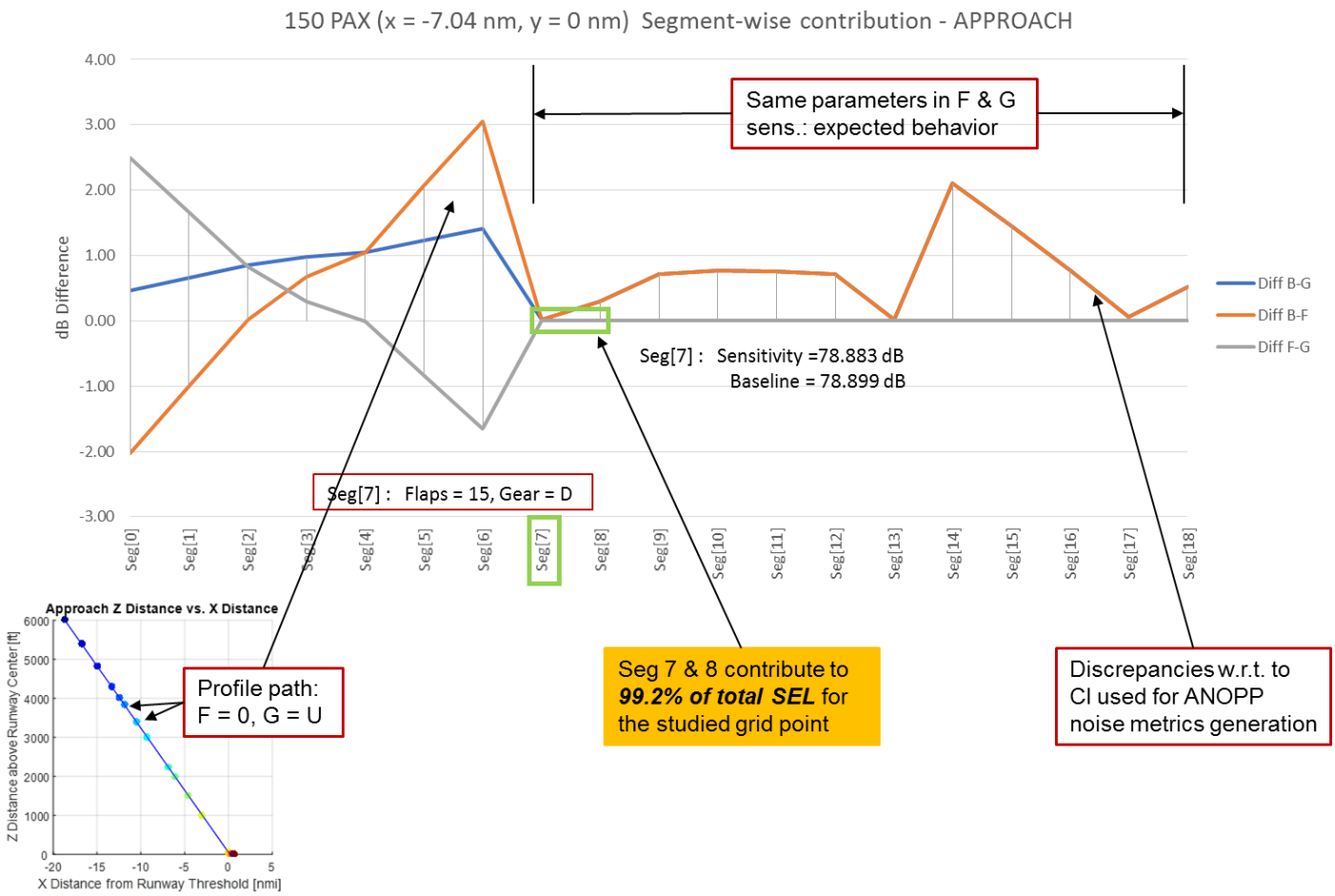

Figure 29. Segment-wise contribution – APPROACH 150 PAX

Table 8. Segment-wise contribution research

Flight path differences				Grid 150 pax, x = -7.04 , y = 0						
Flap Base	Flap Sens	G Base	G Sens	Segment	gear	Flap	base	*Diff B-G*	*Diff B-F*	*Diff F-G*
15	0	D	U	Seg[0]	13.902	16.400	14.372	0.47	-2.03	2.498
15	0	D	U	Seg[1]	18.086	19.750	18.748	0.66	-1.00	1.664
15	0	D	U	Seg[2]	22.827	23.658	23.682	0.85	0.02	0.831
15	0	D	U	Seg[3]	24.834	25.136	25.810	0.98	0.67	0.302
15	0	D	U	Seg[4]	25.430	25.427	26.476	1.05	1.05	-0.003
15	0	D	U	Seg[5]	34.992	34.162	36.226	1.23	2.06	-0.830
15	0	D	U	Seg[6]	43.463	41.817	44.872	1.41	3.06	-1.646
15	15	D	D	Seg[7]	78.883	78.883	78.899	0.02	0.02	0.000
15	15	D	D	Seg[8]	73.257	73.257	73.558	0.30	0.30	0.000
15	15	D	D	Seg[9]	58.835	58.835	59.556	0.72	0.72	0.000
15	15	D	D	Seg[10]	40.998	40.998	41.767	0.77	0.77	0.000
15	15	D	D	Seg[11]	31.707	31.707	32.461	0.75	0.75	0.000
15	15	D	D	Seg[12]	10.334	10.334	11.046	0.71	0.71	0.000
15	15	D	D	Seg[13]	9.739	9.739	9.754	0.02	0.02	0.000
15	15	D	D	Seg[14]	9.132	9.132	11.237	2.11	2.11	0.000
15	15	D	D	Seg[15]	8.396	8.396	9.854	1.46	1.46	0.000
15	15	D	D	Seg[16]	7.714	7.714	8.487	0.77	0.77	0.000
15	15	D	D	Seg[17]	7.079	7.079	7.135	0.06	0.06	0.000
15	15	D	D	Seg[18]	6.508	6.508	7.035	0.53	0.53	0.000

Seg 7 & 8 contribute to 99.2% of total SEL for the studied grid point

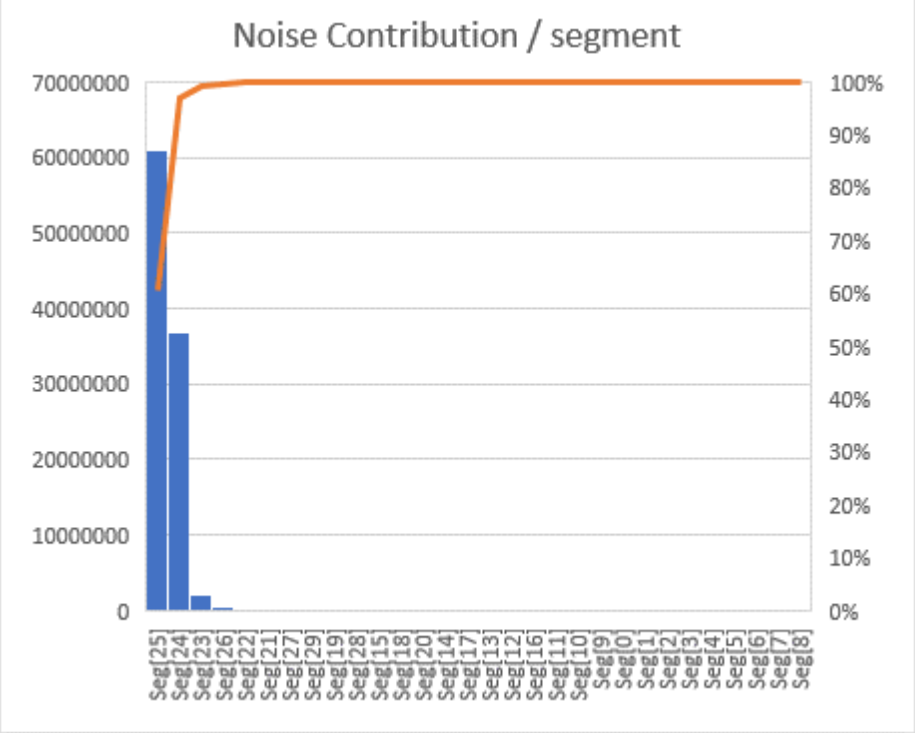

Figure 30. Pareto plot for an NPD+C notional departure

Publications
A journal paper submitted to the AIAA Journal of Aircraft is expected from the research effort. Arturo Santa-Ruiz is the first author of the paper.

Outreach Efforts
Meetings with the ASCENT team were scheduled for subsequent work.

Awards
None.

Student Involvement
Kenneth Decker and Arturo Santa-Ruiz were intimately involved in the day-to-day activities on this research. Kenneth worked on Task 1 in obtaining correct NPD+C input vehicles and developed appropriate plotting scripts. Arturo developed and coded the AEDT NPD+C program and algorithm, included the segment-to-grid-point logic, performed Task 2 & Task 3, and analyzed results.

Project 045 Takeoff/Climb Analysis to Support AEDT APM Development

Georgia Institute of Technology

Project Lead Investigator

Prof. Dimitri Mavris
Professor Dimitri N. Mavris
Director
Aerospace Systems Design Laboratory
School of Aerospace Engineering
Georgia Institute of Technology
Phone: (404) 894-1557
Fax: (404) 894-6596
Email: dimitri.mavris@ae.gatech.edu

Dr. Michelle R. Kirby, Co-PI
Chief, Civil Aviation Research Division
Aerospace Systems Design Laboratory
School of Aerospace Engineering
Georgia Institute of Technology
Phone: (404) 385-2780
Fax: (404) 894-6596
Email: michelle.kirby@ae.gatech.edu

University Participants

Georgia Institute of Technology (GT)

- P.I.(s): Prof. Dimitri Mavris, Dr. Michelle R. Kirby (Co-PI)
- FAA Award Number: 13-C-AJFE-GIT, Amendment 020 and 035
- Period of Performance: August 15, 2016 to August 14, 2018

Project Funding Level

FAA funded amount is $250,000 for the period of performance of August 15, 2016 to August 14, 2017. The Georgia Institute of Technology has agreed to a total of $250,000 in matching funds. Subsequently, the FAA funded amount is $75,000 for the period of performance of August 15, 2017 to August 14, 2018. The Georgia Institute of Technology has agreed to a total of $75,000 in matching funds. This total includes salaries for the project director, research engineers, graduate research assistants and computing, financial and administrative support. The institute has also agreed to provide equipment funds as well as tuition remission for the students paid for by state funds.

Investigation Team

Prof. Dimitri Mavris, Dr. Michelle Kirby, Dr. Don Lim, Dr. Yongchang Li, Dr. Holger Pfaender, Dr. Matthew Levine, and Mr. Jim Brooks. Graduate Students: Vu Ngo and Ameya Behere.

Project Overview

Accurate modeling of aircraft performance is a key factor in estimating aircraft noise, emissions and fuel burn. Within the Aviation Environmental Design Tool (AEDT), many assumptions are made for aircraft performance modeling with respect to aircraft weight and departure procedure coupled with the fact that, typically the aircraft departure is modeled assuming full rated takeoff power/thrust is used. As operations around airports continue to evolve, there is a need to examine those assumptions and to improve the modeling accuracy with flight data. In recent years, flight data has been used more and more to enhance models and bring model estimation even closer to reality. Research is needed to build on prior work with a view to develop a robust set of recommendations for improved estimation processes for takeoff weight, reduced thrust takeoffs, and departure profiles within AEDT.

Task #1: Literature Review and AEDT APM Evaluation

Georgia Institute of Technology

Objective(s)

Review the body of existing literature on estimating the takeoff and climb out performance of aircraft using flight data including several ACRP projects 02-41, 02-37, and 02-55 and also ASCENT Project 35 and the AEDT APM.

Research Approach

Using the existing body of work and Georgia Tech's detailed aircraft and engine modeling knowledge, the AEDT APM algorithms will be systematically evaluated to identify areas of improvement in current modeling methods. For all relevant APM assumptions, the team will identify the assumption in question, the validity of the physics behind the APM assumption, suggested improvements, and any issues in data availability or modeling fidelity associated with the suggested improvements. This analysis of APM assumptions will be critical in identifying tuning methods and calibrating AEDT performance to measured flight data.

The objective of ACRP 02-41 was to produce guidance to include the effects of reduced takeoff thrust in the emissions inventory calculations and to develop a Takeoff Thrust-Setting Estimator Tool (TTREAT) based on statistical analyses of extensive takeoff thrust data supplied by airlines. TTREAT was validated based on US Airways data and concluded that the majority of commercial aircraft use approximately a 15% reduced thrust takeoff. This conclusion is similar to the results of ASCENT Project 35.

The objectives of ACRP 02-37 was to assess the accuracy of general aviation aircraft SEL noise modeling within INM as compared to measured values. The research team focused on examining performance profiles to help identify causes of error and focused on departures using LJ35, GLF4, and EA50 aircraft, where the error was identified as discrepancies between measure and modeled levels of SEL and also altitude. The observations made were that INM modeling for almost all aircraft types computes departure SEL values higher than the measured levels. Also, the INM departure altitudes for the aircraft are higher than actually occurs. It is likely most error in the INM modeling is caused by significant differences between the standard noise and performance profiles (management of thrust, flaps, speed, climb rates and associated noise-power-distance curves) and actual average practice. The general cause for these discrepancies was the use of maximum thrust departures as standard INM input. Two solutions were proposed to correct the takeoff thrust to provide more realistic results and were based on an assumed temperature method (ATM), where ATM is a process where an aircraft Flight Management System (FMS) is asked to compute the thrust required to safely depart the aircraft from a given runway while demanding a decreased level of engine performance. The two solutions are:

- ATM1:
  - Requires determining the specific thrust levels from manufacturer or operator surveys then creating custom profiles to match these inputs
  - Requires updated Thrust Jet data in order to make reduced thrust departure profiles available as standard INM input.
  - Not a preferred option
- ATM2:
  - First uses the INM's internal computation process to determine the aircraft departure profile at an assumed elevated temperature. The resulting departure data are then converted into a static "profile points" style profile which is then input into the INM and run at the normal or average airfield temperature
  - No radar data, measured sound levels, pilot or manufacturer information is needed

- Preferred Option

Each method was applied to a set of aircraft and the noise exposure quantified to show a correction of approximately 2.5 dB for a small set of flights within INM, however the recommendations are applicable to AEDT. ATM2 was recommended as the preferred correction approach since ATM1 required manufacturer's input, but is limited to aircraft types that have hi-temperature coefficients. Similar to ACRP 02-41, reduced thrust takeoff was suggested as an improvement in noise exposure to real world flight and would also affect the trajectory of the departure.

The objective of ACRP 02-55 are to develop: (1) standard model aircraft approach and departure profiles that are not currently in AEDT, (2) methods to model customized aircraft approach and departure profiles using AEDT, and (3) technical guidance for selecting appropriate aircraft approach and departure AEDT profiles, including customized profiles, for specific user situations. At present, the results of this study are not public and will be reviewed once available. However, the objective of modeling departure procedures that are not within AEDT led the GT research team to identify typical departure procedures utilized in real world operations.

FAA AC 91-53A and ICAO PANS OPS Chapter 3 Volume II both contain the minimum safe standards for departure procedures. Both contain the same minimums which are:

1) No thrust cutbacks below 800' AFE, and
2) The level of the thrust cutback will not be less than the Airplane Flight Manual (AFM) thrust required to maintain the minimum engine-out climb gradient.

Both documents recommend that all carriers adopt no more than two procedures for each aircraft type; one for noise abatement of communities close to the airport and one for noise abatement of communities far from the airport. Within FAA AC 91-53A, these are defined as the Close-In and the Distant Procedure, which are similar to ICAO Pans Ops NADP1 and NADP 2 defined in CAEP/7 Working Paper 25. Through discussions with Jim Brooks, NAPD1 and NAPD2 most closely resemble real work departure procedures employed by pilots with a suggested variability in the cutback altitude utilized by different airlines of 800', 1000', and 1500' AFE.

The objective of ASCENT Project 35 was to develop a functional relationship between stage/trip length and takeoff weight that can improve the existing guidance provided for weight estimation; and subsequently to determine the percentage of departures that use reduced thrust and the level of reduced thrust that is used for the departure. The project focused on analyzing major US carrier flight data of four engine/airframe combinations, specifically:

- B757-200/PW2037
- B737-800/CFM56-7B26
- B767-400ER/CF680C2/B8F
- B767-300ER/CF680C2/B6F
-

A series of statistical regressions were conducted to determine the most appropriate functional form to estimate takeoff weight. An example of the results for the B737-800 is depicted in Figure 1 along with the assumption for takeoff weight (TOW) within the AEDT Fleet dB. As evident, the assumed TOW within AEDT is an underestimation of real world operations.

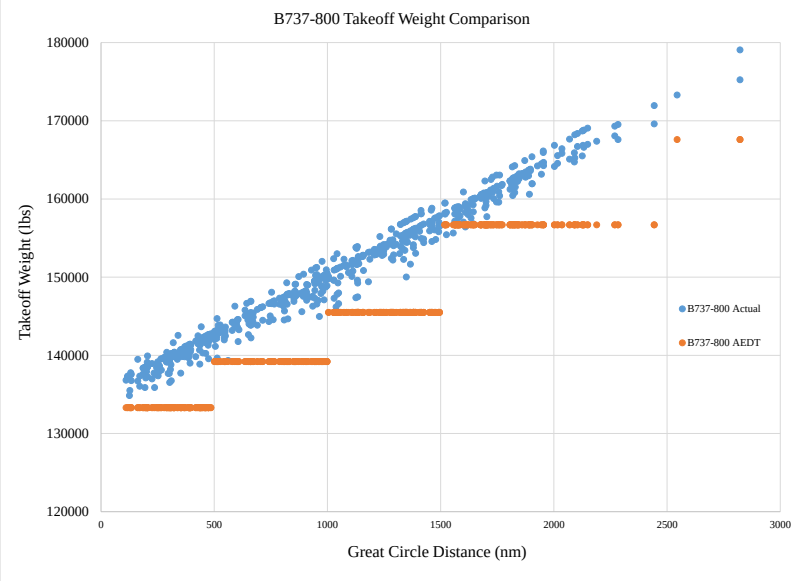

Figure 1. Takeoff Weight Variation with Great Circle Distance

Within AEDT, the manufacturers provide a series of performance and noise coefficients to define their aircraft as guided by BADA and SAE-AIR-1845. SAE-AIR-1845 is the Aircraft Noise and Performance (ANP) database which covers from takeoff and climb performance up to 10,000'. As part of the ANP data, the manufactures provide takeoff weights based on the guidelines in Figure 2 as defined by the AEDT 2b Technical Manual. The two key observations are that a load factor of 65% is assumed and that the TOW within a Stage Length band is constant in lieu of a continual increase with GCD. Based on the results of ASCENT Project 35, real world TOW are higher than the assumptions utilized in AEDT. The main driver for the TOW discrepancies may be the load factor assumption.

Parameter	Planning Rule
Representative Trip Length	Min Range + 0.70*(Max Range – Min Range)
Load Factor	65% Total Payload.
Fuel Load	Fuel Required for Representative Trip Length + ATA Domestic up to 3,000 nmi and International Reserves for trip length > 3,000 nmi. As an example, typical domestics reserves include 5% contingency fuel, 200 nmi alternate landing with 30 minutes of holding.
Cargo	No additional cargo over and above the assumed payload percentage.

Stage number	Trip length (nmi)	Representative Range (nmi)	Weight
1	0-500	350	lb
2	500-1,000	850	lb
3	1,000-1,500	1,350	lb
4	1,500-2,500	2,200	lb
5	2,500-3,500	3,200	lb
6	3,500-4,500	4,200	lb
7	4,500-5,500	5,200	lb
8	5,500-6,500	6,200	lb
9	6,500-7,500	7,200	lb
10	7,500-8,500	8,200	lb
11	>8,500		lb
M	Maximum range at MTOW		lb

Figure 2. ANP Guidance for Takeoff

The load factor assumption of 65% may be a bit low in comparison to historical data. According to the Bureau of Transportation Statistic (BTS), the average load factor, which includes passengers and belly freight, for all carriers and all airports has steadily increased since 2002[1] as depicted in Figure 3. While this data is an aggregate value, BTS does have load factor data at the aircraft level and also for specific air carriers, but is also slightly different than the load factor definition within AEDT. The project 35 results and the BTS data suggest that a further investigation to the load factor assumption should be conducted. Per the FAA Project Manager, Booz Allen Hamilton (BAH) is currently conducting an investigation to this assumption. When the results are publically available, the GT research team will review and incorporate the results for the aircraft not included in the Project 35 TOW results.

[1] "Load Factor", http://www.transtats.bts.gov/Data_Elements.aspx?Data=5, accessed Dec 20, 2016

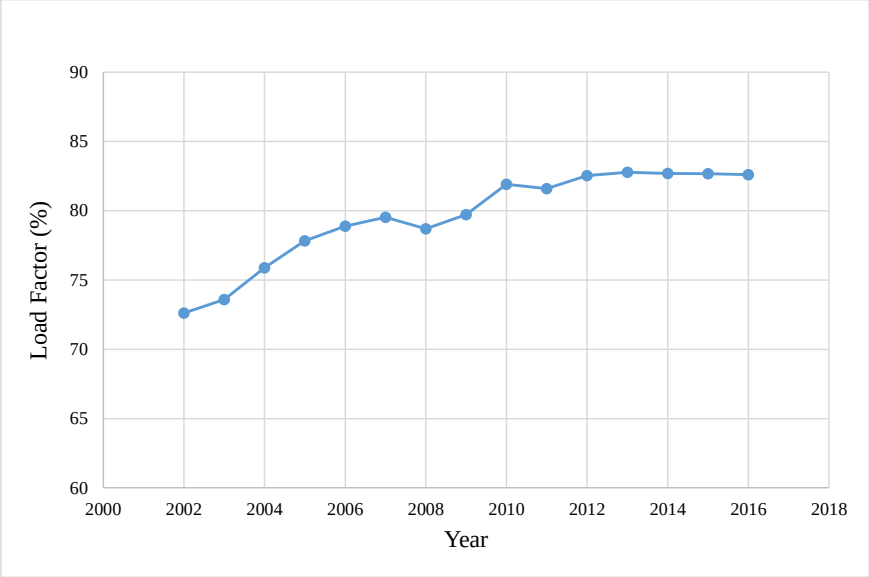

Figure 3. BTS Historical Load Factor

In addition to the load factor assumptions associated with the ANP database, the manufacturers are asked, as part of the standard aircraft noise and performance data submittal form, to provide three departure procedures that are used within AEDT. The guidance of the procedures is defined in the AEDT 2b Technical Manual as defined in Figure 4. In many cases, the "Default" procedure is the same as the ICAO B procedure within the AEDT Fleet dB. For each of these procedures, the manufacturer will fill out the performance of their aircraft based on the form depicted in Figure 5.

Default Procedure[xxxvi] **Modified BBN/AAAI Procedure**	**ICAO A**	**ICAO B**
Takeoff at MaxToPower (full power) and Climb to 1,000 feet AFE	Takeoff MaxToPower (full power)	Takeoff at MaxToPower (full power)
Pitch over and cutback to climb power. Accelerate to zero flaps retracting flaps on schedule (clean configuration)[xxxvii]	Climb at constant speed to 1,500 feet AFE	Climb to 1,000 feet AFE and pitch-over to accelerate at full power to clean configuration
Climb at constant speed to 3,000 feet AFE	Reduce thrust to Climb Power	At Clean Configuration, cutback top climb power
	Climb at constant speed to 3,000 ft AFE	Climb at constant speed to 3,000 ft
Upon achieving 3,000 feet AFE, accelerate to 250 knots[xxxvii]	Accelerate while retracting flaps to Zero (clean configuration)	Upon achieving 3,000 feet AFE, accelerate to 250 kts
	Continue accelerating to 250 knots	
Upon achieving 250 knots, climb to 10,000 feet AFE	Upon achieving 250 knots, climb to 10,000 feet	Upon achieving 250 knots, climb to 10,000 feet

Figure 4. ANP Guidance for Takeoff Departure Procedures Guidance

Stage Number		Procedure Type (Procedural or Points)			Procedure Name	
Segment Type[xxxviii]	Thrust Type[xxxix] (T/C)	Flap Configuration Identifier	Endpoint Altitude (ft AFE)	Rate-of-Climb (ft/min)	Endpoint Speed (KCAS)	Start Thrust[xl] (lb)
Takeoff						lb
Climb			ft			lb
Climb			ft			lb
Accelerate				fpm	kt	lb
Accelerate				fpm	kt	lb
Climb			ft			lb
Climb			ft			lb
Accelerate				fpm	kt	lb
Accelerate				fpm	kt	lb
Climb			10,000			lb

Figure 5. Takeoff Departure Procedures Profile Form

Based on the literature review conducted in Task 1, three elements were identified as the primary drivers for improvement of the APM departure profiles and environmental performance modeling and included the following that will be addressed in the remainder of this project:

- Reduced thrust takeoff of approximately 15%
- Proper takeoff weights as a function of GCD, and
- Proper departure procedure modeling of NADP 1 and 2 versus the existing AEDT STANDARD, ICAO A and ICAO B procedures
-

The standard procedures typically used in AEDT (and previously in INM) for inventory studies correspond to the sequence of segments first described in SAE-AIR-1845[2]. The ICAO-A and ICAO-B procedures are referenced as "ICAO Noise Abatement Take-off Procedure A and/or Procedure B" in ECAC.CEAC Doc29[3], and an ICAO report[4] from 1982 is cited. This nomenclature is abandoned in the CAEP/7 WP/25 Circular on NADP Noise and Emissions Effects and replaced with NADP1 and NADP2, partially because slight variants on previously defined noise abatement departure procedures were introduced. Georgia Tech investigated the similarities and differences between the ICAO-A and ICAO-B procedures currently in AEDT versus the procedures defined in this working paper. ICAO-A and NADP1 procedures were essentially identical, primarily characterized by delaying acceleration/flap retraction segments until the aircraft clears 3000-ft air-field equivalent altitude. ICAO-B and NADP2 procedures were both characterized by completing acceleration/flap retraction segments before the aircraft attains 3000-ft air-field equivalent altitude with one key difference. ICAO-B procedures perform thrust cutback after the acceleration/flap retraction segments are complete, whereas NADP2 procedures perform thrust cutback before initiating acceleration/flap retraction. In his discussions with Delta pilots, Jim Brooks confirmed that the NADP2 procedure is more consistent with the manner the pilots actually fly the procedures.

Task #2: Statistical Analysis of Flight Data

Georgia Institute of Technology

Objective(s)

Literature review and AEDT APM evaluation conducted in Task 1 will identify the key drivers of variations in takeoff weight and takeoff thrust in real-world day-to-day operations, including energy share profiles or hands on pilot approaches to

[2] "Procedure for the Calculation of Airplane Noise in the Vicinity of Airports", SAE-AIR-1845, prepared by SAE Committee A-21, March 1986.
[3] ECAC.CEAC Doc 29, Report on Standard Method of Computing Noise Contours Around Civil Airports, Vol. 2, 3rd ed., Technical Guide, Dec. 2005.
[4] ICAO, 1982. Procedures for Air Navigation Services-aircraft operations: Volume 1, Flight Procedures, Part V — Noise abatement procedures, pages 5-4 to 5-7. Doc 8168-OPS/611, Volume 1, Amendment 2, 1983.

departures to understand the variability in the takeoff procedures that exists in reality. A quantification of the departure of the APM assumptions to real world operations will be conducted for the key drivers identified in Task 1.

Research Approach – Partial Derivative Process

The partial derivative approach focused on the investigation of the impact on terminal area performance due to the changes in assumption for takeoff gross weight, thrust and procedure for standard day sea level condition. The step by step of this process are shown in Figure 6. The approach begins with evaluation of the baseline AEDT STANDARD procedures in terms of noise contour, fuel burn and NOx. After obtaining the baseline results, weight and thrust was varied to gain knowledge about the effect on noise contour, fuel burn and NOx. Next, the vehicle procedure was changed from standard procedure to NADP procedures. The same process was repeated for changes in weight and thrust for the new procedure. The study was performed for three aircraft B737-800, B767-300ER, and B777-200ER for all stage lengths. The overall results for all three vehicles are in the appendix, however for the sake of discussion only B737-800 will be discuss in the main body.

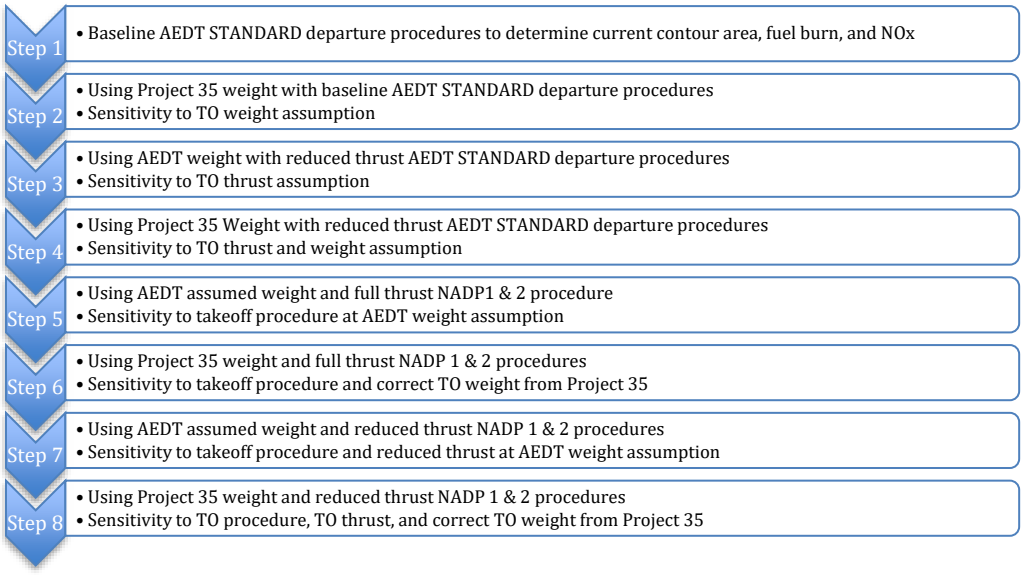

Figure 6: Partial Derivative Approach

Step 1

The first step is to evaluate of the AEDT STANDARD procedures at full takeoff thrust with max climb thrust for all vehicles at sea level condition, for all stage lengths. The AEDT STANDARD procedures parameters are found in AEDT ANP FLEET database. The general STANDARD procedure parameters for B737-800 are defined in Table 1. The plot of the departure profile for STANDARD procedure is also depicted, which can be broken down into segments.

Table 1: STANDARD Procedure

Segment	STANDARD
1	• Takeoff • Flaps 5 • 100% takeoff thrust
2	• Constant speed climb to 1,000 ft
3	• Acceleration step • Specify **ROC$_1$, Vstop$_1$**
4	• Acceleration step • Specify **ROC$_2$, Vstop$_2$** • Flaps 1
5	• Constant speed climb • Clean configuration.
6	• Constant speed climb to 3,000 ft • Reduce thrust to MCLT
7	• Acceleration step to 250 knots • Specify **ROC$_3$**, Vstop = 250 kts
8	• Constant speed climb to 5,500 ft
9	• Constant speed climb to 7,500 ft
10	• Constant speed climb to 10,000 ft

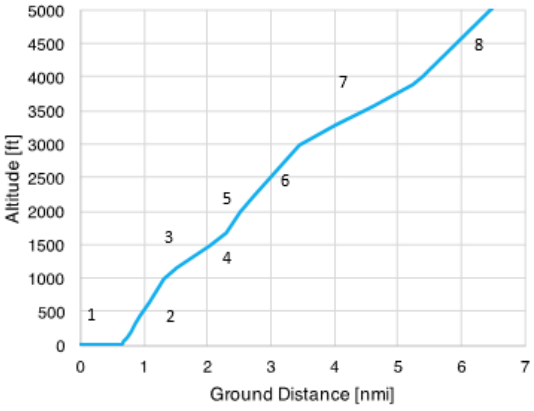

Figure 7: B737-800 STANDARD Procedures

The altitude versus ground distance is a sample of the STANDARD departure procedure as shown in Figure 7, where each of the segment steps are define in the Table 1. An example of stage length 3 STANDARD departure procedure parameters are shown in Figure 8 to Figure 14. Segment 1 is the ground roll and it requires that the takeoff flaps and thrust are specified. The takeoff flaps were set to Flaps 5 and full thrust was used for takeoff as shown in Figure 8. These are defined as STEP_TYPE T (for takeoff), FLAP_ID T_05 (flaps 05) and THR_TYPE T (max takeoff thrust).

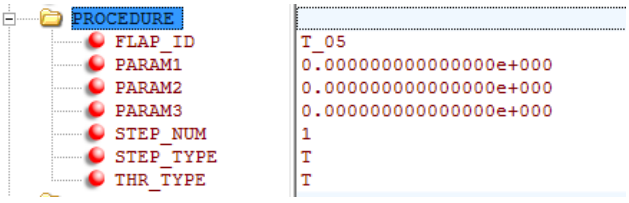

Figure 8: Segment 1 Parameters for Standard Procedure

Segment 2 is constant speed climb to cutback altitude, defined as the aircraft climbing at a constant airspeed until a specific altitude is met. PARAM1 is defined as 1000 ft which is the altitude at the end of the climb. The STEP_TYPE is C, which indicates a constant speed climb, as shown in Figure 9.

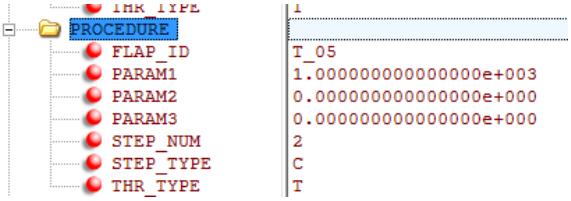

Figure 9: Segment 2 Parameters for STANDARD Procedure

Segment 3 is the first acceleration step, defined as the aircraft climbing and accelerating at a specified rate of climb until the specified airspeed is reached. Figure 10 shows the inputs for each of the relevant parameters. In the prior segment, PARAM1 was the altitude at the end of the climb. However, for the acceleration step (STEP_TYPE A), PARAM1 is the rate of climb in ft/min. PARAM2 is the final velocity (knots), which is the specified airspeed that the vehicle needs to reach at the end of the segment. The rate of climb was set to 1885.7 ft/min and the final velocity was set to 181.7 knots. This final speed corresponds to the flaps retraction schedule.

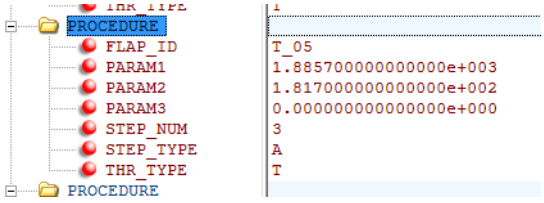

Figure 10: Segment 3 Parameters for STANDARD Procedure

The flap retraction from T_05 to T_01 happens instantaneously between segment 3 and segment 4. Segment 4 is also an acceleration segment where the rate of climb was set to 2112 ft/min and the end velocity is set to 204.8 knots as shown in Figure 11. At the end of segment 4 and before segment 5, the flap are retracted T_01 to T_00 which is the clean configuration.

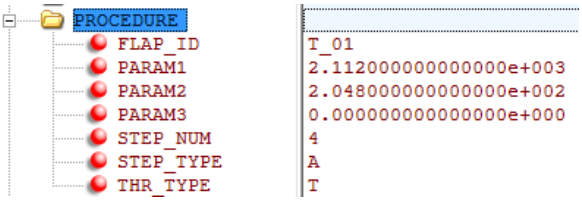

Figure 11: Segment 4 Parameters for STANDARD Procedure

Segment 5 is the constant speed climb where PARAM1 is set to 2040 ft, as shown in Figure 12. Note, this steps is not specified for NADPs procedures.

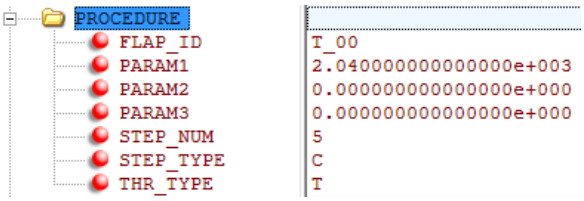

Figure 12: Segment 5 Parameters for STANDARD Procedure

Segment 6 is the constant speed climb, for the STANDARD procedure, cutback occurs at this step. PARAM1 is set to 3000ft and thrust type is set to C (climb thrust), as shown in Figure 13.

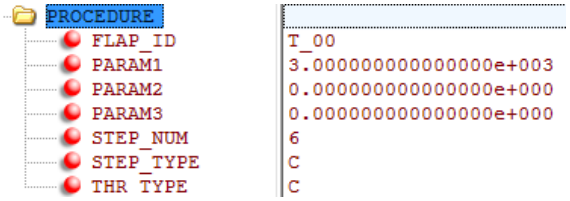

Figure 13: Segment 6 Parameters for STANDARD Procedure

Segment 7 is the final acceleration segment, where the final airspeed PARAM2 is always 250knots for all cases. The thrust type is set to C and PARAM1 is 1891.3 ft/min, as shown in Figure 14.

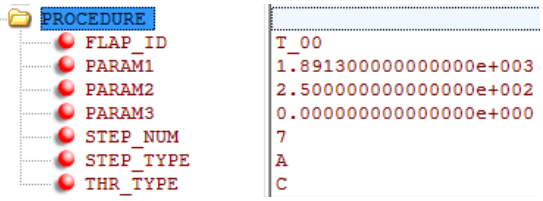

Figure 14: Segment 7 Parameters for STANDARD Procedure

Segments 8, 9, and 10 are the final constant climb segments, where the final altitudes are always 5500, 7500, and 10000 ft for all stage lengths. With these final segments, the entire STANDARD procedure is completely defined. After all the parameters for each segment have been identified for the STANDARD procedure, the aircraft was analyzed for noise, fuel burn, and NOx and tabulate in Table 2 and Table 3 at all stage lengths. This analysis served as the basis of comparisons for assessing the change of takeoff assumptions.

Table 2: Noise Contour Results for B737-800 STANDARD Procedure

Stage Length	70 dB SEL Contour Length [nmi]	70 dB SEL Contour Width [nmi]	70 dB SEL Contour Area [nmi^2]	80 dB SEL Contour Length [nmi]	80 dB SEL Contour Width [nmi]	80 dB SEL Contour Area [nmi^2]	90 dB SEL Contour Length [nmi]	90 dB SEL Contour Width [nmi]	90 dB SEL Contour Area [nmi^2]
1	14.369	4.491	54.156	7.662	2.205	12.159	2.536	0.842	1.474
2	15.160	4.452	57.084	8.104	2.172	12.694	2.655	0.826	1.519
3	16.035	4.414	60.314	8.599	2.152	13.278	2.785	0.807	1.568
4	17.650	4.346	66.305	9.506	2.109	14.345	3.015	0.777	1.660
5	19.327	4.285	72.522	10.445	2.071	15.452	3.273	0.750	1.760

Table 3: Fuel Burn and NOx Results for B737-800 STANDARD Procedures

Stage Length	NOX below 3,000 ft [g]	NOX 3,000 ft to 10,000 ft [g]	Fuel Burn below 3,000 ft [kg]	Fuel Burn 3,000 ft to 10,000 ft [kg]
1	6045.62	6232.65	226.35	264.25
2	6348.99	6570.48	237.54	278.59
3	6680.82	6942.53	249.77	294.38
4	7275.74	7654.39	271.60	324.59
5	7870.57	8394.50	293.37	356.01

Step 2

The second step of the partial derivative approach was to test the impact of the takeoff weight. Within AEDT, weight is defined into stage length bins. The aircraft take-off weight assumption was based on AEDT FLEET database and Project 35[5] results, except for the B777-200ER. Since B777-200ER was not analyzed in Project 35, no operational weights were available. Thus, the alternative weights were calculated based on the maximum payload weight and an operating weight from the Boeing Airport planning document for this aircraft. A 75% payload factor was assumed and it resulted in a constant change in weight being added to the aircraft. Fuel weight was not adjusted. The weight assumption for all three aircrafts which were used for the study are listed in Table 4. For the STANDARD procedure defined in step 1, the vehicle weight was changed from AEDT to the Project 35 weights. The weight change for B737-800 stage length 1 is shown in Figure 15 as an example.

Table 4: AEDT and Project 35 Weight for All Three Aircraft

	B737-800		B767-300ER		B777-200ER	
Stage Length	AEDT Weights [lbs]	P-35 Weights [lbs]	AEDT Weights [lbs]	P-35 Weights [lbs]	AEDT Weights [lbs]	ALT Weights [lbs]
1	133300	137725	265000	278500	429900	441900
2	139200	147590	275500	295600	442400	454400
3	145500	157165	286400	312120	456100	468100
4	156700	167620	305700	328575	483100	495100
5	167600	174203	330000	353100	516400	528400
6			355900	377615	551700	563700
7			367700	402135	589400	601400
8					629500	641500
9					656000	656000

Figure 15: Aircraft Weight Modification in for STANDARD Procedure

For B737-800, as the weight increases from AEDT to Project 35 weight, the contour length and area increased as compared to the baseline for all SEL levels. However, the contour width decreased for all SEL levels is shown in Figure 17. For 70, 80, and 90 dB, increasing the weight resulted in a longer contour, which might be due to the heavier vehicle having a shallower trajectory. This difference in trajectory is shown in Figure 16. Table 5 through Table 7 show the calculated noise metric for baseline and changes in weight for all stage length, the results show an increased in contour length of about 4% to 10% for all SEL levels. There are slight changes in the contour width about less than 1% for SEL 70 and 80 dB. For SEL 90 dB the changes in contour width about 1% to 3%. Overall contour area increases anywhere from 3% to 11% for all SEL levels. Also, increasing the weight increased NOx and fuel burn for all stage lengths is shows in Table 8 and Table 9.

[5] Georgia Institute of Technology, 2016. Airline Flight Data Examination to Improve Flight Performance Modeling-Final Report Project 35.

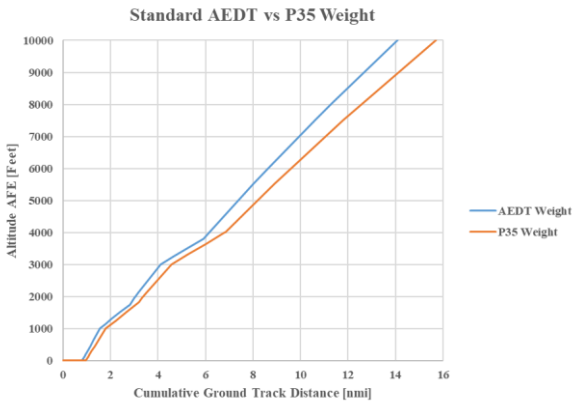

Figure 16: STANDARD AEDT vs. Project 35 Weight for Stage Length 3

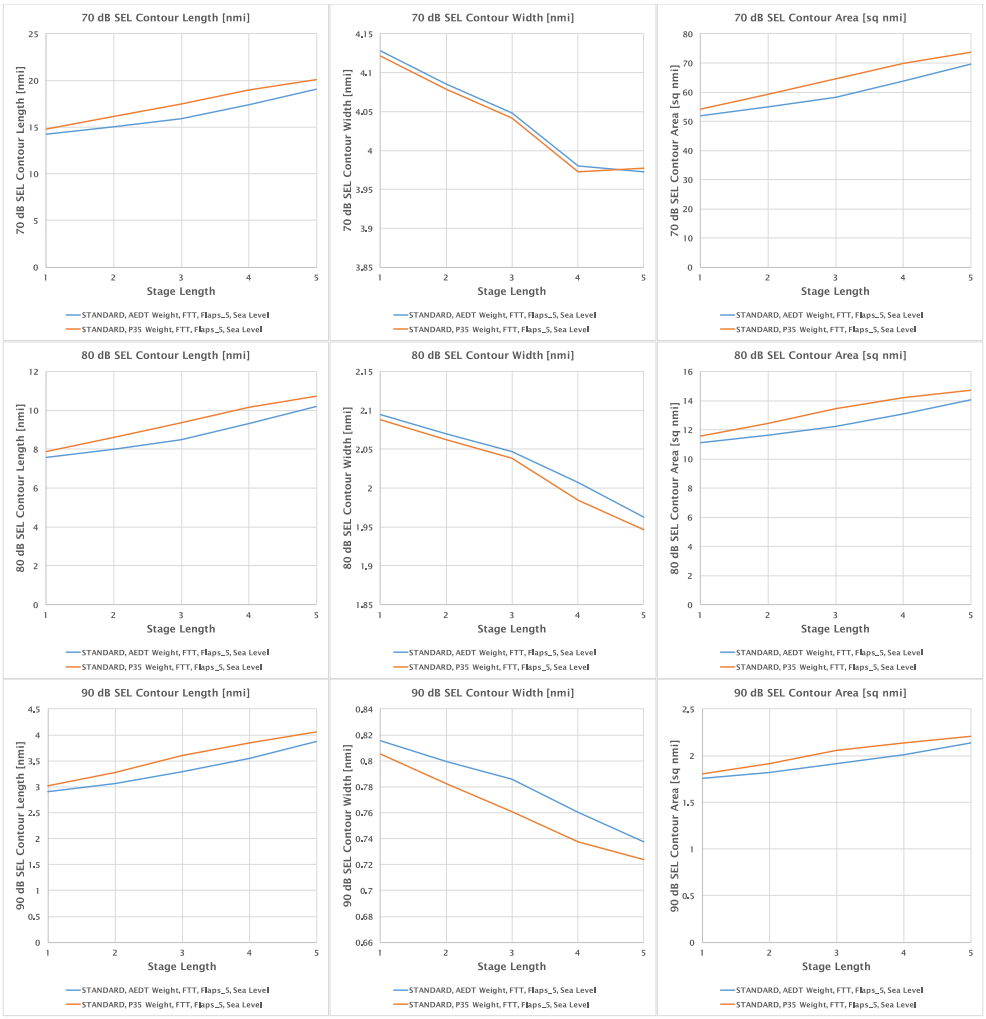

Figure 17: Weight Sensitivity Noise Results

Table 5: Weight Sensitivity SEL 70 dB Metric

Stage Length	STANDARD AEDT FTT Contour Length [nmi]	STANDARD P35 FTT Contour Length [nmi]	Percentage Difference	STANDARD AEDT FTT Contour Width [nmi]	STANDARD P35 FTT Contour Width [nmi]	Percentage Difference	STANDARD AEDT FTT Contour Area [sq. nmi]	STANDARD P35 FTT Contour Area [sq. nmi]	Percentage Difference
1	14.228	14.792	4%	4.128	4.122	0%	52.013	54.232	4%
2	14.998	16.113	7%	4.085	4.078	0%	54.833	59.194	8%
3	15.888	17.511	10%	4.049	4.041	0%	58.125	64.463	11%
4	17.421	19.020	9%	3.980	3.973	0%	63.722	69.895	10%
5	19.050	20.065	5%	3.973	3.978	0%	69.663	73.546	6%

Table 6: Weight Sensitivity SEL 80 dB Metric

Stage Length	STANDARD AEDT FTT Contour Length [nmi]	STANDARD P35 FTT Contour Length [nmi]	Percentage Difference	STANDARD AEDT FTT Contour Width [nmi]	STANDARD P35 FTT Contour Width [nmi]	Percentage Difference	STANDARD AEDT FTT Contour Area [sq. nmi]	STANDARD P35 FTT Contour Area [sq. nmi]	Percentage Difference
1	7.559	7.867	4%	2.095	2.088	0%	11.117	11.553	4%
2	7.985	8.587	8%	2.070	2.062	0%	11.601	12.437	7%
3	8.492	9.370	10%	2.047	2.038	0%	12.219	13.422	10%
4	9.313	10.163	9%	2.007	1.984	-1%	13.100	14.190	8%
5	10.196	10.733	5%	1.962	1.947	-1%	14.046	14.710	5%

Table 7: Weight Sensitivity SEL 90 dB Metric

Stage Length	STANDARD AEDT FTT Contour Length [nmi]	STANDARD P35 FTT Contour Length [nmi]	Percentage Difference	STANDARD AEDT FTT Contour Width [nmi]	STANDARD P35 FTT Contour Width [nmi]	Percentage Difference	STANDARD AEDT FTT Contour Area [sq. nmi]	STANDARD P35 FTT Contour Area [sq. nmi]	Percentage Difference
1	2.909	3.017	4%	0.816	0.805	-1%	1.753	1.803	3%
2	3.068	3.282	7%	0.800	0.783	-2%	1.818	1.916	5%
3	3.285	3.606	10%	0.786	0.761	-3%	1.912	2.057	8%
4	3.550	3.848	8%	0.760	0.737	-3%	2.013	2.133	6%
5	3.874	4.058	5%	0.738	0.724	-2%	2.136	2.209	3%

Table 8: Weight Sensitivity NOx Metric

Stage Length	STANDARD AEDT FTT NOx below 3,000 ft [g]	STANDARD P35 FTT NOx below 3,000 ft [g]	Percentage Difference	STANDARD AEDT FTT NOx 3,000 ft to 10,000 ft [g]	STANDARD P35 FTT NOx 3,000 ft to 10,000 ft [g]	Percentage Difference
1	6441.377491	6702.423261	4%	5479.081	5706.625	4%
2	6761.582634	7266.754357	7%	5787.113	6234.956	8%
3	7168.941787	7909.36733	10%	6125.350	6772.846	11%
4	7957.103434	8685.91611	9%	6551.746	7153.272	9%
5	8582.797272	9022.80602	5%	7221.653	7614.054	5%

Table 9: Weight Sensitivity Fuel Burn Metric

Stage Length	STANDARD AEDT FTT Fuel Burn below 3,000 ft [g]	STANDARD P35 FTT Fuel Burn below 3,000 ft [g]	Percentage Difference	STANDARD AEDT FTT Fuel Burn 3,000 ft to 10,000 ft [g]	STANDARD P35 FTT Fuel Burn 3,000 ft to 10,000 ft [g]	Percentage Difference
1	235.012	244.735	4%	232.659	242.325	4%
2	246.776	265.611	8%	245.762	264.790	8%
3	261.668	289.248	11%	260.150	287.665	11%
4	291.929	319.360	9%	278.414	304.008	9%
5	315.017	331.549	5%	306.898	323.592	5%

Step 3

For this experiment, the takeoff and climb thrust were changed to analyze the effect of thrust on the noise contours. The experiment was run using the STANDARD procedure at sea level condition with AEDT weight. The takeoff thrust was reduced by 15% and climb thrust was reduced by 10%. The derated thrust values for takeoff and climb thrust are based on Project 35. Data from more than a thousand flights gathered for Boeing aircraft showed that the aircraft were taking off with an average between 10% and 15.5% below their maximum takeoff thrust. Therefore, aircraft do not takeoff at maximum takeoff thrust as currently modeled in AEDT. For this study, a 15% reduction of maximum takeoff thrust was utilized. Currently, the climb thrust is set to maximum climb thrust in AEDT. However, based on recommendations by General Electric and Roll Royce, if the nominal takeoff thrust is 90% or higher of the maximum takeoff thrust, maximum climb thrust should be used.[6] [7] For this study, a 15% reduction of max takeoff thrust value was selected, therefore a derated climb thrust of 10% reduction of max climb thrust was selected for the study. Maximum and derated takeoff and climb thrust values are listed in Table 10. The COEFF_E values were changed in the study to simulate a 15% takeoff thrust reduction and 10% reduction in climb thrust, as shown in Figure 18.

Figure 18: COEFF_E Modification for STANDARD Procedure for Reduced Thrust

Table 10: Full and Reduce Thrust Values for All Three Vehicles

	B737-800		B767-300ER		B777-200ER	
Thrust Type	Full Thrust	Reduced Thrust	Full Thrust	Reduced Thrust	Full Thrust	Reduced Thrust
Takeoff, T	26089.1	22175.735	56370	47914.5	93672.6	79621.71
Climb, C	22403.5	20163.15	45480	40932	67093.7	60384.33

The flaps were set to the lowest possible takeoff flaps setting as shown in Table 11. For the B737-800, the flaps were set to Flaps 01. Currently, AEDT models all of the flap settings except for Flaps 01, which is the required takeoff flap setting for B737-800. AEDT requires flap coefficients COEFF_C_D and COEFF_B to be defined in order to enable the vehicle to takeoff at that flap setting. Aircraft trajectories were determined using high fidelity validation data (HFVD) for a B737-800 takeoff with full thrust using Flaps 01 at the following required reference conditions as defined in SAE-AIR-1845:[8]

[6] Donaldson, R., Fischer, D., Gough, J., & Rysz, M. (2007). Economic Impact of Derated Climb on Large Commercial Engines.Proceedings of the Performance and Flight Operations Engineering Conference.
[7] James, W., & O'Dell, P. (2005). Derated Climb Performance In Large Civil Aircraft.Proceedings of the Performance and Flight Operations Engineering Conference.
[8] FAA, 2016. Aviation Environmental Design Tool (AEDT) Version 2c User Guide

1) Wind: 4m/s (8 knots) headwind constant with height above ground
2) Runway Elevation: mean sea level
3) Runway gradient: None
4) Air temperature: 15C (59F)
5) Takeoff gross weight: 85% of maximum takeoff gross weight
6) Landing gross weight: 90% of maximum landing gross weight
7) Number of engines supply thrust along any segment of flight path: 2

Note that SAE-AIR-1845 does not specify thrust conditions for full or reduced engine power, which will likely impact the length of the ground roll.

Table 11: Takeoff Flaps Setting for All Three Vehicles[9]

	B737-800		B767-300ER		B777-200ER	
Flaps	Full Thrust	Reduced Thrust	Full Thrust	Reduced Thrust	Full Thrust	Reduced Thrust
Takeoff Flap	Flap 05	Flap 01	Flap 15	Flap 05	Flap 5	Flap 5

COEFF_B and COEFF_C_D were back calculated using HFVD data. Using SAE-AIR-1845, an "equivalent ground roll" can be calculated by using equation (1):

$$s_g = s_{gear\_up} - \left(\frac{h_{gear\_up}}{|\tan(\gamma)|}\right) \quad (1)$$

where,
γ : Flight path angle at the point where landing gear is retracted
s_{gear_up} : Ground distance
h_{gear_up} : Altitude at the point where landing gear is retracted

Using the calculated ground, COEFF_B was solved as [8]

$$s_g = \frac{B_f \theta \left(\frac{W}{\delta}\right)^2}{N\left(\frac{F_n}{\delta}\right)} \quad (2)$$

where,
s_g: Ground-roll distance
B_f: Ground-roll coefficient, which depends on the flaps setting
θ: Temperature ratio at the airport elevation
δ: Pressure ratio at the airport
$\left(\frac{F_n}{\delta}\right)_2$: Corrected net thrust per engine (lbf) at the end of the takeoff step

The ground roll equation can be simplified by matching the reference conditions specified in SAE-AIR-1845 and assuming the temperature and pressure ratios are equal to 1, resulting in Equation (3).

$$s_g = \frac{B_f W^2}{N(F_n)_2} \quad (3)$$

Rearranging Equation (3)to solve for COEFF_B results in Equation (4).

$$B_f = \frac{s_g N * (F_n)_2}{W^2} \quad (4)$$

[9] ICAO, 2007. Review of Noise Abatement Procedure Research & Development and Implentation Results, pages 9 to 10.

Using Equation (5) for calculating initial climb calibrated airspeed, COEFF_C_D can be back calculated.

$$v_2 = C_f * \sqrt{W} \tag{5}$$

where,
v_2: Initial climb calibrated airspeed
C_f: Takeoff speed coefficient that depends on flap settings
W: Departure profile weight; weight is assumed to remain constant for the entire departure profile

Rearranging Equation (5) in-term of COEFF_C_D results in:

$$C_f = \frac{v_2}{\sqrt{W}} \tag{6}$$

To validate the methodology, the COEFF_B and COEFF_C_D values were calculated for Flaps 05, which is contained in the Fleet DB. The calculated COEFF_B and COEFF_C_D are very similar to the values in AEDT FLEET DB for Flaps 05 as listed in Table 12, therefore this method can be used for calculating COEFF_B and COEFF_C_D for Flaps 1. Using this procedure Flaps 1 coefficient for full and reduce thrust was calculated, the results are listed in Table 13.

Table 12: Flap 05 COEFF_B and COEFF_C_D Calculated Values for Full Thrust

Coefficient	AEDT	Calculated	Percentage Difference
s_g [FT]	N/A	5182.874	N/A
COEFF_B [ft/lb]	0.009633	0.009758	1.30%
COEFF_C_D	0.435043	0.397091	-8.72%

Table 13: Flap 01 COEFF_B and COEFF_C_D Calculated Values for Full and Reduced Thrust

Coefficient	Using Full Thrust Takeoff	Using Reduced Thrust Takeoff
s_g [FT]	7273.1	7360.8
COEFF_B [ft/lb]	0.01359	0.01158
COEFF_C_D	0.41242	0.41424

The reduction of takeoff and climb thrust lead to a longer ground roll and add shallower climb as depicted in Figure 19. As a result, the noise contour lengths increased and the contour width and area decreased for all stage length as shown in Figure 20. Notice that for SEL 70 dB contour length trend does not increase at higher stage lengths, because the departure segment end altitude ends at 10000 ft resulted in the noise contour getting cutoff. The trends are similar for the B767-300ER and B777-200ER.

The tabulated noise results are provided in Table 14 to Table 16. An average decrease of 14% in contour width for SEL 70 dB was observed for all stage lengths. For SEL 80 and 90 dB, an increased in contour length of 3% for SEL 80 dB and between 16% and 23% for SEL 90 dB, because SEL 80 and 90 dB are more sensitive to thrust. There is a significant decrease in the overall noise contour width and area for SEL 80 and 90, for all stage length. NOx and fuel burn below 3,000 feet show an increase over the baseline full thrust takeoff due to the shallower climb out as listed in Table 17 and Table 18. Between 3000 ft and 10000ft there is significant less NOx production, but slight increase in fuel burn.

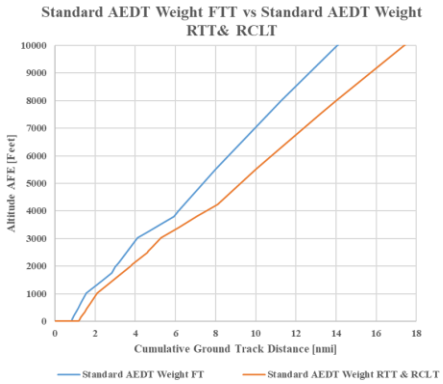

Figure 19: STANDARD Procedure for AEDT Weight Full vs Reduced Takeoff Thrust Trajectory for Stage Length 3

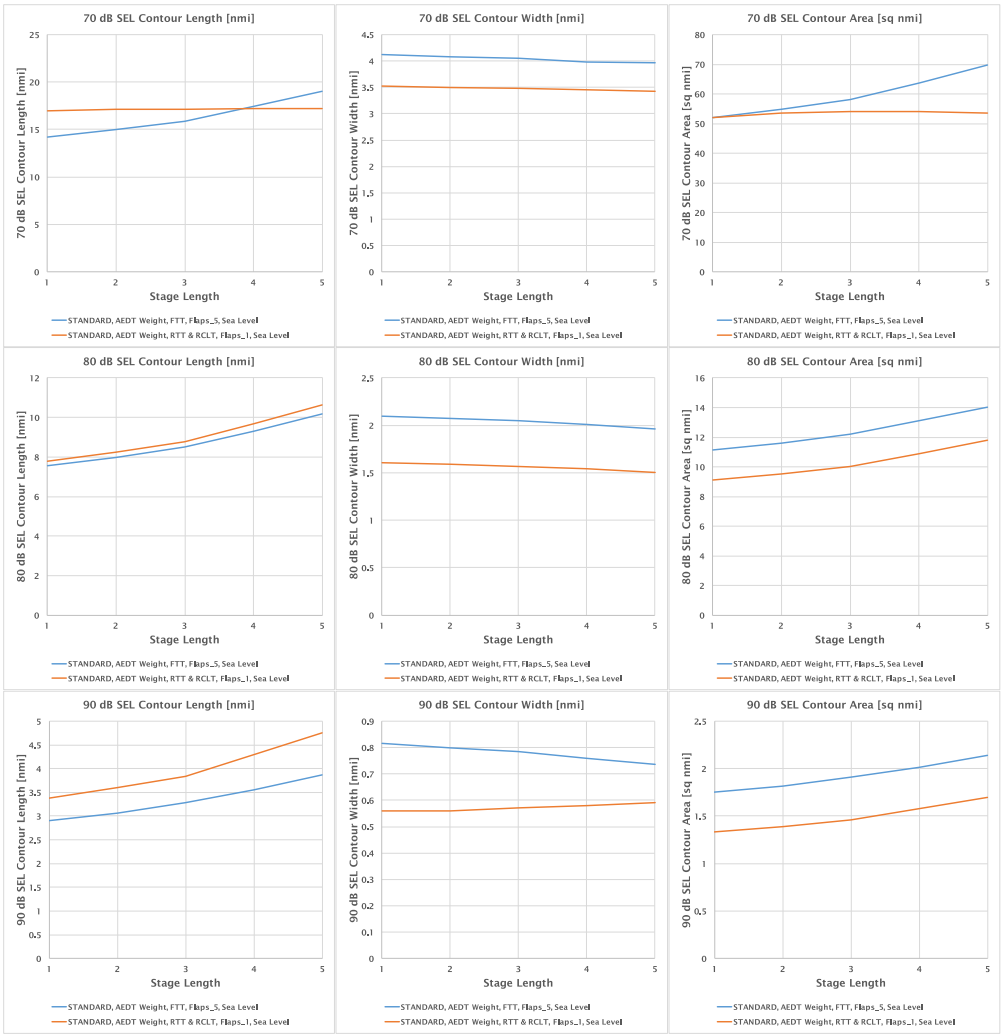

Figure 20: Thrust Sensitivity Noise Results

Table 14: Thrust Sensitivity SEL 70 dB Metric

Stage Length	STANDARD AEDT FTT Contour Length [nmi]	STANDARD AEDT RTT & RCLT Contour Length [nmi]	Percentage Difference	STANDARD AEDT FTT Contour Width [nmi]	STANDARD AEDT RTT & RCLT Contour Width [nmi]	Percentage Difference	STANDARD AEDT FTT Contour Area [sq. nmi]	STANDARD AEDT RTT & RCLT Contour Area [sq. nmi]	Percentage Difference
1	14.228	16.970	19%	4.128	3.520	-15%	52.013	52.050	0%
2	14.998	17.160	14%	4.085	3.490	-15%	54.833	53.620	-2%
3	15.888	17.170	8%	4.049	3.480	-14%	58.125	53.940	-7%
4	17.421	17.200	-1%	3.980	3.450	-13%	63.722	53.960	-15%
5	19.050	17.220	-10%	3.973	3.420	-14%	69.663	53.580	-23%

Table 15: Thrust Sensitivity SEL 80 dB Metric

Stage Length	STANDARD AEDT FTT Contour Length [nmi]	STANDARD AEDT RTT & RCLT Contour Length [nmi]	Percentage Difference	STANDARD AEDT FTT Contour Width [nmi]	STANDARD AEDT RTT & RCLT Contour Width [nmi]	Percentage Difference	STANDARD AEDT FTT Contour Area [sq. nmi]	STANDARD AEDT RTT & RCLT Contour Area [sq. nmi]	Percentage Difference
1	7.559	7.790	3%	2.095	1.610	-23%	11.117	9.110	-18%
2	7.985	8.250	3%	2.070	1.590	-23%	11.601	9.540	-18%
3	8.492	8.760	3%	2.047	1.570	-23%	12.219	10.020	-18%
4	9.313	9.690	4%	2.007	1.540	-23%	13.100	10.900	-17%
5	10.196	10.640	4%	1.962	1.500	-24%	14.046	11.790	-16%

Table 16: Thrust Sensitivity SEL 90 dB Metric

Stage Length	STANDARD AEDT FTT Contour Length [nmi]	STANDARD AEDT RTT & RCLT Contour Length [nmi]	Percentage Difference	STANDARD AEDT FTT Contour Width [nmi]	STANDARD AEDT RTT & RCLT Contour Width [nmi]	Percentage Difference	STANDARD AEDT FTT Contour Area [sq. nmi]	STANDARD AEDT RTT & RCLT Contour Area [sq. nmi]	Percentage Difference
1	2.909	3.380	16%	0.816	0.560	-31%	1.753	1.330	-24%
2	3.068	3.600	17%	0.800	0.560	-30%	1.818	1.390	-24%
3	3.285	3.840	17%	0.786	0.570	-27%	1.912	1.460	-24%
4	3.550	4.290	21%	0.760	0.580	-24%	2.013	1.580	-22%
5	3.874	4.760	23%	0.738	0.590	-20%	2.136	1.700	-20%

Table 17: Thrust Sensitivity NOx Metric

Stage Length	STANDARD AEDT FTT NOx below 3,000 ft [g]	STANDARD AEDT RTT & RCLT NOx below 3,000 ft [g]	Percentage Difference	STANDARD AEDT FTT NOx 3,000 ft to 10,000 ft [g]	STANDARD AEDT RTT & RCLT NOx 3,000 ft to 10,000 ft [g]	Percentage Difference
1	6441.377491	7350.469767	14%	5479.081	4937.643	-10%
2	6761.582634	7765.169042	15%	5787.113	5296.844	-8%
3	7168.941787	8226.378587	15%	6125.350	5628.586	-8%
4	7957.103434	9320.46483	17%	6551.746	6010.076	-8%
5	8582.797272	10163.54645	18%	7221.653	6687.051	-7%

Table 18: Thrust Sensitivity Fuel Burn Metric

Stage Length	STANDARD AEDT FTT Fuel Burn below 3,000 ft [g]	STANDARD AEDT RTT & RCLT Fuel Burn below 3,000 ft [g]	Percentage Difference	STANDARD AEDT FTT Fuel Burn 3,000 ft to 10,000 ft [g]	STANDARD AEDT RTT & RCLT Fuel Burn 3,000 ft to 10,000 ft [g]	Percentage Difference
1	235.012	322.661	37%	232.659	235.320	1%
2	246.776	340.738	38%	245.762	252.313	3%
3	261.668	360.817	38%	260.150	268.160	3%
4	291.929	409.512	40%	278.414	286.410	3%
5	315.017	446.284	42%	306.898	318.744	4%

Step 4

Using the STANDARD procedure define in step 1, the aircrafts weight were changed from AEDT weights to Project 35 weights and the takeoff and climb thrust were reduced as in Step 3, which resulted in a much shallower climb out trajectory as depicted in Figure 21. The takeoff flaps were set to the lowest possible flap setting permissible for takeoff. For B737-800, increasing the weight and reducing the thrust resulted in an increase in the contour length and a decrease in the contour width for all SEL dB level as shown in Figure 22. However, the contour area increased for SEL 70 dB, but decreased for SEL 80 and 90dB as shown in Figure 22. An increase in contour length is due to the shallower climb as depicted in Figure 21.

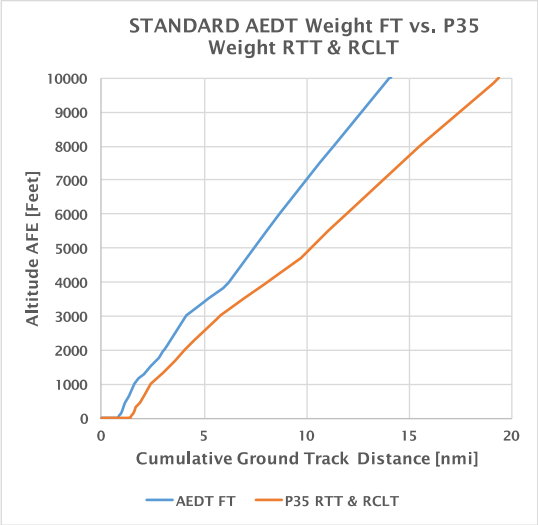

Figure 21: STANDARD AEDT Weight FT vs. Project 35 Weight RTT & RCLT for Stage Length 3

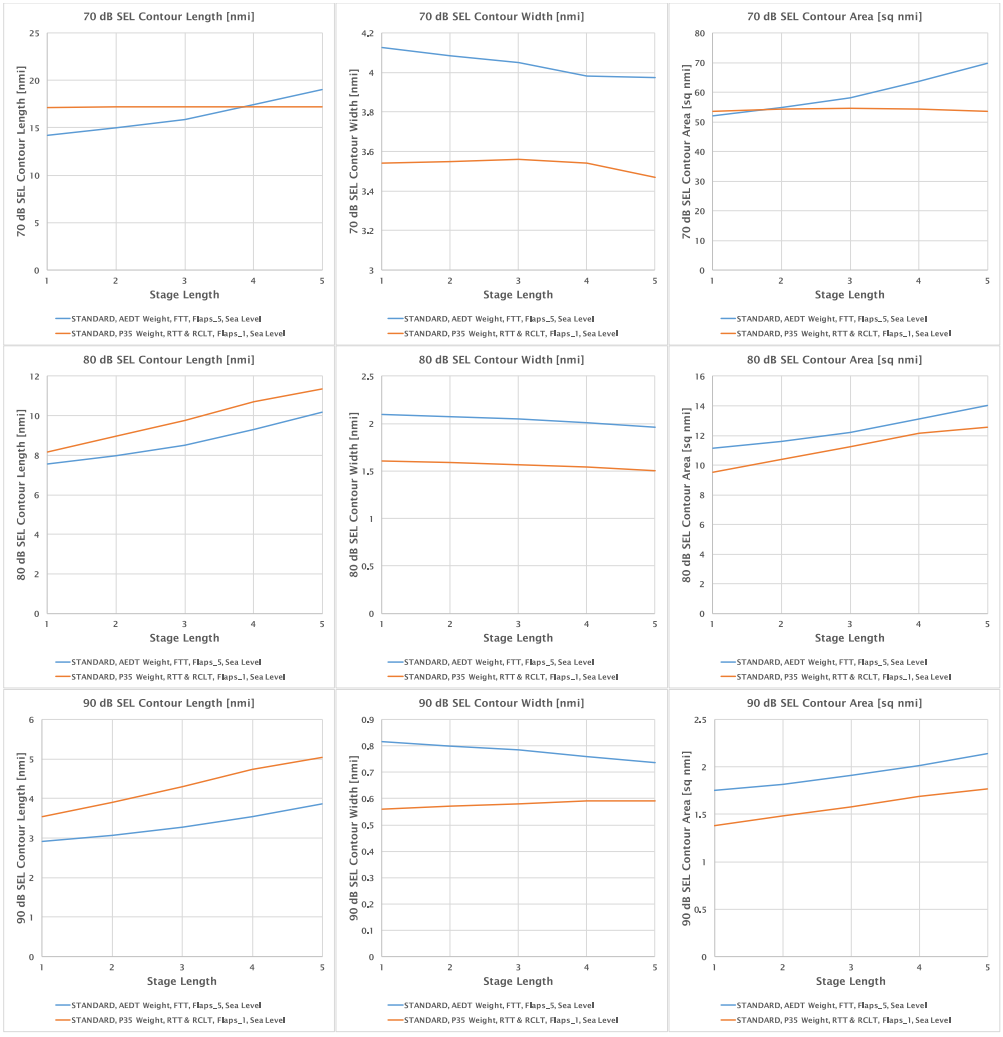

Figure 22: Weight and Thrust Sensitivity Noise Results

The calculated contour noise metrics are listed in Table 19 to Table 21. Note that there is a significant increase in contour length for SEL for SEL 70 dB of 21% at lower stage lengths. However, the contour does not increase further after stage length 1, because the noise contour was cut off due to the end altitude for the departure procedure end at 10000 ft. There are significant changes for SEL 70 dB contour width of 11% to 14% decrease overall. SEL 80 and 90 dB have an increased contour length and decreased in contour width and area. There is a significant increase in NOx and fuel burn below 3000 ft as listed in Table 22 and Table 23, due to the shallower climb due to heavier weight resulted in longer period of times for the aircraft to reach 3000 ft.

Table 19: Weight and Thrust Sensitivity SEL 70 dB Metric

Stage Length	STANDARD AEDT FTT Contour Length [nmi]	STANDARD P35 RTT & RCLT Contour Length [nmi]	Percentage Difference	STANDARD AEDT FTT Contour Width [nmi]	STANDARD P35 RTT & RCLT Contour Width [nmi]	Percentage Difference	STANDARD AEDT FTT Contour Area [sq. nmi]	STANDARD P35 RTT & RCLT Contour Area [sq. nmi]	Percentage Difference
1	14.228	17.160	21%	4.128	3.540	-14%	52.013	53.660	3%
2	14.998	17.180	15%	4.085	3.550	-13%	54.833	54.410	-1%
3	15.888	17.200	8%	4.049	3.560	-12%	58.125	54.600	-6%
4	17.421	17.220	-1%	3.980	3.540	-11%	63.722	54.300	-15%
5	19.050	17.230	-10%	3.973	3.470	-13%	69.663	53.660	-23%

Table 20: Weight and Thrust Sensitivity SEL 80 dB Metric

Stage Length	STANDARD AEDT FTT Contour Length [nmi]	STANDARD P35 RTT & RCLT Contour Length [nmi]	Percentage Difference	STANDARD AEDT FTT Contour Width [nmi]	STANDARD P35 RTT & RCLT Contour Width [nmi]	Percentage Difference	STANDARD AEDT FTT Contour Area [sq. nmi]	STANDARD P35 RTT & RCLT Contour Area [sq. nmi]	Percentage Difference
1	7.559	8.150	8%	2.095	1.610	-23%	11.117	9.530	-14%
2	7.985	8.950	12%	2.070	1.590	-23%	11.601	10.370	-11%
3	8.492	9.760	15%	2.047	1.570	-23%	12.219	11.240	-8%
4	9.313	10.720	15%	2.007	1.540	-23%	13.100	12.140	-7%
5	10.196	11.370	12%	1.962	1.500	-24%	14.046	12.560	-11%

Table 21: Weight and Thrust Sensitivity SEL 90 dB Metric

Stage Length	STANDARD AEDT FTT Contour Length [nmi]	STANDARD P35 RTT & RCLT Contour Length [nmi]	Percentage Difference	STANDARD AEDT FTT Contour Width [nmi]	STANDARD P35 RTT & RCLT Contour Width [nmi]	Percentage Difference	STANDARD AEDT FTT Contour Area [sq. nmi]	STANDARD P35 RTT & RCLT Contour Area [sq. nmi]	Percentage Difference
1	2.909	3.540	22%	0.816	0.560	-31%	1.753	1.380	-21%
2	3.068	3.910	27%	0.800	0.570	-29%	1.818	1.480	-19%
3	3.285	4.300	31%	0.786	0.580	-26%	1.912	1.580	-17%
4	3.550	4.740	34%	0.760	0.590	-22%	2.013	1.690	-16%
5	3.874	5.040	30%	0.738	0.590	-20%	2.136	1.770	-17%

Table 22: Weight and Thrust Sensitivity NOx Metric

Stage Length	STANDARD AEDT FTT NOx below 3,000 ft [g]	STANDARD P35 RTT & RCLT NOx below 3,000 ft [g]	Percentage Difference	STANDARD AEDT FTT NOx 3,000 ft to 10,000 ft [g]	STANDARD P35 RTT & RCLT NOx 3,000 ft to 10,000 ft [g]	Percentage Difference
1	6441.378	7713.759	20%	5479.081	5112.940	-7%
2	6761.583	8483.530	25%	5787.113	5690.379	-2%
3	7168.942	9267.492	29%	6125.350	6194.513	1%
4	7957.103	9391.562	18%	6551.746	7541.325	15%
5	8582.797	10823.022	26%	7221.653	7030.133	-3%

Table 23: Weight and Thrust Sensitivity Fuel Burn Metric

Stage Length	STANDARD AEDT FTT Fuel Burn below 3,000 ft [g]	STANDARD P35 RTT & RCLT & RCLT Fuel Burn below 3,000 ft [g]	Percentage Difference	STANDARD AEDT FTT Fuel Burn 3,000 ft to 10,000 ft [g]	STANDARD P35 RTT & RCLT Fuel Burn 3,000 ft to 10,000 ft [g]	Percentage Difference
1	235.012	338.517	44%	232.659	243.720	5%
2	246.776	372.050	51%	245.762	271.024	10%
3	261.668	406.190	55%	260.150	295.071	13%
4	291.929	408.801	40%	278.414	359.150	29%
5	315.017	475.102	51%	306.898	335.093	9%

Step 5

Currently, AEDT only models STANDARD procedures, but typically, pilots fly using a noise abatement departure procedure (NADP). FAA AC 91-53A and ICAO PANS OPS Chapter 3 Volume II both contain the minimum safe standards for departure procedures. Both documents recommend that all carriers adopt no more than two procedures for each aircraft type; one for noise abatement of communities close to the airport (NADP1) and one for noise abatement of communities far from the airport (NADP-2) as depicted in Figure 23. These procedures are not modeled within AEDT. Therefore, the NADP procedures were modeled based on HFVD. All three aircraft take-off procedures were modeled at STANDARD day sea level conditions. The differences between the existing procedures in AEDT and the new procedures are thrust, cutback altitudes, and the flap retraction schedule. The AEDT STANDARD procedure for the three aircraft was changed to NADP 1 & 2 procedure. The procedure defined in Figure 23 is different from Table 1, because the HFVD procedures use energy share percentage instead of specifying rates of climb. Since the energy share percentage value does not change for the three aircraft, as shown in Figure 24, the rates of climb do not need to be estimated.

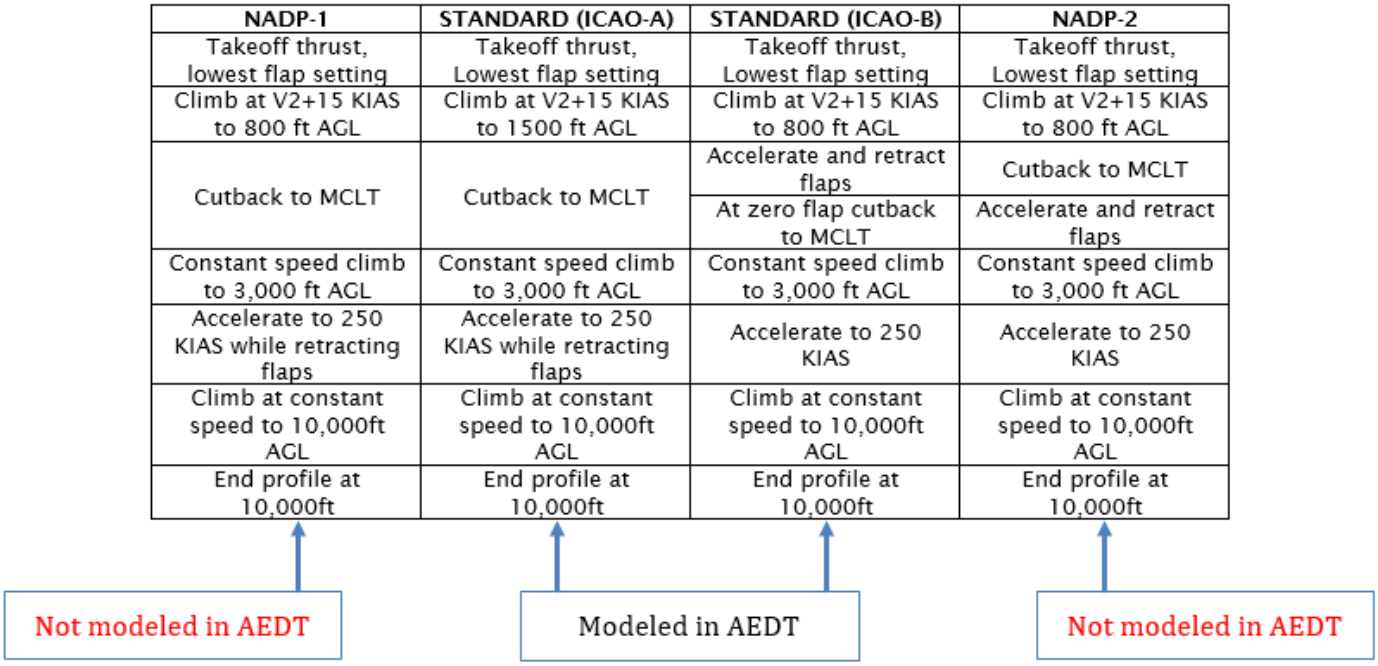

Figure 23: STANDARD and NADPs Procedures

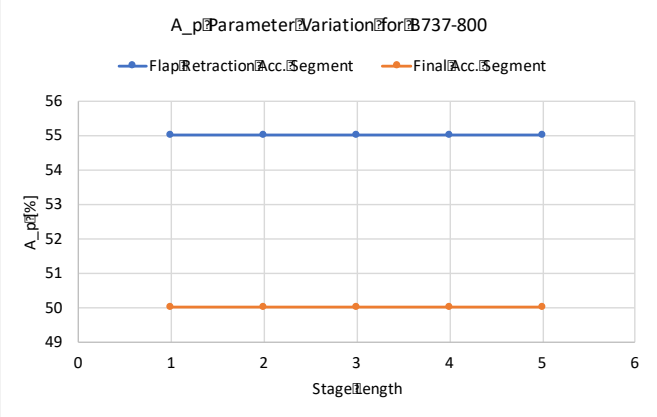

Figure 24: Energy Share Percentage

Energy share percentages of 55% before and 50% after flap retraction are used for the acceleration segment. Table 24 is a sample of NADP-1 procedure parameters defined for the B737-800 at stage length 1. The Flap_ID is the flap setting which in this case is Flaps 5 for B737-800 for takeoff. PARAM1 is the rate of climb for acceleration segment and altitude for constant speed climb segment. The type of segment is denoted in STEP_TYPE, where C is constant speed climb, while A and P are the acceleration climb steps. STEP_TYPE P is for defining energy share percentage for PARAM1 and for STEP_TYPE A, the PARAM1 is the rate of climb (ft/min). PARAM2 is the final velocity in knots.

Table 24: NADP-1 Procedure Parameters

Segment	Flap_ID	PARAM1	PARAM2	PARAM3	STEP_TYPE	THR_TYPE
1	T_05	0	0	0	T	T
2	T_05	1000	0	0	C	T
3	T_05	3000	0	0	C	C
4	T_05	55	175.3	0	P	C
5	T_01	55	209	0	P	C
6	T_00	50	250	0	P	C
7	T_00	5500	0	0	C	C
8	T_00	7500	0	0	C	C
9	T_00	10000	0	0	C	C

Since energy share percentage does not change, the only parameter that varies with stage length is the velocity at the end of the acceleration segment. The velocity at the end of acceleration segment can be acquired from HFVD. However, the end velocity using HFVD is very similar to STANDARD full thrust final velocity parameters. An experiment was performed to check the sensitivity of the noise contours and trajectories when using STANDARD procedure VSTOP parameters for reduced thrust takeoff for NADPs. It was found that the trajectories and contours are nearly identical when using velocities from the STANDARD procedure for NADP-1 and NADP-2.

Step 5 focused on analyzing the changes in noise contour, fuel burn and NOx due to changes in departure procedure for all three vehicles. The vehicle weights were set to AEDT weights, flaps were set to Flap 05, with full takeoff thrust and maximum climb thrust. The noise contour results for B737-800 NADP-1 are shown in Figure 26 and the calculate noise metric are in Table 25 to Table 27. Contour length is slightly longer for SEL 70 and 80 dB, but significantly shorter for SEL 90 dB. Contour width is wider at SEL 70dB, but smaller for SEL 90 dB. The contour width is insensitive to the changes in procedure for SEL 80 dB. Contour area for SEL 70 and 80 dB is larger, but smaller for SEL 90dB. Table 28 and Table 29 shows a 8% to 10% decreased in the fuel burn and NOx below 3000ft, but increase of 15% to 19% in fuel burn and NOx between 3000 ft to 10000 ft. This might be due to NADP-1 procedure cutback to climb thrust earlier than STANDARD procedure as shows in Figure 23.

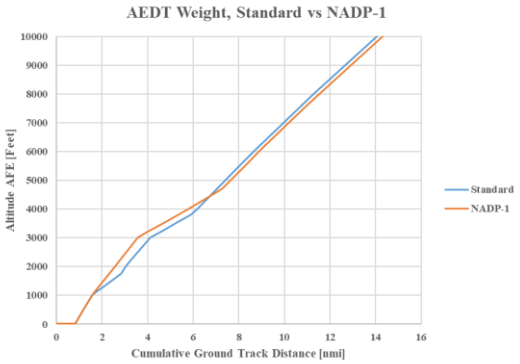

Figure 25: AEDT Weight STANDARD vs NADP-1 Procedure for Full Thrust

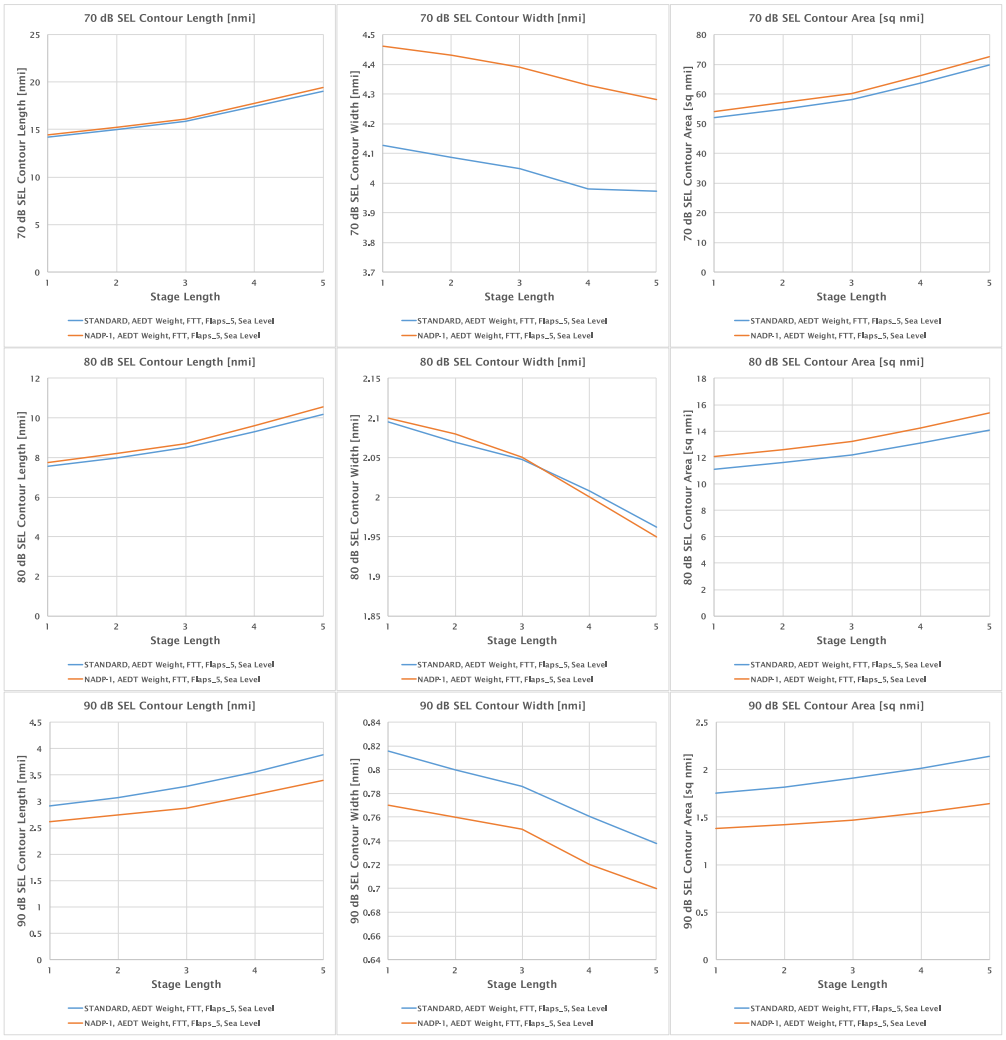

Figure 26: Procedure Sensitivity Noise Results

Table 25: Procedure Sensitivity SEL 70 dB Metric

Stage Length	STANDARD AEDT FTT Contour Length [nmi]	NADP-1 AEDT FTT Contour Length [nmi]	Percentage Difference	STANDARD AEDT FTT Contour Width [nmi]	NADP-1 AEDT FTT Contour Width [nmi]	Percentage Difference	STANDARD AEDT FTT Contour Area [sq. nmi]	NADP-1 AEDT FTT Contour Area [sq. nmi]	Percentage Difference
1	14.228	14.450	2%	4.128	4.460	8%	52.013	54.030	4%
2	14.998	15.250	2%	4.085	4.430	8%	54.833	56.980	4%
3	15.888	16.120	1%	4.049	4.390	8%	58.125	60.230	4%
4	17.421	17.750	2%	3.980	4.330	9%	63.722	66.240	4%
5	19.050	19.440	2%	3.973	4.280	8%	69.663	72.480	4%

Table 26: Procedure Sensitivity SEL 80 dB Metric

Stage Length	STANDARD AEDT FTT Contour Length [nmi]	NADP-1 AEDT FTT Contour Length [nmi]	Percentage Difference	STANDARD AEDT FTT Contour Width [nmi]	NADP-1 AEDT FTT Contour Width [nmi]	Percentage Difference	STANDARD AEDT FTT Contour Area [sq. nmi]	NADP-1 AEDT FTT Contour Area [sq. nmi]	Percentage Difference
1	7.559	7.750	3%	2.095	2.100	0%	11.117	12.050	8%
2	7.985	8.190	3%	2.070	2.080	1%	11.601	12.600	9%
3	8.492	8.690	2%	2.047	2.050	0%	12.219	13.190	8%
4	9.313	9.600	3%	2.007	2.000	0%	13.100	14.260	9%
5	10.196	10.550	3%	1.962	1.950	-1%	14.046	15.360	9%

Table 27: Procedure Sensitivity SEL 90 dB Metric

Stage Length	STANDARD AEDT FTT Contour Length [nmi]	NADP-1 AEDT FTT Contour Length [nmi]	Percentage Difference	STANDARD AEDT FTT Contour Width [nmi]	NADP-1 AEDT FTT Contour Width [nmi]	Percentage Difference	STANDARD AEDT FTT Contour Area [sq. nmi]	NADP-1 AEDT FTT Contour Area [sq. nmi]	Percentage Difference
1	2.909	2.610	-10%	0.816	0.770	-6%	1.753	1.380	-21%
2	3.068	2.740	-11%	0.800	0.760	-5%	1.818	1.420	-22%
3	3.285	2.870	-13%	0.786	0.750	-5%	1.912	1.470	-23%
4	3.550	3.120	-12%	0.760	0.720	-5%	2.013	1.550	-23%
5	3.874	3.390	-12%	0.738	0.700	-5%	2.136	1.640	-23%

Table 28: Procedure Sensitivity NOx Metric

Stage Length	STANDARD AEDT FTT NOx below 3,000 ft [g]	NADP-1 AEDT FTT NOx below 3,000 ft [g]	Percentage Difference	STANDARD AEDT FTT NOx 3,000 ft to 10,000 ft [g]	NADP-1 AEDT FTT NOx 3,000 ft to 10,000 ft [g]	Percentage Difference
1	6441.377	5916.647	-8%	5479.081	6287.650	15%
2	6761.583	6199.107	-8%	5787.113	6648.208	15%
3	7168.942	6506.675	-9%	6125.350	7045.431	15%
4	7957.103	7068.306	-11%	6551.746	7786.112	19%
5	8582.797	7633.095	-11%	7221.653	8554.715	18%

Table 29: Procedure Sensitivity Fuel Burn Metric

Stage Length	STANDARD AEDT FTT Fuel Burn below 3,000 ft [g]	NADP-1 AEDT FTT Fuel Burn below 3,000 ft [g]	Percentage Difference	STANDARD AEDT FTT Fuel Burn 3,000 ft to 10,000 ft [g]	NADP-1 AEDT FTT Fuel Burn 3,000 ft to 10,000 ft [g]	Percentage Difference
1	235.012	224.634	-4%	232.659	266.550	15%
2	246.776	235.092	-5%	245.762	281.840	15%
3	261.668	246.470	-6%	260.150	298.685	15%
4	291.929	267.222	-8%	278.414	330.100	19%
5	315.017	288.059	-9%	306.898	362.705	18%

NADP2 noise results are shows in Figure 28 and calculated noise metric are found in Table 30 and Table 32. There is little to no changes in noise contour length and area for NADP-2 SEL 70 dB compare to STANDARD procedure for all stage length. There is a significant in contour width at earlier stage length, but the different between NADP-2 and STANDARD contour width decreases at higher stage length as shows in Table 30. For SEL 80 dB an increased in about 5% on the overall contour length for all stage length. Table 31 shows a decrease of 12% for contour width and 4% to 6% for contour area. There is a significant decrease for contour length, width and area for SEL 90 dB as shows in Table 32.

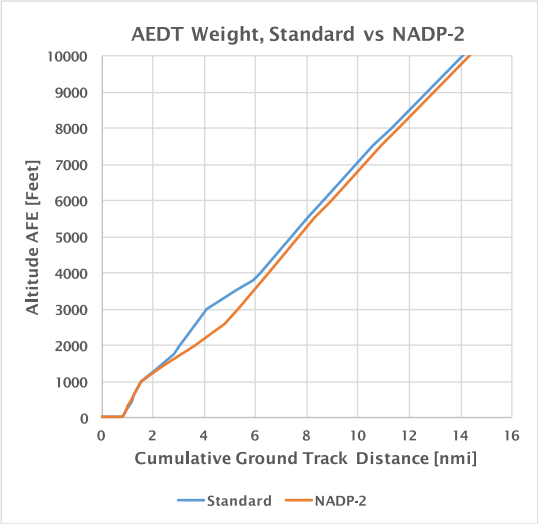

Figure 27: AEDT Weight STANDARD vs NADP-2 Procedure for Full Thrust

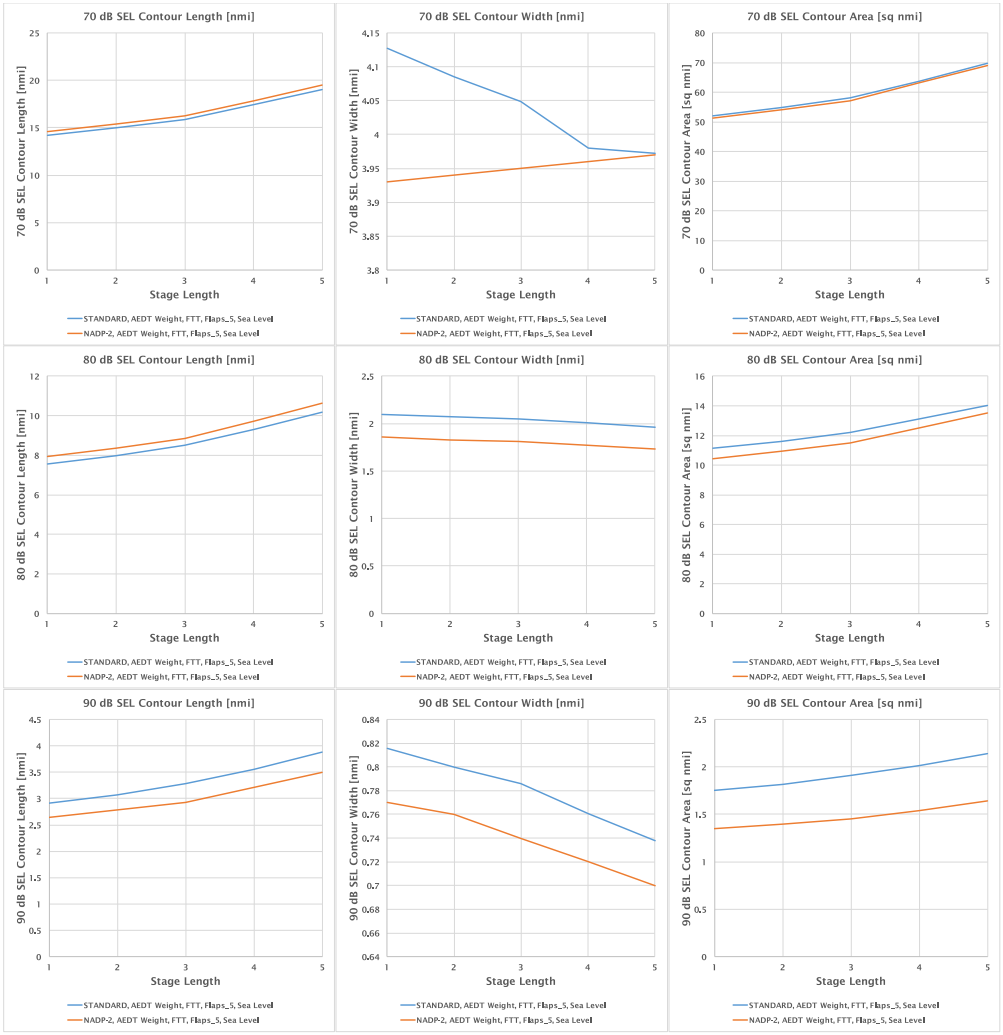

Figure 28: Procedure Sensitivity Noise Results

Table 30: Procedure Sensitivity SEL 70 dB Metric

Stage Length	STANDARD AEDT FTT Contour Length [nmi]	NADP-2 AEDT FTT Contour Length [nmi]	Percentage Difference	STANDARD AEDT FTT Contour Width [nmi]	NADP-2 AEDT FTT Contour Width [nmi]	Percentage Difference	STANDARD AEDT FTT Contour Area [sq. nmi]	NADP-2 AEDT FTT Contour Area [sq. nmi]	Percentage Difference
1	14.228	14.580	2%	4.128	3.930	-5%	52.013	51.160	-2%
2	14.998	15.360	2%	4.085	3.940	-4%	54.833	54.030	-1%
3	15.888	16.230	2%	4.049	3.950	-2%	58.125	57.190	-2%
4	17.421	17.830	2%	3.980	3.960	-1%	63.722	63.050	-1%
5	19.050	19.490	2%	3.973	3.970	0%	69.663	69.070	-1%

Table 31: Procedure Sensitivity SEL 80 dB Metric

Stage Length	STANDARD AEDT FTT Contour Length [nmi]	NADP-2 AEDT FTT Contour Length [nmi]	Percentage Difference	STANDARD AEDT FTT Contour Width [nmi]	NADP-2 AEDT FTT Contour Width [nmi]	Percentage Difference	STANDARD AEDT FTT Contour Area [sq. nmi]	NADP-2 AEDT FTT Contour Area [sq. nmi]	Percentage Difference
1	7.559	7.920	5%	2.095	1.860	-11%	11.117	10.430	-6%
2	7.985	8.360	5%	2.070	1.830	-12%	11.601	10.940	-6%
3	8.492	8.850	4%	2.047	1.810	-12%	12.219	11.490	-6%
4	9.313	9.740	5%	2.007	1.770	-12%	13.100	12.500	-5%
5	10.196	10.640	4%	1.962	1.730	-12%	14.046	13.500	-4%

Table 32: Procedure Sensitivity SEL 90 dB Metric

Stage Length	STANDARD AEDT FTT Contour Length [nmi]	NADP-2 AEDT FTT Contour Length [nmi]	Percentage Difference	STANDARD AEDT FTT Contour Width [nmi]	NADP-2 AEDT FTT Contour Width [nmi]	Percentage Difference	STANDARD AEDT FTT Contour Area [sq. nmi]	NADP-2 AEDT FTT Contour Area [sq. nmi]	Percentage Difference
1	2.909	2.640	-9%	0.816	0.770	-6%	1.753	1.350	-23%
2	3.068	2.780	-9%	0.800	0.760	-5%	1.818	1.400	-23%
3	3.285	2.930	-11%	0.786	0.740	-6%	1.912	1.450	-24%
4	3.550	3.210	-10%	0.760	0.720	-5%	2.013	1.540	-23%
5	3.874	3.490	-10%	0.738	0.700	-5%	2.136	1.640	-23%

There is a significant increase in fuel burn and NOx below 3000 ft, but decrease between 3000 ft and 10000 ft as listed in Table 33 and Table 34.The effect on Fuel burn and NOx is opposite for NADP-2 when compared to NADP-1 procedure. Fuel burn and NOx are higher under 3000ft, but lower above 3000ft when comparing Table 33 and Table 34 to Table 28 and Table 29.

Table 33: Procedure Sensitivity NOx Metric

Stage Length	STANDARD AEDT FTT NOx below 3,000 ft [g]	NADP-2 AEDT FTT NOx below 3,000 ft [g]	Percentage Difference	STANDARD AEDT FTT NOx 3,000 ft to 10,000 ft [g]	NADP-2 AEDT FTT NOx 3,000 ft to 10,000 ft [g]	Percentage Difference
1	6441.377	7063.876	10%	5479.081	4499.245	-18%
2	6761.583	7424.524	10%	5787.113	4769.526	-18%
3	7168.942	7817.392	9%	6125.350	5067.943	-17%
4	7957.103	8535.235	7%	6551.746	5625.374	-14%
5	8582.797	9253.635	8%	7221.653	6203.979	-14%

Table 34: Procedure Sensitivity Fuel Burn Metric

Stage Length	STANDARD AEDT FTT Fuel Burn below 3,000 ft [g]	NADP-2 AEDT FTT Fuel Burn below 3,000 ft [g]	Percentage Difference	STANDARD AEDT FTT Fuel Burn 3,000 ft to 10,000 ft [g]	NADP-2 AEDT FTT Fuel Burn 3,000 ft to 10,000 ft [g]	Percentage Difference
1	235.012	272.460	16%	232.659	191.523	-18%
2	246.776	286.276	16%	245.762	203.030	-17%
3	261.668	301.317	15%	260.150	215.736	-17%
4	291.929	328.773	13%	278.414	239.469	-14%
5	315.017	356.342	13%	306.898	264.105	-14%

Step 6

Similar to step 2, the aircraft weights were changed from AEDT to Project 35 weight for B737-800 and B767-300ER and ALT weight for B777-200ER. The procedure was also changed from STANDARD to the NADP procedures. All the other parameters were kept constant. Changing procedures and weights for B737-800 increased contour length and area for SEL 70 and 80 dB, but decreased for SEL 90 dB as shown in Figure 30. The increase in contour length is due to the shallower trajectory as shown in Figure 29. Contour width is wider for SEL 70 dB, but smaller for SEL 80 and 90 dB as shows in Figure 30. Table 35 and Table 37 shows calculate noise metric for SEL 70, 80,and 90 dB. The results showed there are significant changes to all the noise parameter for all SEL levels, except SEL 80 dB contour width. There little to no changes in contour width for SEL 80 dB. Changing departure procedure and weight, results in significant increase in the overall fuel burn and NOx between 3000 to 10000 ft. However, there is little to no changes for fuel burn and NOx below 3000 ft as shows in Table 38 and Table 39.

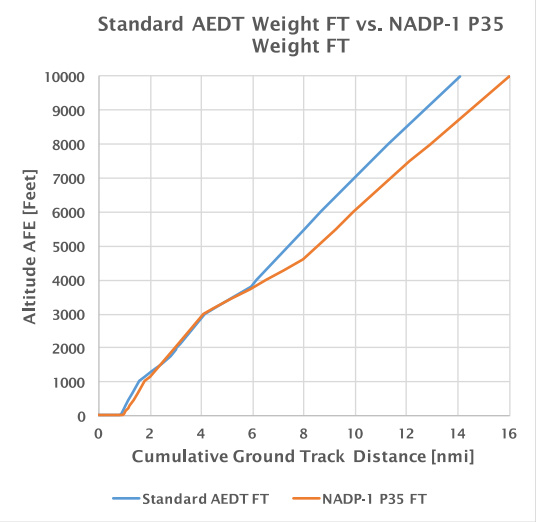

Figure 29: STANDARD AEDT Weight FT vs NADP-1 P35 Weight for Full Thrust

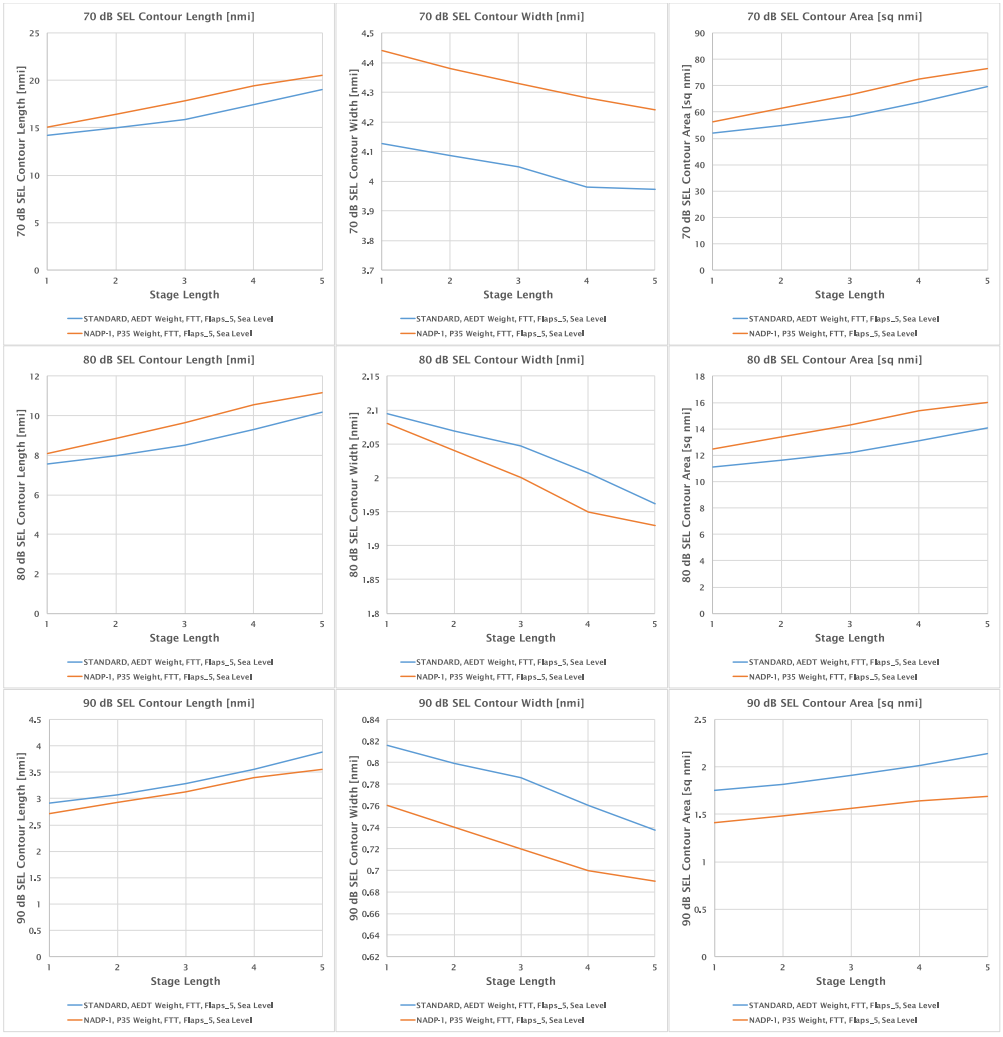

Figure 30: Procedure and Weight Sensitivity Noise Results

Table 35: Procedure and Weight Sensitivity SEL 70 dB Metric

Stage Length	STANDARD AEDT FTT Contour Length [nmi]	NADP-1 P35 FTT Contour Length [nmi]	Percentage Difference	STANDARD AEDT FTT Contour Width [nmi]	NADP-1 P35 FTT Contour Width [nmi]	Percentage Difference	STANDARD AEDT FTT Contour Area [sq. nmi]	NADP-1 P35 FTT Contour Area [sq. nmi]	Percentage Difference
1	14.228	15.050	6%	4.128	4.440	8%	52.013	56.240	8%
2	14.998	16.420	9%	4.085	4.380	7%	54.833	61.340	12%
3	15.888	17.820	12%	4.049	4.330	7%	58.125	66.500	14%
4	17.421	19.440	12%	3.980	4.280	8%	63.722	72.480	14%
5	19.050	20.520	8%	3.973	4.240	7%	69.663	76.430	10%

Table 36: Procedure and Weight Sensitivity SEL 80 dB Metric

Stage Length	STANDARD AEDT FTT Contour Length [nmi]	NADP-1 P35 FTT Contour Length [nmi]	Percentage Difference	STANDARD AEDT FTT Contour Width [nmi]	NADP-1 P35 FTT Contour Width [nmi]	Percentage Difference	STANDARD AEDT FTT Contour Area [sq. nmi]	NADP-1 P35 FTT Contour Area [sq. nmi]	Percentage Difference
1	7.559	8.080	7%	2.095	2.080	-1%	11.117	12.460	12%
2	7.985	8.850	11%	2.070	2.040	-1%	11.601	13.390	15%
3	8.492	9.640	14%	2.047	2.000	-2%	12.219	14.300	17%
4	9.313	10.550	13%	2.007	1.950	-3%	13.100	15.360	17%
5	10.196	11.150	9%	1.962	1.930	-2%	14.046	16.030	14%

Table 37: Procedure and Weight Sensitivity SEL 90 dB Metric

Stage Length	STANDARD AEDT FTT Contour Length [nmi]	NADP-1 P35 FTT Contour Length [nmi]	Percentage Difference	STANDARD AEDT FTT Contour Width [nmi]	NADP-1 P35 FTT Contour Width [nmi]	Percentage Difference	STANDARD AEDT FTT Contour Area [sq. nmi]	NADP-1 P35 FTT Contour Area [sq. nmi]	Percentage Difference
1	2.909	2.710	-7%	0.816	0.760	-7%	1.753	1.410	-20%
2	3.068	2.920	-5%	0.800	0.740	-7%	1.818	1.480	-19%
3	3.285	3.130	-5%	0.786	0.720	-8%	1.912	1.560	-18%
4	3.550	3.390	-5%	0.760	0.700	-8%	2.013	1.640	-19%
5	3.874	3.560	-8%	0.738	0.690	-6%	2.136	1.690	-21%

Table 38: Procedure and Weight Sensitivity NOx Metric

Stage Length	STANDARD AEDT FTT NOx below 3,000 ft [g]	NADP-1 P35 FTT NOx below 3,000 ft [g]	Percentage Difference	STANDARD AEDT FTT NOx 3,000 ft to 10,000 ft [g]	NADP-1 P35 FTT NOx 3,000 ft to 10,000 ft [g]	Percentage Difference
1	6441.377	6126.425	-5%	5479.081	6558.536	20%
2	6761.583	6609.235	-2%	5787.113	7180.958	24%
3	7168.942	7090.749	-1%	6125.350	7819.066	28%
4	7957.103	7633.095	-4%	6551.746	8554.715	31%
5	8582.797	7987.334	-7%	7221.653	9042.302	25%

Table 39: Procedure and Weight Sensitivity Fuel Burn Metric

Stage Length	STANDARD AEDT FTT Fuel Burn below 3,000 ft [g]	NADP-1 P35 FTT Fuel Burn below 3,000 ft [g]	Percentage Difference	STANDARD AEDT FTT Fuel Burn 3,000 ft to 10,000 ft [g]	NADP-1 AEDT FTT Fuel Burn 3,000 ft to 10,000 ft [g]	Percentage Difference
1	235.012	232.394	-1%	232.659	278.036	20%
2	246.776	250.258	1%	245.762	304.433	24%
3	261.668	268.044	2%	260.150	331.497	27%
4	291.929	288.059	-1%	278.414	362.705	30%
5	315.017	301.131	-4%	306.898	383.390	25%

For NADP-2 procedure, increasing in weight resulted shallower climb and longer ground roll as depicted in Figure 31, resulting in longer contour length for SEL 70 and 80 dB, but decrease for SEL 90 dB as showed in Figure 32. For SEL 70 dB, there is significant different in contour width at lower stage length. However at higher stage lengths, there is little to no changes in contour width as shows in Figure 32 and Table 40. There is a significant decrease in contour width for SEL 80 and 90 dB as shows in Table 41 and Table 42. There is an increase in contour area for SEL 70 dB, little to no changes in contour area for SEL 80 dB, and decrease in contour area for SEL 90 dB. Changing procedure and aircraft weight increased the fuel burn and NOx below 3000 ft, but decreased between 3000 ft and 10000 ft as shows in Table 43 and Table 44.

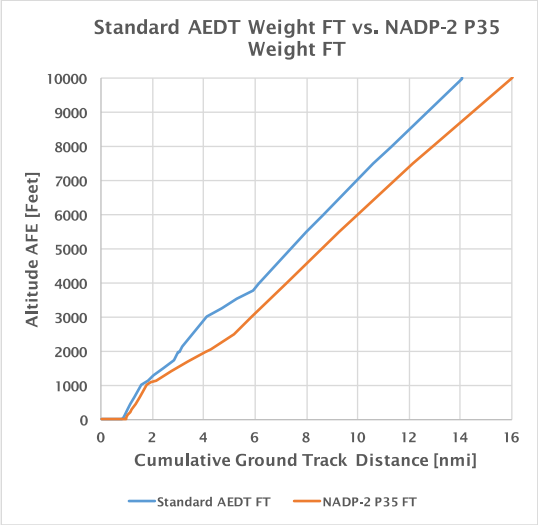

Figure 31: STANDARD AEDT Weight FT vs NADP-2 P35 Weight for Full Thrust

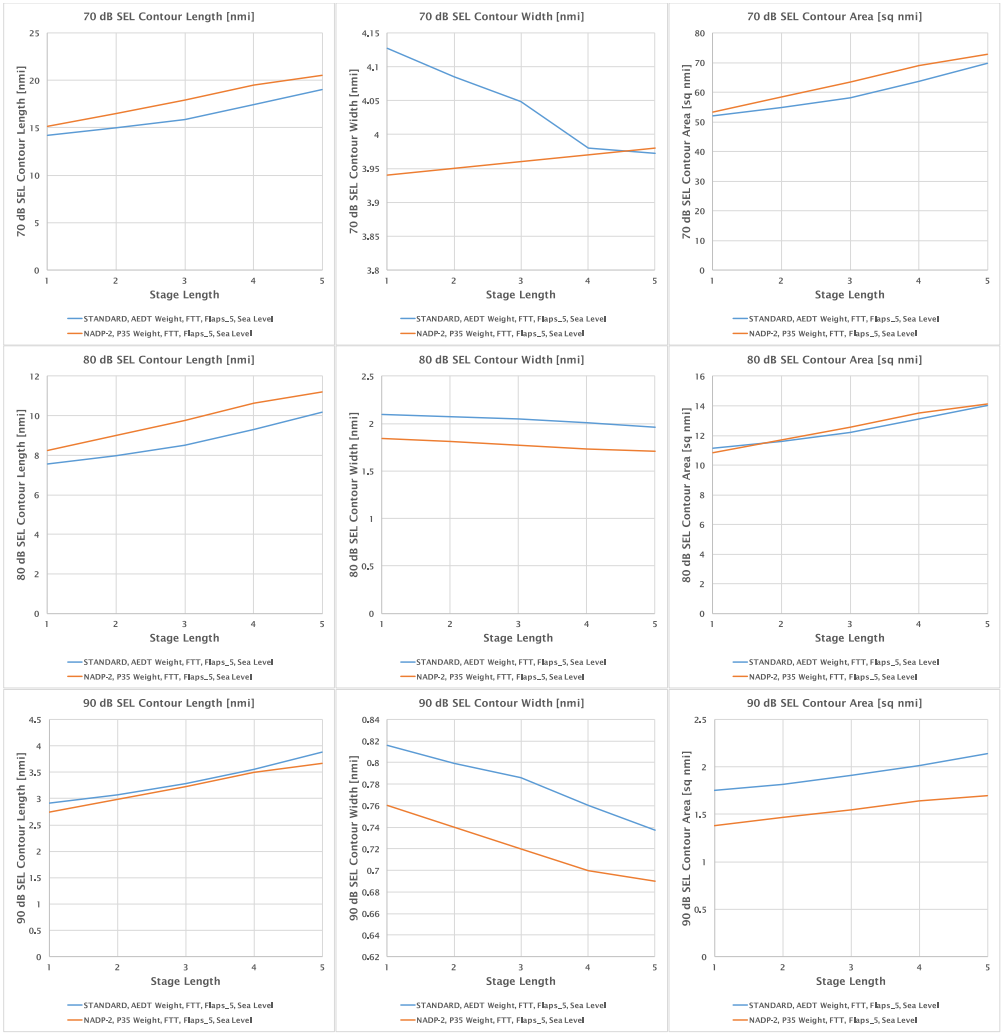

Figure 32: Procedure and Weight Sensitivity Noise Results

Table 40: Procedure and Weight Sensitivity SEL 70 dB Metric

Stage Length	STANDARD AEDT FTT Contour Length [nmi]	NADP-2 P35 FTT Contour Length [nmi]	Percentage Difference	STANDARD AEDT FTT Contour Width [nmi]	NADP-2 P35 FTT Contour Width [nmi]	Percentage Difference	STANDARD AEDT FTT Contour Area [sq. nmi]	NADP-2 P35 FTT Contour Area [sq. nmi]	Percentage Difference
1	14.228	15.160	7%	4.128	3.940	-5%	52.013	53.310	2%
2	14.998	16.520	10%	4.085	3.950	-3%	54.833	58.260	6%
3	15.888	17.900	13%	4.049	3.960	-2%	58.125	63.300	9%
4	17.421	19.490	12%	3.980	3.970	0%	63.722	69.070	8%
5	19.050	20.540	8%	3.973	3.980	0%	69.663	72.880	5%

Table 41: Procedure and Weight Sensitivity SEL 80 dB Metric

Stage Length	STANDARD AEDT FTT Contour Length [nmi]	NADP-2 P35 FTT Contour Length [nmi]	Percentage Difference	STANDARD AEDT FTT Contour Width [nmi]	NADP-2 P35 FTT Contour Width [nmi]	Percentage Difference	STANDARD AEDT FTT Contour Area [sq. nmi]	NADP-2 P35 FTT Contour Area [sq. nmi]	Percentage Difference
1	7.559	8.250	9%	2.095	1.840	-12%	11.117	10.820	-3%
2	7.985	9.010	13%	2.070	1.810	-13%	11.601	11.680	1%
3	8.492	9.770	15%	2.047	1.770	-14%	12.219	12.540	3%
4	9.313	10.640	14%	2.007	1.730	-14%	13.100	13.500	3%
5	10.196	11.210	10%	1.962	1.710	-13%	14.046	14.110	0%

Table 42: Procedure and Weight Sensitivity SEL 90 dB Metric

Stage Length	STANDARD AEDT FTT Contour Length [nmi]	NADP-2 P35 FTT Contour Length [nmi]	Percentage Difference	STANDARD AEDT FTT Contour Width [nmi]	NADP-2 P35 FTT Contour Width [nmi]	Percentage Difference	STANDARD AEDT FTT Contour Area [sq. nmi]	NADP-2 P35 FTT Contour Area [sq. nmi]	Percentage Difference
1	2.909	2.740	-6%	0.816	0.760	-7%	1.753	1.380	-21%
2	3.068	2.980	-3%	0.800	0.740	-7%	1.818	1.470	-19%
3	3.285	3.220	-2%	0.786	0.720	-8%	1.912	1.550	-19%
4	3.550	3.490	-2%	0.760	0.700	-8%	2.013	1.640	-19%
5	3.874	3.670	-5%	0.738	0.690	-6%	2.136	1.700	-20%

Table 43: Procedure and Weight Sensitivity NOx Metric

Stage Length	STANDARD AEDT FTT NOx below 3,000 ft [g]	NADP-2 P35 FTT NOx below 3,000 ft [g]	Percentage Difference	STANDARD AEDT FTT NOx 3,000 ft to 10,000 ft [g]	NADP-2 P35 FTT NOx 3,000 ft to 10,000 ft [g]	Percentage Difference
1	6441.377	7333.63	14%	5479.081	4701.141	-14%
2	6761.583	7949.366	18%	5787.113	5169.285	-11%
3	7168.942	8565.494	19%	6125.350	5649.305	-8%
4	7957.103	9253.635	16%	6551.746	6203.979	-5%
5	8582.797	9700.622	13%	7221.653	6573.292	-9%

Table 44: Procedure and Weight Sensitivity Fuel Burn Metric

Stage Length	STANDARD AEDT FTT Fuel Burn below 3,000 ft [g]	NADP-2 P35 FTT Fuel Burn below 3,000 ft [g]	Percentage Difference	STANDARD AEDT FTT Fuel Burn 3,000 ft to 10,000 ft [g]	NADP-2 AEDT FTT Fuel Burn 3,000 ft to 10,000 ft [g]	Percentage Difference
1	235.012	282.795	20%	232.659	200.119	-14%
2	246.776	306.367	24%	245.762	220.050	-10%
3	261.668	329.930	26%	260.150	240.488	-8%
4	291.929	356.342	22%	278.414	264.105	-5%
5	315.017	373.506	19%	306.898	279.830	-9%

Step 7

For step 7, NADP procedures defined in step 5 were used along with the thrust being reduced by 15% for takeoff and 10% for climb thrust. Aircraft weight was set to AEDT weight and the takeoff flaps setting was set to the lowest possible. This was defined as shown in Table 11. For B737-800, the noise results are shown in Figure 34 and the calculated noise metric are shows in Table 45 to Table 47. Reducing the takeoff and climb thrust lead to longer ground roll and shallower climb as depicted in Figure 33. Shallower climb resulted an increase in contour length for SEL 70 dB. However, for SEL 80 and 90 dB contour length decreases, because SEL 80 and 90 dB are more sensitive to thrust rather than the position of the vehicle. There is little to no changes in contour width and area for SEL 70 dB for all stage length. However, for SEL 80 and 90 dB there is significant decrease in overall contour width and area for all stage length. Changes in procedure and thrust, resulted in a decreased of NOx and increased in fuel burn below 3000 ft as shows in Table 48 and Table 49 for all stage length.

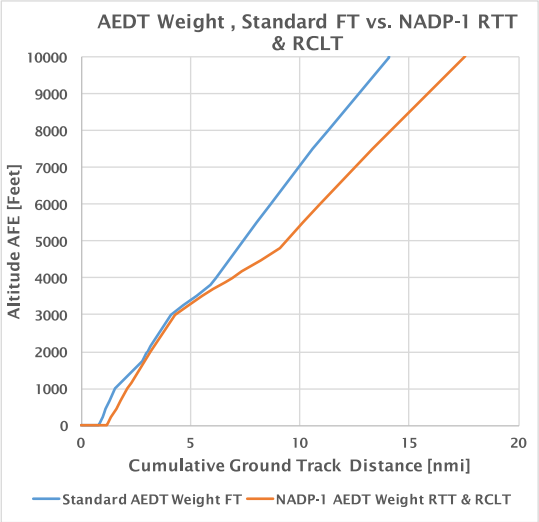

Figure 33: AEDT Weight, STANDARD FT vs NADP-1 RTT & RCLT

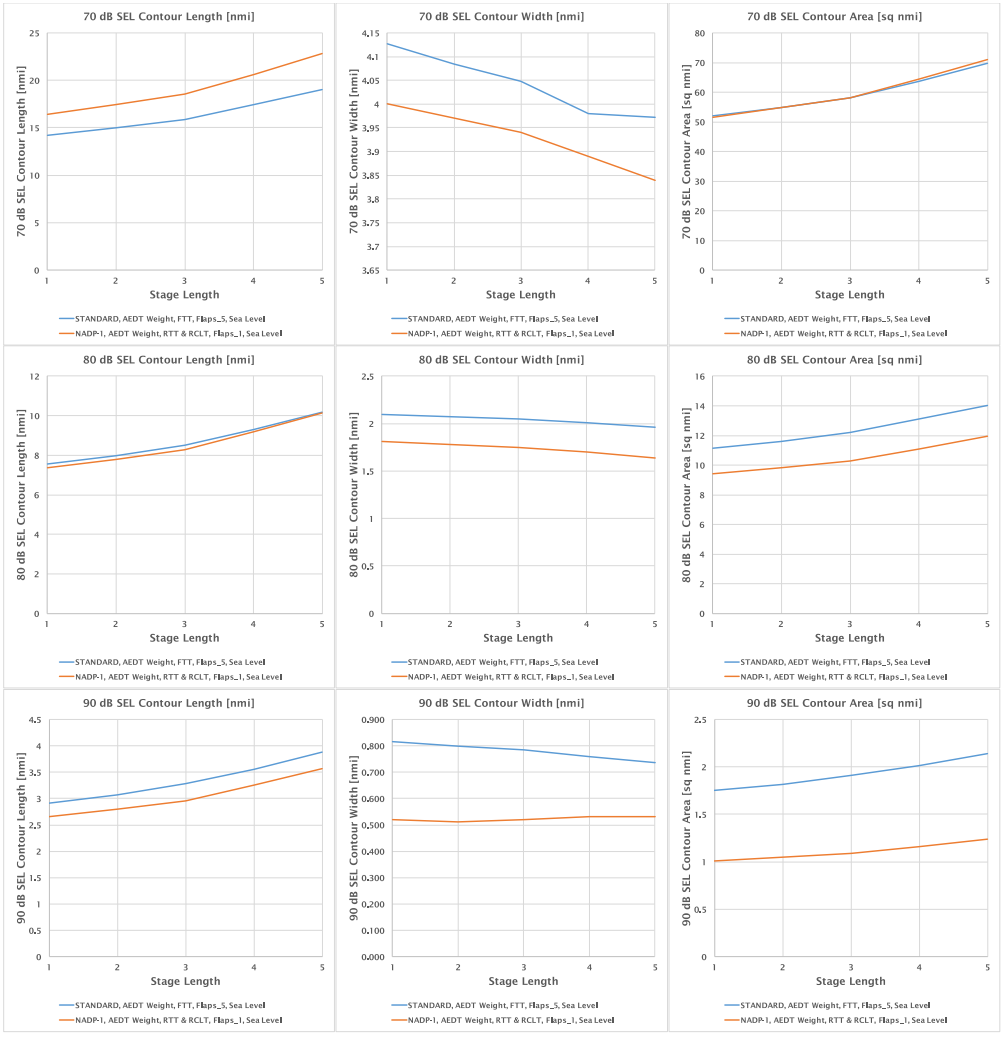

Figure 34: Procedure and Thrust Sensitivity Noise Results

Table 45: Procedure and Thrust Sensitivity SEL 70 dB Metric

Stage Length	STANDARD AEDT FTT Contour Length [nmi]	NADP-1 AEDT RTT & RCLT Contour Length [nmi]	Percentage Difference	STANDARD AEDT FTT Contour Width [nmi]	NADP-1 AEDT RTT & RCLT Contour Width [nmi]	Percentage Difference	STANDARD AEDT FTT Contour Area [sq. nmi]	NADP-1 AEDT RTT & RCLT Contour Area [sq. nmi]	Percentage Difference
1	14.228	16.400	15%	4.128	4.000	-3%	52.013	51.630	-1%
2	14.998	17.410	16%	4.085	3.970	-3%	54.833	54.700	0%
3	15.888	18.530	17%	4.049	3.940	-3%	58.125	58.100	0%
4	17.421	20.630	18%	3.980	3.890	-2%	63.722	64.480	1%
5	19.050	22.840	20%	3.973	3.840	-3%	69.663	71.140	2%

Table 46: Procedure and Thrust Sensitivity SEL 80 dB Metric

Stage Length	STANDARD AEDT FTT Contour Length [nmi]	NADP-1 AEDT RTT & RCLT Contour Length [nmi]	Percentage Difference	STANDARD AEDT FTT Contour Width [nmi]	NADP-1 AEDT RTT & RCLT Contour Width [nmi]	Percentage Difference	STANDARD AEDT FTT Contour Area [sq. nmi]	NADP-1 AEDT RTT & RCLT Contour Area [sq. nmi]	Percentage Difference
1	7.559	7.360	-3%	2.095	1.810	-14%	11.117	9.400	-15%
2	7.985	7.800	-2%	2.070	1.780	-14%	11.601	9.820	-15%
3	8.492	8.280	-3%	2.047	1.750	-15%	12.219	10.270	-16%
4	9.313	9.180	-1%	2.007	1.700	-15%	13.100	11.100	-15%
5	10.196	10.140	-1%	1.962	1.640	-16%	14.046	11.960	-15%

Table 47: Procedure and Thrust Sensitivity SEL 90 dB Metric

Stage Length	STANDARD AEDT FTT Contour Length [nmi]	NADP-1 AEDT RTT & RCLT Contour Length [nmi]	Percentage Difference	STANDARD AEDT FTT Contour Width [nmi]	NADP-1 AEDT RTT & RCLT Contour Width [nmi]	Percentage Difference	STANDARD AEDT FTT Contour Area [sq. nmi]	NADP-1 AEDT RTT & RCLT Contour Area [sq. nmi]	Percentage Difference
1	2.909	2.650	-9%	0.816	0.520	-36%	1.753	1.010	-42%
2	3.068	2.800	-9%	0.800	0.510	-36%	1.818	1.050	-42%
3	3.285	2.950	-10%	0.786	0.520	-34%	1.912	1.090	-43%
4	3.550	3.250	-8%	0.760	0.530	-30%	2.013	1.160	-42%
5	3.874	3.570	-8%	0.738	0.530	-28%	2.136	1.240	-42%

Table 48: Procedure and Thrust Sensitivity NOx Metric

Stage Length	STANDARD AEDT FTT NOx below 3,000 ft [g]	NADP-1 AEDT RTT & RCLT NOx below 3,000 ft [g]	Percentage Difference	STANDARD AEDT FTT NOx 3,000 ft to 10,000 ft [g]	NADP-1 AEDT RTT & RCLT NOx 3,000 ft to 10,000 ft [g]	Percentage Difference
1	6441.377	5545.383	-14%	5479.081	5918.405	8%
2	6761.583	5861.286	-13%	5787.113	6238.139	8%
3	7168.942	6207.151	-13%	6125.350	6592.422	8%
4	7957.103	6841.195	-14%	6551.746	7261.559	11%
5	8582.797	7491.16	-13%	7221.653	7959.436	10%

Table 49: Procedure and Thrust Sensitivity Fuel Burn Metric

Stage Length	STANDARD AEDT FTT Fuel Burn below 3,000 ft [g]	NADP-1 AEDT RTT & RCLT Fuel Burn below 3,000 ft [g]	Percentage Difference	STANDARD AEDT FTT Fuel Burn 3,000 ft to 10,000 ft [g]	NADP-1 AEDT RTT & RCLT Fuel Burn 3,000 ft to 10,000 ft [g]	Percentage Difference
1	235.012	247.908	5%	232.659	281.523	21%
2	246.776	261.992	6%	245.762	296.788	21%
3	261.668	277.417	6%	260.150	313.706	21%
4	291.929	305.704	5%	278.414	345.663	24%
5	315.017	334.743	6%	306.898	379.004	23%

Changes in procedure from STANDARD to NADP-2 and reducing takeoff and climb thrust resulted in longer ground roll and shallower climb as depicted in Figure 35. Shallower climb resulted in longer contour length for SEL 70 dB and decreased in contour width as shows in Figure 36. Reducing thrust resulted in decrease in contour length, width, and area for SEL 80 and 90 dB as shown in Figure 36. Looking at the calculated noise metric values in Table 50 and Table 52, there is little change in contour length for SEL 80 and 90 dB. However, there is a significant decrease in contour width and area. There is little to no change in contour area for SEL 70 dB, but significant increase in contour length and decrease in contour width. Changing from STANDARD procedure to NADP-2 and reducing the takeoff and climb thrust, results in decreased in NOx, but increase in fuel burn as shown in Table 53 and Table 54.

.

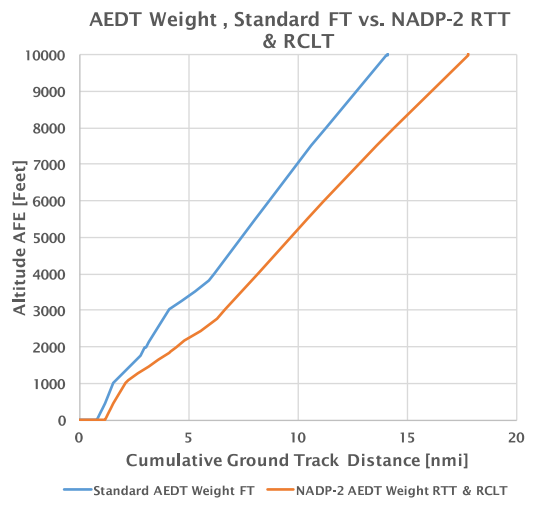

Figure 35: AEDT Weight, STANDARD FT vs NADP-2 RTT & RCLT

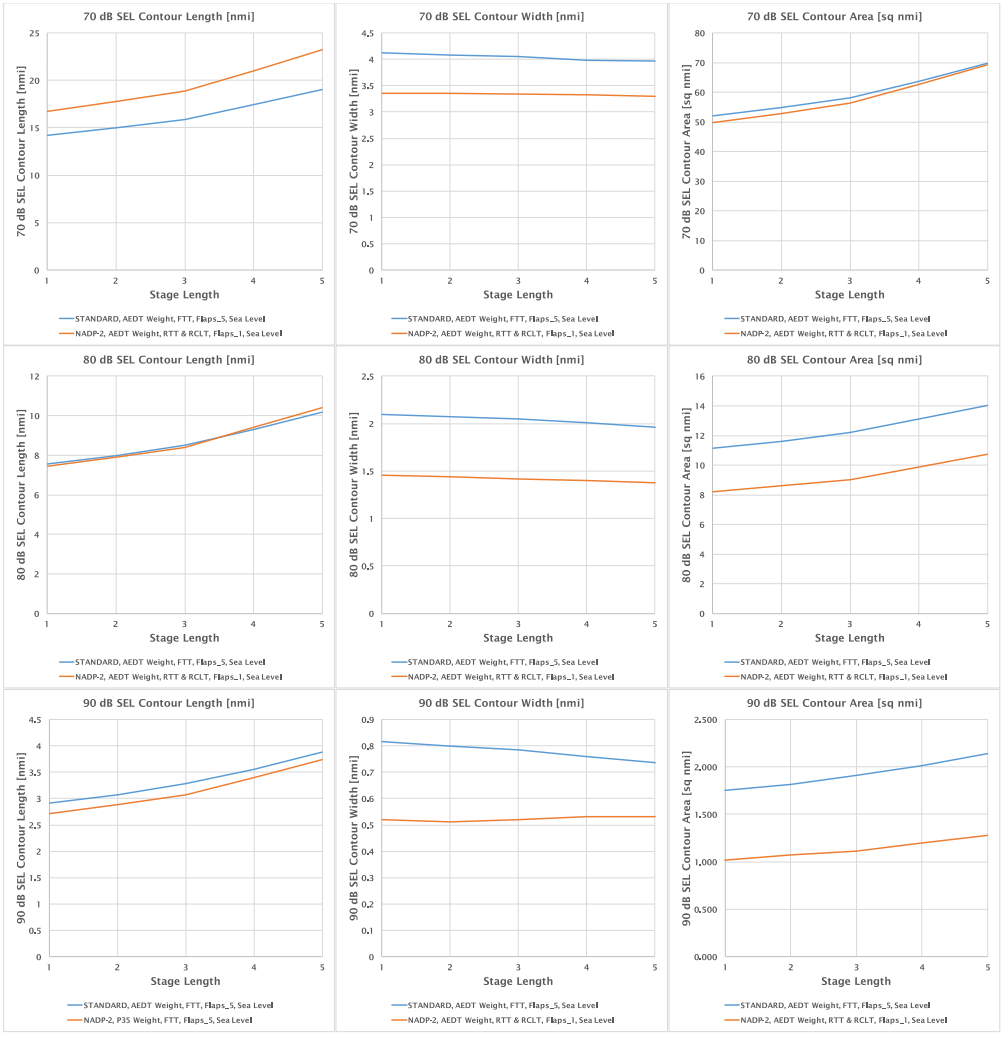

Figure 36: Procedure and Thrust Sensitivity Noise Results

Table 50: Procedure and Thrust Sensitivity SEL 70 dB Metric

Stage Length	STANDARD AEDT FTT Contour Length [nmi]	NADP-2 AEDT RTT & RCLT Contour Length [nmi]	Percentage Difference	STANDARD AEDT FTT Contour Width [nmi]	NADP-2 AEDT RTT & RCLT Contour Width [nmi]	Percentage Difference	STANDARD AEDT FTT Contour Area [sq. nmi]	NADP-2 AEDT RTT & RCLT Contour Area [sq. nmi]	Percentage Difference
1	14.228	16.730	18%	4.128	3.360	-19%	52.013	49.850	-4%
2	14.998	17.750	18%	4.085	3.350	-18%	54.833	52.890	-4%
3	15.888	18.890	19%	4.049	3.340	-18%	58.125	56.260	-3%
4	17.421	21.020	21%	3.980	3.320	-17%	63.722	62.600	-2%
5	19.050	23.240	22%	3.973	3.300	-17%	69.663	69.170	-1%

Table 51: Procedure and Thrust Sensitivity SEL 80 dB Metric

Stage Length	STANDARD AEDT FTT Contour Length [nmi]	NADP-2 AEDT RTT & RCLT Contour Length [nmi]	Percentage Difference	STANDARD AEDT FTT Contour Width [nmi]	NADP-2 AEDT RTT & RCLT Contour Width [nmi]	Percentage Difference	STANDARD AEDT FTT Contour Area [sq. nmi]	NADP-2 AEDT RTT & RCLT Contour Area [sq. nmi]	Percentage Difference
1	7.559	7.440	-2%	2.095	1.460	-30%	11.117	8.190	-26%
2	7.985	7.890	-1%	2.070	1.440	-30%	11.601	8.590	-26%
3	8.492	8.400	-1%	2.047	1.420	-31%	12.219	9.030	-26%
4	9.313	9.410	1%	2.007	1.400	-30%	13.100	9.880	-25%
5	10.196	10.390	2%	1.962	1.380	-30%	14.046	10.730	-24%

Table 52: Procedure and Thrust Sensitivity SEL 90 dB Metric

Stage Length	STANDARD AEDT FTT Contour Length [nmi]	NADP-2 AEDT RTT & RCLT Contour Length [nmi]	Percentage Difference	STANDARD AEDT FTT Contour Width [nmi]	NADP-2 AEDT RTT & RCLT Contour Width [nmi]	Percentage Difference	STANDARD AEDT FTT Contour Area [sq. nmi]	NADP-2 AEDT RTT & RCLT Contour Area [sq. nmi]	Percentage Difference
1	2.909	2.720	-6%	0.816	0.520	-36%	1.753	1.020	-42%
2	3.068	2.890	-6%	0.800	0.510	-36%	1.818	1.070	-41%
3	3.285	3.070	-7%	0.786	0.520	-34%	1.912	1.110	-42%
4	3.550	3.400	-4%	0.760	0.530	-30%	2.013	1.200	-40%
5	3.874	3.740	-3%	0.738	0.530	-28%	2.136	1.280	-40%

Table 53: Procedure and Thrust Sensitivity NOx Metric

Stage Length	STANDARD AEDT FTT NOx below 3,000 ft [g]	NADP-2 AEDT RTT & RCLT NOx below 3,000 ft [g]	Percentage Difference	STANDARD AEDT FTT NOx 3,000 ft to 10,000 ft [g]	NADP-2 AEDT RTT & RCLT NOx 3,000 ft to 10,000 ft [g]	Percentage Difference
1	6441.377	6009.781	-7%	5479.081	5024.006	-8%
2	6761.583	6335.084	-6%	5787.113	5335.536	-8%
3	7168.942	6690.593	-7%	6125.350	5681.548	-7%
4	7957.103	7152.028	-10%	6551.746	6010.581	-8%
5	8582.797	8229.982	-4%	7221.653	6801.334	-6%

Table 54: Procedure and Thrust Sensitivity Fuel Burn Metric

Stage Length	STANDARD AEDT FTT Fuel Burn below 3,000 ft [g]	NADP-2 AEDT RTT & RCLT Fuel Burn below 3,000 ft [g]	Percentage Difference	STANDARD AEDT FTT Fuel Burn 3,000 ft to 10,000 ft [g]	NADP-2 AEDT RTT & RCLT Fuel Burn 3,000 ft to 10,000 ft [g]	Percentage Difference
1	235.012	270.323	15%	232.659	239.352	3%
2	246.776	284.913	15%	245.762	254.226	3%
3	261.668	300.863	15%	260.150	270.748	4%
4	291.929	316.977	9%	278.414	286.433	3%
5	315.017	370.604	18%	306.898	324.231	6%

Step 8

For step 8, the NADP procedures defined in step 5 were used. The aircraft weights were changed from AEDT weights to Project 35 weights and the takeoff and climb thrust were reduced. The takeoff flaps were set to the lowest possible takeoff flap setting. This resulted in longer ground roll and shallower climb as depicted in Figure 37. Shallower climb resulted in longer contour length for SEL 70 as showed in Table 55. Because of the increase in aircraft weight and reduction of takeoff and climb thrust, the contour length of SEL 80 and 90 dB increased as showed in Figure 38 and Table 56 and Table 57. This different can be seen when comparing the noise results for step 8 and step 7. Reduction in thrust reduced the noise contour for all SEL level and all stage lengths. Reduction of thrust resulted in decreases in NOx for below 3000 ft, however increasing in the aircraft weight resulted increasing of fuel burn. The significant changes in NOx and fuel change due to changes in weight can be seen when comparing the fuel burn and NOx results from Table 58 and Table 59 to Table 53 and Table 54.

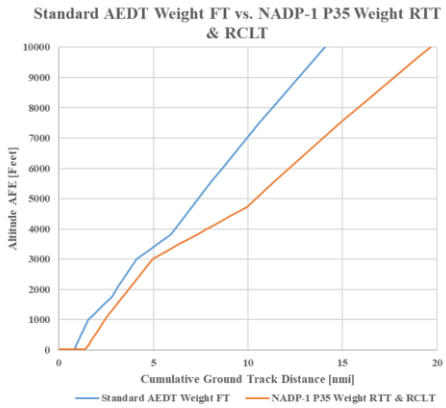

Figure 37: STANDARD AEDT Weight FT vs NADP-1 P35 Weight RTT & RCLT

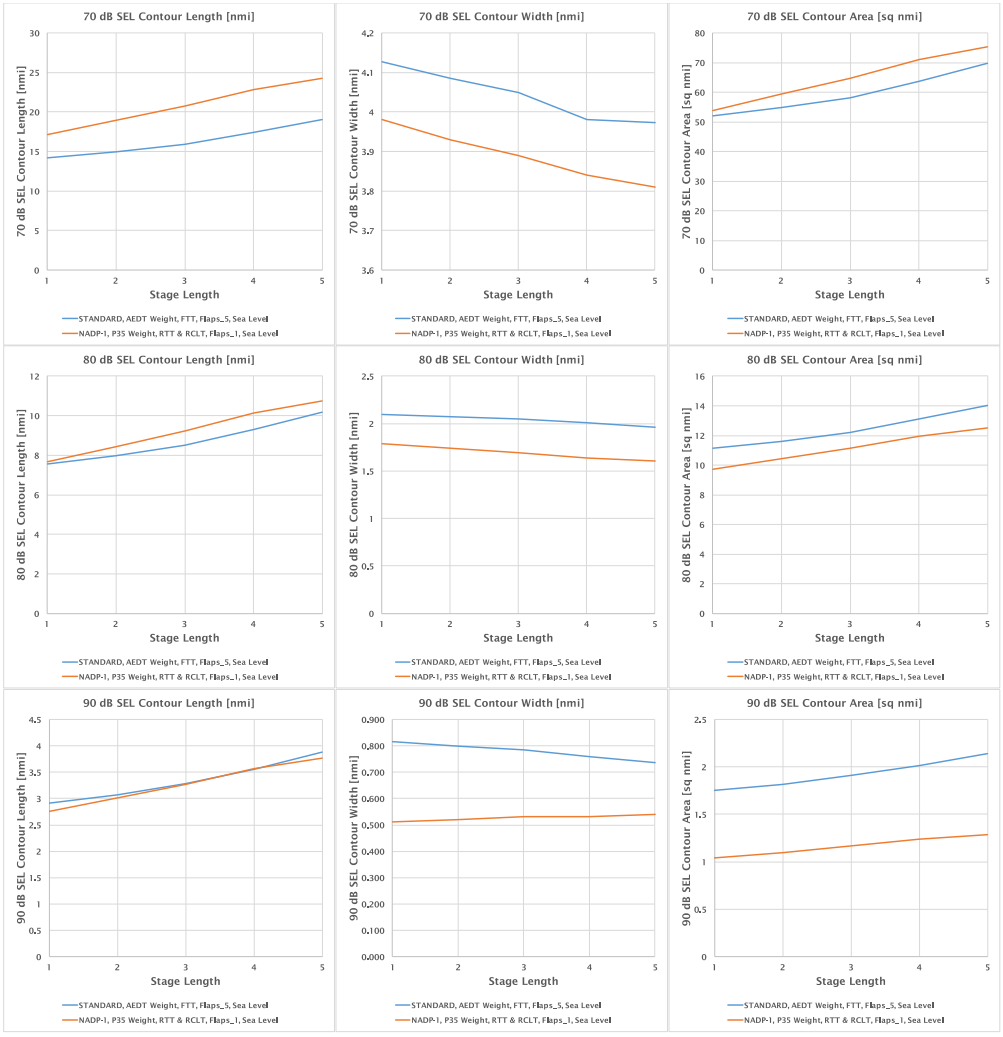

Figure 38: Procedure, Weight and Thrust Sensitivity Noise Results

Table 55: Procedure, Weight and Thrust Sensitivity SEL 70 dB Metric

Stage Length	STANDARD AEDT FTT Contour Length [nmi]	NADP-1 P35 RTT & RCLT Contour Length [nmi]	Percentage Difference	STANDARD AEDT FTT Contour Width [nmi]	NADP-1 P35 RTT & RCLT Contour Width [nmi]	Percentage Difference	STANDARD AEDT FTT Contour Area [sq. nmi]	NADP-1 P35 RTT & RCLT Contour Area [sq. nmi]	Percentage Difference
1	14.228	17.150	21%	4.128	3.980	-4%	52.013	53.920	4%
2	14.998	18.910	26%	4.085	3.930	-4%	54.833	59.260	8%
3	15.888	20.730	30%	4.049	3.890	-4%	58.125	64.760	11%
4	17.421	22.840	31%	3.980	3.840	-4%	63.722	71.140	12%
5	19.050	24.270	27%	3.973	3.810	-4%	69.663	75.400	8%

Table 56: Procedure, Weight and Thrust Sensitivity SEL 80 dB Metric

Stage Length	STANDARD AEDT FTT Contour Length [nmi]	NADP-1 P35 RTT & RCLT Contour Length [nmi]	Percentage Difference	STANDARD AEDT FTT Contour Width [nmi]	NADP-1 P35 RTT & RCLT Contour Width [nmi]	Percentage Difference	STANDARD AEDT FTT Contour Area [sq. nmi]	NADP-1 P35 RTT & RCLT Contour Area [sq. nmi]	Percentage Difference
1	7.559	7.690	2%	2.095	1.790	-15%	11.117	9.710	-13%
2	7.985	8.440	6%	2.070	1.740	-16%	11.601	10.420	-10%
3	8.492	9.220	9%	2.047	1.690	-17%	12.219	11.140	-9%
4	9.313	10.140	9%	2.007	1.640	-18%	13.100	11.960	-9%
5	10.196	10.740	5%	1.962	1.610	-18%	14.046	12.500	-11%

Table 57: Procedure, Weight and Thrust Sensitivity SEL 90 dB Metric

Stage Length	STANDARD AEDT FTT Contour Length [nmi]	NADP-1 P35 RTT & RCLT Contour Length [nmi]	Percentage Difference	STANDARD AEDT FTT Contour Width [nmi]	NADP-1 P35 RTT & RCLT Contour Width [nmi]	Percentage Difference	STANDARD AEDT FTT Contour Area [sq. nmi]	NADP-1 P35 RTT & RCLT Contour Area [sq. nmi]	Percentage Difference
1	2.909	2.760	-5%	0.816	0.510	-37%	1.753	1.040	-41%
2	3.068	3.010	-2%	0.800	0.520	-35%	1.818	1.100	-39%
3	3.285	3.270	0%	0.786	0.530	-33%	1.912	1.170	-39%
4	3.550	3.570	1%	0.760	0.530	-30%	2.013	1.240	-38%
5	3.874	3.770	-3%	0.738	0.540	-27%	2.136	1.290	-40%

Table 58: Procedure, Weight and Thrust Sensitivity NOx Metric

Stage Length	STANDARD AEDT FTT NOx below 3,000 ft [g]	NADP-1 P35 RTT & RCLT NOx below 3,000 ft [g]	Percentage Difference	STANDARD AEDT FTT NOx 3,000 ft to 10,000 ft [g]	NADP-1 P35 RTT & RCLT NOx 3,000 ft to 10,000 ft [g]	Percentage Difference
1	6441.377	5781.331	-10%	5479.081	6157.417	12%
2	6761.583	6322.117	-6%	5787.113	6714.687	16%
3	7168.942	6868.223	-4%	6125.350	7290.366	19%
4	7957.103	7491.16	-6%	6551.746	7959.436	21%
5	8582.797	7902.235	-8%	7221.653	8406.608	16%

Table 59: Procedure, Weight and Thrust Sensitivity Fuel Burn Metric

Stage Length	STANDARD AEDT FTT Fuel Burn below 3,000 ft [g]	NADP-1 P35 RTT & RCLT Fuel Burn below 3,000 ft [g]	Percentage Difference	STANDARD AEDT FTT Fuel Burn 3,000 ft to 10,000 ft [g]	NADP-1 P35 RTT & RCLT Fuel Burn 3,000 ft to 10,000 ft [g]	Percentage Difference
1	235.012	258.426	10%	232.659	292.934	26%
2	246.776	282.541	14%	245.762	319.544	30%
3	261.668	306.910	17%	260.150	347.039	33%
4	291.929	334.743	15%	278.414	379.004	36%
5	315.017	353.132	12%	306.898	400.372	30%

The STANDARD procedure was changed to NADP-2 procedure and takeoff and climb thrust was reduced by 15% and 10%. The takeoff weight were changed from AEDT to Project 35 weight and takeoff flaps was set to the lowest possible takeoff flaps setting. This resulted in longer ground roll and shallower climb as shown in Figure 39. Shallower climb resulted in increased contour length for all SEL levels as shows in Figure 40. Reduction of the thrust resulted in decreased of contour width for all SEL levels. Overall there is slight increases in contour area for SEL 70 dB, and significant decrease in contour area for SEL 80 and 90 dB as showed Table 60 and Table 62. The STANDARD procedure was changed to NADP-2 procedure and takeoff and climb thrust was reduced by 15% and 10%. The takeoff weight was changed from AEDT to Project 35 weight and takeoff flaps was set to the lowest possible takeoff flaps setting. There is little to no change in NOx as listed in Table 63, however significant changes in fuels burn as listed in Table 64.

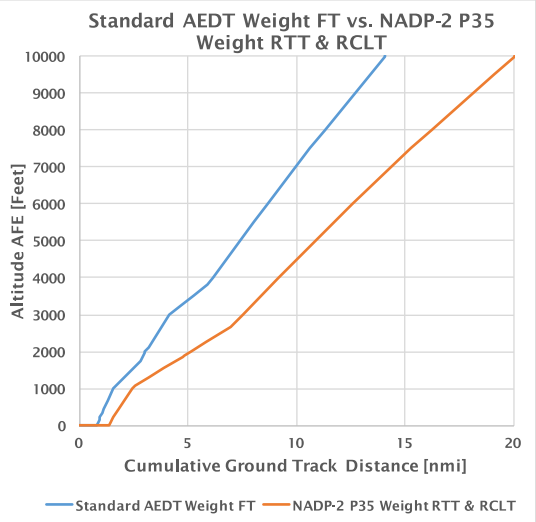

Figure 39: STANDARD AEDT Weight FT vs NADP-2 P35 Weight RTT & RCLT

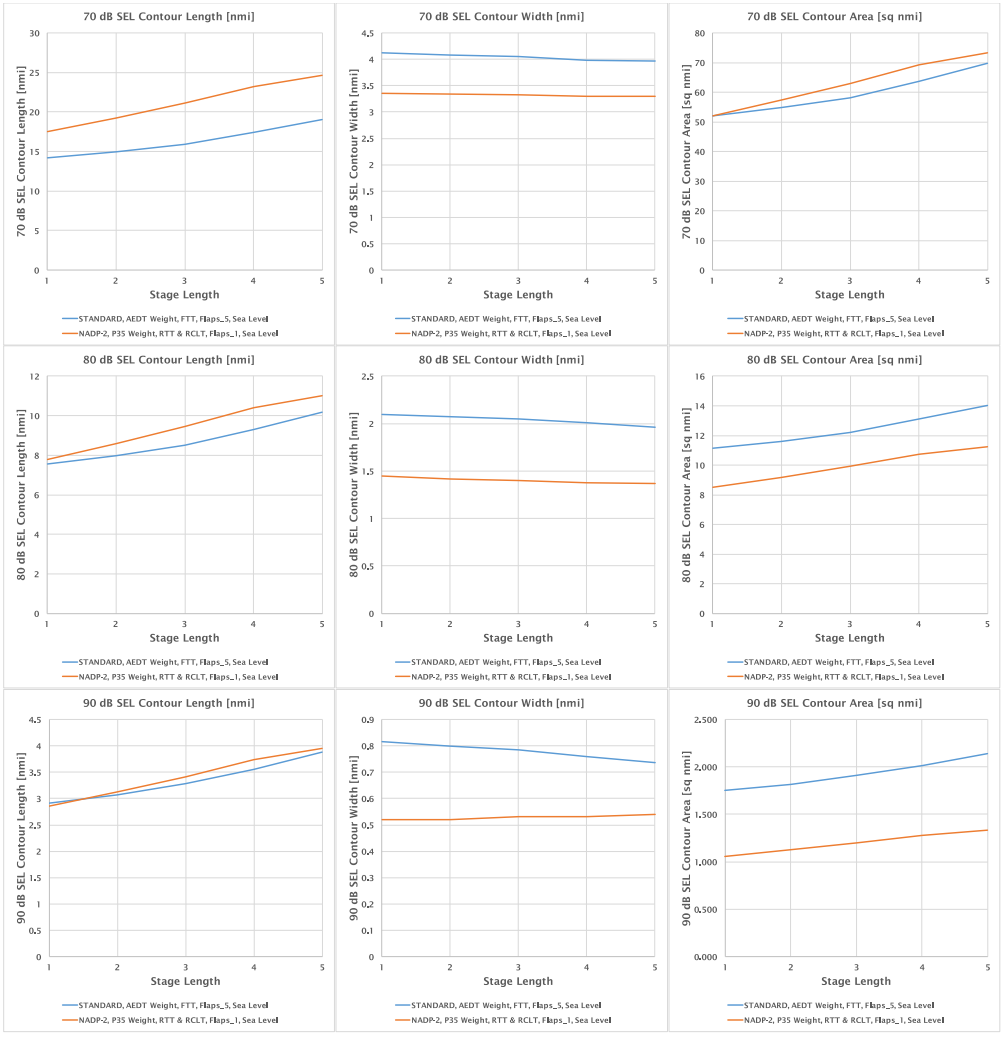

Figure 40: Procedure, Weight and Thrust Sensitivity Noise Results

Table 60: Procedure, Weight and Thrust Sensitivity SEL 70 dB Metric

Stage Length	STANDARD AEDT FTT Contour Length [nmi]	NADP-2 P35 RTT & RCLT Contour Length [nmi]	Percentage Difference	STANDARD AEDT FTT Contour Width [nmi]	NADP-2 P35 RTT & RCLT Contour Width [nmi]	Percentage Difference	STANDARD AEDT FTT Contour Area [sq. nmi]	NADP-2 P35 RTT & RCLT Contour Area [sq. nmi]	Percentage Difference
1	14.228	17.500	23%	4.128	3.350	-19%	52.013	52.120	0%
2	14.998	19.270	28%	4.085	3.340	-18%	54.833	57.400	5%
3	15.888	21.110	33%	4.049	3.320	-18%	58.125	62.870	8%
4	17.421	23.240	33%	3.980	3.300	-17%	63.722	69.170	9%
5	19.050	24.680	30%	3.973	3.290	-17%	69.663	73.370	5%

Table 61: Procedure, Weight and Thrust Sensitivity SEL 80 dB Metric

Stage Length	STANDARD AEDT FTT Contour Length [nmi]	NADP-2 P35 RTT & RCLT Contour Length [nmi]	Percentage Difference	STANDARD AEDT FTT Contour Width [nmi]	NADP-2 P35 RTT & RCLT Contour Width [nmi]	Percentage Difference	STANDARD AEDT FTT Contour Area [sq. nmi]	NADP-2 P35 RTT & RCLT Contour Area [sq. nmi]	Percentage Difference
1	7.559	7.780	3%	2.095	1.450	-31%	11.117	8.490	-24%
2	7.985	8.570	7%	2.070	1.420	-31%	11.601	9.180	-21%
3	8.492	9.450	11%	2.047	1.400	-32%	12.219	9.910	-19%
4	9.313	10.390	12%	2.007	1.380	-31%	13.100	10.730	-18%
5	10.196	11.010	8%	1.962	1.370	-30%	14.046	11.250	-20%

Table 62: Procedure, Weight and Thrust Sensitivity SEL 90 dB Metric

Stage Length	STANDARD AEDT FTT Contour Length [nmi]	NADP-2 AEDT RTT & RCLT Contour Length [nmi]	Percentage Difference	STANDARD AEDT FTT Contour Width [nmi]	NADP-2 AEDT RTT & RCLT Contour Width [nmi]	Percentage Difference	STANDARD AEDT FTT Contour Area [sq. nmi]	NADP-2 AEDT RTT & RCLT Contour Area [sq. nmi]	Percentage Difference
1	2.909	2.850	-2%	0.816	0.520	-36%	1.753	1.060	-40%
2	3.068	3.130	2%	0.800	0.520	-35%	1.818	1.130	-38%
3	3.285	3.410	4%	0.786	0.530	-33%	1.912	1.200	-37%
4	3.550	3.740	5%	0.760	0.530	-30%	2.013	1.280	-36%
5	3.874	3.950	2%	0.738	0.540	-27%	2.136	1.330	-38%

Table 63: Procedure, Weight and Thrust Sensitivity NOx Metric

Stage Length	STANDARD AEDT FTT NOx below 3,000 ft [g]	NADP-2 P35 RTT & RCLT NOx below 3,000 ft [g]	Percentage Difference	STANDARD AEDT FTT NOx 3,000 ft to 10,000 ft [g]	NADP-2 P35 RTT & RCLT NOx 3,000 ft to 10,000 ft [g]	Percentage Difference
1	6441.377	6253.094	-3%	5479.081	5243.264	-4%
2	6761.583	6810.3	1%	5787.113	5800.045	0%
3	7168.942	7589.803	6%	6125.350	6146.187	0%
4	7957.103	8229.982	3%	6551.746	6801.334	4%
5	8582.797	8647.649	1%	7221.653	7243.456	0%

Table 64: Procedure, Weight and Thrust Sensitivity Fuel Burn Metric

Stage Length	STANDARD AEDT FTT Fuel Burn below 3,000 ft [g]	NADP-2 P35 RTT & RCLT Fuel Burn below 3,000 ft [g]	Percentage Difference	STANDARD AEDT FTT Fuel Burn 3,000 ft to 10,000 ft [g]	NADP-2 P35 RTT & RCLT Fuel Burn 3,000 ft to 10,000 ft [g]	Percentage Difference
1	235.012	281.236	20%	232.659	249.858	7%
2	246.776	306.234	24%	245.762	276.406	12%
3	261.668	341.833	31%	260.150	292.945	13%
4	291.929	370.604	27%	278.414	324.231	16%
5	315.017	389.383	24%	306.898	345.346	13%

Task #3: Develop Aircraft State Estimator and APM Enhancement Recommendations

Georgia Institute of Technology

Objective(s)

Once the AEDT APM limitations were understood in Task 1 and the reduced flight dataset from Task 2, work could begin to develop a state estimator for vehicle weight, takeoff thrust, and payload factor as a function of ambient conditions and measured profile. AEDT will be tuned using the developed state estimator to predict the state variables. Keeping in mind that simplicity is desired, a methodology will be developed that is capable of tuning AEDT APM aircraft takeoff weight, takeoff thrust, and climb thrust both with and without detailed trajectory data. The methodology will be focused on AEDT APM, however, EDS models will also be tuned to understand how differences in the EDS and AEDT aircraft performance models impact the tuned state estimates.

Each of the prior tasks will culminate into a set of recommendations for enhancing the performance of AEDT in this research report.

Research Approach

Ideally, a simple, straight-forward implementation scheme will be developed that would not rely on Original Equipment Manufacturers (OEMs) to provide new Fleet DB coefficient definitions for BADA3 and BADA4 currently in AEDT2b. As the results of each task are acquired, insight to the most appropriate implementation scheme will evolve and be reviewed with the FAA Project Manager. Georgia Tech anticipates the following will be generated as a result of this research:

- Report detailing physics and modeling gaps in current AEDT APM algorithms with suggestions for enhancements
- Analysis of flight data and development of statistical correlation between flight data and aircraft state where possible
- Methodology to automatically calibrate aircraft state (thrust, weight) to available data
- Methodology to implement different departure procedures

The annual report summarizes the preliminary findings and recommendations. Since the project is on-going, the recommendations will be updated as more data become available. Table 65 is a high level summary of the findings based on the results from previous tasks and the potential methods to improve the APM, which will be discussed in more detail in this section. For the three areas of takeoff Gross Weight (GW), thrust, and departure procedures, the first two columns of the table describe the gaps between the AEDT assumptions and the reality and the impact of the modeling gaps to the environmental metric calculations. The next two columns list the methods to improve AEDT and the potential sources of data that are needed to implement the methods.

It is envisioned that improving AEDT's current APM assumptions will be achieved in two steps as illustrated in Figure 41. The end goal of this project is to support a successful implementation of new GW, thrust, and departure procedure to the next generation of AEDT, designated as AEDT 3, which is planned to be released in September 2018. Understanding this objective and the timeline, it is extremely important to provide a practical and feasible solution that can be implemented and tested in a timely manner. The first step in the method development is identification and collection of the real world data to come up with improved APM assumptions. While the data collected in the previous projects reviewed in Task 1 have been very useful for understanding the issues with GW, thrust, and departure procedures, the data used for those projects were limited to a handful of aircraft types from a couple of airlines. In order to update the APM assumptions in AEDT 3 for the majority of key aircraft types at minimum, it is necessary to conduct a more comprehensive data collection effort. As such, the research team has identified potential sources of data for each of the APM parameters and has been coordinating with the FAA and other entities to gather more data in parallel to methods development. The report discusses the current status and the next steps of these efforts.

Table 65. Summary of the Findings and Recommendations

APM Assumptions	AEDT vs Reality (What's the problem?)	Importance (Does it matter?)	Changes to AEDT (how?)	Potential Data Source (by how much?)
Weight	• AEDT uses Stage Length (SL) bins • AEDT tends to underestimate GW by ~%5 for low SLs • AEDT may overestimate GW for high SLs	• **Medium** (-5 to +10%) difference in noise contour areas • NOx and FB (-5 to +10%)	• Update the GW/load factor (LF) assumption for each bin AND/OR • Reduce the bin size OR • Use a continuous function(s)	• IATA (GW) • BTS (Payload) • CAEP (LF) • SAPOE • AWABS • Users
Thrust	• AEDT uses 100% thrust • Airlines use reduced takeoff thrust when possible (~95% of the time) • Typically limited at 25% reduction • About 15% reduction on average, but can be as much as 40%	• **High** (Up to 40+%) difference in noise contour areas • NOx (-1%) • FB (+8%)	• Change the thrust coefficient E for takeoff and climb in the THRUST_JET table • Change all Acceleration segments into Percent Acceleration segments in the PROCEDURES table	• IATA • Commercial runway analysis programs by FLYAPG.com • Project 35 → ACARS • Volpe → FDR • Physics based calculations • TTREAT • Users
Departure Procedures	• Most aircraft in AEDT have STANDARD, ICAO-A, and B Procedures • Airlines use NADP1 and 2 Procedures	• **Medium** (1~10%) difference in noise contour areas • NOx and FB (+5 to +19%)	• Rename the ICAO-A and B procedures to NADP1 and 2 • Adjust the segment steps • Convert ROC to Energy Share percent • Interpolate the VSTOP for different GW	• IATA • ICAO PANS-OPS • ICAO 2007 NADP Survey

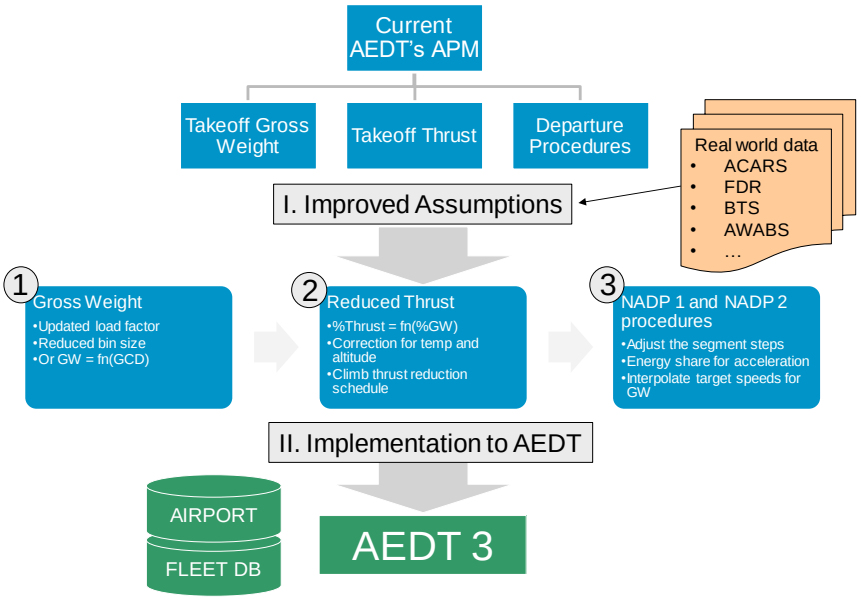

Figure 41. A Two-Step Approach to Improve AEDT's Modeling Accuracy

Development of a Thrust Prediction Model

Factors that Impact the Takeoff Thrust Setting

In order to better reflect the actual takeoff and climb thrust usage in day-to-day operations, it is important to understand how the actual thrust levels for each takeoff is determined. There are four categories of factors that lead to the selection of thrust setting for each departure as listed in Figure 42: thrust available, thrust required, a regulatory limit, and pilot choice. Thrust available is basically the maximum thrust that the engines on the aircraft can produce given atmospheric condition. Thrust required is determined by two aircraft performance constraints: takeoff field length and second segment climb gradient. The thrust required is the minimum thrust level that can be used to safely depart at an aircraft for given weight, runway condition, weather, etc. When the required thrust is less than the available thrust, an opportunity to use reduced thrust takeoff thrust arises. For example, if the available thrust is 100,000 lbs and the require thrust is 70,000 lbs, it is technically safe to use any thrust setting between 70,000 to 100,000 lbs to takeoff. However, the regulation limits the use of reduced thrust takeoff up to 25% of maximum thrust using assumed temperature method. Therefore, the pilot should actually choose a thrust level greater than 75,000 lbs. The pilot in command has final authority to choose any thrust level between 75,000 lbs to 100,000 lbs that he/she thinks most appropriate. Typically, pilots choose a thrust setting greater than the minimum thrust level offered to them. This process sounds quite complicated, but the process is very well established and being performed every time an aircraft departs. Airlines have a team of engineers perform the analysis for the pilots. There are FAA certified commercial software available on mobile devices like iPads that perform this runway analysis.

For the purpose of predicting the average takeoff thrust usage, performing full-blown runway analysis is not feasible nor necessary. Instead, the objective of this research is to develop a simple, general model that works for majority of the aircraft types in AEDT. In addition, AEDT can provide an option for the users to input the takeoff thrust settings they would like to model with their own thrust data for specific flights.

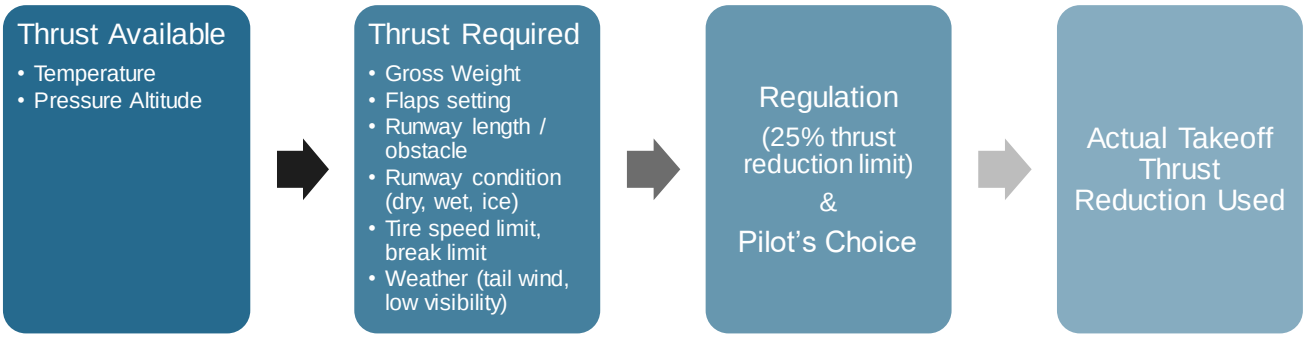

Figure 42. Four Factors of Takeoff Thrust Determination

Review of Takeoff Thrust Data Sources

The first step to develop a method that predicts takeoff thrust was to identify the potential sources of takeoff thrust data. The team considered the following five different types of flight data that might be able to provide takeoff thrust information. Among them, the ACARS data from ASCENT project 35 and AWABS data are most appropriate for the purpose of the project. Following sections provide preliminary analysis results using the dataset.

- Flight Planning
  - Includes actual GW, but no thrust
  - May include the specification of the thrust parameters that pilots are recommended to use
- Aircraft Communications Addressing and Reporting System (ACARS)
  - Includes actual GW and %Reduced Thrust data
  - No runway, no pressure alt, temperature may not be as accurate as AWABS
- AWABS (Dispatch data)
  - Accurate GW, runway, pressure alt, temperature, thrust setting data
  - No thrust, no info on actual pilot choice

- FDR / Flight Operations Quality Assurance (FOQA)
  - Need to estimate thrust based on fuel flow or other engine parameters
  - Best for departure procedures
- Radar Data
  - ACRP Project 02-41 attempted to use radar data, hi-fi weather, and BADA performance data to obtain engine thrust → very hard to obtain reliable thrust data

As mentioned earlier, the objective of ACRP 02-41 was to produce guidance to include the effects of reduced takeoff thrust in their emissions inventory calculations and to develop a Takeoff Thrust-Setting Estimator Tool (TTREAT) based on statistical analyses of extensive takeoff thrust data supplied by airlines. Specifically, ACRP 02-41 used flight planning and FDR data to either collect or drive takeoff thrust. In fact, none of the above five data types directly gives the thrust values. Rather, they provide some engine and aircraft performance parameters and atmospheric conditions that can be used to derive thrust. Figure 43 below is based on a plot from the ACRP 02-41 Technical Report. ACRP 02-41 used 747-400 FDR data to estimate takeoff thrust level used (% of max thrust available) based on fuel flow and other atmospheric conditions (temperature and pressure). Each point on the plot represents a combination of takeoff thrust and weight for an individual 747-400 takeoff. While the % thrust values are not completely accurate, the plot shows a very strong correlation between %Thrust and takeoff weight. It also shows that the thrust values didn't go below 75% even at very low weight. Another observation is that some takeoffs used the maximum thrust regardless of the weights. Finally, for a given weight, most takeoff thrusts could vary by about 10%. Based on the observations made here, a four step method that estimates takeoff thrust as a function of aircraft weight is proposed in the next section

Figure from ACRP 02-41 Technical Report

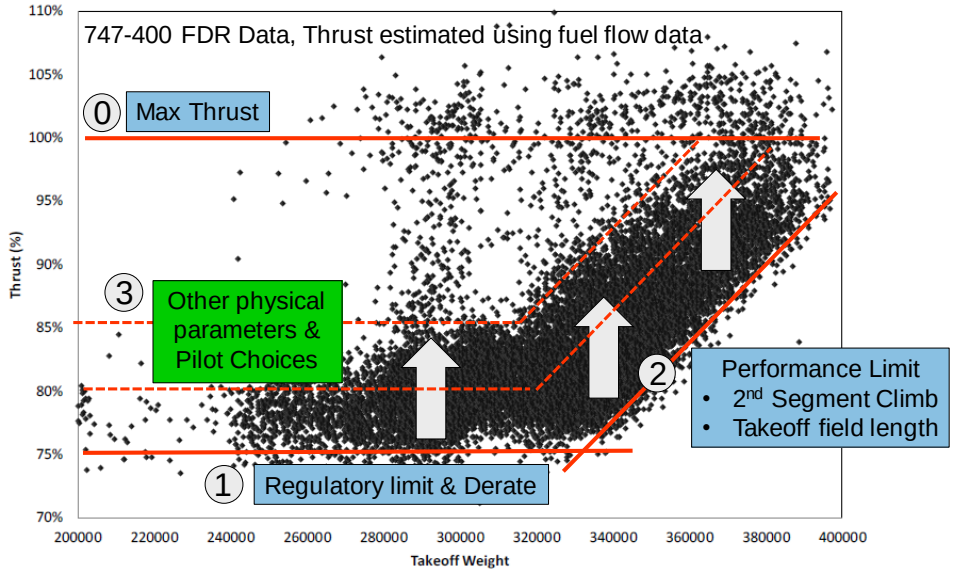

Figure 43. Schematic Diagram of the Takeoff Thrust Model

Proposed Takeoff Thrust Estimation Method:
The method proposed here is based on the observations made with limited aircraft takeoff thrust data. The assumption is that the flight physics, regulations, airline policy on reduced thrust takeoff, and pilot's practice are more or less consistent across aircraft types, regulatory authorities, airlines, and pilots. The method will be refined as more data become available and new trends are observed. The method prescribes the relationship between $\%Thrust_{adj}$ at the standard sea level condition and %GW. The %thrust is the ratio of actual thrust level used for the takeoff to the maximum thrust level available at the given atmospheric condition. $\%Thrust_{adj}$ is the ratio of actual thrust level used for the takeoff to maximum thrust level available at the sea level standard day condition. The %GW is defined as the ratio of the actual takeoff gross weight to the certified maximum takeoff gross weight (MTOW).

1. Maximum Thrust
    - Use the current AEDT's 100% thrust as an option
2. Regulatory Limit & Derates:
    - Set the lower thrust limit by regulation
        - For a 25% thrust reduction limit, the lower bound for %thrust is set at 75%
    - Some aircraft have derate (e.g. TO, TO1, TO2) options
        - Further thrust reduction is done by assumed temperature method up to 25%
        - TO2 with the highest assumed temp can give 40% thrust reduction
        - Set the lower limit at 60% of the max thrust in this case
3. Performance Limit:
    - Define a line (intercept and slope) to represent the thrust limit determined by aircraft performance constraints.
4. Add Margins to the limit sets in Step 2 and 3
    - The lower thrust limits set in Step 2 and 3 can be directly used for the aggressive thrust reduction option
    - Since the pilots typically are offered three takeoff thrust settings including the lower limits, shift the lines from 2) and 3) up by a certain percent (e.g. 5% and 10%) to create moderate and conservative thrust reduction options

A reduced thrust takeoff is typically followed by a reduced thrust in the initial climb segment. Although the pilot can choose to use full climb thrust after a reduced thrust in the takeoff segment, the FMS automatically selects a reduced climb schedule based on the takeoff thrust setting. Otherwise, it is possible to experience an increase in the thrust level at thrust cut-back. The research team recommends the follow climb thrust reduction schedule as shown in Table 66.

Table 66. Recommended Climb Thrust Reduction Schedule[10, 11, 12, 13]

Takeoff Thrust	Climb Thrust
Takeoff Derate < 5%	Use Max Climb Thrust
Takeoff Derate between 5-15%	Derate climb by 20% up to 10,000 feet
Takeoff Derate > 15%	Derate climb by 20% up to 10,000 feet

Application of the Thrust Correction Model in AEDT

The current version of AEDT calculates the engine thrust for a departure operation using the SAE-AIR-1845 method. The thrust coefficients in the ANP database are populated to calculate the thrust for the ANP aircraft ID and for the thrust type (either takeoff or climb) defined in the departure procedure. The SAE-AIR-1845 method calculates the thrust based on the sea level static thrust and corrects it for speed, pressure altitude, and temperature. The current plan of implanting thrust correction to model reduced thrust takeoff is to correct the sea level static thrust (defined by COEFF_E) using a multiplying factor (MF). The formula to calculate MF is provided in Table 67.

[10] GE, "Economic Impact of Derated Climb on Large Commercial Engines"
[11] RR, "Derated Climb Performance In Large Civil Aircraft"
[12] Boeing, "737 Flight Manual"
[13] Interview with Delta Chief Flight Instructor on xx-xx-2017

Table 67. Multiplying Factor for Thrust Correction

Thrust Correction for Reduced Thrust Takeoff COEFF_E_new = COEFF_E *MF **Multiplying Factor (MF)** If Temp <=30 degC, MF = %Thrust_adj(%GW) / alpha If Temp > 30 degC, MF = %Thust_adj(%GW) /alpha * beta where, beta = [1 – COEEF_H/COEFF_E*(TC -30)] alpha = thrust lapse rate with altitude beta = thrust reduction rate at high temp %Thrust_adj(%GW) = a + b*%GW alpha and beta are calculated using AEDT coefficients

Preliminary Takeoff Thrust Model of Boeing 737-800

The takeoff thrust prediction method proposed in the previous section is applied here to Boeing 737-800. In order to successfully build and test a model for the aircraft types in AEDT, a large number of actual flight data including the following parameters are needed:

- Actual takeoff weight
- Actual takeoff used or %takeoff thrust used
- Airport temperature and pressure altitude

The research team has not yet identified any dataset that includes all these parameters. Among the different types of flight data examined, the ACARS data and AWABS data from ASCENT Project 35 found to be the closest to meet the data requirements. The ACARS data from Project 35 includes the actual takeoff weight and %Thrust reduction (FNRED). It also includes airport temperature, but it does not provide pressure altitude. Instead, it provides the airport elevation, which was used in the following analysis. AWABS data provides all above except the actual thrust or %Thrust used. Instead, it gives a set of assumed temperatures that can be used for each of the gross weights.

A preliminary version of the thrust model for Boeing 737-800 was developed using the ACARS data from Project 35. The dataset included the first ACARS report from 62,981 flights. A statistical analysis was performed to understand the distributions of the key performance parameters. Figure 44 shows histograms and summary statics of %Thrust, airport temperature, airport elevation, and the longest runway length. The %Thrust varied from 59.8% to 103.6% with the mean value of 85%. The temperature varied from -8 to 117 degrees Fahrenheit. About 25% of flights occurred when the temperature was higher than 84 degrees Fahrenheit. The airport elevation varied from 4 ft to 7316 ft, while 75% of the departure occurred from airports below 1026 ft. About 97.5% of departures took place from airports with the longest runways longer than 8400 ft.

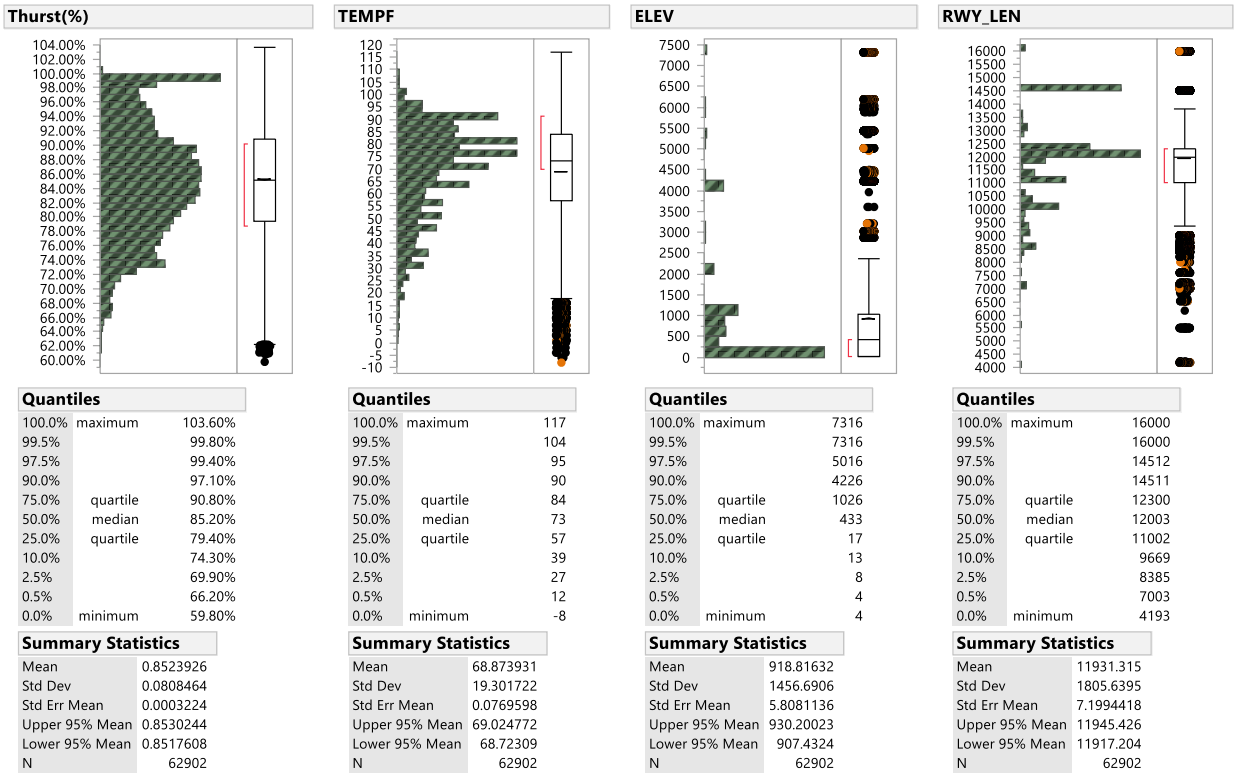

Figure 44. Statistics from the B737-800 ACARS Data

As the first step %GW was calculated by normalizing the takeoff gross weight with the MTOW. Here the MTOW of 174,000 was assumed. %Thrust values were calculated by subtracting the FNRED from 100. Then $\%Thrust_{adj}$ was calculated by: $\%Thrust_{adj}$ = %Thrust/alpha, where, alpha = thrust lapse rate with pressure altitude.

Due to the lack of pressure altitude information in the ACARS dataset, the airport elevation was used instead. The relationship between $\%Thrust_{adj}$ and %GW for B737-800 is shown in Figure 45. With the adjusted thrust and GW, a simplified takeoff thrust model, $\%Thrust_{adj}(\%GW) = a + b*\%GW$, was developed by applying the method proposed in the previous sections. The thrust model is illustrated on the figure and summarized in Table 68.

Table 68. Summary of the Findings and Recommendations

Thrust Types	Options	a (intercept)	b (slope)
Maximum Thrust	None	1	0
Regulatory Limit & Derate For %GW < 0.7	Low	0.6	0
	Medium	0.67	0
	High	0.74	0
Performance Constraints For %GW ≥ 0.7	Low	0.07	0.94
	Medium	0	0.94
	High	-0.07	0.94

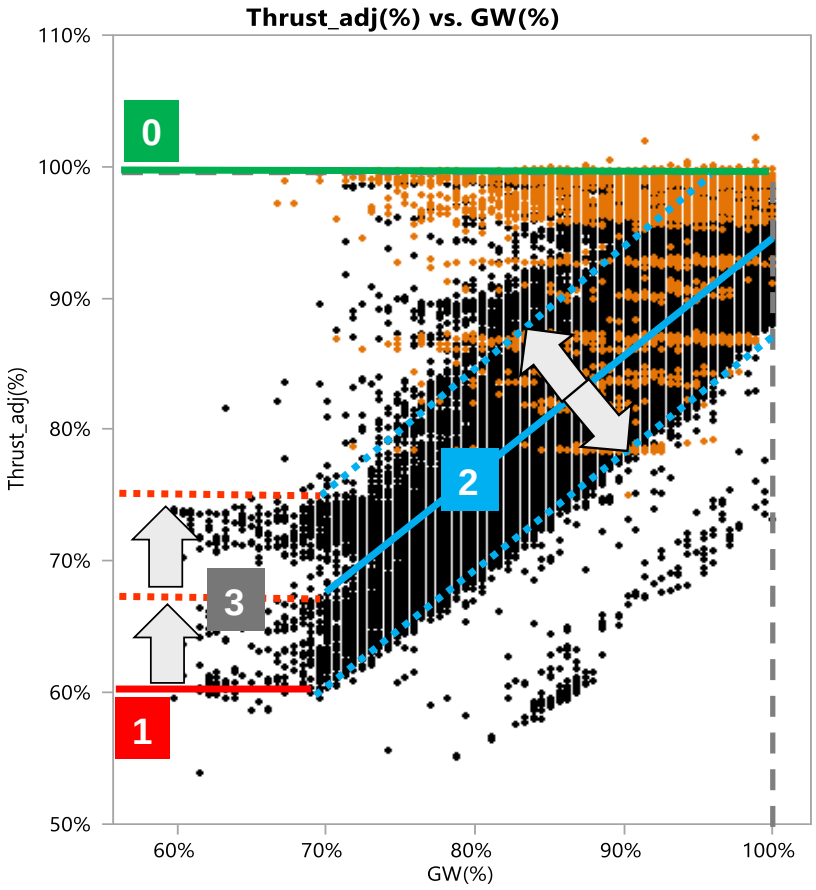

Figure 45. %Thrust$_{adj}$ vs %GW for B737-800

Development of a Takeoff Weight Prediction Method

Previous studies summarized in the literature review section showed the gap between the takeoff weight assumptions in AEDT and the reality. General observation was that AEDT tends to underestimate the weight by about 5%. Takeoff gross weight of an aircraft is comprised of three weight components: Operating Empty Weight (OEW), payload weight, and fuel weight. It is possible that the differences in all these three weight categories contribute to the differences in the gross weight between AEDT and the reality. Coming up with new weight assumptions requires collection of such weight data for majority of aircraft types flown by majority of airlines for an extended period of time. The goal of this research is to develop a new weight assumption that better represents an *average* takeoff weight for each of the aircraft types in AEDT in order to improve calculation of environmental impacts. The success of such a task largely relies on the accessibility of reliable and extensive takeoff weight data. The team has reviewed potential sources of such data including flight planning, ACARS, the BTS T-100, and AWABS. The team currently has some flight planning and ACARS data from one airline for a couple of aircraft types. The dataset includes the takeoff weight information for each flight. While the dataset is extremely valuable providing insights and a means to validate the method later on, it is not possible to use a dataset of an aircraft type for estimating the takeoff weight of other aircraft types. Therefore, the team is coordinating with the FAA to obtain the average payload data that ICAO has been collecting. Alternatively, the team can use the BTS T-100 data. Both the ICAO and T-100 data only provide average payload values. The ICAO data is supposed to be global, but the T-100 data is limited to US operations. Since those datasets only give average payload values, the OEW and fuel weight should be obtained separately to calculate the gross weight. Otherwise, only the payload portion of the gross weight can be updated in AEDT and keeping the current OEW and fuel weights. Though it is easier, the latter approach can lead to underestimation of the gross weight.

Once the gross weight (or just the payload or load factor) data is gathered, the data needs to be processed to be able to update the AEDT's weight assumptions. A handful of different options can be devised depending on the desired level of data aggregation. Currently, AEDT aggregates the takeoff weight of all departure operations for an aircraft type within a stage length. Therefore, one option to improve AEDT's accuracy is to update that representative weight by calculating the average of all the gross weights for each stage length for each aircraft type. This option will ensure that the new AEDT weights match the average weight of all departures for a stage length bin. AEDT currently uses the stage length bins with either 500 nm or 1000 nm width. Due to the wide ranges of flight distances represented by a stage length bin, even the updated assumption won't be able to model the average takeoff weights for a particular OD pair. The gap between the AEDT's weight assumption and the reality can be further reduced by increasing the level of granularity. Five different options below cover the spectrum of solutions that maintains the current level of aggregation (Option 1) to the option of modeling each weight for each flight (Option 5).

Option 1: Maintain the current stage length approach, updating the GW assumptions for each stage length and aircraft type
Option 2: Calculate average GW for finer stage length bins (e.g. 250 nm width)
Option 3: Use different GW assumptions for each SL and Departure Airport
Option 4: Model GW as a continuous function(s) of GCD
Option 5: Model GW for each flight (the users should provide the schedule data including the GW for each flight)

Generally speaking, the modeling accuracy, data requirements, and computational expense increase with the option number. Table 69 provides the initial qualitative assessments of the five weight prediction options with respect to the evaluation criteria. As the next step, the five options could be implemented to model an average day of departures at the ATL airport to provide a quantitative assessment depending on the level of resources available.

Table 69. Options for Takeoff Weight Assumptions, Expected Accuracy, Data Requirement, and Implementation Feasibility

Potential NEW GW Solutions	Computational Burden	Accuracy	Data Req.	Potential Data source/Current Status / Feasibility
AEDT	Baseline One run for each SL and Origin (74 runs*)	Off by 6% on Average*	Baseline (65% LF assumption for all SL and aircraft types	ANP DB includes GW info for 127 commercial aircraft types
Option 1-b: Update LF for each aircraft type	Same as the baseline	May not capture average GW at certain SL bins (high std. dev)	Avg LF or GW for all SL for each aircraft	BTS T-100 can be used for this option for aircraft types used in the US / NONE at the moment / highly feasible in a couple of months
Option 1-c: Different LF assumptions for different SLs	Same as the baseline	Match average GW of all flights in the SL bin (high std. dev) Accounts for MTOW and fuel limits	Avg LF or GW for each SL and aircraft	BTS T-100 can be used for this option for aircraft types used in the US / NONE at the moment / highly feasible in a couple of months
Option 2: Different LF assumptions for sub-SL Bins	Baseline x number of sub-SL bins	Match average GW of all flights in the sub-SL bin (med std. dev) Accounts for MTOW and fuel limits	Avg LF or GW for each sub-SL and aircraft	BTS T-100 can be used for this option for aircraft types used in the US / NONE at the moment / highly feasible in a couple of months
Option 3: Different LF sub-SL bins and Departure Airport	Baseline x number of sub-SL bins	Match average GW of flights in a stage length for the airport (low std. dev) Accounts for MTOW and fuel limits Accounts for runway length and elevation impact to GW	Avg LF or GW for each sub-SL, airport, and aircraft	BTS T-100 has all this info for US flights / NONE at the moment / may not be feasible getting airport level data for international and small US airports
Option 4: Continuous Function(s) of GCD	2.4 times the baseline* One run for each OD pair	Lines with kinks can account for MTOW and fuel limits Does not model airport to airport GW variation	Raw or avg. GW and GCD data GW vs GCD models for each aircraft	BTS T-100 can be used for this option + MTOW and fuel capacity data / regression models of 737-800, 767-300ER, 767-400ER, and 757-200 from P35 / not sure yet
Option 5: GW of each flight	280 times the baseline*	Match both average and individual GW	GW data for all the flights a study is modeling	Users should use their own data for a real study / Entire 737-800 and 767-300ER flight from year 2015? by an airline for test purposes

Qualitative Evaluation Score	
1	Worst
2	Not desirable
3	Okay
4	Good
5	Best

Development of a Process to Implement New Weight, Thrust, and Departure Procedures in AEDT

The final aspect of the research is to determine how to implement the modified weight, thrust, and departure procedure into the AEDT procedural definitions based on the data analysis and methods. Per the AEDT Technical Manual guidance for the departure procedure, it appears the flexibility exists to define any type of procedure. GT has developed a process with which a new aircraft with different weight, thrust, and procedure assumptions can easily be inserted into AEDT. The process illustrated in Figure 46 provides a step-by-step instruction on 1) to extract the current APM assumptions of the aircraft of interest, 2) to change the assumptions in an Excel or an XML file, 3) to update the AEDT's Fleet DB by running SQL scripts, 4) to select the new aircraft in the AEDT GUI, and 5) to run a metric result using the new aircraft. A word document that details all these steps has already been draft. The document will be refined as the team progresses to a larger scale test and will be provided to the FAA.

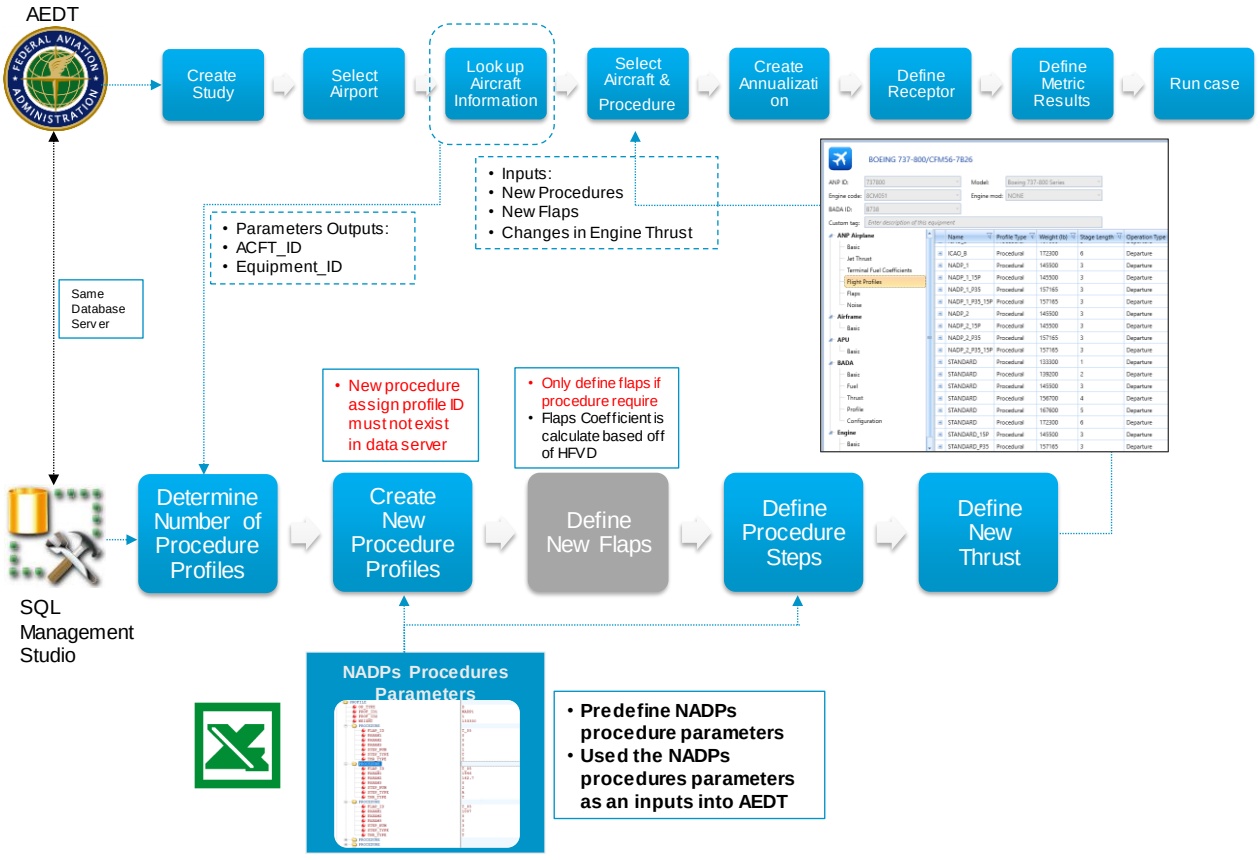

Figure 46. Process of Adding NEW GW, Thrust, and Procedures to AEDT

Milestone(s)
No specific milestones are associated with this project. However, significant progress is being made towards understanding the implications of the APM assumptions for departure.

Major Accomplishments
Significant insight to the impact of the APM assumptions have been obtained through the partial derivative sensitivity approach.

Identification of various implementation options to the APM and the Fleet dB

Publications
None

Outreach Efforts
Bi-weekly calls with the Project Managers. ASCENT annual meeting. FAA Noise workshop. FAA External tools calls.

Awards
None

Student Involvement
Vu Ngo and Ameya Behere – Graduate Research Assistant, Georgia Institute of Technology

Plans for Next Period
The primary focus for the next period will be:
- Implementation of each sensitivity assumption to AEDT
- Assessment of new assumptions at the airport level

Appendix

B737-800

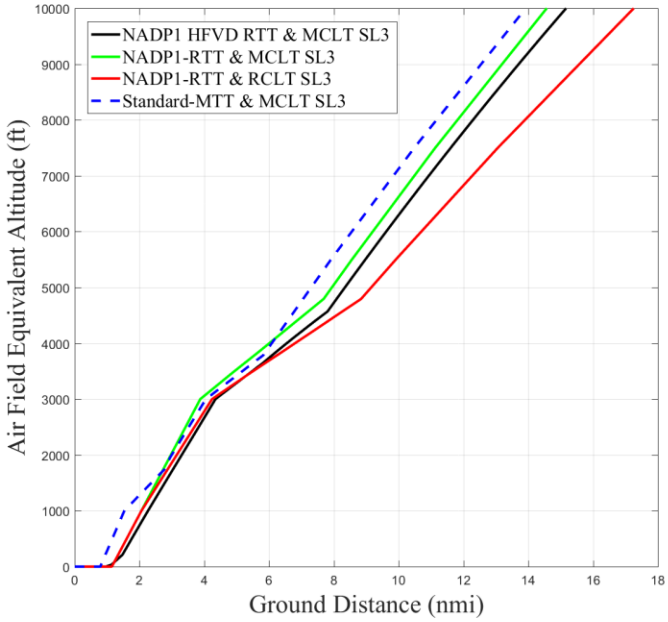

Figure 47: Altitude vs Ground Distance for B737-800 Trajectory Comparison for Stage Length 3 NADP1

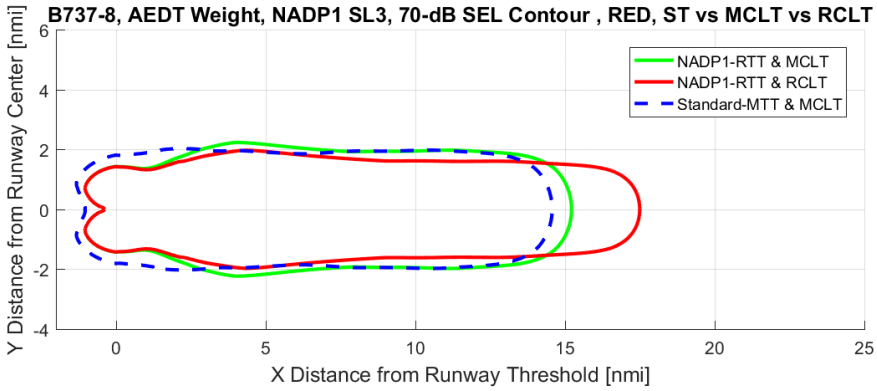

Figure 48: B737-800 Noise Contour Comparison at SEL 70dB for Stage Length 3 NADP1

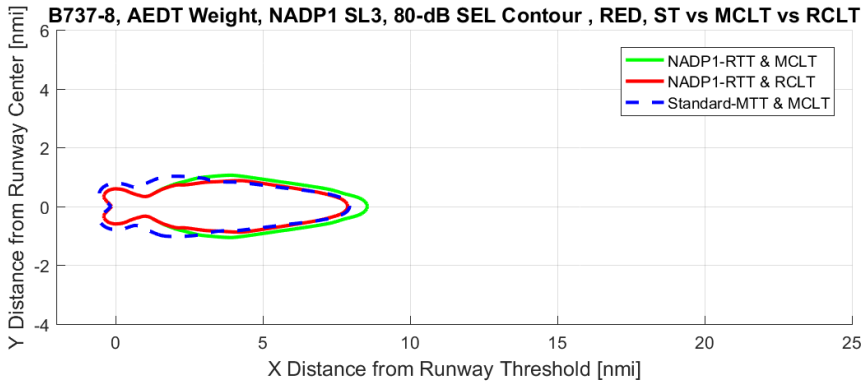

Figure 49: B737-800 Noise Contour Comparison at SEL 80dB for Stage Length 3 NADP1

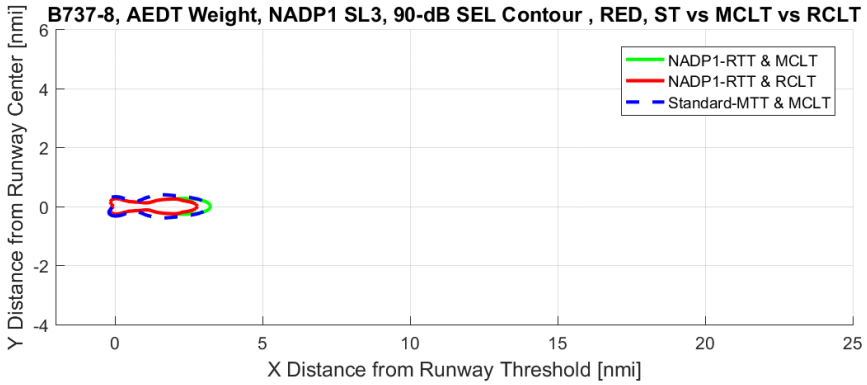

Figure 50: B737-800 Noise Contour Comparison at SEL 90dB for Stage Length 3 NADP1

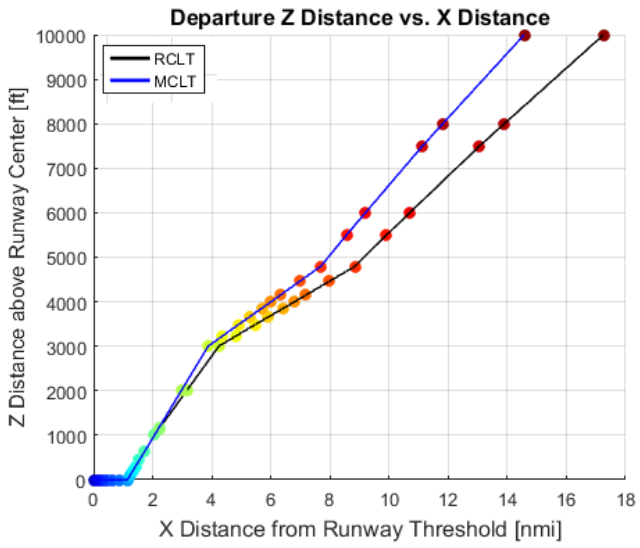

Figure 51: Detailed Altitude vs Ground Distance for B737-800 Stage Length 3 NADP-1

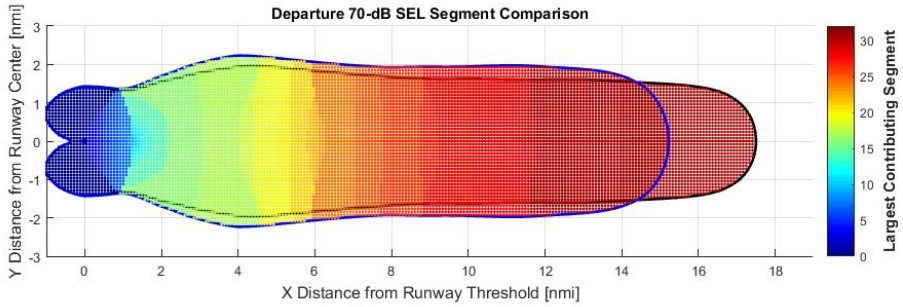

Figure 52: Detailed B737-800 Noise Contour Comparison at SEL 70dB at Stage Length 3 NADP-1

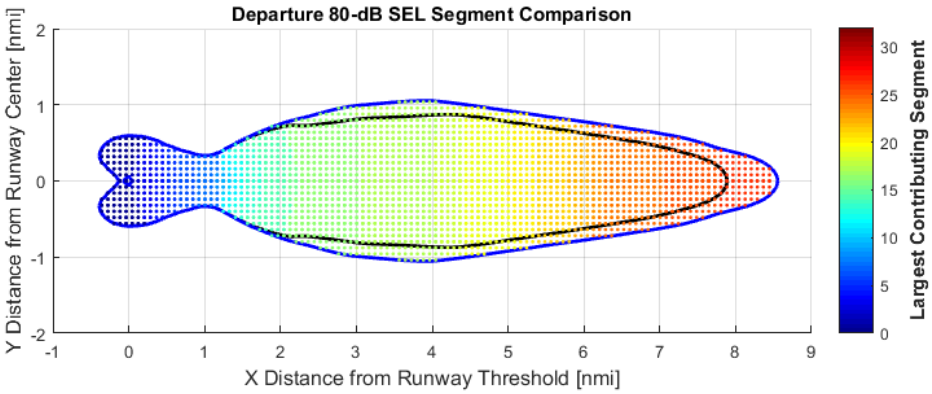

Figure 53: Detailed B737-800 Noise Contour Comparison at SEL 80dB at Stage Length 3 NADP-1

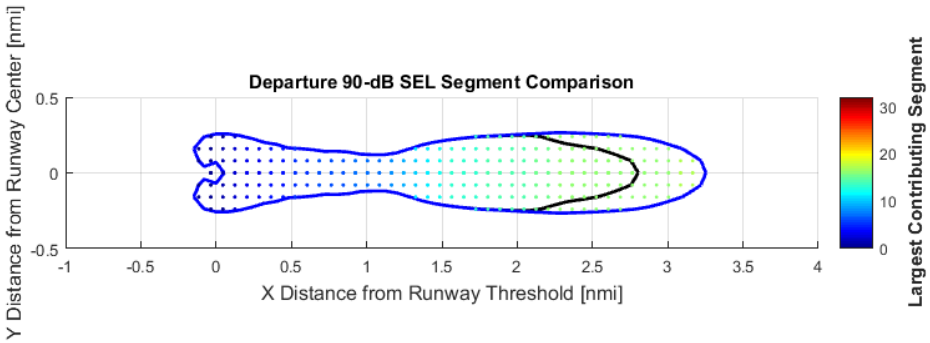

Figure 54: Detailed B737-800 Noise Contour Comparison at SEL 90dB at Stage Length 3 NADP-1

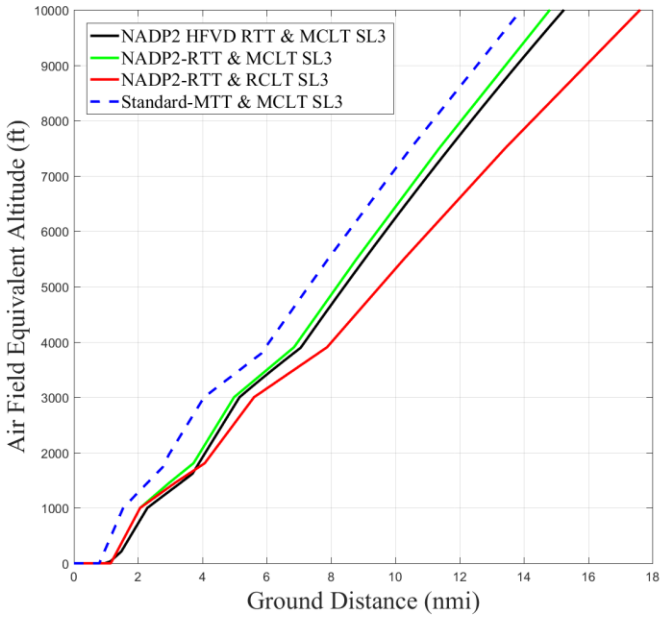

Figure 55: Altitude vs Ground Distance for B737-800 Trajectory Comparison for Stage Length 3 NADP2

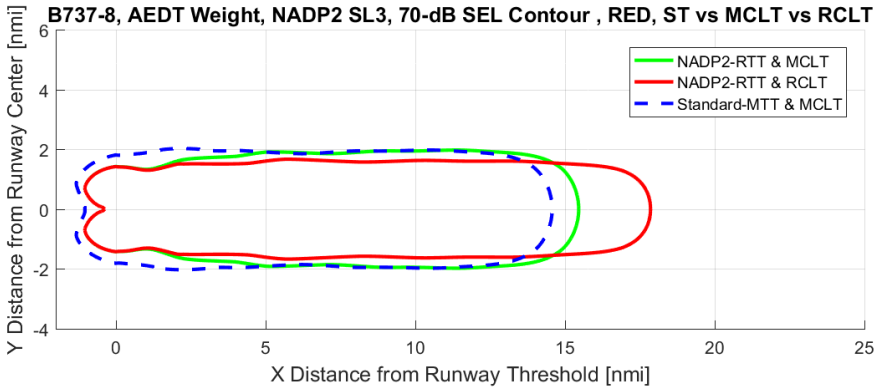

Figure 56: B737-800 Noise Contour Comparison at SEL 70dB for Stage Length 3 NADP2

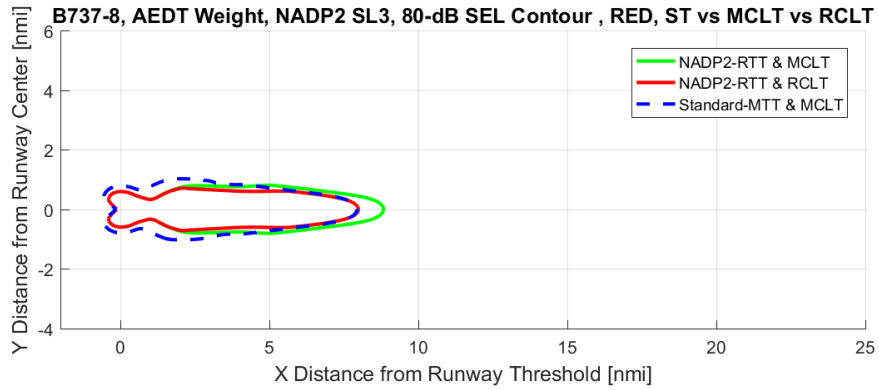

Figure 57: B737-800 Noise Contour Comparison at SEL 80dB for Stage Length 3 NADP2

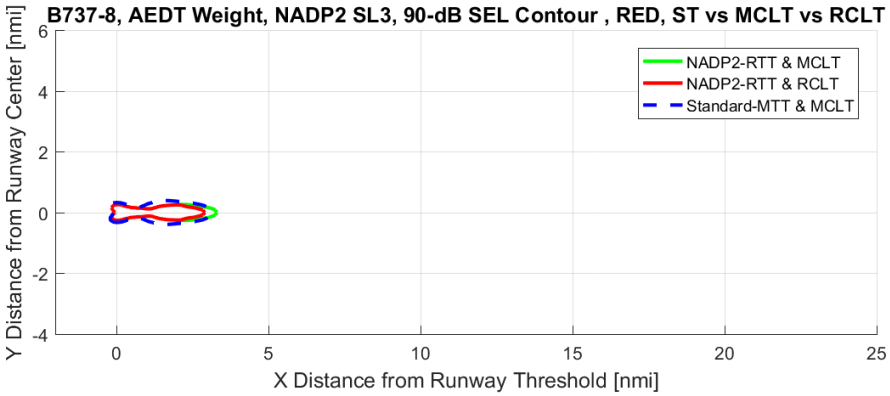

Figure 58: B737-800 Noise Contour Comparison at SEL 90dB for Stage Length 3 NADP2

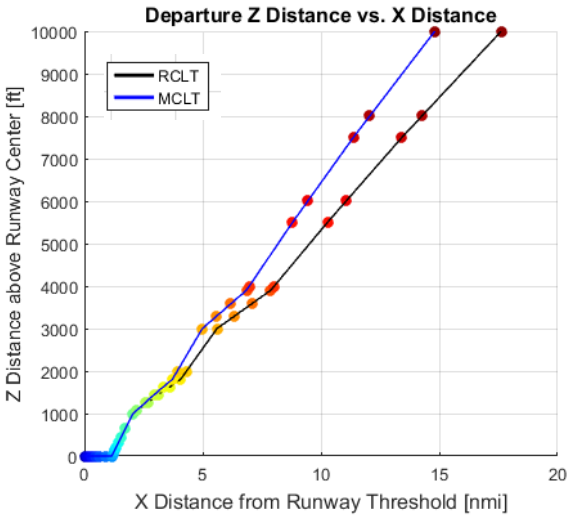

Figure 59: Detailed Altitude vs Ground Distance for B737-800 Stage Length 3 NADP-2

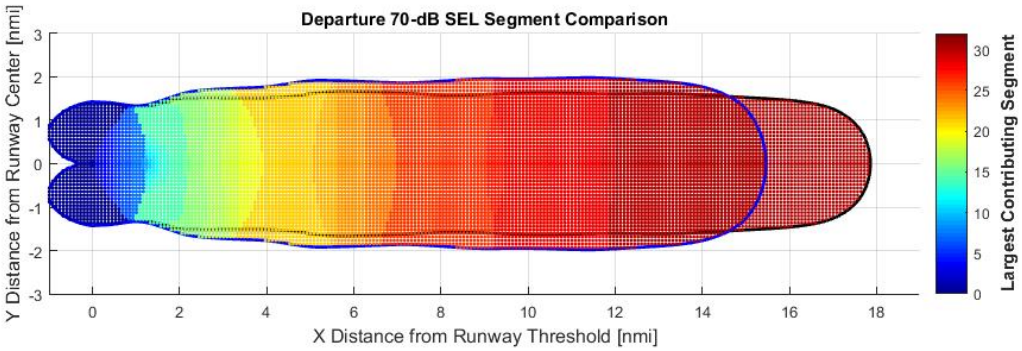

Figure 60: Detailed B737-800 Noise Contour Comparison at SEL 70dB at Stage Length 3 NADP-2

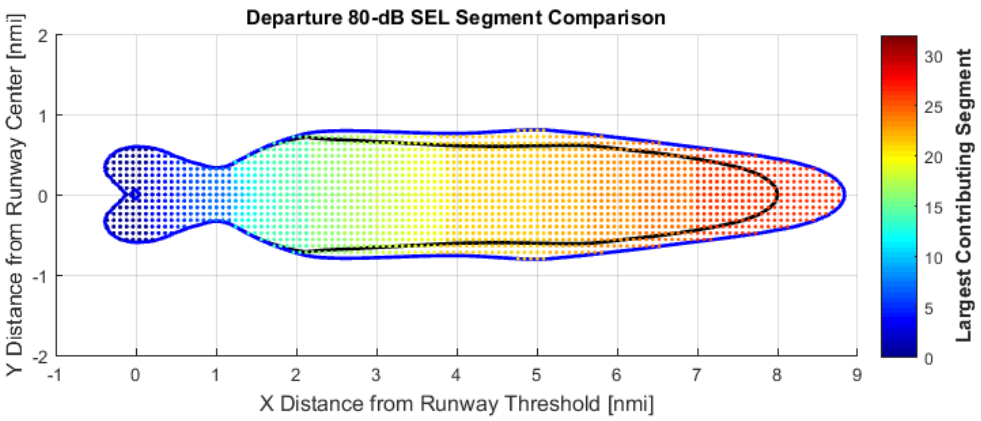

Figure 61: Detailed B737-800 Noise Contour Comparison at SEL 80dB at Stage Length 3 NADP-2

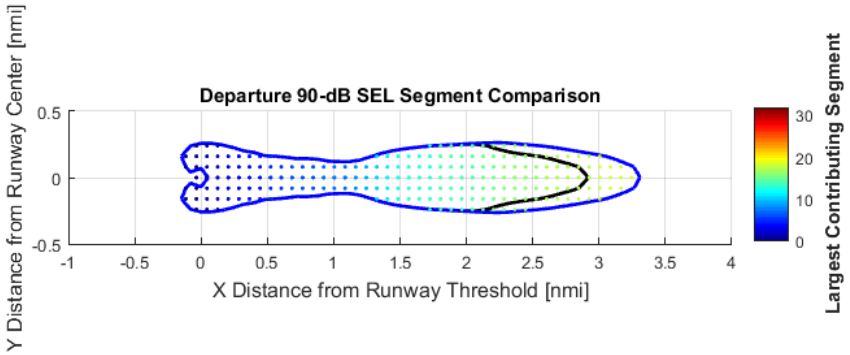

Figure 62: Detailed B737-800 Noise Contour Comparison at SEL 90dB at Stage Length 3 NADP-1

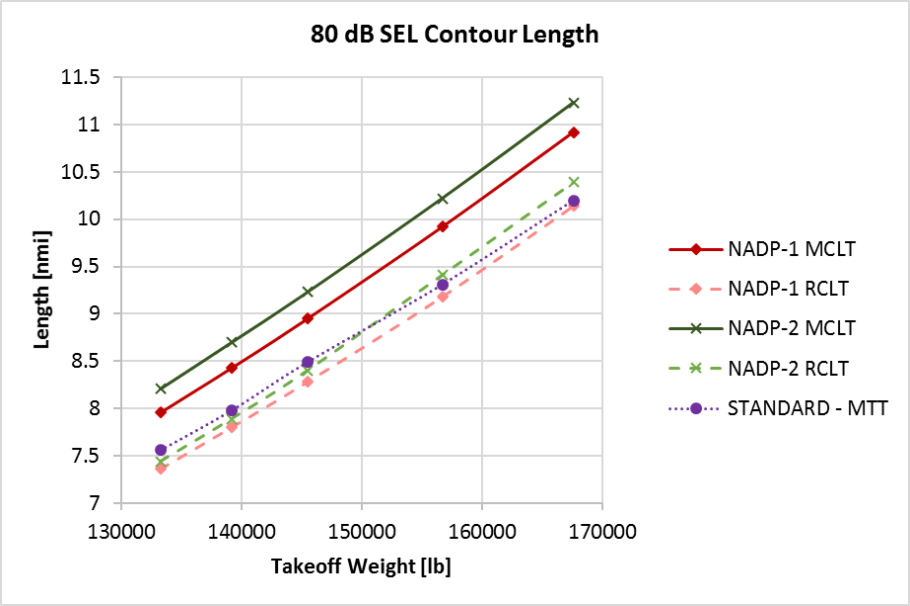

Figure 63: B737-800 Contour Length Comparison for SEL 80dB

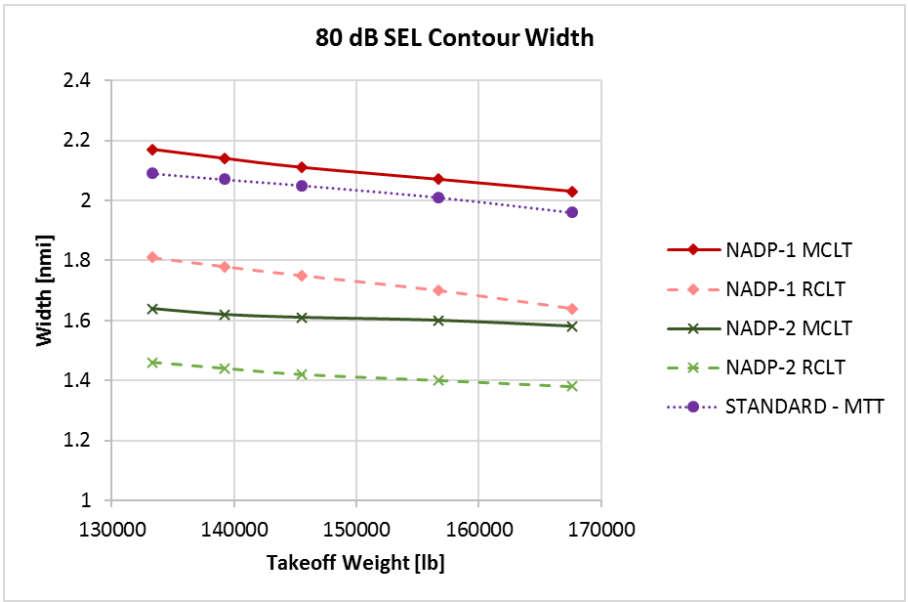

Figure 64: B737-800 Contour Width Comparison for SEL 80dB

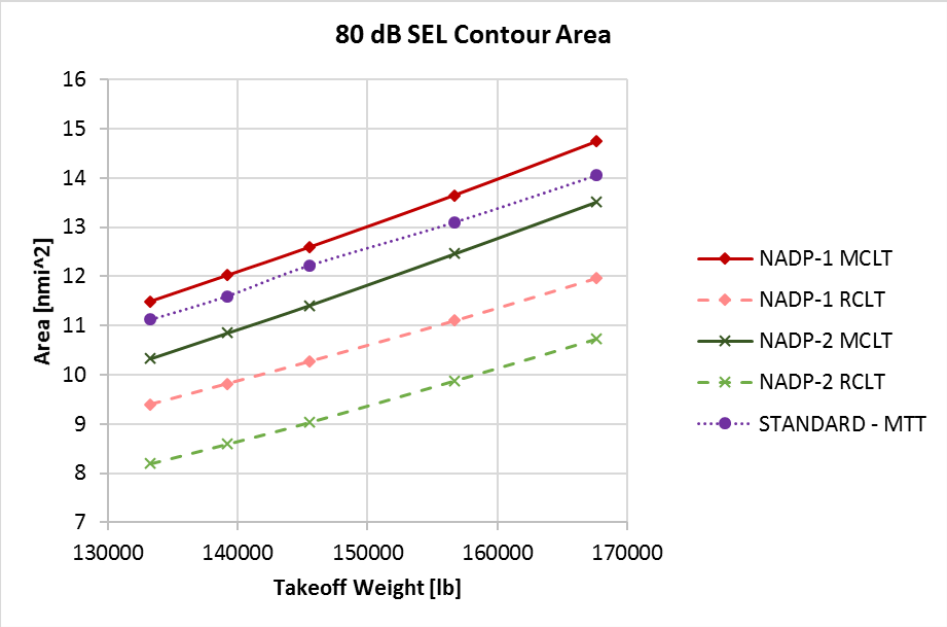

Figure 65: B737-800 Contour Area Comparison for SEL 80dB

Project 046 Surface Analysis to Support AEDT APM Development

Massachusetts Institute of Technology and Massachusetts Institute of Technology Lincoln Laboratory

Project Lead Investigator

Hamsa Balakrishnan
Associate Professor
Aeronautics and Astronautics
Massachusetts Institute of Technology
77 Massachusetts Ave., 33-328
Cambridge, MA 02139
617-253-6101
hamsa@mit.edu

University Participants

Massachusetts Institute of Technology

- P.I.(s): Hamsa Balakrishnan
- FAA Award Number: 13-C-AJFE-MIT, Amendment No. 021
- Period of Performance: July 7, 2016 to Aug. 31, 2017
- Task(s):
    - Phase 1
    - 1.1. Assess AEDT aircraft surface performance modeling needs
    - 1.2. Develop enhanced aircraft surface performance models
    - 1.3. Validate enhanced aircraft surface performance models
    - 1.4. Recommend AEDT APM enhancements
    - Phase 2
    - 2.1. Extend analysis to broader range of aircraft types that serve US domestic operations
    - 2.2. Extend analysis on airport-specific differences that significantly impact surface fuel burn to more US airports
    - 2.3. Identify AEDT surface APM enhancements to support emissions and noise inventories
    - 2.4. Recommend AEDT APM enhancements & Coordination with AEDT APM Developers

Project Funding Level

$75,000 FAA funding and $75,000 matching funds. Source of match is approximately $75,000 all from MIT.

Investigation Team

Prof. Hamsa Balakrishnan, Co-Principal Investigator (MIT)
Dr. Tom Reynolds, Co-Principal Investigator (Lincoln Laboratory, via separate contract)
Yashovardhan Chati (Graduate student)
Sandeep Badrinath (Graduate student)

Project Overview

The current taxi phase models in the Aviation Environmental Design Tool (AEDT) make a number of simplifying assumptions that reduce the accuracy of their fuel burn and emissions predictions. Firstly, AEDT's current model assumes a constant engine specific thrust level (and resulting fuel flow rate) during taxi, determined from engine manufacturer certification data [1]. However, this assumption can be significantly different than actual characteristics during operational conditions for a given aircraft because of factors such as the age of the engine (as the engine gets older the amount of fuel it burns changes), as well as pilot technique (chosen taxi thrust level or "riding the brakes" instead of throttling down the engines when coming to a stop). Secondly, default taxi times are often assumed to be consistent with the standard certification Landing and Take-Off (LTO) cycle which assumes 26 minutes of taxi time on the airport surface, typically broken into 19 min taxi-out and 7 min taxi-in. Clearly different airports may have very different taxi times depending on topology, configuration, congestion levels, etc. which can lead to a large range of different taxi times. Using empirical data to determine realistic taxi time distributions can be effective, but these distributions need to be updated regularly to capture evolving airport conditions. Finally, the fuel burn contribution in the non-movement area from the gate time, pushback and engine start events (including engine and auxiliary power unit (APU) contributions) are typically neglected but can be quite significant. This project addresses these three issues by leveraging empirical data to build statistical and predictive models of fuel flow for a given airport and aircraft type. These analyses are designed to capture "first order" enhancements to provide recommendations for future development of tools such as AEDT.

Task Progress and Plans

Objectives

The objective of this research project is to identify and evaluate "first order" methods for improving taxi performance modeling in AEDT in order to better reflect actual operations. This objective will be met through analyses using surface surveillance (ASDE-X) and ASPM taxi time datasets, in combination with a statistical analysis of Flight Data Recorder (FDR) archives and other operational fuel burn data. Subsequent research phases may address potential higher order enhancement areas.

Research Approach

Task 1.1: Assess AEDT aircraft surface performance modeling needs: This task included soliciting input from stakeholders (including FAA AEE sponsors, AEDT developers, users, etc.) and related research (e.g., ACRP studies 02-45 [2] and 02-27 [3]) on known gaps and associated needs in current aircraft surface modeling capabilities. We conducted a discussion with AEDT developers and users (at the FAA and Volpe) to discuss gaps identified during the literature review and from ACRP studies 02-45 and 02-27. We also familiarized ourselves with the AEDT APM's current capabilities. In addition, prior research into high fidelity aircraft surface modeling was, and will continue to be, assessed and leveraged as appropriate. The three specific need areas identified were (1) enhanced models of fuel flow rates during taxi; (2) refined airport taxi time estimates; and (3) improved estimates of gate, pushback and engine start fuel burn.

Task 1.2: Develop enhanced aircraft surface performance models: This task involves developing refined models that account for the three needs identified in Task 1.1.

Enhancing fuel flow modeling: Figure 1 shows a typical fuel flow rate profile (post-pushback and engine start) during taxi-out. It can be seen that the fuel flow rate profile (red curve) can be divided into two distinct regions: a baseline region and a fuel flow spike region. The baseline region is characterized by an almost constant (low variation) fuel flow rate having a low value. The fuel flow spike region is characterized by spikes in the fuel flow rate with values greater than the baseline fuel flow rate. Therefore, these two fuel flow rate regions need to be modeled separately.

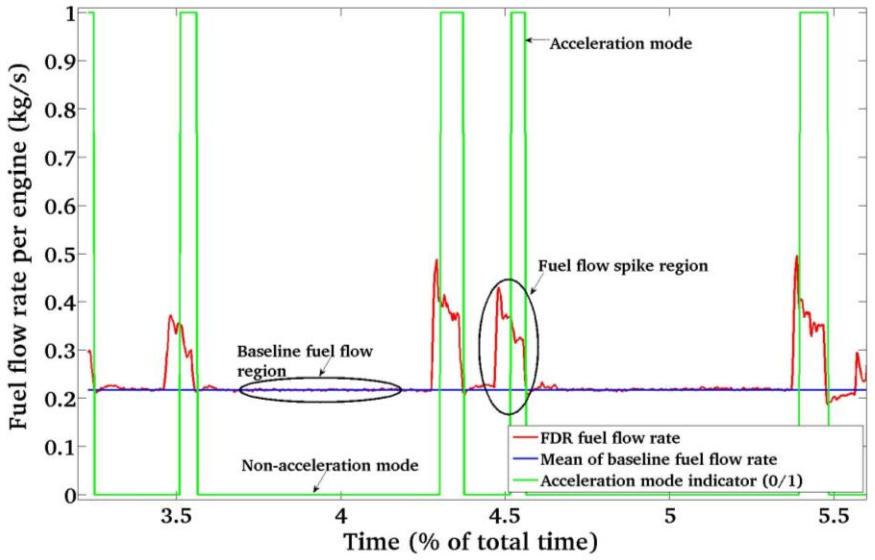

Figure 1. Typical fuel flow rate profile in taxi-out.

Table 1 shows different characteristics of the baseline fuel flow region for two example aircraft types: the A330-343 and the B777-300ER extracted from operational FDRs data. It can be seen that, on an average, more than 90% of the taxi-out fuel consumption occurs during the baseline fuel flow region. Therefore, in the current work, only the baseline fuel flow region is modeled and the fuel flow spikes are neglected. Figure 1 also shows a mean baseline fuel flow rate (in blue) obtained by averaging the baseline fuel flow rates for a particular taxi-out operation.

Table 1. Characteristics of the baseline fuel flow region. The table shows the mean and the range of time spent and fuel mass consumed in the baseline fuel flow region, as a percentage of the total time and fuel burn in taxi-out.

Aircraft type	Time (%)		Fuel burn (%)	
	Mean	Range	Mean	Range
A330-343	94.1	76.1 – 100.0	91.0	68.0 – 100.0
B777-300ER	93.0	77.4 – 100.0	91.0	73.0 – 100.0

The values of aircraft acceleration during taxi are generally not explicitly recorded in the trajectory data. Hence, the raw trajectory data are smoothed in order to estimate the variables of interest (such as acceleration mode, shown in green in Figure 1). Finally, the mean baseline fuel flow rate per engine in taxi-out (blue curve in Figure 1) is regressed against the mean values of the selected predictor variables. An Ordinary Least Squares (OLS) regression approach is found to be sufficient to develop this simplistic model (which is still based on the same functional form as the current AEDT model). Table 2 shows the OLS-derived equations for modeling the fuel flow rate in taxi-out for the two example aircraft types, the A330-343 and the B777-300ER. The training sets used to determine these equations comprised of 118 A330s and 83 B777s.

Table 2. OLS regression equations to model fuel flow rate per engine during taxi-out.

A/C Type	Baseline-1 Model Equation
A330-343	$\dot{m}_{f_{\text{taxi}}} = 0.779\dot{m}_{f_{\text{ICAO,taxi}}}\delta_\infty\theta_\infty^{0.350} \approx 0.779\dot{m}_{f_{\text{ICAO,taxi}}}$
B777-300ER	$\dot{m}_{f_{\text{taxi}}} = 0.753\dot{m}_{f_{\text{ICAO,taxi}}}\delta_\infty\theta_\infty^{0.717} \approx 0.753\dot{m}_{f_{\text{ICAO,taxi}}}$

We also compare the predictions from such baseline fuel flow modeling with the estimates provided by AEDT, which uses the ICAO fuel burn indices in conjunction with the Boeing Fuel Flow Correction. The model evaluation is conducted using an independent test set comprising of the entire taxi-out trajectory (i.e., the time elapsed between pushback and takeoff)

of 37 A330s and 25 B777s. The results are shown in Table 3, and suggest that significant benefits may be achieved through such a data-driven methodology.

Table 3. Performance of the OLS-based baseline fuel flow rate models and the AEDT model to predict fuel flow rates on unseen test data during taxi-out.

A/C Type	Mean error (%)		Mean absolute error (%)	
	OLS Model	AEDT	OLS Model	AEDT
A330-343	-3.3	36	6.3	39.4
B777-300ER	-1.8	42.6	2.7	43.2

Enhancing taxi time estimates: Airport-specific taxi out times are available in AEDT but have been found to be outdated. For this part of the study, taxi times were collected from the FAA's Aviation System Performance Metrics (ASPM). This dataset contains flight-specific taxi out times, available to the nearest minute. ASPM data from flights across 25 major US airports was aggregated for dates between October 2016 and September 2017, to provide a more recent model of the distribution of taxi out times at a given airport. This analysis could be extended to other US or international airports as needed.

Figure 2 below shows the updated taxi out time distributions for three sample airports: New York LaGuardia (LGA), Charlotte Douglas (CLT) and Washington Reagan (DCA). As expected, the times vary significantly within and between airports. For this particular set of airports, LGA is seen to have the longest peak and most varied taxi-out time; this is not surprising given the high congestion levels at LGA. The peak in the total taxi-out time distributions for LGA, CLT, and DCA are 18, 15, and 13 minutes, respectively. Compared to the standard 19 minutes of taxi-out time assumed from the LTO cycle (shown by the dashed magenta line in Figure 2), these correspond to errors of 5.3%, 26.7%, and 46.2% of the typical taxi out times for these particular airports. This is indicative of the impact the LTO 19-minute taxi time has on the accuracy of the calculated fuel burn based on the simplified taxi time.

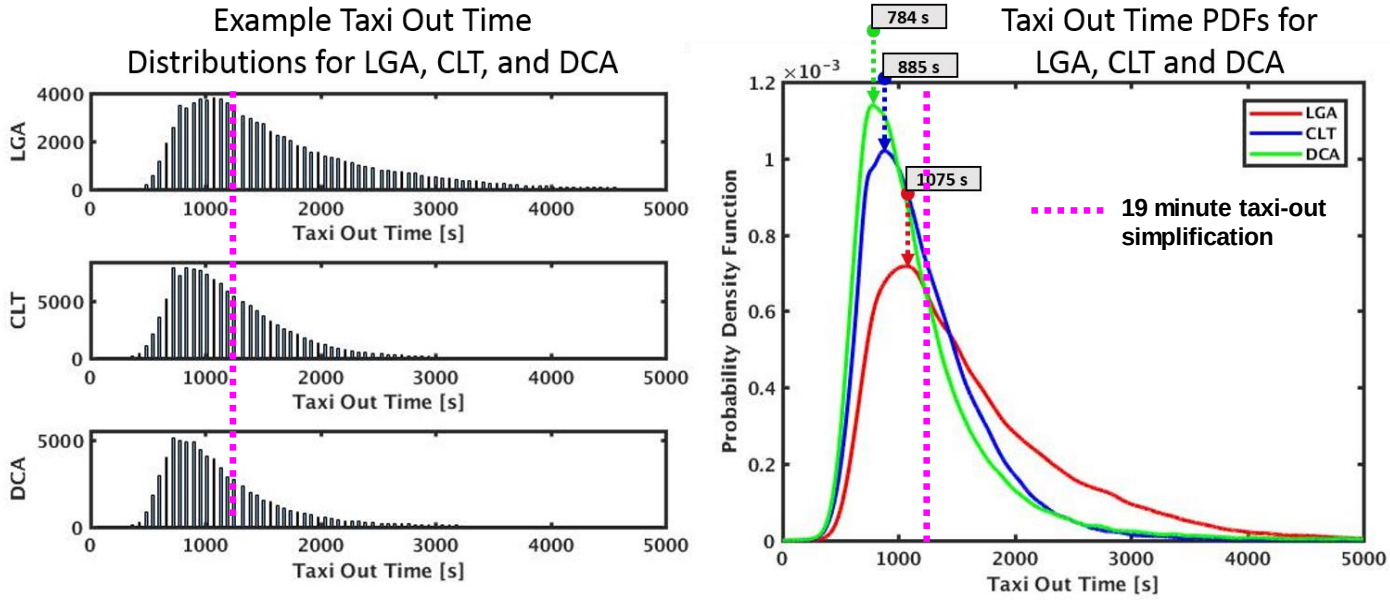

Figure 2. Example ASPM taxi-out time distributions for LGA, CLT and DCA airports

Adding Gate, Push-back & Engine Start Fuel Estimates: In order to establish a more accurate model of the fuel burn at a given airport, the fuel consumed during engine startup up, as well as the APU contribution at the gate, pushback, and engine startup is also investigated in this study. Differences in fuel burn for these phases across different airports were found to be

negligible, however the fuel burn distributions were found to vary significantly between different aircraft types. For this analysis, data from FDR was available for a European carrier for a selection of aircraft types. This contains a record over time of information specific to a flight, including fuel burn and velocity.

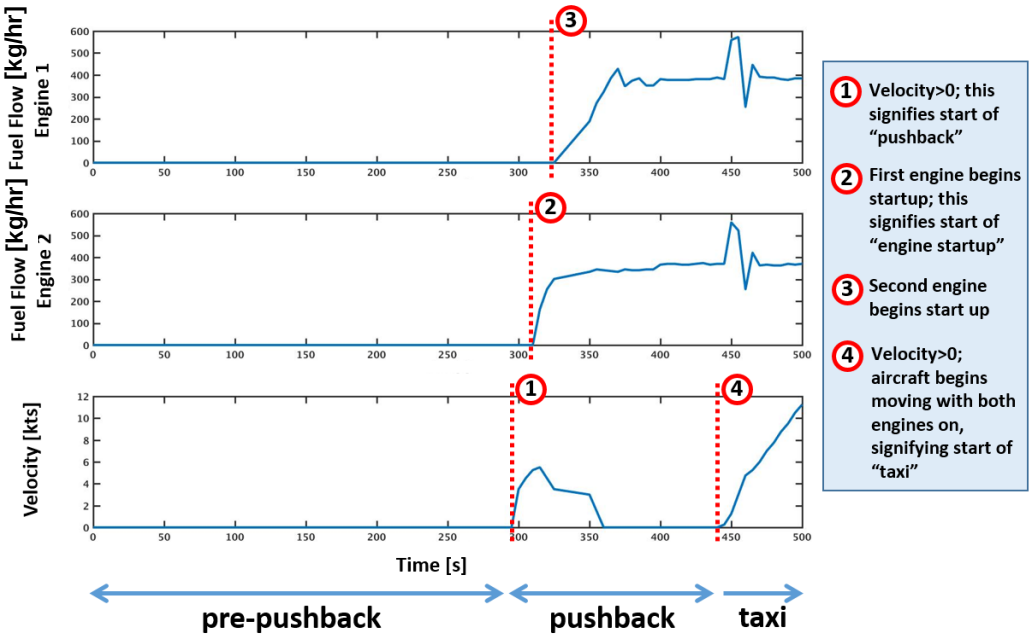

Figure 3. Example FDR data for a single flight gate, engine and push-back events

Figure 3 above shows the raw FDR data for a sample flight. For this part of the analysis, the flight was broken up into multiple segments, as the gate, pushback, and engine start have different APU and engine fuel burn settings. APU fuel burn rates were obtained from the ACRP 02-25 guidance document [3], which groups aircraft into categories (Narrow Body, Wide Body, Jumbo Wide Body, Regional Jet, and Turbo Prop) and gives the APU settings for the "no load" (gate), "environmental control systems" (pushback), and "main engine start" conditions for each aircraft category. The APU is turned on while still at the gate in the "no load" condition, after the aircraft has been disconnected from the gate's electricity. Through discussion with an experienced commercial pilot, it was determined that the APU is first turned on typically between 10-15 minutes before pushing back from the gate at large US airports. Therefore, for all aircraft, the gate time was assumed to be 12.5 minutes, although different assumptions may be appropriate at other airports, for example where off-gate stands are more common. Pushback was defined from the point at which the aircraft began to move back from the gate, until the point at which one of the engines began burning fuel. As can be seen in Figure 3, most aircraft begin starting the first engine while still in the process of pushback by the tug from the gate, before halting and completing engine startup with the remaining engines. Engine startup was defined from the end of pushback to when the aircraft begins to move for taxi after all engines have started up and post-engine checklists are complete.

Much of the work incorporated pre-processing the data before performing the statistical analysis, as many of the flights had corrupted data, such as non-zero fuel or velocity at the beginning of the track. Once tracks had been corrected for these issues, the fuel burn totals for the gate/pushback/engine start processes were aggregated over all the flights of a given aircraft type available in the FDR data as a statistical approach to building the fuel burn histograms from historical data. The resulting fuel burn distributions for the types studied are shown in Figure 4.

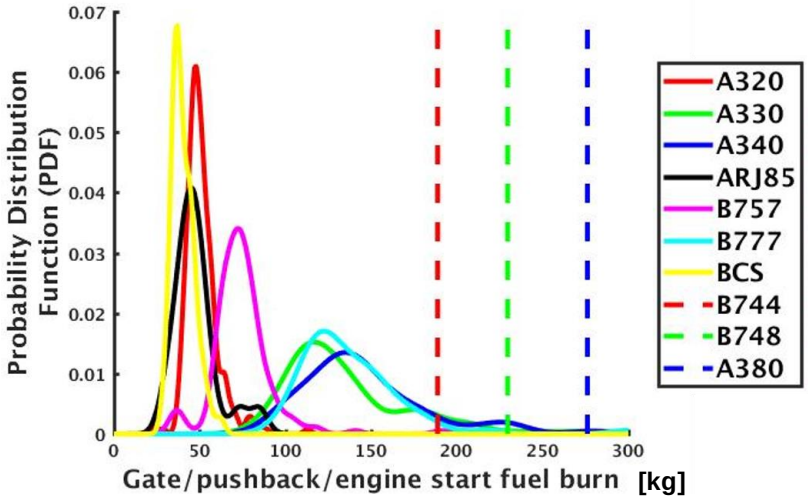

Figure 4. PDF curves for gate, pushback, and engine start fuel burn by aircraft type

The relationship between fuel burn and aircraft size was then investigated as a means to predict the fuel burn of the flights not within the FDR dataset. The maximum takeoff weight was used for each data type, pulled from the BADA 3.6 dataset. The total fuel burned during gate/pushback/engine start was seen to be linearly related to the weight of the aircraft type, and this correlation was used to then predict the approximate fuel burn for aircraft types not available in the FDR data set. Estimates for some example types using the observed correlation are presented as dashed lines in Figure 4.

Task 1.3: Validate enhanced aircraft surface performance models: A subset of the ASDE-X and FDR data archives were held back from the enhanced model development activity in the previous step so it can be used as independent validation data. For example, fuel burn profiles (and baseline fuel flow rates) were estimated using the enhanced models developed from the previous step and compared to the estimates direct from FDR data. Table 3 showed the model performance on the independent training sets. This analysis also demonstrated that the incorporation of fuel flow spikes corresponding to acceleration events during taxi contribute to a second-order impact on the fuel burn.

Task 1.4: Identify and recommend "first order" AEDT APM enhancements: As mentioned earlier, this phase identified and recommended the incorporation of the three first-order impacts mentioned above, namely, (1) enhancing models of fuel flow rates during taxi; (2) refining airport taxi time estimates; and (3) improving estimates of gate, pushback and engine start fuel burn.

Task 2.1: Extend Phase 1 analysis to broader range of aircraft types that serve US domestic operations: The Phase 1 analysis has shown how an aircraft's fuel flow profile can be estimated from the ASDE-X surveillance data, if available. A key finding was that significant improvements would be had by refining the taxi time estimates, as well as by improving the baseline fuel flow rate.

These models to-date were built using fuel flow rate data from a European carrier, including its operations at 6 US airports. However, these US operations correspond only to flights of the Airbus A330/340 and the Boeing 777. In the next phase, we will extend these approaches to analyze the A4A data obtained by the AEE, which includes the total surface fuel consumption for each of nearly 3.3 million domestic US flights between 2012-2015. This data set is also more representative of US operations, with 38% of the flights being flown by the Boeing 737. We therefore propose to use this dataset in Phase 2 to develop and validate baseline fuel burn indices for these different aircraft types. In addition, we hope to consider the typical fleet mixes at various airports to produce a lookup table that would reflect the fuel burn indices. Such a table, in combination with a table of average taxi times under different meteorological conditions, will enable the estimation of taxi fuel burn even in the absence of ASDE-X data. When such ASDE-X data is available, it can be used directly with the revised baseline fuel burn indices to obtain improved estimated of taxi fuel consumption.

Task 2.2: Extend to more US airports Phase 1 findings on airport-specific differences that significantly impact surface fuel burn: Phase 1 analysis has shown that there can be significant differences between airports which impact fuel burn prediction methods and hence potential recommendations for AEDT. For example, these differences between airports include surveillance coverage, pushback operations and airport topology. The first phase of analysis has highlighted differences at a small number of airports and for a limited set of gates at those airports. In Task 1, we have described how this analysis can be extended to airports with different aircraft fleet mixes.

Another key finding in Phase 1 was that the gate, push-back and engine start events do have a significant impact on the surface fuel burn. While this analysis was based on a limited number of airports, it suggested that the engine-startup fuel and times, and pushback times, are primarily dependent on aircraft-specific standard operating procedures and not airport-dependent (although APU fuel burn may be more airport dependent given gate procedure differences). This suggests that the existing analysis can be extended to cover a broader range of aircraft types and airports in Phase 2.

Figure 5 gives an initial proposal of tasking to make proposed enhancements. FDR archives and appropriate regressions will be used to establish look-up tables of push-back and engine start fuel burn for different aircraft types. These data can be used together with the fleet mix at any given airport under investigation to get the total push-back and engine start fuel burn. The FDR and ASDE-X data can be used to develop enhanced taxi fuel flow models for the main aircraft types of interest as previously discussed. These can be multiplied by updated taxi-out/in time distributions based on updated ASPM analysis.

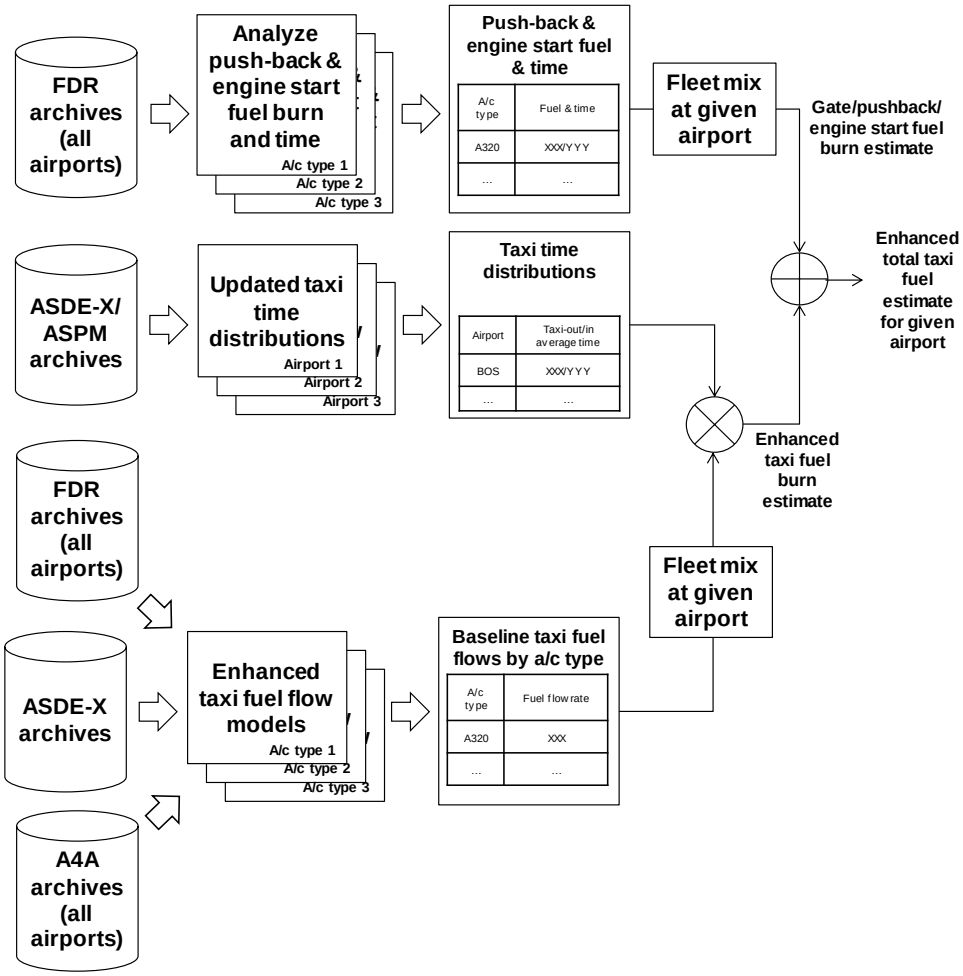

Figure 5. Proposed Phase 2 analysis activities.

Task 2.3: Identify AEDT surface APM enhancements to support emissions and noise inventories
The work to date has focused on the enhancement of AEDT surface APM to support fuel burn models. We will conduct a preliminary study (based on prior literature) to identify potential first-order effects in the modeling of emissions and noise. For example, the spikes in fuel burn caused by acceleration events (and the modeling of the corresponding variations in thrust) are expected to be of particular interest in this task.

Task 2.4: Recommend AEDT APM enhancements & Coordination with AEDT APM Developers
Based on the modeling enhancements developed from this process, specific targeted recommendations for AEDT APM improvements for the surface domain will be made. Coordination will be required throughout with the primary AEDT APM developers—i.e., Volpe and ATAC—to ensure that the research is practical and will directly inform enhancements to the APM.

Milestone(s)
Phase 1 (Tasks 1.1-1.4) was carried out between July 2016-Aug 2017. Phase 2 (Tasks 2.1-2.4) are now ongoing.

Publications
E. Clemons, T.G. Reynolds, S. Badrinath, Y. Chati and H. Balakrishnan. Enhancing Aircraft Fuel Burn Modeling on the Airport Surface. Submitted to the AIAA Aviation 2018 Conference.

Outreach Efforts
Presentations at the FAA-AEE Tools/Analysis Coordination Meetings.

Awards
Yashovardhan Chati and Hamsa Balakrishnan. Best Paper in Trajectory and Queue Management Track, ATM R&D Seminar 2017, Seattle, WA.

Student Involvement
Graduate students have been involved in all aspects of this research.

Plans for Next Period
Completion of Tasks 2.1-2.4.

References
[1] International Civil Aviation Organization (ICAO), “ICAO aircraft engine emissions databank.” [Online database], cited 12 February 2014.

[2] ACRP 02-45, “Methodology to Improve EDMS/AEDT Quantification of Aircraft Taxi/Idle Emissions”, Transportation Research Board, 2016.

[3] ACRP 02-25, “Handbook for Evaluating Emissions and Costs of APUs and Alternative Systems”, Transportation Research Board, 2012.

Project 048 Analysis to Support the Development of an Engine nvPM Emissions Standard

Massachusetts Institute of Technology

Project Lead Investigator

Steven Barrett
Associate Professor
Department of Aeronautics & Astronautics
Massachusetts Institute of Technology
77 Massachusetts Ave
Building 33-316
Cambridge, MA 02139
617-452-2550
sbarrett@mit.edu

University Participants

Massachusetts Institute of Technology

- P.I.: Prof. Steven Barrett
- Co-PI: Dr. Raymond Speth
- FAA Award Number: 13-C-AJFE-MIT, Amendment Nos. 027 and 036
- Period of Performance: July 8, 2016 to Aug. 31, 2018 (Reporting here with the exception of funding level and cost share only for the period October 1, 2016 to September 30, 2017).
- Tasks:
    - Task 1: Write a detailed scientific background of the APMT-I tools suite
    - Task 2: Map emissions from a short-list of representative engines to all engine/airframe combinations
    - Task 3: Evaluate metrics from the CAEP/WG3/PMTG for evaluating an engine's nvPM performance
    - Task 4: Verify technology response provided by engine manufacturers
    - Task 5: Evaluate proposed fuel sensitivity corrections and ambient conditions corrections
    - Task 6: Evaluate the current nvPM modeling approaches available to CAEP and assess uncertainty contributions

Project Funding Level

$350,000 FAA funding and $350,000 matching funds. Sources of match are approximately $105,000 from MIT, plus 3rd party in-kind contributions of $87,000 from University College London and $158,000 from Oliver Wyman Group.

Investigation Team

Principal Investigator: Prof. Steven Barrett
Co-Principal Investigator: Dr. Raymond Speth
Co-Investigators: Dr. Jayant Sabnis
Graduate Students: Akshat Agarwal

Project Overview

This projects aims to provide support to the FAA Office of Environment and Energy (AEE) in developing an emissions standard for non-volatile Particulate Matter (nvPM). The analyses will be further used to inform the International Civil Aviation Organization's Committee on Aviation Environmental Protection (ICAO-CAEP) in developing a global standard for nvPM emissions. The analyses will cover both US NAS-wide and global bases covering the costs and benefits from an economic and environmental (air quality, climate and noise) perspective. The main goals for this project include:

- Writing a scientific overview of the Aviation environmental Portfolio Management Tool's Impact (APMT-I) suite of analysis tools.
- Mapping emissions from a short-list of representative engines to a broader list of engine/airframe combinations.
- Evaluating metrics developed by CAEP Working Group 3 PM Task Group (CAEP/WG3/PMTG) important for evaluating an engine/airframe's nvPM emissions performance.
- Using the initial metrics and stringency options, independently verify the technology response provided by engine manufacturers.
- Evaluating proposed fuel sensitivity corrections and ambient conditions corrections.
- Evaluating the current nvPM modeling approaches available to CAEP, as well as investigating the potential of using number emissions to estimate health impacts. The tools will be further developed to incorporate a number of uncertainties relevant to the nvPM modeling approach.

Task #1: Write a Detailed Scientific Background of the APMT-I Tools Suite

Massachusetts Institute of Technology

Objective(s)

This task involves writing a detailed overview of the scientific background and uncertainty estimations used in the noise, air quality and climate models within the APMT-I tools suite. These papers are intended for presentation to the CAEP Modeling and Databases Group (MDG) to inform the decision to add cost-benefit analysis to the CAEP modeling procedure, which only considers cost-effectiveness analysis at this stage.

Research Approach

The APMT-I tools suite consists of models to analyze the noise, air quality and climate impacts of aviation emissions. Each model moves from estimated emissions or noise sources to monetized impacts in order to compare and contrast the various costs and environmental benefits of a particular policy. The papers are written to provide a detailed resource for understanding the scientific background, modeling assumptions and uncertainty analyses used within the APMT-I models. The papers will be written in 4 sections covering each of the APMT-I models (air quality, climate and noise) and an additional section on the advantages of using cost-benefit analyses on top of cost-effectiveness.

Milestone(s)

All documentation (three model papers and one on cost-benefit analysis) have been completed, refined by FAA project managers, and presented to MDG.

Major Accomplishments

Task complete.

Outreach Efforts

Regular presentations were made to MDG's ad-hoc group on cost-benefit analysis, highlighting the scientific methods, assumptions and benefits of using the APMT-Impacts tool suite and the associated cost-benefit analysis architecture.

Student Involvement

Graduate student Akshat Agarwal was primarily responsible for writing the reviews and presenting them to MDG.

Plans for Next Period

Task complete.

Task #2: Map Emissions from a Short-List of Representative Engines to All Engine/Airframe Combinations

Massachusetts Institute of Technology

Objective(s)

The objective of this task is to develop mappings between a short-list of representative engines that were analyzed during the measurement campaign and engine/airframe combinations currently in operation. This mapping will be used to develop an nvPM emissions inventory and identify the engine/aircraft combinations that may fail a particular stringency option.

Research Approach

A major improvement from historic smoke/PM standards developed by CAEP is the use of a new measurement method to more precisely estimate nvPM emissions from aircraft engines. The measurement campaign will focus on a subset of all available aircraft engines. However, to model the effect of an emissions standard on the current fleet of aircraft, it is crucial to have estimates of nvPM emissions from the full range of engines currently in use. This requires a mapping between measured and available engines.

The mapping has required regular iteration with engine manufacturers communicating their own mappings and MIT has been responsible for ensuring this mapping is reasonable, providing scientific and data-driven justifications. This mapping has now been completed, verified by both OEMs, MIT and the FAA. The final step in this process is calculating the nvPM emissions (mass and number) for each of the “modeled” engines and ensure that they lie in the range that is expected. This process will allow for the use of these engines in understanding OEM responses to stringency options.

Milestone(s)

The mapping process has been completed and agreed upon by all parties involved.

Major Accomplishments

The mapping process has been completed and agreed upon by OEMs and the FAA. We have estimated the nvPM emissions from the mapped engines and are submitting information papers to WG3 to verify the emissions levels and associated uncertainties.

Publications

We will be presenting a paper at the CAEP11 WG3 meeting in Paris this November, which will cover the methods used to estimate nvPM emissions from the fleet of mapped engines and a finalized database of values that can be used by modelers.

Student Involvement

Graduate student Akshat Agarwal is primarily responsible for conducting the mappings.

Plans for Next Period

Present information paper to WG3. Expected to be completed by November 30, 2017.

Task #3: Evaluate Metrics from the CAEP/WG3/PMTG for Evaluating an Engine's Nvpm Performance

Massachusetts Institute of Technology

Objective(s)

The objective of the third task involves independently evaluating the metrics developed by the Particulate Matter Task Group of CAEP Working Group 3 (CAEP/WG3/PMTG). The aim is to identify the key issues relevant to describing nvPM emissions performance.

Research Approach

Throughout the winter, WG3 was tasked with selecting an appropriate metric that can be used to regulate nvPM mass and number emissions. The aim was to identify parameters that would define any trends found in the experimentally data submitted by OEMs, while maintaining similar parameters for both mass and number emissions. An array of options was presented by the MIT team as well as other groups within WG3. Our focus was in trying to identify trends in the datasets and use this to develop the metric options. This is the analogous approach to NO_x emissions, where OPR is used as an explanatory variable since it is a fundamental parameter that leads to higher combustor temperatures and thus higher NO_x formation rates. For nvPM mass and number emissions, this exercise was found to be challenging and no engine-level parameters (e.g. F_{00} or OPR) were found to explain the trends seen in the received data. This is because nvPM emissions are dependent not only on temperatures and pressures, but also the internal design of the combustor, which can vary substantially between manufacturers and engine size.

After numerous analyses and discussions, the metric system was accepted by the group. On top of deciding the correct metric values, WG3 also had to decide on which correction factors to apply. When measuring nvPM emissions, numerous particles can be absorbed by the flow lines that bring the exhaust emissions to the measurement equipment, so-called system losses. In addition, variations in ambient conditions and fuel properties can alter the measured emissions. It was thus necessary to study which corrections were appropriate to include and the MIT team approached this by studying the effect on uncertainties, and the extent to which system losses increased the uncertainty of the metric value was demonstrated. This work was presented at the WG3 meeting in Tokyo, Japan in May, aiding the group to achieve consensus.

Milestone(s)

Metric value analysis completed and presented to WG3.

Major Accomplishments

Task Complete.

Publications

CAEP11-WG3-PMTG05-IP01, Effect of correction and uncertainty, May 2017, WG3 Tokyo.

Outreach Efforts

Regular presentations were made to the metrics ad-hoc group with the aim of helping the group come to consensus on the best metric values to use. These presentations were made regularly from January to March of 2017. A final presentation on uncertainties was made in May in Tokyo.

Student Involvement

Graduate student Akshat Agarwal was primarily responsible for studying the OEM data and identifying a range of parameters to use. He also led the presentation in Tokyo to understand the effects of various corrections and uncertainties in the data.

Plans for Next Period

Task Complete.

Task #4: Verify Technology Response Provided by Engine Manufacturers

Massachusetts Institute of Technology

Objective(s)

The objective of this task is to independently verify the technology response provided by the engine manufacturers and assist the FAA in developing consensus.

Research Approach

OEMs have supplied technology responses to WG3 in October 2017. The technology responses identify the predicted cost to OEMs of reducing nvPM mass or number by a pre-determined amount and also present potential emissions' trade-offs with other species. For example, RQL engines are expected to trade-off NO_x emissions with nvPM mass. Our role is to use our expertise to understand whether these responses are justified and provide feedback to the FAA on how to improve these responses. In addition to consulting in-house experts, we are also approaching the problem using the range of data available in the ICAO emissions data bank (EDB). Historic NO_x standards have led to combustor technologies gradually reducing NO_x emissions while maintaining high fuel performance. The EDB also collects smoke number (SN) information, which has been shown to be well correlated with nvPM mass emissions. Thus, we can identify changes in SN due to improvements in combustor technology that lead to a reduction in NO_x emissions. We are currently processing this dataset and understanding some of the trends presented.

Milestone(s)

EDB data has been processed and we are aiming to present to the FAA in early November.

Outreach Efforts

Initial discussions with FAA have begun and we will continue this process to assist the group in coming to consensus on the technology responses.

Student Involvement

Akshat Agarwal is primarily responsible for analyzing the EDB data and will lead the effort to presenting first to the FAA and then to WG3.

Plans for Next Period

This task is expected to be completed following the November WG3 meeting.

Task #5: Evaluate Proposed Fuel Sensitivity Corrections and Ambient Conditions Corrections

Massachusetts Institute of Technology

Objective(s)

The fifth task for this project involves conducting an independent evaluation of the proposed fuel sensitivity corrections and ambient conditions corrections.

Research Approach

While metric values were being agreed upon in WG3, it was also necessary to develop models that could correct variations in nvPM emissions measurements due to changes in fuel composition. The group had already been accustomed to various approaches to this correction using fuel hydrogen content as the proxy. We began this process using in-house expertise (Speth et al. 2015), with presentations to WG3 in May in Tokyo of an alternative approach that used fuel aromatics content. We have since worked with other members of WG3, led by Dr Prem Lobo, to reconcile the different approaches. This collaborative work led to an additional modeling approach developed by Raymond Speth and presented to WG3 in July in Ann Arbor. After receiving feedback from WG3 on this approach, we will continue to work with Dr Lobo to identify an approach for treating fuel sensitivity that can achieve consensus within WG3.

Milestone(s)
Presented the potential use of fuel aromatics content instead of fuel hydrogen content in Tokyo. Collaborated with Dr Prem Lobo to develop an alternative modeling approach using fuel hydrogen content and presented this approach in Ann Arbor.

Publications
CAEP11-WG3-PMTG5-IP03, Fuel sensitivity corrections for nvPM measurements, May 2017, WG3 Tokyo.
CAEP11-WG3-PMTG6-WP14, Fuel sensitivity corrections factors for nvPM mass and number, July 2017, WG3 Ann Arbor MI.

Outreach Efforts
Regular presentations have been made to the FAA and the metrics ad-hoc group within PMTG. These efforts are aimed at disseminating preliminary results, engaging in discussions about the approach and receiving feedback from WG3.

Student Involvement
Graduate student Akshat Agarwal is collaborating on the data analyses for this task.

Plans for Next Period
The planned analysis of fuel sensitivity was completed in with the presentations in July 2017. Analysis of refinements to the approach to be used by PMTG will be evaluated on an as-needed basis throughout the duration of the project.

Task #6: Evaluate the Current Nvpm Modeling Approaches Available to CAEP and Assess Uncertainty Contributions
Massachusetts Institute of Technology

Objective(s)
The objectives for this task involve assessing the modeling capabilities available to CAEP for estimating the environmental impacts of aviation (air quality, climate and noise) and their potential for incorporating additional measurements available from the new nvPM measurement system. In addition, we aim to include additional uncertainties from the new measurement system that have previously not been included.

Research Approach
In the final task, we not only aim to quantify the environmental impact of an nvPM emissions standard, but also attempt to quantify the various uncertainty contributions due to the new measurement methods. The nvPM emissions tests are conducted at ground level because of their ease in comparison to high-speed, cruise-altitude measurements. However, in order to evaluate the effects of cruise-altitude emissions on other atmospheric processes, e.g., contrail formation, these ground level test data must be mapped to cruise conditions. This has been addressed in historic models such as the FOX model (Stettler et al. 2013)for nvPM emissions, who used a correlation developed by Dopelheuer and Lecht (1998). In this task, we will evaluate the applicability of these models for the new method of measuring nvPM emissions, quantifying the uncertainty of the measurements.

The next part of this task involves ensuring the advanced nvPM measurement capabilities can be used to model the environmental impacts of an nvPM emissions standard. The new nvPM measurement system allows for the estimation of number emissions. These are important for estimating the health impacts of nvPM exposure and will be incorporated in addition to the mass-based exposure response functions that are currently used. We will also study the uncertainties associated with the differential toxicity between the various types of PM species. Finally, we will study the uncertainties in the climate model due to the direct black carbon warming impact and the warming due to contrails.

Milestone(s)
The cost-benefit analysis requires the generation of emissions datasets in a format that can be run through the APMT-Impacts air quality and climate models. We have received preliminary datasets that represent landing and take-off (LTO) emissions on a global scale from Volpe. The format of this requires us to pre-process the data such that they can seamlessly run through our air quality and climate models. We have developed the processes to automatically pre-process

the datasets and are currently working on running them through our air quality model. Upon receiving the full-flight data, we will be able to run simulations through our climate model as well.

Outreach Efforts

We have presented our preliminary results to the FAA and will continue to update them as we work through our modeling chain and receive additional data from Volpe.

Student Involvement

Graduate student Akshat Agarwal is primarily responsible for conducting the analyses.

Plans for Next Period

We aim to complete this task by August 31, 2018.

References

Dopelheuer, A., and M. Lecht. 1998. "Influence of Engine Performance on Emission Characteristics." In *Symposium of the Applied Vehicle Technology Pane-Gas Turbine Engine Combustion, Emissions and Alternative Fuels, Lisbon, Portugal*. Citeseer.

Speth, Raymond L., Carolina Rojo, Robert Malina, and Steven R. H. Barrett. 2015. "Black Carbon Emissions Reductions from Combustion of Alternative Jet Fuels." *Atmospheric Environment*.

Stettler, Marc E. J., Adam M. Boies, Andreas Petzold, and Steven R. H. Barrett. 2013. "Global Civil Aviation Black Carbon Emissions." *Environmental Science & Technology* 47 (18):10397–404.

Publications Index

Project 001

Twenty five graduate students and one undergraduate student involved.

Publications

- Brant, Kristin; Garcia-Perez, Manuel; Geleynse, Scott; Wolcott, Michael; and Zhang, Xiao., "The Alcohol to Jet Conversion Strategy for Drop in Biofuels: Evaluation of Technicla Aspects and Economics," November 2017
- Tanzil, A.H.; Zhang X.; Wolcott M.; and Garcia-Perez, M., "Evaluation of Biorefinery Alternatives for the production of jet Fuels in a Dry Corn Ethanol Plant," To be submitted to Biofuels, Bioproducts and Biorefinery, 2018
- Martinkus, N. Rijkhoff, S.A.M., Hoard, S.A., Shi, W., Smith, P., Gaffney, M., & Wolcott, M. (submitted, R&R). Biorefinery Site Selection Using a Stepwise Biogeophysical and Social Analysis Approach. Biomass and Bioenergy.
- Rijkhoff, S.A.M., Hoard, S., Gaffney, M., Smith, P. (submitted). Communities Ready for Takeoff: Integrating Social Assets for Biofuel Site-selection Modeling. Politics and Life Sciences.
- Smith, P.M., Gaffney, M.J., Shi, W., Hoard, S., Ibarrola Armendariz, I., Mueller, D.W., 2017. Drivers and barriers to the adoption and diffusion of sustainable jet fuel (SJF) in the U.S. Pacific Northwest. Journal of Air Transport Management, 58, 113-124.
- Zhao, Xin, Guolin Yao, and Wallace E. Tyner. "Quantifying breakeven price distributions in stochastic techno-economic analysis." Applied Energy 183 (2016) 318-326.
- Bann, Seamus J., Robert Malina, Pooja Suresh, Matthew Pearlson, Wallace E. Tyner, James I. Hileman, and Steven Barrett. "The costs of production of alternative jet fuel: A harmonized stochastic assessment." Bioresource Technology 227 (2017), 179-187.
- Yao, Guolin, Mark D. Staples, Robert Malina, and Wallace E. Tyner. "Stochastic techno-economic analysis of alcohol-to-jet fuel production." Biotechnology for Biofuels 10:18 (2017), 13 pages.
- Taheripour, F., Cui, H., & Tyner, W. E. (2017). An Exploration of Agricultural Land use Change at the Intensive and Extensive Margins: Implications for Biofuels Induced Land Use Change. In Z. Qin, U. Mishra, & A. Hastings (Eds.), Bioenergy and Land Use Change: American Geophysical Union (Wiley).
- Taheripour, F., Zhao, X., & Tyner, W. E. (2017). The impact of considering land intensification and updated data on biofuels land use change and emissions estimates. Biotechnology for biofuels, 10(1), 191.
- Perkis, David F., and Wallace E. Tyner. "Developing a Cellulosic Aviation Biofuel Industry in Indiana: A Market and Logistics Analysis." Energy, forthcoming 2017.
- Staples, M.D., R. Malina, P. Suresh, J.I. Hileman, S.R.H. Barrett (*in revision*) "Aviation CO_2 emission reductions from the use of alternative jet fuels." *Energy Policy*.
- T. Galligan, M. Staples, R. Speth, S. Barrett. "The potential of bio- and waste- derived jet fuel to reduce US aviation sector emissions in 2050" (in preparation)

Reports

- CAEP/11-AFTF/4-IP/04, Calculation of core default LCA values for selected pathways under CORSIA, presented at AFTF/4, June 2017, Montreal, Canada
- CAEP/11-AFTF/4-WP/02, Progress update on core LCA task, presented at AFTF/4, June 2017 Montreal, Canada.
- CAEP/11-AFTF/3-IP/02, Core LCA Task Group – study of pathway aggregation, February 2017, Montreal, Canada.
- CAEP/11-AFTF/3-WP/02, Progress update on core LCA task group, February 2017, Montreal, Canada.
- CAEP/11-AFTF/2-IP/04, Core LCA Task Group – study of pathway aggregation, October 2016 Montreal, Canada.
- CAEP/11-AFTF/2-WP/02, Report on Core LCA Task, October 2016, Montreal, Canada.
- CAEP/11-AFTF/2-IP/03, Guidance Document for Calculation and Submission of Alternative Jet Fuel Lifecycle Analysis Data for Default Values under the Global Market-based Measure, October, 2016, Montreal, Canada.
- CAEP/11 ILUC Task Group. Development of Test Model Simulations to Be Used in Studying Induced Land Use Change from Aviation Biofuels Production. CAEP/11-AFTF/2-WP/3. Oct 2016.
- CAEP/11 ILUC Task Group. Preliminary Simulation Test Results for Estimation of Land Use Change Emission Values for Aviation Biofuels Production. CAEP/11-AFTF/3-WP/4. Jan 2017.
- CAEP/11 ILUC Task Group. Preliminary GTAP-BIO Simulation Results for Estimation of Land Use Change Emission Values for Aviation Biofuels Production. CAEP/11-AFTF/4-WP/06. May 2017.

- CAEP/11 ILUC Task Group. Summary Comparison of GTAP-BIO and GLOBIOM Models and Results. CAEP/11-AFTF/4-IP/07. May 2017.
- T. Galligan, "The potential of bio- and waste- derived jet fuel to reduce aviation sector emissions in 2050," Master of Science thesis, Department of Aeronautics and Astronautics, Massachusetts Institute of Technology, 2017.

Presentations

- Tanzil, AH, Geleynse S, Garcia-Perez M, Zhang X, Wolcott M: Alternative Jet Fuel Production in Integrated Biorefuneries Using Existing Dry Corn Mill: Cost Reduction Opportunities. ASCENT Meeting, September 27-28, 2016
- Mueller, D., Hoard, S., Sanders, C., & Gaffney, M. The Community Assets and Attributes Model: Refining and Updating Measurements for Social Assets. Fall 2017 ASCENT Advisory Committee Meeting. Alexandria, VA.
- Mueller, D., Hoard, S., Sanders, C., Gaffney, M., & Smith, P. Strategic Applications of the Community Assets and Attribute Model. Washington State University Sustainability Fair. Pullman, WA.
- Long-Term Alternative Jet Fuel Production in the United States. Presented by Mark Staples at ASCENT biannual meeting in September 2017, Alexandria, VA.
- Long-Term Alternative Jet Fuel Production in the United States. Presented by Timothy Galligan on teleconference with Jim Hileman, Fabio Grandi, Dan Williams of the FAA, September 19, 2017.
- Long-Term Alternative Jet Fuel Production in the United States. Presentation given on weekly ASCENT-1 teleconference, May 1, 2017.
- National assessment of alternative jet fuel production potential. Poster presented at ASCENT biannual meeting in April 2017, Alexandria, VA.

Project 002

Four undergraduate students involved.

Project 003

No publications or students to report.

Project 005

No publications or students to report.

Project 008

No publications or students to report.

Project 010

Thirteen graduate students involved.

Publications

- T. W. Lukaczyk, A. D. Wendorff, M. Colonno, E. Botero, T. D. Economon, J. J. Alonso, T. H. Orra, and C, Ilario, "SUAVE: An Open-Source Environment for Multi-Fidelity Conceptual Vehicle Design," 16th AIAA/ISSMO Multidisciplinary Analysis and Optimization Conference, doi:10.2514/6.2015-3087, June, 2015.

- Ogunsina, K., Chao, H., Kolencherry, N., Moolchandani, K., Crossley, W. A., and DeLaurentis, D. A., "A Model of Aircraft Retirement and Acquisition Decisions Based On Net Present Value Calculations," 17th AIAA Aviation Technology, Integration, and Operations Conference, 2017.

Project 011(A)

Four graduate students involved.

Publications

- "Development of Rapid Fleet-Wide Environmental Assessment Capability," AIAA AVIATION Forum, 2017. DOI: 10.2514/6.2017-3339

Presentations

- 1/25/2017: Briefing to FAA Joint University Program research update meeting
- 4/17/2017: Joint briefing to FAA and MITRE to discuss tool development pathway
- 4/18/2017: Briefing to ASCENT Advisory Board
- 6/5/2017: Presentation at AIAA Aviation Conference in Denver, CO.

Project 017

Publications

- McGuire, S., Witte, M., Kallarackal, A., Basner, M.: Pilot study examining the effects of aircraft noise on sleep in communities near Philadelphia International airport. Poster at the 31st Anniversary Meeting of the Associated Professional Sleep Societies, Boston, June 11-15, 2016.
- Basner, M., McGuire, S.: Pilot study examining the effects of aircraft noise on sleep in communities near Philadelphia International airport. Presentation at the 12th ICBEN Congress on Noise as a Public Health Problem, Zurich, Switzerland, June 18-22, 2017.
- Müller, U., Elmenhorst, E.-M., Mendolia, F., Quehl, J., Basner, M., McGuire, S., Aeschbach, D.: A comparison of the effects of night time air traffic noise on sleep at Cologne/Bonn and Frankfurt Airport after the night flight ban. Presentation at the 12th ICBEN Congress on Noise as a Public Health Problem, Zurich, Switzerland, June 18-22, 2017.
- McGuire, S., Müller, U., Elmenhorst, E.-M., Mendolia, F., Aeschbach, D., Basner, M.: Cross-country comparison of aircraft noise-induced sleep disturbance. Poster at the 12th ICBEN Congress on Noise as a Public Health Problem, Zurich, Switzerland, June 18-22, 2017.
- McGuire, S., Basner, M.: Development of a methodology for field studies on the effects of aircraft noise on sleep. Presentation at the 173rd Meeting of the Acoustical Society of America and the 8th Forum Acusticum, Boston, MA, June 25-29, 2017.

Project 018

Three graduate students involved.

Publications

- Penn SL, Boone ST, Harvey BC, Heiger-Bernays W, Tripodis Y, Arunachalam S, Levy JI. Modeling variability in air pollution-related health damages from individual airport emissions. Environ Res 156: 791-800 (2017).

Project 019

One graduate student involved.

Publications

- Arter, C. A. & Arunachalam, S. (2017). Calculating Second Order Sensitivity Coefficients for Airport Emissions in the Continental U.S. Using CMAQ-HDDM. Presented at the 2017 ASCENT Advisory Board Meeting, Washington, D.C.
- Arter, C. A. & Arunachalam, S. (2017). Calculating Second Order Sensitivity Coefficients for Airport Emissions in the Continental U.S. Using CMAQ-HDDM. Poster session presented at the 2017 North Carolina BREATHE Conference, Raleigh, NC.
- Arter, C. A. & Arunachalam, S. (2017). Calculating Second Order Sensitivity Coefficients for Airport Emissions in the Continental U.S. Using CMAQ-HDDM. Poster session presented at the 2017 University of North Carolina Chapel Hill Climate Change Symposium, Chapel Hill, NC.
- Arter, C. A. & Arunachalam, S. (2017). Using Higher Order Sensitivity Approaches to Assess Aircraft Emissions Impacts on O3 and PM2.5. Poster session presented at the 2017 Annual CMAS Conference, Chapel Hill, NC.

Presentations

- Presentation at bi-annual ASCENT stakeholder meetings in Spring and Fall 2017, Alexandria, VA.
- Presentation to FAA and investigators during monthly Tools telecons
- Presentation to New York City Metro Area Energy and Air Quality Data Gaps Workshop, organized by NYSERDA, Columbia University, May 2017

Project 020

Three graduate students involved.

Project 021

Two graduate students involved.

Publications

- Grobler, C., Allroggen, F., Agarwal, A., Speth, R., Staples, M., Barrett, S. (2017). APMT-I Climate version 24 Algorithm Description Document, Laboratory of Aviation and the Environment.
- Grobler, C., Wolfe, P., Allroggen, F., Barrett, S. (2017). Interim Derived Climate Metrics, Laboratory of Aviation and the Environment.

Project 022

One graduate student involved.

Publications

- Zhang and Wuebbles, Evaluation of FAA Climate Tools: APMT. Report for the FAA, December 2016
- Zhang and Wuebbles, Evaluating the regional impact of aircraft emissions on climate and the capabilities of simplified climate model. Master's thesis, University of Illinois, July 2017

Project 023

No publications or students to report.

Project 024(B)

One graduate student involved.

Publication

- Abrahamson, J. P., Zelina, J., Andac, M. G., & Vander Wal, R. L. (2016). Predictive Model Development for Aviation Black Carbon Mass Emissions from Alternative and Conventional Fuels at Ground and Cruise. Environmental Science & Technology, 50(21), 12048-12055.
- Abrahamson, J. P., Vander Wal, R. L., (2017). Gas turbine nvPM formation and oxidation semi-empirical model for commercial aviation. Paper 2E19. Topic: Gas Turbine Combustion. 10th US National Meeting of the Combustion Institute, The University of Maryland, College Pak, MD April 23rd - 26th, 2017.

Presentations

- Vander Wal, R. L. Abrahamson, J. P., ASCENT Project No. 24B, Emissions data analysis for CLEEN, ACCESS and other tests. FAA Center of excellence for alternative jet fuels and environment. Contractor's workshop. Alexandria, VA. Sept. 27th- 28th, 2016.
- Abrahamson, J. P., Vander Wal, R. L., PM Emissions Analysis and Predictive Assessment: Update on nvPM predictive modeling from conventional and alternative jet fuels. Aviation Emissions Council (AEC) WEBEX seminar. Feb. 23rd, 2017.
- 5. Vander Wal, R. L., Abrahamson, J. P., nvPM Emissions Analysis and Predictive Summary. Poster Presentation. Project 24B Report. FAA Center of Excellence for Alternative Jet Fuels & Environment (FAA COE AJFE). Alexandria, VA April 18th - 19th, 2017.
- 6. Abrahamson, J. P., Vander Wal, R. L., (2017). Gas turbine nvPM formation and oxidation semi-empirical model for commercial aviation. Paper 2E19. Topic: Gas Turbine Combustion. 10th US National Meeting of the Combustion Institute, The University of Maryland, College Park, MD April 23rd - 26th, 2017.

Project 025

One graduate student involved

Publications

- D. F. Davidson, Y. Zhu, J. Shao, R. K. Hanson, "Ignition Delay Time Correlations for Distillate Fuels," Fuel 187 26–32 (2017).
- R. Xu, D. Chen, K. Wang, Y. Tao, J.K. Shao, T. Parise, Y. Zhe, S. Wang, R. Zhao, D.J. Lee, F.N. Egolfopoulos, D.F. Davidson, R.K. Hanson, C.T. Bowman and H. Wang, "HyChem Model for Petroleum-Derived Jet Fuels," 10th U. S. National Combustion Meeting, April 23-26, 2017, College Park, Maryland.
- R. Xu, H. Wang, D.F. Davidson, R.K. Hanson, C.T. Bowman, F.N. Egolfopoulos, "Evidence Supporting a Simplified Approach to Modeling High-Temperature Combustion Chemistry," 10th U. S. National Combustion Meeting, April 23-26, 2017, College Park, Maryland.
- J.K. Shao, D.F. Davidson and R.K. Hanson, "Shock Tube Study of Jet Fuel Pyrolysis and Ignition at Elevated Pressure," 10th U. S. National Combustion Meeting, April 23-26, 2017, College Park, Maryland.
- K. Wang, R. Xu, T. Parise, J.K. Shao, D.F. Davidson, R.K. Hanson, H. Wang, C.T. Bowman, "Evaluation of a Hybrid Chemistry Approach for Combustion of Blended Petroleum and Bio-derived Jet Fuels," 10th U. S. National Combustion Meeting, April 23-26, 2017, College Park, Maryland.
- K. Wang, R. Xu, T. Parise, J.K. Shao, D.J. Lee, A. Movaghar, D.F. Davidson, R.K. Hanson, H. Wang, C.T. Bowman and F.N. Egolfopoulos, "Combustion Kinetics of Conventional and Alternative Jet Fuels using a Hybrid Chemistry (HyChem) Approach," 10th U. S. National Combustion Meeting, April 23-26, 2017, College Park, Maryland.

Project 027

Thirteen graduate students involved.

Publications

- E. Mayhew, C. Mitsingas, B. McGann, T. Lee, T. Hendershott, S. Stouffer, P. Wrzesinski, A. Caswell, Spray Characteristics and Flame Structure of Jet A and Alternative Jet Fuels, AIAA SciTech, AIAA-2017-0148, 2017

- Chterev, N. Rock, H. Ek, B. Emerson, J. Seitzman, T. Lieuwen, D. Noble, E. Mayhew, T. Lee, Simultaneous High Speed (5 kHz) Fuel-PLIE, OH-PLIF and Stereo PIV Imaging of Pressurized Swirl-Stabilized Flames using Liquid Fuels, AIAA SciTech, AIAA-2017-0152, 2017
- Chterev, I., Rock, N., Ek, H., Emerson B., Seitzman J., Jiang, N., Roy, S., Lee, T., Gord, T., and Lieuwen, T. 2017. Simultaneous Imaging of Fuel, OH, and Three Component Velocity Fields in High Pressure, Liquid Fueled, Swirl Stabilized Flames at 5 kHz. Combustion and Flame. 186, pp. 150-165.
- Rock, N., Chterev, I., Smith, T., Ek, H., Emerson, B., Noble, D., Seitzman, J. and Lieuwen, T., 2016, June. Reacting Pressurized Spray Combustor Dynamics: Part 1—Fuel Sensitivities and Blowoff Characterization. In ASME Turbo Expo 2016: Turbomachinery Technical Conference and Exposition (pp. V04AT04A021-V04AT04A021). American Society of Mechanical Engineers.
- Chterev, I., Rock, N., Ek, H., Smith, T., Emerson, B., Noble, D.R., Mayhew, E., Lee, T., Jiang, N., Roy, S. and Seitzman, J.M., 2016, June. Reacting Pressurized Spray Combustor Dynamics: Part 2—High Speed Planar Measurements. In ASME Turbo Expo 2016: Turbomachinery Technical Conference and Exposition (pp. V04AT04A020-V04AT04A020). American Society of Mechanical Engineers.
- Wei, S., Sforzo, B., and Seitzman, J., 2017, "High Speed Imaging of Forced Ignition Kernels in Non-Uniform Jet Fuel/Air Mixtures," ASME Turbo Expo 2017: Turbomachinery Technical Conference and Exposition, Charlotte, NC, USA
- Sforzo, B., Wei, S., and Seitzman, J., 2017, "Non-premixed Ignition of Alternative Jet Fuels," AIAA SciTech Forum, Grapevine, Texas, USA
- N. Schorn, D. Blunck, "Flame Stability of Turbulent Premixed Jet Flames of Large Hydrocarbon Fuels," Western States Section of the Combustion Institute Meeting, Laramie, WY (2017).
- A. Fillo, J. Bonebrake, D. Blunck, "Impact of Fuel Chemistry and Stretch Rate on the Global Consumption Speed of Large Hydrocarbon Fuel/Air Flames," 10th US Combustion Meeting, College Park, ME (2017).
- Fillo, Aaron, M.S., Thesis, "The Global Consumption Speeds of Premixed Large- Hydrocarbon Fuel/Air Turbulent Bunsen Flames," Oregon State University.

Project 028

No publications or students to report.

Project 029

Four graduate students involved.

Publications

- "Effect of Aviation Fuel Type and Fuel Injection Conditions on Non-Reacting Spray Characteristics of Hybrid Air Blast Fuel Injector," Timo Buschhagen, Robert Z. Zhang, Sameer V. Naik, Carson D. Slabaugh, Scott E. Meyer, Jay P. Gore, and Robert P. Lucht, presented at the 2016 AIAA SciTech Meeting, San Diego, CA, 4-8 January 2016, Paper Number AIAA 2016-1154.
- "Large-Eddy Simulations of Fuel Injection and Atomization of a Hybrid Air-Blast Atomizer," P. C. May, M. B. Nik, S. E. Carbajal, S. Naik, J. P. Gore, R. P. Lucht, and M. Ihme, presented at the 2016 AIAA SciTech Meeting, San Diego, CA, 4-8 January 2016, Paper Number AIAA 2016-1393.
- "Spray Measurements at Elevated Pressures and Temperatures Using Phase Doppler Anemometry," A. J. Bokhart, D. Shin, R. Gejji, T. Buschhagen, S. V. Naik, R. P. Lucht, J. P. Gore, P. E. Sojka, and S. E. Meyer, presented at the 2017 AIAA SciTech Meeting, Grapevine, TX, 8-13 January 2017, Paper Number AIAA-2017-0828,.
- "Spray Characteristics at Lean Blowout and Cold Start Conditions using Phase Doppler Anemometry," A. J. Bokhart, D. Shin, N. Rodrigues, S. V. Naik, R. P. Lucht, J. P. Gore, P. E. Sojka, and S. E. Meyer, to be presented at the 2018 AIAA SciTech Meeting, Kissimmee, Florida, 8-12 January 2018.

Presentations

- "Effect of Aviation Fuel Type and Fuel Injection Conditions on Non-Reacting Spray Characteristics of Hybrid Air Blast Fuel Injector," Timo Buschhagen, Robert Z. Zhang, Sameer V. Naik, Carson D. Slabaugh, Scott E. Meyer, Jay P. Gore, and Robert P. Lucht, presented at the 2017 AIAA SciTech Meeting, San Diego, CA, 4-8 January 2016

- "Large-Eddy Simulations of Fuel Injection and Atomization of a Hybrid Air-Blast Atomizer," P. C. May, M. B. Nik, S. E. Carbajal, S. Naik, J. P. Gore, R. P. Lucht, and M. Ihme, presented at the 2016 AIAA SciTech Meeting, San Diego, CA, 4-8 January 2016.
- "Spray Measurements at Elevated Pressures and Temperatures Using Phase Doppler Anemometry," A. J. Bokhart, D. Shin, R. Gejji, T. Buschhagen, S. V. Naik, R. P. Lucht, J. P. Gore, P. E. Sojka, and S. E. Meyer, presented at the 2017 AIAA SciTech Meeting, Grapevine, TX, 8-13 January 2017, Paper Number AIAA-2017-0828,.
- "Spray Characteristics at Lean Blowout and Cold Start Conditions using Phase Doppler Anemometry," A. J. Bokhart, D. Shin, N. Rodrigues, S. V. Naik, R. P. Lucht, J. P. Gore, P. E. Sojka, and S. E. Meyer, to be presented at the 2018 AIAA SciTech Meeting, Kissimmee, Florida, 8-12 January 2018.

Project 031(A)

Publications

- "Evaluation of LanzaTech/PNNL Ethanol-to-Jet (LT/PNNL ATJ) Synthetic Paraffinic Kerosene Fuels and Blends Phase 1 Research Report," 2016.
- "Evaluation of High Freeze Point HEFA as Blending Component for Aviation Jet Fuels," ASTM Research Report Version 1.1, 2017.

Project 031(B)

One graduate student involved.

Project 033

Two graduate students involved.

Project 034

Three graduate students and two undergraduate student involved.

Publications

- Colket, Meredith B., Joshua S. Heyne, Mark Rumizen, James T. Edwards, Mohan Gupta, William M. Roquemore, Jeffrey P. Moder, Julian M. Tishkoff, and Chiping Li. 2017. "An Overview of the National Jet Fuels Combustion Program." AIAA Journal, https://doi.org/10.2514/1.J055361.
- Heyne, Joshua S., Colket, Meredith B., , Rumizen, Mark, Edwards, James T., Gupta, Mohan, Roquemore, William M., Moder, Jeffrey P., and Li, Chiping. 2017. "Year 2 of the National Jet Fuels Combustion Program: Moving Towards a Streamlined Alternative Jet Fuels Qualification and Certification Process. Grapevine, TX: American Institute of Aeronautics and Astronautics. (AIAA 2017-0145) https://doi.org/10.2514/6.2017-0145.
- Stachler, Robert D., Joshua S. Heyne, Scott D. Stouffer, Joseph D. Miller, and William M. Roquemore. 2017. "Investigation of Combustion Emissions from Conventional and Alternative Aviation Fuels in a Well-Stirred Reactor." In 55th AIAA Aerospace Sciences Meeting. Grapevine, TX: American Institute of Aeronautics and Astronautics.

Presentations

- Stachler, Robert D., Joshua S. Heyne, Scott D. Stouffer, Joseph D. Miller, and William M. Roquemore. 2017. "Investigation of Combustion Emissions from Conventional and Alternative Aviation Fuels in a Well-Stirred Reactor." 55th AIAA Aerospace Sciences Meeting. Grapevine, TX: American Institute of Aeronautics and Astronautics.
- Stachler, Robert D., Joshua S. Heyne, Scott D. Stouffer, Joseph D. Miller, and William M. Roquemore. 2016. "Investigation of Combustion Emissions from Conventional and Alternative Aviation Fuels in a Well-Stirred Reactor." 12th Annual Dayton Engineering Sciences Symposium. Dayton, OH: ASME.

- Carson, Jeremy, Joshua S. Heyne, Scott D. Stouffer, and Tyler Hendershott. 2016. “On the Relative Importance of Fuel Properties on LBO Behavior.” 12th Annual Dayton Engineering Sciences Symposium. Dayton, OH: ASME.
- Carson, Jeremy and Joshua S. Heyne. 2017. “Updates on the Relative Importance of Fuel Properties on LBO Behavior.” 42nd Dayton-Cincinnati Aerospace Sciences Symposium. Dayton, OH: AIAA.
- Peiffer, Erin, Joshua S. Heyne. 2017. “LBO, Ignition, and Spray Feature Importances from Year 3 of the National Jet Fuels Combustion Program.” 13th Annual Dayton Engineering Sciences Symposium. Dayton, Ohio: ASME.

Project 036

Three graduate students involved

Publications

- Yongchang Li, Don Lim, Michelle Kirby, Dimitri Mavris, George Noel, Uncertainty Quantification Analysis of the Aviation Environmental Design Tool in Emission Inventory and Air Quality Modeling, Submitted to AVIATION 2018 conference.
- Dongwook, Lim, Yongchang Li, Matthew J Levine, Michelle R Kirby, Dimitri, Mavris, Parametric Uncertainty Quantification of Aviation Environmental Design Tool, Submitted to AVIATION 2018 conference.
- Junghyun Kim, Dongwook Lim, Yongchang Yi, Michelle Kirby, and Dimitri Mavris, Parametric Study of Noise Impact on the Airspace over the Acadia National Park using Time-Audible metric in AEDT, Submitted to AVIATION 2018 conference.

Project 37

No publications or students to report.

Project 038

One graduate student involved.

Project 039

Two graduate students involved.

Presentations

- Going Bigger: Capturing PAH Chemistry in RMG *May 23, 2017,* Mengjie Liu, Kehang Han, William H. Green, “Overview of RMG developments to improve thermochemistry estimation for polycyclic species and general handling of aromaticity for kinetics.” International Conference on Chemical Kinetics. Presentation, manuscript in preparation. FAA support was acknowledged.

Project 040

Three graduate students involved.

Project 041

Two graduate students involved.

Project 042

Five graduate students involved.

Publications

- Gregory Busch, Jimmy Tai, Dimitri Mavris, Ruxandra Duca, and Ratheesvar Mohan, “Sensitivity analysis of supersonic Mach cut-off flight,” J. Acoust. Soc. Am.,Vol. 141, No. 5, Pt. 2, 3565 (2017).

Presentations

- Autumn ASCENT COE Meeting 2016: Alexandria, Virginia – Sept. 27-29, 2017
- Spring ASCENT COE Meeting 2017: Alexandria, Virginia – April 18-20, 2017
- ASA Acoustics 2017: Boston, Massachusetts – June 24-27, 2017
- Autumn ASCENT Meeting 2017 & ASCENT Noise Working Group: Alexandria, Virginia – Sept. 26-28, 2017
- Z. Huang and V. W. Sparrow, "Preliminary assessment and extension of an existing Mach cut-off model," Poster for the Penn State Center for Acoustics and Vibration (CAV) Spring Workshop, University Park, PA, April 25-26, 2017.

Project 043

Two graduate students involved.

Project 045

Two graduate students involved.

Project 046

Publications

- E. Clemons, T.G. Reynolds, S. Badrinath, Y. Chati and H. Balakrishnan. Enhancing Aircraft Fuel Burn Modeling on the Airport Surface. Submitted to the AIAA Aviation 2018 Conference.

Project 048

One graduate student involved.

Reports

- CAEP11-WG3-PMTG05-IP01, Effect of correction and uncertainty, May 2017, WG3 Tokyo
- CAEP11-WG3-PMTG5-IP03, Fuel sensitivity corrections for nvPM measurements, May 2017, WG3 Tokyo.
- CAEP11-WG3-PMTG6-WP14, Fuel sensitivity corrections factors for nvPM mass and number, July 2017, WG3 Ann Arbor MI.

Project Funding Allocations by Federal Fiscal Year

Breakout by Project

Project		Funding Based on award date				
		2014	2015	2016	2017	Total
001	Alternative Jet Fuel Supply Chain Analysis	$1,599,943	$1,425,000	$1,498,749	$1,855,461	$6,379,153
002	Ambient Conditions Corrections for Non-Volatile PM Emissions Measurements	$2,800,000	$750,000	-$147,766	$725,500	$4,127,734
003	Cardiovascular Disease and Aircraft Noise Exposure	$200,000	$200,000	$200,000	$340,000	$940,000
004	Estimate of Noise Level Reduction	$150,000	-	-	-	$150,000
005	Noise Emission and Propagation Modeling	$212,000	$200,000	-	-	$412,000
006	Rotorcraft Noise Abatement Operating Conditions Modeling	$250,326	-	-	-	$250,326

007	Civil, Supersonic Over Flight, Sonic Boom (Noise) Standards Development	$100,000	$200,000	-	-	$300,000
008	Noise Outreach	$30,000	$50,000	$75,000	$25,000	$180,000
010	Aircraft Technology Modeling and Assessment	$899,979	$200,000	$310,000	$669,567	$2,079,546
011	Rapid Fleet-wide Environmental Assessment Capability	$600,000	$270,000	$300,000	-	$1,170,000
012	Aircraft Design and Performance Assessment Tool Enhancement	$90,000	-	-	-	$90,000
013	Micro-Physical Modeling & Analysis of ACCESS 2 Aviation Exhaust Observations	$200,000	-	-	-	$200,000
014	Analysis to Support the Development of an Aircraft CO2 Standard	$520,000	-	-	-	$520,000
017	Pilot Study on Aircraft Noise and Sleep Disturbance	$154,000	$343,498	$266,001	$134,924	$898,423

018	Health Impacts Quantification for Aviation Air Quality Tools	$150,000	$150,000	$200,000	$270,000	$770,000
019	Development of Aviation Air Quality Tools for Airport-Specific Impact Assessment: Air Quality Modeling	$320,614	$369,996	-	$625,378	$1,315,988
020	Development of NAS wide and Global Rapid Aviation Air Quality	$150,000	$200,000	$250,000	$250,000	$850,000
021	Improving Climate Policy Analysis Tools	$150,000	$150,000	$150,000	$150,000	$600,000
022	Evaluation of FAA Climate Tools	$150,000	$30,000	$75,000	$100,000	$355,000
023	Analytical Approach for Quantifying Noise from Advanced Operational Procedures	-	$296,711	$250,000	$250,000	$796,711
024	Emissions Data Analysis for CLEEN, ACCESS, and Other Recent Tests	$244,975	-	$75,000	-	$319,975

025	National Jet Fuels Combustion Program – Area #1: Chemical Kinetics Combustion Experiments	-	$615,000	$210,000	$200,000	$1,025,000
026	National Jet Fuels Combustion Program – Area #2: Chemical Kinetics Model Development and Evaluation	-	$200,000	-	-	$200,000
027	National Jet Fuels Combustion Program – Area #3: Advanced Combustion Tests	-	$1,010,000	$580,000	$265,000	$1,855,000
028	National Jet Fuels Combustion Program – Area #4: Combustion Model Development and Evaluation	-	$470,000	$55,000	-	$525,000
029	National Jet Fuels Combustion Program – Area #5: Atomization Tests and Models	-	$640,000	$360,000	$150,000	$1,150,000

030	National Jet Fuels Combustion Program – Area #6: Referee Swirl-Stabilized Combustor Evaluation/Support	-	$349,949	-	-	$349,949
031	Alternative Jet Fuels Test and Evaluation	-	$489,619	$744,891	$999,512	$2,234,022
032	Worldwide LCA of GHG Emissions from Petroleum Jet Fuel	-	$150,000	-	-	$150,000
033	Alternative Fuels Test Database Library	-	$199,624	$119,794	$165,000	$484,418
034	National Jet Fuels Combustion Program – Area #7: Overall Program Integration and Analysis	-	$234,999	$635,365	$192,997	$1,063,361
035	Airline Flight Data Examination to Improve flight Performance Modeling	-	$150,001	-	-	$150,001

036	Parametric Uncertainty Assessment for AEDT2b	-	$65,000	$175,000	$380,000	$620,000
037	CLEEN II Technology Modeling and Assessment	-	$200,000	$150,000	$170,000	$520,000
038	Rotorcraft Noise Abatement Procedures Development	-	$150,000	$150,000	$150,000	$450,000
039	Nephthalene Removal Assessment	-	-	$200,000	$290,000	$490,000
040	Quantifying Uncertainties in Predicting Aircraft Noise in Real-world Situations	-	-	$218,426	$200,000	$418,426
041	Identification of Noise Acceptance Onset for Noise Certification Standards of Supersonic Airplane	-	-	$160,000	$221,000	$381,000

042	Acoustical Model of Mach Cut-off	-	-	$255,000	$150,000	$405,000
043	Noise Power Distance Re-Evaluation	-	-	$150,000	$75,000	225,000
045	Takeoff/Climb Analysis to Support AEDT APM Development	-	-	$250,000	$75,000	$325,000
046	Surface Analysis to Support AEDT APM Development	-	-	$75,000	$75,000	$150,000
048	Analysis to Support the Development of an Engine nvPM Emissions Standards	-	-	$150,000	$200,000	$350,000

Breakout by University*

	Funding Based on award year					
University	**2013**	**2014**	**2015**	**2016**	**2017**	**Total**
Boston University	$5,000	$350,000	$350,000	$400,000	$610,000	$1,715,000
Georgia Institute of Technology	$5,000	$1,660,000	$1,625,001	$1,435,000	$1,468,500	$6,193,501
Massachusetts Institute of Technology	$10,000	$1,153,927	$1,179,073	$ 1,855,000	$1,690,000	$5,888,000
Missouri University of Science and Technology	$5,000	$2,800,000	$750,000	-$147,766	$725,500	$4,132,734
Oregon State University	$5,000	-	$160,000	$80,000	$59,000	$304,000
Pennsylvania State University	$5,000	$862,301	$766,711	$958,426	$890,424	$3,482,862
Purdue University	$5,000	$389,979	$1,030,000	$763,750	$747,067	$2,935,796
Stanford University	$5,000	$380,000	$1,155,000	$345,000	$200,000	$2,085,000

University of Dayton	$5,000	-	$906,196	$1,349,087	$1,192,509	$3,452,792
University of Hawaii	$10,000	-	$75,000	$100,000	$125,000	$310,000
University of Illinois	$5,000	$349,943	$553,000	$375,000	$265,000	$1,547,943
University of North Carolina	$5,000	$320,614	$369,996	-	$625,378	$1,320,988
University of Pennsylvania	$5,000	$154,000	$343,498	$266,001	$134,924	$903,423
University of Tennessee	$5,000	$200,000	$100,000	$100,000	$225,000	$630,000
University of Washington	$5,000	$60,000	$29,997	$15,000		$109,997
Washington State University	$20,000	$974,228	$864,968	$725,961	$796,039	$3,381,196

Breakout by State*

	Funding Based on award year					
State	**2013**	**2014**	**2015**	**2016**	**2017**	**Total**
California	$5,000	$380,000	$1,155,000	$345,000	$200,000	2,085,000
Georgia	$5,000	$1,660,000	$1,625,001	$1,435,000	$1,468,500	$6,193,501
Hawaii	$10,000	-	$75,000	$100,000	$125,000	$310,000
Illinois	$5,000	$349,943	$553,000	$375,000	$265,000	$1,547,943
Indiana	$5,000	$389,979	$1,030,000	$763,750	$747,067	$2,935,796
Massachusetts	$15,000	$1,503,927	$1,529,073	$2,255,000	$2,300,000	$7,603,000
Missouri	$5,000	$2,800,000	$750,000	-$147,766	$725,500	$4,132,234
North Carolina	$5,000	$320,614	$369,996	-	$625,378	$1,320,988
Ohio	$5,000	-	$906,196	$1,349,087	$1,192,509	$3,452,792
Oregon	$5,000	-	$160,000	$80,000	$59,000	$304,000
Pennsylvania	$10,000	$1,016,301	$1,110,209	$1,224,427	$1,025,348	$4,386,285
Tennessee	$5,000	$200,000	$100,000	$100,000	$225,000	$630,000
Washington	$25,000	$1,034,228	$894,965	$740,961	$796,039	$3,491,193

*Totals include administrative funds not associated with specific NFOs